

Hydrogen Bonding—New Insights

CHALLENGES AND ADVANCES IN
COMPUTATIONAL CHEMISTRY AND PHYSICS

Volume 3

Series Editor:

JERZY LESZCZYNSKI

Department of Chemistry, Jackson State University, USA

The titles published in this series are listed at the end of this volume.

Hydrogen Bonding—New Insights

Edited by

SŁAWOMIR J. GRABOWSKI

Department of Physics and Chemistry

University of Łódź

Poland

 Springer

A C.I.P. Catalogue record for this book is available from the Library of Congress.

ISBN-10 1-4020-4852-1 (HB)
ISBN-13 978-1-4020-4852-4 (HB)
ISBN-10 1-4020-4853-X (e-book)
ISBN-13 978-1-4020-4853-1 (e-book)

Published by Springer,
P.O. Box 17, 3300 AA Dordrecht, The Netherlands.

www.springer.com

Printed on acid-free paper

All Rights Reserved

©2006 Springer

No part of this work may be reproduced, stored in a retrieval system, or transmitted in any form or by any means, electronic, mechanical, photocopying, microfilming, recording or otherwise, without written permission from the Publisher, with the exception of any material supplied specifically for the purpose of being entered and executed on a computer system, for exclusive use by the purchaser of the work.

PREFACE

Hydrogen bond is a unique interaction whose importance is great in chemical and bio-chemical reactions including life processes. The number of studies on H-bonding is large and this is reflected by a vast number of different monographs and review articles that cover these phenomena. Hence the following question arises: what is the reason to edit the next book concerning hydrogen bond. The answer is simple, recent numerous studies and the quick and large development of both experimental as well as theoretical techniques cause that old monographs and review articles become quickly out of date.

It seems that presently the situation is similar to that one in the 1980s. Before that time the H-bond was understood in the sense of the Pauling definition as an electrostatic in nature interaction concerning three atoms—hydrogen atom located between two other electronegative ones and bounded stronger to one of them. Few studies were published where the authors found interactions which at least partly fulfill the classical definition of H-bond, as for example the Suttor studies in 1964 on C–H···Y interactions in crystals. However, since C-atom in the proton-donating bond is not electronegative thus these systems are not in line with the classical definition. Also the other “typical” features of H-bonds for C–H···Y systems are not always fulfilled. No surprisingly, only when the study of Taylor and Kennard (1982, *J. Am. Chem. Soc.* 104, 5063) based on the refined statistical techniques applied for the data taken from the Cambridge Structural Database appeared, the existence of C–H···Y hydrogen bonds was commonly accepted. And since that time there was a forceful “jump” on the number of H-bond studies. Among others the C–H···Y, X–H···C and C–H···C interactions were investigated and their features were also compared with the so-called conventional hydrogen bonds. However, it is worth mentioning that very often the controversies and discussions are related to different meaning of H-bond and with the use of different definitions of that interaction. What are the unique features of H-bond interaction? We hope that the reader will find an answer within the chapters of this volume.

One can ask another important question: what is the current situation on investigations on H-bond? Recently, different kinds of interactions are analyzed which may be classified as hydrogen bonds; one can mention dihydrogen bonds or blue-shifting hydrogen bonds. There are new various theoretical methods. One of the most important tools often recently applied in studies on H-bonds is the “atoms in molecules” theory (AIM). It is worth mentioning the studies on the nature of H-bond interaction since the following questions arise

very often: are the H-bonds electrostatic in nature according to the Pauling definition? What are differences between different kinds of H-bonds since the H-bond energy ranges from a fraction to tens of kcal/mol? Is this energy difference the reason why very weak H-bonds are different in nature than the very strong ones? One can provide a lot of examples on new topics, new theoretical methods and new experimental techniques recently used in studies on H-bond interactions.

In this volume mainly the theoretical studies are presented, however also examples of experimental results are included and all the computational results are strongly related to experimental techniques. The most important topics considered in the recent studies on hydrogen bond are discussed in this volume, such problems as: how to estimate the energy of intramolecular H-bonds, covalency of these interactions, the distant consequences of H-bond since in earlier studies usually only the X-H...Y H-bridge was analyzed (X-H is the proton-donating bond and Y is an acceptor), the differences between H-bond and van der Waals interactions from one side and covalent bonds from the other side, the use of the Bader theory to analyze different kinds of H-bonds, the influence of weak H-bonds upon structure and function of biological molecules, etc. There are also topics related to the experimental results: crystal structures, infrared and NMR techniques and many others.

It is obvious that in the case of such broad research area as hydrogen bond interactions it is very difficult to consider all aspects and discuss all problems. However, the authors of the chapters made an effort to consider all current topics and recent techniques applied in the studies of this important phenomenon. As an editor of this volume, I would like to thank the authors for their outstanding work. Their excellent contributions collected in this volume provide the readers the basis to systematize knowledge on H-bond interaction and new insights into hydrogen bonding.

Sławomir J. Grabowski
Łódź, Poland
December 2005

COLOR PLATE SECTION

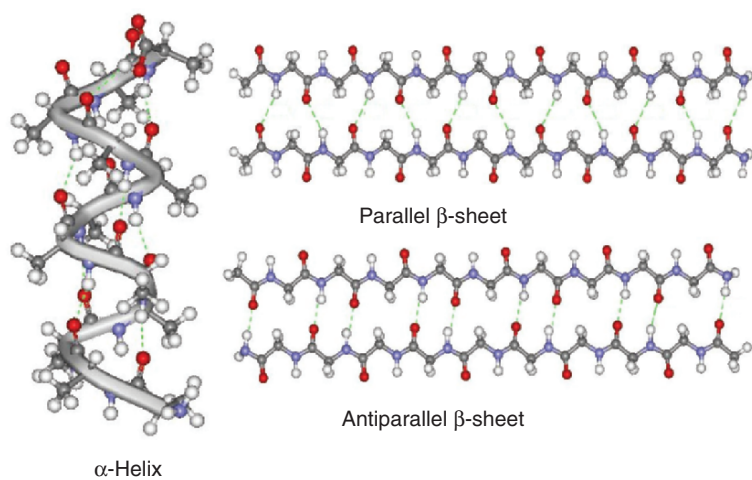


Figure 1-2. Hydrogen bonding in various protein secondary structures.

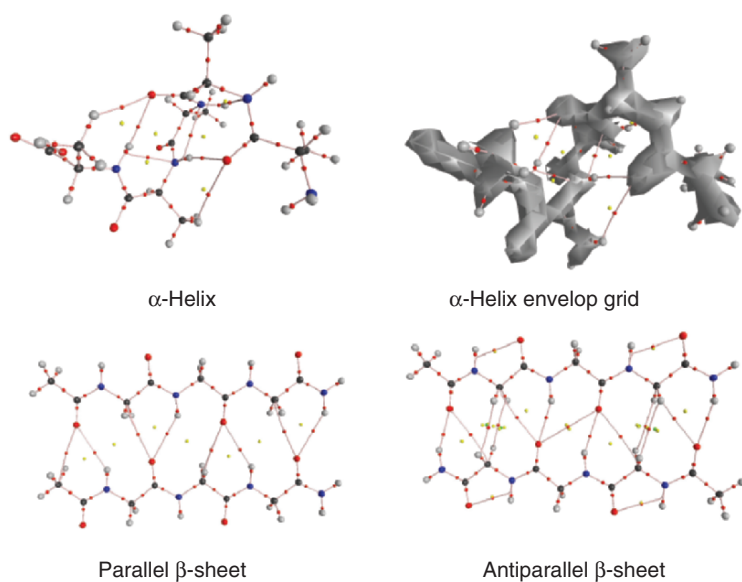


Figure 1-11. Molecular topographies of secondary structures of protein obtained from theoretical electron density. (Results from Ref. [325].)

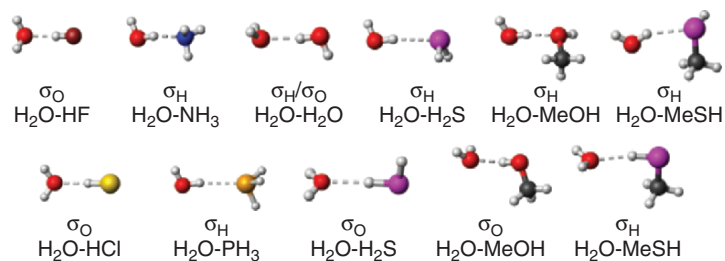


Figure 4-2. Structures of the hydrogen-bonded complexes of H_2O .

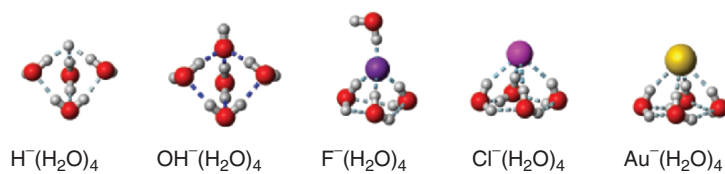


Figure 4-8. Structures of hydrated anion clusters.

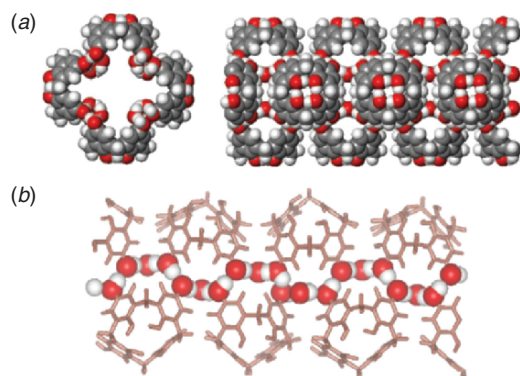


Figure 4-11. Longitudinal H-bond relay comprised of CHQs and water. (a) Tubular polymer structure of a single nanotube obtained with x-ray analysis for the heavy atoms and with ab initio calculations for the H-orientations (top and side views). (b) One of four pillar frames of short H-bonds represents a 1-D H-bond relay composed of a series of consecutive OH groups [hydroxyl groups ($-\text{OH}$) in CHQs and the OHs in water molecules]. Reproduced by permission of American Chemical Society: Ref. [54].

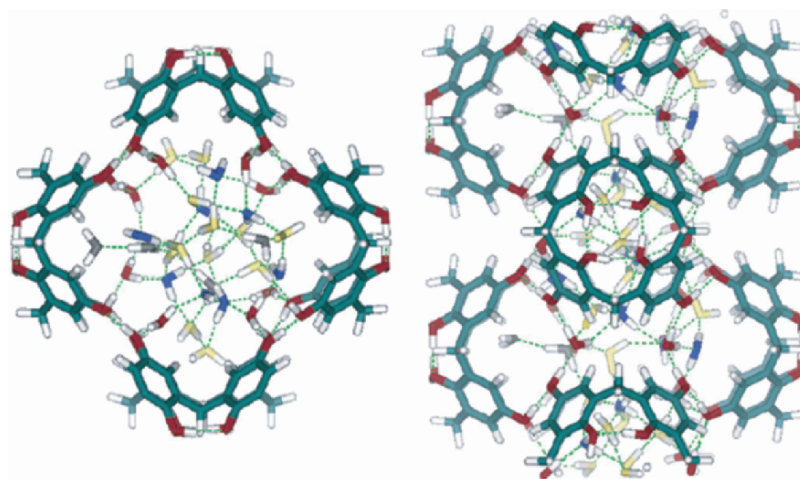


Figure 4-12. The water network in a single tube (top and side views). The top view (left) shows 8 bridging water molecules in red, 8 first-hydration shell water molecules in blue, 12 second-hydration shell water molecules in yellow, and 4 third-hydration shell water molecules in gray, while the side view shows twice those in the top view. Reproduced by permission of American Chemical Society: Ref. [54].

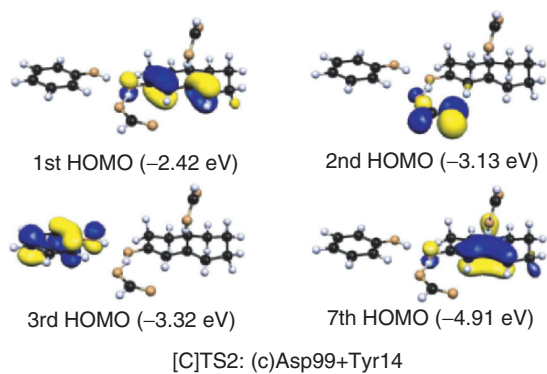


Figure 4-13. Schematic representation of reaction mechanism and HOMO energy levels of transition state (TS) of KSI.

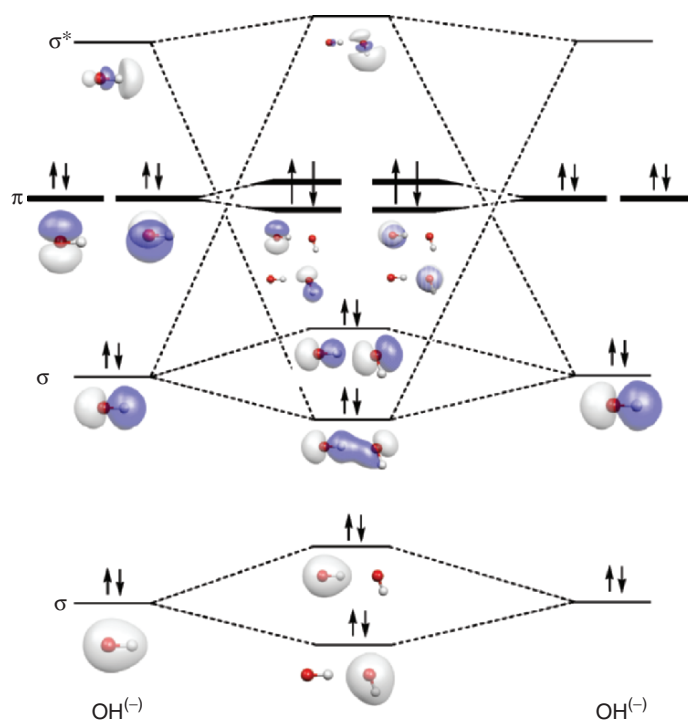


Figure 5-19. Orbital diagram of the interaction between two $\text{OH}^{(-)}$ anions with their $\text{O-H}\cdots\text{O}$ contact at the same geometry than the $\text{O-H}\cdots\text{O}$ bond in the water dimer. See text for details.

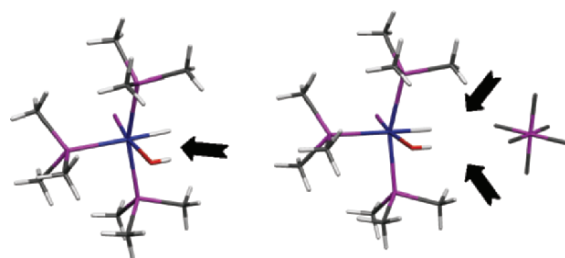


Figure 6-4. The x-ray structure of $[\text{IrH}(\text{OH})(\text{PMe}_3)_4][\text{PF}_6]$: cation (left) and cation and anion (right).

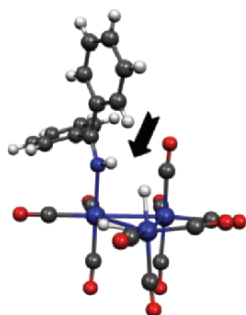


Figure 6-5. The x-ray structure of $[\text{Os}_3(\text{CO})_{10}\text{H}(\mu - \text{H})(\text{HN} = \text{CPh}_2)]$.

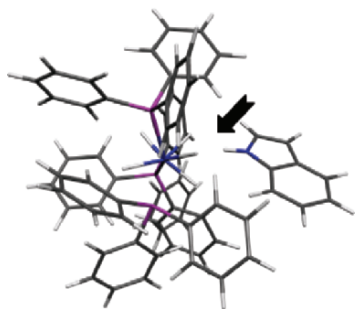


Figure 6-6. The neutron diffraction structure of $[\text{ReH}_5(\text{PPh}_3)_3]\cdot\text{indole-benzene}$.

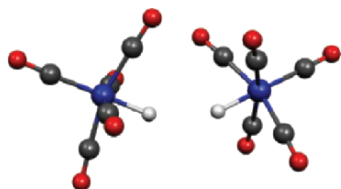


Figure 6-7. The neutron diffraction structure of $[\text{MnH}(\text{CO})_5]$ dimer.

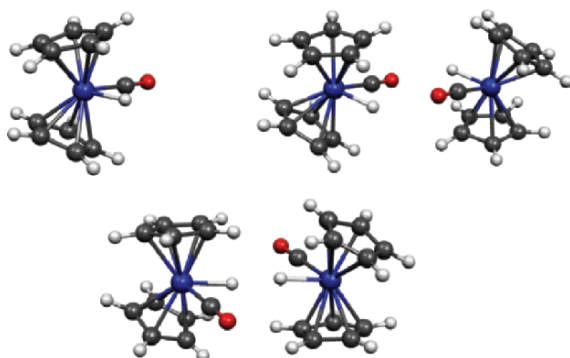


Figure 6-8. The x-ray structure of the monomer $[(\eta^5 - \text{C}_5\text{H}_5)_2\text{MoH}(\text{CO})]^+$ (top, left), the monoclinic form (top, right) and the triclinic form (bottom).

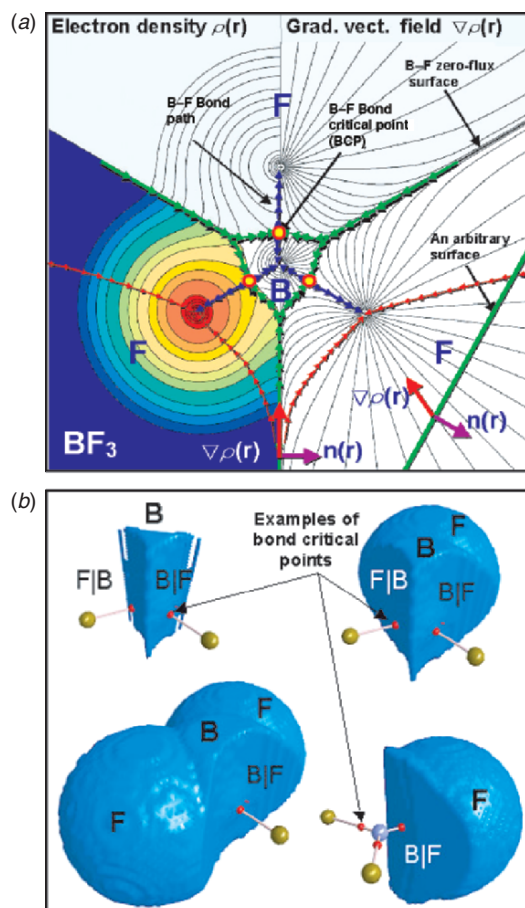


Figure 9-1. (a) Plot of the electron density distribution (left) and of the associated gradient vector field of the electron density (right) in the molecular plane of BF_3 . The lines connecting the nuclei (denoted by the blue arrows) are the lines of maximal density in space, the B-F bond paths, and the lines delimiting each atom (green arrows) are the intersection of the respective interatomic zero-flux surface with the plane of the drawing. The density contours on the left part of the figure increase from the outermost 0.001 au isodensity contour in steps of 2×10^n , 4×10^n , and 8×10^n au with n starting at -3 and increasing in steps of unity. The three bond critical points (BCPs) are denoted by the small red circles on the bond paths. One can see that an arbitrary surface does not satisfy the dot product in Eq. 1 since in this case the vectors are no longer orthogonal. (b) Three-dimensional renderings of the volume occupied by the electron density with atomic fragments in the BF_3 molecule up to the outer 0.002 au isodensity surface. The interatomic zero-flux surfaces are denoted by the vertical bars between the atomic symbols, F|B. The large spheres represent the nuclei of the fluorine atoms (golden) and of the boron atom (blue-grey). The lines linking the nuclei of bonded atoms are the bond paths and the smaller red dots represent the BCPs.

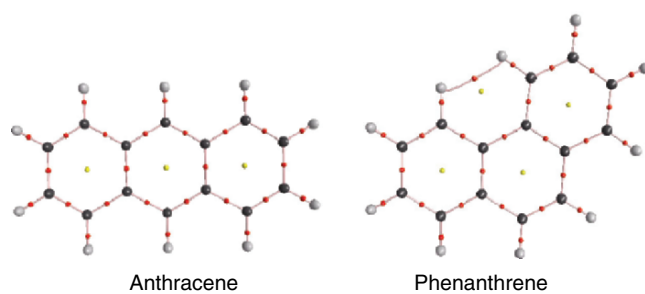


Figure 9-3. Molecular graphs of the two isomers anthracene and phenanthrene. The lines linking the nuclei are the bond paths, the red dots on the bond paths are the BCPs, and the yellow dots are the ring critical points (RCPs). The H–H bond path between H4 and H5 exists only in phenanthrene.

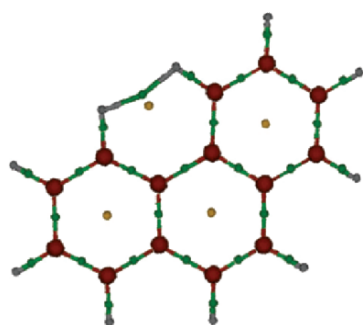


Figure 9-5. The virial graph of phenanthrene.

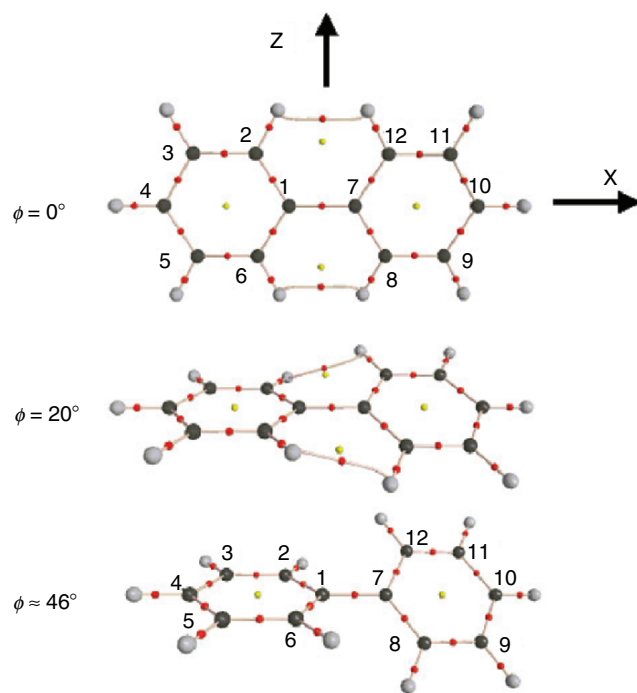


Figure 9-6. Molecular graphs of biphenyl as functions of the dihedral angle between the ring planes (ϕ). The coordinate system is indicated along with the atom numbering system. Hydrogen atoms take the same number as the carbon atoms to which they are bonded. At the critical value of $\phi \approx 27^\circ$ there is a sudden “catastrophic” change in structure with the rupture of the two H–H bond paths (H2–H12 and H6–H8).

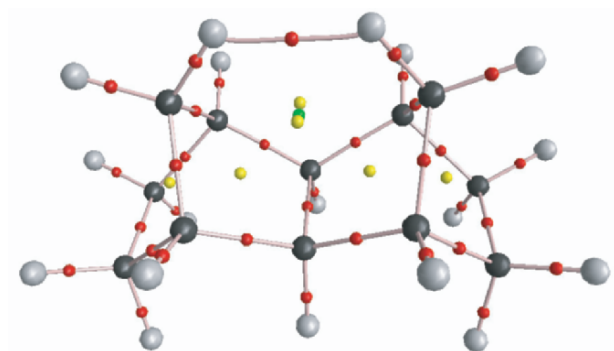


Figure 9-9. The calculated molecular graph of *exo, exo*-tetracyclo[6.2.1.1^{3,6}.0^{2,7}] dodecane which consists of two fused norbornanes rings. The H–H bond path links the nuclei of the two bridgehead hydrogen atoms. This results in the closure of two rings concomitant with the appearance of two ring critical points (yellow) and a cage critical point between them (green).

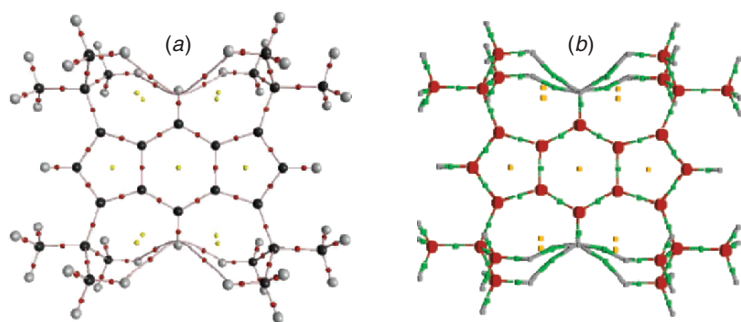


Figure 9-10. The calculated molecular graph (a) and its corresponding virial graph (b) of tetra-*tert*-butylindacene.

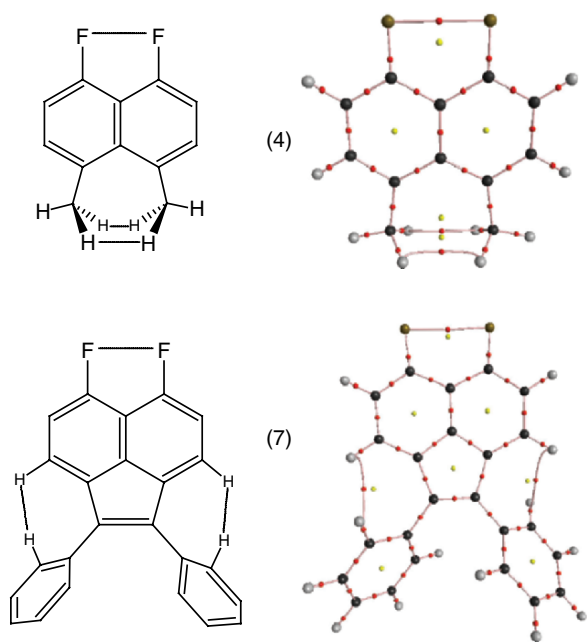


Figure 9-11. The chemical structure and the molecular graph of compounds (4) and (7) exhibiting $C(sp^3)-H \cdots H-C(sp^3)$ and $C(sp^2)-H \cdots H-C(sp^2)$ bond paths, respectively (adapted after Ref. [40]).

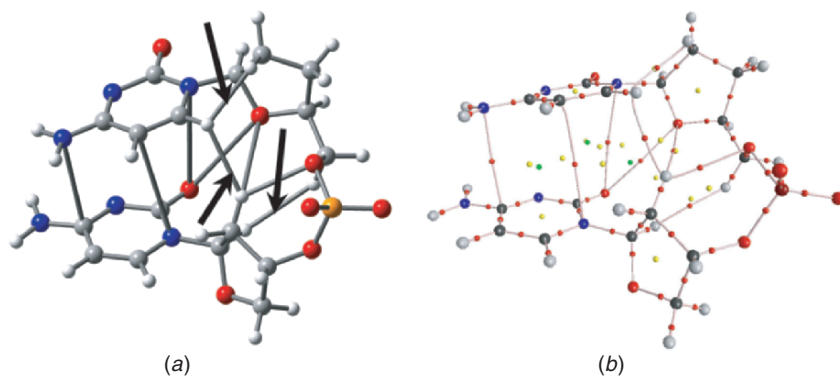


Figure 9-12. An idealised (a) and actual (b) molecular graph of a piece of DNA consisting of two consecutive cytosine bases attached to the phosphate-sugar backbone along a strand of DNA showing the several closed-shell interactions including three H-H bond paths (indicated by the arrows). (Adapted after Ref. [27].)

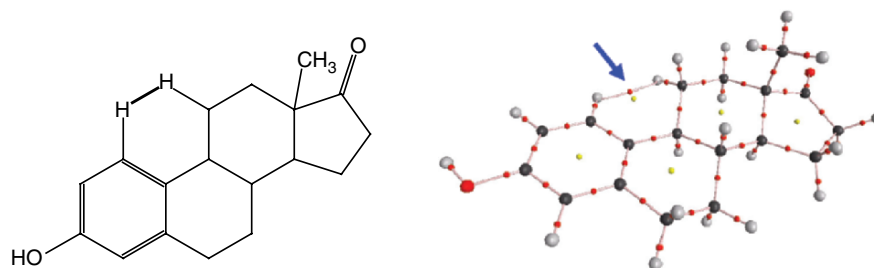


Figure 9-13. Example of a H-H bond path in biological molecules. The chemical structure and the molecular graph of the hormone estrone (the blue arrow indicates the H-H bond path) (adapted from Ref. [133]).

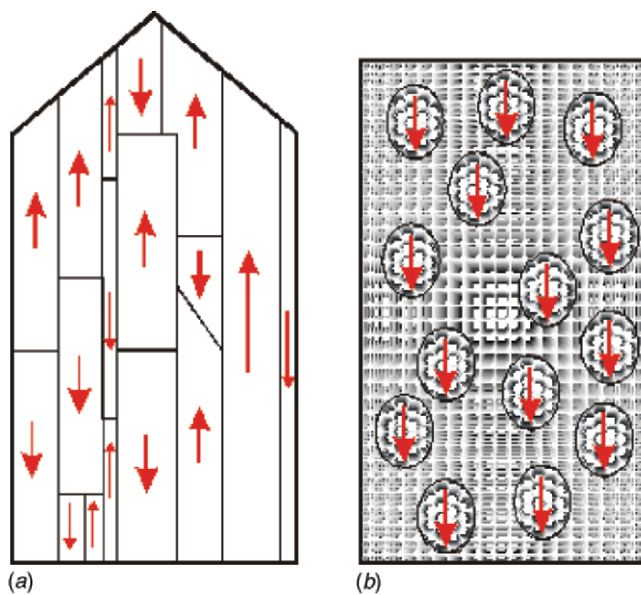


Figure 13-3. A schematic illustration of the domain structure in a ferroelectric crystal (a), and of a relaxor with the polarization of nanoregions pooled in one direction (b).

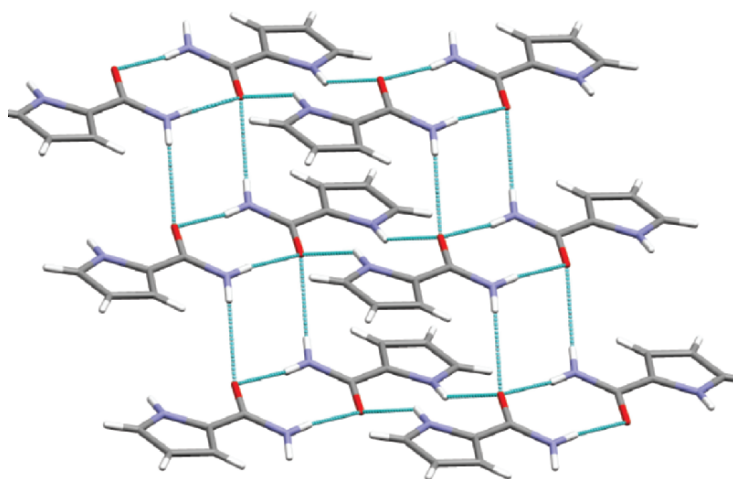


Figure 14-12. Pyrrrole-2-Carboxamide—crystal structure motif containing centrosymmetric dimers with double N-H...O H-bonds.

CONTENTS

Preface	v
1. Characterization of Hydrogen Bonding: From van der Waals Interactions to Covalency	1
<i>R. Parthasarathi and V. Subramanian</i>	
2. Intramolecular Hydrogen Bonds. Methodologies and Strategies for Their Strength Evaluation	51
<i>Giuseppe Buemi</i>	
3. Changes of Electron Properties in the Formation of Hydrogen Bonds	109
<i>Luis F. Pacios</i>	
4. Weak to Strong Hydrogen Bonds	149
<i>Han Myoung Lee, N. Jiten Singh, and Kwang S. Kim</i>	
5. The Nature of the C–H···X Intermolecular Interactions in Molecular Crystals. A Theoretical Perspective	193
<i>Juan J. Novoa, Fernando Mota, and Emiliana D’Oria</i>	
6. Weak Hydrogen Bonds Involving Transition Elements	245
<i>Maria José Calhorda</i>	
7. Contribution of CH···X Hydrogen Bonds to Biomolecular Structure	263
<i>Steve Scheiner</i>	
8. Neutral Blue-Shifting and Blue-Shifted Hydrogen Bonds	293
<i>Eugene S. Kryachko</i>	
9. Hydrogen–Hydrogen Bonding: The Non-Electrostatic Limit of Closed-Shell Interaction Between Two Hydrogen Atoms. A Critical Review	337
<i>Chérif F. Matta</i>	
10. Potential Energy Shape for the Proton Motion in Hydrogen Bonds Reflected in Infrared and NMR Spectra	377
<i>Gleb S. Denisov, Janez Mavri, and Lucjan Sobczyk</i>	
11. Molecular Geometry—Distant Consequences of H-Bonding	417
<i>Tadeusz M. Krygowski and Joanna E. Zachara</i>	

12. Topology of X-Ray Charge Density of Hydrogen Bonds.....	441
<i>Tibor S. Koritsanszky</i>	
13. Structure–Property Relations for Hydrogen-Bonded Solids	471
<i>A. Katrusiak</i>	
14. Unrevealing the Nature of Hydrogen Bonds: π -Electron Delocalization Shapes H-Bond Features. Intramolecular and Intermolecular Resonance-Assisted Hydrogen Bonds.....	487
<i>Sławomir J. Grabowski and Jerzy Leszczynski</i>	
Index	513

CHAPTER 1

CHARACTERIZATION OF HYDROGEN BONDING: FROM VAN DER WAALS INTERACTIONS TO COVALENCY

*Unified picture of hydrogen bonding based
on electron density topography analysis*

R. PARTHASARATHI and V. SUBRAMANIAN

Chemical Laboratory, Central Leather Research Institute, Adyar, Chennai 600 020, India

Abstract This chapter reviews different aspects of hydrogen bonding (H-bonding) interaction in terms of its nature, occurrence, and other characteristic features. H-bonding is the most widely studied noncovalent interaction in chemical and biological systems. The state-of-art experimental and theoretical tools used to probe H-bonding interactions are highlighted in this review. The usefulness of electron density topography in eliciting the strength of the H-bonding interactions in a variety of molecular systems has been illustrated.

Keywords: Hydrogen bond; AIM; electron density; Laplacian of electron density; water; DNA; protein.

1 INTRODUCTION

Hydrogen bonding (H-bonding) is an intensively studied interaction in physics, chemistry and biology, and its significance is conspicuous in various real life examples [1]. Understanding of H-bonding interaction calls for inputs from various branches of science leading to a broad interdisciplinary research. Numerous articles, reviews, and books have appeared over 50 years on this subject. As a complete coverage of the voluminous information on this subject is an extremely difficult task, some recent findings are presented in this chapter.

The multifaceted nature of H-bonding interaction in various molecular systems has been vividly explained in the classical monographs on this interesting topic [2, 3]. Different quantum chemical approaches which predict the structure, energetics, spectra, and electronic properties of H-bonded complexes

were systematically presented in the monograph by Scheiner [4]. These monographs cover several important aspects of H-bonding, indicating the mammoth research activity in this field. It is clearly evident from the history of H-bonding that Pauling's book on *The Nature of the Chemical Bond* attracted the attention of the scientific community [5]. Currently, the term "Hydrogen Bonding" includes much of the broader spectrum of interactions found in gas, liquid, and solid states in addition to the conventional ones. In order to investigate this interaction, several experimental and theoretical methods have been used [1–4]. With the advances in experimental and computational techniques, it is now possible to investigate the nature of H-bonding interaction more meticulously. Bader's theory of atoms in molecules (AIM) [6] is one of the widely used theoretical tools to understand the H-bonding interaction. The present review is focused on applications of AIM theory and its usefulness in delineating different types of H-bonded interaction.

The outline of this chapter is as follows: The chapter begins with the classical definition of H-bonding. Its importance in molecular clusters, molecular solvation, and biomolecules are also presented in the first section. A brief overview of various experimental and theoretical methods used to characterize the H-bonding is presented in the second section with special emphasis on Bader's theory of AIM [6]. Since AIM theory has been explained in numerous reviews and also in other chapters of this volume, the necessary theoretical background to analyze H-bonding interactions is described here. In the last section, the salient results obtained from AIM calculations for a wide variety of molecular systems are provided. The power of AIM theory in explaining the unified picture of H-bonding interactions in various systems has been presented with examples from our recent work.

1.1 Classical Definition and Criteria of Hydrogen Bonding

H-bond is a noncovalent, attractive interaction between a proton donor X–H and a proton acceptor Y in the same or in a different molecule:



According to the conventional definition, H atom is bonded to electronegative atoms such as N, O, and F. Y is either an electronegative region or a region of electron excess [1–5, 7]. However, the experimental and theoretical results reveal that even C–H can be involved in H-bonds and π electrons can act as proton acceptors in the stabilization of weak H-bonding interaction in many chemical systems [3, 4]. In classical H-bonding, there is a shortening of X \cdots Y distance, if X–H is H-bonded to Y. The distance between X \cdots Y is less than the sum of the van der Waals radii of the two atoms X and Y. H-bonding interactions lead to increase in the X–H bond distance. As a consequence, a substantial red shift (of the order of 100 cm⁻¹) is observed in the fundamental X–H stretching vibrational frequencies. Formation of the X–H \cdots Y bond

decreases the mean magnetic shielding of proton involved in the H-bonding thus leading to low field shift [8, 9]. The low field shift in H-bonded complexes is about few parts per million and the anisotropy of the proton magnetic shielding can be increased by as much as 20 parts per million [10–12].

The strength of the strong H-bonding interactions ranges from 15.0 to 40 kcal/mol [1–4]. For the moderate (conventional) and weak H-bonds, the strengths vary from 4–15 to 1–4 kcal/mol, respectively. The strength of H-bonded interactions in diverse molecular systems has been classified [2, 13, 14]. Desiraju has proposed a unified picture of the H-bonding interactions in various systems and the concept of “hydrogen bridge” [14]. The three types of H-bonding interactions which are most often discussed in the literature are weak, moderate, and strong. The properties of these three types are listed in Table 1.

The H-bond strength depends on its length and angle and hence, it has directionality. Nevertheless, small deviations from linearity in the bond angle (up to 20°) have marginal effect on H-bond strength. The dependency of the same on H-bond length is very important and has been shown to decay exponentially with distance. The question on “what is the fundamental nature of hydrogen bond?” has been the subject of numerous investigations in the literature [1–4]. In a classical sense, H-bonding is highly electrostatic and partly covalent. From a rigorous theoretical perspective, H-bonding is not a simple interaction. It has contributions from electrostatic interactions (acid/base), polarization (hard/soft) effects, van der Waals (dispersion/repulsion: intermolecular electron correlation) interactions and covalency (charge transfer)[14].

1.2 Nature of Conventional and Improper or Blue Shifting Hydrogen Bonding

It is evident from the conventional definition of H-bonding that formation of X–H···Y bond is accompanied by a weakening of the covalent X–H bond with concomitant decrease of X–H stretching frequency [1–4, 13, 14]. This red shift

Table 1. General characteristics of the three major types of H-bonds. The numerical information shows the comparative trends only [13]

H-bond parameters	Strong	Moderate	Weak
Interaction type	Strongly covalent	Mostly electrostatic	Electrostatic/dispersed
Bond lengths (H···Y[Å])	1.2–1.5	1.5–2.2	>2.2
Lengthening of X–H (Å)	0.08–0.25	0.02–0.08	<0.02
X–H Vs. H···Y	X–H ≈ H···Y	X–H < H···Y	X–H << H···Y
H-bond length (X···Y [Å])	2.2–2.5	2.5–3.2	>3.2
Directionality	Strong	Moderate	Weak
H-bond angles (°)	170–180	>130	>90
H-bond strength (kcal/mol)	15–40	4–15	<4
Relative Infrared shift (cm ⁻¹)	25%	10–25%	<10%

belongs to one of the most important characteristics of the H-bonding interaction. Its other signature is the considerable increase in the intensity of the spectral band connected with X–H stretching frequency. In addition, there is a nonnegligible electron density transfer from a proton acceptor to a donor [15]. Electron density is transferred from the proton acceptor (lone pair) to the σ^* -antibonding orbital of X–H bond, which causes a weakening and elongation of this bond and a decrease in the X–H stretch frequency.

On the contrary, there are some typical situations, wherein the X–H bond gets compressed and the corresponding X–H stretching vibration is shifted to a higher frequency. This type is called as blue shifting or improper or anti-H-bonding. A review on this appeared recently [16]. One of the first experimental evidences of blue shift in X–H stretching frequency upon formation of a complex was observed by Sandorfy and coworkers [17]. The other experimental evidence for blue shift was noted by Arnold and coworkers who measured the blue shift of C–H stretch of chloroform–triformylmethane complexation [18]. In 1997, Boldeshul et al. have reported the blue shift in the H-bonded complexes of haloforms with various proton acceptors [19]. The first theoretical study on blue shifted H-bonded systems has been performed by Hobza et al. [20]. Subsequently numerous theoretical studies have been carried out to understand the blue shifted H-bonding interaction [21–45]. The electronic basis for improper H-bonding has been analyzed by Alabugin et al. [46]. The observed structural reorganization of X–H bond in both proper and improper H-bonding arises from a balance of hyperconjugative bond weakening and rehybridization bond strengthening. Improper H-bonding is likely to be seen only when the X–H bond elongating hyperconjugative $n(Y) \rightarrow \sigma^*(X-H)$ interaction is relatively weak. When the hyperconjugative interaction is weak and the X-hybrid orbital in X–H bond is able to undergo a sufficient change in hybridization and polarization, rehybridization dominates leading to a shortening of the X–H bond and a blue shift in the X–H stretching frequency. It has been shown that improper H-bonding is not an unexpected aberration but rather a logical consequence of Bent's rule in structural organic chemistry, which predicts an increase in s-character in X–H bonds upon H-bond formation, because H becomes more electropositive during this process [46].

1.3 Hydrogen Bonding in Molecular Dimers

Numerous H-bonded homodimers and heterodimers have been investigated using ab initio electronic structure calculations and density functional theory (DFT)-based methods [1–4]. Various aspects of H-bonding starting from classical definition to H-bonded dimers have been discussed in one of the earlier reviews by Kollman and Allen [47]. Water dimer is a typical example used to explain the H-bonding interaction. The structure of the water dimer was analyzed by a molecular beam electric resonance experiment [48, 49]. Almost all theoretical methods developed so far have been employed to predict the

structure and energetics of H-bonding interaction in water [1–4, 50–63]. All types of basis sets including Pople’s and Dunning’s correlation consistent basis sets have been used to calculate the structure and energetics of the water dimer [64]. The predictive power of the DFT-based methods have also been systematically analyzed by taking the water dimer as an example. The calculated H-bond strength in the water dimer obtained from various levels of calculations is represented in Table 2.

It is evident from the large scale ab initio molecular orbital calculations that the best estimate of strength of H-bond energy of water dimer is 5.0 ± 0.1 kcal/mol [58]. Correcting this value for zero-point and temperature effects yields the value around $\Delta H(375) = -3.2 \pm 0.1$ kcal/mol. This value is within the error limits of the best experimental estimate of -3.6 ± 0.5 kcal/mol. From the analysis of DFT results, it is found that the hybrid methods provide overall description of properties of the H-bonded water dimer [64].

Extensive work on the H-bonding in dimers is presented in previous original articles and reviews [1–4, 7, 13, 65–74]. Dimers of methanol, formaldehyde, formamide, formic acid, acetic acid, *N*-methylacetamide, phenol, etc., have been studied using a variety of quantum chemical methods. Some of these dimers have been chosen as model systems to understand the H-bonding interactions in biomolecules. Geometries, energetics, vibrational frequencies, and electronic properties of H-bonded dimers were investigated [4]. The strengths of O–H···O–H, O–H···N–H, N–H···O–C, C–H···O–C, π ···O–H, π ···H–N, π ···H–C, and π – π interactions have been predicted from these calculations. The analysis clearly depicts the presence of different kind of interactions found in the various homodimer and heterodimer models. From these studies, it is possible to understand the multifarious interactions in stabilization and structure of biomolecules.

Table 2. Counterpoise corrected stabilization energy (kcal/mol) of the water dimer calculated at different levels of theory

Basis set	Methods			
	HF	MP2	CCSD(T)	DFT(B3LYP)
6-31G*	4.75	5.12	–	4.75
6-31G**	4.56	4.69	–	5.1
6-31 + G**	4.44	4.81	–	5.24
6-31 + +G**	4.42	4.79	–	5.22
6-311 + +G**	4.27	4.48	–	5.07
cc-pVDZ	3.6	3.9	3.7	–
cc-pVTZ	3.5	4.4	4.3	4.5
cc-pVQZ	3.5	4.7	4.7	4.6
aug-cc-pVDZ	3.5	4.3	4.3	4.5
aug-cc-pVTZ	3.5	4.6	4.7	4.6
aug-cc-pVQZ	3.5	4.8	4.9	4.6

1.4 Hydrogen Bonding in Molecular Hydration and Microsolvation

Solvation of neutral and charged molecules is a process which is of fundamental importance to many phenomena in chemistry and biology [75]. In the literature, molecular hydration, molecular solvation, and microsolvation are the frequently used terms to describe the interaction of solvent molecules with solute. In order to study the solvation process, isolated size-selected clusters of the type $M-S_n$ have been frequently used as models to characterize the stepwise molecular hydration of molecule (M) by solvent (S). The fruitful combination of mass spectrometric and other spectroscopy techniques on the experimental side, and electronic structure calculations on the other side has been shown to be a powerful strategy [76]. Several investigations describing the solvation of molecules using different quantum chemical calculations and classical approaches have been reported [77–80]. In the prediction of effect of solvation, two approaches viz continuum solvation model (implicit solvation) and direct interaction of solvent molecules with solute (discrete model) have been used [80, 81]. The continuum solvation model treats the solvent as a continuous dielectric medium that reacts with solute charge distribution. Self-consistent reaction field (SCRF) model developed from the original works of Born–Onsager and Kirkwood is now used for modeling the bulk effect of solvation [82–86]. Various implicit models employed to treat molecular solvation or hydration have been reviewed in detail [77–80]. However, continuum models do not take into account of the specific H-bonding interactions of solvent molecules with solutes. In order to elicit the molecular hydration process, explicit interaction of solvent molecules with the solute has been considered. To probe these interactions, a variety of models have been proposed. Buckingham–Fowler model [87], Molecular Mechanics for Clusters (MMC) and Dykstra [88], Alhambra, Luque and Orozco model [89], Polarizable Atomic Multipole Model [90], and Electrostatic Potential for Intermolecular Complexation (EPIC) [91, 92] are some of the popular strategies used to study these weak interactions in solute–solvent.

EPIC model originated from the pioneering work of Gadre and his group and it exploits rich topographical features of molecular electrostatic potential (MESP) [91–98]. Several theoretical methodologies combined with MESP topography have been used to investigate molecular hydration processes [97–104]. Recently, the success of the EPIC model along with other quantum chemical investigations on explicit molecular hydration processes has been reviewed by Gadre et al. [98]. MESP topography of molecules has been found to give information on the probable sites of water molecule interaction in the both polar and nonpolar molecules. Different classes of examples starting from small molecules to large clusters have been investigated in detail using EPIC and quantum chemistry tools. In the microsolvation of nonpolar molecules, benzene was used as a prototype molecule. Numerous experimental and theoretical methods have been employed to understand the hydration process in benzene.

Experimental and theoretical results on microsolvation of benzene were summarized by Brutschy [105]. Infrared (IR) spectral investigations of benzene–(H₂O)₈ have clearly revealed the changes in the structural features of water clusters in the presence of benzene. Zwier has reported the detailed analysis on the IR spectra of large size solvated clusters [106].

The structures and properties of isolated, solvated, and complexed nucleic acid bases have been reviewed by Leszczynski [107]. Interaction of water molecules with various DNA bases, base pairs, and DNA stacks has also been studied to understand structure, nonplanarity bases, tautomerism, and stability. Gadre et al. have also studied the solvation of biomolecules using the EPIC-based docking followed by ab initio and DFT methods [98]. The gas phase hydration of cytosine base, cytosine–cytosine H-bonded base pairs (CC), and cytosine–cytosine stacked dimer (C/C) using ab initio calculations have been reported by our group [108, 109]. Using the topological features of MESP, starting geometries for ab initio calculations have been generated using the EPIC model for interaction of water molecules with cytosine (C), cytosine–cytosine H-bonded pair (CC), and stacked dimer (C/C). The calculated interaction energies of hydrated stacked C/C dimer are numerically higher than that predicted for hydrated CC pair and the difference in the energy ranges from 1 to 2.5 kcal/mol at all levels of calculations explored [109]. Hence, it has been concluded that the stacked C/C dimer hydrates better than the H-bonded base pair, which is in agreement with the experimental evidence [110].

In addition to the microsolvation, the effect of solvation on the reaction has also been modeled by Re and Morokuma [111]. They demonstrated the significance of molecular solvation using the two-layered ONIOM method. The S_N2 pathway between CH₃Cl and OH[−] ion in microsolvated clusters with one or two water molecules has been studied. This work highlighted the role of solvent in the chemical reaction and also the power of ONIOM model to predict complex systems. All these studies have undoubtedly brought out the significance of H-bonding in solute–solvent interaction, chemical reactivity, and molecular solvation phenomenon.

1.5 Hydrogen Bonding in Biological Systems

1.5.1 In DNA and RNA base pairing

It is well documented that the H-bonding interaction is important for the structure and function of biomolecules [112, 113]. H-bonding in α -helical and β -sheet structures in proteins by Pauling et al. [114], DNA base pairs by Watson and Crick [115], and triple helix of collagen by Ramachandran and Kartha [116], and simultaneously by Rich and Crick [117] have opened a new branch of science known as “structural biology.” The H-bonding interactions in nucleic acids play a crucial role in the double helical structure of DNA and RNA along with stacking interactions facilitating molecular recognition via

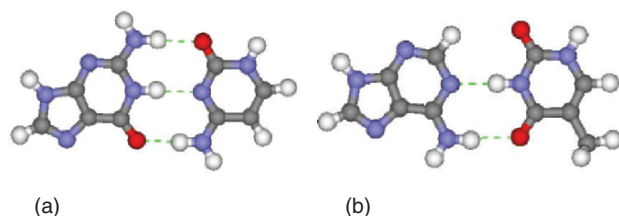


Figure 1. Hydrogen-bonded (a) G·C and (b) A·T DNA base pairs.

replication processes and protein synthesis [113]. Extensive theoretical methodologies have been used to derive information about the H-bonding in DNA base pairing and base stacking [118–134]. The representative H-bonded G·C and A·T DNA base pairs are shown in Fig. 1. The *ab initio* calculation on the G·C and A·T pairs provides the required information about the strength of H-bonding in these systems and the respective binding energies are 20.0 and 17.0 kcal/mol [118]. H-bonding is mainly accountable for the DNA–ligand recognition phenomenon and the studies on molecular recognition help to design new drug molecules [135].

Water is an essential part in the biomacromolecular system, which is mainly responsible for the structure and functions of nucleic acids, proteins, and other constituents of cell [136–138]. Both proteins and DNA are generally hydrated. It is well known that the conformation of DNA is sensitive to hydration, and presence of salts and ligand molecules [112, 138]. The nucleic acids have three levels of water structure. About 12 water molecules per nucleotide are involved in the primary hydration shell [107, 112, 137, 138]. The water molecules present in the primary shell are impermeable to cations and do not form ice on freezing. The secondary level is permeable to cations and forms ice on freezing and third level is the completely disordered, so-called bulk water. Several theoretical studies have been carried out on the level of hydration on DNA bases, base pairs, base stacks, and double helical DNA [107, 121, 131, 139]. Both the experimental and molecular simulation studies have clearly brought out the importance of hydration in DNA and RNA structures [140–147].

1.5.2 Hydrogen bonding in protein secondary structure

H-bonding is the most important interaction governing protein structure, folding, binding, enzyme catalysis, and other properties. The basic secondary structural elements in protein structure are α -helix, β -sheet, γ -turn, π -helix, etc., which are stabilized by H-bonding interactions [1–3, 113, 136]. H-bonding in α -helix and β -sheet is presented in Fig. 2. α -Helix is a result of intramolecular H-bonded interaction between C = O group of the i th peptide residue with N–H group of the $i + 4$ th residue in the peptide or protein sequence. In both the parallel and antiparallel β -sheets, the C = O of one peptide chain H-bonds with

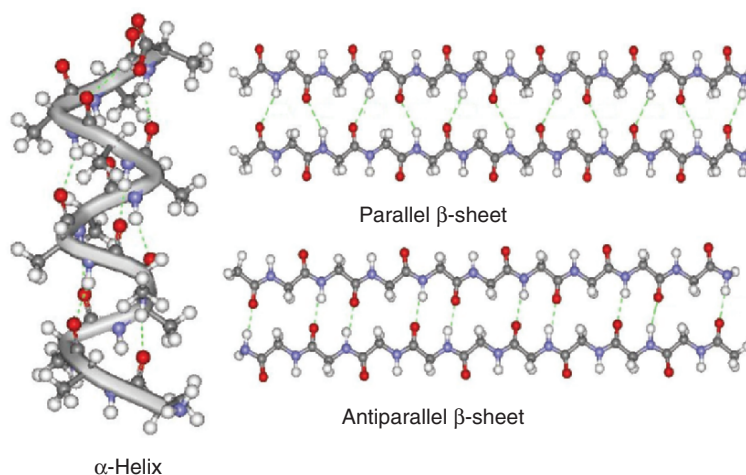


Figure 2 (see color section). Hydrogen bonding in various protein secondary structures.

N–H of the other chain in a unique fashion. H-bonding interaction along with other noncovalent interactions is mainly accountable for the interaction of DNA and protein with other molecules.

Making and breaking of H-bonding in a dynamics situation profoundly influence the rates of dynamics equilibria, which are of paramount importance for the biological activity of proteins [148]. The solvation dynamics of water structure around the protein have been studied in great detail with a view to gain insight into protein folding and enzyme action [84]. It was observed from the atomistic simulation on the explicitly solvated protein that the structural relaxation of protein–water H-bonds is much slower than that of the water–water H-bonds [149].

1.6 Hydrogen Bonding in Crystal Engineering

Crystal structure arises as a result of intermolecular interactions and packing. The packing interaction is a convolution of a large number of strong and weak interactions, each of which influences the other closely [3]. Small changes in the molecular structure lead to observable changes in the crystal structure. Generally, there is no obvious relationship between molecular structure and crystal structure. In crystal engineering, attempts have been made to design molecular systems which could throw light on how molecular structure is related to crystal structure. Both the strong and weak H-bonded interactions play a dominant role in engineering of crystals. The role of weak H-bonded interactions in various molecules and crystals has been dealt with in a recent monograph [3].

2 EXPERIMENTAL AND THEORETICAL METHODS IN UNRAVELING H-BONDED COMPLEXES

2.1 Experimental Methods

The descriptions of the structure, energy, and dynamics of H-bonds continue to be a formidable task for both experimental and theoretical investigations. IR and nuclear magnetic resonance (NMR) techniques have become routine tools to analyze H-bonding interactions in various systems [1–4, 150]. The vibrational modes of molecules in the H-bonded state are affected in several ways. The proton involved in H-bonding interaction exhibits down field shift. Spectroscopic information obtained from these techniques has been used to probe H-bonding interactions.

Various experimental methods used to investigate the H-bonded clusters in gas phase are described in the earlier reviews [150–152]. Since molecular clusters are produced in supersonic beams in the gas phase under collision free conditions, they are free from perturbation of many-body interactions. The spectroscopic characterization of these clusters has less complexity. Hence, high level quantum chemical calculations on these clusters can be directly compared with the experimental values. Due to advent of laser-based techniques, it is currently possible to study the size and mass selective molecular clusters produced in supersonic beam. The combination of high resolution spectroscopy along with the mass and size selective strategies has enabled the scientific community to look at the intrinsic features of H-bonding. Principles behind the method of size selection, beam spectroscopy, and experimental setup have also been thoroughly described in an earlier thematic issue in “chemical review” [105, 150–152].

Challenges in experiments and theory to probe the noncovalent interactions in the weakly bonded clusters have been critically reviewed by Muller-Dethlefs and Hobza [150]. They highlighted the importance of microwave, vibrational rotation tunneling (VRT), REMPI and hole burning, and zero kinetic energy (ZEKE) spectroscopies in probing the noncovalent interactions in molecular clusters in gas phase [150]. IR spectroscopy of size-selected water and methanol clusters was discussed by Buck and Huisken [151]. Brutschy [105] has provided an account on the structural aspects of aromatic molecules surrounded by several polar molecules using IR double resonance laser spectroscopy (IR/R2PI ion depletion spectroscopy) along with the important computational results [105]. Neusser and Siglow have discussed the applications of high resolution ultraviolet (UV) spectroscopy to study the neutral and ionic H-bonded clusters [152]. Mikami have brilliantly exploited the beam spectroscopy to study the H-bonded clusters in the gas phase [153–163]. From their studies, it is possible to gain new insight into the structure and dynamics of H-bonded phenol and protonated water clusters. IR spectroscopy study on $\text{H}_3\text{O}^+(\text{H}_2\text{O})_n$ by them clearly elucidated that the small-sized clusters develop into a two-

dimensional network whereas large clusters with $n \geq 21$ form nanometer-scaled cages [163].

Recently, large $(\text{H}_2\text{O})_n$ clusters with ranges n from 20 to 1960 have been investigated by Steinbach et al. using photofragment spectroscopy [164, 165]. They measured the vibrational spectra of the size-selected water hexamer and identified the H-bonded open book arrangement in the cluster with temperature range from 40 to 60 K [165]. Jordan, Zwier and their collaborators have made several noteworthy contributions to this contemporary area by successful combination of sophisticated experimental and theoretical methods to a large number of H-bonded clusters [106, 166–177]. Their studies include neutral and charged water clusters in various structural environments. The IR spectra have been used to probe the issues related to solvation of Eigen vs. Zundel cation [173]. Headrick et al. have reported how the vibrational spectrum of protonated water clusters evolves in size ranging from 2 to 11 water molecules [177]. IR signature bands indicated the limiting forms of embedded Eigen or Zundel forms in the respective spectra.

2.2 Theoretical Methods

A variety of theoretical methodologies are available at different theoretical levels and accuracy. Different quantum chemical methods used to analyze H-bonding interactions have been systematically discussed by Scheiner in his monograph [4]. Starting from semi-empirical molecular orbital methods, Hartree–Fock (HF), and post-HF methodologies have been employed to study H-bonding. HF method treats the exchange term appropriately and thus it predicts reasonably the electrostatic contribution to the strength of H-bonding. The need for treatment of post-HF techniques for H-bonded systems has been observed as discussed in recent monographs [1–4]. The inclusion of electron correlation and hence intermolecular dispersion energy becomes considerably important for the prediction of strength of the H-bonding. Møller–Plesset (MP2), coupled-cluster singles doubles (CCSD), and CCSD with noniterative triples correction (CCSD (T)) methods are widely used methodologies to investigate H-bonding interactions. The implementation of DFT formalism in the Gaussian package has made it possible to investigate the utility of several exchange and correlational functionals in the prediction of H-bonding [178, 179]. Recently, Zhao and Truhlar have investigated the usefulness of DFT functionals in the prediction of H-bonding [180]. It is a well-known fact that the basis set used in the calculation significantly influences the calculated bond length, bond angle, electronic properties, interaction energy, and vibrational spectra [180]. Hence, theoretically, different combinations of methodologies and basis sets have been applied to obtain reliable estimates of geometrical parameters and energetics of H-bonded systems. In addition, the interaction energy obtained from these calculations needs to be corrected for basis set superposition error (BSSE) as suggested by Boys and Bernardi [181].

Recently, Hobza has reviewed various theoretical methods used to predict the stabilization energies of extended H-bonding systems [150, 182]. The capability of resolution of identity (RI) MP2 method has been assessed with Dunning's correlation consistent basis sets. The need for BSSE corrections for geometries, vibrational frequencies, and other properties of extended H-bonded systems has been stressed. The failure of DFT-based methods to describe the dispersion energy component in the prediction of H-bonding of extended aromatic systems has also been illustrated [182].

However, for molecules of real life interest, for example DNA, protein, and DNA-protein complexes, it is impossible to carry out such higher level calculations. The necessity for the alternative theoretical approaches to handle some of the large molecules has been recognized early and the application of force field based strategies in unraveling the structure and H-bonding in biomolecules is well known [183–185]. Molecular mechanics (MM) and molecular dynamics (MD) have been used to study the structure and dynamics of biomolecules. AMBER, OPLS, and CVFF, etc., are some of the force fields used in the simulation of biomolecules in realistic environment. In addition to the Lennard-Jones 6–12 potential in describing the nonbonded interaction using the force field approach, a 10–12 potential function of the type

$$(2) \quad v(r) = \frac{A}{r^{12}} - \frac{B}{r^{10}}$$

is also used to represent the H-bonding interaction. The realistic simulation of biomolecules requires an appropriate description of solvent environment around the biomolecules [186–191]. To carry out realistic simulation of biomolecules in water, different transferable interaction potentials (TIP) have been generated by Jorgensen et al. [192].

2.3 Characterization of Hydrogen Bonds

Bader's theory of AIM offers a convenient means of looking at H-bonding interaction in various intermolecular and intramolecular systems [6]. One of the advantages of the AIM theory is that one can obtain information on changes in the electron distribution as a result of either bond formation or complex formation. In the following section, the significant features of theory of AIM are discussed from the point of view of characterization of H-bonding interactions.

2.3.1 AIM theory in the characterization of H-bonds

The theory of AIM allows one to study the concept of chemical bond and the bond strength in terms of electron density distribution function [6, 193]. It exploits the topological features of electron density and thereby a definition of chemical bonding through bond path and bond critical point (BCP). A BCP (it is a point at which gradient vector vanishes, $\nabla\rho(\mathbf{r}) = 0$) is found between the

two nuclei of the molecule in equilibrium geometry, which is considered to be connected by a chemical bond. Bader’s group has immensely contributed to the development of the AIM theory and its applications to intermolecular interactions [6]. Popelier and coworkers have employed the AIM theory to address several important chemical issues [194–196]. Numerous studies have been made on various systems to characterize the van der Waals and H-bonded interactions using the AIM theory [6, 26, 38, 43, 197–216]. Several criteria based on the AIM theory have been proposed to investigate conventional and nonconventional H-bonds [198]. The topological descriptors obtained from the AIM theory and electron localization function can be successfully employed to distinguish weak, medium, and strong H-bonds in various molecular systems. Grabowski and coworkers have used Bader’s theory to study the H-bonding in various systems [26, 43, 198–201, 203, 216–219]. It has also been used to investigate intramolecular resonance assisted H-bonds and π -electron delocalization [220], and to understand the interactions of He, Ne, and Ar with hydrogen fluoride and hydrogen chloride [221]. The dihydrogen-bonded complexes have also been studied using the AIM theory employing high level post-HF theory [222–224].

The molecular electron density distribution $\rho(\mathbf{r})$ can be extracted from the corresponding many particle wave function $\psi(x_1, x_2, \dots, x_N)$ as

$$(3) \quad \rho(\mathbf{r}) = N \sum_{\sigma} \int |\psi(x_1, x_2, \dots, x_N)|^2 d^3\mathbf{r}_2 \dots d^3\mathbf{r}_N$$

Here, the summation runs over all spin coordinates, integration over all but one spatial coordinate (x stands for position and spin) and N is the total number of electrons. Within the simplest HF framework, wherein the wave function ψ is expressed in the form of a Slater determinant constructed from the molecular orbital which are, in turn, expressed as linear combinations of the basis functions $\{\phi_i\}$, $\rho(\mathbf{r})$ assumes the form

$$(4) \quad \rho(\mathbf{r}) = \sum_{\mu\nu} P_{\mu\nu} \phi_{\mu}(\mathbf{r}) \phi_{\nu}^*(\mathbf{r})$$

where P stands for the electron density–bond order matrix. It can be shown that $\frac{1}{2}P$ would be an idempotent in orthonormal basis. The electron density and Laplacian of electron density at BCP are denoted as $\rho(r_c)$ and $\nabla^2\rho(r_c)$, respectively. The bond path and associated properties of $\rho(r_c)$ at BCP are used to characterize covalent, ionic bonding, H-bonding, and van der Waals interactions.

2.3.2 Properties of electron density for weakly bonded complexes

Bader and Essen have observed the different categories of CP [225]. They concluded that the hallmark of “shared” (i.e., covalent) interactions is the high value of the electron density at BCP of order $>10^{-1}$ a.u. The curvatures

of $\rho(r_c)$ are usually large. The Laplacian of the electron density ($\nabla^2\rho(r_c)$) is a measure of local concentrations of electron density and may be positive or negative having the order of $\rho(r_c)$. A negative value of $\nabla^2\rho(r_c)$ denotes electron concentration at a particular point whereas a positive value of $\nabla^2\rho(r_c)$ implies depletion of the same. It is evident from the previous AIM analysis that for H-bonded systems, noble-gas dimers and ionic systems, $\rho(r_c)$ is quite small ($\sim 10^{-2}$ a.u. or less for H-bonded complexes and 10^{-3} a.u. for van der Waals complexes) and the Laplacian is positive [6].

2.3.3 Integrated properties of electron density and Popelier's criteria

Topological atoms are defined according to the theory of AIM as regions in space consisting of bundle of electron density gradient path attracted to a nucleus. Due to its firm theoretical footing in quantum mechanics, AIM can be considered as a partitioning scheme to understand the properties of atoms in molecules and in intermolecular complexation. In addition to the topographical features of electron density, Popelier proposed some criteria to gain insight into H-bonding interactions [196, 224]. These include: (1) correct topological pattern (BCP and gradient path), (2) appropriate values of electron density at BCP, (3) proper value of Laplacian of electron density at the BCP, and (4) mutual penetration of hydrogen and acceptor atoms. Criteria pertaining to integrated properties of hydrogen atoms involved in the H-bonding include (5) an increase of net charge, (6) an energetic destabilization, (7) a decrease in dipolar polarization, and finally (8) a decrease in atomic volume.

2.3.4 Grabowski's Δ_{com} measure of hydrogen bonding

Grabowski and coworkers have made a detailed AIM analysis on H-bonded molecular systems [26, 43, 198–203, 216–220, 222, 223, 226, 227]. In these studies, different aspects of conventional and nonconventional H-bonds, dihydrogen, and partial H-bonds have been investigated. Despite the greater variability of systems which are classified as H-bonds, it is possible to spell out criteria for the H-bonding interaction using the AIM theory. Based on the systematic analysis of several dimers, a new measure of H-bond strength has been proposed using the properties of proton donating bond [227]. It is based on the geometrical and topological parameters of the X–H bond:

$$\Delta_{\text{com}} = \left\{ [r_{\text{X-H}} - r_{\text{X-H}}^0 / r_{\text{X-H}}^0]^2 + [(\rho_{\text{X-H}}^0 - \rho_{\text{X-H}}) / \rho_{\text{X-H}}^0]^2 + [(\nabla^2 \rho_{\text{X-H}} - \nabla^2 \rho_{\text{X-H}}^0) / \nabla^2 \rho_{\text{X-H}}^0]^2 \right\}^{1/2} \quad (5)$$

where $r_{\text{X-H}}$, $\rho_{\text{X-H}}$, and $\nabla^2_{\rho_{\text{X-H}}}$ correspond to the parameters of proton donating bond involved in H-bonding, i.e., the bond length, electronic density at X–H BCP, and the Laplacian of that density, respectively, and $r_{\text{X-H}}^0$, $\rho_{\text{X-H}}^0$, and $\nabla^2 \rho_{\text{X-H}}^0$ correspond to the same parameters of X–H bond not involved in H-bond formation. The parameter describing H-bond strength may be based only on geometrical data:

$$(6) \quad \Delta_{\text{geo}} = (r_{\text{X-H}} - r_{\text{X-H}}^0)/r_{\text{X-H}}^0$$

or only on topological parameters:

$$(7) \quad \Delta_{\text{el}} = (\rho_{\text{X-H}}^0 - \rho_{\text{X-H}})/\rho_{\text{X-H}}^0$$

or on Laplacian values:

$$(8) \quad \Delta_{\text{lap}} = |(\nabla^2 \rho_{\text{X-H}} - \nabla^2 \rho_{\text{X-H}}^0)/\nabla^2 \rho_{\text{X-H}}^0|$$

Good relationship between the Δ_{com} and the H-bond strength of various dimers has revealed that it can be used as a reliable measure of the strength of the same.

3. ELECTRONIC STRUCTURE CALCULATIONS ON HYDROGEN-BONDED MOLECULAR SYSTEMS

3.1 Hydrogen Bonding in Water Clusters

Water is a major chemical constituent of the planet's surface and as such it has been indispensable for the genesis of life on the earth [228]. It plays a key role in many biological and chemical reactions. H-bonds between H₂O molecules provide the cohesive force that makes water a liquid at room temperature and favors extreme ordering of water molecules in ice. H-bonding is responsible for the observed unusual properties of water. Hence, water has received more attention than any other substance by researchers. Numerous experimental and theoretical investigations have been carried on H-bonded water clusters to gain insight into fascinating physical and chemical properties of water [50–64, 150, 229–236].

In this section, salient results on structure, energetics, and different arrangements of (H₂O)_n clusters are presented. Although, the state-of-art spectroscopic and theoretical methodologies have been used to study H-bonding in water clusters, the quantification of H-bonding interaction in these clusters is rather complex. The complexity mainly arises due to numerous local minima on the potential energy surface of water clusters and the number of H-bonds which increases as the size of the clusters increases. The concept of cooperativity of H-bonding in water clusters has been formulated by Frank and Wen [237]. Its implications were discussed in a recent review [230].

Several ab initio and DFT calculations have been made on the water dimer [50–64, 233, 235]. The strength of the H-bonding in water dimer is 5.5 ± 0.7 kcal/mol [235]. The water trimer can exist in cyclic arrangement as well as in open chain conformation with linear H-bonds. In the case of the tetramer, previous theoretical calculations have predicted four H-bonded cyclic structures with S₄ symmetry corresponding to the global minimum [235]. This observation has also been supported by the IR spectra of various (H₂O)₄ complexes with benzene and VRT spectra of (H₂O)₄ and (D₂O)₄ [238, 239].

Cyclic H-bonding and the energy minimum structures of $(\text{H}_2\text{O})_n$ with $n \leq 5$ were investigated using different quantum chemical methods without any uncertainty [235, 240]. Water clusters adopt interesting structural pattern when n changes from 5 to 6. The transition from the planar two-dimensional structure to the three-dimensional structural arrangements emerges from $n = 6$ onwards. Hexameric water clusters adopt cyclic ring, bag, prism, cage, and open book structures. All theoretical calculations predict at least four nearly isoenergetic isomers for hexamer. The actual minimum energy structure depends on the rigor of calculation and inclusion of the zero-point energy (ZPE) corrections [235]. Saykally and coworkers have performed the first measurement on water hexamer using the VRT spectroscopy at 5 K [229, 241]. The rotational constants of hexamer were in accordance with the calculated values for the cage isomer. The ring isomer of the water hexamer in liquid helium was detected at 0.4 K [242]. All other spectroscopic experiments were not size selective and did not reveal any conclusion about the isomer. From the theoretical front, there is an interesting temperature effect, which is based on the fact that isomers with lower vibrational frequencies should be preferred at higher temperature because of the entropy effects. For $n = 7$, a cubelike structure with a corner missing is found to be the most stable. This structure has ten H-bonds and has a stabilization energy of 60.53 kcal/mol at the HF/6-31G(d,p) level, with a dipole moment (μ) of 1.35 D [235].

Semi-empirical potential has been used by Plummer to study small water clusters [233]. Wales et al. have employed empirical potential to simulate water clusters with $n \leq 21$ [234]. Extensive ab initio calculations using the HF/6-31G(d,p) and HF/6-311++G(2d,2p) levels and basis sets have been carried out for several possible and the most stable structures of water clusters $(\text{H}_2\text{O})_n$, $n = 8-20$ by Sathyamurthy and coworkers [235]. It was found that the most stable geometries arise from a fusion of tetrameric and pentameric H-bonded rings.

In this section, characterization of H-bonding of water clusters using the AIM approach is presented. Computational details of AIM analysis of water clusters are given elsewhere [243]. Stabilization energies (SEs) of all water clusters have been calculated using the supermolecule approach and corrected for BSSE using the counterpoise (CP) procedure suggested by Boys and Bernardi [181]

$$(9) \quad \text{SE} = E_{\text{complex}} - \sum_{i=1}^n E_i$$

where E_{complex} , E_i , and n represent the total energy of the complex, total energy of monomer and the number of monomers in the clusters, respectively. For the analysis of the strength of H-bonding, $|\text{SE}|$ is only considered. The values of SE, the number of H-bonds (nHB), $\rho(r_c)$, and $\nabla^2\rho(r_c)$ at H-bond CPs (HBCPs) are shown in Table 3. In addition, the number of HBCPs, ring CPs (RCPs), and

Table 3. Number of hydrogen bonds (nHB), hydrogen bond critical points (nHBCP), ring critical points (nRCPs), cage critical points (nCCPs), stabilization energies (SEs, kcal/mol), range of electron density ($\rho(r_c)$), and Laplacian of electron density ($\nabla^2\rho(r_c)$) for the most stable water clusters

Molecule	nHB	nHBCP	nRCP	nCCP	SE ^a	$\rho(r_c)(e/a_0^3)$	$\nabla^2\rho(r_c)(e/a_0^5)$
(H ₂ O) ₂	1	1			5.5	0.02	0.0157
(H ₂ O) ₃	3	3	1		17.1	0.02081–0.02219	0.01681–0.01783
(H ₂ O) ₄	4	4	1		29.1	0.02708	0.0229
(H ₂ O) ₅	5	5	1		37.7	0.0269–0.02815	0.02329–0.02463
(H ₂ O) ₆ prism	9	9	5	1	49.6	0.015–0.03317	0.01288–0.02373
(H ₂ O) ₇	10	10	5	1	60.53	0.01436–0.03462	0.01266–0.0303
(H ₂ O) ₈	12	12	6	1	76.01	0.02014–0.03231	0.01601–0.0279
(H ₂ O) ₉	13	13	6	1	85.05	0.02064–0.03204	0.01645–0.02824
(H ₂ O) ₁₀	15	15	7	1	96.75	0.01779–0.03433	0.0144–0.03025
(H ₂ O) ₁₁	16	18	8	1	105.69	0.01147–0.03136	0.01386–0.02706
(H ₂ O) ₁₂	20	20	11	2	122.39	0.01859–0.03127	0.01556–0.02687
(H ₂ O) ₁₃	21	21	11	2	128.33	0.01863–0.03186	0.01513–0.02749
(H ₂ O) ₁₄	23	23	12	2	144.78	0.01207–0.03043	0.01107–0.03032
(H ₂ O) ₁₅	25	25	13	2	154.82	0.01654–0.03406	0.01386–0.02994
(H ₂ O) ₁₆	28	28	16	3	169.33	0.01745–0.03142	0.01486–0.02707
(H ₂ O) ₁₇	29	30	17	3	176.51	0.01492–0.03147	0.01264–0.02707
(H ₂ O) ₁₈	31	32	18	3	188.64	0.01588–0.03145	0.01349–0.02706
(H ₂ O) ₁₉	33	33	18	3	199.69	0.01114–0.03421	0.01264–0.0274
(H ₂ O) ₂₀	36	36	21	4	216.28	0.01872–0.03148	0.01553–0.02709

Results from Ref. 243

^a HF/6-31G(d,p) BSSE-corrected stabilization energies from Ref. 235

cage CPs (CCPs) is also tabulated along with SEs taken from the previous investigation [235]. The molecular graphs of water clusters are shown in Fig. 3. In general, it is possible to note that the number of H-bonds in each water cluster corresponds to the number of HBCPs. It can be noted from Table 3 that the values of $\rho(r_c)$ and $\nabla^2\rho(r_c)$ at these HBCPs are in accordance with that proposed by Bader for these interactions [6].

Since O–H···O H-bonding interactions are similar for all the clusters, it is expected that the values of $\rho(r_c)$ are identical. However, close scrutiny of the values reveals that $\rho(r_c)$ is not the same in all the clusters. As the cluster size increases, the $\rho(r_c)$ values decrease due to the presence of multiple H-bonded interactions. The presence of RCPs (W₃ onwards) and CCPs (W₆ onwards) in the molecular graphs of water clusters shows the ability of electron density topography analysis in the characterization of ring and cage structures. It is evident from the previous investigations that fusion of tetrameric and pentameric rings is responsible for the stability of water clusters and as a result (H₂O)_n, $n = 8, 12, 16$, and 20 are found to be cuboids while $n = 10$ and 15 are pentameric fused rings [235]. Other structures have cuboids or pentameric fused structures or combinations of these two motifs. However, it can be noted from Fig. 3 that for (H₂O)₁₇ and (H₂O)₁₈, there is an extra HBCP indicating

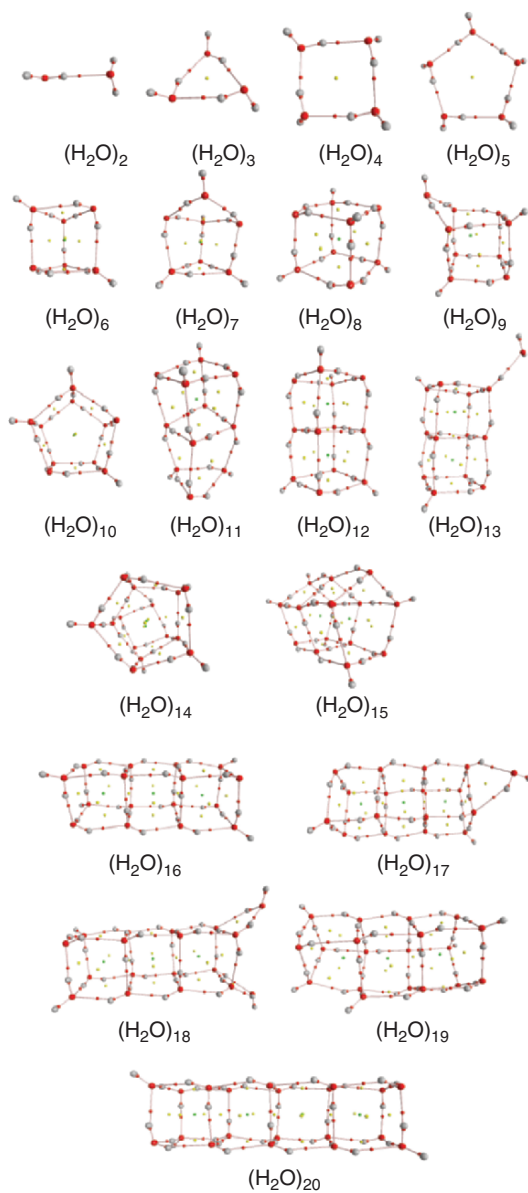


Figure 3. Molecular electron density topographies of water clusters (Results from Ref. 243.)

additional interactions of similar magnitude stabilizing the respective clusters. When one water molecule is added to the $(\text{H}_2\text{O})_{16}$, the 17th water molecule does not exactly interact at the middle but at the side of the cuboid. Similarly the 18th water molecule interacts with the other side of the cuboid in $(\text{H}_2\text{O})_{17}$,

forming a stable $(\text{H}_2\text{O})_{18}$ cluster as depicted in Fig. 3. Further addition of two water molecules to $(\text{H}_2\text{O})_{18}$ leads to cuboids structure for $(\text{H}_2\text{O})_{20}$ cluster as shown in Fig. 3. Grabowski's Δ_{com} measure of H-bonding [227], charge transfer interactions from natural bond orbital (NBO) analysis, and the NMR shielding parameters are also found to be extremely helpful in the understanding of H-bonded interactions in various water clusters [243].

The relationship between various parameters used to describe the strength of H-bonding has been addressed [198–203, 216–220, 222, 223] in the earlier investigations. An attempt has been made to obtain possible relationship between the sum of the $\rho(r_c)$ and $\nabla^2\rho(r_c)$ at the HBCP in water clusters. The amplitude of $\rho(r_c)$ at each HBCP has been summed over to get the total $\rho(r_c)$ for each H-bonded cluster and regression analysis has been performed. It has been found that the calculated total electron density $\rho(r_c)$ at HBCPs of water clusters varies linearly with their SE. The total $\nabla^2\rho(r_c)$ at HBCPs also exhibits similar trend with the SE. The linear relationship between the SE and the sum of electron density at the HBCPs is shown in Fig. 4. The linear relationships between the SE and the sum of the electron density at the HBCPs and the sum of Laplacian at the HBCPs are given below:

$$(10) \quad \text{SE} = 263.50 \sum \rho(r_c)$$

$$(11) \quad \text{SE} = 319.28 \sum \nabla^2\rho(r_c)$$

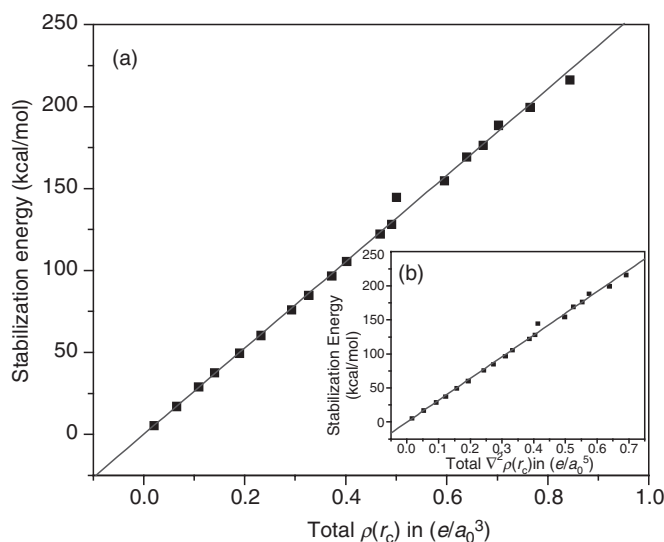


Figure 4. Relationship between stabilization energy (HF/6-31G(d, p)) and (a) total $\rho(r_c)$ and (b) total $\nabla^2\rho(r_c)$ (inset) for water clusters.

The additivity of electron density at the HBCPs in multiple H-bonded (36 HBCPs) systems is clearly evident from Fig. 4. The correlation coefficient for the same is 0.99. Although, the connection between $\rho(r_c)$ and strength of H-bonded complex with single H-bond is already known, we have demonstrated the additivity of electron density at the HBCPs for the multiple H-bonded systems [244, 245].

3.2 Hydrogen Bonding in Water-Mediated Network and Mixed Clusters

It is well known that water-mediated interaction stabilizes structure of biomolecules [1, 138, 247–250]. Therefore, several model molecular systems have been chosen to probe the water-mediated interactions in biomolecules and a large amount of experimental and theoretical work has been published over the years on this subject [78, 138, 251–258]. Since phenol is the simplest aromatic alcohol resembling chromophore of an aromatic amino acid, hydration of phenol molecules has been studied to understand H-bonding and solute–solvent interaction in biological systems. Several experimental and theoretical calculations have been made on the phenol–water clusters [259–273]. Recently, we have made a comprehensive analysis on structure, stability, and H-bonding interaction in phenol (P_{1-4}), water (W_{1-4}), and phenol–water (P_mW_n ($m = 1-3$, $n = 1-3$, $m + n \leq 4$)) clusters using ab initio and DFT methods [245]. In this section, electronic structure calculations combined with AIM analysis on phenol–water clusters are presented.

The calculated stabilization energies (see Table 4) for clusters with similar H-bonding pattern reveal that H-bonding in water clusters is stronger than in

Table 4. Number of H-bonds (nHB) and SE for P_m , W_n , and P_mW_n clusters as obtained from different levels of calculation using 6-31G* basis set

Clusters	nHB		SE (kcal/mol)		
	Primary	Secondary	HF	MP2	DFT/B3LYP
P_2	1	2	4.3	5.7	4.8
W_2	1	–	4.7	5.2	5.4
PW	1	1	6.3	7.3	7.7
P_3	3	1	12.8	17.7	15.6
W_3	3	–	14.1	16.6	18.9
PW_2	3	–	14.5	17.1	18.9
P_2W	3	–	13.5	16.8	17.0
P_4	4	4	22.2	31.6	27.9
W_4	4	–	25.3	30.7	35.2
PW_3	4	1	25.0	30.1	33.6
P_2W_2	4	2	24.9	31.1	32.7
P_3W	4	2	23.6	30.9	30.4

Reproduced with permission from Ref. 245 © American Chemical Society, 2005

phenol clusters. However, fusion of phenol and water clusters in tetrameric ring arrangements leads to stability that is akin to that of $(\text{H}_2\text{O})_4$. The molecular electron density topographies of various phenol–water clusters are presented in Fig. 5. The values of $\rho(r_c)$ and $\nabla^2\rho(r_c)$ for the H-bonds present in these clusters are listed in Table 5. It is clear from Fig. 5 that there are BCPs corresponding to the secondary weak H-bonding interaction in P_2 , PW , P_3 , P_4 , P_2W_2 , PW_3 , and P_3W clusters. It is also clear from Table 5 and Fig. 5 that the presence of secondary weak H-bonding adds to the stability of different phenol and phenol–water clusters. The formation of a ring structure in W_3 , P_3 , and the mixed clusters PW_2 and P_2W is evident from the presence of ring critical points. In phenol trimer, it is possible to identify $\text{C-H}\cdots\pi$ interaction, in addition to the three $\text{O-H}\cdots\text{O}$ H-bonding interactions. In the case of P_4 and the mixed tetramers, the basic $\text{O-H}\cdots\text{O}$ H-bonded core structure is analogous to that of W_4 . The existence of the additional $\text{C-H}\cdots\text{O}$, weak $\text{C-H}\cdots\text{C}$ and $\text{C-H}\cdots\text{H}$ interactions can be seen in all the mixed clusters.

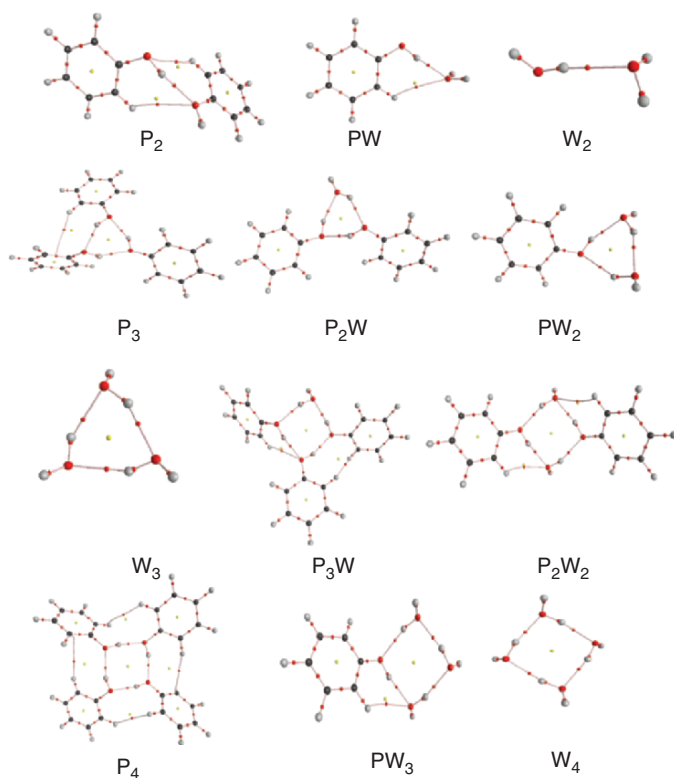


Figure 5. Molecular topographies of phenol, water, and phenol–water clusters as obtained from theoretical electron density. (Reproduced with permission from Ref. 245 © American Chemical Society, 2005.)

Table 5. Electron density ($\rho(r_c)$) and Laplacian of electron density ($\nabla^2\rho(r_c)$) for various phenol-water clusters

Clusters	$\rho(r_c)(e/a_0^3)$	$\nabla^2\rho(r_c)(e/a_0^5)$	$\rho(r_c)(e/a_0^3)$	$\nabla^2\rho(r_c)(e/a_0^5)$
	Primary hydrogen bond		Secondary hydrogen bond	
P ₂	0.021	0.019	0.003–0.004	0.004–0.005
W ₂	0.021	0.018	–	–
PW	0.025	0.022	0.004	0.005
P ₃	0.021–0.022	0.019–0.020	0.002	0.002
W ₃	0.022–0.024	0.019–0.020	–	–
PW ₂	0.017–0.028	0.015–0.024	–	–
P ₂ W	0.018–0.027	0.016–0.023	–	–
P ₄	0.025–0.028	0.022–0.024	0.002–0.003	0.002–0.003
W ₄	0.029	0.025	–	–
PW ₃	0.024–0.033	0.020–0.028	0.005	0.005
P ₂ W ₂	0.025–0.032	0.022–0.027	0.005	0.005
P ₃ W	0.024–0.033	0.021–0.028	0.003–0.004	0.002–0.005

Reproduced with permission from Ref. 245 © American Chemical Society, 2005

It is found that the total electron density ($\Sigma\rho(r_c)$) and total Laplacian of electron density ($\Sigma\nabla^2\rho(r_c)$) at all HBCPs bear a linear relationship with the SE for all the H-bonded clusters as illustrated in Fig. 6. A linear regression analysis yields

$$(12) \quad SE = 212.6 \sum \rho(r_c)$$

$$(13) \quad SE = 248.2 \sum \nabla^2\rho(r_c)$$

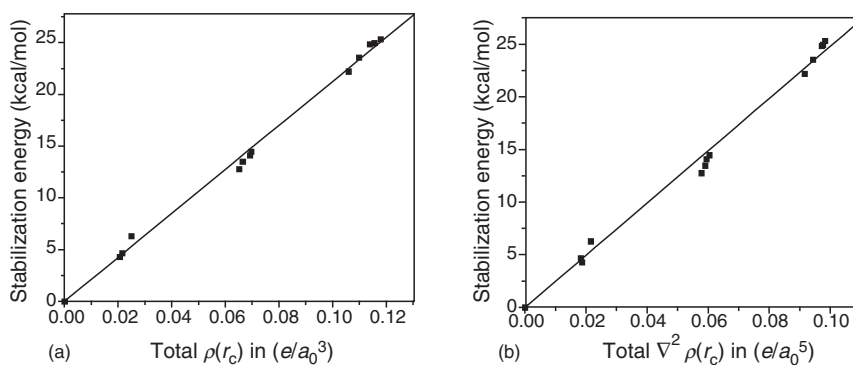


Figure 6. Relationship between stabilization energy (HF/6-31G^{*}) and (a) total $\rho(r_c)$ and (b) total $\nabla^2\rho(r_c)$ for phenol, water, and phenol-water clusters. (Reproduced with permission from Ref. 245 © American Chemical Society, 2005.)

The correlation coefficient is nearly unity in both the cases. It can be seen from Fig. 6a,b that the H-bonded clusters having $|SE|$ in the range of 5–25 kcal/mol show three sets of clusters in the electron density region between 0.020 and $0.125e/a_0^3$ corresponding to the dimers, trimers, and tetramers, respectively. It is interesting to observe from the linear fit that the total density of the phenol and phenol–water mixed clusters is comparable to that of the water clusters.

The formation of a H-bond leads to a subtle increase in the electron density at the HBCPs. This increased electron density translates into a greater strength of H-bonding in the clusters. Cubero et al. have used the AIM theory to distinguish H-bonding from anti-H-bonding and have provided an atomic rationale for the blue shifting [274]. Their results showed that the H-bonding criteria based on the AIM theory are met by the nonconventional dihydrogen-bonding as in $C-H \cdots H$ also. However, they found that in order to differentiate H-bonding from anti-H-bonding, it is necessary to supplement Popelier's criteria with necessary information on the changes in electron density and other properties of the donor X–H bond, upon complexation [196, 224]. Recently, the electron density deformation AIM analysis has been applied to investigate H-bonding patterns in metalated nucleobase complexes [275]. The usefulness of integrated atomic properties of hydrogen atoms has been used to understand the nature of H-bonding in various clusters.

The loss of electron density on hydrogen atoms has been used as one of the criteria for H-bonding. Charges on hydrogen atoms in isolated phenol and water molecules and in the clusters have been computed by integrating the electron density in the appropriate hydrogen atom region partitioned by the AIM theory. The resulting values clearly show that the hydrogen nuclei are deshielded upon H-bond formation. The magnitude of this effect ranges from 0.04 to 0.08 a.u. for different clusters. Another criterion of H-bonding is the energy destabilization of hydrogen atom and can be derived from the difference between atomic energies of the hydrogen atoms in the clusters and the isolated molecules. It was found that H-bond formation inevitably destabilizes the hydrogen atoms that are involved in the bonding.

As pointed out by Popelier et al. the first moment and atomic volume of H atom involved in the H-bonding decreases by 0.02–0.05 a.u. and 5–9 a.u., respectively, in different phenol–water clusters. It is evident from the above illustrations that electron density topography analysis clearly elicits H-bonded interactions in microsolvated and water-mediated clusters [245].

3.3 Ionic Hydrogen Bonding

The strength of ionic hydrogen bond (IHB) ranges from 5 to 35 kcal/mol. These strong interactions are implicated in ionic crystals and clusters, ion solvation, electrolytes, and acid–base chemistry. The importance of this interaction in proton solvation, surface phenomenon, self-assembly process in supramolecular chemistry, and biomolecular structure and function has also been

recognized. Recently, basic insights that have been obtained in the past four decades on IHB have been reviewed [276]. A comprehensive summary on the thermochemistry and its structural implications obtained from ab initio calculations were also presented. In this section, some of the important results from the ab initio calculations on IHB are given.

The formation of IHB involves partial proton transfer from the donor to the acceptor. When a proton interacts with a single water molecule, it forms a strong covalent bond with the oxygen to form the hydronium ion (H_3O^+), known as Eigen cation [277]. It is a key species in the transfer of protons between molecules in the aqueous acid–base chemistry. The hydronium ion is of C_{3v} symmetry and O–H bond dissociation energy is 260 kcal/mol. The interaction of a water molecule with the hydronium ion leads to the H_5O_2^+ , Zundel ion, [278, 279] with 34.39 kcal/mol of energy [280]. From the accurate ab initio calculations on H_5O_2^+ , it was found that equilibrium geometry has C_2 symmetry with O–O bond length of 2.38 Å. Large clusters involving Eigen and Zundel cations as well as hydroxyl ion with H_2O have been investigated in detail [161, 163, 168, 172–174, 177, 231, 276, 281–305]. The main focus in many of these studies was on: (1) proton-transfer mechanism, (2) structure of first solvation shell in the Eigen and Zundel, and (3) computation of high quality interaction potential to describe the clusters. These studies revealed the stepwise development of solvation and about four to six solvent molecules are involved in this process. Since H-bonding sites in the clusters are not blocked, protonated water clusters exhibit infinite network. The presence of cyclic and branched H-bonded network can also be observed in these clusters.

From these studies several interesting results on structure and energetics of $\text{H}_3\text{O}^+(\text{H}_2\text{O})_n$ clusters have been observed. Since the cause for the anomalously high rate of proton transfer in bulk water was identified as the difference between first and second solvation shells, the characterization and quantification of individual strength of the interaction in them are extremely important [283]. In this context, the AIM theory can act as a useful tool in differentiating the first and second solvation shells of the protonated water clusters. In this section, the utility of AIM analysis in unraveling the strength of H-bonded interaction when water molecules interact with Eigen cation in a stepwise manner is explained [297]. The ground state geometries of the $\text{H}_3\text{O}^+(\text{H}_2\text{O})_n$ ($n = 1-3,6$) (henceforth referred to as $\text{H}_3\text{O}^+\text{W}_n$) were obtained using the MP2/6-311++G** method. The calculated SEs for various protonated water clusters are presented in Table 6 along with the number of H-bonds and H-bond distances. The electron density topographical features of protonated water clusters are shown in Fig. 7. The value of $\rho(r_c)$ for the $\text{H}_3\text{O}^+\text{W}_1$ is 0.161 a.u. (Table 7). Stepwise addition of second water to the same leads to sudden decrease in the electron density values at the HBCPs. Marginal changes in the $\rho(r_c)$ can be seen from the values shown in Table 7 for the addition of third water to the protonated cluster. As found in the previous studies, three water molecules are sufficient to form the first solvation shell in the case of H_3O^+ . In

Table 6. Calculated stabilization energies (MP2/6-311++G** level) for various protonated water clusters

Cluster	Number of H-bonds (distances in Å)	SE (kcal/mol)
H ₃ O ⁺ W	1 (1.2)	49.99
H ₃ O ⁺ W ₂	2 (1.5)	58.27
H ₃ O ⁺ W ₃	3 (1.5)	75.23
H ₃ O ⁺ W ₆	6 (1.5–1.7)	111.1

Results from Ref. 297

order to quantify the strength of H-bond formed in the second solvation shell, three water molecules are added further to form the structures as depicted in Fig. 7. The calculated $\rho(r_c)$ values at the second shell H-bonds are all the same and of the order of 0.030 a.u. which is approximately 50% less than that found in the primary hydration shell. The strength of the first H-bond formed in the H₃O⁺W₁ is 49.99 kcal/mol. The SE per H-bond in the H₃O⁺W₂ is ~29 kcal/mol in agreement with the decrease in $\rho(r_c)$ values. For the completed first solvation shell structure (H₃O⁺W₃), the energy per H-bond is 25.6 kcal/mol and is reflected in the corresponding drop in the $\rho(r_c)$ values. The energy per H-bond in the second solvation shell is ~18 kcal/mol in accordance with the decrease in the $\rho(r_c)$ at various HBCPs. The AIM analysis clearly distinguishes the first shell and second shell, and quantifies the strength of the interaction of H₂O with H₃O⁺.

The hydroxide ion (OH⁻) is another important ionic species in aqueous chemistry. Solvation of OH⁻ ion has been actively probed by various experimental and theoretical techniques [276, 283, 288, 289–305]. However, when

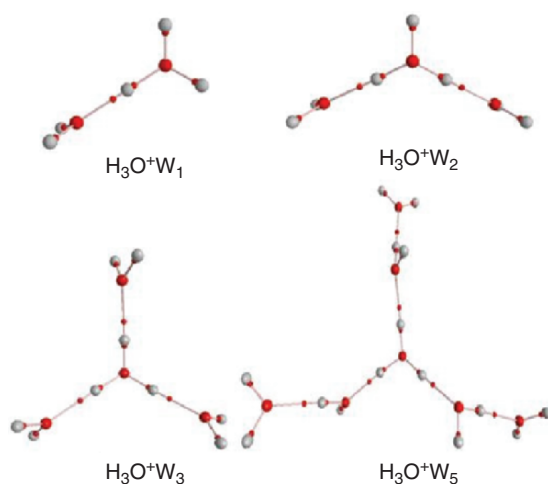


Figure 7. Molecular topographies of protonated water clusters. (Results from Ref. 297.)

Table 7. Electron density ($\rho(r_c)$) and Laplacian of electron density ($\nabla^2\rho(r_c)$) at HBCP for various protonated water clusters in first and second solvation shells

Cluster	Solvation shell	$\rho(r_c)$ (e/a_0^3)	$\nabla^2\rho(r_c)$ (e/a_0^5)
H ₃ O ⁺ W	First	0.1607	-0.1077
H ₃ O ⁺ W ₂	First	0.0739	0.0467
		0.0739	0.0467
H ₃ O ⁺ W ₃	First	0.0575	0.0456
		0.0575	0.0456
		0.0575	0.0456
H ₃ O ⁺ W ₆	First	0.0644	0.0467
		0.0641	0.0468
		0.0641	0.0467
	Second	0.0335	0.0352
		0.0337	0.0356
		0.0335	0.0356

Results from Ref. 297

compared to proton solvation, relatively less number of research work has been carried out on the hydroxide ion. Earlier experiments showed that the water clusters with OH⁻ (henceforth denoted as OH⁻W_n) are less stable than the corresponding protonated ions, but nevertheless, they are still reasonably long-living aggregates.

There has been long standing uncertainty about the number of water molecules in the primary hydration shell of the OH⁻ ions in chemistry. Theoretical calculations indicate that three water molecules complete the first solvation shell and the onset of second solvation shell is seen in the OH⁻(H₂O)₄ [288]. In this section a scrutiny of H-bonding in OH⁻W_n clusters has been performed with the help of AIM theory [305]. The calculated stabilization energies (MP2/6-311++G^{**}) of OH⁻W_{n=1-4} are presented in Table 8 and molecular graphs of the same clusters are shown in Fig. 8. It can be seen from Fig. 8 that three water molecules are sufficient enough to form the primary solvation shell of OH⁻ ion. The onset of second solvation shell is evident with inclusion of the fourth water molecule. Successive formation of the H-bonds shows that the first two bonds

Table 8. Calculated stabilization energies (kcal/mol) for OH⁻W_{n=1-4} clusters

Cluster	Number of H-bonds (distances in Å)		SE
	OH ⁻ ...W	W...W	
OH ⁻ W ₁	1 (1.38)		32.18
OH ⁻ W ₂	2 (1.54)		49.30
OH ⁻ W ₃	3 (1.5-1.7)	1 (2.5)	65.52
OH ⁻ W ₄	4 (1.73)	4 (2.47)	222.12

Results from Ref. 305

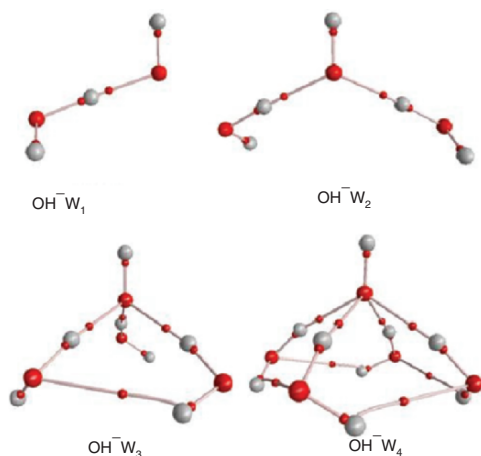


Figure 8. Molecular topographies of $\text{OH}^-W_{n=1-4}$ clusters. (Results from Ref. 305.)

are stronger than the next, revealing the presence of strong and medium interactions in these clusters. It is interesting to note the changes in the electron density properties upon stepwise addition of water molecules (Table 9). In addition to the primary ionic H-bonds between OH^- and water, other water-water interactions do stabilize these clusters in contrast to the corresponding H_3O^+W_n clusters. The OH^-W_3 has interesting electron density topography. Presence of additional interaction between the two water molecules can be observed from the molecular graphs of OH^-W_3 . A H-bonding interaction can be seen from the molecular graphs of OH^-W_3 along with the three primary IHBS.

Table 9. Electron density ($\rho(r_c)$) and Laplacian of electron density ($\nabla^2\rho(r_c)$) for $\text{OH}^-W_{n=1-4}$ clusters

Clusters	Electron density (e/a_0^3)	Laplacian of electron density (e/a_0^5)	Electron density (e/a_0^3)	Laplacian of electron density (e/a_0^5)
	$\text{OH}^- \cdots \text{W}$		$\text{W} \cdots \text{W}$	
OH^-W_1	0.1003	0.0287		
OH^-W_2	0.0648	0.0427		
	0.0648	0.0427		
OH^-W_3	0.057	0.0422	0.00797	0.0075
	0.0424	0.0368		
	0.0548	0.0419		
OH^-W_4	0.0401	0.0356	0.00896	0.0084
	0.04	0.0355	0.00903	0.0085
	0.0401	0.0356	0.00896	0.0084
	0.04	0.0355	0.00904	0.0085

Results from Ref. 305

The presence of ring CP ensures the ringlike topology in $\text{OH}^- \text{W}_3$. The $\text{O} \cdots \text{H}$ distance is 2.5 Å. In the case of $\text{OH}^- \text{W}_4$, further four additional H-bonding interactions stabilize the cluster. The cyclic structural frame work generated by the additional interactions adds to the stability of the cluster. The $\text{O} \cdots \text{H}$ distance in $\text{OH}^- \text{W}_4$ decreases when compared to the same in other clusters. The covalent characters of IHBs are clearly evident from the values of $\rho(r_c)$ at HBCPs (Tables 7 and 9). The analysis of results shows that the extent of covalency is significantly more for protonated water clusters than $\text{OH}^- \text{W}_n$. The exploration of various factors stabilizing the IHB clusters using AIM approach has clearly brought out the nature of interaction in the first and second solvation shells, and the other secondary interactions.

3.4 Hydrogen Bonding Interaction in DNA Base Pairs

Since H-bonding interaction is one of the important factors in the stabilization of DNA double helix, numerous theoretical and experimental investigations have been carried out on the strength of H-bonding interaction between DNA bases [1–4, 112, 138]. Sponer, Hobza, and Leszczynski have made several significant contributions to predict the strength of the H-bonding interactions [118–121].

In this section, the utility of the AIM theory in understanding the H-bonding in DNA base pairs is discussed [244]. GCWC, GG1, GCNEW, CC, GG3, GA1, GT1, GT2, AC1, GC1, AC2, GA3, TAH, TARH, TAWC, TARWC, AA1, GA4, TC2, TC1, AA2, TT2, TT1, TT3, GA2, GG4, AA3, and 2aminoAT of DNA are the various canonical and noncanonical base pairs considered for AIM analysis in terms of the $\rho(r_c)$, $\nabla^2\rho(r_c)$, and integrated atomic properties of hydrogen atoms involved in H-bonding. The details of calculation and analysis are described in our earlier investigation [244]. The molecular topographies for the H-bonded GCWC and TAWC are shown in Fig. 9.

All the canonical and noncanonical base pairs are bonded such that the imino group of the base forms H-bond either with N atom or with O atom of the other base. All the base pairs studied possess $\text{N}-\text{H} \cdots \text{Y}$ type of hydrogen bond, where Y is the general representation for the atoms N and O. The HBCPs have been observed between one of the H atom of the imino group and Y atom. All bases are paired by two H-bonds except for GCWC and 2aminoAT, which have three H-bonds between them. The calculated values of $\rho(r_c)$ and positive sign of $\nabla^2\rho(r_c)$ for various DNA base pairs indicate the presence of closed shell kind of interaction between the two bases governing the pairing [244]. The SE (calculated at MP2/6-31G*(0.25)) for various base pairs has been taken from the earlier work of Sponer et al. [118]. Figure 10 shows the variation of total electron density at the BCP vs. the stabilization energy of various base pairs of DNA. The linear relationship obtained is given below:

$$(14) \quad \text{SE} = 315.555 \sum \rho(r_c) \text{ at HBCP} + 2.676$$

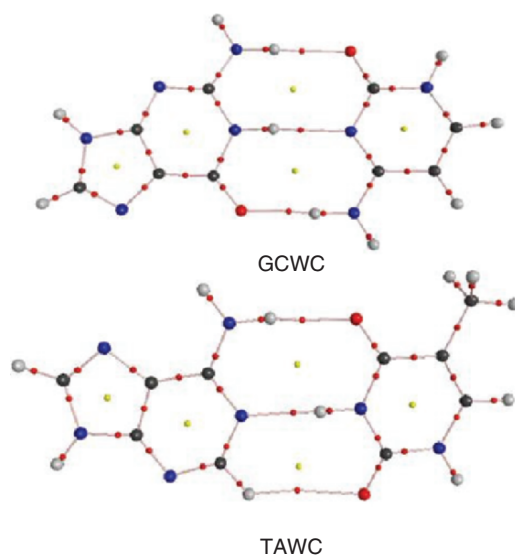


Figure 9. Molecular topographies of DNA base pairs GCWC and TAWC obtained from theoretical electron density. (Reproduced with permission from Ref. 244 © American Chemical Society, 2004.)

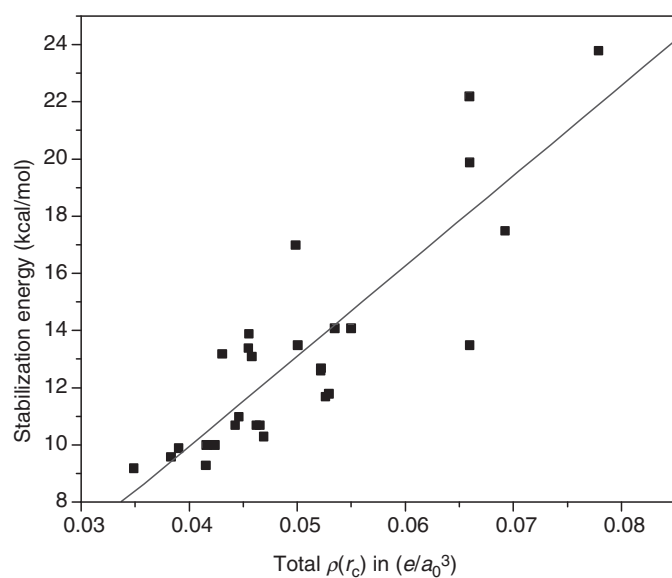


Figure 10. Relationship between stabilization energy and total $\rho(r_c)$ of the DNA base pairs. (Reproduced with permission from Ref. 244 © American Chemical Society, 2004.)

The correlation coefficient of 0.859 for this indicates the existence of reasonable linear relationship between $\rho(r_c)$ and stabilization energy. The effectiveness of $\rho(r_c)$ to explain H-bonding interaction between DNA bases is evident from the linear relation. Generally, these relationships have been developed for series of homologous model systems, which have good linear relationship between stabilization energy and electron density at the HBCP. Although, DNA base pairs do not constitute such a homologous system, $\rho(r_c)$ exhibits reasonably good linear relation with the stabilization energy.

It can be seen from Fig. 10 that the H-bonded base pairs having their SE in the range of 5–15 kcal/mol show clustering in the density region between 0.030 and $0.055e/a_0^3$ and exhibit good linear relationship with their stabilization energy. Similar to electron density variation, the total $\nabla^2\rho(r_c)$ at HBCP exhibits meaningful relationship depicting the more depletion of electron density at the hydrogen-bonded region of the base pairs with numerically more stabilization energy. The linear fit is

$$(15) \quad SE = 383.116 \sum \nabla^2\rho(r_c) \text{ at HBCP} + 1.182$$

The correlation coefficient is 0.827. Further calculations have also highlighted the importance of Poplier's criteria, concerning integrated atomic properties like charge, energy, volume, and first moment of the H-bonded hydrogen atoms in the DNA bases and in the H-bonded base pairs. The change (Δ) of the corresponding properties arising upon pairing has also made. The electron density topography analysis has also confirmed the presence of secondary interactions in various DNA base pairs that would influence the stability of base pairs. It is possible to obtain BCP in the secondary interaction regions in the case of GG3, GA1, TAH, TARH, TAWC, TARWC, TC2, and TC1 for which HF/6-31G** level calculations [118] have also supported the presence of secondary interaction. It is interesting to note that the presence of a third weak interaction stabilizes different AT pairs [244].

3.5 Hydrogen Bonding Interaction in Polypeptides

Ramachandran's stereochemical plot (ϕ - ψ diagram) of dipeptides has been widely used to predict the secondary structures of proteins [306–309]. It is well known that the calculations on the polypeptides are limited by the number of atoms and hence high level ab initio and DFT calculations have been possible recently only. Several theoretical calculations with different levels of accuracy have been made on the polypeptides to study the ϕ - ψ plot distribution, H-bonding interactions, and stability [1–4, 308–322]. In the stability of polypeptides and proteins, H-bond plays an important role in the formation of the secondary structures such as the α -helix, β -sheet, etc., and higher-order structures [1–4]. Quantum chemical calculations on some of the secondary structures in peptides and proteins (β -sheets, β -turns, and γ -turns) at the HF and MP2 levels have been performed with special emphasis to the H-bonded structures

[310]. Most of the electronic structure calculations have concentrated on (1) the structure, (2) long-range interaction, (3) peptide–water interaction, and (4) electronic properties. These studies have also affirmed the central role played by the H-bonding interactions in protein. The possibility of the AIM theory to analyze a polypeptide or a particular portion of a peptide has been described [6, 323, 324]. The existence of H-bond in the peptides has been confirmed by the presence of corresponding bond path in the electron density. Properties associated with the path have also been characterized in terms of $\rho(r_c)$ at HBCPs and ring CPs.

The H-bonding interactions in α -helical and β -sheet model peptides have been studied using the AIM approach [325]. The wave function generated from the ab initio and DFT calculations has been used to generate electron density topography of polyalanine in α -helix conformation and polyglycine in β -sheet conformation at various lengths of amino acid units. The representative topographical features are shown in Fig. 11. It can be observed that the existence of HBCPs and corresponding bond paths confirms the H-bonding found between the i and $i + 4$ residues of α -helical polyalanine. The value of electron density and the Laplacian of electron density at these points are typically of the order of 10^{-2} and 10^{-3} a.u., respectively [6]. For parallel and antiparallel β -sheets, electron density topography features are shown in Fig. 11. It is possible to note from the molecular graph that intermolecular H-bonding between the two chains is evident and the values of electron density parameters are also in the range stipulated by Bader's theory [6].

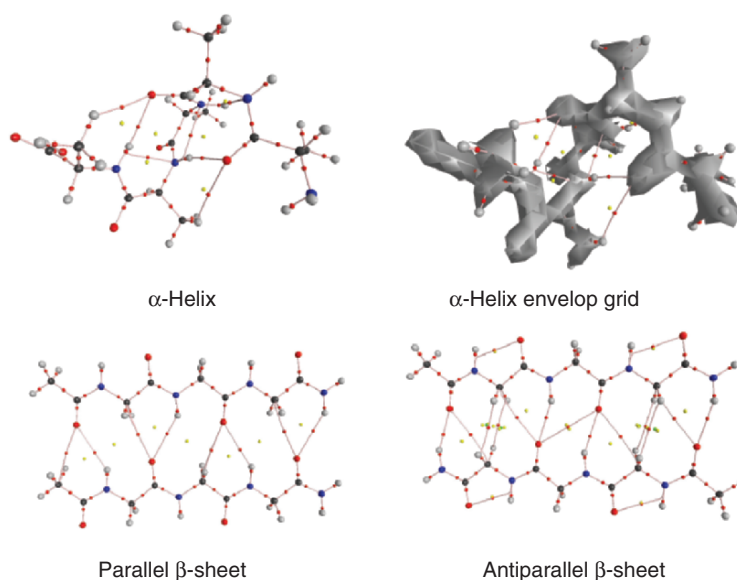


Figure 11 (see color section). Molecular topographies of secondary structures of protein obtained from theoretical electron density. (Results from Ref. 325.)

However, in addition to the H-bonding interaction other secondary interactions which lead to further stability are also evident. RCPs indicate the existence of closed rings in the formation of β -sheets. The values of electron density at the HBCPs and associated topographical features clearly discriminate the nature of primary and secondary interactions found in the basic building blocks of proteins. The cooperativity and long-range effects of H-bonding interactions in the secondary structural elements of protein can be explained by electron density topography analysis [325].

3.6 Relationship Between Strength of H-Bonding and Electron Density

It is well established that topological parameters are quite useful in delineating H-bonding interactions [6]. There are several interesting reports in the literature that $\rho(r_c)$ at HBCPs and H-bond distance exhibits a linear relationship [198–201, 203]. It has been illustrated through various examples presented in the previous sections that $\rho(r_c)$ and $\nabla^2\rho(r_c)$ display linear relationship with the H-bond strength [244–246]. The additivity of $\rho(r_c)$ at the HBCP has also been established by taking multiple H-bonded systems [244]. With a view to developing a more general model to describe the linear relationship between electron density at the HBCPs and the strength of H-bond, 94 different representative model H-bonded complexes of water clusters [243] (Table 3), phenol–water clusters [245] (Tables 4 and 5), ionic water clusters [297, 305] (Tables 6–9), DNA base pairs [244], and various H-bonded complexes [327] (Table 10) have been chosen. The plot presented in Fig. 12 clearly reveals the linear relationship between SEs and $\rho(r_c)$ for the diverse set of H-bonded systems irrespective of results obtained from various levels of calculations. The correlation coefficient close to unity suggests that it is possible to derive the strength of H-bond from electron density values at HBCPs. This observation is of great value for the experimentalist carrying out AIM analysis using electron density data obtained from various diffraction techniques:

$$(16) \quad SE = 267.97 \sum \rho(r_c)$$

3.7 From van der Waals Interactions to Covalency: AIM Perspective

Numerous attempts have been made to classify the various types of H-bonding interactions found in the literature [1–4]. Gilli and Gilli have made one such attempt using Electrostatic–Covalent H-Bond Model (ECHBM) derived from the systematic analysis of structural and spectroscopic data of a large number of O–H···O–H-bonds [326]. According to this model, weak H-bonds are electrostatic in nature but become increasingly covalent with increasing strength. Using the crystal structure data based on H-bonding in small molecules and biomolecules, there are several attempts to analyze the H-bonding pattern and strength.

Table 10. Stabilization energy (SE) (MP2/aug-cc-pVDZ) and electron density ($\rho(r_c)$) for various H-bonded complexes

H-bonded complexes	SE (kcal/mol)	$\rho(r_c)(e/a_0^3)$
H ₃ O ⁺ ... H ₂ O	49.7	0.1517
OH ⁻ ... H ₂ O	31.7	0.0883
NH ₃ ... NH ₄ ⁺	28.6	0.0667
NH ₄ ⁺ ... H ₂ O	19.8	0.0453
NH ₃ ... HF	12.4	0.0482
NH ₃ ... HCl	9.33	0.0497
HCN ... HF	6.88	0.0266
C ₆ H ₅ OH ... H ₂ O	6.28	0.0262
CH ₃ OH ... CH ₃ OH	5.22	0.0264
CH ₃ OH ... H ₂ O	5.16	0.0198
HCl ... H ₂ O	5.09	0.0258
NH ₂ COH ... H ₂ O	4.85	0.0193
CHOH ... H ₂ O	4.81	0.0234
HCN ... HCl	4.68	0.0211
PH ₃ ... HF	4.48	0.0196
H ₂ O ... H ₂ O	4.46	0.022
C ₂ H ₄ ... HF	4.16	0.0183
PH ₃ ... HCl	3.08	0.0163
PH ₃ ... H ₂ O	2.17	0.0119
H ₂ S ... H ₂ S	1.55	0.0102
SH ₂ ... HF	1.54	0.0093
H ₂ S ... PH ₃	1.37	0.0091
HCl ... HCl	1.22	0.0068
SeH ₂ ... HF	0.91	0.0093
CH ₄ ... NH ₃	0.54	0.0073
CH ₄ ... HF	0.25	0.0047
CH ₄ ... SH ₂	0.23	0.0045
CH ₄ ... Ar	0.11	0.0038

Results from Ref. 327

In a recent illuminating article, Desiraju suggested the term hydrogen bridge to meaningfully represent the H-bond [14]. Since the H-bonding strength ranges from van der Waals to covalent limit, hydrogen bridge is a better description of the interaction without any borders. This new nomenclature can in principle describe exhaustively the variations found in H-bonding interactions in gas, liquid, and solid states, and the corresponding relative significances of covalent, electrostatic, and van der Waals (vdW) contributions.

An attempt has been made in our group to study the concept of interaction without borders using the properties of $\rho(r_c)$ at HBCPs [327]. A diverse class of intermolecular complexes having strength in the range from van der Waals to covalent limit has been chosen to develop a unified picture of the nature of H-bond. SEs and electron density topographical parameters have been computed at MP2/aug-cc-pVDZ level. The schematic diagram shown in Fig. 13 depicts the relationships between SE and $\rho(r_c)$ which explain the

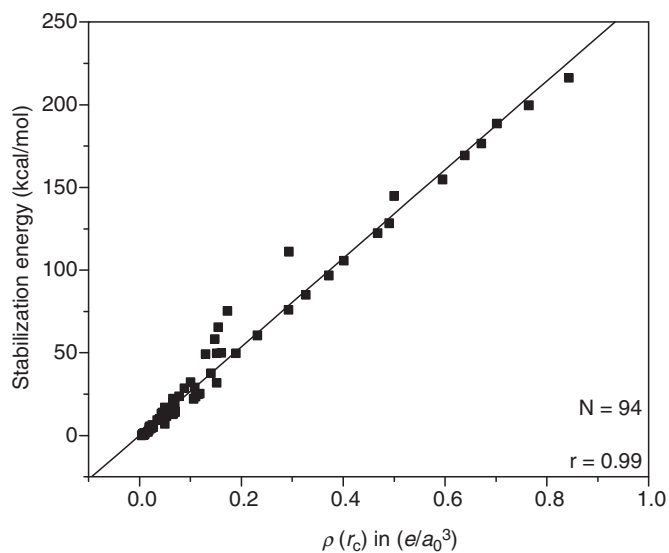


Figure 12. Relationship between stabilization energy and $\rho(r_c)$ for 94 different sets of H-bonded complexes.

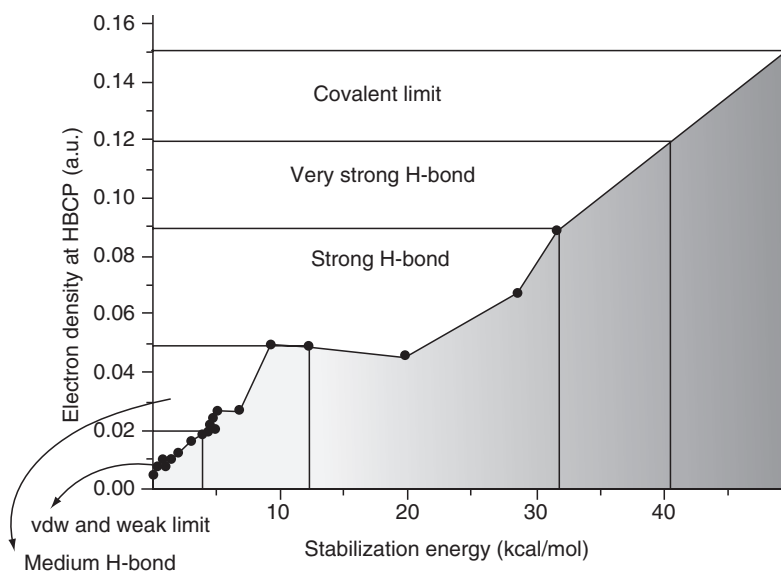


Figure 13. Classification of various types of hydrogen-bonded interactions based on stabilization energy and $\rho(r_c)$. (Results from Ref. 327.)

smooth transition in the H-bond strength from van der Waals to covalent limit. It is worth mentioning that $\rho(r_c)$ at the HBCPs describes the borderless nature of H-bonding interaction found in various molecular complexes. It is clearly evident that $\rho(r_c)$ in various H-bonded interactions follows the order given below:

$\rho(r_c)$ in covalent limit $> \rho(r_c)$ in strong $> \rho(r_c)$ in medium $> \rho(r_c)$ in weak

It is appropriate to mention here that a generalized picture of H-bonded interaction has emerged from the electron density properties at HBCPs.

4. CONCLUDING REMARKS

The main objective of this review is to summarize various aspects of H-bonding interaction starting from its classical definition. From the classical view, H-bonds are electrostatic and partly covalent. The concept of H-bonds has been relaxed to include weak interactions with electrostatic character. In the limiting situation, weak interactions have considerable dispersive–repulsive character and merge into van der Waals interactions. As a result, we observe a great variety of H-bonding interactions without borders. It is currently possible to understand these interactions without borders in the different types of H-bonding with the help of various experimental and theoretical methods. It is illustrated in this chapter that the theory of AIM efficiently describes H-bonding and the concept of the same without border. A unified picture of H-bonding interaction arises from the analysis of electron density topological features at the HBCPs. The results presented here have also demonstrated that the composite nature of the H-bonded interaction can be quantified with the help of electron density and Laplacian of electron density values at the HBCPs. With the development of AIM tools to investigate the experimental electron density from diffraction techniques, it is highly practical for experimentalists to carry out these studies for intermolecular complexes. As a consequence, it is possible to forecast a tremendous growth in characterizing H-bonded interaction using the theory of AIM.

H-bonding has made great impact in various branches of science and hence numerous reports and articles have appeared in the recent past. Therefore, it is not possible to include all the research reports and corresponding references here. All the electronic structure and AIM calculations have been carried out using the G98W [328] and AIM 2000 [329] packages.

ACKNOWLEDGMENTS

The work presented in this chapter was in part supported by the grant received from CSIR, New Delhi, and CLRI, Chennai, India. Authors wish to thank their teachers and mentors Dr. T. Ramasami, Director, CLRI, and Prof. N. Sathyamurthy, IIT, Kanpur for their valuable comments and suggestions and stimulating discussions on various aspects of research. Results presented here

are part of a collaborative research project between CLRI and IIT Kanpur. One of the authors (VS) wishes to thank Prof. S. R. Gadre, Pune University for introducing him to molecular hydration and MESP. It is a pleasure to thank Prof. Jerzy Leszczynski, President's Distinguished Fellow for his kind collaboration and support. Authors thank Prof. S. Grabowski for his invitation to contribute to this volume and his valuable comments. The authors wish to express their gratitude to all the members of Chemical Laboratory for their support and cooperation. One of the authors (VS) dedicates this chapter to his research supervisor Dr. T. Ramasami, Director, CLRI.

REFERENCES

1. G. A. Jeffrey and W. Saenger, *Hydrogen Bonding in Biology and Chemistry* (Springer-Verlag, Berlin, 1991).
2. G. A. Jeffrey, *An Introduction to Hydrogen Bonding* (Oxford University Press, New York, 1997).
3. G. R. Desiraju and T. Steiner, *The Weak Hydrogen Bond in Structural Chemistry and Biology* (Oxford University Press, Oxford, 1999).
4. S. Scheiner, *Hydrogen Bonding. A Theoretical Perspective* (Oxford University Press, Oxford, 1997).
5. L. Pauling, *The Nature of the Chemical Bond* (Cornell University Press, Ithaca, New York, 1960).
6. R. F. W. Bader, *Atoms in Molecules: A Quantum Theory* (Oxford, Clarendon, 1990).
7. A. D. Buckingham, A. C. Legon, and S. M. Roberts, *Principles of Molecular Recognition* (Blackie Academic & Professional, London, 1993).
8. J. A. Pople, W. G. Schneider, and H. J. Bernstein, *High Resolution Nuclear Magnetic Resonance* (McGraw-Hill, New York, 1959), Chap. 15.
9. P. A. Kollman, Hydrogen bonding and donor-acceptor interactions, in: *Applications of Electronic Structure Theory*, edited by H. F. Schaefer III (Plenum, New York, 1977), pp. 109–152.
10. A. Pines, D. J. Ruben, S. Vega, and M. Mehring, New approach to high-resolution proton NMR in solids: deuterium spin decoupling by multiple-quantum transitions, *Phys. Rev. Lett.* **36**, 110–113 (1976).
11. J. F. Hinton, P. Guthrie, P. Pulay, and K. Wolinski, *Ab initio* quantum mechanical calculation of the chemical shift anisotropy of the hydrogen atom in the (H₂O)₁₇ water cluster, *J. Am. Chem. Soc.* **114**, 1604–1605 (1992).
12. D. B. Chesnut, Structures, energies, and NMR shieldings of some small water clusters on the counterpoise corrected potential energy surface, *J. Phys. Chem. A* **106**, 6876–6879 (2002).
13. T. Steiner, The hydrogen bond in the solid state, *Angew. Chem. Int. Ed.* **41**, 48–76 (2002).
14. G. R. Desiraju, Hydrogen bridges in crystal engineering: interactions without borders, *Acc. Chem. Res.* **35**, 565–573 (2002).
15. A. E. Reed, L. A. Curtiss, and F. Weinhold, Intermolecular interactions from a natural bond orbital, donor-acceptor viewpoint, *Chem. Rev.* **88**, 899–926 (1988).
16. P. Hobza and Z. Havlas, Blue-shifting hydrogen bonds, *Chem. Rev.* **100**, 4253–4264 (2000).
17. G. T. Trudeau, J. M. Dumas, P. Dupuis, M. Guerin, and C. Sandorfy, Intermolecular interactions and anesthesia: infrared spectroscopic studies, *Top. Curr. Chem.* **93**, 91–125 (1980).
18. M. Buděšínský, P. Fiedler, and Z. Arnold, Triformylmethane: an efficient preparation, some derivatives, and spectra, *Synthesis* **1989**, 858–860 (1989).
19. I. E. Boldeshul, I. F. Tsymboal, E. V. Ryltsev, Z. Latajka, and A. J. Barnes, Reversal of the usual $\nu(\text{C}\cdots\text{H}/\text{D})$ spectral shift of haloforms in some hydrogen-bonded complexes, *J. Mol. Struct.* **436–437**, 167–171 (1997).

20. P. Hobza, V. Spirko, H. L. Selzle, and E. W. Schlag, Anti-hydrogen bond in the benzene dimer and other carbon proton donor complexes, *J. Phys. Chem. A* **102**, 2501–2504 (1998).
21. E. Cubero, M. Orozco, and F. J. Luque, Electron density topological analysis of the C–H···O anti-hydrogen bond in the fluoroform–oxirane complex, *Chem. Phys. Lett.* **310**, 445–450 (1990).
22. P. Hobza and Z. Havlas, The fluoroform···ethylene oxide complex exhibits a C–H···O anti-hydrogen bond, *Chem. Phys. Lett.* **303**, 447–452 (1999).
23. P. Hobza, V. Špirko, Z. Havlas, K. Buchhold, B. Reimann, H. Barth, and B. Bernhard, Anti-hydrogen bond between chloroform and fluorobenzene, *Chem. Phys. Lett.* **299**, 180–186 (1999).
24. B. J. v. Veken, W. A. Herrebout, R. Szostak, D. N. Shchepkin, Z. Havlas, and P. Hobza, The nature of improper, blue-shifting hydrogen bonding verified experimentally, *J. Am. Chem. Soc.* **123**, 12290–12293 (2001).
25. B. Reimann, K. Buchhold, S. Vaupel, B. Brutschy, Z. Havlas, V. Spirko, and P. Hobza, Improper, Blue-shifting hydrogen bond between fluorobenzene and fluoroform, *J. Phys. Chem. A* **105**, 5560–5566 (2001).
26. S. Scheiner, S. J. Grabowski, and T. Kar, Influence of hybridization and substitution on the properties of the CH···O hydrogen bond, *J. Phys. Chem. A* **105**, 10607–10612 (2001).
27. E. S. Kryachko, T. Zeegers-Huyskens, Theoretical study of the CH···X[−] interaction of fluoromethanes and chloromethanes with fluoride, chloride, and hydroxide anions, *J. Phys. Chem. A* **106**, 6832–6838 (2002).
28. Y. Tatamitani, B. Liu, J. Shimada, T. Ogata, P. Ottaviani, A. Maris, W. Caminati, J. L. Alonso, Weak, improper, C–O···H–C hydrogen bonds in the dimethyl ether dimer, *J. Am. Chem. Soc.* **124**, 2739–2743 (2002).
29. X. Li, L. Liu, and H. B. Schlegel, On the physical origin of blue-shifted hydrogen bonds, *J. Am. Chem. Soc.* **124**, 9639–9647 (2002).
30. K. Hermansson, Blue-shifting hydrogen bonds, *J. Phys. Chem. A* **106**, 4695–4702 (2002).
31. J. M. Fan, L. Liu, and Q. X. Guo, Substituent effects on the blue-shifted hydrogen bonds, *Chem. Phys. Lett.* **365**, 464–472 (2002).
32. W. Zierkiewicz, D. Michalska, Z. Havlas, and P. Hobza, Study of the nature of improper blue-shifting hydrogen bonding and standard hydrogen bonding in the X₃CH···OH and XH···OH₂ complexes (X = F, Cl, Br, I): a correlated *ab initio* study, *Chem. Phys. Chem.* **3**, 511–518 (2002).
33. M. G. Govender and T. A. Ford, Hydrogen bonds, improper hydrogen bonds and dihydrogen bonds, *J. Mol. Struct. (Theochem)* **630**, 11–16 (2003).
34. G. Zhou, J. L. Zhang, N. B. Wong, and A. Tian, Theoretical study of the blue-shifting intramolecular hydrogen bonds of nitro derivatives of cubane, *J. Mol. Struct. (Theochem)* **639**, 43–51 (2003).
35. Z. Xu, H. Li, C. Wang, T. Wu, and S. Han, Is the blue shift of C–H vibration in DMF–water mixture mainly caused by C–H···O interaction? *Chem. Phys. Lett.* **394**, 405–409 (2004).
36. S. K. Rhee, S. H. Kim, S. Lee, and J. Y. Lee, C–H···X interactions of fluoroform with ammonia, water, hydrogen cyanide, and hydrogen fluoride: conventional and improper hydrogen bonds, *Chem. Phys.* **297**, 21–29 (2004).
37. A. Karpfen, The interaction of fluorosilanes with hydrogen fluoride clusters: strongly blue-shifted hydrogen bonds, *J. Mol. Struct. (Theochem)* **710**, 85–95 (2004).
38. P. Koldaivel and V. Nirmala, Study of proper and improper hydrogen bonding using Bader’s atoms in molecules (AIM) theory and NBO analysis, *J. Mol. Struct.* **694**, 33–38 (2004).
39. A. J. Barnes, Blue-shifting hydrogen bonds—are they improper or proper? *J. Mol. Struct.* **704**, 3–9 (2004).
40. P. Lu, G. Q. Liu, and J. C. Li, Existing problems in theoretical determination of red-shifted or blue-shifted hydrogen bond, *J. Mol. Struct. (Theochem)* **723**, 95–100 (2005).
41. S. C. Wang, P. K. Sahu, and S. L. Lee, Intermolecular orbital repulsion effect on the blue-shifted hydrogen bond, *Chem. Phys. Lett.* **406**, 143–147 (2005).

42. X. Wang, G. Zhou, A. Tian, and N. B. Wong, *Ab initio* investigation on blue shift and red shift of C–H stretching vibrational frequency in $\text{NH}_3 \cdots \text{CH}_n\text{X}_{4-n}$ ($n = 1, 3$, X = F, Cl, Br, I) complexes, *J. Mol. Struct. (Theochem)* **718**, 1–7 (2005).
43. S. Wojtulewski and S. J. Grabowski, Blue-shifting C–H...Y intramolecular hydrogen bonds – DFT and AIM analyses, *Chem. Phys.* **309**, 183–188 (2005).
44. W. Zierkiewicz, P. Jurecka, and P. Hobza, On differences between hydrogen bonding and improper blue-shifting hydrogen bonding, *Chem. Phys. Chem.* **6**, 609–617 (2005).
45. A. Karpfen and E. S. Kryachko, Strongly blue-shifted C–H stretches: interaction of formaldehyde with hydrogen fluoride clusters, *J. Phys. Chem. A* **109**, 8930–8937 (2005).
46. I. V. Alabugin, M. Manoharan, S. Peabody, and F. Weinhold, Electronic basis of improper hydrogen bonding: a subtle balance of hyperconjugation and rehybridization, *J. Am. Chem. Soc.* **125**, 5973–5987 (2003).
47. P. A. Kollman and L. C. Allen, Theory of the hydrogen bond, *Chem. Rev.* **72**, 283–303 (1972).
48. T. R. Dyke, K. M. Mack, and J. S. Muentzer, The structure of water dimer from molecular beam electric resonance spectroscopy, *J. Chem. Phys.* **66**, 498–510 (1977).
49. J. A. Odutola and T. R. Dyke, Partially deuterated water dimers: microwave spectra and structure, *J. Chem. Phys.* **72**, 5062–5070 (1980).
50. E. Honegger and S. Leutwyler, Intramolecular vibrations of small water clusters, *J. Chem. Phys.* **88**, 2582–2595 (1988).
51. B. J. Smith, D. J. Swanton, J. A. Pople, H. F. Schaefer III, and L. Random, Transition structures for the interchange of hydrogen atoms within the water dimer, *J. Chem. Phys.* **92**, 1240–1247 (1990).
52. C. Millot and A. J. Stone, Towards an accurate intermolecular potential for water, *Mol. Phys.* **77**, 439–462 (1992).
53. S. S. Xantheas and T. H. Dunning Jr., *Ab initio* studies of cyclic water clusters $(\text{H}_2\text{O})_n$, $n = 1–6$. I. Optimal structures and vibrational spectra, *J. Chem. Phys.* **99**, 8774–8792 (1993).
54. K. Laasonen, M. Parrinello, R. Car, C. Lee, and D. Vanderbilt, Structures of small water clusters using gradient-corrected density functional theory, *Chem. Phys. Lett.* **207**, 208–213 (1993).
55. S. J. Chakravorty and E. R. Davidson, The water dimer: correlation energy calculations, *J. Phys. Chem.* **97**, 6373–6383 (1993).
56. S. Scheiner, *Ab initio* studies of hydrogen bonds: the water dimer paradigm, *Annu. Rev. Phys. Chem.* **45**, 23–56 (1994).
57. S. S. Xantheas, *Ab initio* studies of cyclic water clusters $(\text{H}_2\text{O})_n$, $n = 1–6$. II. Analysis of many-body interactions, *J. Chem. Phys.* **100**, 7523–7534 (1994).
58. M. W. Feyereisen, D. Feller, and D. A. Dixon, Hydrogen bond energy of the water dimer, *J. Phys. Chem.* **100**, 2993–2997 (1996).
59. D. A. Estrin, L. Paglieri, G. Corongiu, and E. Clementi, Small clusters of water molecules using density functional Theory, *J. Phys. Chem.* **100**, 8701–8711 (1996).
60. S. S. Xantheas, On the importance of the fragment relaxation energy terms in the estimation of the basis set superposition error correction to the intermolecular interaction energy, *J. Chem. Phys.* **104**, 8821–8824 (1996).
61. J. K. Gregory and D. C. Clary, Structure of water clusters. The contribution of many-body forces, monomer relaxation, and vibrational zero-point energy, *J. Phys. Chem.* **100**, 18014–18022 (1996).
62. M. Schütz, G. Rauhut, and H. J. Werner, Local treatment of electron correlation in molecular clusters: structures and stabilities of $(\text{H}_2\text{O})_n$, $n = 2–4$, *J. Phys. Chem. A* **102**, 5997–6003 (1998).
63. C. Millot, J. C. Soetens, M. T. C. M. Costa, M. P. Hodges, and A. J. Stone, Revised anisotropic site potentials for the water dimer and calculated properties, *J. Phys. Chem. A* **102**, 754–770 (1998).
64. W. Koch and M. C. Holthausen, *A Chemist's Guide to Density Functional Theory* (Wiley-VCH: Wiley VCH Verlag GmbH, New York, 2001).

65. L. A. Curtiss and M. Blander, Thermodynamic properties of gas-phase hydrogen-bonded complexes, *Chem. Rev.* **88**, 827–841 (1988).
66. A. D. Buckingham, P. W. Fowler, and J. M. Hudson, Theoretical studies of van der Waals molecules and intermolecular forces, *Chem. Rev.* **88**, 963–988 (1988).
67. W. A. Sokalski, P. C. Hariharan, and J. J. Kaufman, A self-consistent field interaction energy decomposition study of 12 hydrogen-bonded dimers, *J. Phys. Chem.* **87**, 2803–2810 (1983).
68. M. J. Frisch, J. E. Del Bene, J. S. Binkley and H. F. Schaefer III, Extensive theoretical studies of the hydrogen-bonded complexes $(\text{H}_2\text{O})_2$, $(\text{H}_2\text{O})_2\text{H}^+$, $(\text{HF})_2$, $(\text{HF})_2\text{H}^+$, F_2H^- , and $(\text{NH}_3)_2$, *J. Chem. Phys.* **84**, 2279–2289 (1986).
69. F. Sim, A. St. Amant, I. Papai, and D. R. Salahub, Gaussian density functional calculations on hydrogen-bonded systems, *J. Am. Chem. Soc.* **114**, 4391–4400 (1992).
70. M. Kieninger and S. Sunai, Density functional studies on hydrogen-bonded complexes, *Int. J. Quantum Chem.* **52**, 465–478 (1994).
71. C. Mijoule, Z. Latajka, and D. Borgis, Density functional theory applied to proton-transfer systems. A numerical test, *Chem. Phys. Lett.* **208**, 364–368 (1993).
72. T. Zhu and W. Yang, Structure of the ammonia dimer studied by density functional theory, *Int. J. Quantum Chem.* **49**, 613–623 (1994).
73. K. Kim and K. D. Jordan, Comparison of density functional and MP2 calculations on the water monomer and dimer, *J. Phys. Chem.* **98**, 10089–10094 (1994).
74. I. A. Topol, S. K. Burt, and A. A. Rashin, Can contemporary density functional theory yield accurate thermodynamics for hydrogen bonding? *Chem. Phys. Lett.* **247**, 112–119 (1995).
75. W. T. Keeton and J. L. Gould, *Biological Science* (W.W. Norton & Co., New York, 1993).
76. N. Solca and O. Dopfer, Prototype microsolvation of aromatic hydrocarbon cations by polar ligands: IR spectra of benzene⁺-*L*_n clusters (L) H₂O, CH₃OH, *J. Phys. Chem. A* **107**, 4046–4055 (2003).
77. J. Tomasi and M. Persico, Molecular interactions in solution: an overview of methods based on continuous distributions of the solvent, *Chem. Rev.* **94**, 2027–2094 (1994).
78. C. J. Cramer and D. G. Truhlar, Implicit solvation models: equilibria, structure, spectra, and dynamics, *Chem. Rev.* **99**, 2161–2200 (1999).
79. M. Orozco and F. J. Luque, Theoretical methods for the description of the solvent effect in biomolecular systems, *Chem. Rev.* **100**, 4187–4226 (2000).
80. J. Tomasi, B. Mennucci, and R. Cammi, Quantum mechanical continuum solvation models, *Chem. Rev.* **105**, 2999–3094 (2005).
81. A. J. Parker, Protic–dipolar aprotic solvent effects on rates of bimolecular reactions, *Chem. Rev.* **69**, 1–32 (1969).
82. L. Onsager, Electric moments of molecules in liquids, *J. Am. Chem. Soc.* **58**, 1486–1493 (1936).
83. J. G. Kirkwood, The dielectric polarization of polar liquids, *J. Chem. Phys.* **7**, 911–919 (1939).
84. M. A. Wong, M. J. Frisch, and K. B. Wiberg, Solvent effects. 2. Medium effect on the structure, energy, charge density, and vibrational frequencies of sulfamic acid, *J. Am. Chem. Soc.* **114**, 523–529 (1992).
85. K. V. Mikkelsen, H. Agren, H. J. A. Jensen, and T. Helgaker, A Multiconfigurational self-consistent reaction-field method, *J. Chem. Phys.* **89**, 3086–3095 (1988).
86. M. V. Basilevsky and G. E. Chudinov, Dynamics of charge transfer chemical reactions in a polar medium within the scope of the Born–Kirkwood–Onsager model, *Chem. Phys.* **157**, 327–344 (1991).
87. A. D. Buckingham and P. W. Fowler, Do electrostatic interactions predict structures of van der Waals molecules? *J. Chem. Phys.* **79**, 6426–6428 (1983).
88. C. E. Dykstra, Molecular mechanics for weakly interacting assemblies of rare gas atoms and small molecules, *J. Am. Chem. Soc.* **111**, 6168–6174 (1989).
89. C. Alhambra, F. J. Luque, and M. Orozco, Molecular solvation potential. A new tool for the quantum mechanical description of hydration in organic and bioorganic molecules, *J. Phys. Chem.* **99**, 3084–3092 (1995).

90. P. Ren and J. W. Ponder, Polarizable atomic multipole water model for molecular mechanics simulation, *J. Phys. Chem. B* **107**, 5933–5947 (2003).
91. S. S. Pundlik and S. R. Gadre, Structure and stability of DNA base trimers: an electrostatic approach, *J. Phys. Chem. B* **101**, 9657–9662 (1997).
92. S. R. Gadre and R. N. Shirsat, *Electrostatics of Atoms and Molecules* (Universities Press (India), Hyderabad, 2000).
93. S. R. Gadre, K. Babu, and A. P. Rendell, Electrostatics for exploring hydration patterns of molecules. 3. Uracil, *J. Phys. Chem. A* **104**, 8976–8982 (2000).
94. S. R. Gadre and S. S. Pundlik, Complementary electrostatics for the Study of DNA base-pair interactions, *J. Phys. Chem. B* **101**, 3298–3303 (1997).
95. S. P. Gejji, C. H. Suresh, L. J. Bartolotti, and S. R. Gadre, Electrostatic potential as a harbinger of cation coordination: CF_3SO_3^- Ion as a model example, *J. Phys. Chem. A* **101**, 5678–5686 (1997).
96. C. H. Suresh and S. R. Gadre, A novel electrostatic approach to substituent constants: doubly substituted benzenes, *J. Am. Chem. Soc.* **120**, 7049–7055 (1998).
97. A. D. Kulkarni, K. Babu, S. R. Gadre, and L. J. Bartolotti, Exploring hydration patterns of aldehydes and amides: *ab initio* Investigations, *J. Phys. Chem. A* **108**, 2492–2498 (2004).
98. S. R. Gadre, M. M. Deshmukh, and R. P. Kalagi, Quantum chemical investigations on explicit molecular hydration, *Proc. Indian Natl. Sci. Acad.* **70**, 709–724 (2004).
99. E. Scrocco and J. Tomasi, in: *Advances in Quantum Chemistry*, edited by P. O. Lowdin (Academic, New York, 1978), Vol. 2.
100. J. Tomasi, R. Bonaccorsi, and R. Cammi, in: *Theoretical Models of Chemical Bonding*, edited by Z. B. Maksic (Springer, Berlin, 1990).
101. P. Politzer, in: *Chemical Applications of Atomic and Molecular Electrostatic Potentials*, edited by P. Politzer, and D. G. Truhlar (Plenum, New York, 1981).
102. K. Morokuma and K. Kitaura, in: *Chemical Applications of Atomic and Molecular Electrostatic Potentials*, edited by P. Politzer, and D. G. Truhlar (Plenum, New York, 1981), pp. 215–242.
103. P. A. Kollman, in: *Chemical Applications of Atomic and Molecular Electrostatic Potentials*, edited by P. Politzer, and D. G. Truhlar (Plenum, New York, 1981).
104. J. N. Murray and K. D. Sen (Eds.), *Molecular Electrostatic Potential: Concepts and Applications* (Elsevier, New York, 1996).
105. B. Brutschy, The Structure of microsolvated benzene derivatives and the role of aromatic substituents, *Chem. Rev.* **100**, 3891–3920 (2000).
106. T. S. Zwier, The spectroscopy of solvation in hydrogen-bonded aromatic clusters, *Ann. Rev. Phys. Chem.* **47**, 205–241 (1996).
107. J. Leszczynski, Isolated, solvated and complexed nucleic acid bases: structures and properties, *Adv. Mol. Struct. Res.* **6**, 209–265 (2000).
108. V. Subramanian, D. Sivasenan, and T. Ramasami, The role of solvent on the base stacking properties of the stacked cytosine dimer, *Chem. Phys. Lett.* **290**, 189–192 (1998).
109. D. Sivasenan, K. Babu, S. R. Gadre, V. Subramanian, and T. Ramasami, Does a stacked DNA base pair hydrate better than a hydrogen-bonded one? An *ab initio* study, *J. Phys. Chem. A* **104**, 10887–10894 (2000).
110. N. I. Nakano and S. J. Igarashi, Molecular interactions of pyrimidines, purines, and some other heteroaromatic compounds in aqueous media, *Biochemistry* **9**, 577–583 (1970).
111. S. Re and K. Morokuma, An ONIOM study of chemical reactions in micro-solvation cluster: $(\text{H}_2\text{O})_n\text{CH}_3\text{Cl} + \text{OH}^-(\text{H}_2\text{O})_m (n + m = 1, 2)$, *J. Phys. Chem. A* **105**, 7185–7197 (2001).
112. W. Saenger, *Principles of Nucleic Acid Structure* (Springer-Verlag, New York, 1984).
113. G. E. Schulz and R. H. Schirmer, *Principles of Protein Structure* (Springer-Verlag, New York, 1979).
114. L. Pauling, R. B. Corey, and H. R. Branson, The structure of proteins; two hydrogen-bonded helical configurations of the polypeptide chain, *Proc. Natl. Acad. Sci. USA* **37**, 205–211 (1951).

115. J. D. Watson and F. H. C. Crick, Molecular structure of nucleic acids: a structure for deoxyribose nucleic acid, *Nature* **171**, 737–738 (1953).
116. G. N. Ramachandran and G. Kartha, Structure of collagen, *Nature* **174**, 269–270 (1954).
117. A. Rich and F. H. C. Crick, The structure of collagen, *Nature* **176**, 915–916 (1955).
118. J. Sponer, J. Leszczynski, and P. Hobza, Structures and energies of hydrogen-bonded DNA base pairs. A nonempirical study with inclusion of electron correlation, *J. Phys. Chem.* **100**, 1965–1974 (1996).
119. J. Sponer, J. Leszczynski, and P. Hobza, Hydrogen bonding and stacking of DNA bases: a review of quantum-chemical *ab initio* studies, *J. Biomol. Struct. Dyn.* **14**, 117–135 (1996).
120. J. Sponer, J. Leszczynski, and P. Hobza, Nature of nucleic acid–base stacking: nonempirical *ab initio* and empirical potential characterization of 10 stacked base dimers. Comparison of stacked and H-bonded base pairs, *J. Phys. Chem.* **100**, 5590–5596 (1996).
121. P. Hobza and J. Leszczynski, Structure, energetics, and dynamics of the nucleic acid base pairs: nonempirical *ab initio* calculations, *Chem. Rev.* **99**, 3247–3276 (1999).
122. M. Kabelac and P. Hobza, Potential energy and free energy surfaces of all ten canonical and methylated nucleic acid base pairs: molecular dynamics and quantum chemical *ab initio* studies, *J. Phys. Chem. B* **105**, 5804–5817 (2001).
123. F. Ryjacek, O. Engkvist, J. Vacek, M. Kratochvil, and P. Hobza, Hoogsteen and stacked structures of the 9-methyladenine···1-methylthymine pair are populated equally at experimental conditions: *ab initio* and molecular dynamics study *J. Phys. Chem. A* **105**, 1197–1202 (2001).
124. J. Sponer, J. Leszczynski, and P. Hobza, Hydrogen bonding, stacking and cation binding of DNA bases, *J. Mol. Struct. (Theochem)* **573**, 43–53 (2001).
125. R. Amutha, V. Subramanian, and Balachandran Unni Nair, Free energy calculation for DNA bases in various solvents using Flory–Huggins theory, *Chem. Phys. Lett.* **335**, 489–495 (2001).
126. P. Hobza and J. Sponer, Toward true DNA base-stacking energies: MP2, CCSD(T), and complete basis set calculations, *J. Am. Chem. Soc.* **124**, 11802–11808 (2002).
127. P. Jurecka and P. Hobza, True stabilization energies for the optimal planar hydrogen-bonded and stacked structures of guanine···cytosine, adenine···thymine, and their 9- and 1-methyl derivatives: complete basis set calculations at the MP2 and CCSD(T) levels and comparison with experiment, *J. Am. Chem. Soc.* **125**, 15608–15613 (2003).
128. P. Jurecka and P. Hobza, Potential energy surface of the cytosine dimer: MP2 complete basis set limit interaction energies, CCSD(T) correction term, and comparison with the AMBER force field, *J. Phys. Chem. B* **108**, 5466–5471 (2004).
129. J. Sponer, P. Jurecka, and P. Hobza, Accurate interaction energies of hydrogen-bonded nucleic acid base pairs, *J. Am. Chem. Soc.* **126**, 10142–10151 (2004).
130. I. Dabkowska, H. V. Gonzalez, P. Jurecka, and P. Hobza, Stabilization energies of the hydrogen-bonded and stacked structures of nucleic acid base pairs in the crystal geometries of CG, AT, and AC DNA steps and in the NMR geometry of the 5'-d(GCGAAGC)-3' hairpin: complete basis set calculations at the MP2 and CCSD(T) levels, *J. Phys. Chem. A* **109**, 1131–1136 (2005).
131. M. Kabelac, L. Zendlova, D. Reha, and P. Hobza, Potential energy surfaces of an adenine-thymine base pair and its methylated analogue in the presence of one and two water molecules: molecular mechanics and correlated *ab initio* Study, *J. Phys. Chem. B* **109**, 12206–12213 (2005).
132. B. Brauer, R. B. Gerber, M. Kabelac, P. Hobza, J. M. Bakker, A. G. Abo Riziq, and M. S. de Vries, Vibrational spectroscopy of the G···C base pair: experiment, harmonic and anharmonic calculations, and the nature of the anharmonic couplings, *J. Phys. Chem. A* **109**, 6974–6984 (2005).
133. A. Perez, J. Sponer, P. Jurecka, P. Hobza, F. J. Luque, and M. Orozco, Are the hydrogen bonds of RNA (AU) stronger than those of DNA (AT)? A quantum mechanics study, *Chemistry* **11**, 5062–5066 (2005).

134. P. Mignon, S. Loverix, J. Steyaert, and P. Geerlings, Influence of the pi-pi interaction on the hydrogen bonding capacity of stacked DNA/RNA bases. *Nucleic Acids Res.* **33**, 1779–1789 (2005).
135. W. Guschlbauer and W. Saenger, *DNA-Ligand Interactions: From Drugs to Proteins* (Plenum, New York, 1987).
136. A. L. Lehninger, D. L. Nelson, and M. M. Cox, *Lehninger Principles of Biochemistry* (Worth Publishers, New York, 2000).
137. B. Wolf and S. Hanlon, Structural transitions of deoxyribonucleic acid in aqueous electrolyte solutions. II. The role of hydration, *Biochemistry* **14**, 1661–1670 (1975).
138. W. Saenger, Structure and dynamics of water surrounding biomolecules, *Annu. Rev. Biophys. Chem.* **16**, 93–114 (1987).
139. M. K. Shukla and J. Leszczynski, Excited states of nucleic acid Bases, in: *Computational Chemistry: Reviews of Current Trends*, edited by J. Leszczynski (World Scientific, Singapore, 2003), Vol. 8, pp. 249–344.
140. M. A. Young, B. Jayaram, and D. L. Beveridge, Intrusion of counterions into the spine of hydration in the minor groove of B-DNA: fractional occupancy of electronegative pockets, *J. Am. Chem. Soc.* **119**, 59–69 (1997).
141. D. Sprous, M. A. Young, and D. L. Beveridge, Molecular dynamics studies of the conformational preferences of a DNA double helix in water and an ethanol/water mixture: theoretical considerations of the A \rightleftharpoons B transition, *J. Phys. Chem. B* **102**, 4658–4667 (1998).
142. N. Spackova, T. E. Cheatham III, F. Ryjacek, F. Lankas, L. van Meervelt, P. Hobza, and J. Sponer, Molecular dynamics simulations and thermodynamics analysis of DNA–drug complexes. Minor groove binding between 4',6-diamidino-2-phenylindole and DNA duplexes in solution, *J. Am. Chem. Soc.* **125**, 1759–1769 (2003).
143. B. Jayaram, D. Sprous, M. A. Young, and D. L. Beveridge, Free energy analysis of the conformational preferences of A and B forms of DNA in solution, *J. Am. Chem. Soc.* **120**, 10629–10633 (1998).
144. D. Vlieghe, J. Sponer, and L. V. Meervelt, Crystal structure of d(GGCCAATTGG) complexed with DAPI reveals novel binding mode, *Biochemistry* **38**, 16443–16451 (1999).
145. D. M. Blakaj, K. J. McConnell, D. L. Beveridge, and A. M. Baranger, Molecular dynamics and thermodynamics of protein–RNA interactions: mutation of a conserved aromatic residue modifies stacking interactions and structural adaptation in the U1A-stem loop 2 RNA complex, *J. Am. Chem. Soc.* **123**, 2548–2551 (2001).
146. H. E. L. Williams and M. S. Searle, Structure, dynamics and hydration of the nogalamycin–d(ATGCAT)₂ complex determined by NMR and molecular dynamics simulations in solution, *J. Mol. Biol.* **290**, 699–716 (1999).
147. M. Zacharias and H. Sklenar, Conformational analysis of single-base bulges in A-form DNA and RNA using a hierarchical approach and energetic evaluation with a continuum solvent model, *J. Mol. Biol.* **289**, 261–275 (1999).
148. W. H. A. Fersht, *Structure and Mechanism in Protein Science: A Guide to Enzyme Catalysis and Protein Folding* (W. H. Freeman and Company, New York, 1999).
149. B. Bagchi, Water dynamics in the hydration layer around proteins and micelles, *Chem. Rev.* **105**, 3197–3219 (2005).
150. K. Muller-Dethlefs and P. Hobza, Noncovalent interactions: a challenge for experiment and theory, *Chem. Rev.* **100**, 143–168 (2000).
151. U. Buck and F. Huisken, Infrared spectroscopy of size-selected water and methanol clusters, *Chem. Rev.* **100**, 3863–3890 (2000).
152. H. J. Neusser and K. Siglow, High-resolution ultraviolet spectroscopy of neutral and ionic clusters: hydrogen bonding and the external heavy atom effect, *Chem. Rev.* **100**, 3921–3942 (2000).
153. Y. Matsumoto, T. Ebata, and N. Mikami, Structures and vibrations of 2-naphthol-(NH₃)_n ($n = 1-3$) hydrogen-bonded clusters investigated by IR–UV double-resonance spectroscopy, *J. Mol. Struct.* **552**, 257–271 (2000).

154. N. Guchhait, T. Ebata, and N. Mikami, Vibrational spectroscopy for size-selected fluorene-(H₂O)_{n=1,2} clusters in supersonic jets, *J. Phys. Chem. A* **104**, 11891–11896 (2000).
155. G. N. Patwari, T. Ebata, and N. Mikami, Evidence of dihydrogen bond in gas phase: phenol–borane–dimethylamine complex, *J. Chem. Phys.* **113**, 9885–9888 (2000).
156. T. Ebata, M. Kayano, S. Sato, and N. Mikami, Picosecond IR–UV pump-probe spectroscopy. IVR of OH stretching vibration of phenol and phenol dimer, *J. Phys. Chem. A* **105**, 8623–8628 (2001).
157. A. Fujii, G. N. Patwari, T. Ebata, and N. Mikami, Vibrational spectroscopic evidence of unconventional hydrogen bonds, *Int. J. Mass Spectrom.* **220**, 289 (2002).
158. A. Fujii, T. Ebata, and N. Mikami, Direct observation of weak hydrogen bonds in micro-solvated phenol: infrared spectroscopy of OH stretching vibrations of phenol–CO and –CO₂ in S₀ and D₀, *J. Phys. Chem. A* **106**, 10124–10129 (2002).
159. G. N. Patwari, T. Ebata, and N. Mikami, Dihydrogen bonded phenol–borane–dimethylamine complex: an experimental and theoretical study, *J. Chem. Phys.* **116**, 6056–6063 (2002).
160. H. Kawamata, T. Maeyama, and N. Mikami, First observation of ionic π -hydrogen bonds; vibrational spectroscopy of dihydrated paphtalene anion (Nph[−](H₂O)₂), *Chem. Phys. Lett.* **370**, 535–541 (2003).
161. M. Miyazaki, A. Fujii, T. Ebata, and N. Mikami, Infrared spectroscopy of hydrated benzene cluster cations, [C₆H₆–(H₂O)_n]⁺ (n = 1–6): structural changes upon photoionization and proton transfer reactions, *Phys. Chem. Chem. Phys.* **5**, 1137–1148 (2003).
162. Y. Yamada, T. Ebata, M. Kayano, and N. Mikami, Picosecond IR–UV pump-probe spectroscopic study of the dynamics of the vibrational relaxation of jet-cooled phenol. I. Intramolecular vibrational energy redistribution of the OH and CH stretching vibrations of bare phenol, *J. Chem. Phys.* **120**, 7400–7409 (2004).
163. M. Miyazaki, A. Fujii, T. Ebata, and N. Mikami, Infrared spectroscopic evidence for protonated water clusters forming nanoscale cages, *Science* **304**, 1134–1137 (2004).
164. C. Steinbach, P. Andersson, J. K. Kazimirski, U. Buck, V. Buch, and T. A. Beu, Infrared predissociation spectroscopy of large water clusters: a unique probe of cluster surfaces, *J. Phys. Chem. A* **108**, 6165–6174 (2004).
165. C. Steinbach, P. Andersson, M. Melzer, J. K. Kazimirski, U. Buck, and V. Buch, Detection of the book isomer from the OH-stretch spectroscopy of size selected water hexamers, *Phys. Chem. Chem. Phys.* **6**, 3320–3324 (2004).
166. K. Kim, K. D. Jordan, and T. S. Zwier, Low-energy structures and vibrational frequencies of the water hexamer: comparison with benzene (H₂O)₆, *J. Am. Chem. Soc.* **116**, 11568–11569 (1994).
167. T. S. Zwier, The Infrared spectroscopy of hydrogen-bonded clusters: chains, cycles, cubes, and three-dimensional networks, In: *Advances in Molecular Vibrations and Collision Dynamics*, edited by J. M. Bowman (JAI, Greenwich, 1998), pp. 249–280.
168. P. Ayotte, G. H. Weddle, G. G. Bailey, M. A. Johnson, F. Vila, and K. D. Jordan, Infrared spectroscopy of negatively charged water clusters: evidence for a linear Network, *J. Chem. Phys.* **110**, 6268–6277 (1999).
169. C. J. Gruenloh, F. C. Hagemeister, and T. S. Zwier, Size and conformation-selective infrared spectroscopy of neutral hydrogen-bonded clusters, in: *Recent Theoretical and Experimental Advances in Hydrogen-Bonded Clusters*, edited by S. S. Xantheas (Kluwer, The Netherlands, 2000), pp. 83–99.
170. G. M. Florio, C. J. Gruenloh, R. C. Quimpo, and T. S. Zwier, The infrared spectroscopy of hydrogen-bonded bridges: I. 2-Pyridone–(water)_n and 2-hydroxypyridine–(water)_n, n = 1,2, *J. Chem. Phys.* **113**, 11143–11153 (2000).
171. J. R. Carney, A. Fedorov, J. R. Cable, and T. S. Zwier, The infrared spectroscopy of H-bonded bridges stretched across the *cis*-amide group: I. Water bridges, *J. Phys. Chem. A* **105**, 3487–3497 (2001).
172. T. S. Zwier, Laser Spectroscopy of jet-cooled biomolecules and their water-containing clusters: water bridges and molecular conformation, *J. Phys. Chem. A* **105**, 8827–8839 (2001).

173. J. W. Shin, N. I. Hammer, E. G. Diken, M. A. Johnson, R. S. Walters, T. D. Jaeger, M. A. Duncan, R. A. Christie, and K. D. Jordan, Infrared signature of structures associated with the $H^+(H_2O)_n$ ($n = 6$ to 27) clusters, *Science* **304**, 1137–1140 (2004).
174. T. S. Zwier, The structure of protonated water clusters, *Science* **304**, 1119–1120 (2004).
175. J. R. Clarkson, E. Baquero, A. V. Shubert, E. M. Myshakin, K. D. Jordan, and T. S. Zwier, Laser-initiated shuttling of a water molecule between H-bonding sites, *Science* **307**, 1443–1446 (2005).
176. K. Diri, E. M. Myshakin, and K. D. Jordan, The role of vibrational anharmonicity on the binding energies of water clusters, *J. Phys. Chem.* **109**, 4005–4009 (2005).
177. J. M. Headrick, E. G. Diken, R. S. Walters, N. I. Hammer, R. A. Christie, J. Cui, E. M. Myshakin, M. A. Duncan, M. A. Johnson, and K. D. Jordan, Spectral signatures of hydrated proton vibrations in water clusters, *Science* **308**, 1765–1769 (2005).
178. P. Hohenberg and W. Kohn, Inhomogeneous electron gas, *Phys. Rev. B* **136**, 864–871 (1964).
179. W. Kohn and L. J. Sham, Self-consistent equations including exchange and correlation effects, *Phys. Rev. A* **140**, 1133–1135 (1965).
180. Y. Zhao and D. G. Truhlar, Hybrid meta density functional theory methods for thermochemistry, thermochemical kinetics, and noncovalent interactions: the MPW1B95 and MPWB1K models and comparative assessments for hydrogen bonding and van der Waals interactions, *J. Phys. Chem. A* **108**, 6908–6918 (2004).
181. S. F. Boys and F. Bernardi, The calculation of small molecular interaction by the differences of separate total energies. Some procedures with reduced errors, *Mol. Phys.* **19**, 553–556 (1970).
182. P. Hobza, Theoretical studies of hydrogen bonding, *Annu. Rep. Prog. Chem. Sect. C: Phys. Chem.* **100**, 3–27 (2004).
183. A. R. Leach, *Molecular Modelling: Principles and Applications* (Prentice Hall, Upper Saddle River, NJ, 2001).
184. C. J. Cramer, *Essentials of Computational Chemistry: Theories and Models* (Wiley, Chichester, UK, 2004).
185. P. A. Kollman, Free energy calculations: applications to chemical and biochemical phenomena, *Chem. Rev.* **93**, 2395–2417 (1993).
186. P. A. Kollman, I. Massova, C. Reyes, B. Kuhn, S. Huo, L. Chong, M. Lee, T. Lee, Y. Duan, W. Wang, O. Donini, P. Cieplak, J. Srinivasan, D. A. Case, and T. E. Cheatham III, Calculating structures and free energies of complex molecules: combining molecular mechanics and continuum models, *Acc. Chem. Res.* **33**, 889–897 (2000).
187. P. A. Kollman, Advances and continuing challenges in achieving realistic and predictive simulations of the properties of organic and biological molecules, *Acc. Chem. Res.* **29**, 461–469 (1996).
188. A. H. Elcock, D. Sept, and J. A. McCammon, Computer simulation of protein–protein interactions, *J. Phys. Chem. B* **105**, 1504–1518 (2001).
189. D. A. Case, Molecular Dynamics and NMR spin relaxation in proteins, *Acc. Chem. Res.* **35**, 325–331 (2002).
190. C. F. Wong and J. A. McCammon, Protein simulation and drug design, *Adv. Protein Chem.* **66**, 87–121 (2003).
191. J. M. Briggs, T. J. Marrone, and J. A. McCammon, Computational science new horizons and relevance to pharmaceutical design, *Trends Cardiovasc. Med.* **6**, 198–203 (1996).
192. W. L. Jorgensen, J. Chandrasekhar, J. D. Madura, R. W. Impey, and M. L. Klein, Comparison of simple potential functions for simulating liquid water, *J. Chem. Phys.* **79**, 926–935 (1983).
193. R. F. W. Bader, A Bond Path: A universal indicator of bonded interactions, *J. Phys. Chem. A* **102**, 7314–7323 (1998).
194. P. L. A. Popelier, *Atoms in Molecules. An Introduction* (Prentice-Hall, Harlow, UK, 2000).

195. P. L. A. Popelier, On the full topology of the Laplacian of the electron density, *Coord. Chem. Rev.* **197**, 169–189 (2000).
196. U. Koch and P. L. A. Popelier, Characterization of C–H–O hydrogen bonds on the basis of the charge density, *J. Chem. Phys.* **99**, 9747–9754 (1995).
197. R. G. A. Bone and R. F. W. Bader, Identifying and analyzing intermolecular bonding interactions in van der Waals molecules, *J. Phys. Chem.* **100**, 10892–10911 (1996).
198. S. J. Grabowski, *Ab initio* calculations on conventional and unconventional hydrogen bonds—Study of the hydrogen bond strength, *J. Phys. Chem. A* **105**, 10739–10746 (2001).
199. S. J. Grabowski, Hydrogen bonding strength—measures based on geometric and topological parameters, *J. Phys. Org. Chem.* **17**, 18–31 (2004).
200. S. Wojtulewski and S. J. Grabowski, *Ab initio* and AIM studies on intramolecular dihydrogen bonds, *J. Mol. Struct.* **645**, 287–294 (2003).
201. S. Wojtulewski and S. J. Grabowski, Unconventional F–H··· π hydrogen bonds—*ab initio* and AIM study, *J. Mol. Struct.* **605**, 235–240 (2002).
202. W. D. Arnold and E. Oldfield, The chemical nature of hydrogen bonding in proteins via NMR: *J*-couplings, chemical shifts, and AIM theory, *J. Am. Chem. Soc.* **122**, 12835–12841 (2000).
203. S. J. Grabowski, An estimation of strength of intramolecular hydrogen bonds—*ab initio* and AIM studies, *J. Mol. Struct.* **562**, 137–143 (2001).
204. M. T. Carroll and R. F. W. Bader, An analysis of the hydrogen bond in base-hydrogen fluoride complexes using the theory of atoms in molecules, *Mol. Phys.* **65**, 695–722 (1988).
205. F. J. Luque, J. M. Lopez, M. L. de la Paz, C. Vicent, and M. Orozco, Role of intramolecular hydrogen bonds in the intermolecular hydrogen bonding of carbohydrates, *J. Phys. Chem. A* **102**, 6690–6696 (1998).
206. L. Gonzalez, O. Mó, and M. Yañez, Density functional theory study on ethanol dimers and cyclic ethanol trimers, *J. Chem. Phys.* **111**, 3855–3861 (1999).
207. E. Espinosa, E. Molins, and C. Lecomte, Hydrogen bond strengths revealed by topological analyses of experimentally observed electron densities, *Chem. Phys. Lett.* **285**, 170–173 (1998).
208. Yu. A. Abramov, On the possibility of kinetic energy density evaluation from the experimental electron-density distribution, *Acta Crystallogr. A* **53**, 264–271 (1997).
209. O. Mó, M. Yañez, and J. Elguero, Cooperative (nonpairwise) effects in water trimers: an *ab initio* molecular orbital study, *J. Chem. Phys.* **97**, 6628–6638 (1992).
210. O. Mó, M. Yañez, and J. Elguero, Cooperative effects in the cyclic trimer of methanol. An *ab initio* molecular orbital study, *J. Mol. Struct. (Theochem)* **314**, 73–81 (1994).
211. I. Rozas, I. Alkorta, and J. Elguero, Unusual hydrogen bonds: H··· π interactions, *J. Phys. Chem. A* **101**, 9457–9463 (1997).
212. L. Gonzalez, O. Mó, M. Yañez, and J. Elguero, Very strong hydrogen bonds in neutral molecules: the phosphinic acid dimers, *J. Chem. Phys.* **109**, 2685–2693 (1998).
213. M. Peters, I. Rozas, I. Alkorta, and J. Elguero, DNA triplexes: a study of their hydrogen bonds, *J. Phys. Chem. B* **107**, 323–330 (2003).
214. R. F. W. Bader and D. J. Bayles, Properties of atoms in molecules: group additivity, *J. Phys. Chem. A* **104**, 5579–5589 (2000).
215. P. L. A. Popelier, L. Joubert, and D. S. Kosov, Convergence of the electrostatic interaction based on topological atoms, *J. Phys. Chem. A* **105**, 8254–8261 (2001).
216. S. Wojtulewski and S. J. Grabowski, DFT and AIM studies on two-ring resonance assisted hydrogen bonds, *J. Mol. Struct. (Theochem)* **621**, 285–291 (2003).
217. L. Checinska and S. J. Grabowski, Partial hydrogen bonds: structural studies on thioureidoalkylphosphonates, *J. Phys. Chem. A* **109**, 2942–2947 (2005).
218. M. Domagala and S. J. Grabowski, C–H···N and C–H···S hydrogen bonds—influence of hybridization on their strength, *J. Phys. Chem. A* **109**, 5683–5688 (2005).
219. S. J. Grabowski, W. A. Sokalski, and J. Leszczynski, How short can the H···H intermolecular contact be? New findings that reveal the covalent nature of extremely strong interactions, *J. Phys. Chem. A* **109**, 4331–4341 (2005).

220. S. J. Grabowski, π -Electron delocalisation for intramolecular resonance assisted hydrogen bonds, *J. Phys. Org. Chem.* **16**, 797–802 (2003).
221. V. Subramanian, D. Sivanesan, J. Padmanabhan, N. Lakshminarayanan, and T. Ramasami, Atoms in molecules: application to electronic structure of van der Waals complexes, *Proc. Indian Acad. Sci. (Chem. Sci.)* **111**, 369–375 (1999).
222. S. J. Grabowski, High-level *ab initio* calculations of dihydrogen-bonded complexes, *J. Phys. Chem. A* **104**, 5551–5557 (2000).
223. S. J. Grabowski, Study of correlations for dihydrogen bonds by quantum-chemical calculations, *Chem. Phys. Lett.* **312**, 542–547 (1999).
224. P. L. A. Popelier, Characterization of a dihydrogen bond on the basis of the electron density, *J. Phys. Chem. A* **102**, 1873–1878 (1998).
225. R. F. W. Bader and H. Essen, The characterization of atomic interactions, *J. Chem. Phys.* **80**, 1943–1960 (1984).
226. R. W. Gora, S. J. Grabowski, and J. Leszczynski, Dimers of formic acid, acetic acid, formamide and pyrrole-2-carboxylic acid: an *ab initio* study, *J. Phys. Chem. A* **109**, 6397–6405 (2005).
227. S. J. Grabowski, A new measure of hydrogen bonding strength—*ab initio* and atoms in molecules studies, *Chem. Phys. Lett.* **338**, 361–366 (2001).
228. P. Ball, *H₂O: A Biography of Water* (Weidenfeld & Nicolson, London, 1999).
229. K. Liu, J. D. Cruzan, and R. J. Saykally, Water clusters, *Science* **271**, 929–933 (1996).
230. R. Ludwig, Water: from clusters to the bulk, *Angew. Chem. Int. Ed.* **40**, 1808–1827 (2001).
231. Ph. Wernet, D. Nordlund, U. Bergmann, M. Cavalleri, M. Odelius, H. Ogasawara, L. Å. Näslund, T. K. Hirsch, L. Ojamäe, P. Glatzel, L. G. M. Pettersson, and A. Nilsson, The structure of the first coordination shell in liquid water, *Science* **304**, 995–999 (2004).
232. D. J. Wales and M. P. Hodges, Global minima of water clusters (H₂O)_n, $n \leq 21$, described by an empirical potential, *Chem. Phys. Lett.* **286**, 65–72 (1998).
233. P. L. M. Plummer, Applicability of semi-empirical methods to the study of small water clusters: cubic structures for (H₂O)_n ($n = 8, 12, 16$), *J. Mol. Struct. (Theochem)* **417**, 35 (1997).
234. D. J. Wales, Structure, dynamics, and thermodynamics of clusters: tales from topographic potential surfaces, *Science* **271**, 925–929 (1996).
235. S. Maheshwary, N. Patel, N. Sathyamurthy, A. D. Kulkarni, and S. R. Gadre, Structure and stability of water clusters (H₂O)_n, $n = 8–20$: an *ab initio* investigation, *J. Phys. Chem. A* **105**, 10525–10537 (2001).
236. D. J. Anick, Zero point energy of polyhedral water clusters, *J. Phys. Chem. A* **109**, 5596–5601 (2005).
237. H. S. Frank and W. Y. Wen, Ion–solvent interaction. Structural aspects of ion–solvent interaction in aqueous solutions: a suggested picture of water structure, *Disc. Faraday Soc.* **24**, 133–140 (1957).
238. J. D. Cruzan, L. B. Braly, K. Liu, M. G. Brown, J. G. Loeser, and R. J. Saykally, Quantifying hydrogen bond cooperativity in water: VRT spectroscopy of the water tetramer, *Science* **271**, 59–62 (1996).
239. J. D. Cruzan, L. B. Braly, K. Liu, M. G. Brown, J. G. Loeser, and R. J. Saykally, Terahertz laser vibration–rotation tunneling spectroscopy of the water tetramer, *J. Phys. Chem. A* **101**, 9022–9031 (1997).
240. J. Kim and K. S. Kim, Structures, binding energies, and spectra of isoenergetic water hexamer clusters: extensive *ab initio* studies, *J. Chem. Phys.* **109**, 5886–5895 (1998).
241. K. Liu, M. G. Brown, C. Carter, R. J. Saykally, J. K. Gregory, and D. C. Clary, Characterization of a cage form of the water hexamer, *Nature* **381**, 501–503 (1996).
242. K. Nauta and R. E. Miller, Formation of cyclic water hexamer in liquid helium: the smallest piece of ice, *Science* **287**, 293–295 (2000).
243. R. Parthasarathi, V. Subramanian, and N. Sathyamurthy, Electron density topography, NMR and NBO analysis on water clusters and water chains (results to be published).

244. R. Parthasarathi, R. Amutha, V. Subramanian, B. U. Nair, and T. Ramasami, Bader's and reactivity descriptors' analysis of DNA base pairs, *J. Phys. Chem. A* **108**, 3817–3828 (2004).
245. R. Parthasarathi, V. Subramanian, and N. Sathyamurthy, Hydrogen bonding in phenol, water, and phenol–water clusters, *J. Phys. Chem. A* **109**, 843–850 (2005).
246. R. Parthasarathi and V. Subramanian, Stacking interactions in benzene and cytosine dimers: from molecular electron density perspective, *Struct. Chem.* **16**, 243–255 (2005).
247. E. Westhof and D.L. Beveridge, Hydration of Nucleic Acids, in: *Water Science Reviews 5*, edited by F. Franks (Cambridge University Press, Cambridge, 1990), pp. 24–136.
248. E. Westhof, Structural water bridges in nucleic acids, in: *Water and Biological Macromolecules*, edited by E. Westhof (CRC Press, Boca Raton, FL, 1993), pp. 226–243.
249. H. M. Berman and B. Schneider, Nucleic acid hydration, in: *Handbook of Nucleic Acid Structure*, edited by S. Neidle (Oxford University Press, Oxford, 1999), pp. 295–312.
250. B. Luisi, DNA–protein interactions at high resolution, in: *DNA–Protein Structural Interactions*, edited by D. M. J. Lilley (IRL Press, Oxford, 1995), pp. 1–48.
251. G. Hummer, A. E. Garcia, and D. M. Soumpasis, Hydration of nucleic acid fragments: comparison of theory and experiment for high-resolution crystal structures of RNA, DNA, and DNA–drug complexes, *Biophys. J.* **68**, 1639–1652 (1995).
252. M. Orozco, E. Cubero, X. Barril, C. Colominas, and F. J. Luque, Nucleic acid bases in solution, in: *Computational Molecular Biology*, edited by J. Leszczynski (Elsevier, Amsterdam, 1999), Vol. 8, pp. 119–166.
253. L. Gorb and J. Leszczynski, Current trends in modeling interactions of DNA fragments with polar solvents, in: *Computational Molecular Biology*, edited by J. Leszczynski (Elsevier, Amsterdam, 1999), Vol. 8, pp. 167–209.
254. S. R. Holbrook, C. Cheong, I. Tinoco Jr., and S. H. Kim, Crystal structure of an RNA double helix incorporating a track of non-Watson–Crick pairs, *Nature* **353**, 579–581 (1991).
255. C. C. Correll, B. Freeborn, P. B. Moore, and T. A. Steitz, Metals, motifs, and recognition in the crystal structure of a 5 S rRNA domain, *Cell* **91**, 705–712 (1997).
256. M. Brandl, M. Meyer, and J. Sühnel, Quantum-chemical study of a water-mediated uracil–cytosine base-pair, *J. Am. Chem. Soc.* **121**, 2605–2606 (1999).
257. M. Brandl, M. Meyer, and J. Sühnel, Water-mediated base-pairs in RNA: a quantum-chemical study, *J. Phys. Chem. A* **104**, 11177–11187 (2000).
258. C. Schneider, M. Brandl, and J. Sühnel, Molecular dynamics simulation reveals conformational switching of water-mediated uracil–cytosine base-pairs in an RNA duplex, *J. Mol. Biol.* **305**, 659–667 (2001).
259. T. Ebata, A. Fujii, and N. Mikami, Vibrational spectroscopy of small-sized hydrogen-bonded clusters and their ions, *Int. Rev. Phys. Chem.* **17**, 331–361 (1998).
260. T. Ebata, A. Fujii, and N. Mikami, Structures of size selected hydrogen-bonded phenol–(H₂O)_n clusters in S₀, S₁ and ion, *Int. J. Mass Spectrom.* **159**, 111–124 (1996).
261. T. Watanabe, T. Ebata, M. Fujii, and N. Mikami, OH stretching vibrations of phenol–(H₂O)_n (n = 1–3) complexes observed by IR–UV double-resonance spectroscopy, *Chem. Phys. Lett.* **215**, 347–352 (1993).
262. D. Feller and M. W. Feyereisen, *ab initio* study of hydrogen bonding in the phenol–water system, *J. Comp. Chem.* **14**, 1027–1035 (1993).
263. A. Oikawa, H. Abe, N. Mikami, and M. Ito, Solvated phenol studied by supersonic jet spectroscopy, *J. Phys. Chem.* **87**, 5083–5090 (1983).
264. M. Gerhards and K. Kleinermanns, Structure and vibrations of phenol(H₂O)₂, *J. Chem. Phys.* **103**, 7392–7400 (1995).
265. T. Burgi, M. Schutz, and S. Leutwyler, Intermolecular vibrations of phenol–(H₂O)₃ and d₁-phenol–(D₂O)₃ in the S₀ and S₁ states, *J. Chem. Phys.* **103**, 6350–6361 (1995).
266. T. Watanabe, T. Ebata, S. Tanabe, and N. Mikami, Size-selected vibrational spectra of phenol–(H₂O)_n (n = 1–4) clusters observed by IR–UV double resonance and stimulated Raman–UV double resonance spectroscopies, *J. Chem. Phys.* **105**, 408–419 (1996).

267. H. Watanabe and I. Iwata, Theoretical studies of geometric structures of phenol–water clusters and their infrared absorption spectra in the O–H stretching region, *J. Chem. Phys.* **105**, 420–431 (1996).
268. T. Ebata, N. Mizuochi, T. Watanabe, and N. Mikami, OH stretching vibrations of phenol–(H₂O)₁ and phenol–(H₂O)₃ in the S₁ state, *J. Phys. Chem.* **100**, 546–550 (1996).
269. Y. Dimitrova, Theoretical study of structures and stabilities of hydrogen-bonded phenol–water complexes, *J. Mol. Struct. (Theochem)* **455**, 9–21 (1998).
270. H. H. Y. Tsui and T. V. Mourik, *Ab initio* calculations on phenol–water, *Chem. Phys. Lett.* **350**, 565–572 (2001).
271. D. M. Benoit and D. C. Clary, Quantum simulation of phenol–water clusters, *J. Phys. Chem. A* **104**, 5590–5599 (2000).
272. D. M. Benoit, A. X. Chavagnac, and D. C. Clary, Speed improvement of diffusion quantum Monte Carlo calculations on weakly bound clusters, *Chem. Phys. Lett.* **283**, 269–276 (1998).
273. M. Yi and S. Scheiner, Proton transfer between phenol and ammonia in ground and excited electronic states, *Chem. Phys. Lett.* **262**, 567–572 (1996).
274. E. Cubero, M. Orozco, P. Hobza, and F. J. Luque, Hydrogen bond versus anti-hydrogen bond: a comparative analysis based on the electron density topology, *J. Phys. Chem. A* **103**, 6394–6401 (1999).
275. J. Gu, J. Wang, and J. Leszczynski, H-bonding patterns in the platinated guanine–cytosine base pair and guanine–cytosine–guanine–cytosine base tetrad: an electron density deformation analysis and AIM study, *J. Am. Chem. Soc.* **126**, 12651–12660 (2004).
276. M. Meot-Ner (Mautner), The ionic hydrogen bond, *Chem. Rev.* **105**, 213–284 (2005).
277. M. Eigen, Proton transfer, acid–base catalysis, and enzymatic hydrolysis. Part I: elementary processes, *Angew. Chem. Int. Ed.* **3**, 1–19 (1964).
278. P. Schuster, G. Zundel, and C. Sandorfy (Eds.), *The Hydrogen Bond. Recent Developments in Theory and Experiments* (North-Holland, Amsterdam, 1976).
279. G. Zundel, Hydrogen Bonds with large proton polarizability and proton transfer processes in electrochemistry and biology, *Adv. Chem. Phys.* **111**, 1–218 (2000).
280. L. Ojamae, I. Shavitt, and S. J. Singer, Potential energy surfaces and vibrational spectra of H₃O⁺ and larger hydrated proton complexes, *Int. J. Quantum Chem.* **56**, 657–668 (1995).
281. Y. Xie, R. B. Remington, and H. B. Schaefer, The protonated water dimer: extensive theoretical studies of H₅O₂⁺, *J. Chem. Phys.* **101**, 4878–4884 (1994).
282. E. F. Valeev and H. F. Schaefer, The protonated water dimer: Brueckner methods remove the spurious C₁ symmetry minimum, *J. Chem. Phys.* **108**, 7197–7201 (1998).
283. M. Tuckerman, K. Laasonen, M. Sprik, and M. Parinello, *Ab initio* molecular dynamics simulation of the solvation and transport of hydronium and hydroxyl ions in water, *J. Chem. Phys.* **103**, 150–161 (1995).
284. U. W. Schmitt and G. A. Voth, The computer simulation of proton transport in water, *J. Chem. Phys.* **111**, 9361–9381 (1999).
285. R. A. Christie and K. D. Jordan, Theoretical investigation of the H₃O⁺(H₂O)₄ cluster, *J. Phys. Chem. A* **105**, 7551–7558 (2001).
286. A. L. Sobolewski and W. Domcke, *Ab initio* investigation of the structure and spectroscopy of hydronium–water clusters, *J. Phys. Chem. A* **106**, 4158–4167 (2002).
287. R. A. Christie and K. D. Jordan, Finite temperature behavior of H⁺(H₂O)₆ and H⁺(H₂O)₈, *J. Phys. Chem. B* **106**, 8376–8381 (2002).
288. W. H. Robertson, E. G. Diken, E. A. Price, J. W. Shin, and M. A. Johnson, Spectroscopic determination of the OH[−] solvation shell in the OH[−]·(H₂O)_{*n*} clusters, *Science* **299**, 1367–1372 (2003).
289. D. Asthagiri, L. R. Pratt, J. D. Kress, and M. A. Gomez, Hydration and mobility of HO[−](aq), *Proc. Natl. Acad. Sci.* **101**, 7229–7233 (2004).
290. M. P. Hodges and A. J. Stone, Modeling small hydronium–water clusters, *J. Chem. Phys.* **110**, 6766–6672 (1999).

291. G. Corongiu, R. Kelterbaum, and E. Kochanski, Theoretical studies of $\text{H}^+(\text{H}_2\text{O})_5$, *J. Phys. Chem.* **99**, 8038–8044 (1995).
292. Y. Xie and H. F. Schaefer, Hydrogen bonding between the water molecule and the hydroxyl radical ($\text{H}_2\text{O} \cdot \text{HO}$): the global minimum, *J. Chem. Phys.* **98**, 8829–8834 (1993).
293. B. Wang, H. Hou, and Y. Gu, Density functional study of the hydrogen bonding: $\text{H}_2\text{O} \cdot \text{HO}$, *Chem. Phys. Lett.* **303**, 96–100 (1999).
294. J. M. Khalack and A. P. Lyubartsev, Solvation structure of hydroxyl radical by Car–Parrinello molecular dynamics, *J. Phys. Chem. A* **109**, 378–386 (2005).
295. M. W. Palascak and G. C. Shields, Accurate experimental values for the free energies of hydration of H^+ , OH^- , and H_3O^+ , *J. Phys. Chem. A* **108**, 3692–3694 (2004).
296. S. Hamad, S. Lago, and J. A. Mejias, A computational study of the hydration of the OH radical, *J. Phys. Chem. A* **106**, 9104–9113 (2002).
297. R. Parthasarathi, V. Subramanian, and N. Sathyamurthy, Structure, stability and solvation shell of H_3O^+ and H_5O_2^+ clusters (results to be published).
298. M. Meot-Ner and C. V. Speller, Filling of solvent shells about ions. 1. Thermochemical criteria and the effects of isomeric clusters, *J. Phys. Chem.* **90**, 6616–6624 (1986).
299. N. Agmon, Mechanism of hydroxide mobility, *Chem. Phys. Lett.* **319**, 247–252 (2000).
300. W. R. Busing and D. F. Hornig, Restrictions on chemical kinetic models, *J. Chem. Phys.* **65**, 284–292 (1961).
301. D. Schiøberg and G. Zundel, Very polarizable hydrogen bonds in solutions of bases having infrared absorption continua, *J. Chem. Soc., Faraday Trans.* **69**, 771–781 (1973).
302. N. B. Librovich, V. P. Sakun, and N. D. Sokolov, H^+ and OH^- ions in aqueous solutions—vibrational spectra of hydrates, *Chem. Phys.* **39**, 351–366 (1979).
303. B. Chen, I. Ivanov, J. M. Park, M. Parrinello, and M. L. Klein, Solvation structure and mobility mechanism of OH^- : a Car–Parrinello molecular dynamics investigation of alkaline solutions, *J. Phys. Chem. B* **106**, 12006–12016 (2002).
304. B. Chen, M. J. Park, I. Ivanov, G. Tabacchi, M. L. Klein, and M. Parrinello, First-principles study of aqueous hydroxide solutions, *J. Am. Chem. Soc.* **124**, 8534–8535 (2002).
305. R. Parthasarathi, V. Subramanian, and N. Sathyamurthy, Electron density analysis on hydroxide ion solvation (results to be published).
306. G. N. Ramachandran, C. Ramakrishnan, and V. Sasisekharan, Stereochemistry of polypeptide chain configurations, *J. Mol. Biol.* **7**, 95–99 (1963).
307. G. N. Ramachandran and V. Sasisekharan, Conformation of Polypeptides and proteins, In: *Advances in protein chemistry*, edited by J. C. B. Anfinsen M. L. Anson, J. T. Edsall, and F. M. Richards, (Academic press, New York, 1968) Vol. 23, pp. 283–438.
308. B. Pullman and A. Pullman, *Advances in Protein Chemistry* (Academic, New York, 1974).
309. T. Head-Gordon, M. Head-Gordon, M. J. Frisch, C. L. Brooks, and J. A. Pople III, Theoretical study of blocked glycine and alanine peptide analogs, *J. Am. Chem. Soc.* **113**, 5989–5997 (1991).
310. K. Moehle, M. Gussmann, A. Rost, R. Cimraglia, and H. -J. Hofmann, Correlation energy, thermal energy, and entropy effects in stabilizing different secondary structures of peptides, *J. Phys. Chem. A* **101**, 8571–8574 (1997).
311. X. Wu and S. Wang, Helix folding of an alanine-based peptide in explicit water, *J. Phys. Chem. B* **105**, 2227–2235 (2001).
312. M. Torrent, D. Mansour, E. P. Day, and K. Morokuma, Quantum chemical study on oxygen-17 and nitrogen-14 nuclear quadrupole coupling parameters of peptide bonds in alpha-helix and beta-sheet proteins, *J. Phys. Chem. A*, **105**, 4546–4557 (2001).
313. C. Aleman, On the Ability of modified peptide links to form hydrogen bonds, *J. Phys. Chem. A* **105**, 6717–6723 (2001).
314. R. Wiczorek and J. J. Dannenberg, Hydrogen-bond cooperativity, vibrational coupling, and dependence of helix stability on changes in amino acid sequence in small 3_{10} -helical peptides. A density functional theory study, *J. Am. Chem. Soc.* **125**, 14065–14071 (2003).

315. Y. D. Wu and Y. L. A. Zhao, Theoretical study on the origin of cooperativity in the formation of 3_{10} - and α -helices, *J. Am. Chem. Soc.* **123**, 5313–5319 (2001).
316. S. Jang, S. Shin, and Y. Pak, Molecular dynamics study of peptides in implicit water: ab initio folding of β -hairpin, β -sheet, and $\beta\beta\alpha$ -motif, *J. Am. Chem. Soc.* **124**, 4976–4977 (2002).
317. R. Wiczorek and J. J. Dannenberg, H-bonding cooperativity and energetics of α -helix formation of five 17-amino acid peptides, *J. Am. Chem. Soc.* **125**, 8124–8129 (2003).
318. A. V. Morozov, T. Kortemme, and D. Baker, Evaluation of models of electrostatic interactions in proteins, *J. Phys. Chem. B* **107**, 2075–2090 (2003).
319. S. Gnanakaran and A. E. Garcia, Validation of an all-atom protein force field: from dipeptides to larger peptides, *J. Phys. Chem. B* **107**, 12555–12557 (2003).
320. D. Liu, T. Wytttenbach, P. E. Barran, and M. T. Bowers, Sequential hydration of small protonated peptides, *J. Am. Chem. Soc.* **125**, 8458–8464 (2003).
321. P. Bour and T. A. Keiderling, Structure, spectra and the effects of twisting of β -sheet peptides. A density functional theory study, *J. Mol. Struct. (Theochem)* **675**, 95–105 (2004).
322. R. Wiczorek and J. J. Dannenberg, Comparison of fully optimized α - and 3_{10} -helices with extended β -strands. An ONIOM density functional theory study, *J. Am. Chem. Soc.* **126**, 14198–14205 (2004).
323. C. Chang and R. F. W. Bader, Theoretical construction of a polypeptide, *J. Phys. Chem.* **96**, 1654–1662 (1992).
324. P. L. A. Popelier and R. F. W. Bader, Effect of twisting a polypeptide on its geometry and electron distribution, *J. Phys. Chem.* **98**, 4473–4481 (1994).
325. R. Parthasarathi and V. Subramanian, Bader's electron density analysis on secondary structures of protein (results to be published).
326. G. Gilli and P. Gilli, Towards an unified hydrogen-bond theory, *J. Mol. Struct.* **552**, 1–15 (2000).
327. R. Parthasarathi, V. Subramanian, and N. Sathyamurthy, Hydrogen Bonding without Borders: An Atoms-in-Molecules Perspective. *J. Phys. Chem. A* **110**, 3349–3351 (2006).
328. M. J. Frisch, G. W. Trucks, H. B. Schlegel, G. E. Scuseria, M. A. Robb, J. R. Cheeseman, V. G. Zakrzewski, J. A. Montgomery Jr., R. E. Stratmann, J. C. Burant, S. Dapprich, J. M. Millam, A. D. Daniels, K. N. Kudin, M. C. Strain, O. Farkas, J. Tomasi, V. Barone, M. Cossi, R. Cammi, B. Mennucci, C. Pomelli, C. Adamo, S. Clifford, J. Ochterski, G. A. Petersson, P. Y. Ayala, Q. Cui, K. Morokuma, D. K. Malick, A. D. Rabuck, K. Raghavachari, J. B. Foresman, J. Cioslowski, J. V. Ortiz, B. B. Stefanov, G. Liu, A. Liashenko, P. Piskorz, I. Komaromi, R. Gomperts, R. L. Martin, D. J. Fox, T. Keith, M. A. Al-Laham, C. Y. Peng, A. Nanayakkara, C. Gonzalez, M. Challacombe, P. M. W. Gill, B. G. Johnson, W. Chen, M. W. Wong, J. L. Andres, M. Head-Gordon, E. S. Replogle, and J. A. Pople, Gaussian 98, revision A.7 (Gaussian Inc., Pittsburgh, PA, 1998).
329. F. Biegler-Konig, J. Schonbohm, R. Derdau, D. Bayles, and R. F. W. Bader, AIM 2000, Version 1 (Bielefeld, Germany, 2000).

CHAPTER 2

INTRAMOLECULAR HYDROGEN BONDS. METHODOLOGIES AND STRATEGIES FOR THEIR STRENGTH EVALUATION

GIUSEPPE BUEMI

Dipartimento di Scienze Chimiche, Università di Catania, Viale Andrea Doria nr.6 I-95125 Catania, Italy. E-mail: gbuemi@dipchi.unict.it

Abstract The classification of the various types of hydrogen bonds as well as the strategies and the theoretical methods for calculating their energies are presented. The main attention is devoted to the homo- and heteronuclear conventional intramolecular hydrogen bonds involving oxygen, nitrogen, sulphur and halogens, for which a survey on the literature results is depicted. The anharmonicity effect on the O–H stretching mode frequency and the dependence of the hydrogen bond strength estimates on the basis set extension are also briefly discussed.

Keywords: Hydrogen bond; calculation methods; calculation strategies; basis set effect; anharmonicity.

1 INTRODUCTION

Nowadays to write a chemical formula as H-H by joining together the atomic symbols with a hyphen between them is an instinctive gesture and the concept of “chemical bond” is nearly as natural as to breathe. But behind this state of art there is the hard work of numerous researchers who laid the foundations for the modern chemistry. It is therefore right, before undertaking a discussion on hydrogen bonding, to remember, among others, Jöns Jacob Berzelius, who introduced the symbols of the chemical elements [1] together with Archibald Scott Couper [2] and August Kekulé von Stradonitz [3], who, independently from each other but in parallel, recognized that carbon atoms can link directly to one another to form carbon chains, and indicated the whole of strengths constituting the glue between the two atoms by means of straight lines linking the symbols of the elements. It is well known that chemical bonds can be ionic or covalent, single, double or triple, and each of them is characterized by a

bond length, whose entity ranges from about 1.2 to about 1.55 Å. The hydrogen bond is conceptually different because at least three atoms are involved but it is extremely important for understanding many chemical properties. Usually, three dots are used for indicating the hydrogen bridges and Huggins in 1937 was among the earliest to use this notation [4, 5].

1.1 Description and Classification of Hydrogen Bonds

More than 80 years have lapsed from the far 1920, when the concept of “hydrogen bond” was born [6–9]. During this long period innumerable papers and books have been written on this subject, since the hydrogen bond is of capital importance in all fields of chemistry and biochemistry owing that it governs conformational equilibria, chemical reactions, supramolecular structures, life processes, molecular assemblies and so on [10–21]. But, as Huggins wrote, ‘*it is also of great importance in physics, crystallography, mineralogy, geology, meteorology, and various other -ologies*’ [22].

The hydrogen bond is weaker than a common chemical bond, and can be encountered in solid, liquid and gas phases. It is commonly represented as $X-H \cdots Y$, where X and Y are atoms having electronegativity higher than that of hydrogen (e.g., O, N, F, Cl, S). The X–H group is termed “electron acceptor” or “hydrogen bond donor”, whilst Y is the “electron donor” or “hydrogen bond acceptor”. The electronegative X atom attracts electrons from the electron cloud of the hydrogen atom which remains partially positively charged and, in turn, attracts a lone pair of electron of the Y atom. So it is generally said that the hydrogen bond is due to attractive forces between partial electric charges having opposite polarity. Indeed, it is true that weak hydrogen bonds are mainly electrostatic in nature, but this is no longer true for strong hydrogen bonds, where delocalization effects and dispersion forces play a very important role.

The hydrogen bond donor and the hydrogen bond acceptor can belong to the same molecule or to two different molecules: the former case is known as “intramolecular hydrogen bond” (Fig. 1), the latter as “intermolecular hydrogen bond” (Fig. 2). Obviously, the intramolecular hydrogen bond is necessarily a bent bond whereas the intermolecular one is generally linear or nearly linear.

A typical effect due to the intermolecular hydrogen bonds is the increase of the alcohol boiling points with respect to those of other compounds having analogous molecular weight. The higher strength of the intermolecular hydrogen bond involving the OH group with respect to those involving the SH one is responsible for the higher boiling point of water with respect to that of hydrogen sulphide. The decrease in density of water upon freezing is also a hydrogen bond consequence since the crystalline lattice of ice is a regular array of H-bonded water molecules spaced farther apart than in liquid phase. To be not forgotten also the capital role that weak hydrogen bonds play in the medicine field, being responsible of the association between proteins and a

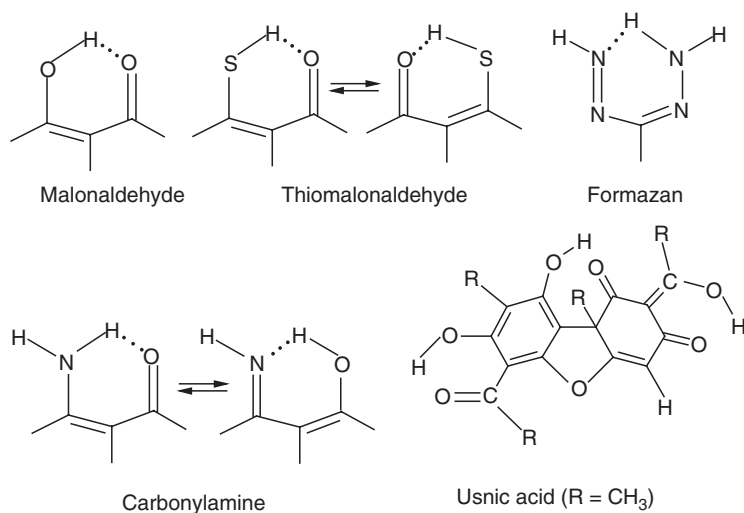


Figure 1. Some molecules exhibiting intramolecular hydrogen bonds.

great variety of molecules having anaesthetic power, as halothane, ethrane, isoflurane, fluorane, etc [23–25]. Also the human hair shape (curly hair, wavy hair, straight hair, etc.) depends on the hydrogen bonds involving the SH groups of cysteine ($\text{HO}-\text{CO}-\text{CH}(\text{NH}_2)-\text{CH}_2-\text{SH}$) which is a component of alpha-keratin.

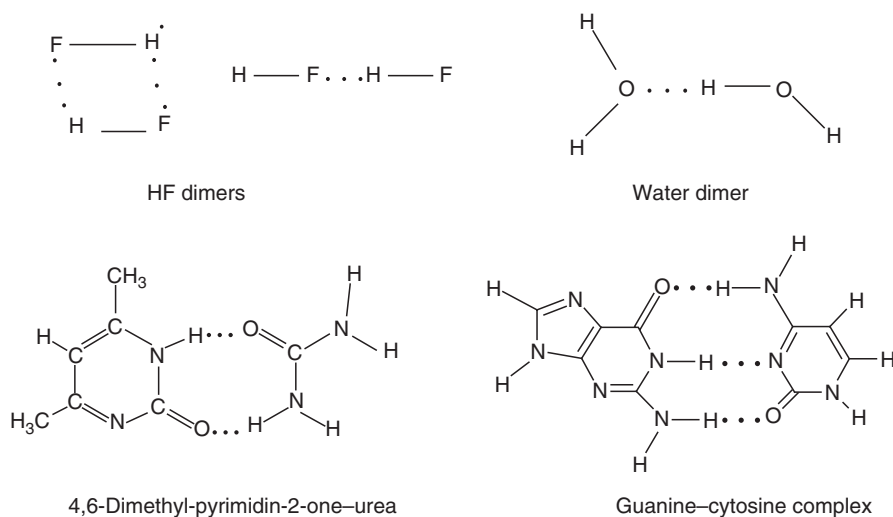


Figure 2. Some molecules exhibiting intermolecular hydrogen bonds.

More than one hydrogen bond can be formed at once. For example, the adduct between 4,6-dimethyl-pyrimidin-2-one and urea derives its stability from two, intermolecular, non-equivalent N–H···O(=C) bridges [26, 27], and the physical properties of usnic acid are strongly affected by its three intramolecular hydrogen bridges located in three different molecular areas and having different strengths [28, 29].

Malonaldehyde (propanedial or β -hydroxypropenal or β -hydroxy-acrolein) is the smallest molecule exhibiting a strong intramolecular hydrogen bond, which allows to close a hexatomic ring (chelate ring). Here the hydrogen-bonded atoms are connected through a conjugated framework which allows a charge flow from hydrogen to the oxygen atom, so enhancing the hydrogen bridge strength. Such bridges are known also as resonance-assisted hydrogen bonds (RAHB) [30, 31] and will be discussed later in the following.

Beyond these “classical” or “conventional” hydrogen bonds, “unconventional” or “non-conventional” interactions are also possible [32] (some examples are shown in Fig. 3).

The hydrogen bond between the C–H group with oxygen was first proposed by Sutor in the early 1960s [33, 34] and looked in disbelief by the scientific community, even if indications that the C–H group could be involved in hydrogen bond go back to the far 1930s [35, 36]. Researches over the years have evidenced the existence of numerous new types of interactions. In 1995 the concept of “dihydrogen bond” was introduced [37] in order to explain certain

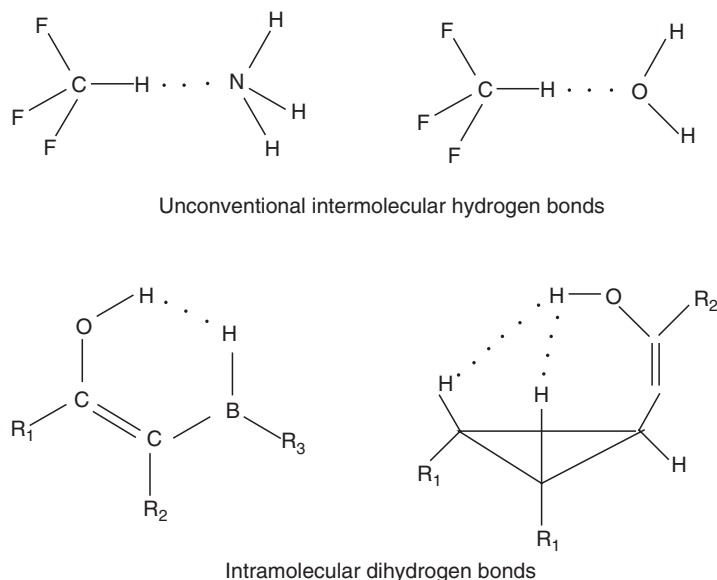


Figure 3. Examples of inter- and intramolecular non-conventional hydrogen bonds.

interactions where a H atom, positively charged, is directly donated to another H atom, negatively charged ($X-H \cdots H-Y$), which occur in systems containing boron or transition metals [38–43]. A typical, widely studied, case is the BH_3NH_3 dimer complex, which contains two dihydrogen bonds differing in strength (bent $B-H \cdots H$ and linear $N-H \cdots H$ arrangements) [44–47]. In 1998, Hobza and Špirko [48] suggested the existence of a new type of interaction identified in benzene dimers and other benzene complexes. It was termed “anti-hydrogen bond” and, later, “blue shifting hydrogen bond”, because, in contrast with classical hydrogen bridges, it is characterized by a C–H bond shortening and a blue shifting of the C–H stretching frequency, as confirmed experimentally too. [49, 50] In absence of experimental data, it is a hard task to distinguish between blue shift and red shift because it has been noted that contrasting results can be obtained from B3LYP and MP2 calculations [51].

The labels “non-conventional” and/or “improper” derive just from the nature of the hydrogen bond donor and hydrogen bond acceptor groups, which are different from those involved in the classical hydrogen bridges. Some examples are given in Fig. 3. On this ground, several classes of non-conventional hydrogen bridges can be distinguished: those in which a non-conventional donor is involved (e.g., the C–H group) [52–54]; those having a non-conventional acceptor, as a C atom or a π -system [55–57]; those in which both the donor and acceptor are non-conventional groups [58–60]; the dihydrogen bonds, formed between a protic X–H group and a hydridic H–Y group, in which the interaction occurs between two H atoms, one of which accepts electrons and the other provides them: $X^{\delta-} - H^{\delta+} \cdots H^{\delta-} - Y^{\delta+}$ [61–64]. To these ones the “inverse” hydrogen bonds can be added, formed by X–H groups with reverse polarity ($X^{\delta+} - H^{\delta-}$), where a H atom will provide electrons and another non-hydrogen atom will accept them (e.g., $Li-H \cdots Li-H$, $H-Be-H \cdots Li-H$) [32, 65, 66].

New types of bridges are continually proposed, as, e.g., the $\pi \cdots H^+ \cdots \pi$ interactions [67] and monoelectron dihydrogen bond, $H \cdots e \cdots H$ [68–71]. This latter (for which hydrogen bond energies ranging from 1.758 to 3.122 kcal/mol have been calculated in the $H_3C \cdots HF$ complex [71]) has been found in water cluster complexes with Li and Na, in HF complexes with the methyl radical and in various HF cluster anions. According to theoretical predictions, the hydrogen fluoride trimer anion $(FH)_2\{e\} \cdots (HF)$ exhibits also exceptionally large static first hyperpolarizability, [72] analogously to what occurs in the water trimer anion [73].

Nowadays the non-conventional hydrogen bridges are the subjects of a fascinating research field and the related papers in the literature are as many numerous as those concerning the classical ones, thus the references here cited are only an extremely small part of the literature and the most recent published papers are preferably reported. However, we must beware of vision of improper hydrogen bonds everywhere a H atom is a little closer to another atom and, in this regard, careful verifications must be done to avoid to get the wrong end of

the stick. A good suggestion to unravel oneself in the modern hydrogen bond jungle is to follow the rules proposed by Bader on the ground of the atoms in molecules (AIM) theory (Refs. 74–79 and therein), which is an extension of quantum mechanics properly defining an atom as an open system [76].

1.2 The AIM Rules for Hydrogen Bonds Recognition

The theory of AIM offers a self-consistent way to partition any system in its atomic fragments and to extract chemical informations, hidden in the wave function Ψ , from the electron density ρ and its gradient vector $\nabla\rho$. Neglecting mathematical details, for which the inquisitive reader is remanded to the cited original papers, it suffices to know that a sequence of infinitesimal gradient vectors traces a “gradient path”, whose starting point can be infinity or some special point in the molecule. Typically they are attracted to a point in space, called an “attractor”. All nuclei are attractors in the gradient vector field of the density and the collection of gradient paths each nucleus attracts is called an “atomic basin”. A point in space where $\nabla\rho$ vanishes is called “critical point” (CP). Some gradient paths do not start from infinity but from a special point appearing somewhere in between two nuclei and are termed “bond critical point” (BCP). It is characterized by one positive and two negative curvatures of ρ . Two gradient paths, each starting at the bond critical point and terminating at a nucleus, are called “atomic interaction line” (AIL). If all forces on all the nuclei vanish, the atomic interaction line becomes a “bond path” (BP): this is a line linking two bonded nuclei and allows to define a “bond”. A collection of bond paths is called a “molecular graph”, which is a representation of the bonding interactions. The topological analysis and evaluation properties can be performed by using the MORPHY [80] and PROAIM [81] programs.

By analysing patterns in the topology and values of ρ and its Laplacian, $\nabla^2\rho$, at the bond critical points, the following rules to ascertain the presence or not of a hydrogen bond have been deduced [79]:

- (a) a BCP proving the existence of a hydrogen bond must be topologically found;
- (b) at the BCP points the charge density (ρ) should be small and the Laplacian of the charge density ($\nabla^2\rho$) should be positive;
- (c) the hydrogen (H) and the acceptor (B) atoms must penetrate each other.
- (d) The hydrogen atom loses electrons, i.e., its population decreases; the phenomenon can be related to the descreening of the hydrogen-bonded protons as observed in the NMR chemical shifts;
- (e) the hydrogen atom must be destabilized in the complex, this destabilization, $\Delta E(\text{H})$, is the difference in total atomic energy between the hydrogen in the hydrogen-bonded complex and in the monomer;
- (f) the dipolar polarization of H must decrease upon formation of the hydrogen bond;
- (g) the volume of H should decrease upon complex formation.

The penetration quantification needs the knowledge of the non-bonding radii of the H and of the acceptor atom (r_{H}^0 and r_{B}^0 , which are the distances from the respective nuclei to a given ρ contour in each monomer) and the bonding radii (r_{H} and r_{B} , which are the distances between the respective nuclei and the hydrogen bond BCP). The penetrations of H and B (Δr_{H} and Δr_{B}) are defined as

$$\Delta r_{\text{H}} = r_{\text{H}}^0 - r_{\text{H}} \quad \text{and} \quad \Delta r_{\text{B}} = r_{\text{B}}^0 - r_{\text{B}}$$

The application of the penetration rule is hampered for intramolecular hydrogen bonds because the reference hydrogen given by the monomer is lacking, however, if a fragment of the molecule can be isolated (via cutting and capping) and used as a monomer-like reference, the criteria can be successfully applied.

1.3 Experimental Evidences of Hydrogen Bond Presence

From the experimental point of view, the existence of a hydrogen bridge can be easily recognized by some peculiar changes in the molecular geometry and in some chemical–physical properties. In particular:

- (a) The X–H bond length becomes longer than the common X–H bonds, whereas the X···Y and H···Y distances are shorter than the sum of the van der Waals radii of the X, Y and H atoms involved in the hydrogen bridge.
- (b) The X–H···Y angle is mostly in the range 140–150° for hexatomic chelate rings and in the range 115–130° for the pentatomic ones.
- (c) In presence of a conventional hydrogen bridge, the frequencies of the XH (and C=O) stretching mode vibration are red-shifted with respect to the corresponding values recorded in a hydrogen bond free compound. The entity of the shift is strictly related to the strength of the hydrogen bridge. On the contrary, in presence of a non-conventional hydrogen bond a shortening of the X–H bond length and a blue shift of its vibration frequency are observed.
- (d) Proton experiencing hydrogen bond undergoes deshielding, which, in turn, causes a downfield of its chemical shift. For many compounds, it has been found that deshielding increases linearly with $r_{\text{O}\cdots\text{O}}$ decreasing whilst the potential function changes from a double to a single minimum well. Very useful correlations between the experimental (and/or theoretical) hydrogen bond distances or hydrogen bond strength and NMR chemical shifts have been also found [82–90].

2 CALCULATION OF THE MOLECULAR ENERGY: SEMIEMPIRICAL AND AB INITIO METHODS

For evaluating the hydrogen bond strength it is necessary to calculate the energy of the molecule under study, which implies also the optimization of the molecular geometry. Consequently, the first step of the study is the choice

of the most suitable method for the energy evaluation, which, in turn, is conditioned by the available computational resources (computer power, hard disk capacity, RAM dimension, and so on), on the dimension (number of atoms) of the molecule to be handled and on the required level of calculations. Even if description of mathematical development of the various approaches is out of the aim of the present review, we think that a brief background is useful for understanding the quality of the results.

In quantum chemistry, the calculation of the energy of a molecule implies the solution of the well-known Schrödinger equation

$$(1) \quad \hat{H}\Psi = E\Psi$$

where \hat{H} is the Hamiltonian operator and Ψ is the wave function obeying to the restrictions required by the quantum mechanics postulates. The operator \hat{H} is the sum of the kinetic (T) and potential (V) energies; therefore it represents the total energy of the system. Remembering that the kinetic energy can be written as a function of the moment and that the quantum mechanical momentum operator is $-i\hbar(\partial/\partial q_i)$, the Hamiltonian for a single-particle three-dimensional system in cartesian coordinates is

$$(2) \quad \hat{H} = T + V = -\frac{\hbar^2}{8\pi^2m} \left(\frac{\partial^2}{\partial x^2} + \frac{\partial^2}{\partial y^2} + \frac{\partial^2}{\partial z^2} \right) + V(x, y, z)$$

\hbar being the Plank constant and m the mass of the particle. The differential operator in parentheses in Eq. 2 is the Laplacian operator ∇^2 , so that Eq. 1 can be simply written as

$$(3) \quad -\frac{\hbar^2}{8\pi^2m} \nabla^2\Psi + V(x, y, z)\Psi = E\Psi$$

For n -particles three-dimensional system, Eq. 3, becomes

$$(4) \quad -\sum_{i=1}^n \frac{\hbar^2}{8\pi^2m_i} \nabla^2\Psi + V(x_1, y_1, z_1, \dots, x_n, y_n, z_n)\Psi = E\Psi$$

The above equation is the time-independent Schrödinger equation for the considered system, which, therefore, is implicitly a conservative system. The above equation cannot be analytically solved and only approximate solutions are possible.

Following the Hartree–Fock method and the iterative SCF (self-consistent field) approach, very good Ψ can be obtained. This Ψ is the product of mono-electronic functions (which take into account also the spin coordinate and are named spin-orbitals) each describing the electron motion under the effect of a coulombian field generated by the nuclei and by the other $n - 1$ electrons. The variation theorem ensures that the energy associate with the approximated ground state wave function is always greater than, or at the most equal to, the exact energy value. Ab initio methods are based on the procedure in summary described, which implies the calculation of innumerable integrals

and made impossible its application even to systems having modest number of atoms without computer's help.

To bypass this problem in the past years, when computers were not available or their performances were inadequate, numerous and very approximate methods were developed for studying the various molecular properties. Such methods were improved over the years keeping pace with the development of the computer engineering science progress and today a simple personal computer is also able to perform high level ab initio calculations. The calculation methods can be therefore grouped into two main classes termed "semiempirical" (for some reviews on the earlier methods, see [91, 92]) and "ab initio". The well-known Huckel [93–95], Extended Huckel [96], CNDO [97], INDO [98], NDDO [97], NNDO [99], PCILO [100, 101], MM4 and its previous versions (Refs. 102, 103 and therein cited), ECEPP [104], MINDO [105], MNDO and MNDOC (Modified Neglect of Diatomic Overlap) [106–108], AM1 (Austin Model One) [109], PM3 and PM5 (MNDO Parameterization 3 or 5) [110–112] belong to the former class (for a review describing the parallel progress of theoretical methods and computers development, see Ref. 113). The label, "semiempirical" means that these methods use some parameters derived from experimental data to simplify calculations. They are very quick and require only small disk space, but not all the molecular properties can be predicted in a satisfactory way. For example, CNDO (Complete Neglect of Differential Overlap) computes very good charge densities and dipole moments, whereas INDO (Intermediate Neglect of Differential Overlap) was mainly used in its spectroscopic version (INDO/S) for predicting the electronic transition energies. MINDO and MNDO, in their standard versions, give acceptable thermochemical predictions but are not able to predict rotation barriers. AM1 and PM3 are improvements of MNDO; they are also able to describe hydrogen-bonded systems but the resulting hydrogen bond energies (E_{HBS}) are generally underestimated. Modified MNDO versions, explicitly devoted to improve hydrogen bond predictions, were also published (MNDO/H) [114, 115] but with scarce or contrasting success [116–120]. On the other hand, semiempirical approaches are very useful when one must handle very big molecules, as protein systems (the most recent AM1, PM3 and PM5 versions [121] are able to handle more than 90,000 of atoms).

The ab initio methods use no experimental parameters in their computations but are much more onerous than the semiempirical ones, both for time consuming and for hard disk capacity requirements. The onerousness increases on increasing the molecular dimensions and the level of sophistication, i.e., the extension of the basis set adopted for calculations. Among the most used ab initio computation packages, we remember here the GAUSSIAN 03 [122], GAMESS [123] and SPARTAN [124].

The basis set is needed for a mathematical description of the orbitals within a system and a good basis set is necessary to obtain a good energy quality. The orbitals are built up through linear combination of gaussian functions, which are

referred as “primitives” and their numbers appear in the basis set name. So, the minimal STO-3G basis set approximates Slater orbitals (STO = Slater Type Orbitals) by employing three gaussian primitives for each basis function. A split valence basis set increases the number of basis functions per atom, so that a change of the orbital size (but not its shape) is possible. The so-called polarized basis sets add d functions to C and f functions to transition metals: they are indicated with an asterisk (e.g., 6-31G* or also as 6-31G(d)). The presence of a second asterisk indicates that p functions are added to the H atom (e.g., 6-31G** or also as 6-31G(d,p)). To allow orbital expansion for occupying a large region of space, diffuse function can be added to the basis set. They are important for improving the description of electrons which are far from the nucleus and their presence is indicated with a “+”. A double plus means that diffuse functions are also added to H (e.g., 6-31+G(d) or 6-31++(G(d))). Since the Hartree–Fock SCF wave function takes into account the interaction between electrons in an average way whilst the motion of electrons is correlated with each other, the resulting energy is in error. It must be corrected by adding a term named “correlation energy”, which can be calculated by various approaches.

Nowadays basis sets less extended than the 6-31G one are no longer used for medium size systems, but in the basis set choice the memory resources of the available computers are essential. In particular, the calculation of correlation energy at MP2 level (second order Møller–Plesset perturbation theory [125]) requires time and noticeable hard disk capacity, but, alternatively, very good results can be obtained with modest computer performances by using functionals (many people use the B3LYP [126–128] one) following the Density Functional Theory (DFT). Very recently, the X3LYP functional has been developed [129, 130], which is an extended hybrid functional combined with the Lee–Yang–Parr correlation functional.

Even if basis set descriptions are easily available on all the user manuals accompanying ab initio computation package, we will give here some short news on the most used bases:

- (a) the 6-31G**, which includes polarization functions, and 6-311++G(d,p) (Ref. 131 and therein), which include polarization and diffuse functions;
- (b) the cc-pVDZ (double zeta) and the cc-pVTZ (triple zeta) Dunning’s correlated consistent basis set [132–134], which can be augmented with diffuse function inclusion (aug-cc-pVDZ, aug-cc-pVTZ); quadruple, quintuple and sextuple zeta are available too, but are too onerous and, in our opinion, not advisable for very limited energy improvement.

High-level calculations can be performed by means of the G2 (Ref. 135 and therein), G2(MP2) (Ref. 136 and therein), G3 [137–139], G3MP2 and G3MP3 [140, 141] G3B3 and G3MP2B3 [142] methods of Pople and coworkers, as well as the complete basis set CBS-APNO [143], CBS-Q (Ref. 144 and therein) and CBS-QB3 of Montgomery, Peterson et al [145]. All of them compute the energy of a molecular system through multi-steps internal predefined calculations in order to improve the energy accuracy and to reduce, as far as possible, the

mean absolute deviation from a set of more of a hundred of experimental energies (dissociation energies, ionization potentials, etc.). The G2 energy, based on the MP2(FULL)/6-31G* geometry (all electrons are considered, MP2=FULL), is given by

$$E = E[\text{MP4}/6\text{-}311\text{G}(\text{d},\text{p})] + \Delta E(+) + \Delta E(2\text{df}) + \Delta + \Delta E(\text{QCI}) + \text{HLC} + \text{ZPE}$$

where

- (a) $\Delta E(+)$, $\Delta E(2\text{df})$ and Δ are corrections arising from the use of limited basis sets;
- (b) $\Delta E(\text{QCI})$ is the correlation energy contribution calculated at the fourth order Møller–Plesset perturbation theory [125] and quadratic configuration interaction (QCI [146, 147]) including single and double substitutions (QCISD)

$$\Delta E(\text{QCI}) = E[\text{QCISD}(\text{T})/6\text{-}311\text{G}(\text{d},\text{p})] - E[\text{MP4}/6\text{-}311\text{G}(\text{d},\text{p})]$$

- (c) HLC (high level correction) = $-An_\alpha - Bn_\beta$ ($A = 4.81$ mh, $B = 0.19$ mh), n_α and n_β being the number of alpha and beta valence electrons, respectively;
- (d) ZPE is the zero point correction energy calculated by scaling by 0.8930 the vibration frequencies resulting from 6-31G(d) basis set.

The G2(MP2) [136] is a modification of G2 approach [135] which entails significant savings in computing expenses and memory resources maintaining high level results. It reduces the calculation of $\Delta E(+)$, $\Delta E(2\text{df})$ and Δ to a single step and uses MP2 instead of MP4, so that the G2(MP2) energy is

$$E = E[\text{QCISD}(\text{T})/6\text{-}311\text{G}(\text{d},\text{p})] + \text{ZPE} + \text{HLC} + \Delta_{\text{MP2}}$$

being

$$\Delta_{\text{MP2}} = E[\text{MP2}/6\text{-}311 + \text{G}(3\text{df},2\text{p})] - E[\text{MP2}/6\text{-}311\text{G}(\text{d},\text{p})]$$

The CBS-Q method is based on the same philosophy of G2 and requires the following calculations [144]:

- (a) UHF/6-31G⁺ geometry optimization and frequencies;
- (b) MP2(FC)/ 6-31G⁺ optimized geometry;
- (c) UMP2/6-311+G(3d2f,2df,2p) energy and CBS extrapolation;
- (d) MP4(SDQ)/6-31+G(d(f)p) energy;
- (e) QCISD(T)/6-31+ G⁺ energy.

The 6-31G⁺ basis is a modification of the 6-31G* one obtained through combination of the 6-31G sp functions with the 6-31G** polarization exponents. The CBS-Q total energy is given by

$$E(\text{CBSQ}) = E(\text{UMP2}) + \Delta E(\text{CBS}) + \Delta E(\text{MP4}) + \Delta E(\text{QCI}) + \Delta E(\text{ZPE}) + \Delta E(\text{emp}) + \Delta E(\text{spin})$$

where $\Delta E(\text{CBS})$ is obtained from the CBS extrapolation (Ref. 148 and therein)

$$\Delta E(\text{MP4}) = E[\text{MP4}(\text{SDQ})/6\text{-}31 + \text{G}(\text{d}(\text{f})\text{p})] - E[\text{MP2}/6\text{-}31 + \text{G}(\text{d}(\text{f})\text{p})]$$

and

$$\Delta E(\text{QCI}) = E[\text{QCISD}(\text{T})/6\text{-}31 + \text{G}^+]$$

$\Delta E(\text{emp})$ and $\Delta E(\text{spin})$ are an empirical correction and the spin contamination correction terms, respectively, whose detailed calculation is given in Ref. 145.

The CBS-QB3 is a modification of the CBS-Q method, in which steps (b) and (c) are replaced with a B3LYP/6-31G⁺ geometry optimization, following the DFT.

G3 is an evolution of G2 theory, in which the following main changes were made:

- (a) the 6-311G(d) basis set used as starting point for the MP4 and QCISD(T) single point calculations is substituted with the 6-31G(d) basis;
- (b) the 6-311+G(3df,2p) basis used in G2 at MP2 level was modified to include more polarization functions for the second row (3d2f), less on the first row (2df), and other changes to improve uniformity. This basis is termed G3 large (for more details see Ref. 137).

A variance of G3 is the G3S method [149], which replaces the additive HLC of G3 theory by a multiplicative scaling of the correlation and Hartree-Fock parts of the G3 energy. The best results of these methods give errors within 1 kcal/mol with respect to the experimental reference data. A comparison of their performances is given in Refs. 150, 151.

3 DEFINITION AND EVALUATION OF THE HYDROGEN BOND STRENGTH

3.1 Intermolecular Hydrogen Bonds

The hydrogen bond energy, E_{HB} , is not physically observable and therefore it is not directly measurable. It is possible, however, to obtain theoretical estimates provided that a zero point in the energy scale is defined. In the case of *intermolecular* hydrogen bond, E_{HB} is the difference between the energy of the adduct and the sum of the energies of the separate component molecules. Unfortunately, the adduct contains more orbitals than each monomer and this produces an artificial lowering of its energy with respect to those of the isolated molecules. This occurrence is known as *Basis Set Superposition Error* (BSSE), whose entity depends on the extension of the basis set adopted for calculations and could not be negligible if the basis set extension is modest. Various techniques have been suggested to minimize this error, but date the most used approach is the a posteriori counterpoise correction scheme (CP) suggested by Boys and Bernardi [152].

Another method for BSSE elimination is the Chemical Hamiltonian Approach (CHA) formulated in 1983 by Mayer, whose basis idea is the a priori exclusion of BSSE (Ref. 153 and therein cited) and in which every

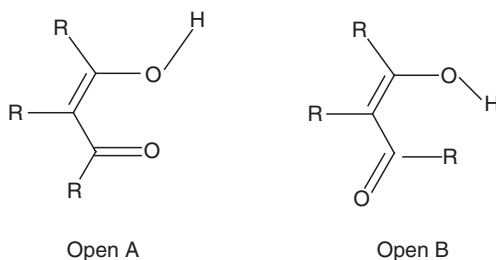
atom is treated as an independent subunit. In other words, the method allows to identify and to omit those terms of the Hamiltonian, which cause the BSSE effect. Since the method was found not appropriate for describing strong interactions, it was successively improved [154, 155]. Despite the different approaches, the a priori BSSE-free CHA method usually gives results similar to those obtainable by the a posteriori CP BSSE correction scheme.

3.2 Intramolecular Hydrogen Bonds

The strength of an *intramolecular* hydrogen bond is generally defined as the stability difference between the *chelate* and *open* conformations, this latter being assumed as hydrogen bond free. Here BSSE is absent, even if according to Jensen, a “basis set effect”, which can be considered as an intramolecular BSSE “is always present when comparing energies of two different systems. As the functions follow the nuclei, the basis set is different for each geometrical configuration. This effect is small and is almost always ignored” [156].

A recent paper suggests the use of Extremely Localized Molecular Orbitals (ELMO) to prevent BSSE instead of correcting the energies [157]. We do not believe that the basis set effect is important in the intramolecular E_{HB} estimate, especially if extended basis sets are used.

Two types of reference open conformations are possible, depending on if the OH (open A) or the C=O (open B) groups are rotated by 180° . It is implicit in this definition that the open conformation is assumed as the origin (zero point) of the E_{HB} scale and the resulting energies will be different, depending on if the former or the latter reference conformation is adopted. Some considerations are, however, to be made for well understanding the meaning and the reliability of the numbers that will go to handle.



- (a) The difference between the energies of the chelate and open conformations includes terms that are bound to different geometrical parameters in the two cases (e.g., in malonaldehyde, at B3LYP/6-311++G(d,p) level, the COH and CCC angles are about 103° and 130° in the chelate and about 109° and 125° in the open forms, respectively).
- (b) The intramolecular hydrogen-bonded molecules are generally planar because the hydrogen bond damps the strain present in the chelate ring. In their open form this strain is no longer balanced and in some cases the

molecule tends to deviate from planarity (generally remarkable torsion occurs around the C–C bond) as observed in malonamide, nitromalonamide and in 3-*t*-butyl- and 3-phenyl-acetylacetone [158–160].

- (c) The open A conformation is by far the most commonly used zero point reference in the E_{HB} evaluation. It is preferred because it preserves the *cis* configuration of the two C=C bonds present in the chelate structure. In any case it must be remembered that the “open A” form identifies a zero point and the “open B” one another, different, “zero point” in the E_{HB} scale. Comparison between E_{HB} values referring to different (non-homogeneous) scales is meaningless.

The entity of an intramolecular hydrogen bond is affected not only by the electronegativity of the heteroatoms involved in the bridge but also by the size of the chelate ring. So, E_{HB} of a hydrogen bridge closing a six-membered ring is higher than that of a pentatomic ring (e.g., in the *ortho*-halophenols), where the possible conjugation contribution is weaker and the X–H···Y angle narrower (in the range of 120° or less).

3.3 The Zero Point Vibration Energy Correction

All calculation methods furnish energies referring to a single molecule in its ground state, in vacuum and 0°K, neglecting the vibrations occurring in the molecular system. According to quantum mechanic theory, the vibration energy of an oscillator does not vanish in the ground state but it assumes the $0.5h\nu$ value, termed “zero point vibrational energy” (ZPVE). The calculated electronic energy of a molecule having n vibrational degrees of freedom must therefore be corrected by summing the quantity

$$E_{\text{ZPVE}} = \frac{1}{2} \sum_{i=1}^n h\nu_i$$

which can be obtained by performing a post-Hartree–Fock frequencies calculation after the geometry optimization process. A thermochemical analysis, at 1 atmosphere of pressure and 298.15°K (using the principal isotope for each element type), is also carried out in all frequency calculations, but it is possible to change these options by specifying suitable different temperature, pressure and isotopes. It is fundamental, however, that the frequencies are calculated with the same basis set and the same correlation energy procedure adopted for the geometry optimization. So, for example, it is meaningless to add the ZPVE calculated at Hartree–Fock level (HF) to the energy evaluated at MP2 or B3LYP level (and yet similar corrections have been made for acetylacetone [161, 162]).

In our opinion, ZPVE correction is also discommended when a transition state (which often is a first-order saddle point) is handled because the contribution due to the degree of freedom corresponding to the negative frequency is ignored. Now, if the negative frequency is small the error could be small, vice

versa the error is not negligible if the frequency is high. The question is delicate in the case of low barrier hydrogen bonds (LBHB), i.e., in the case of compounds showing hydrogen bridges with very short O \cdots O (or X \cdots Y in general) distances, where the ΔE between the most stable C_S conformation and the symmetric C_{2V} one is very small. For example, in nitromalonamide the symmetric conformation is 5.4 (B3LYP/6-311++G(d,p)) or 4.9 kJ/mol (B3LYP/6-31G**), more stable than the asymmetric one after ZPVE correction, but negative frequencies of -646.8 and -511.5 cm^{-1} (corresponding to a ZPE of 3.87 and 3.06 kJ/mol) are predicted by the two basis sets, respectively [163]. At B3LYP/cc-pVDZ level of theory, the C_S conformation is 0.31 kJ/mol more stable than the C_{2V} one, which, on the contrary, becomes 4.9 kJ/mol more stable than the former after ZPVE correction [164]. In such situation, the discussion on the most stable conformation is a non-sense. Indeed, since E_{HB} is the ΔE between the open and chelate conformations, the cumulative ZPVE correction effect on the hydrogen bond strength is small and limited to few kJ/mol units, whereas it is important for the determination of the barrier to the proton transfer process. This barrier in nitromalonamide, without considering ZPVE correction, amounts to only 1.39 kJ/mol [159] at B3LYP/6-311++G(d,p) level, both in gas and in aqueous solution.

3.4 Semiempirical Relationships

As it previously pointed out, the (“non-observable”) hydrogen bond strength is strictly connected to other observables, as $\Delta\delta$, O–H torsional and vibrational frequencies and O \cdots O distances. Very good correlations of the chemical shifts of ^1H , as well as of ^{17}O and ^{13}C of the carbonyl groups, have been found both for primary and secondary 1,2-disubstituted enamines [86] and for cyclic and acyclic N-aryl enamines [165]. Excellent linear correlations were found between chemical shift tensors and bond distances in solid, too [83]. After fitting 59 full O–H \cdots O hydrogen bond lengths measured in small molecules by high resolution X-ray crystallography, the following empirical equation for obtaining O \cdots O distances (error within ≤ 0.05 Å) from chemical shifts was given (Refs. 166, 167 and therein) ($r_{\text{O}\cdots\text{O}}$ in Å, δ in ppm).

$$r_{\text{O}\cdots\text{O}} = 5.04 - 1.16 \ln \delta + 0.0447\delta$$

In order to correlate the spectroscopic observables to the E_{HB} , several semi-empirical relationships have been suggested in the past years.

Analysis of NMR spectra of some *ortho*-substituted phenol derivatives allowed to draw the following relationship between $\Delta\delta$ and E_{HB} :

$$\Delta\delta = -0.4 \pm 0.2 + E_{\text{HB}}$$

($\Delta\delta$ is relative to phenol in part per million, E_{HB} in kcal/mol) proposed in 1975 [168]. According to the theory of Altman et al. [169, 170], the difference of

chemical shift of the hydrogen-bonded protons and deuterons in the ^1H - and ^2H -NMR spectrum, $\Delta[\delta(^1\text{H}) - \delta(^2\text{H})]$, is bound to the category of hydrogen bond. The hydrogen bridge will be weak if $\Delta[\delta(^1\text{H}) - \delta(^2\text{H})]$ is near zero, whilst negative and positive values correspond to strong and very strong hydrogen bonds, respectively. Some literature data (Tetramethylsilane reference) [171], mainly concerning β -diketone derivatives, are collected in Table 1.

A good linear correlation exists between the OH stretching mode frequency and the $\text{O}\cdots\text{O}$ distance for the weak hydrogen bonds ($r_{\text{O}\cdots\text{O}}$ range 2.9–3.4 Å), which deviates from linearity for strong and very strong hydrogen bonds [172].

Several equations for fitting the curves obtained by plotting a graph of ν_{OH} versus $r_{\text{O}\cdots\text{O}}$ (showing exponential shape) and, in turn, the energy corresponding to each frequency were also developed. Among these we remember the Lippincott–Schroeder [173, 174], the Reid [175] and the Bellamy–Owen [176] potential energy functions.

The Lippincott–Schroeder relationship, at first deduced for the linear $\text{O}-\text{H}\cdots\text{O}$ bridge, describes the hydrogen bond in terms of a covalent resonance system involving the $\text{X}^-\text{H}-\text{Y}^+$ and $\text{X}-\text{H}:\text{Y}$ structures. Later it was extended to other homo- ($\text{S}-\text{H}\cdots\text{S}$, $\text{N}-\text{H}\cdots\text{N}$) and heteronuclear ($\text{O}-\text{H}\cdots\text{S}$, $\text{S}-\text{H}\cdots\text{O}$, $\text{N}-\text{H}\cdots\text{O}$, $\text{O}-\text{H}\cdots\text{N}$) bridges [174]. Briefly, the E_{HB} s are calculated as a function of the $\text{X}\cdots\text{Y}$ distance and the $\text{X}-\text{H}\cdots\text{Y}$ angle as

$$E_{\text{HB}} = f[d(\text{X}\cdots\text{Y}), \alpha(\text{X}-\text{H}\cdots\text{Y}), p_i]$$

where p_i is a set of empirical parameters characteristic of the hydrogen bond type. It has been successfully used by Gilli et al. [177–179], who produced also a computational package available on request [180]. However, it has been also pointed out that the Lippincott–Schroeder potential is able to reproduce the shape of the protonic potential in $\text{O}-\text{H}\cdots\text{N}$ systems in gas phase only if some of its parameters are calibrated to fit high level ab initio data [181].

Table 1. Isotope effect on the chemical shifts of some hydrogen-bonded protons (data extracted from Ref. 171)

Compound	$\delta(^1\text{H})$ (ppm)	$\Delta[\delta(^1\text{H}) - \delta(^2\text{H})]$ (ppm)
Malonaldehyde	13.99	+0.42
Acetylacetone (pentane-2,4-dione)	15.58 (Neat)	+0.50
2,4-Phenyl-acetylacetone	17.61 (C_6H_6)	+0.72
	15.52 (CCl_4)	+0.45
3-Methyl-acetylacetone	15.02 (C_6H_{12})	+0.45
Hexafluoro-acetylacetone	13.1 (Neat)	+0.30
3-Propyl-acetylacetone	16.75 (Neat)	+0.66
3-(4-Methoxyphenyl)-acetylacetone	16.65 (Neat)	+0.31
Salicyl aldehyde	11.0 (CH_2Cl_2)	+0.06
	11.03 (CDCl_3)	-0.03

The Reid potential function [175] is derived by the Lippincott–Schroeder one, with the aim of a better description of the O–H···O bonds and takes into account also the OH and O···O stretching motions.

The Bellamy–Owen relationship [176] is based on the calculations of the van der Waals forces by means of a 6–12 Lennard–Jones potential function, which can be written as

$$\varphi(r) = 4\varepsilon_0 \left[\left(\frac{d}{r} \right)^{12} - \left(\frac{d}{r} \right)^6 \right]$$

where ε_0 is the depth of the hole and d is the distance at which the energy vanishes. The d values were firstly based on the collision diameter of molecules in gas phase and subsequently modified to fit the experimental plots. The proposed empirical correlation to the frequency shift of the donor stretching mode is

$$\Delta\nu_s = 50 \left[\left(\frac{d}{r} \right)^{12} - \left(\frac{d}{r} \right)^6 \right]$$

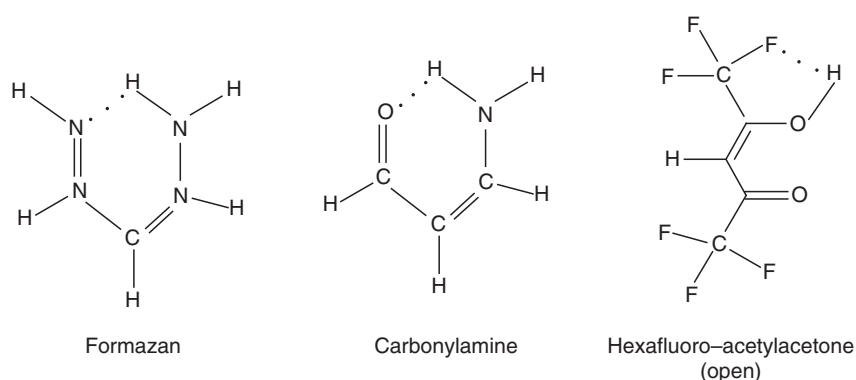
and d assumes the values of 3.2, 3.35, 3.4, 3.6, 3.85 and 3.9 for the F–H···F, O–H···O, N–H···F, N–H···O, N–H···N, O–H···Cl and N–H···Cl bridges, respectively. When applied to 3-(3,4,5-trimethylphenyl)pentane-2,4-dione [182], a E_{HB} of 110 ± 10 kJ/mol was estimated.

Although in many cases the deduced energies are sufficiently satisfactory, such functions must be used with caution. It has been proved that in intramolecular O–H···O bridge the low X–H stretching mode frequency may be a consequence of the molecular symmetry instead of a very large increase of the E_{HB} , and it has been also inferred that the maximum E_{HB} increment on $r_{\text{O}\cdots\text{O}}$ shortening is about 30 kJ/mol [183]. In the C_{2v} structure, which should exhibit the strongest hydrogen bond, $r_{\text{O}\cdots\text{O}}$ is in the range 2.3–2.4 Å. If the hydrogen-bonded atoms are connected through a π -conjugated framework, as in β -diketones, the charge flow from hydrogen to oxygen increases in consequence of the enhanced conjugation so contributing to the hydrogen bond strengthening (RAHB). It is also to be remembered that the very short O···O (or X···Y, in general) distance may be governed by peculiar geometrical situations, as steric effects are caused by repulsive interactions between cumbersome substituent groups. When the hydrogen bond strengthening is no longer able to balance the increased strain deriving from $r_{\text{O}\cdots\text{O}}$ shortening the chelate ring begins to lose its planarity.

3.5 Strategies for E_{HB} Calculation and Comprehension

E_{HB} is classically defined as the energy difference between the open and chelate conformations, i.e., it denotes the stabilization experienced by the open conformation when the OH group rotates by 180° to close a hexatomic or pentatomic

chelate ring. But, what happens when an open conformation does not exist? Examples are formazan and carbonylamine, whose most stable conformers are shown in the scheme, and all molecules in which the donor is the amino group, whose 180° rotation gives back the starting chelate form. In addition, in some cases, it happens that the open form is stabilized by another hydrogen bond which distorts the strength obtained for the O–H···O bridge. An example is hexafluoro-acetylacetone, in which the hydroxyl interacts with a fluorine atom of the adjacent CF_3 group giving rise to a weak O–H···F bridge [184].



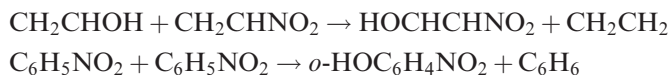
To bypass these problems it has been tried to use the rotation barriers for obtaining E_{HB} estimates. In fact, it has been observed during our studies that the rotation barrier (RB) of a hydrogen-bonded OH group is higher than that of a free OH, because when the rotation starts it must overcome the E_{HB} . Thereby it can be written that the rotation barrier is given by

$$\text{RB} = E_{\text{HB}} + \text{actual RB}$$

Consequently, E_{HB} is the difference between the OH barrier calculated in the chelate conformation and the same barrier calculated in a molecule structurally close to the examined compound but hydrogen bond free. In most of our calculations, the reference molecule was attained by substituting the hydrogen bond acceptor fragment with a H atom. When tested on malonaldehyde and acetylacetone the approach worked very well [185]. The method was then applied with discrete success to many other molecules as formazan [186], carbonylamine [187], hexafluoro-acetylacetone [184], glyoxaloxime [188], 2-nitroresorcinol, 4,6-dinitroresorcinol and 2-nitrophenol in vacuum and in solution [189], malonamide and nitromalonamide [158] and *ortho*-halophenols [190].

Another approach for E_{HB} evaluation exploits the stabilization energy obtainable by considering thermochemistry of appropriate isodesmic reactions for calculating the isodesmic (from greek: $\iota\sigma\sigma\varsigma$ = equal and $\delta\epsilon\zeta\omicron\mu$ = bond) reaction's enthalpy (ΔH_{iso}) [191–193]. Reagents and products in such reactions

must have the same number of carbon (in similar valence state) and hydrogen atoms and equal number of double and single bonds. Adoption of extended basis set is suggested. By using the following isodesmic reactions and MP2/6-31G** calculations:



Varnali and Hargittai found energies of 30 and 12 kJ/mol for the intramolecular hydrogen bond formation in 2-nitrovinyl alcohol and 2-nitro phenol, respectively [194]. They are far from 57.45 and 50.07 kJ/mol, respectively, obtained according to the classical procedure at B3LYP/6-31G** level [189]. To be remembered that the isodesmic reaction technique cannot be used for activation barriers and that different energies will be predicted by different isodesmic reactions.

4 ENERGETICS OF HYDROGEN BONDS

According to Hibbert and Emsley [171], from the relative positions of the hydrogenated and deuterated compound in the potential energy well and from the $r_{\text{O}\cdots\text{O}}$ shortening with respect to the sum of van der Waals radii, three kinds of hydrogen bonds can be identified: *weak* (energy in the range 10–50 kJ/mol), *strong* (energy in the range 50–100 kJ/mol), *very strong* (energy higher than 100 kJ/mol).

Following the analysis of Gilli [31] concerning the nature of the homonuclear hydrogen bond, the O–H \cdots O bridges can be grouped in five classes, labelled as:

- (a) (–)CAHB, [–O \cdots H \cdots O–][–] (negative charge-assisted H-bonds);
- (b) (+)CAHB, [=O \cdots H \cdots O=]⁺ (positive charge-assisted H-bonds);
- (c) RAHB, [–O–H \cdots O=] (resonance-assisted H-bonds);
- (d) PAHB, [\cdots (R)O–H \cdots O–(R)O–H \cdots] (polarization-assisted H-bonds);
- (e) IHB, [–O–H \cdots O<] (isolated H-bonds, non-charged, non-resonant, non-cooperative H-bonds).

Strong hydrogen bonds (termed also Lower Barrier Hydrogen Bonds, LBHBs) [195] belong to the first three classes, whereas the moderate and weak ones are grouped in the fourth and fifth classes, respectively. The first two classes include the N–H \cdots O[–], O–H \cdots N[–] and N–H⁺ \cdots O bridges too, whilst the N–H \cdots O and O–H \cdots N ones belong to the third class.

As previously mentioned, the electrostatic character is maximum in a weak X–H \cdots Y hydrogen bond, whereas a strong hydrogen bond is a mixture of both covalent and electrostatic contributions. Gilli et al. [178] pointed out that the covalent part increases “while the difference of proton affinities, $\Delta\text{PA} = \text{PA}(\text{X}^-) - \text{PA}(\text{Y})$, or acidity constants, $\Delta pK_a = pK_a(\text{X} - \text{H}) - pK_a(\text{X} - \text{Y}^+)$, is approaching zero and, when this limit is achieved, very strong and symmetrical X \cdots H \cdots Y bonds are formed which are better classified

as a three-center-four-electron covalent bonds, that is a 1:1 mixture of the two $X-H\cdots Y \leftrightarrow X\cdots H-Y$ VB resonance forms". In these conditions, the system lies in a symmetric single well and shows the shortest possible $X\cdots Y$ distance.

Anyway, it must be said that the RAHB concept has been just lately questioned on the ground of theoretical and NMR studies [196, 197].

4.1 The O-H \cdots O Bridges

Among the O-H \cdots O intramolecular hydrogen bonds, those of β -diketone enols are resonance assisted and characterized by a low barrier in the proton transfer pathway between two equivalent tautomeric forms, through the H-centred (C_{2v}) conformation representing the transition state (Fig. 4).

Malonaldehyde is undoubtedly the most studied among these compounds (see, e.g., Refs. 183, 198–203 and therein). The barrier height for its proton transfer interconversion was calculated as about 15.2 kJ/mol [183] at MP2/6-31G** level, in good agreement with the literature theoretical data [204–206] and lower than the upper limit of 25 kJ/mol suggested by NMR studies [207]. In its derivatives, the E_{HB} increases with the dimensions of the substituent groups and with their electron withdrawing or donating power. At the best of our knowledge, the highest E_{HB} estimate in the diketones family is that of nitromalonamide (113.6–116.3 kJ/mol at MP2/cc-pVTZ and B3LYP/cc-pVDZ levels, respectively [164]), mainly because its chelate conformation is stabilized by two additional, weaker, (H)N-H \cdots O(N) hydrogen bridges occurring between the NO₂ and the neighbouring amino groups [158, 159]. Neutron diffraction spectra accompanied by theoretical investigations showed that the molecular geometry is very close to the C_{2v} symmetry ($r_{O\cdots O} = 2.39\text{\AA}$) whereas the enol hydrogen vibrates nearly freely with a frequency of $\sim 2000\text{ cm}^{-1}$ in a nearly symmetric single-minimum potential curve [164]. The potential energy curves for the proton transfer pathway, calculated at B3LYP/6-311++G(d,p) level (Fig. 5) confirm this conclusion [159].

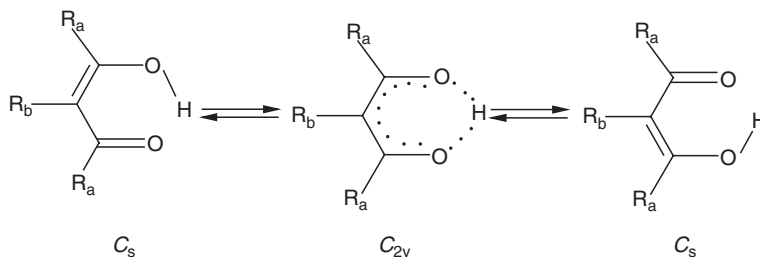


Figure 4. Tautomeric conformations of β -diketones.

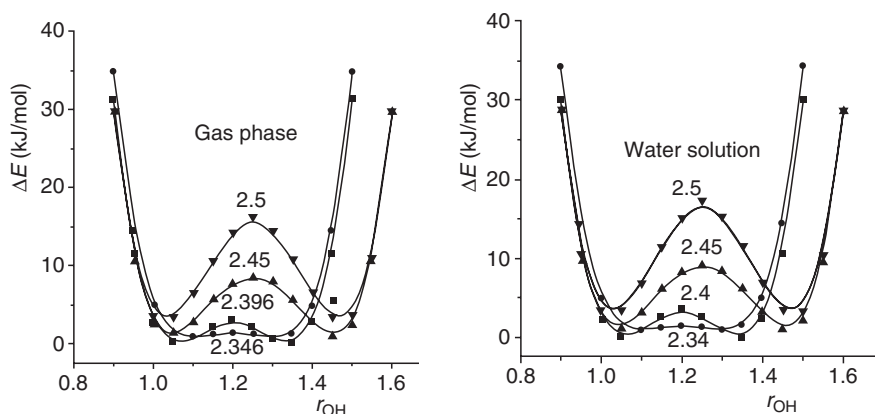


Figure 5. Potential energy curves versus r_{O-H} in vacuum and in water solution for some frozen $r_{O...O}$ values of nitromalonamide. (Reprinted from Ref. 159 with permission from Elsevier.)

The extent of delocalization inside the hydrogen-bonded ring can be represented by the “coupling parameter”, λ , introduced by Gilli et al. [30] defined as

$$\lambda = 1 - \frac{|Q|}{0.320}$$

where $|Q| = q_1 + q_2$, $q_1 = r_{C-O} - r_{C=O}$ and $q_2 = r_{C-C} - r_{C=C}$; $\lambda = 1$ denotes a fully π -delocalization whereas $\lambda = 0$ denotes a fully π -localization.

A slightly different parameter, termed “resonance parameter”, Δ_{rp} , has been introduced by Grabowski [208] for describing the resonance within the RAHB systems. It is defined as

$$\Delta_{rp} = 0.5[(\Delta d_1^o - \Delta d_1^c)/\Delta d_1^o + (\Delta d_2^o - \Delta d_2^c)/\Delta d_2^o]$$

where

$$\begin{aligned} \Delta d_1^o &= |d_{C-C} - d_{C=C}|^o & \Delta d_2^o &= |d_{C-O} - d_{C=O}|^o \\ \Delta d_1^c &= |d_{C-C} - d_{C=C}|^c & \Delta d_2^c &= |d_{C-O} - d_{C=O}|^c \end{aligned}$$

and the superscripts refer to the open and chelate conformations, respectively. It correlates very well with Gilli’s λ -parameter (Fig. 6a).

In the same paper [208] an approach for partitioning the E_{HB} into two terms (the “ring closure energy” and the “ π -delocalization energy”, as schematized in Fig. 7) was also suggested.

The ring closure energy (Fig. 7) is the $|\Delta E|$ between the energy of the open conformation (E_O) and the energy of the chelate conformation having the same geometry of the open one (E'), i.e., it is the energy gained by the system when its chelate ring is closed. The second term is the $|\Delta E|$ between E' and the energy of the full optimized chelate conformation (E_C), i.e., it is the energy gained by

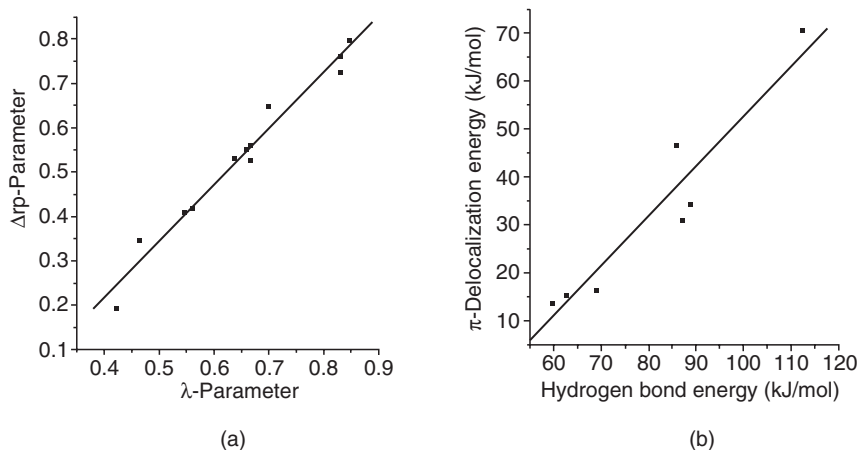


Figure 6. Correlation between λ -parameter and $\Delta\rho$ -parameter (a) and between the π -electron delocalization and the hydrogen bond energy (b). (Reprinted from Ref. 158 with permission from Elsevier.)

the system evolving towards its most stable structure. Analysis of ρ values obtained by the AIM method showed that this term is mainly bound to the “ π -delocalization energy”.

The results of the above procedure, when applied to the malonaldehyde derivatives [158], evidence some important peculiarities (Table 2). A good linear correlation between the π -delocalization energy versus E_{HB} (Fig. 6b) is found only if the values deduced from full planarity imposition to the open form are

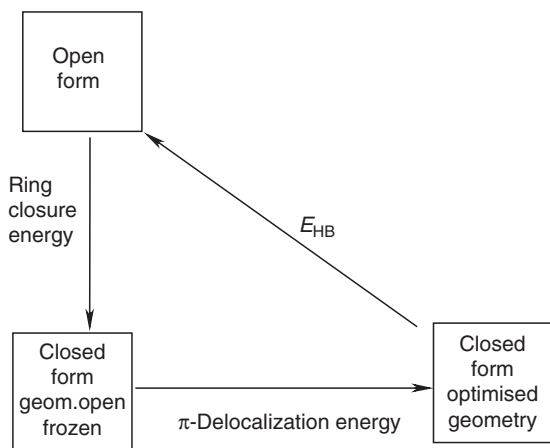


Figure 7. Scheme of E_{HB} partition according to Ref. 208.

Table 2. Grabowski π -delocalization energies (kJ/mol) and resonance parameters for the O–H···O bridges of some malonaldehyde derivatives, calculated at B3LYP/6-31G** level (reprinted from Ref. 158 with permission from Elsevier)

Compound	$r_{O\cdots O}$ (Å) ^a	E_{RC} ^b	π -Energy ^c	λ ^d	Δr_p ^e	E_{HB}
Malonaldehyde	2.555 (2.865)	47.53	15.31	0.560	0.417	62.84
2-Amino-MDA	2.554 (2.850)	52.96	16.21	0.463	0.345	69.17
3-Amino-MDA	2.558 (2.828)	46.08	13.60	0.546	0.408	59.68
4-Amino-MDA	2.443 (2.849)	56.93	34.09	0.846	0.796	88.89
3-Nitro-MDA	2.534 (2.789)	46.42	13.53	0.422	0.193	59.95
Malonamide	2.474 (2.824)	56.58	30.70	0.667	0.561	87.28
Nitromalonamide	2.380 (2.704)	42.15	70.18	0.829	0.760	111.81
NO ₂ rotated by 90°	2.479 (2.848)	39.36	46.47	0.659	0.550	85.83
Open form forced to full planarity						
Malonamide	2.474 (2.794)	63.89	30.09	0.667	0.526	93.98
Nitromalonamide	2.380 (2.515)	96.04	20.72	0.829	0.724	116.77
NO ₂ rotated by 90°	2.479 (2.737)	74.56	21.64	0.638	0.531	96.20
<i>t</i> -Butyl-acetylacetone	2.359 (2.424)	78.29	15.65	0.700	0.647	93.94

^a Values in parentheses refer to the open conformation

^b E_{RC} = ring closure energy

^c Grabowski π -delocalization energy

^d Gilli's parameter

^e Grabowski's resonance parameter

ruled out. Indeed, the strongly different resonance and ring closure energies found when the nitromalonamide and 3-*t*-butyl-acetylacetone open conformations were forced to full planarity indicate that they are strictly intercorrelated and affected by spurious terms connected with the strain amount inside the chelate ring. In fact, the planarity loss implies also a resonance loss (weakening of the π -electron flow) and a lowering of the repulsion terms with respect to the unstable full planar open structure with a consequent decrease of the π -delocalization and a simultaneous decrease of the ring closure energies. The effect is much less evident in malonamide since here the deviation from planarity is lesser than in nitromalonamide, even if, in both molecules, the E_{HB} values are by far less affected by non-planarity than the related ring closure and π -delocalization terms.

For the examined molecules, a good correlation was found between E_{HB} and the OH stretching mode frequencies (Fig. 8a) as well as between the electron population along the O···H axis and the same OH stretching mode frequencies (Fig. 8b).

In the energy partition scheme proposed by Gomak [209], the conformation resulting after 180° rotation around the C=C bond of the chelate form is assumed as zero point for the E_{HB} scale and the resonance stabilization energy is identified with the ΔE between this and the classic open conformation (open A in Sect. 3.2). For malonaldehyde, it amounts to 20.2 kJ/mol (MP4/6-311G(d,p)//MP2/6-31G(d,p) without ZPVE correction), i.e., about 5 kJ/mol higher than

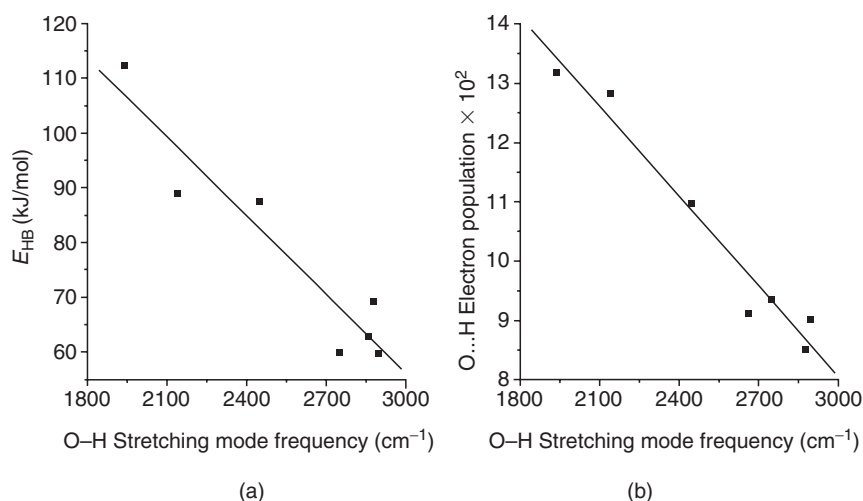
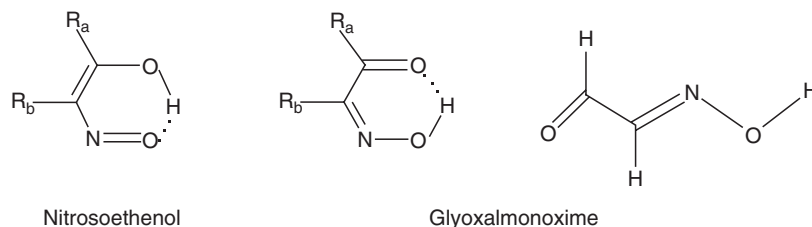


Figure 8. Graphs of E_{HB} (a) and O...H electron population (b) versus ν_{OH} . (Reprinted from Ref. 158 with permission from Elsevier.)

that obtained at B3LYP/6-31G** level (see Table 2) according to Grabowski's scheme, and 8.7 kJ/mol higher than the value obtained by Grabowski (MP2/6-311++G**) [208].

B3LYP/6-311++G(d,p) calculations have shown that in diketones with two resonance-assisted hydrogen bonds, as 2,4-dihydroxy-but-2-ene-4-diol, no rise of the resonance effect is noted and the π -delocalization energy of the closed-open conformations is greater than in the most stable conformers with two closed rings [210].

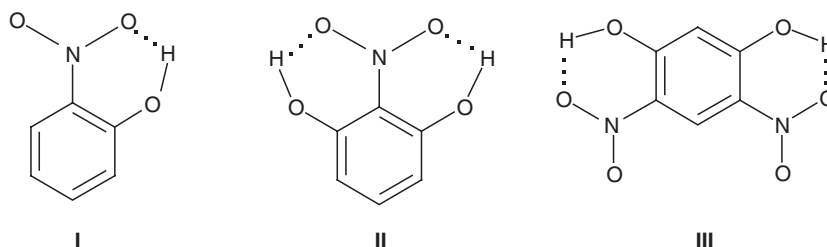
Substitution of the malonaldehyde C=O framework with a N=O group gives rise to nitrosoethenol and/or glyoxalmonoxime molecules, which are interesting systems for investigating the E_{HB} changes in the new O-H...O hydrogen bridges.



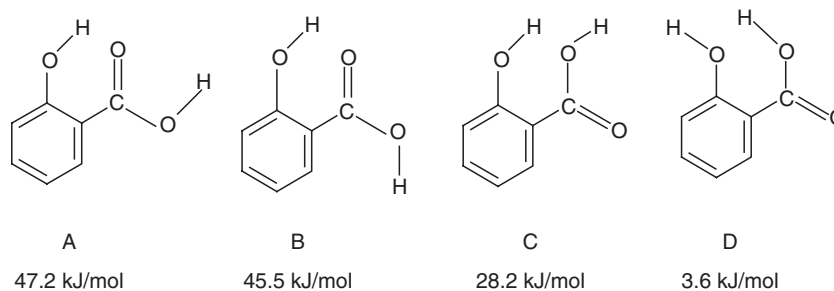
The main remark is that the linear, hydrogen bond free, *s-Trans-Anti-Trans* (TAT) is the most stable conformations of glyoxalmonoxime, both at B3LYP/6-31G** and MP2/6-31G** level of calculations [188]. The strength of the

O–H···O bridge of the chelate conformation is 26.29 kJ/mol (MP2) and 22.53 kJ/mol (B3LYP), respectively, whilst in nitrosoethenol it rises to 58.79 kJ/mol [188]. All these energies nearly halve in water.

The single O–H···O hydrogen bond present in 2-nitrophenol, **I** ($r_{\text{O}\cdots\text{O}} = 2.562 \text{ \AA}$, $E_{\text{HB}} = 50.1 \text{ kJ/mol}$), is about 6 kJ/mol stronger than those of 2-nitroresorcinol, **II** ($r_{\text{O}\cdots\text{O}} = 2.542 \text{ \AA}$), and nearly equal to that of 4,6-dinitro-resorcinol, **III** ($r_{\text{O}\cdots\text{O}} = 2.558 \text{ \AA}$, $E_{\text{HB}} = 49.8 - 52.0 \text{ kJ/mol}$, depending on if it is calculated with respect to the *syn-anti* or *anti-anti* reference conformations) (B3LYP/6-31G** calculations [189]).



In catechol (2-hydroxyphenol) [211, 212], and in the parent guaiacol [211], a hydrogen bond enthalpy amounting to about 21 kJ/mol was calculated (B3LYP/6-31+G(3,pd), which proves that the strength of a hydrogen bridge closing a pentatomic ring (O–H···O angle in the range of 120° or less) is much weaker than in β -diketones (O–H···O angle ranging from 140° to 150°). It halves in aprotic dipolar solvents as acetonitrile or acetone and practically vanishes in strong dipolar solvents as ethanol or water [211]. However, the most recent investigation accompanied by AIM analysis excludes the presence of intramolecular hydrogen bond in catechol and in 1,2-ethanediol [213].

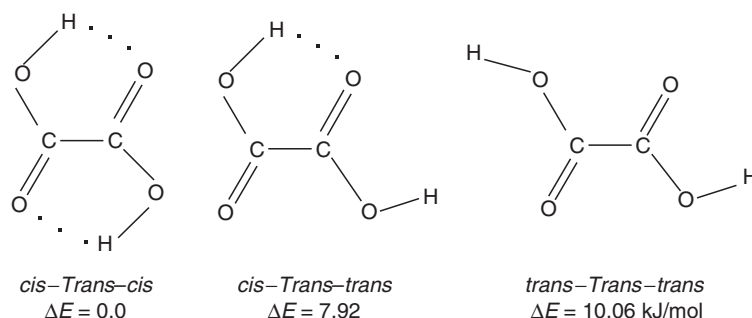


Four conformations showing O–H···O hydrogen bridge are possible for salicylic acid, the most stable of them is here labelled A [214] and is followed by C at 16.9 kJ/mol higher energy, according to B3LYP/6-311+G(2d,p) predictions. E_{HB} (47.2 kJ/mol) is practically equal to that calculated at B3LYP/6-311+G(d) level (46.5 kJ/mol) by Kwon [215] and negligibly lower than found for salicylaldehyde (48.7 kJ/mol) [216].

The intramolecular hydrogen bridges in the amino acid are generally weak. According to the most recent theoretical study [217], at least five types of intramolecular hydrogen bonds involving the OH group were found in the series of 74 unique stable conformations of serine ($\text{HOOC}-\text{CHNH}_2-\text{CH}_2\text{OH}$) identified after optimization of all the 324 possible trial structures:

- (a) $\text{CH}_2\text{OH}\cdots\text{O}(\text{H})-\text{C}=\text{O}$
- (b) $\text{CH}_2\text{OH}\cdots\text{O}=\text{C}-\text{OH}$
- (c) $\text{CH}_2\text{OH}\cdots\text{NH}_2$
- (d) $\text{O}=\text{C}-\text{OH}\cdots\text{OH}-\text{CH}_2$
- (e) $\text{O}=\text{C}-\text{OH}\cdots\text{NH}_2$

The ΔE between the most and the less stable conformations is 59.4 kJ/mol (B3LYP/6-311+G**) but the four most stable conformers, stabilized by the above cited *E*-type hydrogen bridges, lie in an energy range lower than 4.2 kJ/mol. Analogous hydrogen bond interactions governing the most stable conformations were found in Ref. 218.



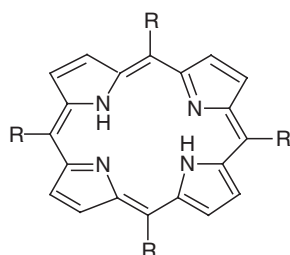
Two $\text{O}-\text{H}\cdots\text{O}$ hydrogen bonds closing five-membered chelate rings are those recognized in the *cis-Trans-cis* conformation of oxalic acid. According to the most recent theoretical study [219] at MP2/6-311++G** level of calculations, their overall strength is 10.06 kJ/mol. The *trans-Cis-trans* (*tCt*) conformation is about 2 kJ/mol over the *trans-Trans-trans* (*tTt*) one, so it can be argued that the *trans* accommodation of the double bonds is favoured by conjugation. A similar result was found in 3-formyl-malonaldehyde [220]. The expected equivalence of the two hydrogen bonds is not supported by the reported ΔE values; very likely they are mutually reinforced and the breakage of one of them strongly weakens the remaining one, owing also to the concurrent collapse of the ring conjugation. Indeed, it must be pointed out that the above ΔE s, notwithstanding calculated according to the classic procedure (rotation of the OH group(s) by 180°), are not comparable with E_{HB} scale of β -diketones because the *cis-Trans-trans* and the *trans-Trans-trans* conformations of oxalic acid are stabilized by one and two $\text{O}-\text{H}\cdots\text{O}$ hydrogen bridge(s), respectively, of the carboxylic framework(s) closing a four-membered ring. The strength of this bridge in formic acid, calculated at B3LYP/6-311++G(d,p) level, is

19.1 kJ/mol. An analogous situation is that of pyruvic and glyoxylic acids [221, 222]. Use of the rotation barriers in these cases could contribute to get more realistic E_{HB} estimates.

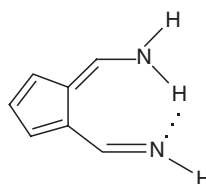
4.2 The N–H···N Bridges

The N–H···N intramolecular hydrogen bridges are generally weaker than the O–H···O ones. In formazan [186] the calculated (MP2/6-31G**) N···N and N···H distances are 2.586 and 1.851 Å, respectively (2.599 and 1.858 Å at B3LYP/6-31G** level) but, as already mentioned, E_{HB} cannot be obtained according to the classic procedure because the amino group prevents the formation of the hydrogen bond free open conformation. Following the rotation barrier approach [185], it was argued that its most probable value should be in the range of 30 kJ/mol.

Porphyrins and aminoderivatives of formylfulvene contain N–H···N bridges too, but in this case also their strength is not valuable according to the classic approach.



R = bulky alkyl groups



N-N'-diphenyl-6-aminofulvene-2-aldimine

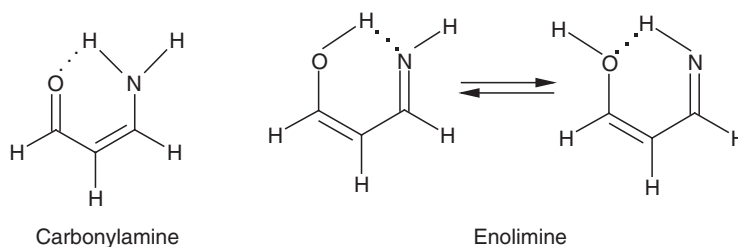
However, the 6-aminofulvene-2-aldimines, where the central hydrogen is rapidly exchanged between the two amino nitrogen atoms [223], are hypothesized to be LBHB systems with a double well potential and have been studied by the isotopic perturbation of equilibrium technique [224–226]. The lowest barrier to proton transfer calculated at B3LYP/6-31G* level was 18.8 kJ/mol (7.3 kJ/mol after zero-point energy correction) in strong contrast with the 49.4 kJ/mol coming from HF/6-311G** results [224].

4.3 The Heteronuclear Hydrogen Bridges

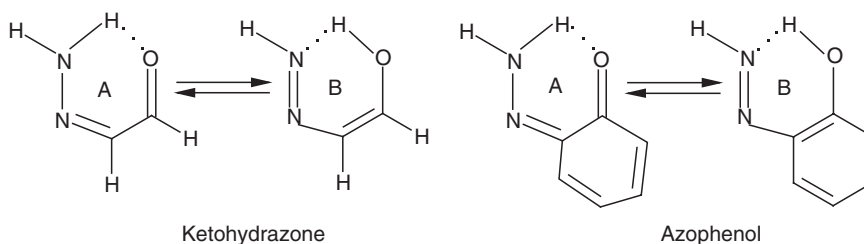
When different heteroatoms are involved in the donor and acceptor groups the hydrogen bond is named “heteronuclear”. Its strength is generally weaker than that of the homonuclear one and depends strongly on the proton affinity of the donor and acceptor groups, the strongest ones being those in which the proton affinity difference (ΔPA) vanishes [178]. Some of these intramolecular hydrogen bond classes are briefly discussed here.

4.3.1 The N–H···O and O–H···N Bridges

Typical intramolecular hydrogen bridges involving nitrogen and oxygen are those present in carbonylamine (3-amino-acrolein or 4-amino-3-penten-2-one, in the following labelled CA) and enolimine (EI) [187, 227, 228]. CA is the most stable among the four possible conformations, but, once again, its N–H···O hydrogen bond strength cannot be estimated according to the classic convention even if it has been deduced that the most probable value is in the range of 30 kJ/mol [187, 227]. In the analogous bridge of enolimine, E_{HB} is 11.2–13.0 kJ/mol at B3LYP/6-31G** and MP2/6-31G** level, respectively [187], and 18.6 kJ/mol according to MP2/6-31G* calculations [227]. On the contrary, E_{HB} values of 76.7 [227], 71.86 ($r_{\text{O}\cdots\text{N}} = 2.548 \text{ \AA}$, B3LYP/6-31G**) and 68.67 kJ/mol ($r_{\text{O}\cdots\text{N}} = 2.580 \text{ \AA}$, MP2/6-31G**) [187] (confirmed by the rotation barrier method) are reported in the literature for the O–H···N bridge of enolimine. They suggest that this bridge is a little stronger than the O–H···O bridge of malonaldehyde.

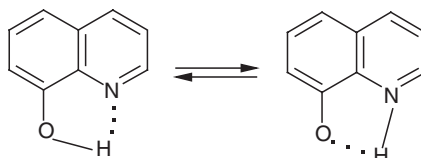


Very interesting is the keto-hydrazone system, in which the tautomer A is more stable than its azoenol B one, owing to the greater proton affinity of nitrogen with respect to oxygen. The stability order reverses if a phenylene moiety is fused with the H-bonded ring, whilst the fusion with a naphthalene ring makes A and B tautomers nearly isoenergetic (a loss of the resonance energy of the aromatic ring occurred [Ref. 179 and therein]). The N···O distance lowers from the range of 2.67 Å to 2.50–2.52 Å.



The strength of the O–H···N bridge of 8-hydroxyquinoline in gas phase [229] was found to be ~32.6 kJ/mol at DFT MPW1K/6-311++G(2d,3p)/MPW1K/

6-311++G(d,p) level ($r_{\text{N}\cdots\text{H}} = 2.098 \text{ \AA}$, $r_{\text{O}\cdots\text{N}} = 2.686 \text{ \AA}$) in good agreement with the experimental value of about 25 kJ/mol deduced on the ground of the OH stretching frequencies [230]. It lowers to 21.8 kJ/mol in acetone and 10.8 kJ/mol in water (PCM calculations [229]).

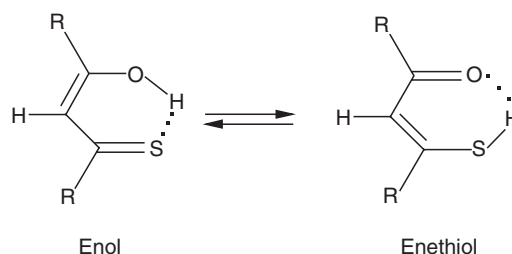


A barrier of about 20 kcal/mol (about twice that of 8-mercaptoquinoline) has been calculated for transferring the proton from O to N, both in vacuum and in water solution. The pentatomic chelate ring and the OH stretching frequency (3418 cm^{-1}) [231] justify the weakness of the bridge.

4.3.2 The Hydrogen Bonds Involving Sulphur

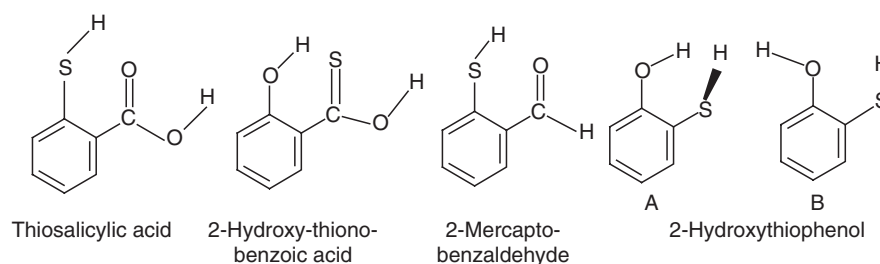
The S atom can form a variety of intramolecular hydrogen bonds, as the S–H \cdots S, S–H \cdots O and O–H \cdots S, the latter being the strongest one. The S–H \cdots S bridge of dithiomalonaldehyde and dithioacetylacetone (for which no experimental information exists at the best of our knowledge), is by far weaker than the O–H \cdots O one of malonaldehyde and acetylacetone. At MP2/6-31G** level of theory its E_{HB} was calculated as 5.59 kJ/mol in the former ($r_{\text{S}\cdots\text{S}} = 3.421 \text{ \AA}$, $r_{\text{S}-\text{H}} = 1.349 \text{ \AA}$, $r_{\text{S}\cdots\text{H}} = 2.209 \text{ \AA}$) and 6.39 kJ/mol in the latter compounds ($r_{\text{S}\cdots\text{S}} = 3.371 \text{ \AA}$, $r_{\text{S}-\text{H}} = 1.354 \text{ \AA}$, $r_{\text{S}\cdots\text{H}} = 2.133 \text{ \AA}$), which become 13.23 ($r_{\text{S}\cdots\text{S}} = 3.377 \text{ \AA}$, $r_{\text{S}-\text{H}} = 1.393 \text{ \AA}$, $r_{\text{S}\cdots\text{H}} = 2.107 \text{ \AA}$) and 14.60 kJ/mol ($r_{\text{S}\cdots\text{S}} = 3.324 \text{ \AA}$, $r_{\text{S}-\text{H}} = 1.403 \text{ \AA}$, $r_{\text{S}\cdots\text{H}} = 2.023 \text{ \AA}$) at B3LYP/6-31G** level [232]. The barrier to the proton transfer process is about 15 kJ/mol in both molecules at MP2 level and 7.3–7.5 kJ/mol when the B3LYP functional was adopted. Insertion of the cumbersome *t*-butyl group in position 3 produces a shortening (0.070 Å at MP2 and 0.053 Å at B3LYP level) of the S \cdots S distance whilst E_{HB} lessens by about 4 kJ/mol, regardless of the approach adopted for the correlation energy calculation. This means that the S \cdots S shortening is accompanied by a strain increase inside the chelate ring, which cannot be quite damped by the hydrogen bridge. Very likely the weakening is bound to the greater dimension and lower electronegativity of the S atom with respect to oxygen.

Thiomalonaldehyde and thioacetylacetone can exist in the enol and enethiol tautomeric forms, the enol being the most stable one (Refs. 233, 234 and therein). According to high level calculations [235], the enethiol tautomer becomes slightly favoured (0.84 kJ/mol at MP2/6-31+G(d,p) and G2(MP2) level of calculations) after correlations inclusion and/or ZPVE correction.



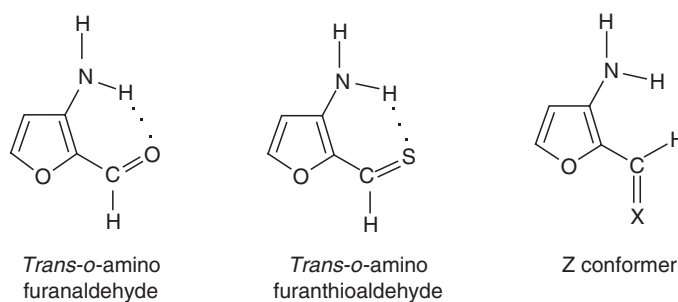
The strength of the O–H···S bridge was estimated as 47.7 kJ/mol whereas that of the S–H···O is about 8.8 kJ/mol [235], only slightly higher than the above cited value of the S–H···S bridge obtained at MP2/6-31G** level. The barrier for the *enol* → *enethiol* tautomerization process is 13.39 kJ/mol (G2(MP2)) and is strongly depending on the correlation energy (inclusion of correlation effects decreases the barrier height by a factor of 5). B3LYP/6-31G** calculations predicted E_{HB} of 61.1 and 65.7 kJ/mol for the O–H···S bridges of thiomalonaldehyde and thioacetylacetone (63.8 and 56.8 kJ/mol at MP2 level), not far from 62.8 and 72.9 kJ/mol obtained for the O–H···O bridge of malonaldehyde and acetylacetone [185]. The same basis predicted strengths of 10.9 and 7.6 kJ/mol (B3LYP) for the S–H···O bridges, which lower to 7.4 and 3.6 kJ/mol if correlation energies are evaluated at MP2 level. The rotation barrier method reproduces very well the strengths of the O–H···S bridges evaluated according to the classic method but fails when applied to the S–H···O or S–H···S ones [185]. Obviously, the above E_{HB} values change under substituent effects depending on their nature, position and electron withdrawing or donating power [236].

The IR spectra of thiosalicylic acid and its S-methylated compounds exclude that intramolecular hydrogen bonds involving S are formed since only OH single bands of the *cis*-carboxyl structure are observed [237].



In 2-hydroxy-thiono-benzoic acid, the B3LYP/6-311+G(d) E_{HB} value of the O–H···S bond is 41.1 kJ/mol [215] but falls to 6.4 (B3LYP/6-311+G*) or 7.45 kJ/mol (B3LYP/6-31+G*) in the S–H···O bridge of 2-mercapto-benzaldehyde [216]. The structure A of 2-hydroxythiophenol, in which the SH group assumes a *gauche* position, is energetically favoured to B. The strength of

the O–H···S bridge is about 14.2 kJ/mol whilst that of the S–H···O bridge in B is 4.9 kJ/mol (B3LYP/6-31+G*) [212].



The strength of the N–H···O bridge of *ortho*-amino-furanaldehyde, calculated as 26.02 kJ/mol at B3LYP/6-31+G* level (with respect to the Z conformer) was found about 5 kJ/mol lower than that of the N–H···S hydrogen bond of *ortho*-amino-furanthioaldehyde (30.92 kJ/mol) [238]. Such values become 14.06 and 16.86 kJ/mol, respectively, when calculated in DMSO solution ($\epsilon = 46.7$) following the Onsager self-consistent reaction field method.

The S–H···N intramolecular hydrogen bond of 8-mercaptoquinoline has been studied recently in the gas phase and in solution [239]. Its strength (difference of sums of electronic and thermal enthalpies including ZPVE corrections) is about 9.6 kJ/mol in vacuum and 6.09 kJ/mol in aqueous solution (MPW1K/6-311++G(d,p)). The barrier height (10.585 kcal/mol) suggests that the proton transfer from S to N occurs with difficulty whilst the opposite process is practically spontaneous.

S–H···S bridges are also present in the highly flexible 1,2-ethanedithiol, for which ten local minima have been theoretically recognized [240, 241]. The energy differences of all these rotamers fall in the range of 15 kJ/mol and a complex equilibrium mixture of several rotameric forms of the molecule exists in gas phase. The difficulty in selecting an appropriate hydrogen bond free reference conformation does not allow to deduce well-defined E_{HB} values, which, however, were roughly estimated to fall in the range 5.7–6.5 kJ/mol (HF/6-31G**), i.e., nearly equal to the 6.29 kJ/mol deduced for the S–H···O bridge of mercaptoethanol [242], which, in turn, is in good agreement with the 7.53 kJ/mol value reported in Ref. 243.

4.3.3 Hydrogen Bonds Involving Halogens

The intramolecular hydrogen bonds involving halogens are rather weak. Some O–H···F bridges, theoretically recognized in secondary conformations of hexafluoro- and trifluoro-acetylacetone, show strengths in the range of 10 kJ/mol or less [184] and still weaker are those found in 3,3,3-trifluoro-propanol [244]. Ab initio results evidencing the effects of the hydrogen bond on the geometrical parameters of 2-trifluoro-methylvinyl-alcohol [245], 2-trifluoromethyl-

resorcinol, 2,6-bis(trifluoromethyl)-phenol [246] and 2-trifluoromethyl-phenol [247] are available in the literature. In these molecules the $O \cdots F$ distances range from 2.66 to 2.77 Å ($r_{H \cdots F}$ from 1.853 to 1.983 Å), with $O-H \cdots F$ angles nearby 137–140°. Where reported, E_{HB} is strongly affected by the technique adopted for its calculations. So, in 2-trifluoro-methylvinyl alcohol ($r_{O \cdots F} = 2.73$ Å, $r_{H \cdots F} = 1.96$ Å) the ZPVE corrected E_{HB} estimated on the ground of hypothetical isodesmic reactions (3.1 kJ/mol (MP2/6-31+G**)) is in contrast with the ΔE between the *chelate* and *open* structures (20.3 kJ/mol) even if this latter was calculated at HF/6-31G** level [245]. The theoretical E_{HB} value found for the *ortho*-fluorophenol hydrogen bridge (12.2 kJ/mol [248] at MP2/6-31+G**//MP2/6-31G**+ZPVE level is nearly twice the experimental value (6.8 kJ/mol, deduced from far IR spectra torsional frequencies) [249] and in contrast with the ≈ 2 kJ/mol energy difference between the *cis* and *trans* conformers deduced from gas electron diffraction spectra [250].

According to MP2/cc-pVDZ calculations, a weak intramolecular hydrogen bridge ($r_{F \cdots H} = 2.526$ Å, $E_{HB} \approx 7.9$ kJ/mol) seems to be responsible for the greater stability of the *gauche* conformation of 2,2,2-trifluoroethanol with respect to the *trans* one, although it is not confirmed by AIM calculations since no atomic interaction line (AIL) linking the hydroxyl hydrogen and a fluorine atom was found [251].

The most stable conformations of 3-fluorobutan-1-ol and 3,3-difluorobutan-1-ol (Fig. 9) exhibit an intramolecular $O-H \cdots F$ hydrogen bridge whose strength was estimated as 14.9 kJ/mol in the former and 10.3 kJ/mol in the latter compound, respectively (B3LYP/6-311++G(3df,2p)//B3LYP/6-31G+G(d,p) [252]. For an analogous bridge in 1-fluoro-cyclopropane-carboxylic acid, a strength of roughly 15 kJ/mol was deduced after MP2/6-311++G(d,p) and B3LYP/aug-cc-pVTZ calculations [253]. Bearing in mind that the $O \cdots F$ distance is practically the same as the sum of the van der Waals radii of F and O, that the bridge closes a pentatomic ring with a $F \cdots H-O$ angle of 118.8° and that the ΔE with respect to the open conformation is only 1.7 kJ/mol, the above estimate could be too generous.

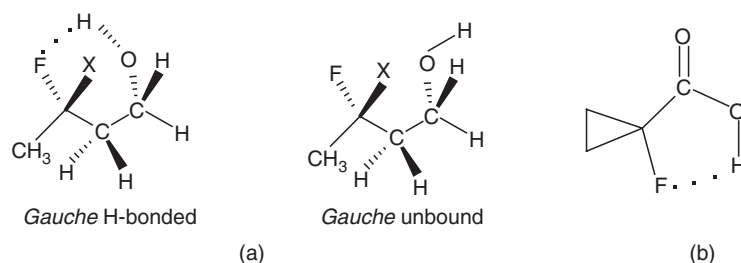
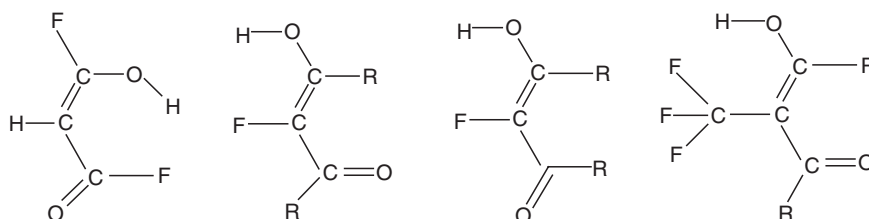


Figure 9. (a) H-bonded and unbound *gauche* forms of 3-fluorobutan-1-ol (X = H) and 3,3-difluorobutan-1-ol (X = F). (b) The $O-H \cdots F$ hydrogen bridge in 1-fluoro-cyclopropane-carboxylic acid.

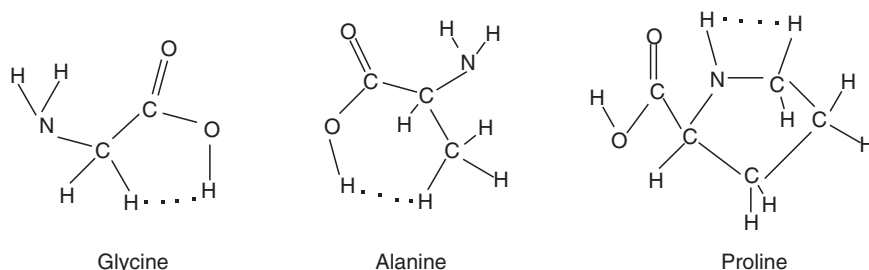
DFT calculations and different basis set adoption predicted an upper limit energy in the range of 20 kJ/mol for the hydrogen bridges between O–H and halogens in 2-halophenols; the strengths smoothly increase within the series $F < Cl < Br < I$ [254] (this trend is opposite to that of the halogens electronegativity) but changes on changing the adopted basis set [255].

The O–H···F bridges in the following conformations of malondialdehyde and acetylacetone are characterized by E_{HB} ranging from 15 to 28 kJ/mol [185].



4.3.4 Intramolecular Dihydrogen Bonds

The intermolecular dihydrogen bonds have been and are widely treated in the literature, whilst by far less numerous are the paper concerning the intramolecular dihydrogen bonds, perhaps because less numerous are the possibilities of such interactions. The possibility of intramolecular dihydrogen bonds in amino acids has been explored from the theoretical point of view in the recent years [64, 256] and rules for their characterization have been suggested [256].



Here examples of four- (proline), five- (glycine) and six-member chelate rings (alanine) are shown, for which E_{HB} ranging from 1.4 (alanine) to 2.1–2.5 kcal/mol (glycine and proline) was estimated. Indeed, we have some doubts that such intramolecular dihydrogen bonds can really exist and also the AIM results appear to be not sufficiently clear.

In a recent study on the intramolecular dihydrogen bridges of 2-cyclopropyl ethanol derivatives [64] (for the molecular scheme see Fig. 3), calculations predicted that the open conformations are more stable than the closed ones and the observed interactions are probably only H···H van der Waals contacts although the “analysis of the parameters derived from the Bader theory shows that such O–H···H–C contacts may be classified as H-bonds”. More convincing is the

situation in the MDA-similar system having a B–H bond as proton acceptor (see scheme in Fig. 3) [62] where E_{HB} ranging from 4.22 to 4.93 kcal/mol ($R_1 = R_2 = R_3 = \text{H}$) or from 5.55 to 7.35 kcal/mol ($R_1 = \text{Cl}$, $R_2 = \text{H}$, $R_3 = \text{Na}$) was found for the $\text{O}-\text{H}^{+\delta}\cdots^{-\delta}\text{H}$ system at different levels of calculation.

Unconventional intramolecular hydrogen bonds involving the double or triple bonds π -electron have been found in 1-amino-1-ethynylcyclopropane [257], 2-cyclopropylideneethanol [258], 2-furan-methanethiol [259], 2-furane-methanol [260] and other similar compounds. A weak H-bond has been also observed in cyclopropane–methanethiol between the H atom of the thiol group and the “quasi- π ” electrons of the cyclopropyl ring, able to act as proton acceptors [261]. It is noteworthy to mention also possible non-conventional intramolecular hydrogen bond in the most stable conformation of 3-butene-selenol [262] in gas phase, occurring between the H atom of the selenol group and the π -electron of the double bond. The interaction is very weak and its actual existence is debatable, at least in our opinion, in default of further investigations evidencing typical hydrogen bond characteristics.

5 E_{HB} DEPENDENCE ON THE CALCULATION LEVEL

Since the calculated energy of a molecule depends on the extension of the basis set and on the inclusion or not on the correlation energy, also the energy of the hydrogen bridge depends on the theoretical degree of sophistication from which it derives. To get the hang of this dependence, it is useful to analyse the results obtained for malonaldehyde and some of its derivatives. As it can be seen from data collected in Table 3, the highest energies are predicted by the less extended basis sets and decrease on increasing the basis set extension, whilst in most cases they increase when correlation energy is taken into account. E_{HB} s calculated by the B3LYP functional are higher than those calculated at MP2 level. Addition of diffuse functions (aug-cc-pVXZ bases) also causes decreasing of the E_{HB} , but modest changes occur when the cc-pVQZ basis is adopted, at least in the few compounds here examined. It is, however, to be pointed out that the hydrogen bond strengthening in the MDA derivatives is also bound to the nature and conjugation ability of the substituent groups in positions 2 and 4 and to the steric effects between these groups and the substituent group in position 3 (for the numbering system see the scheme of nitromalonamide).

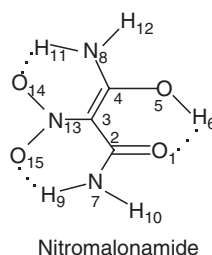


Table 3. $r_{O...O}$ distances (Å) and E_{HB} (kJ/mol, without ZPVE correction) dependence on the basis set and correlation energy for some compounds with strong and very strong intramolecular hydrogen bond. Values without bibliographic references are Author's unpublished data. Values in brackets were obtained forcing the open conformation to full planarity

	HF/3-21G		MP2/3-21G		HF/6-31G**		MP2/6-31G**	
	$r_{O...O}$	E_{HB}	$r_{O...O}$	E_{HB}	$r_{O...O}$	E_{HB}	$r_{O...O}$	E_{HB}
Malonaldehyde ^a	2.605	66.41 ^a	2.604	70.46 ^a	2.681	52.08 ^a	2.592	58.61 ^a
Malonamide	2.487	115.45	2.516	113.22	2.562	91.4	2.508	79.7 [86.6]
Nitromalonamide	2.383	136.89	2.431	129.86	2.424	101.68	2.395	112.82
Acetylacetone	2.570	76.70 ^b	2.583	77.09 ^a	2.627	63.09 ^a	2.559	67.94 ^a
		B3LYP/ 6-31G**		HF/6-311 ++G(d,p)		MP2/6-311 ++G(d,p)		B3LYP/6-311 ++G(d,p)
Malonaldehyde	2.555	62.84 ^a	2.697	46.56	2.585	50.81 ^c	2.587	54.14 ^c
Malonamide	2.474	87.28 ^d	2.499	72.08	2.575	75.17	2.504	79.1 ^c
Nitromalonamide	2.380	[93.09]	2.433	[79.91]	2.387	[78.35]	2.396	107.28 ^c
Acetylacetone	2.519	111.81 ^d	2.635	92.16	2.547	86.13	2.544	66.38
				[101.43]		[104.51]		
		HF/ cc-pVDZ		B3LYP/ cc-pVDZ		HF/ aug-cc-pVDZ		B3LYP/ aug-cc-pVDZ
Malonaldehyde	2.682	49.64	2.544	62.35	2.686	46.00	2.566	53.98
Malonamide	2.556	74.23	2.465	86.60	2.568	71.90	2.494	79.66
Nitromalonamide	2.427	[79.16]	2.383	[92.08]	2.438	[76.25]	2.400	[84.26]
Acetylacetone	2.626	99.65	2.513	113.83	2.626	94.80	2.530	103.33
		[105.48]		[116.39]		[100.30]		[106.44]
		HF/ cc-pVQZ		B3LYP/ cc-pVQZ		HF/ aug-cc-pVQZ		B3LYP/ aug-cc-pVQZ
Malonaldehyde	2.681	45.75	2.573	53.45	2.683	44.78	2.571	53.03
Malonamide	2.561	72.38	2.492	79.02	2.562	72.48	2.493	78.23
Nitromalonamide	2.428	[76.69]	2.394	[83.69]	–	[81.52]	–	–
Acetylacetone	2.622	94.35	2.535	101.92	2.622	55.77	2.533	64.03
		[100.15]		[107.18]				

^a Ref. 160

^b The value reported in Ref. 160 is wrong

^c Ref. 159

^d Ref. 158

These interactions push the oxygen atoms closer to each other and cause the shortening of the O...O distance not only with consequent increase of conjugation inside the chelate ring but also with a simultaneous strain increase. That inside the chelate ring there are remarkable repulsions, partially damped by the hydrogen bridge, can be easily deduced by analysing the geometrical parameters as well as the behaviour of the open conformations. The bond angles at C2

and C3 and O4 of the chelate ring in fact enlarge when the hydrogen bridge is broken for going to the open conformation. The strain rises excessively if a *t*-butyl group is attached in position 3 of acetylacetone, so that the hydrogen bridge is no longer able to damp it and the molecule loses its planarity through rotation around the C–C and/or C–O single bonds, unless restrictions are imposed. In nitromalonamide and malonamide non-planar open conformations are predicted, consequently the related hydrogen bond energies evaluated as stability difference between chelate and open forms are polluted by the too different geometrical parameters. From Table 3 it can be seen that imposition of full planarity implies from 3 to 9 kJ/mol increase in E_{HB} , which are modest quantities on percentage basis but makes extremely difficult, or impossible, any attempt for separating the conjugative from other energy contributions.

In many respects, an unusual situation is shown by the weakly hydrogen-bonded *ortho*-halophenols (five-membered chelate ring), whose E_{HB} , on the ground of the available experimental data, deduced from far IR rotation spectrum [249] and from the temperature dependence of the infrared OH stretching band intensities [263, 264] should decrease on going from F to I (Table 4). In contrast to these, the OH stretching mode frequencies measured in gas phase [264] and in dilute CCl_4 solution [254] decrease in the same direction, so indicating that E_{HB} should increase on passing from F to I. Indeed, the trend paralleling the halogens electronegativity scale is theoretically predicted only by the less extended basis sets (3-21G, CEP-121G and LANL2DZ, at HF, MP2 or B3LYP levels [255]) whilst the available results at high level of calculation (G2MP2 and CBS-QB3) suggest no direct linear relationship with the halogens electronegativity order. An important role in this behaviour is certainly played by the repulsive energy terms and the strain inside the pentatomic ring (inter alia, the calculated O...X distances in most of the halophenol open conformations are shorter than in the closed ones), very likely bound to the increasing atomic dimensions, whose trend is reverse to that of the electronegativity power. Although the anomalous trend of these O–H...X hydrogen bonds has been interpreted in terms of the populations of the electron localization function basins (ELF)[265], the problem deserves further investigations with inclusion of the iodine derivative when extended basis sets for iodine will be available.

6 THE IR SPECTRA AND THE ANHARMONICITY EFFECT

As previously seen, when an inter- or intramolecular hydrogen bond is present the stretching mode frequency of the donor X–H group is red-shifted with respect to that of the same group when hydrogen bond free. It is however to bear in mind that the ν_{XH} values calculated at the Hartree–Fock level and according to the harmonic oscillator model are more or less overestimated owing that they suffer for the same known systematic errors (due to the neglect of the electron correlation); therefore a scale factor, depending on the adopted

Table 4. $r_{O...X}$ distances (Å) and E_{HB} (kJ/mol) dependence on the basis set and correlation energy for compounds with weak intramolecular hydrogen bonds: halophenols. Values in parentheses are ZPVE corrected (Ref. 255)

	MP2/6-31G**		B3LYP/6-31G**		B3LYP/6-311++G(d,p)	
	$r_{O...X}$	E_{HB}	$r_{O...X}$	E_{HB}	$r_{O...X}$	E_{HB}
2-F-phenol	2.718	13.19 (12.40)	2.710	13.14	2.731	12.24 (11.33)
2-Cl-phenol	3.022	11.77 (11.20)	3.016	13.00	3.011	12.90 (12.41)
2-Br-phenol	3.123	15.14 (14.61)	3.108	16.50	3.119	13.43 (13.06)
	HF/cc-pVDZ		HF/aug-cc-pVDZ		MP2/6-311++G(d,p)	
2-F-phenol	2.708	12.40 (11.71)	2.715	11.78 (11.06)	2.737	10.47
2-Cl-phenol	3.012	12.44 (11.88)	3.013	12.56 (12.00)	3.002	10.40
2-Br-phenol	3.130	11.70 (11.15)	3.133	11.52 (11.03)	3.115	11.10
	HF/cc-pVTZ		HF/aug-cc-pVTZ		HF/cc-pVQZ	
2-F-phenol	2.707	10.99 (10.34)	2.706	10.87 (10.23)	2.704	10.74
2-Cl-phenol	2.998	12.34 (11.68)	2.997	12.34 (11.72)	2.995	11.65
2-Br-phenol	3.117	11.45 (10.86)	3.116	11.51 (10.96)	3.116	10.89
	G2MP2		G2		CBS-QB3	
	$r_{O...O}$	E_{HB}	$r_{O...O}$	E_{HB}	$r_{O...O}$	E_{HB}
2-F-phenol	2.718	11.22	2.718	11.19	2.722	11.47
2-Cl-phenol	3.024	12.47			3.003	13.01
2-Br-phenol	3.120	12.60			3.111	12.41
	Experimental					
	E_{HB} (Ref. 249)		E_{HB} (Ref. 264)		$\lambda(\text{cm}^{-1})$ (Ref. 264)	
2-F-phenol	6.82		–		3635	
2-Cl-phenol	6.82		14.27		3583	
2-Br-phenol	6.40		13.10		3562	
2-I-phenol	5.52		11.51		3538	

basis set, is suggested for correcting frequencies as well the zero point vibration energy [266]. Another error source is the vibration anharmonicity. It is well known, in fact, that in malonaldehyde the strong anharmonicity of the motion along the OH stretching coordinate and the mixing of this with other vibration modes make very difficult the interpretation of the broad band experimentally detected in the range between 2800 and 3100 cm^{-1} [267, 268], now fixed at 2856 cm^{-1} [269]. The most recent Gaussian computation package (Gaussian03) [122] allows calculations of the IR spectra taking into account the anharmonicity effects [270, 271] and it has given very good agreement between theoretical and experimental findings in the case of pyrrole and furan [272], azabenzene [273], uracil and 2-thiouracil [274].

Our most recent calculations on malonaldehyde [159] gave excellent agreement with experiment without using scale factors (Table 5). The OH frequency

Table 5. Calculated (B3LYP/6311++G(d,p) and experimental IR frequencies (cm^{-1}) of malonaldehyde (reprinted from Ref. 159 with permission from Elsevier)

$\nu_{\text{harm}}^{\text{a}}$	$\nu_{\text{anharm}}^{\text{a}}$	$\nu_{\text{exp}}^{\text{b}}$	ν_{harm}	ν_{anharm}	$\nu_{\text{exp}}^{\text{b}}$
3214 (3163) C ₃ H	3086 (3012)	3040	999	993	998
3206 (3226) OH + C ₄ H	2810 (2798) ^c	2856	892	880	890
3154 (3116) C ₄ H + OH	2881 (2870)	2960	517	517	512
2973 (2955) C ₂ H	2802 (2752)	2858	269	255	282
1695 (1664)	1654 (1617)	1655	1037	1028	1028
1619 (1571)	1570 (1498)	1593	1009	998	981
1473 (1462)	1443 (1423)	1452	900	931	873
1400	1367	1358	786	769	766
1392	1314	1346	392	404	384
1287	1266	1260	284	294	252
1115	1103	1092			

^a Values in parentheses refer to water solution (where the coupling with the C₄H vibration is practically absent). ΔG_{solv} is 17.7 and 52.8 kJ/mol, for the chelate and open conformations, respectively. E_{HB} decreases from 54.1 to 16.5 kJ/mol on going from vacuum to aqueous solution

^b Ref. 269

^c In solution 3426 cm^{-1} (harmonic) and 3128 cm^{-1} (anharmonic)

(2810 cm^{-1}) agrees rather well with the value of 2832.7 cm^{-1} [275] obtained after anharmonicity correction by the vibrational-self-consistent-field (VSCF) method, with that of 2825 cm^{-1} obtained by the two-dimensional potential energy surface function of Tayyari et al. [276], and with the four-dimensional model study of Došlić and Kühn [277]. The entity of the anharmonicity effect is in the range of 500 cm^{-1} . Less good agreement exists for the amino group frequencies of malonamide (keto conformation).

A recent paper on [233] thioacetylacetone at cc-pVTZ level of calculations showed that in this molecule the anharmonicity effect is about 600 cm^{-1} and the OH stretching frequency of the enol conformation shifts from 2862 to 2188 cm^{-1} , whereas the vapour experimental value is 2500 cm^{-1} . In any case we think that future IR spectra calculations must necessarily be carried out following the anharmonic model, even if they are much more onerous than the harmonic ones, especially if correlation at MP2 level is taken into account.

7 HYDROGEN BONDS AND ν_{OH} IN SOLUTION

In solution the chemical–physical properties of a molecule can be very different than in gas phase, being strictly connected to the solute–solvent interactions, which, in turn, are highly depending on the solute and solvent polarity, dispersion forces and so on (solvent effect). One of the resulting consequences is the weakening of the hydrogen bond and the shift of the *keto* \leftrightarrow *enol* tautomeric equilibrium towards the *keto* form on increasing the dipole moment of the solvent.

The theoretical description of the solute–solvent interactions is not simple. Two self-consistent reaction field (SCRF) methods are mainly used for predicting the effect of the solvent on the solute molecule properties: the Onsager model [278] and the polarized continuum model (PCM-SCRF) initially devised by Tomasi and coworkers [279–281] and progressively implemented by Barone et al. (see, e.g., references in the G03 User’s Reference accompanying the G03 program). In both approaches the solute molecule is placed into a cavity. In the former model the cavity is spherical and the solvent is approximated to a homogeneous polarizable medium having a constant dielectric permittivity, whereas the solute molecular charge distribution is treated approximately as an electric dipole located at the cavity centre. Problems affecting the results are the choice of the cavity radius and the fact that most molecules (especially the planar ones) are far from the spherical form. Moreover, a system having no permanent dipole moment will not exhibit solvent effects. In the PCM model, the cavity is formed by the envelope of spheres centred on each atom or on the atomic groups [282–284], so that it is modelled on the solute shape. Inside the cavity the dielectric constant is the same as in the vacuum whereas outside it is that of the selected solvent. Specific solute–solvent effects are not taken into account at this level of calculations. The UAHF (United Atom for Hartree–Fock) radii are recommended for the molecular cavity building [285, 286].

Results obtained at various levels of calculations on a wide variety of compounds evidence modest changes of bond lengths and bond angles on passing from vacuum to solution, but the hydrogen bond strength reduces progressively on increasing the solvent permittivity. In water ($\epsilon = 78.4$), E_{HB} is predicted to be, on an average, about 50–60% lower than in gas phase [159, 187–190]. From Raman spectra it was deduced that the weak intramolecular hydrogen bond of catechol disappears in water, ethanol and acetone solutions [287]. Solvent specific effects do not produce remarkable change in the hydrogen bond strength [159]. Addition of 1–4 water molecules variously located in the neighbouring of the catechol groups of 4-nitro-catechol has not modified the relative stability of its three possible conformations with respect to vacuum [288]. B3LYP/6-311G(d,p) results concerning several push–pull conjugated compounds predict that, on passing from vacuum to carbon tetrachloride, the OH stretching mode frequency increases slightly if the hydrogen bond occurs with an oxygen atom and decreases when the bonds occurs with a nitrogen atom [289]; in any case, analogously to E_{HB} , also the $\Delta\nu$ values are bound to the solvent polarity and permittivity. Recent B3LYP/6-311++G(d,p) calculations in water solution predict a $\Delta\nu$ of $+20\text{ cm}^{-1}$ with respect to vacuum for the harmonic OH stretching mode of malonaldehyde (-12 cm^{-1} if anharmonicity is taken into account, see Table 5) and -10 cm^{-1} for the same harmonic mode of nitromalonamide [159].

Also the rotation barriers are predicted to decrease on going from gas phase to solution. Some of them concerning the OH and the nitro group are reported in Table 6.

Table 6. OH and NO₂ rotation barriers (kJ/mol) in some malonaldehyde derivatives (B3LYP/6-311++G(d,p)), (Table 10 in Ref. 159, partially reprinted with permission from Elsevier)

	OH Barrier		NO ₂ Barrier	
	Gas phase	Aqueous solution	Gas phase	Aqueous solution
3-Nitro-malonaldehyde	89.95	63.05	35.32	33.07
Malonamide C _s	87.78	58.69	–	–
Nitromalonamide C _s	117.81	60.92	74.40	58.89
NO ₂ rotated by 90°	85.38	56.27	–	–
Nitromalonamide C _{2v}	–	–	79.45	63.55

8 INTRAMOLECULAR HYDROGEN BONDS IN CALIXARENES

Calixarenes are a fascinating class of cyclooligomers having three-dimensional concave surface and relatively rigid structure. Their name derives just from their calyx-form (but various other suggestive forms can be properly constructed) able to act as a host for other molecules (e.g., fullerenes, ions and so on) and have assumed capital importance for their use in analytic chemistry (where are used as ion-selective electrode and electrochemical as well as optical sensors) [290], medicine and other fields. In medicine they assume particular importance because can be used in cancer treatments as non-toxic molecules to carry a toxic payload to the cancer cells.

A simple calixarene built up with four phenol units linked via methylene bridges is shown in Fig. 10 (substitution of the methylene junctions with S atoms gives rise to the class of thiocalixarenes). Cooperative networks of intramolecular hydrogen bonds (circular array of hydrogen bonds, observed also in cyclodextrins) play a capital role in the cavity shape as well as in the conformational features of the macrocyclic skeleton [291–293]. Encapsulation of other molecules in the cavity is also controlled by hydrogen bonds [294].

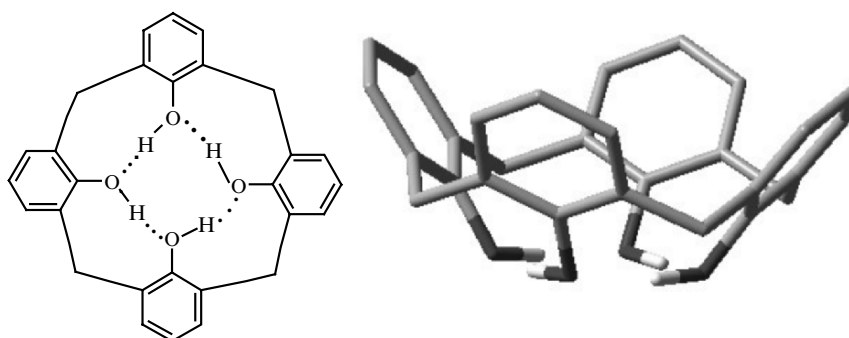


Figure 10. Molecular scheme of calix[4]arene and its spatial shape.

Although E_{HB} values are lacking, IR and $^1\text{H-NMR}$ spectra give clear evidence of hydrogen bond presence in calix[n]arenes. The frequency of the OH stretching mode ranges from $\sim 3150\text{ cm}^{-1}$ for the cyclic tetramer to ~ 3300 for the cyclic pentamer and in the range of $2700\text{--}3000\text{ cm}^{-1}$ in N-benzyl substituted homoazacalixarenes, where a rather strong O–H \cdots N bridge is present, as revealed also by the $^1\text{H-NMR}$ spectra low-field shifted OH signals (10.7–11.6 ppm) [295]. In the cone conformer of calix[4]arene, optimized at B3LYP/6-31G** level of calculation, $r_{\text{O-H}} = 0.991\text{ \AA}$, $r_{\text{O-O}} = 2.645\text{ \AA}$ and $\delta_{\text{O}\cdots\text{H-O}} = 164.6^\circ$ were predicted [296]. In the same paper the temperature dependence of the hydrogen bond array flip-flop was studied and an activation enthalpy of 36.8 kJ/mol was found, whilst the average activation energy per single hydrogen bond is 11.5–11.9 kJ/mol (the hydroxyl ^1H chemical shift is 10.2 ppm). The OH stretching mode vibration band was found at 3173 cm^{-1} (CCl_4 solution) and shifts at 3310 cm^{-1} in the corresponding thioxacalixarene [297], so evidencing a weakening of the cooperative H bond in thiocalixarenes, attributable to an increase of the macrocyclic size when sulphide bridges replace the methylene ones and/or to the formation of bifurcated O–H \cdots S hydrogen bonds. The cumulative strength of the hydrogen bond array decreases also in calix[5]arenes and higher membered rings. A mention is due to the head-to-tail hydrogen-bonded belt, formed by intramolecular C=O \cdots HN hydrogen bonds observed along the wide rim of urea functionalized resorcinarenes [298].

Finally, even though the matter is beyond the aim of the present topic, a short mention is due to pseudorotaxanes, rotaxanes, catenanes and similar compounds (Refs. 299–303 and therein), to which conventional and/or unconventional hydrogen bridges confer peculiar characteristics making them extremely important in supramolecular and nanotechnologies chemistry for constructing molecular machines.

9 CONCLUSIONS

The present survey of hydrogen bonds in general and intramolecular hydrogen bonds in particular opens a breathtaking panorama of fascinating problems difficult to solve but not covering the entire field of the wide hydrogen bond world. The statement that a hydrogen bond exists each time the X \cdots Y and H \cdots Y distances are shorter than the sum of the van der Waals radii of the involved atoms could be necessary but not sufficient when one is on the border line of their limit values. In particular, when E_{HB} is very low can we still say that there is a hydrogen bond or the result is only the balance of casual attractive and repulsive interactions? The location of bond critical points, atomic interaction lines, bond paths and so on, following the AIM method, gives substantial help in replying to this question. However, in the case of intramolecular hydrogen bonds the main problem is to establish a well-defined E_{HB} scale, i.e., to find a well-defined hydrogen bond free reference point, or any other something, representing the zero point in the E_{HB} scale, as much possible

independent of the nature of the hydrogen bond and of the class of compounds one is examining. Only under this condition a significant comparison between the strengths of the hydrogen bridges of different compounds can be possible. An energy partition to identify the main terms contributing to the strength of the bridge could be a probable direction, but the additivity of the various possible but interdepending energy terms is to be demonstrated. Archimedes said: “give me a place to stand and I’ll move the world”. Well, for us the *place to stand* is an absolute and universal definition of the zero point in the intramolecular E_{HB} scale. We are aware that the solution of this problem is a very hard task, but, to make the situation less serious than it is and to hold out hope, we must remember the definition of “invention”: *invention is something that all people considered impossible to realize, until a person who was not informed about this dogma, created it.*

ACKNOWLEDGMENTS

The author greatly acknowledges Elsevier Ltd. for permission of reprinting some figures and tables from Refs. 158, 159 and 189.

Financial support from the Italian Ministero dell’Istruzione, dell’Università e della Ricerca (MIUR), Roma, and from the University of Catania is also gratefully acknowledged.

REFERENCES

1. Berzelius, J.J., Essay on the cause of chemical proportions, and on some circumstances relating to them: together with a short and easy method of expressing them, *Ann. Philos.*, **2**, 443–454 (1813).
2. Couper, A.S., On a new chemical theory, *Philos. Mag.*, **16**, 104–116 (1858). Available on Internet at <http://web.lemoyne.edu/~giunta/couper/couper.html>.
3. Details at the internet address:- www.chemheritage.org/classroom/chemach/chemsynthesis/, or, search Archibald Scott Couper and August Kekulé von Stradonitz.
4. Bhat, R.G., and Gudihal, R., Dots, dashes and hydrogen bonds, *Curr. Science*, **85**, 839 (2003).
5. Huggins, M.L., Hydrogen bridges in organic compounds, *J. Org. Chem.*, **1**, 407–456 (1936).
6. Latimer, W.M., and Rodebush, W.H., Polarity and ionization from the standpoint of the Lewis theory of valence, *J. Am. Chem. Soc.*, **42**, 1419–1433 (1920).
7. Huggins, M.L., Atomic structure, *Science*, **55**, 459–60 (1922).
8. Huggins, M.L., Electronic structure of atoms, *J. Phys. Chem.*, **26**, 601–625 (1922).
9. Huggins, M.L., Atomic radii. I, *Phys. Rev.*, **19**, 346–353 (1922).
10. Jeffrey, G.A., and Saenger, W., *Hydrogen bonding in biological structures*, Springer, Berlin, 1991.
11. Jeffrey, G.A., *An introduction to hydrogen bonding*, Oxford University Press, New York, 1997.
12. Desiraju, G., and Steiner, T., *The weak hydrogen bond in structural chemistry and biology*, Oxford University Press, Oxford 1999.
13. Weinhold, F., Nature of H-bonding in clusters, liquids and enzymes: an ab initio, natural bond orbital perspective, *J. Mol. Struct.: Theochem*, **398–399**, 181–197 (1997).
14. Kojić-Prodić, B., Štefanić, Z., and Žinić, M., Hydrogen bonding and molecular assemblies, *Croat. Chem. Acta*, **77**, 415–425 (2004).

15. Nangia, A., Organic nanoporous structures, *Curr. Opin. Solid State Mat. Sci.*, **5**, 115–122 (2001).
16. Vicente, V., Martin, J., Jiménez-Barbero, J., Chiara, J.L., and Vicent, C., Hydrogen-bonding cooperativity: using an intramolecular hydrogen bond to design a carbohydrate derivative with a cooperative hydrogen-bond donor centre, *Chem. Eur. J.*, **10**, 4240–4251 (2004).
17. Luisi, B., Orozco, M., Sponer, J., Luque, F.J., and Shakked Z., On the potential role of the amino nitrogen atom as a hydrogen bond acceptor in macromolecules, *J. Mol. Biol.*, **279**, 1123–1136 (1998).
18. Casadesús, R., Moreno, M., González-Lafont, Á., Lluch, J.M., and Repasky, M.P., Testing electronic structure methods for describing intermolecular H \cdots H interactions in supramolecular chemistry, *J. Comput. Chem.*, **25**, 99–105 (2004).
19. Ramon, V., Hydrogen-bonding templated assemblies, *Struct. Bonding (Berlin)*, **111**, 85–137 (2004).
20. Schuster, P., and Wolschann, P., Hydrogen bonding: from small clusters to biopolymers, *Monatsh. Chem.*, **130**, 947–960 (1999).
21. Katrusiak, A., Macroscopic and structural effects on hydrogen bond transformation, *Crystallogr. Rev.*, **9**, 91–133 (2003).
22. Huggins, M.L., 50 Years of hydrogen bond theory, *Angew. Chem. Int. Ed.*, **10**, 147–151 (1971).
23. Sándorfy, C., Hydrogen bonding and anaesthesia, *J. Mol. Struct.*, **708**, 3–5 (2004).
24. Miller, K.W., The nature of sites of general anaesthetic action, *Brit. J. Anaesth.*, **89**, 17–31 (2002).
25. Liu, R., Pidikiti, R., Ha, C.-E., Petersen, C.E., Bhagavan, N.V., and Eckenhoff, R.G., The role of electrostatic interactions in human serum albumin binding and stabilization by halothane, *J. Biol. Chem.*, **277**, 36373–36379 (2002).
26. Emsley, J., Ma Lewina, Y.Y., Hursthouse, M.B., Karaulov, S.A., and Motevalli, M., β -Diketone interactions. Part 11. The hydrogen bonded adduct 4,6-dimethylpyrimidin-2-one-urea (DMP.U) from the reaction of pentane-2,4-dione and urea, *J. Chem. Soc. Perkin Trans. 2*, 1077–1080 (1990).
27. Buemi, G., 4,6-Dimethylpyrimidin-2-one-urea adduct: ab initio and semi-empirical study of the intermolecular hydrogen bonding, *Boll. Acc. Gioenia Sci. Nat., Catania*, **26**, 309–322 (1993).
28. Norrestam, R., von Glehn, M., and Wachtmeister, C.A., Three-dimensional structure of usnic acid, *Acta Chem. Scand. Ser. B*, **28**, 1149–1152 (1974).
29. Buemi, G., and Zuccarello, F., Molecular conformations, hydrogen bond strengths and electronic structure of usnic acid. An AM1 and CNDO/S study, *J. Mol. Struct.: Theochem*, **209**, 89–99 (1990).
30. Gilli, G., Bellucci, F., Ferretti, V., and Bertolasi, V., Evidence for resonance-assisted hydrogen bonding from crystal–structure correlations on the enol form of β -diketone fragment, *J. Am. Chem. Soc.*, **111**, 1023–1028 (1989).
31. Gilli, G., and Gilli, P., Towards an unified hydrogen-bond theory, *J. Mol. Struct.*, **552**, 1–15 (2000).
32. Alkorta, I., Rozas, I., and Elguero, J., Non-conventional hydrogen bonds, *Chem. Soc. Rev.*, **27**, 163–170 (1998).
33. Sutor, D.J., The C–H \cdots O hydrogen bond in crystals, *Nature*, **195**, 68–69 (1962).
34. Sutor, D.J., Evidence for the existence of C–H \cdots O hydrogen bonds in crystals, *J. Chem. Soc.*, 1105–110 (1963).
35. Glasstone, S., The structure of some molecular complexes in the liquid phase, *Trans. Faraday Soc.*, **33**, 200–214 (1937).
36. Dippy, J.F., The dissociation constants of monocarboxylic acids; their measurement and their significance in theoretical organic chemistry, *Chem. Rev.*, **25**, 151–211 (1939).
37. Richardson, T.B., de Gala, S., and Crabtree, R.H., Unconventional hydrogen bonds: intermolecular B–H \cdots H–N interactions, *J. Am. Chem. Soc.*, **117**, 12875–12876 (1995).

38. Lee, J.C., Peris, E., Rheingold, A.L., and Crabtree, R.H., An unusual type of H \cdots H interaction: Ir–H \cdots H–O and Ir–H \cdots H–N hydrogen bonding and its involvement in σ -bond metathesis, *J. Am. Chem. Soc.*, **116**, 11014–11019 (1994).
39. Park, S., Ramachandran, R., Lough, A.J., and Morris, R.H., A new type of intramolecular H \cdots H \cdots H interaction involving N–H \cdots H(Ir) \cdots H–N atoms. Crystal and molecular structure of [IrH(η^1 –SC₅H₄NH) $2(\eta^2$ –SC₅H₄N) (PCy₃)]BF₄–072CH₂Cl₂, *J. Chem. Soc. Chem. Commun.*, 2201–2202 (1994).
40. Peris, E., Lee, J.C., Rambo, J.R., Eisenstein, O., and Crabtree, R.H., Factors affecting the strength of X–H \cdots H–M hydrogen bonds, *J. Am. Chem. Soc.*, **117**, 3485–3491 (1995).
41. Epstein, L.M., and Shubina, E.S., New types of hydrogen bonding in organometallic chemistry, *Coordin. Chem. Rev.*, **231**, 165–181 (2002).
42. Epstein, L.M., Belkova, N.V., Gutsul, E.I., and Shubina, E.S., Spectral features of unconventional hydrogen bonds and proton transfer to transition metal hydrides, *Polish. J. Chem.*, **77**, 1371–1383 (2003).
43. Custelcean, R., and Jackson, J., Dihydrogen bonding: structures, energetics and dynamics, *Chem. Rev.*, **101**, 1963–1980 (2001).
44. Popelier, P.L.A., Characterization of a dihydrogen bond on the basis of the electron density, *J. Phys. Chem. A*, **102**, 1873–1878 (1998).
45. Li, J., Zhao, F., and Jing, F., B–H δ – σ bond as dihydrogen bond acceptor: some theoretical observation and predictions, *J. Chem. Phys.*, **116**, 25–32 (2002).
46. Kar, T., and Scheiner, S., Comparison between hydrogen and dihydrogen bonds among H₃BNH₃, H₂BNH₂ and NH₃, *J. Chem. Phys.*, **119**, 1473–1482 (2003).
47. Meng, Y., Zhou, Z., Duan, C., Wang, B., and Zhong, Q., Non-conventional hydrogen bonding interaction of BH₃NH₃ complexes: a comparative theoretical study, *J. Mol. Struct.: Theochem*, **713**, 135–144 (2005).
48. Hobza, P., and Špirko, V., Anti-hydrogen bond in the benzene dimer and other carbon proton donor complexes, *J. Phys. Chem. A*, **102**, 2501–2504 (1998).
49. Van der Veken, B.J., Herrebout, W.A., Szostak, R., Shchepkin, D.N., Havlas, Z., and Hobza, P., The nature of improper blue-shifting hydrogen bonding verified experimentally, *J. Am. Chem. Soc.*, **123**, 12290–12293 (2001).
50. Hobza, P., Špirko V., Havlas, Z., Buchhold, K., Reimann, B., Barth, H.-D., and Brutschy, B., Anti-hydrogen bond between chloroform and fluorobenzene, *Chem. Phys. Lett.*, **299**, 180–186 (1999).
51. Lu, P., Liu, G.-Q., and Li, J.-C., Existing problems in theoretical determination of red-shifted or blue-shifted hydrogen bond, *J. Mol. Struct.: Theochem*, **723**, 95–100 (2005).
52. Scheiner, S., Gu, Y., and Kar, T., Evaluation of the H-bonding properties of the CH \cdots O interactions based upon NMR spectra, *J. Mol. Struct.: Theochem*, **500**, 441–452 (2000).
53. Gu, Y., Kar, T., and Scheiner, S., Fundamental properties of the CH \cdots O interaction: is it a true hydrogen bond? *J. Am. Chem. Soc.*, **121**, 9411–9422 (1999).
54. Desiraju, G.R., The C–H \cdots O bond: structural implications and supramolecular design, *Acc. Chem. Res.*, **29**, 441–449 (1996).
55. Chandra, A.K., and Nguyen, M.T., Quantum chemical study of the hydrogen bonded C₄H₂ \cdots HCl complex, *J. Chem. Res. Synop.*, 216–217 (1997).
56. Allen, F.H., Hoy, V.J., Howard, J.A.K., Thalladi, V.R., Desiraju, G.R., Wilson, C.C., and McIntyre, G.J., Crystal engineering and correspondence between molecular and crystal structures. Are 2- and 3-aminophenols anomalous? *J. Am. Chem. Soc.*, **119**, 3477–3480 (1997).
57. Sumathi, R., and Chandra, A.K., Quantum chemical study of hydrogen-bonded CH₂ = C = O \cdots HX and CH₂ = C = CH₂ \cdots HX (X=Cl, F) complexes, *Chem. Phys. Lett.*, **271**, 287–295 (1997).
58. Grabowski, S.J., Simulation of the orthorhombic crystal structure of acetylene using atom-atom potential calculations, *J. Chem. Res. Synop.*, 534–535 (1996).

59. Grabowski, S.J., and Wilamowski, J., Synthesis, crystal structure and intramolecular interactions of 2-methyl-3-(2-methylphenyl)but-1-ene-1,1-dicarbonitrile (MMBD), *Austr. J. Chem.*, **49**, 951–954 (1996).
60. Philp, D., and Robinson, J.M.A., A computational investigation of cooperativity in weakly hydrogen-bonded assemblies, *J. Chem. Soc. Perkin Trans. 2*, 1643–1650 (1998).
61. Grabowski, S.J., Study of correlations for dihydrogen bonds by quantum-chemical calculations, *Chem. Phys. Lett.*, **312**, 542–547 (1999).
62. Grabowski, S.J., Theoretical evidence for a new kind of intramolecular dihydrogen bond, *Chem. Phys. Lett.*, **327**, 203–208 (2000).
63. Grabowski, S.J., High level ab initio calculations of dihydrogen-bonded complexes, *J. Phys. Chem. A*, **104**, 5551–5557 (2000).
64. Palusiak, M., and Grabowski, S.J., Are the O–H···H–C intramolecular systems of 2-cyclopropyl ethanol and its derivatives classified as dihydrogen bonds? Ab initio and DFT study, *J. Mol. Struct.: Theochem*, **674**, 147–152 (2004).
65. Rozas, I., Alkorta, I., and Elguero, J., Inverse hydrogen-bonded complexes, *J. Phys. Chem. A*, **101**, 4236–4244 (1997).
66. Steiner, S., The hydrogen bond in the solid state, *Angew. Chem. Int. Ed.*, **41**, 48–76 (2002).
67. Grabowski S.J., Sokalski, W.A., and Leszczynski, J., Is a $\pi \cdots H^+ \cdots \pi$ complex hydrogen bonded? *J. Phys. Chem. A*, **108**, 1806–1812 (2004).
68. Tsurusawa, T., and Iwata, S., Electron-hydrogen bonds and OH harmonic frequency shifts in water cluster complexes with a group I metal atom, $M(H_2O)_n$ ($M = Li$ and Na), *J. Chem. Phys.*, **112**, 5705–5710 (2000).
69. Hao, X.-Y., Li, Z.-R., Wu, D., Wang, Y., Li, Z.-S., and Sun, C.-C., A theoretical prediction on intermolecular mono-electron dihydrogen bond $H \cdots e \cdots H$ in the cluster anion $(FH)_2\{e\} \cdots (HF)_2$, *J. Chem. Phys.*, **118**, 83–86 (2003).
70. Hao, X.-Y., Li, Z.-R., Wu, D., Wang, Y., Li, Z.-S., and Sun, C.-C., The evolution of the mono-electron dihydrogen bond $H \cdots e \cdots H$ in the symmetric and asymmetric cluster anions $(FH)_n\{e\} \cdots (HF)_n$, *J. Chem. Phys.*, **118**, 10939–10943 (2003).
71. Wang, B.-Q., Li, Z.-R., Wu, D., Hao, X.-Y., Li, R.-J., and Sun, C.-C., Single-electron hydrogen bonds in the methyl radical complexes $H_3C \cdots HF$ and $H_3C \cdots HCCH$: an ab initio study, *Chem. Phys. Lett.*, **375**, 91–95 (2003).
72. Li, Y., Li, Z.-R., Wu, D., Li, R.-Y., Hao, X.-Y., and Sun, C.-C., An ab initio prediction of the extraordinary static first hyperpolarizability for the electron solvated cluster $(FH)_2\{e\} \cdots (HF)$, *J. Phys. Chem. B*, **108**, 3145–3148 (2004).
73. Chen, W., Li, Z.-R., Wu, D., Gu, F.-L., Hao, X.-Y., Wang, B.-Q., Li, R.-J., and Sun, C.-C., The static polarizability and first hyperpolarizability of the water trimer anion: ab initio study, *J. Chem. Phys.*, **121**, 10489–10494 (2004).
74. Bader, R.F.W., *Atoms in molecules. A quantum theory*, Clarendon, Oxford, 1990.
75. Bader, R.F.W., A quantum theory of molecular structure and its applications, *Chem. Rev.*, **91**, 893–928 (1991).
76. Bader, R.F.W., Principle of stationary action and the definition of a proper open system, *Phys. Rev. B*, **49**, 13348–13356 (1994).
77. Koch, U., and Popelier, P.L.A., Characterization of C–H–O hydrogen bonds on the basis of the charge density, *J. Phys. Chem.*, **99**, 9747–9754 (1995).
78. Popelier, P.L.A., Characterization of dihydrogen bond on the basis of the electron density, *J. Phys. Chem.*, **102**, 1873–1878 (1998).
79. Popelier, P.L.A., *Atoms in molecules. An introduction*, Prentice, Pearson Education, Essex, England, 2000.
80. Program MORPHY, written from scratch by Popelier, P.L.A., available via plapl100@cus.cam.ac.uk.

81. Program PROAIM, Biegler-König, Bader, R.F.W., and Tang, T.-H., Calculation of the average properties of atoms in molecules. II, *J. Comput. Chem.*, **3**, 317–328 (1982); modified by Keit, T.A., and Cheeseman J.R.
82. Liepins, E., Petrova, M.V., Gudriniece, E., Paulins, J., and Kuznestov, S.L., Relationships between ^1H , ^{13}C and ^{17}O NMR chemical shifts and H/D isotope effects on ^{13}C and ^{17}O nuclear shielding in intramolecular hydrogen bonded systems, *Magn. Res. Chem.*, **27**, 907–915 (1989).
83. Berglund, B., and Vaughan, R.W., Correlations between proton chemical shift tensors, deuterium quadrupole couplings and bond distances to hydrogen bonds in solids, *J. Chem. Phys.*, **73**, 2037–2043 (1980).
84. Jeffrey, G.A., and Yeon, Y., The correlation between hydrogen-bond lengths and proton chemical shifts in crystals, *Acta Crystallogr. Sect. B*, **42**, 410–413 (1986).
85. Kumar, G.A., and McAllister, M.A., Theoretical investigation of the relationship between proton NMR chemical shift and hydrogen bond strength, *J. Org. Chem.*, **63**, 6968–6972 (1998).
86. Bertolasi, V., Gilli, P., Ferretti, V., and Gilli, G., Intramolecular O–H...O hydrogen bonds assisted by resonance. Correlation between crystallographic data and ^1H NMR chemical shifts, *J. Chem. Soc. Perkin Trans. 2*, 945–952 (1997).
87. Benedict, H., Limbach, H.-H., Wehlan, M., Fehlhammer, W.-P., Golubev, N.S., and Janoschek, R., Solid state ^{15}N NMR and theoretical studies of primary and secondary geometric H/D isotope effects on low-barrier NHN-hydrogen bonds, *J. Am. Chem. Soc.*, **120**, 2939–2950 (1998).
88. Sack, I., Goldbourn, A., Vega, S., and Buntkowsky, G., Deuterium REDOR: principles and applications for distance measurements, *J. Magn. Res.*, **138**, 54–65 (1999).
89. Kawahara, S.-I., Kojima, C., Taira, K., and Uchimaru, T., A theoretical study of correlation between hydrogen bond stability and J-coupling through a hydrogen bond, *Helv. Chim. Acta*, **86**, 3265–3273 (2003).
90. Emmler, T., Gieschler, S., Limbach, H.H., and Buntkowsky, G., A simple method for the characterization of OHO-hydrogen bonds by ^1H -solid state NMR spectroscopy, *J. Mol. Struct.*, **700**, 29–38 (2004).
91. Jug, K., On the development of semiempirical methods in the MO formalism, *Theor. Chim. Acta*, **14**, 91–135 (1968).
92. Jaffè, H.H., All-valence-electron semiempirical self-consistent field calculations, *Acc. Chem. Res.*, **2**, 136–143 (1969).
93. Hückel, E., Quantum-theoretical contributions to the benzene problem. I. The electron configuration of benzene and related compounds, *Z. Physik.*, **70**, 204–286 (1931).
94. Hückel, E., Quantum theoretical contributions to the problem of aromatic and non-saturated compounds. III, *Z. Physik.*, **76**, 628–648 (1932).
95. Hückel, E., Theory of free radicals of organic chemistry, *Trans. Faraday Soc.*, **30**, 40–52 (1934).
96. Hoffmann, R., An extended Huckel theory. I. Hydrocarbons, *J. Chem. Phys.*, **39**, 1397–1412 (1963).
97. Pople, J.A., Santry, D.P., and Segal, G.A., Approximate self-consistent molecular orbital theory. I. Invariant procedures, *J. Chem. Phys.*, **43**, S129–S135 (1965).
98. Pople, J.A., Beveridge, D.L., and Dobosh, P.A., Approximate self consistent molecular-orbital theory. V. Intermediate neglect of differential overlap, *J. Chem. Phys.*, **47**, 2026–2033 (1967).
99. Baird, N. Colin, Modified SCF-MO method for pi electrons. Neglect of nonbonded differential overlap, *Mol. Phys.*, **18**, 39–47 (1970).
100. Diner, S., Malrieu, J.P., and Clavarie, P., Localized bond orbitals and the correlation problem. I. Perturbation calculation of ground state energy, *Theor. Chim. Acta*, **13**, 1–17 (1969).
101. Malrieu, J.P., Clavarie, P., and Diner, S., Localized bond orbitals and the correlation problem. II. Application to π -electron systems, *Theor. Chim. Acta*, **13**, 18–45 (1969).
102. Burkert, U., and Allinger, N.L., Molecular mechanics, ACS Monograph 177, Am. Chem. Soc. Washington, D.C., 1982.

103. Allinger, N.L., Chen, K., and Lii, J.-H., An improved force field (MM4) for saturated hydrocarbons, *J. Comp. Chem.*, **17**, 642–668 (1996).
104. Momany, F.A., McGurie, R.F., Burgess, A.W., and Scheraga, H.A., Energy parameters in polypeptides. VII. Geometric parameters, partial atomic charges, nonbonded interactions and intrinsic torsional potentials for the naturally occurring amino acids, *J. Phys. Chem.*, **79**, 2361–2381 (1975).
105. Bingham, R.C., Dewar, M.J.S., and Lo, D.H., Ground state of molecules. XXV. MINDO/3. An improved version of the MINDO semiempirical SCF-MO method, *J. Am. Chem. Soc.*, **97**, 1285–1293 (1975).
106. Dewar, M.J.S., and Thiel, W., Ground state of molecules. 38. The MNDO method, *J. Am. Chem. Soc.*, **99**, 4899–4907 (1977).
107. Dewar, M.J.S., and Thiel, W., Ground state of molecules. 39. MNDO results for molecules containing hydrogen, carbon, nitrogen, and oxygen, *J. Am. Chem. Soc.*, **99**, 4907–4917 (1977).
108. Thiel, W., The MNDOC method, a correlated version of the MNDO model, *J. Am. Chem. Soc.*, **103**, 1413–1420 (1981).
109. Dewar, M.J.S., Zoebisch, E.G., Healy, E.F., and Stewart, J.J.P., AM1: a new general purpose quantum mechanical molecular model, *J. Am. Chem. Soc.*, **107**, 3902–3909 (1985).
110. Stewart, J.J.P., Optimization of parameters for semiempirical methods. I. Method, *J. Comp. Chem.*, **10**, 209–220 (1989).
111. Stewart, J.J.P., Optimization of parameters for semiempirical methods. II. Applications, *J. Comp. Chem.*, **10**, 221–264 (1989).
112. Vendrame, R., Coluci, V.R., and Galvão, D.S., Comparative parametric method 5 (PM5) study of *trans*-stilbene, *J. Mol. Struct.: Theochem*, **686**, 103–108 (2004).
113. Bolcer, J.D., and Hermann, R.B., The development of computational chemistry in the United States, *Rev. Comput. Chem. vol. 5, p. 1*, Lipkowitz, K.B., and Boyd, D.B. Editors. VCH Publishers Inc., New York, 1994.
114. Burstein, K. Ya., and Isaev, A., MNDO calculations on hydrogen bonds. Modified function for core–core repulsion, *Theor. Chimica Acta*, **64**, 397–401 (1984).
115. Rios, M.A., and Rodríguez, J., Semiempirical study of compounds with OH–O intramolecular hydrogen bond, *J. Comput. Chem.*, **13**, 860–866 (1992).
116. Koller, J., Harb, V., Hodoscek, M., and Hadzi, D., MNDO and MNDO/H calculations on hydrogen bonds. A comparison with ab initio and CNDO/2 methods, *J. Mol. Struct.: Theochem*, **23**, 343–350 (1985).
117. Koller, J., and Hadzi, D., MNDO/H and AM1 calculations on the formic acid-methylamine complexes, *J. Mol. Struct.: Theochem*, **59**, 533–541 (1989).
118. Rodríguez, J., Semiempirical study of compounds with intramolecular O–H···O hydrogen bonds. II. Further verification of a modified MNDO method, *J. Comput. Chem.*, **15**, 183–189 (1994).
119. Casadesús, R., Moreno, M., González-Lafont, Á., Lluch, J.M., and Repasky, M.P., Testing electronic structure methods for describing intermolecular H···H interactions in supramolecular chemistry, *J. Comp. Chem.*, **25**, 99–105 (2004).
120. Stewart, J.J.P., Comparison of the accuracy of semiempirical and some DFT methods for predicting heats of formation, *J. Mol. Model.*, **10**, 6–12 (2004).
121. Stewart, J.J.P., MOPAC 2002, Fujitsu Limited, Tokyo, Japan (<http://www.cachesoftware.com/mopac/index.shtml>).
122. Frisch, M.J., Trucks, G.W., Schlegel, H.B., Scuseria, G.E., Robb, M.A., Cheeseman, J.R., Montgomery, J.A. Jr., Vreven, T., Kudin, K.N., Burant, J.C., Millam, J.M., Iyengar, S.S., Tomasi, J., Barone, V., Mennucci, B., Cossi, M., Scalmani, G., Rega, N., Petersson, G.A., Nakatsuji, H., Hada, M., Ehara, M., Toyota, K., Fukuda, R., Hasegawa, J., Ishida, M., Nakajima, T., Honda, Y., Kitao, O., Nakai, H., Klene, M., Li, X., Knox, J.E., Hratchian, H.P., Cross, J.B., Adamo, C., Jaramillo, J., Gomperts, R., Stratmann, R.E., Yazyev, O., Austin, A.J., Cammi, R., Pomelli, C., Ochterski, J.W., Ayala, P.Y., Morokuma, K., Voth,

- G.A., Salvador, P., Dannenberg, J.J., Zakrzewski, V.G., Dapprich, S., Daniels, A.D., Strain, M.C., Farkas, O., Malick, D.K., Rabuck, A.D., Raghavachari, K., Foresman, J.B., Ortiz, J.V., Cui, Q., Baboul, A.G., Clifford, S., Cioslowski, J., Stefanov, B.B., Liu, G., Liashenko, A., Piskorz, P., Komaromi, I., Martin, R.L., Fox, D.J., Keith, T., Al-Laham, M.A., Peng, C.Y., Nanayakkara, A., Challacombe, M., Gill, P.M.W., Johnson, B., Chen, W., Wong, M.W., Gonzalez, C., and Pople, J.A., *Gaussian 03*, Gaussian Inc., Pittsburgh PA, 2003 (<http://www.gaussian.com/>).
123. Schmidt, M.W., Baldridge, K.K., Boatz, J.A., Elbert, S.T., Gordon, M.S., Jensen, J.H., Koseki, S., Matsunaga, N., Nguyen, K.A., Su, S., Windus, T.L., Dupuis, M., and Montgomery, J.A. Jr., General atomic and molecular electronic structure system, *J. Comput. Chem.*, **14**, 1347–1363 (1993) (<http://www.msg.ameslab.gov/GAMESS/GAMESS.html>).
 124. Carpenter, J.E., Baker, J., Hehre, W.J., and Khan, S.D., Wavefunction Inc. (1980) Irvine, CA., The SPARTAN system (<http://www.wavefun.com>).
 125. Møller, C., and Plesset, M.S., Note on the approximation treatment for many-electron systems, *Phys. Rev.*, **46**, 618–622 (1934).
 126. Becke, A.D., Density-functional exchange energy approximation with correct asymptotic behavior, *Phys. Rev.*, **A38**, 3098–3100 (1988).
 127. Becke, A.D., Density-functional thermochemistry. III. The role of exact exchange, *J. Chem. Phys.*, **98**, 5648–5652 (1993).
 128. Lee, C., Yang, W., and Parr, R.G., Development of the Colle–Salvetti correlation energy formula into a functional of the electron density, *Phys. Rev.*, **B37**, 785–789 (1988).
 129. Xu, X., and Goddard, W.A. III., The X3LYP extended density functional for accurate descriptions of nonbond interactions, spin states, and thermochemical properties., *Proc. Natl. Acad. Sci. U.S.A.*, **101**, 2673–2677 (2004).
 130. Xu, X., and Goddard, W.A. III., Bonding properties of the water dimer: a comparative study of density functional theories, *J. Phys. Chem. A*, **108**, 2305–2313 (2004).
 131. Hariharan, P.C., and Pople, J.A., Influence of polarization functions on MO hydrogenation energies, *Theor. Chim. Acta*, **28**, 213–222 (1973).
 132. Dunning, T.H. Jr., Gaussian basis sets for use in correlated molecular calculations. I. The atoms boron through neon and hydrogen, *J. Chem. Phys.*, **90**, 1007–1023 (1989).
 133. Woon, D.E., and Dunning, T.H. Jr., Gaussian basis sets for use in correlated molecular calculations. IV. Calculation of static electrical response properties, *J. Chem. Phys.*, **100**, 2975–2988 (1994).
 134. Wilson, A.K., Woon, D.E., Peterson, K.A., and Dunning, T.H. Jr., Gaussian basis sets for use in correlated molecular calculations. IX. The atoms gallium through krypton, *J. Chem. Phys.*, **110**, 7667–7676 (1999).
 135. Curtiss, L.A., Raghavachari, K., Trucks, G.W., and Pople, J.A., Gaussian-2 theory for molecular energies of first and second-row compounds, *J. Chem. Phys.*, **94**, 7221–7230 (1991).
 136. Curtiss, L.A., Raghavachari, K., and Pople, J.A., Gaussian-2 theory using reduced Møller–Plesset orders, *J. Chem. Phys.*, **98**, 1293–1298 (1993).
 137. Curtiss, L.A., Raghavachari, K., Redfern, P.C., Rassolov, V., and Pople, A.J., Gaussian-3 (G3) theory for molecules containing first and second-row elements, *J. Chem. Phys.*, **109**, 7764–7776 (1998).
 138. Curtiss, L.A., Redfern, P.C., Rassolov, V., Kedziora, G., and Pople, J.A., Extension of Gaussian-3 theory to molecules containing third-row atoms K, Ca, Ga–Kr, *J. Chem. Phys.*, **114**, 9287–9295 (2001).
 139. Curtiss, L.A., and Raghavachari, K., Gaussian-3 and related methods for accurate thermochemistry, *Theor. Chem. Acc.*, **108**, 61–70 (2002).
 140. Curtiss, L.A., Redfern, P.C., Raghavachari, K., Rassolov, V., and Pople, A.J., Gaussian-3 theory using reduced Møller–Plesset order, *J. Chem. Phys.*, **110**, 4703–4709 (1999).

141. Curtiss, L.A., Redfern, P.C., Raghavachari, K., and Pople, A.J., Gaussian-3 theory: a variation based on third order perturbation theory and an assessment for the contribution of core-related correlation, *Chem. Phys. Lett.*, **313**, 600–607 (1999).
142. Baboul, A.G., Curtiss, L.A., Redfern, P.C., and Raghavachari, K., Gaussian-3 theory using density functional geometries and zero-point energies, *J. Chem. Phys.*, **110**, 7650–7657 (1999).
143. Montgomery, J.A. Jr., Ochterski, J.W., and Petersson, G.A., A complete basis set model chemistry. IV. An improved atomic pair natural orbital method, *J. Chem. Phys.*, **101**, 5900–5909 (1994).
144. Ochterski, J.W., Petersson, G.A., and Montgomery, J.A. Jr., A complete basis set model chemistry. V. Extensions to six or more heavy atoms, *J. Chem. Phys.*, **104**, 2598–2619 (1996).
145. Montgomery, J.A. Jr., Frisch, M.J., Ochterski, J.W., and Petersson, G.A., A complete basis set model chemistry. VI. Use of density functional geometries and frequencies, *J. Chem. Phys.*, **110**, 2822–2827 (1999).
146. Petersson, G.A., Tensfeldt, T.G., and Montgomery, J.A. Jr., A complete basis set model chemistry. III. The complete basis set-quadratic configuration interaction family of methods, *J. Chem. Phys.*, **94**, 6091–6101 (1991).
147. Pople, J.A., Head-Gordon, M., and Raghavachari, K., Quadratic configuration interaction. A general technique for determining electron correlation energies, *J. Chem. Phys.*, **87**, 5968–5975 (1987).
148. Petersson, G.A., and Al-Laham, M.A., A complete basis set model chemistry. II. Open-shell systems and the total energies of the first-row atoms, *J. Chem. Phys.*, **94**, 6081–6090 (1991).
149. Curtiss, L.A., Raghavachari, K., Redfern, P.C., and Pople, J.A., Gaussian-3 theory using scaled energies, *J. Chem. Phys.*, **112**, 1125–1130 (2000).
150. Ochterski, J.W., Petersson, G.A., and Wiberg, K.B., A comparison of model chemistries, *J. Am. Chem. Soc.*, **117**, 11299–11308 (1995).
151. Pickard IV, F.C., Pokon, E.K., Liptak, M.D., and Shields, G.C., Comparison of CBS-QB3, CBS-APNO, G2 and G3 thermochemical predictions with experiment for formation of ionic clusters of hydronium and hydroxide ions complexed with water, *J. Chem. Phys.*, **122**, 024302–1–024302–7 (2005).
152. Boys, S.F., and Bernardi, F., The calculation of small molecular interactions by the difference of separate total energies. Some procedures with reduced errors, *Mol. Phys.*, **19**, 553–566 (1970).
153. Mayer, I., Towards a “chemical” Hamiltonian, *Intern. J. Quantum Chem.*, **23**, 341–363 (1983).
154. Halász, G.J., Vibók, Á., Suhai, S., and Mayer, I., Toward a BSSE-free description of strongly interacting systems, *Intern. J. Quantum Chem.*, **89**, 190–197 (2002).
155. Mayer, I., Interrelations between the a priori and a posteriori BSSE correction schemes, *Intern. J. Quantum Chem.*, **100**, 559–566 (2004).
156. Jensen, F., The magnitude of intramolecular basis set superposition error, *Chem. Phys. Lett.*, **261**, 633–636 (1996).
157. Fornili, A., Sironi, M., and Raimondi, M., Determination of extremely localized molecular orbitals and their application to quantum mechanics/molecular mechanics methods and to the study of intramolecular hydrogen bonding, *J. Mol. Struct.: Theochem*, **632**, 157–172 (2003).
158. Buemi, G., and Zuccarello, F., DFT study of the intramolecular hydrogen bonds in the amino and nitro-derivatives of malonaldehyde, *Chem. Phys.*, **306**, 115–129 (2004).
159. Buemi, G., and Zuccarello, F., Theoretical study of malonamide and nitromalonamide in vacuum and in water solution, *J. Mol. Struct.: Theochem*, **719**, 137–148 (2005).
160. Buemi, G., and Zuccarello, F., Importance of steric effect on the hydrogen bond strength of malonaldehyde and acetylacetone 3-substituted derivatives. An ab initio study, *Electr. J. Theor. Chem.*, **2**, 302–314 (1997).
161. Dannenberg, J.J., and Rios, R., Theoretical study of the enolic forms of acetylacetone. How strong is the H-bond? *J. Phys. Chem.*, **98**, 6714–6718 (1994).

162. Wong, F.M., Keefe, J.R., and Wu, W., The strength of a low-barrier hydrogen bond in water, *Tetrahedron Lett.*, **43**, 3561–3564 (2002).
163. Buemi, G., unpublished results.
164. Madsen, G.K.H., Wilson, C., Nymand, T.M., McIntyre, G.J., and Larsen, F.K., The structure of nitromalonamide: a combined neutron-diffraction and computational study of a very short hydrogen bond, *J. Phys. Chem. A*, **103**, 8684–8690 (1999).
165. Zhuo, J.-C., NMR of enamines. Part 3— ^1H , ^{13}C and ^{17}O NMR spectroscopic studies of acyclic and cyclic N-aryl enamines: substituent effects and intramolecular hydrogen bonding, *Magn. Res. Chem.*, **35**, 311–322 (1997).
166. Harris, T.K., Zhao, K., and Mildvan, A.S., NMR studies of strong hydrogen bonds in enzymes and in a model compound, *J. Mol. Struct.*, **552**, 97–109 (2000).
167. Zhao, Q., Abeygunawardana, C., Gittis, A.G., and Mildvan, A.S., Hydrogen bonding at the active site of Δ^5 -3-ketosteroid isomerase, *Biochemistry*, **36**, 14616–14626 (1997).
168. Shaefer, T., A relationship between hydroxyl proton chemical shifts and torsional frequencies in some ortho-substituted phenol derivatives, *J. Phys. Chem.*, **79**, 1888–1890 (1975).
169. Altman, L.A., Lungani, D., Gunnarsson, G., Wennerström, H., and Forsén, S., Proton, deuterium and tritium. Nuclear magnetic resonance of intramolecular hydrogen bonds. Isotope effect and the shape of the potential energy function, *J. Am. Chem. Soc.*, **100**, 8264–8266 (1978).
170. Gunnarsson, G., Wennerström, H., Egan, W., and Forsén, S., Proton and deuterium NMR of hydrogen bonds: relationship between isotope effects and the hydrogen bond potential, *Chem. Phys. Lett.*, **38**, 96–99 (1976).
171. Hibbert, F., and Emsley, J., Hydrogen bonding and chemical reactivity, *Adv. Phys. Org. Chem.*, **26**, 255–379 (1990).
172. Ratajczak, H., and Orville-Thomas, W.J., Hydrogen-bond studies. I. Relation between vibrational frequencies and bond length in O–H \cdots O hydrogen bonded systems, *J. Mol. Struct.*, **1**, 449–461 (1968).
173. Lippincott, E.R., and Schroeder, R., One-dimensional model of the hydrogen bond, *J. Chem. Phys.*, **23**, 1099–1106 (1955).
174. Schroeder, R., and Lippincott, E.R., Potential function model of hydrogen bonds. II, *J. Phys. Chem.*, **61**, 921–928 (1957).
175. Reid, C., Semiempirical treatment of the hydrogen bond, *J. Chem. Phys.*, **30**, 182–190 (1959).
176. Bellamy, L.J., and Owen, A.J., A simple relationship between the infra-red stretching frequencies and the hydrogen bond distances in crystals, *Spectrochim. Acta*, **25A**, 329–333 (1969).
177. Gilli, P., Bertolasi, V., Ferretti, V., and Gilli, G., Covalent nature of the strong homonuclear hydrogen bond. Study of the O–H \cdots O system by crystal structure correlation methods, *J. Am. Chem. Soc.*, **116**, 909–915 (1994).
178. Gilli, P., Bertolasi, V., Pretto, L., Ferretti, V., and Gilli, G., Covalent versus electrostatic nature of the strong hydrogen bond: discrimination among single, double and asymmetric single-well hydrogen bonds by variable temperature X-ray crystallographic methods in β -diketone enol RAHB systems, *J. Am. Chem. Soc.*, **126**, 3845–3855 (2004).
179. Gilli, P., Bertolasi, V., Pretto, L., Antonov, L., and Gilli, G., Variable-temperature X-ray crystallographic and DFT computational study of the N–H \cdots O/N \cdots H–O tautomeric competition in 1-(aryloxy)-2-naphthols. Outline of a transition-state hydrogen bond theory, *J. Am. Chem. Soc.*, **127**, 4943–4953 (2005).
180. Gilli, P., Bertolasi, V., Ferretti, V., and Gilli, G., Chemical classification and H-bond energy evaluation for the heteronuclear intermolecular N–H \cdots O bond. Comparison with the homonuclear O–H \cdots O case (<http://www.xray.cz/ecm-cd/ecm/abstract/all/311.htm>).
181. Vener, M.V., How reliable is the Lippincott–Schroeder potential for the O–H \cdots N hydrogen bonded fragment in the gas phase? *Chem. Phys. Lett.*, **244**, 89–92 (1995).
182. Emsley, J., Ma, Lewina Y.Y., Nyburg, Stanley C., Parkins, and Adrian, W., β -Diketone interactions. Part 12. The structure and properties of 3-(3,4,5-trimethyl-phenyl)pentane-2,

- 4-dione, C₁₄H₁₈O₂; the hydrogen bond energy of the enol tautomers of β -diketones, *J. Mol. Struct.*, **240**, 59–67 (1990).
183. Buemi, G., and Zuccarello, F., Ab initio study of the potential energy well of malondialdehyde on varying the O...O distance, *J. Chem. Soc. Faraday Trans.*, **92**, 347–351 (1996).
184. Buemi, G., Ab initio DFT study of hydrogen bridges in hexafluoro-acetylacetone, trifluoro-acetyl-acetone and some 3-substituted derivatives, *J. Mol. Struct.: Theochem*, **499**, 21–34 (2000).
185. Buemi, G., and Zuccarello, F., Is the intramolecular hydrogen bond energy valuable from rotation barriers? *J. Mol. Struct.: Theochem*, **581**, 71–85 (2002).
186. Buemi, G., Zuccarello, F., Venuvanalingam, P., Ramalingam, M., and Ammal, S.S.C., Ab initio study of formazan and 3-nitro-formazan, *J. Chem. Soc. Faraday Trans.*, **94**, 3313–3319 (1998).
187. Buemi, G., Zuccarello, F., Venuvanalingam, P., and Ramalingam, M., Ab initio study of tautomerism and hydrogen bonding of β -carbonylamine in the gas phase and in water solution, *Theor. Chem. Acc.*, **104**, 226–234 (2000).
188. Ramalingam, M., Venuvanalingam, P., Swaminathan, J., and Buemi, G., Ab initio and DFT studies on conformations, hydrogen bonding and electronic structures of glyoxal-monoxime and its methyl derivatives, *J. Mol. Struct.: Theochem*, **712**, 175–185 (2004).
189. Buemi, G., Ab initio DFT study of the rotation barriers and competitive hydrogen bond energies (in gas phase and water solution) of 2-nitroresorcinol, 4,6-dinitroresorcinol, and 2-nitrophenol in their neutral and deprotonated conformations, *Chem. Phys.*, **282**, 181–195 (2002).
190. Buemi, G., Ab initio study of 2,4-dihalosubstituted malonaldehyde and 2-halo-phenols in gas phase and solution, *Chem. Phys.*, **277**, 241–256 (2002).
191. Hehre, W.J., Ditchfield, R., Radom, L., and Pople, J.A., Molecular orbital theory of the electronic structure of organic compounds. V. Molecular theory of bond separation, *J. Am. Chem. Soc.*, **92**, 4796–4801 (1970).
192. Rozas, I., Alkorta, I., and Elguero, J., Intramolecular hydrogen bonds in ortho-substituted hydroxybenzenes and in 8-substituted 1-hydroxy-naphthalenes: can a methyl group be an acceptor of hydrogen bonds? *J. Phys. Chem. A*, **105**, 10462–10467 (2001).
193. Wiberg, K.B., and Ochterski, J.W., Comparison of different ab initio models for calculating isodesmic reaction energies for small ring and related compounds, *J. Comput. Chem.*, **18**, 108–114 (1997).
194. Varnali, T., and Hargittai, I., Geometrical consequences of resonance-assisted hydrogen bonding in 2-nitrovinyl alcohol and indication of a slight attractive O...H interaction in 2-nitroethanol. An ab initio molecular orbital investigation, *J. Mol. Struct.: Theochem*, **388**, 315–319 (1996).
195. Cleland, W.W., and Krevoy, M.M., Low-barrier hydrogen bonds and enzymic catalysis, *Science*, **264**, 1887–1890 (1994).
196. Alkorta, I., Elguero, J., Mo, O., Yanez, M., and Del Bene, J.E., Do coupling constants and chemical shifts provide evidence for the existence of resonance-assisted hydrogen bonds? *Mol. Phys.*, **102**, 2563–2574 (2004).
197. Alkorta, I., Elguero, J., Mo, O., Yanez, M., and Del Bene, J.E., Are resonance-assisted hydrogen bonds ‘resonance assisted’? A theoretical NMR study, *Chem. Phys. Lett.*, **411**, 411–415 (2005).
198. Barone, V., and Adamo, C., Proton transfer in the ground and lowest excited states of malonaldehyde: a comparative density functional and post-Hartree–Fock study, *J. Chem. Phys.*, **105**, 11007–11019 (1996).
199. Delchev, V.B., and Mikosch, H., An ab initio study of the rotamers and rotations of propane-1,3-dial by DFT and SCF calculations, *Monatsh. Chem.*, **132**, 223–233 (2001).

200. Continho-Neto, M.D., Viel, A., and Manthe, U., The ground state tunneling splitting of malonaldehyde: accurate full dimensional quantum dynamics calculations, *J. Chem. Phys.*, **121**, 9207–9210 (2004).
201. Tew, O.P., Handy, N.C., and Carter, S., The vibrations and tunnelling of malonaldehyde on a Møller–Plesset surface, *Mol. Phys.*, **102**, 2217–2226 (2004).
202. Wolf, K., Mikenda, W., Nusterer, E., and Schwarz, K., Proton motion in malonaldehyde: an ab initio molecular dynamics study, *J. Mol. Struct.*, **448**, 201–207 (1998).
203. Wolf, K., Mikenda, W., Nusterer, E., Schwarz, K., and Ulbricht, C., Proton transfer in malonaldehyde: an ab initio projector augmented wave molecular dynamics study, *Chem. Eur. J.*, **4**, 1418–1427 (1998).
204. Pichierri, F., Effect of fluorine substitution on the proton transfer barrier in malonaldehyde. A density functional theory study, *Chem. Phys. Lett.*, **376**, 781–787 (2003).
205. Tuckerman, M.E., and Marx, D., Heavy-atom skeleton and proton tunneling in “intermediate barrier” hydrogen bonds, *Phys. Rev. Lett.*, **86**, 4946–4949 (2001).
206. Sadhukhan, S., Muñoz, D., Adamo, C., and Scuseria, G.E., Predicting proton transfer barriers with density functional methods, *Chem. Phys. Lett.*, **306**, 83–87 (1999).
207. Brown, R.S., Tse, A., Nakashima, T., and Haddon, R.C., Symmetries of hydrogen-bonded enol forms of diketones as determined by X-ray photoelectron spectroscopy, *J. Am. Chem. Soc.*, **101**, 3157–3162 (1979).
208. Grabowski, S.J., π -Electron delocalisation for intramolecular resonance assisted hydrogen bonds, *J. Phys. Org. Chem.*, **16**, 797–802 (2003).
209. Gomak, V.V., Ab initio study of intra- and intermolecular H-bond energies in π -conjugated molecular systems, *J. Mol. Struct.: Theochem*, **726**, 213–224 (2005).
210. Wojtulewski, S., and Grabowski, S.J., DFT and AIM studies on two-ring resonance assisted hydrogen bonds, *J. Mol. Struct.: Theochem*, **621**, 285–291 (2003).
211. Lithoxidou, A.T., and Bakalbassis, E.G., PCM study of the solvent and substituent effects on the conformers, intramolecular hydrogen bonds and bond dissociation enthalpies of 2-substituted phenols, *J. Phys. Chem. A*, **109**, 366–377 (2005).
212. Chung, G., Kwon, O., and Kwon, Y., Theoretical study on 1,2-dihydroxybenzene and 2-hydroxythiophenol: intramolecular hydrogen bonding, *J. Phys. Chem. A*, **101**, 9415–9420 (1997).
213. Mandado, M., Graña, A.M., and Mosquera, R.A., Do 1,2-ethanediol and 1,2-dihydroxybenzene present intramolecular hydrogen bond? *Phys. Chem. Chem. Phys.*, **6**, 4391–4396 (2005).
214. Chen, C., and Shyu, S.-F., Conformers and intramolecular hydrogen bonding of the salicylic acid monomer and its anions, *J. Mol. Struct.: Theochem*, **536**, 25–39 (2001).
215. Kwon, Y., Theoretical study on salicylic acid and its analogues: intramolecular hydrogen bonding, *J. Mol. Struct.: Theochem*, **532**, 227–237 (2000).
216. Chung, G., Kwon, O., and Kwon, Y., Theoretical study on salicylaldehyde and 2-mercapto-benzaldehyde: intramolecular hydrogen bonding, *J. Phys. Chem. A*, **102**, 2381–2387 (1998).
217. Miao, R., Jin, C., Yang, G., Hong, J., Zhao, C., and Zhu, L., Comprehensive density functional theory study on serine and related ions in gas phase: conformations, gas phase basicities and acidities, *J. Phys. Chem. A*, **109**, 2340–2349 (2005).
218. Gronert, S., and O’Hair, R.A.J., Ab initio studies of amino acid conformations. 1. The conformers of alanine, serine and cysteine, *J. Am. Chem. Soc.*, **117**, 2071–2081 (1995).
219. Mohajeri, A., and Shakerin, N., The gas-phase acidity and intramolecular hydrogen bonding in oxalic acid, *J. Mol. Struct.: Theochem*, **711**, 167–172 (2004).
220. Buemi, G., and Zuccarello, F., Molecular conformations and intramolecular hydrogen bonding of 3-formylmalonaldehyde and 3-formylacetylacetone. An ab initio study, *Electr. J. Theor. Chem.*, **2**, 118–129 (1997).
221. Yang, X., Orlova, G., Zhou, X.J., and Leung, K.T., A DFT study of the radical, monomer and dimer of α -keto pyruvic acid: equilibrium structures and vibrational analysis of stable conformers, *Chem. Phys. Lett.*, **380**, 34–41 (2003).

222. Chen, C., and Shyu, S.-F., Theoretical study of glyoxylic and pyruvic acids: rotamers and intramolecular hydrogen bonding, *J. Mol. Struct.: Theochem*, **503**, 201–211 (2000).
223. Miller-Westeroff, U., Evidence against nonclassical aromaticity in hydrogen-bonded systems. 6-Aminofulvene-2-aldimines, *J. Am. Chem. Soc.*, **92**, 4849–4855 (1970).
224. Claramunt, R.M., Sanz, D., Alarcón, S.H., Torralba, M.P., Elguero, J., Foces-Foces, C., Pietrzak, M., Langer, U., and Limbach, H.-H., 6-Aminofulvene-1-alimine: a model molecule for the study of intramolecular hydrogen bonds, *Angew. Chem. Int. Ed.*, **40**, 420–423 (2001).
225. Perrin, C.L., and Ohta, B.K., Symmetry of O–H–O and N–H–N hydrogen bonds in 6-hydroxy-2-formylfulvene and 6-aminofulvene-2-aldimines, *Bioorg. Chem.*, **30**, 3–15 (2002).
226. Perrin, C.L., and Ohta, B.K., Symmetry of NHN hydrogen bonds in solution, *J. Mol. Struct.*, **644**, 1–12 (2003).
227. Tayyari, S.F., Fazli, M., and Milani-Nejad, F., Molecular conformation and intramolecular hydrogen bonding in 4-amino-3-penten-2-one, *J. Mol. Struct.: Theochem*, **541**, 11–15 (2001).
228. Richardson, A.D., Hedberg, K., Wiberg, K.B., and Rablen, P.R., Internal hydrogen bonding in gaseous 3-aminoacrolein: an electron-diffraction investigation augmented by ab initio calculations of its molecular structure and conformational composition, *J. Mol. Struct.*, **445**, 1–11 (1998).
229. Shchavlev, A.E., Pankratov, A.N., and Shalabay, A.V., DFT computational studies on rotation barriers, tautomerism, intramolecular hydrogen bond and solvent effects in 8-hydroxyquinoline, *Int. J. Quantum Chem.*, **106**, 876–886 (2006).
230. Badger, G.M., and Moritz, A.G., Intramolecular hydrogen bonding in 8-hydroxyquinoline, *J. Chem. Soc.*, 3437–3442 (1958).
231. Krishnakumar, V., and Ramasamy, R., DFT studies and vibrational spectra of isoquinoline and 8-hydroxyquinoline, *Spectrochim. Acta*, **61A**, 673–683 (2005).
232. Buemi, G., and Zuccarello, F., Ab initio study of the potential energy well of dithiomalonaldehyde on varying the S···S distance, *J. Mol. Struct.: Theochem*, **506**, 213–221 (2000).
233. Posokhov, Y., Gorski, A., Spanget-Larsen, J., Duus, F., Hansen, P.E., and Waluk, J., Thioacetylacetone: structural and vibrational assignments, *Chemphyschem*, **5**, 495–502 (2004).
234. Buemi, G., Molecular geometries and hydrogen bonding of acetylacetone and its monothioanalogs studied by the ab initio method, *Boll. Acc. Gioenia Sci. Nat., Catania*, **26**, 323–333 (1993).
235. Gonzalez, L., Mó, O., and Yáñez, M., High level ab initio calculations on the intramolecular hydrogen bond in thiomalonaldehyde, *J. Phys. Chem.*, **101A**, 9710–9719 (1997).
236. Gonzalez, L., Mó, O., and Yáñez, M., Substituent effects on the strength of intramolecular hydrogen bond of thiomalonaldehyde, *J. Org. Chem.*, **64**, 2314–2321 (1999).
237. Mori, N., Kaido, S., Suzuki, K., Nakamura, M., and Tsuzuki, Y., Intramolecular hydrogen bonds. XVII. Intramolecular hydrogen bonding involving the mercapto group as a hydrogen donor, *Bull. Chem. Soc. Jap.*, **44**, 1858–1864 (1971).
238. Kwon, Y., Theoretical studies on *o*-aminofuranaldehyde and *o*-aminofuranthioaldehyde in reaction field: C–C rotational barriers and intramolecular hydrogen bonding, *J. Mol. Struct.: Theochem*, **496**, 217–226 (2000).
239. Shchavlev, A.E., Pankratov, A.N., and Shalabay, A.V., Theoretical studies on the intramolecular hydrogen bond and tautomerism of 8-mercaptoquinoline in the gaseous phase and in solution using modern DFT methods, *J. Phys. Chem. A*, **109**, 4137–4148 (2005).
240. Marstokk, K.-M., and Moellendal, H., Structural and conformational properties of 1,2-ethanedithiol as studied by microwave spectroscopy and ab initio calculations, *Acta Chem. Scand.*, **51**, 653–663 (1997).
241. Bultinck, P., Goeminne, A., and Van de Vondel, D., Ab initio conformational analysis of ethane-1,2-dithiol, *J. Mol. Struct.: Theochem*, **334**, 101–107 (1995).
242. Buemi, G., Conformational analysis of ethane-1,2-dithiol and mercaptoethanol. An ab initio SCF HF/3-21G* and 6-31G** study, *Phosphorus, Sulfur Silicon*, **84**, 239–247 (1993).

243. Shagidullin, R.R., Chernova, A.V., and Plyamovaty, A.Kh., Intramolecular hydrogen bonds and the conformations of mercaptoethanol molecules, *Izvestiya Akademii Nauk SSSR, Seriya Khimicheskaya*, 711–714 (1989).
244. Marstokk, K.-M., and Moellendal, H., Microwave spectrum, intramolecular hydrogen bonding, conformational properties and quantum chemical calculations for 3,3,3-trifluoropropanol, *Acta Chem. Scand.*, **53**, 202–208 (1999).
245. Kovács, A., and Hargittai, I., Hydrogen bonding interactions of the trifluoromethyl group: 2-trifluoromethylvinyl alcohol, *Int. J. Quantum Chem.*, **62**, 645–652 (1997).
246. Kovács, A., and Hargittai, I., Hydrogen bonding in 2-trifluoromethylresorcinol and 2,6-bis(trifluoromethyl)phenol and its geometrical consequences, *J. Mol. Struct.: Theochem*, **455**, 229–238 (1998).
247. Kovács, A., Kolossváry, I., Csonka, G.I., and Hargittai, I., Theoretical study of intramolecular hydrogen bonding and molecular geometry of 2-trifluoromethylphenol, *J. Comput. Chem.*, **17**, 1804–1819 (1996).
248. Kovács, A., Macsári, I., and Hargittai, I., Intramolecular hydrogen bonding in fluorophenol derivatives: 2-fluorophenol, 2,6-difluorophenol, and 2,3,5,6-tetrafluoro-hydroquinone, *J. Phys. Chem. A*, **103**, 3110–3114 (1999).
249. Carlsson, G.L., Fateley, W.G., Manocha, A.S., and Bentley, F.F., Torsional frequencies and enthalpies of intramolecular hydrogen bonds of *o*-halophenols, *J. Phys. Chem.*, **76**, 1553–1557 (1972).
250. Vajda, E., and Hargittai, I., Molecular structure of 2-fluorophenol and 2,6-difluorophenol from gas-phase electron diffraction, *J. Phys. Chem.*, **97**, 70–76 (1993).
251. Senent, M.L., Niño, A., Muñoz-Caro, C., Smeyers, Y.G., Domínguez-Gómez, R., and Orza, J.M., Theoretical study of the effect of hydrogen-bonding on the stability and vibrational spectrum of isolated 2,2,2-trifluoroethanol and its molecular complexes, *J. Phys. Chem. A*, **106**, 10673–10680 (2002).
252. Krusic, P.J., Marchione, A.A., Davidson, F., Kaiser, M.A., Kao, C.-P.C., Richardson, R.E., Bothelo, M., Waterland, R.L., and Buck, R.C., Vapour pressure and intramolecular hydrogen bonding in fluorotelomer alcohols, *J. Phys. Chem. A*, **109**, 6232–6241 (2005).
253. Møllendal, H., Leonov, A., and de Meijere, A., A microwave and quantum chemical study of the conformational properties and intramolecular hydrogen bonding of 1-fluoro-cyclopropanecarboxylic acid, *J. Phys. Chem. A*, **109**, 6344–6350 (2005).
254. Simperler, A., Lampert, H., and Mikenda, W., Intramolecular interactions in ortho-substituted phenols: survey of DFT-B3LYP calculated data, *J. Mol. Struct.*, **448**, 191–199 (1998).
255. Buemi, G., Basis set effects on the energy of intramolecular O–H···Halogen hydrogen bridges in ortho-halo-phenols and 2,4-dihalo-malonaldehyde, *Chem. Phys.*, **300**, 107–117 (2004).
256. Pakiari, A.H., and Jamshidi, Z., Intra-molecular dihydrogen bond in the amino acid, *J. Mol. Struct.: Theochem*, **685**, 155–161 (2004).
257. Marstokk, K.-M., de Meijere, A., Wagner-Gillen, K., and Møllendal, H., The structural and conformational properties of 1-amino-1-ethynylcyclopropane as studied by microwave spectroscopy and quantum chemical calculations. *J. Mol. Struct.*, **509**, 1–9 (1999).
258. Brase, S., Klæboe, P., Marstokk, K.-M., de Meijere, A., Møllendal, H., and Nielsen, C.J., Conformational properties of 2-cyclopropylideneethanol as studied by microwave, infrared and Raman spectroscopy and by ab initio computations, *Acta Chem. Scand.*, **52**, 1122–1136 (1998).
259. Marstokk, K.-M., and Møllendal, H., Microwave spectrum, conformational equilibrium, intramolecular hydrogen bonding and ab initio calculations for 2-furanmethanethiol (furfuryl mercaptan), *Acta Chem. Scand.*, **48**, 298–305 (1994).
260. Marstokk, K.-M., and Møllendal, H., Microwave spectrum, conformational equilibrium, and ab initio calculations for 2-furanmethanol (furfuryl alcohol), *Acta Chem. Scand.*, **48**, 25–31 (1994).

261. Marstokk, K.-M., and Møllendal, H., A microwave and ab initio study of the conformational properties and intramolecular hydrogen bonding of cyclopropane-methanethiol, *Acta Chem. Scand.*, **45**, 354–360 (1991).
262. Petitprez, D., Demaison, J., Włodarczyk, Guillemin, J.-C., and Møllendal, H., 3-Butene-selenol—the first example of a selenol with an intramolecular hydrogen bond as studied by microwave spectroscopy and quantum chemical calculations, *J. Phys. Chem. A*, **108**, 1403–1408 (2004).
263. Okuyama, M., and Ikawa, S.-I., Intramolecular hydrogen bond and molecular conformation. Part 3—effect of temperature and pressure on the IR spectra of *o*-halophenols in dilute solutions, *J. Chem. Soc. Faraday Trans.*, **90**, 3065–3069 (1994).
264. Lin, T.-S., and Fishman, E., Enthalpies of intramolecular hydrogen bonds of *o*-halophenols and deuterated *o*-halophenols in the vapour phase, *Spectrochim. Acta Part A*, **23**, 491–500 (1967).
265. Silvi, B., Kryachko, E.S., Tishchenko, O., Fuster, F., and Nguyen, M.T., Key properties of monohalogen substituted phenols: interpretation in terms of the electron localization function, *Mol. Phys.*, **100**, 1659–1675 (2002).
266. Foresman, J.B., and Frisch, A.E., *Exploring chemistry with electronic structure methods*, Second Edition, Gaussian Inc., Pittsburg, USA, 1996.
267. Seliskar, C., and Hoffmann, R.E., On the infrared spectrum of malonaldehyde, a tunnelling hydrogen-bonded molecule, *J. Mol. Spectr.*, **96**, 146–155 (1982).
268. Smith, Z., Wilson, E.B., and Duerst, R.W., The infrared spectrum of gaseous malonaldehyde (3-hydroxy-2-propenal), *Spectrochim. Acta*, **39A**, 1117–1129 (1983).
269. Tayyari, S.F., and Milani-Nejad, F.F., On the reassignment of vibrational frequencies of malonaldehyde, *Spectrochim. Acta*, **54A**, 255–263 (1998).
270. Carbonniere, P., Lucca, T., Pouchan, C., Rega, N., and Barone, V., Vibrational computations beyond the harmonic approximation: performances of the B3LYP density functional for semirigid molecules, *J. Comput. Chem.*, **26**, 384–388 (2005).
271. Carbonniere, P., and Barone, V., Performances of different functionals in the computation of vibrational spectra beyond the harmonic approximation, *Chem. Phys. Lett.*, **399**, 226–229 (2004).
272. Barone, V., Vibrational spectra of large molecules by density functional computations beyond the harmonic approximation: the case of pyrrole and furan, *Chem. Phys. Lett.*, **383**, 528–532 (2004).
273. Barone, V., Accurate vibration spectra of large molecules by density functional computations beyond the harmonic approximation: the case of azabenzenes, *J. Phys. Chem. A*, **108**, 4146–4150 (2004).
274. Barone, V., Festa, G., Grandi, A., Rega, N., and Sanna, N., Accurate vibrational spectra of large molecules by density functional computation beyond the harmonic approximation: the case of uracil and 2-thiouracil, *Chem. Phys. Lett.*, **388**, 279–283 (2004).
275. Alparone, A., and Millefiori, S., Anharmonic vibrational spectroscopic investigation of malonaldehyde, *Chem. Phys.*, **290**, 15–25 (2003).
276. Tayyari, S.F., Tabrizi, M.Z., Tayyari, F., and Milani-Nejad, F., A two dimensional double minimum potential function for bent hydrogen bonded systems, I-malonaldehyde, *J. Mol. Struct.: Theochem*, **637**, 171–181 (2003).
277. Došlić, N., and Kühn, O., The intramolecular hydrogen bond in malonaldehyde as seen by infrared spectroscopy. A four-dimensional model study, *Z. Phys. Chem.*, **237**, 1507–1524 (2003).
278. Onsager, L., Electric moments of molecules in liquids, *J. Am. Chem. Soc.*, **58**, 1486–1493 (1936).
279. Miertus, S., Scrocco, E., and Tomasi, J., Electrostatic interaction of a solute with a continuum. A direct utilization of ab initio molecular potentials for the prevision of solvent effects, *Chem. Phys.*, **55**, 117–129 (1981).

280. Miertus, S., and Tomasi, J., Approximate evaluations of the electrostatic free energy and internal energy changes in solution processes, *Chem. Phys.*, **65**, 239–245 (1982).
281. Tomasi, J., and Persico, M., Molecular interactions in solution: an overview of methods based on continuous distributions of the solvent, *Chem. Rev.*, **94**, 2027–2094 (1994).
282. Pascual-Ahuir, J.L., Silla, E., and Tuñón, I., GEPOL: an improved description of molecular surfaces. III. A new algorithm for the computation of a solvent-excluding surface, *J. Comp. Chem.*, **15**, 1127–1138 (1994).
283. Cossi, M., Mennucci, B., and Cammi, R., Analytical first derivatives of molecular surfaces with respect to nuclear coordinates, *J. Comp. Chem.*, **17**, 57–73 (1996).
284. Cossi, M., Barone, V., Cammi, R., and Tomasi, J., Ab initio study of solvated molecules: a new implementation of the polarizable continuum model, *Chem. Phys. Lett.*, **255**, 327–335 (1996).
285. Barone, V., Cossi, M., and Tomasi, J., A new definition of cavities for the computation of solvation free energies by the polarizable continuum model, *J. Chem. Phys.*, **107**, 3210–3221 (1997).
286. Barone, V., and Cossi, M., Quantum calculations of molecular energies and energy gradients in solution by a conductor solvent model, *J. Phys. Chem. A*, **102**, 1995–2001 (1998).
287. López Navarrete, J.T., and Ramírez, F.J., A study by Raman spectroscopy and the semiempirical AM1 method on several 1,2-dihydroxybenzene solutions, *Spectrochim. Acta*, **49A**, 1759–1767 (1993).
288. Cornard, J.-P., and Merlin, J.-C., Molecular structure and spectroscopic properties of 4-nitrocatechol at different pH: UV–visible, Raman, DFT and TD-DFT calculations, *Chem. Phys.*, **309**, 239–249 (2005).
289. Bouchy, A., Rinaldi, D., and Rivail, J.-L., Solvent effect on intramolecular hydrogen bonds in push–pull conjugated molecules, *Int. J. Quantum Chem.*, **96**, 273–281 (2004).
290. McMahon, G., O'Malley, S., Nolan, K., and Diamond, D., Important calixarene derivatives—their synthesis and applications, *ARKIVOC*, 23–31 (2003).
291. Casnati, A., Sciotto, D., and Arena, G., Water soluble calixarenes, in *Calixarenes 2001*, Asfari, Z., Böhmer, V., Harrowfield, J., and Vicens, J., Editors, Kluwer Academic Publishers, London, pp. 440–456, 2001.
292. Gutsche, C.D., *Stoddart J.F. Editor, Calixarenes*, The Royal Soc. of Chemistry, Cambridge, Great Britain, pp. 54, 78,79, 1989.
293. Rudkevich, D.M., Intramolecular hydrogen bonding in calixarenes, *Chem. Eur. J.*, **6**, 2679–2686 (2000).
294. Cho, Y.L., Rudkevich, D.M., Shinanyuk, A., Rissanen, K., and Rebeck, J. Jr, Hydrogen bonding effects in calyx[4]arene capsules, *Chem. Eur. J.*, **6**, 3788–3796 (2000).
295. Masci, B., Homooxa- and homoaza-calixarenes, in *Calixarenes 2001*, Asfari, Z. Böhmer, V., Harrowfield, J. and Vicens, I., Editors, Kluwer Academic Publishers, Dordrecht, 2001, pp.235–249.
296. Lang, J., Deckerová, V., Czernek, J., and Lhoták, P., Dynamics of circular hydrogen bond array in calix[4]arene in non polar solvent: a nuclear magnetic resonance study, *J. Chem. Phys.*, **122**, 044506–1–0044506–11 (2005).
297. Kovalenko, V.I., Chernova, A.V., Borisoglebskaya, E.I., Katsyuba, S.A., Zverev, V.V., Shagidullin, R.R., Antipin, I.S., Solov'eva, S.E., Stoikov, I.I., and Kononov, A.I., Cooperative intramolecular hydrogen bond and conformations of thiocalix[4]arene molecules, *Russian Chem. Bull.*, **51**, 825–827 (2002).
298. Hayashida, O., Ito, J.-I., Matsumoto, S., and Hamachi, I., Preparation and unique circular dichroism phenomena of urea-functionalized self-folding resorcinarenes bearing chiral termini through asymmetric hydrogen-bonding belts, *Org. Biomol. Chem.*, **3**, 654–660 (2005).
299. Reuter, C., Schmieder, R., and Vögtle, F., From rotaxanes to knots. Templating, hydrogen bond patterns, and cyclochirality, *Pure Appl. Chem.*, **72**, 2233–2241 (2000).

300. Schalley, C.A., Weilandt, T., Brueggemann, J., and Voegtle, F., Hydrogen-bond-mediated template synthesis of rotaxanes, catenanes and knotanes, *Top. Curr. Chem.*, **248**, 141–200 (2005).
301. Badjić, J.D., Balzani, V., Credi, A., Lowe, J.N., Silvi, S., and Stoddart, J.F, A mechanically interlocked bundle, *Chem. Eur. J.*, **10**, 1926–1935 (2004).
302. Tseng, H.-R., Vignon, S.A., Celestre, P.C., Perkins, J., Jeppesen, J.O., Di Fabio, A., Ballardini, R., Gandolfi, M.T., Venturi, M., Balzani, V., and Stoddart, J.F, Redox-controllable amphiphilic [2]rotaxanes, *Chem. Eur. J.*, **10**, 155–172 (2004).
303. Harada, A., Cyclodextrin-bases molecular machines, *Acc. Chem. Res.*, **34**, 456–464 (2001).

CHAPTER 3

CHANGES OF ELECTRON PROPERTIES IN THE FORMATION OF HYDROGEN BONDS

Spatial study of descriptors computed from the ab initio electron density and the electron localization function

LUIS F. PACIOS

Unidad de Química y Bioquímica, Dep. Biotecnología, E.T.S.I. Montes, Universidad Politécnica de Madrid, E-28040 Madrid, Spain

Abstract The purpose of this chapter is to provide a theoretical analysis of the changes occurring in the molecular electron distribution of two monomers at different distances as they move closer to form a hydrogen bond. The study focuses on properties computed from electron densities, electrostatic potentials, and electron localization functions obtained in quantum correlated calculations for dimers linked by N–H···O and O–H···O hydrogen bonds. The variation of these properties with the intermolecular distance allows to explore changes in the electron distribution of the interacting molecules and gain thus insight into the electronic nature of the interactions that underlie hydrogen bonding. Since the goal is to identify essential features, the study concentrates on conventional H-bonds which are central representative examples of the interaction.

Keywords: Hydrogen bonding; electron density; electrostatic potential; electron localization function; topological descriptors; atomic charges.

1 INTRODUCTION

Since about 1990 new types of interactions identified now as hydrogen bonds have considerably widened the range of associated energies to cover more than two orders of magnitude [1–11]. A continuum of strengths [1, 5, 11] exists ranging from a few tenths of kcal/mol for weak H-bonds [2–4] that are hardly distinguishable from van der Waals interactions to a few tens of kcal/mol for strong H-bonds [6–10] that exhibit features typical of covalent bonds. The energy range 2–15 kcal/mol, traditionally assigned to hydrogen bonding as a whole, is today representative of what one could call “classical” H-bonds like those involving N–H or O–H donor groups and N or O acceptor atoms.

Although with fluctuating intensity, hydrogen bonding has been the subject of research for nearly one century [11]. If the importance of classical H-bonds for a vast number of chemical systems has been the main reason for this long-lasting interest, new H-bonds have triggered a renewed activity in scientific fields that range from solid state [5] to biology [12]. Particularly interesting in this regard are the new perspectives opened by H-bonds at both ends of the strength spectrum for protein chemistry. Although unequivocal evidence for the existence of weak H-bonds with C–H donor groups was already presented in 1982 [13], their role in proteins, discovered in 1995 [14], might help to explain as yet unsolved problems in protein structure, stability, and folding [12, 15, 16]. Short strong H-bonds (SSHBs) with low barriers to proton transfer and the so-called low-barrier H-bonds (LBHBs) were observed in gas phase long ago [17] but the proposal that they could play a role in enzymatic catalysis was suggested in 1992 [18]. Although SSHBs and LBHBs are not the same thing [9, 19], the existence of strong H-bonds (with or without low barrier to H transfer) in active sites of enzymes has been largely confirmed and their properties used to explain a variety of observations in proteins [20, 21] and catalytic processes [22–24].

1.1 Nature of Hydrogen Bond

As “new” H-bonds have been responsible for the intense revival of hydrogen bonding research carried over the last 10 or 15 years, classical H-bonds are also now studied from a broader perspective. Even the most classical of H-bonds, namely $\text{O}-\text{H}\cdots\text{O}$ and $\text{N}-\text{H}\cdots\text{O}$, have been recently under debate [25–33]. Experimental measurements of Compton profile anisotropies of ordinary ice [25] and urea crystals [26] were first interpreted as direct evidence for partial covalency of H-bonds [25, 27]. This interpretation was contested by alternative explanations in terms of antisymmetrization of the product of monomer wave functions [28] or as a result of calculations using maximally localized Wannier functions [29]. This controversy, however, has demonstrated that the measured Compton profiles in solid water and urea cannot be explained without considering the quantum nature of the interaction underlying hydrogen bonding in these systems [30]. Moreover, other reports have directly pointed out some degree of covalent character for the 27 representative $\text{O}-\text{H}\cdots\text{O}$ bonds of the 7 phases of ice [31].

Protein chemistry provides again an illustrative example of the new light cast on conventional H-bonds. Baker and coworkers [32, 33] have used the geometric characteristics of H-bonds in a dataset of 698 high-resolution protein crystal structures to develop an orientation-dependent hydrogen bonding potential. Upon analyzing more than 100,000 H-bonds (most of them $\text{N}-\text{H}\cdots\text{O}$ backbone–backbone links), these authors concluded that quantum effects are utterly essential to explain the spatial orientation of these H-bonds [32] and even stated explicitly their partial covalent nature [33].

As a consequence of all this research, the complexity of hydrogen bonding has increased dramatically in recent years. It is already not possible to consider any $A-H \cdots B$ hydrogen bond as an electrostatic interaction between a strongly polar group $A^{\delta-}-H^{\delta+}$ on the one side and an atom $B^{\delta-}$ on the other side, with A and B electronegative elements restricted mainly to N, O, and halogens, as most chemistry and biochemistry textbooks still do when the topic is introduced. In spite of the great amount of data provided by new experimental observations and theoretical calculations, the ultimate nature of hydrogen bonding is not revealed yet. Insofar as the term “H-bond” refers nowadays to a much broader phenomenon than recognized before, it is unlikely that one single unified description should be able to cover all the interactions currently grouped under that label. It seems more appropriate to focus on categories of H-bonds searching for properties that characterize them as unambiguously as possible. While quantum calculation is the obvious theoretical methodology for this purpose, one still needs to extract useful information from quantum results [34].

1.2 Analyses of Quantum Results

There is a general agreement that accurate quantum studies on hydrogen bonds require flexible basis sets, i.e., triple- ζ with at least one set of diffuse and polarization functions (especially on H atoms: it is surprisingly frequent to find in the literature calculations that exclude these functions from hydrogens) and treatment of electron correlation by means of either wave function-based or DFT-based methods [34–41]. Since these requirements have rendered useless much of the outdated theoretical material published before 1990, one can consider that the efforts to characterize hydrogen bonding from a quantum viewpoint are more or less 15 years old (see the historical comments in Ref. 5).

In order to investigate the essential features of the interaction underlying hydrogen bonding, data provided by quantum results can be roughly grouped into three broad categories: geometries, energies, and electron properties [34, 35, 41]. This chapter focuses on the latter. Given that the electron density $\rho(\mathbf{r})$ at an optimized geometry contains the essential quantum information of a system, the molecular $\rho(\mathbf{r})$ (an observable and experimentally measurable quantity [42]) is the main object to analyze. Electron populations obtained from conventional schemes [43] or more elaborate natural bond orbital (NBO) analyses [44] (strictly a wavefunction-dependent not a density-dependent approach) give insight into the electron nature of the H-bonded molecular aggregates. However, the quantum theory of atoms in molecules (AIM) developed by Bader and collaborators [45, 46] is the formalism most frequently used in recent years to analyze $\rho(\mathbf{r})$. The tools provided by this approach have proven so useful in extracting chemical information from quantum results that a great deal of work has been devoted to

the applications of the AIM theory to hydrogen bonding. The subject not only has been presented in numerous reviews and articles [2, 5, 20, 31, 40, 41, 47–49], but it has also been covered in the other chapters of this volume, so an introductory outline is not necessary here.

The continuous electron density plus the discrete set of nuclei define the total charge density $D(\mathbf{r})$ of a molecular system. The electrostatic potential $U(\mathbf{r})$ [50–52] is related to $D(\mathbf{r})$ through Poisson's equation:

$$(1) \quad \nabla^2 U(\mathbf{r}) = -4\pi D(\mathbf{r})$$

This relation suggests that $U(\mathbf{r})$ can be regarded as a fundamental quantity which explains the use of electrostatic potentials to lay down guidelines on hydrogen bonding research [51, 53]. For instance, the positions of minima of $U(\mathbf{r})$ associated with H-accepting (or electron donating) centers in isolated molecules were shown to predict successfully sites and directionality of H-bonds in a number of systems [51]. It was also found that there is a complementarity between regions of positive potential around donor groups and regions of negative potential for acceptor groups (see Sect. 3.3) [11, 53]. Very recently, the electrostatic potential at selected atomic sites has been used as an index to quantify the reactivity of molecules with respect to H-bond formation [54, 55]. Although properties based on $U(\mathbf{r})$ have an obvious interest to explore molecular interactions, reports dealing with H-bond applications are scarce in the last years. The computational effort required to calculate ab initio electrostatic potentials (see Sect. 2.2.4) and the more complex topology of $U(\mathbf{r})$ [56] as compared with that of $\rho(\mathbf{r})$ on the one side, and the great success of AIM analyses of electron density (much easier to compute) on the other side, are probably the reasons for the relative scarcity of electrostatic potential applications in current hydrogen bonding research.

In 1994, Silvi and Savin [57] proposed a new approach to explore chemical bonds using topological techniques similar to those of Bader's theory applied to a relatively simple function of $\rho(\mathbf{r})$: the electron localization function (ELF), $\eta(\mathbf{r})$ (its definition and meaning are outlined in Sect. 2.2.5). This function was earlier introduced to provide a description of electron localization independent on orbitals [58]. Similar to what the AIM theory does for $\rho(\mathbf{r})$, the topological analysis of the $\eta(\mathbf{r})$ gradient vector field yields basins of attractors that allow partitioning the molecular space into domains. However, unlike domains of $\rho(\mathbf{r})$ which are atomic in nature, domains of $\eta(\mathbf{r})$ are explicitly associated with bond or lone electron pairs in consistency with the Lewis description in terms of electron pairs [57]. The topological analysis of the ELF, which may be viewed as a complement to Bader's theory, has rendered fruitful applications on a variety of molecular problems (representative examples may be found elsewhere [59–62]). Applications to H-bond complexes have begun to appear recently [63, 64].

1.3 Dependence on the Intermolecular Distance

The variation with the intermolecular distance of electron properties as monomers initially separated move closer until a H-bond forms between them gives an especially useful insight into the nature of the interaction. However, the vast majority of reports dealing with analyses of quantum results refer to properties at equilibrium geometries so that relationships between H-bond distances and electron descriptors are usually established by considering different systems at their observed or computed equilibrium structures. We started a research program intended to investigate the dependence on the intermolecular distance of a variety of properties obtained from $\rho(\mathbf{r})$ and $\eta(\mathbf{r})$ as well as geometry data and other descriptors [65–72]. This work, that initially regarded classical H-bonds [65–69], has been recently extended to strong H-bonds and associated proton transfer processes [70–72]. A related report by Espinosa et al. on dimers involving acceptor groups with fluorine has also been recently published [73].

This chapter presents an overview of the variation with the intermolecular distance of electron properties computed from the electron density $\rho(\mathbf{r})$, electrostatic potential $U(\mathbf{r})$, and ELF $\eta(\mathbf{r})$. The terms associated with energy components are not mentioned deliberately to avoid preconceptions which are unfortunately so frequent when decomposition schemes (necessarily artificial in molecular orbital calculations) are used to investigate hydrogen bonding. On the contrary, this discussion focuses on subtle changes occurring in the electron distribution of the system as monomers interact at closer distances until a H-bond is formed. Since the ultimate goal is gaining insight into the physical nature of hydrogen bonding, the study concentrates on classical N–H···O and O–H···O bonds because they are central examples representative of the interaction and any particular effect is thus, in principle, precluded. This research will be extended in the near future toward both weak and strong sides of the broad H-bond spectrum described above.

2 COMPUTATIONAL BACKGROUND

This overview analyzes the electron redistribution that takes place in two interacting monomers upon H-bond formation. The systems selected (shown in Fig. 1) focus on the two most important classical H-bonds, O–H···O and N–H···O, and cover both donor and acceptor roles of every monomer. They are the following: (a) water dimer (WD), (b) methanol–water complex (MW), (c) water–methanol complex (WM), (d) formic acid dimer (FAD), (e) formamide dimer (FD), and (f) formamide–formic acid complex (FFAC). Systems (a)–(c) are bound by one single O–H···O bond whereas cyclic dimers (d)–(f) are linked by two H-bonds. In FAD and FD homodimers, both monomers behave simultaneously as donor and acceptor while in the FFAC heterodimer, formamide and formic acid play competing roles.

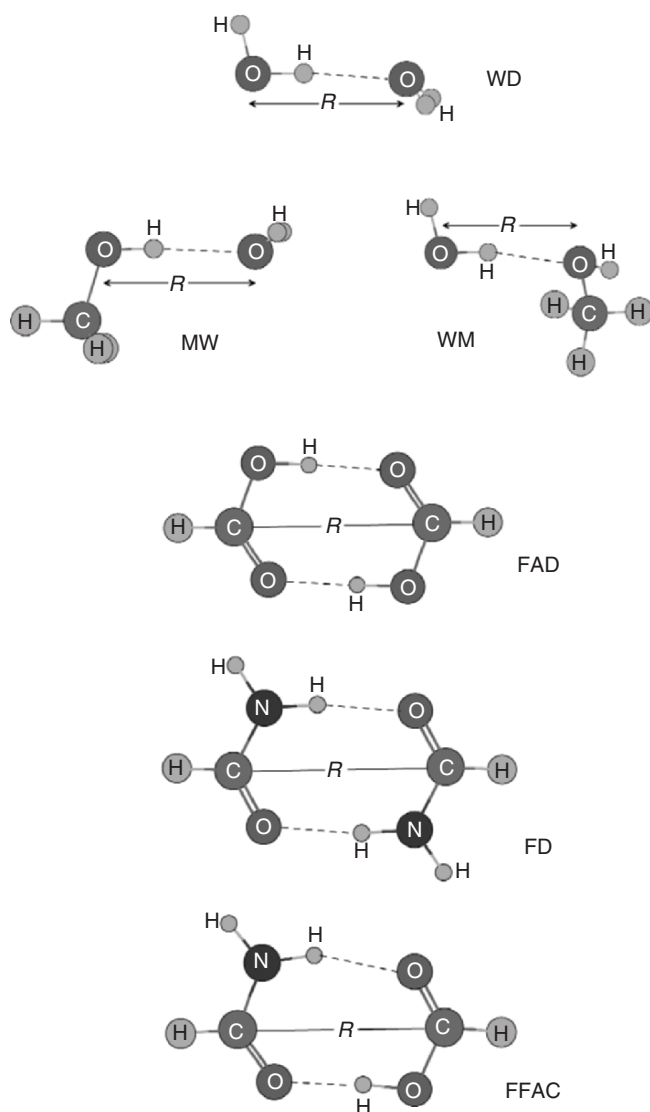


Figure 1. Equilibrium geometries of dimers with O-H...O and N-H...O hydrogen bonds.

2.1 Quantum Calculations

Ab initio MP2/6-311++G(d,p) calculations were performed to obtain geometries and electron densities. The perturbative MP2 approach is one of the wavefunction-based methods most frequently used to include electron correlation and its well-gained reputation needs no further comments. The basis set

chosen is the smallest one that includes all the requirements needed to treat H-bonds: triple- ζ plus one set of diffuse and polarization functions in all the atoms [34, 35, 38]. Although the rapidly increasing capabilities of computers allow applying this level of theory to H-bond systems of moderate size, it is still computationally too demanding to be routinely used. DFT methods are obvious candidates for overcoming this problem, but, though the popular B3LYP hybrid approach gives very good results in many H-bond systems [37, 66, 67], the known deficiency of DFT to describe dispersion effects is a drawback to take into consideration [39].

Equilibrium and nonequilibrium geometries were optimized in redundant internal coordinates using analytic gradients without symmetry constraints. Since this study focuses on electron properties, no correction for basis set superposition error (BSSE) was made in the optimizations (we have reported before BSSE-corrected energies for these dimers [66–68]). Once the equilibrium structures shown in Fig. 1 were found, five nonequilibrium geometries were optimized for every dimer at fixed intermolecular distances R (see Fig. 1: note that this variable is $R(\text{O}\cdots\text{O})$ for WD, MW, and WM, and $R(\text{C}\cdots\text{C})$ for FAD, FD, and FFAC) with values 0.2 Å shorter and 0.2, 0.4, 0.8, and 1.6 Å longer than equilibrium R_{eq} . In what follows, these geometries will be referred to in all the figures by indicating the $R - R_{\text{eq}}$ difference as X -axis. Electron densities $\rho(\mathbf{r})$ were then obtained in single-point calculations at the six optimized structures of every complex. Geometries and electron densities were computed with GAUSSIAN03 [74].

2.2 Electron Properties

The following sections describe the electron properties analyzed.

2.2.1 Topological descriptors of the electron density

Critical points (CPs) of the electron density, r_c , are points where the gradient of $\rho(\mathbf{r})$ vanishes. The sign of the eigenvalues of the Hessian of $\rho(\mathbf{r})$ calculated at r_c sets the topological category of any CP: a bond critical point (BCP) is a $(3, -1)$ point and the local value of a property X computed at it, $X(r_c) = X_c$, is a topological descriptor which can be used to characterize the type of bonding [45, 46]. According to the AIM theory, the essential condition to detect an $\text{A}-\text{H}\cdots\text{B}$ hydrogen bond is the existence of a $(3, -1)$ BCP at the $\text{H}\cdots\text{B}$ path and some of its properties have been proposed to set the criteria to characterize hydrogen bonding [41, 46–48, 75]. Location and characterization of BCPs as well as the calculation of local properties (electron density, ρ_c , Laplacian of $\rho(\mathbf{r})$, $\nabla^2\rho_c$, and total energy density, H_c) were accomplished with EXTREME, a module of the AIMPAC suite [76]. Numerical grids to render electron density isocontour maps were computed with CHECKDEN, a program that reads WFN output files generated by GAUSSIAN (and other packages as well) and calculates a variety of electron functions [77].

2.2.2 AIM atomic charges

According to the AIM theory, an “atom” is defined as a region of space bounded by a surface that is not crossed by any gradient vectors of $\rho(\mathbf{r})$ (the so-called zero-flux property) [45]. A molecular system is thus partitioned into atomic basins whose boundaries are such surfaces. Integration of the electron density over an atomic basin A gives its total electron population N_A so that the net atomic charge is $q_A = Z_A - N_A$. Koch and Popelier proposed the use of q_H in one of their criteria to characterize H-bonds [75] and very recently, Bader and Matta have emphasized the quantum observable nature of the AIM charges and their central role in a wide range of experimentally measurable properties [78]. Numerical integration of $\rho(\mathbf{r})$ over AIM basins was done with PROAIM, the integration module of AIMPAC [76].

2.2.3 NBO populations

The NBO method makes use of the first-order reduced density matrix to optimally transform a given wave function into localized form corresponding to one-center (lone pair) and two-center (bond) elements of the conventional Lewis picture (a comprehensive overview of the NBO method exists [79]). Although much less applied to hydrogen bonding than other theoretical tools, the usefulness of NBO analyses to highlight the nonelectrostatic nature of H-bonds was demonstrated by Weinhold in 1997 [44]. More recently, NBO data have been shown to reveal interesting features in the covalent–hydrogen bonding transition occurring in proton transfer associated with strong H-bond complexes [72]. Natural orbitals obtained from MP2/6-311++G(d,p) wave functions of the systems in Fig. 1 were used to compute NBO charges and electron lone pair populations with the program NBO 4.M [80] implemented in the Q-CHEM package [81].

2.2.4 Electrostatic potentials

The electrostatic potential $U(\mathbf{r})$ created at \mathbf{r} by a molecular system composed of a set of nuclei located at \mathbf{R}_A with nuclear charges Z_A and a continuous electron density $\rho(\mathbf{r}')$ is expressed by [50–52]

$$(2) \quad U(\mathbf{r}) = \sum_A \frac{Z_A}{|\mathbf{R}_A - \mathbf{r}|} - \int \frac{\rho(\mathbf{r}')}{|\mathbf{r}' - \mathbf{r}|} d\mathbf{r}'$$

Equation 2 is simply an expression of Coulomb’s law in atomic units and gives the energy acting on a unit positive charge located at \mathbf{r} due to the net electrostatic effect arising from positive point charges of nuclei and the negative charge distribution of electrons. The sign of $U(\mathbf{r})$ in any particular region will depend on whether nuclear or electron effects are dominant there. H-bond systems display complementary regions of positive potential around donor groups and negative potential around acceptor groups [11, 53]. The electrostatic potential at a nucleus, U_0 , is also a quantity of interest inasmuch as

rigorous expressions relating U_0 with energies of atoms and molecules have been known for years [50]. Values of U_0 at selected sites, particularly hydrogen nuclei, have been used as descriptor indexes for the H-bond formation [54, 55]. It follows from Eq. 2 that the electrostatic potential at a nucleus is given by

$$(3) \quad U_0 = - \int \frac{\rho(\mathbf{r})}{\mathbf{r}} d\mathbf{r}$$

Although the rigorous evaluation of $U(\mathbf{r})$ (i.e., all of the integrals arising from the electronic term in Eq. 2 being calculated exactly) was in the past hampered by the computational effort involved, it has become easily affordable thanks to the capabilities of modern computers. However, if a molecular system has tens of atoms, basis sets include polarization functions with $\ell \geq 2$, and grids of points large enough to probe representative regions of space are required, the computational burden is still so heavy even by current standards that the use of ab initio electrostatic potentials remains far from routine in hydrogen bonding research.

The rigorous calculation of $U(\mathbf{r})$ was performed at selected planes for systems in Fig. 1 with CHECKDEN [77] using 2D grids with step size of 0.05 Å, which in some cases amounts to more than 32,000 points. This program has also been used to calculate values at nuclei of electrostatic potentials, U_0 , and electron densities, ρ_0 .

2.2.5 Electron localization functions

The ELF originally proposed by Becke and Edgecombe [58] is defined as

$$(4) \quad \eta(\mathbf{r}) = \left[1 + \left(\frac{T - T_W}{T_{TF}} \right)^2 \right]^{-1}$$

with

$$T = \frac{1}{2} \sum_i |\nabla \varphi_i(\mathbf{r})|^2, \quad T_W = \frac{1}{8} \frac{|\nabla \rho(\mathbf{r})|^2}{\rho(\mathbf{r})}, \quad T_{TF} = \frac{3}{10} (3\pi^2)^{2/3} \rho(\mathbf{r})^{5/3}$$

Assuming a density ρ constructed with orbitals φ_i , T defines the actual kinetic energy density of the system while T_W and T_{TF} are the von Weizsäcker (W) and Thomas–Fermi (TF) kinetic energy functionals, respectively [82]. Whereas the TF functional gives the kinetic energy of a homogeneous electron gas, the W functional accounts for inhomogeneity corrections through the presence of $\nabla \rho$ and gives the local kinetic energy of a bosonic-like system, i.e., a system of noninteracting particles of density ρ without the Pauli repulsion [58]. Therefore, for a system of fermions with the same ρ , the difference $T - T_W$ can be interpreted as the local excess of kinetic energy due to the Pauli repulsion and, choosing T_{TF} as the scaling factor, one can quantify locally the repulsion between electrons due to the exclusion principle in kinetic terms. The ELF can

thus be viewed as a measure of local electron localization [58] with values restricted to $0 \leq \eta(\mathbf{r}) \leq 1$ because of the normalized Lorentzian-type definition, Eq. 4. In regions where electrons are alone or form opposite spin pairs, the Pauli repulsion is low, $T - T_W$ is small, and $\eta(\mathbf{r})$ is close to 1, with upper limit $\eta(\mathbf{r}) = 1$ corresponding to perfect localization. Contrarily, at boundaries between such regions, there is a high probability of same spin pairs, $T - T_W$ is high, and $\eta(\mathbf{r}) \rightarrow 0$. The value $\eta(\mathbf{r}) = \frac{1}{2}$ corresponds to electron delocalization in regions with gas-like-pair probability at which $T = T_W \pm T_{TF}$. Graphical representations of electron localization for the H-bond systems in Fig. 1 were obtained by plotting isosurfaces of the ELF computed with CHECKDEN [77].

The topological analysis of the $\eta(\mathbf{r})$ gradient vector field yields CPs that enable partitioning the molecular space into basins of attractors [57]. There are basically two types of basins: core basins around nuclei and valence basins in the remaining space [59]. Whereas a core basin, labeled $C(A)$, is necessarily centered on one single atom A , a valence basin is characterized by its synaptic order, defined as the number of cores to which it is connected. There are disynaptic valence basins $V(A, B)$ shared by A and B atoms and monosynaptic valence basins $V(A)$ containing one electron lone pair in atom A [59–62]. For instance, water molecule has one core basin $C(O)$, two disynaptic valence basins $V(O, H_1)$ and $V(O, H_2)$, and two monosynaptic valence basins $V_1(O)$ and $V_2(O)$ for the two lone pairs of oxygen. This characterization of domains of $\eta(\mathbf{r})$ has thus a clear chemical signification explicitly associated with bond or lone electron pairs which complements the topological analysis of $\rho(\mathbf{r})$ provided by the AIM theory. From a quantitative point of view, a localization basin (core or valence) is characterized by the integrated values of some operators \hat{A} over the basin: $\hat{A} = 1$ yields simply its volume while integrating $\hat{A} = \rho(\mathbf{r})$ gives the electron population of the basin.

The topological analysis of the ELF and the calculation of integrated properties were performed with the TOPMOD package [83]. A step interval of 0.07 bohr was chosen in each space direction to set 3D grids of ELF basins. For the systems in Fig. 1, this gives place to a number of points per geometry between 3.8×10^7 and 9.4×10^7 depending on the intermolecular distance.

3 VARIATION OF ELECTRON PROPERTIES

Mutual interaction between two approaching molecules produces changes in their electron distributions. If a hydrogen bonding complex is eventually formed, these changes will be mainly concentrated at the immediate environment of the H-bond. The variation with the intermolecular distance of properties chosen to probe the whole electron distribution will provide essential information to infer the nature of the interaction. This is the purpose of this section that addresses properties presented in Sect. 2.2 for the classical H-bonds shown in Fig. 1. In what follows, the six geometries corresponding to $R - R_{eq}$ intermolecular distances indicated in Sect. 2.1 will be investigated for every system. Table 1 presents some reference data for their equilibrium ($R - R_{eq} = 0$) geometries.

Table 1. Distances in A–H··O hydrogen bonds (Å) and energies (kcal/mol) for equilibrium geometries of the H-bond systems in Fig. 1

Dimer	A	$r(\text{A–H})$	$R(\text{H} \cdots \text{O})$	$R(\text{A} \cdots \text{O})$	ΔE^a	ΔE^b
WD	O	0.9656	1.950	2.914	6.03	5.05
MW	O	0.9643	1.942	2.906	6.11	4.72
WM	O	0.9676	1.894	2.856	6.62	5.36
FAD	O	0.9897	1.726	2.716	14.3	14.0
FD	N	1.023	1.898	2.915	13.3	12.8
FFAC	N	1.020	1.940	2.927	14.5	14.3
FFAC	O	0.9943	1.692	2.685		

^a MP2/6-311++G(d,p) BSSE-uncorrected values of $|E(\text{dimer}) - E(\text{monomers})|$

^b B3LYP/6-311++G(d,p) BSSE-corrected dissociation energies from Refs. 66 and 67

3.1 Electron Density: Topological Descriptors

Hydrogen bonding complexes present electron distributions that exhibit isocontours of high density enclosing both monomers. This is illustrated in Fig. 2 by plotting isodensity maps for a single H-bond complex (MW) and a dimer with two H-bonds (FD). To assess the degree of electron density sharing between monomers one should recall that $\rho = 0.001$ or 0.002 a.u. (two outermost isocontours in Fig. 2) have been proposed as outer limits to define molecular size and shape [45, 84]. In spite of the different strengths of H-bonds in MW and FD (see Table 1), both complexes show the same $\rho = 0.02$ a.u. value for the largest (within the set drawn) isocontour that encloses both monomers, an electron density one order of magnitude larger than the outer isocontour taken to set molecular size and shape.

That large sharing of $\rho(\mathbf{r})$ between monomers (not usually highlighted in hydrogen bonding studies) is accompanied by a local electron redistribution that leaves the proton partially deshielded. This electron deficiency of hydrogen becomes apparent in the $\rho(\mathbf{r})$ value at the nucleus, $\rho_0(\text{H})$, plotted in Fig. 3. Note how the deficiency is greater, i.e., $\rho_0(\text{H})$ is lower, for O–H··O bonds in FAD and FFAC, and increases more sharply near equilibrium. These two curves not only show the lowest $\rho_0(\text{H})$ in this plot but they also exhibit the greatest difference with respect to monomer values (formic acid in this case). If one considers that shorter intermolecular distances could be associated with stronger H-bonds and that these two bonds have the shortest O··O distances (see Table 1), their larger electron deficiency at the H nucleus should also indicate stronger hydrogen bonding.

A similar effect is found for the electron density at A–H donor groups. Values of $\rho(\mathbf{r})$ at the BCP of this covalent bond plotted in Fig. 4 show again a slight deficiency with respect to isolated monomers, although with a smaller magnitude than $\rho_0(\text{H})$. The shape of these curves is also similar to those of Fig. 3, which suggests that a closer proximity between monomers is accompanied by small losses of electron density that are felt at H-donor bonds as well as at the position of the H nucleus.

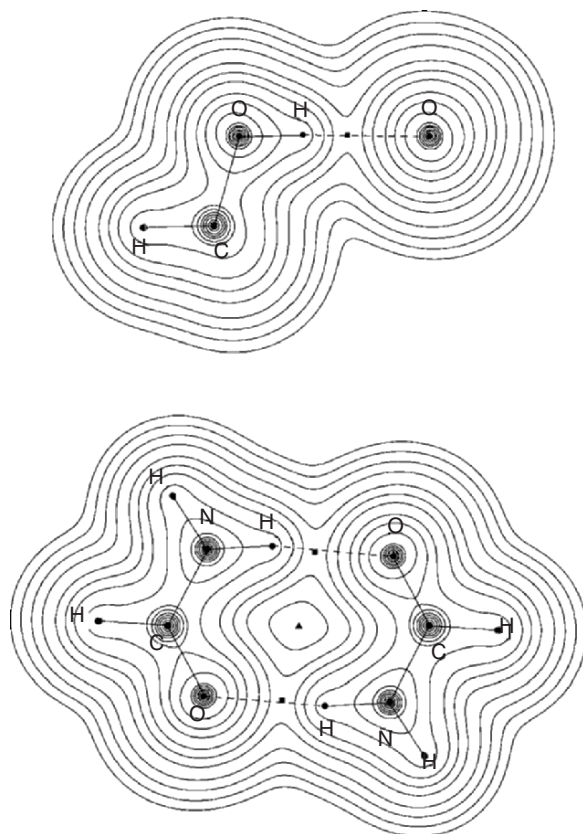


Figure 2. Electron density isocontour maps for MW (top) and FD (bottom) at equilibrium geometries. Nuclear positions are represented as circles, intermolecular BCPs as squares, and the RCP as a triangle. Outermost contour has $\rho = 0.001$ a.u. and remaining contours equal 2×10^n , 4×10^n , and 8×10^n a.u., with $n = -3, -2, -1, 0, 1,$ and 2 .

The local value of $\rho(\mathbf{r})$ at the BCP of H-bond $\text{H} \cdots \text{B}$ paths is one of the most frequently used topological descriptors in hydrogen bonding studies. For instance, one of the Koch–Popelier criteria [46, 75] to characterize H-bonds establishes the range $\rho_c = 0.002\text{--}0.040$ a.u. for equilibrium structures. The fact that it correlates with H-bond energies has led to treat this parameter as a measure of hydrogen bonding strength [41, 85, 86]. Reports for a large set of complexes have shown an exponential increase of ρ_c with shorter H-bond distances [85, 86] and the same behavior has been found for different distances within a given system [66–70, 73]. If one recalls the known exponentially decaying behavior of the electron density at long distances [45, 82], greater values of ρ_c at interatomic regions are expected for stronger local bonding. Fig. 5 plots the variation of ρ_c with the $\text{H} \cdots \text{O}$ distance. The increase of ρ_c seen

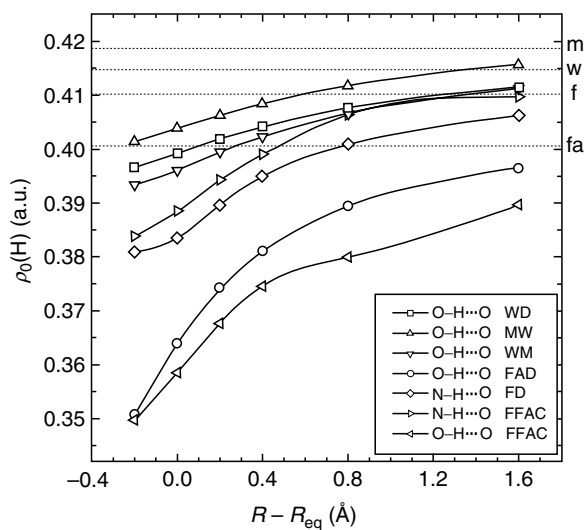


Figure 3. Change of $\rho(\mathbf{r})$ at the H nucleus. Dotted lines represent values in the isolated monomers (m: methanol, w: water, f: formamide, fa: formic acid).

in this figure is in contrast to the decrease of $\rho(\mathbf{r})$ at the H nucleus (Fig. 3) and at the A–H covalent BCPs (Fig. 4). All the curves in Fig. 5 rise exponentially with shorter R rather similarly except again the O–H...O bonds in FAD and FFAC that not only increase markedly but also show near R_{eq} values larger than the

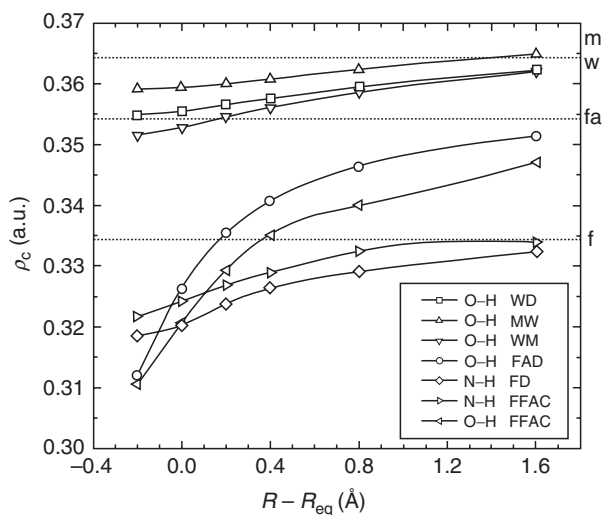


Figure 4. Change of $\rho(\mathbf{r})$ at the A–H covalent BCP of H-donor groups. Dotted lines represent values in the isolated monomers (m: methanol, w: water, fa: formic acid, f: formamide).

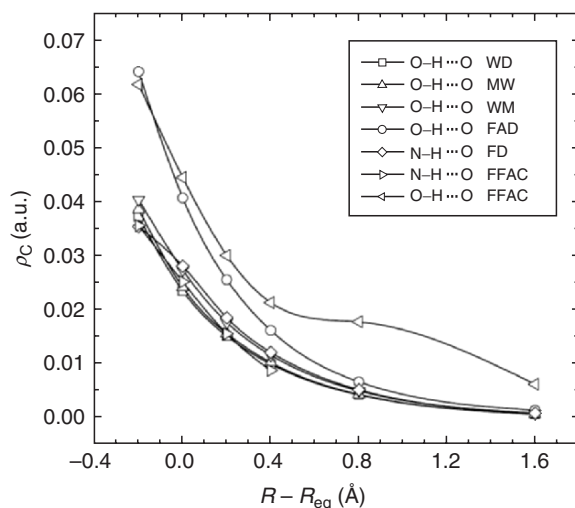


Figure 5. Change of $\rho(\mathbf{r})$ at the H \cdots O hydrogen BCP.

upper limit of Koch–Popelier criterion, an additional evidence in support of their greater strength pointed out above. The peculiar shape of the O–H \cdots O curve in FFAC is due to the sudden change found for this complex at intermediate distances at which the presumably weaker N–H \cdots O bond breaks (this curve stops at $R - R_{eq} = 0.4\text{\AA}$ in Fig. 5) while the stronger O–H \cdots O bond remains though exhibiting altered features [67, 87].

If values of ρ_c at the two bond paths of A–H \cdots O indicate that the electron redistribution decreases $\rho(\mathbf{r})$ in the covalent bond A–H and increases it in the hydrogen bond H \cdots O as A \cdots O intermolecular distance shortens, the Laplacian of $\rho(\mathbf{r})$ tells how this redistribution affects the bond environment locally. Let us recall that in the AIM theory, strong shared-shell interatomic interactions (such as covalent bonding) are characterized by local concentration of charge ($\nabla^2\rho(\mathbf{r}) < 0$) and thus the BCPs of covalent bonds have negative $\nabla^2\rho_c$, whereas weak closed-shell interactions (such as hydrogen bonding) exhibit local depletion of charge ($\nabla^2\rho(\mathbf{r}) > 0$) and the BCPs of H-bonds have positive $\nabla^2\rho_c$. According to other Koch–Popelier criteria, these values must be in the range $\nabla^2\rho_c = 0.02\text{--}0.15$ a.u. [46, 75].

Values of $\nabla^2\rho_c$ at the BCPs of A–H covalent and H \cdots O hydrogen bonds are displayed in Figs. 6 and 7, respectively. The O–H \cdots O bonds in FAD and FFAC exhibit again a different behavior to the rest of the H-bonds in both figures. In fact, the hydroxyl group of formic acid is the only covalent bond in Fig. 6 that increases $\nabla^2\rho_c$ at closer proximity between monomers whereas changes for hydroxyl in water and methanol, and for the N–H bond in formamide are nearly negligible. Since the local concentration of charge in the vicinity of equilibrium decreases noticeably only for these two stronger

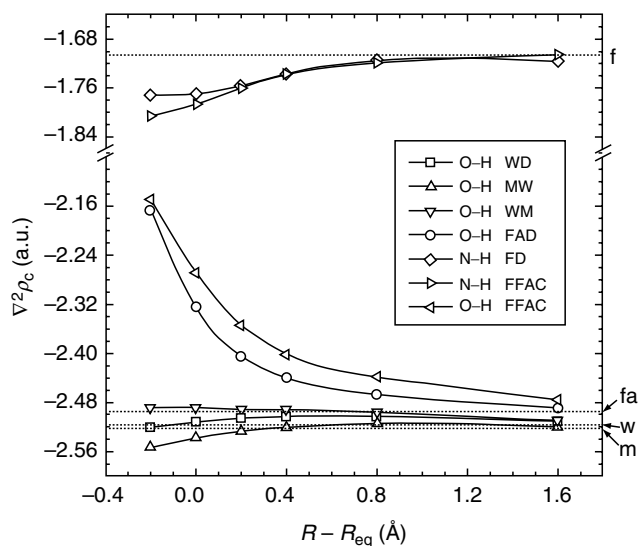


Figure 6. Change of $\nabla^2\rho(\mathbf{r})$ at the A-H covalent BCP of donor groups. Dotted lines represent values in the isolated monomers (f: formamide, fa: formic acid, w: water, m: methanol).

H-bonds (see their step rise from $R - R_{eq} = 0.4\text{\AA}$ inward in Fig. 6) while the rest of the H-donor covalent bonds suffer nearly no depletion of charge, only for these two O-H \cdots O hydrogen bonds, one should properly speak of *shifts* of electron density in the H-donor groups.

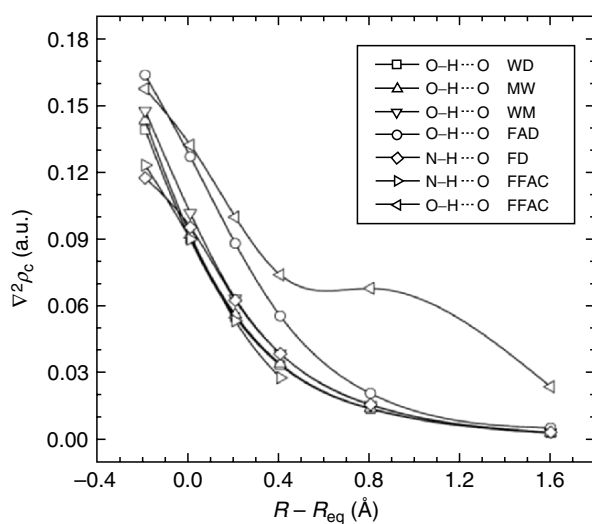


Figure 7. Change of $\nabla^2\rho(\mathbf{r})$ at the H \cdots O hydrogen BCP.

The Laplacian of $\rho(\mathbf{r})$ at the H-bond CP plotted in Fig. 7 is in all cases within the Koch–Popelier range, and, except for the scale, changes of $\nabla^2\rho_c$ show a rather similar pattern to changes of ρ_c in Fig. 5. Both ρ_c and $\nabla^2\rho_c$ increase rapidly in the proximity of R_{eq} , i.e., larger electron densities are accompanied by increased depletion of charge in the H···O paths. To interpret this observation correctly one should recall that the Laplacian of the electron density at a point is the trace of the Hessian matrix of $\rho(\mathbf{r})$, i.e., the sum of its three eigenvalues or local curvatures of the density at the point. The sign of $\nabla^2\rho_c$ at a $(3, -1)$ BCP is the result of adding one positive curvature (ρ is a minimum) along the interaction line (bond path) and two negative curvatures (ρ is a maximum) at the plane perpendicular to the interaction line. For hydrogen bonds, $\nabla^2\rho_c > 0$ is determined by the positive curvature of ρ along the H-bond paths as closed-shell interactions are characterized by relative depletion of charge in the interatomic perpendicular surface [45]. At shorter intermolecular distances in Figs. 5 and 7, the minimum value of ρ at the H-bond path is larger (ρ_c increases) and the concentration of charge at the perpendicular plane is smaller (negative curvatures decrease and $\nabla^2\rho_c$ is more positive). Nevertheless, the small magnitude of $\nabla^2\rho_c$ in Fig. 7 for these classical H-bonds is in contrast to the great changes of this topological descriptor for strong H-bonds. As we have recently demonstrated [72], the variation of $\nabla^2\rho_c$ in the transit from covalent to hydrogen bonding associated to proton transfer occurring along a strong H-bond connects continuously the covalent regime (as that plotted in Fig. 6) with the hydrogen bonding regime (as that of Fig. 7) after reaching a small maximum near the region where $\nabla^2\rho_c = 0$ [72].

The local value of the total energy density at a point \mathbf{r} , $H(\mathbf{r})$, is another useful topological descriptor that provides supplementary information about the nature of the interaction at \mathbf{r} . The total energy density $H(\mathbf{r})$ is the sum of the kinetic energy density $G(\mathbf{r})$, a positive quantity, and the potential energy density $V(\mathbf{r})$, a negative quantity, both densities related with the Laplacian of $\rho(\mathbf{r})$ through the local expression for the virial theorem [45, 46]:

$$(5) \quad V(\mathbf{r}) + 2G(\mathbf{r}) = \frac{1}{4}\nabla^2\rho(\mathbf{r})$$

When integrated over the full space or over a basin, the integral of $\nabla^2\rho(\mathbf{r})$ vanishes and Eq. 5 takes the usual form of the virial theorem. If \mathbf{r} is a BCP r_c , the sign of $H(r_c) = H_c = G_c + V_c$ shows whether the positive kinetic or the negative potential contribution is dominant. When there is an excess of kinetic energy, $\nabla^2\rho_c > 0$ in Eq. 5 and $\rho(\mathbf{r})$ is concentrated towards the nuclei as found in closed-shell interactions such as hydrogen bonding. A dominance of potential energy leading to $\nabla^2\rho_c < 0$ in Eq. 5 may be viewed as the consequence of accumulating charge at the BCP, as found in covalent bonds. Therefore, in bonds with any degree or covalent character, $|V_c| > G_c$ and $H_c < 0$, whereas $H_c > 0$ is always indicative of purely closed-shell interactions. Bonds with H_c negative but $|V_c| < 2G_c$ are termed *partially* covalent [20, 31].

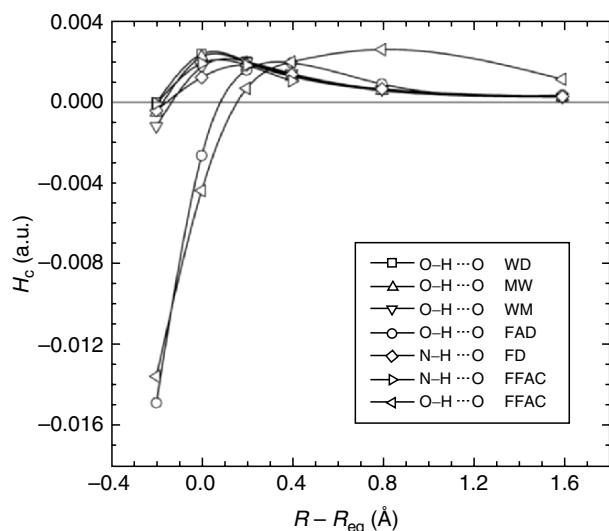


Figure 8. Change of $H_c(r)$ at the $H \cdots O$ hydrogen BCP.

Figure 8 plots the evolution of H_c at the $H \cdots O$ bond paths. The $O-H \cdots O$ bonds in FAD and FFAC show once again a different behavior entering the negative domain of H_c at R longer than R_{eq} and then falling abruptly. On the contrary, the rest of the H-bonds keep their positive H_c until the equilibrium separation and only at the closer $R_{eq} - 0.2$ distance they start to exhibit very small negative H_c . As a consequence, $O-H \cdots O$ in FAD and FFAC are the only H-bonds showing $H_c < 0$ at R_{eq} . Table 2 presents local values of kinetic and potential energy densities at the hydrogen BCP as well as H_c itself for geometries corresponding to these two shorter intermolecular distances. In agreement with the observation that $\nabla^2 \rho_c > 0$ for all the systems at all the distances

Table 2. Energy (G_c : kinetic, V_c : potential, H_c : total) densities (a.u.) at the $H \cdots O$ hydrogen BCP of systems in Fig. 1 at the equilibrium distance R_{eq} and at $R_{eq} - 0.2A$

Dimer	H-bond	R_{eq}			$R_{eq} - 0.2$		
		G_c	V_c	H_c	G_c	V_c	H_c
WD	O-H...O	0.02050	-0.01817	0.00233	0.03532	-0.03535	-0.00003
MW	O-H...O	0.02115	-0.01896	0.00219	0.03688	-0.03740	-0.00052
WM	O-H...O	0.02410	-0.02239	0.00171	0.03862	-0.03979	-0.00117
FAD	O-H...O	0.03484	-0.03745	-0.00261	0.05617	-0.07081	-0.01464
FD	N-H...O	0.02301	-0.02181	0.00120	0.03022	-0.03063	-0.00041
FFAC	N-H...O	0.02096	-0.01908	0.00188	0.03133	-0.03141	-0.00008
FFAC	O-H...O	0.03786	-0.04217	-0.00431	0.05331	-0.06667	-0.01336

considered (see Fig. 7) and according to Eq. 5, if $H_c < 0$ the condition $|V_c| < 2G_c$ must be fulfilled. In fact, Table 2 shows that this inequality holds so that H-bonds exhibiting negative H_c at some intermolecular separations should be considered to display *partial* covalent character. A behavior noticed in Fig. 8 is that H_c takes significant values only in the proximity of the equilibrium reaching the maxima just at R_{eq} except for the O–H···O bonds in FAD and FFAC. These stronger H-bonds show large potential energy effects that compensate the greater kinetic contributions near R_{eq} (see Table 2) thus leading to $H_c < 0$ in that region, but they exhibit positive H_c values distinctly larger than the rest of the H-bonds at long distances (especially O–H···O in FFAC). Both observations illustrate the dominance of kinetic effects in the associated electron redistribution.

3.2 AIM Charges and NBO Populations

The most conventional picture of any A–H···B hydrogen bond is probably the electrostatic point-charge image $A^{\delta-}-H^{\delta+}\cdots B^{\delta-}$ that highlights the role of electronegativity of atoms directly involved. For the classical H-bonds and regardless of the complexity of the image suggested by electron effects, one should expect such a qualitative charge arrangement. Changes with R of the difference between dimer and monomer atomic charges in A–H···O bonds are plotted for the H-donor atom A (N, O) in Fig. 9, for H-acceptor O in Fig. 10, and for H in Fig. 11, while the corresponding monomer values are listed in Table 3 for reference. In what follows, the results of integrating $\rho(\mathbf{r})$ over AIM

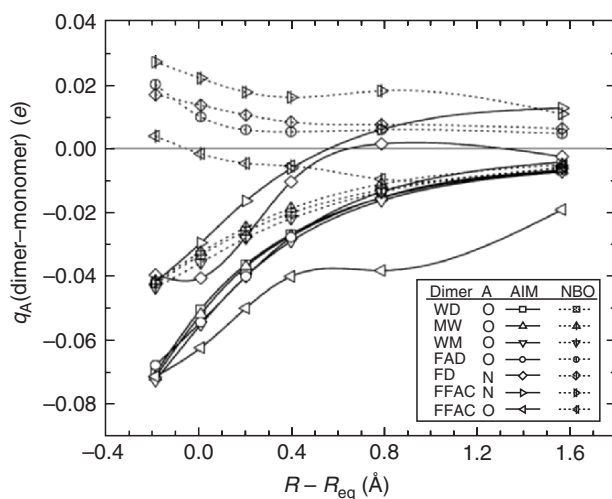


Figure 9. Change with respect to monomer values of the atomic charge of atom A in A–H···O hydrogen bonds.

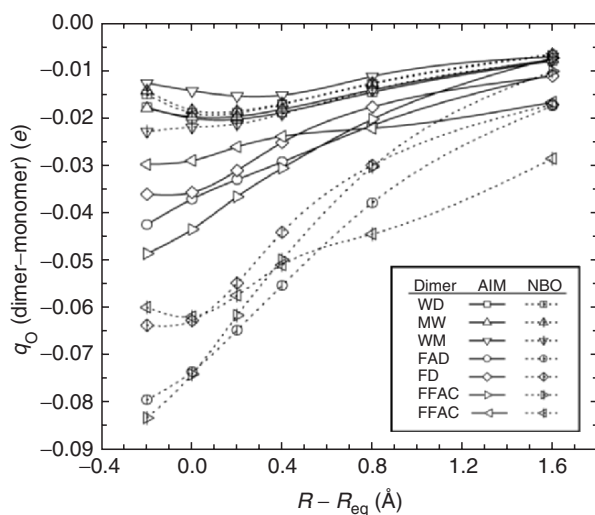


Figure 10. Change with respect to monomer values of the atomic charge of oxygen in A-H...O hydrogen bonds.

basins and those of adding NBO populations ascribed to atoms are discussed together. Given the rather different nature of AIM and NBO atomic charges, their common features discussed in this overview reveal essential characteristics of bonding, avoiding thus artificial issues so frequent when dealing with other

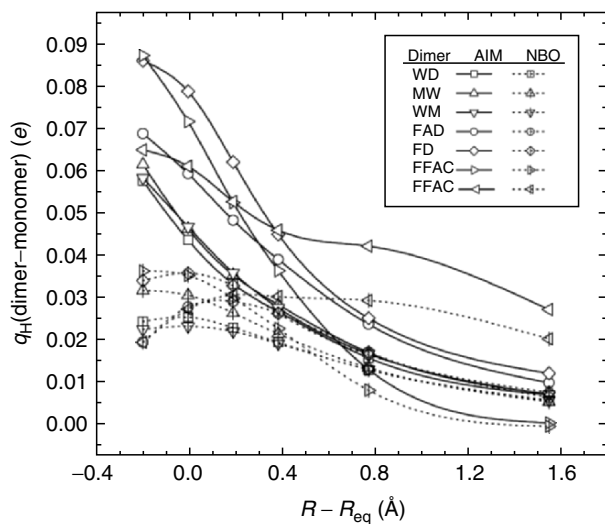


Figure 11. Change with respect to monomer values of the atomic charge of hydrogen in A-H...O hydrogen bonds.

Table 3. Monomer atomic charges (e) of the atoms involved in A–H···O hydrogen bonds

Monomer	A	AIM			NBO		
		q_A	q_H	q_O	q_A	q_H	q_O
Water	O	-1.1328	0.5664	-1.1328	-0.8977	0.4488	-0.8977
Methanol	O	-1.0941	0.5577	-1.0941	-0.7178	0.4430	-0.7178
Formic acid	O	-1.1279	0.5971	-1.1244	-0.6683	0.4714	-0.5362
Formamide	N	-1.2238	0.4261	-1.1308	-0.8099	0.3898	-0.5619

electron populations based upon less elaborate approaches (see the recent discussion by Bader and Matta on the meaning of “atomic charges” in Ref. 78).

The changes of curvature seen in some curves of FFAC are due to the changes suffered by this complex described above. When both monomers in FFAC separate from equilibrium, the N–H···O bond breaks leaving the system bound by the single O–H···O bond. This process involves a particular electron redistribution at intermediate distances which in turn gives rise to local alterations, but, except for some wiggles in that region, this specific change has no effect on the general trends studied, so that, as it has been addressed in separate papers [67, 87], it will not be further considered in this overview.

With the only exception of the donor atom A in FAD, FD, and FFAC for which there is a qualitative discrepancy between AIM and NBO results, trends shown by all the charges in Figs. 9–11 comply with the $A^{\delta^-} - H^{\delta^+} \dots B^{\delta^-}$ picture. Regarding the donor atom A in Fig. 9, AIM predicts a steady increase in its negative charge as the monomers move closer, with all the oxygens showing nearly identical variation. Since AIM charges give populations of atomic basins of $\rho(\mathbf{r})$, the electron redistribution occurring at all the intermolecular distances is felt as continuous changes of q with R (this remark is of course also valid for Figs. 10 and 11). NBO predicts a similar trend only for systems with one single H-bond whereas for cyclic dimers with two H-bonds, q_A changes very little with R and only near the equilibrium it shows slight differences decreasing its negative value by less than $0.02e$. This makes the disagreement with AIM scarcely significant, especially when one considers that both methods agree in predicting similar trends for changes of charges in H···O. In fact, AIM and NBO q_O curves in Fig. 10 are essentially identical for WD, MW, and WM, and exhibit rather similar patterns for FAD, FD, and FFAC (note the identical sequence shown by AIM and NBO curves of these complexes in the inner region). This H-acceptor atom increases its negative charge at all the intermolecular separations. If for AIM charges this variation may be viewed as the direct consequence of the repeatedly mentioned electron redistribution, the greater sensitivity of NBO charges for H-acceptor atoms as compared with H-donor atoms suggests a possible effect due to electron lone pairs. In fact, since NBO one-center atomic charges include population of lone pairs on that center, this difference between electronegative A and O atoms

points to a distinct role played by the lone pairs of oxygen. One of the traditional views of hydrogen bonding has been the involvement of a lone pair of the H-acceptor $B^{\delta-}$ atom in the interaction. The variation of NBO charges plotted in Fig. 10 is consequent on that role which is further explored below using the information provided by the ELF (see Sect. 3.4).

Figure 11 shows that hydrogen loses charge increasing thus its positive charge $H^{\delta+}$ upon closer approximation between monomers. This well-known effect constitutes another Koch–Popelier criterion [46, 75] and is one of the main characteristics of the interaction. The AIM curves in Fig. 11 split into systems with one single H-bond and systems with two H-bonds, with q_H values in these cyclic dimers also showing a slightly different behavior in $O-H \cdots O$ and $N-H \cdots O$ bonds. Since AIM charges are obtained integrating $\rho(\mathbf{r})$ over atomic basins, and H basins suffer greatest spatial changes due to their location between A and O basins in molecular space, the magnitude of the variation of q_H with R is in general the largest one of the three atoms in H-bonds. The NBO values of q_H are not very different to AIM values at long and intermediate distances in Fig. 11, but in the proximity of equilibrium, they are smaller than AIM and have a magnitude more similar to q_A (Fig. 9) than to q_O (Fig. 10). Since NBO charges are one-center natural populations, this is consistent with the direct connection between H and A atoms in the covalent bond A–H.

Comparison between the variation of AIM and NBO atomic charges reflects the magnitude of effects associated to hydrogen bonding at different intermonomer distances. Atomic basins of $\rho(\mathbf{r})$ extend over the whole molecular space of the system [45, 46] so that the AIM basins of the three atoms in $A-H \cdots O$ feel a subtle electron redistribution that changes in a continuous manner with R . These changes are revealed in continuous variation of the associated populations as indicated by the comparable magnitude of AIM values for A, H, and O atoms at any distance. On the contrary, the variation of NBO charges depends on the molecular orbital effects directly felt by the bonded atoms. This implies that the magnitude of the variation of the NBO charges is smaller than that of the AIM charges, and as discussed above, the behavior of oxygen is different due to the role of its lone pairs. Although the AIM and NBO analyses provide distinct information that gives rise to distinct individual atomic features, they agree closely in predicting the spatial evolution of net electron charges of monomer partners at the whole range of intermolecular distances, as Fig. 12 clearly illustrates.

These net charges are obtained by adding all the atomic charges in every monomer. According to the Lewis concept of an acid as an electron acceptor and a base as an electron donor, H-donor monomers in Fig. 12 gain charge ($q < 0$) and H-acceptor monomers lose charge ($q > 0$). Water and methanol in single H-bond complexes show small net charges about $0.015e$ at R_{eq} and $0.025e$ at $R_{eq} - 0.2\text{\AA}$, whereas FFAC exhibits larger charges about $0.040e$ at R_{eq} and $0.045e$ at $R_{eq} - 0.2\text{\AA}$. The negative value in this complex belongs to formic acid that behaves as the net H-donor acid while formamide is the positive net H-acceptor base, in agreement with the aforementioned data

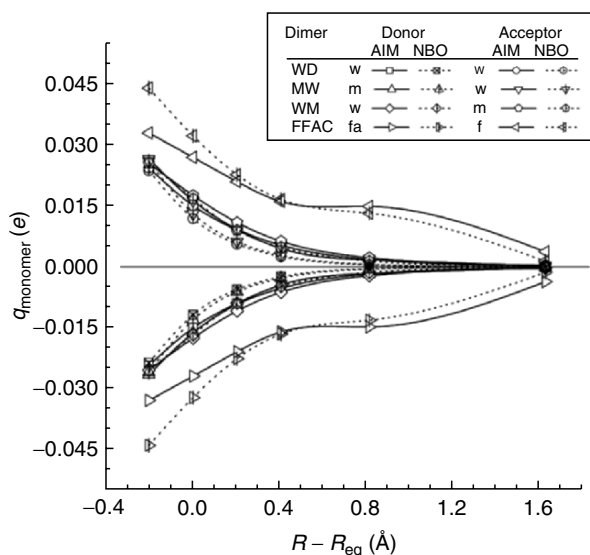


Figure 12. Change of the net charge of the monomers.

indicating that $\text{O-H}\cdots\text{O}$ is stronger than $\text{N-H}\cdots\text{O}$ in FFAC. Note besides the rather different behavior of this system at intermediate and long distances. Whereas the rest of the complexes show noticeable charges only at the close proximity of equilibrium, FFAC reveals hydrogen bonding effects as soon as the monomers begin to approximate, and even at distances 1.2 \AA longer than R_{eq} they present net charges comparable to those of the single H-bond systems. FAD and FD are symmetric dimers in which both monomers behave simultaneously as H-donor (acid) and H-acceptor (base), and have thus net charge zero at any distance. As a final consideration regarding charge effects, the excellent agreement between the AIM and NBO curves in Fig. 12 indicates that despite the different type of information provided by both methods, they are able to identify a coincident response of hydrogen bonding partners to charge transfer effects underlying the interaction.

3.3 Electrostatic Potentials

The value of the electrostatic potential $U(\mathbf{r})$ created by a molecular system at a point \mathbf{r} gives the electrostatic energy on a unit positive charge located at \mathbf{r} and the sign indicates whether the nuclear or the electron term in Eq. 2 is dominant there. $U(\mathbf{r})$ is a useful property to study reactivity given that an approaching electrophile will be attracted to negative regions (particularly to points with most negative values), where the electron distribution effect is dominant. Experimental $U(\mathbf{r})$ computed with electron densities obtained from X-ray diffraction data has been used to explore the electrophilicity of hydrogen bonding functional groups

[11, 88]. The study of experimental and theoretical $U(\mathbf{r})$ shows that H-donor and H-acceptor properties of molecules are revealed by positive and negative regions, respectively, so that the formation of a H-bond can be regarded as the consequence of a complementarity between the electrostatic potentials [11, 53]. At H-bond distances, however, these regions superimpose and cancel in the intermolecular region [53, 88].

This complementarity between electrostatic potentials is illustrated for a single H-bond complex (MW) in Fig. 13 and a dimer with two H-bonds (FD) in Fig. 14. As it is readily noticed in these plots, $U(\mathbf{r})$ for H-donor and H-acceptor monomers merges into one common positive region around the H-bond embracing both partners in complexes. These maps show also features that relate the electrostatic potential to the NBO charges discussed in Sect. 3.2 and ELF properties addressed in Sect. 3.4 with regard to electron lone pairs of H-acceptor oxygen. Isolated water (Fig. 13b) and formamide (Fig. 14a or 14b) monomers exhibit negative regions around oxygen that clearly points to two lone pairs as sites of electrophilic attack. These regions enclose two minima in water (innermost negative contours in Fig. 13b) and are symmetrically located around O nucleus while in formamide the presence of the NH_2 group distorts that symmetry slightly (compare the shapes of both negative regions around O in Fig. 14a or 14b). Upon hydrogen bonding, one of those negative regions remains virtually unchanged whereas the other suffers distinct changes: its extension decreases in MW (above acceptor oxygen in Fig. 13c) and nearly disappears in FD (see the very small two-lobe negative region in the bond ring interior in Fig. 14c). Changes with respect to isolated monomers displayed by the negative part of $U(\mathbf{r})$ in H-bond complexes are in agreement with the expected direct involvement of one of the lone pairs of H-acceptor oxygen in the interaction.

Figure 15 plots electrostatic potentials for MW and FD at geometries corresponding to an intermolecular distance 0.8 \AA longer than R_{eq} . The remarkable similarity of these maps with those of equilibrium in Figs. 13c and 14c illustrates the long distance behavior of the electrostatic complementarity between monomers. However, it is interesting to consider the magnitude of $U(\mathbf{r})$ in the intermonomer region to gauge the electrostatic differences due to different intermolecular distances. As for the set of isocontours plotted in these maps, the innermost value of $U(\mathbf{r})$ that embraces both monomers in MW is 80 kcal/mol at R_{eq} (Fig. 13c) and 20 kcal/mol at $R_{\text{eq}} + 0.8$ (Fig. 15a), whereas for FD, these values are 100 kcal/mol at R_{eq} (Fig. 14c) and 20 kcal/mol at $R_{\text{eq}} + 0.8$ (Fig. 15b). The proximity to equilibrium structures becomes thus apparent in the magnitude of the electrostatic potential in the electropositive region surrounding the H-bond. Save for this quantitative difference in the arrangement of $U(\mathbf{r}) > 0$ isocontours, the division of space into negative and positive regions is rather similar in both geometries as the virtually identical shapes of $U(\mathbf{r}) = 0$ border reveal. These considerations indicate that, upon hydrogen bonding, the electrostatic potential suffers a rearrangement similar to the electron density redistribution discussed before.

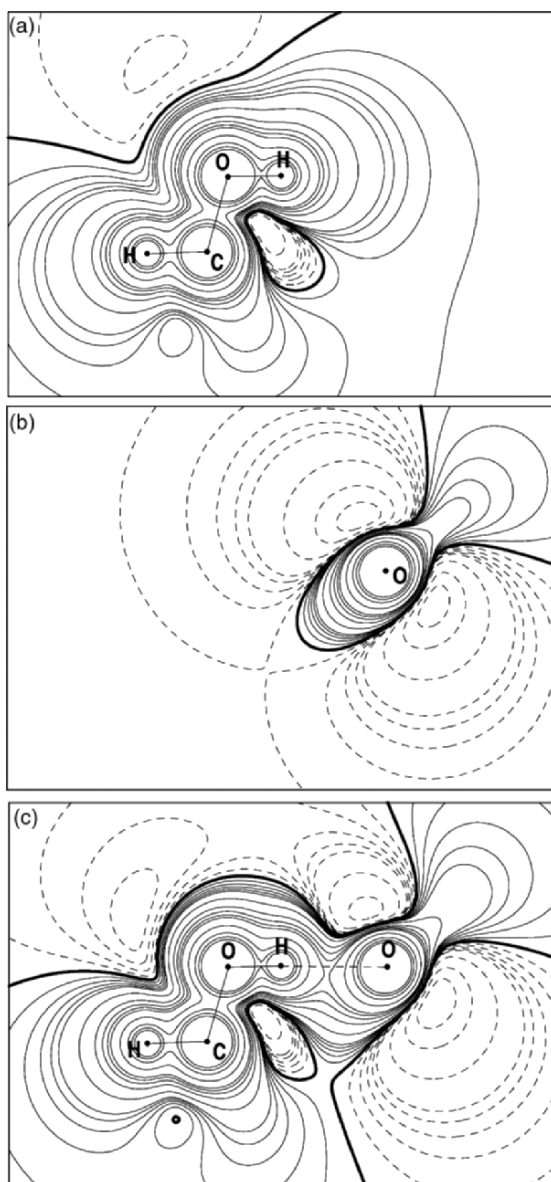


Figure 13. Electrostatic potential isocontour maps at the plane of O–H···O bond for MW at equilibrium. Contours are $U(\mathbf{r}) = \pm p \times 10^n$ ($p = 2, 4, 6, 8, 10$, $n = 0, 1, 2$) kcal/mol, increasing (full lines positive) and decreasing (dashed lines negative) from contour $U(\mathbf{r}) = 0.0$ (bold line): (a, b) Isolated monomers (a: methanol, b: water) at the complex geometry. (c) Complex.

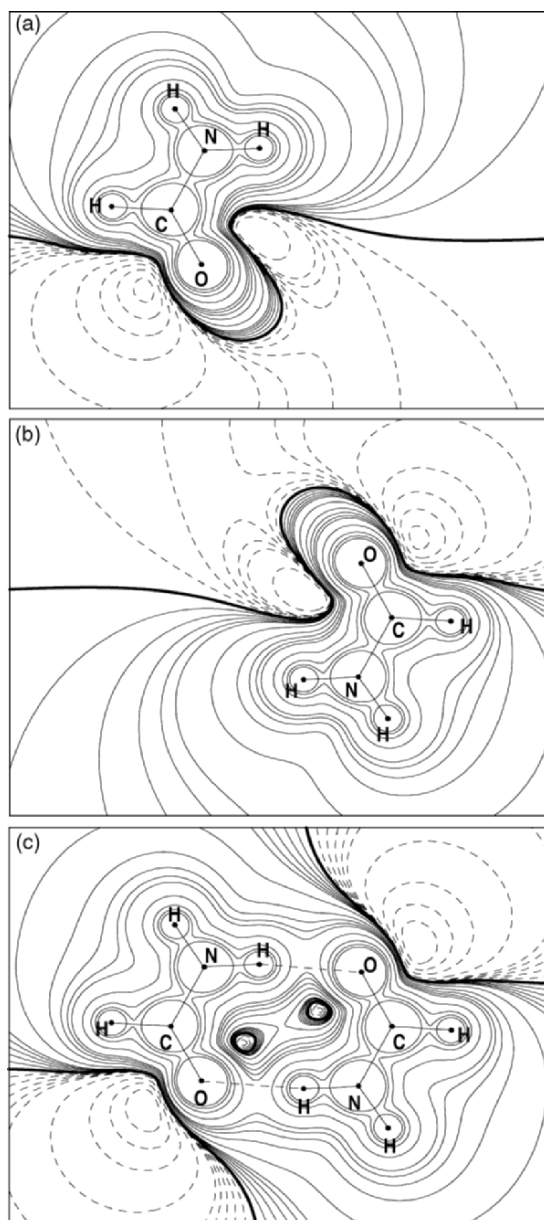


Figure 14. Electrostatic potential isocontour maps for FD at equilibrium: (a, b) Isolated formamide monomers at the dimer geometry. (c) Dimer. Contours as in Fig. 13.

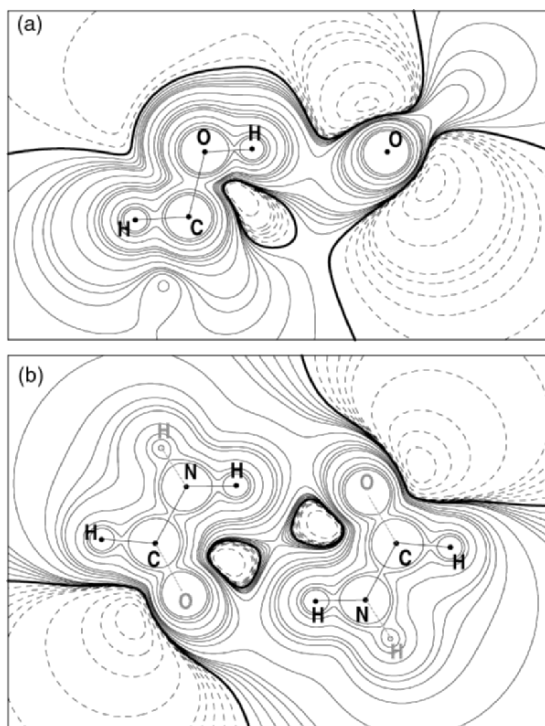


Figure 15. Electrostatic potential isocontour maps for MW (a) and FD (b) at $R_{\text{eq}} + 0.8$ geometries. Gray lines and symbols in (b) indicate out of plane atoms. Contours as in Fig. 13.

Information provided by the spatial distribution of electrostatic potentials is supplemented with local values of $U(\mathbf{r})$ at selected atomic sites. The electrostatic potential at a nucleus, U_0 defined in Eq. 3, is a quantity which can be used as a reactivity parameter in the spirit of AIM topological descriptors. Linear correlations between H-bond energies and U_0 calculated at the sites of donor and acceptor atoms have been reported for a series of H-bond complexes [55]. However, the most general descriptor regarding U_0 is that computed at the hydrogen site, $U_0(\text{H})$. Excellent linear relationships between $U_0(\text{H})$ and H-bond energies that include terms arising from decomposition schemes have been used to investigate hydrogen bonding abilities of molecules with a variety of functional groups [54]. The variation of $U_0(\text{H})$ plotted in Fig. 16 is in close agreement with changes of $\rho_0(\text{H})$ displayed in Fig. 3. Due to the expression of U_0 , Eq. 3, the electron deficiency at the proton position (see Fig. 3) is noticed now as a decreased, i.e., less negative, electrostatic potential at the nucleus. This decrease rises exponentially with shorter distances for most of the H-bonds investigated and at $R_{\text{eq}} + 0.8 \text{ \AA}$, values of $U_0(\text{H})$ in the complexes are already much larger than in the monomers. The sequence of values at R_{eq} for $U_0(\text{H})$ in

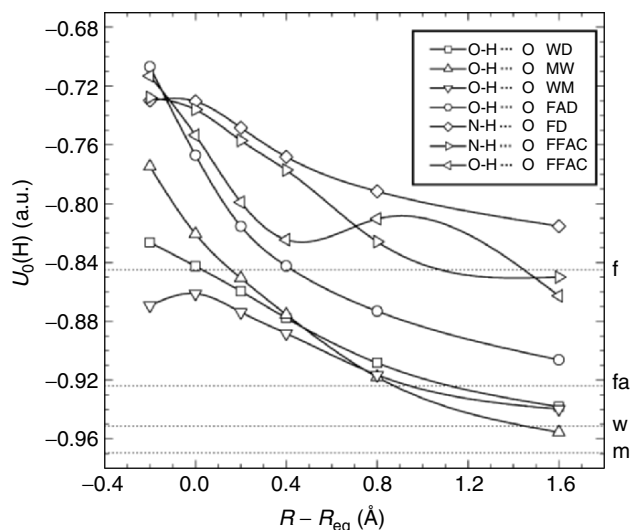


Figure 16. Change of $U(\mathbf{r})$ at the H nucleus. Dotted lines represent values in the isolated monomers (f: formamide, fa: formic acid, w: water, m: methanol).

Fig. 16 and $\rho_0(\text{H})$ in Fig. 3 is the same but if one looks at the scale in both plots (recall that for an isolated hydrogen atom, $U_0 = -1$ a.u.), the electrostatic potential at the H nucleus is a more sensitive descriptor than the electron density. This is highlighted by expressing $\rho_0(\text{H})$ and $U_0(\text{H})$ values at R_{eq} as relative changes with respect to monomer values. For the system showing the smallest deviation from monomers, WD, the deficiency of $\rho_0(\text{H})$ amounts to 3.7% and the decrease of $U_0(\text{H})$ to 11.4%. For the system with the largest deviation from monomers, O-H...O bond in FFAC, relative changes of $\rho_0(\text{H})$ and $U_0(\text{H})$ are 9.7% and 18.5%, respectively.

3.4 Electron Localization Function

The description of the electron redistribution that accompanies formation of H-bonds considered up to this point is now supplemented with information provided by the ELF. Spatial distributions of $\eta(\mathbf{r})$ are displayed in Figs. 17 and 18 in the form of isocontour maps at selected planes of MW and FD, respectively. These plots show the most prominent feature of changes suffered by the ELF upon hydrogen bonding: the mutual “pressure” exerted by H-donor and H-acceptor groups. To understand this feature calls for considering first the localization domains of monomeric species involved in A-H...O bond. Valence disynaptic basins $V(\text{A}, \text{H})$ in H-donor monomers occupy less space than valence monosynaptic basins $V(\text{O})$ in H-acceptor monomers [63], i.e., in protonated basins $V(\text{A}, \text{H})$ the localization is higher than in basins $V(\text{O})$

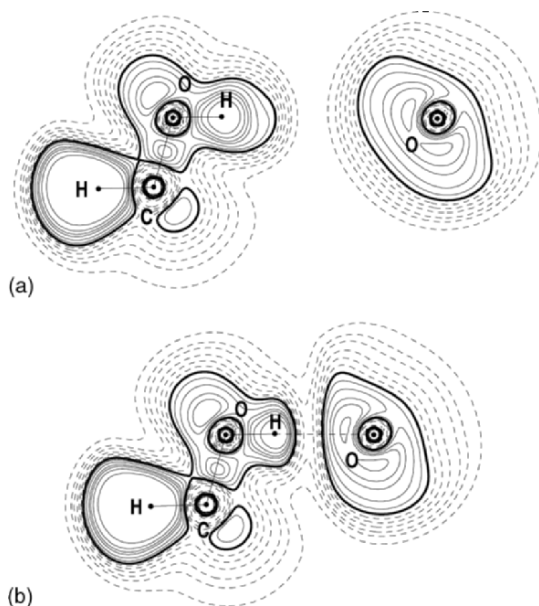


Figure 17. Electron localization function isocontour maps at the plane containing O–H···O bond in MW. The following isocontours of $\eta(\mathbf{r})$ are drawn (starting at the outermost one): 0.01, 0.05, 0.1, 0.2, 0.3, 0.4 (dashed lines), 0.5 (bold line), 0.6, 0.7, 0.8, 0.85, 0.9, and 0.95 (full lines): (a) Isolated monomers (left: methanol, right: water) at the orientation of the complex at equilibrium. (b) MW at equilibrium geometry.

corresponding to lone pairs of oxygen. Although ELF basins are not shown in Figs. 17 and 18, the different space occupied by these domains is readily noticed: compare the region around the O–H bond of isolated methanol with the region around oxygen of isolated water in MW (Fig. 17a) or the regions around N–H bond and carbonyl oxygen of isolated formamides in FD (Fig. 18a). As Silvi and Savin have pointed out [57], ELF basins give a qualitative picture of valence shell electron pair repulsion (VSEPR) domains. In agreement with the assumptions of the VSEPR model [89, 90] regarding localization of electron pairs in molecular geometry, lone pairs occupy more space than bond pairs though bonds with H are a special case because the associated space can be much larger if the other atom is not electronegative (compare for instance the regions around O–H and C–H bonds of isolated methanol in Fig. 17a).

Hydrogen bond formation reduces volume of $V(\text{A}, \text{H})$ and $V(\text{O})$ domains in isolated monomers (see Figs. 19 and 20) because the electron localization increases in the interaction. Besides, the mutual Pauli repulsion of pairs along the region surrounding A–H···O link in the complex flattens their opposite boundary isosurfaces of $\eta(\mathbf{r})$ as it is readily noticed in Figs. 17b and 18b. Although, as discussed below, the changes shown by regions of donor A–H bonds and acceptor lone pairs are slightly different because a

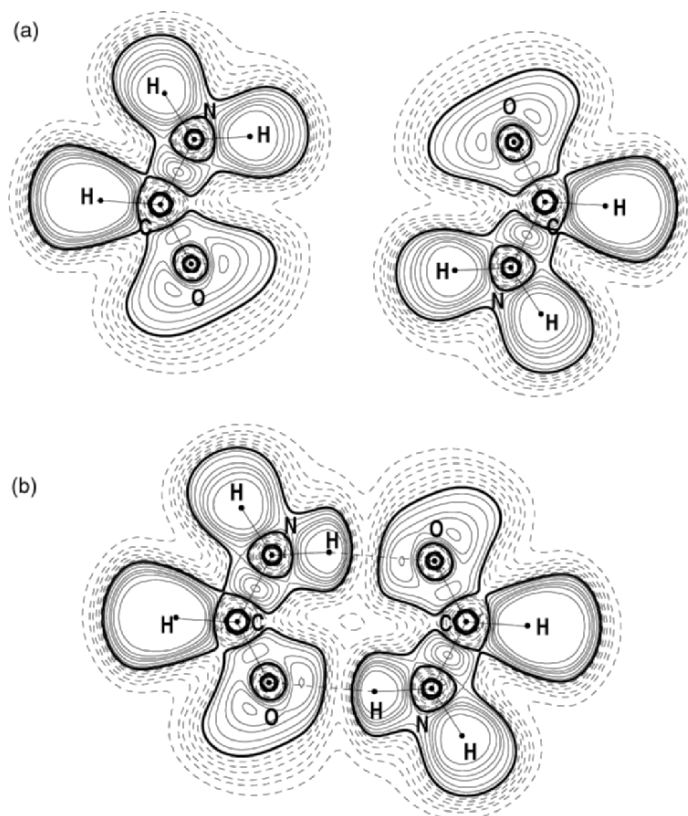


Figure 18. Electron localization function isocontour maps for FD: (a) Isolated formamide monomers at the orientation of the dimer at equilibrium. (b) FD at equilibrium geometry. Contours as in Fig. 17.

bond pair and a lone pair have distinct localization domains, this mutual pressure between donor and acceptor groups due to the Pauli repulsion can be viewed as an effect of the mutual penetration of the hydrogen and acceptor atoms prescribed by Koch and Popelier in their criteria to characterize hydrogen bonds [46, 75].

As anticipated on the basis of this mutual pressure, the volumes of $V(A, H)$ and $V(O)$ basins must decrease upon hydrogen bonding. On the other side, although one should expect lower populations associated to smaller volumes, the possibility of charge transfer as a consequence of localization changes predicted by the ELF [63] can give rise to a different behavior. To assess the magnitude of these effects we analyze now the variation of volumes and electron populations of these two basins as well as those of the second monosynaptic basin $V(O)$ corresponding to the other lone pair of oxygen not directly involved in hydrogen bonding.

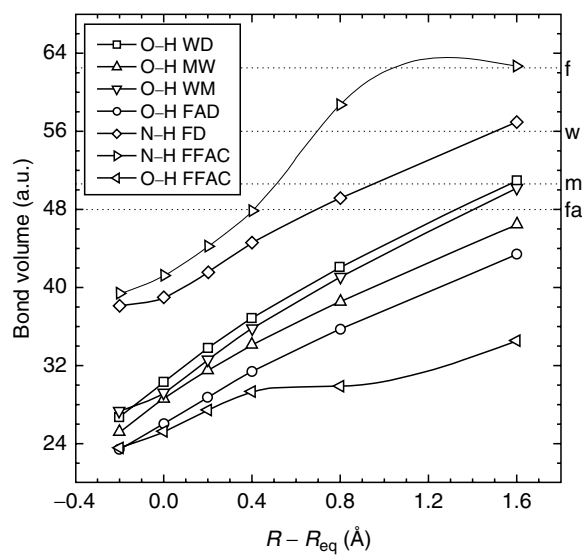


Figure 19. Change of volume of the bond pair ELF basin of A-H donor bond. Dotted lines are values in the monomers (f: formamide, w: water, m: methanol, fa: formic acid).

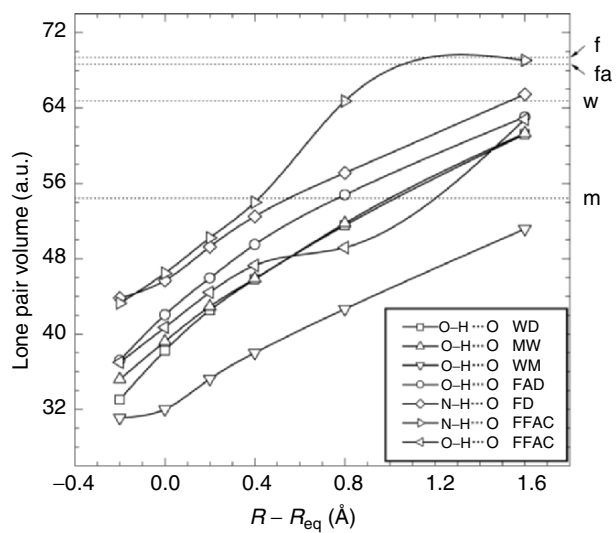


Figure 20. Change of volume of the lone pair ELF basin of O involved in H bond. Dotted lines are values in the monomers (f: formamide, fa: formic acid, w: water, m: methanol).

Figures 19 and 20 plot the variation of volume of $V(A, H)$ and $V(O)$ basins whereas Fig. 21 plots volumes of the second monosynaptic $V(O)$ basin corresponding to the lone pair of oxygen not directly involved in H-bond. Save for the above-mentioned local wiggles of FFAC at intermediate R , the large contraction of localization domains revealed by Figs. 19 and 20 illustrates the magnitude of the mutual pressure exerted by $V(A, H)$ and $V(O)$ basins. This effect is felt at long distances as it is apparent by the fact that all the curves are already well below monomer values at $R_{\text{eq}} + 1.6 \text{ \AA}$. The great contraction with respect to isolated monomers demonstrates that this change of volume is one of the most sensitive properties to hydrogen bonding effects. As for results plotted in Figs. 19 and 20, the decrease of the volume of the disynaptic basins at R_{eq} is about 45% for the O–H bonds and 35% for the N–H bonds while the contraction of monosynaptic basins is about 40% for the acceptor lone pairs in the O–H...O bonds and about 33% for the N–H...O bonds. On the contrary, the volume of the second lone pair basin of oxygen shown in Fig. 21 changes very little remaining nearly constant until distances close to R_{eq} . Complexes with one single H-bond exhibit slight decreases of volume (about 1% for WD and WM and 5% for MW) whereas this second $V(O)$ basin expands about 5% in cyclic systems. This slight expansion can be seen as a consequence of structural constraints existing in the ring planar geometries of these systems: compare the freedom to orient in space of both the lone pair domains of the acceptor oxygen in MW (Fig. 17b) with its restricted orientation in FD (Fig. 18b). However, irrespective of whether this monosynaptic basin contracts or expands, its

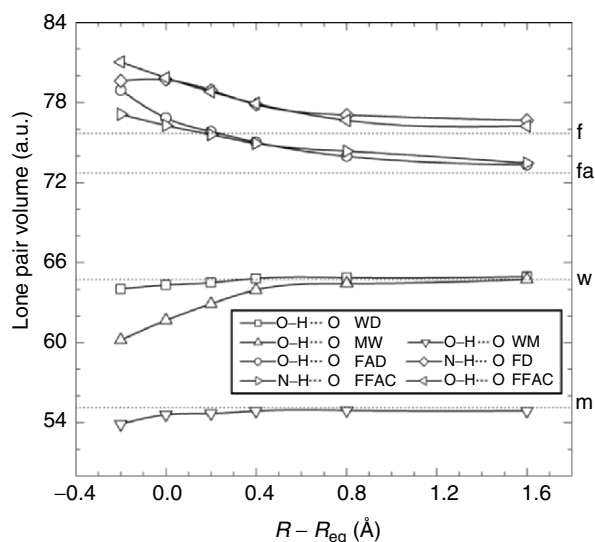


Figure 21. Change of volume of the lone pair ELF basin of O not involved in H bond. Dotted lines are values in the monomers (f: formamide, fa: formic acid, w: water, m: methanol).

changes are insignificant when compared with those of localization basins involved in hydrogen bonding.

As properties related with electron density and electrostatic potential suggest, the formation of a H-bond involves some charge transfer between the interacting monomers. Analyses of the ELF allow to investigate the amount of charge transfer due to electron delocalization between $V(A, H)$ and $V(O)$ basins. According to the Lewis point of view, the expected net effect of intermolecular charge transfer should be an increase of $V(A, H)$ population and an electron loss in the $V(O)$ basin. The variation of $V(A, H)$ and $V(O)$ populations is plotted in Figs. 22 and 23, respectively, whereas that of the second lone pair basin of oxygen is displayed in Fig. 24. A first point to note in these plots is that unlike volumes, populations keep a well-separated grouping around reference monomer values. As expected, A–H bond population increases at closer approximation between monomers with a noticeable change of slope at R about 0.4 \AA longer than R_{eq} (Fig. 22). In a parallel manner, lone pair population of acceptor oxygen decreases at shorter R with a similar change of slope also at $R_{\text{eq}} + 0.4 \text{ \AA}$ (Fig. 23). If one considers that both basins undergo large contraction and that despite its smaller volume, the $V(A, H)$ population increases at shorter distances, this gain of charge can be viewed as the dominant effect due to electron delocalization between the donor and the acceptor. The magnitude of this increase of charge at equilibrium is $0.015e$ in WD and WM, $0.030e$ in MW, and $0.093\text{--}0.098e$ in complexes with two H-bonds.

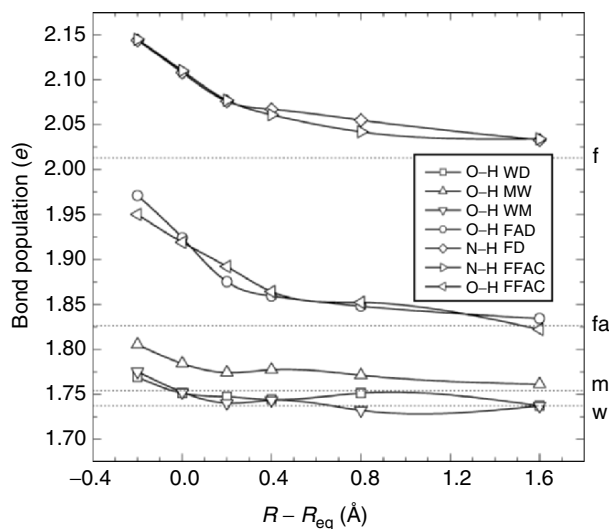


Figure 22. Change of the bond ELF basin population of A–H donor bond. Dotted lines are values in the monomers (f: formamide, fa: formic acid, m: methanol, w: water).

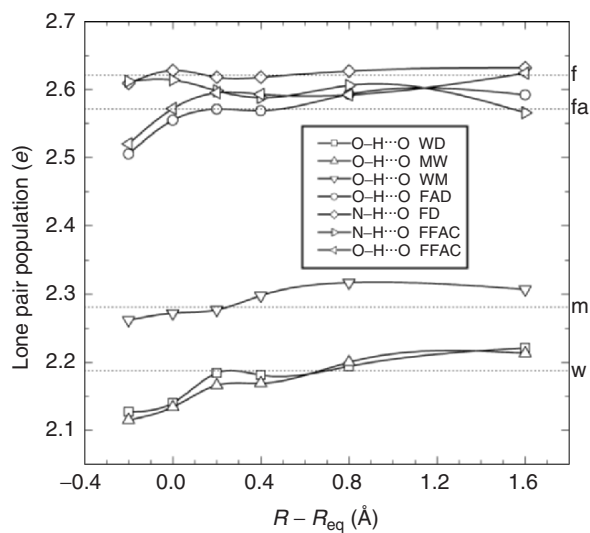


Figure 23. Change of the lone pair ELF basin population of O involved in the H bond. Dotted lines are values in the monomers (f: formamide, fa: formic acid, m: methanol, w: water).

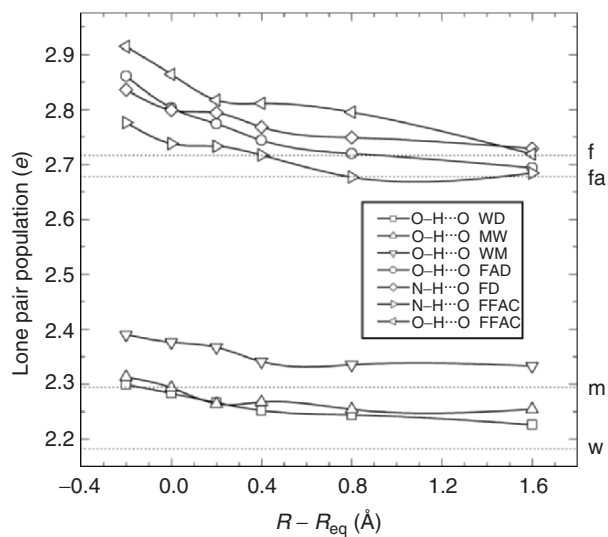


Figure 24. Change of the lone pair ELF basin population of O not involved in the H bond. Dotted lines are values in the monomers (f: formamide, fa: formic acid, m: methanol, w: water).

The variation of charge for monosynaptic basins associated to both lone pairs of acceptor oxygen is involved to a greater extent due to the existence of other disynaptic basins that permit electron transfer between valence localization domains in this atom. Thus, the magnitude of the loss of charge for the lone pair participating in H-bond (Fig. 23) at R_{eq} is $0.05e$ in WD, MW, and O–H···O bond in FFAC, $0.01e$ in WM, and $0.015e$ in FAD, but for the two N–H···O bonds, this population increases by $0.01e$ in FD and $0.04e$ in FFAC. The second monosynaptic basin population of the lone pair not involved in H-bond (Fig. 24) increases by larger amounts of charge: about $0.10e$ in WD and MW, $0.08e$ in WM, FD, and N–H···O bond in FFAD, and $0.13e$ in FAD and O–H···O bond in FFAD. The net effect for localization domains around oxygen is thus a gain of charge made at the expense of the adjacent disynaptic basins.

Note finally the magnitude of populations associated to localization domains. In the monomeric species, the $V(\text{A}, \text{H})$ population for the O–H bonds is about $1.75e$ in water and methanol, and $1.83e$ in formic acid while for the N–H bond in formamide it is $2.0e$. The added population of both $V(\text{O})$ lone pair basins of oxygen is $4.37e$ in water, $4.58e$ in methanol, $5.25e$ in formic acid, and $5.34e$ in formamide. On the basis of these monomeric values, the H-donor ability must increase as the charge associated to A–H decreases and thus hydroxyl must be a better donor than N–H. The H-acceptor ability of oxygen must increase as the charge associated to its lone pairs increases and thus the carbonyl oxygen (in formamide and formic acid) must be a better acceptor than the hydroxyl oxygen (in methanol and water). Taking into account even the small quantitative differences in all these populations, the stronger H-bond must be O–H···O in FFAC, as other evidence presented before in this overview has already suggested. It is noteworthy that populations obtained from space domains defined in terms of electron localization agree in describing the hydrogen bonding abilities of functional groups that form the most common types of classical H-bonds.

4 CONCLUDING REMARKS

The interaction between two monomers that move nearer until a stable H-bond complex is formed provokes changes in their electron distribution which can be probed by comparing the electron properties of the complex with the monomer values. This study has been presented in this overview by means of *ab initio* quantum calculations for complexes linked by conventional N–H···O and O–H···O hydrogen bonds at different intermolecular distances R . The changes with the distance of a number of properties obtained from the electron density $\rho(\mathbf{r})$, AIM and NBO atomic charges, electrostatic potentials $U(\mathbf{r})$, and the ELF $\eta(\mathbf{r})$ can be succinctly summarized as follows.

4.1 Properties of $\rho(\mathbf{r})$

At shorter R , the monomers share increasingly higher contours of $\rho(\mathbf{r})$ but the local electron redistribution at the region of the A–H···O bond gives rise to a deficiency at the position of H, leaving the proton deshielded, and to a small loss of density at the A–H covalent bond. The value of ρ_c at BCPs in H···O paths increases exponentially with shorter R but the rise of its positive Laplacian indicates that $\rho(\mathbf{r})$ decreases at the plane perpendicular to the H···O line. The electron redistribution is dominated by kinetic effects (G_c dominates over V_c at every R) but all the bonds show $H_c < 0$ (a “partially covalent” feature) at R immediately shorter than R_{eq} while the two stronger O–H···O bonds have $H_c < 0$ even at R_{eq} .

4.2 AIM and NBO Atomic Charges

Both methods predict for donor (A) and acceptor (O) atoms negative charges that increase at shorter R , this variation being more marked for systems with two H-bonds. The particular features shown by NBO values of q_O indicate an involvement of lone pairs of oxygen at all the distances. Hydrogen atom loses charge displaying positive values of q_H that increase at shorter R . This charge is more sensitive to the type of H-bond than the q_A and q_O charges, with stronger H-bonds showing greater positive q_H . Although AIM and NBO may slightly differ in providing local features at certain R , both methods predict virtually identical net charges for monomers in the complex at all the distances. These net charges identify the magnitude of the roles as H-donor (acid) of the monomer with net charge $q < 0$ and H-acceptor (base) of the monomer with net charge $q > 0$, in agreement with the Lewis electron view of acid–base interactions.

4.3 Properties of $U(\mathbf{r})$

The electrostatic potential shows a complementarity between positive regions of H-donor groups and negative regions of the H-acceptor atom that merge into one common positive region around the A–H···O bond in the complex. The involvement of one of the lone pairs of oxygen is revealed in the maps of $U(\mathbf{r})$ by a noticeable difference between the two electronegative regions that surround this atom in the complex. At long distances, there is a space distribution of $U(\mathbf{r})$ rather similar in size and shape to that found at R_{eq} but the magnitude of positive contours that embrace both partners in the complex rises noticeably at shorter R . However, the division of molecular space into negative and positive regions made by $U = 0$ contour is nearly identical at all the intermolecular distances. The electrostatic potential at the H nucleus, $U_0(\text{H})$, is a rather sensitive descriptor that amplifies the electron deficiency suffered by H atom in the interaction. $U_0(\text{H})$ decreases (gets less negative)

exponentially at shorter R but even at long distances, its values display very large changes with respect to those of the monomers.

4.4 Properties of $\eta(\mathbf{r})$

Upon hydrogen bonding, ELF domains associated to H-donor and H-acceptor groups exert a mutual pressure due to the Pauli repulsion between electron pairs that flattens the localization domains along the H \cdots O link. This effect of mutual penetration of H and O atoms can also be identified in the local distributions of $\rho(\mathbf{r})$ and $U(\mathbf{r})$. Volume of ELF basins $V(\text{A}, \text{H})$ and $V(\text{O})$ for the lone pair involved in the H-bond decreases dramatically even at long distances. On the contrary, volume of the second $V(\text{O})$ basin for the lone pair of O not involved in the H-bond remains nearly constant. Despite the great contraction of $V(\text{A}, \text{H})$ basins, their electron populations increase as R decreases with a steeper slope near R_{eq} that is more pronounced in complexes with two H-bonds. The $V(\text{O})$ populations for lone pairs of oxygen also increase at shorter R , but, in this case, it occurs as an effect made at the expense of other adjacent valence basins. In any event, if one considers the large contractions of space associated to ELF domains involved in hydrogen bonding, the gains of charge of $V(\text{A}, \text{H})$ and $V(\text{O})$ basins should be viewed as the dominant effect due to electron localization between the H-donor and the H-acceptor. Finally, it is noteworthy that the populations obtained from the ELF domains agree in describing the different hydrogen bonding abilities of functional groups that form the most common types of classical H-bonds discussed in this overview.

ACKNOWLEDGMENTS

The author thanks Drs. Pedro C. Gómez and Óscar Gálvez for their fruitful collaboration and friendship. Financial support by Dirección General de Investigación, Ministerio de Ciencia y Tecnología of Spain, Project No. BQU2002-04005 is gratefully acknowledged.

REFERENCES

1. F. Hibbert and J. Emsley, Hydrogen bonding and chemical reactivity, *Adv. Phys. Org. Chem.* **26**, 255–379 (1990).
2. I. Alkorta, I. Rozas, and J. Elguero, Non-conventional hydrogen bonds, *Chem. Soc. Rev.* **27**, 163–170 (1998).
3. G. R. Desiraju and T. Steiner, *The Weak Hydrogen Bond in Structural Chemistry and Biology* (Oxford University Press, Oxford, 1999).
4. M. J. Calhorda, Weak hydrogen bonds: theoretical studies, *Chem. Commun.* 801–809 (2000).
5. T. Steiner, The hydrogen bond in the solid state, *Angew. Chem. Int. Ed.* **41**, 48–76 (2002).
6. P. Gilli, V. Ferretti, V. Bertolasi, and G. Gilli, Evidence for resonance-assisted hydrogen bonding. Covalent nature of the strong homonuclear hydrogen bond. Study of the O–H \cdots O system by crystal structure correlation methods, *J. Am. Chem. Soc.* **116**, 909–915 (1994).

7. G. A. Kumar and M. A. McAllister, Theoretical investigation of the relationship between proton NMR chemical shift and hydrogen bond strength, *J. Org. Chem.* **63**, 6968–6972 (1998).
8. L. Gonzalez, O. Mo, M. Yañez, and J. Elguero, Very strong hydrogen bonds in neutral molecules: the phosphinic acid dimers, *J. Chem. Phys.* **109**, 2685–2693 (1998).
9. L. C. Remer and J. H. Jensen, Toward a general theory of hydrogen bonding: the short, strong hydrogen bond $[\text{HOH}\cdots\text{OH}]^-$, *J. Phys. Chem. A* **104**, 9266–9275 (2000).
10. S. Humbel, Short strong hydrogen bonds: a valence bond analysis, *J. Phys. Chem. A* **106**, 5517–5520 (2002).
11. G. A. Jeffrey, *An Introduction to Hydrogen Bonding* (Oxford University Press, New York, 1997).
12. M. S. Weiss, M. Brandl, J. Sühnel, D. Pal, and R. Hilgenfeld, More hydrogen bonds for the (structural) biologist, *Trends Biochem. Sci.* **26**, 521–523 (2001).
13. R. Taylor and O. Kennard, Crystallographic evidence for the existence of C–H \cdots O, C–H \cdots N, and C–H \cdots Cl hydrogen bonds, *J. Am. Chem. Soc.* **104**, 5063–5070 (1982).
14. Z. S. Derewenda, L. Lee, and U. Derewenda, The occurrence of C–H \cdots O hydrogen bonds in proteins, *J. Mol. Biol.* **252**, 248–262 (1995).
15. M. M. Brandl, M.S. Weiss, A. Jabs, J. Sühnel, and R. Hilgenfeld, C–H $\cdots\pi$ interactions in proteins, *J. Mol. Biol.* **307**, 357–377 (2001).
16. T. Steiner and G. Koellner, Hydrogen Bonds with π -acceptors in proteins: frequencies and role in stabilizing local 3D structures, *J. Mol. Biol.* **305**, 535–557 (2001).
17. A. C. Legon, D. J. Millen, and S. C. Rogers, Spectroscopic investigation of hydrogen bonding interactions in the gas phase. I. The determination of geometry, dissociation energy, potential constants and electric dipole moment of the hydrogen-bonded hetero-dimer HCN–HF from its microwave rotational spectrum, *Proc. R. Soc. London A* **370**, 213–237 (1980).
18. W. W. Cleland, Low-barrier hydrogen bonds and low fractionation factor bases in enzymatic reactions, *Biochemistry* **31**, 317–319 (1992).
19. S. Scheiner and T. Kar, The nonexistence of specially stabilized hydrogen bonds in enzymes, *J. Am. Chem. Soc.* **117**, 6970–6975 (1995).
20. W. D. Arnold and E. Oldfield, The chemical nature of hydrogen bonding in proteins via NMR: *J*-couplings, chemical shifts, and AIM theory, *J. Am. Chem. Soc.* **122**, 12835–12841 (2000).
21. A. S. Mildvan, M. A. Massiah, T. K. Harris, G. T. Marks, D. H. T. Harrison, C. Viragh, P. M. Reddy, and I. M. Kovach, Short, strong hydrogen bonds on enzymes: NMR and mechanistic studies, *J. Mol. Struct.* **615**, 163–175 (2002).
22. W. W. Cleland, P. A. Frey, and J. A. Gerlt, The low barrier hydrogen bond in enzymatic catalysis, *J. Biol. Chem.* **273**, 25529–25532 (1998).
23. W. W. Cleland, Low-barrier hydrogen bonds and enzymatic catalysis, *Arch. Biochem. Biophys.* **382**, 1–5 (2000).
24. C. N. Schutz and A. Warshel, The low barrier hydrogen bond (LBHB) proposal revisited: the case of the Asp \cdots His pair in serine proteases, *Proteins* **55**, 711–723 (2004).
25. E. D. Isaacs, A. Shukla, P. M. Platzman, D. R. Hamann, B. Barbiellini, and C. A. Tulk, Covalency of the hydrogen bond in ice: a direct X-ray measurement, *Phys. Rev. Lett.* **82**, 600–603 (1999).
26. A. Shukla, E. D. Isaacs, D. R. Hamann, and P. M. Platzman, Hydrogen bonding in urea, *Phys. Rev. B* **64**, 052101 1–4 (2001).
27. A. Hellemans, Getting to the bottom of water, *Science* **283**, 614–615 (1999).
28. T. K. Ghanty, V. N. Staroverov, P. R. Koren, and E. R. Davidson, Is the hydrogen bond in water dimer and ice covalent? *J. Am. Chem. Soc.* **122**, 1210–1214 (2000).
29. A. H. Romero, P. L. Silvestrelli, and M. Parrinello, Compton scattering and the character of the hydrogen bond in ice I_h , *J. Chem. Phys.* **115**, 115–123 (2001).
30. B. Barbiellini and A. Shukla, Ab initio calculations of the hydrogen bond, *Phys. Rev. B* **66**, 235101 1–5 (2002).

31. S. Jenkins and I. Morrison, The chemical character of the intermolecular bonds of seven phases of ice as revealed by ab initio calculation of electron densities, *Chem. Phys. Lett.* **317**, 97–102 (2000).
32. T. Kortemme, A.V. Morozov, and D. Baker, An orientation-dependent hydrogen bonding potential improves prediction of specificity and structure for proteins and protein–protein complexes, *J. Mol. Biol.* **326**, 1239–1259 (2003).
33. A. V. Morozov, T. Kortemme, K. Tsemekhman, and D. Baker, Close agreement between the orientation dependence of hydrogen bonds observed in protein structures and quantum mechanical calculations, *Proc. Natl. Acad. Sci. USA* **101**, 6946–6951 (2004).
34. S. Scheiner, *Hydrogen Bonding. A Theoretical Perspective* (Oxford University Press, Oxford, 1997).
35. J. E. Del Bene, Hydrogen bonding: 1. In: *The Encyclopedia of Computational Chemistry*, edited by P.v.R. Schleyer, N. L. Allinger, T. Clark, J. Gasteiger, P. A. Kollman, H. F. Schaefer III, and P. R. Schreiner (Wiley, Chichester, UK, 1998), Vol. 2, pp. 1263–1271
36. A. K. Rappe and E. R. Bernstein, Ab initio calculation of nonbonded interactions: are we there yet? *J. Phys. Chem. A* **104**, 6117–6128 (2000).
37. A. D. Rabuck and G. E. Scuseria, Performance of recently developed kinetic energy density functionals for the calculation of hydrogen binding strengths and hydrogen-bonded structures, *Theor. Chem. Acc.* **104**, 439–444 (2000).
38. J. E. Del Bene and M. J. T. Jordan, What a difference a decade makes: progress in ab initio studies of the hydrogen bond, *J. Mol. Struct. (Theochem)* **573**, 11–23 (2001).
39. J. Ireta, J. Neugebauer, and M. Scheffler, On the accuracy of DFT for describing hydrogen bonds: dependence on the bond directionality, *J. Phys. Chem. A* **108**, 5692–5598 (2004).
40. S. J. Grabowski, Ab initio calculations on conventional and unconventional hydrogen bonds—study of the hydrogen bond strength, *J. Phys. Chem. A* **105**, 10739–10746 (2001).
41. S. J. Grabowski, Hydrogen bonding strength—measures based on geometric and topological parameters, *J. Phys. Org. Chem.* **17**, 18–31 (2004).
42. P. Coppens, *X-Ray Charge Densities and Chemical Bonding* (Oxford University Press, Oxford, 1997).
43. A. van der Vaart and K. M. Merz, Charge transfer in small hydrogen bonded clusters, *J. Chem. Phys.* **116**, 7380–7388 (2002).
44. F. Weinhold, Nature of H-bonding in clusters, liquids, and enzymes: an ab initio, natural bond orbital perspective, *J. Mol. Struct. (Theochem)* **398–399**, 181–197 (1997).
45. R. F. W. Bader, *Atoms in Molecules. A Quantum Theory* (Clarendon, Oxford, 1990).
46. P. Popelier, *Atoms in Molecules. An Introduction* (Prentice-Hall, Harlow, UK, 2000).
47. P. L. A. Popelier, F. M. Aicken, and S. E. O'Brien, Atoms in molecules. In: *Chemical Modelling: Applications and Theory*, edited by A. Hinchliffe (The Royal Society of Chemistry, London, 2000), Vol. 1, Chapter 3, pp. 143–198.
48. P. L. A. Popelier and P. J. Smith, Quantum topological atoms. In: *Chemical Modelling: Applications and Theory*, edited by A. Hinchliffe (The Royal Society of Chemistry, London, 2002), Vol. 2, Chapter 8, pp. 391–448.
49. J. Poater, X. Fradera, M. Sola, M. Duran, and S. Simon, On the electron-pair nature of the hydrogen bond in the framework of the atoms in molecules theory, *Chem. Phys. Lett.* **369**, 248–255 (2003).
50. P. Politzer and D. G. Truhlar (Eds.), *Chemical Applications of Atomic and Molecular Electrostatic Potentials* (Plenum, New York, 1981).
51. P. Politzer and J. S. Murray, Molecular electrostatic potentials and chemical reactivity. In: *Reviews in Computational Chemistry*, edited by K. B. Lipkowitz and D. B. Boyd (VCH Publishers, New York, 1991), Vol. 2, Chapter 7, pp. 273–312.
52. P. Politzer and J. S. Murray, The fundamental nature and role of the electrostatic potential in atoms and molecules, *Theor. Chem. Acc.* **108**, 134–142 (2002).

53. M. D. Ryan, Effect of hydrogen bonding on molecular electrostatic potentials. In: *Modeling the Hydrogen Bond*, edited by D. A. Smith (American Chemical Society, Washington, 1994), ACS Symposium Series 569, Chapter 4.
54. V. Dimitrova, S. Ilieva, and B. Galabov, Electrostatic potential at atomic sites as a reactivity descriptor for hydrogen bonding. Complexes of monosubstituted acetylenes and ammonia, *J. Phys. Chem. A* **106**, 11801–11805 (2002).
55. B. Galabov, P. Bobadova-Parvanova, S. Ilieva, and V. Dimitrova, The electrostatic potential at atomic sites as a reactivity index in the hydrogen bond formation, *J. Mol. Struct. (Theochem)* **630**, 101–112 (2003).
56. M. Leboeuf, A. M. Koster, K. Jug, and D. R. Salahub, Topological analysis of the molecular electrostatic potential, *J. Chem. Phys.* **111**, 4893–4905 (1999).
57. B. Silvi and A. Savin, Classification of chemical bonds based on topological analysis of electron localization functions, *Nature* **371**, 683–686 (1994).
58. A. D. Becke and K. E. Edgecombe, A simple measure of electron localization in atomic and molecular systems, *J. Chem. Phys.* **92**, 5397–5403 (1990).
59. S. Noury, F. Colonna, A. Savin, and B. Silvi, Analysis of the delocalization in the topological theory of chemical bond, *J. Mol. Struct.* **450**, 59–68 (1998).
60. F. Fuster and B. Silvi, Determination of protonation sites in bases from topological rules, *Chem. Phys.* **252**, 279–287 (2000).
61. B. Silvi, The synaptic order: a key concept to understand multicenter bonding, *J. Mol. Struct.* **614**, 3–10 (2002).
62. B. Silvi, How topological partitions of the electron distribution reveal delocalization, *Phys. Chem. Chem. Phys.* **6**, 256–260 (2004).
63. F. Fuster and B. Silvi, Does the topological approach characterize the hydrogen bond? *Theor. Chem. Acc.* **104**, 13–21 (2000).
64. F. Fuster, B. Silvi, S. Berski, and Z. Latajka, Topological aspects of protonation and hydrogen bonding: the dihydrogen bond case, *J. Mol. Struct.* **555**, 75–84 (2000).
65. O. Galvez, P. C. Gomez, and L. F. Pacios, Approximate kinetic energy density for intermolecular regions in hydrogen bond dimers, *Chem. Phys. Lett.* **337**, 263–268 (2001).
66. O. Galvez, P. C. Gomez, and L. F. Pacios, Variation with the intermolecular distance of properties dependent on the electron density in hydrogen bond dimers, *J. Chem. Phys.* **115**, 11166–11184 (2001).
67. O. Galvez, P. C. Gomez, and L. F. Pacios, Variation with the intermolecular distance of properties dependent on the electron density in cyclic dimers with two hydrogen bonds, *J. Chem. Phys.* **118**, 4878–4895 (2003).
68. L. F. Pacios, Topological descriptors of the electron density and the electron localization function in hydrogen bond dimers at short intermonomer distances, *J. Phys. Chem. A* **108**, 1177–1188 (2004).
69. L. F. Pacios, Change with the intermolecular distance of electron properties of hydrogen bond dimers at equilibrium and non-equilibrium geometries, *Struct. Chem.* **16**, 223–241 (2005).
70. L. F. Pacios and P. C. Gomez, Dependence of calculated NMR proton chemical shifts on electron density properties in proton-transfer processes on short strong hydrogen bonds, *J. Phys. Chem. A* **108**, 11783–11792 (2004).
71. P. C. Gomez and L. F. Pacios, Environmental effects on proton transfer in a strong hydrogen bond dimer: the 4-methyl-imidazole-aspartate case, *Phys. Chem. Chem. Phys.* **7**, 1374–1381 (2005).
72. L. F. Pacios, O. Galvez, and P. C. Gomez, Variation of geometries and electron properties along proton transfer in strong hydrogen bond complexes, *J. Chem. Phys.* **122**, 214307 1–11 (2005).
73. E. Espinosa, I. Alkorta, J. Elguero, and E. Molins, From weak to strong interactions: a comprehensive analysis of the topological and energetic properties of the electron density distribution involving X–H···F–Y systems, *J. Chem. Phys.* **117**, 5529–5542 (2002).

74. M. J. Frisch, G. W. Trucks, H. B. Schlegel, G. E. Scuseria, M. A. Robb, J. R. Cheeseman, J. A. Montgomery Jr., T. Vreven, K. N. Kudin, J. C. Burant, J. M. Millam, S. S. Iyengar, J. Tomasi, V. Barone, B. Mennucci, M. Cossi, G. Scalmani, N. Rega, G. A. Petersson, H. Nakatsuji, M. Hada, M. Ehara, K. Toyota, R. Fukuda, J. Hasegawa, M. Ishida, T. Nakajima, Y. Honda, O. Kitao, H. Nakai, M. Klene, X. Li, J. E. Knox, H. P. Hratchian, J. B. Cross, V. Bakken, C. Adamo, J. Jaramillo, R. Gomperts, R. E. Stratmann, O. Yazyev, A. J. Austin, R. Cammi, C. Pomelli, J. W. Ochterski, P. Y. Ayala, K. Morokuma, G. A. Voth, P. Salvador, J. J. Dannenberg, V. G. Zakrzewski, S. Dapprich, A. D. Daniels, M. C. Strain, O. Farkas, D. K. Malick, A. D. Rabuck, K. Raghavachari, J. B. Foresman, J. V. Ortiz, Q. Cui, A. G. Baboul, S. Clifford, J. Cioslowski, B. B. Stefanov, G. Liu, A. Liashenko, P. Piskorz, I. Komaromi, R. L. Martin, D. J. Fox, T. Keith, M. A. Al-Laham, C. Y. Peng, A. Nanayakkara, M. Challacombe, P. M. W. Gill, B. Johnson, W. Chen, M. W. Wong, C. Gonzalez, and J. A. Pople, *Gaussian 03*, Revision C.02 (Gaussian Inc., Wallingford, CT, 2004).
75. U. Koch and P. L. A. Popelier, Characterization of C–H–O hydrogen bonds on the basis of the charge density, *J. Chem. Phys.* **99**, 9747–9754 (1995).
76. F. W. Biegler-Konig, R. F. W. Bader, and T. H. Tang, Calculation of the average properties of atoms in molecules. II, *J. Comput. Chem.* **3**, 317–328 (1982).
77. L. F. Pacios, CHECKDEN: a computer program to generate 1D, 2D and 3D grids of functions dependent on the molecular ab initio electron density, *Comput. Biol. Chem.* **27**, 197–209 (2003).
78. R. F. W. Bader and C. F. Matta, Atomic charges are measurable quantum expectation values: a rebuttal of criticisms of QTAIM charges, *J. Phys. Chem. A* **108**, 8385–8394 (2004).
79. F. Weinhold, Natural bond orbital methods. In: *The Encyclopedia of Computational Chemistry*, edited by P. v. R. Schleyer, N. L. Allinger, T. Clark, J. Gasteiger, P. A. Kollman, H. F. Schaefer III, and P. R. Schreiner (Wiley, Chichester, UK, 1998), Vol. 3, pp. 1792–1811.
80. E. D. Glendening, J. K. Badenhoop, A. E. Reed, J. E. Carpenter, and F. Weinhold, *NBO 4.0* (Theoretical Chemistry Institute, University of Wisconsin, Madison, 1999).
81. J. Kong, C. A. White, A. I. Krylov, C. D. Sherrill, R. D. Adamson, T. R. Furlani, M. S. Lee, A. M. Lee, S. R. Gwaltney, T. R. Adams, C. Ochsenfeld, A. T. B. Gilbert, G. S. Kedziora, V. A. Rassolov, D. R. Maurice, N. Nair, Y. Shao, N. A. Besley, P. E. Maslen, J. P. Dombroski, H. Dachsel, W. M. Zhang, P. P. Korambath, J. Baker, E. F. C. Byrd, T. Van Voorhis, M. Oumi, S. Hirata, C. P. Hsu, N. Ishikawa, J. Florian, A. Warshel, B. G. Johnson, P. M. W. Gill, M. Head-Gordon, and J. A. Pople, Q-Chem 2.0: a high-performance ab initio electronic structure program, *J. Comput. Chem.* **21**, 1532–1548 (2000).
82. R. G. Parr and W. Yang, *Density Functional Theory of Atoms and Molecules* (Oxford University Press, New York, 1989).
83. S. Noury, X. Krokidis, F. Fuster, and B. Silvi, Computational tools for the electron localization function topological analysis, *Comput. Chem.* **23**, 597–604 (1999).
84. P. G. Mezey, *Shape in Chemistry. An Introduction to Molecular Shape and Topology* (VCH Publishers, New York, 1993).
85. E. Espinosa, E. Molins, and C. Lecomte, Hydrogen bond strengths revealed by topological analyses of experimentally observed electron densities, *Chem. Phys. Lett.* **285**, 170–173 (1998).
86. E. Espinosa and E. Molins, Retrieving interaction potentials from the topology of the electron density distribution: the case of hydrogen bonds, *J. Chem. Phys.* **113**, 5686–5694 (2000).
87. L. F. Pacios, Computational study of a hydrogen bond break process: the case of the formamide-formic acid complex, *J. Comput. Chem.* in press (2006).
88. R. F. Stewart and B. M. Craven, Molecular electrostatic potentials from crystal diffraction. The neurotransmitter γ -aminobutyric acid, *Biophys. J.* **65**, 998–1005 (1993).
89. R. J. Gillespie, *Molecular Geometry* (Van Nostrand, London, 1972).
90. R. J. Gillespie and P. L. A. Popelier, *Chemical Bonding and Molecular Geometry. From Lewis to Electron Densities* (Oxford University Press, New York, 2001).

CHAPTER 4

WEAK TO STRONG HYDROGEN BONDS

HAN MYOUNG LEE, N. JITEN SINGH, and KWANG S. KIM

National Creative Research Initiative Center for Superfunctional Materials, Department of Chemistry, Division of Molecular and Life Sciences, Pohang University of Science and Technology, San 31, Hyojadong, Namgu, Pohang 790-784, Korea. E-mail: kim@postech.ac.kr

Abstract We review various types of hydrogen bond characteristics based on our theoretical work of diverse chemical systems. The systems include water clusters, hydrated clusters, enzymes, ionophores/receptors, and assembled molecules such as organic nanotubes. Special features of weak, normal, short, short strong H-bonding are discussed in terms of structures, interaction energies, and spectra. Various π -type H-bonds are also discussed.

Keywords: Hydrogen bonds; hydrated clusters; receptors; enzymes; ab initio calculations.

1 INTRODUCTION

Intermolecular interactions are important in understanding organic, organo-metallic and biomolecular structures, supramolecular assembly, crystal packing, reaction selectivity/specificity, molecular recognition, and drug–receptor interactions [1]. Based on these interaction forces, not only theoretical design but also experimental realization of novel functional molecules, nanomaterials, and molecular devices has become possible [2]. Thus, the study of the fundamental intermolecular interactions is very important for aiding self-assembly synthesis and nanomaterials design as well as for understanding molecular cluster formation [3]. Among various types of molecular interactions, the hydrogen bond (H-bond) is the most vital interaction force both in biology and chemistry. For instance, water which is the most abundant and essential substance on our planet and proteins and DNA which are the most important substances in biosystems are held basically by networks of H-bonds. The H-bond energy ranges from 1 to 30 kcal/mol. Since H-bonds can be easily formed and broken depending on the given environment, they are considered to have “on or off” functions in biology [1].

Recent progress both in theoretical and experimental methods has shown many new interesting facts about the H-bonding. Then, these H-bond interactions have been applied to the biological and material chemistry [3–8]. H-bonds have often been used for self-assembling macromolecular architecture such as capsules, nanotubes, biomaterials, wires, etc [4]. The charge transfer (CT) through the H-bonded networks of a wire form has been chemically and biochemically explored [5]. The charged and ionic H-bond interactions have been applied to the recognition of ions by receptors/ionophores [6]. Many biological systems such as proteins, membranes, RNA, and DNA show functions related to multiple H-bonded frames [7].

As various aspects of H-bonds have already been covered previously, interested readers can find many books [1–2] and reviews [8, 9] concerning this topic. Regarding H-bonds, *ab initio* molecular orbital calculations have become a powerful approach to study H-bonded cluster systems as well as the fundamental binding energies of the single H-bonds. This is in part because theoretical investigations make it easy to explore potential energy surface of diverse conformations and to deduce important electronic energy components such as electrostatic, inductive, dispersive, charge transfer, and repulsive interactions, as well as their influences on the structures, spectra, and interaction energies. Depending on the nature of H-bonds, it can have different proportions of these energy components. Thus, in this review, we summarize our theoretical work done on many different chemical systems (water clusters, π -systems, organic nanotubes, enzymes, drugs, and receptors), which exhibit wide variety of different H-bonding characteristics such as normal, short, short strong, and weak π -type H-bonds. Some of the pertinent issues which will be addressed in the course of this review are the following: (1) typical H-bonds in water clusters, (2) H-bonds, (3) ionic H-bonds in enzymes and bio-receptors, (4) cooperative effect of H-bonds, and (5) normal vs. strong hydrogen bonds.

2 THEORETICAL APPROACH

2.1 Calculation Methods

We used the density functional methods using Becke three parameters with Lee–Yang–Parr functionals (B3LYP) and the *ab initio* methods using Moller–Plesset second-order perturbation theory (MP2) to obtain the geometries, binding energies, and IR frequencies. The coupled cluster calculations with singles and doubles excitations (CCSD) and those including perturbative triples excitations [CCSD(T)] were often carried out for more accurate calculations. The basis sets we employed are 6-31+G*, 6-311++G**, aug-cc-pVDZ' (to be shorted as aVDZ') where the diffuse functions for H and the d diffuse functions for other atoms are deleted from the aug-cc-pVDZ basis set, aug-cc-pVDZ (to

be shorted as aVDZ), aug-cc-pVTZ (to be shorted as aVTZ), aug-cc-pVDZ+(2s2p/2s) (to be shorted as aVDZ+), and aug-cc-pVTZ+(2s2p/2s) (to be shorted as aVTZ+).

The basis set superposition error (BSSE) correction was made. As previously experienced, full BSSE correction tends to underestimate binding energies unless large basis sets are used to take into account most of electron correlation energy. The interaction energies are reported as the median value of the BSSE-corrected and BSSE-uncorrected values (i.e., half-BSSE-corrected binding energies ($-\Delta E_c$)) which can be considered as the lower and upper limits, respectively [9]. Although the BSSE-corrected values are more rigorous in theoretical viewpoint, the energy obtained from incomplete basis sets is underestimated due to the lack of insufficient electron correlation energy which in most cases tends to be empirically compensated partially by BSSE. In particular, it should be noted that the BSSE-uncorrected H-bond distance is somewhat too short, so that the full BSSE correction underestimates the binding energy due to the overestimated repulsion at the distance (toward the hard wall region) shorter than the optimal H-bond distance. The zero-point-energy (ZPE)-corrected binding energies ($-\Delta E_0$ and D_0) and enthalpies (ΔH_{298}) and free energies (ΔG_{298}) at room temperature and 1 atm are also reported. The charge analysis is done using natural bond orbital (NBO) [10] analysis. HOMOs and LUMOs are investigated. In order to consider the solvent effect, the relative interaction energy in the given solvent (dielectric constant ϵ) ($\delta\Delta E_{\text{sol}}$) was obtained by using the isodensity surface polarized continuum model (IPCM). The molecular orbital (MO) analysis was done using the Posmol package [11].

2.2 Decomposition of Interaction Energy

In order to analyze the interaction energy component, the symmetry-adapted perturbation theory (SAPT) [12] calculations were performed. SAPT have been used to analyze the interaction energies in terms of electrostatic, induction, dispersion, and exchange interaction components. The SAPT interaction energy (E_{int}) has been analyzed up to the second-order symmetry adapted perturbation theory: the electrostatic energy (E_{elst}) consisting of $E_{\text{elst}}^{(10)}$ and $E_{\text{elst,resp}}^{(12)}$, induction (E_{ind}) which equals $E_{\text{ind,resp}}^{(20)}$, dispersion (E_{disp}) which equals $E_{\text{disp}}^{(20)}$, and exchange repulsion (E_{exch}) which equals $E_{\text{exch}}^{(10)} + E_{\text{exch}}^{(11)} + E_{\text{exch}}^{(12)} + E_{\text{exch-ind,resp}}^{(20)} + E_{\text{exch-disp}}^{(20)}$. The superscripts (n_1n_2) denote orders in perturbation theory with respect to intermolecular and intramolecular interaction operators, respectively. The subscript “resp” indicates the term including coupled-perturbed HF response ($\delta E_{\text{int,resp}}^{\text{HF}}$). One distinct advantage of SAPT over supermolecular approach is that each term in the perturbation series can be physically interpreted:

$$\begin{aligned}
E_{\text{tot}} &= E_{\text{es}} + E_{\text{exch}} + E_{\text{ind}} + E_{\text{disp}} + \delta E_{\text{int,resp}}^{\text{HF}} \\
&= E_{\text{es}} + E_{\text{exch}}^* + E_{\text{ind}}^* + E_{\text{disp}}^* + \delta E_{\text{int,resp}}^{\text{HF}},
\end{aligned}$$

where

$$\begin{aligned}
E_{\text{es}} &= E_{\text{es}}^{(10)} + E_{\text{es,resp}}^{(12)}, \\
E_{\text{ind}} &= E_{\text{ind}}^{(20)}, \\
E_{\text{disp}} &= E_{\text{disp}}^{(20)}, \\
E_{\text{exch}} &= E_{\text{exch}}^{(10)} + E_{\text{exch}}^{(11)} + E_{\text{exch}}^{(12)} + E_{\text{exch,ind,resp}}^{(20)} + E_{\text{exch,disp}}^{(20)}, \\
E_{\text{ind}}^* &= E_{\text{ind}}^{(20)} + E_{\text{exch,ind,resp}}^{(20)}, \\
E_{\text{disp}}^* &= E_{\text{disp}}^{(20)} + E_{\text{exch,disp}}^{(20)},
\end{aligned}$$

and

$$E_{\text{exch}}^* = E_{\text{exch}}^{(10)} + E_{\text{exch}}^{(11)} + E_{\text{exch}}^{(12)}.$$

Here, the superscript “*” indicates the effective energy component.

3 H-BOND IN WATER CLUSTERS

A water molecule favors four H-bond interactions. Neutral water clusters are determined mainly by the H-bond interactions and strains between water molecules. Structures, energetics, and electronic and spectroscopic properties of small water clusters have been well investigated [13–15]. Each water molecule in clusters can be classified as “d”, “a”, “da”, “aa”, “dd”, “daa”, “dda”, and “ddaa” types, where “d” and “a” indicate H-donor and H-acceptor, respectively.

The lowest-energy water clusters from water dimer to dodecamer and their interaction energies are presented in Fig. 1 and Table 1. The water tetramer, pentamer, and octamer are relatively stable with respect to the water dimer, hexamer, and heptamer. The trimer to pentamer has global minimum energy structures of cyclic ring conformation. The hexamer has five isoenergetic conformations. The high level calculations show that the cage structure has the lowest energy, followed by book, prism, cyclic, and bag structures (the energies of which are 30.76, 30.70, 30.54, 30.19, 30.10 kcal/mol, respectively, in $-\Delta E_0$ at the MP2/HZ4P(2fg/2d)++ level) [14h]. Indeed, the cage structure, which is the most stable conformer of neutral water hexamer near 0 K was experimentally observed [16]. The nearly isoenergetic conformer, book structure, was also observed recently [17]. In addition, the slightly higher energy conformer of cyclic structure was observed in Ar matrix [18].

Water-containing clusters tend to have different H-bond framework at high temperature. Generally, the temperature–entropy effect decreases the number of H-bond interactions. Especially, the H-bond clusters with some angle strain are affected by temperature. So, the cyclic ring or book structures are more stable at high temperatures, while at low temperatures 3-D structures (cage and prism)

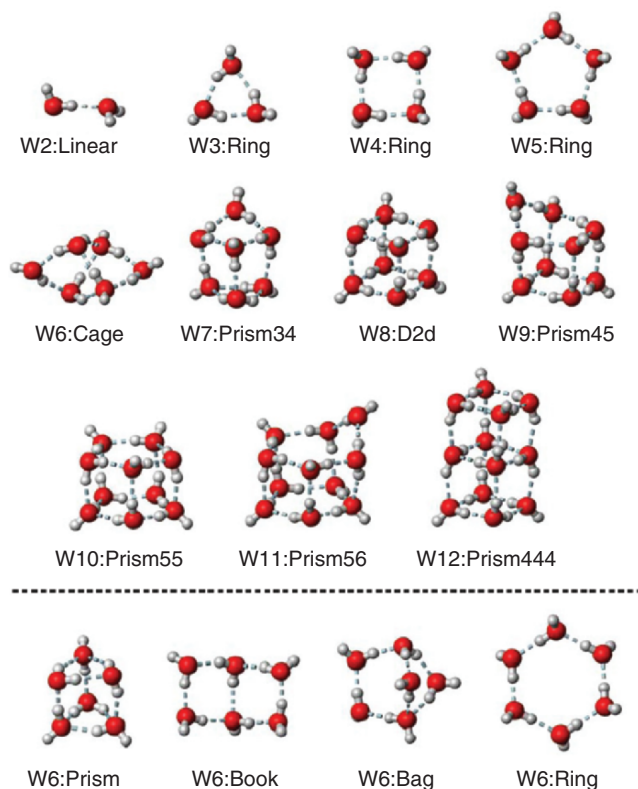


Figure 1. The lowest-energy neutral water cluster structures (W₂₋₁₂ at 0 K) and four other iso-energetic isomers of neutral water hexamer.

are more stable (Fig. 1). This aspect is related to the phase transition between 1-D or 2-D and 3-D structures. The 1-D structures are less H-bonded and 3-D structures are more H-bonded. This conformational change is important in the generation of excess-electron-bound water clusters. At low temperatures, in comparison with other sizes, the interaction energies of water hexamer and heptamer are relatively weak due to the molecular strain. The water hexamer cage conformer has a highly strained structure with cyclic tetrameric H-bond interactions, and the heptamer cluster structure has a unit of cyclic trimeric H-bond interaction. At low temperatures, the caged structures with more H-bond interactions are favorable, while at high temperatures the cyclic structures with less H-bond interactions are favorable. This trend sometimes appears in IR spectra of aqua clusters. So, the entropy-driven effect has to be well understood to identify their structures and coordinations using IR spectra, because the computationally estimated IR spectrum using the low-energy structure can be different from the experimental one observed at a finite temperature.

Table 1. Interaction energies (kcal/mol) of neutral water clusters (H_2O) $_{n=2-12}$ ^a

n	Structure	#HB	MP2/TZ2P++			MP2/aug-cc-pVDZ+(2s2p/2s)			
			$-\Delta E_e \pm \text{BSSE}/2$	$-\Delta E_0$	$-\Delta H_{298}$	$-\Delta E_e \pm \text{BSSE}/2$	$-\Delta E_0$	$-\Delta H_{298}$	$-\Delta G_{50}$
2	Linear	1	4.88 ± 0.33	2.58	3.13	4.85 ± 0.42	2.55	3.10	2.04
3	Ring	3	15.11 ± 0.89	9.38	11.27	15.14 ± 1.24	9.40	11.30	8.00
4	Ring	4	26.72 ± 1.75	18.06	20.93	26.56 ± 2.20	17.90	20.78	15.46
5	Ring	5	35.17 ± 2.42	24.30	27.65	34.90 ± 2.90	24.03	27.38	20.70
6	Cage	8	43.48 ± 2.98	30.52	34.29	44.45 ± 4.03	30.18	34.70	25.71
7	Prism34	10	55.24 ± 3.66	37.89	43.39	55.85 ± 5.14	38.50	44.00	32.96
8	D2d	12	70.06 ± 4.68	48.68	55.75	70.86 ± 6.61	49.44	56.54	42.64
9 ^a	Prism45	9	79.14 ± 5.39	55.69	63.27	80.20 ± 7.19	56.16	63.75	48.46
10 ^a	Prism55	10	90.07 ± 6.13	63.48	72.14	91.37 ± 8.18	64.13	72.78	55.32
11 ^a	Prism56	11	98.67 ± 6.82	69.66	78.99	99.86 ± 9.09	70.12	79.46	60.37
12 ^a	Prism444	12	112.59 ± 7.54	79.41	90.13	115.50 ± 10.1	81.54	92.26	70.47

^a The thermodynamic corrections were made using the B3LYP/6-311++G** values. For $n \leq 8$, all the geometries were fully optimized, while for $n \geq 9$, the single point energy calculations were carried out for MP2/TZ2P++ and MP2/aug-cc-pVDZ+(2s2p/2s) on the MP2/TZ2P optimized geometries. Italic data are corrected by 13.3% BSSE of MP2/TZ2P++

Generally, single H-donor water molecules (“da” or “daa” waters) have strong H-bond interactions in neutral water clusters. This aspect appears in IR spectra for O–H stretch frequencies as strong red-shifts. The red-shifts of O–H stretch frequencies monotonically increase up to the hexamer ring structure owing to the increase in the strength of H-bond interaction by the decrease of bond angle strains (Table 2). However, this H-bond strength is saturated at the hexamer, and so the heptamer and octamer ring conformers have red-shifts similar to the hexamer. These red-shifted values with respect to those of water monomer reflect the strength of H-bond interactions between water molecules. The cyclic pentamer cluster shows $\sim 540\text{ cm}^{-1}$ red-shifted frequencies corresponding to “da” water, while the hexamer-cage shows $\sim 670\text{ cm}^{-1}$ red-shifted frequencies, corresponding to “daa”-type water. The large shifts are due to the strong polarization effect by the H-bonds.

The order of red-shifts of OH stretching frequencies with respect to the average value of ν_3 and ν_1 of the water molecule in the water dimer to dodecamer is “da”(ν_3) < “daa”(ν_3) < “dda”(ν_3) < “ddaa”(ν_3) < “ddaa”(ν_1) \approx < “dda”(ν_1) < “da”(ν_1) < “daa”(ν_1). The IR intensities of double proton donor-type waters (“dda” and “ddaa”) in asymmetric OH stretching modes (ν_3) are strong, while the intensities of single donor-type waters (“da” and “daa”) are strong in symmetric OH stretching modes (ν_1). The order of red-shifts of bending frequencies with respect to that of monomer is “ddaa” > “dda” > “daa” \approx “da”. In the cases of undecamer and dodecamer, the ranges of $-\delta\nu_3$ and $-\delta\nu_1$ of “ddaa”-type are 209–299 cm^{-1} and 245–496 cm^{-1} , and that of $\delta\nu_2$ of “ddaa”-

Table 2. B3LYP/6-311++G** vibrational frequency shifts (with respect to the monomer frequencies ν_3 and ν_1) and IR intensities (average in parentheses) of $(\text{H}_2\text{O})_{n=2-8}$

n	Conf.	$-\delta\nu_3$			$-\delta\nu_1$		
		“da”	“daa”	“dda”	“dda”	“da”	“daa”
2	Linear		“a”: 8 (9)	“d”: 30 (8)	“a”: 3 (2)		“d”: 112 (33)
3	Ring	27–33 (8)					188–257 (37)
4	Ring	37–38 (7)				310–442 (74)	
5	Ring	32–39 (7)				339–488 (89)	
6	Ring	36–37 (7)				344–499 (97)	
	Book	34–38 (7)	47 (8)	199 (40)	235 (32)	253–473 (100)	552 (28)
	Bag	28–45 (8)	47 (5)	257 (68)	200 (58)	176–539 (79)	611 (40)
	Cage	26–45 (8)	39–43 (7)	176–208 (36)	143–226 (32)	295–342 (60)	385–617 (76)
	Prism	26–37 (7)	38–41 (7)	147–190 (26)	122–260 (36)		275–639 (59)
7	Prism ³⁴	31 (6)	39–42 (7)	137–242 (39)	155–280 (37)	414 (62)	289–707 (79)
	Ring	28–39 (7)				334–484 (98)	
8	D2d		44 (6)	230–275 (56)	185–204 (21)		519–604 (89)
	Ring	29–30 (7)				323–472 (101)	

For $n = 1$, $\nu_3 = 3921$ (57) and $\nu_1 = 3816$ (9). Frequencies are in cm^{-1} ; IR intensities in 10 km/mol. If $\delta\nu_1 = \delta\nu_3$, it means that ν_1 is smaller than ν_3 by 105 cm^{-1} . The red-shift is defined with respect to the average value (3868 cm^{-1}) of ν_1 and ν_3 (i.e., $-\delta\nu_3 - 52$ and $-\delta\nu_1 + 52\text{ cm}^{-1}$)

type is $93\text{--}135\text{ cm}^{-1}$. The values of $-\delta\nu_3$ and $-\delta\nu_1$ of “dda”-type are $66\text{--}242\text{ cm}^{-1}$ and $181\text{--}436\text{ cm}^{-1}$, and that of $\delta\nu_2$ of “dda”-type is $46\text{--}138\text{ cm}^{-1}$.

4 H-BOND IN POLAR SYSTEMS

To investigate the H-bond, it is essential to study the interaction of the water molecule interacting with other molecular species (Y) (Fig. 2). For the lowest energy conformers of water–Y complexes, the binding energies (D_0 at MP2/aVTZ) for the first hydrides: HF (σ_O), $\text{H}_2\text{O}(\sigma_H/\sigma_O)$, $\text{NH}_3(\sigma_H)$, and MeOH (σ_H) are 6.11, 3.04, 4.50, and 4.32 kcal/mol, respectively (Table 3). In the case of water dimer, the σ -type includes both σ_H and σ_O types. For the second-row hydrides, the binding energies (D_0) of a water molecule interacting with HCl (σ_O), H_2S (σ_H), PH_3 (σ_H), and MeSH (σ_H) are 4.02, 2.38, 1.57, and 3.16 kcal/mol, respectively.

Ammonia has strong proton affinity, thus has strong H-bond interactions with the water monomer compared with the interaction in the water dimer. In $\text{NH}_3\text{--H}_2\text{O}$ interaction, polarizable lone-pair electrons in NH_3 make NH_3 better H-accepting than H_2O . H_2S is a weaker proton-acceptor than H_2O and plays a role of H-donor in $\text{H}_2\text{O--H}_2\text{S}$ interaction. The third elements P and S atoms have relatively weak H-bond interactions due to large atomic radius.

In the hydrogen halide acid–water clusters [19], water plays a role of H-acceptor, while in anion–water clusters [20], water acts as H-donor. Good acids provide protons more easily than stable anions. Their properties are strongly related to the stabilization of dissociated ions by the hydration effect. The anionic systems have strong proton affinity which gives a strong H-bond interaction. In the case of charged systems [20, 21], the charge highly increases the strength of H-bond interaction due to the strong electrostatic interaction. In the protonated systems, the hydronium cation is a better proton donor than the ammonium cation [22], so hydronium has stronger H-bond interaction than ammonium. The positively charged systems have stronger H-bond interactions than the negatively charged ones. The positively charged atom can easily interact with the water O atom at a shorter distance, while the negatively

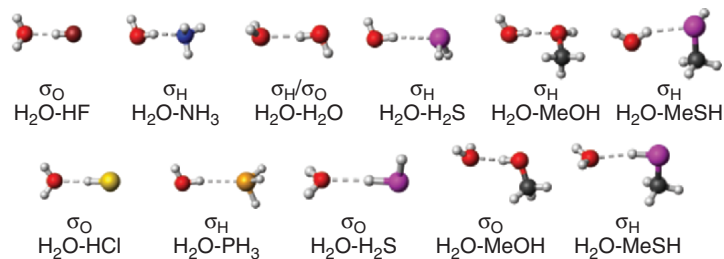


Figure 2 (see color section). Structures of the hydrogen-bonded complexes of H_2O .

Table 3. Binding energies SAPT interaction energies, and selected distances of the water-Y complexes (Y: HF, H₂O, NH₃, MeOH, HCl, H₂S, PH₃, MeSH) at the MP2/6-31+G* [MP2/aug-cc-pVDZ][MP2/aug-cc-pVTZ//MP2/aug-cc-pVDZ] levels^a

	H ₂ O-HF	H ₂ O-H ₂ O	H ₂ O-NH ₃	H ₂ O-MeOH
ΔE_c	σ_O {-8.88 ± 0.54}	σ {-5.17 ± 0.46}	σ_H {-6.71 ± 0.46}	σ_O {-5.23 ± 0.52}
ΔE_0	{-6.11}	{-3.04}	{-4.50}	{-3.62}
ΔH_{298}	{-7.19}	{-3.51}	{-5.55}	{-3.65}
	H ₂ O-HCl	H ₂ O-H ₂ S	H ₂ O-PH ₃	H ₂ O-MeSH
ΔE_c	σ_O {-6.06 ± 0.75}	σ_H {-3.98 ± 0.61}	σ_H {-2.89 ± 0.51}	σ_O {-2.74 ± 0.41}
ΔE_0	{-4.02}	{-2.38}	{-1.73}	{-0.92}
ΔH_{298}	{-4.80}	{-2.54}	{-1.69}	{-1.20}

^a All energies are in kcal/mol; ΔE_c is the median of the BSSE-corrected and -uncorrected values which can be considered as the upper and lower bounds for the interaction energy, respectively, and the value after ± is half the BSSE. ΔE_0 is the ZPE-corrected ΔE_c . ΔH_{298} is the half BSSE-corrected binding enthalpy at 298 K and 1.0 atm

charged atom interacts with only a few H atom without full coordination, due to the presence of an excess electron that requires a large vacant space around the anion for stabilization as well as the repulsions between crowded H atoms of water.

Some interesting N-containing aromatic rings were theoretically and experimentally investigated for their H-bond interactions with water molecules [23]. Pyridine, which has sp^2 -hybridized nitrogen atom and resonance effect, has stronger H-bonding interaction than those of ammonia–water, imine–water, and furan–water systems. This is because the lone-pair electrons of pyridine are less-stabilized and less-delocalized (“localization effect”) in the HOMO, while the lone-pair electrons of furan are delocalized and stabilized at the HOMO (π -electrons occupy carbon atom’s HOMO). Pyridine is a good proton-acceptor and therefore plays actively in the H-bond interaction. Pyrrole shows strong σ -H bond interactions with water due to resonance effect and acidity, and also weak π -H-bond interactions with water molecules. In the latter case, the lone-pair electrons are delocalized around the aromatic ring by the resonance effect. The carbon/ π -electrons are compatible with lone-pair electrons of water molecules. The pictures of their π -type interactions with water show the π -H interaction. Thus, in the next section, we discuss the details of weak π -H interactions.

5 H-BOND IN π -SYSTEMS

Novel H-bond involving aromatic rings have been an important subject in the last decade [4]. The comparison of π -type H-bond interaction with the traditional water–water σ -type H-bond interaction should be very interesting. The interaction energies of ethylene–water π -H bond and water–water H-bond interactions were calculated to be 2.84 ± 0.59 and 4.89 ± 0.41 kcal/mol at the MP2/aVDZ level, where the lower and upper limits are the BSSE-corrected and -uncorrected values, respectively.

For the ethene–water and water–water SAPT interaction energies (MP2/aVDZ) without ZPE correction (ΔE_e ; -2.0 and -4.1 kcal/mol, respectively), the electrostatic components are -3.9 and -8.4 kcal/mol, the first-order exchange components are 5.5 and 8.5 kcal/mol, the second-order induction terms are -2.7 and -2.9 kcal/mol, and the second-order dispersion energies are -2.4 and -2.3 kcal/mol, respectively. The π -systems have low-energy LUMOs and polarizable electrons occupied in the higher energy molecular orbitals. The π -systems can play a role of good electron-donating group. Therefore, with respect to the electrostatic interaction energy of π -H-bond interaction, the exchange component is highly repulsive. While the exchange component of water–water H-bond interaction is in the magnitude similar to the electrostatic interaction, the induction energy of π -H-bond interaction has relatively large energy component. The dispersion interaction is also relatively large due to the diffuse and polarizable π -electron density in the π -H-bond interaction.

Here we particularly discuss the case of phenol systems in comparison with water molecules (i.e., phenol vs. water molecule interacting with various molecules: σ -type, π -type, and χ -type H-bonds), because of their similarity in interaction with other molecular species while they are π - and σ -systems. The nature of interactions of phenol with various molecules (Y: the first hydrides (HF, H₂O, NH₃), the second hydrides (HCl, H₂S, PH₃), and the analogs of H₂O and H₂S (MeOH, MeSH)) is investigated (Fig. 3 and Table 4). In addition, we find that phenol can also involve in π -H interaction (to be denoted as π -type) and both π -H and $\sigma(\sigma_{\text{H}}/\sigma_{\text{O}})$ interactions (to be denoted as χ -type ($\chi_{\text{H}}/\chi_{\text{O}}$)). We made our efforts to investigate the π conformers as well as to investigate the difference between σ_{H} and σ_{O} conformations. We compared the conformational energetics depending on $\sigma_{\text{H}}, \sigma_{\text{O}}, \pi, \chi_{\text{HO}}$, and

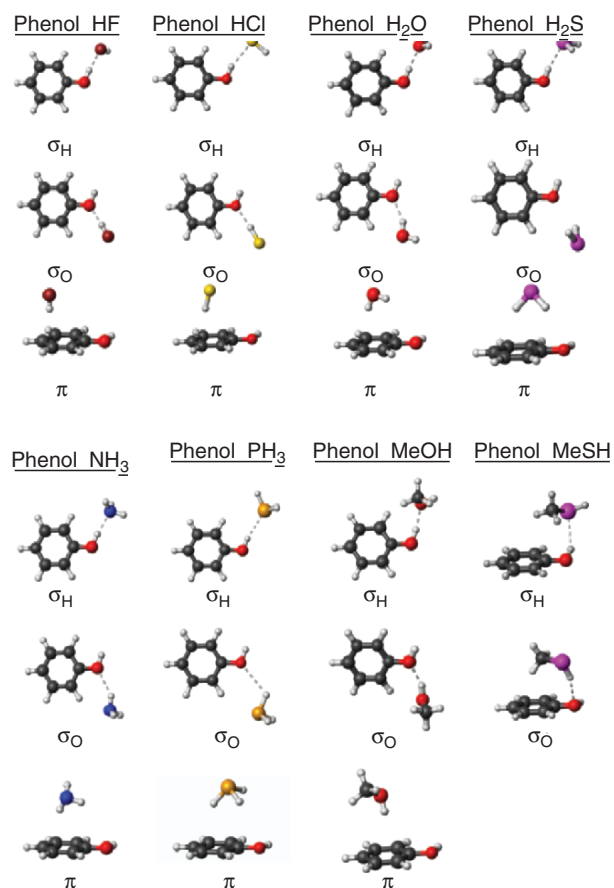


Figure 3. Structures of the hydrogen-bonded complexes of phenol. Reproduced by permission of American Chemical Society: Ref. [24].

Table 4. Binding energies of the phenol-Y complexes (Y: HF, H₂O, NH₃, MeOH, HCl, H₂S, PH₃, MeSH) at the MP2/aug-cc-pVTZ//MP2/aug-cc-pVDZ levels^a

	Phenol-HF			Phenol-H ₂ O		
ΔE_c	σ_H	σ_O	π	σ_H	σ_O	π
ΔE_0	{-3.99 ± 0.60}	{-8.08 ± 0.78}	{-5.70 ± 1.04}	{-7.32 ± 0.74}	{-5.05 ± 0.73}	{-4.48 ± 1.03}
ΔH_{298}	{-2.47}	{-6.39}	{-4.06}	{-5.58}	{-3.63}	{-3.44}
	{-2.82}	{-7.34}	{-4.62}	{-5.64}	{-3.58}	{-3.08}
		Phenol-NH ₃		Phenol-MeOH		
ΔE_c	σ_H	σ_O	π	σ_H	σ_O	π
ΔE_0	{-9.56 ± 0.79}	{-3.77 ± 0.69}	{-3.59 ± 1.08}	{-9.00 ± 1.18}	{-5.83 ± 1.01}	{-6.36 ± 1.62}
ΔH_{298}	{-7.20}	{-2.59}	{-2.83}	{-7.49}	{-4.84}	{-5.42}
	{-7.84}	{-2.34}	{-2.84}	{-7.35}	{-5.00}	{-4.97}
		Phenol-HCl		Phenol-H ₂ S		
ΔE_c	σ_H	σ_O	π	σ_H	σ_O	π
ΔE_0	{-3.23 ± 0.76}	{-6.08 ± 1.13}	{-6.36 ± 1.52}	{-5.15 ± 1.05}	{-4.11 ± 0.68}	{-5.34 ± 1.35}
ΔH_{298}	{-2.11}	{-4.44}	{-5.02}	{-3.94}	{-3.08}	{-4.33}
	{-2.78}	{-5.60}	{-5.34}	{-3.71}	{-2.76}	{-4.03}
		Phenol-PH ₃		Phenol-MeSH		
ΔE_c	σ_H	σ_O	π	χ_H	χ_O	
ΔE_0	{-4.58 ± 0.95}	{-2.10 ± 0.73}	{-4.70 ± 1.34}	{-8.04 ± 2.02}	{-6.59 ± 1.97}	
ΔH_{298}	{-3.49}	{-1.63}	{-3.66}	{-6.93}	{-5.54}	
	{-3.14}	{-1.43}	{-3.39}	{-6.72}	{-5.18}	

^a See the footnote of Table 3

χ_O -type interactions and analyzed their energy components (electrostatic, induction, dispersion, and exchange repulsion energies). In addition, by studying the corresponding water–Y complexes, we compared them with phenol–Y complexes.

In going from HF to H₂O to NH₃, the σ_H binding energy “ D_0 ” increases from 2.5 to 5.6 to 7.2 kcal/mol, the σ_O binding energy decreases from 6.4 to 3.6 to 2.6 kcal/mol, and the π binding energy decreases from 4.1 to 3.4 to 2.8 kcal/mol. Although MeOH can be considered to be similar to H₂O, the phenol–MeOH binding energy (σ_H : 7.5, σ_O : 4.8, χ : 5.4 kcal/mol) is much larger than the phenol–H₂O energy due to the extra dispersion energy for the π -H interaction by the Me group. For the second-row hydrides, from HCl to H₂S to PH₃, the σ_H binding energy increases (2.1, 3.9, 3.5 kcal/mol), while the σ_O binding energy decreases (4.4, 3.1, 1.6 kcal/mol) and the π -binding energy also decreases (5.0, 4.3, 3.7 kcal/mol). In the case of MeSH, the χ_H and χ_O binding energies (6.9 and 5.5 kcal/mol) are large due to large dispersion energies. In the cases of the first hydrides, the σ_O complex of HF is ca. 4 kcal/mol more stable than the σ_H conformer, while the σ_H conformers of H₂O and NH₃ are more stable than the corresponding σ_O ones by ca. 2 and 5 kcal/mol, respectively. On the other hand, in the second hydride systems, the π complexes are slightly more stable (by only a fraction of 1 kcal/mol) than, but compete with the σ_O complex for HCl and the σ_H complexes for H₂S and PH₃. The H-bonding types of the global minimum energy structures are σ_O for HF, σ_H for H₂O, NH₃, PH₃, and MeOH, π for HCl, H₂S, and PH₃, and χ_H for MeSH. Thus, HF favors σ_O -type H-bonding, while H₂O, NH₃, and MeOH favor σ_H -type H-bonding. On the other hand, HCl, H₂S, and PH₃ favor π -type H-bonding, which are slightly favored over σ_O , σ_H , σ_H -type bonding, respectively. MeSH favors χ_H -type which has characters of both π and σ_H . Phenol–Y complexes are compared with water–Y complexes. In the water–Y complexes where σ_O/σ_H -type involves the H-bond by the water O/H atom, HF and HCl favor σ_O -type, H₂O involves both σ_O/σ_H -type, and H₂S, NH₃, PH₃, MeOH, and MeSH favor σ_H -type. Except for HF, other seven species have larger binding energy with phenol than H₂O. The details are given in Ref. [24].

In the phenol–Y clusters, the SAPT interaction energies E_{int} are dominated by attractive electrostatic E_{int} and repulsive exchange energies. However, in the case of π complexes where the electrostatic and exchange interactions are weaker, the dispersion and induction energies become important among the interaction energy components. E_{int} is correlated with E_{ind} , while it is hard to find a good correlation between E_{int} and $E_{\text{elst}}/E_{\text{disp}}/E_{\text{exch}}$. This is because the sum of E_{elst} and E_{disp} tends to cancel out E_{exch} . It is partially related with the trend that not only E_{disp} is already well correlated with E_{exch} but also the main interaction E_{elst} needs to be balanced by E_{exch} . These energy components could be affected by the substituents of benzene, which could provide various magnitudes of the interaction energy [9]. The comparison of the phenol–Y system with the water–Y system is in Ref. [24].

As the vibrational spectroscopy is an indispensable tool for successful identification and characterization of H-bonds [25], we have studied the phenolic O–H stretch and the intermolecular stretch which are highly sensitive to the molecular environment by virtue of specific (H-bonding) and non-specific interactions. To correct the overestimation of harmonic frequencies, a single scale factor of 0.96 was used to scale all frequencies. Henceforth, the scaled frequencies are discussed unless otherwise stated. It should be noted in Table 5 that the OH stretch mode of phenol (ν_{OH}) as the proton-donor (σ_{OH} conformers) undergoes drastic red-shift along with sharply increased intensity, while those of phenol as the proton-acceptor (σ_{O} conformers) and π conformers hardly change. The small red-shifts for phenolic O–H stretch in the case of phenol–HF and phenol–HCl complexes (in comparison with other phenol–Y heterodimers) can be understood from the weak basicity of HF/HCl monomers. The red-shifts which are proportional to H-bond strengths tend to follow the basicity order of the interacting molecule Y.

The MP2/6-31+G* [MP2/aVDZ] intermolecular stretching frequencies (ν_{int}) for the σ_{H} complexes of phenol interacting with H₂O, NH₃, and MeOH are predicted to be 183 [163], 198 [190], and 198 [187] cm⁻¹ respectively, which

Table 5. Calculated and experimental vibrational frequency shifts (cm⁻¹) of phenolic O–H stretch ($\delta\nu_{\text{OH}}$) and intermolecular stretch modes (ν_{int}) for phenol–Y complexes at the MP2/6-31+G* [MP2/aug-cc-pVDZ] levels. Experimental data are from Ref. [26]

	Phenol–HF				Phenol–HCl		
	σ_{H}	σ_{O}	π	σ_{H}	σ_{O}	π	
$\delta\nu_{\text{OH}}$	-2 [-35]	12 [7]	-1 [-3]		-15 [-44]	1 [-4]	0 [-3]
$\Gamma\nu_{\text{OH}}$	4.4 [4.9]	1.5 [1.4]	1.2 [1.2]		4.4 [5.0]	1.2 [1.2]	1.1 [1.1]
ν_{int}	125 [113]	187 [178]	115 [125]		81 [84]	118 [115]	81 [95]
	Phenol–H ₂ O				Phenol–H ₂ S		
	σ_{H}	σ_{O}	π	Expt	σ_{H}	σ_{O}	π
$\delta\nu_{\text{OH}}$	-120 [-173]	4 [1]	2 [1]	-132	-90 [-138]	-4 [-7]	-3 [-7]
$\Gamma\nu_{\text{OH}}$	10.1 [10.4]	1.1 [1.0]	1.1 [1.1]		8.8 [9.5]	1.0 [1.0]	1.1 [1.1]
ν_{int}	177 [157]	150 [131]	102 [99]	155	98 [102]	84 [88]	74 [92]
	Phenol–NH ₃				Phenol–PH ₃		
	σ_{H}	σ_{O}	π	Expt	σ_{H}	σ_{O}	π
$\delta\nu_{\text{OH}}$	-340 [-419]	3 [-3]	0 [-2]	-362	-104 [-125]	-2 [-4]	0 [-5]
$\Gamma\nu_{\text{OH}}$	18.6 [19.6]	0.9 [0.9]	1.0 [1.0]		8.7 [8.7]	0.9 [0.9]	1.0 [0.9]
ν_{int}	198 [190]	119 [118]	90 [122]	164	92 [92]	58 [62]	67 [86]
	Phenol–MeOH				Phenol–MeSH		
	σ_{H}	σ_{O}	π	Expt	χ_{H}	χ_{O}	
$\delta\nu_{\text{OH}}$	-171 [-232]	6 [-3]	-2 [-6]	-201	-105 [-142]	-7 [-10]	
ν_{int}	190 [179]	150 [134]	108 [118]	162	111 [119]	82 [94]	

agree well with the corresponding observed values [26a–c, 27] 155, 164, and 162 cm^{-1} . The red-shift of phenolic O–H stretching frequency relative to that of bare phenol ($-\delta\nu_{\text{OH}}$) is well correlated with the O–H bond elongation upon H-bond formation in σ_{H} complexes. The predicted red-shifts $-\delta\nu_{\text{OH}}$ for the above three σ_{H} complexes (120 [173], 340 [419] and 171 [232] cm^{-1} respectively) compare well with the corresponding experimental values [26a–c, 27] (132, 362, and 201 cm^{-1} , respectively). It should also be noted that the intensity ratio is 10–20-fold for the first-row hydride and MeOH, and 5–10-fold for the second-row hydrides and MeSH. This drastic enhancement in intensity was already proven in experiments of phenol with H_2O and NH_3 . [26d] It is very clear that for H_2O , NH_3 , and MeOH, only the σ_{H} conformers which are the lowest energy structures can explain the observed characteristic spectra, since their σ_{O} and π conformers hardly show frequency shifts and intensity changes in the calculations. As our calculated results are in good agreement with the available experimental data, we may predict that the lowest energy conformers of σ_{O} phenol–HF and π phenol–HCl/ H_2S / PH_3 /MeSH would show minimal red-shift for $-\delta\nu_{\text{OH}}$. In addition, the intermolecular stretching frequency ν_{int} for σ_{O} phenol–HF is predicted to be 187 [178] cm^{-1} , those for π phenol–HCl/ H_2S / PH_3 are predicted to be 81 [95], 74 [92], and 67 [86] cm^{-1} , respectively, and that for the χ_{H} phenol–MeSH is 111 [119] cm^{-1} .

6 EDGE-TO-FACE AROMATIC INTERACTIONS AND SUBSTITUENT EFFECTS

Aromatic interactions are known to play a significant role in stabilizing protein tertiary structures, enzyme–substrate complexes, organic supra molecules, and organic nanomaterials [4, 9, 28–33]. Therefore, a clear understanding of these interactions in terms of nanorecognition [34, 35] is of importance for the design of novel supramolecular systems and nanomaterials. Various studies on the benzene dimer have focused on the face-to-face (stacked), displaced face-to-face (displaced stacked), and edge-to-face (T-shaped) structures [36–40]. Of these, the latter two are much more stable, with the last being slightly more stabilized. Hence, the displaced stacked conformers are often found in organic crystals and nanomaterials, and the edge-to-face conformers are frequently found in biological systems. Since the conformational changes between T-shape and stacked conformers could be utilized as precursors of nanomechanical devices [41] such as molecular vessels for drug delivery and nanosurgery, the understanding of edge-to-face interaction between the edge H atom of an axial aromatic ring and the center of the facial aromatic ring is of importance.

It is generally known that the substituent effect on the aromatic ring is related to both the inductive effect caused by the substituent (electron-localization factor) and the resonance effect (electron-delocalization factor) [42]. These effects are highly correlated to Hammett's constants [43]. In terms of the

inductive effects, the NH_2 , OH , F , Cl , Br , CN , and NO_2 groups are electron-acceptors, while CH_3 is an electron-donor. However, in terms of resonance effects, the NH_2 , OH , F , Cl , Br , and CH_3 groups are electron-donors, while CN and NO_2 are electron-acceptors. NH_2 and OH have some of the electron-accepting inductive effects due to the electronegativity of N and O atoms, but their electron-donating resonance effects are dominating. Although the F , Cl , and Br groups have some of the electron-donating resonance effects, the electron-accepting inductive effects are dominating. Therefore, the F , Cl , Br , CN , and NO_2 groups have negative Hammett's constants as electron-acceptors, while the NH_2 , OH , and CH_3 groups have positive Hammett's constants as electron-donors. We compare edge-to-face interactions (T-shaped structure) of variously substituted aromatic systems on model systems I and II with substituted axial and facial benzenes, respectively (Fig. 4).

Table 6 lists the interaction energies (ΔE) and interphenyl distances ($d_{\text{H}\phi}$) along with the Hammett constants (σ_p). δE and δd_{H} are the relative values for the substituted systems with respect to the unsubstituted benzene dimer. The relative values are depicted in Fig. 5. The absolute binding energy of the benzene dimer depends seriously on the levels of theory and basis sets. The binding energy ($-\Delta E$) of MP2/6-31 + G^* , MP2/6-311 + G^* , MP2/aVDZ, MP2/aVTZ, MP2/aVQZ, CCSD/aVDZ', and CCSD(T)/aVDZ' are 1.60, 2.31, 3.20, 3.44, 3.53, 1.10, and 1.56 kcal/mol, respectively. Therefore, the MP2/aVTZ value would be near the complete basis limit (CBS) which is estimated to be ~ 3.6 kcal/mol, while the CCSD(T)/aVDZ' value is far from the CBS value since the CCSD(T) calculations would require much larger basis sets to describe the CBS value than the MP2 calculations. If we consider the CCSD(T)/aVDZ' binding energy is 1.28 kcal/mol smaller than the MP2/aVDZ' value, the CCSD(T) CBS binding energy could be estimated to be only ~ 2.3 kcal/mol.

Although the absolute binding energy depends seriously on the levels of theory and basis sets, it is interesting to note that the relative binding energies of the substituted aromatic systems do not significantly change, partially due to

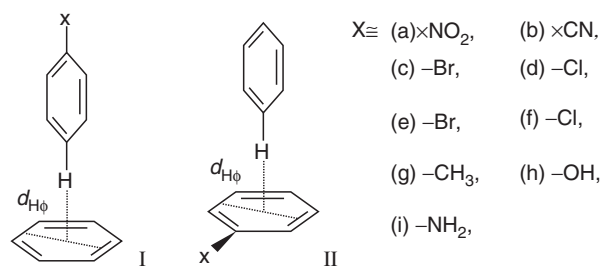


Figure 4. Model systems for aromatic edge-to-face interactions with various substituents. The CH atoms at the *para*-position of the axial (vertical) ring is constrained to be along the axis passing through the center of the facial (horizontal) ring and to be perpendicular to the facial ring. Reproduced by permission of American Chemical Society: Ref. [42].

Table 6. Relative interaction energies ($\delta\Delta E$) and interphenyl charge transfer (δq_{CT}) for the edge-to-face aromatic interactions (types I and II), and the Hammett substituent constants (σ_p) for p -C₆H₅X^a

Type I: X	Strong electron-accepting										Strong electron-donating									
	NO ₂	CN	Br	Cl	F	CH ₃	OH	NH ₂	(H)	(H)	NO ₂	CN	Br	Cl	F	CH ₃	OH	NH ₂	(H)	(H)
$\delta\Delta E$: MP2/6-31+G*	-0.68	-0.59	-0.31	-0.26	-0.22	0.05	0.04	0.15	(ΔE : -1.60)									0.15		
MP2/6-311++G**	-0.63	-0.57	-0.27	-0.23	-0.18	0.06	0.06	0.17	(ΔE : -2.31)									0.17		
MP2/aVDZ	-0.65	-0.61	-0.33	-0.30	-0.18	0.05	0.06	0.06	(ΔE : -3.20)									0.15		
MP2/aVTZ	-0.68	-0.63	-0.34	-0.32	-0.19	0.04	0.03	0.18	(ΔE : -3.44)									0.18		
CCSD(T)/aVDZ'	-0.67	-0.57	-0.26	-0.24	-0.18	0.06	0.03	0.13	(ΔE : -1.56)									0.13		
ΔE_{soln} : MP2/6-31+G*	-0.55	-0.44	-0.18	-0.18	-0.17	0.03	0.06	0.10	(ΔE_{soln} : -1.47)									0.10		
σ_p	0.78	0.66	0.23	0.23	0.06	-0.17	-0.37	-0.66	0									-0.66		
Type II: X	CN	NO ₂	F	Cl	Br	OH	CH ₃	NH ₂	(H)	CN	NO ₂	F	Cl	Br	OH	CH ₃	NH ₂	(H)	(H)	
ΔE : MP2/6-31+G*	0.38	0.38	0.31	0.26	0.22	0.04	-0.24	-0.36	(ΔE : -1.60)									-0.36		
MP2/6-311++G**	0.34	0.32	0.27	0.18	0.11	-0.02	-0.32	-0.39	(ΔE : -2.31)									-0.39		
MP2/aVDZ	0.34	0.31	0.30	0.10	0.03	-0.05	-0.37	-0.58	(ΔE : -3.20)									-0.58		
MP2/aVTZ	0.37	0.32	0.26	0.09	0.01	-0.05	-0.37	-0.60	(ΔE : -3.44)									-0.60		
CCSD(T)/aVDZ'	0.37	0.35	0.26	0.20	0.19	-0.01	-0.21	-0.37	(ΔE : -1.56)									-0.37		
ΔE_{soln} : MP2/6-31+G*	0.24	0.30	0.24	0.15	0.12	0.05	-0.23	-0.21	(ΔE_{soln} : -1.47)									-0.21		

^a All these values were obtained with BSSE correction. The relative interaction energies in the chloroform solvent (dielectric constant $\epsilon = 4.9$) ($\delta\Delta E_{\text{soln}}$) were obtained using isodensity surface polarized continuum model (IPCM). The interphenyl distances $d_{\text{H}\cdots\text{H}}$ of MP2/6-31+G* optimized geometries were re-optimized with the BSSE-corrected MP2/aug-cc-pVDZ calculations. Energies are in kcal/mol. The values in the table (except for those in parentheses for the cases of X=H for which the absolute values are given) are relative values with respect to the T-shaped benzene dimer. σ_p is Hammett's substituent constant for the *para*-position, defined as the acidity of *p*-substituted benzoic acid at 25°C. It should be noted that all the relative energies at different levels of theory are consistent, while their absolute magnitudes vary depending on the levels of theory.

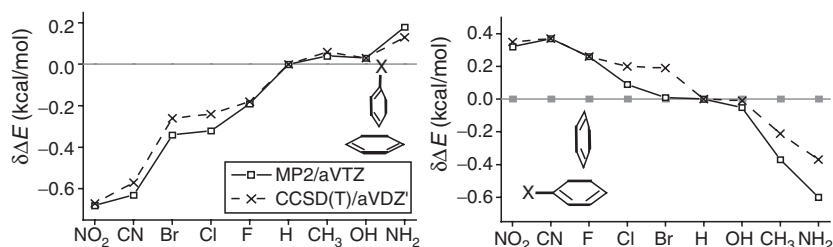


Figure 5. Relative values of interaction energies ($\delta\Delta E/\delta\Delta E_{\text{sol}}$ for the gas/solution phase; in kcal/mol) for types I and II with respect to the benzene dimer: $\Delta E/\Delta E_{\text{sol}} = -3.20/-1.47$ kcal/mol. Reproduced by permission of American Chemical Society: Ref. [42].

the cancellation errors. For example, the relative energies are almost the same within 0.02 kcal/mol for both CCSD(T)/aVDZ' and CCSD/aVDZ' (thus, the latter values have not been reported in Table 1), while the absolute binding energies of the former are consistently ~ 0.46 kcal/mol larger than those of the latter. Similarly, the MP2 binding energies are quite different depending on the basis set used, but the relative energy differences are almost same. The relative binding energies at the CCSD(T) level are similar to those at the MP2 level regardless of the basis set employed. In this regard, it is clear that the relative energies can be predicted in a reliable way. In this regard, though all the results are consistent, there can be subtle errors up to ~ 0.1 kcal/mol (or at most ~ 0.2 kcal/mol in the worst situation). In consideration that our results are based on geometries at the BSSE-corrected MP2/aVDZ level, we discuss our results in terms of MP2/aVDZ values [and MP2/aVTZ//MP2/aVDZ values in brackets], unless otherwise specified.

The interaction energy increase/decrease due to the monosubstitution of the benzene dimer is no more than 0.65/0.34 [0.68/0.37] kcal/mol in the gas phase. This value becomes much smaller (0.55/0.24 kcal/mol) in the chloroform solvent (dielectric constant $\epsilon = 4.9$). This small energy difference agrees with experiments [31, 35a]. Although the edge-to-face interaction energy at the CCSD(T)/CBS level is ~ -1.5 kcal/mol, these small energy changes should not be simply neglected, since the sum of a large number of these interaction terms could be significant in multisubstituted aromatic systems, in particular, in the cases when strong interactions are not present.

Based on the predicted interaction energies, we find that for type I, the electron-accepting strength of the axial aromatic ring is in the order $\text{NO}_2 > \text{CN} > \text{Br} > \text{Cl} > \text{F} > \text{H} > \text{CH}_3 > \text{OH} > \text{NH}_2$ in both the gas phase and the chloroform solution. For type II, the electron-donating strength of the facial aromatic ring is in the order $\text{CN} < \text{NO}_2 < \text{F} < \text{Cl} < \text{Br} < \text{H} < \text{OH} < \text{CH}_3 < \text{NH}_2$ in the gas phase, and in the order $\text{NO}_2 < \text{CN} < \text{F} < \text{Cl} < \text{Br} < \text{OH} < \text{H} < \text{NH}_2 \approx \text{CH}_3$ in the chloroform solution. Therefore, the order in binding strength of type I for NO_2 and CN in the gas phase, that for Br , Cl , and F in both gas and solution phases, and that for CH_3 and OH in the gas phase, and

that for CH₃ and NH₂ in the chloroform solution are changed into type II. It should be noted that though the systems with electron-accepting substituents (NO₂, CN, Br, Cl, F) favor type I, those with electron-donating substituents (NH₂, CH₃, OH) favor type II; then the substitution can strengthen the binding, compared to the unsubstituted benzene dimer.

For type I, the binding strength increases as the substituent changes from strong electron-donor to strong electron-acceptor. The trend for δE shows a good correlation between the free energy and the Hammett constant. Indeed, we also find that δE are correlated with the Hammett constant at *para*-position (σ_p). The interaction for type I can thus be correlated with the charge transfer effect or polarizability-driven inductive effect. Thus, for type I, the polarizability-driven inductive effect would be important. For type I, a strong electron-accepting/donating group of the NO₂/NH₂ substituent increases/decreases the binding strength by 0.65/0.15 [0.68/0.18] kcal/mol compared to the unsubstituted case. The solvent effect for type I does not change the order in binding strength in the gas phase, but slightly decreases the absolute binding energy and the relative binding energy differences.

For type II, the increased/decreased π -electron density by the electron-donating/accepting substituent NH₂/CN increases/decreases the binding strength by 0.58/0.34 [0.60/0.37] kcal/mol. The solvent effect changes the order in binding strength between NO₂ and CN and the order between CH₃ and NH₂. The largest/smallest binding energy in solution is 1.70/1.17 kcal/mol (for CH₃/NO₂), while that in the gas phase is 3.79/2.86 kcal/mol (for NH₂/CN). The maximum binding energy gain/loss by substituent in the benzene dimer is only 0.23/0.30 kcal/mol in the solvent, in contrast to significant gain/loss in the gas phase by 0.38/0.36 kcal/mol at MP2/6-31 + G* (0.58/0.34 kcal/mol at MP2/aVDZ). Although in solution CN/CH₃ is a more effective electron-acceptor/donor than NO₂/NH₂, the overall trend in solvent is similar to that in the gas phase. In addition, considering the halide groups which are electron-acceptors, the F-substituent system is more stabilized than the Cl/Br-substituent systems, so this trend is opposite to that in type I. Similarly, the OH group is less effective than the CH₃ group. In addition to the charge transfer from the facial to axial rings, the CH- π interaction in type II depends on the electron density around the center of a substituted facial aromatic ring which is very sensitive to the exchange repulsion and dispersion energy.

For the complexes involving both types I and II, the interaction energies are found to be nearly additive. The complex with the facial aminobenzene and the axial nitrobenzene gives the interaction energy gain by 1.18 kcal/mol over the dimer. This value is close to the sum (1.23 kcal/mol) of the interaction energy gain (0.65 kcal/mol) for the axial nitrobenzene interacting with the benzene and that (0.58 kcal/mol) for the facial aminobenzene interacting with the benzene. The complex with the facial cyanobenzene and the axial nitrobenzene gives the interaction energy gain by 1.16 kcal/mol over the dimer, close to the sum of the

two separate contributions ($0.61 + 0.58 = 1.19$ kcal/mol). Thus, the edge-to-face interactions can be enhanced as much as 1.2 kcal/mol by both axial and facial substitutions.

The substituent effect of the interaction energies and energy components for types I and II is listed in Table 7. In the benzene dimer, we find that the total interaction energy (E_{tot}) is -2.49 kcal/mol, and the electrostatic energy (E_{es}), induction energy (E_{ind}), dispersion energy (E_{disp}), and exchange repulsion (E_{exch}) are -2.04 , -1.00 , -4.56 , and 5.47 kcal/mol, respectively, and E_{ind}^* , E_{disp}^* , and E_{exch}^* are -0.23 , -4.10 , and -4.24 kcal/mol, respectively. Therefore, the dispersion is the dominating interaction component for any substituents in both types, since the substitution effect changes within ~ 0.7 kcal/mol.

While the total interaction energies and their energy components widely vary depending on the levels of calculation, the relative energies little depend on them. Therefore, the relative energies (δE_{tot} , δE_{es} , δE_{exch} , δE_{ind} , δE_{disp}) of the substituted systems with respect to the benzene dimer are considered to be reliable. For both types, it is interesting to note that though the main energy component of E_{tot} is E_{disp} , the main energy component of δE_{tot} is δE_{es} . For type I, δE_{tot} is well described simply by δE_{es} among the four components (δE_{es} , δE_{exch} , δE_{ind} , δE_{disp}). Since the electrostatic energy plays a key role in type I, the electrostatic energy-driven polarization (induction) is well correlated with E_{tot} . We particularly note that $\delta E_{\text{es}+\text{ind}}^*$ ($= \delta E_{\text{es}} + \delta E_{\text{ind}}^*$) is almost the same with δE_{tot} , since the three terms of δE_{disp}^* , δE_{exch}^* , and δE_{HF} ($\delta E_{\text{disp}}^* + \delta E_{\text{exch}}^* + \delta E_{\text{HF}} = \delta E_{\text{disp}}^* + \delta E_{\text{exch}}^* + \delta E_{\text{HF}}$) almost cancel out. Thus, the total

Table 7. Substituent effect (relative energy with respect to the basis set at the MP2/aVDZ' level) of the interaction energies and energy components (kcal/mol) for the edge-to-face aromatic interactions (types I and II) by SAPT decomposition

Type I: X	NO ₂	CN	Cl	OH	NH ₂	(H)
δE_{tot}	-0.77	-0.66	-0.28	0.05	0.19	(E_{tot} : -2.49)
δE_{es}	-0.59	-0.55	-0.25	0.05	0.20	(E_{es} : -2.04)
δE_{ind}^*	-0.17	-0.13	-0.05	0.01	0.02	(E_{ind}^* : -0.23)
δE_{disp}^*	-0.17	-0.18	-0.09	0.01	0.02	(E_{disp}^* : -4.10)
δE_{exch}^*	0.26	0.30	0.14	-0.03	-0.08	(E_{exch}^* : 4.24)
$\delta E_{\text{es}+\text{ind}}^*$	-0.76	-0.68	-0.29	0.06	0.22	($E_{\text{es}+\text{ind}}^*$: -2.27)
$\delta E_{\text{disp}^*+\text{exch}^*+\delta\text{HF}}$	-0.01	0.02	0.01	-0.01	-0.03	($E_{\text{disp}^*+\text{exch}^*+\delta\text{HF}}$: -0.21)
Type II: X	NO ₂	CN	Cl	OH	NH ₂	(H)
δE_{tot}	0.33	0.34	0.13	-0.03	-0.45	(E_{tot} : -2.49)
δE_{es}	0.50	0.52	0.26	-0.04	-0.54	(E_{es} : -2.04)
δE_{ind}^*	0.08	0.08	0.04	0.00	-0.05	(E_{ind}^* : -0.23)
δE_{disp}^*	-0.16	-0.16	-0.22	-0.18	-0.50	(E_{disp}^* : -4.10)
δE_{exch}^*	-0.18	-0.19	0.07	0.16	0.70	(E_{exch}^* : 4.24)
$\delta E_{\text{es}+\text{disp}^*+\text{exch}^*}$	0.16	0.17	0.11	-0.06	-0.34	($E_{\text{es}+\text{disp}^*+\text{exch}^*}$: -1.90)

energy change by the substituent effect in type I is represented by the sum of δE_{es} and δE_{ind}^* . One can easily note a good correlation between δE_{tot} and δE_{es} as well as an excellent agreement between δE_{tot} and $\delta E_{\text{es+ind}}^*$.

For type II, δE_{tot} is the most correlated with δE_{es} among the four components. In addition, $\delta E_{\text{es+disp}^*+\text{exch}^*}$ ($= \delta E_{\text{es}} + \delta E_{\text{disp}}^* + \delta E_{\text{exch}}^*$) is also correlated with δE_{tot} (Fig. 4). Thus, the substituent effect in type II is complicated. The decrease/increase of the electron density of the facial rings by large/small charge transfer due to the electron-donor/acceptor should significantly decrease/increase δE_{ind} , but this change is less significant than the changes of δE_{disp}^* and δE_{exch}^* . Upon substitution, δE_{disp}^* are all greater in magnitude than that of the benzene dimer, probably because the total amount of electron population of the facial benzene ring increases (since the H atom depletes the electron density of the facial aromatic ring as a strong electron-acceptor, in comparison with nonhydrogen atoms). While the electron-donor/acceptor with increased/decreased charge transfer shows increased/decreased binding energy, the sum of δE_{ind} , δE_{exch}^* , and δE_{disp}^* reasonably differentiates various edge-to-face interactions for type II.

Figure 6 shows interesting polarization effects on the occupied molecular orbitals of strong electron-donor (NH_2^-) and strong electron-acceptor (NO_2^-) substituted aromatic rings relative to the benzene ring for types I and II. The benzene gives only minor polarization from the facial ring to the axial ring. For type I, the strong electron-accepting group NO_2 withdraws electron (which results in strong stabilization), whereas the electron-donating group NH_2 forbids the electron withdrawing (which results in destabilization). Therefore, the polarization due to the electron-donating/accepting power affects the edge-to-face interaction energy. This effect is very important in type I. In type II, the electrostatic interaction plays also an important role, and, subsequently, the polarization is correlated with the electrostatic energy. The facial NO_2 -substituted aromatic ring forbids the electron-transfer-driven polarization to the axial ring (which results in destabilization), whereas the facial NH_2 -substituted aromatic ring allows strong polarization to the vertical ring (which results in strong stabilization). It is also interesting to note that the polarization for the facial Cl/Br/F-substituted aromatic ring in type II is slightly weaker than or similar to that for the benzene-dimer system. However, other effects (dispersion and exchange in addition to the electrostatic energy) are also important in type II, as discussed earlier.

It is interesting to compare the edge-to-face interactions for the T-shaped aromatic–aromatic complexes with those for the T-shaped structure with an aromatic ring and a counterpart such as H_2 , H_2O , HCl , and HF . In this case, H_2 would involve mainly dispersion and induction energies; the benzene involves dispersion, quadrupole–driven polarization, and quadrupole–quadrupole interaction energies; H_2O , HCl , and HF would involve dispersion, dipole–driven polarization, and dipole–quadrupole interaction energies. The dipole moments of H_2O , HCl , and HF along the axial direction are 1.13, 1.18, and 1.84 Debye,

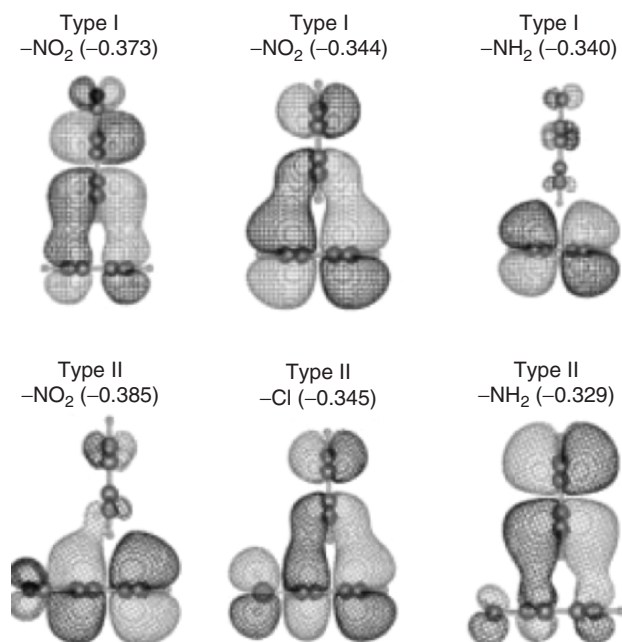


Figure 6. The occupied molecular orbitals of types I (top) and II (bottom) involving with the charge transfer. Orbital energies in parentheses are given in au. In contrast to the benzene dimer which shows a moderate charge transfer ($q_{\text{CT}} = -0.0133$ au; $\delta q_{\text{CT}} = 0$ as a reference system), in the cases of type I the strong electron-accepting NO_2 group in the axial aromatic ring shows increased electron-transfer toward the axial aromatic ring ($\delta q_{\text{CT}} = -0.0017$ au), whereas the strong electron-donating NH_2 group shows decreased charge transfer ($\delta q_{\text{CT}} = 0.0007$ au). In the cases of type II, the strong electron-accepting NO_2 groups in the facial aromatic rings show decreased charge transfers ($\delta q_{\text{CT}} = 0.00142$ au), while the strong electron-donating NH_2 group shows increased charge transfer ($\delta q_{\text{CT}} = -0.00103$ au). Reproduced by permission of American Chemical Society: Ref. [42].

respectively. While the H_2 does not give significant interaction energy gain/loss depending on the substituted benzene, the quadrupole-driven electrostatic effect in the benzene shows marginal energy differences, and the dipole-driven electrostatic effects in H_2O , HCl , and HF show large energy differences depending upon substitution (Fig. 7). In the case of H_2O , the difference in the edge-to-face interaction energy between the NO_2^- - and NH_2 -cases is 2.1 kcal/mol. In the case of HF -aromatic systems, this difference is further enhanced as much as 2.6 kcal/mol. The energy difference between $\text{NO}_2^-/\text{NH}_2$ -substituted benzene–water system and the benzene–water system is 1.3/–0.8 kcal/mol; thus, these large energy differences would be useful for the design of novel supramolecular systems and novel molecular devices. Even though the difference in the aromatic–aromatic systems is not large, the sum of a large number of interactions in the absence of H-bonding type interactions would be of

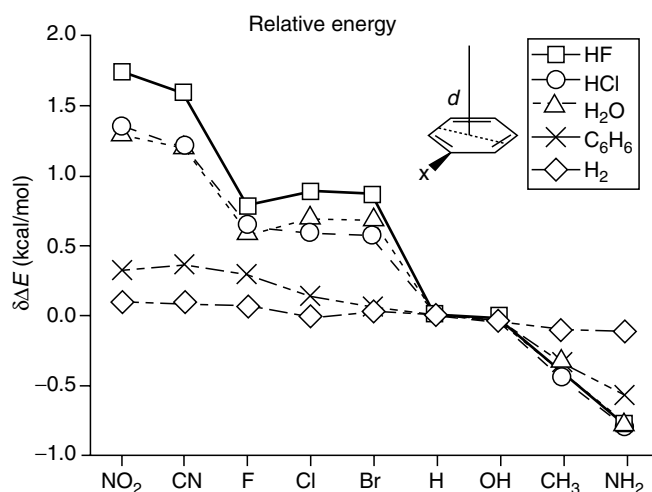


Figure 7. Relative interaction energies ($\delta\Delta E$ in kcal/mol) for the T-shape conformers of the substituted aromatic ring with H_2 , benzene, H_2O , HCl , and HF . Reproduced by permission of American Chemical Society: Ref. [42].

importance to play a key role, which can be evidenced from the fact that the aromatic–aromatic π stacking which has the interaction energy comparable to the edge-to-face interaction plays a key role in crystal packing.

7 H-BONDS IN HYDRATION AND COORDINATION CHEMISTRY

The diffuse electron-rich lone pair of electrons of negatively charged ions provides diverse hydration and coordination chemistry as shown in Fig. 8. Although the anions have different numbers of lonepair electrons, they show tri- or tetra-coordinations. A hydroxide ion forms trihydrated structure using three lone pairs. The tetraordinated hydroxide anion is isoenergetic to the tricoordinated hydroxide ion, and is observed in larger clusters. The tetrahydrated fluoride ion has an internal state near 0 K, but as temperature increases to the room temperature, water–water H-bond breaking appears with tetrahedral coordination using four lone pairs of electrons due to the entropy effect [20]. On the other

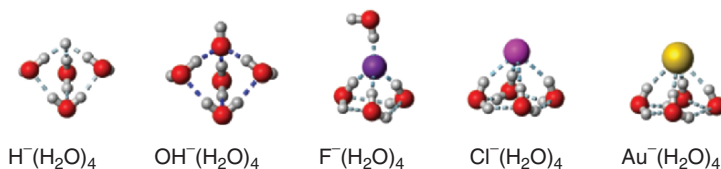


Figure 8 (see color section). Structures of hydrated anion clusters.

hand, the tetrahydrated chloride ion has a surface bound state even at room temperature [20]. A chloride ion has weak ion–water interactions in comparison to a fluoride ion. Strongly electronegative small ions form strong H-bonds with water molecules, which are larger than the water–water binding energy, due to the strong electrostatic interactions. While a cation has very strong electrostatic interaction, an anion has slightly weaker electrostatic interaction because the presence of an excess electron requires a large space for stabilization (i.e., to lower the kinetic energy of the excess electron).

8 COOPERATIVE EFFECT IN SHORT H-BOND

Although, in general sense, the cooperativity applies to all intermolecular interactions, it is particularly important in H-bond interaction because of the relay effect of hydrogen atoms. The H-bond distance tends to decrease as the cluster size increases. The typical characteristics of cooperative effects show the shorter X \cdots H distance, longer X–H distance, larger chemical shift, and large red-shifts of the O–H vibrational frequency.

8.1 Linear H-Bonded Chains

A number of studies have been devoted to investigate the property of linear H-bonded chains such as HF, HCN, and H₂O systems. Mostly, the HF dimer has been served as a hydrogen bond model. Experiments show that the bent dimer and cyclic hexamer are stable in cluster. In crystalline hydrogen fluoride, HF forms infinite chain structure by strong hydrogen bond (F \cdots F distance of 2.47 Å which is \sim 0.25 Å shorter than the normal F \cdots F distance of 2.72 Å in the finite system HF \cdots HF) [44]. Guedes et al. [45] have investigated the characteristics of cyclic HF and HCl clusters, and showed that the hydrogen-bond cooperativity is related to electronic sharing and delocalization through electron density difference. Rincon et al. [46] also showed that the cooperative effect is related to electron delocalization between monomer units through the analysis of the topology of electron density.

Cooperative effects in H₂O appear as gradual shortening of hydrogen bond distance from dimer (2.98 Å) to liquid (\sim 2.8 Å) to ice (\sim 2.75 Å) [47]. Beside the studies of liquid water and ice, a lot of theoretical studies have been devoted to water chains [48–50]. Suhai calculated the bond distance and average H-bond energy in the infinite water chain as 2.73 Å and 6.30 kcal/mol, respectively, which is comparable to experimental results on ice (2.74 Å and 6.7 kcal/mol) [48]. Hermansson et al. [49] investigated the polarization of the individual water molecules in finite and infinite H-bonded chains, and showed that the induced dipole moment in the middle of the long chain is about twice those at the ends. The additional dipole moments are created by charge transfer from acceptor to donor. Masella and Flament [50] investigated the cooperative effects in cyclic trimers comprised of water and methanol.

8.2 Short H-Bond in Organic Crystals and Peptides

The cooperativity of H-bond plays an important role in determining the structures of molecular crystals and biological molecules. Cyclohexane-1,3-dione forms sheet, which has long chains of hydrogen bond with most solvents (forms 6:1 cocrystal with benzene) [51]. Dannenberg et al [52]. explained this by comparing asymptotic interaction energy of the infinite chain and cyclic hexamer. Comparing differences between urea and 1,3-cyclohexanedione under external electric field, they found that the short distance in urea is reasonably described by the electrostatic interaction and the polarization effect, but 1,3-cyclohexanedione is not.

The cooperative effects in secondary protein structures, helix and sheet have been reported [53]. The linear chain of formamide which resembles peptides has large cooperativity in H-bond, which is 2.5 times that of formamide dimer. For the parallel and antiparallel sheet in secondary protein structures, there was no cooperativity in the parallel direction, while significant cooperativity exists in perpendicular direction. In methanol solvent system, the cooperative effects were reduced, indicating that the cooperativity is due to the polarization effect.

8.3 Diol and Dione

We considered two different linear chainlike H-bond relays, poly-1,2-ethanediols and 1,3-propanedione (Fig. 9) [54]. The geometries on the plane were optimized up to the decamer at the B3LYP/6-31G* level, and up to hexamer at the MP2/6-31G* level. The binding energy of infinite chain was obtained on the basis of the exponential decay plot (Fig. 10).

In the case of the dimer, 1,3-propanedione has larger H-bond energy (12.3 kcal/mol) than 1,2-ethanediol (5.9 kcal/mol) at the B3LYP level. Based on the exponential decay plot, the H-bond energies in the infinite chains of 1,3-propanedione and 1,2-ethanediol are 24.4 and 9.8 kcal/mol, respectively,

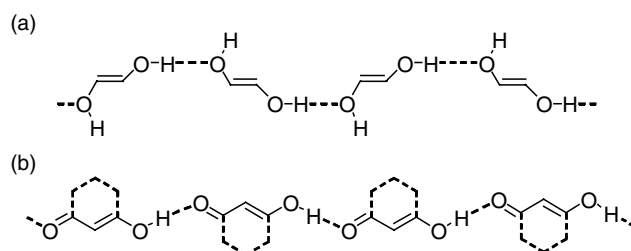


Figure 9. Schematic of 1-D H-bonds relays. (a) 1-D H-bond relay of poly-1,2-ethanediols (diols). (b) 1-D H-bond relay of poly-1,3-propanedione (diones). Reproduced by permission of American Chemical Society: Ref. [54].

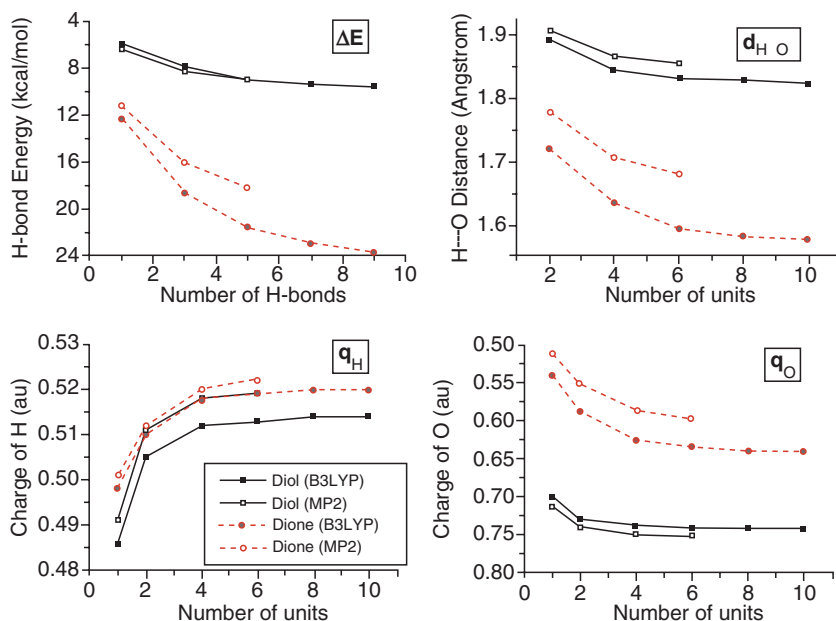


Figure 10. ZPE-uncorrected H-bond interaction energies (ΔE_e), H...O distances ($d_{H...O}$), and atomic charges of H and O atoms of the central H-bond (q_H , q_O) in the 1-D H-bond relay of 1,2-ethanediols and 1,3-propanediol. Reproduced by permission of American Chemical Society: Ref. [54].

which increased by 12.0 and 3.9 kcal/mol, respectively, than those of the dimers. Also, bond distances are shortened by 0.07 and 0.15 Å, respectively. MP2 results are comparable with B3LYP results. Change of NBO atomic charge shows that the polarization is mainly responsible for this cooperativity. H-bond between diones is stronger with the larger cooperativity effect than that of diols.

8.4 Short H-Bonds for Organic Nanotubes and the Solvent Effect

We recently synthesized calix[4]hydroquinone (CHQ) nanotubes, which are assembled by 1-D short hydrogen bonds (SHBs) (Fig. 11) [4]. Hydrogen bond length in CHQ is about 2.65 Å, which is almost 0.2 Å shorter than that of normal hydrogen bond. For cluster systems, we have carried out B3LYP and MP2 calculations. To investigate the periodic systems including solvent, we have carried out plane wave density functional theory (PW-DFT) using generalized gradient approximation (GGA) of Perdew and Wang [55], and the Vanderbilt pseudopotentials [56].

1-D SHB in CHQ nanotubes involves three kinds of H-bond between hydroquinone (Q_h) and water (W). We denote the complex with a H-donor and a H-acceptor as $D > A$. The $W > Q_h$, $Q_h > Q_h$, and $Q_h > W$ in Fig. 12 have bond

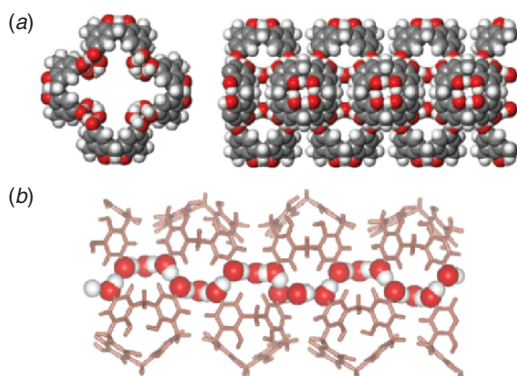


Figure 11 (see color section). Longitudinal H-bond relay comprised of CHQs and water. (a) Tubular polymer structure of a single nanotube obtained with X-ray analysis for the heavy atoms and with ab initio calculations for the H-orientations (top and side views). (b) One of the four pillar frames of short H-bonds represents a 1-D H-bond relay composed of a series of consecutive OH groups [hydroxyl groups (–OH) in CHQs and the OHs in water molecules]. Reproduced by permission of American Chemical Society: Ref. [54].

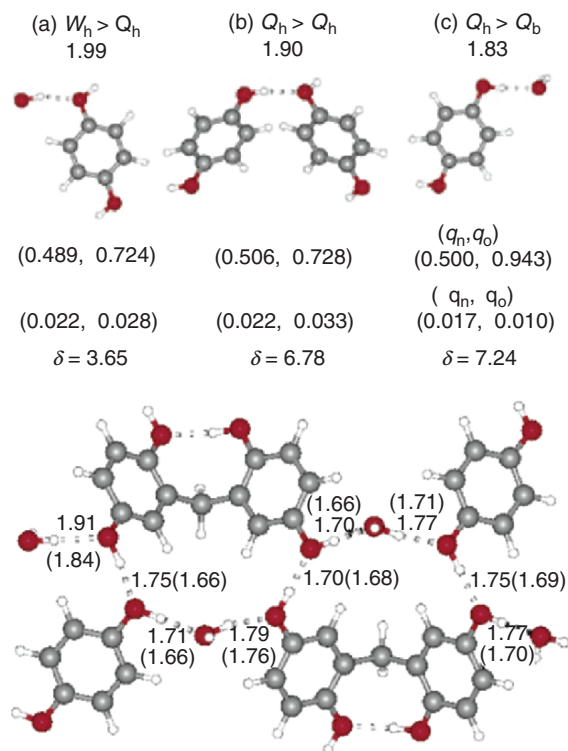


Figure 12 (Continued).

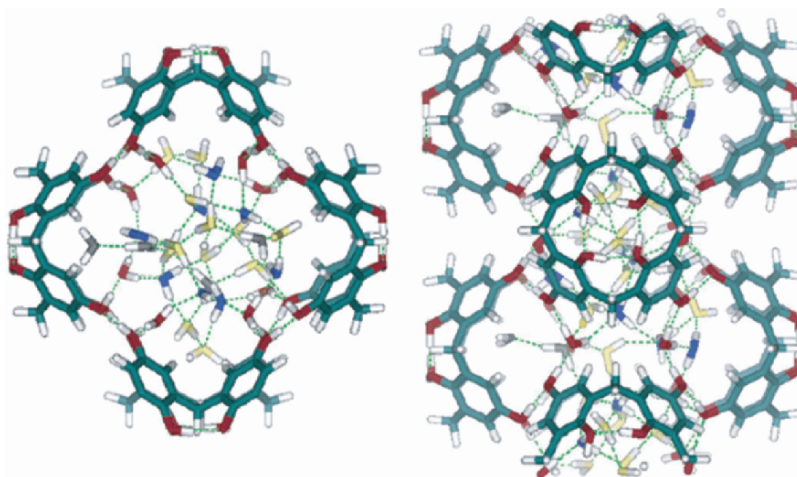


Figure 12 cont'd (see color section). Short H-bonds in CHQ nanotubes in the top figures are three types of H-bonding involved with 1-D H-bonds of CHQ nanotubes [(a) $W_b > Q_h$, (b) $Q_h > Q_h$, and (c) $Q_h > W_h$]. The H-bond distances (\AA), atomic charges (q_H and q_O in au), and their changes with respect to the values of the isolated systems (δ_{q_H} and δ_{q_O} in au), and proton chemical shifts (d in ppm) are given at the B3LYP/6-31G* level. The middle figure is the nine H-bonds relay system showing short H-bonds in a fragment of CHQ nanotube. The bottom figure is the water network in a single tube (top and side views). The top view (left) shows 8 bridging water molecules in red, 8 first-hydration shell water molecules in blue, 12 second-hydration shell water molecules in yellow, and 4 third-hydration shell water molecules in gray, while the side view shows twice those in the top view. Reproduced by permission of American Chemical Society: Ref. [54].

energies of 5.4, 6.3, 8.6 kcal/mol, respectively (B3LYP/6-31G*). These values are similar to MP2/6-31G* results of 5.6, 7.8, and 8.5 kcal/mol and PW-DFT results of 5.6, 4.6, and 8.4 kcal/mol. Case $Q_h > W$ has ~ 0.15 \AA shorter O \cdots H bond distance and ~ 3 kcal/mol larger binding energy than case $W > Q_h$. From orbital interpretation of hydrogen bond, a H atom is likely to stabilize the lone-pair electrons of water oxygen atom more than those of hydroquinone oxygen atom.

In order to investigate the effect of SHB in CHQ nanotubes, we have performed calculations with the increasing number of H-bonds. On the basis of exponential decay plot, the asymptotic H-bond energies for $W > Q_h$, $Q_h > Q_h$, and $Q_h > W$ in infinite H-bond relay are estimated to be 11, 11, and 12 kcal/mol, respectively. The average value of these H-bond energies is 11.3 kcal/mol, which is 4.5 kcal/mol higher than the normal H-bond.

We have calculated the average bond energy gain in the infinite SHB array (E_{shb}) and the solvent effect in bond energy (E_{sol}) using the partition scheme. In this case, E_{shb} is -3.9 kcal/mol and E_{sol} is 1.2 kcal/mol. Thus average HB energy per SHB in the presence of solvent water molecule is 8.9 kcal/mol, which is 2.7 kcal/mol larger than normal H-bond energy.

9 SHORT STRONG H-BOND IN ENZYME CATALYSIS

Short strong H-bond (SSHB)[57, 58] is characterized by their large hydrogen bond energies (>10 kcal/mol), short distances (<2.6 Å), and large downfield shift of NMR resonances (>15 ppm). In low dielectric organic solvents, unusual physicochemical properties have been observed for a number of hydrogen bonds between two partners with an equal pK_a .

The proposal that SSHB plays a key role in the enzymatic catalysis has been highly debated in recent years [59]. One of the examples for the role of SSHB in enzymatic reaction can be found in Δ^5 -3-ketosteroid isomerase (KSI) which is a paradigm for fast enzymatic reactions [60]. KSI catalyzes the conversion of $\beta\gamma$ - to α,β -unsaturated steroidal ketones via a dienolate intermediate at a nearly diffusion-controlled rate. During the reactions, Asp38 serves as a base for abstracting the C4 β -proton of the steroid substrate, while Tyr14 (H-bonded by Tyr55) and Asp99 serve as catalytic residues by providing H-bonds to the oxyanion (C3-O or O3) of the dienolate intermediate (Fig. 13).

The calculated results about energy profile of the wild type system [57] indicate that the barriers for the first step (ES \rightarrow TS1 \rightarrow EI1; abstraction of the proton from the substrate) and the third step (EI2 \rightarrow TS3 \rightarrow EP; donation of the proton to the substrate) are very similar and crucial in energy, while the second step (EI1 \rightarrow TS2 \rightarrow EI2; rotation of Asp38) is not significant in energy so that total reaction is eventually a two-step mechanism. In the presence of Tyr14 or Asp99, the transition states TS1 and TS3 are lowered by ~ 6 kcal/mol. This result implies that the catalytic effect of the two residues is almost equivalent. When Tyr14 and Asp99 were introduced simultaneously, TS1 and TS3 are lowered by ~ 10 kcal/mol. Intermediate states (EIs: EI1 and EI2) and TS2 are stabilized by ~ 15 kcal/mol, suggesting that the two functional groups contribute cooperatively to the stabilization of EIs and TS2.

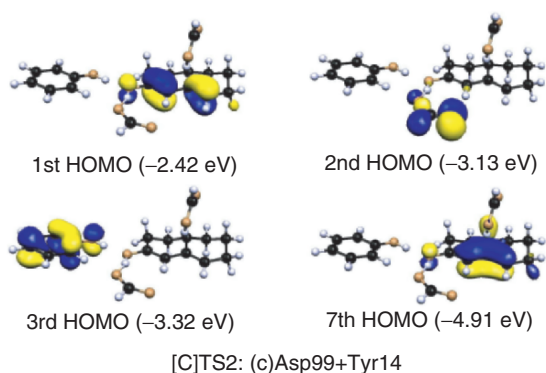
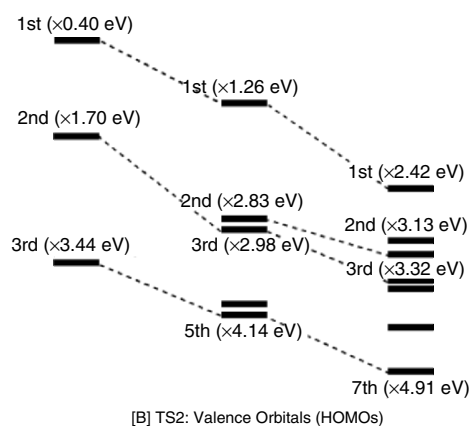
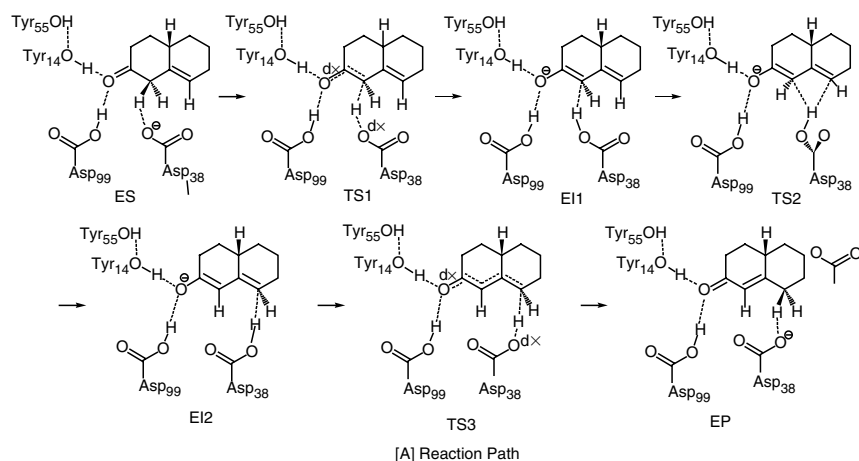


Figure 13 (see color section). Schematic representation of reaction mechanism and HOMO energy levels of transition state (TS) of KSI.



In the structure of the active sites in the complex with the intermediate analogs, the hydrogen bond distances between O3 and Tyr14 or Asp99 are ~ 2.6 Å, which is slightly shorter than those (~ 2.8 Å) of the structure in complex with the product analog [57] (Table 8). NMR spectroscopic investigations also indicate that in the D38N mutant KSI, the H-bond between the catalytic residues and equilenin exhibits a large downfield shifted peak (>16 ppm) [60, 61].

Table 8. Distances (Å) between O_{residue} and O3 along the reaction path (Fig. 13) in wild type of KSI

Residue	ES	TS1	EI1	TS2	EI2	TS3	EP
Tyr14	2.68	2.64	2.55	2.51	2.55	2.61	2.67
Asp99	2.75	2.66	2.60	2.55	2.58	2.65	2.71

The distances between O_{residue} and O3 ($d[\text{O}_r\text{--O3}]$) along the reaction path (Table 8) [57] indicate that even though normal H-bonds are formed between residues and substrate at the starting and ending point of reaction, they are converted to short strong one during the reaction where $d[\text{O}_r\text{--O3}]$ is reduced by $\sim 0.2 \text{ \AA}$, in accordance with the experimental results.

10 H-BOND IN RECEPTORS/IONOPHORES

Host-guest complexes play an important role in biological processes, and H-bonds play a crucial role in the molecular recognition phenomena. In this context, by utilizing hydrogen bond interaction, various ionophores/receptors with selective binding affinity of specific ions have been designed, and demonstrated by experiments [6, 62–65]. Usually, H-bonds in those receptors are in competition with the interaction of polar solvents with ions. Therefore, the most important strategy in designing receptors/ionophores is to know how to optimize the H-bond between receptor and ion in the presence of solvent molecules. Some MD simulation studies for receptors/ionophores involving ions and solvents are available [66].

10.1 H-Bond in the Selective Receptor for Ammonium Ion (NH_4^+) over Potassium Ion (K^+)

The recognition of NH_4^+ has attracted lots of interest since ammonium-containing compounds are very important in chemical, biological, and physiological molecular systems [63]. One of the major problems in the selective recognition of NH_4^+ over K^+ arises from their nearly equivalent sizes. Since the $\text{p}K_{\text{a}}$ of NH_4^+ is 9.0, the subunit to recognize NH_4^+ should be strong proton-withdrawing to strengthen the charged H-bonds [67]. Figure 14 shows schematics of the

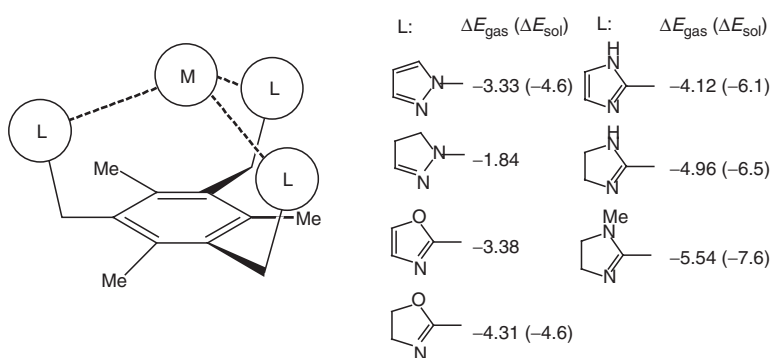


Figure 14. Schematics of the receptors with different subunits L (L = interacting moiety of the receptor) and their relative affinities (kcal/mol) of various ammonium receptors for NH_4^+ over K^+ . ΔE_{sol} for selected receptors in CHCl_3 solution were obtained using the IPCM method. Reproduced by permission of American Chemical Society: Ref. [63(a)].

receptors with the respective interaction energies in the gas phase and CH_3Cl_3 solution for the tripodal receptor with various subunits to selectively recognize NH_4^+ over K^+ . The interaction energy in solvent was calculated using the static isodensity surface polarized continuum model (IPCM) method.

Apart from the recognition efficacy in solvent, the receptors need to possess solvent access-blocking groups (such as Me). In this way, the coordination number of the receptors is limited to no more than 4. Since NH_4^+ and K^+ favor the coordination numbers of 4 and 6, respectively [68], NH_4^+ is solvated in three sites by the receptor and in one site by solvent, while K^+ is solvated in three sites by the receptor and in three sites by solvent. Thus, NH_4^+ tends to be inside the receptor much more than K^+ which tends to be solvated by solvent.

10.2 Ionic H-Bonds in Receptors for Anions

With an aid of supramolecular chemistry, recognizing and sensing anionic species have recently emerged as a key research field [6, 62–65]. In particular, the development of receptors capable of selectively recognizing a specific anion is quite intriguing. To enhance the sensing efficacy and selectivity of anions in solvent, strong ionic H-bond has been frequently harnessed. In this regard, several selective receptors utilizing ionic H-bonds will be introduced.

Recently, we have designed the tripodal receptors (**1–3** in Fig. 15) with 1,3-disubstituted imidazolium ring subunit which can form $(\text{C}-\text{H})^+ \cdots \text{X}^-$ hydrogen bonds with anions [6] in contrast with the common practice that most positively ionic anion receptors were designed to form $(\text{N}-\text{H})^+ \cdots \text{X}^-$ hydrogen bonds. ^1H NMR titration experiment was performed to investigate anion binding properties of hosts. Upon addition of chloride anion to host **1**, significantly large downfield shifts ($\Delta\delta > 0.94$ ppm) were observed for the proton of C(2) which is in between two N atoms of imidazolium subunit. This suggests complexation of the anion by CH hydrogen bonds. Although both hosts **1** and **2** show higher affinities for the chloride anion than bromide, the affinity and the selectivity

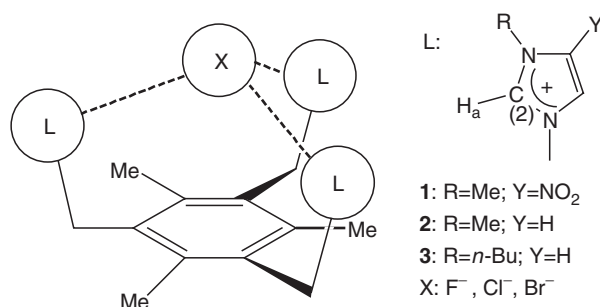


Figure 15. Schematics of tripodal receptors for halide ions.

Table 9. Association constants (K_a) and binding free energies (ΔG°) for 1:1 complexes of host **1**–**3** (Fig. 15) with anions in DMSO- d_6 at 298 K^a

Hosts	Anions ^b	K_a (M ⁻¹)	$-\Delta G_{298}^0$
1	Cl ⁻	4800	5.02
	Br ⁻	490	3.67
2	F ⁻	1300	4.25
	Cl ⁻	1100	4.15
	Br ⁻	180	3.07
3	F ⁻	2400	4.61
	Cl ⁻	1500	4.33

^aEstimated errors <10%. Anions used in this assay were in the form of their tetrabutylammonium salts. $-\Delta G_{298}^0$ is in kcal/mol

of host **1** for halide anions are much higher than those of host **2** (Table 9). This is a consequence of stronger (C–H)⁺ ··· X⁻ hydrogen bonds by more electron-deficient imidazolium moieties as well as more enhanced charge–dipole interaction by the NO₂ group.

In spite of the enhanced affinity for halide anions, the recognition of F⁻ was not accomplished through ionic H-bond with host **1**, because of the nucleophilic reaction of F⁻ on C(2) or the abstraction of the C(2)-hydrogen, thereby unable to observe the C(2)-proton peak upon addition of F⁻ on **1** in DMSO/CH₃CN. For the complex of host **2** and F⁻, ab initio calculations predicted that F⁻ forms shorter and more linear H-bond with host **2** than Cl⁻ or Br⁻, so that F⁻ shows higher binding energies both in the gas and polar solvent phases. In polar solvent with dielectric constant of acetonitrile ($\epsilon = 36.64$), the calculated binding energies of **2** with F⁻ and Cl⁻ decrease to only ~20 kcal/mol, while they are larger than 200 kcal/mol in the gas phase. This indicates that the cationic imidazolium receptor interacts with polar solvent so that its effective charges on C(2) diminish, and its ability of forming ionic H-bond with anions decreases. This trend is confirmed again in the experimental results in 1:1 mixture of DMSO- d_6 and acetonitrile- d_3 or DMSO- d_6 solvent. In these highly polar solvent, F⁻ interacts moderately with host **3**, while the butyl groups block the direct interaction of F⁻ with solvent molecules and reduce the microenvironmental polarity around the binding site.

Recently, by extending this approach, a receptor of anthracene derivative with two imidazolium moieties, which show selective binding affinity for H₂PO₄⁻ over other halide anions and anion-induced quenching of the fluorescence by the photo-induced electron-transfer (PET) mechanism was reported (Host **4a** in Fig. 16) [65]. However, further investigation shows that F⁻ forms 2:1 complex with receptor on each ionic H-bonding site. In addition to (C–H)⁺ ··· F⁻ bonding (1.63 Å), due to the high flexibility of the receptor site of host **4a**, the hydrogen atom connecting CH₂ between the anthracene and imidazolium moiety also interacts with F⁻ at a distance of 2.29 Å. On the other hand, host **4b** favors H₂PO₄⁻ over F⁻ in polar acetonitrile solvent. For both hosts **4a** and **4b**, their H₂PO₄⁻ ··· (H–C)⁺ distances

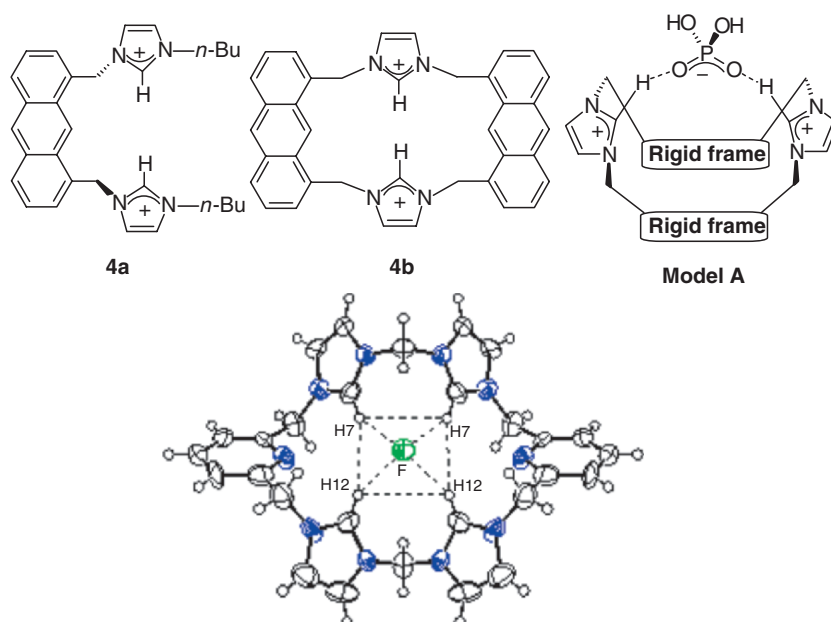


Figure 16. Molecular systems (model A: **4a**, **4b**) and calix[4]imidazolium[2]pyridine (**5**) designed for the recognition of H_2PO_4^- and F^- , respectively. (Reproduced by permission of American Chemical Society for 4a, 4b and Model A; Ref. [65(a),(b)], and WILEY-VCH Verlag GmbH & Co for 5; Ref. [65(c)].)

are almost same, and so are the $\text{F}^- \cdots (\text{H}-\text{C})^+$ distances (1.7 and 1.6 Å, respectively). In the case of host **4b**, however, the $\text{F}^- \cdots (\text{H}_2\text{C})$ interaction becomes negligible (>3 Å). Consequently, the greater rigidity of host **4b** enhances the binding selectivity toward H_2PO_4^- (Fig. 16). Very recently, we have also designed calix[4]imidazolium compound (**5** in Fig. 16), which selectively binds the F^- ion through the $\text{F}^- \cdots (\text{H}-\text{C})^+$ interaction thereby forming 1:1 stoichiometric complex [65c]. Unlike the fluoride anion, the chloride and bromide anions do not fit in the center of the cavity of **5** since they are larger and favor nonspherical or surface conformations in order to keep the extra electron in a large empty space. The density functional calculation on the conformation analysis and predicted binding affinities were in good agreement with the experiments.

10.3 H-Bond in Amphi-Ionophores

Cyclic polypeptides [69] can interact with both cations through C=O moieties and anions through N-H moieties (Fig. 17). In structures **6** and **7**, both carbonyl and amide groups are nearly on the same cylindrical surface, i.e., nearly parallel to the principal axis. Upon complexation with an ion, the cyclic peptides are found to have two types of binding: one at the center ($n\cdot\mathbf{I}$ where n

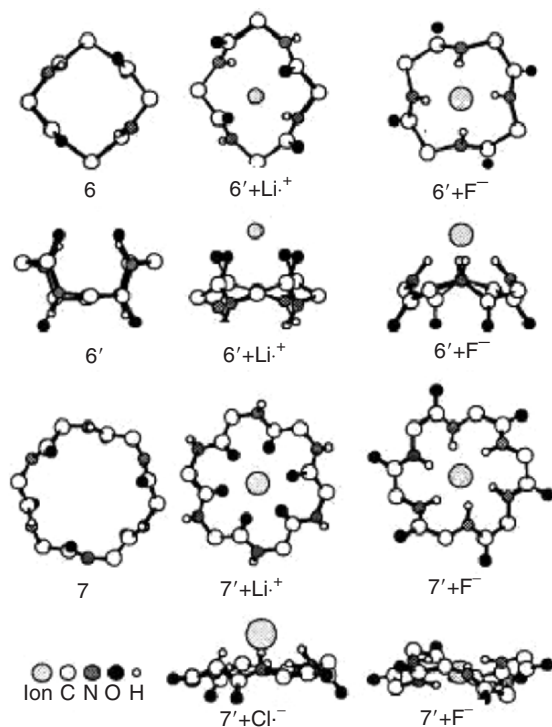


Figure 17. Selected structures of cyclic peptides (glycine) and their ion complexes. Reproduced by permission of American Chemical Society: Ref. [69(a)].

denotes cyclic peptides and **I** denotes an ion) and the other above the molecular plane ($n'\cdot\mathbf{I}$). In the presence of cation, carbonyl dipole moieties tend to point inward (toward the cation), while, in the presence of an anion, amide dipole moieties point inward, forming H-bond. The type of binding is decided by the size of ions and the cavity of cyclic peptides. If an ion is small and the cyclic peptides is sufficiently large, then $n\cdot\mathbf{I}$ type complex is formed. Otherwise, $n'\cdot\mathbf{I}$ type complexation is observed. When **7** binds with F^- , it prefers the $n\cdot\mathbf{I}$ type binding. In the case of Cl^- , however, the complex changes its geometry to $n'\cdot\mathbf{I}$. In $7'\cdot\text{Cl}^-$, the $\text{Cl}^- \cdots \text{H}$ distances are 2.57 Å for three H atoms and 2.68 Å for the remaining three H atoms with supplementary angle ϕ equal to 30° and 37° , respectively.

11 CONCLUDING REMARKS

The hydrogen atom, the most simplest and abundant atom in the universe, is involved in one of the most complex and flexible bonding in both chemical and biological systems, giving its special features including wide range inter-

action energies, cooperativity effect, proton exchange through the H-bonds, self-assembly of molecular tubes and layers, and multiply H-bonded frames in biological molecules. We have illustrated diverse H-bonding characteristics with the analysis of each energy component. Normally, the proton-accepting and proton-donating capability (electronegativity, electron affinity, ionization potential, acidity, and basicity) gives combinatorially strong H-bond interactions. The understanding of diverse H-bonds would be useful for the developments of various functional molecular systems. Indeed, utilizing the cooperative vs. competitive effect of H-bonds, we have been successful in designing various hydrogen-bonded ionophores, receptors, supramolecules, nanomaterials, and nanodevices [34, 70]. Therefore, we hope that the present review of the H-bonding would be useful for understanding the role of H-bonding in molecular and biomolecular systems.

ACKNOWLEDGMENTS

This research was supported by KOSEF(CRI) and partly by BK21.

REFERENCES

- (a) G. A. Jeffrey, and W. Saenger, *Hydrogen Bonding in Biological Structures*. Springer-Verlag (1991). (b) G. A. Jeffrey, *An Introduction to Hydrogen Bonding*, D. G. Truhlar, editor, Oxford University Press., Oxford (1997). (c) E. C. Hulme, editor, *Receptor-Ligand Interactions: A Practical Approach*, Oxford University Press, Oxford (1992).
- (a) D. A. Smith, editor, *Modeling the Hydrogen Bond in ACS symp. ser. 569*, American Chemical Society, New York (1994). (b) S. Scheiner, *Hydrogen Bonding. A Theoretical Perspective*, Oxford University Press, Oxford (1997). (c) G. R. Desiraju, and T. D. Steiner, *The Weak Hydrogen Bond: In Structural Chemistry and Biology (International Union of Crystallography Monographs on Crystallography, 9)*, Oxford University Press, Oxford (1999).
- (a) P. Tarakeshwar, and K. S. Kim, Nanorecognition. In: *Encyclopedia of Nanoscience and Nanotechnology*, H. S. Nalwa, editor, American Science Publishers, New York, **7**, 367–404 (2004). (b) F. P. Schmidtchen, and M. Berger, Artificial organic host molecules for anions, *Chem. Rev.* **97**, 1609–1646 (1997). (c) P. Tarakeshwar, H. S. Choi, and K. S. Kim, Olefinic vs. aromatic π -H interaction: a theoretical investigation of the nature of interaction of first-row hydrides with ethene and benzene, *J. Am. Chem. Soc.* **123**, 3323–3331 (2001). (d) F. Auer, D. W. Schubert, M. Stamm, T. Arnebrant, A. Swietlow, M. Zizlsperger, and B. Sellergren, Switchable assembly of stable, ordered molecular layers, *Chem. Eur. J.* **5**, 1150–1159 (1999). (e) H. G. Kim, C.-W. Lee, S. Yun, B. H. Hong, Y.-O. Kim, D. Kim, H. Ihm, J. W. Lee, E. C. Lee, P. Tarakeshwar, S.-M. Park, and K. S. Kim, An electrochemically controllable nanomechanical molecular system utilizing edge-to-face and face-to-face aromatic interactions, *Org. Lett.* **4**, 3971–3974 (2002). (f) G. Wulff, T. Gross, and R. Schonfeld, Enzyme models based on molecularly imprinted polymers with strong esterase activity, *Angew. Chem., Int. Ed.* **36**, 1962–1964 (1997). (g) A. P. Sukharevsky, I. Read, B. Linton, A. D. Hamilton, and D. H. Waldeck, Experimental measurements of low-frequency intermolecular host-guest dynamics, *J. Phys. Chem. B* **102**, 5394–5403 (1998).
- (a) B. H. Hong, J. Y. Lee, C.-W. Lee, J. C. Kim, S. C. Bae, and K. S. Kim, Self-assembled organic nanotube arrays with infinitely long one-dimensional H-bonds, *J. Am. Chem. Soc.* **123**, 10748–10749 (2001). (b) B. H. Hong, S. C. Bae, C.-W. Lee, S. Jeong, and K. S. Kim, Ultrathin

- single-crystalline silver nanowire arrays formed in an ambient solution phase, *Science* **294**, 348–351 (2001). (c) K. S. Kim, S. B. Suh, J. C. Kim, B. H. Hong, P. Tarakeshwar, J. Y. Lee, Y. Kim, S. Yun, E. C. Lee, H. J. Ihm, H. G. Kim, J. W. Lee, J. K. Kim, H. M. Lee, D. Kim, C. Cui, J. W. Lee, S. J. Youn, C. Y. Kim, H. Y. Chung, H. S. Choi, C.-W. Lee, S. J. Cho, S. Jeong, and J.-H. Cho, Assembling phenomena of calix[4]hydroquinone nanotube bundles by one-dimensional short hydrogen bonding and displaced π - π stacking, *J. Am. Chem. Soc.* **124**, 14268–14279 (2002). (d) S. B. Suh, B. H. Hong, P. Tarakeshwar, S. J. Youn, S. Jeong, and K. S. Kim, Electronic structure of silver subnanowires in self-assembled organic nanotubes: density functional calculations, *Phys. Rev. B* **67**, 241402(R) 1–4 (2003).
5. (a) R. Mittal, and A. Howard, Orientational defects on a hydrogen-bonded chain, *Phys. Rev. B* **53**, 14171–14187 (1996). (b) H. S. Mei, M. E. Tuckerman, D. E. Sagnella, and M. L. Klein, Quantum nuclear ab initio molecular dynamics study of water wires, *J. Phys. Chem. B* **102**, 10446–10458 (1998).
 6. (a) S. Yun, H. Ihm, H. G. Kim, C.-W. Lee, B. Indrajit, K. S. Oh, Y. J. Gong, J. W. Lee, J. Yoon, H. C. Lee, and K. S. Kim, Molecular recognition of fluoride anion: benzene-based tripodal imidazolium receptor, *J. Org. Chem.* **68**, 2467–2470 (2003). (b) H. Ihm, S. Yun, H. G. Kim, J. K. Kim, and K. S. Kim, Tripodal nitro-imidazolium receptor for anion binding driven by (C–H)⁺X[–] hydrogen bonds, *Org. Lett.* **4**, 2897–2900 (2002).
 7. (a) K. S. Kim, and E. Clementi, Energetics and hydration structures of a solvated gramicidin a transmembrane channel for K⁺ and Na⁺ cations, *J. Am. Chem. Soc.* **107**, 5504–5513 (1985). (b) H. S. Son, B. H. Hong, C.-W. Lee, S. Yun, and K. S. Kim, A new type of helix pattern in poly-alanine peptide, *J. Am. Chem. Soc.* **123**, 514–515 (2001).
 8. (a) P. A. Kollman, and L. C. Allen, Theory of the hydrogen bond, *Chem. Rev.* **72**, 283–303 (1972). (b) B. Chen, I. Alkorta, I. Rozas, and J. Elguero, Non-conventional hydrogen bonds, *Chem. Soc. Rev.* **27**, 163–170 (1998). (c) P. Hobza, and Z. Havlas, Blue-shifting hydrogen bonds, *Chem. Rev.* **100**, 4253–4264 (2000). (d) P. E. S. Wormer, and A. van der Avoird, Intermolecular potentials, internal motions, and spectra of van der Waals and hydrogen-bonded complexes, *Chem. Rev.* **100**, 4109–4144 (2000). (e) P. Tarakeshwar and K. S. Kim, Comparison of the nature of p and conventional H-bonds: a theoretical investigation, *J. Mol. Struct.* **615**, 227–228 (2002). (f) P. Tarakeshwar, H. M. Lee, and K. S. Kim, Insight into theoretical investigations of aqueous clusters in *Reviews of Modern Quantum Chemistry*, Vol. II, Sen, K. D., editor, World Scientific, Singapore, 1642–1683. (2002). (g) C. L. Perrin, and J. B. Nielson, “Strong” hydrogen bonds in chemistry and biology, *Annu. Rev. Phys. Chem.* **48**, 511–544 (1997). (h) M. Mautner, The ionic hydrogen bond, *Chem. Rev.* **105**, 213–284 (2005).
 9. K. S. Kim, P. Tarakeshwar, and J. Y. Lee, Molecular clusters of π -systems: theoretical studies of structures, spectra and origin of interaction energies, *Chem. Rev.* **100**, 4145–4185 (2000).
 10. (a) J. E. Carpenter, and F. Weinhold, Analysis of the geometry of the hydroxymethyl radical by the “different hybrids for different spins” natural bond orbital procedure, *J. Mol. Struct. (Theochem)* **169**, 41–62 (1988). (b) J. E. Carpenter, PhD thesis, University of Wisconsin, WI (1987). (c) J. P. Foster, and F. Weinhold, Natural hybrid orbitals, *J. Am. Chem. Soc.* **102**, 7211–7218 (1980). (d) A. E. Reed, and F. Weinhold, Natural bond orbital analysis of near-Hartree-Fock water dimer, *J. Chem. Phys.* **78**, 4066–4073 (1983). (e) A. E. Reed, R. B. Weinstock, and F. Weinhold, Natural population analysis, *J. Chem. Phys.* **83**, 735–746 (1985). (f) A. E. Reed, L. A. Curtiss, and F. Weinhold, Intermolecular interactions from a natural bond orbital, donor-acceptor viewpoint, *Chem. Rev.* **88**, 899–926 (1988).
 11. S. J. Lee, H. Y. Chung, and K. S. Kim, An easy-to-use three-dimensional molecular visualization and analysis program: POSMOL, *Bull. Korean. Chem. Soc.* **25**, 1061–1064 (2004).
 12. B. Jeziorski, R. Moszynski, A. Ratkiewicz, S. Rybak, K. Szalewicz, and H. L. Williams, *Methods and Techniques in Computational Chemistry: METECC-94, Medium Size Systems*, Vol. B, Clementi, E., editor, STEF, Cargliari (1993).
 13. (a) H. M. Lee, S. B. Suh, J. Y. Lee, P. Tarakeshwar, and K. S. Kim, Structures, energies, vibrational spectra, and electronic properties of water monomer to decamer, *J. Chem. Phys.*

- 112, 9759–9772 (2000); **114**, 3343 (2001). (b) H. M. Lee, S. B. Suh, and K. S. Kim, Structures, energies, and vibrational spectra of water undecamer and dodecamer: ab initio study, *J. Chem. Phys.* **114**, 10749–10756 (2001); **115**, 7331 (2002).
14. (a) K. S. Kim, M. Dupuis, G. C. Lie, and E. Clementi, Revisiting small clusters of water molecules, *Chem. Phys. Lett.* **131**, 451–456 (1986). (b) B. J. Mhin, H. S. Kim, H. S. Kim, J. W. Yoon, and K. S. Kim, Ab initio studies of the water hexamer: near degenerate structures, *Chem. Phys. Lett.* **176**, 41–45 (1991). (c) K. S. Kim, B. J. Mhin, U.-S. Choi, and K. Lee, Ab initio studies of the water dimer using large basis sets: the structure and thermodynamic energies, *J. Chem. Phys.* **97**, 6649–6662 (1992). (d) B. J. Mhin, S. J. Lee, and K. S. Kim, Water cluster distribution with respect to pressure and temperature in the gas phase, *Phys. Rev. A* **48**, 3764–3770 (1993). (e) B. J. Mhin, J. Kim, S. Lee, J. Y. Lee, and K. S. Kim, What is the global minimum energy structure of the water hexamer? Importance of nonadditive interactions, *J. Chem. Phys.* **100**, 4484–4486 (1994). (f) J. Kim, B. J. Mhin, S. J. Lee, and K. S. Kim, Entropy-driven structures of the water octamer, *Chem. Phys. Lett.* **219**, 243–246 (1994). (g) J. Kim, J. Y. Lee, S. Lee, B. J. Mhin, and K. S. Kim, Harmonic vibrational frequencies of the water monomer and dimer: comparison of various levels of ab initio theory, *J. Chem. Phys.* **102**, 310–317 (1995). (h) J. Kim and K. S. Kim, Structures, binding energies, and spectra of isoenergetic water hexamer clusters: extensive ab initio studies, *J. Chem. Phys.* **109**, 5886–5895 (1998). (i) J. Kim, D. Majumdar, H. M. Lee, and K. S. Kim, Structures and energetics of the water heptamer: comparison with the water hexamer and octamer, *J. Chem. Phys.* **110**, 9128–9134 (1999).
15. (a) C. Steinbach, P. Andersson, J. K. Kazimirski, U. Buck, V. Buch, and T. A. Beu, Infrared predissociation spectroscopy of large water clusters: a unique probe of cluster surfaces, *J. Phys. Chem. A* **108**, 6165–6174 (2004). (b) Y. Lilach, V. Buch, and M. Asscher, Formation and dynamics of water clusters on Ru(001), *J. Chem. Phys.* **119**, 11899–11905 (2003). (c) V. Buch, and J. P. Devlin, A new interpretation of the OH-stretch spectrum of ice, *J. Chem. Phys.* **110**, 3437–3443 (1999). (d) C. J. Burnham, and S. S. Xantheas, Development of transferable interaction models for water. I. Prominent features of the water dimer potential energy surface, *J. Chem. Phys.* **116**, 1479–1492 (2002). (e) S. S. Xantheas, M. A. Miller, B. E. Applegate, and R. E. Miller, The formation of cyclic water complexes by sequential ring insertion: experiment and theory, *J. Chem. Phys.* **117**, 1109–1122 (2002). (f) M. E. Fajardo, and S. Tam, Observation of the cyclic water hexamer in solid parahydrogen, *J. Chem. Phys.* **115**, 6807–6810 (2001).
16. (a) K. Liu, M. G. Brown, C. Carter, R. J. Saykally, J. K. Gregory, and D. C. Clary, Characterization of a cage form of the water hexamer, *Nature* **381**, 501–503 (1996). (b) F. Huisken, M. Kaloudis, and A. Kulcke, Infrared spectroscopy of small size-selected water clusters, *J. Chem. Phys.* **104**, 17–25 (1996). (c) J. B. Paul, C. P. Collier, J. J. Scherer, A. O’Keefe, and R. J. Saykally, Direct measurement of water cluster concentrations by infrared cavity ringdown laser absorption spectroscopy, *J. Phys. Chem. A* **101**, 5211–5214 (1997).
17. C. Steinbach, P. Andersson, M. Melzer, J. K. Kazimirski, U. Buck, and V. Buch, Detection of the book isomer from the OH-stretch spectroscopy of size selected water hexamers, *Phys. Chem. Chem. Phys.* **6**, 3320–3324 (2004).
18. K. Nauta and R. E. Miller, Formation of cyclic water hexamer in liquid helium: the smallest piece of ice, *Science* **287**, 293–295 (2000).
19. (a) S. Odde, B. J. Mhin, S. Lee, H. M. Lee, and K. S. Kim, Dissociation chemistry of hydrogen halides in water, *J. Chem. Phys.* **120**, 9524–9535 (2004). (b) S. Re. Y. Osamura, Y. Suzuki, and H. F. Schaefer III, Structures and stability of hydrated clusters of hydrogen chloride, $\text{HCl}(\text{H}_2\text{O})_n$, $n = 1–5$, *J. Chem. Phys.* **109**, 973–977 (1998). (c) E. M. Cabaleiro-Lago, J. M. Hermida-Ramon, and J. Rodriguez-Otero, Computational study of the dissociation of H–X acids ($X = \text{F}, \text{Cl}, \text{Br}, \text{I}$) in water clusters, *J. Chem. Phys.* **117**, 3160–3168 (2002).
20. (a) A. T. Blades, P. Jayaweera, M. G. Ikononou, and P. Kebarle, Studies of alkaline earth and transition metal M^{++} gas phase ion chemistry, *J. Chem. Phys.* **92**, 5900–5906 (1990).

- (b) L. Perera, and M. L. Berkowitz, Stabilization energies of Cl^- , Br^- , and I^- ions in water clusters, *J. Chem. Phys.* **99**, 4222–4224 (1993); **100**, 3085–3093 (1994). (c) M. Roeselova, G. Jacoby, U. Kaldor, and P. Jungwirth, Relaxation of chlorine anions solvated in small water clusters upon electron photodetachment: the three lowest potential energy surfaces of the neutral $\text{Cl} \cdot \text{H}_2\text{O}$ complex, *Chem. Phys. Lett.* **293**, 309–316 (1998). (d) J. Baik, J. Kim, D. Majumdar, and K. S. Kim, Structures, energetics, and spectra of fluoride–water clusters $\text{F}^-(\text{H}_2\text{O})_n$, $n = 1-6$: ab initio study, *J. Chem. Phys.* **110**, 9116–9127 (1999). (e) D. Majumdar, J. Kim, and K. S. Kim, Charge transfer to solvent (CTTS) energies of small $\text{X}^-(\text{H}_2\text{O})_{n=1-4}$ ($\text{X} = \text{F}, \text{Cl}, \text{Br}, \text{I}$) clusters: ab initio study, *J. Chem. Phys.* **112**, 101–105 (2000). (f) J. Kim, H. M. Lee, S. B. Suh, D. Majumdar, and K. S. Kim, Comparative ab initio study of the structures, energetics and spectra of $\text{X}^-(\text{H}_2\text{O})_{n=1-4}$ [$\text{X} = \text{F}, \text{Cl}, \text{Br}, \text{I}$] clusters, *J. Chem. Phys.* **113**, 5259–5272 (2000). (g) H. M. Lee, and K. S. Kim, Structures and spectra of iodide–water clusters $\text{I}^-(\text{H}_2\text{O})_n$, $n = 1-6$: ab initio study, *J. Chem. Phys.* **114**, 4461–4471 (2001). (h) M. Masamura, Structures, energetics, and spectra of $\text{OH}^-(\text{H}_2\text{O})_n$ and $\text{SH}^-(\text{H}_2\text{O})_n$ clusters, $n = 1-5$: ab initio study, *J. Chem. Phys.* **117**, 5257–5263 (2002). (i) H. M. Lee, D. Kim, and K. S. Kim, Structures, spectra, and electronic properties of halide–water pentamers and hexamer, $\text{X}^-(\text{H}_2\text{O})_{5,6}$ ($\text{X} = \text{F}, \text{Cl}, \text{Br}, \text{I}$): ab initio study, *J. Chem. Phys.* **116**, 5509–5520 (2002). (j) F. Vila, and K. D. Jordan, Theoretical study of the dipole-bound excited states of $\text{I}^-(\text{H}_2\text{O})_4$, *J. Phys. Chem. A* **106**, 1391–1397 (2002). (k) S. Odde, C. Pak, H. M. Lee and K. S. Kim, Aqua dissociation nature of cesium hydroxide, *J. Chem. Phys.* **121**, 204–208 (2004). (l) N. Grishina, and V. Buch, Structure and dynamics of orientational defects in ice I, *J. Chem. Phys.* **120**, 5217–5225 (2004). (m) H. M. Lee, S. B. Suh, P. Tarakeshwar, and K. S. Kim, Origin of the magic numbers of water clusters with an excess electron, *J. Chem. Phys.* **122**, 044309-1-6 (2005).
21. (a) H. M. Lee, P. Tarakeshwar, J. Park, M. R. Kolaski, Y. J. Yoon, H. Yi, W. Y. Kim, and K. S. Kim, Insights into the structures, energetics, and vibrations of monovalent cation–(water) $_{1-6}$ clusters, *J. Phys. Chem. A* **108**, 02949–02958 (2004). (b) J. Kim, S. Lee, S. J. Cho, B. J. Mhin, and K. S. Kim, Structures, energetics, and spectra of aqua-sodium(I): thermodynamic effects and nonadditive interactions, *J. Chem. Phys.* **102**, 839–849 (1995). (c) H. M. Lee, S. K. Min, E. C. Lee, J. H. Min, S. Odde, and K. S. Kim, Hydrated copper and gold monovalent cations: ab initio study, *J. Chem. Phys.* **122**, 064314-1-10 (2005).
22. (a) Y.-S. Wang, H.-C. Chang, J.-C. Jiang, S. H. Lin, Y. T. Lee, and H.-C. Chang, Structures and isomeric transitions of $\text{NH}_4^+(\text{H}_2\text{O})_{3-6}$: from single to double rings, *J. Am. Chem. Soc.* **120**, 8777–8788 (1998). (b) J.-C. Jiang, Y.-S. Wang, H.-C. Chang, S. H. Lin, Y. T. Lee, G. Niedner-Schatteburg, and H.-C. Chang, Infrared spectra of $\text{H}^+(\text{H}_2\text{O})_{5-8}$ clusters: evidence for symmetric proton hydration, *J. Am. Chem. Soc.* **122**, 1398–1410 (2000).
23. (a) C. Pak, H. M. Lee, J. C. Kim, D. Kim, and K. S. Kim, Theoretical investigation of normal to strong hydrogen bonds, *Struct. Chem.* **16**, 187–202 (2005). (b) M. H. Abraham, P. P. Duce, and D. V. Prior, Hydrogen bonding. Part 9. Solute proton donor and proton acceptor scales for use in drug design, *J. Chem. Soc. Perkin Trans. II* 1355–1375 (1989). (c) M. H. Abraham, Scales of solute hydrogen-bonding: their construction and application to physicochemical and biochemical processes, *Chem. Soc. Rev.* **22**, 73–83 (1993).
24. I. Bandyopadhyay, H. M. Lee, and K. S. Kim, Phenol vs. water molecule interacting with various molecules: σ -type, π -type, and χ -type hydrogen bonds, interaction energies and their energy components, *J. Phys. Chem. A* **109**, 1720–1728 (2005).
25. (a) P. Hobza, V. Sopirko, Z. Havlas, K. Buchhold, B. Reinmann, H.-D. Barth, and B. Brutschy, Anti-hydrogen bond between chloroform and fluorobenzene, *Chem. Phys. Lett.* **299**, 180–186 (1999). (b) P. Hobza, C. Riehn, A. Weicherit, and B. Brutschy, Structure and binding energy of the phenol dimer: correlated ab initio calculations compared with results from rotational coherent spectroscopy, *Chem. Phys.* **283**, 331–339 (2002). (c) J.-W. Shin, N. I. Hammer, E. G. Diken, M. A. Johnson, R. S. Walters, T. D. Jaeger, M. A. Duncan, R. A. Christie, and K. D. Jordan, Infrared signature of structures associated with the $\text{H}^+(\text{H}_2\text{O})_n$ ($n = 6$ to 27) clusters, *Science* **304**, 1137–1140 (2004). (d) M. Miyazaki, A. Fujii, T. Ebata, and

- N. Mikami, Infrared spectroscopic evidence for protonated water clusters forming nanoscale cages, *Science* **304**, 1134–1137 (2004). (e) S. B. Suh, H. M. Lee, J. Kim, J. Y. Lee, and K. S. Kim, Vibrational spectra and electron detachment energy of the anionic water hexamer, *J. Chem. Phys.* **113**, 5273–5277 (2000). (f) R. Wu, and B. Brutschy, Study on the structure and intra- and intermolecular hydrogen bonding of 2-methoxyphenol-(H₂O)_n (*n* = 1,2), *Chem. Phys. Lett.* **390**, 272–278 (2004).
26. (a) M. Sodupe, A. Oliva, and J. Bertran, Theoretical study of the ionization of phenol–water and phenol–ammonia hydrogen-bonded complexes, *J. Phys. Chem. A* **101**, 9142–9151 (1997). (b) A. Schiefke, C. Deussen, C. Jacoby, M. Gerhards, M. Schmitt, K. Kleinermanns, and P. Hering, Structure and vibrations of the phenol–ammonia cluster, *J. Chem. Phys.* **102**, 9197–9204 (1995). (c) S. Tanabe, T. Ebata, M. Fujii, and N. Mikami, OH stretching vibrations of phenol-(H₂O)_n (*n* = 1–3) complexes observed by IR-UV double-resonance spectroscopy, *Chem. Phys. Lett.* **215**, 347–352 (1993). (d) D. Michalska, W. Zierkiewicz, D. C. Bien'ko, W. Wojciechowski, and T. Zeegers-Huyskens, “Troublesome” vibrations of aromatic molecules in second-order Moller–Plesset and density functional theory calculations: infrared spectra of phenol and phenol-OD revisited, *J. Phys. Chem. A* **105**, 8734–8739 (2001).
27. (a) M. Schmitt, H. Muller, U. Henrichs, M. Gerhards, W. Perl, C. Deussen, and K. Kleinermanns, Structure and vibrations of phenol–CH₃OH(CD₃OD) in the electronic ground and excited state, revealed by spectral hole burning and dispersed fluorescence spectroscopy, *J. Chem. Phys.* **103**, 584–594 (1995). (b) M. Schmitt, J. Kupper, D. Spangenberg, and A. Westphal, Determination of the structures and barriers to hindered internal rotation of the phenol–methanol cluster in the S₀ and S₁ states, *Chem. Phys.* **254**, 349–361 (2000). (c) K. Muller-Dethlefs, Applications of ZEKE spectroscopy, *J. Electron Spectrosc. Relat. Phenom.* **75**, 35–46 (1995). (d) J. Kupper, A. Westphal, and M. Schmitt, The structure of the binary phenol–methanol cluster: a comparison of experiment and ab initio theory, *Chem. Phys.* **263**, 41–53 (2001).
28. (a) S. K. Burley, and G. A. Petsko, Aromatic–aromatic interaction: a mechanism of protein structure stabilization, *Science* **229**, 23–28 (1985). (b) S. K. Burley, and G. A. Petsko, Weakly polar interactions in proteins, *Adv. Protein Chem.* **39**, 125–189 (1988). (c) S. K. Burley, and G. A. Petsko, Electrostatic interactions in aromatic oligopeptides contribute to protein stability, *Trends Biotechnol.* **7**, 354–359 (1989).
29. (a) K. O. Bornsen, H. L. Selzle, and E. W. Schlag, Spectra of isotopically mixed benzene dimers: details on the interaction in the vdW bond, *J. Chem. Phys.* **85**, 1726–1732 (1986). (b) P. Hobza, H. L. Selzle, and E. W. Schlag, Floppy structure of the benzene dimer: ab initio calculation on the structure and dipole moment, *J. Chem. Phys.* **93**, 5893–5897 (1990).
30. (a) C. A. Hunter, and J. K. M. Sanders, The nature of pi–pi interactions, *J. Am. Chem. Soc.* **112**, 5525–5534 (1990). (b) C. A. Hunter, Arene–arene interactions: electrostatic or charge transfer? *Angew. Chem., Int. Ed.* **32**, 1584–1586 (1993). (c) C. A. Hunter, Meldola Lecture. The role of aromatic interactions in molecular recognition, *Chem. Soc. Rev.* **23**, 101–109 (1994). (d) F. J. Carver, C. A. Hunter, D. J. Livingstone, J. F. McCabe, and E. M. Seward, Substituent effects on edge-to-face aromatic interactions, *Chem. Eur. J.* **8**, 2848–2859 (2002).
31. F. Cozzi, M. Cinquini, R. Annunziata, T. Dwyer, and T. S. Siegel, Polar/pi interactions between stacked aryls in 1,8-diarylnaphthalenes, *J. Am. Chem. Soc.* **114**, 5729–5733 (1992).
32. (a) S. Paliwal, S. Geib, and C. S. Wilcox, Molecular torsion balance for weak molecular recognition forces. Effect of “tilted-T” edge-to-face aromatic interactions on conformational selection and solid-state structure, *J. Am. Chem. Soc.* **116**, 4497–4498 (1994). (b) E. Kim, S. Paliwal, and C. S. Wilcox, Measurements of molecular electrostatic field effects in edge-to-face aromatic interactions and CH–π interactions with implications for protein folding and molecular recognition, *J. Am. Chem. Soc.* **120**, 11192–11193 (1998).
33. (a) K. D. Schladetzky, T. S. Haque, and S. H. Gellman, Structural characterization of thioclophanes that promote edge-to-face aromatic–aromatic geometries, *J. Org. Chem.* **60**, 4108–4113 (1995). (b) S. H. Gellman, introduction: molecular recognition, *Chem. Rev.* **97**, 1231–1232

- (1997). (c) C.-Y. Kim, P. P. Chabdra, A. Jain, and D. W. Christanson, Fluoroaromatic–fluoroaromatic interactions between inhibitors bound in the crystal lattice of human carbonic anhydrase II, *J. Am. Chem. Soc.* **123**, 9620–9627 (2001). (d) H. Lee, C. B. Knobler, and M. F. Hawthorne, A Hydrogen-bonded [(mercuracarborand-water)₂-benzene] π -sandwich complex, *Angew. Chem., Int. Ed.* **40**, 3058–3060 (2001). (e) E. A. Meyer, R. K. Castellano, and F. Diederich, Interactions with aromatic rings in chemical and biological recognition, *Angew. Chem., Int. Ed.* **42**, 1210–1250 (2003).
34. (a) K. S. Kim, P. Tarakeshwar, and H. M. Lee, De novo theoretical design of functional nanomaterials and molecular devices. In: *Dekker Encyclopedia of Nanoscience and Nanotechnology*, Schwarz, J. A., Contescu, C., Putyera, K., editors, Marcel Dekker, NY, **3**, 2423–2433 (2004). (b) P. Tarakeshwar, D. Kim, H. M. Lee, S. B. Suh, and K. S. Kim, Theoretical approaches to the design of functional nanomaterials. In: *Computational Materials Science*, Leszczynski, J., editor, *Theoretical and Computational Chemistry Series*, Elsevier, Amsterdam, **15**, 119–170 (2004).
35. K. S. Kim, P. Tarakeshwar, and H. M. Lee. In: *Theory and Applications of Computational Chemistry: the First 40 Years, a Volume of Technical and Historical Perspectives*, Dykstra, C. E., Frenking, G., Kim, K.S., Scuseria G., editors, Elsevier Publishers, Amsterdam (2005).
36. (a) T. Ren, Y. Jin, K. S. Kim, and D. H. Kim, Aromatic–aromatic ring interaction revisited with model compounds of wilcox, *J. Biomol. Struct. Dyn.* **15**, 401–405 (1997). (b) B. H. Hong, J. Y. Lee, S. J. Cho, S. Yun, and K. S. Kim, Theoretical study of the conformations and strain energies of $[n, n]$ metaparacyclophanes: indication of stable edge-to-face and displaced face-to-face conformers for $n = 4$, *J. Org. Chem.* **64**, 5661–5665 (1999). (c) K. S. Kim, P. Tarakeshwar, and J. Y. Lee, Olefinic vs aromatic π -H interaction: a theoretical investigation of the nature of interaction of first-row hydrides with ethene and benzene, *J. Am. Chem. Soc.* **123**, 3323–3331 (2001).
37. (a) W. L. Jorgensen, and D. L. Severance, Aromatic–aromatic interactions: free energy profiles for the benzene dimer in water, chloroform, and liquid benzene, *J. Am. Chem. Soc.* **112**, 4768–4774 (1990). (b) D. Heidrich, Do isopropyl and tert-butyl cations form π complexes with benzene? *Angew. Chem., Int. Ed.* **41**, 3208–3210 (2002).
38. (a) P. Hobza, and J. Sponer, Toward true DNA base-stacking energies: MP2, CCSD(t), and complete basis set calculations, *J. Am. Chem. Soc.* **124**, 11802–11808 (2002). (b) P. Hobza, H. L. Selzle, and E. W. Schlag, Potential energy surface for the benzene dimer. Results of ab initio CCSD(T) calculations show two nearly isoenergetic structures: T-shaped and parallel-displaced, *J. Phys. Chem.* **100**, 18790–18794 (1996). (c) P. Hobza, H. L. Selzle, and E. W. Schlag, Potential energy surface of the benzene dimer: ab initio theoretical study, *J. Am. Chem. Soc.* **116**, 3500–3506 (1994). (d) P. Hobza, H. L. Selzle, and E. W. Schlag, Structure and properties of benzene-containing molecular clusters: nonempirical ab initio calculations and experiments, *Chem. Rev.* **94**, 1767–1785 (1994).
39. (a) S. V. Lindeman, D. Kosynkin, and J. K. Kochi, Unusually Short (C–H... π) hydrogen bonds for effective supramolecular (aromatic/aromatic) organization in edge-to-face motifs, *J. Am. Chem. Soc.* **120**, 13268–13269 (1998). (b) B. Brutschy, The structure of microsolvated benzene derivatives and the role of aromatic substituents, *Chem. Rev.* **100**, 3891–3920 (2000). (c) S. Tsuzuki, K. Honda, T. Uchimaru, M. Mikami, and K. Tanabe, Origin of attraction and directionality of the π/π interaction: model chemistry calculations of benzene dimer interaction, *J. Am. Chem. Soc.* **124**, 104–112 (2002). (d) Y. Wang, and X. Hu, A quantum chemistry study of binding carotenoids in the bacterial light-harvesting complexes, *J. Am. Chem. Soc.* **124**, 8445–8451 (2002). (e) S. Scheiner, T. Kar, and J. Pattanayak, Comparison of various types of hydrogen bonds involving aromatic amino acids, *J. Am. Chem. Soc.* **124**, 13257–13264 (2002).
40. (a) M. S. Sinnokrot, E. F. Valeev, and C. D. Sherrill, Estimates of the ab initio limit for π – π interactions: the benzene dimer, *J. Am. Chem. Soc.* **124**, 10887–10893 (2002). (b) M. S. Sinnokrot, and C. D. Sherrill, Unexpected substituent effects in face-to-face π -stacking interactions, *J. Phys. Chem. A* **107**, 8377–8379 (2003).

41. (a) H. G. Kim, C.-W. Lee, S. Yun, B. H. Hong, Y.-O. Kim, D. Kim, H. Ihm, J. W. Lee, E. C. Lee, P. Tarakeshwar, S.-M. Park, and K. S. Kim, An electrochemically controllable nanomechanical molecular system utilizing edge-to-face and face-to-face aromatic interactions, *Org. Lett.* **4**, 3971–3974 (2002). (b) T. K. Manojkumar, H. S. Choi, B. H. Hong, P. Tarakeshwar, and K. S. Kim, *p*-benzoquinone–benzene clusters as potential nanomechanical devices: a theoretical study, *J. Chem. Phys.* **121**, 841–846 (2004).
42. E. C. Lee, B. H. Hong, J. Y. Lee, J. C. Kim, D. Kim, Y. Kim, P. Tarakeshwar, and K. S. Kim, Substituent effects on the edge-to-face aromatic interactions, *J. Am. Chem. Soc.*, **127**, 4530–4537 (2005).
43. (a) L. P. Hammett, Some relations between reaction rates and equilibrium constants, *Chem. Rev.* **17**, 125–136 (1935). (b) S. H. Pines, *Organic Chemistry*, McGraw-Hill, New York (1987). (c) T. W. G. Solomons, editor, *Organic Chemistry*, Wiley, New York (1996).
44. B. J. Howard, T. R. Dyke, and W. Klemperer, The molecular beam spectrum and the structure of the hydrogen fluoride dimer, *J. Chem. Phys.* **81**, 5417–5425 (1984).
45. R. C. Guedes, P. C. D. Couto, and B. J. Cabral, Binding energy, structure, and vibrational spectra of (HCl)_{2–6} and (HF)_{2–10} clusters by density functional theory, *J. Chem. Phys.* **118**, 1272–1281 (2003).
46. L. Rincon, R. Almeida, D. Garcia-Aldea, and H. D. Riega, Hydrogen bond cooperativity and electron delocalization in hydrogen fluoride clusters, *J. Chem. Phys.* **114**, 5552–5561 (2001).
47. (a) A. K. Soper, F. Bruni, and M. A. Ricci, Site–site pair correlation functions of water from 25 to 400°C: revised analysis of new and old diffraction data, *J. Chem. Phys.* **106**, 247–254 (1997). (b) S. W. Peterson, and H. A. Levy, A single-crystal neutron diffraction study of heavy ice, *Acta Crystallogr.* **10**, 70–76 (1957).
48. (a) S. Suhai, Cooperative effects in hydrogen bonding: fourth-order many-body perturbation theory studies of water oligomers and of an infinite water chain as a model for ice, *J. Chem. Phys.* **101**, 9766–9782 (1994). (b) S. Suhai, Density functional studies of the hydrogen-bonded network in an infinite water polymer, *J. Phys. Chem.* **99**, 1172–1181 (1995).
49. (a) K. Hermansson, and M. Alfredsson, Molecular polarization in water chains, *J. Chem. Phys.* **111**, 1993–2000 (1999). (b) L. Ojamae, and K. Hermansson, Ab initio study of cooperativity in water chains: binding energies and anharmonic frequencies, *J. Phys. Chem.* **98**, 4271–4282 (1994).
50. M. Masella, and J. P. Flament, Relation between cooperative effects in cyclic water, methanol/water, and methanol trimers and hydrogen bonds in methanol/water, ethanol/water, and dimethylether/water heterodimers, *J. Chem. Phys.* **108**, 7141–7151 (1998).
51. M. C. Etter, Z. Urbanczyk-Lipkowska, D. A. Jahn, and J. Frye, Solid-state structural characterization of 1,3-cyclohexanedione and of a 6:1 cyclohexanedione-benzene cyclamer complex, a novel host–guest species, *J. Am. Chem. Soc.* **108**, 5871–5876 (1986).
52. (a) J. J. Dannenberg, Cooperativity in hydrogen bonded aggregates. Models for crystals and peptides, *J. Mol. Struct.* **615**, 219–226 (2002). (b) S. Simon, M. Duran, and J. J. Dannenberg, Effect of basis set superposition error on the water dimer surface calculated at Hartree–Fock, Møller–Plesset, and density functional theory levels, *J. Phys. Chem. A* **103**, 1640–1643 (1999). (c) A. Masunov, and J. J. Dannenberg, Theoretical study of urea and thiourea. 2. chains and ribbons, *J. Phys. Chem. B* **104**, 806–810 (2000). (d) J. J. Dannenberg, L. Haskamp and A. Masunov, Are hydrogen bonds covalent or electrostatic? A molecular orbital comparison of molecules in electric fields and h-bonding environments, *J. Phys. Chem. A* **103**, 7083–7086 (1999).
53. Y.-L. Zhao and Y.-D. Wu, A theoretical study of β -sheet models: is the formation of hydrogen-bond networks cooperative? *J. Am. Chem. Soc.* **124**, 1570–1571 (2002).
54. S. B. Suh, J. C. Kim, Y. C. Choi, S. Yun, and K. S. Kim, Nature of one-dimensional short hydrogen bonding: bond distances, bond energies, and solvent effects, *J. Am. Chem. Soc.* **126**, 2186–2193 (2004).

55. (a) Y. Wang, and J. P. Perdew, Spin scaling of the electron–gas correlation energy in the high-density limit, *Phys. Rev. B* **43**, 8911–8916 (1991). (b) J. P. Perdew, and Y. Wang, Accurate and simple analytic representation of the electron–gas correlation energy, *Phys. Rev. B* **45**, 13244–13249 (1992).
56. D. Vanderbilt, Soft self-consistent pseudopotentials in a generalized eigenvalue formalism, *Phys. Rev. B* **41**, 7892–7895 (1990).
57. (a) K. S. Kim, K. S. Oh, and J. Y. Lee, Catalytic role of enzymes: short strong H-bond-induced partial proton shuttles and charge redistributions, *Proc. Natl. Acad. Sci. U.S.A.* **97**, 6373–6378 (2000). (b) K. S. Oh, S.-S. Cha, D.-H. Kim, H.-S. Cho, N.-C. Ha, G. Choi, J. Y. Lee, P. Tarakeshwar, H. S. Son, K. Y. Choi, B.-H. Oh, and K. S. Kim, Role of catalytic residues in enzymatic mechanisms of homologous ketosteroid isomerases, *Biochemistry* **39**, 13891–13896 (2000). (c) K. S. Kim, D. Kim, J. Y. Lee, P. Tarakeshwar, and K. S. Oh, Catalytic mechanism of enzymes: preorganization, short strong hydrogen bond, and charge buffering, *Biochemistry* **41**, 5300–5306 (2002). (d) H.-S. Cho, N.-C. Ha, G. Choi, H.-J. Kim, D. Lee, K. S. Oh, K. S. Kim, W. Lee, K. Y. Choi, and B.-H. Oh, Crystal structure of delta Δ^5 -3-ketosteroid isomerase from *Pseudomonas testosteroni* in complex with equilenin settles the correct hydrogen bonding scheme for transition state stabilization, *J. Biol. Chem.* **274**, 32863–32868 (1999). (e) T. K. Manojkumar, C. Cui, and K. S. Kim, Theoretical insights into the mechanism of acetylcholinesterase-catalyzed acylation of acetylcholine, *J. Comput. Chem.* **26**, 606–611 (2005).
58. (a) W. W. Cleland, and M. M. Kreevoy, Low-barrier hydrogen bonds and enzymic catalysis, *Science* **264**, 1887–1890 (1994). (b) P. A. Frey, S. A. Whitt, and J. B. Tobin, A low-barrier hydrogen bond in the catalytic triad of serine proteases, *Science* **264**, 1927–1930 (1994).
59. (a) Z. R. Wu, S. Ebrahimian, M. E. Zawrotny, L. D. Thornburg, G. C. Perez-Alvarado, P. Brothers, R. M. Pollack, and M. F. Summers, Solution structure of 3-oxo-delta5-steroid isomerase, *Science* **276**, 415–418 (1997). (b) A. Warshell, and A. Parazyan, Energy considerations show that low-barrier hydrogen bonds do not offer a catalytic advantage over ordinary hydrogen bonds, *Proc. Natl. Acad. Sci. U.S.A.* **93**, 13665–13670 (1996).
60. (a) S. W. Kim, S.-S. Cha, H.-S. Cho, J.-S. Kim, N.-C. Ha, M.-J. Cho, S. Joo, K.-K. Kim, K. Y. Choi, and B.-H. Oh, High-resolution crystal structures of Δ^5 -3-ketosteroid isomerase with and without a reaction intermediate analogue, crystal structure and enzyme mechanism of 5-3-ketosteroid isomerase from *Pseudomonas testosteroni*, *Biochemistry* **36**, 14030–14036 (1997). (b) H.-S. Cho, G. Choi, K. Y. Choi, and B.-H. Oh, Crystal structure and enzyme mechanism of Δ^5 -3-ketosteroid isomerase from *Pseudomonas testosteroni*, *Biochemistry* **37**, 8325–8330 (1998).
61. (a) Q. Zhao, C. Abeygunawardana, P. Talalay, and A. S. Mildvan, NMR evidence for the participation of a low-barrier hydrogen bond in the mechanism of Δ^5 -3-ketosteroid isomerase, *Proc. Natl. Acad. Sci. U.S.A.* **93**, 8220–8224 (1996). (b) Y. K. Li, A. Kuliopulos, A. S. Mildvan, and P. Talalay, Environments and mechanistic roles of the tyrosine residues of Delta.5-3-ketosteroid isomerase, *Biochemistry* **32**, 1816–1824 (1993). (c) I. P. Petrounia, and R. M. Pollack, Substituent effects on the binding of phenols to the D38N mutant of 3-oxo- Δ^5 -steroid isomerase. A probe for the nature of hydrogen bonding to the intermediate, *Biochemistry* **37**, 700–705 (1998).
62. (a) J. Y. Kwon, N. J. Singh, H. N. Kim, S. K. Kim, K. S. Kim, and J. Y. Yoon, Fluorescent GTP-sensing in aqueous solution of physiological pH, *J. Am. Chem. Soc.* **126**, 8892–8893 (2004). (b) S. Yun, Y.-O. Kim, D. Kim, H. G. Kim, H. Ihm, J. K. Kim, C.-W. Lee, W. J. Lee, J. Yoon, K. S. Oh, J. Yoon, S.-M. Park, and K. S. Kim, Rational design of biologically important chemosensors: a novel receptor for selective recognition of acetylcholine over ammonium cations, *Org. Lett.* **5**, 471–474 (2003). (c) T. K. Manojkumar, D. Kim, and K. S. Kim, Theoretical studies on hydroquinone-benzene clusters, *J. Chem. Phys.* **122**, 014305–5 (2005). (d) E. C. Lee, B. H. Hong, J. Y. Lee, J. C. Kim, D. Kim, Y. Kim, P. Tarakeshwar, and K. S. Kim, Substituent effects on the edge-to-face aromatic interactions, *J. Am. Chem. Soc.* **127**, 4530–4537 (2005).

63. (a) K. S. Oh, C.-W. Lee, H. S. Choi, S. J. Lee, and K. S. Kim, Origin of the high affinity and selectivity of novel receptors for NH_4^+ over K^+ : charged hydrogen bonds vs cation- π interaction, *Org. Lett.* **2**, 2679–2681 (2000). (b) P. Buhlmann, E. Pretsch, and E. Bakker, Carrier-based ion-selective electrodes and bulk optodes. 2. Ionophores for potentiometric and optical sensors, *Chem. Rev.* **98**, 1593–1688 (1998).
64. (a) T. Mizuno, W.-H. Wei, L. R. Eller, and J. L. Sessler, Phenanthroline complexes bearing fused dipyrrolylquinoxaline anion recognition sites: efficient fluoride anion receptors, *J. Am. Chem. Soc.* **124**, 1134–1135 (2002). (b) S. Yamaguchi, S. Akiyama, and K. Tamao, Colorimetric fluoride ion sensing by boron-containing π -electron systems, *J. Am. Chem. Soc.* **123**, 11372–11375 (2001). (c) P. Jr. Anzenbacher, K. Jursiková, V. M. Lynch, P. A. Gale, and J. L. Sessler, Calix[4]pyrroles containing deep cavities and fixed walls. Synthesis, structural studies, and anion binding properties of the isomeric products derived from the condensation of p-hydroxyacetophenone and pyrrole, *J. Am. Chem. Soc.* **121**, 11020–11021 (1999). (d) S. C. McCleskey, M. J. Griffin, S. E. Schneider, J. T. McDevitt, and E. V. Anslyn, Differential receptors create patterns diagnostic for ATP and GTP, *J. Am. Chem. Soc.* **125**, 1114–1115 (2003). (e) L. Baldini, A. J. Wilson, J. Hong, and A. D. Hamilton, Pattern-based detection of different proteins using an array of fluorescent protein surface receptors, *J. Am. Chem. Soc.* **126**, 5656–5657 (2004). (f) C. Schmuck, and L. Geiger, Dipeptide binding in water by a de novo designed guanidino-carbonylpyrrole receptor, *J. Am. Chem. Soc.* **126**, 8898–8899 (2004).
65. (a) S. K. Kim, N. J. Singh, S. J. Kim, H. G. Kim, J. K. Kim, J. W. Lee, K. S. Kim, and J. Yoon, New fluorescent photoinduced electron transfer chemosensor for the recognition of H_2PO_4^- , *Org. Lett.* **5**, 2083–2086 (2003). (b) J. Yoon, S. K. Kim, N. J. Singh, J. W. Lee, Y. J. Yang, K. Chellappan, and K. S. Kim, Highly effective fluorescent sensor for H_2PO_4^- , *J. Org. Chem.* **69**, 581–583 (2004). (c) K. Chellappan, N. J. Singh, I.-C. Hwang, J. W. Lee, and K. S. Kim, A calix[4]imidazolium[2]pyridine as an anion receptor, *Angew. Chem., Int. Ed.* **44**, 2899–2903 (2005); *Angew. Chem.* **117**, 2959–2963 (2005). (d) J. Yoon, S. K. Kim, N. J. Singh, and K. S. Kim, Imidazolium Receptors for the Recognition of Anions, *Chem. Soc. Rev.* **35**, 355–360 (2006).
66. (a) H. S. Choi, S. B. Suh, S. J. Cho, and K. S. Kim, Ionophores and receptors using cation- π interactions: collarenes. *Proc. Natl. Acad. Sci. U.S.A.* **95**, 12094–12099 (1998). (b) C. Chipot, B. Maigret, D. A. Pearlman, and P. A. Kollman, Molecular dynamics potential of mean force calculations: a study of the toluene-ammonium π -cation interactions, *J. Am. Chem. Soc.* **118**, 2998–3005 (1996). (c) J. W. Caldwell, and P. A. Kollman, Cation- π interactions: nonadditive effects are critical in their accurate representation, *J. Am. Chem. Soc.* **117**, 4177–4178 (1995).
67. A. Streitwieser, C. H. Heathcock, and E. M. Kosower, *Introduction to Organic Chemistry*, 4th ed., Macmillan, New York, 1101 (1992).
68. H. M. Lee, J. Kim, S. Lee, B. J. Mhin, and K. S. Kim, Aqua-potassium(I) complexes: ab initio study, *J. Chem. Phys.* **111**, 3995–4004 (1999).
69. (a) K. S. Kim, C. Cui, and S. J. Cho, Novel amphi-ionophores, *J. Phys. Chem. B* **102**, 461–463 (1998). (b) S. B. Suh, C. Cui, H. S. Son, J. S. U. Y. Won, and K. S. Kim, Novel amphi-ionophore in aqueous solution: cyclohexaalanyl, *J. Phys. Chem. B* **106**, 2061–2064 (2002).
70. K. S. Kim, From gas phase clusters to nanomaterials: an overview of theoretical insights, *Bull. Korean Chem. Soc.* **24**, 757–762 (2003).

CHAPTER 5

THE NATURE OF THE C–H···X INTERMOLECULAR INTERACTIONS IN MOLECULAR CRYSTALS. A THEORETICAL PERSPECTIVE

JUAN J. NOVOA, FERNANDO MOTA and EMILIANA D'ORIO

Departament de Química Física, Facultat de Química and CERQT, Parc Científic, Universitat de Barcelona, Av. Diagonal 647, 08028-Barcelona, Spain. E-mail: juan.novoa@ub.edu

Abstract The different C–H···X interactions are analyzed in this chapter. They are compared with the other types of hydrogen bonds, especially O–H···O ones. Theoretical tools are presented, among them the “atoms in molecules” theory (AIM). The H-bond motifs existing in crystals are presented. The evidences that C–H···X interactions may be often classified as H-bonds are discussed. Etter’s graph set analysis is also used to describe the structure of complex aggregates.

Keywords: Hydrogen bonds; van der Waals interactions; C–H···X interactions; ab initio calculations; AIM theory; crystal structures.

1 INTRODUCTION

Intermolecular interactions (the interaction between molecules [1]) are the driving force behind the formation and structure (also called crystal packing) of molecular crystals. Therefore, one key step in our pathway toward a rational design of molecular crystals is to understand the nature of the most common intermolecular interactions found in these solids, and learning how to control their strength and directionality. This is particularly relevant in molecular crystals that can pack in more than one way (called polymorphs [2]), as different polymorphs sometimes present different macroscopic properties (magnetism, conductivity, etc.) and many of these macroscopic properties are governed by the relative orientations of the molecules within the crystal [2]. Each polymorph is a local minimum in the free energy hypersurface of the crystal structures, and results from a compromise of all intermolecular interactions that could exist among the molecules that form the crystal (some of

them necessarily attractive, while others can be repulsive). Understanding the nature of the intermolecular interactions helps to rationalize the existence of these local minima and their structure. In the long run it should also help to find forms of controlling the structure of these polymorphs. This is the final goal of crystal engineering [3, 4], one of the branches of supramolecular chemistry [5].

One of the most common intermolecular interactions in molecular crystals, particularly in organic molecular crystals or those involving organic ligands, is the so-called C–H···X interaction. These interactions involve a C–H group of one molecule and an X atom of a second molecule, oriented in such a way that they make a short H···X contact. We will show below that there is more than one type of C–H···X intermolecular interactions. *Some of them present the properties of a hydrogen bond, while others do not* (for instance, not all interactions are attractive and to be a bond the interaction must be energetically attractive). Those having hydrogen bond properties are part of the subclass of hydrogen bonds (defined here as all A–H···X interactions having hydrogen bond properties) called weak hydrogen bonds.

In this work, we will review the results from accurate quantum chemical calculations of systems that present C–H···X interactions, with the aim of improving the current insight about the nature of the C–H···X intermolecular interactions in molecular crystals. A monography [6, 7] and some reviews [8, 9] have been published recently in the literature on this subject. They were mostly focused on geometrical trends extracted from the analysis of the crystals deposited in the Cambridge Crystallographic Database [10], although one review was mainly focused on theoretical studies [11], following a different perspective than that taken here. It is also worth mentioning a monography dedicated to theoretical studies of hydrogen bonds [12], where C–H···X interactions were also treated.

2 INTERMOLECULAR BONDS

2.1 What a Bond Is?

The hydrogen bond nature of the C–H···X interactions has been a controversial issue in the literature in old and more recent times. Therefore, to properly address such a point, we will begin by reviewing the current knowledge about what a hydrogen bond is. This will drive us into the nature of a bond.

Among the many available definitions in the literature for hydrogen bonds [9, 13–15]¹ the one we believe is the most functional is the following one, which is a reformulation of Pimentel and McClellan's [15] original definition: we can say that an A–H···B intermolecular interaction is a hydrogen bond when: (1)

¹ They discuss extensively many of the known definitions.

there is evidence of a bond, and (2) this bond involves the H atom covalently bonded to A. This definition relies on our capability of identifying the existence of a bond and that this bond is made between the H and B atoms. We address these nontrivial issues in the following paragraphs².

The most complete definition of a bond, later used by others, was given by Pauling [14]: “There is a chemical bond between two atoms or group of atoms in case that the forces acting between them are such as to lead to the formation of an aggregate with sufficient stability to make it convenient for the chemist to consider it as an independent molecular species.” Then he lists the bonds that fit such a definition: the covalent bond, the ionic bond, the coordination bond, and “even the weak bond that holds together the two O₂ molecules in O₄,” that is, the intermolecular bond. Later on in the book, he also talks about the hydrogen bond². According to this definition, *the key for the existence of a bond is the energetic stability of the bonded system*. Therefore, only energetically attractive interactions can be bonds.

This definition takes us naturally to the following question: are all attractive interactions bonds? which can be rewritten as: where do we put the bonds? This issue is faced in complex molecules and intermolecular aggregates, and originates in the fact that Pauling’s definition (except for the trivial case of a diatomic molecule) only allows to identify the existence of a bond, but not the atoms involved in it. We can illustrate the problem in two examples, selected as prototypes of intramolecular and intermolecular bonds: where do we plot the bonds in benzene and in water dimer?

This theory associates the existence of bonds with certain topological features of the electron density of the aggregate: a bond, either intramolecular or intermolecular, requires the presence of a (3,–1) bond critical point in the electron density. These are points where the gradient of the electron density is zero, there are three nonzero eigenvalues in the Hessian of the density, two of them being negative while the remaining one is positive, and the line of maximum density links the two bonded atoms. Intermolecular bond critical points differ from intramolecular ones in the value of the electron density at the bond critical point (much smaller in intermolecular bonds), and on the value of the Laplacian (the sum of the diagonal elements of the second derivative of the density), which is positive in intermolecular bonds. Using this theory, one can find in benzene six C–H and six C–C intramolecular bond critical points (see Fig. 1). This allows us to plot the structure of this molecule as a six-membered ring with only bonds in the sides. For water dimer one obtains two intramolecular O–H bonds within each molecule, and only one intermolecular bond of the O–H···O type. This bond has all the features required for a hydrogen bond (the dimer is stable, see Fig. 2, and the H and O atoms

² Linus Pauling, in page 449 of Ref. [14], provided an interesting definition: “It was recognized some decades ago that under certain conditions an atom of hydrogen is attracted by rather strong forces to two atoms, instead of only one, so that it may be considered to be acting as a bond between them. This is called the hydrogen bond. Other names, such as hydrogen bridge, have also been used.”

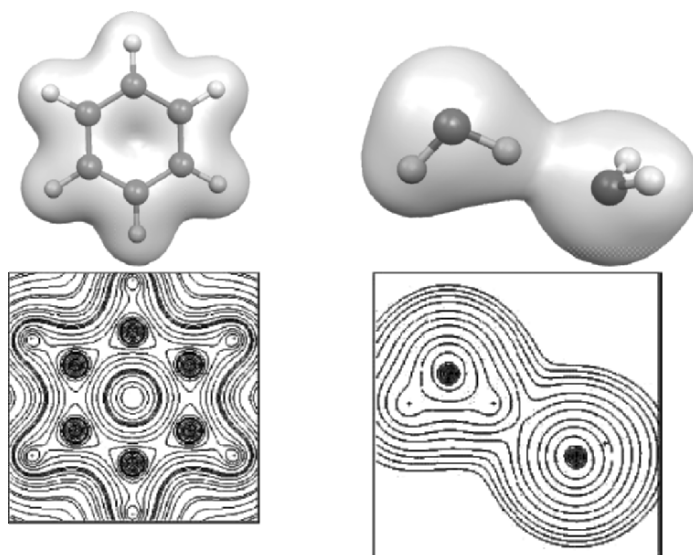


Figure 1. Upper row: Electron density of the benzene molecule (left) and the water dimer (right); the contour of 0.02 a.u. has been plotted in both cases. Lower row: Cut of the electron density along the plane of the benzene (left) and along the plane of the leftmost water molecule (right), showing the details of the density; the bond critical points are the zones of minimum density placed between the bonds.

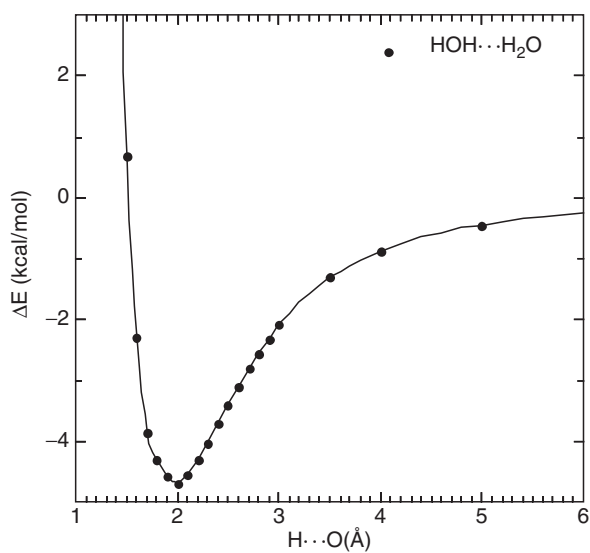


Figure 2. Interaction energy curve of two water molecules oriented as shown in Fig. 1. The curve has been computed at the MP2/aug-cc-pVTZ level. The interaction energy has been corrected by the BSSE.

are involved in the O–H···O bond, see Fig. 1). These results agree well with the conventional view of the bond in these two chemical entities. Systematic studies show that the AIM method is a reliable tool to identify bonds in complex aggregates.

Once we have identified all the bonds present in these two chemical entities, it is worth to make some considerations about their physical meaning. A rigorous analysis of the interaction energy in benzene and the water dimer (that can also be extended to other systems) indicates that the bonds identified by the AIM theory are not the only energetically stable interactions present in these systems (in the water dimer this can be easily shown by simple electrostatic considerations, the dominant component of the interaction energy [17]). Therefore, we have to conclude that the bonds that we normally draw to describe the structure of chemical systems just indicate *the most important attractive interactions found between the constituents of these systems*. Such a definition makes bonds powerful tools when rationalizing the stability of a given structure (how many bonds are made and their energy) or its reactivity (what bonds have to be broken to react and how much energy is required). The same idea is valid for intermolecular bonds, although the smaller energetic stability of intermolecular bonds makes less robust these structures (the reason behind the presence of many minima in the potential energy surface of many crystals). However, even in these cases, the bond concept is useful to understand the energetic stability of the minima and the feasibility of their transformation into another minima. Bonds talk about energy in approximate ways, and energy is the driving force of chemical transformations. Therefore, although up to now the properties of intermolecular bonds are not so clear-cut as in intramolecular bonds, we believe that it is more informative than not using it at all and just talk about molecule–molecule interactions [18], as to rationalize molecule–molecule interactions one has to turn down into bonds. We also think that it is better than purely geometrical alternatives that lack a clear energetic meaning, and that there is no sound quantum chemical reason to change it for a similar concept, bridges [19].³ The topological identification of bonds in aggregates using AIM can also be done using the experimental data about the electronic density obtained in some X-ray diffraction experiments [20]. For instance, correlations have been found in some compounds between the H···X distance and the electron density

³ This work proposed to use again the term hydrogen bridge instead of hydrogen bond, on the basis that “If the term bond has other hallowed connotations in chemistry, it might be far preferable to refer to hydrogen bonds as hydrogen bridges, for so different are they from covalent bonds. . . . The terminology of a hydrogen bridge does not carry with it the unnecessary and incorrect implication that a hydrogen bond is like a covalent bond but only much weaker.” In our opinion, the term bond is flexible enough to include all known classes of energetically stable interactions, and does not assume any consideration about its nature. Within its classes it includes the ionic bond and the covalent bond. Hydrogen bonds are just one more type, whose nature is partly ionic and partly covalent, in a degree that changes with the specific hydrogen bond. So, there is no sound quantum chemical reason to substitute bonds by bridges at this moment.

at the bond critical point [21], density and strength [22], and also between the H...X distance and the strength of the hydrogen bond [23].

Consistent with the above considerations, one should be careful in distinguishing among *contacts*, *interactions*, and *bonds* when looking at intermolecular interactions in crystals (and other aggregates). While *contacts* is a geometrical term that only refers to the metric of some of the atoms in a given interaction between two molecules, interaction implies that one is talking about the energy for that contact, and bond implies that such interaction is attractive and one of the energetically dominant.

2.2 Nature of the Intermolecular Bonds

Theoretical studies carried out over the years on the nature of the intermolecular bonds have shown that they are always energetically stabilizing along some orientation, and follow a Morse-like curve like chemical bonds, although the minimum is located at longer distances and a lot less energetic.

A very useful tool to rationalize the nature of these intermolecular bonds will be the analysis of the dominant components of the interaction energy. Using classical mechanics, when the two molecules are far enough the interaction energy between two molecules A and B fixed in the space can be approximated as the electrostatic interaction energy (E_{el}) between two sets of multipoles [1, 24, 25]. The leading terms of the electrostatic interaction energy between two undistorted A and B molecules can be written as a power series:

$$\begin{aligned}
 E_{\text{el}} = & \frac{1}{4\pi\epsilon_0} \frac{q_A q_B}{r} - \frac{1}{(4\pi\epsilon_0)} \frac{q_A \mu_B}{r^2} \cos \theta \\
 (1) \quad & - \frac{1}{(4\pi\epsilon_0)} \frac{\mu_A \mu_B}{r^4} (2 \cos \theta_1 \cos \theta_2 - \sin \theta_1 \sin \theta_2 \cos \phi) - \dots
 \end{aligned}$$

Notice that other terms, like the charge–quadrupole term can also be important in some complexes. In this expression, r is the distance between the two centers of mass of the two molecules, θ_1 and θ_2 the angles between the dipole of each molecule (placed in their center of mass) and the axis that links their center of mass, and ϕ the dihedral angle of the dipoles around that axis. In this expression, the first term, called the *charge–charge term*, is only found when the two fragments have net charge (q_A and q_B) different from zero. The second term, called the *charge–dipole term*, is only present when one of the fragments has a nonzero net charge and the other a nonzero permanent dipole (μ_B). Finally, the third term is called the *dipole–dipole term*, only present when the two molecules have a non-null permanent dipole. Therefore, (1) can also be written as

$$(2) \quad E_{\text{el}} = E(q,q) + E(q,\mu) + E(\mu,\mu) + \dots$$

At the typical equilibrium distances for intermolecular interactions (1.2–3 Å), when the two fragments are charged, the first term dominates over the remaining two (due to its $1/r$ dependence). When one fragment is charged and the

other is neutral but has a non-negligible dipole, the second term is the dominant one ($1/r^2$ dependence). For the interaction between two neutral fragments that present a non-negligible dipole moment, the third term is the dominant one (with a $1/r^4$ dependence). Examples of each type of domination are the interaction between ions in ionic salts, ion–solvent interactions, and solvent–solvent interactions. Note that Eqs. 1 and 2 do not take into account the polarization effect of one molecule due to the presence of the other, which depends on the polarizability. However, they can be accounted using the proper analytical expressions [1, 24, 25].

A simplified form of Eq. 1 can be used when the A and B molecules are freely rotating (for instance, when they are part of a liquid or a gas, and the temperature is high enough). In this case, one can average over the angles and obtain an expression that only depends on r , whose three terms retain their physical meaning:

$$(3) \quad E_{\text{el}} = \frac{1}{4\pi\epsilon_0} \frac{q_A q_B}{r} - \frac{1}{(4\pi\epsilon_0)^2} \frac{1}{6kT} \frac{q_A^2 \mu_B^2}{r^4} - \frac{1}{(4\pi\epsilon_0)^2} \frac{2}{3kT} \frac{\mu_A^2 \mu_B^2}{r^6} - \dots$$

Due to its simplicity, Eq. 3 is more widely used in qualitative analysis. However, because molecules in crystals are fixed bodies in the space, Eq. 1 is more appropriate for molecules in crystals.

The above equations should only be rigorously applied for molecules at large distances. However, for dimers or aggregates close to their equilibrium distances, the objects of our usual interest, one should resort to better formulations. One of these, which has a solid Quantum Mechanical foundation, is the so-called intermolecular perturbation theory (IMPT) [26]. This is a perturbative method that provides a rigorous expression for the interaction energy of two molecules that present a small but non-negligible overlap between their orbitals (note: this perturbative approach sometimes diverges when the orbital overlap becomes very large, so it is convenient to check that the addition of all energy components given by the IMPT method is similar to the interaction energy computed using a nonperturbative approach, for instance by subtracting the energy of the dimer and the fragments). The IMPT interaction energy (E_{int}) is obtained as the sum of the following five components:

$$(4) \quad E_{\text{int}} = E_{\text{er}} + E_{\text{el}} + E_{\text{p}} + E_{\text{ct}} + E_{\text{disp}}$$

The first term (E_{er}) is the *exchange–repulsion component*, a combination of the Pauli repulsion that two electrons feel when forced to be in the same region of the space, and the attractive exchange component (overall, it has a net repulsive character). The second term (E_{el}) is the *electrostatic component*, associated to the electrostatic interaction of two fragments whose electronic distribution is frozen to their values when isolated. The next two terms (E_{p} and E_{ct}) are the *polarization* and *charge-transfer components*, respectively. The first one is associated to the polarization of the electronic distribution of the fragments due to the presence of

the second fragment, and the second to transferences of electronic charge from one fragment to the other when the fragment's electronic distributions are allowed to relax. Finally, the last term (E_{disp}) is the *dispersion component*, a nonclassical term whose existence is due to the correlated motions of the electrons (the closest classical image is the interaction between the instantaneous dipole moments induced in the fragments by the electron motions).

As the IMPT method was designed to analyze the interaction energy of closed-shell molecules, it does not include terms that can describe the formation of bond. Whenever there are unpaired electrons in the molecules, there is one extra term, whose origin can be traced to the pairing of electrons responsible for the formation of bonds. Thus we can call it the *bond component* (identified as E_{bond}).

As we will see below (Table 1), the exchange–repulsion term is always repulsive, particularly at short distances (this is the term responsible of the existence of the so-called repulsive well, which is determinant in defining the distance of closest approach between two molecules). Consequently, the energetic stability of the intermolecular interactions is associated to the last four terms of Eq. 4. Previous studies [26] have shown that in most cases the electrostatic component dominates over the polarization and the charge-transfer components (see Table 1 for examples). Thus, *the energetic stability of an intermolecular interaction can be rationalized by looking at the sign and size of the electrostatic and dispersion terms*. In such rationalization, the sign and size of the electrostatic term can be analyzed with the help of Eqs. 1–3.

2.3 Types of Intermolecular Bonds

All the known intermolecular bonds can be classified in one of the following three main categories, according to the nature of the interaction: *ionic bonds*, *hydrogen bonds*, and *van der Waals bonds*. Their main characteristics are:

– *Ionic bonds* are the intermolecular bonds in which one of the species has a net charge (this is, by definition, an ion). The prototypical example is the $\text{Na}^+ \cdots \text{Cl}^-$ interaction, but the ion–solvent interactions are also within this

Table 1. Value of the energetic components of the interaction energy for the indicated systems, computed using the IMPT method. E_{el} , E_{er} , E_{p} , E_{ct} , and E_{disp} are, respectively, the electrostatic, exchange-repulsion, polarization, charge-transfer, and dispersion components. E_{tot} is the sum of these components and E_{MP2} is the BSSE-corrected interaction energy, shown to serve as reference to calibrate the quality of the IMPT calculation. The MP2 intermolecular optimum distance is also shown (r_{opt}). Distances are given in Å and energies in kcal/mol

System	r_{opt}	E_{el}	E_{er}	E_{p}	E_{ct}	E_{disp}	E_{tot}	E_{MP2}
$\text{Na}^+ \cdots \text{Cl}^-$	2.412	−142.3	25.4	−10.5	−1.4	−35.5	−164.3	−128.0
$\text{HO-H} \cdots \text{H}_2\text{O}$	1.990	−6.7	5.0	−0.7	−0.5	−2.0	−3.9	−4.2
$\text{Ar} \cdots \text{Ar}$	3.842	−0.04	0.15	0.00	0.00	−0.28	−0.16	−0.16

class. The energy of these interactions is dominated by the electrostatic term (Table 1), particularly by the charge–charge or charge–dipole term. These bonds require that the two ions involved are of opposite charge, as otherwise the interaction is repulsive (and thus fails to satisfy the criteria of energetic stability required for an interaction to be a bond).

– *Hydrogen bonds* are intermolecular bonds showing an A–H···X topology. In most cases it involves the so-called proton donor (A–H) group pointing to the region of accumulation of electronic density on the proton acceptor group (X), like the location of the lone-pair electrons or the bonding π -electrons. It implies the existence of a H···X bond critical point between the H and X atoms. The prototypical example is the O–H···O bond found in water dimers. However, it is worth pointing that one can also have this topology and bond properties in aggregates where one or two of the molecules participating in the interaction have net charge (therefore, the stable ion-solvent interactions presenting an A–H···X topology should be included here). When the bond involves neutral dimers the dominant term in the interaction energy (Table 1) is the dipole–dipole term (Eqs. 1–3), but this is not always the case when the fragments are charged.

– *van der Waals bonds* are intermolecular bonds where two atoms A and B that present strong electronic localization (lone pairs, π -orbitals) are connected by an A···B bond critical point. These bonds originate from the dispersion terms (Table 1) and are usually the weakest of all possible bonds. A prototypical example is the bond in the Ar₂ dimer, or the bond between aromatic molecules piled in π -stacks, so often found in many molecular crystals. In complex geometrical arrangements, one can check if a hydrogen bond or a van der Waals bond is formed by looking at the topology of the bond critical points computed by an AIM analysis (for one example, see Ref. 27).

All the known intermolecular interactions can be classified within one of these three groups. Whenever there is more than one option, we suggest to look at the dominant component of the interaction energy and use it to classify the molecule (for instance the Ar···Ar interaction is a van der Waals interaction—in fact a bond, as it is energetically stable, but K⁺···K⁺, which is isoelectronic, is an ionic interaction—it is not a bond, as it is energetically destabilizing).

3 HYDROGEN BOND

3.1 Identification of Its Presence

Once we have established what a hydrogen bond is and its relative position within the possible intermolecular bonds, we can focus our attention in the forms conventionally used to identify its presence. Besides the *direct* criteria described before as part of defining its nature (compute the energy of the interaction and search for a H···X bond critical point in the A–H···X

interactions), over the years there have been indirect criteria taken as evidence of the presence of hydrogen bonds [28, 29], which we summarize in the following sections.

3.1.1 Geometry [3, 7, 9, 30]

- The A–H···X bonds show a preference for a collinearity of the A–H donor group and the X acceptor group (that is, the $\langle \text{A–H} \cdots \text{X} \text{ angle} \rangle$ tends to be close to 180°), a fact that distinguishes these bonds from van der Waals bonds. This is illustrated in Fig. 3.
- In some cases, the acceptor group X also shows some angular preference, which can be identified with the position of the electron lone pairs (the prototypical example is the O–H···O=C interaction).

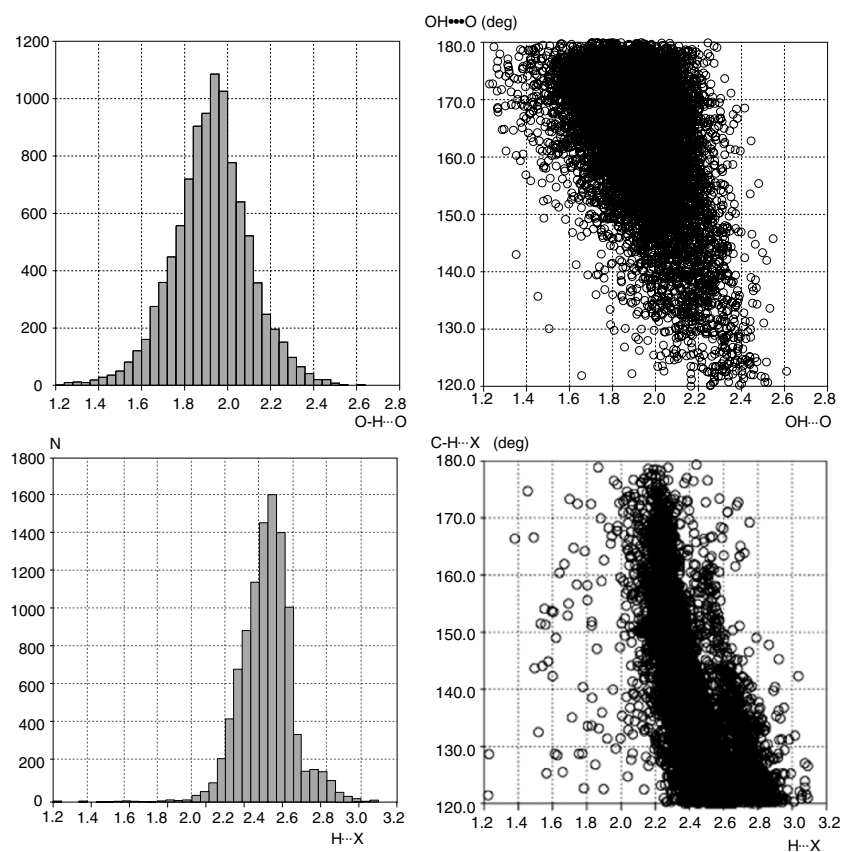


Figure 3. Distribution of H···X distances (left) and scatterplot of the A–H···X angles versus the H···X distances for the crystal structures deposited in version 5.26 of the Cambridge Crystallographic Database (November 2004). *Upper row:* O–H···O contacts. *Lower row:* C–H···O contacts. The van der Waals radii of hydrogen and oxygen are 1.2 and 1.52 Å.

- The H···A distances are usually shorter than the sums of the van der Waals radii of H and A (the van der Waals radii are tabulated in Ref. 31). This is the case of hydrogen bonds where A and X are strongly electronegative (O–H···O, for instance), but the situation is not so clear when less electronegative atoms are present, as in the C–H···O bonds (see Fig. 3). It is very common to use cut-off distances based on van der Waals radii to identify hydrogen bonds. However, recently the use of relaxed thresholds that add 0.5 Å (or even more) to the sum of van der Waals radii [30] has been suggested.
- Recent studies have also suggested that one should also relax the value of the threshold angle used as cut-off value for acceptable hydrogen bonds. Thus, in C–H···X, angles up to 90° have been suggested [9] as recommended thresholds, although the same author suggests that the cut-off angle should be lowered to 130° for O–H···X bonds.

3.1.2 Energy

By doing calorimetry or mass-spectrometry experiments, it is possible to measure the interaction energy for stable aggregates [28, 29]. These are complex techniques and experimental values are available only for a few hydrogen bonded dimers. It is also possible to measure the sublimation heat [32] of crystals, which can be equated to the combined interaction energy of all intermolecular interactions found in the crystal [33]. However, nowadays, the most reliable technique to measure the interaction energy of aggregates is performing quantum chemical calculations [34–36] using the appropriate method and basis set. Typically, the reported values lie within the 0.2–39.0 kcal/mol energy range [7].

3.1.3 Rotational spectroscopy of gas-phase complexes [37]

It provides information about the geometry isolated hydrogen bonded dimer. It also provides information about the strength of the dimer.

The gas-phase equilibrium geometry of the hydrogen bonded dimers was found to coincide with the axis of the lone-pair electrons or, when they are not available, with the direction of the π -bonding pairs.

3.1.4 IR Spectroscopy [28, 38]

The classic technique used to study the hydrogen bond in condensed phases, both in solution and the solid state. The hydrogen bond is manifested by a decrease in the value of the A–H stretching ($\Delta\nu_{\text{AH}}$) with respect to the free A–H value, together with a broadening of this vibrational band.

In some cases, the so-called blue-shifted hydrogen bond, the shift of the A–H stretching frequency is toward higher wave numbers. The reasons for this exceptional behavior have been now properly rationalized [39].

Isotopic shift of that band ($\Delta\nu_{\text{AH}}/\Delta\nu_{\text{AD}} \neq 1$).

Good correlations have been found between the shift and the strength of the bond, for instance, for hydrogen bonds in solution $\Delta H = -0.31(\Delta\nu_{\text{OH}})^{1/2}$ [7].

Information about “nearly isolated” hydrogen bonded dimers can be obtained by matrix-isolation techniques, which provide information on the geometries and energy for hydrogen bonded dimers frozen in an inert matrix [40, 41].

3.1.5 NMR spectroscopy [28, 29, 42]

The ^1H chemical shift moves downfield (in some cases up to 20 ppm), and $\text{A}\cdots\text{X}$ distance versus shift correlations have been established, based on ^1H solid-state NMR measurements and geometries from neutron crystal structures. These correlations have also been successfully applied to hydrogen bonds in the liquid state [43]. The shift is also known to be proportional to the number of hydrogen bonds [21].

3.2 Types of Hydrogen Bonds Relevance of the Monomer Charge

There are many ways of classifying the hydrogen bonds. One of the most extended forms was suggested by Jeffrey [38], where hydrogen bonds are classified according to their relative strength compared to “normal” hydrogen bonds (taken as those found in water dimers and similar compounds). The normal hydrogen bonds constitute the so-called *moderate* group, with energies in the range 4–15 kcal/mol. Hydrogen bonds with energies above these values form the *strong* group, while those with values below form the weak group. The classification is in some sense arbitrary, as the selection of the range of energies covered by the normal group is in many ways a matter of personal taste.

Looking at the structural features of the list of bonds whose energy is known (see, for instance, Table 1 for reference [9], where the strongest dimers are $\text{F}-\text{H}\cdots\text{F}^-$ or $\text{HO}-\text{H}\cdots\text{F}^-$, with energies close to 40 kcal/mol, and the weakest dimer is $\text{HO}-\text{H}\cdots\text{Cl}^-$, with an energy of 13.5 kcal/mol) one concludes that in all strong hydrogen bonds one of the fragments has a net charge, that is, we are dealing with *charge*··*neutral interactions*. As shown in Table 2, the reason for the extra stability of these bonds compared to that found in the

Table 2. Value of the energetic components of the interaction energy (in kcal/mol) for the indicated systems, computed using the IMPT method. E_{el} , E_{er} , E_{p} , E_{ct} , and E_{disp} are, respectively, the electrostatic, exchange–repulsion, polarization, charge-transfer, and dispersion components. E_{tot} is the sum of these components and E_{MP2} is the BSSE-corrected interaction energy, shown to serve as reference to calibrate the quality of the IMPT calculation. The MP2 optimum distance (in Å) is also shown. The basis set used is the aug-cc-pVTZ

System	$r_{\text{H}\cdots\text{O}}$	E_{el}	E_{er}	E_{p}	E_{ct}	E_{disp}	E_{tot}	E_{MP2}
$\text{HO}-\text{H}\cdots\text{F}^-$	1.587	−32.7	21.9	−7.8	−3.2	−6.1	−27.9	−26.1
$\text{HO}-\text{H}\cdots\text{OH}_2$	1.990	−6.7	5.0	−0.7	−0.5	−2.0	−3.9	−4.2
$\text{H}_3\text{C}-\text{H}\cdots\text{OH}_2$	2.627	−0.7	1.1	−0.2	−0.1	−0.7	−0.6	−0.6

water dimer is the increased strength of the electrostatic term. With the help of Eqs. 1–3, one can associate that behavior to the presence of a ion–dipole electrostatic term, dominant term in the energy, which adds to the dipole–dipole electrostatic term. Therefore, one can consider these strong hydrogen bonds as *charge-assisted hydrogen bonds*. This fact also suggests that one could get stronger hydrogen bonds than those currently reported by allowing the two fragments involved in the hydrogen bond to present charges of opposite sign, as this will also add a charge–charge contribution (the design of these complexes has some difficulties, as one has to avoid the transfer of the proton from the proton donor to the proton acceptor group). In any case, this is a first indication that the charge of the monomers that constitute the dimer is key in defining its interaction energy.

When similar considerations are applied to the normal and weak hydrogen bonds, one finds that in all of them the fragments have no net charge, that is, they are *neutral···neutral interactions*. An analysis of the energetic components of moderate and weak hydrogen bonds reveals that the main difference between them relies on the relative importance of the electrostatic and dispersion terms. In fact, without the dispersion contribution the C–H···O bond present in the methane···water complex would not exist, as the interaction energy would become destabilizing and the dimer will dissociate into its monomers. This fact, surprising when first reported [44], is a clear manifestation that *not all hydrogen bonds are just electrostatic in nature*, as it has been sometimes (incorrectly) stated.

The importance of the charge in determining the strength (and even the nature) of the A–H···X interactions is illustrated in Table 3 in the particular case of the O–H···O interactions. The values reported in this table correspond to the O–H···O complexes obtained by successive deprotonation of the water dimer, preserving the geometry of the remaining atoms in the aggregate (that is, the geometrical features of the O–H···O interaction in all the complexes is the same) [45]. This study shows that the O–H···O interactions presenting the same geometry can be attractive or repulsive, depending on the net charge of the monomers. Consequently, the geometry of an O–H···O contact is not

Table 3. Value of the energetic components of the interaction energy computed using the IMPT method. E_{el} , E_{er} , E_{p} , E_{ct} , and E_{disp} are, respectively, the electrostatic, exchange–repulsion, polarization, charge-transfer, and dispersion components. E_{tot} is the sum of these components (all values in kcal/mol). The 6–31+G(2d,p) basis set was used. The geometry of the (H₂O)₂ dimer is the optimum MP2/aug-cc-pVDZ

System	E_{el}	E_{er}	E_{p}	E_{ct}	E_{disp}	E_{tot}
HO–H···OH ₂	–8.9	6.9	–0.7	–0.7	–1.7	–5.2
O–H ^(–) ···OH ₂	2.4	10.0	–1.1	–0.9	–2.3	8.1
HO–H···OH ^(–)	–23.9	11.1	–4.1	–2.1	–2.6	–21.6
O–H ^(–) ···OH ^(–)	90.5	12.6	–5.9	–3.2	–3.6	90.4

indicative of its nature, as it has been sometimes (incorrectly) assumed when analyzing crystals.

Although the $\text{OH}^{(-)} \cdots \text{OH}^{(-)}$ interactions are not energetically stable when the complex is isolated, they are found in crystal, as in the NaOH crystal, due to the stabilizing effect of the cation \cdots anion interactions. This is clearly shown when the distribution of $\text{O}-\text{H} \cdots \text{O}$ and $\text{OH}^{(-)} \cdots \text{O}^{(-)}$ interactions found in the Cambridge Crystallographic Database is analyzed [46]. Fig. 4 shows such an analysis as a function of the $\text{O} \cdots \text{O}$ distance, while Fig. 5 shows the same analysis as a function of the $\text{H} \cdots \text{O}$ distance (notice that the second analysis is expected to be less accurate, as many of the structures are obtained from X-ray diffraction, and thus the position of the hydrogens is not so well characterized as those of the heavy atoms). The reason for the existence of $\text{OH}^{(-)} \cdots \text{O}^{(-)}$ interactions in crystals is that the sum of cation \cdots anion interactions overweight the sum of the anion \cdots anion and cation \cdots cation repulsions. As a consequence, the crystal is energetically stable, in fact, more stable than crystals of neutral components, as manifested in the tables of sublimation heats of structurally similar crystals [32]. As the crystal packing is a compromise between many interactions, the resulting geometry of the $\text{OH}^{(-)} \cdots \text{O}^{(-)}$ interaction can be identical to that found in energetically stable $\text{O}-\text{H} \cdots \text{O}$ interactions (notice the similar ranges of distances for the neutral \cdots neutral and anion \cdots anion distribution of Fig. 4). However, as shown in Table 3, none of the anion \cdots anion complexes are energetically stable, so they are not bonds. Therefore, *one has to pay attention to the net charge of the monomers when analyzing intermolecular interactions*. For instance, one should distinguish

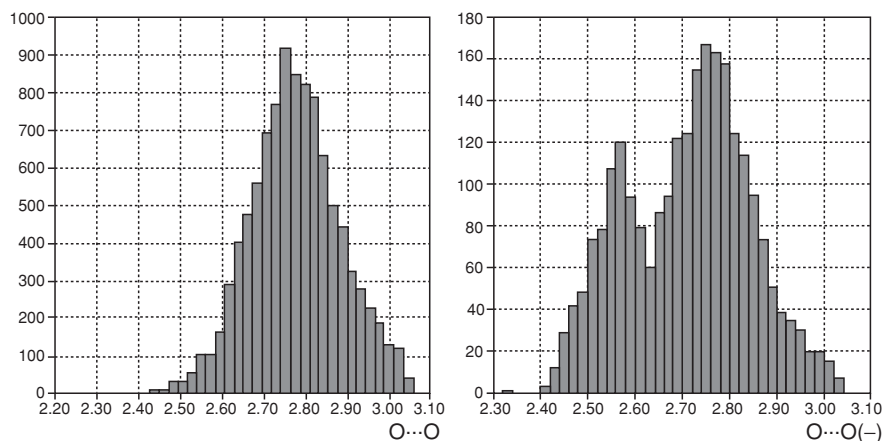


Figure 4. Number of contacts as a function of the $\text{O} \cdots \text{O}$ distance for the $\text{O}-\text{H} \cdots \text{O}$ contacts. *Left:* Neutral \cdots neutral contacts. *Right:* Neutral \cdots anion and anion \cdots anion contacts (the left peak is that due to the anion \cdots anion contacts). The analysis was done on the crystal structures deposited in version 5.26 of the Cambridge Crystallographic Database (November 2004). The van der Waals radii of oxygen are 1.52 Å.

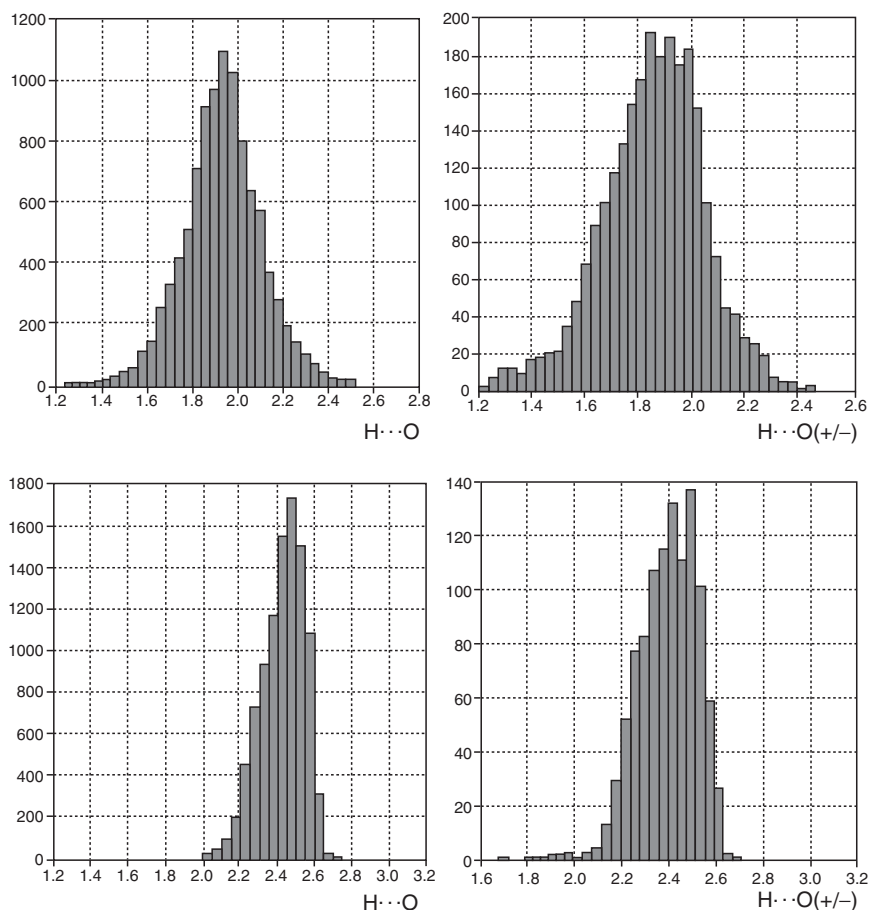


Figure 5. Number of contacts versus the H···O distances for the O–H···O contacts (*upper row*) and the C–H···O contacts (*lower row*). In each row, the left diagram collects the data for neutral···neutral contacts, while those in the right diagram refer to anion···anion contacts. The analysis was done on the crystal structures deposited in version 5.26 of the Cambridge Crystallographic Database (November 2004). The van der Waals radii of hydrogen and oxygen are 1.2 and 1.52 Å.

between O–H···O and OH⁽⁻⁾···O⁽⁻⁾ interactions. This different nature gives rise to differences in the crystal structures, which are manifested in statistical analysis of crystal structures [46]. For instance (see Fig. 4) the OH⁽⁻⁾···O⁽⁻⁾ interactions present a distribution with the O···O distance whose maximum is located at a shorter distance than the maximum of the O–H···O interactions. This behavior is also observed in O···H distributions (Fig. 5). In weaker contacts (Fig. 4 plots the C–H···O and C–H⁽⁻⁾···O⁽⁻⁾ distributions) such an effect is not so clear.

3.3 Computational Methodology

As a result of many studies [47–49], it has been concluded that an accurate description of the hydrogen bond properties (geometry and energy, particularly) in moderate bonds, as that in the water dimer, requires the use of large and flexible basis sets and also methods that include the electron correlation. Good results are also found when using the proper nonlocal exchange-correlation density (DFT) functionals [50–52], among them the B3LYP functional [53].⁴ This is clearly shown by looking at the data for the water dimer in Tables 4 and 5 (Table 4 lists the data computed with various basis set using the Hartree–Fock (HF) and second order Moller–Plesset (MP2) methods [34], while Table 5 lists the data computed with various methods using the aug-cc-pVTZ basis set [54];^{5,6} the data have been taken from Ref. 47). For this dimer, the experimental geometry [55] and interaction energy [56] have been determined experimentally.

It is worth pointing here that we are looking at formation energies (the difference between the optimum energy of the complex and the optimum energy of the monomers) and that bonding energies differ from the interaction energies (the difference between the optimum energy of the complex and the energy of the monomers at the same geometry than they have in the complex) by the relaxation energy of the monomers. In most moderate and weak hydrogen bonds, the relaxation energy is small and the interaction and bonding energies

Table 4. Formation energy of the water dimer (values in parenthesis are BSSE-corrected) computed [47] using the Hartree–Fock (HF) and second order Moller–Plesset (MP2) methods with the indicated basis set. All values are in kcal/mol. The experimental value is -5.44 ± 0.7 kcal/mol [56]

Basis set	Number of functions	HF	MP2
cc-pVDZ	48	−5.75 (−3.70)	−7.30 (−3.93)
aug-cc-pVDZ	82	−3.79 (−3.55)	−5.71 (−4.32)
cc-pVTZ	116	−4.37 (−3.55)	−6.04 (−4.40)
aug-cc-pVTZ	184	−3.61 (−3.54)	−5.10 (−4.64)
cc-pVQZ	230	−3.90 (−3.57)	−5.45 (−4.67)
aug-cc-pVQZ	344	−3.60 (−3.56)	−5.05 (−4.81)
cc-pV5Z	402	−3.66 (−)	

⁴ B3LYP is a density functional obtained by taking the three parameter non-local exchange functional of Becke and the non-local correlation functional of Lee–Yang–Parr.

⁵ cc-pVxZ is the correlation consistent basis set from double up to quintuple zeta quality (the quality is indicated by the x, which can be D, T, Q, and 5, for double, triple, quadruple, and quintuple zeta quality).

⁶ aug-cc-pVxZ is the correlation consistent basis set that includes diffuse functions. The quality of the basis set is indicated following the same convention than in the cc-pVxZ basis sets.

Table 5. Formation energy of the water dimer (values in parenthesis are BSSE-corrected) computed [47] using the aug-cc-pVTZ and the indicated methods [34]. All values are in kcal/mol

Basis set	Formation energy	
HF	–3.61 (–3.54)	
MP2	–5.10 (–4.64)	
MP4	–5.14 (–4.66)	
QCISD	–4.89 (–4.46)	
QCISD(T)	–5.16 (–4.69)	
B3LYP	–4.36 (–4.31)	This work

are nearly the same (or the same). Formation energies are the values measured experimentally. When these values are corrected by the zero-point energy (ZPE) one obtains the value of D_0 .

The results of Table 4 are plotted in Fig. 6 to allow a better visualization of their trends. The following conclusions can be reached:

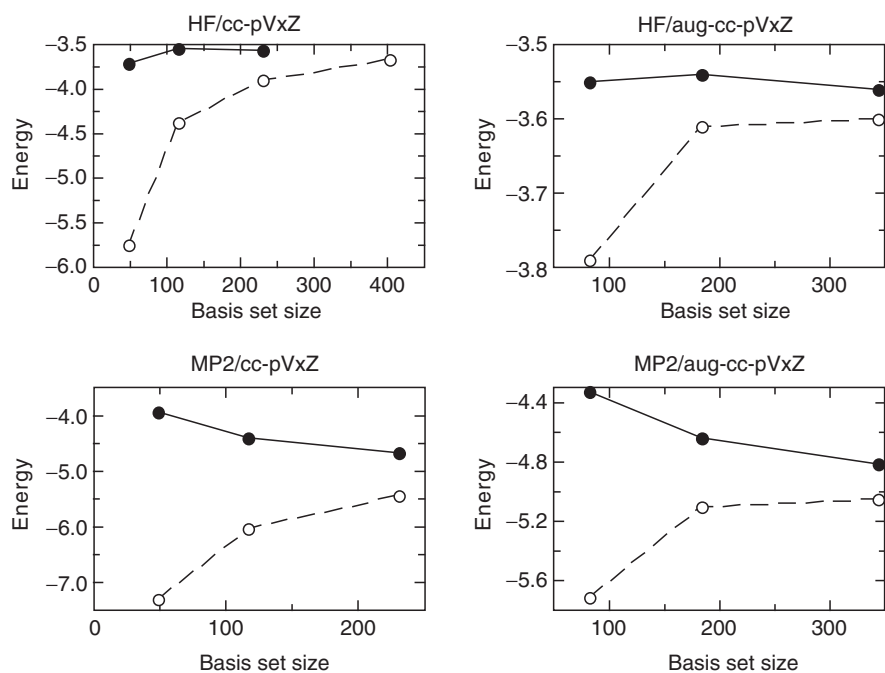


Figure 6. Dependence of the HF and MP2 formation energy (in kcal/mol) on the basis set size. Upper row: HF for the cc-pVxZ and aug-cc-pVxZ basis sets. Lower row: MP2 values for the same basis sets. Empty symbols are for formation energies whose BSSE has not been corrected, while filled circles are for BSSE-corrected values (see text).

- a. The formation energies present a non-negligible basis set superposition error (BSSE) [57]. This error diminishes as the basis set quality is improved, being larger in the MP2 than the HF energies (for the same basis set).⁷
- b. The BSSE-corrected formation energies (the correction has been done using the counterpoise method [57]) show less dependence on the basis set quality than the uncorrected values. The convergence is from above, indicating a tendency of the counterpoise method to overestimate the BSSE for small basis sets. Studies have shown that for large and flexible basis set the BSSE becomes negligible and the BSSE-corrected formation energy is close to the experimental value [58–61]. Thus, it is recommended to look at the BSSE-corrected values, when comparing data from calculations where different basis sets have been used: the same suggestion is done to compare results for different systems. In doing this, one should check if the basis set is very small and the counterpoise method is overestimating the BSSE-error.
- c. The HF and MP2 BSSE values are much smaller in the aug-cc-pVxZ than in the cc-pVxZ basis set.
- d. By exponential fitting it is possible to obtain a limit value for the HF and MP2 energies. These two methods provide different limits: -3.55 kcal/mol in the HF method, and -5.05 kcal/mol in the MP2 method.
- e. The MP4 and QCISD(T) methods give formation energies similar to the MP2 method. Multireference methods are not usually needed to describe hydrogen bonds (they are only needed when near degeneration situations are expected, as in the Be₂ dimer, where the s and p states of the Be atoms are nearly degenerate; see, for instance, Ref. 44).
- f. The B3LYP functional gives values similar to the MP2 method, at much lower computational effort. This is particularly true when looking at the BSSE-corrected data, and opens the door to use the proper DFT functionals on larger clusters having hydrogen bonds of similar nature. As we will see below, the quality of the DFT functionals decreases when one works with weak hydrogen bonds, for instance, C–H···O bonds. Studies have been done to assess the quality of the usual DFT functionals in describing the hydrogen bonds [52]. Also interesting is the fact that the BSSE errors of DFT formation energies are close to the HF values, and much smaller than the MP2 values [52].

4 HYDROGEN BONDS IN CRYSTALS

4.1 Introduction

Up to now, we have focused our attention on the properties of hydrogen bonds in simple model complexes where only one isolated bond exists. Crystals are

⁷ In the counterpoise method the interaction energy is computed by subtracting the energy of dimers and monomers using in both cases the basis set of the dimer. To obtain formation energies one also has to take into account the relaxation energy of the monomers from their geometry in the dimer to their optimum geometry.

more complex entities. Most crystals of interest are made of complex molecules, where more than one proton donor and proton acceptor groups are present. One has to find forms of identifying which bonds are really made in a rigorous way. In many cases, such identification has been done by looking at the geometry of the A–H···X contacts, but a proper tool already exists, by applying the AIM method to the crystal or the molecular complexes that exist within the crystal. This tool can also be helpful to differentiate when they are ionic, hydrogen bond, or van der Waals [27].

Besides the previous considerations, the mere existence of a crystal or aggregate requires that the participant molecules can form more than one bond with different molecules. The topology of these bonds has been found to be an important tool to analyze and distinguish between different polymorphic forms. When one molecule can form more than one bond then the cooperativity between these bonds becomes an important issue. Thus, the interaction energy of a carboxylic acid in its ring conformation is more than twice that found in the linear conformation (both conformers are plotted in Fig. 8).

All these issues will be addressed in this section, after looking at the types and strength of the hydrogen bonds that can be found in crystals. We will do so by looking at the O–H···O interactions found in crystals deposited in the Cambridge Crystallographic Database whose structure has been obtained using neutron-diffraction.

4.2 The O–H···O Interactions in Crystals

The O–H···O hydrogen bond plays a capital role in the study of hydrogen bonds: it is the reference against which other bonds are compared to test their hydrogen bonded nature. Therefore, we decided that the O–H···O properties in crystal should be investigated first.

In order to investigate the main features of the properties of the O–H···O interaction in crystals, we evaluated [61] the interaction energy of all dimeric complexes showing O–H···O contacts with the metric of hydrogen bonds. These complexes were located on crystals whose structure was determined by neutron-diffraction, as in this form the position of the H atoms can be determined with accuracy.

We selected all the intermolecular contacts of the type QA–O₁–H···O₂–QA having a H···O₂ distance in the 1.2–2.1 Å range and an O₁···O₂ distance in the 2.3–2.9 Å range (QA is any element of the periodic table except the metallic ones, lanthanides, actinides, and noble gases). The ⟨O₁–H···O₂ angle was also restricted to be between 120° and 180°. No charge was specified on any of the atoms. Among all the obtained structures, we further restricted our search to those having no disorder. We found 63 crystals that fulfilled all these requirements. Using their crystal geometry, the interaction energy was computed for each of these dimeric complexes at the MP2/6–31+G(d) level. For a further

characterization of the interaction, the components of the interaction energy were determined using the IMPT method.

Many of these 63 crystals are polymorphic forms. We selected only one of them as a representative of all. We also discarded crystals of very large molecules, to make possible our calculations. We thus ended in 36 crystals. As many of these crystals presented more than one complex satisfying the metrics, we ended in computing the interaction energy of 45 complexes (see Ref. 61) for details of the complexes, the geometric parameters, and the interaction energies).

The complexes were classified in groups according to the net charge on the monomers, as this property was shown before to play an important role in defining the nature of the A–H···X interactions. The following groups were found: (1) N···N *group*, where the two molecules are neutral and nonzwitterionic (zwitterions: formally neutral molecules, but where two regions, of strong positive and strong negative charge localization, can be found), (2) N···ZW *group*, where one of the molecules is a zwitterion and the other is a neutral nonzwitterionic molecule, (3) ZW···ZW *group*, where both molecules are zwitterions, (4) q···N *group*, where one of the molecules has a net charge (+ or –) and the other is a neutral nonzwitterionic one, and (5) q···q *group*, where both molecules have net charge, not necessarily of the same sign and/or size. As the N···ZW group has only one member, in the plots it will be included within the ZW···ZW group.

Figure 7 plots, separated by groups, the interaction energy and H···O distance for each of the 45 complexes. The energy span of these interactions goes from –160 to 190 kcal/mol, values much wider than those reported before

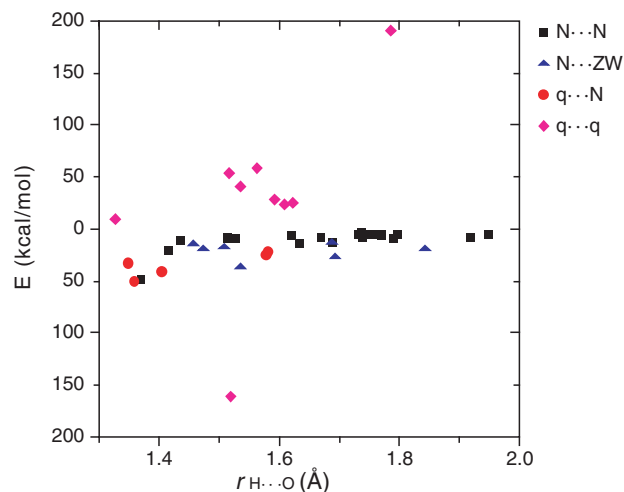


Figure 7. Values of the interaction energy (computed at the MP2/6–31+G(d) level) and H···O distance for each of the 45 complexes found to fulfill the metrics expected for an O–H···O interaction to be a hydrogen bond.

on model dimmers [7, 9], and that also contain unstable interactions. The following ranges are valid within each group (all values in kcal/mol): (1) N···N *group*: (–3.4, –48.5), (2) N···ZW *group*: just has one value –36.0, (3) ZW···ZW *group*: (–12.6, –27.0), (4) q···N *group*: (–21.6, –50.8), (5) q···q *group*: (190, –160). Therefore, while the first four groups only present energetically stable O–H···O interactions, the q···q *group* contains many interactions that present the metric expected for hydrogen bonds but are energetically unstable, that is, they cannot be considered hydrogen bonds.

The data in Fig. 7 also demonstrate the failure of the so-called “strength–length” empirical relation (which can be stated as “the shorter the contact, the stronger it should be”). This is a widely used structure–energy correlation employed when analyzing crystal packings. The very wide range of energies that one finds at the same distance is a clear demonstration that such correlation does not work for the O–H···O interactions found in neutron-diffraction crystal structures.

Very useful information about the nature of these O–H···O interactions can be obtained by looking at the components of the interaction energy computed [61] using the IMPT method [26]. Table 6 presents the values of these components for some representative cases. These results show that the most important term in defining the size and sign of the interaction is the electrostatic component, which represents most of the interaction energy in the OH···O interactions of the q···q type. In the remaining types, the charge is also the largest one, followed in many cases by an important dispersion component, in general larger than the polarization and charge-transfer components. Notice that all these values refer to interaction energies.

4.3 Graph Sets: Motifs

A very useful tool in describing the complexities of the networks of hydrogen bonds in aggregates is to perform a graph set analysis of the hydrogen bond networks and define the *packing motifs*, a procedure first introduced by Etter [62, 63]. According to this procedure, any complex network of hydrogen bonds can be reduced to combinations of simple patterns: *chain*, *rings*, *self* (for intramolecular bonds), and *finite* (for patterns not propagated over the crystal), respectively, represented by the letters **C**, **R**, **S**, and **D**, shown in Fig. 8. The specification of a pattern is done using the following convention $\mathbf{L}_{d^a(n)}$, where **L** is a letter designating the simple pattern (either **C**, **R**, **S**, or **D**), the subscript d indicates the number of hydrogen bond donor groups in the pattern, the superscript a that indicates the number of hydrogen bond acceptor groups in the pattern, and n is the number of atoms in the pattern. Patterns containing only one type of hydrogen bond are called *motifs*. Originally hydrogen bonds were recognized using distance cut-off criteria, but a more strict form would be using the AIM method. These concepts can be easily extended to dimeric or more complex aggregates.

Table 6. Values of the H···O distance (in Å), IMPT energy components of the interaction energy (in kcal/mol; E_{el} , E_{er} , E_p , E_{ct} , and E_{disp} are, respectively, the electrostatic, exchange–repulsion, polarization, charge-transfer, and dispersion components, while E_{tot} is the sum of these components), type of hydrogen bond (four groups are present in this table: N···N where both fragments are neutral, ZW···ZW where both are zwitterions, q···N and q···q; in the last two groups, the charge in each fragment is indicated), and the BSSE-corrected MP2 interaction energy (E_{MP2}). Each complex is identified by the REFCODE of the crystal where the complex is found, sometimes followed by a number when different complexes are found within the same crystal

REFCODE	$r_{(H\cdots O)}$	E_{el}	E_{er}	E_{pol}	E_{ct}	E_{disp}	E_{tot}	Type	E_{MP2}
ACYGLI11	1.529	-26.12	25.77	-4.68	-4.68	-4.42	-14.13	N···N	-10.13
KECYBU02 -dim1	1.435	-24.49	37.12	-7.11	-5.23	-16.17	-19.88	N···N	-11.03
KECYBU02 -dim2	1.514	-21.71	28.22	-4.67	-3.87	-11.71	-13.74	N···N	-7.56
LYXOSE01	1.793	-11.50	10.63	-1.47	-1.78	-2.25	-6.37	N···N	-4.99
NALCYS02	1.513	-25.10	27.08	-4.33	-5.58	-4.43	-12.36	N···N	-9.02
OXALAC06	1.918	-9.45	8.02	-1.15	-0.72	-3.94	-7.24	N···N	-7.84
PERYTO10	1.790	-25.23	19.74	-2.24	-2.72	-4.58	-15.03	N···N	-9.18
RESORA	1.756	-14.84	14.29	-1.66	-1.51	-7.02	-10.74	N···N	-4.99
SUCACB02	1.688	-35.27	33.57	-5.46	-4.34	-14.52	-26.02	N···N	-13.42
UREAOH12	1.669	-19.46	19.07	-2.93	-2.30	-6.87	-12.49	N···N	-8.45
UREXPO11	1.619	-19.51	21.72	-3.19	-2.52	-6.65	-10.15	N···N	-6.38
UROXAL01	1.416	-43.13	46.15	-9.54	-6.18	-22.03	-33.73	N···N	-20.50
AEPHOS02	1.535	-73.80	59.05	-12.62	-8.50	-72.23	-111.10	ZW···ZW	-35.96
DLASPA02	1.508	-34.03	27.36	-6.62	-5.82	-4.18	-23.29	ZW···ZW	-17.31
DLSERN11	1.692	-46.93	30.15	-6.44	-4.20	-16.97	-44.39	ZW···ZW	-26.95
HOPROL12	1.843	-26.09	10.48	-3.05	-2.48	-2.54	-23.68	ZW···ZW	-19.30
KECROT01	1.348	-46.90	53.58	-17.07	-9.14	-30.08	-49.61	(-1)···N	-33.71
KHDFRM12	1.270	-70.93	72.05	-22.64	-12.02	-33.06	-66.60	(-1)···N	-48.70
KOXPY12	1.579	-35.32	28.86	-8.87	-4.78	-10.41	-30.43	(-2)···N	-25.23
NAOXAP11	1.582	-30.92	28.11	-8.70	-4.80	-10.43	-26.76	(-2)···N	-21.55
TGLYSU11 -dim2	1.406	-26.18	54.44	15.49	-13.48	-22.41	-23.12	(+1)···N	-41.56
18183(hco3-)	1.562	45.95	31.26	-7.80	-4.52	-11.34	53.55	(-1)···(-1)	58.89
EDATAR01	1.784	188.03	11.61	-8.55	-4.96	-2.73	183.40	(-2)···(-2)	190.02
LGLUTA	1.624	16.33	14.76	-3.94	-2.49	-2.64	22.02	(+1)···(+1)	25.32
NHOXAL02	1.537	25.37	31.44	-7.73	-4.23	-11.63	33.22	(-1)···(-1)	40.88
PUTRDP11	1.517	33.49	29.03	-7.87	-4.61	-11.21	38.83	(-1)···(-1)	52.13
TGLYSU11 -dim1	1.520	-155.10	31.44	-14.39	-6.16	-12.38	-156.60	(-2)···(+1)	-159.99

The list of all motifs found in a crystal constitutes the first-level or unitary graph set of that crystal, and is a sort of fingerprint of a crystal that can help to distinguish between different polymorphs of the same crystal (for instance Form 2 of the iminodiacetic acid crystal contains six motifs and its first-level graph set is $N_1 = \mathbf{DDC}(5)\mathbf{C}(5)\mathbf{C}(8)\mathbf{C}(8)$, while Form 1 has only three motifs and its first-level graph set is $N_1 = \mathbf{C}(5)\mathbf{C}(8)\mathbf{R}_2^2(10)$).

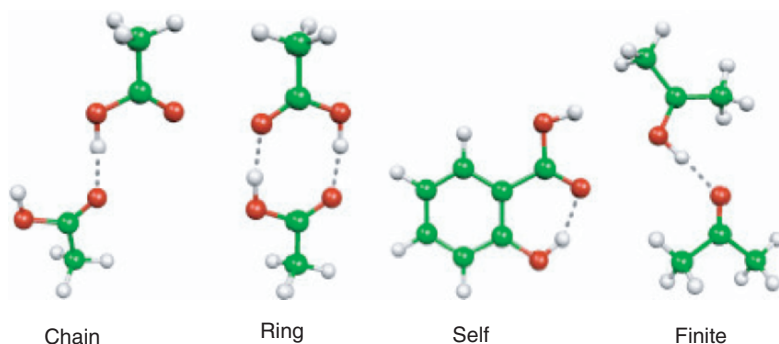


Figure 8. Basic types of motifs in Etter's graph set analysis [43, 44]. Represented from left to right is a $C(4)$, $R_2^2(8)$, S and D motif.

The use of motifs allows to have a rigorous, yet simple, language for the description of hydrogen bonds in molecules. Etter's rules can also be extended to allow a similar topological analysis of van der Waals bonds or even ionic bonds, thus having a full first-level graph set of the full intermolecular bonds within an aggregate. One can also use the motifs as conceptual tools to understand the structure of aggregates and crystals. This implies changing the concept of "bond" by the concept of "motif" as the driving force of our analysis. This is the idea behind the concept of *supramolecular synthons* [64], defined as energetically robust motifs that serve as the basis for the crystal structure by propagation of their structure. Again, a proper analysis of crystals in these terms also requires the computation of the strength of the implied motifs (obtained from the interaction energy of the molecules of the motif). In motifs presenting multiple bonds this calculation is even more straightforward than computing the interaction energy of the bonds that define the motif (due to the cooperative effects and that sometimes it is difficult to find realistic model systems where the bonds are properly represented). An understanding of the properties of the synthons requires a proper identification of the bonds that define the supramolecular synthon, and a good estimation of their energy (which can be done, in a first approach, by adding the energies of the constituent bonds, if possible corrected by the cooperative effects).

The interest of Etter's graph set analysis in describing the structural features of aggregates can be demonstrated with the following example, which corresponds to one of the *bc* planes of the NANQUO02 crystal [65] (see Fig. 9), where the name corresponds to the REFCODE of the crystal in the Cambridge Crystallographic Database [10]. However, the same analysis could be applied to an isolated aggregate.

The NANQUO02 crystal results from the aggregation of the 3,4-*bis*(dimethylamino)-3-cyclobutene-1,2-dione neutral molecules. Each molecule presents

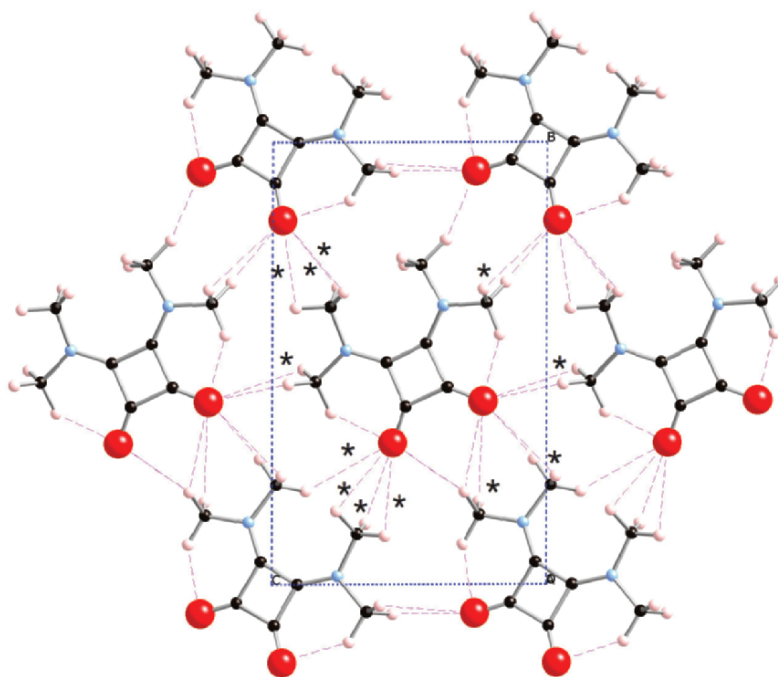


Figure 9. View along the a -axis of one of the bc planes of the NANQUO02 crystal. The dotted lines show the shortest distance $C-H \cdots O$ contacts. Notice that some of these contacts do not present bond-critical points and are not bonds. For the central molecule, we have marked with an * those $C-H \cdots O$ contacts that are not bonds. There are also short $C-H \cdots O$ contacts between adjacent planes, not shown in the figure.

two $C=O$ acceptor groups and four methyl groups, each one having three $C-H$ proton donor groups. The central molecule makes 21 $C-H \cdots O$ contacts in the 2.0–3.5 Å range. An AIM analysis of the electron density [65] shows that only nine of them are $C-H \cdots O$ bonds. Therefore, the 12 nonbonding $C-H \cdots O$ contacts are short because of the packing that the crystal presents but are not responsible for the energetic stability of the packing. However, they can affect the crystal packing; their destabilizing interaction avoids the two molecules participating in the short contact getting closer.

Using Etter's rules, the topological connections that form the hydrogen bonds can be classified as $R_2^2(9)$ (identified in Fig. 10 as $R(9)$, for simplicity), S , and $C(7)$. One of the $R_2^2(9)$ motifs is more complex as it presents a bifurcated $C-H \cdots O$ bond against the two acceptor groups. Thus, it is composed of two $R_2^1(6)R_1^2(5)$ motifs sharing one of their sides. The overall packing that these motifs induce is easily described as $R_2^2(9)$ dimers, laterally connected by the $C(7)$ motifs. The S motifs only help to make the geometry of the molecules more strongly coplanar.

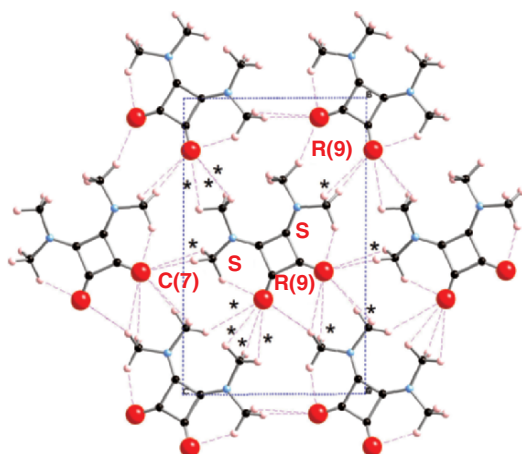


Figure 10. Motifs found within the NANQUO02 crystal. For simplicity of representation, the $\mathbf{R}_2^2(9)$ motifs are indicated as $\mathbf{R}(9)$.

4.4 Cooperativity

Many of the properties of n interconnected hydrogen bonds are different than that of n -times the sum of each individual bond. This effect is called *cooperativity*, and originates in the polarization that is induced in the donor and acceptor groups of one molecule due to the participation of this molecule in other hydrogen bonds. Such an effect makes that the strength estimated for the bonds in the isolated dimers (or isolated motifs) is smaller than that found in aggregates where multiple bonds can be found.

The importance of cooperative effects (sometimes called nonadditive effects) on bonds found in aggregates can be understood by comparing the experimental formation energy of the OH···O bond in an isolated water dimer (-5.44 kcal/mol [56]) against the formation energy per water molecule of the same bond in ice at 0 K (-11.3 kcal/mol [66]). While dimers can be formed with only one intermolecular bond, the transition from isolated dimers to crystals is only possible when the molecules that form the dimer can also form more intermolecular bonds with other molecules. For instance, in ice I_h polymorph (the polymorphic form of solid water at normal pressure and temperature), each water molecule makes four hydrogen bonds, two as donor and two as acceptor.

Cooperative effects are also found when doing calculations. They are clearly manifested by looking at the data of Table 7 and Fig. 11 where the formation energy per water molecule computed for $(\text{H}_2\text{O})_n$ clusters using good quality basis sets and methods that work well on the water dimer is presented. The curves can be fitted by an $A + B/n$ expression (A and B are constants) and

Table 7. Formation energy *per water molecule* computed for various $(\text{H}_2\text{O})_n$ clusters at the HF/aug-cc-pVDZ [49], MP2/aug-cc-pVDZ [49], and BLYP/TZVP levels [67]. The first two sets are BSSE-corrected results, while those for the BLYP data are noncorrected values (for a DFT calculation with a basis set of this quality, the BSSE is expected to be very small [52]). All values in kcal/mol

Complex	HF	MP2	BLYP
$(\text{H}_2\text{O})_2$	-1.83	-2.32	-2.63
$(\text{H}_2\text{O})_3$	-3.67	-4.62	-5.58
$(\text{H}_2\text{O})_4$	-4.88	-6.08	-7.56
$(\text{H}_2\text{O})_5$	-5.19		-8.03
$(\text{H}_2\text{O})_6$	-5.40		-8.13
$(\text{H}_2\text{O})_7$			-8.56
$(\text{H}_2\text{O})_8$			-9.64
$(\text{H}_2\text{O})_9$			-9.18
$(\text{H}_2\text{O})_{10}$			-9.43
$(\text{H}_2\text{O})_{12}$			-10.12
$(\text{H}_2\text{O})_{16}$			-10.40
$(\text{H}_2\text{O})_{20}$			-10.57

converge to -11.39 kcal/mol as the size n is increased. Such a value is close to the experimental formation energy per water molecule of ice at 0 K (-11.3 kcal/mol [66]). This fact is consistent with studies on infinite polymers [68] (imposing periodic boundary conditions); a formation energy per hydrogen bond of -5.48 kcal/mol was found at the HF level, which becomes -6.84 kcal/

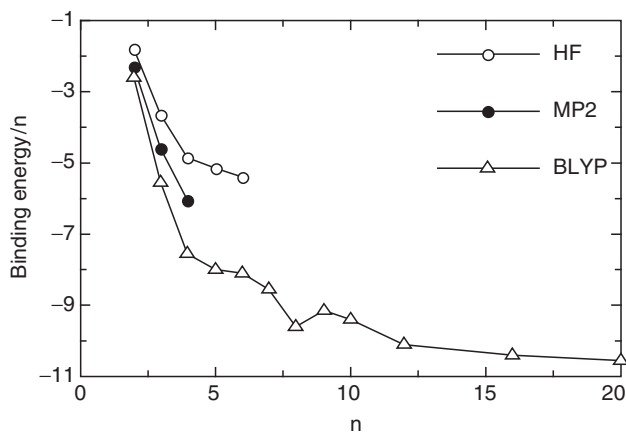


Figure 11. Variation of the bonding energy per molecule (in kcal/mol) with the size of the $(\text{H}_2\text{O})_n$ cluster. Three results have been computed at the following levels: HF/aug-cc-pVDZ [49], MP2/aug-cc-pVDZ [49], and BLYP/TZVP levels [67].

mol at the MP2 level (at the HF and MP2 levels the formation energy per hydrogen bond is -3.6 kcal/mol and -4.50 kcal/mol, respectively). We thus have a clear indication that these computational methods can reproduce the strength of the O–H···O hydrogen bond in isolated dimers and in molecular aggregates.

Cooperative effects are proportional to the polarizability of the molecules that participate in the aggregate. They can be computed but no good theory is currently available to estimate them. In the meantime, for qualitative analysis one can still use the values for bonds obtained in isolated dimers and motifs, specially if they are done on systems that present a similar polarizability.

5 THE NATURE OF THE C–H···X INTERACTIONS IN CRYSTALS

5.1 C–H···O Interactions

The prototypical example of C–H···X weak hydrogen bonds is found in the C–H···O interactions. As illustrated above in Figs. 9 and 10, not all C–H···O interactions present all the features that one would expect for a hydrogen bond, but many of them do and it is appropriate to call them C–H···O hydrogen bonds. Another example of C–H···O interactions that do not present all the properties of a hydrogen bond is found when the contact is made between anionic monomers, hereafter identified as the C–H⁽⁻⁾···O⁽⁻⁾ interaction. Here we will focus our attention on those C–H···O interactions that can be classified as bonds, and in the next section we will address our attention to those that are not hydrogen bonds.

After some initial controversy [69], enough conclusive spectroscopic [70, 71] and crystallographic [72] evidence provided support to the hydrogen bond nature of the C–H···O interactions, and today there is a general consensus on such hydrogen bonded nature [73, 74]. Such consensus is also supported by theoretical calculations. Thus, the methane–water complex is energetically stable and in its optimum MP2/aug-cc-pVDZ geometry shows a C–H···O bond critical point (see Fig. 12). Therefore, like in the O–H···O bond found in the water dimer, the two conditions required by the definition of hydrogen bond are also fulfilled here.

There is a consensus that C–H···O bonds energy are typically similar to those of van der Waals bonds [38] or just a bit stronger than these bonds (a maximum value of 2 kcal/mol has been suggested as threshold for a typical C–H···O bond [74]). A look at the most representative results published on C–H···O interactions (Table 8) suggests that such threshold should be increased a bit (the maximum BSSE-corrected result at the MP2 level is 6.9 kcal/mol), but in any case, these values are weaker than the energy scale reported before for O–H···O bonds (Table 6 and Fig. 7). This explains that these bonds are commonly accepted to play the role of secondary interactions in aggregates and crystals [74]. However, due to the use of small basis sets in

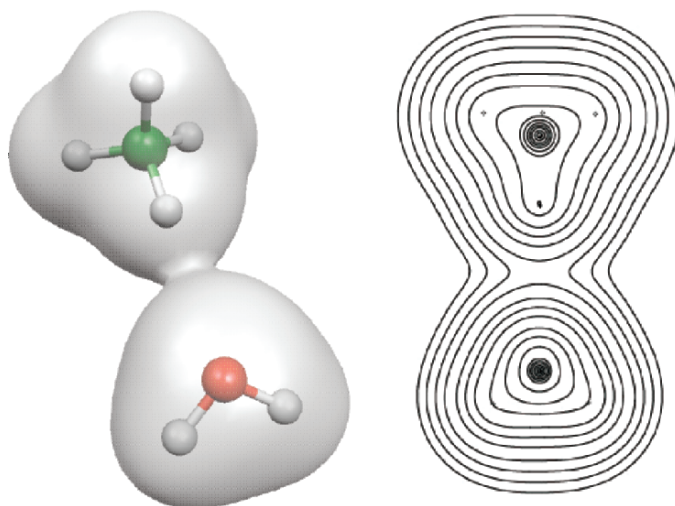


Figure 12. Left: Optimum geometry of the methane–water complex, showing the electron density surface of 0.005 a.u. Right: Cut of the electronic density in the C–H···O plane, showing the position of the H···O bond critical point.

some of the calculations, the results lack a uniform quality, a fact that makes difficult doing comparisons between different complexes.

5.2 Methodology for the Calculation of C–H···O Interactions

As in the case of moderate hydrogen bonds, we tested the quality of the most popular methods and basis sets, using as test system, the methane–water complex (Fig. 13), at the optimum computed at the MP2/aug-cc-pVDZ level. Table 9 lists the MP2 interaction energy results obtained with various basis sets (these results are also plotted in Fig. 14), while Table 10 lists the values obtained with various methods and the aug-cc-pVDZ basis set (notice that the formation energy and interaction energy are nearly identical for these weakly interacting complexes, as the fragments have a nearly identical geometry when isolated or in the complex). As in the O–H···O case, the data in Table 9 and Fig. 14 show the convergence of the MP2 values towards a limit value (in this case, 0.59 kcal/mol) as the basis set quality is improved. Notice that the BSSE-corrected MP2 interaction energy computed with a valence triple-zeta plus polarization and diffuse basis set as 6–311+G(d,p) is only half of that value. Concerning the evaluation of the methods, Table 10 shows that the MP2 method gives similar results to the MP4 or CCSD(T). However, the HF and B3LYP methods fail to produce energetically stable dimers when the BSSE-error is corrected and gives values of the BSSE-uncorrected energy that are too weak.

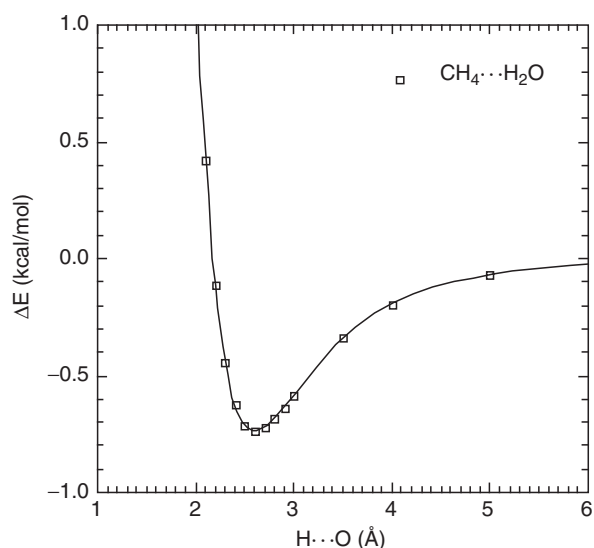


Figure 13. Interaction energy curve of a methane–water complex oriented as shown in Fig. 12. The curve has been computed at the MP2/aug-cc-pvTZ level and the interaction energy has been corrected by the BSSE.

Table 8. Theoretical data available on the literature about C–H···X interactions. The complex, method and basis set, H···O optimum distance, and non-BSSE corrected (E) and BSSE-corrected (E_{CP}) formation energies are given for each complex, together with the reference from which the data are extracted (the references are given at the end of this table ordered from less to more recent)

Complex	Method/basis set	$r_{(\text{H}\cdots\text{X})}$	E	E_{CP}	Reference
(CH ₃) ₂ NCOH···	MP2/aug-cc-pVDZ	1.799	−8.95	−8.12	REF26
HNCO(CH ₃) ₂					
C ₂ H ₂ ···C ₆ H ₆	MP2/6-31g(d,p)		−1.6		REF23
C ₂ H ₂ ···C ₂ H ₂	MP2/DZP	3.008	−0.43	−0.35	REF4
C ₂ H ₂ ···C ₂ H ₂	HF/6-311++g**	3.073	−0.69	−0.58	REF28
C ₂ H ₂ ···C ₂ H ₂	MP2/6-31g**	2.62		−0.9	REF14
C ₂ H ₂ ···CH ₃ Ph	MP2/6-31g**	2.77		−1.4	REF14
C ₂ H ₂ ···CH ₄	MP2/6-311+g(3df,2p)	2.724	−0.57	−0.07	REF25
	B3LYP/6-311+g(3df,2p)	3.131	−0.50	−0.28	
C ₂ H ₂ ···NH ₃	MP2/6-311+g(3df,2p)	2.275	−3.34	−2.20	REF25
	B3LYP/6-311+g(3df,2p)	2.308	−3.37	−2.22	
C ₂ H ₂ ···NH ₃	MP2/6-311+g(3df,2p)	2.608	−1.17	−0.50	REF25
	B3LYP/6-311+g(3df,2p)	2.740	−1.17	−0.45	
C ₂ H ₂ ···O ₃	MP2/D95++(d,p)	2.798	−1.76	−0.85	REF11
C ₂ H ₂ ···OCH ₂	MP2/D95++(d,p)	2.251	−3.57	−2.26	REF11
C ₂ H ₂ ···OH ₂	MP2/6-31++g(2d,2p)	2.198	−3.46	−2.51	REF15
	MP4/6-31++g(2d,2p)		−3.70	−2.48	

(Continued)

Table 8. —(Continued)

Complex	Method/basis set	$r_{(H...X)}$	E	E_{cp}	Reference
$C_2H_2 \cdots OH_2$	MP2/6-311+g(3df,2p)	2.184	-2.63	-1.65	REF25
	B3LYP/6-311+g(3df,2p)	2.228	-2.65	-1.70	
$C_2H_2 \cdots OH_2$	MP2/6-311+g(3df,2p)	2.454	-1.00	-0.36	REF25
	B3LYP/6-311+g(3df,2p)	2.596	-1.03	-0.41	
$C_2H_2 \cdots OH_2$	HF/6-311++g**	2.278	-2.50	-2.05	REF28
$C_2H_2 \cdots OH_2$	MP2/D95++(d,p)	2.191	-3.93	-2.73	REF11
$C_2H_2 \cdots SH_2$	MP2/6-311+g(3df,2p)	2.837	-1.29	-0.60	REF25
	B3LYP/6-311+g(3df,2p)	2.958	-1.34	-0.67	
$C_2H_2 \cdots SH_2$	MP2/6-311+g(3df,2p)	3.187	-0.55	-0.14	REF25
	B3LYP/6-311+g(3df,2p)	3.399	-0.57	-0.02	
$C_2H_3(NH_2)_3 \cdots OH_2$	MP2/6-311+g(2d,2p)		-1.28	-0.85	REF21
$C_2H_3(OH)_3 \cdots OH_2$	MP2/6-311+g(2d,2p)		-3.09	-2.65	REF21
$C_2H_3F_3 \cdots OH_2$	MP2/6-311+g(2d,2p)		-1.01	-0.63	REF21
$C_2H_4(NH_2)_2 \cdots OH_2$	MP2/6-311+g(2d,2p)		-1.14	-0.73	REF21
$C_2H_4(OH)_2 \cdots OH_2$	MP2/6-311+g(2d,2p)		-2.69	-2.27	REF21
$C_2H_4 \cdots OH_2$	MP2/6-31++g(2d,2p)	2.472	-1.50	-0.94	REF15
	MP4/6-31++g(2d,2p)		-1.57	-0.93	
$C_2H_4F_2 \cdots OH_2$	MP2/6-311+g(2d,2p)		-0.83	-0.46	REF21
$C_2H_5(NH_2) \cdots OH_2$	MP2/6-311+g(2d,2p)		-1.02	-0.64	REF21
$C_2H_5(OH) \cdots OH_2$	MP2/6-311+g(2d,2p)		-1.08	-0.74	REF21
$C_2H_5F \cdots OH_2$	MP2/6-311+g(2d,2p)		-0.70	-0.35	REF21
$C_2H_6 \cdots NH_3$	MP2/6-311+g(3df,2p)	2.809	-0.62	-0.21	REF25
	B3LYP/6-311+g(3df,2p)	3.076	-0.60	-0.12	
$C_2H_6 \cdots OH_2$	MP2/6-311+g(2d,2p)		-0.63	-0.32	REF21
$C_2H_6 \cdots OH_2$	MP2/6-311+g(3df,2p)	3.738	-0.50	-0.07	REF25
	B3LYP/6-311+g(3df,2p)	3.968	-0.50	-0.02	
$C_6H_6 \cdots C_6H_6$	HF/STO-g + 1/r ⁶	3.97		-5.26	REF2
$C_6H_6 \cdots C_6H_6$	MP2/6-311g(2d,2p)		-5.75	-3.20	REF17
$C_6H_6 \cdots C_6H_6$	NEMO	5.21	-1.7		REF18
$C_6H_6 \cdots C_6H_6$	NEMO	5.19	-1.2		REF18
$C_6H_6 \cdots C_6H_6$	MP2/aug-cc-pvVTZ _(C) / cc-pVDZ _(H)		-2.96		REF19
	MP4/aug-cc-pVDZ _(C) / cc-pVDZ _(H)		-2.48		
	CCSD(T)/aug-cc-pVDZ _(C) / cc-pVDZ _(H)		-2.17		
	MP2/6-31g(d,p)		-1.2		REF23
$CCl_2H_2 \cdots Cl^-$	MP2/6-31+g(d,p)	2.288	-13.82	-11.74	REF30
$CCl_2H_2 \cdots F^-$	MP2/6-31+g(d,p)	1.545	-23.59	-23.16	REF30
$CCl_2H_2 \cdots OH^-$	MP2/6-31+g(d,p)	1.607	-	-	REF30
			24.34	22.75	
$CCl_2H_2 \cdots OH_2$	HF/4-31g + 1/r ⁶			-6.4	REF3
$CCl_2H_2 \cdots OH_2$	MP2/6-31+g(d,p)	2.227 ^c		-3.78	REF29
		3.388 ^c			
$CCl_3H \cdots C_6H_6$	MP2/6-31g(d,p)		-3.2		REF23
$CCl_3H \cdots Cl^-$	MP2/6-31+g(d,p)	2.126	-18.24	-15.0	REF30
$CCl_3H \cdots F^-$	MP2/6-31+g(d,p)	1.379	-31.04	-32.68	REF30
$CCl_3H \cdots H_2O$	MP2/6-31+g(d,p)	2.077		-3.68	REF29

Complex	Method/basis set	$r_{(H\cdots X)}$	E	E_{cp}	Reference
CCl ₃ H···OH [−]	MP2/6–31+g(d,p)	1.431	−32.42	−33.07	REF30
CCl ₃ H···OH ₂	HF/4–31g + 1/r ⁶			−8.1	REF3
CCl ₃ H···OH ₂	MP2/aug-cc-pVDZ		−3.79	−2.96	This work
CCl ₄ ···OH ₂	HF/4–31g + 1/r ⁶			−1.1	REF3
CClH ₃ ···OH ₂	HF/4–31g + 1/r ⁶			−5.6	REF3
CClH ₃ ···OH ₂	MP2/6–31+g(d,p)	2.437 ^c		−2.76	REF29
		2.599 ^c			
CF ₂ H ₂ ···CH ₂ O	HF/aug-cc-pVDZ			−1.79	REF24
	MP2/aug-cc-pVDZ			−2.04	
	B3LYP/6–311+g(d,p)			−1.89	
CF ₂ H ₂ ···CH ₃ OH	HF/aug-cc-pVDZ			−1.89	REF24
	MP2/aug-cc-pVDZ			−2.52	
	B3LYP/6–311+g(d,p)			−2.63	
CF ₂ H ₂ ···Cl [−]	MP2/6–31+g(d,p)	2.467	−12.54	−11.52	REF30
CF ₂ H ₂ ···F [−]	MP2/6–31+g(d,p)	1.699	−20.22	−20.41	REF30
CF ₂ H ₂ ···OH [−]	MP2/6–31+g(d,p)	1.802	−21.03	−20.36	REF30
CF ₂ H ₂ ···OH ₂	MP2/6–311+g(2d,2p)		−1.86	−1.48	REF21
CF ₂ H ₂ ···OH ₂	HF/aug-cc-pVDZ			−1.85	REF24
	MP2/aug-cc-pVDZ			−2.24	
	B3LYP/6–311+g(d,p)			−2.48	
CF ₂ H ₂ ···OH ₂	MP2/6–31+g(d,p)	2.39		−2.13	REF13
CF ₂ H ₂ ···OH ₂	MP2/6–31+g(d,p)	2.408 ^c		−3.40	REF29
		2.249 ^c			
CF ₃ H···Cl [−]	MP2/6–31+g(d,p)	2.252	−16.62	−15.11	REF30
CF ₃ H···F [−]	MP2/6–31+g(d,p)	1.537	−27.65	−29.26	REF30
CF ₃ H···H ₂ O	MP2/6–31+g(d,p)	2.164		−3.72	REF29
CF ₃ H···OH [−]	MP2/6–31+g(d,p)	1.625	−27.59	−27.82	REF30
CF ₃ H···OH ₂	MP2/6–311+g(2d,2p)		−2.87	−2.45	REF21
CF ₃ H···OH ₂	MP2/6–31g(d,p)	2.28		−3.16	REF13
CFH ₃ ···CH ₃ F ^a	MP2(fc)/6–31+g(d,p)	2.461 ^d		−1.36	REF30
		2.461 ^d			
CFH ₃ ···CH ₂ O	HF/aug-cc-pVDZ			−0.90	REF24
	MP2/aug-cc-pVDZ			−1.20	
	B3LYP/6–311+g(d,p)			−0.97	
CFH ₃ ···CH ₃ OH	HF/aug-cc-pVDZ			−0.89	REF24
	MP2/aug-cc-pVDZ			−1.42	
	B3LYP/6–311+g(d,p)			−1.34	
CFH ₃ ···OH ₂	MP2/6–311+g(2d,2p)		−1.04	−0.71	REF21
CFH ₃ ···OH ₂	HF/aug-cc-pVDZ			−0.89	REF24
	MP2/aug-cc-pVDZ			−1.23	
	B3LYP/6–311+g(d,p)			−1.28	
CFH ₃ ···OH ₂	MP2/6–31g(d,p)	2.51		−1.41	REF13
CFH ₃ ···OH ₂	MP2/6–31+g(d,p)	2.620 ^c		−3.76	REF29
		2.016 ^c			
CFH ₃ ···OH ₂	MP2/6–31+g(d,p)	2.620		−3.76	REF29
CH ₃ NH ₂ ···OH ₂	MP2/DZP'		−0.61		REF16
CH ₃ NH ₃ ⁺ ···OH ₂	MP2/DZP'		−9.3		REF16
CH ₄ ···C ₅ NH ₅	MP2/6–31g(d,p)			0.65	REF22

(Continued)

Table 8. —(Continued)

Complex	Method/basis set	$r_{(\text{H}\cdots\text{X})}$	E	E_{cp}	Reference
$\text{CH}_4 \cdots (\text{OH}_2)_n$	MP2/6-31++g** $n = 1$			-0.37	REF12
	$n = 2$			-0.61	
	$n = 3$			-0.86	
$\text{CH}_4 \cdots \text{Br}^{-\text{b}}$	MP2/6-31++g(d,p)	4.074	-2.96	-1.76	REF7
$\text{CH}_4 \cdots \text{C}_5\text{NH}_5$	MP2/6-31g(d,p)			1.87	REF22
$\text{CH}_4 \cdots \text{C}_6\text{H}_6$	MP2/6-31g(d,p)		-0.4		REF23
$\text{CH}_4 \cdots \text{CH}_2\text{O}$	HF/aug-cc-pVDZ			-0.14	REF24
	MP2/aug-cc-pVDZ			-0.46	
	B3LYP/6-311+g(d,p)			-0.14	
$\text{CH}_4 \cdots \text{CH}_3\text{OH}$	HF/aug-cc-pVDZ			-0.16	REF24
	MP2/aug-cc-pVDZ			-0.63	
	B3LYP/6-311+g(d,p)			-0.30	
$\text{CH}_4 \cdots \text{Cl}^-$	MP2/6-31++g(d,p)	3.838	-4.23	-2.15	REF7
$\text{CH}_4 \cdots \text{Cl}^-$	MP2/6-31+g(d,p)	2.730	-2.45	-1.58	REF30
$\text{CH}_4 \cdots \text{CN}^-$	MP2/6-311++g(2d,2p)	2.678	-2.43	-2.17	REF9
$\text{CH}_4 \cdots \text{F}^-$	MP2/6-31++g(d,p)	3.028	-6.06	-5.26	REF7
$\text{CH}_4 \cdots \text{F}^-$	MP2/6-31+g(d,p)	1.955	-5.57	-4.78	REF30
$\text{CH}_4 \cdots \text{HC}_2\text{H}$	MP2/6-311+g**	3.22	-0.58		REF6
$\text{CH}_4 \cdots \text{HCH}_3$	MP2/6-311+g**	2.74	-0.20		REF6
$\text{CH}_4 \cdots \text{I}^{-\text{b}}$	MP2/6-31++g(d,p)	4.246	-2.34	-1.14	REF7
$\text{CH}_4 \cdots \text{NC}^-$	MP2/6-311++g(2d,2p)	2.451	-2.83	-2.45	REF9
$\text{CH}_4 \cdots \text{OH}^-$	MP2/6-31+g(d,p)	2.040	-5.90	-4.55	REF30
$\text{CH}_4 \cdots \text{OH}_2$	STO-3g		-1.81		REF1
$\text{CH}_4 \cdots \text{OH}_2$	MP2/SZ(3P+bond,P)		-0.69	-0.49	REF5
$\text{CH}_4 \cdots \text{OH}_2$	HF/4-31g + 1/r ⁶			-0.7	REF3
$\text{CH}_4 \cdots \text{OH}_2$	MP2/6-31++g(2d,2p)	2.631	-0.86	-0.42	REF15
	MP4/6-31++g(2d,2p)		-0.95	-0.43	
	MP2/6-311+g(2d,2p)		-0.51	-0.25	REF21
$\text{CH}_4 \cdots \text{OH}_2$	HF/aug-cc-pVDZ			-0.16	REF24
	MP2/aug-cc-pVDZ			-0.43	
	B3LYP/6-311+g(d,p)			-0.26	
$\text{CH}_4 \cdots \text{OH}_2$	MP2/6-311+g**	2.70	-1.08		REF6
$\text{CH}_4 \cdots \text{OH}_2$	MP2/6-31++g(2d,2p)	2.676	-0.72	-0.42	REF8
$\text{CH}_4 \cdots \text{OH}_2$	MP2/DZP		-0.53		REF16
$\text{CH}_4 \cdots \text{OH}_2$	MP2/S		-0.49		REF10
$\text{CH}_4 \cdots \text{OH}_2$	MP2/6-31+g(d,p)	2.507		-0.29	REF29
$\text{CH}_4 \cdots \text{SeH}_2$	MP2/6-311g**	4.34	-0.26		REF6
$\text{CH}_4 \cdots \text{SH}_2$	MP2/SZ(3P+bond,P)		-0.82	-0.67	REF5
$\text{CH}_4 \cdots \text{SH}_2$	MP2/6-31++g(2d,2p)	3.260		-0.24	REF20
$\text{CH}_4 \cdots \text{SH}_2$	MP2/6-311g**	3.96	-0.48		REF6
$\text{CH}_4 \cdots \text{TeH}_2$	MP2/3-21g	3.75	-0.93		REF6
$\text{H}_2\text{NCOH} \cdots \text{H}_2\text{NCOH}$	MP2/aug-cc-pVTZ	2.320	-3.12	-2.39	REF26
$\text{HCO}_2\text{H} \cdots \text{O}_2\text{HCH}$	HF/6-311++g**	1.864	-6.09	-5.74	REF28
$\text{MePy}^+ \cdots \text{O}_2\text{P}(\text{OMe})_2^{\text{a}}$	MP2/6-311++g**	2.079 ^c	-93.1	-88.1	REF27
		1.956 ^c			
		2.241 ^c			
		2.528 ^c			

Complex	Method/basis set	$r_{(\text{H}\cdots\text{X})}$	E	E_{cp}	Reference
MePy ⁺ ···O ₂ P(OMe) ₂ ^a	MP2/6-311++g**	1.931 ^f 1.810 ^f	–84.2	–79.6	REF27
MePy ⁺ ···OMe ₂ ^a	MP2/6-311++g**	2.050 ^g 2.311 ^g	–12.2	–10.0	REF27
MePy ⁺ ···OMe ₂ ^a	MP2/6-311++g**	2.004	–9.2	–7.5	REF27
NCH···O ₃	MP2/D95++(d,p)	2.680	–2.18	–1.48	REF11
NCH···OCH ₂	MP2/D95++(d,p)	2.106	–4.97	–3.90	REF11
NCH···OH ₂	MP2/D95++(d,p)	2.051	–6.22	–4.95	REF11

^a Complexes where the interaction energies were calculated taking into account the ZPE: DE+ZPE

^b Values obtained with use of pseudopotential cores

^c R₂²(5) complex forming a ring with two O···H bonds

^d R₂¹(6) complex forming a ring with two O···H bonds

^e R₂¹(6)R₂¹(4)R₂¹(6) complex forming three rings with four O···H bonds

^f R₂²(7) complex forming a ring with two O···H bonds

^g R₂¹(6) complex forming a ring with two O···H bonds

- REF1 Ungemach, S. R. and Schaefer, H. F. (1974) The weak attraction between water and methane, *J. Am. Chem. Soc.*, **96**, 7898–7901
- REF2 Karlström, G., Linse, P., Wallqvist, A. and Johnson B. (1983) Intermolecular potentials for H₂O–C₆H₆ and the C₆H₆–C₆H₆ system calculates in an ab initio SCF CI approximation, *J. Am. Chem. Soc.*, **105**, 3777–3782
- REF3 Hobza, P. and Sandorfy, C. (1984) Quantum chemical and statistical thermodynamic investigation of anesthetic activity. 3. The interaction between CH₄, CH₃ClCH₂Cl₂, CHCl₃, CCl₄ and an O–H···O hydrogen bond., *Can. J. Chem.*, **62**, 606–609
- REF4 Alberts, I. L., Rowlands, T. W. and Handy, N. C. (1988) Stationary points on the potential energy surfaces of (C₂H₂)₂, (C₂H₂)₃ and (C₂H₄)₂, *J. Chem. Phys.*, **88**, 3811–3816
- REF5 Woon, D. E., Zeng, P. and Beck, D. R. (1990) Ab initio potentials and pressure second virial coefficients for CH₄–H₂O and CH₄–H₂S, *J. Phys. Chem.*, **93**, 7808–7812
- REF6 Novoa, J. J., Whangbo, M.-H. and Williams, J. M. (1990) Ab initio computational study of the C–H···donor and C–H···anion contact interactions in organic donor salts, *Mol. Cryst. Liq. Cryst.*, **181**, 25–42
- REF7 Novoa, J. J., Whangbo, M.-H. and Williams J. M. (1991) Interaction energies associated with short intermolecular contacts of C···H bonds. 4. Ab initio computational study of C–H···anion interactions in CH₄···X[–] (X = F, Cl, Br, I), *Chem. Phys. Lett.*, **180**, 241–248
- REF8 Novoa, J. J., Tarron, B., Whangbo, M.-H. and Williams, J. M. (1991) Interaction energies associated with short intermolecular contacts of C–H bonds. Ab initio computational study of the C–H···O contact interaction in CH₄···OH₂, *J. Chem. Phys.*, **95**, 5179–5186
- REF9 Novoa, J. J., Whangbo, M.-H. and Williams, J. M. (1991) Interaction energies associated with short intermolecular contacts of C–H bonds. Structure and energetics of the interactions between CH₄ and CN[–], *Chem. Phys. Lett.*, **177**, 483–490.
- REF10 Szeceśniak, M. M., Chalasinski, G., Cybulski, S. M. and Cieplak, P. (1992) Ab initio study of the potential energy surface of CH₄–H₂O, *J. Chem. Phys.*, **98**, 3078–3089
- REF11 Turi, L. and Dannenberg, J. J. (1993) Molecular orbital studies of C–H···O hydrogen-bonded complexes, *J. Phys. Chem.*, **97**, 7899–7909
- REF12 Novoa, J. J., Costans, P. and Whangbo, M.-H. (1993) On the Strength of the C–H···O hydrogen bond and eclipsed arrangement of the methyl group in a tricyclic orthoamide trihydrate, *Angew. Chem. Int. Ed. Engl.*, **32**, 588–889
- REF13 Alkorta, I. and Maluendes, S. (1995) Theoretical study of CH···O hydrogen bonds in H₂O–CH₃F, H₂O–CH₂F₂, and H₂O–CHF₃, *J. Phys. Chem.*, **99**, 6457–6460

- REF14 Steiner, T., Starikov, E. B., Amado, A. M. and Teixeira-Dias, J. J. C. (1995) Weak hydrogen bonding. Part 2. The hydrogen bonding nature of short C–H··· π contacts: crystallographic, spectroscopic and quantum mechanical studies of some terminal alkynes, *J. Chem. Soc. Perkin Trans.*, **2**, 1321–1326
- REF15 Rovira, M. C., Novoa, J. J., Whangbo, M.-H. and Williams, J. M. (1995) Ab initio computation of the potential energy surfaces of the water···hydrocarbon complexes H₂O···C₂H₂, H₂O···C₂H₄ and H₂O···CH₄: minimum energy structures, vibrational frequencies and hydrogen bond energies, *Chem. Phys.*, **200**, 319–335
- REF16 van Mourik, T. and van Duijneveldt, F. B. (1995) Ab initio calculations on the C–H···O hydrogen-bonded systems CH₄–H₂O, CH₃NH₂–H₂O, CH₃NH₃⁺–H₂O, *J. Mol. Struct.: Theochem.*, **341**, 63–73
- REF17 Tsuzuki, S., Uchimaru, T., Mikami, M. and Tanabe K. (1996) Basis set effects on the calculated bonding energies of neutral benzene dimers: importance of diffuse polarization functions, *Chem. Phys. Lett.*, **252**, 206–210
- REF18 Spirko, V., Engkvist, O., Soldán, P., Sezle, H. L., Schlag, W. and Hobza, P. (1999) Structure and vibrational dynamics of the benzene dimer, *J. Chem. Phys.*, **111**, 572–582
- REF19 Hobza, P., Sezle, H. L. and Schlag, W. (1996) Potential energy surface for benzene dimer. Results of ab initio CCSD(T) calculations show two nearly isoenergetic structures: T-shaped and parallel-displaced, *J. Phys. Chem.*, **100**, 18790–18794
- REF20 Novoa, J. J. and Rovira, M. C. (1997) Strength and directionality of the C(sp³)–H···S(sp³) interaction. Ab initio study using the H₂S···CH₄ model complex., *Chem. Phys. Lett.*, **279**, 140–150
- REF21 Novoa, J. J. and Mota, F. (1997) Substituent effects in intermolecular C(sp³)–H O(sp³) contacts: how strong can a C(sp³)–HO(sp³) hydrogen bond be? *Chem. Phys. Lett.*, **266**, 23–30
- REF22 Samanta, U., Chakrabarti, P. and Chandrasekhar, J. (1998) Ab initio study of energetics of X–H··· π (X = N, O and C) interactions involving a heteroaromatic ring, *J. Phys. Chem.*, **102**, 8964
- REF23 Cubero, E., Orozco, M., Hobza, P. and Luque, F. J. (1999) Hydrogen bond versus anti-hydrogen bond: a comparative analysis based on the electron density topology, *J. Phys. Chem. A*, **103**, 6394–6401
- REF24 Gu, Y., Kar, T. and Scheiner, S. (1999) Fundamental properties of the CH···O interaction: is it a true hydrogen bond? *J. Am. Chem. Soc.*, **121**, 9411–9422
- REF25 Hartmann, M., Wetmore, S. D. and Radom, L. (2001) C–H···X hydrogen bonds of acetylene, ethylene, and ethane with first- and second-row hydrides, *J. Phys. Chem. A*, **105**, 4470–4479
- REF26 Vargas, R., Garza, J., Friesner, R. A., Stern H., Hay, B. J. and Dixon, A. D. (2001) Strength of N–H···O=C and C–H···O=C Bonds in formamide and N-methylacetamide dimers, *J. Phys. Chem. A*, **105**, 4936–4968
- REF27 Raymo, F. M., Bartberger, M. D., Houk, K. N. and Stoddart, J. F. (2001) The magnitude of [C–H···O] hydrogen bonding in molecular and supramolecular assemblies, *J. Am. Chem. Soc.*, **123**, 9264–9267
- REF28 Grabowski, S. J. (2001) Ab initio calculations on conventional and unconventional hydrogen bonds—study of the hydrogen bonds strength, *J. Phys. Chem. A*, **105**, 10739–10746
- REF29 Kryachko, E. S. and Zeegers-Huyskens, T. (2001) Theoretical study of the C–H···O interaction in fluoromethanes·H₂O and chloromethanes·H₂O complexes, *J. Phys. Chem. A*, **105**, 7118–7125
- REF30 Kryachko, E. S. and Zeegers-Huyskens, T. (2002) Theoretical study of the C–H···X[–] interaction of fluoromethanes and chloromethanes with fluoride, chloride and hydroxide anions, *J. Phys. Chem. A*, **106**, 6832–6838
- REF31 Kryachko, E. S. and Scheiner, S. (2004) C–H···F Hydrogen bonds of fluoromethanes, *J. Phys. Chem. A*, **108**, 2527–2535

Table 9. C–H···O interaction energy computed for the methane–water complex using the MP2 method. The BSSE-uncorrected (E) and BSSE-corrected (E_{CP}) energies are given in kcal/mol. The BSSE is also indicated. The geometry is the optimum MP2/aug-cc-pVTZ geometry

Basis set	E	E_{CP}	BSSE
3-21g	−3.42	−0.42	3.00
6-31g	−1.24	−0.31	0.93
6-31+g	−0.83	−0.27	0.56
6-31+g(d)	−0.80	−0.30	0.50
6-31+g(d,p)	−0.84	−0.34	0.51
6-311++g(d,p)	−0.98	−0.34	0.64
aug-cc-pvdz	−0.91	−0.47	0.44
aug-cc-pvtz	−0.75	−0.55	0.19
aug-cc-pvqz	−0.66	−0.58	0.07
aug-cc-pv5z	−0.63	−0.60	0.03

5.3 Nature of the C–H···O Hydrogen Bonds

As already mentioned above, the stability of the C–H···O in the prototypical methane–water complex originates in the combination of electrostatics and dispersion (see Table 2), the latter terms being similar in strength to the electrostatic term. Thus, the situation is very different to that found in the Ar–Ar van der Waals bond, where the dispersion term (−0.28 kcal) is much stronger than the electrostatic term (−0.04 kcal/mol). As a consequence, the C–H···O hydrogen bond in methane–water retains some of the directionality of the O–H···O bonds. This fact added to the nondominant character of these interactions in

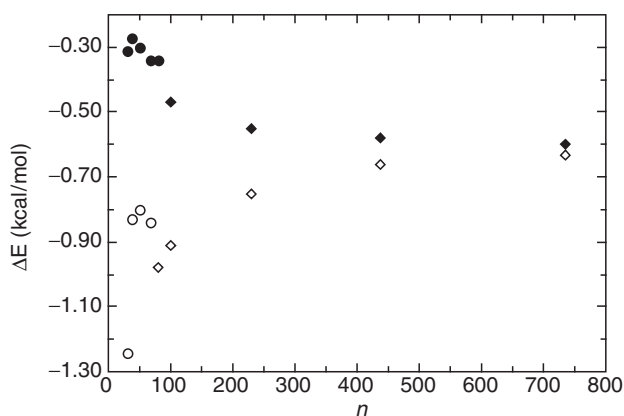


Figure 14. Variation of the MP2 BSSE-uncorrected and BSSE-corrected interaction energies of the methane–water complex with the basis set. Circles indicate results obtained using Pople basis set, while squares indicate results obtained with the aug-cc-pVxZ basis sets. The geometry is the optimum one computed at the MP2/aug-cc-pVTZ level.

Table 10. BSSE-uncorrected (E) and BSSE-corrected (E_{CP}) interaction energies of the methane–water complex. It has been computed using the aug-cc-pVTZ basis set and the indicated methods [34]. All values are in kcal/mol. The geometry is the optimum MP2/aug-cc-pVTZ geometry

Basis set	E	E_{CP}
HF	+0.02	+0.06
MP2	−0.75	−0.55
MP4(SDQ)	−0.69	−0.51
CCSD	−0.68	−0.50
B3LYP	−0.01	+0.02

crystals gives rise to distribution of angles (Fig. 3) where the maximum is clearly not at 180° . However, after applying the “cone correction” to that distribution, the maximum is located at 180° also in the C–H \cdots O contacts [74].

Based on spectroscopic [70] and crystallographic evidence [74], it has been established that the strength of the C–H \cdots O bonds depends on the proton donor acidity and proton acceptor basicity. For instance, the strength changes as C(sp) \cdots H > C(sp²) \cdots H > C(sp³) \cdots H, and also O(sp²) groups give rise to stronger bonds than O(sp³) groups. All of this is also clearly shown in the data listed in Table 11. These values show that the increase in strength is due to an increment in the value of the electrostatic component and of its relative importance with respect to the dispersion component: the electrostatic component in the acetylene–water complex is 2.5 bigger than the dispersion component. The effect on the strength of a C(sp³)–H \cdots O(sp³) bond induced by different substituents was also studied on substituted R₁R₂R₃C–H \cdots OH₂ complexes [75]. A near Hartree–Fock limit basis set was used. The maximum strength was found when R₁ = R₂ = R₃ = OH or F, with MP2 BSSE-corrected values of −2.63 and −2.41 kcal/mol, respectively. Up to now, the strongest C(sp) \cdots H \cdots O(sp³) bonds between neutral fragments were found in the HCN–water complex, −5.0 kcal/mol [77]. It is even stronger than the C(sp²)–H \cdots O(sp²) bond found in cyclic motifs of formamide dimers, with a strength of −2.5 kcal/mol per bond [76] (two C(sp²)–H \cdots O(sp²) bonds are found in an

Table 11. Value of the energetic components of the interaction energy (in kcal/mol) for the indicated systems, computed using the IMPT method. E_{el} , E_{er} , E_p , E_{ct} , and E_{disp} are, respectively, the electrostatic, exchange–repulsion, polarization, charge-transfer, and dispersion components. E_{tot} is the sum of these components and E_{MP2} is the BSSE-corrected interaction energy, shown to serve as reference to calibrate the quality of the IMPT calculation. The MP2 optimum distance (in Å) is also shown. The basis set used is the aug-cc-pVTZ

System	$r_{H\cdots O}$	E_{el}	E_{er}	E_p	E_{ct}	E_{disp}	E_{tot}	E_{MP2}
H ₃ C(sp ³)–H \cdots OH ₂	2.627	−0.7	1.1	−0.2	−0.1	−0.7	−0.6	−0.6
H ₂ CHC(sp ²)–H \cdots OH ₂	2.472	−1.5	1.5	−0.2	−0.1	−1.0	−1.3	−1.1
HCC(sp) \cdots H \cdots OH ₂	2.213	−5.0	4.5	−0.6	−0.3	−2.0	−3.4	−2.7

$R_2^2(8)$ motif, so cooperative effects are expected to be present, reinforcing the strength of its two C–H···O bonds). The effect that the proton acceptor basicity has on the interaction was studied on reference [78].

Concerning other properties that are usually taken as signature of hydrogen bonds, it is found that C–H···O bonds behave like O–H···O hydrogen bonds [77]. For instance, both present the same shifts in the atomic electron populations (the shift depends on the substituent, and it is proportional to the bond strength). The C–H···O bonds also present a shift in the antisymmetric C–H stretching frequency of the complex vibrational spectra, compared to the isolated monomer. However, in the C–H···O bonds the shift is toward positive values (blue shift), while in the O–H···O bonds is towards negative values (red shift). This shift is consistent with that found in experimental studies [79]. The origin of these two different shifts is now well understood [39]. Therefore, we can conclude that the C–H···O bonds found in these complexes can be classified as true hydrogen bonds.

All the C–H···O hydrogen bonds described up to now involve neutral fragments. Therefore, they are members of the N···N class. We also have evaluated the strength of some representative examples for the C–H···O hydrogen bonds of the q···N and q···q classes (Table 12).

5.4 Nature of the C–H···O Interactions That Are Not Bonds

As mentioned before, not all C–H···O interactions fulfill the two requirements for being hydrogen bonds (energetic stability and topological H···O connection), and, consequently, we should not call them hydrogen bonds. Up to now, there are two known cases of C–H···O interactions that are not hydrogen bonds: (1) when the \langle C–H···O angle is far from collinear, or (2) when the C–H···O interaction is made between charged fragments of the same sign.

5.4.1 The \langle C–H···O angle and the hydrogen bond nature of the C–H···O interactions

The possible nonhydrogen bonded nature of some C–H···O interactions was first suggested on C–H···water contacts on the basis that at some orientations the shortest C–H···water contact would be of the H···H type [80]. The authors

Table 12. Value of the BSSE-corrected MP2/aug-cc-pVTZ interaction energy for the indicated systems, computed at their optimum geometry, computed at the MP2/aug-cc-pVTZ (methane–water), or MP2/6-31+G(d) (the other two complexes) levels

Type of hydrogen bond	Model complex	$r_{H\cdots O}$	E_{MP2}
N···N	H ₃ C(sp ³)–H···OH ₂	2.627	–0.55
q···N	H ₃ C(sp ³)–H···OH ^(–)	1.982	–5.77
q···q	N(CH ₃) ₃ C(sp ³)–H ⁽⁺⁾ ···OH ^(–)	1.916	–94.53 ^a

^a Three equivalent C–H···O contacts are made, as the OH sits on top of the C_{3v} axis

attributed a repulsive nature to the H···H contacts (this is very unlikely to be the case, as collinear H···H interactions are energetically stabilizing even in the H₂ and (CH₄)₂ dimers [81]). However, only with the use of the AIM theory, it is possible to test the bonding or nonbonding nature of one contact in circumstances where the presence of simultaneous short contacts with many atoms makes almost impossible to reach a conclusion just following qualitative considerations.

The power of the AIM analysis was already illustrated before on the NANQUO02 crystal (Figs. 9 and 10), thus making unnecessary further presentations here. An analysis of this crystal shows the presence of 27 unique C–H···O contacts below 3.0 Å, all made by methyl groups. By doing an AIM analysis [65], one finds that only 23 of them have a hydrogen bond nature (the authors did their assignment on the basis of the existence of a bond critical point, the energetic stability of the dimers, and the fulfillment of the Koch–Popelier criteria [82] by these critical points, a series of empirical properties satisfied by most critical points that show hydrogen bond properties). It is worth pointing here that Espinosa et al. [22], using data on 83 A–H···X hydrogen bonded complexes, found that the hydrogen bond interaction energy (E_{HB}) may be correlated with the electronic potential energy at the bond critical point ($V(\mathbf{r}_{\text{CP}})$) by the expression

$$(5) \quad E_{\text{HB}} = 0.5V(\mathbf{r}_{\text{CP}})$$

At the same time, they found that E_{HB} and the H···O distance ($r_{\text{H}\cdots\text{O}}$) were related by the following expression:

$$(6) \quad E_{\text{HB}} = -25.3 \times 10^3 \exp[-3.6r_{\text{H}\cdots\text{O}}]$$

As this curve always provides negative values, its validity implies that when a H···O critical point is found in hydrogen bonded complexes, it is always a bond, as it is energetically stabilizing according to Eq. 6.

The absence of hydrogen bonded nature in 4 of the 27 C–H···O contacts of NANQUO02 has been attributed to the $\langle\text{C–H}\cdots\text{O}\rangle$ angle of these 4 contacts; they have values around 95°, while the hydrogen bond contacts have values between 120° and 180°. However, calculations on an isolated methane–formaldehyde complex [27] show that one can only find three simultaneous H···O bond critical points with a methyl group when the methyl C_{3v} axis is aligned with the formaldehyde C_{2v} axis. Otherwise, for all values of the $\langle\text{C–H}\cdots\text{O}\rangle$ angle in the 90–180° range only one bond critical point is found. This explains why only one critical point is found in some cases. On the above basis, the absence of critical points from two of the methyl groups (see Fig. 10) cannot be justified by the value of the $\langle\text{C–H}\cdots\text{O}\rangle$ angle and must just be attributed to the crystal packing that avoids the presence of these points.

We can finally comment on the validity of the AIM analysis of bond critical point in solids. Its validity has been recently questioned [18, 83] on the basis of a recent finding that the topological features of the electron density of a complex

or aggregate can be described remarkably well by the superposition of spherical densities of the independent atoms [83] (the so-called promolecular density, obtained as the sum of atomic densities in an independent atom model). However, it has been recently reported that for NANQUO02 the independent atom model and the experimental density present different bond critical points in 4 out of 19 intermolecular bonds. Such a fact puts into question the general validity of the independent atom model.

5.4.2 C–H···O interaction between charged fragments of the same sign

The first manifestation that the charge in the fragments could be important in determining the nature of the C–H···O interaction was found [84] in the mixed-valence $[(\eta^6 - \text{C}_6\text{H}_6)_2\text{Cr}]^+[\text{Cr}(\text{OCH}_3)]^-$ salt. The packing of this salt (Fig. 15) presents two types of short C–H···O contacts: (1) C–H⁽⁺⁾···O⁽⁻⁾ between cations and anions, the four shortest within the 2.40–2.45 Å range, (2) C–H⁽⁻⁾···O⁽⁻⁾ between anions, the shortest one presenting a H···O distance of 2.381 Å.

If these two C–H···O interactions were of the same nature, one would expect that the shortest would be energetically more stabilizing (in agreement with the strength–length correlation). However, in good agreement with our previous findings, HF/LANL2DZ calculations found the interaction between the two anions to be energetically unstable by +58 kcal/mol; the interaction between adjacent cations and anions is energetically stabilizing by –128 kcal/mol [84]. The cation···anion interactions present two $\mathbf{R}_2^2(7)$ motifs, each composed of two C(sp²)–H···O interactions. Thus, the strength of each of these interactions is +32 kcal/mol. A topological analysis reveals that all of them present H···O bond critical points, thus they are C–H···O hydrogen bonds. However,

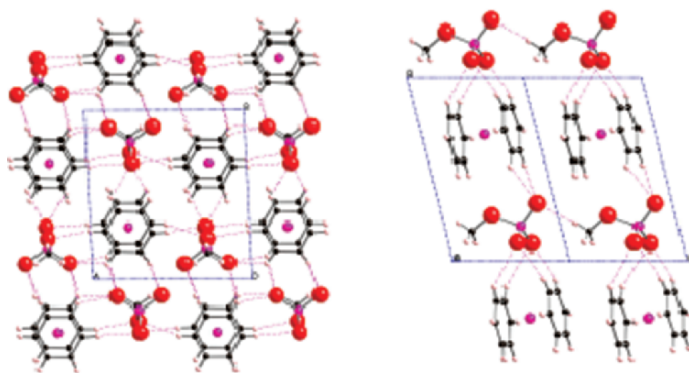


Figure 15. Packing of the mixed-valence $[(\eta^6 - \text{C}_6\text{H}_6)_2\text{Cr}]^+[\text{Cr}(\text{OCH}_3)]^-$ salt. *Left*: View along the c -axis, showing the short C–H⁽⁺⁾···O⁽⁻⁾ contacts between cations and anions. *Right*: View along the c -axis, showing the short C–H⁽⁺⁾···O⁽⁻⁾ contacts between cations and anions and the short C–H⁽⁻⁾···O⁽⁻⁾ contacts between anions.

the anion \cdots anion interaction only shows one possible C–H \cdots O interaction, thus the +58 kcal/mol value is a direct measure of such interaction. Due to its unstable energetic interaction energy, this interaction is not a bond (therefore, it is not a hydrogen bond). The crystal stability arises in the fact that the cation \cdots anion interactions (–128 kcal/mol) overcome the cation \cdots cation and anion \cdots anion repulsions (+52 and +58 kcal/mol, respectively).

The nonbonded nature of the A–H \cdots X interactions between charged fragments of the same sign was later on reported for the O–H \cdots O interactions found between deprotonated dicarboxylic acids. The first case was detected [46] in the KHC_2O_4 ionic crystal (REFCODE name KHOXAL11). The packing of this crystal presents only one C(5) motif that connects the anions (Fig. 16). This motif presents short O–H \cdots O interactions with a H \cdots O distance of 1.654 Å. However, the interaction energy between two adjacent HC_2O_4^- anions is +39 kcal/mol (HF/6-31+G(2d,2p) calculation), and this interaction cannot be a bond. Other cases were found on larger deprotonated dicarboxylic acids [85–88]. All the OH \cdots O interactions between anions computed up to now are energetically unstable.

The analysis of the components of the interaction energy for the O–H \cdots O interactions found between two adjacent HC_2O_4^- anions (Table 13), placed at the geometry that they have in the KHOXAL11 crystal, reveals that the main change that takes place when going from the $\text{HC}_2\text{O}_4^{(-)}\cdots\text{HC}_2\text{O}_4^{(-)}$ interactions to the $\text{H}_2\text{C}_2\text{O}_4\cdots\text{HC}_2\text{O}_4^{(-)}$ or $\text{H}_2\text{C}_2\text{O}_4\cdots\text{H}_2\text{C}_2\text{O}_4$ interactions is a change in the sign of the electrostatic component. Using Eqs. 1–4 the change can be traced down to the charge–charge term.

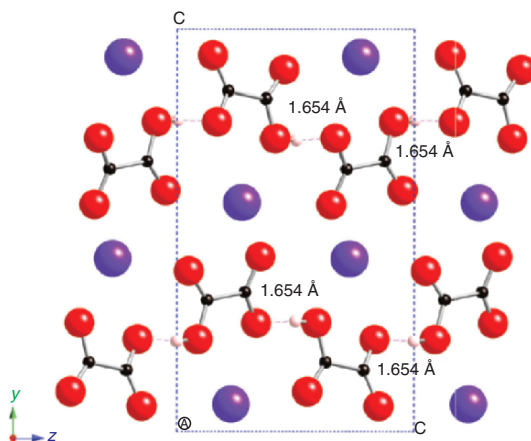


Figure 16. Packing of the KHC_2O_4 salt (KHOXAL11) viewed along the a -axis. The distance and position of the shortest O–H \cdots O contact is also shown.

Table 13. Value of the energetic components of the interaction energy computed using the IMPT method for the indicated complexes. E_{el} , E_{er} , E_p , E_{ct} , and E_{disp} are, respectively, the electrostatic, exchange–repulsion, polarization, charge-transfer, and dispersion components. E_{tot} is the sum of these components (all values in kcal/mol). The 6-31+G(2d,p) basis set was used. The geometry of the (H₂O)₂ dimer is the optimum MP2/aug-cc-pVDZ. For the other three complexes, the geometry is taken from the geometry of the (HC₂O₄)₂ dimer found in the KHOXAL11 crystal, adding one or two protons on the appropriate place of the carboxylate group (the statistical average position in crystals containing –COOH groups)

System	E_{el}	E_{er}	E_p	E_{ct}	E_{disp}	E_{tot}
HO–H···OH ₂	–8.9	6.9	–0.7	–0.7	–1.7	–5.2
H ₂ C ₂ O ₄ ···H ₂ C ₂ O ₄	–26.1	36.0	–4.6	–5.5	–13.3	–14.5
H ₂ C ₂ O ₄ ···HC ₂ O ₄ ^(–)	–41.9	36.2	–9.0	–6.8	–15.1	–36.6
HC ₂ O ₄ ^(–) ···HC ₂ O ₄ ^(–)	16.7	40.4	–8.8	–6.6	–15.8	25.9

5.4.3 Why interaction between charged fragments of the same sign shows the same features than bonds? Charge-induced bonds

On theoretical grounds, the nonattractive nature of the A–H···X interactions between charged fragments of the same sign does not imply a change in some of the properties usually taken as signature of a hydrogen bond. Such surprising behavior, also detected experimentally [89–91], is discussed in detail below. The presence of these signatures was improperly taken as an indication of the hydrogen bonded nature of the A–H···X interactions between charged fragments of the same sign.

Despite the net repulsive character of the interaction between two anions (or two cations), there are experimental reports indicating the presence in solids and liquids of short-contact cation···cation or anion···anion dimers that present the signatures usually associated to the existence of a bond. An example of anion···anion interactions having the signatures of a bond is found in some TCNE[–] ionic crystals (TCNE = tetracyanoethylene) [92–94]. In these crystals, the TCNE[–]···TCNE[–] dimers have C–C distances larger than 2.9 Å, but the dimers are diamagnetic due to the pairing of the unpaired electron sitting on each radical (each TCNE[–] is a doublet). The TCNE[–]···TCNE[–] dimers also show other properties usually associated to the formation of covalent C–C bonds (UV–vis shifts, IR spectra, etc.). A system presenting cation···cation interactions showing the signature of bonds is the [Au{C(NHMe)₂}₂] (PF₆) · 0.5(acetone) crystal [95], where the [Au{C(NHMe)₂}₂]⁺ cations form dimers (whose shortest Au^I···Au^I distance is around 3.4 Å) that present the same luminescent properties found in attractive aurophilic interactions [96].

The presence of short-distance cation···cation or cation···cation dimers in ionic crystals can be explained as resulting from propagating energetically stable cation_nanion_m aggregates along the symmetry elements of the crystal. The energetic stability of these cation_nanion_m aggregates results from the sum of cation···anion interactions, which overcomes the sum of the cation···cation and anion···anion repulsions. As a consequence of this stability, pairs of cations or

anions are placed at distances where the orbitals can present a non-negligible overlap. Such induced overlap induces the formation of bonding and antibonding combinations of the overlapped orbitals, like in energetically stable dimers. Consequently, the cation_{*n*}anion_{*m*} aggregates present an orbital diagram identical to that found in stable dimers (where bonds between the monomers are formed), although the origin of the diagram is different in both cases. Such a similarity in electronic structure explains that all properties which are connected with this electronic structure are also similar: UV-visible shifts, IR-shifts, NMR-shifts, and many other properties taken as signature of a bond. Figure 17 illustrates

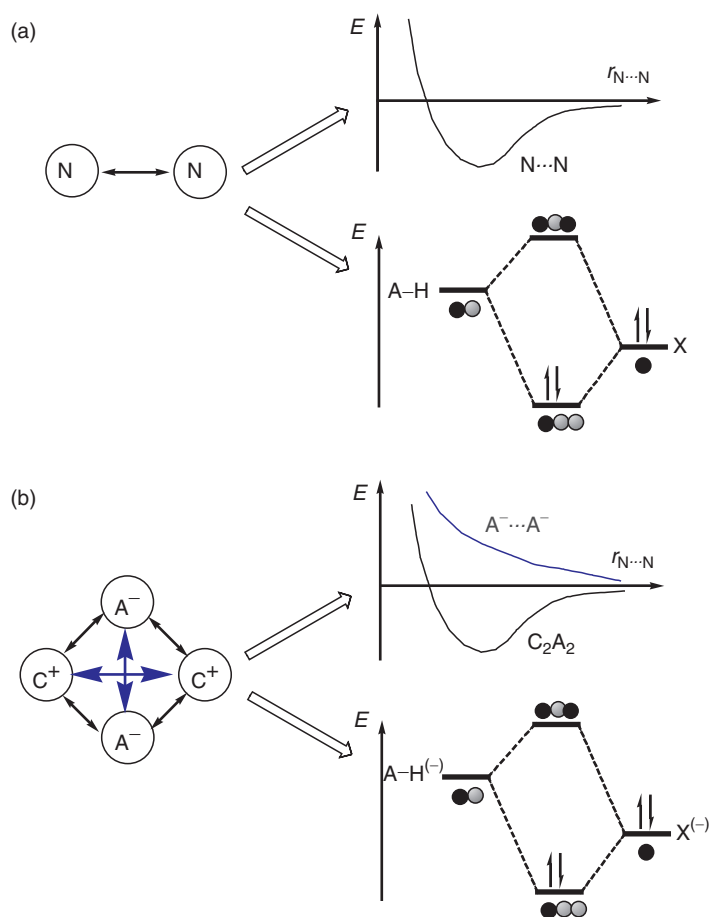


Figure 17. Comparison of the interaction energy curve and orbital diagram of an attractive $N...N$ dimer presenting an $A-H...X$ hydrogen bond (a), with the curve and diagram for an $A-H^{(-)}...X^{(-)}$ interaction found when two C^+ cations induce the interaction of two A^- anions (b). Notice the repulsive character of the $A^-...A^-$ interaction, and the attractive character of the overall interactions in the C_2A_2 aggregate.

these similarities and their different origins for a pair of anions (A^-) that due to the presence of cations (C^+) make short $A-H^{(-)} \cdots X^{(-)}$ contacts.

Most of the interactions between fragments of the same charge present an interaction energy curve that is repulsive at all distances (we have seen that in very large ions or when the charge is strongly localized the interaction energy curve can present a metastable local minimum [97]). Consequently, they cannot be called as bonds. However, as they present the signatures associated to bonds, it is possible to call them *charged-mediated bonds* [93–95], stressing their bonding properties and keeping in mind the supramolecular origin of these interactions (they require a $cation_n anion_m$ aggregate where the $cation \cdots anion$ interactions could overweigh the $cation \cdots cation$ and $anion \cdots anion$ repulsions).

The similarity between the orbital diagrams of $A-H \cdots X$ and $A-H^{(-)} \cdots X^{(-)}$ interactions is illustrated in Figs. 18 and 19 for the $(FH)_2$ and $(OH^{(-)})_2$ dimers, both placed in such a way that both $A-H \cdots X$ contacts have the same geometry (that found in the minimum of the water dimer [47]). The FH molecule is a closed-shell singlet with its eight valence electrons placed in a σ -bonding,

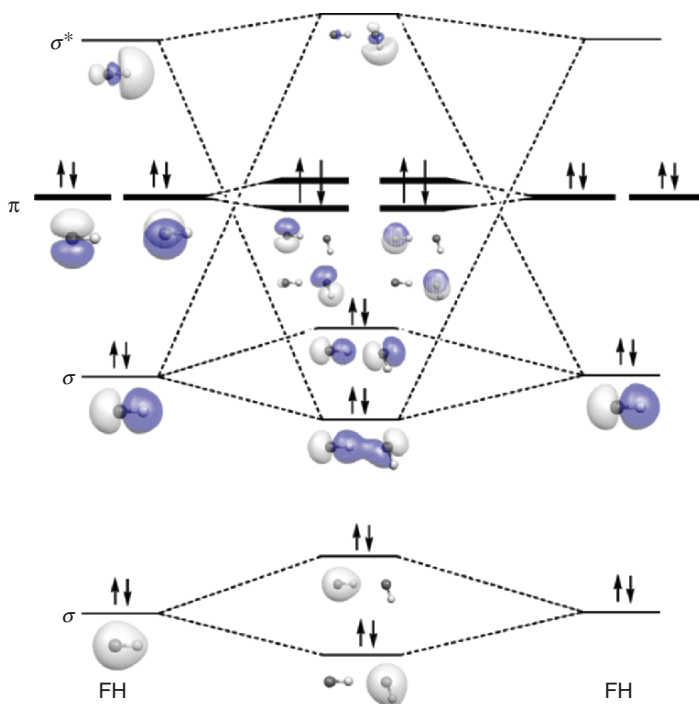


Figure 18. Orbital diagram of the interaction between two FH molecules placed with their $F-H \cdots F$ bond at the same geometry than the $O-H \cdots O$ bond in the water dimer. See text for details.

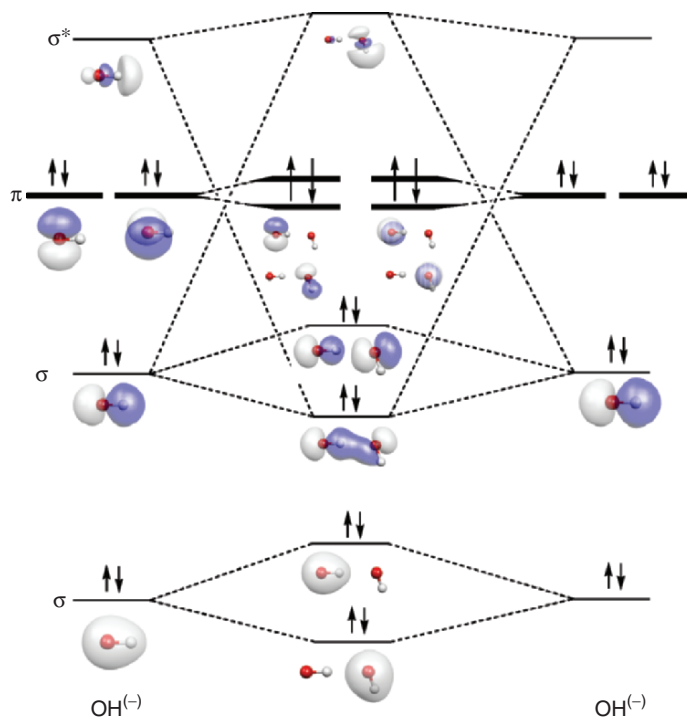


Figure 19 (see color section). Orbital diagram of the interaction between two $\text{OH}^{(-)}$ anions with their $\text{O-H}\cdots\text{O}$ contact at the same geometry than the $\text{O-H}\cdots\text{O}$ bond in the water dimer. See text for details.

σ -nonbonding, and two π -nonbonding orbitals. Besides, there is a σ -antibonding orbital that will play a decisive role in the $\text{A-H}\cdots\text{X}$ and $\text{A-H}^{(-)}\cdots\text{X}^{(-)}$ interactions. The $\text{OH}^{(-)}$ anion is isoelectronic to FH and has the same electronic structure. When two FH or $\text{OH}^{(-)}$ fragments interact, their orbitals overlap and bonding, nonbonding, and antibonding combinations are obtained, each with a different energy. However, the two diagrams are basically identical. The only difference is in the total energy associated to these diagrams: while the $(\text{FH})_2$ dimer is stable against its dissociation into two FH fragments, the $(\text{OH}^{(-)})_2$ dimer is not stable, and it will only be found in the presence of cations. Although not shown here, when the two cations are added the diagram of Fig. 19 remains the same, although the orbital energies are shifted toward more stable values.

5.5 Other C-H \cdots X Interactions

The concepts described above for the C-H \cdots O interactions can be extended to other C-H \cdots X interactions. Consequently, we will not carry out a detailed study of these interactions, but just will give the most relevant details.

Besides the C–H···O interactions, the most relevant C–H···X interactions are the C–H···N, C–H···S and C–H··· π interactions (see Table 8 for a complete set of results). The trends for the C–H···N contacts found in crystals were first analyzed by Taylor and Kennard [72] in their seminal paper, where they also concluded that there was enough evidence to consider them as hydrogen bonds. These authors also attributed a hydrogen bond nature to the C–H···N and C–H···S contacts.

The C–H···S interactions are found in many molecular crystals presenting conducting and superconducting properties [98–100]. These interactions were found to be hydrogen bonded and belonging to the N···N or q···N class. The interaction energy of the C–H···O hydrogen bond was evaluated on the methane–SH₂ complex at the MP2 level using basis sets of up to near Hartree–Fock limit quality [101]. The best BSSE-corrected value is –0.42 kcal/mol, that is, similar to the interaction energy of the methane–water complex. No detailed studies exist on the q···N or q···q types.

The relevance of C–H··· π interactions in many supramolecular systems has made them the subject of specific monographies [6]. In these interactions the acceptor is constituted by the region where the π -electrons are located (double, triple bonds, or aromatic π -rings). The best known π -acceptors are phenyl rings, double and triple C–C bonds, cyano groups, and pyridyl rings. The hydrogen bonded nature of the C(sp)–H··· π interactions in the acetylene–acetylene [102] and HCN–acetylene [103] complexes has been established by a combination of experimental techniques (gas-phase rotational spectroscopy [37] and IR techniques). Theoretical studies on C(sp)–H··· π complexes have been carried out for a long time [104] and have shown the energetic stability of these complexes in orientations where short C(sp)–H··· π contacts are found (a summary of these results is found in Table 8). The presence of H··· π bond critical points has also been demonstrated for the most relevant examples of C(sp)–H··· π interactions [105] of the N···N type (no studies have been carried out up to now on the q···N or q···q classes). Combined crystallographic–theoretical studies on the complexes found in crystals [106, 107] have found C(sp)–H··· π interactions of the N···N type whose interaction energies are within –0.1 to –2.0 kcal/mol. Consequently, we can safely conclude that the C–H··· π interactions are hydrogen bonds.

The strengths of the most relevant examples of C(sp)–H··· π hydrogen bonds are shown in Table 14. These strengths follow the trend C(sp)–H > C(sp²)–H > C(sp³)–H already shown in other C–H···X hydrogen bonds. Such a trend is consistent with statistical studies of crystal structures [108]. Notice that these values indicate that benzene is a worse donor than acetylene, but is a much better acceptor. This is relevant to understand the structure of aromatic compounds presenting an edge-to-face orientation (that is C(sp²)–H bond), as those found in many acetylene-derivatives or phenyl complexes and crystals [6, 7]. When cooperative effects are possible (as in the “six-fold phenyl embrace” topology [109]), it can be a major driving force in the packing.

Table 14. BSSE-uncorrected (E) and BSSE-corrected (E_{CP}) interaction energies for the most relevant classes of C–H $\cdots\pi$ hydrogen bonds. First two columns show the values obtained using the MP2/6–31+G(2d,p) basis set at the optimum geometry of these complexes obtained with the same method. Second two columns (when available) collect the MP2/aug-cc-pVTZ results obtained on geometries computed also at that level. All values are in kcal/mol (values from Ref. 105)

Complex	E	E_{CP}	E	E_{CP}
Ethane–ethene	–0.92	–0.55		
Acetylene–ethene	–1.79	–1.29	–2.03	–1.56
Benzene–ethene	–1.49	–0.80		
Acetylene–acetylene	–1.83	–1.23	–1.98	–1.56
Acetylene–benzene	–3.96	–2.59		
Benzene–benzene ^a	–5.04	–1.84		

^a MP2/6–31+G(d) calculation

Table 15. Values of the electrostatic (E_{el}), exchange–repulsion (E_{er}), polarization (E_{pol}), charge-transfer (E_{ct}), and dispersion (E_{disp}) components of the interaction energy, as given by the IMPT method, computed for the indicated complexes using the 6–31+G(2d,2p) basis set. The sum of all components is also given in the last column (E_{tot}). All the energies are in kcal/mol

Complex	E_{el}	E_{er}	E_{pol}	E_{ct}	E_{disp}	E_{tot}
Acetylene–acetylene	–2.21	2.35	–0.15	–0.24	–1.07	–1.32
Acetylene–water	–4.63	3.25	–0.42	–0.32	–1.22	–3.34
Water–water	–9.18	7.31	–0.77	–0.76	–1.97	–5.37

The analysis of the components of the interaction energy (Table 15) shows that the C–H $\cdots\pi$ bonds have a nature similar to that found in OH \cdots O and C–H \cdots O hydrogen bonds [105], although closer to the second type of hydrogen bonds. Thus, the interaction energy is dominated by the electrostatic component, but with an important weight of the dispersion term.

6 SUMMARY

The results from theoretical calculations demonstrate that C–H \cdots O interactions of the N \cdots N, and q \cdots N class are hydrogen bonds. Up to now there are no reports of C–H \cdots O interactions where zwitterions are present. On the other hand, C–H \cdots O interactions of the q \cdots q class where the two charged fragments have the same sign are found to be nonattractive, thus failing to comply with the stability criteria that all bonds must present according to Pauling’s definition.² Thus, they cannot be considered as hydrogen bonds. Even so, we showed that they present the same orbital diagrams as hydrogen bonds. Therefore, we cannot distinguish between attractive and repulsive C–H \cdots O interactions by looking at many of the properties usually taken as signatures of bonds (shifts in the IR, UV, or NMR spectral properties, for instance).

The reasons for such behavior have been analyzed in detail by looking at the components of the interaction energy obtained from IMPT computations. This allows to trace the nonattractive nature of O–H···O and C–H···O interactions of the q··q class to the strong repulsive nature of the electrostatic term in these complexes. The analysis was done on model dimers and also on complexes extracted from molecular crystals. The statistical trends that these two interactions present in crystals were also analyzed.

We have also used Etter's graph set analysis to describe the structure of complex aggregates where more than one bond is found, and advocated for the use of the bond analysis in these complexes as a tool to understand their structure and energetic stability. Bonds in dimers, aggregates, and crystals can be located by doing an AIM analysis of the electron density (recent studies have shown that not always the promolecule model gives the same result than when using the real electron density) and then checking that the obtained bond critical points correspond to energetically stabilizing interactions (in some ionic crystals one can find bond critical points and interaction energies that are not stabilizing).

ACKNOWLEDGMENTS

The authors acknowledge the support over the years of the "Ministerio de Ciencia y Tecnología" and "CIRIT" for funding (the latest contracts being BQU2002-04587-C02-02 and 2001SGR-0044). They also thank CEPBA-IBM Research Institute, CEPBA, and CESCO for allocation of CPU time in their computers. E. D'O. also acknowledges the Spanish "Ministerio de Educación y Ciencia" for the award of his Ph.D. grant.

REFERENCES

1. Israelachvili, J. (1992) *Intermolecular and Surface Forces*, 2nd edition, Academic, London.
2. Bernstein, J. (2002) *Polymorphism in Molecular Crystals*, Clarendon, Oxford.
3. Desiraju, G. R. (1989) *Crystal Engineering. The Design of Organic Solids*, Elsevier, Amsterdam.
4. Braga, D., Grepioni, F. and Orpen, G. (1999) *Crystal Engineering: From Molecules and Crystals to Materials*, Kluwer, Dordrecht.
5. Lehn, J. M. (1995) *Supramolecular Chemistry. Concepts and Perspectives*, VCH, Weinheim.
6. Nishio, M., Hirota, M. and Umezawa, Y. (1998) *The CH/π Interaction. Evidence, Nature, and Consequences*, Wiley-VCH, New York.
7. Desiraju, G. R. and Steiner, T. (1999) *The Weak Hydrogen Bond in Structural Chemistry and Biology*, Oxford University Press, Oxford.
8. Desiraju, G. (1991) The C–H···O hydrogen bond in crystals. What is it? *Acc. Chem. Res.* **24**, 290–296.
9. Steiner, T. (2002) The hydrogen bond in the solid state, *Angew. Chem. Int. Ed.* **41**, 48–76.
10. Allen, F. H. (2002) The Cambridge Structural Database: a quarter of a million crystal structures and rising, *Acta Crystallogr. B*, **58**, 380–388.
11. Calhorda, J. M. (2000) Weak hydrogen bonds: theoretical studies, *Chem. Commun.* 801–809.
12. Scheiner, S. (1997) *Hydrogen Bonding. A Theoretical Perspective*, Oxford University Press, New York.

13. Aakeroy, C. B. and Seddon, K. R. (1993) The hydrogen bond and crystal engineering, *Chem. Soc. Rev.* **22**, 397–407.
14. Pauling, L. (1960) *The Nature of the Chemical Bond*, 3rd edition, Cornell University Press, Ithaca.
15. Pimentel, G. C. and McClellan, A. L. (1960) *The Hydrogen Bond*, W. H. Freeman, San Francisco.
16. Bader, R. F. (1990) *Atoms in Molecules. A Quantum Theory*, Clarendon, Oxford.
17. Braga, D., Maini, L., Grepioni, F., Mota, F., Rovira, C. and Novoa, J. J. (2000) Interanionic $(^-)\text{OH}\cdots\text{O}^{(-)}$ interactions: a solid-state study of the ring and chain motifs, *Chem. Eur. J.* **6**, 4536–4551.
18. Dunitz, J. and Gavezzotti, A. (2005) Molecular recognition in organic crystals: directed intermolecular bonds or nonlocalized bonding? *Angew. Chem. Int. Ed.* **44**, 1766–1787.
19. Desiraju, G. R. (2002) Hydrogen bridges in crystal engineering: interactions without borders, *Acc. Chem. Res.* **35**, 565–573.
20. Tsirelson, V. G. and Ozerov, R. P. (1996) Institute of Physics Publishing, Bristol.
21. Alkorta, I and Elguero, J. (1999) Theoretical study of strong hydrogen bonds between neutral molecules: the case of the amine oxides and phosphine oxides as hydrogen bond acceptors, *J. Phys. Chem. A* **103**, 272–279.
22. Espinosa, E., Molins, E. and Lecomte, C. (1998) Hydrogen bond strengths revealed by topological analyses of experimentally observed electron densities, *Chem. Phys. Lett.* **285**, 170–173.
23. Grabowski, S. J. (2001) Ab initio calculations on conventional and unconventional hydrogen bonds—study of the hydrogen bond strength, *J. Phys. Chem. A* **105**, 10739–10746.
24. Maitland, G. C., Rigby, M., Smith, E. B. and Wakeham, W. (1981) *Intermolecular Forces. Their Origin and Determination*, Clarendon Oxford.
25. Stone, A. J. (1996) *The Theory of Intermolecular Forces*, Clarendon Oxford.
26. Hayes, I. C. and Stone, A. J. (1984) An intermolecular perturbation theory for the region of moderate overlap, *J. Mol. Phys.* **53**, 83–105.
27. Novoa, J. J., Lafuente, P. and Mota, F. (1998) Are non-linear C–H \cdots O contacts hydrogen bonds or van der Waals interactions? Establishing the limits between hydrogen bonds and van der Waals interactions, *Chem. Phys. Lett.* **290**, 519–525.
28. Pimentel, G. C. and McClellan, A. L. (1971) Hydrogen bonding, *Ann. Rev. Phys. Chem.* **22**, 347–385.
29. Hibbert, F. and Emsley, J. (1990) Hydrogen bonding and chemical reactivity, *Adv. Phys. Org. Chem.* **26**, 255–379.
30. Jeffrey, G. A. and Saenger, W. (1991) *Hydrogen Bonding in Biological Structures*, Springer, Berlin.
31. Bondi, A. (1964) van der Waals volumes and radii, *J. Phys. Chem.* **68**, 441–452.
32. Chickos, J. S. and Acree, Jr. W. E. (2002) Enthalpies of sublimation of organic and organo-metallic compounds, *J. Phys. Chem. Ref. Data* **31**, 537–698.
33. Gavezzotti, A. (1998) The crystal packing of organic molecules: challenge and fascination below 1000 Da, *Cryst. Rev.* **7**, 5–121.
34. Szabo, A. and Ostlund, N. S. (1982) *Modern Quantum Chemistry: Introduction to Advanced Electronic Structure Theory*, Macmillan, New York.
35. Parr, R. G. and Yang, W. (1989) *Density-Functional Theory of Atoms and Molecules*, Oxford University Press, New York.
36. Jensen, F. (1998) *Introduction to Computational Chemistry*, John Wiley, New York.
37. Legon, A. C. and Millen, D. J. (1987) Directional character, strength, and nature of the hydrogen bond in gas-phase dimers, *Acc. Chem. Res.* **20**, 39–46.
38. Jeffrey, G. A. (1997) *An Introduction to Hydrogen Bonding*, Oxford University Press, New York.
39. Hobza, P. and Havlas, Z. (2000) Blue-shifting hydrogen bonds, *Chem. Rev.* **100**, 4253–4264.
40. Hallam, H. E. (1973) *Vibrational Spectroscopy of Trapped Species*, John Wiley, New York.

41. Ault, B. S., Balboa, A., Tevault, D. and Hurley, M. (2004) Matrix isolation infrared spectroscopy and theoretical study of the interaction of water and dimethyl methylphosphonate, *J. Phys. Chem. A* **108**, 10094–10098.
42. Brunner, E. and Sternberg, U. (1998) Solid-state NMR investigations on the nature of hydrogen bonds, *J. Prog. NMR Spectrosc.* **32**, 21–57.
43. Shenderovich, I. G., Tolstoy, P. M., Golubev, N. S., Smirnov, S. N., Denisov, G. S. and Limbach, H. H. (2003) Low-temperature NMR studies of the structure and dynamics of a novel series of acid-base complexes of HF with collidine exhibiting scalar couplings across hydrogen bonds, *J. Am. Chem. Soc.* **125**, 11710–11720.
44. Novoa, J. J., Tarron, B., Whangbo, M.-W. and Williams, J. (1991) Interaction energies associated with short intermolecular contacts of C–H bonds. Ab initio computational study of the C–H···O contact interaction in CH₄···OH₂, *J. Chem. Phys.* **95**, 5179–5186.
45. Novoa, J. J., Nobeli, I., Grepioni, F. and Braga, D. (2000) Are all short O–H···O contacts hydrogen bonds? A quantitative look at the nature of O–H···O intermolecular hydrogen bonds, *New. J. Chem.* **24**, 5–8.
46. Braga, D., Grepioni, F. and Novoa, J. J. (1998) Inter-anion OH[−]···O[−] hydrogen bond like interactions: the breakdown of the strength–length analogy, *Chem. Commun.* **18**, 1959–1960.
47. Feller, D. (1992) Application of systematic sequences of wavefunctions to the water dimer, *J. Chem. Phys.* **96**, 6104–6114.
48. Chakravorty, S. J. and Davidson, E. R. (1993) The water dimer: correlation energy calculations, *J. Phys. Chem.* **97**, 6373–6383.
49. Xantheas, S. S. (1994) Ab initio studies of cyclic water clusters (H₂O)_n, n = 1–6. II. Analysis of many-body interactions, *J. Chem. Phys.* **100**, 7523–7534.
50. Sim, F., St-Amant, A., Papai, I. and Salahub, D. R. (1992) Gaussian density functional calculations on hydrogen-bonded systems, *J. Am. Chem. Soc.* **114**, 4391–4400.
51. Kim, K. and Jordan, K. D. (1994) Comparison of density functional and MP2 calculations on the water monomer and dimer, *J. Phys. Chem.* **98**, 10089–10094.
52. Novoa, J. J. and Sosa, C. (1995) Evaluation of the density-functional approximation on the computation of hydrogen-bond interactions, *J. Phys. Chem.* **99**, 15837–15845.
53. Becke, A. D. *J. Chem. Phys.* **98** (1993) 5648; Lee, C., Yang, W. and Parr, R. G., *Phys. Rev. B.* **37** (1988) 785.
54. Dunning, Jr. T. H. (1989) *J. Chem. Phys.* **90**, 1007.
55. Ordutola, J. A. and Dyke, T. R. (1980) Partially deuterated water dimers: microwave spectra and structure *J. Chem. Phys.* **72**, 5062–5070.
56. Kuchitsu, K. and Morino, Y. (1965) Estimation of anharmonic potential constants. I. linear XY₂ molecules, *Bull. Chem. Soc. Jpn.* **38**, 805–816.
57. Boys, S. F. and Bernardi, F. (1970) Calculation of small molecular interactions by differences of separate total energies—some procedures with reduced errors, *Mol. Phys.* **19**, 553–566.
58. Novoa, J. J., Planas, M. and Whangbo, M.-H. (1994) A numerical evaluation of the counterpoise method on hydrogen bonded complexes using near complete basis sets, *Chem. Phys. Lett.* **225**, 240–246.
59. Novoa, J. J., Planas, M. and Rovira, M. C. (1996) On the usefulness of the counterpoise method on hydrogen-bonded complexes: a numerical test using near complete basis sets on H₂O···HF, (H₂O)₂, (HF)₂ and CH₄···H₂O, *Chem. Phys. Lett.* **251**, 33–46.
60. van Duijneveldt, F. B., van der Rijdt, J. G. C. M. and van Lenthe, J. H. (1994) State of the art in counterpoise theory, *Chem. Rev.* **94**, 1873–1885.
61. D’Oria, E. and Novoa, J. J. (2004) The strength–length relationship at the light of ab initio computations: does it really hold? *Cryst. Eng. Comm.*, **64**, 367–376.
62. Etter, M. C. (1990) Encoding and decoding hydrogen bond patterns of organic compounds, *Acc. Chem. Res.* **23**, 120–126.
63. Bernstein, J., Davis, R. E., Shimoni, L. and Chang, N.-L. (1995) Patterns in hydrogen bonding: functionality and graph set analysis in crystals, *Angew. Chem. Int. Ed.* **34**, 1555–1573.

64. Desiraju, G. R. (1995) Supramolecular synthons in crystal engineering—A new organic synthesis, *Angew. Chem. Int. Ed.* **34**, 2311–2327.
65. Gatti, C., May, E., Destro, R. and Cargnoni, F. (2002) Fundamental properties and nature of C–H···O interactions in crystals on the basis of experimental and theoretical charge densities. The case of 3,4-bis(dimethylamino)-3-cyclobutene-1,2-dione (DMACB) crystal, *J. Phys. Chem. A* **106**, 2707–2720.
66. Whalley, E. (1976) *The Hydrogen Bond* (Shuster, P., Zundel, G. and Sandorfy, C., editors), North-Holland, Amsterdam, p. 1427).
67. Lee, C., Chen, H. and Fitzgerald, G. (1995) Chemical bonding in water clusters, *J. Chem. Phys.* **102**, 1266–1269.
68. Suhai, S. (1994) Cooperative effects in hydrogen bonding: fourth order many-body perturbation theory studies of water oligomers and of an infinite chain as a model for ice, *J. Chem. Phys.* **101**, 9766–9782.
69. Donohue, J. (1968) in *Structural Chemistry and Molecular Biology* (Rich, A. and Davidson, N., editors), W. H. Freeman, San Francisco, pp. 459–463.
70. Allerhand, A. and Schleyer, P. v. R. (1963) A survey of C–H groups as proton donors in hydrogen bonding, *J. Am. Chem. Soc.* **85**, 1715–1723.
71. Green, R. D. (1974) *Hydrogen Bonding by C–H groups*, MacMillan, London.
72. Taylor, R. and Kennard, O. (1982) Crystallographic evidence for the existence of C–H···O, C–H···N and C–H···Cl hydrogen bonds, *J. Am. Chem. Soc.* **104**, 5063–5070.
73. Desiraju, G. R. (1991) The C–H···O hydrogen bond in crystals: what is it? *Acc. Chem. Res.* **24**, 290–296.
74. Steiner, T. (1997) Unrolling the hydrogen bond properties of C–H···O interactions, *Chem. Commun.* 727–734.
75. Novoa, J. J. and Mota, F. (1997) Substituent effects in intermolecular C(sp³)–H···O(sp³) contacts: how strong a C(sp³)–H···O(sp³) hydrogen bond can be? *Chem. Phys. Lett.* **266**, 23–30.
76. Vargas, R., Garza, J., Friesner, R. A., Stern, H., Hay, B. P. and Dixon, D. A. (2001) Strength of the N–H···O=C and C–H···O=C bonds in formamide and *N*-methylacetamide dimers, *J. Am. Chem. Soc.* **105**, 4863–4968.
77. Turi, L. and Dannenberg, J. J. (1993) Molecular orbital studies of C–H···O H-bonded complexes, *J. Phys. Chem.* **97**, 7899–7909.
78. Gu, Y., Tar, T. and Scheiner, S. (1999) Fundamental properties of the C–H···O interaction: is it a true hydrogen bond? *J. Am. Chem. Soc.* **121**, 9411–9422.
79. Mizuno, K., Ochi, T. and Shindo, Y. (1998) Hydrophobic hydration of acetone probed by nuclear magnetic resonance and infrared: evidence for the interaction C–H···OH₂, *J. Chem. Phys.* **109**, 9502–9507.
80. Steiner, T. and Saenger, W. (1992) Geometry of C–H···O hydrogen bonds in carbohydrate crystal structures. Analysis of neutron diffraction data, *J. Am. Chem. Soc.* **114**, 10146–10154.
81. Novoa, J. J., Whangbo, M.-H. and Williams, J. M. (1991) Interaction energies associated with short intermolecular contacts of C–H bonds. II Ab initio computational study of the C–H···H–C interactions in methane dimer, *J. Chem. Phys.* **94**, 4835–4841.
82. Koch, U. and Popelier, P. L. A. (1995) Characterization of C–H–O hydrogen bonds on the basis of the charge density, *J. Phys. Chem.* **99**, 9747–9754.
83. Spackman, M. A. (1999) Hydrogen bond energetics from topological analysis of experimental electron densities: recognizing the importance of the promolecule, *Chem. Phys. Lett.* **301**, 425–429.
84. Braga, D., Grepioni, F., Tagliavini, E., Novoa, J. J. and Mota, F. (1998) C–H···O hydrogen bonds in the mixed-valence salt [(η⁶-C₆H₆)₂Cr]⁺[Cr(OCH₃)][−] and the breakdown of the length/strength analogy, *New. J. Chem.* **22**, 755–757.
85. Braga, D., Bazzi, C., Grepioni, F. and Novoa, J. J. (1999) Electrostatic compression on non-covalent interactions: the case of π stacks involving ions, *New. J. Chem.* **23**, 577–579.

86. Braga, D., Maini, L., Grepioni, F., Mota, F., Rovira, C. and Novoa, J. J. (2000) Interanionic ($^{\ominus}$ O–H···O $^{\ominus}$) interactions: a solid-state and computational study of the ring and chain motifs, *Chem. Eur. J.* **6**, 4536–4551.
87. Braga, D., Novoa, J. J. and Grepioni, F. (2001) On the charge delocalization in partially deprotonated polycarboxylic acid anions and zwitterions forming ($^{\ominus}$ O–H···O $^{\ominus}$) interactions in the solid state, *New. J. Chem.* **25**, 226–230.
88. Braga, D., D’Oria, E., Grepioni, F., Mota, F., Novoa, J. J. and Rovira, C. (2002) O–H···O interactions involving doubly charged anions: charge-compression in carbonate-bicarbonate crystals, *Chem. Eur. J.* **8**, 1173–1180.
89. Steiner, T. (1999) Inter-anion O–H···O interactions are classical hydrogen bonds, *Chem. Commun.* 2299–2300.
90. Mascal, M., Marajo, C. E. and Blake, A. J. (2000) Breakdown of the hydrogen bond strength–length analogy: a revision, *Chem. Commun.* 1591–1592.
91. Macchi, P., Iversen, B. B., Sironi, A., Chokoumakas, B. C. and Larsen, F. K. (2000) Breakdown of the hydrogen bond strength–length analogy: a revision *Angew. Chem. Int. Ed.* **39**, 2719–2722.
92. Novoa, J. J., Lafuente, P., Del Sesto, R. and Miller, J. S. (2001) Exceptionally long (>2.9 Å) C–C bonds between [TCNE] $^{\ominus}$ ions: two-electron, four-center $\pi^*-\pi$ C–C bonding in π –[TCNE] $^{\ominus}_2$, *Angew. Chem. Int. Ed.* **40**, 2540–2545.
93. Novoa, J. J., Lafuente, P., Del Sesto, R. and Miller, J. S. (2002), On the existence of long C–C bonds between pairs of anions which repel: when and why? A test case on the [TCNE] $^{\ominus}_2$ dimers found ionic crystals, *Cyrst. Eng. Comm.* **4**, 373–377.
94. Del Sesto, R., Miller, J. S., Novoa, J. J. and Lafuente, P. (2002) Exceptionally long (>2.9 Å) C–C bonding interactions in π –[TCNE] $^{\ominus}_2$ dimers: two-electron, four-center cation-mediated CC bonding interactions involving π^* electrons, *Chem. Eur. J.* **8**, 4894–4908.
95. White-Morris, R. L., Olmstead, M. M., Jiang, F., Tinti, D. S. and Balch, A. L. (2002) Remarkable variations in the luminescence of frozen solutions of [Au{C(NHMe) $_2$ } $_2$](PF $_6$)·0.5(acetone). Structural and spectroscopic studies of the effects of anions and solvents on Gold(I) carbene complexes, *J. Am. Chem. Soc.* **124**, 2327–2336.
96. Schmidbaur, H. (1995) High-carat gold compounds, *Chem. Soc. Rev.* 391–400.
97. D’Oria, E., Braga, D., Grepioni, F. and Novoa J. J. Unpublished results.
98. Williams, J. M., Ferraro, J. R., Thorn, R. J., Carlson, K. D., Geiser, U., Wang, H. H. Kini, A. M. and Whangbo, M.-H. (1992) *Organic Superconductors (Including Fullerenes)*. *Synthesis, Structure, Properties, and Theory*, Prentice Hall, Englewood Cliffs.
99. Ishiguro, T. and Yamaji, K. (1990) *Organic Superconductors*, Springer-Verlag, Berlin.
100. Novoa, J. J., Rovira, M. C., Rovira, C., Veciana, J. and Tarrés, J. (1995) C–H···S and S···S: two major forces in organic conductors, *Adv. Mater.* **7**, 233–237.
101. Rovira, C. and Novoa, J. J. (1997) Strength and directionality of the C(sp 3)–H···S(sp 3) interaction. An ab initio study using the H $_2$ S···CH $_4$ model complex, *Chem. Phys. Lett.* **279**, 140–150.
102. Aldritch, P. D., Kukolich, S. G. and Campbell, E. J. (1983) The structure and molecular properties of the acetylene–HCN complex as determined from rotational spectra, *J. Chem. Phys.* **78**, 3521–3530.
103. Fraser, G. T., Suenram, R. D., Lovas, F. J., Pine, A. S., Hougen, J. T., Leferty, W. J. and Muentzer, J. S. (1988) Infrared and microwave investigations of interconversion tunneling in the acetylene dimer, *J. Chem. Phys.* **89**, 6028–6045.
104. Alberts, I. L., Rowlands, T. and Handy, N. C. (1988) Stationary points on the potential energy surfaces of (C $_2$ H $_2$) $_2$, (C $_2$ H $_2$) $_3$ and (C $_2$ H $_4$) $_2$, *J. Chem. Phys.* **88**, 3811–3816.
105. Novoa, J. J. and Mota, F. (2000) The C–H··· π bonds: strength, identification and hydrogen-bonded nature. A theoretical study, *Chem. Phys. Lett.* **318**, 345–354.
106. Fan, M.-F., Lin, Z., McGrady, J. E. and Mingos, D. M. P. (1996) Novel intermolecular C–H··· π interactions. Ab initio and density functional theory study, *J. Chem. Soc. Perkin Trans. 2*, 563–568.

107. Steiner, T., Starikov, E. B. and Tamm, M. (1996) Weak hydrogen bonding. Part 3. A benzyl group accepting equally strong hydrogen bonds from O–H and C–H donors. 5-Ethynyl-5-H-dibenzo[a,d]cyclohepten-5-ol, *J. Chem. Soc. Perkin Trans. 2*, 67–71.
108. Umezawa, Y. and Nishio, M. (1998) CH/ π interactions as demonstrated in the crystal structure of the guanine-nucleotide binding proteins src homology-2 domains and human growth hormone in complex with their specific ligands, *Bioorg. Med. Chem.* **6**, 493–504.
109. Dance, I. and Scudder, M. (1995) The sextuple phenyl embrace, a ubiquitous concerted supramolecular motif, *Chem. Commun.* 1039–1040.

CHAPTER 6

WEAK HYDROGEN BONDS INVOLVING TRANSITION ELEMENTS

MARIA JOSÉ CALHORDA

Department of Chemistry and Biochemistry, Faculdade de Ciências, Universidade de Lisboa, 1749-016 Lisboa, Portugal. E-mail: mjc@fc.ul.pt

Abstract The most important types of weak, unconventional hydrogen bonds involving transition metals are analyzed and discussed. The metal center acts as an acceptor in the X–H···M intermolecular interactions, the most widely studied example being given by the family of [Co(CO)₄][HNR₃] salts. Many structures were determined, computational approaches and the AIM theory were applied, and the nature of the X–H···M bond has been established as a hydrogen bond. The same X–H···M motif can arise within one molecule, as was observed in a molybdenum complex bearing a phenolic substituent in the cyclopentadienyl ring (O–H···Mo). Heating this complex leads to loss of one ligand, accompanied by an unprecedented oxidative addition of the O–H bond to the metal. The dihydrogen bond, X–H···H–M, is also characteristic of metal hydrides, though analogues containing BH or even CH and SiH have been described. Again, intramolecular and intermolecular interactions exist, the former having been described earlier. Calculations aimed at understanding the nature of such bonds have been performed at several levels of theory, progressively better as time goes on. It changes, for instance, upon going from neutral to cationic complexes. The “first” example of a dihydrogen bond, [IrH(OH)(PMe₃)₄]⁺, with a short H···H contact of 2.40 Å, was found to exhibit instead two weak H···F hydrogen bonds between fluorine atoms of the [PF₆][−] anion and the proton and the hydride. The dihydrogen bond plays a special role in proton transfer reactions involving metal–hydride complexes. The symmetrical dihydrogen bond, M–H···H–M, differs very much from system to system and a thorough analysis is not yet available for most examples.

Keywords: Hydrogen bond; dihydrogen bond; weak hydrogen bonds; BSSE corrections; AIM theory.

1 INTRODUCTION

Hydrogen bonds have made their way into chemistry with Pauling [1] and were described in detail by Jeffrey and Saenger [2], who introduced the concept of weak hydrogen bond. In a classical, strong hydrogen bond there is an

interaction of the type $D-H \cdots A$ ($D-H$ is the donor and A the acceptor), where both D and A are electronegative elements (F, O, N); they are typically two-center bonds and their energy overcomes 10 kcal mol^{-1} . When D is a less electronegative atom (X), the interactions are weaker, less directional, and we enter the realm of the normal to weak hydrogen bonds. The widely studied $C-H \cdots O$ bonds, so common in organometallic complexes and organic species, belong to this group [3]. Changes in the acceptor lead to the so-called unconventional hydrogen bonds: a metal ($X-H \cdots M$) [4], the π electrons of a ring ($C-H \cdots \pi$) [5], a hydride ($X-H \cdots H-M$) [6], or a $H-B$ group ($X-H \cdots H-B$) [7]. In the two latter groups, there is a close contact between two hydrogen atoms, which can be formally considered as one hydride and one proton, since one hydrogen is bound to an electropositive metal or boron, and the second to an electronegative atom. The resulting charges on the hydride and proton allow an electrostatic interaction to take place. These are called the dihydrogen bonds [6]. Interestingly, such close contacts can also be observed in symmetric environments $M-H \cdots H-M$ [8, 6j], where charges cannot explain such an interaction. This brings us to the controversy about the border between hydrogen bonds and van der Waals interactions [9]. Computational studies have been extremely useful to obtain a deeper knowledge about the nature of these weak hydrogen bonds. The improvement of computer power has allowed the systematic use of high quality methods and extended basis sets, since a good estimation of correlation is required to describe the weak bonds between closed shell systems, as found in hydrogen bonds [10]. Basis set superposition errors (BSSE) [11] introduce a significant correction in the calculation of energies and have been considered in most recent studies.

The application of the theory of “atoms in molecules” (AIM) [12] has known a large expansion. It is based on the analysis of the topological properties of the charge density. Bonds are characterized by critical points and as bonds change from covalent to hydrogen bonds [13], for instance, so do the properties of their respective critical points. It becomes therefore possible to assign the type of bond, often an important issue when trying to decide about the presence of a hydrogen bond. For instance, in covalent bonds (open shell interactions), the laplacian of the charge density, $\nabla^2\rho$, is negative in the critical point; it becomes positive for closed shell interactions.

In this work, the unconventional and weak hydrogen bonds that involve transition elements, namely the dihydrogen bond (symmetric and asymmetric) and the $X-H \cdots M$ interactions, will be described and interpreted. More attention will be given to recent results, following an earlier publication [14]. The structures described were taken from the Cambridge Crystallographic Database [15].

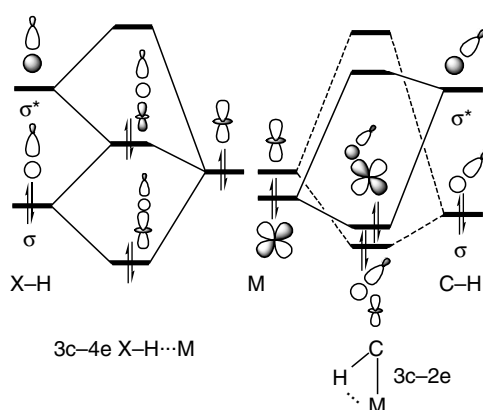
2 HYDROGEN BONDS INVOLVING THE METAL CENTER: $X-H \cdots M$

The short contacts between a metal center and a proton attached to carbon or a more electronegative element, such as N or O, have been known for some time, though their assignment as agostic interactions or hydrogen bonds has

persisted in the literature for some time. In electronic terms, the agostic interaction can be described as a covalent bond with a donation to an electron deficient center and a back donation component (Scheme 1, right side) involving three atoms and two electrons (3c–2e). On the other hand, in the hydrogen bond, there is a weak interaction between closed shells (3c–4e), as shown in Scheme 1, left.

The nature of the agostic bonds was confirmed using the AIM formalism for several electron deficient titanium complexes [16]. More controversial were square planar d^8 species, where a proton from one ligand may approach the metal in an axial direction, but again experiments and calculations did not support the assignment of these $M \cdots H$ interactions as agostic bonds [17, 4c].

Short $X-H \cdots M$ contacts diagnosed as hydrogen bonds were mainly studied by Brammer and coworkers [18], who synthesized and characterized families of salts containing the $[Co(CO)_4]^-$ anion and substituted ammonium cations, having thus obtained a large variety of data allowing an assessment of the effect of substituents. In the anionic complex, the electronically saturated d^{10} cobalt is unlikely to participate in agostic interactions, providing a good acceptor for the formation of hydrogen bonds. Its tetrahedral environment can easily distort to allow for the $Co \cdots H$ close contact. A neutron diffraction study [19] showed that in the $[HNEt_3]^+$ salt the $N-H$ bond is slightly elongated (1.054 Å), and a linear $Co \cdots H-N$ arrangement is observed. Several features of the $D-H \cdots M$ bond, which can be used to define this type of hydrogen bonds, were summarized in a review article [20]. They range from electronic requirements (saturated 18 electron species and electron rich metal centers; acidic protons) to structural (linear $D-H \cdots M$ arrangement) and spectroscopic ones (lowering of the ν_{D-H} stretching frequency in the IR and downfield shift of the 1H NMR chemical shift of the bridging hydrogen atom). Also, an energy



Scheme 1. Comparison of the orbital interaction in the hydrogen (left) and in the agostic bond (right).

decomposition analysis for the O–H···M bond, following Morokuma approach [21], should indicate charge transfer of the metal to H–O, less important electrostatic contribution than in other types of “hydrogen bonds, large contribution of polarization”.

Alkorta et al. [22] used DFT/6–311G++** calculations to analyze the hydrogen bonds in the $[\text{Co}(\text{CO})_4][\text{HD}]$ system, taking smaller hydrogen bond donors (HF, HCN, HNC, $[\text{HNMe}_3]$) and considering also the isoelectronic but neutral $[\text{Ni}(\text{CO})_4]$ acceptor. After the association with the HB donors, the complexes have C_{3v} symmetry, with the $C_{\text{ax}}\text{--M--}C_{\text{eq}}$ angle depending on the strength of the interaction. The $\text{Co}\cdots\text{H}$ distances fall in the range 2.22–2.78 Å, but the $\text{Ni}\cdots\text{H}$ distances are longer, in agreement with the lower calculated interaction energies, although all are within the accepted values for hydrogen bonds. In the case of $[\text{Co}(\text{CO})_4][\text{HNMe}_3]$, the X-ray distance is 3.402 Å and the calculated one 3.30 Å. BSSE corrections were found not to be very significant in these systems. The AIM analysis revealed critical points in the M–C and C–O bonds, and between the metal and the proton. The electron density at the M–C bond critical points (BCPs), ρ_{BCP} , decreases, relative to the free anionic complex, upon interaction with the ammonium cation. The effect is more pronounced in the M–C bond *trans* to the N–H group, the opposite effect being observed for the C–O bonds (increase in ρ_{BCP} , specially at the axial bond) [22]. These trends reflect the loss of electron density at the metal (transfer to the proton), leading to less back donation to the carbonyls, which is more felt at the axial position, and detected also in the charge distribution. In the analysis of the BCPs between the metal and H, besides ρ_{BCP} and the laplacian of the charge density, $\nabla^2\rho$, the energy density (H_{BCP}) was used, since its sign is more sensitive to the nature of the bond. Indeed, it can be positive or negative (as found in the study of $[\text{Co}(\text{CO})_4][\text{HD}]$), for bonds exhibiting a positive laplacian. ρ_{BCP} is $\sim 10^{-2}$ a.u., but H_{BCP} becomes negative in the weakest interactions (M···H distance longer than sum of van der Waals radii).

The interaction in $[\text{Co}(\text{CO})_4][\text{NMPH}]$, where NMP is *N*-methylpiperazine (Fig. 1), has been studied [23], based on the DFT [24] (ADF [25] program) and MP2 [26] calculations.

There is a good quality X-ray structure determination (low temperature data) [27], and, while the relevant dimer does not appear to be too large and therefore

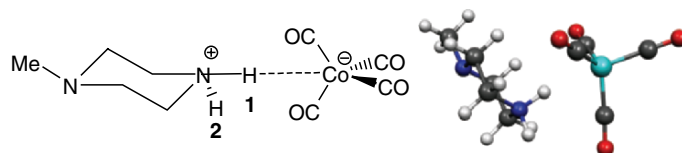


Figure 1. Interaction between the two ions in $[\text{Co}(\text{CO})_4][\text{NMPH}]$ (left) and ADF optimized structure (right).

can be calculated, the structure is complicated by the presence of several independent ions in the unit cell. Indeed, there are five units, $[\text{Co}(\text{CO})_4]_2[\text{NMP}_3\text{H}_2]$, joined by $\text{N-H}\cdots\text{Co}$ and $\text{N-H}\cdots\text{N}$ hydrogen bonds. Each protonated NMP binds both a Co complex (H1) and the neutral NMP (H2), forming a small chain. The ADF optimized structure of $[\text{Co}(\text{CO})_4][\text{NMPH}]$ agrees relatively well with the X-ray data, as shown by the $\text{Co}\cdots\text{H}$ distance of 2.539 Å (2.523 Å), N-H of 1.093 Å (1.05 Å), Co-C_{ax} of 1.776 Å (1.764 Å), Co-C_{eq} of 1.776–1.758 Å (1.775–1.744 Å), respectively. The $\text{C}_{\text{ax}}\text{-Co-C}_{\text{eq}}$ angle was calculated as $\sim 105^\circ$, close to the X-ray value 106.7° . An energy decomposition analysis [28] was carried out on the ADF optimized structure and the result is shown in Table 1.

The bonding energy (BE) can be decomposed into several terms: Pauli repulsion (ΔE_{Pauli}), electrostatic (ΔE_{elec}), and orbital interactions (ΔE_{oi}), representing, respectively, the Pauli repulsion between occupied orbitals of the fragments, the electrostatic interaction between fragments (an attractive term), and the two-electron stabilizing interactions between occupied levels of one fragment and empty levels of the other. The final term, ΔE_{prep} , represents the energy required to take each fragment from its geometry in the molecule to the lowest energy state. In the absence of ΔE_{prep} , the energy required to break the bond without allowing relaxation of the fragments is obtained (E_{int}). It is interesting to notice that although the electrostatic interaction is the major contributor to the interaction energy [21], there is also an attractive term corresponding to a covalent interaction (E_{orb}). The preparation energy is small for both fragments, despite the need to distort the Co complex away from its tetrahedral structure.

B–H bonds can also participate in similar interactions, as observed in the crystal structure of bis{bis(3-*tert*-butyl-5-isopropylpyrazol)hydroborato}-cobalt(II) complex, where two nitrogen atoms of each pyrazolyl ligand bind the metal in a square planar arrangement and the two B–H units approach axially ($\text{Co}\cdots\text{H}$ distance 1.95 Å). The involvement of the B–H bond is also reflected in

Table 1. Energy decomposition for the interaction between $[\text{Co}(\text{CO})_4]^-$ and $[\text{NMPH}]^+$ (energies in kcal mol^{-1})

(1) E_{Pauli}	23.90	
(2) E_{elec}	-90.02	
$E_{\text{steric}} = (1) + (2)$		-66.12
(3) E_{orb}	-26.32	
$E_{\text{int}} = (1) + (2) + (3)$		-92.44
(4) $\Delta E_{\text{prep}}[\text{Co}(\text{CO})_4]^-$	1.74	
(5) $\Delta E_{\text{prep}}[\text{NMPH}]^+$	2.16	
$\Delta E_{\text{prep}} = (4) + (5)$	3.9	
Bonding energy		-88.54

the lowering of the $\nu_{\text{B-H}}$ frequencies, compared with the values for terminal BH bonds [29].

Another interesting example, dealing with an O-H...M interaction, draws the attention to the role of hydrogen bonds in reactivity [30]. The product of the reaction between $[\text{Mo}(\text{PMe}_3)_6]$ and 2,6- $\text{Ph}_2\text{C}_6\text{H}_3\text{OH}$ is shown in Fig. 2 and the short O-H...M contact is highlighted. The Mo...H distance is 2.76(3) Å, the Mo...O distance 3.571(2) Å and the Mo...H-O arrangement is close to linear (172°). Although this complex is stable in solution, it loses PMe_3 when heated to 80°, and undergoes oxidative addition of the O-H bond. The last aspect is the most relevant one, since oxidative addition of the bond involved in the hydrogen bridge had never been observed in other related species.

The interaction observed in $[\text{RuH}_3(\text{SiCl}_2\text{Me})(\text{PPh}_3)_3]$, Ru-H...Si, can be considered the reverse of those described above [31]. The structure of the complex is shown in Fig. 3.

The Ru-H bond distances are typical (1.68, 1.54, 1.59 Å) for this kind of bond, revealing no lengthening. On the other hand, the Si...H distances (1.94, 1.86, 1.94 Å) suggest a strong interaction with Si. This arrangement can be considered either as an Si-H agostic interaction with Ru, or as an Ru-H...Si hydrogen bond, where Ru-H behaves as the donor and Si as the acceptor, and has been found in other systems. DFT calculations showed that the Ru-H bond electrons are donated to the Si-Cl σ^* orbital, so that the hydrogen bond representation describes the bond in a better way. The presence of a chloride near silicon (Si-Cl bond) is required [32].

The M-H bond in $[(\eta^5\text{-C}_5\text{H}_5)\text{Mo}(\text{CO})_3\text{H}]^+$ has been also shown to behave as a proton donor toward phosphine oxides acting as bases. The formation of the M-H...B species has been studied experimentally by infrared spectroscopy and computationally with DFT calculations. These species are intermediate in the proton transfer process giving rise to ion pairs $\text{M}^- \cdots \text{H}^+ - \text{B}$ [33].

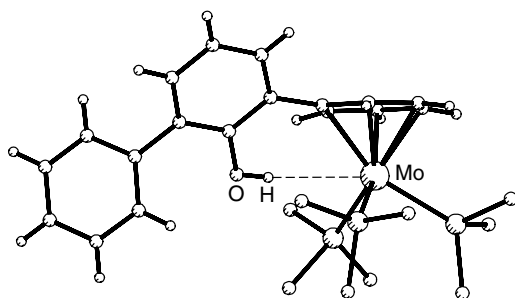


Figure 2. Molybdenum complex depicting a short O-H...Mo contact (the hydrogens of the phosphine ligands were omitted for clarity).

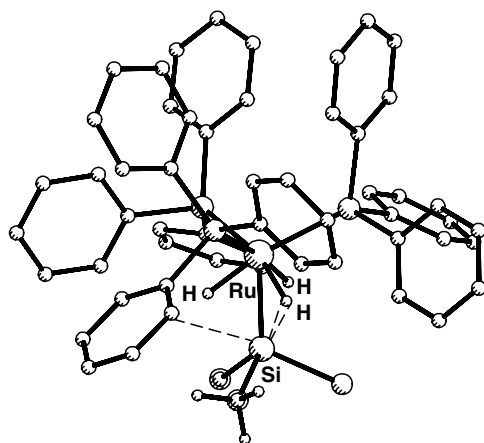
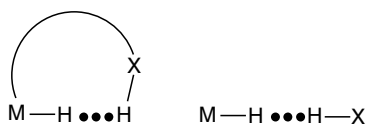


Figure 3. Ruthenium complex showing three short Ru-H...Si contacts (the hydrogens of the phosphine ligands were omitted for clarity).

3 THE DIHYDROGEN BOND X-H...H-M

In this type of interaction, a metal hydride is close to a proton, either in an intramolecular (Scheme 2, left) or in an intermolecular environment (Scheme 2, right).

The first example reported in the literature belonged to the first group and was observed in complex *cis*-[IrH(OH)(PMe₃)₄][PF₆] [34]. The cation is shown in the left side of Fig. 4 and there is a short H...H distance of 2.40(1)Å (neutron



Scheme 2. The intra- and the intermolecular dihydrogen bond.

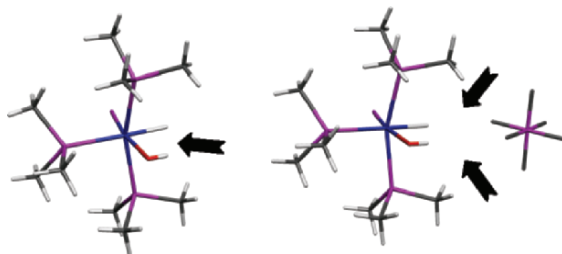


Figure 4 (see color section). The X-ray structure of [IrH(OH)(PMe₃)₄][PF₆]: cation (left) and cation and anion (right).

diffraction structure), with a distorted Ir–O–H angle of 104.4(7)°. A first look would suggest a negative charge at the hydride H(Ir) and a positive charge at the proton H(O), resulting in an electrostatic contribution to the dihydrogen bond. A deeper HF and MP2 study, accompanied by an AIM analysis [35], however, revealed no critical point between the two hydrogen atoms, suggesting that maybe the counter ion also had a role to play [6k]. Indeed, the experimental structure was much better reproduced when the PF₆ anion was introduced in the calculation and two critical points were detected between each H and the two closest fluorine atoms of the anion (Table 2, Fig. 4, right). The calculated charge densities are very small and the Laplacian is positive for the H···F BCP, reflecting the presence of weak hydrogen bonds, while for the O–H bond, there is a large ρ and $\nabla^2\rho$ is negative. Still, no BCP was detected between H1 and H2.

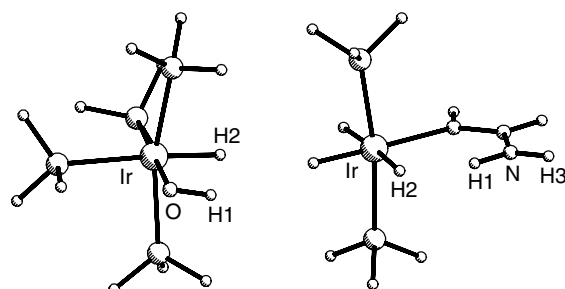
The calculated charges were negative for the hydrides and positive for the protons, both in the cation and in [IrH(OH)(PMe₃)₄][PF₆].

The conclusion was that this complex was not a proper example of a dihydrogen bond, and a search for neutral complexes was carried out, in order to avoid counter ions and the problems they introduced.

A very large family of iridium hydride derivatives, both neutral and cationic, exhibiting dihydrogen bonds was synthesized and characterized by the groups of Crabtree and Morris, and counts among the pioneer examples of these bonds [6]. A DFT study was performed in 1995 using a simple but representative model of the complexes, [IrH₃L(PH₃)₂](L = HNCHNH₂, 2-aminopyridine, etc.), which allowed an estimation of 7.1 kcal mol⁻¹ for the strength of the H···H interaction when L = 2-aminopyridine [6c]. This model complex was selected for another comparative AIM analysis based on HF and MP2 calculations [35], since it was a neutral complex. The close H···H contact observed in the structure of [IrH₃(HNCHNH₂)(PH₃)₂] was shown, by means of AIM, to

Table 2. Charge density ρ and $\nabla^2\rho$ for selected bond critical points of the two model complexes [IrH(OH)(PH₃)₄][PF₆] and [IrH₃(HNCHNH₂)(PH₃)₂] (see numbering in Scheme 3; HF and MP2 results)

Bond	[IrH(OH)(PH ₃) ₄][PF ₆]		[IrH ₃ (HNCHNH ₂)(PH ₃) ₂]	
	ρ	$\nabla^2\rho$	ρ	$\nabla^2\rho$
O/N–H1	0.380	–2.890		
H1···F/N	0.001	0.008	0.344	–2.111
			0.313	–1.675
H2···F	0.002	0.009		
	0.002	0.010		
H1···H2			0.016	0.041
			0.022	0.044
H3–N			0.357	–1.974
			0.331	–1.640



Scheme 3. Numbering scheme for the complexes $[\text{IrH}(\text{OH})(\text{PH}_3)_4]^+$ and $[\text{IrH}_3(\text{HNCHNH}_2)(\text{PF}_3)_2]$.

exhibit a critical point between the two hydrogen atoms H1 and H2 (Scheme 3, Table 2).

Indeed, both ρ and $\nabla^2\rho$ are typical of the characteristic values for hydrogen bonds, with a small ρ and positive laplacian. Notice that although the numbers differ, the qualitative results from HF and MP2 calculations provide the same picture. This finding gives some support to the results described above for $[\text{IrH}(\text{OH})(\text{PH}_3)_4][\text{PF}_6]$, which had to rely on HF data. As the molecule is much larger, it was not possible to perform MP2 calculations at the time [35]. The N–H2 bond involved in the interaction with the hydride differs from the N–H3 bond, which exhibits larger charge density.

More examples of this type of M–H \cdots H–X dihydrogen bond were detected in recent years, in other systems, such as Os₃ trinuclear clusters [36]. One interaction was found in $[\text{Os}_3(\text{CO})_{10}\text{H}(\mu\text{-H})(\text{HN}=\text{CHCH}_3)]$ [36a], where the Os–H \cdots H–N interaction between the terminal hydride and the NH proton was observed by solution NMR. In Fig. 5, the crystal structure of one cluster of this family is represented. The Os–H bond [1.56(5) Å] is among the shortest of its kind, the H \cdots H distance also being very short [1.79(6) Å]. This distance was reproduced by DFT/B3LYP calculations, which also allowed an estimate of the

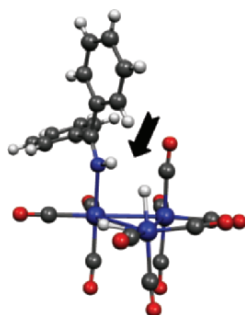


Figure 5 (see color section). The X-ray structure of $[\text{Os}_3(\text{CO})_{10}\text{H}(\mu\text{-H})(\text{HN}=\text{CPh}_2)]$.

H \cdots H interaction energy of about 2.5 kcal mol $^{-1}$, comparable to experimental data [36b].

Besides a range of Os–H \cdots H–N arrangements observed within the basic structure and several nitrogen ligands, the related Os–H \cdots H–S motif was also observed, by solution NMR experiments, in similar clusters containing thiolate ligands [36d].

The related Re $_3$ cluster [Re $_3$ (CO) $_9$ (μ -H) $_4$ (Hpz)] (Hpz = pyrazole) also features a dihydrogen bond, involving a bridging hydride and the N–H bond from pyrazole [37a]. In this cluster, the H \cdots H distance is 2.047 Å, not so short as in the previous Os cluster. It should be noted, however, that the determination of hydrogen positions by X-ray diffraction has some error. In a solid state IR experiment, the authors compared the change in position of the N–H stretching band in the cluster, with respect to a compound where the dihydrogen bond was impossible, namely [Re $_3$ (CO) $_{11}$ (μ -H) $_3$ (Hpz)], where the hydrides lie to the opposite side of the NH bond. Systematic studies of these and other interactions led to the establishment of a relationship between the shifts of the N–H stretching frequencies, when this bond is involved in a hydrogen bond and in the absence of any hydrogen bond, and the strength of the interaction. The 148 cm $^{-1}$ shift indicated a bond strength of 3.1 kcal mol $^{-1}$, which is again a very weak bond.

The DMA analogue (DMA = Me $_2$ NH) [37b] showed a H \cdots H contact of 2.24 Å in the X-ray structure. Combined experiments and DFT calculations led to an estimate of 2.2 kcal mol $^{-1}$ for the interaction energy.

As soon as the intramolecular dihydrogen bond was observed, the search for the intermolecular one started [38]. The first example in the literature was found when [ReH $_5$ (PPh $_3$) $_3$] was cocrystallized with indole, a molecule containing one N–H bond and benzene, as shown in Fig. 6 [38a]. Two hydride ligands are close to the H–N bond, the H \cdots H distances being 2.212(9) Å and 1.734(8) Å, defining a very asymmetric environment. This type of intermolecular dihydrogen bond has been widely studied. Besides the initial interest in observing its

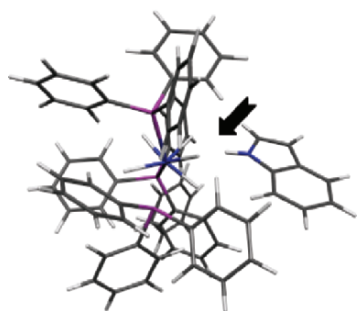


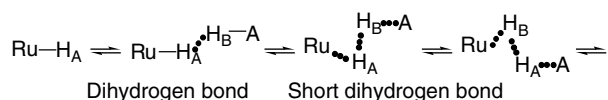
Figure 6 (see color section). The neutron diffraction structure of [ReH $_5$ (PPh $_3$) $_3$] · indole · benzene.

features, it is relevant in many reactions involving proton transfer, where it can assist the reactions, leading to smaller barriers and higher reaction rates. A Ru–H···H–O bond was found to be present in one of the calculated (DFT/B3LYP) transition states for the catalytic hydration of nitriles promoted by $[(\eta^5\text{-C}_9\text{H}_7)\text{Ru}(\text{dppm})\text{H}]$ (dppm = bis(diphenylphosphino)methane), being responsible for lowering the reaction barrier. Other weak hydrogen bonds were detected in this system [39].

The hydrogen transfer between several kinds of proton donors and a large group of transition metal hydrides has been studied in detail by Shubina and coworkers [40]. There are some review papers [40a, b], which cover the earlier work. More recently, other systems have been addressed. In the general mechanism for hydrogen transfer, the HD donor forms a dihydrogen bond with the hydride, and it then rearranges to a dihydrogen (H_2) complex, which may transform into a classical dihydride. $[\text{CpRuH}(\text{CO})(\text{PCy}_3)]$ interacts with proton donors HOR, and the proton is transferred, via an Ru–H···H–O interaction, which ends with the formation of a cationic dihydrogen complex, $[\text{CpRu}(\text{H}_2)(\text{CO})(\text{PCy}_3)]^+[\text{OR}]^-$. The anion can then replace the H_2 ligand, so that formally H was replaced by OR [40c]. The kinetics of the reaction was experimentally studied by low temperature infrared spectroscopy, in different solvents, and complemented by a DFT study. Similar studies were performed with other metal complexes, namely $[\text{Cp}^*\text{FeH}(\text{dppe})]$ [40d], $[\text{ReH}_2(\text{CO})(\text{NO})(\text{PR}_3)]$ and $[\text{ReHCl}(\text{CO})(\text{NO})(\text{PMe}_3)]$ [40f], and $[\text{Cp}_2\text{NbH}_3]$, and transfer of hydrogen was observed [40g]. A remarkable feature of these systems is that the interaction always takes place at hydride, the metal never playing a direct role. In many cases, it is possible, using complementary techniques, to compare the behavior of the system in the solid and in the solution, the M–H···H–X pattern being always present.

Chiral diphosphine ligands (PP*) were used to prepare $[\text{CpRuH}(\text{PP}^*)]$ complexes with the enantiomerically pure or racemic ligand and study their reaction with acids (HBF_4 and HCF_3COO), in order to investigate in detail the kinetics of the proton transfer reaction [41].

It is interesting that when 1 equivalent of HCF_3COO was used, the reaction proceeded via the formation of an intermediate with a very short dihydrogen bond, the H···H distance in the Ru–H···H–O group being estimated, from NMR relaxation times, to be 1.43 Å. This species, the first of its kind, was considered as an intermediate state between the coordinated dihydrogen and the classical dihydrogen bond, formed in the beginning (Scheme 4).



Scheme 4. A proposed mechanism for hydrogen transfer.

In this new intermediate, the hydride and proton character are exchanged between the two hydrogen atoms, the anion jumping from one to the other. The system then continues to react.

The reaction of simpler metal hydrides, such as LiH, with C–H proton donors from several species (CH₄, CH₃F, CH₂F₂, CHF₃, CH₃Cl, CH₂Cl₂, CHCl₃) was systematically studied, using MP2 calculations with large basis sets and an AIM analysis was performed. In all the cases, BCPs were detected between the two hydrogen atoms, characterized by a small charge density and a small, positive laplacian. An energy decomposition analysis indicated that in most cases the electrostatic term was the largest contributor to the attractive interaction (all interactions were attractive at the MP2 level) [42].

The XC–H···H–M interaction was studied for M = Li, Na, K and X = F, Cl, Br, but a different approach was used, so that a direct comparison with the previous examples is not straightforward [43].

Other examples of C–H···H–M short contacts [44] were found in iridium complexes, and the competition between agostic interactions and hydrogen bonds was tested by QMMM calculations for several R groups hanging from an orthometallated benzoquinoline ligand. The agostic structure is favored for *t*-Bu, but the hydrogen bond is preferred by isopropyl [44b].

4 OTHER RELATED DIHYDROGEN BONDS E–H···H–X

Other atoms can replace the metal ion in interactions of the same kind. Boron has been the most studied. For instance, B–H bonds in closed carboranes can undergo interactions with proton donors, which are very similar to those described above and were studied with the same techniques [45]. Other molecules containing boron have been studied both experimentally and theoretically in recent years [46], but their analysis is outside the scope of this work.

5 THE SYMMETRIC DIHYDROGEN BOND M–H···H–M

These systems are particularly intriguing, since electrostatic factors cannot explain the interaction. Among the existing systems, [MnH(CO)₅] [8] is one of the most interesting, since it forms dimers in the solid state [8a], with a H···H distance of 2.292 Å, the angle between the two C–Mn–H axes being 155.8° (Fig. 7). These data were taken from the neutron diffraction study of the α polymorph [8a], which are more reliable than the X-ray values (β polymorph; they were found to be essentially the same) [8b]. The structure of the isolated molecule has also been determined by electron diffraction studies. The dimer was studied by the Extended Hückel (EH) method and the DFT calculations in an earlier work, and the nature of the H···H interaction could be explained as a weakly bound bridging dihydrogen molecule [6j].

More recently, a comparison of the HF and MP2 study of the H···H approach along the experimental angle between the two C–Mn–H axes

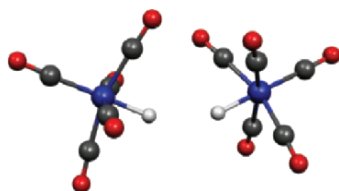


Figure 7 (see color section). The neutron diffraction structure of the $[\text{MnH}(\text{CO})_5]$ dimer.

(155.8°) revealed the importance of correlation [47]. Indeed, while HF calculations lead to increasing repulsion as the $\text{H}\cdots\text{H}$ distance decreases, the MP2 results show the existence of a well-defined minimum for a distance of 1.51 \AA . The shorter than the experimental value is probably due to the relatively small basis set that could be used (6-311G**). The interaction energy was calculated to be $-5.1 \text{ kcal mol}^{-1}$, after the BSSE correction [11]. As expected [48], the correction for this type of interaction was not negligible ($4.6 \text{ kcal mol}^{-1}$). The linear approach of the two $[\text{MnH}(\text{CO})_5]$ molecules was also studied under the same conditions. The equilibrium distance was close to 1 \AA , and the interaction energy was calculated as $12.7 \text{ kcal mol}^{-1}$, after the BSSE correction [47]. Although this energy is much higher than the energy calculated for the nonlinear approach, the geometries were not fully optimized; on the other hand, it is known that MP2 methods tend to lead to too high energies [49]. Therefore, packing forces might be more relevant than the calculated energies suggest. The $\text{H}\cdots\text{OC}$ interaction can also be envisaged in this system and has been observed in other cases [50].

Calculations run along the same lines as above showed a very long $\text{H}\cdots\text{O}$ equilibrium distance of 2.56 \AA and a BSSE-corrected interaction energy of only $0.6 \text{ kcal mol}^{-1}$: no interaction.

This dimer was revisited very recently and an AIM analysis performed [23]. The geometry was fully optimized in C_2 symmetry with ADF/PW91 and single point MP2 calculations were also carried out, in order to obtain more reliable energies. The $\text{H}\cdots\text{H}$ distance was 2.353 \AA , with an OC-Mn-H angle of 155.7° , in good agreement with the neutron data [8a]. The AIM analysis revealed BCPs between the two hydrogens of the dimer, as well as in all the formal covalent bonds. The results from MP2 and B3LYP (Gaussian 03) and ADF/PW91 were qualitatively similar, as can be seen in Table 3.

The most interesting result is that the laplacian for the $\text{H}\cdots\text{H}$ interaction is negative, suggesting that we are in the presence of a (weak) covalent bond. The BCP for the Mn-H bond, expected to be a true covalent bond, is also characterized by a negative laplacian and positive charge density, but the values of ρ are much larger. According to this analysis, one might be tempted to assign the $\text{H}\cdots\text{H}$ bond as a weak covalent bond, making the EH interpretation more realistic.

Table 3. Charge density ρ and $\nabla^2\rho$ for selected bond critical points of the $[\text{MnH}(\text{CO})_5]$ dimer (MP2, B3LYP, and ADF results)

Bond	MP2		B3LYP		ADF	
	ρ	$\nabla^2\rho$	ρ	$\nabla^2\rho$	ρ	$\nabla^2\rho$
H···H	0.008	-0.004	0.007	-0.004	0.007	-0.004
H-Mn	0.108	-0.054	0.114	-0.017	0.113	-0.026

An energy decomposition analysis was also carried out (ADF/PW91; Table 4), and showed, in agreement with the features of the BCP, that the orbital interaction is an important term in the attractive interaction between the two molecules in the dimer, about 25% larger than the electrostatic term. The Pauli repulsion has about the same magnitude as the orbital interaction. The binding energy is only $0.86 \text{ kcal mol}^{-1}$, and all these values are so small, that this interpretation should be tested with other approaches.

This H···H interaction is indeed a very weak one, but it was shown to be more efficient than the H···OC alternative. A very different situation occurs when one of the carbonyl groups is replaced by a triphenylphosphine, where C-H bonds are available, and other kinds of interactions may take place [51]. Indeed, one C-H bond from the phosphine becomes engaged in a C-H···H-Mn interaction. The molecular geometry is comparable to that of $[\text{MnH}(\text{CO})_5]$, with $C_{\text{ax}}-\text{M}-C_{\text{eq}}$ angles larger than 90° , so that carbonyl groups approach the hydride. The Mn-H bond length is $1.573(2) \text{ \AA}$, very close to $1.601(16) \text{ \AA}$ in $[\text{MnH}(\text{CO})_5]$ [8a]. The H···H distance is $2.101(3) \text{ \AA}$. The authors experimentally determined the charge density and its topology, having found BCPs between the two hydrogen atoms in C-H···H-Mn and in the other bonds. For the dihydrogen bond, the laplacian at the BCP was found to be positive, reflecting a closed shell interaction, and the charge density was 0.066. Both values are high, compared to those normally obtained from theoretical calculations of similar bonds [52], including our above result for $[\text{MnH}(\text{CO})_5]$. On the other hand, they found a negative laplacian of the charge density for the BCP in the Mn-H bond [51].

Table 4. Energy decomposition for the interaction between the two $[\text{MnH}(\text{CO})_5]$ molecules in the dimer (ADF; energies in kcal mol^{-1})

(1) E_{Pauli}	1.18	
(2) E_{elect}	-0.87	
$E_{\text{steric}} = (1) + (2)$		-0.31
(3) E_{orb}	-1.17	
$E_{\text{int}} = (1) + (2) + (3)$		-0.86
(4) $\Delta E_{\text{prep}[\text{MnH}(\text{CO})_5]}$	~ 0	
Bonding energy		-0.86

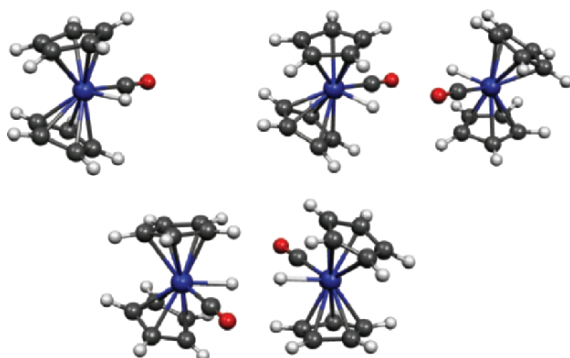


Figure 8 (see color section). The X-ray structure of the monomer $[(\eta^5 - \text{C}_5\text{H}_5)_2\text{MoH}(\text{CO})]^+$ (top, left), the monoclinic form (top, right) and the triclinic form (bottom).

The competition between $\text{H} \cdots \text{H}$ and $\text{H} \cdots \text{OC}$ interaction is particularly striking in the case of the solid state structures containing the $[(\eta^5\text{-C}_5\text{H}_5)_2\text{MoH}(\text{CO})]^+$ complex and $[(\eta^5\text{-C}_5\text{H}_5)\text{Mo}(\text{CO})_3]^-$ as counter ion, shown in Fig. 8. Indeed, short intermolecular contacts between cations could be found, both in the monoclinic form (short $\text{H} \cdots \text{OC}$ distances of 2.511 Å) [50], and in the triclinic form ($\text{Mo}-\text{H} \cdots \text{H}-\text{Mo}$ short distance of 2.234 Å) [53]. The EH calculations suggested the existence of weak hydrogen bonds in both cases, following positive overlap populations. In the monoclinic form ($\text{H} \cdots \text{OC}$), the hydride bears a positive charge (0.164) and the oxygen is negative (-0.662), allowing for an electrostatic interaction. On the other hand, in the triclinic form ($\text{H} \cdots \text{H}$), the bonding situation is similar to that found for the $[\text{MnH}(\text{CO})_5]$ dimer [6j].

This system is being studied at a higher calculation level, in order to determine the energetic, the energy decomposition pattern and perform an AIM analysis.

6 CONCLUSIONS

In recent years, more examples of the unconventional $\text{X}-\text{H} \cdots \text{M}$ or $\text{X}-\text{H} \cdots \text{H}-\text{M}$ hydrogen bonds were found and computational studies were carried out more systematically and using better methods, including in most cases the BSSE correction. The application of the AIM theory to detect BCPs and therefore the presence and nature of bonds also increased significantly. The role of the unconventional hydrogen bonds in several reactions, namely proton transfer, has been emphasized.

The dihydrogen bond has left the scope of the $\text{X}-\text{H} \cdots \text{H}-\text{M}$ interaction with a metal (or B) present, to include interactions such as $\text{X}-\text{H} \cdots \text{H}-\text{C}/\text{Si}$ and become responsible for arrangements in amino acids [54]. Metals are also involved in hydrogen bonds of other types. For instance, coordinated halogens often behave as acceptors in hydrogen bonds [55]. Electronegative atoms, such

as oxygen, or N–H bonds in ligands may also establish strong hydrogen bonds with other complementary groups of the counter ion or the solvent and influence the course of reactions [56].

The importance of all these kinds of hydrogen bonds in crystal engineering to design new structures has been shown in several recent reviews [57].

REFERENCES

1. L. Pauling, *The Nature of the Chemical Bond* (Cornell University Press, Ithaca, NY, 1939).
2. G. A. Jeffrey, W. Saenger, *Hydrogen Bonding in Biological Structures* (Springer-Verlag, Berlin, 1991).
3. (a) T. Steiner (1997) *Chem. Comm.* 727. (b) J. Bernstein, R. E. Davis, L. Shimoni, N.-L. Chang (1995) *Angew. Chem. Int. Ed. Engl.* 34, 1555. (c) T. Steiner (1995) *J. Chem. Soc., Perkin Trans.*, 2, 1315. (d) T. Steiner, E. B. Starikov, A. M. Amado, J. J. C. Teixeira-Dias (1995) *J. Chem. Soc., Perkin Trans.*, 2, 1321. (e) G. R. Desiraju (1991) *Acc. Chem. Res.* 24, 290. (f) Y. Gu, T. Kar, S. Scheiner (1999) *J. Am. Chem. Soc.* 121, 9411. (g) T. Steiner (1999) *Chem. Comm.* 313.
4. (a) L. Brammer, J. M. Charnock, P. L. Goggin, R. J. Goodfellow, A. G. Orpen, T. F. Koetzle (1991) *J. Chem. Soc., Dalton Trans.* 1789. (b) M. C. McCann, R. M. Bullock, R. K. McMullan, P. Sherwood (1992) *Organometallics* 11, 2339. (c) W. Yao, O. Eisenstein, R. H. Crabtree (1997) *Inorg. Chem. Acta* 254, 105.
5. (a) M. Nishio, M. Hirota (1989) *Tetrahedron* 45, 7201. (b) M. Nishio, Y. Umezawa, M. Hirota, Y. Taceuchi (1951) *Tetrahedron* 51, 8665. (c) L. R. Hanton, C. A. Hunter, D. H. Purvis (1992) *J. Chem. Soc., Chem. Comm.* 1134.
6. (a) J. C. Lee Jr., A. L. Rheingold, B. Muller, P. S. Pregosin, R. H. Crabtree (1994) *J. Chem. Soc., Chem. Comm.* 1021. (b) J. C. Lee Jr., E. Peris, A. L. Rheingold, R. H. Crabtree (1994) *J. Am. Chem. Soc.* 116, 11014. (c) E. Peris, J. C. Lee Jr., J. R. Rambo, O. Eisenstein, R. H. Crabtree (1995) *J. Am. Chem. Soc.* 117, 3485. (d) R. H. Crabtree, O. Eisenstein, G. Sini, E. Peris (1998) *J. Organomet. Chem.* 567, 7. (e) R. H. Crabtree, P. E. M. Siegbhan, O. Eisenstein, A. L. Rheingold, T. F. Koetzle (1996) *Acc. Chem. Res.* 29, 348. (f) R. H. Crabtree (1998) *J. Organomet. Chem.* 577, 111. (g) S. Park, R. Ramachandran, A. L. Lough, R. H. Morris (1994) *J. Chem. Soc., Chem. Comm.* 2201. (h) A. L. Lough, S. Park, R. Ramachandran, R. H. Morris (1994) *J. Am. Chem. Soc.* 116, 8356. (i) D.-H. Lee, B. P. Patel, E. Clot, O. Eisenstein, R. Crabtree (1999) *Chem. Comm.* 297. (j) D. Braga, P. de Leonardis, F. Grepioni, E. Tedesco, M. J. Calhorda (1998) *Inorg. Chem.* 37, 3337. (k) D. Braga, F. Grepioni, E. Tedesco, M. J. Calhorda, P. E. M. Lopes (1999) *New J. Chem.* 23, 219. (l) S. Gründemann, A. Kovacevic, M. Albrecht, J. W. Faller, R. H. Crabtree (2002) *J. Am. Chem. Soc.* 124, 10473.
7. (a) T. R. Richardson, S. Gala, R. H. Crabtree (1995) *J. Am. Chem. Soc.* 117, 12875. (b) T. Kar, S. Schneider (2003) *J. Chem. Phys.* 119, 1473. (c) A. Tanwar, S. Pal (2004) *J. Phys. Chem. A* 108, 11838. (d) Y. Meng, Z. Zhou, C. Duan, B. Wang, Q. Zhing (2005) *J. Mol. Struct. (THEOCHEM)* 713, 135.
8. (a) S. J. La Placa, W. C. Hamilton, J. A. Ibers, A. Davison (1969) *Inorg. Chem.* 8, 1928. (b) E. McNeill, F. R. Scholer (1977) *J. Am. Chem. Soc.* 99, 6243.
9. (a) T. Steiner, G. Desiraju (1998) *Chem. Comm.* 891. (b) F. A. Cotton, L. M. Daniels, G. T. Jordan IV, C. A. Murillo (1997) *Chem. Comm.* 1673. (c) R. G. A. Bone, R. F. W. Bader (1996) *J. Phys. Chem.* 100, 10892. (d) M. Mascal (1991) *Chem. Comm.* 303. (e) I. Alkorta, I. Rozas, J. Elguero (1998) *Struct. Chem.* 9, 243.
10. (a) P. Pykkö (1997) *Chem. Rev.* 97, 524. (b) P. Pykkö (1994) in *Crystal Engineering: From Molecules to Crystals to Materials*, D. Braga, F. Grepioni, A. G. Orpen (eds.) (Kluwer Academic Publishers, Dordrecht, 1999, and references therein).
11. B. S. Boys, F. Bernardi (1970) *Mol. Phys.* 19, 553.

12. (a) R. F. W. Bader, *Atoms in Molecules—A Quantum Theory* (Oxford Science Publications, Oxford, 1990). (b) R. F. W. Bader (1991) *Chem. Rev.* 91, 893.
13. (a) M. T. Carroll, C. Chang, R. F. W. Bader (1988) *Mol. Phys.* 63, 387. (b) M. T. Carroll, R. F. W. Bader (1988) *Mol. Phys.* 65, 695.
14. M. J. Calhorda (2000) *Chem. Comm.* 801.
15. F. H. Allen (2002) *Acta Crystallogr.* B58, 380.
16. P. L. A. Popelier, G. Logothetis (1998) *J. Organomet. Chem.* 555, 101.
17. (a) A. J. Canty, G. van Koten (1995) *Acc. Chem. Res.* 28, 406. (b) F. Neve, M. Ghedini, A. Crispini (1992) *Organometallics* 11, 3324. (c) A. Albinati, P. S. Pregosin (1990) *Inorg. Chem.* 29, 1812. (d) A. Albinati, F. Liana, P. S. Pregosin, B. Müller (1994) 33, 2522.
18. J. C. Mareque Rivas, L. Brammer (1999) *Coord. Chem. Rev.* 183, 43.
19. (a) F. Calderazzo, G. Fachinetti, F. Marchetti, P. F. Zanazzi (1981) *J. Chem. Soc., Chem. Comm.* 181. (b) M. C. McCann, R. M. Bullock, R. K. McMullan, P. Sherwood (1992) *Organometallics* 11, 2339.
20. L. Brammer (2003) *Dalton Trans.* 3145.
21. K. Kitaura, K. Morokuma (1976) *Int. J. Quantum Chem.* 10, 325.
22. I. Alkorta, I. Rozas, J. Elguero (2001) *J. Molec. Struct. (THEOCHEM)* 537, 139.
23. M. J. Calhorda, P. D. Vaz, unpublished results.
24. R. G. Parr, W. Yang, *Density Functional Theory of Atoms and Molecules* (Oxford, University Press, New York, 1989).
25. <http://www.scm.com/>
26. C. Møller, M. S. Plesset (1934) *Phys. Rev.* 46, 618.
27. L. Brammer, D. Zhao (1994) *Organometallics* 13, 1545.
28. (a) T. Ziegler, A. Rauk (1979) *Inorg. Chem.* 18, 1755. (b) T. Ziegler, A. Rauk (1978) *Inorg. Chem.* 18, 1758. (c) T. Ziegler, A. Rauk (1977) *Theor. Chim. Acta* 46, 1.
29. P. Ghosh, J. B. Bonanno, G. Parkin (1998) *J. Chem. Soc., Dalton Trans.* 2779.
30. T. Hascall, M.-H. Baik, B. M. Bridgewater, J. H. Shin, D. G. Churchill, R. A. Friesner, G. Parkin (2002) *Chem. Comm.* 2644.
31. N. M. Hardy, F. R. Lemke, L. Bramer (2001) *Organometallics* 20, 5670.
32. (a) G. I. Nikonov, P. Mountford, J. C. Green, P. A. Cooke, M. A. Leech, A. J. Blake, J. A. K. Howard, D. A. Lemenovskii (2000) *Eur. J. Inorg. Chem.* 1917. (b) G. I. Nikonov, I. Kuzmina, S. F. Vyboishchikov, D. A. Lemenovskii, J. A. K. Howard (1999) *Chem. Eur. J.* 5, 2947.
33. V. A. Levina, N. V. Belkova, E. I. Gutsul, D. A. Valyaev, O. A. Fillipov, L. M. Apstein, E. S. Shubina, A. Lledós, Int. Conference "From molecules towards materials," September 3–11, 2005, Nizhny Novgorod, Russia.
34. (a) D. Milstein, J. C. Calabrese, I. D. Williams (1986) *J. Am. Chem. Soc.* 108, 6387. (b) R. C. Stevens, R. Bau, D. Milstein, O. Blum, T. F. Koetzle (1990) *J. Chem. Soc. Dalton Trans.* 1429.
35. M. J. Calhorda, P. E. M. Lopes (2000) *J. Organomet. Chem.* 609, 53.
36. (a) S. Aime, M. Férriz, R. Gobetto (1999) *Organometallics* 18, 2030. (b) S. Aime, E. Diana, R. Gobetto, M. Milanesio, E. Valls, D. Viterbo (2002) *Organometallics* 21, 50. (c) S. Aime, F. Bertone, R. Gobetto, L. Milone, A. Russo, M. J. Stchedroff, M. Milanesio (2002) *Inorg. Chim. Acta* 334, 448. (d) S. Aime, M. R. Chierotti, R. Gobetto, A. Russo, M. J. Stchedroff (2003) *Inorg. Chim. Acta* 351, 251.
37. (a) T. Beringuelli, G. d'Alfonso, M. Panigati, P. Mercandelli, A. Sironi (2002) *Chem. Eur. J.* 8, 5340. (b) M. Panigati, P. Mercandelli, G. d'Alfonso, T. Beringuelli, A. Sironi (2005) *J. Organomet. Chem.* 690, 2044.
38. (a) J. Wessel, J. C. Lee Jr., E. Peris, G. P. A. Yap, J. B. Fortin, J. S. Ricci, G. Sini, A. Albinati, T. F. Koetzle, O. Eisenstein, A. L. Rheingold, R. H. Crabtree (1995) *Angew. Chem. Int. Ed. Engl.* 34, 2507. (b) B. P. Patel, W. Yao, G. P. A. Yap, A. L. Rheingold, R. H. Crabtree (1996) *Chem. Comm.* 991. (c) J. C. Lee Jr., W. Yao, R. H. Crabtree, H. Rügger (1996) *Inorg. Chem.* 35, 695. (d) B. P. Patel, K. Kavallieratos, R. H. Crabtree (1997) *J. Organomet. Chem.* 528, 205. (e) R. Bosque, F. Maseras, O. Eisenstein, B. P. Patel, W. Yao, R. H. Crabtree (1997) *Inorg. Chem.* 36, 5505.

39. W. K. Fung, X. Huang, M. L. Man, S. M. Ng, M. Y. Hung, Z. Lin, C. P. Lau (2003) *J. Am. Chem. Soc.* 125, 11539.
40. (a) L. E. Epstein, E. S. Shubina (2002) *Coord. Chem. Rev.* 231, 165. (b) E. S. Shubina, N. V. Belkova, L. E. Epstein (1997) *J. Organomet. Chem.* 536, 17. (c) N. V. Belkova, M. Besora, L. E. Epstein, A. Lledós, F. Maseras, E. S. Shubina (2003) *J. Am. Chem. Soc.* 125, 7715. (d) N. V. Belkova, P. O. Revin, L. E. Epstein, E. V. Vorontsov, V. I. Bakhmutov, E. S. Shubina, E. Collange, R. Poli (2003) *J. Am. Chem. Soc.* 125, 11106. (e) N. V. Belkova, E. Collange, P. Dub, L. E. Epstein, D. A. Lemenovskii, A. Lledós, O. Maresca, F. Maseras, R. Poli, P. O. Revin, E. S. Shubina, E. V. Vorontsov (2005) *Chem. Eur. J.* 11, 873. (f) N. V. Belkova, E. S. Shubina, E. I. Gutsul, L. E. Epstein, I. L. Eremenko, S. E. Nefedov (2000) *J. Organomet. Chem.* 610, 58. (g) E. V. Bakhmutova, V. I. Bakhmutov, N. V. Belkova, M. Besora, L. E. Epstein, A. Lledós, G. I. Nikonov, E. S. Shubina, J. Tomàs, E. V. Vorontsov (2004) *Chem. Eur. J.* 10, 661.
41. E. Cayuela, F. A. Jalón, B. R. Manzano, G. Espino, W. Weissensteiner, K. Mereiter (2004) *J. Am. Chem. Soc.* 126, 7049.
42. P. Lipkowski, S. Grabowski, T. L. Robinson, J. Leszczynski (2004) *J. Phys. Chem. A* 108, 10865.
43. W. Zierkiewicz, P. Hobza (2004) *PCCP* 6, 5288.
44. (a) T. Richardson, T. F. Koetzle, R. H. Crabtree (1996) *Inorg. Chim. Acta* 250, 69. (b) E. Clot, O. Eisenstein, T. Dubé, J. W. Faller, R. H. Crabtree (2002) *Organometallics* 21, 575.
45. E. S. Shubina, E. V. Bakhmutova, A. M. Filin, I. B. Siaev, L. N. Teplitskaya, A. L. Chistyakov, I. V. Stankevich, V. I. Bakhmutov, V. I. Bregadze, L. E. Epstein (2002) *J. Organomet. Chem.* 657, 155.
46. (a) T. Kar, S. Scheiner (2003) *J. Chem. Phys.* 119, 1473. (b) A. Tanwar, S. Pal (2004) *J. Phys. Chem. A* 108, 11838. (c) Y. Meng, Z. Zhou, C. Duan, B. Wang, Q. Zhong (2005) *J. Mol. Struct. (THEOCHEM)* 713, 135.
47. M. J. Calhorda, P. J. Costa (2002) *CrystEngComm* 4, 1.
48. (a) I. Alkorta, J. Elguero, C. Foces-Foces (1996) *Chem. Comm.* 1633. (b) S. J. Grabowski (2000) *J. Phys. Chem. A* 104, 5551. (c) S. J. Grabowski (2001) *Chem. Phys. Lett.* 338, 361. (d) S. J. Grabowski (2001) *J. Phys. Chem. A* 105, 10739.
49. P. Pyykkö, N. Runeberg, F. Mendizabal (1997) *Chem. Eur. J.* 3, 1451.
50. A. S. Antsyshkina, L. M. Dikareva, M. A. Porai-Koshits, V. N. Ostrikova, Yu. V. Skripkin, O. G. Volpov, A. A. Pasynskii, V. T. Kalinnikov (1985) *Koord. Khim.* 11, 82.
51. Y. A. Abramov, L. Brammer, W. T. Klooster, R. M. Bullock (1998) *Inorg. Chem.* 37, 6317.
52. (a) U. Koch, P. L. A. Popelier (1995) *J. Phys. Chem.* 99, 9747. (b) P. L. A. Popelier (1998) *J. Phys. Chem. A* 102, 1873.
53. J. A. Marsella, J. C. Huffman, K. G. Caulton, B. Longato, J. R. Norton (1982) *J. Am. Chem. Soc.* 104, 6360.
54. H. Pakiari, Z. Jamshidi (2004) *J. Mol. Struct. (THEOCHEM)* 685, 155.
55. (a) G. Aullón, D. Bellamy, L. Brammer, E. A. Bruton, A. G. Orpen (1998) *Chem. Comm.* 653. (b) L. Brammer, E. A. Bruton, P. Sherwood (2001) *Cryst. Growth Des.* 1, 277. (c) F. Zordan, L. Brammer (2004) *Acta Crystallogr. B* 60, 512. (d) L. Brammer, G. M. Espallargas, H. Adams (2003) *CrystEngComm* 5, 343.
56. (a) M. C. Buzzeo, A. H. Iqbal, C. M. Long, D. Millar, S. Patel, M. A. Pellow, S. A. Saddough, A. L. Smenton, J. F. C. Turner, J. D. Wadhawan, R. G. Compton, J. A. Golen, A. L. Rheingold, L. H. Doerrer (2004) *Inorg. Chem.* 43, 7709. (b) H. Mori, E. Miyoshi (2004) *Bull. Chem. Soc. Jpn.* 77, 687. (c) P. Braunstein, Y. Chauvin, S. Mercier, L. Saussine (2005) *C. R. Chimie* 8, 31.
57. (a) L. Brammer, J. C. M. Rivas, R. Atencio, S. Fang, F. C. Pigge (2000) *J. Chem. Soc., Dalton Trans.* 3855. (b) L. Brammer (2004) *Chem. Soc. Rev.* 33, 476. (c) D. Braga, L. Brammer, N. R. Champness (2005) *CrystEngComm* 7, 1.

CHAPTER 7

CONTRIBUTION OF CH...X HYDROGEN BONDS TO BIOMOLECULAR STRUCTURE

STEVE SCHEINER

Department of Chemistry and Biochemistry, Utah State University, Logan, UT 84322-0300, USA.
E-mail: schein@cc.usu.edu

Abstract The history of weak CH...X hydrogen bonds is discussed, beginning with early hints of their existence, to our current understanding of their widespread occurrence. While the presence of such bonds is no longer contested, there is a great deal of uncertainty regarding whether, and to what degree, these weak interactions may contribute to the structure of biomolecules. The ability of quantum calculations to address this issue, and their success to date, are discussed in detail.

Keywords: Quantum chemical; weak H-bonds; proteins; amides; imidazole; benzene; indole; phenol; alanine; nucleic acids.

1 INTRODUCTION

The importance of the hydrogen bond to the structure and function of biological molecules can hardly be overstated. This phenomenon was a primary ingredient even in the original development of such fundamental structural components as the α -helix of proteins and the transmission of the genetic code via DNA base pairing. And indeed, the multitude of ways in which H-bonds are now known to participate in biological function has grown exponentially in the ensuing years.

Whereas the function of standard H-bonds such as NH...O and OH...O is now appreciated, the contributions of weaker interactions remain an active area of inquiry. For example, the approach of a OH-bearing group as a proton donor toward the electron cloud that hovers above an aromatic ring, in a so-called OH... π H-bond, is becoming more widely recognized. A particularly interesting unconventional H-bond makes use of a CH group as a proton donor. Early skepticism about this phenomenon was based primarily on the low electronegativity of carbon, which reduces the partial positive charge that is

believed to be necessary to reside on the H if it is to act as a bridging atom. On the other hand, there are a number of features which can promote the acidity of a CH group. One obvious example is HCN, wherein the triple bond to the N makes this molecule into a potent acid, and one which unquestionably engages in CH \cdots X H-bonding. In a biological context, the pair of amide groups that surround the C $^{\alpha}$ H of each amino acid within a protein ought to be electron-withdrawing enough to accomplish the same feat. The building blocks of nucleic acids and carbohydrates likewise abound in CH groups that are bordered by electronegative atoms; so there is reason to suspect CH \cdots X H-bonds on these biomolecules as well.

2 HISTORICAL RECORD

It is interesting to read the scientific record on the topic of CH \cdots X H-bonds. Probably the earliest tangible evidence for their existence dates to the late 1930s. This sort of interaction was invoked to help explain curious observations concerning mixtures of chloroform with ether in the liquid phase [1], the anomalously high dissociation constants of *o*-toluic and *n*-butyric acids [2], and heat of mixing data [3]. In terms of biologically relevant molecules, an X-ray diffraction analysis of uracil in 1954 found the geometrical earmarks of a CH \cdots O H-bond, with surprisingly short C \cdots O contact distances [4]. The 1960s witnessed the spread and refinement of structural data of biological systems [5], e.g., the collagen triple helix [6] wherein the C $^{\alpha}$ H of amino acids form H-bonds to bound water molecules. Indeed, even in 1963, some authors [7] went so far as to suggest that “it is tempting to speculate as to whether the CH \cdots O hydrogen bond plays as important a part in the structure of biological molecules as the other kinds of H-bonds do.”

Spectroscopic measurements offered another main avenue of experimental information concerning CH \cdots X H-bonds. For many years, one of the hallmarks of a H-bond of the OH \cdots X type was the strong red shift of the OH stretching frequency. It was therefore a surprise when some data first reported in the 1950s [8–12] indicated that CH bonds might behave in the opposite fashion, i.e., shift to the blue. However, these observations were sporadic and were not necessarily characteristic of all such CH \cdots X bonds. Indeed, some of the most systematic work of the 1960s [13] used IR data to solidify the notion of CH \cdots O interactions as true H-bonds. And such sorts of analysis were able to successfully extend the reach of spectroscopic verification of CH \cdots O H-bonds into the realm of biomolecules, e.g., polyglycine and myoglobin [14] at about the same time.

By the mid-1970s, the existence of CH \cdots X H-bonds had achieved general acceptance [15], with verification coming from a range of different measurements that included vapor pressure, azeotrope formation, second virial coefficient, solubility, freezing-point diagrams, enthalpies of mixing, dipole moments, viscosity, refractive index, and electronic, vibrational, and NMR

spectroscopy [16–18]. Likewise, there were a number of studies of nucleic acid structures [19–23] that together offered convincing geometrical evidence that these bonds not only exist, but exert a direct effect upon the structures adopted by these biomolecules.

2.1 Proliferation of the Concept

Once these H-bonds were established in the literature as a real phenomenon, researchers became far more conscientious in terms of looking for signs of them within their collected data. It was at about this point, then, that the literature mushroomed with sightings of $\text{CH}\cdots\text{X}$ H-bonds. In a neutron diffraction study of 113 crystals, Taylor and Kennard [24] found a statistically significant tendency to form short $\text{CH}\cdots\text{O}$ intermolecular contacts. A certain amount of directional character was observed [25] in the $\text{CH}\cdots\text{O}$ bonds of several planar oxygenated aromatics, sufficient to steer structure to a sheet-based β -form. The H-bonding character was further confirmed by a clear relationship between the number of electron-withdrawing Cl atoms on the CH donor and the length of the putative H-bond [26].

In the biological realm, a 1982 survey of 32 neutron diffraction structures of amino acid crystals [27] noted geometrical evidence, especially those involving the C^αH group. Berkovitch-Yellin and Leiserowitz [28] described the role played by $\text{C-H}\cdots\text{O}$ and $\text{C-H}\cdots\text{N}$ interactions in determining molecular packing and conformation. They were seen as instrumental in fixing packing motifs in α -glycine, uracil, and quinone–phenol complexes, among others. It was interesting that their observed $\text{CH}\cdots\text{X}$ bonds included C in all three of its common hybridizations. They attributed the interbilayer arrangement in α -glycine to these bonds. And Parthasarathy et al. [29], made the intriguing claim that $\text{C}^\alpha\text{H}\cdots\text{O}$ bonds were instrumental in the adoption of parallel vs. antiparallel β -sheet structure in a dipeptide crystal. One realizes that a proposal has reached wide acceptance when it makes its appearance in the textbooks. Saenger's 1984 text on nucleic acid structure [30] made several references to $\text{CH}\cdots\text{O}$ H-bonds, mentioning their importance to particular orientations of bases, stability of nucleosides with anti-bases, and even possible interactions of amino acids with base pairs.

The decade of the 1990s saw what could arguably be termed an explosion of studies of the $\text{CH}\cdots\text{X}$ interaction that broadened the sorts of systems that engage in this phenomenon, while better defining it [31, 32]. Alkynes and alkenes were found to participate in such bonds [33–36], as did aryl groups [37–42], and even CH groups present in smaller rings [43, 44], carboranes [45] and even cubyl arrangements [46]. Organometallic systems were also found to contain such bonds on a regular basis [47–49]. Other studies began to outline how the nature of the proton acceptor can influence the strength of this bond [50, 51]. The preponderance of evidence for this sort of interaction at this point

in time is exemplified by a statistical analysis [52] that identified fully 965 examples of the CH \cdots N bond.

2.2 Biological Systems

Studies of these weak H-bonds accelerated in biological systems at about this same time as well. A 1991 survey based on neutron diffraction of 32 zwitterion amino acids [53] noted good evidence for the existence of CH \cdots O=C interactions, a conclusion echoed by analysis of 16 high-precision neutron diffraction sets of α -amino acids [54]. The collagen triple helix, too, showed evidence of C $^{\alpha}$ H \cdots O=C H-bonding, in a pattern identical to that of β -sheets in globular proteins [55]. Other β -sheets displayed geometric evidence of CH \cdots O interactions [56, 57]. Indeed, Fabiola et al. [58] observed CH \cdots O bonds to be quite a widespread occurrence in β -sheets, and disputed the claim that they might simply be the result of mere steric dispositions. The His residue appeared to be a potent CH donor [59–61] as is the proline residue [62]. An extensive survey of known protein structures in 1995 [63] suggested that a large percentage of short C $^{\alpha}$ H \cdots O=C contacts are cohesive, a predecessor of work to come when the authors, accepting that “CH \cdots O may be ubiquitous in macromolecular structures,” went on to ask the important question: “Are they significant energetically?”

Nucleic acids, too, were under intense scrutiny and yielded a large number of CH \cdots X contacts [64–66]. C–H \cdots O bonds were termed a “prime determinant for base pairing specificity” [67], a sentiment that was reinforced by numerous other studies that followed [68–72]. It is not only the bases themselves, but other components of nucleic acids that seem able to participate in these bonds [73]. In an echo of the earlier question regarding proteins, Leonard et al. [74] noted that the exact contribution of these bonds is not known in nucleic acids. Steiner and Saenger [75] extended the concept of weak H-bonds to carbohydrates, calling the CH \cdots O bond a “third, direct cohesive host–guest interaction,” after van der Waals and normal H-bonds. These interactions have been observed repeatedly over the years [76].

3 CENTRAL QUESTION

As of the turn of the millennium, then, there had been countless sightings of CH \cdots X contacts in biological systems of all sorts. And inferences had been drawn that their presence must surely influence the geometries adopted by biomolecules. But a crucial question remained open: just how much do such weak H-bonds actually contribute to the conformations of biomolecules in an energetic sense? Knowledge had advanced to the point that a 2001 summary [77] concluded that CH \cdots O bonds constitute as much as 1/4 of all H-bonds in certain proteins so “can be expected to contribute significantly to the overall

stabilization energy of a protein.” But how much? As framed by investigators at various points in the recent history, “Nothing is known experimentally about the strength of these interactions and how this strength varies with the polarity of the proton donor.” [78] Wahl and Sundaralingam [76] had pointed out that these bonds “do not seem to play only a passive role” but rather “contribute to overall stabilization,” but were unable to be any more quantitative than this. And following an exhaustive survey of RNA geometries from X-ray and NMR data, Brandl et al. [73] had been led to conclude that “despite the occurrence of short $\text{C-H}\cdots\text{X}$ contacts their free energy contribution to RNA stability remains to be assessed.” Even by 2002, it was believed that there had been no experimental quantifications of $\text{CH}\cdots\text{O}$ H-bond energies [79]; “There are few experimental studies of the energetic contribution from any type of $\text{C-H}\cdots\text{O}$ H-bonds in protein or polypeptide systems.” [80] Such energetic quantities are simply not accessible via structural data: “the properties of $\text{CH}\cdots\text{O}$ H-bonds are not readily derived from geometrical parameters in one or a small number of crystal structures, because of significant structural interference from many other interactions.” [81]

Since roughly 2000, the interpretation of experimental data has led to direct inferences concerning the influence of $\text{CH}\cdots\text{X}$ H-bonds upon molecular structure and functions. Neutron diffraction data led Steiner [82] to consider how $\text{CH}\cdots\text{O}$ interactions might actively rotate a methyl group from its preferred staggered arrangement. Investigations by Thalladi et al. [83] led them to conclude that $\text{CH}\cdots\text{N}$ bonds might have structure-steering character, despite their weakness. Echoing this idea, Pigge et al. [84] suggested that a number of these weak H-bonds might perhaps override the effects of the stronger, more classical $\text{O-H}\cdots\text{O}$ and $\text{N-H}\cdots\text{O}$ types. Based upon crystal structure data of lariat and crown ethers, another group [85] found evidence that aryl $\text{CH}\cdots\text{O}$ bonds help to define the conformation and binding character of their complexes. Supramolecular self-assembly is another area where these bonds display some influence [86–88] and they seem to help with formation of inorganic channel structure [89, 90].

Biological systems too have revealed progressively more direct effects upon structure. $\text{CH}\cdots\text{O}$ bonds were taken as a primary cause for the formation of a folded novel β -turn in a model peptide [91] and a source of stability for a new sort of chain reversal motif in an amino acid crystal [92]. Based on a survey of 125 helix–helix interfaces in 11 membrane proteins [93], Engelman’s group claimed that $\text{CH}\cdots\text{O}$ contacts favor parallel right-handed packing of helices, a theme that was soon echoed by Babu et al. [94], extending the registration idea to strands in antiparallel orientation. An extensive survey of 634 proteins identified 111 Schellman motifs that contain $\text{C}^\alpha\text{H}\cdots\text{O}$ [95]; these bonds helped register both α -helices and β -strands. A 2003 work confirmed the importance of these bonds to the adoption of the Schellman motif [96], and went so far as to state there was now “firm evidence in support of the emerging view that

CH \cdots O interactions may contribute significantly in energetic terms in determining folded structures,” but alas, still nothing more quantitative.

High-pressure FTIR measurements in 2003 [97] indicated that C $^{\alpha}$ H \cdots O bonds help stabilize β -sheets. These interactions were also instrumental in the formation of extended β -strands in a chain containing D-chiral residues [98]. A helical hairpin motif was attributed [99] to CH \cdots O bonds between the side chains of one helix and the backbone of another in 2001. The large number (75) of CH \cdots O bonds exceeds the 49 conventional intersubunit H-bonds, indicating that the former contacts determine association and orientation of transmembrane helices in PSI [100]. A detailed survey [101] indicated that these bonds can affect the Trp rotation angle in proteins. These bonds were considered potentially as a driving force for ligand selectivity, as noted in the hydrophobic pocket of retinoic acid receptor RAR γ [102].

There have been attempts to estimate the quantitative contribution of these bonds by experimental means. Unfortunately, such estimates tend to be rather rough, and perhaps worse, tend to conflict with one another. Pierce et al. [103], for example, found that replacement of the NH of a thiazole by CH has little effect on K_i , implying that traditional and CH \cdots O H-bonds are roughly interchangeable in an energetic sense. Kallenbach's group [80] estimated CH \cdots O H-bond strength between Phe and Glu side chains by effects on helicity, via CD and NMR. Curiously, they found an energy of -0.5 kcal for one direction of the bond, but 0 for the other. Yohannan et al. [104] considered a C $^{\alpha}$ H \cdots O (Ala \cdots Thr) bond in bacteriorhodopsin. When the Thr residue was mutated to various other residues, only some of which were capable of forming such a bond, no evidence was found of an energetic loss. They concluded that “the mere presence of these H-bonds does not imply energetic significance,” but allowed that “even if most C $^{\alpha}$ H \cdots O H-bonds are not strongly stabilizing, it is likely that they do play an important role, because they allow closer packing than would be allowed if electron orbital overlaps could not occur.” In contrast, once again, another study in the same year [105] estimated the energy of a C $^{\alpha}$ H \cdots O bond within a protein to be 0.9 kcal.

4 THEORETICAL ANSWERS

It is fortunate that different methods of scientific inquiry frequently have complementary strengths. While experimental techniques are not amenable to extraction of the energetic contributions of a single phenomenon to overall stability of a biological molecule, theoretical methods can approach this question, albeit with some caution required. One early attempt to gauge the energetic contribution of CH \cdots O bonds was based upon a statistical potential [106]. Jiang and Lai estimated that these bonds might contribute an average of 17% of the total interaction energy at protein–protein interfaces, as high as 50% in certain cases. They alleged that these bonds are indispensable to forming a bifurcated H-bond motif between β -strands. However, this use of a

statistical potential is open to question, given its indirect means of assessing the energy.

Quantum chemical techniques offer a much more direct assessment of interaction energies, and have been used to good effect in a wide range of H-bond studies over the years [107]. As a secondary consideration, method development has reached the point where these methods have become increasingly more reliable, even for particularly weak interactions, such as $\text{CH}\cdots\text{O}$ bonds. Of course, no method is perfect, and quantum chemical methods have their share of weaknesses. In the first place, the computer resources needed for any given system rise as third, fourth, or even higher power of the size of the system considered, i.e., the number of atoms included in the model system. There is thus a strong tendency to limit the size of the system. There is a like increase in computer needs that accompany the use of increasingly more sophisticated, and thus more accurate, quantum chemical method. As an upshot, the record of quantum calculations over the years shows a trend toward as small a system as is reasonable to model a given system, and the use of as unsophisticated an approach as is likely to furnish a reasonable answer. Moreover, the vast majority of calculations in the literature pertain to the molecules considered explicitly, i.e., in vacuo. In other words, few quantum calculations take any account of the environment.

It is for this reason that the decade of the 1970s saw a number of considerations of $\text{CH}\cdots\text{X}$ bonds that were carried out for very small systems, with little biological relevance [108–111]. Moreover, these systems were considered by rather crude methods, either semiempirical, or *ab initio* but with small basis sets, and with no inclusion of electron correlation [112–114]. The data was interesting from a comparative point of view, but yielded little in the way of quantitatively useful information. Some of the work became more interesting in the next decade. For example, a SCF/4–31G calculation in 1984, even though crude, suggested that each progressive replacement of a H atom from CH_4 by Cl yields a progressively stronger $\text{CH}\cdots\text{O}$ bond when the chloromethane is paired with OH_2 as acceptor [115]. Indications were found [116] that the very weakly acidic HCCH might form a “true,” albeit weak, H-bond with NH_3 as acceptor. And calculations were made that rationalized the details of a low-temperature crystal structure [117] which revealed a curious eclipsing of hydrogens with N atoms in terms of $\text{CH}\cdots\text{N}$ bonds.

Emboldened by methodological advances, theoreticians began to apply their toolchest to quite a few more $\text{CH}\cdots\text{X}$ systems in the 1990s [118–121]. One of the earliest studies that examined a system with direct biological significance appeared in 1993 wherein Feller and Feyereisen [122], examined the $\text{CH}\cdots\text{O}$ interaction between an aryl CH of phenol (a possible model of the Tyr side chain) and the O of water. However, analysis of this interaction was hampered as it was weaker than, and secondary to, the more conventional $\text{OH}\cdots\text{O}$ H-bond between the same two molecules.

4.1 A Recurring Complication

Indeed, the latter turns out to be a common problem in attempts to elucidate the energy of a particular $\text{CH}\cdots\text{X}$ bond: its weakness tends to make it secondary to stronger, conventional H-bonds. One is thus confronted with the presence of two or more H-bonds, and the puzzle of how to dissect the total interaction energy into the contribution from each. The conundrum is confounded by the fact that each bond induces a certain amount of strain into the other, so even if the total interaction energy could be unambiguously deconvoluted, each H-bond is weaker than it would be if unstrained. As another example of this issue, calculations by Turi and Dannenberg [123] addressed pairs of acetic acid molecules, potential models of Asp and Glu side chains. As illustrated in Fig. 1, one of the minima identified in the surface contains not only a standard $\text{OH}\cdots\text{O}$, but also a $\text{CH}\cdots\text{O}$ bond which is clearly bent from its optimal θ ($\text{CH}\cdots\text{O}$) angle of 180° . Consequently, the authors' estimate of the H-bond energy was necessarily ambiguous, and different means of carrying out this deconvolution varied over the wide range between 0.5 and 1.8 kcal/mol.

Intramolecular $\text{CH}\cdots\text{O}$ interactions suffer from similar problems, which are exacerbated by the inherent ambiguity in determining an interaction energy of a particular interaction, within the context of a single molecule. A typical example is provided by the analysis by Tsuzuki et al. [124] of the $\text{CH}_3\text{OCH}_2\text{CH}_2\text{OCH}_3$ molecule. Some of the conformers are illustrated in Fig. 2. All contain at least one $\text{CH}\cdots\text{O}$ interaction, but there remains the difficulty of assessing the interaction energy of each. After resorting to molecular mechanics, and ab initio computations of other (bimolecular) systems to help with the analysis, the authors arrived at a crude estimate of 1.2–1.4 kcal/mol for each $\text{CH}\cdots\text{O}$.

5 BIOLOGICAL SYSTEMS

There have been a number of systems considered over the years that have biological relevance, and which contain $\text{CH}\cdots\text{X}$ interactions. The sizes of the systems vary considerably, in the sense that in some cases the connection

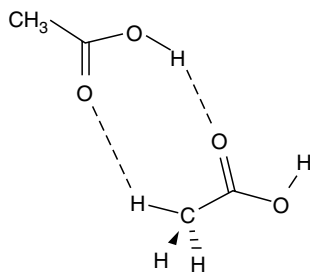


Figure 1. One of the several geometries adopted by acetic acid, indicating both putative $\text{OH}\cdots\text{O}$ and $\text{CH}\cdots\text{O}$ H-bonds by broken line, from Ref. [123].

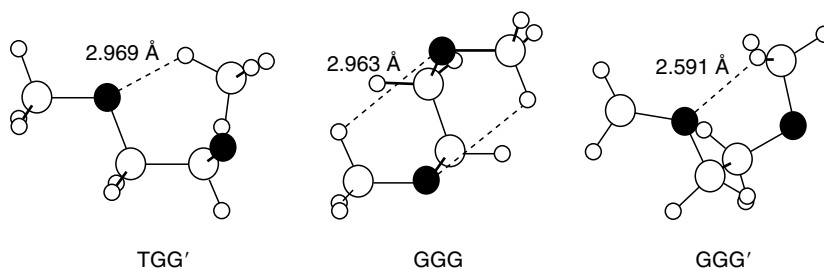


Figure 2. Various conformers of the $\text{CH}_3\text{OCH}_2\text{CH}_2\text{OCH}_3$ molecule calculated with 6-311+G* basis set [124]. O atoms are designated by filled circle, C and H by open circles. $R(\text{H}\cdots\text{O})$ distances indicated for each suspected $\text{CH}\cdots\text{O}$ H-bond.

between the actual system being studied, and the biological system which it is intended to model, are more tenuous than in others. The following summary is organized so as to first describe the results of systems that are related to nucleic acids, and then proteins.

5.1 Nucleic Acids

The stabilizing role of $\text{C}-\text{H}\cdots\text{O}=\text{C}$ contacts in base pairs was evaluated for the Watson-Crick adenine-uracil (AU) pair by Starikov and Steiner [125]. Their ab initio calculations indicated these bonds contributed only about 6% to the total interaction energy. A better estimate might be achieved via the correlated calculations of the dimer of pyrimidine [126] (related to DNA base pairs) like that shown in Fig. 3. This dimer does not contain any conventional H-bonds,

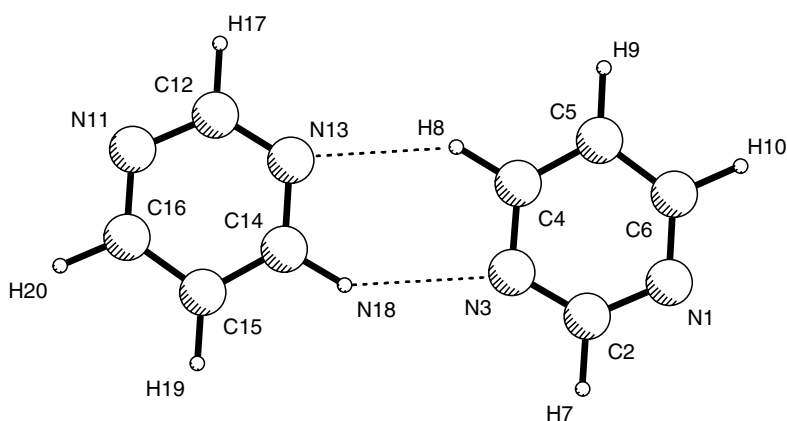


Figure 3. Optimized dimer of pyrimidine [126] as obtained at HF/6-31++G** level. $\text{CH}\cdots\text{N}$ bonds indicated by broken lines.

so the pair of $\text{CH}\cdots\text{N}$ H-bonds may be considered the entirety of the “glue.” One might thus divide the total interaction energy of 3.25 kcal/mol by the number of $\text{CH}\cdots\text{N}$ bonds (2) to arrive at an estimate of 1.6 kcal/mol for each.

A wide assortment of different possible geometries for the uracil dimer were examined [127] in 1998. The most stable of all these contained a pair of $\text{NH}\cdots\text{O}$ bonds, but another was identified, only slightly less stable than the others, in which one of these conventional H-bonds was replaced by $\text{CH}\cdots\text{O}=\text{C}$. There was no way of estimating the energetic contribution of this particular interaction, as it was secondary to the stronger $\text{NH}\cdots\text{O}$ bond. A study of the adenine–thymine pair [128] noted a blue shift of the C–H stretching frequency, an indication of a H-bond, but the authors did not attempt to extract an interaction energy.

Hobza and coworkers [129, 130] later identified a number of base pair combinations, that contained what appeared to be a secondary $\text{CH}\cdots\text{O}$ interaction, some of which are pictured in Fig. 4. The AU pair corresponds to a Watson–Crick arrangement. UU C is so designated as this sort of geometry was first noticed by a group in Calcutta; the UU 7 pair would not occur in nucleic acids as the bridging H would normally be replaced by the connection of the U base to the chain. Of course, these $\text{CH}\cdots\text{O}$ bonds are only one of the several in each pair, and no attempt was made to determine the energy of any separately. The authors carried out analysis of the wave functions and vibrational frequencies but these were aimed primarily toward establishing whether these $\text{CH}\cdots\text{O}$ interactions are cohesive, and whether they obey the normal characteristics of H-bonds, nothing more quantitative regarding energetics.

This so-called Calcutta UU base was the target of another study [131] which also considered AA and UA pairs. The total UU interaction energy was computed to be 7.6 kcal/mol and that of AA 5.0 kcal/mol. In order to extract

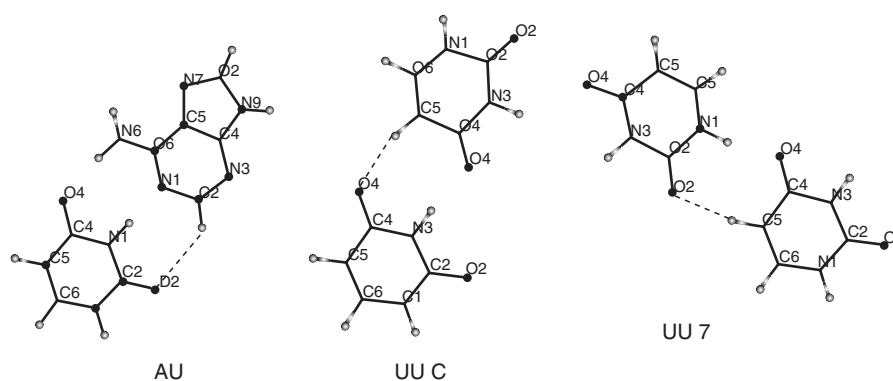


Figure 4. Adenine–Uracil (AU) and Uracil–Uracil (UU) dimers optimized at MP2/6–31G** level [130]. Putative $\text{CH}\cdots\text{O}$ bonds indicated by broken lines.

the energy of the H-bonds themselves, one of the bases in each pair was replaced by formaldehyde. However, the resulting complexes still contained a pair of H-bonds, sidestepping the important question as to the binding energy of any single $\text{CH}\cdots\text{X}$ interaction.

The clusters formed between pyrimidine and a group of water molecules was the subject of calculations coupled to multiphoton ionization measurements [132]. A $\text{CH}\cdots\text{O}$ bond appeared in several of these clusters, but was again secondary to stronger bonds, and there was no estimate of its energetic contribution.

Studies have also been carried out for full nucleosides. A 2001 analysis of the electron density [133] in lamivudine, a nucleoside analog, suggested that the intramolecular $\text{CH}\cdots\text{O}$ contacts were likely H-bonding in nature. However, other than the ability of such interactions to exert some influence upon the conformation, there was no quantitative information forthcoming. A computation of ribonucleosides [134] identified what appeared to be $\text{CH}\cdots\text{O}$ H-bonds in several conformations of guanosine, as based upon analysis of the wave function. But these bonds were only one, minor, component in the set of overall factors that govern the geometry (see Fig. 5), so there was no energy associated with them by the calculations. Likewise, a $\text{CH}\cdots\text{O}$ bond is present in one conformer of glucopyranose [135], but is only one of the four bonds, the others of which are of the stronger $\text{OH}\cdots\text{O}$ type.

In summary, then, there is little quantitative information derived from *ab initio* calculations that pertain to the energetic contribution of $\text{CH}\cdots\text{X}$ bonds to nucleic acid structure. The best data available at present derives from the pyrimidine dimer [126] wherein a value on the order of 1.6 kcal/mol was suggested. However, this quantity pertains to angularly distorted $\text{CH}\cdots\text{N}$ bonds in *vacuo*, with no account taken of the surroundings.

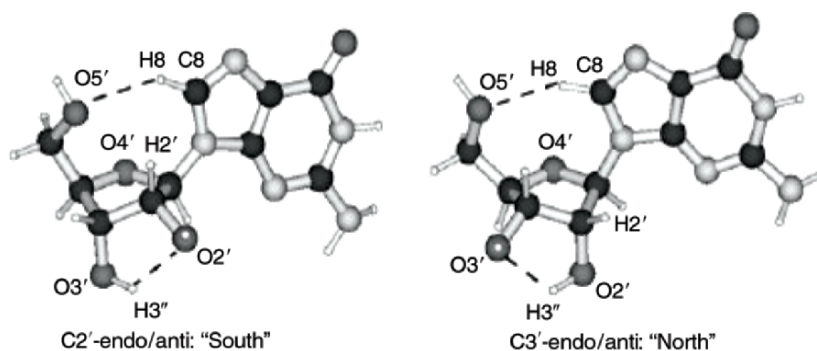


Figure 5. Geometries of guanosine, optimized at B3LYP/6-31G* level [134]. One potential $\text{CH}\cdots\text{O}$ bond is present in each, connecting the C8H8 group with O5'.

5.2 Proteins

As in the case of the nucleic acids, systems that model various segments of proteins tend to vary in both size and relevance to the full systems. One is beset with the same problems that the $\text{CH}\cdots\text{X}$ bonds of interest are typically secondary to stronger conventional H-bonds, and consequently distorted.

5.2.1 Amides and polypeptides

Amides represent probably the smallest sort of model of a peptide group, and have been subject to some scrutiny with regard to $\text{CH}\cdots\text{O}$ potential. The simplest of these is formamide. Note, however, as a caveat, that the bridging CH proton of HCONH_2 is directly bonded to what would represent the peptide C atom. Such a situation would not pertain in a polypeptide backbone where this C atom is bonded to O, N, and C.

A study of dimers of formamide [136] identified a number of structures that represent local minima on the surface. Some of these contain $\text{CH}\cdots\text{O}$ or $\text{CH}\cdots\text{N}$ interactions, but their energetic contributions were not disentangled from several other factors and stronger H-bonds. Hess's group considered [137] complexes pairing formamide with formic acid (a model of Glu and Asp), some of which contained a $\text{CH}\cdots\text{O}$ interaction, as illustrated in Fig. 6. These $\text{CH}\cdots\text{O}$ interactions are again secondary to stronger $\text{NH}\cdots\text{O}$ bonds, and rather distorted as well. Despite these distortions, the authors estimated their energetic contributions in the 2.5–4.0 kcal/mol range.

In a 2001 study of pairs of small amides [138], the CH donors were again bonded directly to the amide C, a CH which does not occur in polypeptides. This work led to estimates of the $\text{CH}\cdots\text{O}$ H-bond energy in the range of

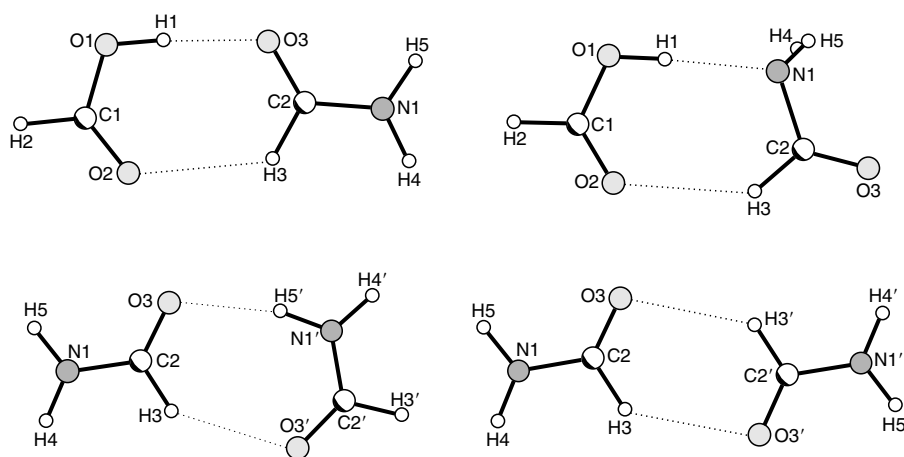


Figure 6. Minima identified on the potential energy surface of the $\text{HCOOH}/\text{HCONH}_2$ pair [137] which contain at least one putative $\text{CH}\cdots\text{O}$ bond.

1.9–2.6 kcal/mol. Other calculations [139] modeled the polypeptide chain by a pair of dimethylformamide molecules, in which one of the CH donors, a methyl group, is bordered on one side by an amide function, closer to the C^αH type that occurs in proteins. The four stable geometries obtained, illustrated in Fig. 7, indicate the difficulty of elucidating the interaction energy of any single such bond, none of which are even close to an optimal linear $\text{CH}\cdots\text{O}$ alignment. Moreover, the H-bonds are of various types in that it is the methyl groups acting as proton donors in configurations 2, 3, and 4, but aldehydic protons in 1. Nonetheless, the authors arrived at an estimate of the $\text{CH}\cdots\text{O}$ energy in the range of 2.1–2.7 kcal/mol. An attempt to extrapolate their result to a more realistic model of a polypeptide led to a rough guess of 3.5–4.5 kcal/mol. Another work was more relevant in that the donor was an aliphatic CH_2 group [140], but this group was again bordered by only one amide instead of two. Moreover, each geometry of the parent molecule contained various H-bonds, each of different type and each with different geometry (all angularly distorted), preventing any sort of unambiguous determination of the $\text{CH}\cdots\text{O}$ interaction energy.

Later work [141] reconsidered *N,N*-dimethylformamide, this time paired with one or more water molecules. Some of the minima, illustrated in Fig. 8, contained $\text{CH}\cdots\text{O}$ bonds emanating from the methyl groups, but also a

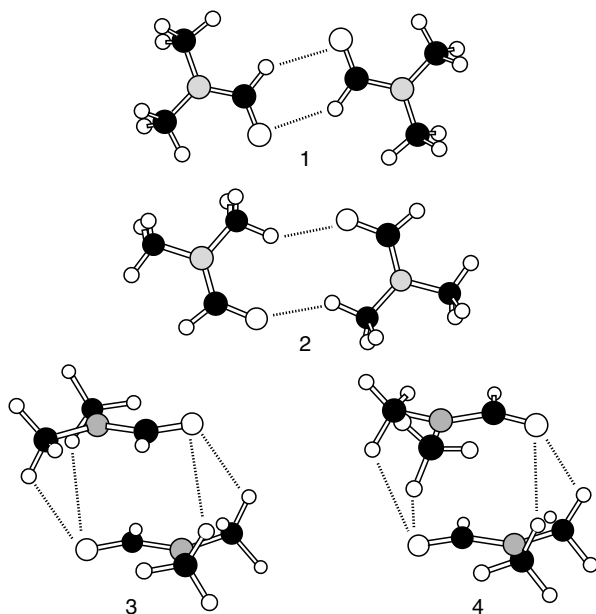


Figure 7. Geometries of the *N,N*-dimethylformamide dimer [139] at the MP2/aug-cc-pTZV level. Suspected H-bonds indicated by broken lines.

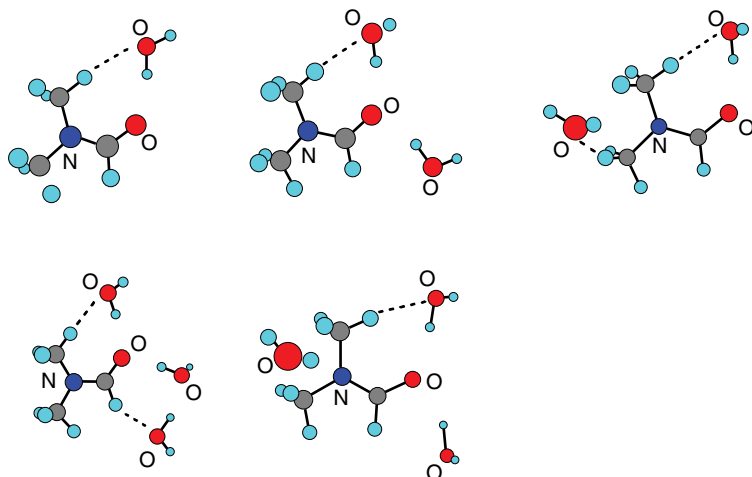


Figure 8. Equilibrium geometries obtained [141] for the complexes of *N,N*-dimethylformamide with one, two, and three water molecules. Broken lines indicate potential $\text{CH}\cdots\text{O}$ bonds. Labels designate O and N atoms.

stronger conventional H-bond. These $\text{CH}\cdots\text{O}$ interactions are explicitly designated by broken lines in Fig. 8, ignoring the conventional bonds which are also present. Unfortunately, the authors focused on vibrational frequencies, ignoring the energetics of the various structures.

Perhaps a superior estimate of the H-bonding ability of the C^αH protons on the polypeptide chain was obtained by a set of calculations [142] that considered as a model the full amino acids. That is, the CH of interest was surrounded on one side by a COOH group and on the other by NH_2 . Different R groups were appended so as to make the $\text{H}_2\text{NC}^\alpha\text{HRCOOH}$ representative of each of a number of different amino acids. Water was used to accept the C^αH proton in each case. The interaction energies are reported in Table 1, wherein each

Table 1. $\text{CH}\cdots\text{O}$ interaction energies for various amino acids combined with a molecule of water, from Ref. [142]

Proton donor	ΔE (kcal/mol)
Gly, R = H	-2.50
Ala, R = CH_3	-2.10
Val, $\text{CH}(\text{CH}_3)_2$	-2.00
Ser, CH_2OH	-2.30
Cys, CH_2SH	-1.90
Lys ⁺ , $(\text{CH}_2)_4\text{NH}_3^+$	-4.92
Asp ⁻ , CH_2COO^-	+1.43

negative quantity refers to an attractive force. It may be seen that most of the interaction energies fall in the neighborhood of 2–2.5 kcal/mol. There is a surprisingly small degree of sensitivity to the nature of the R group. Not surprisingly, the strongest interaction energy is associated with the Lys cation, up to 5 kcal/mol. Note that the anionic Asp residue does not result in an attractive $\text{CH}\cdots\text{O}$ interaction.

Alanine was reinvestigated later, again pairing it with a molecule of water [143]. Quite a number of minima identified on that surface contained a $\text{CH}\cdots\text{O}$ interaction, but unlike the earlier work which isolated the $\text{CH}\cdots\text{O}$ bond as the only H-bond present, these interactions were combined with a stronger conventional H-bond. This combination prevented an assessment of the energetic contribution of either one separate from the other. On the positive side, this work demonstrated that it was possible to submerge such systems in model solvents/proteins, and obtain meaningful results.

Larger systems have been considered as well. For example, a conformational analysis of the alanine dipeptide [144] identified a number of minima on the potential energy surface. All these minima contained what appeared to be internal $\text{CH}\cdots\text{O}$ bonds, but no attempt was made to elucidate the energetic contribution of the bonds. Likewise for an investigation of the conformational preferences of vigabatrin, related to amino acids [145], where some of the minima on the surface contained $\text{CH}\cdots\text{O}$ as secondary interactions.

The dipeptide of alanine has been recently investigated [146]. One of its dimers appears to contain a pair of $\text{CH}\cdots\text{O}$ bonds, both to the same O atom, as designated by the hashed broken lines in Fig. 9. While the authors provided

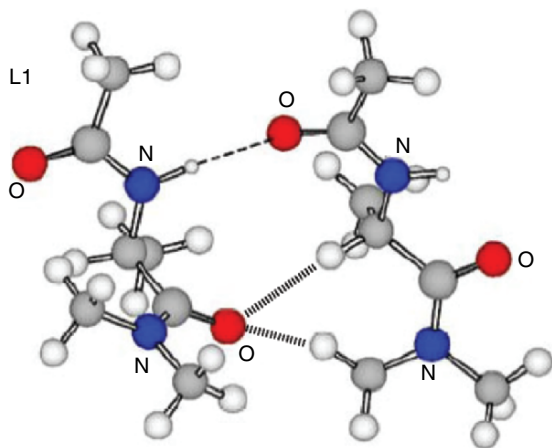


Figure 9. Structure obtained [146] for dimer of Ac-L-Ala-NMe_2 at the B3LYP/6-31+G** level. Hashed broken lines indicate possible presence of $\text{CH}\cdots\text{O}$ bonds.

details of the geometry of this structure, its energy is as usual clouded by the presence of the stronger $\text{NH}\cdots\text{O}$ bond.

5.2.2 Side chains

In addition to the C^αH of the polypeptide backbone, there exist a wealth of amino acid side chains which can donate CH protons to an acceptor, at least in principle. First with regard to the carboxyl groups that characterize the Asp and Glu residues, high pressure studies of mixtures of formic acid and water by Chang et al. [147] were supplemented by *ab initio* calculations. The latter suggested that after the first water molecule has occupied the COOH site of the formic acid, additional waters form $\text{CH}\cdots\text{O}$ bonds with the formic CH. However, there was no attempt made to quantify the energetics of this bond. Moreover, the CH of formic acid would not be present in the Asp and Glu residues where this C is bonded only to O and C atoms. Roy and Thakkar [148] later considered oligomers of formic acid up to the pentamer level. Various geometries were considered, some of which contain $\text{CH}\cdots\text{O}$ bonds. Although there was no configuration in which $\text{CH}\cdots\text{O}$ was the only H-bond present, the authors nevertheless estimated that such bonds contribute on the order of 1.4 kcal/mol to the binding energy.

Some calculations of 4-ethoxybenzaldehyde dimers [149] indicated that both the phenyl and aldehydic protons might be involved in $\text{CH}\cdots\text{O}$ bonds. While there was more than one such bond present in each dimer, there were no stronger bonds present. One could thus make a rough approximation that each such bond might be worth as much as 1.3 kcal/mol. The $\text{CH}\cdots\text{O}$ bond formed between aldehydes was the subject of a later set of computations [150] which focused on the vibrational frequency shifts. While the $\text{CH}\cdots\text{O}$ bonds were all distorted, binding energies on the order of 0.6 kcal/mol were estimated for each such bond. This work concluded that this interaction energy could be increased by the replacement of the nonparticipating H atom of H_2CO by various halides.

More direct contact with proteins was made by Ornstein and Zheng [151], whose 1997 study focused on imidazole, the side chain of the His residue, as well as benzene, serving a similar modeling function for Phe. The authors computed binding energies for $\text{CH}\cdots\text{O}$ bonds at the MP2 level of 1.6 kcal/mol for the benzene \cdots water pair, and 2.0–3.0 kcal/mol for imidazole \cdots water, depending on which CH of the Im was considered. The latter quantities were roughly 30–50% of the analogous classical $\text{NH}\cdots\text{O}$ bonds. In any case, the results are likely to represent overestimates as basis set superposition error was left uncorrected. Indeed, later computations at higher levels and with BSSE corrections [152] yielded $\text{CH}\cdots\text{O}$ binding energies for benzene as proton donor of 1.2–1.7 kcal/mol, depending upon the precise nature of the acceptor.

Similar sorts of calculations [153] indicated that $\text{CH}\cdots\text{O}$ bonds might exist for the imidazole model of His and a proton acceptor O, as indicated in Fig. 10. (Note that the ring contains only one N atom and there are two O atoms on

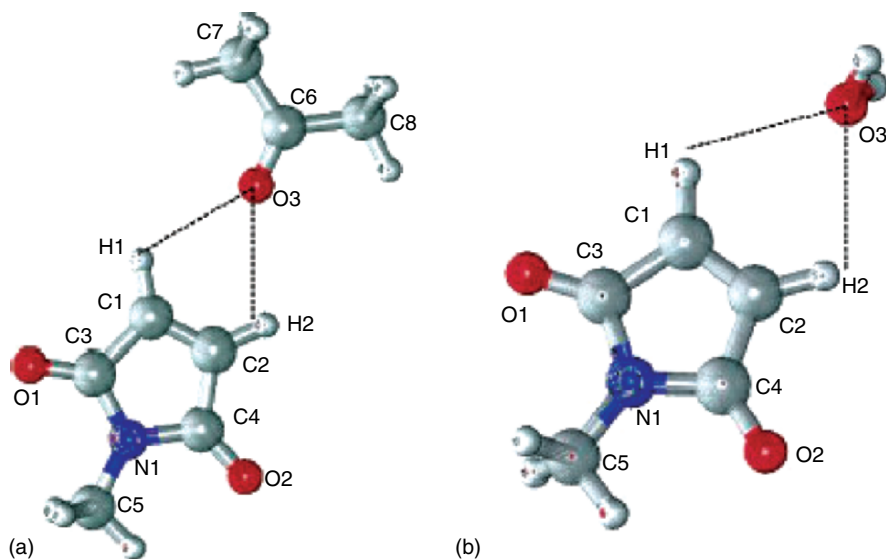


Figure 10. Geometries pairing *N*-methyl maleimide with (a) acetone and (b) water [153], optimized at B3LYP/6-31G* level.

N-methyl maleimide that would not be present in the His residue.) In this case, as there were no conventional H-bonds present, one could at least in principle, consider the H-bond energy of each as roughly half the total interaction energy, which would lead to an estimate of 1.4–1.7 kcal/mol for each. On the other hand, the two $\text{CH}\cdots\text{O}$ bonds are clearly angularly distorted so the numerical value is apt to represent an underestimate.

When phenol, the functional group of the Tyr residue, was paired with water, the optimal geometry was found [154] to contain the expected $\text{OH}\cdots\text{O}$ H-bond. The phenol could serve as either proton donor or acceptor, but in either case, one of the C–H groups of the phenol was in position to form a secondary H-bond as illustrated in Fig. 11. No estimate was made of the energetic contribution of this secondary interaction.

Direct experimental evidence that an aromatic could form a $\text{C–H}\cdots\text{O}$ hydrogen bond was obtained by Mikami's group in 2004 by fluorescence-detected infrared spectroscopy [155], when tetrafluorobenzene was paired with water in the gas phase. Accompanying MP2 calculations led to the geometry pictured in Fig. 12, wherein the bent $\text{CH}\cdots\text{O}$ bond is combined with a $\text{OH}\cdots\text{F}$ interaction.

A set of ab initio computations in 2002 [156] addressed the question of aromatic $\text{CH}\cdots\text{O}$ bond energies more directly. As illustrated in Fig. 13, a water molecule was used as universal proton acceptor, and placed in a position whereby it might form a $\text{CH}\cdots\text{O}$ bond with the CH of both benzene (Phe side chain), and the phenol of Tyr. It is worth stressing that the energetics reported

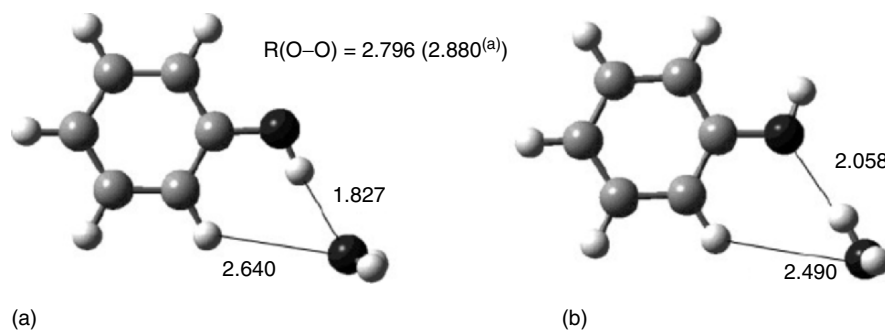


Figure 11. Two complexes of phenol with water [154] wherein water acts as (a) proton acceptor and (b) proton donor to phenol hydroxy, using MP2/6-311G** calculations.

here were unambiguous in the sense that the $CH \cdots O$ bond is the only one present in each configuration, and is undistorted from an optimal linear geometry. Two different CH groups were considered for phenol, both immediately adjacent (*ortho*) to the OH group, and one removed (*meta*). The energies listed in Fig. 13 refer to the H-bond energies for each such configuration, and reveal that this quantity is calculated to be 1.1 kcal/mol for the bare benzene. This quantity is increased a bit, up to 1.3 kcal/mol by the presence of the OH.

This work [156] went on to address other aromatic CH groups as well. In particular, both choices of CH in the imidazole side chain of His were shown to be somewhat stronger proton donors than the phenyl ring, by a factor of about

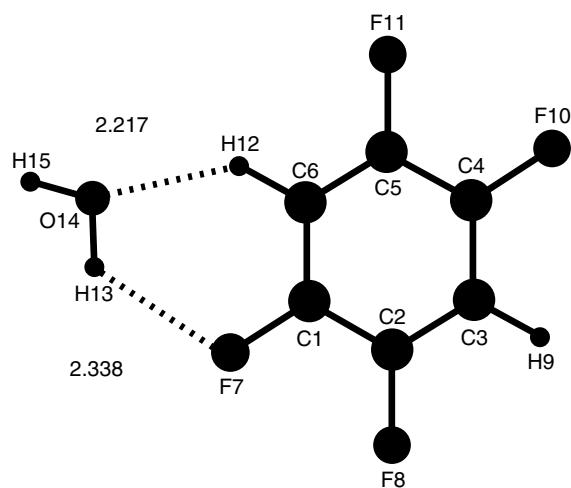


Figure 12. MP2/6-31+G* complex of 1,2,4,5-tetrafluorobenzene with water [155], indicating both $CH \cdots O$ and $OH \cdots F$ interactions.

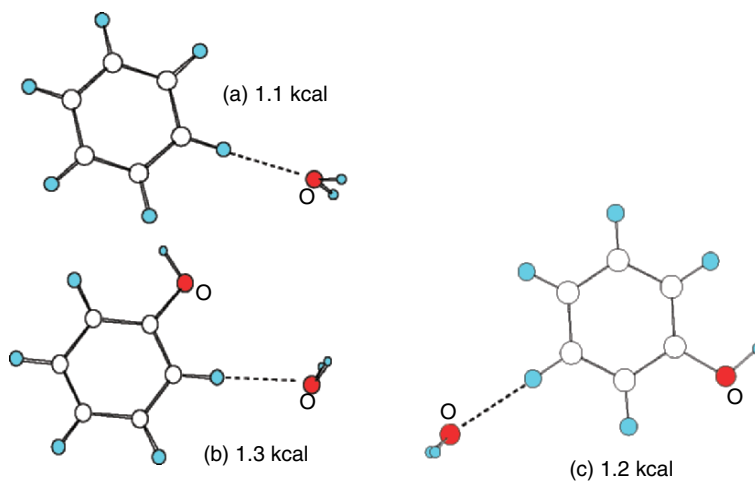


Figure 13. MP2/6-31+G** complexes of water with (a) benzene and (b,c) phenol that contain $\text{CH}\cdots\text{O}$ bonds [156]. Counterpoise-corrected interaction energies included, along with labels on O atoms.

2, as illustrated in Fig. 14. There is only a slight difference between the various CH protons of the His side chain.

What makes a truly large difference is the protonation state of the residue. The His residue is frequently in a charged state, wherein both N atoms are protonated. As reported in Fig. 15, the interaction energies swell up to as large as 11.3 kcal/mol for the $\text{ImH}^+\cdots\text{OH}_2$ system, suggesting that even nominally weak $\text{CH}\cdots\text{O}$ bonds can become extremely strong if one of the two groups is charged. This idea was confirmed by later computations [157] that addressed

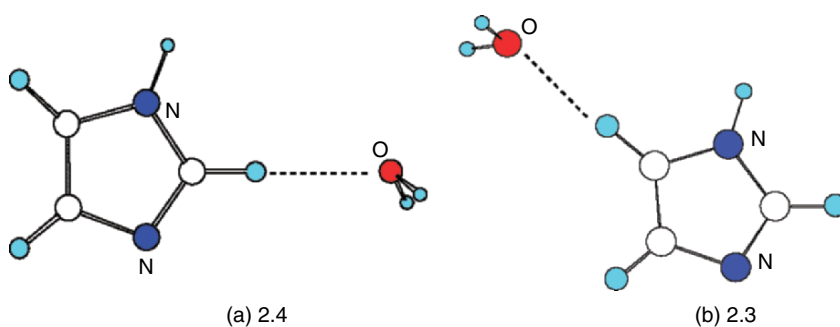


Figure 14. MP2/6-31+G** complexes of water with imidazole that contain $\text{CH}\cdots\text{O}$ bonds [156]. Counterpoise-corrected interaction energies included, along with labels on O and N atoms.

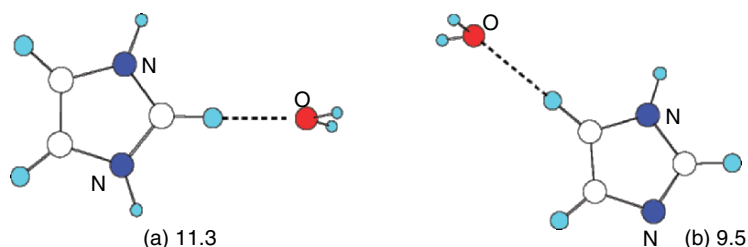


Figure 15. MP2/6-31+G** complexes of water with protonated imidazole that contain CH \cdots O bonds [156]. Counterpoise-corrected interaction energies included, along with labels on O and N atoms.

the potential of imidazole to form H-bonds, including those of CH \cdots O type, when present as a radical cation C₃N₂H₄⁺.

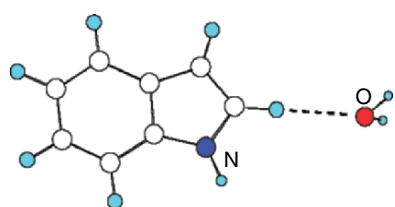
Another aromatic side chain of amino acids that may participate in CH \cdots O interactions is the indole moiety of Trp. Figure 16 illustrates [156] that the strongest such bond, amounting to 2.1 kcal/mol, is associated with the position adjacent to the N atom. Moving over to the other CH in the five-membered ring cuts this H-bond energy in half, as does the use of one of the CH groups of the larger ring. In fact, the latter quantity is approximately equal to that of the bare phenyl.

Guo et al. [158] considered the ability of the C δ H group of Pro to donate a proton to a carbonyl oxygen. Their work centered upon geometries that had in fact been encountered in real proteins, although of course they were forced to perform their calculations on smaller model systems. The interaction energies were not surprisingly highly dependent upon the particular geometry. Values obtained varied from repulsive in certain cases to as much as 4 kcal/mol in others.

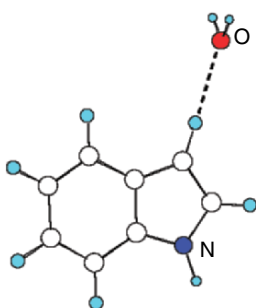
5.3 Other Systems

The interaction between proteins and nucleic acids has been considered as well. Dabkowska et al. [159] began with the most stable tautomers of Gly and uracil, identifying 23 different minima on the surface that characterized their pairing. While most of these configurations, particularly the most stable, contained only conventional H-bonds, several minima did appear to contain either CH \cdots O or CH \cdots N, but no attempt was made to determine the energetic contribution of any individual bonds. These interactions were the subject of another set of calculations [160] which paired a model of the protein backbone with nucleic acids. Some of the minima contained secondary CH \cdots O bonds, along with the more standard H-bonds.

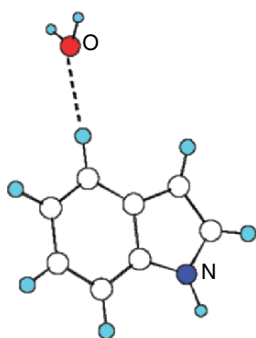
Koch and Popelier [161] later used an “atoms in molecules” analysis to suggest that an internal CH \cdots O bond was instrumental in the geometry



(a) 2.1



(b) 1.1



(c) 0.9

Figure 16. MP2/6-31+G** complexes of water with indole that contain $\text{CH}\cdots\text{O}$ bonds [156]. Counterpoise-corrected interaction energies included, along with labels on O and N atoms.

adopted by an anti-AIDS drug, but were unable to arrive at an energetic estimate. An ambitious 2001 study [162] examined the interaction between bacteriochlorophyll and the carotenoid rhodopsin glucoside. Although not the highest level available, calculations led to estimates of the $\text{CH}\cdots\text{O}$ interaction energy in the neighborhood of 1.5–2.4 kcal/mol, corresponding to the sum of two such bonds.

6 SUMMARY AND FUTURE PERSPECTIVES

It is obvious to the reader at this point that, while there have been a sizable number of *ab initio* studies of CH \cdots X bonds, only a small minority of these calculations have been successful at assessing the energetic contribution of these interactions. The most obvious problem has been the presence of other, normally stronger, conventional H-bonds. The presence of more than one H-bond complicates the extraction of the energetic contribution of any individual bond. Moreover, the stronger bond acts to force the weaker CH \cdots X interaction into a highly deformed geometry, prohibiting an evaluation of what the strength of this bond would be if it were left undistorted.

There is only one value in the literature that pertain to nucleic acids. The bent CH \cdots N bonds in the pyrimidine dimer were estimated [126] to contribute roughly 1.6 kcal/mol each; a larger value would be expected in the absence of this distortion. More information is available that relate to proteins. Although not present *per se* in polypeptides, the amidic CH appears to form H-bonds on the order of 1.9–4.0 kcal/mol [137, 138].

The hydrogens of methyl groups that lie immediately adjacent to an amide function are somewhat closer in character to the C $^{\alpha}$ H groups of polypeptides. Estimates of the strength of the pertinent CH \cdots O bond vary between 2.1 and 4.5 kcal/mol [139]. More accurate representations of the polypeptide C $^{\alpha}$ H H-bond strength derive from full amino acids [142], leading to values in the 2–2.5 kcal/mol range.

There is somewhat more information available for CH \cdots O bonds that model the side chains of protein residues. The aromatic CH of the Phe side chain forms H-bonds with strength in the range of 1.1–1.7 kcal/mol [14, 151–153, 156]. This interaction is strengthened by perhaps 0.1–0.2 kcal/mol when a –OH group is added to the phenyl ring, as in Tyr [156]. The aromatic CH of the imidazole group of His is a somewhat stronger donor, due in large measure to the pair of N atoms in the ring. H-bond energies have been computed between 2.0 and 3.0 kcal/mol [151], with the best value to date of 2.3–2.4 [156]. The CH groups of the indole species of the Trp residue are more variable. The CH \cdots O bond strength has been calculated to be 2.1 kcal/mol for the CH adjacent to the N atom, but only 0.9–1.1 for other CH groups in the same indole ring.

The passage of time will undoubtedly lead in several different directions. It is likely first that researchers will apply progressively more accurate quantum chemical methods to systems that will grow in size, approaching more and more realistic segments of biomolecules. A second avenue toward greater realism will be the displacement of these systems from the isolated *in vacuo* situation, which has been the case in nearly all prior studies, into a medium which better approximates the biological situation. For example, the CH \cdots O bond within a protein might be surrounded by protein groups, or even by a continuous medium which better approximates the environment within a protein interior than does a vacuum. It is especially intriguing to point out the results of a recent study [163]

which found preliminary evidence that, although inherently weaker than a conventional H-bond, a $\text{CH}\cdots\text{O}$ bond may contribute just as much to the energy of folding of a protein. This apparent discrepancy occurs because the $\text{CH}\cdots\text{O}$ bond may suffer less of a “desolvation penalty” than does a traditional H-bond.

REFERENCES

1. Glasstone, S. (1937) The structure of some molecular complexes in the liquid phase, *Trans. Faraday Soc.* **33**, 200–214.
2. Dippy, J.F.J. (1939) The dissociation constants of monocarboxylic acids; their measurement and their significance in theoretical organic chemistry, *Chem. Rev.* **25**, 151–211.
3. Marvel, C.S., Copley, M.J., and Ginsberg, E. (1940) Hydrogen bonds involving the C–H link. XI. Effect of structure on bonding of donor and acceptor molecules, *J. Am. Chem. Soc.* **62**, 3109–3112.
4. Parry, G.S. (1954) The crystal structure of uracil, *Acta Cryst.* **7**, 313–320.
5. Sutor, D.J. (1962) The C–H \cdots O hydrogen bond in crystals, *Nature* **195**, 68–69.
6. Ramachandran, G.N. and Chandrasekharan, R. (1968) Interchain hydrogen bonds via bound water molecules in the collagen triple helix, *Biopolymers* **6**, 1649–1658.
7. Sutor, D.J. (1963) Evidence for the existence of C–H \cdots O hydrogen bonds in crystals, *J. Chem. Soc.* 1105–1110.
8. Pinchas, S. (1955) Infrared absorption of the aldehydic C–H group, *Anal. Chem.* **27**, 2–6.
9. Pinchas, S. (1957) Infrared absorption of aldehydic C–H group. Ortho-substituted benzaldehydes, *Anal. Chem.* **29**, 334–339.
10. Pinchas, S. (1963) Intramolecular hydrogen bonding in *o*-nitrobenzaldehyde and related compounds, *J. Phys. Chem.* **67**, 1862–1865.
11. Schneider, W.G. and Bernstein, H.J. (1956) Molecular association and infra-red spectrum of solid formaldehyde and acetaldehyde, *Trans. Faraday Soc.* **52**, 13–18.
12. Forbes, W.F. (1962) The study of hydrogen bonding and related phenomena by spectroscopic methods. Part VII. Intramolecular hydrogen bonding and steric interactions in *o*-nitrobenzaldehyde and related compounds, *Can. J. Chem.* **40**, 1891–1898.
13. Allerhand, A. and Schleyer, P.v.R. (1963) A survey of C–H groups as proton donors in hydrogen bonding, *J. Am. Chem. Soc.* **85**, 1715–1723.
14. Krimm, S. (1967) Hydrogen bonding of C–H \cdots O=C in proteins, *Science* **158**, 530–531.
15. Green, R.D. (1974) *Hydrogen Bonding by C–H Groups*; Wiley Interscience: New York.
16. Sammes, M.P. and Harlow, R.L. (1976) Intramolecular hydrogen bonds involving polar carbon–hydrogen bonds: infrared and ^1H nuclear magnetic resonance spectra of some cyanomethyl and benzyl sulphones, *J. Chem. Soc. Perkin Trans. II*, 1130–1135.
17. Slasinski, F.M., Tustin, J.M., Sweeney, F.J., Armstrong, A.M., Ahmed, Q.A., and Lorand, J.P. (1976) A survey of structural effects on formation constants in C–H hydrogen bonding, *J. Org. Chem.* **41**, 2693–2699.
18. Hussein, M.A. and Millen, D.J. (1976) Hydrogen bonding in the gas phase. Part 4. Infrared spectroscopic investigation of O–H \cdots O and C–H \cdots N complexes: alcohol + ether and trichloromethane + amine systems, *J. Chem. Soc., Faraday Trans. 2* **72**, 693–699.
19. Sussman, J.L., Seeman, N.C., Kim, S.-H., and Berman, H.M. (1972) Crystal structure of a naturally occurring dinucleoside phosphate: uridylyl 3′–5′-adenosine phosphate. Model for RNA chain folding, *J. Mol. Biol.* **66**, 403–421.
20. Rubin, J., Brennan, T., and Sundaralingam, M. (1972) Crystal and molecular structure of a naturally occurring dinucleoside monophosphate. Uridylyl-(3′–5′)-adenosine hemihydrate. Conformational “rigidity” of the nucleotide unit and models for polynucleotide chain folding, *Biochem.* **11**, 3112–3128.
21. Saenger, W. (1973) Structure and function of nucleosides and nucleotides, *Angew. Chem., Int. Ed. Engl.* **12**, 591–601.

22. Kvick, Å., Koetzle, T.F., and Thomas, R. (1974) Hydrogen bond studies. 89. A neutron diffraction study of hydrogen bonding in 1-methylthymine, *J. Chem. Phys.* **61**, 2711–2719.
23. Takusagawa, F., Koetzle, T.F., Srikrishnan, T., and Parthasarathy, R. (1979) C–H···O interactions and stacking of water molecules between pyrimidine bases in 5-nitro-1(β-D-ribose-luronic acid)-uracil monohydrate [1-(5-nitro-2,4-dioxypyrimidinyl)-β-D-ribofuranic acid monohydrate]: a neutron diffraction study at 80 K, *Acta Cryst.* **B35**, 1388–1394.
24. Taylor, R. and Kennard, O. (1982) Crystallographic evidence for the existence of C–H···O, C–H···N, and C–H···Cl hydrogen bonds, *J. Am. Chem. Soc.* **104**, 5063–5070.
25. Sarma, J.A.R.P. and Desiraju, G.R. (1986) The role of Cl···Cl and C–H···O interactions in the crystal engineering of 4-Å short-axis structures, *Acc. Chem. Res.* **19**, 222–228.
26. Desiraju, G.R. (1989) Distance dependence of C–H···O interactions in some chloroalkyl compounds, *J. Chem. Soc., Chem. Commun.* 179–180.
27. Jeffrey, G.A. and Maluszynska, H. (1982) A survey of hydrogen bond geometries in the crystal structures of amino acids, *Int. J. Biol. Macromol.* **4**, 173–185.
28. Berkovitch-Yellin, Z. and Leiserowitz, L. (1984) The role played by C–H···O and C–H···N interactions in determining molecular packing and conformation, *Acta Cryst.* **B40**, 159–165.
29. Parthasarathy, R., Fridley, S.M., and Srikrishnan, T. (1989) Conformation and hydrogen bonding of *N*-formylmethionyl peptides. II. Crystal and molecular structure of *N*-formyl-L-methionyl-L-phenylalanine, *Int. J. Peptide Protein Res.* **33**, 308–312.
30. Saenger, W. (1984) *Principles of Nucleic Acid Structure*; Springer-Verlag: New York.
31. Steiner, T. (1998) Lengthening of the covalent X–H bond in heteronuclear hydrogen bonds quantified from organic and organometallic neutron crystal structures, *J. Phys. Chem. A* **102**, 7041–7052.
32. Steiner, T. and Desiraju, G.R. (1998) Distinction between the weak hydrogen bond and the van der Waals interaction, *Chem. Commun.* 891–892.
33. Desiraju, G.R. (1990) Strength and linearity of C–H···O bonds in molecular crystals: a database study of some terminal alkynes, *J. Chem. Soc., Chem. Commun.* 454–455.
34. Lutz, B., van der Maas, J., and Kanters, J.A. (1994) Spectroscopic evidence for C–H···O interaction in crystalline steroids and reference compounds, *J. Mol. Struct.* **325**, 203–214.
35. Song, J.-S., Szalda, D.J., and Bullock, R.M. (1996) Ether complexes of tungsten with two different binding modes: an O-bound ether and an η²-(C=C) vinyl ether. Evidence for C–H···O hydrogen bonding of vinylic C–H groups, *J. Am. Chem. Soc.* **118**, 11134–11141.
36. Steiner, T., Lutz, B., van der Maas, J., Veldman, N., Schreurs, A.M.M., Kroon, J., and Kanters, J.A. (1997) Spectroscopic evidence for cooperativity effects involving C–H···O hydrogen bonds: crystalline mestranol, *Chem. Commun.* 191–192.
37. Reddy, D.S., Goud, B.S., Panneerselvam, K., and Desiraju, G.R. (1993) C–H···N mediated hexagonal network in the crystal structure of the 1:1 molecular complex 1,3,5-tricyanobenzene–hexamethylbenzene, *Chem. Commun.* 663–664.
38. Cense, J.M., Agafonov, V., Ceolin, R., Ladure, P., and Rodier, N. (1994) Crystal and molecular structure analysis of flutamide. Bifurcated helicoidal C–H···O hydrogen bonds, *Struct. Chem.* **5**, 79–84.
39. Lewis, F.D., Yang, J.-S., and Stern, C.L. (1996) Crystal structures of secondary arenedicarboxamides. An investigation of arene–hydrogen bonding relationships in the solid state, *J. Am. Chem. Soc.* **118**, 12029–12037.
40. Sharma, C.V.K. and Zaworotko, M.J. (1996) X-ray crystal structure of C₆H₃(CO₂H)₃-1,3,5-1.5(4,4'-bipy): a 'super trimesic acid' chicken-wire grid, *Chem. Commun.* 2655–2656.
41. Marjo, C.E., Scudder, M.L., Craig, D.C., and Bishop, R. (1997) Edge-to-edge aryl C–H···N dimer: a new supramolecular synthon, *J. Chem. Soc. Perkin Trans. II* 2099–2104.
42. Pigge, F.C., Ghasedi, F., and Rath, N.P. (1999) A new inclusion host: an inclusion complex between a 1,2,5-triarolylbenzene host and a benzene guest stabilized by C–H···O hydrogen bonds, *Tetrahedron Lett.* **40**, 8045–8048.

43. Allen, F.H., Lommerse, J.P.M., Hoy, V.J., Howard, J.A.K., and Desiraju, G.R. (1996) The hydrogen-bond C-H donor and γ -acceptor characteristics of three-membered rings, *Acta Cryst.* **B52**, 734–745.
44. Braga, D., Angeloni, A., Grepioni, F., and Tagliavini, E. (1997) Moulding a honeycomb framework around $[\text{Co}(\eta^5\text{-C}_5\text{H}_5)_2]^+$ via charge-assisted $\text{C-H}\cdots\text{O}$ hydrogen bonds, *Chem. Commun.* 1447–1448.
45. Harakas, G., Vu, T., Knobler, C.B., and Hawthorne, M.F. (1998) Synthesis and crystal structure of 9,12-bis-(4-acetylphenyl)- 1,2-dicarbododecaborane(12): self-assembly involving intermolecular carboranyl C-H hydrogen bonding, *J. Am. Chem. Soc.* **120**, 6405–6406.
46. Kuduva, S.S., Craig, D.C., Nangia, A., and Desiraju, G.R. (1999) Cubanecarboxylic acids. Crystal engineering considerations and the role of $\text{C-H}\cdots\text{O}$ hydrogen bonds in determining $\text{OP-H}\cdots\text{O}$ networks, *J. Am. Chem. Soc.* **121**, 1936–1944.
47. Braga, D. and Grepioni, F. (1994) From molecule to molecular aggregation: clusters and crystals of clusters, *Acc. Chem. Res.* **27**, 51–56.
48. Braga, D., Dyson, P.J., Grepioni, F., Johnson, B.F.G., and Calhorda, M.J. (1994) Intramolecular and intermolecular bonding in benzene clusters, *Inorg. Chem.* **33**, 3218–3228.
49. Braga, D., Grepioni, F., Biradha, K., Pedireddi, V.R., and Desiraju, G.R. (1995) Hydrogen bonding in organometallic crystals. 2. $\text{C-H}\cdots\text{O}$ hydrogen bonds in bridged and terminal first-row metal carbonyls, *J. Am. Chem. Soc.* **117**, 3156–3166.
50. Iwaoka, M. and Tomoda, S. (1994) First observation of a $\text{C-H}\cdots\text{Se}$ “hydrogen bond”, *J. Am. Chem. Soc.* **116**, 4463–4464.
51. Steiner, T. (1994) Effect of acceptor strength on $\text{C-H}\cdots\text{O}$ hydrogen bond lengths as revealed by and quantified from crystallographic data, *J. Chem. Soc., Chem. Commun.* 2341–2342.
52. Mascal, M. (1998) Statistical analysis of $\text{C-H}\cdots\text{N}$ hydrogen bonds in the solid state: there are real precedents, *Chem. Commun.* 303–304.
53. Jeffrey, G.A. and Saenger, W. (1991) *Hydrogen Bonding in Biological Structures*; Springer-Verlag: Berlin.
54. Steiner, T. (1995) Weak hydrogen bonding. Part I. Neutron diffraction data of amino acid $\text{C}_\alpha\text{-H}$ suggest lengthening of the covalent C-H bond in $\text{C-H}\cdots\text{O}$ interactions, *J. Chem. Soc. Perkin Trans. II* 1315–1319.
55. Bella, J. and Berman, H.M. (1996) Crystallographic evidence for $\text{C}^\alpha\text{-H}\cdots\text{O} = \text{C}$ hydrogen bonds in a collagen triple helix, *J. Mol. Biol.* **264**, 734–742.
56. Nagarajan, V., Pattabhi, V., Johnson, A., Bobde, V., and Durani, S. (1997) Crystal structures of heterochiral peptides. Part II. *tert*-Boc-valyl-D-alanyl-leucyl-alanyl methoxide, *J. Peptide Res.* **49**, 74–79.
57. Ridder, I.S., Rozeboom, H.J., and Dijkstra, B.W. (1999) Haloalkane dehalogenase from *Xanthobacter autotrophicus* GJ10 refined at 1.15 Å resolution, *Acta Cryst.* **D55**, 1273–1290.
58. Fabiola, G.F., Krishnaswamy, S., Nagarajan, V., and Pattabhi, V. (1997) $\text{C-H}\cdots\text{O}$ hydrogen bonds in β -sheets, *Acta Cryst.* **D53**, 316–320.
59. Derewenda, Z.S., Derewenda, U., and Kobos, P.M. (1994) $(\text{His})\text{C}^\epsilon\text{-H}\cdots\text{O} = \text{C} <$ hydrogen bond in the active sites of serine hydrolases, *J. Mol. Biol.* **241**, 83–93.
60. Ash, E.L., Sudmeier, J.L., Day, R.M., Vincent, M., Torchilin, E.V., Haddad, K.C., Bradshaw, E.M., Sanford, D.G., and Bachovchin, W.W. (2000) Unusual ^1H NMR chemical shifts support $(\text{His})\text{C}^\epsilon\text{-H}\cdots\text{O} = \text{C}$ H-bond: proposal for reaction-driven ring flip mechanism in serine protease catalysis, *Proc. Nat. Acad. Sci., USA* **97**, 10371–10376.
61. Bachovchin, W.W. (2001) Contributions of NMR spectroscopy to the study of hydrogen bonds in serine protease active sites, *Magn. Reson. Chem.* **39**, S199–S213.
62. Chakrabarti, P. and Chakrabarti, S. (1998) $\text{C-H}\cdots\text{O}$ hydrogen bond involving proline residues in α -helices, *J. Mol. Biol.* **284**, 867–873.
63. Derewenda, Z.S., Lee, L., and Derewenda, U. (1995) The occurrence of $\text{C-H}\cdots\text{O}$ hydrogen bonds in proteins, *J. Mol. Biol.* **252**, 248–262.

64. Leonard, G.A., McAuley-Hecht, K., Brown, T., and Hunter, W.N. (1995) Do C–H···O hydrogen bonds contribute to the stability of nucleic acid base pairs? *Acta Cryst.* **D51**, 136–139.
65. Egli, M. and Gessner, R.V. (1995) Stereoelectronic effects of deoxyribose O4' on DNA conformation, *Proc. Nat. Acad. Sci., USA* **92**, 180–184.
66. Berger, I., Egli, M., and Rich, A. (1996) Inter-strand C–H···O hydrogen bonds stabilizing four-stranded intercalated molecules: stereoelectronic effects of O4' in cytosine-rich DNA, *Proc. Nat. Acad. Sci., USA* **93**, 12116–12121.
67. Wahl, M.C., Rao, S.T., and Sundaralingam, M. (1996) The structure of r(UUCGCG) has a 5'-UU-overhang exhibiting Hoogsteen-like trans U···U base pairs, *Nature Struct. Biol.* **3**, 24–31.
68. Metzger, S. and Lippert, B. (1996) A metalated guanine, cytosine base quartet with a novel GC pairing pattern involving H(5) of C, *J. Am. Chem. Soc.* **118**, 12467–12468.
69. Cate, J.H., Gooding, A.R., Podell, E., Zhou, K., Golden, B.L., Kundrot, C.E., Cech, T.R., and Doudna, J.A. (1996) Crystal structure of a group I ribozyme domain: principles of RNA packing, *Science* **273**, 1678–1685.
70. Grune, M., Furste, J.P., Klussmann, S., Erdmann, V.A., and Brown, L.R. (1996) Detection of multiple conformations of the E-domain of 5S rRNA from *Escherichia coli* in solution and in crystals by NMR spectroscopy, *Nucleic Acid Res.* **24**, 2592–2596.
71. Corell, C.C., Freeborn, B., Moore, P.B., and Steitz, T.A. (1997) Metals, motifs, and recognition in the crystal structure of a 5S rRNA domain, *Cell* **91**, 705–712.
72. Sigel, R.K.O., Freisinger, E., Metzger, S., and Lippert, B. (1998) Metalated nucleobase quartets: dimerization of a metal-modified guanine, cytosine pair of *trans*-(NH₃)₂Pt^{II} and formation of CH···N hydrogen bonds, *J. Am. Chem. Soc.* **120**, 12000–12007.
73. Brandl, M., Lindauer, K., Meyer, M., and Sühnel, J. (1999) C–H···O and C–H···N interactions in RNA structures, *Theor. Chem. Acc.* **101**, 103–113.
74. Leonard, G.A., McAuley-Hecht, K., Brown, T., and Hunter, W.N. (1995) Do C–H···O hydrogen bonds contribute to the stability of nucleic acid base pairs? *Acta Cryst.* **D51**, 136–139.
75. Steiner, T. and Saenger, W. (1992) Geometry of C–H···O hydrogen bonds in carbohydrate crystal structures. Analysis of neutron diffraction data, *J. Am. Chem. Soc.* **114**, 10146–10154.
76. Wahl, M.C. and Sundaralingam, M. (1997) C–H···O hydrogen bonding in biology, *Trends Biochem. Sci.* **22**, 97–102.
77. Weiss, M.S., Brandl, M., Sühnel, J., Pal, D., and Hilgenfeld, R. (2001) More hydrogen bonds for the (structural) biologist, *Trends Biochem. Sci.* **26**, 521–523.
78. Musah, R.A., Jensen, G.M., Rosenfeld, R.J., McRee, D.E., Goodin, D.B., and Bunte, S.W. (1997) Variation in strength of an unconventional C–H to O hydrogen bond in an engineered protein cavity, *J. Am. Chem. Soc.* **119**, 9083–9084.
79. Baures, P.W., Beatty, A.M., Dhanasekaran, M., Helfrich, B.A., Perez-Segarra, W., and Desper, J. (2002) Solution and solid-state models of peptide CH···O hydrogen bonds, *J. Am. Chem. Soc.* **124**, 11315–11323.
80. Shi, Z., Olson, C.A., Bell, A.J., and Kallenbach, N.R. (2002) Non-classical helix-stabilizing interactions: C–H···O H-bonding between Phe and Glu side chains in α -helical peptides, *Biophys. Chem.* **101–102**, 267–279.
81. Sarkhel, S. and Desiraju, G.R. (2004) N–H···O, O–H···O, and C–H···O hydrogen bonds in protein-ligand complexes: strong and weak interactions in molecular recognitions, *Proteins* **54**, 247–259.
82. Steiner, T. (2000) Influence of C–H···O interactions on the conformation of methyl groups quantified from neutron diffraction data, *J. Phys. Chem. A* **104**, 433–435.
83. Thalladi, V.R., Smolka, T., Gehrke, A., Boese, R., and Sustmann, R. (2000) Role of weak hydrogen bonds in the crystal structures of phenazine, 5,10-dihydrophenazine and their 1:1 and 3:1 molecular complexes, *New J. Chem.* **24**, 143–147.
84. Pigge, F.C., Zheng, Z., and Rath, N.P. (2000) 1,3,5-triarolylbenzenes are versatile inclusion hosts via C–H···O hydrogen bonding, *New J. Chem.* **24**, 183–185.

85. Meadows, E.S., De Wall, S.L., Barbour, L.J., Fronczek, F.R., Kim, M.-S., and Gokel, G.W. (2000) Structural and dynamic evidence for $\text{C-H}\cdots\text{O}$ hydrogen bonding in lariat ethers: implications for protein structure, *J. Am. Chem. Soc.* **122**, 3325–3335.
86. Lee, H., Knobler, C.B., and Hawthorne, M.F. (2000) Supramolecular self-assembly directed by $\text{C-H}\cdots\text{F}$ interactions, *Chem. Commun.* 2485–2486.
87. George, S., Nangia, A., Muthuraman, M., Bagieu-Beucher, M., Masse, R., and Nicoud, J.-F. (2001) Crystal engineering of neutral *N*-arylpurimidinones and their HCl and HNO_3 adducts with a $\text{C-H}\cdots\text{O}$ supramolecular synthon. Implications for non-linear optics, *New J. Chem.* **25**, 1520–1527.
88. Reyes-Arellano, A., Vega-Ramírez, L., Nájera-Mundo, J.A., Salgado-Zamora, H., Molins, E., Peralta-Cruz, J., and Tamariz, J. (2003) An abnormal $\text{C-H}\cdots\text{O}$ bond directs intermolecular bonding arrangements in bisimines, *J. Mol. Struct.* **655**, 141–148.
89. Ayi, A.A., Choudhury, A., Natarajan, S., and Rao, C.N.R. (2001) Cyclic acetate dimers formed by $\text{C-H}\cdots\text{O}$ hydrogen bonds in an open-framework zinc phosphate-acetate, *New J. Chem.* **25**, 213–215.
90. Moorthy, J.N., Natarajan, R., and Prasenjit Mal, P.V. (2004) Polymorphism of an *o*-anisaldehyde: a novel example of channel-type organization sustained by weak $\text{C-H}\cdots\text{O}$ and $\text{C-H}\cdots\text{N}$ hydrogen bonds, *New J. Chem.* **28**, 1416–1419.
91. Thakur, A.K. and Kishore, R. (2000) Stabilization of a novel β -turn-like motif by non-conventional intramolecular hydrogen-bonding interactions in a model peptide incorporating β -alanine, *Biopolymers* **53**, 447–454.
92. Cheung, E.Y., McCabe, E.E., Harris, K.D.M., Johnston, R.L., Tedesco, E., Raja, K.M.P., and Balaram, P. (2002) $\text{C-H}\cdots\text{O}$ hydrogen bond mediated chain reversal in a peptide containing a γ -amino acid residue, determined directly from powder X-ray diffraction data, *Angew. Chem., Int. Ed. Engl.* **41**, 494–496.
93. Senes, A., Ubarretxena-Belandia, I., and Engelman, D.M. (2001) The $\text{C}_\alpha\text{-HO}$ hydrogen bond: a determinant of stability and specificity in transmembrane helix interactions, *Proc. Nat. Acad. Sci., USA* **98**, 9056–9061.
94. Babu, M.M., Singh, S.K., and Balaram, P. (2002) A $\text{C-H}\cdots\text{O}$ hydrogen bond stabilized polypeptide chain reversal motif at the C terminus of helices in proteins, *J. Mol. Biol.* **322**, 871–880.
95. Singh, S.K., Babu, M.M., and Balaram, P. (2003) Registering α -helices and β -strands using backbone $\text{C-H}\cdots\text{O}$ interactions, *Proteins Struct. Func. Genetics* **51**, 167–171.
96. Aravinda, S., Shamala, N., Bandyopadhyay, A., and Balaram, P. (2003) Probing the role of the $\text{C-H}\cdots\text{O}$ hydrogen bond stabilized polypeptide chain reversal at the C-terminus of designed peptide helices. Structural characterization of three decapeptides, *J. Am. Chem. Soc.* **125**, 15065–15075.
97. Lee, K.M., Chang, H.-C., Jiang, J.-C., Chen, J.C.C., Kao, H.-E., Lin, S.H., and Lin, I.J.B. (2003) $\text{C-H}\cdots\text{O}$ hydrogen bonds in β -sheetlike networks: combined X-ray crystallography and high-pressure infrared study, *J. Am. Chem. Soc.* **125**, 12358–12364.
98. Fabiola, G.G., Bobde, V., Damodharan, L., Patabhi, V., and Durani, S. (2001) Conformational preferences of heterochiral peptides. Crystal structures of heterochiral peptides Boc-(d) Val-(d) Ala-Leu-Ala-OMe and Boc-Val-Ala-Leu(d) Ala-OMe-enhanced stability of β -sheet through $\text{CH}\cdots\text{O}$ hydrogen bonds, *J. Biomol. Struct. Dyn.* **18**, 579–594.
99. Ramagopal, U.A., Ramakumar, S., Sahal, D., and Chauhan, V.S. (2001) *De novo* design and characterization of an apolar helical hairpin peptide at atomic resolution: compaction mediated by weak interactions, *Proc. Nat. Acad. Sci., USA* **98**, 870–874.
100. Loll, B., Raszewski, G., Saenger, W., and Biesiadka, J. (2003) Functional role of $\text{C}^\alpha\text{-H}\cdots\text{O}$ hydrogen bonds between transmembrane α -helices in photosystem I, *J. Mol. Biol.* **328**, 737–747.
101. Petrella, R.J. and Karplus, M. (2004) The role of carbon-donor hydrogen bonds in stabilizing tryptophan conformations, *Proteins Struct. Func. Genetics* **54**, 716–726.

102. Klaholz, B.P. and Moras, D. (2002) C–H···O hydrogen bonds in the nuclear receptor RAR γ —a potential tool for drug selectivity, *Structure* **10**, 1197–1204.
103. Pierce, A.C., Sandretto, K.L., and Bemis, G.W. (2002) Kinase inhibitors and the case for CH···O hydrogen bonds in protein-ligand binding, *Proteins Struct. Func. Genetics* **49**, 567–576.
104. Yohannan, S., Faham, S., Yang, D., Grosfeld, D., Chamberlain, A.K., and Bowie, J.U. (2004) A C α –H···O hydrogen bond in a membrane protein is not stabilizing, *J. Am. Chem. Soc.* **126**, 2284–2285.
105. Arbely, E. and Arkin, I.T. (2004) Experimental measurement of the strength of a C α –H···O bond in a lipid bilayer, *J. Am. Chem. Soc.* **126**, 5362–5363.
106. Jiang, L. and Lai, L. (2002) CH···O hydrogen bonds at protein–protein interfaces, *J. Biol. Chem.* **277**, 37732–37740.
107. Scheiner, S. (1997) *Hydrogen Bonding. A Theoretical Perspective*; Oxford University Press, New York.
108. Morokuma, K. (1971) Molecular orbital studies of hydrogen bonds. III. C=O···H–O hydrogen bond in H₂CO···H₂O and H₂CO···2H₂O, *J. Chem. Phys.* **55**, 1236–1244.
109. van Duijneveldt-van de Rijdt, J.G.C.M. and van Duijneveldt, F.B. (1971) Perturbation calculations on the hydrogen bonds between some first-row atoms, *J. Am. Chem. Soc.* **93**, 5644–5653.
110. Johansson, A., Kollman, P., and Rothenberg, S. (1972) The electronic structure of the HCN dimer and trimer, *Theor. Chim. Acta* **26**, 97–100.
111. Bonchev, D. and Cremaschi, P. (1974) C–H group as proton donor by formation of a weak hydrogen bond, *Theor. Chim. Acta* **35**, 69–80.
112. Johansson, A., Kollman, P., and Rothenberg, S. (1972) Hydrogen bonding and the structure of the HF–HCN dimer, *Chem. Phys. Lett.* **16**, 123–127.
113. Kollman, P., McKelvey, J., Johansson, A., and Rothenberg, S. (1975) Theoretical studies of hydrogen-bonded dimers. Complexes involving HF, H₂O, NH₃, HCl, H₂S, PH₃, HCN, HNC, HCP, CH₂NH, H₂CS, H₂CO, CH₄, CF₃H, C₂H₂, C₄H₄, C₆H₆, F[–], and H₃O⁺, *J. Am. Chem. Soc.* **97**, 955–965.
114. Vishveshwara, S. (1978) Ab-initio molecular orbital studies on CH···X hydrogen bonded systems, *Chem. Phys. Lett.* **59**, 26–29.
115. Hobza, P. and Sandorfy, C. (1984) Quantum chemical and statistical thermodynamic investigations of anesthetic activity. 3. The interaction between CH₄, CH₃Cl, CH₂Cl₂, CHCl₃, CCl₄, and an O–H···O hydrogen bond, *Can. J. Chem.* **62**, 606–609.
116. Frisch, M.J., Pople, J.A., and Del Bene, J.E. (1983) Hydrogen bonds between first-row hydrides and acetylene, *J. Chem. Phys.* **78**, 4063–4065.
117. Seiler, P., Weisman, G.R., Glendening, E.D., Weinhold, F., Johnson, V.B., and Dunitz, J.D. (1987) Observation of an eclipsed C_{sp}³–CH₃ bond in a tricyclic orthoamide; experimental and theoretical evidence for C–H···O hydrogen bonds, *Angew. Chem., Int. Ed. Engl.* **26**, 1175–1177.
118. Novoa, J.J., Whangbo, M.-H., and Williams, J.M. (1990) Ab initio computational study of the C–H···donor and C–H···anion contact interactions in organic donor salts, *Mol. Cryst. Liquid Cryst.* **181**, 25–42.
119. Reynolds, C.H. (1990) Methyl chloride/formic acid van der Waals complex: a model for carbon as a hydrogen bond donor, *J. Am. Chem. Soc.* **112**, 7903–7908.
120. Wiberg, K.B., Waldron, R.F., Schulte, G., and Saunders, M. (1991) Lactones. 1. X-ray crystallographic studies of nonanolactone and tridecanolactone: nature of CH···O non-bonded interactions, *J. Am. Chem. Soc.* **113**, 971–977.
121. Popelier, P.L.A. and Bader, R.F.W. (1992) The existence of an intramolecular C–H–O hydrogen bond in creatine and carbamoyl sarcosine, *Chem. Phys. Lett.* **189**, 542–548.
122. Feller, D. and Feyereisen, M.W. (1993) Ab initio study of hydrogen bonding in the phenol–water system, *J. Comput. Chem.* **14**, 1027–1035.

123. Turi, L. and Dannenberg, J.J. (1993) Molecular orbital study of acetic acid aggregation. 1. Monomers and dimers, *J. Phys. Chem.* **97**, 12197–12204.
124. Tsuzuki, S., Uchimaru, T., Tanabe, K., and Hirano, T. (1993) Conformational analysis of 1,2-dimethoxyethane by ab initio molecular orbital and molecular mechanics calculations: stabilization of the TGG' rotamer by the 1,5 CH_3/O nonbonding attractive interaction, *J. Phys. Chem.* **97**, 1346–1350.
125. Starikov, E.B. and Steiner, T. (1997) Computational support for the suggested contribution of $\text{C-H}\cdots\text{O}=\text{C}$ interactions to the stability of nucleic acid base pairs, *Acta Cryst.* **D53**, 345–347.
126. McCarthy, W., Smets, J., Adamowicz, L., Plokhotnichenko, A.M., Radchenko, E.D., Sheina, G.G., and Stepanian, S.G. (1997) Competition between H-bonded and stacked dimers of pyrimidine: IR and theoretical ab-initio study, *Mol. Phys.* **91**, 513–525.
127. Kratochvil, M., Engkvist, O., Sponer, J., Jungwirth, P., and Hobza, P. (1998) Uracil dimer: potential energy and free energy surfaces. Ab initio beyond Hartree–Fock and empirical potential surfaces, *J. Phys. Chem. A* **102**, 6921–6926.
128. Shishkin, O.V., Sponer, J., and Hobza, P. (1999) Intramolecular flexibility of DNA bases in adenine–thymine and guanine–cytosine Watson–Crick base pairs, *J. Mol. Struct.* **477**, 15–21.
129. Sponer, J. and Hobza, P. (2000) Interaction energies of hydrogen-bonded formamide dimer, formamide dimer, and selected DNA base pairs obtained with large basis sets of atomic orbitals, *J. Phys. Chem. A* **104**, 4592–4597.
130. Hobza, P., Sponer, J., Cubero, E., Orozco, M., and Luque, F.J. (2000) $\text{C-H}\cdots\text{O}$ contacts in the adenine–uracil Watson–Crick and uracil–uracil nucleic acid base pairs: nonempirical ab initio study with inclusion of electron correlation effects, *J. Phys. Chem. B* **104**, 6286–6292.
131. Brandl, M., Meyer, M., and Sühnel, J. (2001) Quantum-chemical analysis of $\text{C-H}\cdots\text{O}$ and $\text{C-H}\cdots\text{N}$ interactions in RNA base pairs—H-bond versus anti-H-bond pattern, *J. Biomol. Struct. Dyn.* **18**, 545–555.
132. Zhang, B., Cai, Y., Mu, X., Lou, N., and Wang, X. (2002) Multiphoton ionization and density functional studies of pyrimidine–(water)_n clusters, *J. Chem. Phys.* **117**, 3701–3710.
133. Fidanza, N.G., Suvire, F.D., Sosa, G.L., Lobayan, R.M., Enriz, R.D., and Peruchena, N.M. (2001) A search for $\text{C-H}\cdots\text{O}$ type hydrogen bonds in Lamivudine (3TC). An exploratory conformational and electronic analysis, *J. Mol. Struct. (Theochem)* **543**, 185–193.
134. Louit, G., Hocquet, A., and Ghomi, M. (2002) Intramolecular hydrogen bonding in ribonucleosides: an AIM topological study of the electronic density, *Phys. Chem. Chem. Phys.* **4**, 3843–3847.
135. Klein, R.A. (2002) Electron density topological analysis of hydrogen-bonding in glucopyranose and hydrated glucopyranose, *J. Am. Chem. Soc.* **124**, 13931–13937.
136. Cabaleiro-Lago, E.M. and Otero, J.R. (2002) Ab Initio and density functional theory study of the interaction in formamide and thioformamide dimers and trimers, *J. Chem. Phys.* **117**, 1621–1632.
137. Neuheuser, T., Hess, B.A., Reutel, C., and Weber, E. (1994) Ab initio calculations of supramolecular recognition modes. Cyclic versus noncyclic hydrogen bonding in the formic acid/formamide system, *J. Phys. Chem.* **98**, 6459–6467.
138. Vargas, R., Garza, J., Friesner, R.A., Stern, H., Hay, B.P., and Dixon, D.A. (2001) Strength of the $\text{N-H}\cdots\text{O}=\text{C}$ and $\text{C-H}\cdots\text{O}=\text{C}$ bonds in formamide and *N*-methylacetamide dimers, *J. Phys. Chem. A* **105**, 4963–4968.
139. Vargas, R., Garza, J., Dixon, D.A., and Hay, B.P. (2000) How strong is the $\text{C}^\alpha\text{-H}\cdots\text{O}=\text{C}$ hydrogen bond? *J. Am. Chem. Soc.* **122**, 4750–4755.
140. Vargas, R., Garza, J., Dixon, D.A., and Hay, B.P. (2000) Conformational analysis of *N,N,N',N'*-tetramethyl succinamide: the role of $\text{C-H}\cdots\text{O}$ hydrogen bonds, *J. Phys. Chem. A* **104**, 5115–5121.
141. Xu, Z., Li, H., Wang, C., Wu, T., and Han, S. (2004) Is the blue shift of C-H vibration in DMF–water mixture mainly caused by $\text{C-H}\cdots\text{O}$ interaction? *Chem. Phys. Lett.* **394**, 405–409.
142. Scheiner, S., Kar, T., and Gu, Y. (2001) Strength of the $\text{C}^\alpha\text{-H}\cdots\text{O}$ hydrogen bond of amino acid residues, *J. Biol. Chem.* **276**, 9832–9837.

143. Zhang, H., Zhou, Z., and Shi, Y. (2004) Density functional theory study of the hydrogen-bonding interaction of 1:1 complexes of alanine with water, *J. Phys. Chem. A* **108**, 6735–6743.
144. Vargas, R., Garza, J., Hay, B.P., and Dixon, D.A. (2002) Conformational study of the alanine dipeptide at the MP2 and DFT levels, *J. Phys. Chem. A* **106**, 3213–3218.
145. Sadlej-Sosnowska, N., Dobrowolski, J.C., Oziminski, W.P., and Mazurek, A.P. (2002) On conformation and hydrogen bonding in vigabatrin amino acid molecule, *J. Phys. Chem. A* **106**, 10554–10562.
146. Broda, M.A., Rospenk, M., Siodlak, D., and Rzeszotarska, B. (2005) Association of model peptides and dehydropeptides: *N*-acetyl-L-alanine and dehydroalanine *N,N'*-dimethylamides, *J. Mol. Struct.* **740**, 17–24.
147. Chang, H.-C., Jiang, J.-C., Chao, M.-C., Lin, M.-S., Lin, S.H., Chen, H.-Y., and Hsueh, H.-C. (2001) Pressure-dependent studies on hydration of the C–H group in formic acid, *J. Chem. Phys.* **115**, 8032–8037.
148. Roy, A.K. and Thakkar, A.J. (2005) Pentamers of formic acid, *Chem. Phys.* **312**, 119–126.
149. Marques, M.P.M., da Costa, A.M.A., and Ribeiro-Claro, P.J.A. (2001) Evidence of C–H···O hydrogen bonds in liquid 4-ethoxybenzaldehyde by NMR and vibrational spectroscopies, *J. Phys. Chem. A* **105**, 5292–5297.
150. Kovács, A., Szabó, A., Nemesok, D., and Hargittai, I. (2002) Blue-shifting C–H···X (X = O, Halogen) hydrogen bonds in the dimers of formaldehyde derivatives, *J. Phys. Chem. A* **106**, 5671–5678.
151. Ornstein, R.L. and Zheng, Y. (1997) Ab initio quantum mechanics analysis of imidazole C–H···O water hydrogen bonding and a molecular mechanics forcefield correction, *J. Biomol. Struct. Dyn.* **14**, 657–665.
152. Kim, K. and Friesner, R.A. (1997) Hydrogen bonding between amino acid backbone and side chain analogues: a high-level ab initio study, *J. Am. Chem. Soc.* **119**, 12952–12961.
153. Wang, B., Hinton, J.F., and Pulay, P. (2003) C–H···O hydrogen bond between *N*-methyl maleimide and dimethyl sulfoxide: a combined NMR and ab initio study, *J. Phys. Chem. A* **107**, 4683–4687.
154. Ahn, D.-S., Park, S.-W., Lee, S., and Kim, B. (2003) Effects of substituting group on the hydrogen bonding in phenol-H₂O complexes: ab initio study, *J. Phys. Chem. A* **107**, 131–139.
155. Venkatesan, V., Fujii, A., Ebata, T., and Mikami, N. (2004) A direct experimental evidence for an aromatic C–H···O hydrogen bond by fluorescence-detected infrared spectroscopy, *Chem. Phys. Lett.* **394**, 45–48.
156. Scheiner, S., Kar, T., and Pattanayak, J. (2002) Comparison of various types of hydrogen bonds involving aromatic amino acids, *J. Am. Chem. Soc.* **124**, 13257–13264.
157. Yan, S. and Bu, Y. (2005) Coupling properties of imidazole dimer radical cation assisted by embedded water molecule: toward understanding of interaction character of hydrogen-bonded histidine residue side-chains, *J. Chem. Phys.* **122**, 184324.
158. Guo, H., Beahm, R.F., and Guo, H. (2004) Stabilization and destabilization of the C^β–H···O = C hydrogen bonds involving proline residues in helices, *J. Phys. Chem. B* **108**, 18065–18072.
159. Dabkowska, I., Rak, J., and Gutowski, M. (2002) Computational study of hydrogen-bonded complexes between the most stable tautomers of glycine and uracil, *J. Phys. Chem. A* **106**, 7423–7433.
160. Alkorta, I. and Elguero, J. (2003) Interaction of protein backbone with nucleic acid bases, *J. Phys. Chem. B* **107**, 5306–5310.
161. Koch, U. and Popelier, P.L.A. (1995) Characterization of C–H–O hydrogen bonds on the basis of the charge density, *J. Phys. Chem.* **99**, 9747–9754.
162. He, Z., Sundström, V., and Pullerits, T. (2001) Intermolecular hydrogen bonding between carotenoid and bacteriochlorophyll in LH2, *FEBS Lett.* **496**, 36–39.
163. Scheiner, S. and Kar, T. (2005) Effect of solvent upon CH···O hydrogen bonds with implications for protein folding, *J. Phys. Chem. B* **109**, 3681–3689.

CHAPTER 8

NEUTRAL BLUE-SHIFTING AND BLUE-SHIFTED HYDROGEN BONDS¹

EUGENE S. KRYACHKO

Department of Chemistry, Bat. B6c, University of Liege, Sart-Tilman, B-4000 Liege 1, Belgium and Bogoliubov Institute for Theoretical Physics, Kiev, 03143 Ukraine. E-mail: eugene.kryachko@ulg.ac.be

Abstract This is a critical review that, first, covers the most important results in the area of blue-shifting hydrogen bonds including their update list containing more than 80 blue-shifting hydrogen-bonded complexes and, second, attempts to classify them on the equal footing with the classical hydrogen bonds and to partly re-examine their origin by means of introducing the concept of the blue-shifted hydrogen bonds.

Keywords: Hydrogen bonding; definition of hydrogen bond; classification of hydrogen bonding interaction; red shift; C–H···B interaction; blue shift; blue-shifting and blue-shifted C–H···B bonds.

Put all your eggs in one basket and – watch that basket.
Mark Twain “Pudd’nhead Wilson”

1 INTRODUCTION

In fact, by the end of the twentieth century almost everyone who ever worked in the theory of hydrogen bonding has believed that its principal nature is well settled and understood. The edge of the last century was marked by the works of Hobza and collaborators [1], Karger et al. [2], and Scheiner and co-workers [3] which suddenly and partially changed our early thoughts and made many of us to somehow doubt on whether everything is in order in the “Kingdom of the Hydrogen Bond,” and inspired us as well to look deeper at the origin of the hydrogen bonding interaction. To comprehend what is precisely out of order right there, we introduce the rules that governed this “Kingdom” until the end of the twentieth century and which will be hereafter referred to as “classical.”

¹ Charged blue-shifting hydrogen and π -hydrogen bonds are not considered in the present review.

2 THE CLASSICAL CONCEPT OF HYDROGEN BOND: RULES

The concept of a classical or conventional hydrogen bond $A-H \cdots B$ that is formed between a conventional hydrogen bond (or proton) donor $A-H$ and a conventional proton acceptor B containing lone-pair sp -electrons was introduced by Moore and Winmill (“weak union,” Ref. [4]), Huggins [5] (who claimed to have been the first to propose hydrogen bonds in 1919 in a thesis to explain tautomerism in acetoacetic acid esters, his later usage of the term “hydrogen bridge” may have coined the German word “Wasserstoffbrücke”), Latimer and Rodebush (“hydrogen nucleus held between 2 octets constitutes a weak “bond,” Ref. [6]), and Pauling [7] at the beginning of the twentieth century. Actually, the idea of a weak specific interaction directly involving the hydrogen atom even goes back to Nernst [8] who discussed a dimeric association of molecules with hydroxyl groups in 1891 and to Werner [9] who introduced ten years later the concept of a minor valence (“Nebervalenz”) as a proper description of hydrogen bonding (see also the related works by Oddo and Puxeddu [10] and Pfeiffer [11]). The hydrogen bond was apparently quoted for the first time by Lewis [12] (“it seems to me that the most important addition to my theory of valence lies in the suggestion of what has become known as the hydrogen bond”) in 1923 and later by Bernal and Megaw [13], and by Huggins [14].

During nearly a century, the concept of the hydrogen bonding interaction has been vastly explored in myriad ways in physics, chemistry, biology, and material science, particularly in supramolecular chemistry (or molecular sociology) (see Refs. [15–30] and references therein). The ubiquitous hydrogen bond, as playing a very important role in nature, still fascinates all scientists who ever worked in this area. Literally, thousands of papers are published every year on hydrogen bonds: for example, a *Chemical Abstract* search for the year 1998 with “hydrogen bond” as the keyword gives 3,707 papers and 13,436 occurrences [31] (see also Ref. [32]).

Within the general theory of hydrogen bonding, A is usually a sufficiently electronegative group that induces a rather polar bond. $O-H$ and $N-H$ groups are typical conventional hydrogen bond donors (generally speaking, $R'-A-H$ where $A = O, N$ and R' is the remainder of the molecule under study). Typical conventional hydrogen bond or proton acceptors are the atoms $F, N, O, P, S, Cl, Se, Br,$ and I which are characterized by larger electronegativities relative to hydrogen and having an unshared electron pair (or molecular groups that contain these atoms). When a hydrogen atom H belonging to the $A-H$ group of one molecule approaches the electronegative atom B sufficiently close, it interacts with B and forms a bond by sharing its proton between A and B . Such bonding (sharing), graphically designated by a dotted line “ \cdots ” rearranges the electron densities of the $A-H$ group and B in such a manner that H partially loses its charge compared to the monomer $A-H$. Within the $A-H \cdots B$ hydrogen

bond, H is treated as a bridging “hydron” $H^{+\delta}$ ($0 \leq \delta < 1$) or, in the extreme case of strong symmetric hydrogen bonds, as a bridging proton H^+ .

The geometric description of a hydrogen (H-) bond $A-H \cdots B$ relies on the two bond lengths, $R(A-H)$ and $r(H \cdots B)$, and the bond angle $\varphi_H \equiv \angle AHB$. $r(H \cdots B)$, defined as the distance between the bridging proton (hydron) and the proton acceptor B, is often called the hydrogen bond separation. It is also useful, especially for those bonds which are characterized by larger deviations of φ_H from π , to define the donor-acceptor distance $r(A \cdots B)$ as another characteristic of a given H-bond. Sometimes, instead of φ_H , the another angle $\psi_H \equiv \pi - \varphi_H$ is also used to directly measure the deviation of $A-H \cdots B$ from collinearity. Spectroscopically, the formation of a hydrogen bond $A-H \cdots B$ gives rise to a new vibrational mode ν_σ that describes the H-bond $A \cdots B$ stretch and perturbs the intermolecular bending modes.

It is usually assumed that a conventional hydrogen bond $A-H \cdots B$ is formed if the following structural and spectroscopic criteria (rules) are obeyed [15–30]:

1. There exists clear evidence for the bond formation $A-H \cdots B$ (“association or chelation” [16]). This might be, for example, the appearance of the H-bond stretching mode $\nu_\sigma(A \cdots B)$. The energy E_{HB} of formation of a hydrogen bond is defined as $E_{HB} \equiv E(A-H \cdots B) - [E(A-H) + E(B)]$. If a hydrogen bond is formed, $E_{HB} < 0$. Another evidence can be based on the energy criteria [18]: the absolute value, $|E_{HB}|$, is larger than the dipolar or London dispersion energies.
2. There exists clear evidence that the formed bond specifically involves a hydrogen atom as bonded to B predominantly along the bond direction $A-H^2$.
3. The $A-H$ bond elongates, i.e.

$$(1) \quad \Delta R(A-H) > 0$$

relative to that in the monomer implying that this covalent bond weakens. A measure of such elongation is

$$(2) \quad \Delta R(A-H) \equiv R_{A-H \cdots B}(A-H) - R_{A-H}(A-H)$$

4. The so-called van der Waals cutoff criterion: the hydrogen bond separation $r(H \cdots B)$ is shorter than the sum of van der Waals radii of H and B, i.e.

$$(3) \quad r(H \cdots B) < w_H + w_B$$

where w_X is the van der Waals radius of X. In addition, the following necessary but insufficient condition is often imposed on $r(A \cdots B)$: a H-bond is formed if $r(A \cdots B) < w_A + w_B$. In some cases, the van der Waals cutoff constraint is too strong from the experimental point of view and it is

² This criterion is not apparently a necessary requisite of a hydrogen bond; see, e.g., Ref. [16].

often substituted by a weaker one: $r(\text{H} \cdots \text{B}) \leq 3.0$ or even 3.2 \AA [20, 21, 23, 25] (see also note [21] in Ref. [25])

5. The proton-stretching vibrational mode $\nu(\text{A-H})$ undergoes a red shift (a downshift to lower wavenumbers) with respect to that in the corresponding monomer, i.e.

$$(4) \quad \Delta\nu(\text{A-H}) \equiv \nu_{\text{A-H}\cdots\text{B}}(\text{A-H}) - \nu_{\text{A-H}}(\text{A-H}) < 0$$

and its IR absorption increases

$$(5) \quad \text{IR}_{\text{A-H}\cdots\text{B}}(\nu(\text{A-H})) / \text{IR}_{\text{A-H}}(\nu(\text{A-H})) > 1$$

The last two criteria, (4) and (5), are the most unequivocal and powerful signs for the formation of the hydrogen bond. $\Delta\nu(\text{A-H})$ and $\text{IR}_{\text{A-H}\cdots\text{B}}(\nu(\text{A-H})) / \text{IR}_{\text{A-H}}(\nu(\text{A-H}))$ are the most important characteristics of H-bonding, its “fingerprints” or “signature” [33], say literally.

6. Proton nuclear magnetic resonance (^1H NMR) chemical shifts in the $\text{A-H} \cdots \text{B}$ hydrogen bond are shifted downfield compared to the monomer, i.e.

$$(6) \quad \Delta\sigma_{\text{iso}}(\text{H}) \equiv \sigma_{\text{iso}}^{\text{A-H}\cdots\text{B}}(\text{H}) - \sigma_{\text{iso}}^{\text{A-H}}(\text{H}) < 0$$

This is another powerful indicator of hydrogen bonding [34]. The negative character of $\Delta\sigma_{\text{iso}}(\text{H})$ is explained by the deshielding of the bridging hydron H that is induced by the formation of the hydrogen bond.

The bridging hydron loses its electron density, that is, becomes more positively charged. Upon formation of a hydrogen bond, there is also a transfer of net charge between the proton donor and the proton acceptor caused by the Coulomb repulsion between the lone-pair electrons of the proton donor and those of the proton acceptor: the electron density flows from lone electron pairs of the proton acceptor B to the σ^* -antibonding molecular orbital of the proton donor A-H [35] (see also Ref. [36]) that induces a larger negative charge on the proton donor and a more positive one on the proton acceptor, and increases the electron density on the σ^* -antibonding molecular orbital of the A-H. This causes a weakening of the A-H bond, its elongation, and a concomitant red-shifting of the $\nu(\text{A-H})$ stretching vibrational mode.

The criteria 1–6 are related to the geometric and spectroscopic features of the interaction upon which crystallographers, molecular spectroscopists, and quantum chemists (with adding the energetic criterion, see Table 1) primarily rely and most widely use, considering them as an evidence of an attractive interaction that involves a rearrangement of the electronic density distribution within a given system. Note that criteria 3–6 can be also treated as an indirect confirmation of criterion 1 and criterion 2, meaning that the set of criteria 1–6 is apparently overcomplete. In addition, there are also other features that are related to the H-bond formation such as, e.g., an increase of the polarity of the

Table 1. Jeffrey's classification of hydrogen bonds [21] (see also Refs. [25, 36–38]). All notations in the first column are defined in the criteria 1–6

Type of H-bond	Strong (proton-shared)	Moderate (medium)	Weak (conventional)
Type of interaction	Strongly covalent, ionic	Dominant electrostatic	Electrostatic and dispersion
$r(\text{H}\cdots\text{B})$, Å	1.2–1.5	1.5–2.2	≥ 2.2
$\Delta R(\text{A}-\text{H})$, Å	0.08–0.25	0.02–0.08	≤ 0.02
$R(\text{A}-\text{H})/r(\text{H}\cdots\text{B})$	≈ 1	< 1	$\ll 1$
$r(\text{A}\cdots\text{B})$, Å	2.2–2.5 (2.6)	2.5 (2.6)–3.2	≥ 3.2
φ_{H}	170–180°	130–170°	90–130°
$ E_{\text{HB}} $, kcal · mol ⁻¹	15–40 (60 [36, 37])	4–15	≤ 4
$\Delta\nu(\text{A}-\text{H})/\nu(\text{A}-\text{H})$, %	25	10–25	≤ 10
$ \Delta\sigma_{\text{iso}}(\text{H}) $, ppm	14–22	< 14	

A–H bond, an increase of the total dipole moment of the system relative to the vector sum of the dipole moments of monomers, etc. However, the features gathered by the criteria 1–6 are quintessential witnesses of the existence of the hydrogen bonding interaction. If they are satisfied, the hydrogen bond A–H \cdots B is formed and A–H is then called a proton donor and B a proton acceptor.

Let us stress once more that the above definition of a hydrogen bond operates with the geometric, spectroscopic, and energetic features of a H-bonded system under consideration. A simpler definition of the hydrogen bond was proposed by Pauling [7]: “... under certain conditions an atom of hydrogen is attracted by rather strong forces to two atoms, instead of only one, so that it may be considered to be acting as a bond between them. This is called the hydrogen bond.” Pauling's definition has been further revisited by Lippert [39] (“A H-bond exists if one hydrogen atom H is bonded to more than one other atom, for instance, to two atoms named X and Y.”), and by Perrin and Nielson [40] (“A hydrogen bond is an attractive interaction between a hydron donor A–H and hydron acceptor B.”), and recently by Steiner [25]³:

(7) AA–H \cdots B interaction is called a hydrogen bond if

(a) it constitutes a local bond and (b) if A–H acts as a proton donor with respect to B.

Hydrogen bonds are classified, according to Table 1, as strong or proton-shared (ion-pair), moderate (medium), and normal or weak (conventional). Strong H-bonds are two-center bonds with short H-bond distances such that $r(\text{A}\cdots\text{B}) \in (2.2 \text{ \AA}, 2.60 \text{ \AA})$ (notice that for very strong H-bonds, $r(\text{A}\cdots\text{B}) < 2.45 \text{ \AA}$). For symmetric strong H-bonds, the graphic notation ‘ \cdots ’ for the hydrogen bonding H \cdots B loses its sense since the involved proton is equally

³ Actually, this definition relies on the definitions of a local bond and a proton donor.

shared and thus centered between A and B (for other strong H-bonds, a shorter distance, either between A and H or between B and H, determines a donor group). They are therefore depicted as A–H–B. Strong hydrogen bonds are practically linear and their H-bond formation energies fall within the range of $15 \text{ kcal} \cdot \text{mol}^{-1} \leq |E_{\text{HB}}| \leq 60 \text{ kcal} \cdot \text{mol}^{-1}$.

Weak or conventional hydrogen bonds are characterized by longer distances $r(\text{A} \cdots \text{B})$ and $r(\text{H} \cdots \text{B})$. Their A–H bonds are slightly elongated relative to the monomeric $R(\text{A–H})$ and their $r(\text{H} \cdots \text{B})$ bond lengths are much longer than a covalent $\text{H} \cdots \text{B}$ distance. The strength of a conventional hydrogen bond $\text{A–H} \cdots \text{B}$ is typically estimated by the electrostatic attraction of the bond dipole A–H with a negative charge on B [18]. Usually, this strength is an order of magnitude weaker than a covalent bond.

The archetypical system with a typical conventional hydrogen bond is the water dimer [41] depicted in Fig. 1. It is solely stabilized by the hydrogen bond $\text{O}_2^{-0.54} \text{–H}_5^{+0.30} \cdots \text{O}_1^{-0.51}$ where the superscripts indicate the corresponding Mulliken charges. The ZPVE-corrected E_{HB} of water dimer amounts to $-2.82 \text{ kcal} \cdot \text{mol}^{-1}$ at the B3LYP/6-311++(2*d*,2*p*) computational level (for the

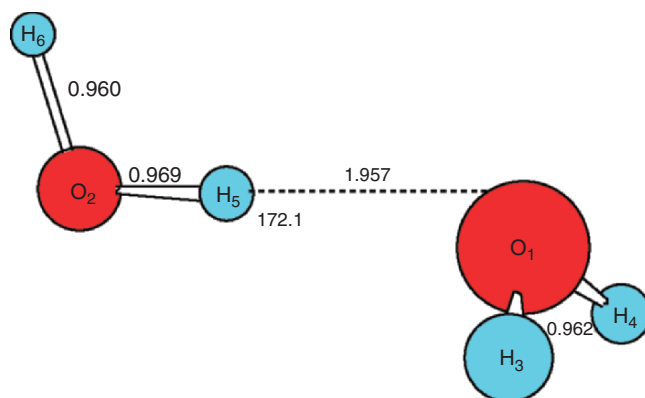


Figure 1. The H-bonded structure of water dimer at the B3LYP/6-311++(2*d*,2*p*) computational level. The distance $r(\text{O}_1 \cdots \text{O}_2) = 2.919 \text{ \AA}$. The Mulliken charges are the following: $\Delta q_{\text{M}}(\text{O}_1) = -0.507$, $\Delta q_{\text{M}}(\text{O}_2) = -0.536$, $\Delta q_{\text{M}}(\text{H}_3) = \Delta q_{\text{M}}(\text{H}_4) = 0.258$, $\Delta q_{\text{M}}(\text{H}_5) = 0.296$, and $\Delta q_{\text{M}}(\text{H}_6) = 0.232|e|$ (to be compared with those of the water monomer: $\Delta q_{\text{M}}(\text{O}_1) = -0.468$ and $\Delta q_{\text{M}}(\text{H}_{3,4}) = 0.234|e|$). The stretching vibrational modes are: $\nu(\text{O}_2\text{–H}_5) = 3707 \text{ cm}^{-1}$ ($330 \text{ km} \cdot \text{mol}^{-1}$), $\nu_{\text{sym}}(\text{O}_1\text{–H}_{3,4}) = 3816 \text{ cm}^{-1}$ ($14 \text{ km} \cdot \text{mol}^{-1}$), $\nu_{\text{asym}}(\text{O}_1\text{–H}_{3,4}) = 3914 \text{ cm}^{-1}$ ($84 \text{ km} \cdot \text{mol}^{-1}$), $\nu(\text{O}_2\text{–H}_6) = 3897 \text{ cm}^{-1}$ ($85 \text{ km} \cdot \text{mol}^{-1}$) (the water monomer is characterized by the stretching modes $\nu_{\text{sym}}(\text{O}_1\text{–H}_{3,4}) = 3821 \text{ cm}^{-1}$ ($7 \text{ km} \cdot \text{mol}^{-1}$) and $\nu_{\text{asym}}(\text{O}_1\text{–H}_{3,4}) = 3923 \text{ cm}^{-1}$ ($62 \text{ km} \cdot \text{mol}^{-1}$)). Throughout the present work, bond lengths are given in Å and bond angles in degree. The electronic energy E (in hartree) and ZPVE (in $\text{kcal} \cdot \text{mol}^{-1}$) of the water monomer and water dimer are the following: $E(\text{H}_2\text{O}) = -76.462041$ and $E((\text{H}_2\text{O})_2) = -152.931994$; $\text{ZPVE}(\text{H}_2\text{O}) = 13.41$, and $\text{ZPVE}((\text{H}_2\text{O})_2) = 28.97$.

computational methodology of the present work see footnote⁴ $\Delta R(\text{O}_2\text{--H}_5)$ as defined in criterion 3 is equal to 0.008 Å. The red shift of the stretching vibrational mode $\nu(\text{O}_1\text{--H}_5)$ caused by the formation of the H-bond in water dimer is equal to 114 cm^{-1} (relative to $\nu_{\text{sym}}(\text{H}_2\text{O})$), that is about 3.0% of the stretching frequency of the water monomer, and the ratio of the IR activities amounts to ca. 47. The NMR chemical shift $\delta\sigma_{\text{iso}}(\text{H}_5)$ of the bridging hydron $\text{H}_5^{+0.30}$ amounts to -3.2 ppm. The formation of the H-bond in this system induces a flow of the electron density that can be traced by the changes in the Mulliken atomic and the Natural Population Analysis (NPA) charges: $\Delta q_{\text{M}}(\text{O}_2) = -0.070$, $\Delta q_{\text{M}}(\text{O}_1) = -0.040$, $\Delta q_{\text{M}}(\text{H}_5) = +0.060$, and $\Delta q_{\text{M}}(\text{H}_3) = \Delta q_{\text{M}}(\text{H}_4) = +0.020$ and $\Delta q_{\text{NPA}}(\text{O}_2) = -0.031$, $\Delta q_{\text{NPA}}(\text{O}_1) = -0.012$, $\Delta q_{\text{NPA}}(\text{H}_5) = +0.022$, and $\Delta q_{\text{NPA}}(\text{H}_3) = \Delta q_{\text{NPA}}(\text{H}_4) = +0.013|e|$.

3 BLUE-SHIFTING C–H···B HYDROGEN BONDS

In fact, as noticed by Hobza and Havlas [1e], “the published definitions of the H-bond are not unambiguous and many exist.” Nowadays, the concept of a hydrogen bond is much broader than it was expected nearly century ago (see Refs. [23, 25, 43–45] and references therein), and that is why it permits, together with the conventional H-bonds, the existence of a wide class of those, say “nonconventional” ones, identified during the last three decades experimentally and theoretically, which do not partially satisfy either the traditional view on the proton donor and proton acceptors or/and the conditions (criteria 1–6). A class of nonconventional hydrogen bonds particularly include the A–H···M ones which are formed, on the one hand, between conventional hydrogen bond donors and electron-rich transition metals M, such as Co, Ru, Rh, Os, Ir, and Pt functioning as weak nonconventional proton acceptors [46], and on the other, between the conventional hydrogen bond donors and clusters of such coinage metals as Ag and Au [47]. A major part of a class of nonconventional hydrogen bonds belongs to the C–H···B bonds, particularly the C–H···O ones [15, 16, 23].

The very first, to our knowledge, reference to C–H···O hydrogen bonds goes back to 1936 when Huggins published his work [14] where he suggested that “If a carbon atom is sufficiently polarized by attachment to one or more electronegative atoms, the hydrogen in question may become loose enough bound to serve as a bridge.” One year later Glasstone [48] suggested that the complex

⁴ These computations were conducted with the *GAUSSIAN 03* package of quantum chemical programs [42]. The Kohn–Sham self-consistent field formalism with the hybrid density functional B3LYP potential was used together with the basis set 6-311++G(2d,2p) for oxygen and hydrogen. All geometrical optimizations were performed with the keywords “Tight” and “Int=UltraFine.” The unscaled harmonic vibrational frequencies, zero-point vibrational energies (ZPVE), and enthalpies were also calculated. The binding energy $E_{\text{b}}[\text{AB}]$ of the complex AB is defined as the energy difference, $E_{\text{b}}[\text{AB}] \equiv |E[\text{AB}] - (E[\text{A}] + E[\text{B}])|$. The ZPVE-corrected binding energies E_{b} are reported throughout this work.

between chloroform and acetone whose existence was known at least from 1914 is formed due to the $\text{Cl}_3\text{C}-\text{H}\cdots\text{O}$ hydrogen bonding.

In 1938 Marvel and co-workers started a series of papers under the title “Hydrogen bonds involving the C–H link” [49] (see also Ref. [50]). In parallel, infrared spectroscopic studies involving chloroform and bromoform were conducted in this period [51] revealing small red shifts of the $\nu(\text{C}-\text{H})$ stretching vibrational modes. The year of 1943 was marked by the first work by Huggins [52] on C–H \cdots O bonds in proteins. As Martin and Derewenda [32] wrote, Huggins’ “idea . . . took over 50 years to resurface but which is now generally accepted” [53].

The first review on the C–H \cdots B hydrogen bonding [54] was quite pessimistic: “So weak is the tendency of the C–H group to form a hydrogen bond that it is manifested only under the influence of activating atoms or groups tending to promote ionization of the hydrogen atom, as in chloroform, hydrogen cyanide and phenyl acetylene.” Clearly, the first evidence of the C–H \cdots B hydrogen bond with B = N was reported four years later [55] (see also the 1960th edition of Ref. [7], p. 458, and Ref. [56]). Dougill and Jeffrey [57] used a term of the C–H \cdots O=C “polarization bonding” for the explanation of the anomalously high melting point of dimethyloxalate. However, the history of the C–H \cdots B hydrogen bonding was not quite successful as that of the classical ones: there were definitely moments in time when the C–H \cdots B bond was not even considered at all as a hydrogen bond. Recall, for example, the response by Donohue to the question “The C–H \cdots O hydrogen bond: what is it? It isn’t!” [58].

The first evidence of the C–H \cdots O hydrogen bonding in organic crystals was reported more than 40 years ago [59], and only in the 1990s this type of interaction was accepted widespread, thanks particularly to theoretical results. C–H \cdots O hydrogen bonds have been recognized as important “bricks” that determine the stability and specificity of biological systems [60]. The intramolecular C–H \cdots O H-bond was first suggested for 1,2-dimethoxyethane in the gas phase [61] in 1979 and confirmed only in 1992 by matrix-isolation infrared spectroscopy [62]. The theoretical study of this molecule has been conducted one year later [63] and demonstrated the importance of the C–H \cdots O hydrogen bonding in the conformational stabilization.

The strength of the C–H \cdots B hydrogen bonds and their stretching modes $\nu(\text{C}-\text{H})$ strongly depend on the nature of the proton donor as $\text{C}(sp)-\text{H} > \text{C}(sp^2)-\text{H} > \text{C}(sp^3)-\text{H}$ and also increases when hydrogen atoms are successively replaced by electron withdrawing groups (Ref. [33]; see also Refs. [23, 43], and Ref. [64] for current computational studies). Surprisingly, the C–H \cdots B hydrogen bonds behave as a “two-headed Janus.” For some category of molecular systems, the C–H \cdots B interaction weakens the C–H bond, that in turn results in its elongation, a concomitant red shift of the stretching vibrational mode $\nu(\text{C}-\text{H})$, and an increase of its IR intensity. In other words, these C–H \cdots O interactions may be definitely referred to the classical hydrogen bonding. For another category of systems with the C–H \cdots O interaction, the

C–H bond is strengthened and its bond length is shortened (see Refs. [1–3, 65–90] and references therein). As a result, the stretching vibrational mode $\nu(\text{C–H})$ is shifted to higher wave numbers, namely, blue-shifted, and its IR intensity is often reduced. This peculiar phenomenon of a shortening of the C–H bond and a blue shifting of the respective $\nu(\text{C–H})$ stretching vibrational mode that definitely contrasts with or even opposite to the conditions 3 and 4 of the classical, conventional hydrogen bonding has drawn great attention during the last years, on both, theoretical and experimental sides, and has been then named as “anti-” or “improper,” or “blue-shifting hydrogen bonding” [1].

As noticed by Barnes [91], the earliest evidence on blue-shifting hydrogen bonds was reported in the 1950s by Pinchas [79], suggesting that the upshift of the aldehydic C–H stretch of *o*-nitrobenzaldehyde and related compounds relative to the corresponding *m*- and *p*-substituted benzaldehydes arises due to the formation of the intramolecular C–H \cdots O hydrogen bonding (see also Ref. [94]). The unusual shifts of the C–H stretching vibrational frequencies to higher wavenumbers were early revealed for fluoroform dissolved in liquefied Ar and N₂ by Golubev et al. [93] in 1977, for fluoroparaffin derivatives containing the CHF₂ groups and dissolved in mixtures of diethyl ether/methylcyclohexane by Sandorfy and co-workers [80] in 1980, for fluoro- and chloroforms by Paulson and Barnes [81] in 1982, for chloroform upon complexation with triformylmethane by Buděšínský et al. [82] ($\nu(\text{C–H})$ of chloroform is blue-shifted from 3021 to 3028 cm⁻¹) in 1989, and later by Tsymbal et al. [83], [87]⁵, Bulanin et al. [84], Tokhadze [85], Boldeskul et al. [86], Chaney et al. [94], Contréras et al. [95], and van der Veken and co-workers. In the work [86], Boldeskul et al. studied the IR spectra in the region of the C–H/D stretches of chloroform, deuteriochloroform, and deuterobromoform which are H-bonded to some molecules containing NO₂, SO₂, COC, and COO proton acceptor groups. The main results of this work [86] are summarized in Table 2.

The current list of blue-shifting hydrogen bonds is quite impressive (see Table 3 which collects most of them, basically those which in some sense have become classical) and it considerably grows each year (interestingly, among more than 1000 articles published in *Journal of Molecular Structure* between 1982 and 1996, only nine were referred to the C–H \cdots B bonding, see Ref. [50]).

⁵ These authors also mentioned the early works on a blue shift of the N–H (H. Lee, S. Ya. Haikin, and V. M. Chulanovski, in *Mol. Spectrosc.*, Vol. 2, G. S. Denisov (Ed.) (Leningrad State University Press, Leningrad, 1973), p. 18; E. V. Ryltsev, I. F. Tsymbal, A. K. Shurubura, and Y. P. Egorov, *Teor. Eksp. Khim. (USSR)* **15**, 273 (1979)) and C–H (R. C. Lord, B. Nolin, and H. D. Stidham, *J. Am. Chem. Soc.* **77**, 1365 (1955); V. E. Borisenko and D. N. Shchepkin, *Opt. Spektrosk. (USSR)* **29**, 46 (1970); H. Kleeberg, C. Eisenberg, and T. Zinn, *J. Mol. Struct.* **240**, 175 (1990)) stretches.

Table 2. Experimental shifts of the $\nu(\text{C-H/D})$ (in cm^{-1}) in the $\text{Cl}_3\text{C-H}\cdots\text{B}$, $\text{Cl}_3\text{C-D}\cdots\text{B}$, and $\text{Br}_3\text{C-D}\cdots\text{B}$ H-bonded complexes [86]. Note that the $\nu(\text{C-H})$ of haloforms appears to be in Fermi resonance with the overtone of the C-H bending vibrational modes. The corresponding corrections for Fermi resonance have been recently made in Ref. [78a] for fluoroform dissolved in liquefied Ar, N_2 , CO, and CO_2 and as shown therein, their effect is rather insignificant

Proton acceptor molecule B	Proton acceptor	$\nu(\text{C-H})$ CHCl_3	$\nu(\text{C-D})$ CDCl_3	$\nu(\text{C-D})$ CDBr_3
Nitromethane	NO_2	+8	+5	+6
Nitrobenzene	NO_2		+5	
Ethyl methylsulfonate	SO_2		+7	+6
3,4-Dimethylthiofiansulphone	SO_2	+8	+3	
<i>p</i> - $\text{CH}_3\text{C}_6\text{H}_4\text{SO}_2\text{NHC}_6\text{H}_{11}$	SO_2		+5	
<i>p</i> - $\text{CH}_3\text{C}_6\text{H}_4\text{SO}_2(\text{O}(\text{CH}_2)_2)_4\text{OH}$	SO_2		+5	+6
	COC		-7	-5
1,2-Dimethoxy-4-bromobenzene	COC		+5	
Ethyl acetate	COO		+3	
Acetic anhydride	COO		+7	

The horns of a dilemma are usually on the same bull.
Spanish proverb

4 BLUE-SHIFTING HYDROGEN BONDS IS A “TRUE” HYDROGEN BOND?

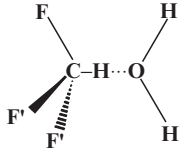
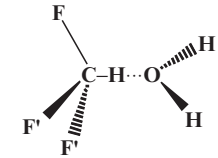
The nature of the $\text{C-H}\cdots\text{B}$ hydrogen bond still remains a rather controversial topic [23, 25, 26, 1–3, 67–78, 87, 91, 100, 103, 119, 122], mainly on the following issues:

- (α) What is the origin of a blue shift of “nonconventional” $\text{C-H}\cdots\text{B}$ bonds or, in the other words, of the biased nature of the proton-“donating” ability of the C-H group?
- (β) Whether the $\text{C-H}\cdots\text{B}$ bonding interaction is similar or different from the classical hydrogen bonding?
- (γ) How $\text{C-H}\cdots\text{B}$ bonds should be correctly classified?
- (δ) What is the upper bound for a blue shift if it does exist?

Evidently, the first issues overlap with each other, and therefore, if (α) would be completely resolved, the latter two are immediately answered. Since (α) is still the problem, we may speculate with the other two, partly shedding light on the former.

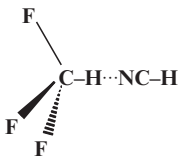
How a blue-shifting H-bond should be correctly classified: as a true or classical, conventional hydrogen bond, or as a van der Waals interaction, although the borderline between a weak hydrogen bonding and van der Waals interactions are not clear-cut (see in particular Ref. [36], p. 105 ff and Ref. [123]) and “the definition of a hydrogen bond is still controversial” (Ref. [123a], p. 149; see also Ref. [124])? Or, alternatively, as a nonconventional, “improper, blue-shifting” hydrogen bond that emphasizes a new type of bonding having “the different origin” from the classical one [1, 67, 87]?

Table 3. List of the neutral C–H···B “nonconventional” hydrogen bonds. The abbreviation “HB” means “hydrogen-bonded.” The MP2 indicates the frozen-core approximation, in contrast to the MP2 (full). A(C–H) indicates the IR activity (in $\text{km} \cdot \text{mol}^{-1}$) of the vibrational mode $\nu(\text{C–H})$

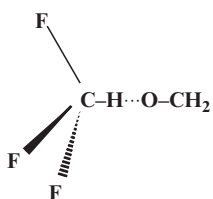
Molecular system/experimental data	Computational data	
Intermolecular C–H···B hydrogen bonding		
I. F₃C–H···OH₂		
(quasi-linear complex; two geometries 1 and 2 are reported)		
		
1 (Refs. [74,100a])	MP2/6-311+G(<i>d,p</i>) [71,100a]: $\angle \text{C–H} \cdots \text{O} = 176.2^\circ$ $\Delta R(\text{C–H}) = -0.0023 \text{ \AA}$ $\Delta E = -4.6 \text{ kcal} \cdot \text{mol}^{-1}$ $\Delta R(\text{C–F}) = 0.0029 \text{ \AA}$ $\Delta R(\text{O–H}) = 0.0009 \text{ \AA}$	$r(\text{O} \cdots \text{H}) = 2.1970 \text{ \AA}$ $\Delta \nu(\text{C–H}) = 37.9 \text{ cm}^{-1}$ $\Delta E_{\text{BSSE}} = -3.3 \text{ kcal} \cdot \text{mol}^{-1}$ $\Delta R(\text{C–F}') = 0.0044 \text{ \AA}$
	MP2/6-31+G(<i>d</i>) [74]: $r(\text{O} \cdots \text{H}) = 2.143 \text{ \AA}$ $\Delta R(\text{C–F}) = 0.004 \text{ \AA}$	$\Delta R(\text{C–H}) = -0.0016 \text{ \AA}$ $\Delta E = -5.2 \text{ kcal} \cdot \text{mol}^{-1}$
2 (Refs.[3, 70, 67a,b, 72b])	MP2/SDD** [67a]: $\angle \text{C–H} \cdots \text{O} = 169.3^\circ$ $\Delta R(\text{C–H}) = -0.0020 \text{ \AA}$ $\Delta E = -3.73 \text{ kcal} \cdot \text{mol}^{-1}$ $\Delta R(\text{C–F}) = 0.0041 \text{ \AA}$	$r(\text{O} \cdots \text{H}) = 2.1532 \text{ \AA}$ $\Delta \nu(\text{C–H}) = 29 \text{ cm}^{-1}$ $\Delta R(\text{C–F}') = 0.0045 \text{ \AA}$
<i>Note:</i> Ref. [101] does not report any unusual frequency shift for this system. Upon imposing the restriction of the linearity of the C–H···O bond of the structure 2 , $\Delta R(\text{C–H}) = -0.002 \text{ \AA}$, $\Delta \nu(\text{C–H}) = 42 \text{ cm}^{-1}$, and $\Delta E_{\text{BSSE}} = -2.3 \text{ kcal} \cdot \text{mol}^{-1}$ (MP2/6-311+G(<i>d,p</i>), Ref. [3])	MP2/6-31G(<i>d,p</i>) [67e]: $\Delta R(\text{C–H}) = -0.0040 \text{ \AA}$	$\Delta \nu(\text{C–H}) = 55 \text{ cm}^{-1}$
$\Delta \nu_{\text{exp}}(\text{C–H}) = 12 \text{ cm}^{-1}$ (fluoroform–water mixture in an argon matrix [81], uncertainty in the assignment [91])	MP2/6-31+G(<i>d,p</i>) [70a]: $\Delta R(\text{C–H}) = -0.0016 \text{ \AA}$ $\Delta E_{\text{BSSE}} = -3.72 \text{ kcal} \cdot \text{mol}^{-1}$ $\Delta R(\text{H} \cdots \text{O}) = 2.164 \text{ \AA}$	$\Delta \nu(\text{C–H}) = 27\text{--}33 \text{ cm}^{-1}$ (isotope effect, see Table 2 of Ref. [71a])
$\Delta \nu_{\text{exp}}^{\text{sym}}(\text{O–H}) = -23 \text{ cm}^{-1}$ [102] $\Delta \nu_{\text{exp}}^{\text{asym}}(\text{O–H}) = -30 \text{ cm}^{-1}$ [102]	MP2/6-311G(<i>d,p</i>) [67b]: $\angle \text{C–H} \cdots \text{O} = 164.0^\circ$ $\Delta R(\text{C–H}) = -0.0023 \text{ \AA}$ $\Delta \nu(\text{C–H}) = 35 \text{ cm}^{-1}$ $\Delta R(\text{C–F}) = 0.0030 \text{ \AA}$	$r(\text{O} \cdots \text{H}) = 2.2024 \text{ \AA}$ $\Delta E = -3.01 \text{ kcal} \cdot \text{mol}^{-1}$ $\Delta R(\text{C–F}') = 0.0057 \text{ \AA}$
	HF/6-311++G(<i>d,p</i>) [72b]: $\Delta R(\text{C–H}) = -0.0023 \text{ \AA}$ $\Delta \nu(\text{C–H}) = 38 \text{ cm}^{-1}$ $\Delta E_{\text{BSSE}} = -3.44 \text{ kcal} \cdot \text{mol}^{-1}$	$\Delta E = -3.82 \text{ kcal} \cdot \text{mol}^{-1}$
	B3LYP/6-311++G(<i>d,p</i>) [72b]: $\Delta R(\text{C–H}) = -0.0009 \text{ \AA}$ $\Delta \nu(\text{C–H}) = 14 \text{ cm}^{-1}$ $\Delta E_{\text{BSSE}} = -3.73 \text{ kcal} \cdot \text{mol}^{-1}$	$\Delta E = -4.25 \text{ kcal} \cdot \text{mol}^{-1}$
	MP2/6-311++G(<i>d,p</i>) [73b]: $\Delta R(\text{C–H}) = -0.0022 \text{ \AA}$ $\Delta \nu(\text{C–H}) = 33 \text{ cm}^{-1}$ $\Delta E_{\text{BSSE}} = -3.37 \text{ kcal} \cdot \text{mol}^{-1}$	$\Delta E = -4.64 \text{ kcal} \cdot \text{mol}^{-1}$

(Continued)

Table 3. —(Continued)

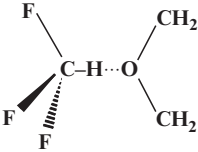
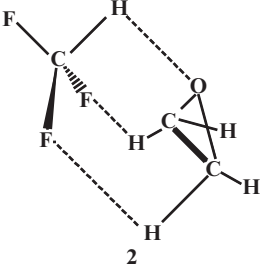
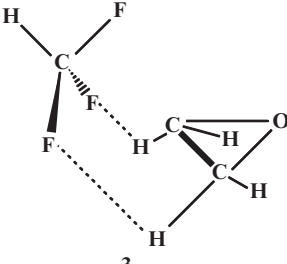
Molecular system/experimental data	Computational data	
II. Cl₃C–H···OH₂ <i>Note:</i> With only few exceptions, chloroform forms complexes with conventional H-bonds; more than 75 of them are collected in Ref. [43]. The complex Br ₃ C–H···OH ₂ also refers to that with conventional H-bond [46b]. A red shift of the ν (C–H) stretch is experimentally observed for the CCl ₃ H–water complex [81,91]. See also Ref. [100p] for the blue-shifting complex Br ₃ C–H···(OH ₂) ₂	MP2/6-311G(<i>d,p</i>) [67b]: \angle C–H···O = 136.6° ΔR (C–H) = –0.0011 Å $\Delta\nu$ (C–H) = 17 cm ^{–1} ΔR (C–Cl) = –0.0033 Å MP2/6-31G(<i>d,p</i>) [67e]: ΔR (C–H) = –0.0002 Å MP2/6-31+G(<i>d,p</i>) [70a]: ΔR (C–H) = –0.0006 Å ΔE_{BSSE} = –3.68 kcal · mol ^{–1} ΔR (H···O) = 2.077 Å	r (O···H) = 2.1900 Å ΔE = –2.99 kcal · mol ^{–1} ΔR (C–Cl') = 0.0050 Å $\Delta\nu$ (C–H) = 8 cm ^{–1} $\Delta\nu$ (C–H) = 16–23 cm ^{–1} (isotope effect, see Table 2 of Ref. [71a])
III. F₃C–H···N≡CH 	MP2/6-311+G(<i>d,p</i>) [100a]: r (N···H) = 2.4021 Å $\Delta\nu$ (C–H) = 36 cm ^{–1} ΔR (C–F) = 0.0031 Å	ΔR (C–H) = –0.0021 Å ΔE = –3.5 kcal · mol ^{–1} ΔR (N–C) = –0.0010 Å
F₃C–H···FH (quasi-linear complex)	MP2/6-311+G(<i>d,p</i>) [71]: \angle C–H···F = 172.9° ΔR (C–H) = –0.0026 Å ΔE = –2.6 kcal · mol ^{–1} MP2/6-31+G(<i>d</i>) [74]: r (F···H) = 2.266 Å ΔR (C–F) = 0.002 Å	r (F···H) = 2.2719 Å $\Delta\nu$ (C–H) = 45.8 cm ^{–1} ΔE_{BSSE} = –1.9 kcal · mol ^{–1} ΔR (C–H) = –0.0020 Å ΔE = –2.6 kcal · mol ^{–1}
IV. F₃C–H···FH (cyclic complex)	MP2/6-311++G(2 <i>d</i> ,2 <i>p</i>) [76a]: \angle C–H···F'' = 112.6° ΔR (C–H) = –0.0007 Å ΔE = –3.3 kcal · mol ^{–1} MP2/aug-cc-pVTZ [76a]: \angle C–H···F'' = 113.3° ΔR (C–H) = –0.0007 Å ΔE = –3.1 kcal · mol ^{–1} ΔR (C–F) = 0.0164 Å ΔR (H–F) = 0.0035 Å	r (F''···H) = 2.6046 Å $\Delta\nu$ (C–H) = 16 cm ^{–1} (9 km · mol ^{–1}) ΔE_{BSSE} = –2.2 kcal · mol ^{–1} ΔR (C–F') = –0.0050 Å r (F''···H) = 2.5757 Å $\Delta\nu$ (C–H) = 15 cm ^{–1} (8 km · mol ^{–1}) ΔE_{BSSE} = –2.5 kcal · mol ^{–1} ΔR (C–F') = –0.0046 Å

Molecular system/ experimental data	Computational data		
V–VII. F₃C–H···B (B = N₂, CO, CO₂) [79a] (see also Ref. [78f]) $\Delta\nu_{\text{exp}}(\text{C–H}; \text{N}_2) = 14.1 \text{ cm}^{-1}$ $\Delta\nu_{\text{exp}}(\text{C–H}; \text{CO}) = 19.1 \text{ cm}^{-1}$ $\Delta\nu_{\text{exp}}(\text{C–H}; \text{CO}_2) = 23.6 \text{ cm}^{-1}$	B	MP2/6-311++G(3df,3pd) [78a]:	
	N ₂	$\Delta R(\text{C–H}) = -0.0010 \text{ \AA}$ $\Delta E_{\text{BSSE}} = 1.54 \text{ kcal} \cdot \text{mol}^{-1}$	$\Delta\nu(\text{C–H}) = 30 \text{ cm}^{-1}$
	CO	$\Delta R(\text{C–H}) = -0.0010 \text{ \AA}$ $\Delta E_{\text{BSSE}} = 1.94 \text{ kcal} \cdot \text{mol}^{-1}$	$\Delta\nu(\text{C–H}) = 26 \text{ cm}^{-1}$
	CO ₂	$\Delta R(\text{C–H}) = -0.0013 \text{ \AA}$ $\Delta E_{\text{BSSE}} = 1.93 \text{ kcal} \cdot \text{mol}^{-1}$	$\Delta\nu(\text{C–H}) = 37 \text{ cm}^{-1}$
	B	B3LYP/6-311++G(3df,3pd) [78a]:	
	N ₂	$\Delta R(\text{C–H}) = -0.0008 \text{ \AA}$	$\Delta\nu(\text{C–H}) = 17 \text{ cm}^{-1}$
	CO	$\Delta R(\text{C–H}) = -0.0008 \text{ \AA}$	$\Delta\nu(\text{C–H}) = 16 \text{ cm}^{-1}$
	CO ₂	$\Delta R(\text{C–H}) = -0.0013 \text{ \AA}$	$\Delta\nu(\text{C–H}) = 27 \text{ cm}^{-1}$
	VIII. F₃C–H···SH₂	MP2/6-311+G(d,p) [71]:	
		$\angle \text{C–H} \cdots \text{S} = 177.9^\circ$ $\Delta R(\text{C–H}) = -0.0016 \text{ \AA}$ $\Delta E = -2.7 \text{ kcal} \cdot \text{mol}^{-1}$	$r(\text{S} \cdots \text{H}) = 2.8290 \text{ \AA}$ $\Delta\nu(\text{C–H}) = 22.5 \text{ cm}^{-1}$ $\Delta E_{\text{BSSE}} = -1.2 \text{ kcal} \cdot \text{mol}^{-1}$
MP2/6-31+G(d) [75]:			
$r(\text{S} \cdots \text{H}) = 2.788 \text{ \AA}$ $\Delta R(\text{C–F}) = 0.002 \text{ \AA}$ $\Delta E = -2.8 \text{ kcal} \cdot \text{mol}^{-1}$		$\Delta R(\text{C–H}) = -0.0013 \text{ \AA}$	
IX. F₃C–H···ClH	MP2/6-311+G(d,p) [71]:		
	$\angle \text{C–H} \cdots \text{Cl} = 119.0^\circ$ $\Delta R(\text{C–H}) = -0.0010 \text{ \AA}$ $\Delta E = -2.5 \text{ kcal} \cdot \text{mol}^{-1}$	$r(\text{Cl} \cdots \text{H}) = 3.0295 \text{ \AA}$ $\Delta\nu(\text{C–H}) = 15.1 \text{ cm}^{-1}$ $\Delta E_{\text{BSSE}} = -1.1 \text{ kcal} \cdot \text{mol}^{-1}$	
	MP2/6-31+G(d) [75]:		
	$r(\text{Cl} \cdots \text{H}) = 2.776 \text{ \AA}$ $\Delta R(\text{C–F}) = 0.0000 \text{ \AA}$	$\Delta R(\text{C–H}) = -0.0015 \text{ \AA}$ $\Delta E = -1.8 \text{ kcal} \cdot \text{mol}^{-1}$	
X. F₃C–H···O=CH₂ (formaldehyde)	HF/6-311++G(d,p) [72b]:		
	$\Delta R(\text{C–H}) = -0.0027 \text{ \AA}$ $\Delta E = -3.31 \text{ kcal} \cdot \text{mol}^{-1}$	$\Delta\nu(\text{C–H}) = 49 \text{ cm}^{-1}$ $\Delta E_{\text{BSSE}} = -3.12 \text{ kcal} \cdot \text{mol}^{-1}$	
	B3LYP/6-311++G(d,p) [72b]:		
	$\Delta R(\text{C–H}) = -0.0016 \text{ \AA}$ $\Delta E = -3.16 \text{ kcal} \cdot \text{mol}^{-1}$	$\Delta\nu(\text{C–H}) = 29 \text{ cm}^{-1}$ $\Delta E_{\text{BSSE}} = -2.98 \text{ kcal} \cdot \text{mol}^{-1}$	
	MP2/6-311++G(d,p) [72b]:		
	$\Delta R(\text{C–H}) = -0.0028 \text{ \AA}$	$\Delta\nu(\text{C–H}) = 46 \text{ cm}^{-1}$	
	$\Delta E = -3.55 \text{ kcal} \cdot \text{mol}^{-1}$	$\Delta E_{\text{BSSE}} = -2.82 \text{ kcal} \cdot \text{mol}^{-1}$	
<i>Note:</i> Upon imposing the restriction of the linearity of the C–H···O bond, $\Delta R(\text{C–H}) = -0.003 \text{ \AA}$, $\Delta\nu(\text{C–H}) = 20 \text{ cm}^{-1}$, and $\Delta E_{\text{BSSE}} = -2.6 \text{ kcal} \cdot \text{mol}^{-1}$ (MP2/6-311+G(d,p), Ref. [68a])			



(Continued)

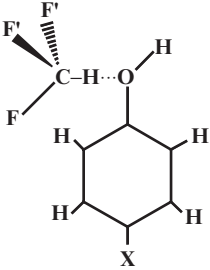
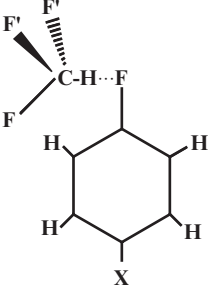
Table 3. —(Continued)

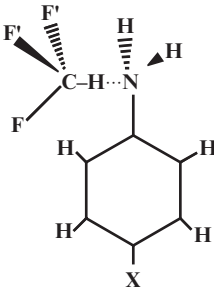
Molecular system/ experimental data	Computational data												
XI. F₃C–H···O(CH₂)₂ (oxirane)  1	MP2/6-31++G(2 <i>d,p</i>) [1a,e]: 1. ‘planar’ 1 : $\Delta R(\text{C–H})$ = -0.0012 \AA $\Delta\nu(\text{C–H}) = 29 \text{ cm}^{-1}$ $\Delta E_{\text{BSSE}} = -3.47 \text{ kcal} \cdot \text{mol}^{-1}$ $\Delta E = -3.45 \text{ kcal} \cdot \text{mol}^{-1}$ 2. nonplanar 2 : $\Delta R(\text{C–H})$ = -0.0029 \AA $\Delta\nu(\text{C–H}) = 43 \text{ cm}^{-1}$ $\Delta E_{\text{BSSE}} = -3.93 \text{ kcal} \cdot \text{mol}^{-1}$ $\Delta E = -3.84 \text{ kcal} \cdot \text{mol}^{-1}$												
<p>Note: The “planar” structure 1 has the C–H···O H-bond. The nonplanar structure 2 with two C–H···F–C bonds and single C–H···O bond reported in Ref. [1a] is not confirmed in Ref. [72b]. Instead, Ref. [72b] reports the existence of another, “reversed” and less stable minimum 3 at the HF/6-311++G(<i>d,p</i>) and MP2/6-311++G(<i>d,p</i>) which splits into two “reversed” minima at the B3LYP/6-311++G(<i>d,p</i>)</p>	HF/6-311++G(<i>d,p</i>) (1) [72b]: $\Delta R(\text{C–H}) = -0.0025 \text{ \AA}$ $\Delta E = -3.80 \text{ kcal} \cdot \text{mol}^{-1}$ $\Delta\nu(\text{C–H}) = 40 \text{ cm}^{-1}$ $\Delta E_{\text{BSSE}} = -3.47 \text{ kcal} \cdot \text{mol}^{-1}$												
	B3LYP/6-311++G(<i>d,p</i>) (1) [72b]: $\Delta R(\text{C–H}) = -0.0007 \text{ \AA}$ $\Delta E = -3.96 \text{ kcal} \cdot \text{mol}^{-1}$ $\Delta\nu(\text{C–H}) = 8 \text{ cm}^{-1}$ $\Delta E_{\text{BSSE}} = -3.54 \text{ kcal} \cdot \text{mol}^{-1}$												
	MP2/6-311++G(<i>d,p</i>) (1) [72b]: $\Delta R(\text{C–H}) = -0.0018 \text{ \AA}$ $\Delta E = -4.89 \text{ kcal} \cdot \text{mol}^{-1}$ $\Delta\nu(\text{C–H}) = 23 \text{ cm}^{-1}$ $\Delta E_{\text{BSSE}} = -3.40 \text{ kcal} \cdot \text{mol}^{-1}$												
	MP2/6-31+G(<i>d</i>) (global minimum 2) [74]: $r(\text{O} \cdots \text{H}) = 2.337 \text{ \AA}$ $\Delta R(\text{C–F}) = 0.002 \text{ \AA}$ $\Delta R(\text{C–H}) = -0.0032 \text{ \AA}$ $\Delta E = -5.7 \text{ kcal} \cdot \text{mol}^{-1}$												
 2	MP2/6-311++G(2 <i>df,2p</i>) (global minimum 2) [89] $\Delta R(\text{C–H}; \text{CF}_3\text{H}) = -0.0031 \text{ \AA}$ $\Delta R(\text{C–H}; \text{C}_2\text{H}_4\text{O}, \text{HB})$ = -0.0005 \AA $\Delta R(\text{C–H}; \text{C}_2\text{H}_4\text{O}, \text{free})$ = -0.0004 \AA $\Delta\nu(\text{C–H}; \text{CF}_3\text{H}) = 50 \text{ cm}^{-1}$ $\Delta\nu(\text{C–H}; \text{C}_2\text{H}_4\text{O}) = 7\text{--}10 \text{ cm}^{-1}$ $\Delta E_{\text{BSSE}} = -3.75 \text{ kcal} \cdot \text{mol}^{-1}$ $\Delta R(\text{O} \cdots \text{H}) = 2.367 \text{ \AA}$ $\Delta R(\text{F} \cdots \text{H}) = 2.683 \text{ \AA}$												
	Rotational constants (in MHz): <table border="1" style="margin-left: 20px;"> <thead> <tr> <th></th> <th>Theory</th> <th>Experiment [90]</th> </tr> </thead> <tbody> <tr> <td>A</td> <td>5362</td> <td>5264.8472(47)</td> </tr> <tr> <td>B</td> <td>1219</td> <td>1177.6737(20)</td> </tr> <tr> <td>C</td> <td>1129</td> <td>1096.6055(19)</td> </tr> </tbody> </table>		Theory	Experiment [90]	A	5362	5264.8472(47)	B	1219	1177.6737(20)	C	1129	1096.6055(19)
	Theory	Experiment [90]											
A	5362	5264.8472(47)											
B	1219	1177.6737(20)											
C	1129	1096.6055(19)											
 3	<p>Note: The experimental rotational constants of the fluoroform-oxirane complex measured in Ref. [89a] are consistent with the two C_s stationary structures. One of them is 2 whereas the other has a bifurcated C–H···F···C–H bond. 2 is the global minimum at the MP2/6-311++G(2<i>df,2p</i>) level [89a]. The latter is the transition structure, distinguished by the energy offset of only 0.22 kcal · mol^{−1} [89a]. The topological analysis of the electron density in 1 is investigated in Ref. [103]</p>												

Molecular system/ experimental data	Computational data	
XII. F₃C–H···O(CH₃)₂ (dimethyl ether) <div style="text-align: center;"> </div>	MP2/6-31+G(d) [74]: $r(\text{O}\cdots\text{H}) = 2.123 \text{ \AA}$ $\Delta R(\text{C-F}) = -0.005 \text{ \AA}$	$\Delta R(\text{C-H}) = -0.0009 \text{ \AA}$ $\Delta E = -5.5 \text{ kcal}\cdot\text{mol}^{-1}$
	MP2/6-31G(d) [87a]: $\Delta R(\text{C-H}) = -0.0015 \text{ \AA}$ $\Delta E = -3.24 \text{ kcal}\cdot\text{mol}^{-1}$ $\Delta R(\text{C-F}) = 0.0048 \text{ \AA}$ $R(\text{H}\cdots\text{O}) = 2.247 \text{ \AA}$	$\Delta\nu(\text{C-H}) = 31 \text{ cm}^{-1}$ $\Delta R(\text{C-F}') = 0.0034 \text{ \AA}$
$\Delta\nu_{\text{exp}}(\text{C-H}) = 17.7 \text{ cm}^{-1}$ [87a]		
<i>Note:</i> $\Delta\nu_{\text{exp}}(\text{C-H}) = 10.6 \text{ cm}^{-1}$ for $\text{ClF}_2\text{C-H}\cdots\text{O}(\text{CH}_3)_2$, $\Delta\nu_{\text{exp}}(\text{C-H}) = 4.8 \text{ cm}^{-1}$ for $\text{Cl}_2\text{FC-H}\cdots\text{O}(\text{CH}_3)_2$, and $\Delta\nu_{\text{exp}}(\text{C-H}) = -8.3 \text{ cm}^{-1}$ for $\text{Cl}_3\text{C-H}\cdots\text{O}(\text{CH}_3)_2$ [87b].		
XIII. F₃C–H···OH–CH=CH₂	HF/6-311++G(3d,3p) [100b]: $\Delta R(\text{C-H}) = -0.0019 \text{ \AA}$ $\Delta E_{\text{BSSE}} = -1.58 \text{ kcal}\cdot\text{mol}^{-1}$	$\Delta\nu(\text{C-H}) = 33.7 \text{ cm}^{-1}$
	MP2/6-311++G(d,p) [100b]: $\Delta R(\text{C-H}) = -0.0023 \text{ \AA}$ $\Delta E_{\text{BSSE}} = -1.70 \text{ kcal}\cdot\text{mol}^{-1}$	$\Delta\nu(\text{C-H}) = 37.4 \text{ cm}^{-1}$
	MP2(full)/6-311+G(d) [100b]: $\Delta R(\text{C-H}) = -0.0025 \text{ \AA}$ $\Delta E_{\text{BSSE}} = -1.77 \text{ kcal}\cdot\text{mol}^{-1}$	$\Delta\nu(\text{C-H}) = 43.0 \text{ cm}^{-1}$
XIV. F₃C–H···N≡CCH₃ (H-bonded minimum) <div style="text-align: center;"> </div>	HF/6-311++G(d,p) [72b]: $\Delta R(\text{C-H}) = -0.0025 \text{ \AA}$ $\Delta E = -3.84 \text{ kcal}\cdot\text{mol}^{-1}$	$\Delta\nu(\text{C-H}) = 41 \text{ cm}^{-1}$ $\Delta E_{\text{BSSE}} = -3.59 \text{ kcal}\cdot\text{mol}^{-1}$
	B3LYP/6-311++G(d,p) [72b]: $\Delta R(\text{C-H}) = -0.0013 \text{ \AA}$ $\Delta E = -4.03 \text{ kcal}\cdot\text{mol}^{-1}$	$\Delta\nu(\text{C-H}) = 18 \text{ cm}^{-1}$ $\Delta E_{\text{BSSE}} = -3.83 \text{ kcal}\cdot\text{mol}^{-1}$
	MP2/6-311++G(d,p) [72b]: $\Delta R(\text{C-H}) = -0.0021 \text{ \AA}$ $\Delta E = -4.50 \text{ kcal}\cdot\text{mol}^{-1}$	$\Delta\nu(\text{C-H}) = 31 \text{ cm}^{-1}$ $\Delta E_{\text{BSSE}} = -3.75 \text{ kcal}\cdot\text{mol}^{-1}$
<i>Note:</i> Ref. [72b] also reports the existence of the “reversed” and less stable minimum which exhibits $\Delta\nu(\text{C-H}) = 6\text{--}7 \text{ cm}^{-1}$		
XV. F₃C–H···OHCH₃	Upon imposing the restriction of the linearity of the C–H···O bond, $\Delta R(\text{C-H}) = -0.002 \text{ \AA}$, $\Delta\nu(\text{C-H}) = 47 \text{ cm}^{-1}$, and $\Delta E_{\text{BSSE}} = -1.8 \text{ kcal}\cdot\text{mol}^{-1}$ (MP2/6-311+G(d,p), Ref. [3])	
XVI. F₃C–H···O₂NCH₃	MP2/6-31G(d,p) [68e]: $\Delta R(\text{C-H}) = -0.0037 \text{ \AA}$	$\Delta\nu(\text{C-H}) = 58 \text{ cm}^{-1}$

(Continued)

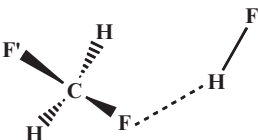
Table 3. —(Continued)

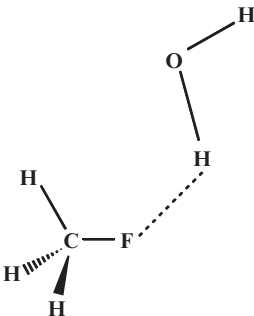
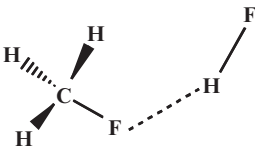
Molecular system/experimental data	Computational data			
XVII–XXIV. F₃C–H··· OH–C₆H₄–4-X [100b]	X	HF/6-311++G(<i>d,p</i>)	MP2/6-31G(<i>d</i>)	
	NH ₂	$\Delta R(\text{C–H}) = -0.0022 \text{ \AA}$ $\Delta \nu(\text{C–H}) = 37.3 \text{ cm}^{-1}$ $\Delta E = -8.9 \text{ kcal} \cdot \text{mol}^{-1}$	$\Delta R(\text{C–H}) = -0.0024 \text{ \AA}$ $\Delta \nu(\text{C–H}) = 43.2 \text{ cm}^{-1}$ $\Delta E = -11.2 \text{ kcal} \cdot \text{mol}^{-1}$	
	CH ₃	$\Delta R(\text{C–H}) = -0.0022 \text{ \AA}$ $\Delta \nu(\text{C–H}) = 36.3 \text{ cm}^{-1}$ $\Delta E = -7.9 \text{ kcal} \cdot \text{mol}^{-1}$	$\Delta R(\text{C–H}) = -0.0024 \text{ \AA}$ $\Delta \nu(\text{C–H}) = 42.9 \text{ cm}^{-1}$ $\Delta E = -10.0 \text{ kcal} \cdot \text{mol}^{-1}$	
	OH	$\Delta R(\text{C–H}) = -0.0023 \text{ \AA}$ $\Delta \nu(\text{C–H}) = 37.3 \text{ cm}^{-1}$ $\Delta E = -7.9 \text{ kcal} \cdot \text{mol}^{-1}$	$\Delta R(\text{C–H}) = -0.0024 \text{ \AA}$ $\Delta \nu(\text{C–H}) = 42.9 \text{ cm}^{-1}$ $\Delta E = -10.6 \text{ kcal} \cdot \text{mol}^{-1}$	
	H	$\Delta R(\text{C–H}) = -0.0021 \text{ \AA}$ $\Delta \nu(\text{C–H}) = 35.6 \text{ cm}^{-1}$ $\Delta E = -7.5 \text{ kcal} \cdot \text{mol}^{-1}$	$\Delta R(\text{C–H}) = -0.0024 \text{ \AA}$ $\Delta \nu(\text{C–H}) = 42.7 \text{ cm}^{-1}$ $\Delta E = -9.7 \text{ kcal} \cdot \text{mol}^{-1}$	
	F	$\Delta R(\text{C–H}) = -0.0021 \text{ \AA}$ $\Delta \nu(\text{C–H}) = 35.7 \text{ cm}^{-1}$ $\Delta E = -6.6 \text{ kcal} \cdot \text{mol}^{-1}$	$\Delta R(\text{C–H}) = -0.0024 \text{ \AA}$ $\Delta \nu(\text{C–H}) = 42.3 \text{ cm}^{-1}$ $\Delta E = -9.1 \text{ kcal} \cdot \text{mol}^{-1}$	
	Cl	$\Delta R(\text{C–H}) = -0.0021 \text{ \AA}$ $\Delta \nu(\text{C–H}) = 34.8 \text{ cm}^{-1}$ $\Delta E = -5.7 \text{ kcal} \cdot \text{mol}^{-1}$	$\Delta R(\text{C–H}) = -0.0024 \text{ \AA}$ $\Delta \nu(\text{C–H}) = 41.8 \text{ cm}^{-1}$ $\Delta E = -9.0 \text{ kcal} \cdot \text{mol}^{-1}$	
	CN	$\Delta R(\text{C–H}) = -0.0019 \text{ \AA}$ $\Delta \nu(\text{C–H}) = 31.4 \text{ cm}^{-1}$ $\Delta E = -4.1 \text{ kcal} \cdot \text{mol}^{-1}$	$\Delta R(\text{C–H}) = -0.0023 \text{ \AA}$ $\Delta \nu(\text{C–H}) = 40.1 \text{ cm}^{-1}$ $\Delta E = -7.2 \text{ kcal} \cdot \text{mol}^{-1}$	
	NO ₂	$\Delta R(\text{C–H}) = -0.0018 \text{ \AA}$ $\Delta \nu(\text{C–H}) = 30.1 \text{ cm}^{-1}$ $\Delta E = -3.9 \text{ kcal} \cdot \text{mol}^{-1}$	diverge	
	XXV–XXXII. F₃C–H··· F–C₆H₄–4-X [100b]	X	HF/6-311++G(<i>d,p</i>)	MP2/6-31G(<i>d</i>)
		NH ₂	$\Delta R(\text{C–H}) = -0.0023 \text{ \AA}$ $\Delta \nu(\text{C–H}) = 37.6 \text{ cm}^{-1}$ $\Delta E = -6.7 \text{ kcal} \cdot \text{mol}^{-1}$	$\Delta R(\text{C–H}) = -0.0030 \text{ \AA}$ $\Delta \nu(\text{C–H}) = 52.5 \text{ cm}^{-1}$ $\Delta E = -5.6 \text{ kcal} \cdot \text{mol}^{-1}$
		CH ₃	$\Delta R(\text{C–H}) = -0.0022 \text{ \AA}$ $\Delta \nu(\text{C–H}) = 35.5 \text{ cm}^{-1}$ $\Delta E = -6.1 \text{ kcal} \cdot \text{mol}^{-1}$	$\Delta R(\text{C–H}) = -0.0029 \text{ \AA}$ $\Delta \nu(\text{C–H}) = 51.4 \text{ cm}^{-1}$ $\Delta E = -4.3 \text{ kcal} \cdot \text{mol}^{-1}$
		OH	$\Delta R(\text{C–H}) = -0.0022 \text{ \AA}$ $\Delta \nu(\text{C–H}) = 35.2 \text{ cm}^{-1}$ $\Delta E = -5.8 \text{ kcal} \cdot \text{mol}^{-1}$	$\Delta R(\text{C–H}) = -0.0029 \text{ \AA}$ $\Delta \nu(\text{C–H}) = 51.2 \text{ cm}^{-1}$ $\Delta E = -4.8 \text{ kcal} \cdot \text{mol}^{-1}$
H		$\Delta R(\text{C–H}) = -0.0021 \text{ \AA}$ $\Delta \nu(\text{C–H}) = 34.2 \text{ cm}^{-1}$ $\Delta E = -5.7 \text{ kcal} \cdot \text{mol}^{-1}$	$\Delta R(\text{C–H}) = -0.0029 \text{ \AA}$ $\Delta \nu(\text{C–H}) = 50.9 \text{ cm}^{-1}$ $\Delta E = -4.7 \text{ kcal} \cdot \text{mol}^{-1}$	
F		$\Delta R(\text{C–H}) = -0.0020 \text{ \AA}$ $\Delta \nu(\text{C–H}) = 31.8 \text{ cm}^{-1}$ $\Delta E = -5.7 \text{ kcal} \cdot \text{mol}^{-1}$	$\Delta R(\text{C–H}) = -0.0028 \text{ \AA}$ $\Delta \nu(\text{C–H}) = 49.2 \text{ cm}^{-1}$ $\Delta E = -4.3 \text{ kcal} \cdot \text{mol}^{-1}$	
Cl		$\Delta R(\text{C–H}) = -0.0019 \text{ \AA}$ $\Delta \nu(\text{C–H}) = 31.1 \text{ cm}^{-1}$ $\Delta E = -4.7 \text{ kcal} \cdot \text{mol}^{-1}$	$\Delta R(\text{C–H}) = -0.0028 \text{ \AA}$ $\Delta \nu(\text{C–H}) = 48.2 \text{ cm}^{-1}$ $\Delta E = -3.9 \text{ kcal} \cdot \text{mol}^{-1}$	
CN		$\Delta R(\text{C–H}) = -0.0015 \text{ \AA}$ $\Delta \nu(\text{C–H}) = 24.5 \text{ cm}^{-1}$ $\Delta E = -3.5 \text{ kcal} \cdot \text{mol}^{-1}$	$\Delta R(\text{C–H}) = -0.0026 \text{ \AA}$ $\Delta \nu(\text{C–H}) = 44.8 \text{ cm}^{-1}$ $\Delta E = -2.7 \text{ kcal} \cdot \text{mol}^{-1}$	
NO ₂		$\Delta R(\text{C–H}) = -0.0014 \text{ \AA}$ $\Delta \nu(\text{C–H}) = 22.5 \text{ cm}^{-1}$ $\Delta E = -3.7 \text{ kcal} \cdot \text{mol}^{-1}$	diverge	

Molecular system/experimental data	Computational data		
XXXIII–XL. F₃C–H···NH₂–C₆H₄–4-X [100b] 	X	HF/6-311++G(<i>d,p</i>)	MP2/6-31G(<i>d</i>)
	NH ₂	$\Delta R(\text{C–H}) = -0.0026 \text{ \AA}$ $\Delta\nu(\text{C–H}) = 39.2 \text{ cm}^{-1}$ $\Delta E = -10.0 \text{ kcal} \cdot \text{mol}^{-1}$	$\Delta R(\text{C–H}) = -0.0026 \text{ \AA}$ $\Delta\nu(\text{C–H}) = 40.7 \text{ cm}^{-1}$ $\Delta E = -10.3 \text{ kcal} \cdot \text{mol}^{-1}$
	CH ₃	$\Delta R(\text{C–H}) = -0.0026 \text{ \AA}$ $\Delta\nu(\text{C–H}) = 38.7 \text{ cm}^{-1}$ $\Delta E = -9.1 \text{ kcal} \cdot \text{mol}^{-1}$	$\Delta R(\text{C–H}) = -0.0025 \text{ \AA}$ $\Delta\nu(\text{C–H}) = 39.7 \text{ cm}^{-1}$ $\Delta E = -9.6 \text{ kcal} \cdot \text{mol}^{-1}$
	OH	$\Delta R(\text{C–H}) = -0.0025 \text{ \AA}$ $\Delta\nu(\text{C–H}) = 37.2 \text{ cm}^{-1}$ $\Delta E = -9.2 \text{ kcal} \cdot \text{mol}^{-1}$	$\Delta R(\text{C–H}) = -0.0025 \text{ \AA}$ $\Delta\nu(\text{C–H}) = 38.9 \text{ cm}^{-1}$ $\Delta E = -9.6 \text{ kcal} \cdot \text{mol}^{-1}$
	H	$\Delta R(\text{C–H}) = -0.0026 \text{ \AA}$ $\Delta\nu(\text{C–H}) = 38.8 \text{ cm}^{-1}$ $\Delta E = -8.4 \text{ kcal} \cdot \text{mol}^{-1}$	$\Delta R(\text{C–H}) = -0.0025 \text{ \AA}$ $\Delta\nu(\text{C–H}) = 39.0 \text{ cm}^{-1}$ $\Delta E = -8.9 \text{ kcal} \cdot \text{mol}^{-1}$
	F	$\Delta R(\text{C–H}) = -0.0024 \text{ \AA}$ $\Delta\nu(\text{C–H}) = 36.3 \text{ cm}^{-1}$ $\Delta E = -7.7 \text{ kcal} \cdot \text{mol}^{-1}$	$\Delta R(\text{C–H}) = -0.0023 \text{ \AA}$ $\Delta\nu(\text{C–H}) = 36.9 \text{ cm}^{-1}$ $\Delta E = -7.9 \text{ kcal} \cdot \text{mol}^{-1}$
	Cl	$\Delta R(\text{C–H}) = -0.0025 \text{ \AA}$ $\Delta\nu(\text{C–H}) = 36.4 \text{ cm}^{-1}$ $\Delta E = -6.9 \text{ kcal} \cdot \text{mol}^{-1}$	$\Delta R(\text{C–H}) = -0.0023 \text{ \AA}$ $\Delta\nu(\text{C–H}) = 36.0 \text{ cm}^{-1}$ $\Delta E = -7.5 \text{ kcal} \cdot \text{mol}^{-1}$
	CN	$\Delta R(\text{C–H}) = -0.0021 \text{ \AA}$ $\Delta\nu(\text{C–H}) = 30.3 \text{ cm}^{-1}$ $\Delta E = -4.8 \text{ kcal} \cdot \text{mol}^{-1}$	$\Delta R(\text{C–H}) = -0.0021 \text{ \AA}$ $\Delta\nu(\text{C–H}) = 33.3 \text{ cm}^{-1}$ $\Delta E = -5.3 \text{ kcal} \cdot \text{mol}^{-1}$
	NO ₂	$\Delta R(\text{C–H}) = -0.0019 \text{ \AA}$ $\Delta\nu(\text{C–H}) = 27.0 \text{ cm}^{-1}$ $\Delta E = -4.3 \text{ kcal} \cdot \text{mol}^{-1}$	diverge
	XLI. F₃Si–H···OH₂	MP2/6-311+G(<i>d,p</i>) [71]: $\angle \text{Si–H} \cdots \text{O} = 78.3^\circ$ $\Delta R(\text{C–H}) = -0.0046 \text{ \AA}$ $\Delta E = -6.2 \text{ kcal} \cdot \text{mol}^{-1}$	$r(\text{O} \cdots \text{H}) = 2.6776 \text{ \AA}$ $\Delta\nu(\text{Si–H}) = 22.2 \text{ cm}^{-1}$ $\Delta E_{\text{BSSE}} = -3.6 \text{ kcal} \cdot \text{mol}^{-1}$
	XLII. F₃Si–H···SH₂	MP2/6-311+G(<i>d,p</i>) [71]: $\angle \text{Si–H} \cdots \text{S} = 83.7^\circ$ $\Delta R(\text{C–H}) = -0.0025 \text{ \AA}$ $\Delta E = -3.1 \text{ kcal} \cdot \text{mol}^{-1}$	$r(\text{S} \cdots \text{H}) = 3.5503 \text{ \AA}$ $\Delta\nu(\text{Si–H}) = 13.6 \text{ cm}^{-1}$ $\Delta E_{\text{BSSE}} = -1.2 \text{ kcal} \cdot \text{mol}^{-1}$
	XLIII. F₃Si–H···NH₃	MP2/6-311+G(<i>d,p</i>) [71]: $\angle \text{Si–H} \cdots \text{N} = 179.8^\circ$ $\Delta R(\text{Si–H}) = -0.0010 \text{ \AA}$ $\Delta E = -2.3 \text{ kcal} \cdot \text{mol}^{-1}$	$r(\text{N} \cdots \text{H}) = 2.6992 \text{ \AA}$ $\Delta\nu(\text{Si–H}) = 1.6 \text{ cm}^{-1}$ $\Delta E_{\text{BSSE}} = -1.4 \text{ kcal} \cdot \text{mol}^{-1}$
	XLIV. F₂HC–H···OH₂ (constraint: a linearity of C–H···O bond) Note: The global minimum is similar to that of CH ₃ F–H ₂ O. It is characterized by the MP2/6-31+G(<i>d,p</i>) interaction energy of $-3.40 \text{ kcal} \cdot \text{mol}^{-1}$ [70a]. Upon imposing the restriction of the linearity of the C–H···O bond, $\Delta R(\text{C–H}) = -0.003 \text{ \AA}$, $\Delta\nu(\text{C–H}) = 26 \text{ cm}^{-1}$, and $\Delta E_{\text{BSSE}} = -2.7 \text{ kcal} \cdot \text{mol}^{-1}$ (MP2/6-311+G(<i>d,p</i>), Ref. [3]). See Refs. [89b,c] for the experimental work	MP2/6-31+G(<i>d,p</i>) [70a]: $\Delta R(\text{C–H}) = -0.0024 \text{ \AA}$ $\Delta\nu(\text{C–H}) = 34–43 \text{ cm}^{-1}$ (isotope effect, see Table 2 of Ref. [70a]) $\Delta E_{\text{BSSE}} = -2.62 \text{ kcal} \cdot \text{mol}^{-1}$ $\Delta R(\text{H} \cdots \text{O}) = 2.254 \text{ \AA}$	

(Continued)

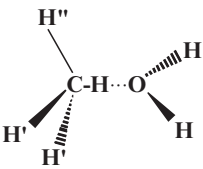
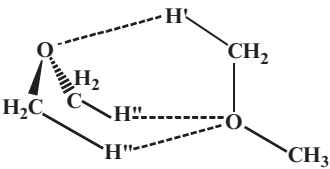
Table 3. —(Continued)

Molecular system/ experimental data	Computational data
XLV. CH₂F₂ ··· HF 	MP2/aug-cc-pVTZ [76b]: $\Delta R(\text{C-H}) = -0.0007, -0.0014 \text{ \AA}$ $\Delta\nu(\text{C-H}) = 13,20 \text{ cm}^{-1}$ $\Delta A(\text{C-H}) = -13, -12 \text{ km} \cdot \text{mol}^{-1}$ $\Delta E = -4.3 \text{ kcal} \cdot \text{mol}^{-1}$ $\Delta E_{\text{BSSE}} = -3.7 \text{ kcal} \cdot \text{mol}^{-1}$ $\Delta R(\text{C-F}) = 0.019 \text{ \AA}$ $\Delta R(\text{C-F}') = -0.0085 \text{ \AA}$ $\Delta R(\text{H-F}) = 0.0063 \text{ \AA}$
XLVI. F₂HC-H ··· O=CH₂	Upon imposing the restriction of the linearity of the C-H ··· O bond, $\Delta R(\text{C-H}) = -0.003 \text{ \AA}$, $\Delta\nu(\text{C-H}) = 24 \text{ cm}^{-1}$, and $\Delta E_{\text{BSSE}} = -2.5 \text{ kcal} \cdot \text{mol}^{-1}$ (MP2/6-311+G(<i>d,p</i>), Ref. [3])
XLVII. F₂HC-H ··· OHCH₃	Upon imposing the restriction of the linearity of the C-H ··· O bond, $\Delta R(\text{C-H}) = -0.002 \text{ \AA}$, $\Delta\nu(\text{C-H}) = 20 \text{ cm}^{-1}$, and $\Delta E_{\text{BSSE}} = -2.4 \text{ kcal} \cdot \text{mol}^{-1}$ (MP2/6-311+G(<i>d,p</i>), Ref. [3])
XLVIII. F₂N-H ··· FH <i>Note:</i> It is mentioned in Ref. [67c] that the full optimization of the complex NF ₂ H-FH leads to the cyclic complex with two H-bonds, N-H ··· F and F-H ··· F. The former is blue-shifted by 17 cm ⁻¹ . The results of Refs. [67c,71] are partially criticized in Ref. [100c] which reports that this complex is cyclic and has the H-bond N-H ··· F which shows a red shift $\Delta\nu(\text{N-H}) = -12 \text{ cm}^{-1}$ at the B3LYP/6-311++G(3df,3pd) computational level and a blue shift $\Delta\nu(\text{N-H}) = 16 \text{ cm}^{-1}$ at MP2(full)/6-311+G(<i>d,p</i>). More recent results [76e] confirm that the cyclic structure is a minimum. At MP2/aug-cc-pVTZ a red shift $\Delta\nu(\text{N-H}) = -8 \text{ cm}^{-1}$ is reported. The global minimum has, however, a conventional F-H ··· N hydrogen bond and no N-H ··· F hydrogen bond. In this global minimum a blue shift $\Delta\nu(\text{N-H}) = 12 \text{ cm}^{-1}$ is obtained (see Table 6 for more details)	MP2/6-311+G(<i>d,p</i>) [71]: $\angle \text{N-H} \cdot \cdot \cdot \text{F} = 136.1^\circ$ $r(\text{F} \cdot \cdot \cdot \text{H}) = 2.1649 \text{ \AA}$ $\Delta R(\text{N-H}) = -0.0003 \text{ \AA}$ $\Delta\nu(\text{N-H}) = 13.4 \text{ cm}^{-1}$ $\Delta E = -4.3 \text{ kcal} \cdot \text{mol}^{-1}$ $\Delta E_{\text{BSSE}} = -3.2 \text{ kcal} \cdot \text{mol}^{-1}$ MP2/6-31G(<i>d,p</i>) [67c] (linear constraint on the N-H ··· F H-bond geometry is imposed): $\Delta R(\text{N-H}) = -0.0011 \text{ \AA}$ $\Delta\nu(\text{N-H}) = 45 \text{ cm}^{-1}$ $\Delta E_{\text{BSSE}} = -3.3 \text{ kcal} \cdot \text{mol}^{-1}$ B3LYP/6-311++G(3df,3pd) [100c]: $\Delta R(\text{N-H}) = 0.002 \text{ \AA}$ $\Delta\nu(\text{N-H}) = -12 \text{ cm}^{-1}$ MP2(full)/6-311+G(<i>d,p</i>) [100c]: $\Delta R(\text{N-H}) = 0.001 \text{ \AA}$ $\Delta\nu(\text{N-H}) = 16 \text{ cm}^{-1}$ MP2/aug-cc-pVTZ [76e] (cyclic structure of [100c]): $\Delta R(\text{N-H}) = 0.002 \text{ \AA}$ $\Delta\nu(\text{N-H}) = -8 \text{ cm}^{-1}$ $\Delta E_{\text{BSSE}} = -3.9 \text{ kcal} \cdot \text{mol}^{-1}$ MP2/aug-cc-pVTZ [76e] (global minimum with N-H ··· F hydrogen bond): $\Delta R(\text{N-H}) = -0.0003 \text{ \AA}$ $\Delta\nu(\text{N-H}) = 12 \text{ cm}^{-1}$ $\Delta E_{\text{BSSE}} = -5.0 \text{ kcal} \cdot \text{mol}^{-1}$

Molecular system/ experimental data	Computational data
XLIX. $F_2P-H \cdots OH_2$	MP2/6-311+G(<i>d,p</i>) [71]: $\angle P-H \cdots O = 105.1^\circ$ $\Delta R(P-H) = -0.0041 \text{ \AA}$ $\Delta E = -3.6 \text{ kcal} \cdot \text{mol}^{-1}$ $r(O \cdots H) = 2.8081 \text{ \AA}$ $\Delta \nu(P-H) = 33.1 \text{ cm}^{-1}$ $\Delta E_{BSSE} = -1.9 \text{ kcal} \cdot \text{mol}^{-1}$
L. $F_2P-H \cdots SH_2$	MP2/6-311+G(<i>d,p</i>) [71]: $\angle P-H \cdots S = 106.5^\circ$ $\Delta R(P-H) = -0.0023 \text{ \AA}$ $\Delta E = -2.8 \text{ kcal} \cdot \text{mol}^{-1}$ $r(S \cdots H) = 3.3731 \text{ \AA}$ $\Delta \nu(P-H) = 18.5 \text{ cm}^{-1}$ $\Delta E_{BSSE} = -1.0 \text{ kcal} \cdot \text{mol}^{-1}$
LI. $F_2P-H \cdots NH_3$	MP2/6-311+G(<i>d,p</i>) [71]: $\angle P-H \cdots N = 108.9^\circ$ $\Delta R(C-H) = -0.0056 \text{ \AA}$ $\Delta E = -3.5 \text{ kcal} \cdot \text{mol}^{-1}$ $r(N \cdots H) = 2.7199 \text{ \AA}$ $\Delta \nu(C-H) = 42.7 \text{ cm}^{-1}$ $\Delta E_{BSSE} = -2.0 \text{ kcal} \cdot \text{mol}^{-1}$
LII. $FH_2C-H \cdots OH_2$ (linear C-H \cdots O bond)	MP2/6-31+G(<i>d,p</i>) [70a]: $\Delta R(C-H) = -0.0019 \text{ \AA}$ $\Delta E_{BSSE} = -1.57 \text{ kcal} \cdot \text{mol}^{-1}$ $\Delta R(H \cdots O) = 2.364 \text{ \AA}$ $\Delta \nu(C-H) = 25-32 \text{ cm}^{-1}$ (isotope effect, see Table 2 of Ref. [70a])
<i>Note:</i> The global minimum of the $CH_3F \cdots H_2O$ complex with $\Delta E = -3.60 \text{ kcal} \cdot \text{mol}^{-1}$ ($3.76 \text{ kcal} \cdot \text{mol}^{-1}$ at the MP2/6-31+G(<i>d,p</i>), Ref. [70a]) has a bent	<i>Note:</i> Upon the constraint of the linearity of the C-H \cdots O bond, $\Delta R(C-H) = -0.002 \text{ \AA}$, $\Delta \nu(C-H) = 22 \text{ cm}^{-1}$, and $\Delta E_{BSSE} = -1.7 \text{ kcal} \cdot \text{mol}^{-1}$ (MP2/6-311+G(<i>d,p</i>), Ref. [3])
	Ref. [105]: $\Delta \nu_{exp}^{asym}(O-H)$ (in cm^{-1}) $CH_3F \cdots HOH$ -11 $CH_3F \cdots DOH$ +5 $CH_3F \cdots HOD$ -64 $CH_3F \cdots DOD$ -12 $\Delta \nu_{exp}^{asym}(O-H)$ (in cm^{-1}) $CH_3F \cdots HOH$ -12 $CH_3F \cdots DOH$ -24 $CH_3F \cdots HOD$ +9 $CH_3F \cdots DOD$ -23 Expt B3LYP/6-311++G(3 <i>df</i> ,3 <i>pd</i>) -15 +12 -64 -15 -37 -46 +9 -23
C-F \cdots H-O hydrogen bond (MP4/(10 <i>s</i> 6 <i>p</i> 4 <i>d</i> /6 <i>s</i> 4 <i>p</i>)/ [5 <i>s</i> 3 <i>p</i> 2 <i>d</i> /3 <i>s</i> 2 <i>p</i>], Ref. [104])	
LIII. $CH_3F \cdots HF$	MP2/aug-cc-pVTZ [76b]: $\Delta R(C-H) = -0.0013, -0.0020 \text{ \AA}$ $\Delta \nu(C-H) = 16, 26, 29 \text{ cm}^{-1}$ $\Delta A(C-H) = -9, -14, -11 \text{ km} \cdot \text{mol}^{-1}$ $\Delta E = -6.1 \text{ kcal} \cdot \text{mol}^{-1}$ $\Delta R(C-F) = 0.0168 \text{ \AA}$ $\Delta E_{BSSE} = -5.5 \text{ kcal} \cdot \text{mol}^{-1}$ $\Delta R(H-F) = 0.0098 \text{ \AA}$
	

(Continued)

Table 3. —(Continued)

Molecular system/ experimental data	Computational data
LIV. FH₂C–H···O=CH₂	Upon imposing the restriction of the linearity of the C–H···O bond, $\Delta R(\text{C–H}) = -0.002 \text{ \AA}$, $\Delta\nu(\text{C–H}) = 19 \text{ cm}^{-1}$, and $\Delta E_{\text{BSSE}} = -1.5 \text{ kcal} \cdot \text{mol}^{-1}$ (MP2/6-311+G(<i>d,p</i>), Ref. [3])
LIV. FH₂C–H···OHCH₃	Under the restriction of the linearity of the C–H···O bond, $\Delta R(\text{C–H}) = 0.001 \text{ \AA}$, $\Delta\nu(\text{C–H}) = 17 \text{ cm}^{-1}$, and $\Delta E_{\text{BSSE}} = -1.4 \text{ kcal} \cdot \text{mol}^{-1}$ (MP2/6-311+G(<i>d,p</i>), Ref. [3])
LVI. H₃C–H···OH₂	MP2/6-31+G(<i>d,p</i>) [70a]: $\Delta R(\text{C–H}) = -0.0004 \text{ \AA}$ $\Delta\nu(\text{C–H}) = 12 \text{ cm}^{-1}$ $\Delta E_{\text{BSSE}} = -0.29 \text{ kcal} \cdot \text{mol}^{-1}$ $\Delta R(\text{H} \cdots \text{O}) = 2.507 \text{ \AA}$
	
LVII. H₃CH₂C–H···OH₂ Note: See also Ref. [100q] for CH ₃ CHO–NH ₃	MP2/6-31G(<i>d,p</i>) [67e] $\Delta R(\text{C–H}) = -0.0010 \text{ \AA}$ $\Delta\nu(\text{C–H}) = 8 \text{ cm}^{-1}$
LVIII. H₃Si–H···NH₃	MP2/6-31G(<i>d,p</i>) [67e]: $\Delta R(\text{C–H}) = -0.0039 \text{ \AA}$ $\Delta\nu(\text{C–H}) = 18 \text{ cm}^{-1}$
LIX. OHC–H···OCH₂ Note: A series of dimers built from substituted formaldehydes CHO _X (X = H, CH ₃ , F, Cl, Br, I) are studied in Ref. [106]	MP2/6-31G(<i>d,p</i>) [67e]: $\Delta R(\text{C–H}) = -0.0046 \text{ \AA}$ $\Delta\nu(\text{C–H}) = 54 \text{ cm}^{-1}$
LX. Acetaldehyde–CO₂ $\Delta\nu_{\text{exp}}(\text{C–H}) = 1.3 \text{ cm}^{-1}$ [107]	MP2/6-31+G(<i>d</i>) [107]: $\Delta E = -2.69 \text{ kcal} \cdot \text{mol}^{-1}$
LXI. [O(CH₃)₂]₂ (dimethyl ether (DME) dimer)	MP2/6-311++G(<i>d,p</i>) [108]: $\Delta R(\text{C–H}') = -0.0001 \text{ \AA}$ $\Delta\nu(\text{C–H}') = 6 \text{ cm}^{-1}$ $\Delta R(\text{C–H}'') = -0.0021 \text{ \AA}$ $\Delta\nu(\text{C–H}'') = 17 \text{ cm}^{-1}$ $\Delta E_{\text{BSSE}} = -2.29 \text{ kcal} \cdot \text{mol}^{-1}$ MP2/6-31G(<i>d</i>) [100]: $\Delta R(\text{C–H}') = -0.002 \text{ \AA}$ $\Delta R(\text{C–H}'') = -0.003 \text{ \AA}$ $\Delta E_{\text{BSSE}} = -0.75 \text{ kcal} \cdot \text{mol}^{-1}$ $R(\text{O} \cdots \text{H}') = 2.436 \text{ \AA}$ $R(\text{O} \cdots \text{H}'') = 2.573 \text{ \AA}$ Note: The formation of larger DME clusters (DME) _{3≤n≤4} and hydrated DME clusters H ₂ O – (DME) _{2≤n≤4} causes the contraction of the C–H bonds involved in the intermolecular C–H···O bondings [110]. Interestingly, the formation of the complex HO–H···O(CH ₃) ₂ between water molecule and DME that solely arises due to the formation of the conventional O–H···O hydrogen bond contracts the C–H bonds of DME by 0.002 Å and blue-shifts their stretches $\Delta\nu(\text{C–H})$ by 12–30 cm ^{−1} (B3LYP/6-31G(<i>d</i>), Ref. [109]). The latter is consistent with the $\Delta\nu_{\text{exp}}(\text{C–H}) = 12\text{--}19 \text{ cm}^{-1}$ (Ref. [111])
	
The ground-state rotational spectrum of the triply H-bonded DME dimer with three C–H···O–C blue-shifting H-bonds has been studied by molecular beam Fourier transform microwave and free jet millimeter wave absorption spectroscopies in Refs. [108,109a]: $\Delta\nu_{\text{exp}}(\text{C–H}) = 13\text{--}21 \text{ cm}^{-1}$, $\Delta E_{\text{exp}} = -1.36 \text{ kcal} \cdot \text{mol}^{-1}$	

Molecular system/ experimental data	Computational data	
LXII. Dimethyl sulfoxide (DMSO) – (H₂O)_{1 ≤ n ≤ 3} $\Delta\nu_{\text{exp}}^{n=3}(\text{C-H}) = 17 \text{ cm}^{-1}$ [112]	<i>n</i>	MP2/6-31G(<i>d,p</i>) [67d] 1 A $\Delta\nu(\text{C-H}) = 1-6 \text{ cm}^{-1}$ $\Delta E_{\text{BSSE}} = -8.27 \text{ kcal} \cdot \text{mol}^{-1}$ 1 B $\Delta\nu(\text{C-H}) = 2-9 \text{ cm}^{-1}$ $\Delta E_{\text{BSSE}} = -2.83 \text{ kcal} \cdot \text{mol}^{-1}$ 1 C $\Delta\nu(\text{C-H}) = 0-8 \text{ cm}^{-1}$ $\Delta E_{\text{BSSE}} = -6.59 \text{ kcal} \cdot \text{mol}^{-1}$ 2 A $\Delta\nu(\text{C-H}) = 7-16 \text{ cm}^{-1}$ 2 B $\Delta\nu(\text{C-H}) = 1-12 \text{ cm}^{-1}$ 3 $\Delta\nu(\text{C-H}) = 8-19 \text{ cm}^{-1}$ (A, B, and C indicate different energy minimum structures, see Figs. 2-4 of Ref. [67d])
LXIII-LXVIII. Cyclic dimers of fluoromethanes [75]: CH ₃ F ··· CH ₃ F $\Delta\nu_{\text{exp}}(\text{C-H}) = 10 \text{ cm}^{-1}$ [105] CH ₃ F ··· CH ₂ F ₂ CH ₃ F ··· CHF ₃ (see Ref. [109b] for a microwave structure) CH ₂ F ₂ ··· CH ₂ F ₂ (see Refs. [109a,112,113] ⁶ for a microwave structure) CH ₂ F ₂ ··· CHF ₃ CHF ₃ ··· CHF ₃ (see also Ref. [114])		MP2/6-31+G(<i>d,p</i>) [75]: $\Delta\nu(\text{C-H}) = 20,20 \text{ cm}^{-1}$ $\Delta A(\text{C-H}) = -27, -11 \text{ km} \cdot \text{mol}^{-1}$ $\Delta E = -1.36 \text{ kcal} \cdot \text{mol}^{-1}$ $\Delta\nu(\text{C-H}) = 26,17 \text{ cm}^{-1}$ $\Delta A(\text{C-H}) = -7, -14 \text{ km} \cdot \text{mol}^{-1}$ $\Delta E = -1.95 \text{ kcal} \cdot \text{mol}^{-1}$ $\Delta\nu(\text{C-H}) = 39,16 \text{ cm}^{-1}$ $\Delta A(\text{C-H}) = -20, -12 \text{ km} \cdot \text{mol}^{-1}$ $\Delta E = -2.30 \text{ kcal} \cdot \text{mol}^{-1}$ $\Delta\nu(\text{C-H}) = 17,18 \text{ cm}^{-1}$ $\Delta A(\text{C-H}) = -28, -12 \text{ km} \cdot \text{mol}^{-1}$ $\Delta E = -1.74 \text{ kcal} \cdot \text{mol}^{-1}$ $\Delta\nu(\text{C-H}) = 19,20 \text{ cm}^{-1}$ $\Delta A(\text{C-H}) = -11, -12 \text{ km} \cdot \text{mol}^{-1}$ $\Delta E = -1.89 \text{ kcal} \cdot \text{mol}^{-1}$ $\Delta\nu(\text{C-H}) = 27,14 \text{ cm}^{-1}$ $\Delta A(\text{C-H}) = -13, -16 \text{ km} \cdot \text{mol}^{-1}$ $\Delta E = -1.67 \text{ kcal} \cdot \text{mol}^{-1}$ $\Delta\nu(\text{C-H}) = 17,17 \text{ cm}^{-1}$ $\Delta A(\text{C-H}) = -23, -3 \text{ km} \cdot \text{mol}^{-1}$ $\Delta E = -1.22 \text{ kcal} \cdot \text{mol}^{-1}$
LXIX. C₂-H₂(A) ··· O₂(T) bond of the Watson-Crick DNA AzT base pair (Refs. [115a,b, 16]; see also Ref. [117])		B3LYP/6-31+G(<i>d</i>) [90] (see also Ref. [117]): $\Delta R(\text{C}_2-\text{H}_2) = 0.0002 \text{ \AA}$ $\Delta\nu(\text{C}_2-\text{H}_2) = 6 \text{ cm}^{-1}$
LXX. Isomers of guanine dimer The isomer K9K7-1 [118] reveals a rather large blue shift of the NH ₂ stretch		HF/6-31G(<i>d,p</i>) [116]: $\Delta\nu_{\text{sym}}(\text{N-H}; \text{harmonic}) = 32 \text{ cm}^{-1}$ $\Delta\nu_{\text{asym}}(\text{N-H}; \text{harmonic}) = 55 \text{ cm}^{-1}$ $\Delta E(\text{K9K7-1}) = -21.92 \text{ kcal} \cdot \text{mol}^{-1}$ MP2/6-31G(<i>d,p</i>) [116]: $\Delta\nu_{\text{sym}}(\text{N-H}; \text{harmonic}) = 90 \text{ cm}^{-1}$ $\Delta\nu_{\text{asym}}(\text{N-H}; \text{harmonic}) = 115 \text{ cm}^{-1}$ $\Delta\nu_{\text{sym}}(\text{N-H}; \text{anharmonic}) = 101 \text{ cm}^{-1}$ $\Delta\nu_{\text{asym}}(\text{N-H}; \text{anharmonic}) = 145 \text{ cm}^{-1}$
Intramolecular C-H ··· B Hydrogen bonding		
LXXI. 1-methoxy-2-(methylthio)ethane $\Delta\nu(\text{C-H}) = 25 \text{ cm}^{-1}$ [66b]		

(Continued)

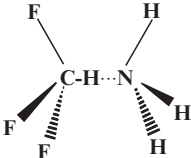
⁶ For the recent study of the potential energy surface of the CH₂F₂ dimer see A. Ebrahimi, H. Roohi, and S. M. Habibi, *J. Mol. Struct. (Theochem)* **684**, 87 (2004).

Table 3. —(Continued)

Molecular system/experimental data	Computational data
LXXII. TG(T G') conformer of 1-methoxy-2-(dimethylamino)ethane $\Delta\nu(\text{C-H}) = 35 \text{ cm}^{-1}$ [63]	
A series of complexes with intramolecular C-H...B (B = O, N, S) H-bonds [119]	
DFT calculations of molecules with intramolecular hydrogen bonds have been performed at the B3LYP/6-31G** computational level [100e]. The investigated 2,6-dinitro-3,5-diaminopyrazine-1-oxide (LLM-105) and its derivatives contain two types of intramolecular H-bonds (the classical, red-shifted, and blue-shift H-bonds) and thus two types of intramolecular H-bonded rings. The electron density transfer mechanisms on the basis of natural bond orbital (NBO) analysis have been suggested	
Blue-shifted intramolecular H-bonds in aromatic <i>N</i> -sulfinylamines with <i>ortho</i> -C-H bonds [120]	
Exceptional blue-shifted Rg-H...B complexes [121]	

On the one hand, there exists a rather impressive amount of computational and experimental evidences, mainly gathered in Tables 2 and 3, that definitely and reasonably corroborates that the “blue-shifting” C-H...B bond behaves distinctly different from the conventional hydrogen bond, primarily concerning the criteria 3 and 5 as the most important characteristics of the latter. It is claimed [1, 67, 87] that the different origin of the blue-shifting H-bond stems from a two-step mechanism that underlies its formation. The first step consists in a flow of the electron density from the proton acceptor to the remote (nonparticipating) part of the proton donor (e.g., to the highly electronegative fluorine atoms of CF₃H) rather than to the A-H σ^* -antibonding molecular orbital (this viewpoint is disputed in Refs. [100b, 100j]). The second step involves a structural reorganization of the proton donor submolecule resulting in contraction of the A-H bond and thus produces some shifts of the vibrations of the remote part of the proton donor. Hobza and Havlas [1a] (see also Refs. [93, 125, 69d, 78a]) suggest that for fluoroform involved in some C-H...O bonds such as F₃C-H...O(CH₂)₂ (**XI**, Table 3), the blue shift originates from a negative sign of the dipole moment derivative $\partial\mu_{\text{CHF}_3}/\partial r_{\text{CH}}$ determining the response of the fluoroform to an external electric field. The latter is, therefore,

Table 4. A complement list to Table 3 consisting of the conventional hydrogen bonds closely related to the nonconventional ones (for the additional H-bonded systems see Refs. [64,69])

Molecular system/experimental data	Computational data
F₃C–H···NH₃  $\Delta\nu_{\text{exp}}(\text{C-H}) = -12 \text{ cm}^{-1}$ [102]	MP2/6-311+G(<i>d,p</i>) [71,100a] (see also Ref. [78a] for the MP2/6-311++G(3 <i>df</i> ,3 <i>pd</i>): $\angle\text{C-H}\cdots\text{N} = 179.7^\circ$ $r(\text{N}\cdots\text{H}) = 2.2937 \text{ \AA}$ $\Delta R(\text{C-H}) = -0.0003 \text{ \AA}$ $\Delta\nu(\text{C-H}) = -1 \text{ to } -2 \text{ cm}^{-1}$ $\Delta E = -5.3 \text{ kcal}\cdot\text{mol}^{-1}$ $\Delta E_{\text{BSSE}} = -3.9 \text{ kcal}\cdot\text{mol}^{-1}$ $\Delta R(\text{C-F}) = 0.0051 \text{ \AA}$ $\Delta R(\text{N-H}) = 0.0024 \text{ \AA}$ MP2/6-31+G(<i>d</i>) [74]: $r(\text{N}\cdots\text{H}) = 2.234 \text{ \AA}$ $\Delta R(\text{C-H}) = 0.0012 \text{ \AA}$ $\Delta R(\text{C-F}) = 0.006 \text{ \AA}$ $\Delta E = -6.1 \text{ kcal}\cdot\text{mol}^{-1}$ MP2/aug-cc-pVDZ [100a]: $r(\text{N}\cdots\text{H}) = 2.2804 \text{ \AA}$ $\Delta R(\text{C-H}) = 0.0005 \text{ \AA}$ $\Delta\nu(\text{C-H}) = -13 \text{ cm}^{-1}$ $\Delta E = -5.3 \text{ kcal}\cdot\text{mol}^{-1}$ $\Delta R(\text{C-F}) = 0.0052 \text{ \AA}$ $\Delta R(\text{N-H}) = 0.0003 \text{ \AA}$
F₂N–H···OH₂	MP2/6-31G(<i>d,p</i>) [67c]: $\Delta R(\text{N-H}) = 0.0033 \text{ \AA}$ $\Delta\nu(\text{N-H}) = -37 \text{ cm}^{-1}$ $\Delta E_{\text{BSSE}} = -6.2 \text{ kcal}\cdot\text{mol}^{-1}$
F₂N–H···NH₃	MP2/6-31G(<i>d,p</i>) [67c]: $\Delta R(\text{N-H}) = 0.0100 \text{ \AA}$ $\Delta\nu(\text{N-H}) = -165 \text{ cm}^{-1}$ $\Delta E_{\text{BSSE}} = -8.7 \text{ kcal}\cdot\text{mol}^{-1}$

considerably different compared to conventional proton donors and this might likely explain the very nature of the blue-shifting phenomenon [1a, 69d]. On the contrary, the dipole moment derivative $\partial\mu_{\text{CHF}_3}/\partial r_{\text{CH}}$ is reported to be positive for the F₃C–H···NH₃ system which is a typical conventional hydrogen bond (Table 4 and Ref. [78a]). Moreover, it appears that a negative sign of $\partial\mu_{\text{CHF}_3}/\partial r_{\text{CH}}$ is actually a necessary precondition for the blue shift that is caused by the electric field only at rather large intermolecular distances [72a]. Hermansson suggested [72a] that in the vicinity of the equilibrium, the blue shift mainly originates from the Pauli exchange repulsion: "... the reasons for the blue-shifting C–H bonds lie in the sign of the dipole moment derivative with respect to the stretching coordinate combined with electronic exchange overlap at moderate and shorter H-bonded distances" [72a]. Liu and Schlegel [71] assume that the Pauli exchange repulsion balances the electrostatic attraction and precisely this balance serves as the main origin of the blue shift (see also Refs. [1a, 67e, 100b, 100j]).

Let us, for instance, consider the fluoroform molecule acting as the proton donor in the majority of blue-shifting H-bonded systems (**I–XL**, Table 3). Its carbon atom is highly polarized by the three electron-withdrawing fluorine atoms and hence carries a large positive charge. The latter induces a significant

attraction between C and B, in addition to the typical H \cdots B interaction. This attraction causes a shortening of the C \cdots B separation and therefore, the H of the C–H \cdots B approaches closer to B and “feels” a considerable Pauli exchange repulsion that “pulls” it out off B and finally leads to the C–H contraction.

Regarding the role of the dispersion forces in the origin of the blue shift, Hobza and Havlas [1a] assume that its contribution is quite negligible, as though Pejov and Hermansson [72b] suggest that it might even cause a small red shift (for discussion see Refs. [67e, 100a]).

Weinhold and co-workers [74] offer the following picture underlying the mechanism of the blue shift: the bond length $R(\text{A–H})$ is controlled by a balance of two main and opposite effects. One of them is the hyperconjugative interaction $n(\text{B}) \rightarrow \sigma^*(\text{A–H})$ that is responsible for elongation of the A–H bond, whereas the other is the increase in the s character of the hybrid molecular orbital at A accompanying the polarization of the A–H bond. If the latter effect dominates, the A–H bond contracts and $\nu(\text{A–H})$ undergoes a blue shift. If the former dominates, the red shift of $\nu(\text{A–H})$ occurs (see also Ref. [100a]).

This viewpoint contrasts with some previous works [1b, 3, 70a] demonstrating that the electron density distributions of blue-shifting H-bonded systems are not essentially different from those of the conventional ones (see also Ref. [67e]). Additionally, there is also an early suggestion regarding the $\text{F}_3\text{C–H}\cdots\text{OH}_2$ system (**I**, Table 3) that its blue shift results from the charge transfer to the fluorine atoms [1e]. This is one facet of the blue-shifting story that basically emphasizes the essential distinctions between the “nonconventional, blue-shifting” and conventional hydrogen bonds.

Another facet is related to the viewpoint, expressed by Scheiner and co-workers [3, 68], Dannenberg and co-workers [69], and Kryachko and Zeegers-Huyskens [70], that the conventional, red-shifting and nonconventional, blue-shifting hydrogen bonds are not fundamentally different from each other. A blue shift in the latter solely arises due to a combination of a variety of effects including the electrostatic, polarization, charge transfer, dispersion, and exchange/steric repulsion forces between the proton donor and proton acceptor (see also Ref. [73c], p. 5617; Ref. [72a], p. 4702; and Refs. [71, 74, 99]). One can therefore treat the conventional and blue-shifting H-bonds as similar in their basic nature exhibiting either a red or blue shift of the $\nu(\text{A–H})$ stretch as a consequence of the balance between opposite factors [3, 68b, 70a, 74, 77]. This point of view necessarily demands to revisit the classical definition of true hydrogen bonding, especially in re-examining or even removing the conditions 3 and 4, or extending their domains to the negative values for $\Delta R(\text{A–H})$ and $\Delta \nu(\text{A–H})$, and below 1 for $\text{IR}_{\text{A–H}\cdots\text{B}}(\nu(\text{A–H}))/\text{IR}_{\text{A–H}}(\nu(\text{A–H}))$. Apparently, such viewpoint is meaningful for the following three reasons, say the least. First: almost all known blue-shifting H-bonded systems involve the classical

proton acceptors which, under another circumstances (viz., with the conventional proton donors), participate in formation of the classical H-bonds. Second: the C–H proton donor in a sense behaves like a “two-headed Janus”: almost all proton donors which demonstrate blue shifts under some conditions (particularly those involving sp^3 -hybridized carbon atoms) may in contrast exhibit red shifts under changed conditions (see, e.g., Table 4 for few examples). And the third: there does not exist any exceptional H-bonded system that still undermines the standard mode of thinking accepted within the H-bonded community on that the A–H bond elongation concomitantly red-shifts the $\nu(\text{A–H})$ stretch and, oppositely, the A–H bond contraction induces a blue shift of the $\nu(\text{A–H})$ mode [1, 67, 71] (notice that the computational uncertainty revealed in Ref. [100c] for the $\text{F}_2\text{N–H}\cdots\text{FH}$ system (XLVIII, Table 3) is resolved in Ref. [76e]).

The outlined discussion mainly focuses on the problems of (β), that is, whether the C–H \cdots B bonding interaction is similar or different from the classical hydrogen bonding and (δ) how C–H \cdots B bonds should be correctly classified and actually relies on the definition of the hydrogen bond that operates with its geometric, spectroscopic, and energetic features. Invoking instead the alternative definition proposed in the general form by Steiner [25] (see Proposal (7) in Sect. 2), we can unify the conventional and nonconventional hydrogen bonds under the general concept of the hydrogen bond. This, in turn, allows us to straightforwardly generalize Jeffrey’s classification (Table 1) as follows (Table 5).

Despite the fact that the proposed classification based on the H-bond definition (7) unambiguously resolves the aforementioned problems (β) and (δ), it does not however give the complete answer on (α) what is the origin of a blue shift of nonconventional C–H \cdots B bonds or, in the other words, of the biased nature of the proton-donating ability of the C–H group? The latter is a main concern of the following section where it is shown that this problem is much deeper than earlier thought.

Table 5. The “symmetrized” generalization of Jeffrey’s classification of hydrogen bonds

Type of H-bond	Strong	Moderate	Weak
$r(\text{H}\cdots\text{B})$, Å	1.2–1.5	1.5–2.2	≥ 2.2
$ \Delta R(\text{A–H}) $, Å	0.08–0.25	0.02–0.08	≤ 0.02
$R(\text{A–H})/r(\text{H}\cdots\text{B})$	≈ 1	< 1	$\ll 1$
$r(\text{A}\cdots\text{B})$, Å	2.2–2.6	2.6–3.0	$\geq \sim 3.0$
$ E_{\text{HB}} $, kcal·mol ⁻¹	15–40 (60 [36,37])	4–15	≤ 4
$ \Delta\nu(\text{A–H}) /\nu(\text{A–H})$, %	~ 25	~ 10 – ~ 25	$\leq \sim 10$

The purpose of computing is insight, not numbers. R. W. Hamming “Numerical Methods for Scientists and Engineers”, 2nd Ed., McGraw-Hill, 1973

5 THE CONCEPT OF BLUE-SHIFTED HYDROGEN BOND

5.1 Introductory Background

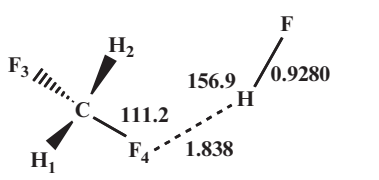
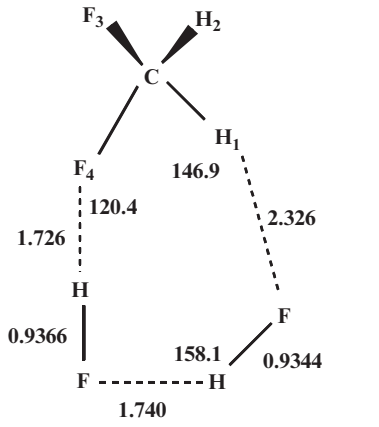
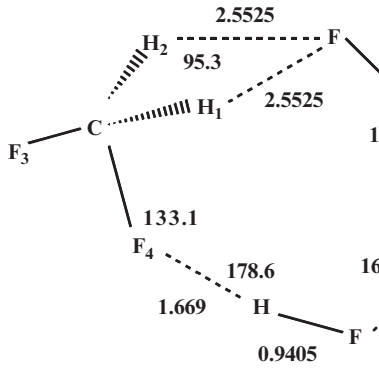
Upon a closer inspection of Table 3, we conclude that many of the reported nonconventional, blue-shifting hydrogen-bonded complexes are formed either by at least two bonds, one of which is the C–H···B bond and the other is the C–X···B' where X indicates a halogen (mainly fluorine) or oxygen atom, or by a single C–X···B' bond (actually, the latter case cannot be adequately referred to the C–H···B bond; see below for the discussion). To this class belong, for instance, the following systems: **IV**: F₃C–H···FH; **XI** (structure **2**): F₃C–H···O(CH₂)₂; **XII**: F₃C–H···O(CH₃)₂; **XLV**: CH₂F₂···HF; **LII**: FH₂C–H···OH₂; **LIII**: CH₃F···HF, **LIX**: CH₂O···CH₂O, and likely also **IX**: F₃C–H···ClH. For the systems of the former subclass, the C–X···B' hydrogen bond is stronger than the C–H···B one. Interestingly, no matter whether the latter is formed, the C–H bond(s) of such systems contracts compared to that in the monomer and its stretching vibrational mode $\nu(\text{C–H})$ undergoes a blue shift. That is why the systems belonging to the former subclass are hereafter referred as “blue-shifted” H-bonded ones [77a, b]. The complexes between fluoromethanes and (HF)_n molecules treated in Sec. 5.2 are the remarkable examples of both subclasses. It is also worth in this regard to recall the old experiment by Nelander [126] who demonstrated that $\nu(\text{C–H})$ of the complexes between the formaldehyde molecule and hydrogen bromide, chlorine, and iodine chloride undergo significant blue shifts which are larger in nitrogen than in argon matrices.

5.2 Complexes of Fluoromethanes CH₂F₂ and CH₃F with (HF)₁ ≤ n ≤ 3

Let us first consider the dimers **XLV**: CH₂F₂···HF and **LIII**: CH₃F···HF that are formed between fluoromethane and hydrogen fluoride [76b]. Their global minimum structures displayed in Table 6 are open complexes due to the absence of the C–H···F hydrogen bonds. In these complexes, the HF monomer is approximately oriented along the direction of the lone pair of the fluorine atom involved in the formation of the C–F···H–F *halogen–hydrogen* bond. Therefore, these dimers CH₂F₂···HF (**XLV**) and CH₃F···HF (**LIII**) neither belong to the blue-shifting nor blue-shifted complexes, but rather to the complexes with the single conventional C–F₄···H–F halogen–hydrogen bond (precisely, the second subclass in Sect. 5.1) [76b]. The C–F₄ bond of CH₂F₂ and CH₃F acts as a proton acceptor in the C–F₄···H–F bond (see the corresponding structures in Table 6). Its formation causes an elongation of the C–F₄ bond by 17–19 mÅ.

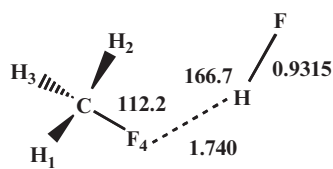
A striking feature of the complexes CH₂F₂···HF and CH₃F···HF is that while the C–F₄ bond is lengthened, the noninteracting C–H bonds of CH₂F₂ and CH₃F are shortened by 1.3–2.0 and 0.7–1.4 mÅ and the C–H stretches are blue-shifted by 16–29 and 13–20 cm⁻¹, respectively (Table 6). Put in the other

Table 6. The selected neutral blue-shifted hydrogen bonds. For the notations see the legend to Table 3

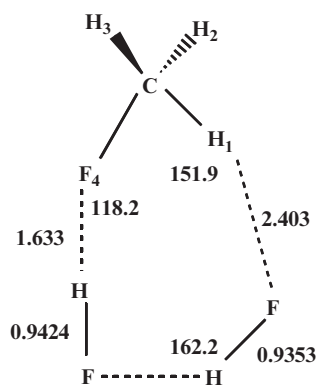
<p style="text-align: center;">XLV. CH₂F₂...HF</p> 	<p>MP2/aug-cc-pVTZ [76b]:</p> $\Delta R(\text{C-H}_1) = -0.0014 \text{ \AA}$ $\Delta R(\text{C-H}_2) = -0.0007 \text{ \AA}$ $\Delta \nu(\text{C-H}) = 13, 20 \text{ cm}^{-1}$ $\Delta A(\text{C-H}) = -13, -12 \text{ km} \cdot \text{mol}^{-1}$ $\Delta E = -4.3 \text{ kcal} \cdot \text{mol}^{-1}$ $\Delta E_{\text{BSSE}} = -3.7 \text{ kcal} \cdot \text{mol}^{-1}$ $\Delta R(\text{C-F}_4) = 0.0190 \text{ \AA}$ $\Delta R(\text{C-F}_3) = -0.0085 \text{ \AA}$
<p style="text-align: center;">LXXIII. CH₂F₂...(HF)₂</p> 	<p>MP2/aug-cc-pVTZ [76b]:</p> $\Delta R(\text{C-H}_1) = -0.0019 \text{ \AA}$ $\Delta R(\text{C-H}_2) = -0.0020 \text{ \AA}$ $\Delta \nu(\text{C-H}) = 24, 38 \text{ cm}^{-1}$ $\Delta A(\text{C-H}) = -13, -21 \text{ km} \cdot \text{mol}^{-1}$ $\Delta E = -7.7 \text{ kcal} \cdot \text{mol}^{-1}$ $\Delta E_{\text{BSSE}} = -6.7 \text{ kcal} \cdot \text{mol}^{-1}$ $\Delta R(\text{C-F}_4) = 0.0304 \text{ \AA}$ $\Delta R(\text{C-F}_3) = -0.0100 \text{ \AA}$
<p style="text-align: center;">LXXIV. CH₂F₂...(HF)₃</p> 	<p>MP2/aug-cc-pVTZ [76b]:</p> $\Delta R(\text{C-H}_1) = -0.0038 \text{ \AA}$ $\Delta R(\text{C-H}_2) = -0.0038 \text{ \AA}$ $\Delta \nu(\text{C-H}) = 43, 58 \text{ cm}^{-1}$ $\Delta A(\text{C-H}) = -23, -16 \text{ km} \cdot \text{mol}^{-1}$ $\Delta E = -6.3 \text{ kcal} \cdot \text{mol}^{-1}$ $\Delta E_{\text{BSSE}} = -5.2 \text{ kcal} \cdot \text{mol}^{-1}$ $\Delta R(\text{C-F}_4) = 0.0333 \text{ \AA}$ $\Delta R(\text{C-F}_3) = -0.0113 \text{ \AA}$
<p style="text-align: center;">LIII. CH₃F...HF</p>	

(Continued)

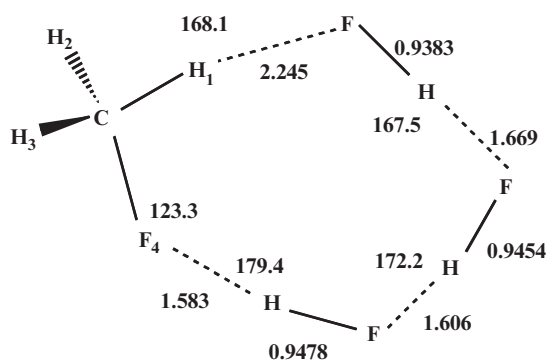
Table 6. —(Continued)

LXXV. CH₃F... (HF)₂

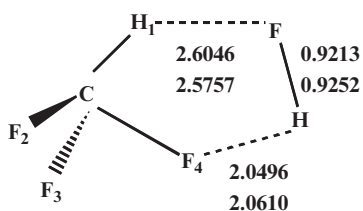
MP2/aug-cc-pVTZ [76b]:
 $\Delta R(\text{C}-\text{H}_{1,3}) = -0.0020 \text{ \AA}$
 $\Delta R(\text{C}-\text{H}_2) = -0.0013 \text{ \AA}$
 $\Delta \nu(\text{C}-\text{H}) = 16, 26, 29 \text{ cm}^{-1}$
 $\Delta A(\text{C}-\text{H}) = -9, -14, -11 \text{ km} \cdot \text{mol}^{-1}$
 $\Delta E = -6.1 \text{ kcal} \cdot \text{mol}^{-1}$
 $\Delta E_{\text{BSSE}} = -5.5 \text{ kcal} \cdot \text{mol}^{-1}$
 $\Delta R(\text{C}-\text{F}_4) = 0.0168 \text{ \AA}$

LXXVI. CH₃F... (HF)₃

MP2/aug-cc-pVTZ [76b]:
 $\Delta R(\text{C}-\text{H}_1) = -0.0020 \text{ \AA}$
 $\Delta R(\text{C}-\text{H}_{2,3}) = -0.0027 \text{ \AA}$
 $\Delta \nu(\text{C}-\text{H}) = 22, 39, 40 \text{ cm}^{-1}$
 $\Delta A(\text{C}-\text{H}) = -6, -13, -22 \text{ km} \cdot \text{mol}^{-1}$
 $\Delta E = -9.8 \text{ kcal} \cdot \text{mol}^{-1}$
 $\Delta E_{\text{BSSE}} = -8.8 \text{ kcal} \cdot \text{mol}^{-1}$
 $\Delta R(\text{C}-\text{F}_4) = 0.0278 \text{ \AA}$



MP2/aug-cc-pVTZ [76b]:
 $\Delta R(\text{C}-\text{H}_1) = -0.0028 \text{ \AA}$
 $\Delta R(\text{C}-\text{H}_2) = -0.0026 \text{ \AA}$
 $\Delta R(\text{C}-\text{H}_3) = -0.0032 \text{ \AA}$
 $\Delta \nu(\text{C}-\text{H}) = 26, 42, 52 \text{ cm}^{-1}$
 $\Delta A(\text{C}-\text{H}) = 0, -14, -20 \text{ km} \cdot \text{mol}^{-1}$
 $\Delta E = -8.1 \text{ kcal} \cdot \text{mol}^{-1}$
 $\Delta E_{\text{BSSE}} = -7.0 \text{ kcal} \cdot \text{mol}^{-1}$
 $\Delta R(\text{C}-\text{F}_4) = 0.0321 \text{ \AA}$

IV. $F_3C-H \cdots FH$ 

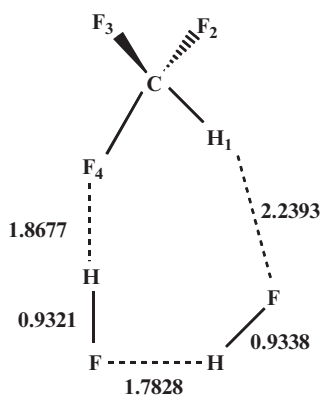
(the upper entry corresponds to MP2/6-311++G(2d,2p) and the lower to MP2/aug-cc-pVTZ)

MP2/6-311++G(2d,2p) [76a]:

$$\begin{aligned} \Delta R(C-H_1) &= -0.0007 \text{ \AA} \\ \Delta \nu(C-H_1) &= 16 \text{ cm}^{-1} \\ \Delta A(C-H_1) &= -15 \text{ km} \cdot \text{mol}^{-1} \\ \Delta E &= -3.3 \text{ kcal} \cdot \text{mol}^{-1} \\ \Delta E_{\text{BSSE}} &= -2.2 \text{ kcal} \cdot \text{mol}^{-1} \\ \Delta R(C-F_4) &= 0.0172 \text{ \AA} \\ \Delta R(C-F_{2,3}) &= -0.0050 \text{ \AA} \end{aligned}$$

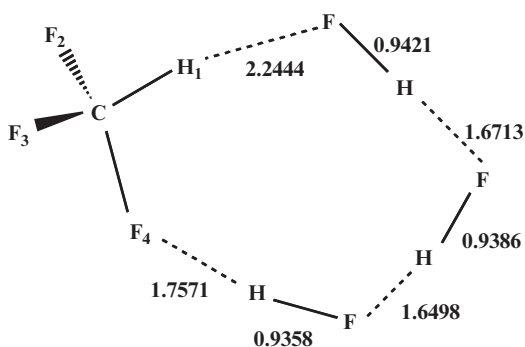
MP2/aug-cc-pVTZ [76a]:

$$\begin{aligned} \Delta R(C-H_1) &= -0.0007 \text{ \AA} \\ \Delta \nu(C-H_1) &= 15 \text{ cm}^{-1} \\ \Delta A(C-H_1) &= -14 \text{ km} \cdot \text{mol}^{-1} \\ \Delta E &= -3.1 \text{ kcal} \cdot \text{mol}^{-1} \\ \Delta E_{\text{BSSE}} &= -2.5 \text{ kcal} \cdot \text{mol}^{-1} \\ \Delta R(C-F_4) &= 0.0164 \text{ \AA} \\ \Delta R(C-F_{2,3}) &= -0.0046 \text{ \AA} \end{aligned}$$

LXXVII. $CHF_3 \cdots (HF)_2$ 

MP2/aug-cc-pVTZ [76a]:

$$\begin{aligned} \Delta R(C-H_1) &= -0.0012 \text{ \AA} \\ \Delta \nu(C-H_1) &= 30 \text{ cm}^{-1} \\ \Delta A(C-H_1) &= -20 \text{ km} \cdot \text{mol}^{-1} \\ \Delta E &= -10.9 \text{ kcal} \cdot \text{mol}^{-1} \\ \Delta E_{\text{BSSE}} &= -9.4 \text{ kcal} \cdot \text{mol}^{-1} \\ \Delta R(C-F_4) &= 0.0303 \text{ \AA} \\ \Delta R(C-F_{2,3}) &= -0.0076 \text{ \AA} \end{aligned}$$

LXXVIII. $CHF_3 \cdots (HF)_3$ 

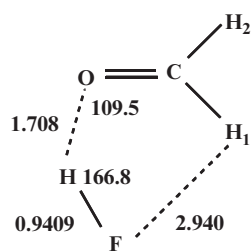
MP2/aug-cc-pVTZ [76a]:

$$\begin{aligned} \Delta R(C-H_1) &= -0.0039 \text{ \AA} \\ \Delta \nu(C-H_1) &= 60 \text{ cm}^{-1} \\ \Delta A(C-H_1) &= -19 \text{ km} \cdot \text{mol}^{-1} \\ \Delta E &= -20.1 \text{ kcal} \cdot \text{mol}^{-1} \\ \Delta E_{\text{BSSE}} &= -17.5 \text{ kcal} \cdot \text{mol}^{-1} \\ \Delta R(C-F_4) &= 0.0318 \text{ \AA} \\ \Delta R(C-F_{2,3}) &= -0.0074 \text{ \AA} \end{aligned}$$

LXXIX. $H_2CO \cdots HF$

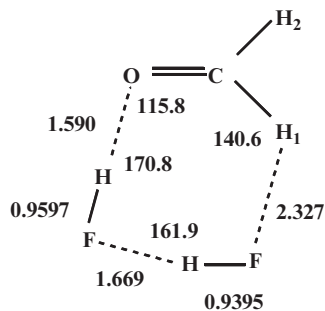
(Continued)

Table 6. —(Continued)

LXXIX. $\text{H}_2\text{CO} \cdots \text{HF}$ 

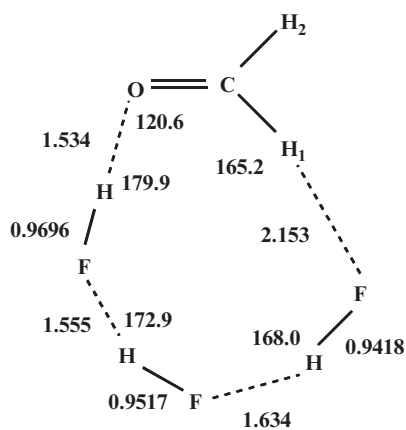
MP2/aug-cc-pVTZ [76d]:

$$\begin{aligned} \Delta R(\text{C}-\text{H}_1) &= -0.0035 \text{ \AA} \\ \Delta R(\text{C}-\text{H}_2) &= -0.0046 \text{ \AA} \\ \Delta \nu_{\text{sym}}(\text{C}-\text{H}) &= 44 \text{ cm}^{-1} \\ \Delta A_{\text{sym}}(\text{C}-\text{H}_1) &= -23 \text{ km} \cdot \text{mol}^{-1} \\ \Delta \nu_{\text{asym}}(\text{C}-\text{H}) &= 68 \text{ cm}^{-1} \\ \Delta A_{\text{asym}}(\text{C}-\text{H}_1) &= -49 \text{ km} \cdot \text{mol}^{-1} \\ \Delta E &= -8.6 \text{ kcal} \cdot \text{mol}^{-1} \\ \Delta E_{\text{BSSE}} &= -7.9 \text{ kcal} \cdot \text{mol}^{-1} \\ \Delta R(\text{C}-\text{O}) &= 0.0058 \text{ \AA} \end{aligned}$$

LXXX. $\text{H}_2\text{CO} \cdots (\text{HF})_2$ 

MP2/aug-cc-pVTZ [76d]:

$$\begin{aligned} \Delta R(\text{C}-\text{H}_1) &= -0.0058 \text{ \AA} \\ \Delta R(\text{C}-\text{H}_2) &= -0.0057 \text{ \AA} \\ \Delta \nu_{\text{sym}}(\text{C}-\text{H}) &= 63 \text{ cm}^{-1} \\ \Delta A_{\text{sym}}(\text{C}-\text{H}_1) &= +10 \text{ km} \cdot \text{mol}^{-1} \\ \Delta \nu_{\text{asym}}(\text{C}-\text{H}) &= 101 \text{ cm}^{-1} \\ \Delta A_{\text{asym}}(\text{C}-\text{H}_1) &= -76 \text{ km} \cdot \text{mol}^{-1} \\ \Delta E &= -13.8 \text{ kcal} \cdot \text{mol}^{-1} \\ \Delta E_{\text{BSSE}} &= -12.8 \text{ kcal} \cdot \text{mol}^{-1} \\ \Delta R(\text{C}-\text{O}) &= 0.0103 \text{ \AA} \end{aligned}$$

LXXXI. $\text{H}_2\text{CO} \cdots (\text{HF})_3$ 

MP2/aug-cc-pVTZ [76d]:

$$\begin{aligned} \Delta R(\text{C}-\text{H}_1) &= -0.0069 \text{ \AA} \\ \Delta R(\text{C}-\text{H}_2) &= -0.0061 \text{ \AA} \\ \Delta \nu_{\text{sym}}(\text{C}-\text{H}) &= 67 \text{ cm}^{-1} \\ \Delta A_{\text{sym}}(\text{C}-\text{H}_1) &= +250 \text{ km} \cdot \text{mol}^{-1} \\ \Delta \nu_{\text{asym}}(\text{C}-\text{H}) &= 118 \text{ cm}^{-1} \\ \Delta A_{\text{asym}}(\text{C}-\text{H}_1) &= -69 \text{ km} \cdot \text{mol}^{-1} \\ \Delta E &= -13.0 \text{ kcal} \cdot \text{mol}^{-1} \\ \Delta E_{\text{BSSE}} &= -11.8 \text{ kcal} \cdot \text{mol}^{-1} \\ \Delta R(\text{C}-\text{O}) &= 0.0118 \text{ \AA} \end{aligned}$$

words: if a given, say “spectator” C–F₄ bond of CH₂F₂ and CH₃F that participates in the C–F₄···H–A halogen–hydrogen bond elongates, the nonparticipating C–H bonds of CH₂F₂ and CH₃F which are remote from the contact region are shortened (to some extent, it partially resembles the aforementioned two-step mechanism [1, 67, 87]). This straightforwardly implies that a shortening of the C–H bonds and blue shifts of their stretching vibrational modes of those fluoromethanes that occur under elongation of the C–F₄ while it participates in the formation of the halogen–hydrogen bond is the *intrinsic characteristic* of CH₂F₂ and CH₃F. We call this characteristic as a “negative response” (or precisely, an “intrinsic negative response”) [76f]. This is actually the feature which, as we believe, underlies the subclass of blue-shifted hydrogen bonds listed in Table 6 that particularly includes the most stable and cyclic complexes of CH₂F₂···(HF)₂ (LXXIII), CH₂F₂···(HF)₃ (LXXIV), CH₃F···(HF)₂ (LXXV), and CH₃F···(HF)₃ (LXXVI). In addition to C–F···H–F halogen–hydrogen bonds, they possess C–H···F–H hydrogen bonds between the fluoromethane and the (HF)₂ or (HF)₃ moiety.

The formation of the C–F···H–F halogen–hydrogen bond in the complexes LXXIII–LXXVI is accompanied by a further elongation of the C–F₄ proton acceptor bond by ~28–32 mÅ. All C–H bonds undergo a contraction ranging from 1.9 to 3.8 mÅ, thus demonstrating the typical feature of blue-shifting hydrogen bonds. All C–H stretching frequencies are therefore blue-shifted from 22 to 58 cm⁻¹. Summarizing: the important, if not a primary cause of the $\nu(\text{C–H})$ blue shifts in these complexes LXXIII–LXXV is the elongation of the C–F₄ proton acceptor bond relative to that in the isolated fluoromethane as a consequence of formation of a halogen–hydrogen bond.

A theory has only the alternative of being wrong or right. A model has a third possibility: it may be right but irrelevant. Manfred Eigen, in “The Physicist’s Concept of Nature”, J. Mehra (Ed.), Reidel, Dordrecht, 1973.

5.3 The Origin of Intrinsic Negative Response: Theoretical Force-Field Model

5.3.1 Prelude

One of the major corollaries that we deduce from the list of the nonconventional H-bonded systems collected in Tables 3 and 6 is that fluoromethanes act as the proton donors in a majority of the blue-shifting and blue-shifted hydrogen-bonded systems. Notice that the quintessential distinction between the blue-shifting and blue-shifted hydrogen bonds lies in the following. The former has only nonconventional A–H···B bond(s), that is, the bond whose donor A–H sub-bond contracts under the A–H···B bond formation and whose corresponding stretching mode $\nu(\text{A–H})$ undergoes a blue shift with respect to the isolated donor molecule. In contrast, the latter, which comprises of the

interacting molecule M_I and molecule M_{II} , has at least one conventional H-bond $A_1-H_1 \cdots B_1$ and at least one nonconventional $A_2-H_2 \cdots B_2$ where $B_1 \cup A_2-H_2 \in M_I$ and $B_2 \cup A_1-H_1 \in M_{II}$, and is therefore cyclic. Note that in the blue-shifted complexes of fluoromethanes ($\equiv M_I$)- M_{II} , the $A_1-H_1 \cdots B_1$ is of the $A_1-H_1 \cdots F_4-C$ type (see Table 6).

It is demonstrated in Sect. 5.2 that the C-H bonds of the fluoromethanes CH_2F_2 and CH_3F are contracted under elongation of the C-F₄, and this is their intrinsic characteristic. This effect is called an intrinsic negative response. The first conjecture is that fluoroform CF_3H does also belong to the subclass of molecules characterized by an intrinsic negative response.

The most stable and cyclic complexes of $F_3CH \cdots F-H$ (IV), $F_3CH \cdots (HF)_2$ (LXXVII), and $F_3CH \cdots (HF)_3$ (LXXVIII) having both the C-F \cdots H-F halogen-hydrogen bonds and the C-H \cdots F-H ones are shown in Table 6 (Ref. [76a]). The formation of the former elongates the C-F₄ proton acceptor bond by $\sim 16-32$ mÅ whereas the nonparticipating C-F_{2,3} bonds are contracted by $\sim 5-8$ mÅ. The C-H₁ bond is also shortened by $0.7-3.9$ mÅ and its stretch becomes blue-shifted by $15-60$ cm⁻¹.

The *second conjecture* is the following: the whole class of molecules with a negatively response may form blue-shifted complexes with molecules containing the conventional proton donor(s). In order to understand the origin of a negative response of fluoromethanes, we propose the following physical model based on their harmonic force fields [76f] (notice that the idea of the force field was also invoked for blue-shifting hydrogen bonds by Qian and Krimm [73]).

Let us consider a fluoromethane molecule CH_nF_{4-n} ($1 \leq n \leq 3$). It possesses nine independent degrees of freedom four of which are the radial ones associated with the four existing bonds, either of C-H or C-F types. The remaining five degrees of freedom are angular related to the bond angles. According to Refs. [76a-b], the angular degrees of freedom undergo sufficiently small changes while CH_nF_{4-n} ($1 \leq n \leq 3$) interacts, for example, with $(HF)_m$ ($1 \leq m \leq 3$), and thus will be neglected within the proposed model.

5.3.2 Harmonic ansatz

Within the harmonic approximation that neglects the angular degrees of freedom, the potential energy function of CH_nF_{4-n} ($1 \leq n \leq 3$) in the vicinity of its ground-state equilibrium geometry casts as

$$(8) \quad U_n^h(\{x_i^{(n)}\}_{i=1}^4) = (1/2) \sum_{j=1}^4 \mathbf{k}_{ij}^{(n)} x_i^{(n)} x_j^{(n)}$$

where the bond displacement $x_i^{(n)} \equiv r_i - r_{ie}$, r_{ie} is the equilibrium length of the i th bond, $x_1^{(n)}, \dots, x_n^{(n)}$ correspond to the C-H bonds and $x_{n+1}^{(n)}, \dots, x_4^{(n)}$ to the C-F ones. In Eq. 8, $\mathbf{K}^{(n)} \equiv (\mathbf{k}_{ij}^{(n)})_{1 \leq i, j \leq 4}$ is the harmonic force constant matrix of CH_nF_{4-n} ($1 \leq n \leq 3$). Notice that the force constant matrix $\mathbf{K}^{(n)}$ is symmetric and reflects the point-group symmetry of CH_nF_{4-n} , viz.,

$$\begin{aligned}
n = 1(\text{CHF}_3): & \quad \mathbf{k}_{12}^{(1)} = \mathbf{k}_{13}^{(1)} = \mathbf{k}_{14}^{(1)}, \quad \mathbf{k}_{22}^{(1)} = \mathbf{k}_{33}^{(1)} = \mathbf{k}_{44}^{(1)}, \quad \mathbf{k}_{23}^{(1)} = \mathbf{k}_{24}^{(1)} = \mathbf{k}_{34}^{(1)}, \\
n = 2(\text{CH}_2\text{F}_2): & \quad \mathbf{k}_{11}^{(2)} = \mathbf{k}_{22}^{(2)}, \quad \mathbf{k}_{13}^{(2)} = \mathbf{k}_{14}^{(2)} = \mathbf{k}_{23}^{(2)} = \mathbf{k}_{24}^{(2)}, \quad \mathbf{k}_{33}^{(2)} = \mathbf{k}_{44}^{(2)}, \\
n = 3(\text{CH}_3\text{F}): & \quad \mathbf{k}_{11}^{(3)} = \mathbf{k}_{22}^{(3)} = \mathbf{k}_{33}^{(3)}, \quad \mathbf{k}_{12}^{(3)} = \mathbf{k}_{13}^{(3)} = \mathbf{k}_{23}^{(3)}, \quad \mathbf{k}_{14}^{(3)} = \mathbf{k}_{24}^{(3)} = \mathbf{k}_{34}^{(3)}.
\end{aligned}$$

The values of matrix elements of $\mathbf{K}^{(n)}$ ($1 \leq n \leq 3$) evaluated by means of the MP2/6-311++G(2d,2p) and MP2/aug-cc-pVTZ methods are collected in Table 7.

Let us assume that the spectator C–F₄ bond has a length $x_4^{(n)} = x_0^{(n)}$ determined by the formation of the (C)F₄···H–A hydrogen bond. This converts $U_n^h(\{x_i^{(n)}\}_{i=1}^4)$ into a reduced potential energy function [76f]

$$(9) \quad U_n^h(\{x_i^{(n)}\}_{i=1}^3; x_0^{(n)}) = (1/2) \sum_{i,j=1}^3 \mathbf{k}_{ij}^{(n)} x_i^{(n)} x_j^{(n)} + (1/2) x_0 \sum_{i=1}^3 \mathbf{k}_{ij}^{(n)} x_i^{(n)} x_j^{(n)}$$

which parametrically depends on $x_0^{(n)}$ (notice that the constant term $(1/2) \mathbf{k}_{44}^{(n)} (x_0^{(n)})^2$ is removed in Eq. 9). We assume that $u_n^h(\{x_i^{(n)}\}_{i=1}^3; x_0^{(n)})$ has an extremum at $\{x_{i0}^{(n)}\}_{i=1}^3$. The latter linearly depend on $x_0^{(n)}$ because of the chosen harmonic ansatz and obey the following system of linear algebraic equations (the superscript (n) is removed for simplicity):

$$(10) \quad \begin{aligned} \mathbf{k}_{11}x_{10} + \mathbf{k}_{12}x_{20} + \mathbf{k}_{13}x_{30} &= -\mathbf{k}_{14}x_0, \\ \mathbf{k}_{12}x_{10} + \mathbf{k}_{22}x_{20} + \mathbf{k}_{23}x_{30} &= -\mathbf{k}_{24}x_0, \\ \mathbf{k}_{13}x_{10} + \mathbf{k}_{23}x_{20} + \mathbf{k}_{33}x_{30} &= -\mathbf{k}_{34}x_0. \end{aligned}$$

The solutions of (10) are simply expressed in terms of the ratios of the corresponding minors, viz.,

$$(11) \quad x_{i0} = -(\Delta_i/\Delta)x_0, \quad i = 1, 2, 3$$

where

$$\Delta = \begin{vmatrix} \mathbf{k}_{11} & \mathbf{k}_{12} & \mathbf{k}_{13} \\ \mathbf{k}_{12} & \mathbf{k}_{22} & \mathbf{k}_{23} \\ \mathbf{k}_{13} & \mathbf{k}_{23} & \mathbf{k}_{33} \end{vmatrix}, \quad \Delta_1 = \begin{vmatrix} \mathbf{k}_{14} & \mathbf{k}_{12} & \mathbf{k}_{13} \\ \mathbf{k}_{24} & \mathbf{k}_{22} & \mathbf{k}_{23} \\ \mathbf{k}_{34} & \mathbf{k}_{23} & \mathbf{k}_{33} \end{vmatrix}, \quad \Delta_2 = \begin{vmatrix} \mathbf{k}_{11} & \mathbf{k}_{14} & \mathbf{k}_{13} \\ \mathbf{k}_{12} & \mathbf{k}_{24} & \mathbf{k}_{23} \\ \mathbf{k}_{13} & \mathbf{k}_{34} & \mathbf{k}_{33} \end{vmatrix}, \quad \Delta_3 = \begin{vmatrix} \mathbf{k}_{11} & \mathbf{k}_{12} & \mathbf{k}_{14} \\ \mathbf{k}_{12} & \mathbf{k}_{22} & \mathbf{k}_{24} \\ \mathbf{k}_{13} & \mathbf{k}_{23} & \mathbf{k}_{34} \end{vmatrix}$$

are equal to:

$$(12a) \quad \begin{aligned} n = 1: \\ \Delta &= (\mathbf{k}_{22} - \mathbf{k}_{23})[\mathbf{k}_{11}(\mathbf{k}_{22} + \mathbf{k}_{23}) - 2\mathbf{k}_{12}^2] \\ \Delta_1 &= \mathbf{k}_{12}(\mathbf{k}_{22} - \mathbf{k}_{23})^2, \quad \Delta_2 = \Delta_3 = (\mathbf{k}_{22} - \mathbf{k}_{23})(\mathbf{k}_{11}\mathbf{k}_{23} - \mathbf{k}_{12}^2); \end{aligned}$$

$$(12b) \quad \begin{aligned} n = 2: \\ \Delta &= (\mathbf{k}_{11} - \mathbf{k}_{12})[\mathbf{k}_{33}(\mathbf{k}_{11} + \mathbf{k}_{12}) - 2\mathbf{k}_{13}^2] \\ \Delta_1 &= \Delta_2 = (\mathbf{k}_{11} - \mathbf{k}_{12})(\mathbf{k}_{33} - \mathbf{k}_{34})\mathbf{k}_{13} \\ \Delta_3 &= (\mathbf{k}_{11} - \mathbf{k}_{12})[\mathbf{k}_{34}(\mathbf{k}_{11} + \mathbf{k}_{12}) - 2\mathbf{k}_{13}^2]; \end{aligned}$$

$$\begin{aligned}
 n = 3: \\
 (12c) \quad \Delta &= (\mathbf{k}_{11} - \mathbf{k}_{12})[\mathbf{k}_{11}(\mathbf{k}_{11} + \mathbf{k}_{12}) - 2\mathbf{k}_{12}^2] \\
 \Delta_1 = \Delta_2 = \Delta_3 &= (\mathbf{k}_{11} - \mathbf{k}_{12})^2 \mathbf{k}_{14}
 \end{aligned}$$

and tabulated in Table 7. Using this table, one finally obtains

$$(13a) \quad n = 1: \quad x_{1o} = -0.024x_o, \quad x_{2o} = x_{3o} = -0.117x_o;$$

$$(13b) \quad n = 2: \quad x_{1o} = x_{2o} = -0.032x_o, \quad x_{3o} = -0.130x_o;$$

$$(13c) \quad n = 3: \quad x_{1o} = x_{2o} = x_{3o} = -0.036x_o$$

Since all intramolecular coupling force constants \mathbf{k}_{ij} ($i \neq j$) are positive and $\mathbf{k}_{ij}/\mathbf{k}_{nn} \ll 1$ (see Table 7), we approximate the minors as

$$(12a') \quad n = 1: \quad \Delta \approx \mathbf{k}_{11}\mathbf{k}_{22}^2, \quad \Delta_1 \approx \mathbf{k}_{12}\mathbf{k}_{22}^2, \quad \Delta_2 = \Delta_3 \approx \mathbf{k}_{11}\mathbf{k}_{22}\mathbf{k}_{23};$$

$$(12b') \quad n = 2: \quad \Delta \approx \mathbf{k}_{11}^2\mathbf{k}_{33}, \quad \Delta_1 = \Delta_2 \approx \mathbf{k}_{11}\mathbf{k}_{33}\mathbf{k}_{13}, \quad \Delta_3 \approx \mathbf{k}_{11}^2\mathbf{k}_{34};$$

$$(12c') \quad n = 3: \quad \Delta \approx \mathbf{k}_{11}^3, \quad \Delta_1 = \Delta_2 = \Delta_3 \approx \mathbf{k}_{11}^2\mathbf{k}_{14}$$

The latter leads to the approximate values of the exact solutions (13):

$$(13a') \quad n = 1: x_{1o}/x_o \approx -\mathbf{k}_{12}/\mathbf{k}_{11} \approx -0.031, \quad x_{2o}/x_o = x_{3o}/x_o \approx -\mathbf{k}_{23}/\mathbf{k}_{22} \approx -0.134;$$

$$(13b') \quad n = 2: x_{1o}/x_o = x_{2o}/x_o \approx -\mathbf{k}_{13}/\mathbf{k}_{11} \approx -0.037, \quad x_{3o}/x_o \approx -\mathbf{k}_{34}/\mathbf{k}_{33} \approx -0.132;$$

$$(13c') \quad n = 3: x_{1o}/x_o = x_{2o}/x_o = x_{3o}/x_o \approx -\mathbf{k}_{14}/\mathbf{k}_{11} \approx -0.036$$

Concluding, all the ratios x_{io}/x_o ($i = 1, 2, 3$) are negative, and therefore, all fluoromethanes are characterized by a negative response, meaning that if a given spectator C–F₄ bond stretches, i.e. $x_o^{(n)} > 0$, each fluoromethane ‘responds’ by shortening of all other C–H and C–F bonds, viz.,

$$(14) \quad r_i = r_{ie} - (\Delta_i/\Delta)(r_4 - r_{4e}), \quad (\Delta_i/\Delta) > 0 \quad (i = 1, 2, 3)$$

It directly follows from Eqs. 13a–c that fluoroform features the largest negative response for its C–H bonds whereas methylene fluoride is characterized by the largest negative response for its nonparticipating C–F bond. Since the estimations given in Eq. 13' are very close to the corresponding exact solutions 13, we conclude that a negative response of the whole series of fluoromethanes to the stretched spectator C–F bond originates from the positivity of the intramolecular coupling force constants \mathbf{k}_{ij} ($i \neq j$) > 0 ($\mathbf{k}_{ii} > 0$ due to stability of a given fluoromethane), precisely: the larger is the intermolecular coupling (under the given $\mathbf{k}_{ii} > 0$), the larger is a negative response, and the larger is a blue shift of the respective C–H stretch. We finally define the so-called harmonic response factors $\alpha_{hi}^{(n)} \equiv \Delta_i^{(n)}/\Delta^{(n)}$ which measure the strengths of the negative response of CH_nF_{4–n} ($1 \leq n \leq 3$): a negative response takes a place if $\alpha_{hi}^{(n)} > 0$.

5.3.3 Generalization to formaldehyde

We believe that the concept of the negative response and the physical model behind it can be rather useful to predict whether a given molecule M containing

$B_1 \cup A_2-H_2 \in M$ belongs to a subclass of blue-shifted H-bonded systems while interacting with another molecule $M' \in B_2 \cup A_1-H_1$ and forming one conventional H-bond $A_1-H_1 \cdots B_1$ and at least one nonconventional $A_2-H_2 \cdots B_2$. Let us explain this suggestion in more details invoking the H_2CO as an example (see Refs. [76d–f]).

Within the harmonic approximation, the potential energy of H_2CO in the vicinity of its ground-state equilibrium geometry is represented by

$$U_{H_2CO}^h(R, r, r') = (1/2)F_{11}S_1^2 + F_{12}(S_1S_2 + S_1S_3) + (1/2)F_{22}(S_2^2 + S_3^2) + F_{23}S_2S_3 \quad (15)$$

where $R \equiv R(C=O)$, $r \equiv R(C-H)$, $r' \equiv R(C-H')$, $S_1 \equiv (R-R_e)/R_e$, $S_2 \equiv (r-r_e)/r_e$, $S_3 \equiv (r'-r'_e)/r'_e$, and the subscript “e” stands for the equilibrium

Table 7. The harmonic force constants (mdyne·Å⁻¹) of CH_nF_{4-n} ($1 \leq n \leq 3$) evaluated within the MP2/aug-cc-pVTZ and MP2/6-311++G(2d,2p) approaches [76f]

	CHF ₃	CHF ₃	CH ₂ F ₂	CH ₂ F ₂	CH ₃ F	CH ₃ F
	MP2/aug-cc-pVTZ	MP2/6-311++G(2d,2p)	MP2/aug-cc-pVTZ	MP2/6-311++G(2d,2p)	MP2/aug-cc-pVTZ	MP2/6-311++G(2d,2p)
k_{11}	5.621 5.684 ^a	5.693	5.502 5.745 ^a	5.571	5.491 5.590 ^a	5.540
k_{12}	0.177 0.132 ^a	0.176	0.039 0.021 ^a	0.040	0.031 0.020 ^a	0.035
k_{22}	6.474 5.567 ^a	6.283	5.502 5.587 ^a	5.571	5.491 5.605 ^a	5.540
k_{23}	0.865 0.867 ^a	0.857	0.203 0.169 ^a	0.202	0.031 0.022 ^a	0.035
k_{13}	0.865 0.138 ^a	0.857	0.203 -0.130 ^a	0.202	0.031 0.020 ^a	0.035
k_{33}	6.474 6.702 ^a	6.283	6.098 5.736 ^a	5.903	5.491 5.605 ^a	5.540
k_{34}	0.865 0.885 ^a	0.857	0.807 0.729 ^a	0.795	0.198 0.147 ^a	0.197
k_{14}	0.177 0.137 ^a	0.177	0.203 0.226 ^a	0.202	0.198 0.136 ^a	0.197
k_{44}	6.474 6.746 ^a	6.283	6.098 6.417 ^a	5.903	5.776 5.164 ^a	5.586
Δ	231.060	220.220	184.141	182.743	165.634	170.014
Δ_1	5.380		5.868		5.905	5.970
		5.182		5.707		
Δ_2	27.109		5.868		5.905	5.970
		26.305		5.707		
Δ_3	27.109		23.980		5.905	5.970
		26.305		24.219		

^a The selected force constants of the optimized structures $CH_nF_{4-n}-(HF_2)$ ($1 \leq n \leq 3$; see the structures LXXIII, LXXV, and LXXVII in Table 6)

(see, e.g., Ref. [127]). Since the equilibrium structure of H_2CO in the ground electronic state is characterized by C_{2h} symmetry, we define the symmetry-adapted relative stretching displacements $Q_{23} \equiv (S_2 + S_3)/2$ and $q_{23} \equiv S_2 - S_3$, and rewrite $U^h(R, r, r')$ as

$$(16) \quad U_{\text{H}_2\text{CO sym}}^h(\mathbf{R}, Q_{23}, q_{23}) = (1/2)F_{11}S_1^2 + 2F_{12}S_1Q_{23} + (F_{22} + F_{23})Q_{23}^2 + (1/4)(F_{22} - F_{23})q_{23}^2$$

Let us consider the C=O bond as a spectator bond fixed at some length R_0 that corresponds to $S_1^0 \equiv (R_0 - R_e)/R_e$. $U_{\text{H}_2\text{CO sym}}^h(\mathbf{R}, Q_{23}, q_{23})$ transforms then to the reduced form

$$(17) \quad u_{\text{H}_2\text{CO sym}}^h(Q_{23}; R_0) = 2F_{12}S_1^0Q_{23} + (F_{22} + F_{23})Q_{23}^2$$

that determines a function of Q_{23} parametrically depending on R_0 via S_1^0 . Notice that the last term on the rhs of Eq. 16 is removed as decoupled from S_1 . An extremum of $u_{\text{H}_2\text{CO sym}}^h(Q_{23}; R_0)$ is attained at $Q_{23}^0 = Q_{23}^0(S_1^0)$ which satisfies the following linear algebraic equation:

$$(18) \quad F_{12}S_1^0 + (F_{22} + F_{23})Q_{23}^0 = 0.$$

Therefore,

$$(19) \quad Q_{23}^0 = -[F_{12}/(F_{22} + F_{23})]S_1^0 \equiv -\alpha_h S_1^0$$

where α_h is a so-called harmonic response factor introduced here by analogy with Sect. 5.3.2. Substituting the values of the harmonic force constants $F_{12} = 0.714$, $F_{22} = 2.964$, and $F_{23} = 0.086$ aJ given in Ref. [127] into Eq. 19 yields $\alpha_h = 0.234$ [76d].

Therefore, since the ratio $Q_{23}^0/S_1^0 (S_1^0 > 0)$ is negative or, equivalently, the harmonic response factor is positive, an elongation of the spectator C=O bond causes a contraction of the C–H bonds. Obviously, a positivity of the harmonic response factor is completely determined by the sign of the intramolecular coupling F_{12} . Table 6 demonstrates that formaldehyde H_2CO forms nonconventional blue-shifted hydrogen bonds with hydrogen fluoride clusters $(\text{HF})_{2 \leq m \leq 3}$ [76d].

With hydrogen fluoride, formaldehyde interacts quite strongly, forming a stable dimeric complex **LXXIX** (Table 6) with the binding energy of ca. $-8 \text{ kcal} \cdot \text{mol}^{-1}$, that indicates a strong $\text{F}-\text{H} \cdots \text{O}=\text{C}$ hydrogen bond. The distance $r(\text{H}_1 \cdots \text{F})$ of about 2.94 \AA slightly exceeds the sum of the van der Waals radii of F and H ($\sim 2.90 \text{ \AA}$), hence their contact $\text{C}-\text{H}_1 \cdots \text{F}$ cannot be definitely treated as a hydrogen bond, according to the rule 4. However, together with the remote C–H₂ bond, the C–H₁ one, undergoes substantial changes relative to the isolated H_2CO molecule: their bond lengths are shortened by 3.5 and 4.6 mÅ and their symmetric and asymmetric stretching modes are blue-shifted

by 44 and 68 cm^{-1} . We may thus conclude that it is definitely the formation of the $\text{F-H}\cdots\text{O}=\text{C}$ hydrogen bond that causes an elongation of the $\text{C}=\text{O}$ bond by about 0.006 Å and simultaneously contracts both C-H bonds, and considerably blue shifts their stretches.

The complexes $\text{H}_2\text{CO}\cdots(\text{HF})_2$ (**LXXX**) and $\text{H}_2\text{CO}\cdots(\text{HF})_3$ (**LXXXI**) are cyclic, characterized by the planar, C_s -symmetric equilibrium structures and the binding energies amounting, respectively, to $-12.8 \text{ kcal}\cdot\text{mol}^{-1}$ and $-11.8 \text{ kcal}\cdot\text{mol}^{-1}$ (see Table 6). In addition to the strong, conventional and red-shifted hydrogen bonds $\text{F-H}\cdots\text{O}=\text{C}$ and $\text{F-H}\cdots\text{F}$, they possess the blue-shifted $\text{C-H}_1\cdots\text{F}$ contact since $r(\text{H}_1\cdots\text{F}) = 2.33 \text{ Å}$ in **LXXX** and 2.15 Å in **LXXXI**. Both C-H bonds in the complexes **LXXX** and **LXXXI** are considerably contracted that correlates with a further elongation of the $\text{C}=\text{O}$ bond as the ring size increases. Relative to the monomer, the $\nu_{\text{sym}}(\text{C-H})$ and $\nu_{\text{asym}}(\text{C-H})$ undergo enormous blue shifts equal, correspondingly, to 63 cm^{-1} and **101** cm^{-1} for (**LXXX**), and 67 cm^{-1} and **118** cm^{-1} for (**LXXXI**) [76d]. These are the *largest theoretical blue shifts* obtained so far for $\text{C-H}\cdots\text{F}$ nonconventional hydrogen bonds (together with the complex $\text{H}_2\text{CO}\cdots(\text{HF})_4$ whose $\Delta\nu_{\text{sym}}(\text{C-H})$ and $\Delta\nu_{\text{asym}}(\text{C-H})$ reach **+77** and **+127** cm^{-1} , respectively [76d]). It is worth finally mentioning that in comparison with the dimer **LXXIX**, the infrared intensities of $\nu_{\text{sym}}(\text{C-H})$ and $\nu_{\text{asym}}(\text{C-H})$ of the trimer **LXXX** are correspondingly larger and lower.

Why did it stop where it did?
Cheshire Cat
Lewis Carrol "Alice in Wonderland"

6 CONCLUSIONS AND PERSPECTIVES

The aim of the present review is mainly threefold. First of all, it is considered as an attempt to consolidate the conventional and nonconventional, blue-shifting hydrogen bonds by modifying the obsolete classification of the former ones in order to include the latter. Second, it provides the most complete list of $\text{C-H}\cdots\text{B}$ nonconventional hydrogen bonds gathering more than 80 systems. Third, it discusses the concept of blue-shifted hydrogen bonds which form a quite large subclass of the blue-shifting ones and whose intramolecular coupling(s) play the predominant role in the blue shifts of their C-H stretching vibrational frequencies. Finally, it presents some cyclic $\text{H}_2\text{CO}\cdots(\text{HF})_{1\leq n\leq 3}$ clusters which are primarily stabilized by the strong $\text{F-H}\cdots\text{O}=\text{C}$ and $\text{F-H}\cdots\text{F}$ hydrogen bonds and which reveal unusually large blue shifts of the C-H stretching modes, exceeding 100 cm^{-1} and thus comparable, by the absolute value, with the red shift of the archetypical water dimer with its typical classical hydrogen bond. We believe that the force-field model proposed in Sect. 5.3 will be a useful tool to predict new blue-shifted hydrogen bonds.

ACKNOWLEDGMENT

The author gratefully thanks Slawomir Grabowski for his invitation, Françoise Remacle for warm hospitality and F.R.F.C. 2.4562.03F (Belgium) for fellowship. I would like also to thank Sonia Melikova, Thérèse Zeegers-Huyskens, Pavel Hobza, Alfred Karpfen, Camille Sandorfy, and Steve Scheiner for exciting discussions.

REFERENCES

1. (a) P. Hobza and Z. Havlas, *Chem. Phys. Lett.* **303**, 447 (1999); (b) E. Cubero, M. Orozco, P. Hobza, and F. J. Luque, *J. Phys. Chem. A* **103**, 6394 (1999); (c) P. Hobza, V. Spirko, Z. Havlas, K. Buchhold, B. Reimann, H. D. Barth, and B. Brutschy, *Chem. Phys. Lett.* **299**, 180 (1999); (d) P. Hobza, V. Špirko, H. L. Selzle, and E. W. Schlag, *J. Phys. Chem. A* **102**, 2501 (1998); (e) P. Hobza and Z. Havlas, *Chem. Rev.* **100**, 4253 (2000).
2. N. Karger, A. M. Amorim da Costa, and P. J. A. Ribeiro-Claro, *J. Phys. Chem. A* **103**, 8672 (1999).
3. Y. Gu, T. Kar, and S. Scheiner, *J. Am. Chem. Soc.* **121**, 9411 (1999).
4. T. S. Moore and T. F. Winmill, *J. Chem. Soc.* **101**, 1635 (1912).
5. M. Huggins, *Thesis* (University of California, 1919).
6. W. M. Latimer and W. H. Rodebush, *J. Am. Chem. Soc.* **42**, 1419 (1920).
7. L. Pauling, *The Nature of the Chemical Bond* (Cornell University Press, Ithaca, 1939). See also L. Pauling, *Proc. Natl. Acad. Sci. USA* **14**, 359 (1928).
8. W. Nernst, *Z. Phys. Chem.* **8**, 110 (1891).
9. A. Werner, *Liebigs Ann. Chem.* **322**, 261 (1902).
10. G. Oddo and E. Puxeddu, *Gazz. (ii)* **36**, 1 (1906).
11. P. Pfeiffer, *Ann.* **398**, 137 (1913).
12. G. N. Lewis, *Valence and Structure of Atoms and Molecules* (Chemical Catalog, New York, 1923). Ch. 12.
13. J. D. Bernal and H. D. Megaw, *Proc. Roy. Soc. London A* **151**, 384 (1935).
14. M. L. Huggins, *J. Org. Chem.* **1**, 407 (1936). See also M. L. Huggins, *Angew. Chem. Int. Ed. Engl.* **10**, 147 (1971).
15. D. Hadži and H. W. Thompson (Eds.), *Hydrogen Bonding* (Pergamon Press, London, 1959).
16. C. G. Pimentel and A. L. McClellan, *The Hydrogen Bond* (Freeman, San Francisco, 1960). See also G. C. Pimentel and A. L. McClellan, *Annu. Rev. Phys. Chem.* **22**, 347 (1971).
17. W. C. Hamilton and J. A. Ibers, *Hydrogen Bonding in Solids* (Benjamin, New York, 1968).
18. P. A. Kollman and L. C. Allen, *Chem. Rev.* **72**, 283 (1972).
19. P. Schuster, G. Zundel, and C. Sandorfy (Eds.), *The Hydrogen Bond. Recent Developments in Theory and Experiments* (North-Holland, Amsterdam, 1976).
20. G. A. Jeffrey and W. Saenger, *Hydrogen Bonding in Biological Structures*, 2nd edition (Springer, Berlin, 1994).
21. G. A. Jeffrey, *An Introduction to Hydrogen Bonding* (Oxford University Press, Oxford, 1997).
22. S. Scheiner, *Hydrogen Bonding. A Theoretical Perspective* (Oxford University Press, Oxford, 1997).
23. G. R. Desiraju and T. Steiner, *The Weak Hydrogen Bond in Structural Chemistry and Biology* (Oxford University Press, Oxford, 1999). See also (a) G. R. Desiraju, *Acc. Chem. Res.* **29**, 441 (1996); (b) G. R. Desiraju, *Chem. Commun.* 2995 (2005).
24. P. Schuster, in *Intermolecular Interactions: from Diatomics to Biopolymers*, B. Pullman (Ed.) (Wiley, Chichester, 1978). p. 363.
25. T. Steiner, *Angew. Chem. Int. Ed.* **41**, 48 (2002).
26. T. Steiner and G. R. Desiraju, *Chem. Commun.* 891 (1998).

27. M. S. Gordon and J. H. Jensen, *Acc. Chem. Res.* **29**, 536 (1996).
28. C. Sandorfy, *Top. Curr. Chem.* **120**, 41 (1984).
29. S. Scheiner, in *Pauling's Legacy—Modern Modelling of the Chemical Bond*, Z. B. Maksic and W. J. Orville-Thomas (Eds.) (Elsevier, Amsterdam, 1977), Vol. 6 p. 571.
30. (a) J. E. Del Bene, in *The Encyclopedia of Computational Chemistry*, P. v. R. Schleyer, N. L. Allinger, T. Clark, J. Gasteiger, P. A. Kollman, H. F. Schaefer III, and P. R. Schreiner (Eds.) (Wiley, Chichester, 1998), Vol. 2. p. 1263; (b) J. E. Del Bene and M. J. T. Jordan, *Int. Rev. Phys. Chem.* **18**, 119 (1999); (c) J. E. Del Bene, in *Recent Theoretical and Experimental Advances in Hydrogen Bonded Clusters, NATO ASI Series C, Vol. 561*, S. S. Xantheas (Ed.) (Kluwer, Dordrecht, 2000), p. 309; (d) J. E. Del Bene and M. J. T. Jordan, *J. Mol. Struct. (Theochem)* **573**, 11 (2001).
31. E. Arunan, *Curr. Sci.* **77**, 1233 (1999).
32. T. W. Martin and Z. S. Derewenda, *Nat. Struct. Biol.* **6**, 403 (1999).
33. A. Allerhand and P. v. R. Schleyer, *J. Am. Chem. Soc.* **85**, 1715 (1963).
34. (a) J. F. Hinton and K. Wolinski, in *Theoretical Treatments of Hydrogen Bonding*, D. Hadži (Ed.) (Wiley, Chichester, 1997), p. 75; (b) E. D. Becker, in *Encyclopedia of Nuclear Magnetic Resonance*, D. M. Grant and R. K. Harris (Eds.) (Wiley, New York, 1996), p. 2409.
35. C. A. Coulson, *Res. Appl. Ind.* **10**, 149 (1957).
36. P. Schuster, in *The Hydrogen Bond. Recent Developments in Theory and Experiments* (North-Holland, Amsterdam, 1976), Vol. I. Theory, Ch.2.
37. I. G. Kaplan, *Theory of Molecular Interactions. Studies in Physical and Theoretical Chemistry*, (Elsevier, Amsterdam, 1986), Vol. 42.
38. M. Meot-Ner (Mautner), *Chem. Rev.* **105**, 213 (2005).
39. E. Lippert, in *The Hydrogen Bond. Recent Developments in Theory and Experiments*, (North-Holland, Amsterdam, 1976), Vol. I. Theory. Ch. 1.
40. C. L. Perrin and J. B. Nielson, *Annu. Rev. Phys. Chem.* **48**, 511 (1997).
41. S. Scheiner, *Annu. Rev. Phys. Chem.* **45**, 23 (1994) and references therein.
42. M. J. Frisch, G. W. Trucks, H. B. Schlegel, G. E. Scuseria, M. A. Robb, J. R. Cheeseman, J. A. Montgomery, Jr., T. Vreven, K. N. Kudin, J. C. Burant, J. M. Millam, S. S. Iyengar, J. Tomasi, V. Barone, B. Mennucci, M. Cossi, G. Scalmani, N. Rega, G. A. Petersson, H. Nakatsuji, M. Hada, M. Ehara, K. Toyota, R. Fukuda, J. Hasegawa, M. Ishida, T. Nakajima, Y. Honda, O. Kitao, H. Nakai, M. Klene, X. Li, J. E. Knox, H. P. Hratchian, J. B. Cross, C. Adamo, J. Jaramillo, R. Gomperts, R. E. Stratmann, O. Yazyev, A. J. Austin, R. Cammi, C. Pomelli, J. W. Ochterski, P. Y. Ayala, K. Morokuma, G. A. Voth, P. Salvador, J. J. Dannenberg, V. G. Zakrzewski, S. Dapprich, A. D. Daniels, M. C. Strain, O. Farkas, D. K. Malick, A. D. Rabuck, K. Raghavachari, J. B. Foresman, J. V. Ortiz, Q. Cui, A. G. Baboul, S. Clifford, J. Cioslowski, B. B. Stefanov, G. Liu, A. Liashenko, P. Piskorz, I. Komaromi, R. L. Martin, D. J. Fox, T. Keith, M. A. Al-Laham, C. Y. Peng, A. Nanayakkara, M. Challacombe, P. M. W. Gill, B. Johnson, W. Chen, M. W. Wong, C. Gonzalez, and J. A. Pople, *GAUSSIAN 03* (Revision A.1), Gaussian, Inc., Pittsburgh, PA, 2003.
43. R. D. Green, *Hydrogen Bonding by C-H Groups* (Macmillan, London, 1974).
44. L. J. Prins, D. N. Reinhoudt, and P. Timmerman, *Angew. Chem. Int. Ed.* **40**, 2382 (2001).
45. (a) R. H. Crabtree, P. E. M. Siegbahn, O. Eisenstein, A. L. Rheingold, and T. F. Koetzle, *Acc. Chem. Res.* **29**, 348 (1996); (b) R. H. Crabtree, *J. Organomet. Chem.* **577**, 111 (1998).
46. (a) L. Brammer, M. C. McCann, R. M. Bullock, R. K. McMullan, and P. Sherwood, *Organometallics* **11**, 2339 (1992); (b) S. G. Kazarian, P. A. Hanley, and M. Poliakov, *J. Am. Chem. Soc.* **115**, 9069 (1993); (c) A. Albinati, F. Lianza, P. S. Pregosin, and B. Müller, *Inorg. Chem.* **33**, 2522 (1994); (d) Y. Gao, O. Eisenstein, and R. H. Crabtree, *Inorg. Chim. Acta* **254**, 105 (1997); (e) L. Brammer, D. Zhao, F. T. Lapidó, and J. Braddock-Wilking, *Acta Crystallogr. Sect. B* **53**, 680 (1995); (f) D. Braga, F. Grepioni, and G. R. Desiraju, *Chem. Rev.* **98**, 1375 (1998); (g) E. S. Shubina, N. V. Belkova, and L. M. Epstein, *J. Organomet. Chem.* **17**, 536 (1997); (h) G. Orlova and S. Scheiner, *Organometallics* **17**, 4362 (1998); (i) L. M. Epstein and E. S. Shubina, *Ber.*

- Bunsenges. Phys. Chem.* **102**, 359 (1998); (j) L. M. Epstein and E. S. Shubina, *Coord. Chem. Rev.* **231**, 165 (2002); (k) L. Brammer, *Dalton Trans.* 3145 (2003); (l) N. V. Belkova, E. S. Shubina, and L. M. Epstein, *Acc. Chem. Res.* **38**, 624 (2005); and references therein.
47. (a) E. S. Kryachko and F. Remacle, in *Theoretical Aspects of Chemical Reactivity*, A. Torro-Labbe (Ed.), Vol. 16 of *Theoretical and Computational Chemistry*, P. Politzer, (Ed.) (Elsevier, Amsterdam, 2005); (b) E. S. Kryachko and F. Remacle, *Chem. Phys. Lett.* **404**, 142 (2005); (c) E. S. Kryachko and F. Remacle, *Nano Lett.* **5**, 735 (2005); (d) E. S. Kryachko, A. Karpfen, and F. Remacle, *J. Phys. Chem. A* **109**, 7309 (2005); (e) E. S. Kryachko and F. Remacle, in *Progress in Theoretical Chemistry and Physics*, J. Maruani and S. Wilson (Eds.) (Springer, Dordrecht, 2005); (f) E. S. Kryachko and F. Remacle, *J. Phys. Chem. B* **109**, 22746 (2005).
48. S. Glasstone, *Trans. Faraday Soc.* **33**, 200 (1937).
49. (a) G. F. Zellhoefer, M. J. Copley, and C. S. Marvel, *J. Am. Chem. Soc.* **60**, 1337 (1938); (b) G. F. Zellhoefer and M. J. Copley, *Ibid.* **60**, 1343 (1938); (c) M. J. Copley and C. E. Holley, Jr., *J. Chem. Soc.* **61**, 1599 (1939); (d) M. J. Copley, G. F. Zellhoefer, and C. S. Marvel, *J. Am. Chem. Soc.* **60**, 2666 (1938); (e) M. J. Copley, G. F. Zellhoefer, and C. S. Marvel, *Ibid.* **60**, 2714 (1938); (f) M. J. Copley, G. F. Zellhoefer, and C. S. Marvel, *Ibid.* **61**, 3550 (1939); (g) M. J. Copley, G. F. Zellhoefer, and C. S. Marvel, *Ibid.* **62**, 227 (1940); (h) C. S. Marvel, F. C. Dietz, and M. J. Copley, *Ibid.* **62**, 2273 (1940); (i) C. S. Marvel, M. J. Copley, and E. Ginsberg, *Ibid.* **62**, 3109 (1940); (j) C. S. Marvel, M. J. Copley, and E. Ginsberg, *Ibid.* **62**, 3263 (1940); (k) M. J. Copley, E. Ginsberg, G. F. Zellhoefer, and C. S. Marvel, *Ibid.* **63**, 254 (1941); (l) C. S. Marvel and J. H. Harkema, *Ibid.* **63**, 1609 (1941).
50. G. A. Jeffrey, *J. Mol. Struct.* **485–486**, 293 (1999).
51. (a) W. Gordy, *Phys. Rev.* **50**, 115 (1936); (b) W. Gordy, *J. Am. Chem. Soc.* **60**, 605 (1938); (c) W. Gordy, *Nature* **142**, 831 (1938); (d) W. Gordy, *J. Chem. Phys.* **7**, 93 (1939); (e) W. Gordy, *Ibid.* **7**, 163 (1939); (f) A. M. Buswell, W. H. Rodebush, and M. F. Roy, *J. Am. Chem. Soc.* **60**, 2528 (1938); (g) W. Gordy and S. C. Stanford, *J. Chem. Phys.* **8**, 170 (1940); (h) S. C. Stanford and W. Gordy, *J. Am. Chem. Soc.* **63**, 1094 (1941).
52. M. L. Huggins, *Chem. Rev.* **32**, 195 (1943).
53. (a) Z. S. Derewenda, L. Lee, and U. Derewenda, *J. Mol. Biol.* **252**, 248 (1995); (b) M. C. Wahl and M. Sundaralingam, *Trends Biochem. Sci.* **22**, 97 (1997).
54. I. Hunter, *Ann. Rep. Prog. Chem.* **43**, 141 (1947).
55. W. J. Dulmage and W. N. Lipscomb, *Acta Cryst.* **4**, 330 (1951).
56. F. V. Smallcross and G. B. Carpenter, *Acta Cryst.* **11**, 490 (1958).
57. M. W. Dougill and G. A. Jeffrey, *Acta Cryst.* **6**, 831 (1953).
58. J. Donohue, in *Selected Topics in Hydrogen Bonding in Structural Chemistry and Molecular Biology*, A. Rich and N. Davidson (Eds.) (Freeman, San Francisco, 1948). p. 443.
59. (a) D. J. Sutor, *Nature* **195**, 68 (1962); (b) D. J. Sutor, *J. Chem. Soc.* 1105 (1963).
60. (a) R. A. Musah, G. M. Jensen, R. J. Rosenfeld, D. E. McRee, and D. B. Goodin, *J. Am. Chem. Soc.* **119**, 9083 (1997); (b) Y. Mandel-Gutfreund, H. Margalit, R. L. Jernigan, and V. B. Zhurkin, *J. Mol. Biol.* **277**, 1129 (1998); (c) A. Senes, I. Ubarretxena-Belandia, and D. M. Engelman, *Proc. Natl. Acad. Sci. U.S.A.* **98**, 9056 (2001); (d) S. Yohannan, S. Faham, D. Yang, D. Grosfeld, A. K. Chamberlain, and T. U. Bowie, *J. Am. Chem. Soc.* **126**, 2284 (2004); (e) R. Taylor and O. Kennard, *J. Am. Chem. Soc.* **104**, 5063 (1982); (f) M. C. Wahl, *Trends Biochem. Sci.* **22**, 97 (1997); (g) G. A. Leonard, K. McAuley-Hecht, T. Brown, and W. N. Hunter, *Acta Cryst. Sect. D* **51**, 136 (1995); (h) T. Steiner, *Acta Cryst. Sect. D* **51**, 93 (1995); (i) P. Raveendran and S. L. Wallen, *J. Am. Chem. Soc.* **124**, 12590 (2002); (j) B. Wang, J. F. Hinton, and P. Pulay, *J. Phys. Chem. A* **107**, 4683 (2003) and references therein.
61. E. E. Astrup, *Acta Chem. Scand. A* **33**, 655 (1979).
62. H. Yoshida, I. Kaneko, H. Matsuura, Y. Ogawa, and M. Tasumi, *Chem. Phys. Lett.* **196**, 601 (1992). See also H. Yoshida, T. Tanaka, and H. Matsuura, *Chem. Lett.* 637 (1996).
63. S. Tsuzuki, T. Uchimarui, K. Tanabe, and T. Hirano, *J. Phys. Chem.* **97**, 1346 (1993).

64. (a) L. Turi and J. J. Dannenberg, *J. Phys. Chem.* **99**, 639 (1995); (b) T. Steiner, *New J. Chem.* 1099 (1998); (c) M. Brandl, K. Lindauer, M. Meyer, and J. Sühnel, *Theor. Chem. Acc.* **101**, 103 (1999); (d) M. J. Calhorda, *Chem. Commun.* 801 (2000); (e) M. Hartmann, S. D. Wetmore, and L. Radom, *J. Phys. Chem A* **105**, 4470 (2001); (f) S. Scheiner, S. J. Grabowski, and T. Kar, *Ibid.* **105**, 10607 (2001); (g) S. J. Grabowski, *J. Phys. Org. Chem.* **17**, 18 (2004) and references therein.
65. (a) H. Yoshida, T. Harada, T. Murase, K. Ohno, and H. Matsuura, *J. Phys. Chem. A* **101**, 1731 (1997); (b) T. Harada, H. Yoshida, K. Ohno, and H. Matsuura, *Chem. Phys. Lett.* **362**, 453 (2002).
66. P. J. A. Ribeiro-Claro, M. P. M. Marques, and A. M. Amado, *Chem. Phys. Chem.* **3**, 599 (2002).
67. (a) P. Hobza and Z. Havlas, *Theor. Chem. Acc.* **108**, 325 (2002); (b) W. Zierkiewicz, D. Michalska, Z. Havlas, and P. Hobza, *Chem. Phys. Chem.* **3**, 511 (2002); (c) P. Hobza, *Int. J. Quantum Chem.* **90**, 1071 (2002); (d) E. Mrázková and P. Hobza, *J. Phys. Chem. A* **107**, 1032 (2003); (e) W. Zierkiewicz, P. Jurečka, and P. Hobza, *Chem. Phys. Chem.* **6**, 609 (2005); (f) W. Zierkiewicz and P. Hobza, *Phys. Chem. Chem. Phys.* **6**, 5288 (2004); (g) J. Chocholousova, V. Spirko, and P. Hobza, *Ibid.* **6**, 37 (2004); (h) P. Hobza, *Ibid.* **3**, 2555 (2001).
68. (a) S. Scheiner, Y. Gu, and T. Kar, *J. Mol. Struct. (Theochem)* **500**, 441 (2000); (b) S. Scheiner and T. Kar, *J. Phys. Chem. A* **106**, 1784 (2002); (c) S. Scheiner, T. Kar, and J. Pattanayak, *J. Am. Chem. Soc.* **124**, 13257 (2002); (d) Y. Gu, T. Kar, and S. Scheiner, *J. Mol. Struct.* **552**, 17 (2000); (e) S. Scheiner and T. Kar, *J. Phys. Chem. B* **109**, 3681 (2005); (f) T. Kar and S. Scheiner, *J. Phys. Chem. A* **108**, 9161 (2004); (g) S. Scheiner, T. Kar, and Y. Gu, *J. Biol. Chem.* **276**, 9832 (2001); (h) S. Scheiner, *J. Phys. Chem. B* **109**, 16132 (2005).
69. (a) J. J. Dannenberg, *J. Mol. Struct. (Theochem)* **401**, 279 (1997); (b) J. J. Dannenberg, L. Haskamp, and A. Masunov, *J. Phys. Chem. A* **103**, 7083 (1999); (c) P. Salvador, S. Simon, M. Duran, and J. J. Dannenberg, *J. Chem. Phys.* **113**, 5666 (2000); (d) A. Masunov, J. J. Dannenberg, and R. H. Contreras, *J. Phys. Chem. A* **105**, 4737 (2001).
70. (a) E. S. Kryachko and T. Zeegers-Huyskens, *J. Phys. Chem. A* **105**, 7118 (2001); (b) E. S. Kryachko and T. Zeegers-Huyskens, *Ibid.* **106**, 6832 (2002); (c) E. S. Kryachko and T. Zeegers-Huyskens, *Ibid.* **107**, 7546 (2003); (d) E. S. Kryachko and T. Zeegers-Huyskens, *J. Mol. Struct.* **615**, 251 (2002).
71. X. Li, L. Liu, and H. B. Schlegel, *J. Am. Chem. Soc.* **124**, 9639 (2002).
72. (a) K. Hermansson, *J. Phys. Chem. A* **106**, 4695 (2002); (b) L. Pejov and K. Hermansson, *J. Chem. Phys.* **119**, 313 (2003).
73. (a) W. Qian and S. Krimm, *J. Phys. Chem. A* **106**, 6628 (2002); (b) W. Qian and S. Krimm, *Ibid.* **106**, 11663 (2002); (c) W. Qian and S. Krimm, *Ibid.* **109**, 5608 (2005).
74. I. V. Alabugin, M. Manoharan, S. Peabody, and F. Weinhold, *J. Am. Chem. Soc.* **125**, 5973 (2003).
75. E. Kryachko and S. Scheiner, *J. Phys. Chem. A* **108**, 2527 (2004).
76. (a) A. Karpfen and E. S. Kryachko, *J. Phys. Chem. A* **107**, 9724 (2003); (b) A. Karpfen and E. S. Kryachko, *Chem. Phys.* **310**, 77 (2005); (c) A. Karpfen, *J. Mol. Struct. (Theochem)* **710**, 85 (2004); (d) A. Karpfen and E. S. Kryachko, *J. Phys. Chem. A* **109**, 8930 (2005); (e) A. Karpfen, *J. Mol. Struct. (Theochem)* **753**, 203 (2005); (f) A. Karpfen and E. S. Kryachko, *Chem. Phys. Cederbaum Festschrift* (in press).
77. S. Scheiner, in *Advances in Molecular Structure Research*, M. Hargittai and I. Hargittai (Eds.) (JAI Press, Stamford, CT, 2000) Vol. 6. pp. 159–207.
78. (a) S. M. Melikova, K. S. Rutkowski, P. Rodziewicz, and A. Koll, *Chem. Phys. Lett.* **352**, 301 (2002); (b) P. Rodziewicz, K. S. Rutkowski, S. M. Melikova, and A. Koll, *Chem. Phys. Chem.* **6**, 1282 (2005); (c) K. S. Rutkowski, P. Rodziewicz, S. M. Melikova, W. A. Herrebout, B. J. van der Veken, and A. Koll, *Chem. Phys.* **313**, 225 (2005); (d) S. M. Melikova, K. S. Rutkowski, P. Rodziewicz, and A. Koll, *J. Mol. Struct.* **705**, 49 (2004); (e) K. S. Rutkowski, S. M. Melikova, D. N. Shchepkin, P. Lipkowski, and A. Koll, *Chem. Phys. Lett.* **325**, 425 (2000); (f) P. Rodziewicz, S. M. Melikova, K. S. Rutkowski, and F. Buda, *Chem. Phys. Chem.* **6**, 1719 (2005).

79. (a) S. Pinchas, *Anal. Chem.* **27**, 2 (1955); (b) S. Pinchas, *Ibid.* **29**, 334 (1957); (c) S. Pinchas, *Chem. Ind. (London)* 1451 (1959); (d) S. Pinchas, *J. Phys. Chem.* **67**, 1862 (1963).
80. G. Trudeau, J.-M. Dumas, P. Dupuis, M. Guérin, and C. Sandorfy, *Top. Curr. Chem.* **93**, 91 (1980).
81. S. L. Paulson and A. J. Barnes, *J. Mol. Struct.* **80**, 151 (1982). See also S. L. Paulson, Ph.D. Thesis (University of Salford, 1984).
82. M. Buděšínský, P. Fiedler, and Z. Arnold, *Synthesis* 858 (1989).
83. I. F. Tsymbal, E. V. Ryltsev, I. E. Boldeskul, and B. G. Lysak, *Khim. Fiz. (USSR)* **12**, 988 (1993).
84. M. O. Bulanin, T. D. Kolomiitsova, V. A. Kondaurov, and S. M. Melikova, *Opt. Spektrosk. (USSR)* **68**, 763 (1990).
85. K. G. Tokhadze, in *Molecular Cryospectroscopy*, Adv. Spectrosc. R. J. H. Clark and R. E. Hester (Eds.) (Wiley, Chichester, 1993), Vol. 23. p. 160.
86. I. E. Boldeskul, I. F. Tsymbal, E. V. Ryltsev, Z. Latajka, and A. J. Barnes, *J. Mol. Struct.* **436-437**, 167 (1997).
87. (a) B. J. van der Veken, W. A. Herrebout, R. Szostak, D. N. Shchepkin, Z. Havlas, and P. Hobza, *J. Am. Chem. Soc.* **123**, 12290 (2001); (b) S. N. Delanoye, W. A. Herrebout, and B. J. van der Veken, *Ibid.* **124**, 11854 (2002); (c) W. A. Herrebout, S. M. Melikova, S. N. Delanoye, K. S. Rutkowski, D. N. Shchepkin, and B. J. van der Veken, *J. Phys. Chem. A* **109**, 3038 (2005); (d) W. A. Herrebout, S. M. Delanoye, and B. J. van der Veken, *Ibid.* **108**, 6059 (2004); (e) S. N. Delanoye, W. A. Herrebout, and B. J. van der Veken, *J. Am. Chem. Soc.* **124**, 7490 (2002); (f) T. van den Kerkhof, A. Bouwen, W. A. Herrebout, and B. J. van der Veken, *Phys. Chem. Chem. Phys.* **6**, 358 (2004).
88. M. Blatchford, P. Raveendran, and S. L. Wallen, *J. Am. Chem. Soc.* **124**, 14818 (2002).
89. (a) J. L. Alonso, S. Antolínez, S. Blanco, A. Lessari, J. C. López, and W. Caminati, *J. Am. Chem. Soc.* **126**, 3244 (2004); (b) W. Caminati, S. Melandri, I. Rossi, and P. G. Favero, *J. Am. Soc.* **121**, 10098 (1999); (c) W. Caminati, S. Melandri, M. Schnell, D. Banser, J.-U. Grabow, and J. L. Alonso, *J. Mol. Struct.* **742**, 87 (2005).
90. H. Matsuura, H. Yoshida, M. Hieda, S.-ya Yamanaka, T. Harada, K. Shin-ya, and K. Ohno, *J. Am. Chem. Soc.* **125**, 13910 (2003).
91. A. J. Barnes, *J. Mol. Struct.* **704**, 3 (2004).
92. W. G. Schneider and H. J. Bernstein, *Trans. Faraday Soc.* **52**, 13 (1956).
93. N. S. Golubev, T. D. Kolomiitsova, S. M. Melikova, and D. N. Shchepkin, in *Teoret. Spektrosk. Izv. Akad. Nauk SSSR* 78 (1977).
94. J. D. Chaney, C. R. Goss, K. Folting, B. D. Santarsiero, and M. D. Hollingsworth, *J. Am. Chem. Soc.* **118**, 9432 (1996).
95. R. H. Contréras, J. E. Peralta, C. G. Giribet, M. C. Ruiz de Azua, and J. C. Faceli, *Annu. Rep. NMR Spectrosc.* **41**, 55 (2000).
96. H. M. T. Nguyen, M. T. Nguyen, J. Peeters, and T. Zeegers-Huyskens, *J. Phys. Chem. A* **108**, 11101 (2004).
97. P. Kolandaivel and V. Nirmala, *J. Mol. Struct.* **694**, 33 (2004).
98. (a) P. J. A. Ribeiro-Claro, M. P. M. Marques, and A. M. Amado, *Chem. Phys. Chem.* **3**, 599 (2002). (b) P. J. A. Ribeiro-Claro, M. G. B. Drew, and V. Félix, *Chem. Phys. Lett.* **356**, 318 (2002).
99. R. Souda, H. Kawanowa, M. Kondo, and Y. Gotoh, *J. Chem. Phys.* **120**, 5723 (2004).
100. (a) S. K. Rhee, S. H. Kim, S. Lee, and J. Y. Lee, *Chem. Phys.* **297**, 21 (2004); (b) J.-M. Fan, L. Liu, and Q.-X. Guo, *Chem. Phys. Lett.* **365**, 464 (2002); (c) P. Lu, G.-Q. Liu, and J.-C. Li, *J. Mol. Struct. (Theochem)* **723**, 95 (2005); (d) H.-C. Chang, J.-C. Jiang, C.-W. Chuang, J.-S. Lin, W.-W. Lai, Y.-C. Yang, and S. H. Lin, *Chem. Phys. Lett.* **410**, 42 (2005); (e) W. D. He, G. Zhou, N. B. Wong, A. M. Tian, and X. P. Long, *J. Mol. Struct. (Theochem)* **723**, 217 (2005); (f) S. C. Wang and S. L. Lee, *Chem. Phys. Lett.* **406**, 143 (2005); (g) X. Wang, G. Zhou, A. M. Tian, and N. B. Wong, *J. Mol. Struct. (Theochem)* **718**, 1 (2005); (h) H. C. Chang, J. C.

- Jiang, C. C. Su, L. C. Lu, C. J. Hsiao, C. W. Chuang, and S. H. Lin, *J. Phys. Chem. A* **108**, 11001 (2004); (i) Z. Xu, H. R. Li, C. M. Wang, T. Wu, and S. J. Han, *Chem. Phys. Lett.* **394**, 405 (2004); (j) Y. Fang, J.-M. Fan, L. Liu, X.-S. Li, and Q.-X. Guo, *Chem. Lett.* 116 (2002); (k) Y. Feng, S. W. Zhao, L. Liu, J. T. Wang, X. S. Li, and Q. X. Guo, *J. Phys. Org. Chem.* **17**, 1099 (2004); (l) Y. Feng, L. Liu, J. T. Wang, X. S. Li, and Q. X. Guo, *Chem. Commun.* 88 (2004); (m) R. Zhang, H. Li, Y. Lei, and S. Han, *J. Mol. Struct.* **693**, 17 (2004); (n) W.-D. He, G. Zhou, N.-B. Wong, A.-M. Tian, and X.-P. Long, *J. Mol. Struct. (Theochem)* **723**, 217 (2005); (o) G. Zhou, J.-L. Zhang, N.-B. Wong, and A. Tian, *Ibid.* **639**, 43 (2003); (p) W. Wang, A. Tian, and N.-B. Wong, *J. Phys. Chem. A* **109**, 8035 (2005); (q) Y. Yong, W. Zhang, S. Pei, J. Shao, W. Huang, and X. Gao, *J. Mol. Struct. (Theochem)* **732**, 33 (2005).
101. I. Alkorta and S. Maluendes, *J. Phys. Chem.* **99**, 6457 (1995).
102. A. Kaldor and I. M. Mills, *Spectrochim. Acta A* **20**, 523 (1964).
103. E. Cubero, M. Orozco, and F. J. Luque, *Chem. Phys. Lett.* **310**, 445 (1999). See also P. Kolandaivel and V. Nirmala, *J. Mol. Struct.* **694**, 33 (2004).
104. J. E. Monat, R. R. Toczylowski, and S. M. Cybulski, *J. Phys. Chem. A* **105**, 9004 (2001).
105. Y. Futami, S. Kudoh, M. Takayanagi, and M. Nakata, *Chem. Phys. Lett.* **357**, 209 (2002).
106. A. Kovacs, A. Szabo, D. Nemcsok, and I. Hargittai, *J. Phys. Chem. A* **106**, 5671 (2002).
107. M. A. Blatchford, P. Raveendran, and S. L. Wallen, *J. Am. Chem. Soc.* **124**, 14818 (2002).
108. Y. Tatamitani, B. Liu, J. Shimada, T. Ogata, P. Ottaviani, A. Maris, W. Caminati, and J. Alonso, *J. Am. Chem. Soc.* **124**, 2739 (2002).
109. (a) W. Caminati, S. Melandri, P. Moreschini, and P. G. Favero, *Angew. Chem. Int. Ed. Engl.* **38**, 2924 (1999); (b) W. Caminati, J. C. Lopez, J. L. Alonso, and J.-U. Grabow, *Angew. Chem. Int. Ed. Engl.* **44**, 3841 (2005).
110. S. Vijayakumar and P. Kolandaivel, *J. Mol. Struct.* **734**, 157 (2005).
111. A. J. Barnes and T. R. Beech, *Chem. Phys. Lett.* **94**, 568 (1983).
112. K. Mizuno, S. Imafuji, T. Ochi, T. Ohta, and S. Meada, *J. Phys. Chem. B* **104**, 11001 (2000).
113. S. Blanco, J. C. López, A. Lesarri, and J. L. Alonso, *J. Mol. Struct.* **612**, 255 (2002).
114. S. Tsuzuki, T. Uchimarui, M. Mikami, and S. Urata, *J. Phys. Chem. A* **107**, 7962 (2003).
115. (a) E. S. Kryachko and J. R. Sabin, *Int. J. Quantum Chem.* **91**, 695 (2003); (b) E. S. Kryachko, in *Fundamental World of Quantum Chemistry: A Tribute Volume to the Memory of Per-Olov Löwdin*, E. J. Brändas and E. S. Kryachko (Eds.) (Kluwer, Dordrecht, 2003), Vol. 2. pp. 583–629.
116. P. Hobza and V. Spirko, *Phys. Chem. Chem. Phys.* **5**, 1290 (2003).
117. P. Hobza, J. Spöner, E. Cubero, M. Orozco, and F. J. Luque, *J. Phys. Chem. B* **104**, 6286 (2000).
118. E. Nir, Ch. Janzen, P. Imhof, K. Kleinermanns, and M. S. de Vries, *Phys. Chem. Chem. Phys.* **4**, 740 (2002).
119. S. Wojtulewski and S. J. Grabowski, *Chem. Phys.* **309**, 183 (2005).
120. H. M. Muchall, *J. Phys. Chem. A* **105**, 632 (2001).
121. (a) A. Lignell, L. Khriachtchev, M. Pettersson, and M. Räsänen, *J. Chem. Phys.* **117**, 961 (2002); (b) A. Lignell, L. Khriachtchev, M. Pettersson, and M. Räsänen, *Ibid.* **118**, 11120 (2003); (c) S. A. C. McDowell, *Ibid.* **118**, 4066 (2003); (d) S. A. C. McDowell, *Phys. Chem. Chem. Phys.* **5**, 808 (2003); (e) S. A. C. McDowell, *Chem. Phys. Lett.* **368**, 649 (2003); (f) S. A. C. McDowell, *J. Chem. Phys.* **118**, 7283 (2003); (g) S. A. C. McDowell, *Ibid.* **119**, 3711 (2003); (h) S. A. C. McDowell and A. D. Buckingham, *Spectrochim Acta Part A* **61**, 1603 (2005); (i) S. A. C. McDowell and A. D. Buckingham, *Mol. Phys.* **103**, 257 (2005); (j) S. A. C. McDowell, *J. Mol. Struct. (Theochem)* **625**, 243 (2003); (k) S. A. C. McDowell, *Ibid.* **674**, 227 (2004); (l) S. A. C. McDowell, *Ibid.* **715**, 73 (2005); (m) I. V. Alabugin, M. Manoharan, and F. A. Weinhold, *J. Phys. Chem. A* **108**, 4720 (2004).
122. (a) R. K. Castellano, *Curr. Org. Chem.* **8**, 845 (2004); (b) F. A. Cotton, L. M. Daniels, G. T. Jordan IV, and C. A. Murillo, *Chem. Commun.* 1673 (1997).

123. (a) C. Rovira and J. J. Novoa, *Chem. Phys. Lett.* **279**, 140 (1997); (b) J. J. Novoa, P. Lafuente, and F. Mota, *Ibid.* **290**, 519 (1998).
124. C. B. Aakeröy and K. R. Seddon, *Chem. Soc. Rev.* **22**, 397 (1993).
125. V. V. Bertcev, N. S. Golubev, and D. N. Shchepkin, *Opt. Spectrosk. (USSR)* **40**, 951 (1977).
126. B. Nelander, *J. Mol. Struct.* **69**, 59 (1980).
127. D. C. Burleigh, A. B. McCoy, and E. L. Sibert III, *J. Chem. Phys.* **104**, 480 (1998).

CHAPTER 9

HYDROGEN–HYDROGEN BONDING: THE NON-ELECTROSTATIC LIMIT OF CLOSED-SHELL INTERACTION BETWEEN TWO HYDROGEN ATOMS. A CRITICAL REVIEW

CHÉRIF F. MATTA

*Department of Chemistry, Dalhousie University, Halifax, Nova Scotia, Canada B3H 4J3 and
Department of Chemistry, McMaster University, Hamilton, Ontario, Canada L8S 4M1.*

Abstract This chapter reviews some of the recent work about hydrogen–hydrogen bonding (an essentially non-electrostatic closed-shell interaction) and contrasts it with dihydrogen bonding (a predominantly electrostatic closed-shell interaction). These two modes are shown to represent the two extremes of a continuum of closed-shell interactions between pairs of hydrogen atoms in molecules.

Keywords: Hydrogen bonding; hydrogen–hydrogen bonding; dihydrogen bonding; topology of the electron density; quantum theory of atoms in molecules (QTAIM); bond path.

A class must be defined in terms of observable properties, and this often introduces difficulties of two kinds. The first difficulty is associated with the fact that most properties can vary continuously, at least from a practical viewpoint, so that clean-cut separations of things are often somewhat arbitrary. . . . The other difficulty concerns the fact that it is often necessary to amend definitions many times in order that the class may continue to be useful [1].

E. B. Wilson, Jr. (1952)

1 INTRODUCTION

In a typical first year textbook, the hydrogen bond is introduced as a largely electrostatic interaction in which a negatively charged heteroatom **X** is covalently bonded to a positively charged hydrogen atom which in turn attracts another negatively charged heteroatom **B**. The hydrogen bond is, thus, symbolically denoted by $\mathbf{X}^{\delta-}-\mathbf{H}^{\delta+}\cdots\mathbf{Y}^{\delta-}-\mathbf{Z}^{\delta+}$, where the **X–H** group is known as

the hydrogen donor (or electron acceptor) and atom **Y**, which usually possesses a lone pair, as the hydrogen acceptor (or electron donor). The stabilisation arising from hydrogen bonding is primarily a result of Coulombic attraction which also imparts this bonding interaction with its directional nature.

In addition to this broad class of “conventional” hydrogen bonds, several non-conventional variants also exist in nature [2–7]. For example, hydrogen bonds occur in systems with non-conventional hydrogen acceptors, such as isonitriles [8, 9], carbanions [10, 11], carbenes and silynes [12], π -systems [8, 9, 13]. Non-conventional hydrogen bonds also include those known as hydridic, also termed “inverse hydrogen bonds” since they are characterised by an inverted polarity [9], that is $\text{X}^{\delta+}-\text{H}^{\delta-}\cdots\text{Y}^{\delta+}$, and a newly characterised $\pi\cdots\text{H}^{\delta+}\cdots\pi$ bonding interaction [14]. Koch and Popelier presented for the first time a complete characterisation of the hydrogen bond on the basis of the topological properties of the electron density [15].

The domain of the hydrogen bond was further enlarged with the discovery of the *dihydrogen bond* in the 1990s by Crabtree et al. [16–21] and by others [22–24]. These groups reported unusually short $\text{H}\cdots\text{H}$ contacts, $d_{\text{H}\cdots\text{H}} = 1.7\text{--}2.2\text{ \AA}$ (significantly shorter than twice the van der Waals radius of a hydrogen atom, $\sim 2.4\text{ \AA}$) [25], in X-ray crystallographic structures of organometallics. The dihydrogen bonds are generally of the type $\text{X}^{\delta-}-\text{H}^{\delta+}\cdots\text{H}^{\delta-}-\text{M}^{\delta+}$ [19], where **M** is a metal atom such as Ir, and **X** is an electronegative atom such as O or N [17], or of the type $\text{N}^{\delta-}-\text{H}^{\delta+}\cdots\text{H}^{\delta-}-\text{B}^{\delta+}$ as revealed by neutron diffraction crystallography of BH_3NH_3 [18, 20].

The dihydrogen bond is thus a type of hydrogen bond in which the acceptor happens to be a hydrogen atom bearing a negative charge due to its bonding to a less electronegative atom such as a metal atom. The qualifier “dihydrogen” is a good choice since, in my opinion, it stresses the fact that this is a hydrogen bonding interaction, it just happens to have a second hydrogen as the acceptor. As any other hydrogen bond, a major source of stability in the dihydrogen bonds is electrostatic including for example dominant dipole–monopole and dipole–dipole contributions. The dihydrogen bond is the subject of considerable current theoretical [3, 26–40] and chemical informatics [41] interest and has been fully characterised based on the topological properties of the electron density [26].

In contrast to this largely electrostatic and rather directional interaction, evidence also suggests that a closed-shell stabilising interaction can occur between hydrogen atoms that are electrically neutral, close to electrical neutrality, or bearing identical or similar charges. The identity or similarity of these charges is due to molecular symmetry or similarity of the electronic environment, respectively, of the two hydrogen atoms involved in this bonding. To my knowledge, the earliest definitive low temperature neutron diffraction crystallographic report of a very short intramolecular $\text{H}\cdots\text{H}$ contact ($d_{\text{H}\cdots\text{H}} = 1.713(3)\text{ \AA}$, in norbornene derivatives) was published as early as 1983 [42]. In another experimental study, Reid et al [43], were able to obtain an isotropic interaction potential for $(\text{CH}_4)\cdots(\text{CH}_4)$ from crossed molecular

beam experiments with $D_e \sim 0.40$ kcal/mol at a carbon–carbon separation ($d_{C\dots C}$) of 4.02 Å, data consistent with a previous, also isotropic, experimental determination ($D_e \sim 0.35$ kcal/mol at $d_{C\dots C} = 4.18$ Å) [44]. These results were reproduced in a theoretical study in the cases of two (out of six) possible arrangements of the CH₄ dimer (D_{2h} and D_{3d}) [45]. For these two geometries, D_e was found to be 0.22 and 0.30 kcal/mol with an equilibrium $d_{C\dots C}$ separation of 4.256 and 3.765 Å, respectively [45], at the MP2/6-311G(2d,2p) level of theory after correction for basis set superposition error (BSSE) by the counterpoise (CP) method [46, 47]. MP2 calculations performed on the remaining geometrical arrangements with a variety of basis sets, with and without BSSE correction, showed that all (CH₄) \cdots (CH₄) complexes are bound (with energies ranging from 0.06 to 0.43 kcal/mol, the shortest $d_{H\dots H}$ in each system ranging from 2.226 to 3.447 Å, and $d_{C\dots C}$ from 3.765 to 4.868 Å) [45].

Thus, based on energetic considerations obtained from experiment and from theory, it becomes clear that systems with C–H \cdots H–C in which there is no net electrical charges on the hydrogen atoms (or very small charges of the same sign) can exhibit energetic stability, potentials typical of bound systems, and stable equilibrium geometries. The absence, identity, or close similarity of the electrical charges on the hydrogen atoms obviously sets this type of interaction apart from dihydrogen bonding, or for that matter, from hydrogen bonding all together. On these grounds, interactions of the type C–H \cdots H–C deserve a separate class since they cannot be regarded as variants of the hydrogen bond, lacking, as they do, a donor and an acceptor. We have suggested, therefore, to refer to this interaction as *hydrogen–hydrogen bonding* [48] (or in short, H–H bonding) to distinguish it from dihydrogen bonding. The qualifier “hydrogen–hydrogen” emphasises the similarity of these two atoms by listing them on an equal footing.

Several experimental [42, 49–56], theoretical [27, 48, 57–62], and informatics [41] studies report intermolecular [41, 50, 51, 54–56, 60] and intramolecular [27, 40, 42, 48, 49, 52, 53, 57–59, 61, 62] H–H bonding interactions, the majority referring to it as “dihydrogen bonding”, and some referring to it as a non-bonding repulsive interaction [57] or “non-bonded distance” [42]. In this chapter we will review some of the evidence showing that this interaction is indeed stabilising, and hence should be described as a “bonding interaction”. It is unfortunate that, so far, the majority of publications about closed-shell interactions between a pair of hydrogen atoms do not discriminate between H–H bonding and dihydrogen bonding and lump them together under the designation “dihydrogen bonding”. One of the goals of this chapter is to encourage authors and educators to clearly indicate which end of the continuum they refer to, since H–H bonding is qualitatively different than dihydrogen bonding.

In the spirit of the opening quote of this chapter, the quantum theory of atoms in molecules (QTAIM) [63] has been extensively applied to classify and understand bonding interactions in terms of a quantum mechanical observable: the electron density $\rho(\mathbf{r})$. In this chapter we will take advantage of this theory to

draw the distinction between the two ends of the hydrogen–hydrogen bonding–dihydrogen bonding continuum, with a particular focus on the former.

In view of the explosion of literature on the topic, and despite my best effort, I may have missed important and/or relevant literature. If this is so, I do apologise to the reader and to the author(s) whom I could have missed unintentionally. Some of the material here complements [64] what has already been published (see in particular Ref. [48]) and effort was made to keep duplication at a minimum.

2 SOME BASIC CONCEPTS OF THE QUANTUM THEORY OF ATOMS IN MOLECULES (QTAIM)

Parallel to the exciting reports about new types of hydrogen–hydrogen interactions, a paradigm shift was (and is) taking place in interpretative theoretical chemistry. Since the publication of Bader’s classic monograph in 1990 [63], the quantum theory of atoms in molecules (QTAIM) has become a standard tool for the interpretation of theoretical and experimental [65–69] electron density distribution maps. The theory and its applications have been reviewed on a number of occasions by its principal author [63, 70–78] and by others [65–67, 69, 79–84]. A brief reminder of some of the basic concepts of QTAIM will be presented here with the sole purpose of keeping this chapter self-contained, but the interested reader is referred to the previously cited literature for in-depth treatments.

The starting point in QTAIM is the topology of the electron density $\rho(\mathbf{r})$. The topology of the density dictates a natural partitioning of the molecular space into disjoint, generally mononuclear regions (with the uncommon exception when non-nuclear attractors are present [85, 86]), which are identified as atoms in molecules, or AIMS. The atoms in a molecule are bounded by *surfaces of zero-flux* in the gradient vector field of the electron density, i.e., the surfaces bounding each atom are not crossed by any of the gradient vectors ($\nabla\rho(\mathbf{r})$) at any point belonging to the surface (see Fig. 1). A zero-flux surface is also sometimes referred to as an *interatomic surface* (IAS). All points belonging to a zero-flux surface satisfy the condition:

$$(1) \quad \nabla\rho(\mathbf{r}) \cdot \mathbf{n}(\mathbf{r}) = 0$$

where \mathbf{r} is the position vector and $\mathbf{n}(\mathbf{r})$ is the unit vector normal to the surface.

Figure 1a is a plot of the electron density and its associated gradient vector field of a planar molecule BF_3 in the molecular plane. The figure illustrates how the zero-flux surfaces partition the molecular space into disjoint mononuclear regions, namely *atomic basins*, and how such surfaces differ from an arbitrary surface for which $\nabla\rho(\mathbf{r}) \cdot \mathbf{n}(\mathbf{r}) \neq 0$. The left half of Fig. 1a is a contour plot of the electron density $\rho(\mathbf{r})$, the contours increase in value as they approach the nuclei. Each contour line is a line with a constant value of the electron density.

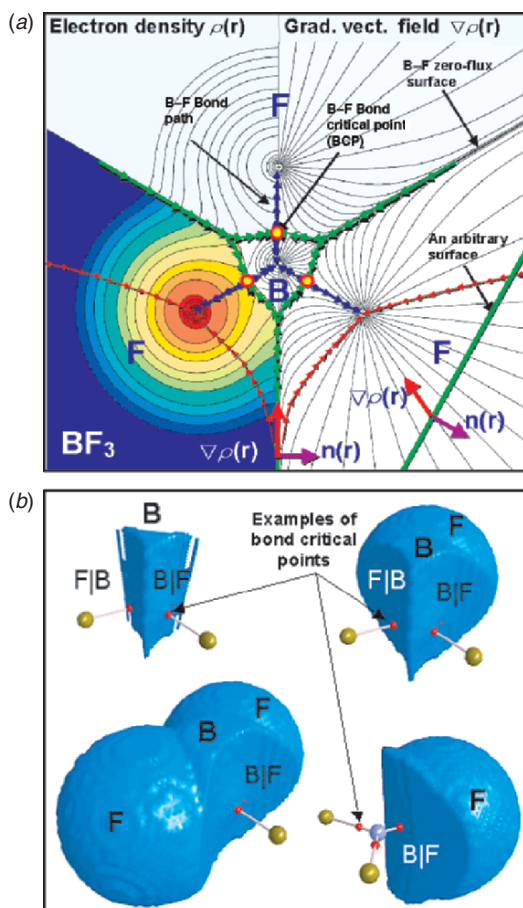


Figure 1 (see color section). (a) Plot of the electron density distribution (left) and the associated gradient vector field of the electron density (right) in the molecular plane of BF_3 . The lines connecting the nuclei (denoted by the blue arrows) are the lines of maximal density in space, the B–F bond paths, and the lines delimiting each atom (green arrows) are the intersection of the respective interatomic zero-flux surface with the plane of the drawing. The density contours on the left part of the figure increase from the outermost 0.001 au isodensity contour in steps of 2×10^n , 4×10^n , and 8×10^n au with n starting at -3 and increasing in steps of unity. The three bond critical points (BCPs) are denoted by the small red circles on the bond paths. One can see that an arbitrary surface does not satisfy the dot product in Eq. 1 since in this case the vectors are no longer orthogonal. (b) Three-dimensional renderings of the volume occupied by the electron density with atomic fragments in the BF_3 molecule up to the outer 0.002 au isodensity surface. The interatomic zero-flux surfaces are denoted by the vertical bars between the atomic symbols, F|B. The large spheres represent the nuclei of the fluorine atoms (golden) and of the boron atom (blue-grey). The lines linking the nuclei of bonded atoms are the bond paths and the smaller red dots represent the BCPs.

The right half of Fig. 1a depicts the gradient vector field $\nabla\rho(\mathbf{r})$ associated with the density. The gradient vector lines represent the directions of steepest ascent from infinity and converging onto the nuclei (with the exception of the finite set of lines that terminate, each, at a bond critical point which is defined below). It is immediately apparent from the figure that the gradient vector field lines partition the molecular space into four separate atomic basins, three fluorine basins and one boron basin at the centre of the figure (in Fig. 1a, the atomic basin of one fluorine atom is shaded in grey, another is coloured, the third as well as the central boron atoms are left without shading or colours).

QTAIM provides a definitive answer to the question of whether two atoms are bonded or not even in ambiguous cases [87, 88] and, as a consequence, the molecular graph, i.e., the chemical *structure*, is readily defined by this theory. Two atoms are bonded if their nuclei are linked in space by a line of maximal electron density termed the *bond path* [89, 90] (see Fig. 1). A single bond path links the nuclei of chemically bonded atoms irrespective of the mode of the bonding: covalent (single or multiple), hydrogen, van der Waals, ionic, metallic, etc. The properties of the electron density determined at the point of lowest density along the bond path, where

$$(2) \quad \nabla\rho = \mathbf{i}\frac{\partial\rho}{\partial x} + \mathbf{j}\frac{\partial\rho}{\partial y} + \mathbf{k}\frac{\partial\rho}{\partial z} = \vec{\mathbf{0}}$$

are a basis for the classification of bonding interactions both qualitatively (covalent/shared, polar-covalent, or closed-shell) and quantitatively (bond order/bond strength) [63]. Points in the electron density satisfying Eq. 2 are termed *critical points* (CPs) and the critical point that falls on the bond path between the nuclei of two bonded atoms is called *bond critical point* (BCP). It is at the BCP that the bond path intersects with the zero-flux interatomic surface shared by the two bonded atoms (see Fig. 1).

Thus, while “a bond” has no definition in physics and is not an observable, a bonding interaction is well characterised in terms of observable physical quantities measured at the BCP. The collection of all bond paths found in a molecule defines the *molecular graph*. Every molecular graph is mirrored in space by a “shadow” graph composed of the lines of maximally negative potential energy density, i.e., lines of “maximal stability” in space, linking the same nuclei which are linked by a bond path [91]. The line of maximally negative potential energy density linking the nuclei of two bonded atoms is termed a “*virial path*” and the shadow graph composed of all the virial paths in a system is referred to as the “*virial graph*”. This line of maximal stability that always connects the same nuclei sharing a bond path brings the chemist’s intuition associating stability to bonding into the realm of physical three-dimensional space.

Traditionally, the full power of quantum mechanics was only applicable to whole undivided (closed) systems such as an isolated molecule, a crystal, an isolated atom, whether unperturbed or bathed in an external field. Before the

inception of QTAIM [92], there seemed to be no way to obtain the quantum expectation value of an operator averaged over an *open quantum system*, that is, a system capable of exchanging matter and energy with its surrounding such as an atom within a molecule.

Bader has shown that the topological partitioning of the molecules into atomic basins coincides with the requirements of formulating quantum mechanics for open systems [93], and in this way all the so-called theorems of quantum mechanics can be derived for an open system [94]. Furthermore, the zero-flux condition, Eq. 1, turns out to be the necessary constraint for the application of Schwinger's principle of stationary action [95] to a part of a quantum system [93]. The successful application of QTAIM to numerous chemical problems has thus deep physical roots since it is a theory which expands and generalises quantum mechanics themselves to include open and total systems, both treated on equal formal footing.

The partitioning of the molecular space into well-defined disjoint atomic basins is a necessary requirement for translating the chemist's intuition of expressing molecular properties in terms of atomic and group contributions. In this manner, the expectation value of an observable averaged over all the molecular space is equal to that obtained from the sum of the expectation values of this operator averaged over all the atoms in the molecule (or in the extended system or crystal), and one can write

$$\begin{aligned}
 \langle \hat{A} \rangle_{\text{molecule}} &= \sum_i^{\text{all atoms in the molecule}} \left(N \int_{\Omega_i} \left\{ \int \frac{1}{2} [\Psi^* \hat{A} \Psi + (\hat{A} \Psi)^* \Psi] d\tau' \right\} d\mathbf{r} \right) \\
 (3) \qquad \qquad \qquad &= \sum_i^{\text{all atoms in the molecule}} \left(\int_{\Omega_i} \rho_A d\mathbf{r} \right) = \sum_i^{\text{all atoms in the molecule}} A(\Omega_i)
 \end{aligned}$$

where $\langle \hat{A} \rangle_{\text{molecule}}$ is the molecular expectation value of the operator \hat{A} , $A(\Omega_i)$ is the average value of the property A over the volume Ω_i of the i th atom in the molecule, the symbol $\int d\tau'$ implies integration over the coordinates of all electrons but one and summation over all spins, and N is the total number of electrons in the molecule.

Equation 3 expresses any global (molecular) property as a sum of atomic contributions, each obtained by averaging the appropriate operator over the volume of the atom. This partitioning takes advantage of the fact that all molecular properties can be expressed in terms of corresponding densities in three-dimensional space $\rho_A(\mathbf{r})$. An atomic population, for example, is the expectation values of the number operator averaged over the atomic basin in questions, and is, thus, a quantum mechanical observable [96, 97]. As a second example, in Sect. 4 we will see how the energy density is used to define the energy of an atom in a molecule.

The QTAIM atomic properties have been applied in numerous fields (see, for example, the reviews in Refs. [70, 96] and references therein). Even molecular vibration-induced changes in QTAIM properties, such as changes in atomic polarisabilities and in atomic dipolar polarisations, have been used for the accurate prediction of Raman [98–101] and infrared [102–104] intensities, respectively.

3 THE CLASSIFICATION OF BONDING INTERACTIONS ACCORDING TO QTAIM

3.1 Electron Density at the Bond Critical Point

The strength of a chemical bond, reflected in its bond order (BO), is strongly correlated to the electron density at the BCP (ρ_b) [63]:

$$(4) \quad \text{BO} = \exp[a(\rho_b - b)]$$

where a and b are constants dependent on the nature of the bonded atoms. Generally, $\rho_b > 0.20$ au for shared or polar interactions (covalent bonding) and < 0.10 au for closed-shell interactions (ionic, van der Waals, hydrogen, dihydrogen, H–H bonding, etc.)

The electron density at the BCP has been shown to be strongly correlated with the binding energy for several hydrogen bonded systems, a separate regression being necessary for each class of hydrogen bonding (see, for example, Refs. [31, 35, 105–109]).

3.2 Laplacian of the Electron Density at the Bond Critical Point

The trace of the diagonalised Hessian matrix is known as the Laplacian which is written explicitly:

$$(5) \quad \nabla^2 \rho(\mathbf{r}) = \nabla \cdot \nabla \rho(\mathbf{r}) = \underbrace{\frac{\partial^2 \rho(\mathbf{r})}{\partial x^2}}_{\lambda_1} + \underbrace{\frac{\partial^2 \rho(\mathbf{r})}{\partial y^2}}_{\lambda_2} + \underbrace{\frac{\partial^2 \rho(\mathbf{r})}{\partial z^2}}_{\lambda_3}$$

When evaluated at the BCP, $\nabla^2 \rho_b$ is the sum of two negative curvatures perpendicular to the bond path (λ_1 and λ_2) and a positive curvature (λ_3) tangent to it (by convention, $|\lambda_1| > |\lambda_2|$). In a shared interaction, the two negative curvatures dominate as density is accumulated between the nuclei, therefore ρ_b is large and $\nabla^2 \rho_b < 0$. In a typical C–H bond, for instance, $\rho_b = 0.29$ au and $\nabla^2 \rho_b = -1.1$ au. On the other hand, in a closed-shell interaction the density is depleted in the region of contact of the two atoms and hence ρ_b is small and $\nabla^2 \rho_b > 0$. A hydrogen bond such as N–(H···O)=C, for example, has $\rho_b = 0.01$ au and $\nabla^2 \rho_b = +0.03$ au. In polar bonding, e.g. C–X (e.g., X = O, N, F), there is a significant charge accumulation between the

nuclei, as in any shared interactions, but the Laplacian in this type of bonding can be of either sign.

3.3 Bond Ellipticity

The ellipticity, defined as $\varepsilon = (\lambda_1/\lambda_2 - 1)$, measures the preferential accumulation of electron density in a given plane containing the bond path at the BCP. When $\varepsilon = 0$, in other words when $\lambda_1 = \lambda_2$, the bond is cylindrically symmetrical. The extent of the departure from cylindrical symmetry measures the π -character of the bonding up to the limit of the “double bond” for which the ellipticity is maximal. The ellipticity decreases again with an increasing triple bond character since at the limit of $\text{BO} = 3$ the bonding regains its cylindrical symmetry (having two perpendicular π -bonding interactions). A carbon–carbon bond with $\varepsilon = 0$ includes $\text{H}_3(\text{C}-\text{C})\text{H}_3$ for example, this value rises to 0.23 in benzene and 0.45 in ethylene to fall back to zero for acetylene.

3.4 Energy Densities at the Bond Critical Point

Energy densities are determined by the one-electron density matrix and when determined at the BCP they provide a means to classify chemical bonding. The potential energy density $\mathcal{V}(\mathbf{r})$, also known as the virial field, is the average effective potential field felt by a single electron at point \mathbf{r} in a many-particle system. At an equilibrium geometry, the integral of $\mathcal{V}(\mathbf{r})$, which is negative everywhere, yields the total potential energy of the molecule. The virial field, the kinetic energy density, and the Laplacian are interrelated through the local expression of the virial theorem, which when written for a stationary state is [63, 77, 93]:

$$(6) \quad \left(\frac{\hbar^2}{4m}\right) \nabla^2 \rho(\mathbf{r}) = 2G(\mathbf{r}) + \mathcal{V}(\mathbf{r})$$

where

$$(7) \quad G(\mathbf{r}) = \frac{\hbar^2}{2m} N \int d\tau' \nabla \Psi^* \cdot \nabla \Psi$$

where $G(\mathbf{r})$ is the gradient kinetic energy density and Ψ is an antisymmetric many-electron wave function.

The application of the local virial theorem at the BCP implies that interactions for which $\nabla^2 \rho_b < 0$ are dominated by a local lowering of the potential energy, while those for which $\nabla^2 \rho_b > 0$ are dominated by a local excess in the kinetic energy (since $G(\mathbf{r}) > 0$ and $\mathcal{V}(\mathbf{r}) < 0$, always).

To compare the kinetic and potential energy densities on an equal standing, instead of the 2:1 virial ratio, Cremer and Kraka [110] evaluate the total electronic energy density at the BCP:

$$(8) \quad H_b = G_b + \mathcal{V}_b$$

which when integrated over the whole space yields the total electronic energy. H_b assumes negative values for all interactions with significant sharing of electrons, its magnitude reflecting the “covalent character” of the interaction [110].

3.5 Electron Delocalisation (Exchange) Between Bonded atoms as a Measure of Bond Order

The bond order traditionally means the number of electron pairs *shared* between two bonded atoms. The sharing of electrons between any two atoms in a molecule is measured by the delocalisation index $\delta(A,B)$. This index is the magnitude of the exchange of the electrons in the basin of atom A with those in the basin of atom B [111]:

$$(9) \quad \delta(A,B) = 2|F^\alpha(A,B)| + 2|F^\beta(A,B)|$$

where

$$(10) \quad \begin{aligned} F^\sigma(A,B) &= - \sum_i \sum_j \int_A d\mathbf{r}_1 \int_B d\mathbf{r}_2 \{ \phi_i^*(\mathbf{r}_1) \phi_j(\mathbf{r}_1) \phi_j^*(\mathbf{r}_2) \phi_i(\mathbf{r}_2) \} \\ &= - \sum_i \sum_j S_{ij}(A) S_{ji}(B) \end{aligned}$$

where $S_{ij}(A) = S_{ji}(A)$ is the overlap integral of two spin orbitals over a region A , and σ represents spin (α or β).

A delocalisation index can be calculated between any two atoms in a molecule, a complex, or a crystal, whether these two atoms are bonded or not. When $\delta(A,B)$ is calculated for two *bonded* atoms it is a measure of the bond order between them [111, 112]. Since ρ_b and the BO are strongly correlated (Eq. 4), Matta and Hernández-Trujillo suggested to calibrate this correlation using the delocalisation index rather than arbitrarily assigned bond orders [113]:

$$(11) \quad \delta(A, B) = \exp[a(\rho_b - b)]$$

3.6 Classification of Bonding Interactions

Bianchi et al. present a concise pictorial summary of the QTAIM characterisation and classification of bonding interactions in the conclusion of their paper about the electron density of $\text{Mn}_2(\text{CO})_{10}$ [114]. Figure 2 is an adaptation (with modifications) of their scheme. The classification is to be taken as a general guide since exceptions and special cases do arise as one attempts to draw a correspondence between classical bonding descriptors (ionic, covalent, etc.) and quantum mechanical quantities.

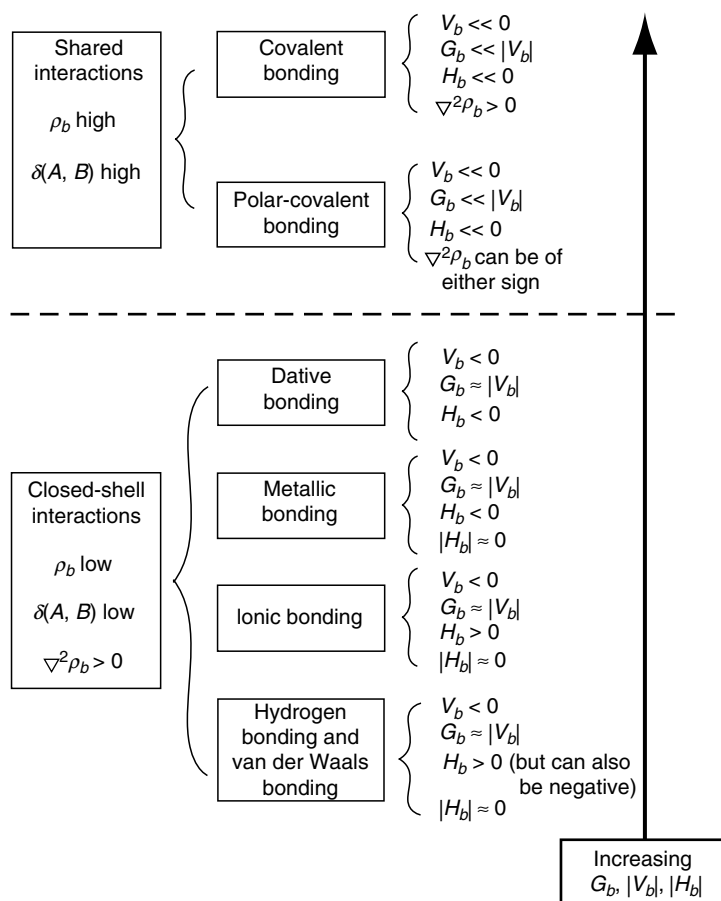


Figure 2. Classification of chemical bonding (adapted with modifications after Ref. [114]).

4 ATOMIC ENERGIES

Since the atomic energies are used to complement the characterisation of the H–H bonding by unravelling regions of local stabilisation or destabilisation within the molecule, a brief discussion of how these energies are obtained is recapped here (see Bader’s book [63] for a complete treatment).

4.1 The Partitioning of the Total Molecular Energy into Atomic Contributions

An expression alternative to Eq. 7 can be written for the kinetic energy density:

$$(12) \quad K(\mathbf{r}) = -\frac{\hbar^2}{4m} N \int d\tau' [\Psi \nabla^2 \Psi^* + \Psi^* \nabla^2 \Psi]$$

the two expressions being related by

$$(13) \quad K(\mathbf{r}) = G(\mathbf{r}) - \frac{\hbar^2}{4m} \nabla^2 \rho(\mathbf{r})$$

From Eq. 13, it is clear that the integral of the kinetic energy densities $K(\mathbf{r})$ and $G(\mathbf{r})$ over an arbitrary volume (ω) would generally yield two different values, since the integral of the term proportional to $\nabla^2 \rho(\mathbf{r})$ does not generally vanish when the integral is over an arbitrary volume. Obtaining two different values for the kinetic energy of the same region of space depending on which (equivalent) expression one uses is clearly physical nonsense. One can therefore say that the kinetic energy is not well-defined for an arbitrary region of space. As a corollary, *the kinetic energy of an open system is well-defined if the integral of the Laplacian over that system vanishes*, since this is the only way that would result in the equality $K(\omega) = G(\omega)$. The Laplacian integral vanishes over the total system (as expected) and only over “proper” open systems, designated as “proper” since they are the only open systems (out of an infinity of possible open systems) for which the kinetic energy is well defined. To see this point more clearly, we write the integral of Eq. 13 over ω :

$$(14) \quad K(\omega) = G(\omega) - \frac{\hbar^2}{4m} N \int_{\omega} d\tau' \nabla \cdot \nabla \rho$$

The volume integral in the right-hand side of Eq. 14 can be transformed into a surface integral:

$$(15) \quad K(\omega) = G(\omega) - \frac{\hbar^2}{4m} N \int dS(\omega, \mathbf{r}) \nabla \rho \cdot \mathbf{n}(\mathbf{r})$$

The second term in the right-hand side vanishes only for systems bounded by a zero-flux surface, i.e., satisfying Eq. 1. Such systems include the total system and proper open systems such as atoms in molecules. A proper open system will be referred to as Ω to distinguish it from an arbitrary bounded region of space ω .

Thus, for a proper open system one can write

$$(16) \quad K(\Omega) = G(\Omega) = T(\Omega)$$

Since the integral of the Laplacian vanishes over Ω , the integral of the local statement of the virial theorem (Eq. 6) over the volume of an atom Ω in a molecule yields the *atomic virial theorem*:

$$(17) \quad -2T(\Omega) = \mathcal{V}(\Omega)$$

where the $\mathcal{V}(\Omega)$ is the total atomic virial.

The atomic electronic energy $E_e(\Omega)$ is

$$(18) \quad E_e(\Omega) = T(\Omega) + \mathcal{V}(\Omega)$$

For systems in equilibrium there are no (Hellmann–Feynman) forces acting on the nuclei and the virial equals the average potential energy of the molecule, i.e., $\mathcal{V} = V$. Under this condition Eq. 17 becomes

$$(19) \quad -2T(\Omega) = V(\Omega)$$

where $V(\Omega)$ is the potential energy of atom Ω , and Eq. 18 becomes

$$(20) \quad E(\Omega) = E_e(\Omega) = T(\Omega) + V(\Omega) = -T(\Omega)$$

where $E(\Omega)$ is the total energy of atom Ω .

Thus, the energy of an atom in a molecule at its equilibrium geometry is obtained from the atomic statement of the virial theorem, $E(\Omega) = -T(\Omega)$. The sum of atomic energies yields, naturally, the total energy of the molecule (obtained directly from the electronic structure calculation) to within a small numerical integration error. This additivity of the atomic energies is expressed:

$$(21) \quad E_{\text{total}} = \sum_{\Omega} E(\Omega).$$

Equation 21 is, truly, a remarkable result by virtue of which the total molecular energy is given an atomic basis. Such partitioning of the total energy is indispensable if one is to understand the atomic origins of the energetic difference between two isomers for example.

4.2 A “Technical” Caveat

The well-known molecular virial theorem is expressed:

$$(22) \quad \gamma = -\frac{V}{T} = 2$$

In an electronic structure calculation, however, Eq. 22 is generally not satisfied exactly and the virial ratio (γ) can sometimes deviate by as much as 0.01 from the ideal value of 2. Due to this deviation of the virial ratio, atomic energy will not sum to yield the molecular energy, i.e., Eq. 21 will not be satisfied to an acceptable accuracy. A numerical rectification for this problem is performed (by default) by the atomic integration software [115–119]. The rectification consists of multiplying each atomic kinetic energy, $T(\Omega)$, by $(1-\gamma)$ rather than by (-1) . These numerically corrected (scaled) atomic energies do satisfy Eq. 21, and their sum equals or is very close to the total molecular energy (within a numerical integration error). The virial corrections generally scale linearly with respect to $T(\Omega)$, being smallest for hydrogen atoms, which—fortunately—leaves the relative stabilities of the atoms unchanged.

In benchmark calculations [48, 120], however, one needs to perform atomic integrations of energy densities obtained from systems which satisfy the molecular virial theorem exactly (see discussion in Ref. [120]). Dr. Keith has written a link [121] for the Gaussian program [122] that implements Löwdin’s scaling of the electronic coordinates [123, 124], the so-called self-consistent

virial scaling (or SCVS), so that the final wave function satisfies the molecular virial theorem, Eq. 22, exactly. Calculations using this link [121] yield wave functions which satisfy the virial theorem to the eighth decimal place.

5 METHOD

In this review, we describe the basic steps in theoretical (molecular, non-periodic) calculations to study the H–H bonding interactions. For the analysis of electron density obtained by high-resolution low-temperature X-ray diffraction experiments coupled with multipolar refinement [125], the reader is referred to the literature [65, 66].

First, a wave function is calculated from first principles using an available electronic structure program such as Gaussian 03 [122]. Second, the topology of the electron density is analysed with software such as AIMPAC [115, 116] or AIM 2000 [118, 119] to locate the critical points and the interatomic zero-flux surfaces. Third, numerical integrations are performed over the atomic basins to obtain the atomic averages of the various quantum mechanical operators. The first and (particularly) the third steps are the most expensive in terms of computer time. The delocalisation indices are then calculated from the atomic overlap matrices (produced in the output of AIMPAC-PROAIM, i.e., the atomic integration files) using AIMDELOC [126]. Molecular graphs and volume renderings can be plotted using AIM 2000 [118].

Since in this work we are also interested in analysing *energies*, particularly atomic energies and the different energy densities evaluated at the BCP, an electronic method which yields a first-order *density matrix* (not just its diagonal elements, that is, the electron density) must be used. Such methods include the Hartree–Fock approximation (HF) and various schemes of post self-consistent field (SCF) configuration interaction methods such as CISD, QCISD, MP2, and so forth. Density functional theory (DFT) is, thus, not a good choice in principle. However, experience has shown that the numerical values and trends are well reproduced by the DFT hybrid functional B3LYP [48]. Further, we have previously shown [48] that the relative ordering of the atomic energies is insensitive to the basis set or to the inclusion of Coulombic correlation. The same insensitivity to the level of theory is also found for bond properties.

As mentioned above, SCVS corrections scale linearly with respect to $T(\Omega)$, and hence its application should not alter the relative stability of the atoms too much. In an SCVS calculation, the electronic coordinates are scaled so as to satisfy the virial theorem while simultaneously re-optimising the geometry.

6 THE CHARACTERISATION OF THE HYDROGEN–HYDROGEN BONDING INTERACTION

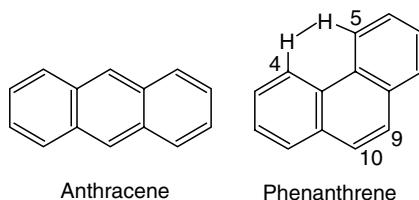
Cioslowski and Mixon [57] reported atomic interaction lines connecting hydrogen atoms separated by short distances ($d_{\text{H}\dots\text{H}} \leq 2.18 \text{ \AA}$) in several polycyclic aromatic hydrocarbons (PAHs). These authors describe this interaction as

“non-bonding repulsive” [57]. While we disagree with this description for reasons that will become apparent shortly, the Cioslowski and Mixon paper is credited for being the first to report the existence of this interaction in angular PAHs and for obtaining functional dependencies between $d_{\text{H}\cdots\text{H}}$ and several properties determined directly at the BCP or derived from them.

Since the H–H is *locally* stabilising (*vide infra*), and since these paths are present in equilibrium geometries where there are no net forces on the nuclei, they will be referred to as “bond paths”. The H–H bond path turns out to be ubiquitous in angular PAHs [48, 57, 58] and in several methylated hydrocarbons [48] serving as a “corset” stabilising structures that otherwise would fly apart [48].

6.1 Case Study I: An Atomic Basis for the Stability of Phenanthrene over its Isomer Anthracene

Our interest in bonding and aromaticity in PAHs [113, 127] led us to revisit the old problem of the stability of phenanthrene relative to its isomer anthracene. Phenanthrene is more stable than anthracene by ~ 5.4 kcal/mol at the RHF/6–31G(*d,p*) level [48], and by 7.8 kcal/mol based on the difference of their empirical resonance energies estimated from heats of combustion [128]. The classical explanation for this difference usually stops at the resonance energy argument.



A resonance energy is a global “property” of a molecule. Therefore, differences between resonance energies of two isomers or conformers cannot provide any information on *regional* or *atomically resolved* relative stabilisation or destabilisation. The quantum theory of atoms in molecules, on the other hand, provides the required atomically resolved partitioning of the total energy, as described in Sect. 4.

To apply QTAIM, one first determines the molecular graph. The molecular graph of phenanthrene [48] exhibits a H–H bond path between the two nuclei of H4 and H5 which are separated by ~ 2.03 Å. The formation of the H–H bond in phenanthrene closes a 6-membered ring (6-MR) and is accompanied by the appearance of a ring critical point (RCP), as required for the satisfaction of the Poincaré–Hopf relationship [63]. In contrast, there are no H–H bond paths in phenanthrene’s isomer anthracene (see the comparison of the molecular graphs in Fig. 3).

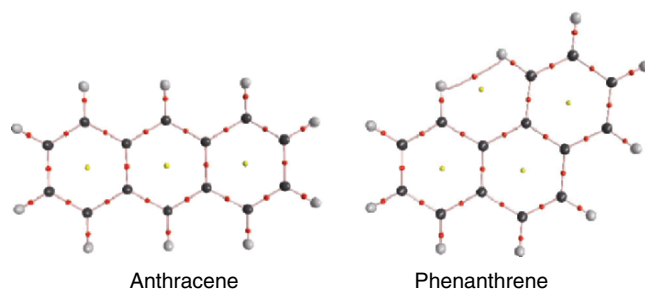


Figure 3 (see color section). Molecular graphs of the two isomers anthracene and phenanthrene. The lines linking the nuclei are the bond paths, the red dots on the bond paths are the BCPs, and the yellow dots are the ring critical points (RCPs). The H–H bond path between H4 and H5 exists only in phenanthrene.

Figure 4 displays the electron density distribution in the molecular plane of anthracene and contrasts it with that of phenanthrene along with the associated gradient vector field of the latter. In this figure, one can see the curved bond path linking the nuclei of the two hydrogen atoms, H4 and H5, in phenanthrene as well as the zero-flux interatomic surface they share, features lacking in the map of anthracene.

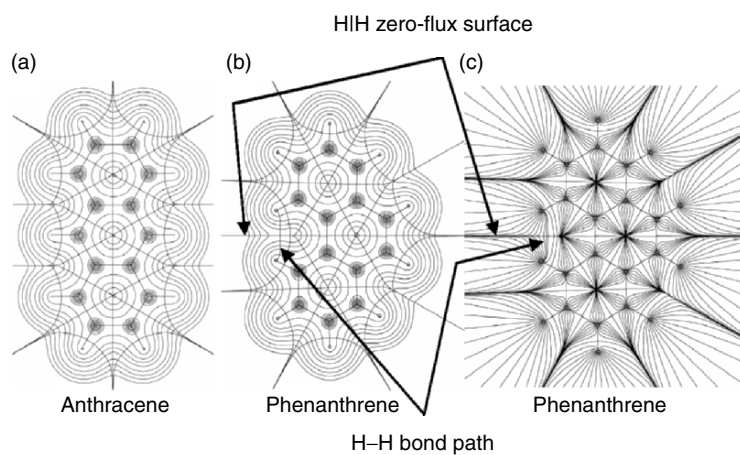


Figure 4. (a and b) Displays of the electron density $\rho(\mathbf{r})$ contours in the molecular plane of anthracene and phenanthrene, respectively. The density increases from the outermost 0.001 au contour in the order 2×10^n , 4×10^n , and 8×10^n au with n starting at -3 and increasing in steps of unity. The intersections of the interatomic zero-flux surfaces with the planes of the figures and the bond paths are superimposed on the plots. (c) A display of the gradient vector field of phenanthrene in the same orientation and plane as in (b). The gradient vector $\nabla\rho(\mathbf{r})$ field clearly shows the shape of each atomic basin and its bounding zero-flux surface.

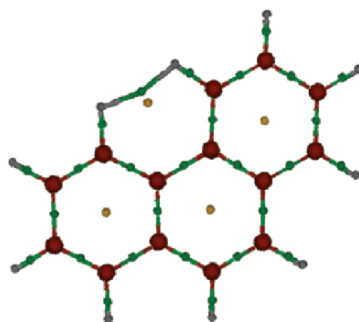


Figure 5 (see color section). The virial graph of phenanthrene.

As mentioned earlier (Sect.2), to each molecular graph there exists a shadow graph in the virial field, consisting of the collection of all the virial paths in the molecule, known as the virial graph. The virial graph and the molecular graph are homeomorphic [91]. The virial graph of phenanthrene (Fig. 5) clearly shows the H–H virial path, a line of maximally stabilising potential energy density in space, linking the nuclei of the two hydrogen atoms H4 and H5.

At the RHF/6–31G(*d,p*) level, the atomic integration reveals that the carbon skeleton of phenanthrene is less stable than in anthracene by ~ 10.5 kcal/mol, at the same time the hydrogen atoms are collectively more stable by ~ 15.9 kcal/mol in phenanthrene compared to anthracene. The net balance yields, of course, the known result that phenanthrene is more stable than anthracene by ~ 5.1 kcal/mol at this level of theory, a value that increases to 6.4 kcal/mol at the MP2 level and 6.9 kcal/mol at the MP2(SCVS) level [48].

In phenanthrene, two hydrogen atoms, H4 and H5, stand out with a significantly lower energy than the other hydrogen atoms (whether gauged against the eight remaining “normal” hydrogen atoms in phenanthrene or against any of the ten hydrogen atoms of anthracene). Gauging the energy of one of these two symmetry-equivalent hydrogen atoms involved in the H–H bonding interaction against the average energy of the eight “normal” hydrogen atoms in this molecule, one gets

$$(23) \quad \left[\sum_{i=1, i \neq 4,5}^{10} \frac{E(H_i)}{8} - E(H_{4 \text{ or } 5}) \right]_{\text{Phenanthr.}} = 6.0 \text{ kcal/mol}$$

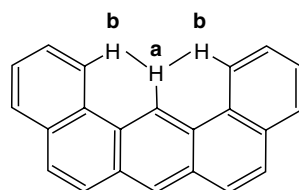
and if we gauge this energy against the hydrogen atoms in anthracene, we get

$$(24) \quad \left[\sum_{i=1}^{10} \frac{E(H_i)}{10} \right]_{\text{Anthr.}} - [E(H_{4 \text{ or } 5})]_{\text{Phenanthr.}} = 6.4 \text{ kcal/mol}$$

which is essentially the same result as in Eq. 23. In sharp contrast, the energies of the remaining hydrogen atoms which are not involved in the H–H bonding

vary very little. Thus, the standard deviation of the atomic energies of the eight “normal” hydrogen atoms in phenanthrene is as little as $\sim\pm 0.5$ kcal/mol, and the corresponding standard deviation of the energies of all the hydrogen atoms in anthracene is even lower being only $\sim\pm 0.3$ kcal/mol. These observations clearly indicate a significant stability imparted to the two hydrogen atoms involved in the H–H bond, that is, H4 and H5 of phenanthrene. These two atoms alone lower the energy of phenanthrene by ~ 12 kcal/mol when compared to anthracene. In other words, the H–H bonding interaction in phenanthrene is accompanied by 12 kcal/mol of local stabilisation at the RHF/6–31G(*d,p*) level (and 9.4 kcal/mol at the B3LYP/6–31G(*d,p*) level) [48].

Dibenz[*a,j*]anthracene possesses two regions similar to the one in which the H–H bonding takes place in phenanthrene, but these two regions share a hydrogen atom (see the chemical structure below). This molecule exhibits two H–H bonding interactions involving this common hydrogen atom [H(a)], H(b)–H(a)–H(b), providing an example of a bifurcated H–H bonding interaction. The remaining hydrogen atoms not involved in the H–H bonding interactions will, once more, be referred to as “normal” hydrogen atoms.



Dibenz[*a,j*]anthracene

At the RHF/6–31G(*d,p*) level, each H(b) is ~ 5.7 kcal/mol more stable than the average normal hydrogen atom. Interestingly, the relative stability of H(a) (-12.8 kcal/mol), which is the terminus of two H–H bonds, is approximately twice that of H(b), the terminus of only one H–H bond [64] (see also Ref. [48]).

6.2 Case Study II: An Atomic Basis for the Stability of Twisted vs. Planar Biphenyl

It is well known that the gas-phase equilibrium geometries of biphenyl and its substituted derivatives are twisted with a significant dihedral angle ϕ between the two ring planes. Gas-phase electron diffraction experiments yield a value of $\phi = 41.6^\circ (\pm 2.0^\circ)$ for the biphenyl molecule [129]. The classical explanation for the twisting of the biphenyl molecule is that the proximal *ortho*-hydrogens repel each other sterically which causes the molecule to twist. This view, also adopted by Cioslowski and Mixon [57], does not hold upon comparing the atomic energies in the planar and twisted conformations of biphenyl as we shall see.

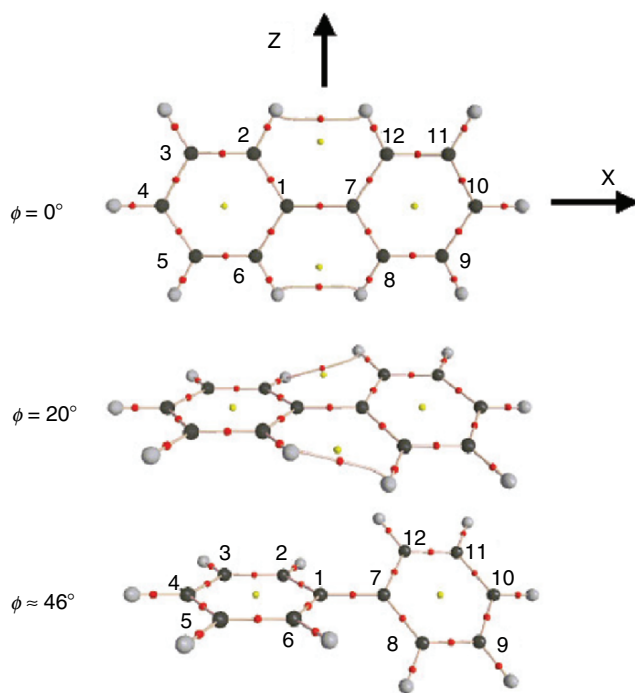


Figure 6 (see color section). Molecular graphs of biphenyl as functions of the dihedral angle between the ring planes (ϕ). The coordinate system along with the atom numbering system. Hydrogen atoms take the same number as the carbon atoms to which they are bonded. At the critical value of $\phi \approx 27^\circ$ there is a sudden “catastrophic” change in structure with the rupture of the two H–H bond paths (H2–H12 and H6–H8).

In the planar conformation, biphenyl exhibits two H–H bond paths connecting the nuclei of the proximal *ortho*-hydrogen atoms (H2–H12 and H6–H8, see Fig. 6). These bond paths persist up to $\phi \sim 27^\circ$ at the RHF/6–31G(*d,p*) level of theory [57]. Figure 6, depicts the biphenyl in three conformations: (1) the planar transition state (TS); (2) an intermediate geometry ($\phi = 20^\circ$) where the BCP exists still, but comes closer in space to the RCP; and (3) the equilibrium (EQU) geometry ($\phi \approx 45.5^\circ$) lacking H–H bond paths. The figure also displays the atom numbering system and the coordinate system.

As the dihedral angle is increased from $\phi = 0^\circ$ to the “critical” value beyond which the bond path vanishes (27°), the H–H BCP and the corresponding 6-MR RCP come closer and closer. The annihilation of the H–H BCP at ca. 27° entails a sudden change in “structure”, a “catastrophe” [130], known as the fold catastrophe [63] (see change in structure in Fig. 6). As the BCP and the RCP approach one another, the property densities evaluated at each CP assume closer and closer values until the two points eventually merge and annihilate each other [57]. The plot in Fig. 7a shows the change in the distance

between the BCP and the RCP (expressed as the z -coordinate) as a function of the dihedral angle ϕ , and the plots in Fig. 7b,c display the electron density and its Laplacian, determined at the two critical points as a function of ϕ and show how the respective values approach one another until the two critical points coalesce and vanish.

The twisted equilibrium geometry of biphenyl ($\phi = 45.5^\circ$) is more stable than the planar TS geometry by 3.4 kcal/mol at the RHF/6-31G(d,p) level. Table 1 is an atom-by-atom comparison of the atomic energies in these two structures; such a comparison is indispensable to establish an atomic basis for their difference in stability. Thus, the table lists the atomic energies of every atom (Ω) in biphenyl in the planar geometry ($E_{0^\circ}(\Omega)$) and in the equilibrium geometry ($E_{45.5^\circ}(\Omega)$) in atomic units and lists their difference in kcal/mol:

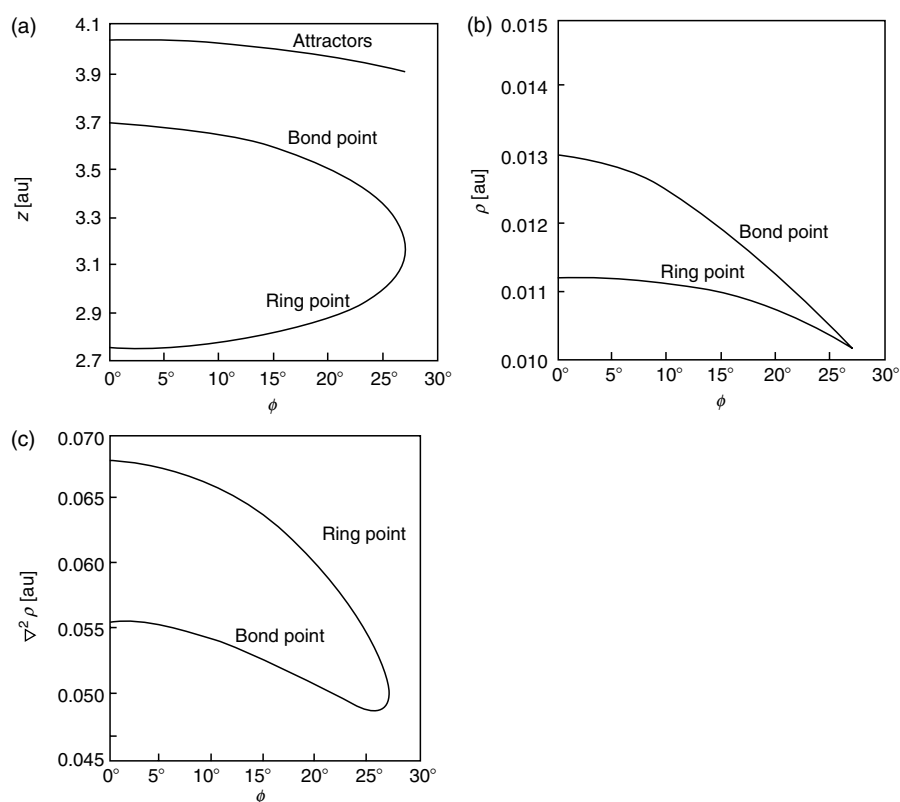


Figure 7. (a) The z -coordinate of the critical points relevant to the H–H bonding interaction as a function of the dihedral angle ϕ in biphenyl (the coordinate system is defined in Fig. 6). (b) The electron density $\rho(\mathbf{r})$ at the BCP and RCP as a function of ϕ . (c) The Laplacian, $\nabla^2 \rho(\mathbf{r})$, at the BCP and RCP as a function of ϕ (reproduced with permission from Ref. [57]).

Table 1. Comparison of the atomic energies of biphenyl in the planar transition state geometry (TS, $\phi = 0^\circ$) vs. the corresponding atomic energies in the equilibrium twisted geometry (EQU, $\phi = 45.49^\circ$)^{a,b}

Atom	$E_{0^\circ}(\Omega)$ (au)	$E_{45.5^\circ}(\Omega)$ (au)	$E_{0^\circ}(\Omega) - E_{45.5^\circ}(\Omega)$ (kcal/mol)
Atoms destabilised in TS			
C1	-37.8145	-37.8502	+22.4
C7	-37.8145	-37.8502	+22.4
H4	-0.6513	-0.6519	+0.4
H10	-0.6513	-0.6519	+0.4
C2	-37.8081	-37.8086	+0.3
C12	-37.8081	-37.8086	+0.3
C6	-37.8082	-37.8086	+0.2
C8	-37.8082	-37.8086	+0.2
Total destabilisation			+46.6
Atoms stabilised in TS			
H2	-0.6647	-0.6523	-7.7
H12	-0.6647	-0.6523	-7.7
H6	-0.6647	-0.6523	-7.7
H8	-0.6647	-0.6523	-7.7
C4	-37.8070	-37.8015	-3.4
C10	-37.8071	-37.8015	-3.5
C3	-37.8046	-37.8031	-1.0
C11	-37.8047	-37.8031	-1.0
C5	-37.8047	-37.8031	-1.0
C9	-37.8047	-37.8031	-1.0
H9	-0.6529	-0.6521	-0.5
H5	-0.6529	-0.6521	-0.5
H3	-0.6529	-0.6521	-0.5
H11	-0.6529	-0.6521	-0.5
Total stabilisation			-43.7
Molecular totals			Differences
$\sum E(\Omega)$ (au)	-460.2673	-460.2718	+2.8
SCF (au)	-460.2664	-460.2719	+3.4

^a Results based on a RHF/6-31G(*d,p*) calculation [64]

^b Atomic numbering corresponds to the numbering indicated in Fig. 6

$$(25) \quad \Delta E(\Omega) = E_{0^\circ}(\Omega) - E_{45.5^\circ}(\Omega)$$

Since atomic energies are always negative, values of $\Delta E(\Omega) > 0$ indicate that the atom is destabilised in the planar TS structure, and values of $\Delta E(\Omega) < 0$ mean that the atom is more stable in the planar TS. Examination of Table 1 reveals that the only two atoms which are considerably destabilised in the planar TS are C1 and C7, the two carbon atoms linking the two rings. These two carbon atoms alone jointly contribute 44.8 kcal/mol (out of the 46.6 kcal/mol) of destabilisation of the TS with respect to the equilibrium geometry. On the other hand, the atoms which are more stable in the planar TS relative to the equilibrium structure are many (the majority of the atoms actually), but the

prime contribution comes from the four symmetry-equivalent *ortho*-hydrogen atoms (H2, H12, H6, and H8). These hydrogen atoms are each 7.7 kcal/mol more stable in the TS than their counterpart in the equilibrium geometry. A bookkeeping of these changes in atomic energy on going from $\phi = 0^\circ$ to $\phi = 45.5^\circ$ should of course recover the $\Delta E(\text{SCF})$ energy favouring the equilibrium geometry. The (small) numerical integration errors are manifested collectively in a small discrepancy between the difference in stability of the two structures (2.8 kcal/mol obtained by summing the differences in atomic energies vs. a $\Delta E(\text{SCF})$ value of 3.4 kcal/mol). At the bottom of Table 1 the SCF total energies of the two biphenyl structures are listed along with the sum of the atomic energies of each structure. The SCF values differ slightly from the sum of the atomic energies of the respective structures due to the accumulation of numerical integration errors. This error is only ~ 0.57 and ~ 0.06 kcal/mol for the planar and the equilibrium structures, respectively, and is of no consequence with regard to any of the conclusions reached here.

From the above, one concludes that the lower stability of the planar TS compared to the twisted equilibrium structure is thus to a large extent driven by two opposing effects: (1) a stabilisation of TS imparted by the four *ortho*-hydrogen atoms involved in the H–H bonding and (2) an overwhelming destabilisation of the TS imparted by the two carbon atoms joining the two rings. The destabilisation of the C1 and C7 carbon atoms in the TS could be the result of the accompanying stretching of the C1–C7 bond in the planar structure by ~ 0.009 Å to accommodate the H–H bonds. Each H–H bond thus contributes 15.4 kcal/mol at the RHF(SCVS)/6–31G(*d,p*), a value that increases to 15.8 kcal/mol upon using the larger basis set (6–311++G(2*d*,2*p*)) and which is 10.4 kcal/mol at the B3LYP/6–31G(*d,p*) DFT level. We will call this energy the H–H *bond stabilisation energy* ($E_{\text{H–H}}$), not to be confused with a “bond energy” or “bond dissociation energy, D_e ”. Unlike D_e , $E_{\text{H–H}}$ refers to the stabilisation imparted by the H–H bond to a region in a molecule and does not refer to, nor carries the usual ambiguities of, the energy needed to break the bond [48].

6.3 Properties of H–H Bonding and How They Differ from Those Characterising Dihydrogen Bonding

The H–H bond has recently been characterised [48]. To avoid repeating what has already been published (at the B3LYP/6–31G(*d,p*) level) [48], Table 2 lists some of the characteristics of the H–H bonding calculated at the RHF/6–31G(*d,p*) [64]. Neither the trends nor the numerical values listed in Table 2 differ significantly from the corresponding values calculated at the B3LYP level. The data in the table clearly indicate a closed-shell interaction characterised by a small ρ_b , a small $\delta(\text{H},\text{H}')$, $\nabla^2\rho_b > 0$, and a very small (but positive) H_b .

We have calculated the bond stabilisation energies for a number of molecules at the B3LYP/6–31G(*d,p*) [48] and at the RHF/6–31G(*d,p*) [64] levels. Table 2 lists $E_{\text{H–H}}$ calculated for a number of polycyclic aromatic hydrocarbons at the

Table 2. Bond properties of some H–H bonding interactions in angular polycyclic aromatic hydrocarbons^a

Molecule ^b	$E_{\text{H-H}}$ (kcal/mol)	$d_{\text{H-H}}$ (Å)	$\delta(\text{H,H}')$	ρ_b (au)	$\nabla^2\rho_b$ (au)	ε	G_b (au)	V_b (au)	H_b (au)
I	–12.0	2.029	0.025	0.0115	0.050	0.466	0.010	–0.007	0.003
II	–5.5	2.174	0.018	0.0098	0.046	1.795	0.009	–0.006	0.003
III	–13.5	1.977	0.027	0.0127	0.055	0.401	0.011	–0.008	0.003
IV	–13.5	2.003	0.026	0.0120	0.052	0.411	0.010	–0.008	0.003
V	–15.4	1.966	0.028	0.0130	0.056	0.370	0.011	–0.009	0.003

^a Results based on a RHF/6–31G(*d,p*) calculation [64]

^b **I** = Phenanthrene; **II** = 9,10-Dihydrophenanthrene; **III** = Chrysene; **IV** = Dibenzo[*a,j*]anthracene; **V** = Planar biphenyl

latter level of theory, since these were not published previously, along with some of the key bond properties. It is remarkable that we find a very good linear correlation between the estimated $E_{\text{H-H}}$ and the listed bond properties, one of these linear relationships, the one with the density at the BCP ρ_b , can be described by the following regression equation:

$$(26) \quad E_{\text{H-H}}(\text{kcal/mol}) = 22.662 - 2934.74 \times \rho_b \text{ (au)} \quad [r^2 = 0.934, S = 1.05 \text{ kcal/mol}, n = 5]$$

where S is the standard error. The plot in Fig. 8 corresponds to this regression equation along with the individual data points.

The detailed comparison contrasting the properties of the H–H bond with those of the dihydrogen bond [48] is distilled here and presented in the form of a tabular summary of the main points in Table 3 (for details, see Ref. [48]).

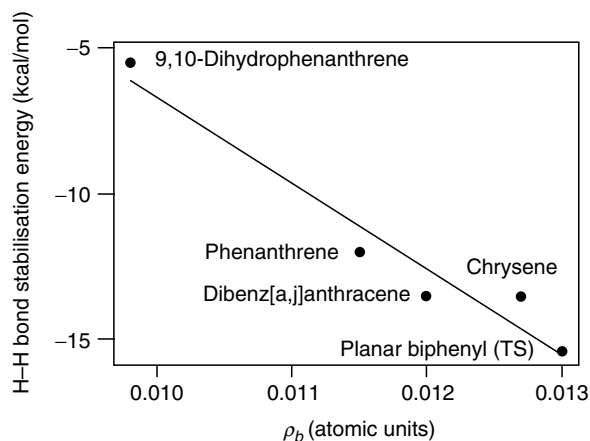


Figure 8. H–H stabilisation energy calculated for some polycyclic aromatic hydrocarbons as a function of the density at the BCP (ρ_b). The regression line is based on Eq. 26.

Table 3. Contrasting H–H bonding and dihydrogen bonding (distilled from Ref. [48])

Comparison criteria	H–H bonding X–H ··· H–Y	Dihydrogen bonding X ^{δ-} –H ^{δ+} ··· H ^{δ-} –Y ^{δ+}
Nature of atoms involved	X, Y are both not highly electronegative, usually both are carbon atoms	X = an electronegative atom such as oxygen or nitrogen Y = an electronegative atom such as metal atom
X–H bond length and vibrational frequency	X–H bond length decreases upon the formation of the bond, and hence its stretching vibration shifts to a higher frequency (blue shift)	X–H bond length increases upon the formation of the dihydrogen bond (as is the case for any hydrogen bond), and thus the stretching vibration of X–H shifts to a lower frequency (red shift)
Electric charges on the hydrogen atoms	Both hydrogen atoms are either electrically neutral or carry minute charges which are usually of similar sign	One of the two hydrogen atoms, the acidic hydrogen, bears a significant positive charge (and thus clearly belongs to the proton donor group) while the other is negatively charged (hydridic) and acts as the proton acceptor
Change in the atomic volume of H upon the formation of the bond	The volume decreases but to a smaller (absolutely and proportionately) than the electropositive hydrogen of the dihydrogen bond. The two hydrogen atoms experience identical or similar change	The volume of the electropositive hydrogen atom is significantly reduced due to the transfer of electronic charge to both the hydridic hydrogen and X. The volume of the hydridic hydrogen, on the other hand, increases
Change in the atomic energies of H upon the formation of the bond	Both hydrogen atoms are stabilised by typically 2 to 7 kcal/mol each	The acidic hydrogen experiences a marked destabilisation of up to 20 to 40 kcal/mol

6.4 The “Direct” Evaluation of the Change in Energy Arising from the Formation of the H|H Interatomic Zero-Flux Surface

To partition the stabilisation experienced by an atom Ω in a molecule in its equilibrium geometry by “bond contributions”, we write the atomic statement of the virial theorem:

$$(27) \quad -2T(\Omega) = \mathcal{V}_b(\Omega) + \mathcal{V}_S(\Omega)$$

where $\mathcal{V}_b(\Omega)$ and $\mathcal{V}_S(\Omega)$ refer to the virial of the Ehrenfest forces exerted on the atomic basin (the basin virial) and on the zero-flux surface(s) bounding the atom (the surface virial), respectively.

For a free unbound atom, the sum $[2T(\Omega) + \mathcal{V}_b(\Omega)]$ vanishes. For a bound atom in a molecule, however, this sum is equal to $-\mathcal{V}_S(\Omega)$, the negative of the

virial of the forces acting on the surface of the atom [63]. Therefore, one can write [63]

$$(28) \quad 2\Delta T(\Omega) + \Delta\mathcal{V}_b(\Omega) = -\mathcal{V}_s(\Omega)$$

where Δ signifies the change in the respective quantity when the atom becomes bound. For a molecule in equilibrium, $\Delta T(\Omega) = -\Delta E(\Omega)$. Substituting this equality into Eq. 28 yields [63]

$$(29) \quad \Delta E(\Omega) - \frac{1}{2}\Delta\mathcal{V}_b(\Omega) = \frac{1}{2}\mathcal{V}_s(\Omega) = \frac{1}{2} \sum_{\Omega' \neq \Omega} \mathcal{V}_s(\Omega|\Omega')$$

where $\Delta E(\Omega)$ is the change in the energy of an atom on going from its free ground state to becoming a bound atom in a molecule. The last equality states that the total surface virial of the bound atom is, in general, equal to a sum of contributions from the different interatomic zero-flux surfaces that this atom, Ω , shares with other atoms to which it is bounded, Ω' . The interatomic surfaces shared between Ω and its bonded neighbours Ω' are denoted by the vertical bar in $(\Omega|\Omega')$. $\mathcal{V}_s(\Omega|\Omega')$ is the virial of the forces acting on the $\Omega|\Omega'$ interatomic surface, i.e., the potential energy contribution to ΔE associated with this surface [63].

For planar biphenyl, $\mathcal{V}_s(\text{H}|\text{H})$ was found to be -14.5 kcal/mol [B3LYP/6-31G(*d,p*)] and -20.6 kcal/mol [RHF(SCVS)6-31G(*d,p*)] [48]. Both values of $\mathcal{V}_s(\text{H}|\text{H})$ exceed the calculated $E_{\text{H-H}}$ of 10.4 and 15.4 kcal/mol at the two levels of theory, respectively, by ca. 5 kcal/mol. This difference is accounted for by a *destabilising* contribution, $\mathcal{V}_s(\text{C}|\text{H}) \approx 2.5$ kcal/mol, from each of the two C–H interatomic surfaces (C|H). Similar results were obtained in the case of phenanthrene, for which $\mathcal{V}_s(\text{H}|\text{H}) = -16.6$ kcal/mol compared to an $E_{\text{H-H}} = -12.8$ kcal/mol [RHF(SCVS)6-31G(*d,p*)] [48]. In both cases, thus, the H–H interatomic surface contributes ~ 5 kcal/mol in excess of the stabilisation energy $E_{\text{H-H}}$, an energy recovered upon the addition of the destabilising contributions from the C|H interatomic surfaces.

6.5 Examples of Intramolecular H–H Bonding Interactions

The H–H bonding interaction is ubiquitous and has been found in a number of systems. The earliest experimental account I am aware of reporting unusually short intramolecular H \cdots H distances is that of Ermer and Mason [42]. These authors find H \cdots H distances as short as 1.754(4) Å and 1.713(3) Å between neighbouring bridgehead hydrogen atoms in fused norbornenes based on low temperature neutron diffraction experiments [42]. Even shorter H \cdots H distances were suggested in another norbornene derivative on the basis of an X-ray diffraction determination ($d_{\text{H}\cdots\text{H}} = 1.62$ Å) [49]. While the latter result awaits confirmation by neutron diffraction, it still indicates that norbornene or norbornane derivatives are candidates for very short, perhaps the shortest, intramolecular H \cdots H distances. The molecular graph of the parent compound in this series (*exo, exo*-tetracyclo[6.2.1.1^{3,6}.0^{2,7}]dodecane) obtained at the

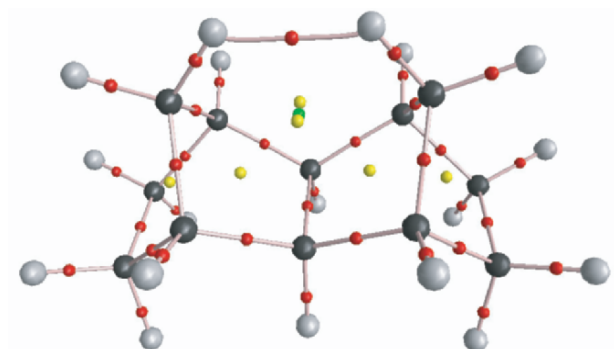


Figure 9 (see color section). The calculated molecular graph of *exo, exo*-tetracyclo[6.2.1.1^{3,6}.0^{2,7}]dodecane which consists of two fused norbornanes rings. The H–H bond path links the nuclei of the two bridgehead hydrogen atoms. This results in the closure of two rings concomitant with the appearance of two ring critical points (yellow) and a cage critical point between them (green).

B3LYP/6-311++G(*d,p*)/AM1 level is displayed in Fig. 9. The bond properties obtained at this level reveal a moderately strong interaction ($d_{\text{H}\cdots\text{H}} = 1.7303 \text{ \AA}$, $\rho_{\text{b}} = 0.0206 \text{ au}$, $\nabla^2\rho_{\text{b}} = +0.0671 \text{ au}$) [131]. Work is underway in our laboratory to completely characterise this interaction in calculated electron density maps, including an analysis of atomic energies [131].

Recently, $E_{\text{H-H}}$ stabilisation energies ranging from 0.8–1.6 kcal/mol in tetra-*tert*-butyltetrahedrane, 4.6 kcal/mol in tetra-*tert*-butycyclobutadiene, and 3.8 kcal/mol in tetra-*tert*-butylindacene were obtained [48]. In the later, each apical hydrogen atoms participates in four H–H bonding interaction, in other words, each apical hydrogen atom is involved in tetrafurcated H–H bonding (see Fig. 10). Since in this molecule there is no “normal hydrogen” that can be used as a reference, the same energy of hydrogen atoms after a 60° rotation of the methyl groups (which results in the disappearance of the H–H bond paths)

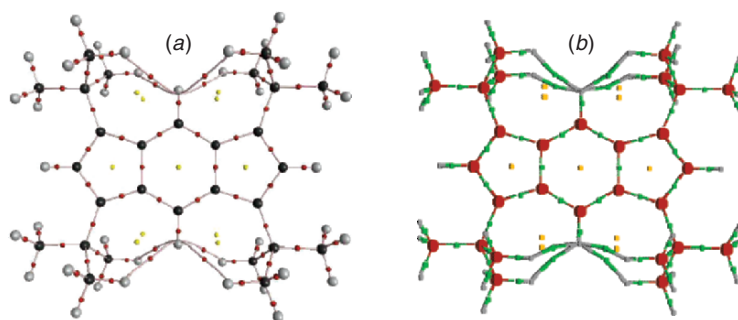
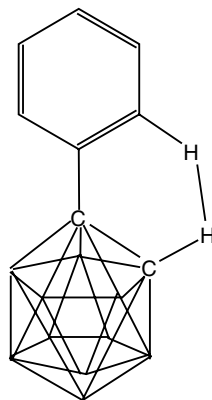


Figure 10 (see color section). The calculated molecular graph (a) and its corresponding virial graph (b) of tetra-*tert*-butylindacene.

was used as the reference [48]. The molecular graph and the topological properties of tetra-*tert*-butylindacene were subsequently closely reproduced by high resolution X-ray crystallography with multipolar refinement [52].

A detailed analysis of atomic energies by Cortés-Guzmán, Hernández-Trujillo, and Cuevas revealed the origin of the 1,3-diaxial interaction [59]. These authors find that the 1,3-*syn*-diaxial interaction between two hydrogen atoms, one belonging to the cyclohexane ring and the other to a methyl substituent, is actually stabilising (locally) and is associated with the formation of a H–H bond path [59]. The overall bookkeeping of the atomic energy, which recovers the $\Delta E(\text{SCF})$ energetic difference between the substituted cyclohexane conformers, indicates that the relative destabilisation of the 1,3-*syn* conformation has its origin in the carbon skeleton. This destabilisation overwhelms the stabilisation accompanying the H–H bonding interaction, and the net result is that the 1,3-*syn* conformer is the least stable [59]. These new findings call, perhaps, for a reconsideration of the junior undergraduate textbook explanation to the effect that the 1,3-diaxial interaction is a “repulsive” interaction and that it is the “reason” for the relative destabilisation of conformations in which it exists.

In another interesting study, Glukhov et al. [61] performed a potential energy scan around the dihedral angle defining the orientation of the plane of a phenyl ring attached to *ortho*-carborane. The scan covered the range from 0° to 90° and was done at 10° steps. They find very small barriers to this rotation (ca. 0.5 kcal/mol) at the RHF/6–31G(*d*) level, which means that this rotation is practically uninhibited [61], a fact consistent with experiment and previous calculations [132].



A cartoon representing 1-Phenyl-0-carborane

Along the “reaction” path, these authors report several H–H interactions of the types $\text{C}_{\text{phenyl}}\text{--H}\cdots\text{H--C}_{\text{carborane}}$ and $\text{C}_{\text{phenyl}}\text{--H}\cdots\text{H--B}_{\text{carborane}}$ which make and break as the phenyl is rotated. All the interactions characterised along the reaction path have positive Laplacians with small magnitude and $0.0093 \text{ au} < \rho_b < 0.0139 \text{ au}$ [61]. It is possible, in my opinion, that the low barrier

reported for this rotation could be partly due to the formation of new H–H stabilising interaction(s) as others are broken during the rotation, effectively cancelling any net stabilisation or destabilisation. This opinion, however, remains to be tested by calculation.

Other interesting examples of H–H interactions were recently observed in a compound with crowded methyl groups (**4**), i.e., $C(sp^3)-H \cdots H-C(sp^3)$, and in another compound (**7**) between crowded aromatic rings, i.e., $C(sp^2)-H \cdots H-C(sp^2)$ [40] (see Fig. 11).

Finally, examples of intramolecular H–H bonding interactions were also found in biological molecules. Based on B3LYP/6–311++G(*d,p*) calculations on model fragments of DNA at their crystallographic geometries, up to ten different H–H bonding interactions have been found and characterised [27]. The interactions characterised include H–H bonding between stacked base-pairs, interactions linking hydrogen atoms in the nucleic acid bases to the DNA backbone, and interactions between pairs of hydrogen atoms belonging to the backbone [27]. Figure 12 provides examples of H–H bonding interactions between the nucleic acid base cytosine and the backbone, and between two hydrogen atoms both of which belong to the backbone [27].

As another biological example, a H–H bonding interaction was found in the electron density of the hormone estrone at its optimised geometry (B3LYP/

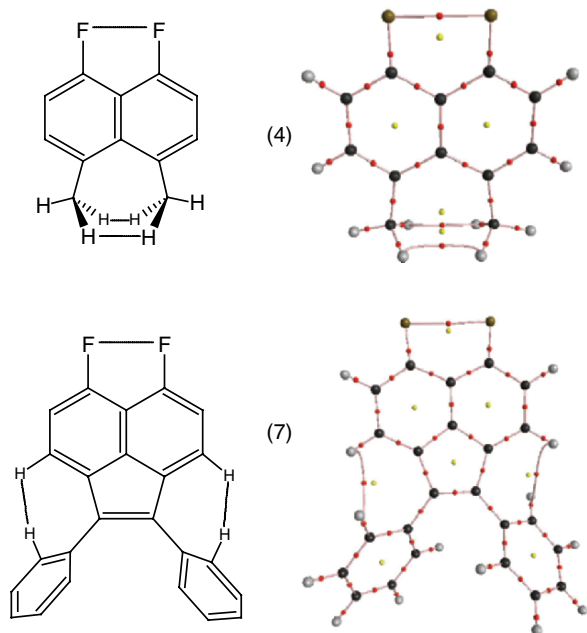


Figure 11 (see color section). The chemical structure and the molecular graph of compounds (**4**) and (**7**) exhibiting $C(sp^3)-H \cdots H-C(sp^3)$ and $C(sp^2)-H \cdots H-C(sp^2)$ bond paths, respectively (adapted after Ref. [40]).

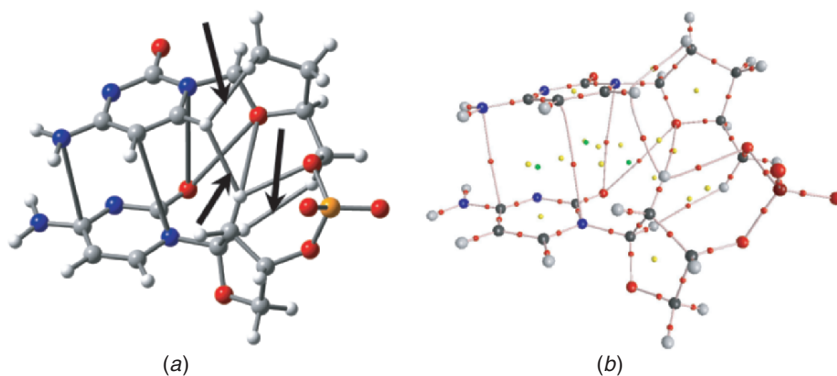


Figure 12 (see color section). An idealised (a) and actual (b) molecular graph of a piece of DNA consisting of two consecutive cytosine bases attached to the phosphate–sugar backbone along a strand of DNA showing the several closed-shell interactions including three H–H bond paths (indicated by the arrows) (adapted after Ref. [27]).

6–31+G(d) [133]. This bond path links the nuclei of two hydrogen atoms separated by ~ 2.50 Å and is characterised by a $\rho_b = 0.0114$ au [133] (see Fig. 9–13).

6.6 Examples of Intermolecular H–H Bonding Interactions

Robertson [50], Knop, and Cameron [51] (RKC) observed and characterised topologically 15 H–H bonding interactions in the crystal structures of tetraphenylborates of dabcoH⁺, guanidinium, and biguanidinium cations. These authors obtain accurate electron density maps determined by multipolar refinement and describe several interesting C–H \cdots H–C intermolecular bond paths, some exhibiting marked and quite unusual curvatures, generally falling within the distance range $d_{\text{H}\cdots\text{H}} = 2.18 - 2.57$ Å [50, 51]. Figure 14 provides two examples of H–H bond paths traced by RKC in experimental electron densities. The longer end of this distance range within which the H–H bonding interactions are observed is interesting since it shows that the H–H bond path can

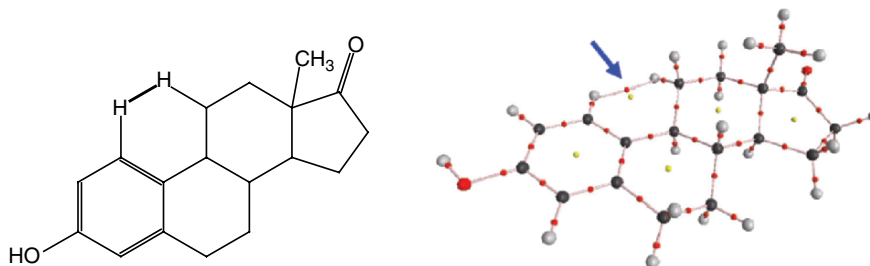


Figure 13 (see color section). Example of a H–H bond path in biological molecules. The chemical structure and the molecular graph of the hormone estrone (the blue arrow indicates the H–H bond path) (adapted from Ref. [133]).

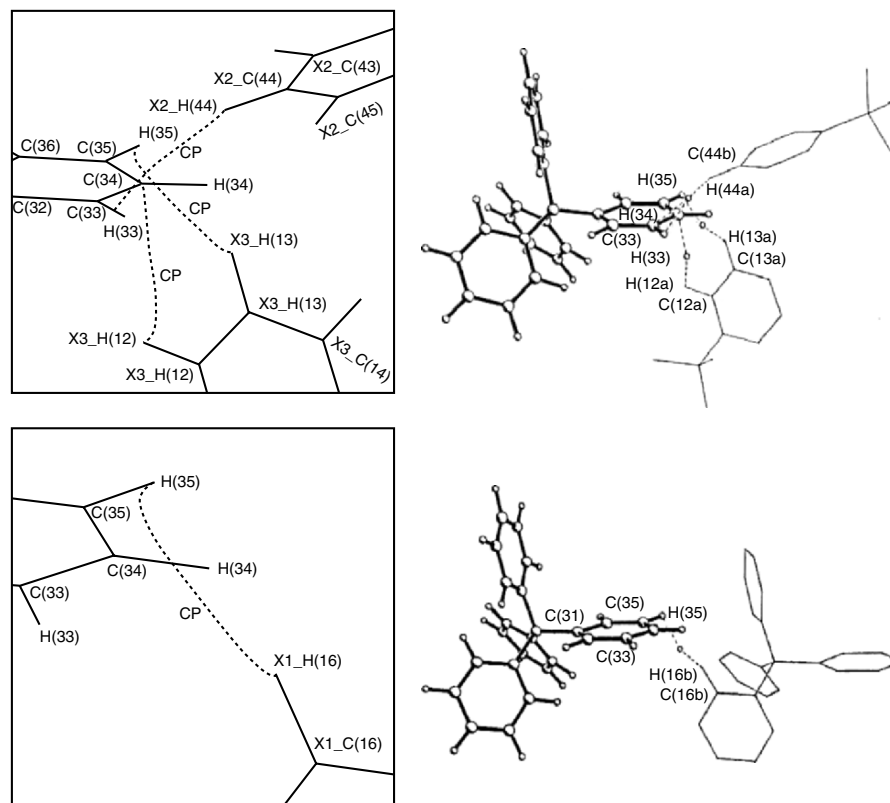


Figure 14. Examples of several intramolecular H–H bond path found by RKC in tetraphenyl borates by high resolution X-ray crystallographic experiments followed by multipolar refinement. “CP” mark the positions of the H–H BCPs. See Refs. [50,51] for details (reproduced with permission from Ref. [50]).

link the nuclei of two hydrogen atoms even if their separation exceeds the sum of their van der Waals radii. To my knowledge, the longest H–H bond path observed experimentally is found intermolecularly between furan molecules in solid furan [60]. The H···H separation in the furan crystal is 3.026 Å, with ρ_b as low as 0.0013 au and $\nabla^2\rho_b = 0.0044$ au [60].

RKC also analysed the results of MP2/6–31G(*d,p*) calculations on a series of 33 small model complexes which represents a range of interactions stretching from the two ends of the scale, namely, from dihydrogen bonding to H–H bonding [51]. Based on these calculations, RKC report several correlations between different topological properties of the dihydrogen and H–H interactions [51]. A particularly interesting correlation is found between the difference in the Mulliken charges of the two hydrogen atoms in the separated monomers ($\Delta\epsilon(H)_m$) and the Laplacian at the H–H BCP. They found that

within the range $0 \text{ e} < \Delta\varepsilon(\text{H})_{\text{m}} < \sim 0.54 \text{ e}$ the Laplacian is positive and of small magnitude ($\sim +0.2 \text{ au} < \nabla^2\rho_{\text{b}} < \sim +1.2 \text{ au}$), they symbolise the interaction in this range by $\text{X}-\text{H}\cdots\text{H}-\text{Y}$ [51]. At $\Delta\varepsilon(\text{H})_{\text{m}} \approx 0.54 \text{ e}$, however, there is a sudden downturn in the relationship and beyond this value the Laplacian assumes negative values of significant magnitudes $\nabla^2\rho_{\text{b}} \sim -22.0 \text{ au}$ to -32.8 au . Accompanying this sudden change in the Laplacian is a sudden shrinking in the $\text{H}\cdots\text{H}$ distance, which can now be as short as 0.738 \AA in the “strong” dihydrogen bonded regime as the one in the $\text{LiH}\cdots\text{HNF}_3^+$ complex [51]. They designate such a system as $\text{X}\cdots\text{H}-\text{H}\cdots\text{Y}$, since now the bond linking the two hydrogen is characterised by the traits of a shared interaction [51], and the system consists essentially of a hydrogen molecule trapped between two charged bracketing groups (the bond length in a hydrogen molecule at its equilibrium position is $\sim 0.734 \text{ \AA}$ at this level of theory [51]).

Several other recent crystallographic evidences of H–H bonding interactions have also appeared in the literature. For example, Pozzi et al.[55] conducted a 100 K single crystal neutron diffraction study of a methoxylated derivative of 1-methyl-2-quinolone. They reported several intermolecular H–H bond paths (among other closed-shell interactions) connecting the individual molecules in the crystals. The $d_{\text{H}\cdots\text{H}}$ between a methene hydrogen of one molecule and a methyl hydrogen of a neighbouring molecule was determined to be $2.290(11) \text{ \AA}$ [55]. Nemes et al.[56] describe several interesting intramolecular short contacts and an extended H–H bonding pattern that appears to contribute in holding a double-chain arrangement based on the results of an X-ray crystallographic study of (9,9'-disubstituted difluorenyl)(dimethyl) derivative of germanium.

Finally, Damodharan and Pattabhi [41] report a search of the Cambridge Structural Database [134–137] for $\text{H}\cdots\text{H}$ contacts which are shorter than 2.40 \AA . They only include good quality X-ray crystallographic determinations ($R_{\text{factor}} < 0.05$) and exclude from their search any $\text{H}\cdots\text{H}$ close contact involving methyl group since free rotation of the methyl can cause the positions of the hydrogen to be highly uncertain. A search of the C–H \cdots H–C interactions, unconstrained by angle, results in 23 hits and shows that both C–H \cdots H angles cluster around $100\text{--}140^\circ$ and that the majority of the $d_{\text{H}\cdots\text{H}}$ tend to be around $2.3\text{--}2.4 \text{ \AA}$ (a $d_{\text{H}\cdots\text{H}}$ as short as 1.95 was found though). On the other hand, a search of the database for N–H \cdots H–N interactions results in 234 hits with a wide range of angular preference of $\sim 60\text{--}170^\circ$, and a preference for $d_{\text{H}\cdots\text{H}}$ of $2.2\text{--}2.4 \text{ \AA}$. The authors conjecture that these interactions may have a role in the stabilisation of the crystals in which they occur intermolecularly.

7 CONCLUSIONS

The hydrogen–hydrogen bonding interaction is a phenomenon that occurs in a wide variety of organic and organometallic molecules, intra- and intermolecularly. We have used the quantum theory of atoms in molecules to classify, characterise, and calculate the local changes in the energy associated with this

interaction. Our analysis shows that this mode of closed-shell chemical bonding can impart a significant *local* stabilising contribution to the systems where it is found, a contribution which can be as high as 12 kcal/mol. The H–H bonding interaction along with its cousin, the dihydrogen bonding interaction, appears to contribute to the stability of several crystalline structures as revealed by chemical informatics [41] (a count including at least ~250 structures from those deposited at the Cambridge Structural Database [134–137] as of 2004).

The H–H and the dihydrogen bonding interactions are shown to be *qualitatively* different, yet there is no sharp demarcation line separating these two modes of chemical bonding. These two distinct modes of closed-shell bonding represent the two ends of a continuum: a non-directional non-electrostatic van der Waals-like interaction (H–H bonding) at one extreme, and a directional electrostatic attraction between a pair of oppositely charged hydrogen atoms (dihydrogen bonding) at the other extreme. Thus, for the sake of precision, authors are encouraged to distinguish between these two modes of bonding in their publications by using the proper term instead of lumping both under the common designation “dihydrogen bonding”. Furthermore, terms such as “steric non-bonded repulsive interactions” must be introduced with caution to our undergraduate students, perhaps gradually abandoned all together, in view of the accumulating evidence of the local stabilising contribution that can be associated with a H–H *bonding* interaction.

Finally, it is hoped that this presentation has sparked the interest of some readers in the quantum theory of atoms in molecules by showing how the topological properties of an experimental observable, the electron density, can be used to classify and categorise chemical bonding, in the spirit of the opening quote of this chapter.

ACKNOWLEDGMENTS

I am indebted to Professor Jesús Hernández-Trujillo (Universidad Nacional Autónoma de México), Professor Russell J. Boyd (Dalhousie University), and Dr. Elizabeth Zhurova and Professor Alan Pinkerton (both at the University of Toledo) for their permission to report here for the first time some previously unpublished data from our joint work. I also thank Dr. Katherine Robertson and Professor T. Stanley Cameron (both at Dalhousie University), Professor Jerzy Cioslowski (University of Szczecin), and the National Research Council of Canada for their permission to reproduce Figs. 14 and 7, respectively. I acknowledge Professor Russell J. Boyd and Mr. David Wolstenholme (Dalhousie University), and Professor Sławomir Grabowski (Łódź University) for their critical reading of the manuscript and helpful suggestions and comments. I am grateful to the Killam Trusts for an Izaak Walter Killam post doctoral fellowship and to McMaster University for an adjunct professorship of chemistry. Those acknowledged are not necessarily in complete agreement with the views espoused in this chapter.

REFERENCES

1. E. B. Wilson. *An Introduction to Scientific Research* (McGraw-Hill Book Co., Inc., New York, 1952).
2. N. V. Belkova, E. S. Shubina, L. M. Epstein. Diverse world of unconventional hydrogen bonds. *Acc. Chem. Res.*; **38**, 624–631 (2005).
3. I. Alkorta, I. Rozas, J. Elguero. Non-conventional hydrogen bonds. *Chem. Soc. Rev.*; **27**, 163–170 (1998).
4. M. J. Calhorda. Weak hydrogen bonds: theoretical studies. *Chem. Commun.*; 801–809 (2000).
5. T. Steiner. The hydrogen bond in the solid state. *Angew. Chem. Int. Ed. Engl.*; **41**, 48–76 (2002).
6. G. R. Desiraju, T. Steiner. *The Weak Hydrogen Bond in Structural Chemistry and Biology* (Oxford University Press, Inc., Oxford, 1999).
7. G. A. Jeffrey. *An Introduction to Hydrogen Bonding* (Oxford University Press, Oxford, 1997).
8. I. Alkorta, I. Rozas, J. Elguero. Isocyanides as hydrogen bond acceptors. *Theor. Chem. Acc.*; **99**, 116–123 (1998).
9. I. Rozas, I. Alkorta, J. Elguero. Inverse hydrogen-bonded complexes. *J. Phys. Chem. A*; **101**, 4236–4244 (1997).
10. J. A. Platts, S. T. Howard, K. Wozniak. Quantum chemical evidence for C–H···C hydrogen bonding. *Chem. Commun.*; 63–64 (1996).
11. J. A. Platts, S. T. Howard. C–H···C Hydrogen bonding involving ylides. *J. Chem. Soc., Perkin Trans. 2*; 2241–2248 (1997).
12. I. Alkorta, J. Elguero. Carbenes and silylenes as hydrogen bond acceptors. *J. Phys. Chem.*; **100**, 19367–19370 (1996).
13. I. Rozas, I. Alkorta, J. Elguero. Unusual hydrogen bonds: H··· π interactions. *J. Phys. Chem. A*; **101**, 9457–9463 (1997).
14. S. J. Grabowski, W. A. Sokalski, J. Leszczynski. Is a π ···H⁺··· π complex hydrogen bonded? *J. Phys. Chem. A*; **108**, 1806–1812 (2004).
15. U. Koch, P. L. A. Popelier. Characterization of C–H—O hydrogen bonds on the basis of the charge density. *J. Phys. Chem.*; **99**, 9747–9754 (1995).
16. R. H. Crabtree. A new type of hydrogen bond. *Science*; **282**, 2000–2001 (1998).
17. J. C. Jr. Lee, E. Peris, A. L. Rheingold, R. H. Crabtree. An unusual type of H···H interaction: Ir–H···H–O and Ir–H···H–N hydrogen bonding and its involvement in σ -metathesis. *J. Am. Chem. Soc.*; **116**, 11014–11019 (1994).
18. T. B. Richardson, S. de Gala, R. H. Crabtree. Unconventional hydrogen bonds: intermolecular B–H···H–N interactions. *J. Am. Chem. Soc.*; **117**, 12875–12876 (1995).
19. R. H. Crabtree, P. E. M. Siegbahn, O. Eisenstein, A. L. Rheingold, T. F. Koetzle. A new intermolecular interaction: unconventional hydrogen bonds with element–hydride bonds as proton acceptor. *Acc. Chem. Res.*; **29**, 348–354 (1996).
20. W. T. Klooster, T. F. Koetzle, P. E. M. Siegbahn, T. B. Richardson, R. H. Crabtree. Study of the N–H···H–B dihydrogen bond including the crystal structure of BH₃NH₃ by neutron diffraction. *J. Am. Chem. Soc.*; **121**, 6337–6343 (1999).
21. R. H. Crabtree. Dihydrogen complexes: some structural and chemical studies. *Acc. Chem. Res.*; **23**, 95–101 (1990).
22. R. C. Stevens, R. Bau, D. Milstein, O. Blum, T. F. Koetzle. Concept of the H(δ^+)···H(δ^-) interaction. A low-temperature neutron diffraction study of cis-[IrH(OH)(PMe₃)₄]PF₆. *J. Chem. Soc., Dalton Trans.*; 1429–1432 (1990).
23. S. Park, R. Ramachandran, A. J. Lough, R. H. Morris. A new type of intramolecular H···H···H interaction involving NH···H(Ir)···HN atoms. Crystal and molecular structure of [IrH(η^1 -SC₃H₄NH)₂(η^3 -SC₅H₄N)(PCy₃)]BF₄·0.72CH₂Cl₂. *J. Chem. Soc., Chem. Commun.*; 2201–2202 (1994).
24. G. J. Kubas. Molecular hydrogen complexes: coordination of a σ bond to transition metals. *Acc. Chem. Res.*; **21**, 120–128 (1988).

25. L. Pauling. *The Nature of the Chemical Bond* (Third Ed.) (Cornell University Press, Ithaca, N.Y., 1960).
26. P. L. A. Popelier. Characterization of a dihydrogen bond on the basis of the electron density. *J. Phys. Chem. A*; **102**, 1873–1878 (1998).
27. C. F. Matta, N. Castillo, R. J. Boyd. Extended weak bonding interactions in DNA: π -stacking (base–base), base–backbone, and backbone–backbone interactions. *J. Phys. Chem. B*; **110**, 563–578 (2006).
28. I. Rozas, I. Alkorta, J. Elguero. Field effects on dihydrogen bonded systems. *Chem. Phys. Lett.*; **275**, 423–428 (1997).
29. I. Alkorta, J. Elguero, O. Mo, M. Yanez, J. E. Del Bene. Ab initio study of the structural, energetic, bonding, and IR spectroscopic properties of complexes with dihydrogen bonds. *J. Phys. Chem. A*; **106**, 9325–9330 (2002).
30. S. J. Grabowski. High-level ab initio calculations of dihydrogen-bonded complexes. *J. Phys. Chem. A*; **104**, 5551–5557 (2000).
31. S. J. Grabowski. Ab initio calculations on conventional and unconventional hydrogen bonds—study of the hydrogen bond strength. *J. Phys. Chem. A*; **105**, 10739–10746 (2001).
32. S. Wojtulewski, S. J. Grabowski. Ab initio and AIM studies on intramolecular dihydrogen bonds. *J. Mol. Struct.*; **645**, 287–294 (2003).
33. P. Lipkowski, S. J. Grabowski, T. L. Robinson, J. Leszczynski. Properties of the C–H \cdots H dihydrogen bond: an ab initio topological analysis. *J. Phys. Chem. A*; **108**, 10865–10872 (2004).
34. S. J. Grabowski, W. A. Sokalski, J. Leszczynski. Nature of X–H δ^+ $\cdots\delta^-$ H–Y dihydrogen bonds and X–H $\cdots\sigma$ interactions. *J. Phys. Chem. A*; **108**, 5823–5830 (2004).
35. S. Grabowski, W. A. Sokalski, J. Leszczynski. How short can the H \cdots H intermolecular contact be? New findings that reveal the covalent nature of extremely strong interactions. *J. Phys. Chem. A*; **109**, 4331–4341 (2005).
36. D. Hugas, S. Simon, M. Duran. Counterpoise-corrected potential energy surfaces for dihydrogen bonded systems. *Chem. Phys. Lett.*; **386**, 373–376 (2004).
37. M. Solimannejad, A. Boutalib. Theoretical investigation of the weakly dihydrogen bonded dimers H $_{2-n}$ X $_n$ AlH \cdots HArF and H $_{2-n}$ X $_n$ AlH \cdots HKrF ($n = 0-2$; X = F, Cl). *Chem. Phys.*; **320**, 275–280 (2006).
38. S. Zhang, H. Li, P. Yang, S. Li. Geometries and properties of guanine–BH $_3$ complex: an investigation with density functional theory (DFT) method. *J. Mol. Struct. (Theochem)*; **682**, 47–53 (2004).
39. C. F. Matta, R. F. W. Bader. An atoms-in-molecules study of the genetically-encoded amino acids. I. Effects of conformation and of tautomerization on geometric, atomic, and bond properties. *Proteins: Struct. Funct. Genet.*; **40**, 310–329 (2000).
40. C. F. Matta, N. Castillo, R. J. Boyd. The characterization of a closed-shell fluorine–fluorine bonding interaction in aromatic compounds on the basis of the electron density. *J. Phys. Chem. A*; **109**, 3669–3681 (2005).
41. L. Damodharan, V. Pattabhi. Weak dihydrogen bond interactions in organic crystals. *Tetrahedron Lett.*; **45**, 9427–9429 (2004).
42. O. Ermer, S. A. Mason. Extremely short non-bonded H \cdots H distances in two derivatives of *exo,exo*-tetracyclo [6.2.1.1 3,6 .O 2,7] dodecane. *J. Chem. Soc., Chem. Commun.*; 53–54 (1983).
43. B. P. Reid, M. J. O’Loughlin, R. K. Sparks. Methane–methane isotropic interaction potential from total differential cross sections. *J. Chem. Phys.*; **83**, 5656–5662 (1985).
44. R. Righini, K. Maki, M. L. Klein. An intermolecular potential for methane. *Chem. Phys. Lett.*; **80**, 301–305 (1981).
45. J. J. Novoa, M. H. Whangboo, J. M. Williams. Interactions energies associated with short intermolecular contacts of C–H bonds. II. Ab initio computational study of the C–H \cdots H–C interactions in methane dimers. *J. Chem. Phys.*; **94**, 4835–4841 (1991).
46. S. F. Boys, F. Bernardi. The calculation of small molecular interactions by the differences of separate total energies. Some procedures with reduced errors. *Mol. Phys.*; **19**, 553–566 (1970).

47. F. B. van Duijneveldt, J. G. C. M. van Duijneveldt-van de Rijdt, J. H. van lenthe. State of the art in counterpoise theory. *Chem. Rev.*; **94**, 1873–1885 (1994).
48. C. F. Matta, J. Hernández-Trujillo, T. H. Tang, R. F. W. Bader. Hydrogen–hydrogen bonding: a stabilizing interaction in molecules and crystals. *Chem. Eur. J.*; **9**, 1940–1951 (2003).
49. S. G. Bodige, D. Sun, A. P. Marchand, N. N. Namboothiri, R. Shukla, W. H. Watson. Short H···H distances in norbornene derivatives. *J. Chem. Cryst.*; **29**, 523–530 (1999).
50. K. N. Robertson. *Intermolecular Interactions in a Series of Organoammonium Tetraphenylborates*; Ph.D. Thesis (Dalhousie University, Halifax, Canada, 2001).
51. K. N. Robertson, O. Knop, T. S. Cameron. C–H···H–C interactions in organoammonium tetraphenylborates: another look at dihydrogen bonds. *Can. J. Chem.*; **81**, 727–743 (2003).
52. C.-C. Wang, T.-H. Tang, L.-C. Wu, Y. Wang. Topological analyses and bond characterization of 1,3,5,7-tetra-*tert*-butyl-*s*-indacene: a weak C_{sp3}–H···H–C_{sp2}-type dihydrogen interaction. *Acta Cryst. A*; **60**, 488–493 (2004).
53. S. J. Grabowski, A. Pfitzner, M. Zabel, A. T. Dubis, M. Palusiak. Intramolecular H···H interactions for the crystal structures of [4-((E)-but-1-enyl)-2,6-dimethoxyphenyl]pyridine-3-carboxylate and [4-((E)-pent-1-enyl)-2,6-dimethoxyphenyl]pyridine-3-carboxylate; DFT calculations on modeled styrene derivatives. *J. Phys. Chem. B*; **108**, 1831–1837 (2004).
54. A. Bacchi, E. Bosetti, M. Carcelli, P. Pelagatti, D. Rogolini. The structural role of the triflate anion in the non-covalent silver polymer [Ag(LOH)₂(CF₃SO₃)(CH₃CN)] LOH = α-(4-pyridyl)benzhydrol. *Eur. J. Inorg. Chem.*; 1985–1991 (2004).
55. C. G. Pozzi, A. C. Fantoni, A. E. Goeta, C. C. Wilson, J. C. Autino, G. Punte. Close shell interactions in 3-ethoxycarbonyl-4-hydroxy-6-methoxymethyleneoxy-1-methyl-2-quinolone: 100 K single crystal neutron diffraction study and ab initio calculations. *J. Mol. Struct.*; **753**, 173–181 (2005).
56. G. C. Nemes, L. Silaghi-Dumitrescu, I. Silaghi-Dumitrescu, J. Escudié, H. Ranaivonjatovo, K. C. Molloy, M. F. Mahon, J. Zukerman-Schpector. Difluorenylsilanes, -germanes, and -stannanes exhibiting an unprecedented parallel arrangement of the fluorene units. *Organometallics*; **24**, 1134–1144 (2005).
57. J. Cioslowski, S. T. Mixon. Universality among topological properties of electron density associated with the hydrogen–hydrogen nonbonding interactions. *Can. J. Chem.*; **70**, 443–449 (1992).
58. C. F. Matta. *Applications of the Quantum Theory of Atoms in Molecules to Chemical and Biochemical Problems*; Ph.D. Thesis (McMaster University, Hamilton, Canada, 2002) (<http://chem.utoronto.ca/~cmatta/>).
59. F. Cortés-Guzmán, J. Hernández-Trujillo, G. Cuevas. The non-existence of repulsive 1,3-diaxial interactions in monosubstituted cyclohexanes. *J. Phys. Chem. A*; **107**, 9253–9256 (2003).
60. M. Montejo, A. Navarro, G. J. Kearley, J. Vázquez, J. J. López-González. Intermolecular charge transfer and hydrogen bonding in solid furan. *J. Am. Chem. Soc.*; **126**, 15087–15095 (2004).
61. I. V. Glukhov, M. Y. Antipin, K. A. Lyssenko. C–C Bond variation in the 1-phenyl-*o*-carborane: steric versus electronic effects. *Eur. J. Inorg. Chem.*; 1379–1384 (2004).
62. A. Vila, R. A. Mosquera. Quantum theory of atoms in molecules analysis on the conformation preferences of vinyl alcohol and related ethers. *J. Phys. Chem. A*; **109**, 6985–6989 (2005).
63. R. F. W. Bader. *Atoms in Molecules: A Quantum Theory* (Oxford University Press, Oxford, U.K., 1990).
64. C. F. Matta, J. Hernández-Trujillo. Unpublished data; (2003).
65. P. Coppens. *X-ray Charge Densities and Chemical Bonding* (Oxford University Press, Inc., New York, 1997).
66. P. Macchi, A. Angelo Sironi. Chemical bonding in transition metal carbonyl clusters: complementary analysis of theoretical and experimental electron densities. *Coord. Chem. Rev.*; **238–239**, 383–412 (2003).

67. T. S. Koritsanszky, P. Coppens. Chemical applications of X-ray charge-density analysis. *Chem. Rev.*; **101**, 1583–1628 (2001).
68. P. Coppens, B. Iversen, F. K. Larsen. The use of synchrotron radiation in X-ray charge density analysis of coordination complexes. *Coord. Chem. Rev.*; **249**, 179–195 (2005).
69. C. Gatti. Chemical bonding in crystals: new directions. *Z. Kristallogr.*; **220**, 399–457 (2005).
70. R. F. W. Bader, C. F. Matta, F. J. Martín. “Atoms in medicinal chemistry”. In: F. Alber, P. Carloni (Eds.). *Medicinal Quantum Chemistry*. (Wiley-VCH, Weinheim, 2003), pp. 201–231.
71. F. Cortés-Guzmán, R. F. W. Bader. Complementarity of QTAIM and MO theory in the study of bonding in donor–acceptor complexes. *Coord. Chem. Rev.*; **249**, 633–662 (2005).
72. R. F. W. Bader. The quantum mechanical basis of conceptual chemistry. *Monatsh Chem.*; **136**, 819–854 (2005).
73. R. F. W. Bader. In: P. v. Schleyer, (Ed.). *Encyclopedia of Computational Chemistry*. (John Wiley and Sons, Chichester, U.K., 1998), pp. 64–86.
74. R. F. W. Bader. 1997 Polanyi award lecture: why are there atoms in chemistry? *Can. J. Chem.*; **76**, 973–988 (1998).
75. R. F. W. Bader, P. L. A. Popelier, T. A. Keith. Theoretical definition of a functional group and the molecular orbital paradigm. *Angew. Chem. Int. Ed. Engl.*; **33**, 620–631 (1994).
76. R. F. W. Bader. A quantum theory of molecular structure and its applications. *Chem. Rev.*; **91**, 893–928 (1991).
77. R. F. W. Bader, T. T. Nguyen-Dang. Quantum theory of atoms in molecules—Dalton revisited. *Adv. Quantum Chem.*; **14**, 63–123 (1981).
78. R. F. W. Bader, T. T. Nguyen-Dang, Y. Tal. A topological theory of molecular structure. *Rep. Prog. Phys.*; **44**, 893–948 (1981).
79. P. L. A. Popelier. *Atoms in Molecules: An Introduction* (Prentice Hall, London, 2000).
80. R. J. Gillespie, P. L. A. Popelier. *Molecular Geometry and Chemical Bonding: From Lewis to Electron Densities* (Oxford University Press, New York, 2001).
81. P. L. A. Popelier, F. M. Aicken, S. E. O’Brien. “Atoms in molecules”. *Chemical Modelling: Applications and Theory, Vol. 1* (The Royal Society of Chemistry, Cambridge, U.K., 2000), pp. 143–198.
82. P. L. A. Popelier, P. J. Smith. “Quantum topological atoms”. *Chemical Modelling: Applications and Theory, Vol. 2* (The Royal Society of Chemistry, Cambridge, U.K., 2002), pp. 391–448.
83. V. Luaña, A. Costales, P. Mori-Sánchez, M. A. Blanco, A. Martín Pendás. Topological properties of the electron density of solids and molecules. Recent developments in Oviedo. *Acta Cryst. A*; **60**, 434–437 (2004).
84. C. F. Matta, R. J. Gillespie. Understanding and interpreting electron density distributions. *J. Chem. Educ.*; **79**, 1141–1152 (2002).
85. C. Gatti, P. Fantucci, G. Pacchioni. Charge density topological study of bonding in lithium clusters. Part I: Planar Li *n* clusters (*n*=4, 5, 6). *Theor. Chem. Acc. (Formerly, Theoret. Chim. Acta)*; **72**, 433–458 (1987).
86. W. L. Cao, C. Gatti, P. J. MacDougall, R. F. W. Bader. On the presence of non-nuclear attractors in the charge distributions of Li and Na clusters. *Chem. Phys. Lett.*; **141**, 380–385 (1987).
87. R. F. W. Bader, C. F. Matta. Bonding to titanium. *Inorg. Chem.*; **40**, 5603–5611 (2001).
88. R. F. W. Bader, C. F. Matta, F. Cortés-Guzmán. Where to draw the line in defining a molecular structure. *Organometallics*; **23**, 6253–6263 (2004).
89. R. F. W. Bader. A bond path: a universal indicator of bonded interactions. *J. Phys. Chem. A*; **102**, 7314–7323 (1998).
90. G. R. Runtz, R. F. W. Bader, R. R. Messer. Definition of bond paths and bond directions in terms of the molecular charge distribution. *Can. J. Chem.*; **55**, 3040–3045 (1977).
91. T. A. Keith, R. F. W. Bader, Y. Aray. Structural homeomorphism between the electron density and the virial field. *Int. J. Quantum Chem.*; **57**, 183–198 (1996).

92. R. F. W. Bader, P. M. Beddall. Virial field relationship for molecular charge distributions and the spatial partitioning of molecular properties. *J. Chem. Phys.*; **56**, 3320–3328 (1972).
93. R. F. W. Bader. Principle of stationary action and the definition of a proper open system. *Phys. Rev. B*; **49**, 13348–13356 (1994).
94. R. F. W. Bader, P. L. A. Popelier. Atomic theorems. *Int. J. Quantum Chem.*; **45**, 189–207 (1993).
95. J. Schwinger. The theory of quantized fields. I. *Phys. Rev.*; **82**, 914–927 (1951).
96. R. F. W. Bader, C. F. Matta. Atomic charges are measurable quantum expectation values: a rebuttal of criticisms of QTAIM charges. *J. Phys. Chem. A*; **108**, 8385–8394 (2004).
97. R. F. W. Bader, P. F. Zou. An atomic population as the expectation value of a quantum observable. *Chem. Phys. Lett.*; **191**, 54–58 (1992).
98. K. M. Gough, H. K. Srivastava, K. Belohorcová. Analysis of Raman trace scattering intensities in alkanes with the theory of atoms in molecules. *J. Chem. Phys.*; **98**, 9669–9677 (1993).
99. K. M. Gough, H. K. Srivastava, K. Belohorcová. Molecular polarizability and polarizability derivatives in cyclohexane analyzed with the theory of atoms in molecules. *J. Phys. Chem.*; **98**, 771–776 (1994).
100. K. M. Gough, H. K. Srivastava. Electronic charge flow and Raman trace scattering intensities for CH stretching vibrations in *n*-pentane. *J. Phys. Chem.*; **100**, 5210–5216 (1996).
101. K. M. Gough, M. M. Yacowar, R. H. Cleve, J. R. Dwyer. Analysis of molecular polarizabilities and polarizability derivatives in H₂, N₂, F₂, CO, and HF, with the theory of atoms in molecules. *Can. J. Chem.*; **74**, 1139–1144 (1996).
102. R. L. A. Haiduke, A. E. de Oliveira, R. E. Bruns. Atomic mean dipole moment derivative and anisotropic contributions to molecular infrared intensity sums. *J. Phys. Chem. A*; **108**, 6788–6796 (2004).
103. P. H. César, S. H. D. M. Faria, J. V. da Silva Jr., R. L. A. Haiduke, R. E. Bruns. A charge–charge flux–dipole flux decomposition of the dipole moment derivatives and infrared intensities of the AB₃ (A = N, P; B = H, F) molecules. *Chem. Phys.*; **317**, 35–42 (2005).
104. R. L. A. Haiduke, R. E. Bruns. An atomic charge–charge flux–dipole flux atom-in-molecule decomposition for molecular dipole-moment derivatives and infrared fundamental intensities. *J. Phys. Chem. A*; **109**, 2680–2688 (2005).
105. R. J. Boyd, S. C. Choi. Hydrogen bonding between nitriles and hydrogen halides and the topological properties of molecular charge distribution. *Chem. Phys. Lett.*; **129**, 62–65 (1986).
106. M. T. Carroll, R. F. W. Bader. An analysis of the hydrogen bond in BASE–HF complexes using the theory of atoms in molecules. *Mol. Phys.*; **65**, 695–722 (1988).
107. E. Espinosa, E. Molins, C. Lecomte. Hydrogen bond strengths related by topological analyses of experimentally observed electron densities. *Chem. Phys. Lett.*; **285**, 170–173 (1998).
108. M. Domagala, S. Grabowski, K. Urbaniak, G. Mloston. Role of C–H···S and C–H···N hydrogen bonds in organic crystal structures—the crystal and molecular structure of 3-methyl-2,4-diphenyl-(1,3)-thiazolidine-5-spiro-2'-adamantane and 3-methyl-2,4,5,5-tetraphenyl-(1,3)-thiazolidine. *J. Phys. Chem. A*; **107**, 2730–2736 (2003).
109. M. Domagala, S. Grabowski. C–H···N and C–H···S hydrogen bonds—influence of hybridization on their strength. *J. Phys. Chem. A*; **109**, 5683–5688 (2005).
110. D. Cremer, E. Kraka. Chemical bonds without bonding electron density—does the difference electron-density analysis suffice for a description of the chemical bond? *Angew. Chem. Int. Ed. Engl.*; **23**, 627–628 (1984).
111. X. Fradera, M. A. Austen, R. F. W. Bader. The Lewis model and beyond. *J. Phys. Chem. A*; **103**, 304–314 (1999).
112. M. A. Austen. *A New Procedure for Determining Bond Orders in Polar Molecules, with Applications to Phosphorus and Nitrogen Containing Systems*; Ph.D. Thesis (McMaster University, Hamilton, Canada, 2003).
113. C. F. Matta, J. Hernández-Trujillo. Bonding in polycyclic aromatic hydrocarbons in terms of the electron density and of electron delocalization. *J. Phys. Chem. A*; **109**, 10798 (2005).

114. R. Bianchi, G. Gervasio, D. Marabello. Experimental electron density analysis of $\text{Mn}_2(\text{CO})_{10}$: metal–metal and metal–ligand bond characterization. *Inorg. Chem.*; **39**, 2360–2366 (2000).
115. F. W. Biegler-König, R. F. W. Bader, T.-H. Tang. Calculation of the average properties of atoms in molecules. II. *J. Comput. Chem.*; **13**, 317–328 (1982).
116. R. F. W. Bader. *AIMPAC*. <http://www.chemistry.mcmaster.ca/aimpac/>.
117. T. Keith (1997). *AIMALL97 (for DOS/Windows)* (private communication).
118. F. W. Biegler-König, J. Schönbohm, D. Bayles. AIM2000—a program to analyze and visualize atoms in molecules. *J. Comput. Chem.*; **22**, 545–559 (2001).
119. F. W. Biegler-König, J. Schönbohm, D. Bayles. “AIM2000 program can be downloaded from Internet at <http://gauss.fh-bielefeld.de/aim2000>”.
120. F. Cortés-Guzmán, R. F. W. Bader. Transferability of group energies and satisfaction of the virial theorem. *Chem. Phys. Lett.*; **379**, 183–192 (2003).
121. T. A. Keith. Link for Gaussian to perform Self-Consistent Virial Scaling (SCVS) of ab-initio calculations. *Private communication* (1997).
122. M. J. Frisch, G. W. Trucks, H. B. Schlegel, G. E. Scuseria, M. A. Robb, J. R. Cheeseman, Jr. J. A. Montgomery, T. Vreven, K. N. Kudin, J. C. Burant, J. M. Millam, S. S. Iyengar, J. Tomasi, V. Barone, B. Mennucci, M. Cossi, G. Scalmani, N. Rega, G. A. Petersson, H. Nakatsuji, M. Hada, M. Ehara, K. Toyota, R. Fukuda, J. Hasegawa, M. Ishida, T. Nakajima, Y. Honda, O. Kitao, H. Nakai, M. Klene, X. Li, J. E. Knox, H. P. Hratchian, J. B. Cross, C. Adamo, J. Jaramillo, R. Gomperts, R. E. Stratmann, O. Yazyev, A. J. Austin, R. Cammi, C. Pomelli, J. W. Ochterski, P. Y. Ayala, K. Morokuma, G. A. Voth, P. Salvador, J. J. Dannenberg, V. G. Zakrzewski, S. Dapprich, A. D. Daniels, M. C. Strain, O. Farkas, D. K. Malick, A. D. Rabuck, K. Raghavachari, J. B. Foresman, J. V. Ortiz, Q. Cui, A. G. Baboul, S. Clifford, J. Cioslowski, B. B. Stefanov, G. Liu, A. Liashenko, P. Piskorz, I. Komaromi, R. L. Martin, D. J. Fox, T. Keith, M. A. Al-Laham, C. Y. Peng, A. Nanayakkara, M. Challacombe, P. M. W. Gill, B. Johnson, W. Chen, M. W. Wong, C. Gonzalez, J. A. Pople, *Gaussian03, Revision B.03* (Gaussian Inc.: Pittsburgh PA, 2003).
123. P.-O. Löwdin. Scaling problem, virial theorem, and connected relations in quantum mechanics. *J. Mol. Spectr.*; **3**, 46–66 (1959).
124. D. E. Magnoli, J. R. Murdoch. Obtaining self-consistent wave functions which satisfy the virial theorem. *Int. J. Quantum Chem.*; **22**, 1249–1262 (1982).
125. N. K. Hansen, P. Coppens. Testing aspherical atom refinement on small molecules data sets. *Acta Cryst.*; **A34**, 909–921 (1978).
126. C. F. Matta. *AIMDELOC: Program to calculate AIM localization and delocalization indices (QCPE0802)*. Quantum Chemistry Program Exchange, Indiana University: IN 2001 (<http://qcpe.chem.indiana.edu/>).
127. C. F. Matta, J. Hernández-Trujillo, R. F. W. Bader. Proton spin–spin coupling and electron delocalisation. *J. Phys. Chem. A*; **106**, 7369–7375 (2002).
128. G. M. Badger. *Aromatic Character and Aromaticity* (Cambridge University Press, Cambridge, 1969).
129. L. V. Vilkov, V. S. Mastryukov, N. I. Sadova. *Determination of the Geometrical Structure of Free Molecules* (English translation) (Mir Publishers, Moscow, 1983).
130. R. Thom. *Structural Stability and Morphogenesis: An Outline of a General Theory of Models (English Translation)* (Adison-Wesley Publishing Company, Massachusetts, 1972).
131. C. F. Matta. *Work in progress, to be published* (2006).
132. P. T. Brain, J. Cowie, D. J. Donohoe, D. Hnyk, D. W. H. Rankin, D. Reed, B. D. Reid, H. E. Robertson, A. J. Welch, M. Hofmann, P. v. R. Schleyer. 1-Phenyl-1,2-dicarba-*closo*-dodecaborane, 1-Ph-1,2-*closo*- $\text{C}_2\text{B}_{10}\text{H}_{11}$. Synthesis, characterization, and structure as determined in the gas phase by electron diffraction, in the crystalline phase at 199 K by X-ray diffraction, and by ab initio computations. *Inorg. Chem.*; **35**, 1701–1708 (1996).
133. E. A. Zhurova, C. F. Matta, N. Wu, V. V. Zhurov, A. A. Pinkerton. Experimental and theoretical electron density study of estrone. *J. Am. Chem. Soc.*; **128**, 8849–8861 (2006).

134. F. H. Allen. The Cambridge Structural Database: a quarter of a million crystal structures and rising. *Acta Crystallogr. B*; **58**, 380–388 (2002).
135. A. G. Orpen. Applications of the Cambridge Structural Database to molecular inorganic chemistry. *Acta Crystallogr. B*; **58**, 398–406 (2002).
136. F. H. Allen, W. D. S. Motherwell. Applications of the Cambridge Structural Database in organic chemistry and crystal chemistry. *Acta Crystallogr. B*; **58**, 407–422 (2002).
137. R. Taylor. Life Science applications of the Cambridge Structural Database. *Acta Crystallogr. D*; **58**, 879–888 (2002).

CHAPTER 10

POTENTIAL ENERGY SHAPE FOR THE PROTON MOTION IN HYDROGEN BONDS REFLECTED IN INFRARED AND NMR SPECTRA

GLEB S. DENISOV¹, JANEZ MAVRI² and LUCJAN SOBCZYK^{3,*}

¹ *Institute of Physics, St. Petersburg State University, Petrodvorets, Ulyanovskaya 1, 198504 Sankt Petersburg, Russia;* ² *National Institute of Chemistry, Hajdrihova 19, SI-1000 Ljubljana, Slovenia;* ³ *Faculty of Chemistry, University of Wrocław, Joliot-Curie 14, 50-383 Wrocław, Poland*

Abstract The importance of the shape of the potential for the proton motion in hydrogen bonds is emphasized in various molecular phenomena. There are discussed such problems as anharmonicity, empirical equations describing potentials, variational solutions of the Schrödinger equation, Car–Parrinello simulation and quantum-dynamical simulation of the proton motion. Critical review is presented with respect to the relationship between the anharmonic potential energy shape and infrared spectra. Possibilities of application of NMR spectra with various nuclei are presented as applied to complexes of neutral molecules and with participation of ions. An attention is also paid to intramolecular hydrogen bonds in such systems like enols of β -diketones.

Keywords: Potential for the proton motion; theoretical treatment; anharmonicity and IR spectra; NMR spectra.

1 INTRODUCTION

The shape of the potential for the proton motion, particularly when the proton is engaged in hydrogen bond formation, is one of the most fascinating problems of molecular physics and chemistry. Because of very low mass the stretching protonic vibrations are characterized by high frequencies and, if independent of additional interactions, they are anharmonic. It is commonly known that expression of quantum-chemical calculations in the harmonic approximation, on various levels of the quantum-mechanical approach, needs the application of some scaling factors [1, 2]. For stretching protonic vibrations this factor is

* L. Sobczyk is the corresponding author.

less than unity: where the calculated frequencies are markedly higher than the experimental ones. The hydrogen bond interaction increases these effects.

The anharmonicity of the stretching protonic vibrations has several effects specific in character for hydrogen bonds. In particular, it leads to coupling with low frequency modes, arising from the bridge stretching vibrations. This phenomenon is of great importance in the relaxation of excited vibrational levels, and thus in broadening of IR bands and in the formation of the substructure of these bands [3]. It also results in the coupling of protonic stretching vibrations with overtones and summation frequencies of modes in the medium frequency range below 1800 cm^{-1} , particularly those which the $\delta(\text{AH})$ and $\gamma(\text{AH})$ protonic deformation vibrations contribute.

In the case of a very strong hydrogen bond the situation becomes much more complicated, in particular when we approach the so-called critical region where a double minimum potential appears. A variety of situations are illustrated in Fig. 1 for the simplified one-dimensional model.

One can expect that particular situation should appear for the double minimum potential with very low barrier. The anharmonicity of the potential in such a critical region is unusual; it can be opposite to that observed in usual hydrogen bonded systems. On the other hand, it is commonly accepted

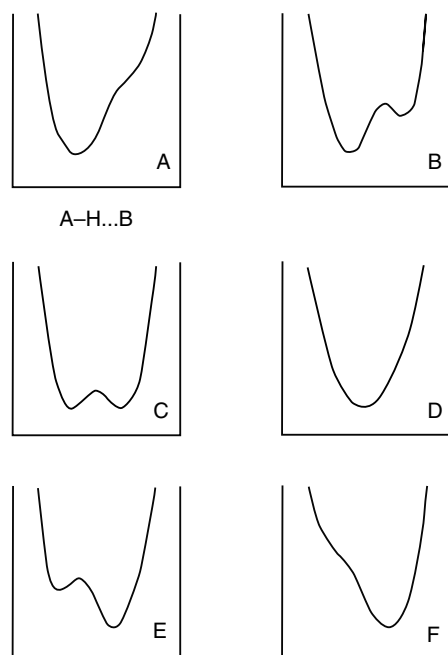


Figure 1. Various one-dimensional potential energy curves for the proton motion in $\text{AH}\cdots\text{B}$ hydrogen bonds.

that low-barrier hydrogen bonds are of great importance in chemistry and enzymology [4]. They will be one of the main topics to be discussed in this chapter.

There are a plethora of isotope effects accompanying hydrogen bond formation [5]. Isotopic substitution leads to a substantial decrease of anharmonicity of stretching vibrations, while also producing major effects when the barrier height is lowered. In this case the fundamental vibrational level is lowered with respect to the barrier top and a marked reduction of the tunnelling effect takes place.

In this review we would like to focus on three main topics:

- Theoretical aspects of the potential energy surface (Sects. 4–7).
- Correlation of infrared spectra with the shape of the potential (Sects. 8–10).
- NMR spectra of hydrogen bonded systems (Sects. 11–14).

The approaches described in Sects. 4–7 and the analytical approaches in the subsequent sections are complementary. Construction of the multidimensional hypersurface on medium high *ab initio* or DFT level and solving the vibrational Schrödinger equation require several thousand hours of CPU time. The obtained expectation values are reliable and usually compare well with the experiment. The approach may, however, be classified as a numerical experiment since there are no analytical solutions.

The application of one-dimensional model potentials provides many insights and helps predict trends, which can be of significant benefit to experimentalists rationalizing their measurements and in designing new experiments.

2 EMPIRICAL EQUATIONS DESCRIBING ONE-AND TWO-DIMENSIONAL POTENTIALS

The one-dimensional potential energy curve describes precisely the electronic term of a system only in the simple case of diatomic molecules. With A–H bonds, where A is part of a multiatom molecule, the diatomic approximation is valid. But in the general case the potential energy as a function of the A–H bond length, $V(r)$, should be expressed using a polynomial expansion

$$(1) \quad V(r) = V(r_e) + \left(\frac{\partial V}{\partial r}\right)_{r=r_e} (r - r_e) + \frac{1}{2!} \left(\frac{\partial^2 V}{\partial r^2}\right)_{r=r_e} (r - r_e)^2 + \frac{1}{3!} \left(\frac{\partial^3 V}{\partial r^3}\right)_{r=r_e} (r - r_e)^3 + \dots$$

where r_e is the equilibrium bond length. The first non-zero square component of the polynomial has the parabolic shape that corresponds to the harmonic potential. However, the A–H bond, especially when forming the hydrogen bond, can never be approximated by a harmonic potential; and higher terms of the polynomial (i.e. cubic, etc.) corresponding to anharmonic potentials should be taken into account. The real potential may also be approximated

by simple functions based on experimental data or on quantum-chemical calculations of the energy for varying r .

The Morse potential, the oldest, and to date the most widely applicable expression, is presented for the diatomic molecule in the form

$$(2) \quad V(r) = D_e[1 - \exp(-a(r - r_e))]^2$$

where constants D_e and a express the depth and width of the potential well, and r_e is the equilibrium distance. The comparison of the harmonic potential with the real anharmonic potential is shown in Fig. 2, where D_o is the dissociation energy and D_e is the bond energy. The Morse potential is much more realistic than the potential function described in the harmonic approximation. The chemical bond described by the Morse function can dissociate. A combination of Morse functions is the basis for the empirical valence bond (EVB) method, which can realistically describe parts of the Born–Oppenheimer (BO) surface responsible for chemical reactivity [6].

The Morse function describes quite satisfactorily the potential where $r > r_e$, but it is less reliable where $r < r_e$ because there is a strong repulsion at small interatomic distances.

A somewhat modified version of the Morse potential was proposed [7] in the form

$$(3) \quad V(r) = D_e[1 - \exp(-n(r - r_e)^2/2r)]$$

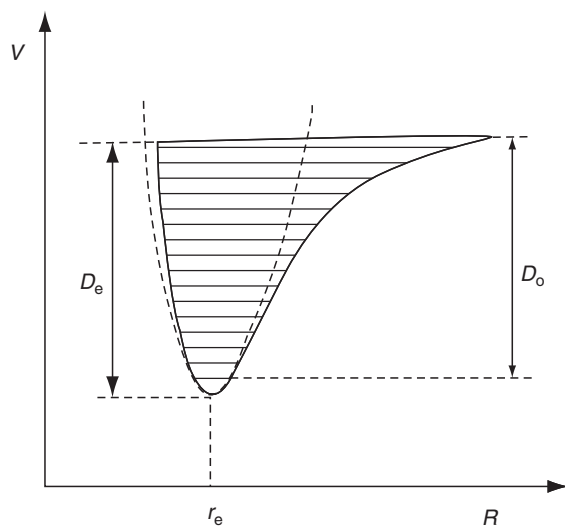


Figure 2. Harmonic (dashed curve) vs. real anharmonic potential $V(r)$ with vibrational levels; r_e is equal to the equilibrium distance.

where the coefficient $n = k_e r_e / D_e$ replaces the parameter a (k_e is the force constant of the stretching vibrations). The diatomic approximation is applicable to AH stretching vibrations, since they can be described as a separate mode due to small mass of a proton and high frequency.

For strong hydrogen bonds a second potential minimum appears, and that leads to a substantial modification of the potential energy curve. The simplest solution of the problem was the application of the double Morse function [8], shown in the form

$$(4) \quad V(r) = D_e \{ \exp[-2a(r - r_e)] - 2 \exp[-a(r - r_e)] \}$$

This has been applied successfully to the analysis of tunnelling phenomena and isotope effects in strongly hydrogen-bonded crystals.

The best description of the one- and the two-dimensional potential is the Lippincott-Schröder equation [7]. The Lippincott-Schröder function consists of three parts assigned to three interaction components V_1, V_2, V_3 , respectively, A-H, $B^+ - H$ (proton transfer state) and $A \cdots B$:

$$(5) \quad \begin{array}{c} V(r', R) = V(r') + V_2(r', R) + V_3(r', R) \\ \downarrow \quad \downarrow \quad \downarrow \\ \text{A-H} \quad \text{B}^+ - \text{H} \quad \text{A} \cdots \text{B} \end{array}$$

The geometrical parameters used in the description of the above components are presented in Fig. 3.

The values of particular components are expressed in the following equations:

$$(6) \quad V_1(r') = D \left[1 - \exp \left(\frac{-n(r - r_o \cos \alpha^2)}{2r' \cos \alpha} \right) \right]$$

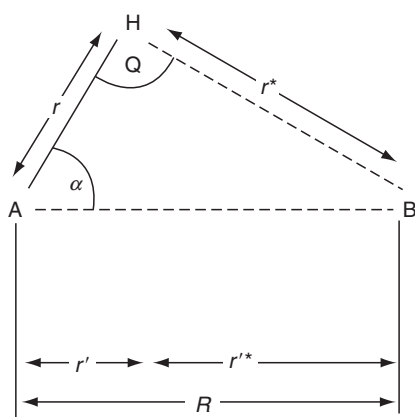


Figure 3. Geometrical parameters used in the Lippincott-Schröder equation.

$$(7) \quad V_2(r', R) = -D \left[\frac{n^*[R - r - r_o^* \cos(\alpha + \Theta)]^2}{2(R - r') \cos(\alpha + \Theta)} \right]$$

$$(8) \quad V_3(r', R) = A(r') \exp(-bR_o) \left\{ \exp \left[-b(R - R_o) - \frac{1}{2}(R_o/R)^m \right] \right\}$$

while

$$A(r') = -n^* D^* \left\{ 1 - [r_o^*/(R_o - r')]^2 \right\} \exp \left[\frac{n^*[R_o - r' - r_o^* \cos(\alpha + \Theta)]^2}{2(R_o - r') \cos(\alpha + \Theta)} \right] \\ \times [2 \cos(\alpha + \Theta) \exp(-bR_o)(b - m/2R_o)]^{-1}$$

where, $n = k_o r_o / D$ (k_o is the force constant of vibration of the free A–H group); $n^* = k^* r^* D^*$, and is related to the B⁺–H group; D and D^* are the A–H and B⁺–H bond energies; b represents the repulsion between A and B while the exponent m is close to unity.

The parameter values of the Lippincott–Schröder equation for the three most common types of hydrogen bonds are summarized in Table 1 [9].

The usefulness of Lippincott–Schröder potential was shown, e.g., in studies of isotope effects and vibrational levels [10].

The fourth-order polynomial proposed for the first time by Somorjai and Hornig [11] appeared to be useful in semiquantitative analysis, and can be expressed in the general form

$$(9) \quad V(r, R) = a_2(R)r^2 + a_3(R)r^3 + a_4(R)r^4$$

where R is the bridge coordinate (the A···B distance) and r is the A–H distance. The coefficients a_2 , a_3 , a_4 are normally a function of R . The first component of the equation expresses the harmonic potential with a single minimum, while the third component presents a symmetrical double minimum potential. The second component describes the asymmetry of the potential. The coefficients a_2 and a_4 can be fitted to experimental spectroscopic correlations for particular types of hydrogen bonds [12]. The equation was successfully applied in a semiquantitative analysis of IR spectra of hydrogen bonded systems [13, 14]. A simple double minimum potential was proposed by Laane [15] in studies on the influence of the

Table 1. Values of the Lippincott–Schröder potential parameters for OH···O, NH···O and N–H···N hydrogen bonds

	OH···O	NH···O	NH···N
D (kcal · mol ⁻¹)	118.6	112.4	112.5
n (10 ⁸ cm ⁻¹)	9.18	8.60	9.01
n^* (10 ⁸ cm ⁻¹)	13.32	13.15	13.49
r_o (Å)	0.97	0.99	1.033
r_o^* (Å)	0.97	0.97	1.038
b (10 ⁸ cm ⁻¹)	4.8	4.8	4.8

barrier height on the IR spectroscopic behaviour of hydrogen bonds. A detailed analysis of the hydrogen and proton transfer processes in hydrogen bonded systems was recently performed based on the modified Lippincott–Schröder potential [16]. This showed good agreement of calculated barrier heights with experimental data and with advanced ab initio calculations.

3 EMPIRICAL VALENCE BOND APPROACH

Ab initio and DFT calculations of the BO surfaces, which are used to describe hydrogen-bonded systems, are computationally demanding. Computational practice has shown that a flexible basis set is required. The Hartree–Fock (HF) level is typically insufficient, and electron correlation must be included. DFT is an attractive alternative to the post HF calculations. The hypersurface is obtained in such a way pointwise. One can fit it to a computationally efficient form that allows for an inexpensive evaluation needed in thermal averaging or calculation of matrix elements when performing vibrational analysis.

The EVB method proposed by Warshel [6] is an elegant and computationally very efficient method of describing the entire BO surface, thus allowing treatment of chemical reactions such as proton transfer in hydrogen bonds. It can also be used in vibrational analysis. In conjunction with the environment described at the molecular mechanics level it was the first QM/MM method. Vibrational analyses of hydrogen bonded systems and of enzymatic catalysis have a lot in common.

In both cases it is necessary to describe parts of the hypersurface relatively high above the minimum. In a typical enzymatic reaction proton transfer is associated with the rearrangement of covalent bonds, where the free energy of activation is about $20 \text{ kcal} \cdot \text{mol}^{-1}$. The vibrational transition $0 \rightarrow 1$ in a hydrogen bond has an OH stretching frequency of 3000 cm^{-1} with a ground vibrational state at $4.3 \text{ kcal} \cdot \text{mol}^{-1}$ and the first excited state at around $12.9 \text{ kcal} \cdot \text{mol}^{-1}$. In EVB the system wave function is represented by two or more resonant forms.

A proton transfer across a heteronuclear hydrogen bond can typically be represented with two resonant forms; one corresponding to the neutral state and the second one corresponding to the ionic state. In the EVB approach a Hamiltonian matrix is constructed. Diagonal matrix elements are usually described by Morse functions, while the off-diagonal elements are either constants or distance dependent functions. Hamiltonian diagonalization gives rise to eigenstates and eigenfunctions. EVB has strong transferability, which is essential for computational support of biocatalysis. Nuclear quantum effects can be easily studied by EVB, since matrix elements necessary for quantum treatment of nuclei can be calculated with minimal CPU time. EVB has been used frequently in studies of hydrogen-bonded systems, including proton transfer reactions in enzymes. For a recent discussion concerning EVB and closely related methods see Ref. [17].

4 VARIATIONAL SOLUTIONS OF THE SCHRÖDINGER EQUATION

Hydrogen bonded systems are highly anharmonic and therefore their computational treatment in a harmonic approximation is of very limited value. On the other hand, rapid progress in advanced experimental techniques, such as the pulse-echo treatment of hydrogen bonding dynamics, requires computational support that should, ideally, be state-resolved. The ideal solution would consist of a numerical solution of the time-dependent Schrödinger equation (SE) for the nuclei. The time-independent SE still provides solutions that are of high value for the interpretation of experimental data. Thus, they are useful for the interpretation of vibrational spectra, or for H/D isotope effects on the chemical shift of hydrogen bonded systems.

A software program was developed for variational solutions of the time-independent SE in one and two dimensions [18]. Extension to more dimensions is straightforward. The first part of the program includes the fitting program (FIT), which allows points calculated by *ab initio* or DFT to be fitted to a computationally efficient and functional form. Proper fitting of the potential energy surface is crucial for the quality of the results. The second part of the program provides for the variational solution of the 2D Schrödinger, using either a shifted Gaussian basis set or a rectangular basis set [19]. The third part of the program calculates the expectation values, includes IR and Raman spectra (XPECT) and plots the results (PLOT). This program was applied to study the nature of the strong hydrogen bond in picolinic acid N-oxide (Fig. 4).

Potential energy surfaces calculated by *ab initio* or DFT are fitted to various functional forms that include: polynomial expansion, linear combination of Gaussians, splines and an EVB form. Proper fitting of the potential energy surface is essential for the calculated eigenvalues and eigenfunctions. In the case of picolinic acid N-oxide we have found satisfactory representation of the two-dimensional potential energy surface (2D PES) by a superposition of about ten shifted Gaussians. Shifted Gaussians or local constants on a rectangular grid were used as basis functions for the variational solution. As a criterion of reliability a given number of eigenvalues below the energy threshold were applied. Several test runs were performed on harmonic oscillators and on the intramolecular strong hydrogen bond in PANO. Only in nearly harmonic systems is the Gaussian basis set more favourable than the grid basis set in terms of CPU time and memory usage. For realistic, anharmonic systems it has been demonstrated that the grid basis set has several advantages over the Gaussian basis set:

- The potential part of the Hamiltonian matrix is diagonal. This becomes important if the potential energy matrix elements are not analytical.
- For sufficiently fine grids, the integration of the potential energy matrix elements can be approximated by the potential function above the centre of the basis function.

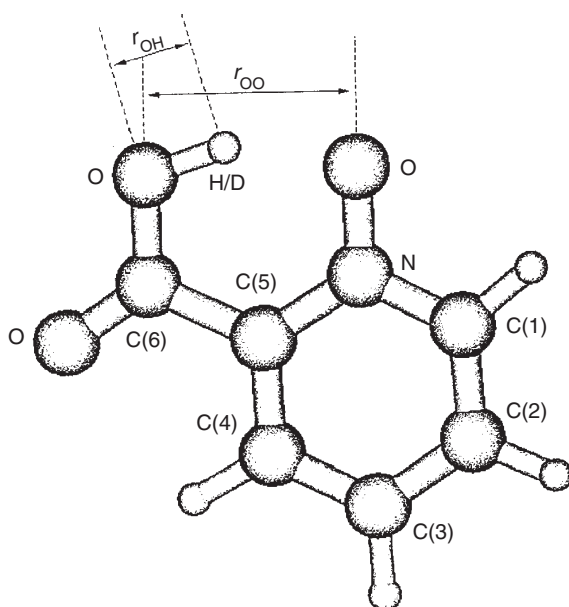


Figure 4. Structure and atom numbering in picolinic acid *N*-oxide.

- The grid basis set requires no orthogonalization. On the other hand, canonical orthogonalization with the Gaussian basis set requires overlap matrix diagonalization and one matrix multiplication.
- The grid basis set procedure is much easier to code.

With multidimensional problems, the grid basis set is more suitable for matrix diagonalization procedures, which yield a desired number of the lowest eigenvalues. Extension of the procedure to three and more dimensions is straightforward.

At this point it is worth emphasizing that the amount of CPU time required to construct the hypersurface depends exponentially on the number of dimensions. If ten points are required for each dimension then for a four-dimensional problem one would need 10,000 points, which is not a computationally trivial problem. Matrix operations involving such large matrices are also not trivial, both in terms of memory and CPU time.

It will be a challenge for the future to solve the Hadžis ABC trio of a strong hydrogen bonded system, representing a four-dimensional problem.

5 CALCULATION OF NMR ISOTOPE EFFECTS

Chemical shifts are the most important molecular responses to external magnetic fields. Chemical shift calculations are extremely sensitive for the applied level of theory. Calculated shift assist the interpretation of the NMR spectra of complex organic compounds [20–25].

In the case of strong hydrogen bonds a quantum nature of the proton motion adds additional complexity to the problem. Obviously, deuteration gives rise to different nuclear wave function for the hydrogen bond motion resulting in changed expected values that include chemical shifts. Traditionally computational studies concerning chemical shift isotope effects were limited only to one dimension: only OH stretching coordinate was concerned. In a recent study the approach to two dimensions was performed [26]. Beside isotopic substitution, the solvent effect was also considered: experiments were performed in chloroform and acetonitrile solution. The effects of solvation were taken into account using the solvent reaction field method of Tomasi and Persico [27]. It is worth emphasizing that the so-obtained hypersurfaces have meaning of free energy hypersurfaces as shown in Fig. 5. To summarize the work, the two-dimensional free energy and chemical shift hypersurfaces were constructed along the OH and OO internal coordinates that are of major importance for the structure and dynamics of hydrogen bonding in PANO. The anharmonic vibrational wave functions and their energies were calculated and used then in the thermal quantum averaging of the chemical shift functions. With minor exceptions, fairly good agreement between the calculated and experimental chemical shifts was found, especially for the relative values, signs and trends of the solvent effect and the isotope effects on chemical shifts. In particular, a good agreement between the experiment and the absolute values for the primary isotope effect was found. Some of the calculated values are in rather poor agreement with the

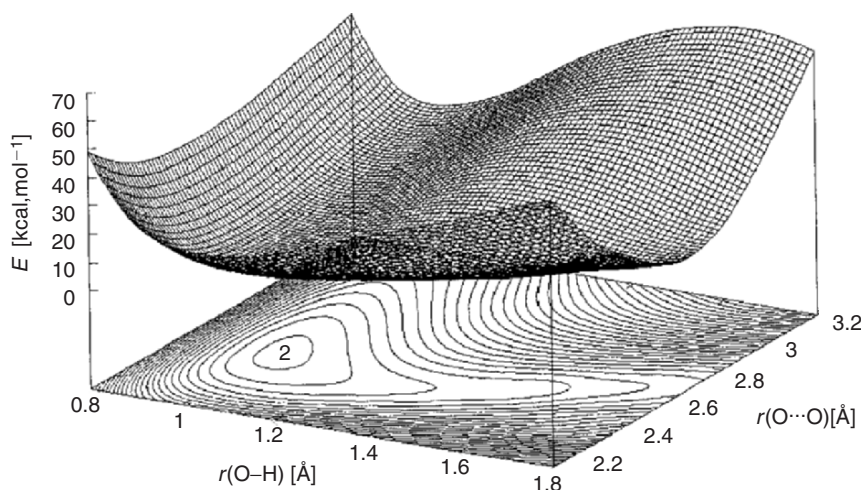


Figure 5. Free energy surface for picolinic acid *N*-oxide in chloroform solution as a function of OH and OO distances calculated on the B3LYP/6-31+G(*d,p*) level. Solvent reaction field method of Tomasi and Persico was used to calculate the free energy of solvation. The applied dielectric permittivity was 4.9.

experiment; this can possibly be attributed to limitations of the applied methods, including the B3LYP functional, the reaction field model and the limited number of vibrational degrees of freedom taken into account. In our study the vibrational SE was solved for the free energy hypersurface. In principle such an approach is methodologically questionable, since the quantization of fast vibrational degrees of freedom is performed over averaged solvent orientational polarization that is at least two orders of magnitude slower. This problem is associated not only with the present approach but is inherent to solvent reaction field in general in the context of solute electron motion vs. solvent dynamics. One believes that the explicit solvent treatment using a QM/MM scheme would improve the results, but we are aware that such an approach would be very CPU demanding. It is definitively a method of choice when dealing with isotope effects in hydrogen bonds in complex environments such as enzymes. All in all our experiment and calculations yield evidence that the hydron distribution in the hydrogen bond has a significant influence on the chemical shifts of all the carbon atoms in the investigated compound. It is illustrated for the C3 atom in Fig. 6.

We are sure that measurements of chemical shifts and associated computational support will play a very important role in the studies of enzyme active sites like in Ref. [28].

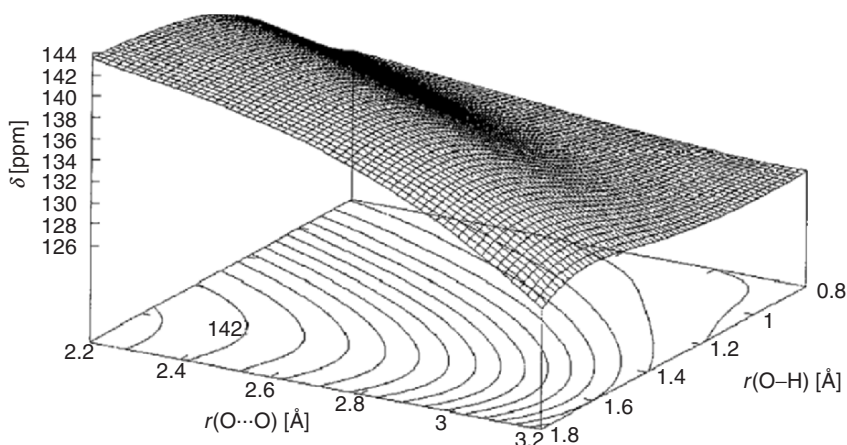


Figure 6. Chemical shift of the C3 atom as a function of OH and OO distance in picolinic acid *N*-oxide, according to Ref. [26]. Reprinted from Ref. [26] by permission granted by the American Chemical Society. For each OH and OO value all other geometry parameters were optimized. The inner contour labelled “2” pertains to the energy value of 2 kcal · mol⁻¹ above the minimum; successive contours are drawn at 2 kcal · mol⁻¹ intervals, according to Ref. [26].

6 CAR-PARRINELLO SIMULATION OF THE STRETCHING OH VIBRATIONS

In this section preliminary results of the Car–Parrinello molecular dynamics of PANO in the solid state are reported [29]. In particular, we are interested in simulation of the broad band associated with the OH stretching motion.

The Car–Parrinello method belongs to the class of the methods called *ab initio* molecular dynamics. These methods solve equations of motion for atomic nuclei, where the forces are calculated quantum-mechanically. The most widely used theory for studying the quantum-mechanical electronic structure problem of solids and larger molecular systems is the density-functional theory of Hohenberg and Kohn in the local-density approximation (LDA). Car and Parrinello’s method [30] is based on the LDA, and uses pseudopotentials and plane wave basis sets, but they added the concept of updating iteratively the electronic wave functions simultaneously with the motion of atomic nuclei (electron and nucleus dynamics are coupled). This is implemented in a standard molecular dynamics paradigm, associating dynamical degrees of freedom with each electronic Fourier component with a small mass. The procedure turned out to be very efficient, especially for the large systems.

The application of the plane wave basis set implies that the periodicity is taken into account and the method is therefore well suited for the simulation of the crystal field effects. For a recent review of Car–Parrinello methodology see Ref. [31]. With Car–Parrinello method the proton motion in PANO including the effects of crystal environment was simulated. The molecular dynamics simulation was carried out at a constant volume, i.e. the unit cell parameters were fixed during the simulation. Fictitious orbital mass was set to 150 a.u. (note that 1 a.u. corresponds to the electron mass) and the propagation time step was set to 2 a.u.

The temperature of the system was controlled using the Nose–Hoover thermostat for the nuclear motion. Target temperature was set to 300 K. The structure of PANO was energy minimized prior to the dynamics run. The simulation consisted of about 300,000 steps, the simulated time was approximately 14.5 ps. Nuclear coordinates were saved to the trajectory file every time step of the simulation. Next, snapshots of the dynamics were extracted from the trajectory every 5,000 steps (approx. 242 fs). In such a way, 50 distinct structures, as generated by the dynamics simulation, were obtained. From each of these structures, two proton potential functions (one per PANO molecule in the unit cell) were acquired by stepwise displacing the H-bonded proton along the line that connects the proton donor and the oxygen nucleus while keeping all the other nuclei frozen; a single point calculation was performed for each proton position. A total number of 100 proton potentials were obtained in such a way.

Anharmonic vibrational energies and wave functions were determined for each of these potentials by solving the vibrational SE. The variational Fourier

Grid Hamiltonian method was used for this purpose. The calculated anharmonic OH stretching frequencies are distributed over a wide range between 1,100 and 2,100 cm^{-1} . The frequency of each individual 0 to 1 vibrational transition is represented as a delta function whose height is proportional to the dipole-driven transition intensity in the approximation of electric harmonicity. The distribution of the frequencies outlines the shape of the broad band attributed to the OH stretching mode. The envelope shown in Fig. 7 was obtained by representing each individual transition as a Gaussian function of a half-width of 50 cm^{-1} centred at the pertinent frequency. Each of the Gaussians was scaled in such a way that its integral was equal to the calculated transition intensity. The calculated envelope of the OH stretching band spans over a very wide range and at least qualitatively matches the experimental broad absorption in the experimental infrared spectrum of solid PANO that is attributed to the OH stretching mode. The peak of the band at about 1,400 cm^{-1} is in good agreement with the estimated centre of the experimental broad absorption [32].

At this point it is worth to emphasize that the spectrum calculated from the velocity autocorrelation function is in disagreement with the experiment. The

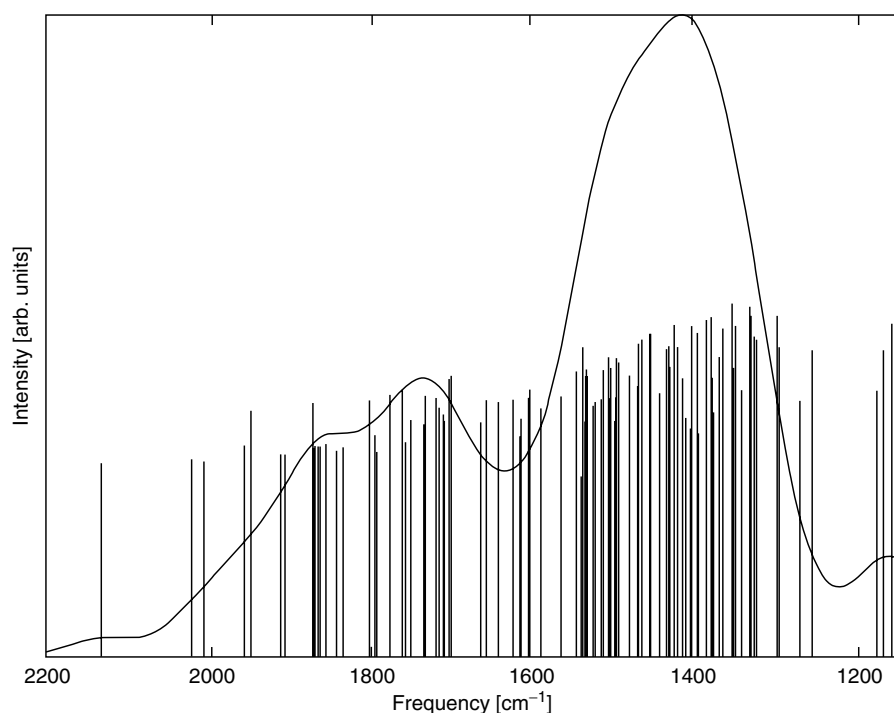


Figure 7. Car-Parrinello calculated envelope for the OH stretching mode in picolinic acid N-oxide in the solid state, according to Ref. [32].

applied methodology can be easily applied to study spectra of hydrogen bonds in solution or in a fluctuating macromolecular environment. Computational costs associated with evaluation of the force and energies, however, still prevent quantum-dynamical simulation of the proton motion using the Car–Parrinello methodology.

7 QUANTUM-DYNAMICAL SIMULATION OF THE PROTON MOTION

In this section we report quantum-dynamical simulation of the proton motion in acetylacetone. Acetylacetone is a medium strong hydrogen bonded system with the OH asymmetric stretching frequency band centred at 2800 cm^{-1} . The system is conjugated, giving rise to weak OH stretching frequency band. The band we simulated using the following strategy. First computationally inexpensive functional form of the potential was constructed. The one-dimensional OH motion was treated by time-dependent SE, while, the rest of the system, including solvent, was treated on the level of molecular mechanics. The density matrix evolution (DME) method is coupled with classical systems [33]. The DME method is based on the coupling of the Liouville–von Neumann equation with which the quantum subsystem is described with the classical equations of motion. For the quantum subsystem a few displaced Gaussian functions are used, what formally corresponds to the application of Gauss–Hermite polynomials that are eigenfunctions for harmonic oscillator. The force acting on the classical subsystem is just its expectation value. The DME method can be contrasted with the surface hopping method where the force originates from the pure quantum states, giving rise to the ad hoc scaling of the velocities of the classical particles in order to preserve the total energy.

The spectrum was calculated from the time-dependent wave function of the proton wave function. The proton potential in acetylacetone was first examined by semiempirical MO methods, *ab initio* methods on the HF and MP2 levels, and by the DFT method using the exchange functional proposed by Becke and the correlation functional of Lee, Yang and Parr. The semiempirical method yields an unreasonably high barrier to the proton transfer. The Hartree–Fock calculations also yield a too high barrier. The MP2 and B3LYP applied with large, flexible basis sets yield a classical barrier of under $3.0\text{ kcal}\cdot\text{mol}^{-1}$. The part of the hypersurface relevant for the proton transfer was explored with the B3LYP/6–311+G(2*d*,2*p*) method yielding a classical barrier of $2.12\text{ kcal}\cdot\text{mol}^{-1}$. Variations in the proton potential with respect to the OO distance and both CO distances were considered. The former influences the barrier height, while the latter introduces asymmetry. The potential was fitted to the two state empirical valence form suitable for quantum-dynamical molecular simulations.

Mixed quantum–classical simulation using the DME method was performed in the gas phase and in a chloroform solution [34]. The effects of deuteration were also considered. The vibrational spectrum was calculated by Fourier

transform of the time-dependent expectation value for the OH bond length. In the present case, we demonstrate by calculations and experimentally that coupling of the proton to the OO and both CO bonds, which are attached to the hydrogen bond (indirect relaxation mechanism), is more important than coupling to the solvent degrees of freedom in determining spectral shape.

The DME method has many possible applications. Inclusion of the external electromagnetic field into the mixed quantum–classical simulation is possible and offers a possibility for computational support of the pulse-echo experiments in the infrared region. See for example Ref. [35].

We hope to apply this method in the near future for enzymatic active centres. Replacement of the polar solvent with a fluctuating macromolecular environment, such as an enzyme, is methodologically a straightforward step but requires a lot of coding efforts. Quantum treatment of the nuclear motion is essential for calculation of the kinetic isotope effects that are of vital importance for enzymology. Very recently the H/D kinetic isotope effect $k_{\text{H}}/k_{\text{D}} = 80$ was simulated with what is in excellent agreement with the experiment [36].

8 MAIN FEATURES OF IR SPECTRA RELATED TO THE ANHARMONIC POTENTIAL ENERGY SHAPE

One of the most important parameters characterizing the specificity of hydrogen bondings and affecting the spectroscopic behaviour of hydrogen-bonded systems is the anharmonicity of $\nu(\text{A-H})$ vibrations. According to Sándorfy [37, 38] the anharmonicity of $\nu(\text{A-H})$ stretching vibrations is defined as being limited to the first overtone. The sign of the X_{12} value is assumed sometimes to be reversed. The data related to the higher order excitations are limited and very rarely discussed:

$$(10) \quad X_{12} = \nu_{01}(\text{AH}) - \frac{1}{2}\nu_{02}(\text{AH})$$

The importance of anharmonicity of $\nu(\text{AH})$ vibrations results first of all from the interpretation of the width and shape of the IR absorption bands. It is almost commonly accepted that the anharmonicity is a source of the coupling phenomena of $\nu(\text{AH})$ vibrations with the low frequency vibrations, mainly of the bridge stretching mode and modes into which the bridge atoms contribute. The theoretical basis for the coupling phenomena was formulated by Marechal and Witkowski [39, 40] and developed taking into account the Fermi resonances by Wójcik [41]. The Fermi resonance is of great importance in analysis of the substructure of the broad absorption which is ascribed to the coupling with overtones and combination modes into which the $\delta(\text{AH})$ and $\gamma(\text{AH})$ vibrations contribute.

Wójcik and coworkers [42] studied in particular the band shape for asymmetric OH stretching vibrations in benzoic acid dimer. The experimental spectra were compared with calculated ones. The calculations were based on

the adiabatic coupling between the high frequency mode (OH), the low frequency mode (OO), resonance between the two hydrogen bonds in the dimer and Fermi resonance between the fundamental asymmetric OH stretching and the overtone of the $\delta(\text{OH})$ bending vibration. Good agreement between the calculated and experimental results for both OH and OD spectra was found.

As follows from the recently performed analyses [3] the shape of the $\nu(\text{AH})$ IR absorption bands results usually from the indirect relaxation of the excited vibrational levels, i.e. through the coupling with the low frequency internal modes which next interact with phonons of the condensed phase. The broad bands are characteristic not only for condensed phases. They are also observed in the gas phase in the case of bulky expanded molecules, which can be treated as a bath. In this case a crucial is the coupling of $\nu(\text{A-H})$ vibrations with low frequency bridge vibrations.

As an example of hydrogen-bonded molecules which play the role of a bath in relaxation of the excited $\nu(\text{A-H})$ vibrational level can be the dimers of phosphinic acids studied in the gas phase at high temperatures [43]. In Fig. 8 the results of investigations of profiles of broad IR bands ascribed to $\nu(\text{OH})$ vibrations with characteristic Hadži's ABC trio are shown. These spectra are very similar to those recorded for strong hydrogen bonds in condensed phases [44].

The example of phosphinic acids illustrates very well the appearance of three submaxima on the envelope of broad bands (continua). Let us note that till now

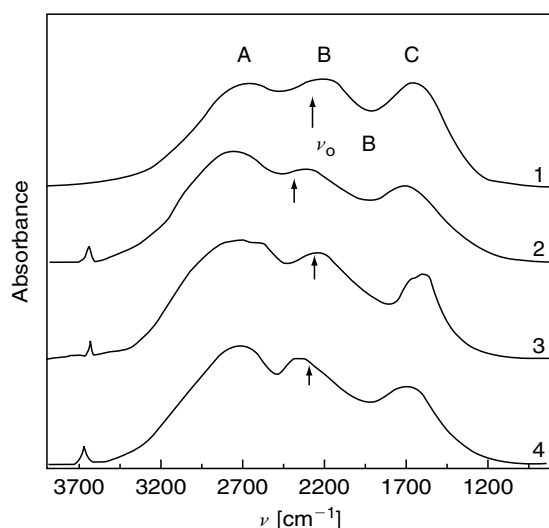


Figure 8. The $\nu(\text{OH})$ bands of R_2POOH dimers in the gas phase: 1— H_2POOH ($T = 345$ K); 2— $(\text{CH}_3)_2\text{POOH}$ (530 K); 3— $(\text{CH}_2\text{Cl})_2\text{POOH}$ (450 K); 4— $(\text{C}_4\text{H}_9\text{O})_2\text{POOH}$ (425 K). The arrows denote the centre of gravity ν_0 of the dimer band, A, B, C denote the components of ABC structure, reprinted from Ref. [43] by permission granted by the Polish Chemical Society.

there is no commonly accepted view with respect to the origin of submaxima or, as many authors believe, two subminima. The latter could correspond to the Fermi resonance with overtones of $\delta(\text{OH})$ and $\gamma(\text{OH})$ vibrations. One should mention here that Zundel [45] has shown that the broad continuum with submaxima can be due to the overlapping of a few transitions resulted from the tunnel splitting for an asymmetric potential energy curve. A confirmation of the rightness of such a point of view could be considerations of Sokolov [46] on the isotope effect which will be discussed later.

In line of the Zundel approach results of calculations for OHO hydrogen bonds based on Eq. 9 could be considered [12, 13]. In calculation it has been assumed, in agreement with commonly accepted theory of the coupling between anharmonic protonic vibrations with the bridge vibrations, that the relaxation of the excited vibrational states undergoes through such low frequency vibrations. However, it has been assumed simultaneously that the bridge vibrations are strongly damped, particularly in condensed phases due to the interaction with phonons. This assumption is consisted with the stochastic model [47] which implies that the hydrogen bond length is modulated over the amplitude of vibrations. However, the shape of the potential is modulated too. In consequence we have to take into account modulation of the barrier height and splitting of the vibrational levels.

The coefficients a_2 and a_4 of Eq. 9 were fitted to experimental correlations between the $\nu(\text{AH})$ frequency and $r(\text{AH})$ bond length and the bridge length. The coefficient a_3 was defined by using the positions of minima and its value was arbitrarily assumed. The calculations were performed for OHO hydrogen bonds for which there are enough data related to the correlation between $\nu(\text{OH})$ and $r(\text{OH})$ and the bridge length.

The evolution of the absorption bands starting from long asymmetric hydrogen bonds to symmetric short ones is shown in Fig. 9. It is seen that separated bands corresponding to various transitions cover the whole infrared region. For short symmetric bridges the probability of the high frequency transitions to higher vibrational level drops almost to zero.

The confrontation of experimental spectra with those predicted in such a way does not provide sufficient agreement. There are several reasons for that. First of all the band widths should be larger when we assume that, in addition to the distribution of the bridge length, additional coupling with other low frequency vibrations takes place, especially with vibrational and translational modes. One should also take into account the direct mechanism of relaxation according to the Zundel polarizability of low-barrier hydrogen bonds [45].

Let us come back to the problem of anharmonicity and its relationship with the hydrogen bond strength and hence the potential energy shape for the proton motion.

There is little known about the correlation between the anharmonicity expressed in Eq. 10 and the interaction strength expressed by concrete parameters, e.g. ΔpK_a . On the other hand, there are in our disposal numerous

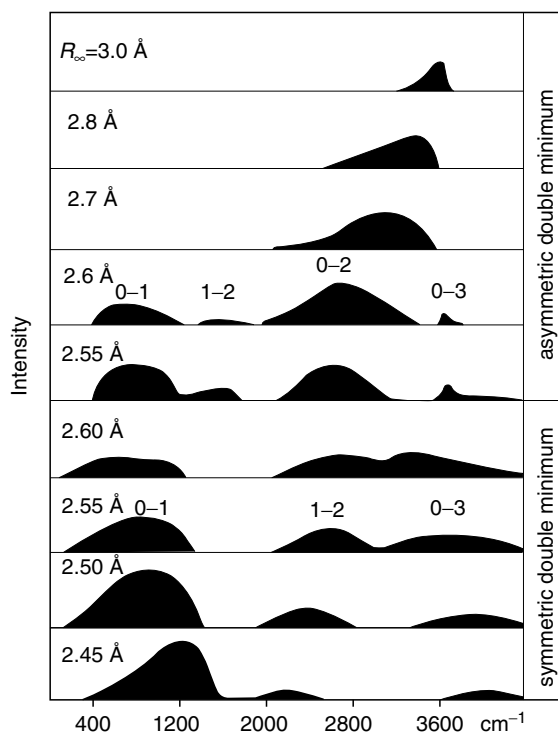


Figure 9. Simulated band profiles for various transitions in OHO hydrogen bonds of varying length, according to Ref. [13].

data related to the $^1\text{H}/^2\text{H}$ isotope effects, which can be correlated with the anharmonicity that will be discussed later.

From the data reported by Rospenk and Zeegers-Huyskens [10] related to complexes formed by phenol derivatives and pyridine it follows that for not very high $\Delta\text{p}K_{\text{a}}$ values X_{12} increases, reaches a maximum and, approaching to the critical region, starts to decrease. The detailed studies performed recently [48] for Mannich bases over broad $\Delta\text{p}K_{\text{a}}$ region are illustrated in Fig. 10. The results unequivocally show that in the critical point a deep minimum appears and the X_{12} value changes the sign. This clearly reflects a substantial change of the shape of the potential energy curve. It becomes steeper than that of the harmonic one. This behaviour seems to be characteristic for very strong hydrogen bonds. In the case of weak hydrogen bonds, as has been shown in Ref. [49], unexpected minimum of X_{12} value is visible. This phenomenon is illustrated in Fig. 11 for a large number of hydrogen-bonded alcohols. The minimum corresponds to $\Delta\nu$ values of the order of 100 cm^{-1} . Such a behaviour should be considered as due to the coupling of $\nu(\text{AH})$ vibrations with $\delta(\text{AH})$ and $\gamma(\text{AH})$ modes which cause the weakening of hydrogen bonds. This result seems to be

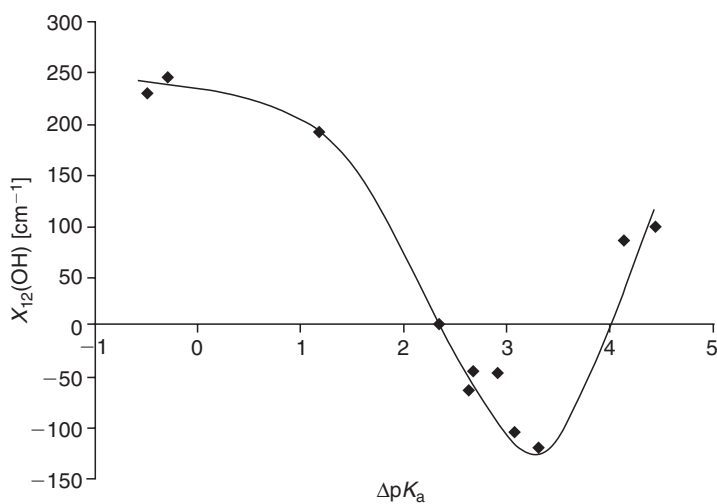


Figure 10. X_{12} values for Mannich bases plotted vs. ΔpK_a , according to Ref. [48].

important in understanding two-dimensional potential energy surfaces. Simultaneously it shows the necessity of taking into account bending vibrations in theoretical analysis.

9 FREQUENCY ISOTOPE EFFECTS

The isotope effects in hydrogen bonded systems reflected in IR spectra were recently reviewed [5]. Here we would like to concentrate our attention on some selected main points.

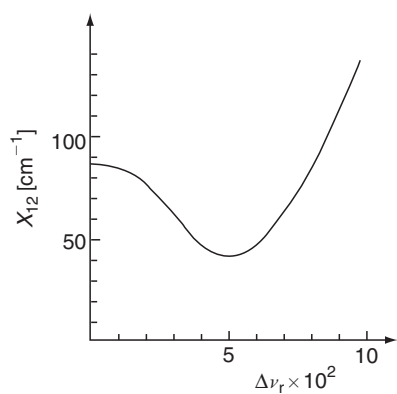


Figure 11. Correlation between the X_{12} value and relative frequency shift $\Delta \nu_r = \Delta \nu(\text{OH})/\nu_o(\text{OH})$ for hydrogen-bonded alcohols, according to Ref. [49].

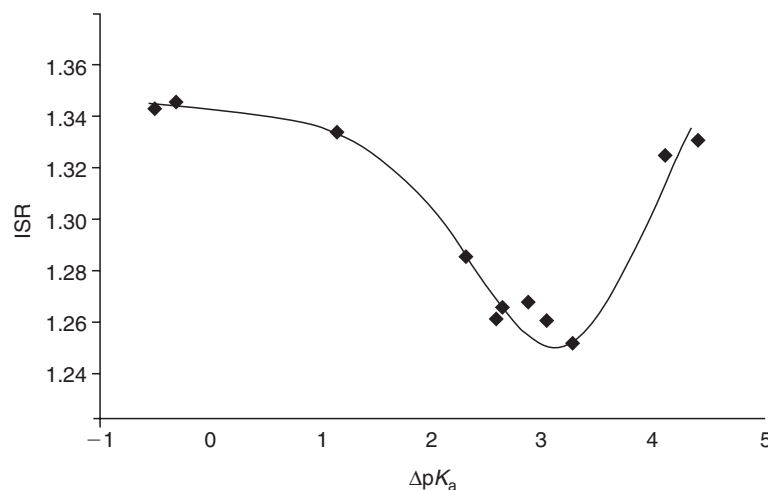


Figure 12. ISR plotted vs. ΔpK_a for Mannich bases, according to Ref. [48].

For all systems containing $\text{OH}\cdots\text{O}$, $\text{OH}\cdots\text{N}$ and $\text{NH}\cdots\text{N}$ hydrogen bonds there are observed deep minima on the plots of isotopic ratio ($\text{ISR} = \nu(\text{AH})/\nu(\text{AD})$) vs. relative shift of the $\nu(\text{AH})$ frequency. This minimum (close to unity) is observed for gravity centre located at $1000\text{--}1500\text{ cm}^{-1}$ that is characteristic of strong hydrogen bonds in condensed media. For strongest hydrogen bonds the ISR value starts to increase reaching $\sqrt{2}$ and even more. However, in the case of intramolecular $\text{OH}\cdots\text{N}$ hydrogen bonds when no continuous broad absorption is observed, the minimum on the plot $\text{ISR} = f(\Delta pK_a)$ is not so deep as can be seen in Fig. 12.

This result can speak in favour of the concept that broad continuous absorption extended to very low frequencies is due to overlapping of a few transitions characterized by different isotopic ratio, as argued by Sokolov [46].

In the critical point characterized by a double minimum potential with a low barrier we have to expect high values of ISR markedly exceeding $\sqrt{2}$ that is connected with unusual anharmonicity. An evidence of that are results of studies on the isotope effect in AH complexes with nitrogen bases in low temperature matrices that have been reviewed in Ref. [50]. In the critical point the ISR value markedly exceeds $\sqrt{2}$ while not far from this point the ISR value is evidently lower than $\sqrt{2}$.

10 LOW-BARRIER HYDROGEN BONDS

Some importance in understanding of unusual behaviour of systems with a symmetrical double minimum potential and low barrier possess the results collected recently for charge assisted $[\text{NHN}]^+$ bridges, particularly in proto-

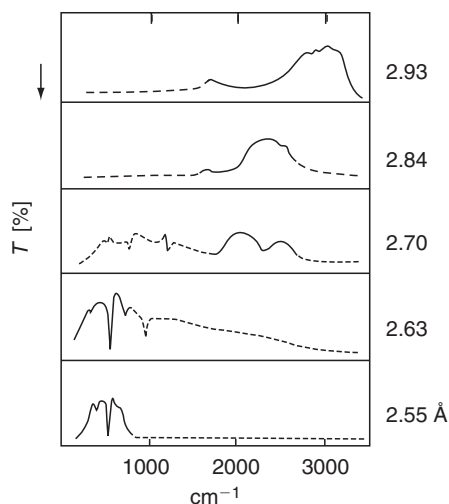


Figure 13. Examples of infrared $\nu[\text{NHN}]$ bands in NHN hydrogen-bonded systems with different N···N bridge length. The dashed parts of curves were obtained after separation of bands ascribed to other internal modes, based on data cited in Ref. [53].

nated proton sponges [51, 52]. The $\nu[\text{NHN}]^+$ absorption bands in protonated naphthalene proton sponges (1,8-*bis*(dimethylamino)-naphthalene (DMAN)), when the symmetric NHN bridges are present, possess unique properties as shown in Fig. 13 comparing with bands corresponding to longer bridges.

For the hydrogen bonds of ca. 2.55 Å length this band is located at extremely low frequencies with an Evans hole assigned to the coupling with NC_3 bending vibrations. For somewhat longer bridges (2.63 or 2.70 Å) a continuous absorption is manifested extending from 100 to 3000 cm^{-1} similarly to those observed for strong OHO or OHN hydrogen bonds. One should mention here that very short charge assisted $[\text{NHN}]^+$ hydrogen bonds are constrained by steric effects.

The *ab initio* and DFT calculations yield the results consistent with experiments related to the bridge length, $\nu[\text{NHN}]$ frequency as well as to isotope effects. Moreover they allow to understand the behaviour of such bridges owing to the possibility of analysis of the potential energy curve and distribution of protonic vibrational levels. The calculated potential energy curve for protonated 2,7-dimethoxy-DMAN is shown in Fig. 14. The MP2 barrier height is 462 cm^{-1} corresponding to 1.32 $\text{kcal} \cdot \text{mol}^{-1}$ that means that zero point energy level for $[\text{NHN}]^+$ is above the barrier. All data related to protonated 2,7-dimethoxy-DMAN are collected in Table 2. From the data in Table 2 it clearly follows that anharmonicity expressed in Eq. 10 is highly negative with unusually high frequency isotopic ratio.

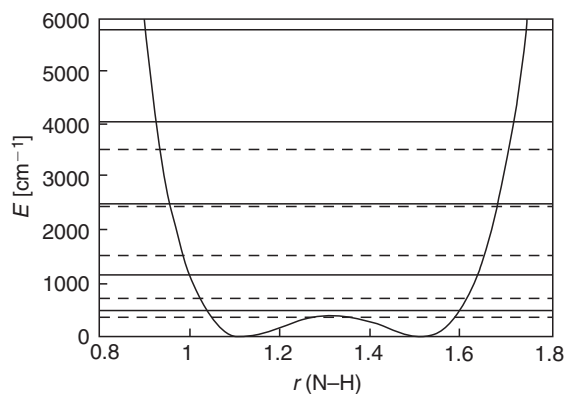


Figure 14. Calculated MP2 one-dimensional potential for protonated 2,7-dimethoxy-DMAN with indicated $\nu[\text{NHN}]^+$ (solid lines) and $\nu[\text{NDN}]^+$ (dashed lines) energy levels, reprinted from Ref. [52] by permission granted by the American Chemical Society.

The behaviour of protonated 2,7-dimethoxy-DMAN is similar to that of other protonated 2,7-disubstituted DMANs as shown in Table 3. The data in this table demonstrate that $[\text{NHN}]^+$ bridge is sensitive to the environment expressed in the buttressing effect exerted by various substituents in positions 2,7. This is well reflected in the geometry of molecules.

It is worth mentioning here that in the case of charge assisted $[\text{NHN}]^+$ hydrogen bonds there was reported only one system with single symmetrical potential, namely protonated 1,6-diazabicyclo[4.4.4]tetradecane [54]. In this case the $\text{N}\cdots\text{N}$ distance is equal to 2.526(3) Å, the shortest known so far. The single minimum potential was confirmed based on primary H/D isotope

Table 2. Theoretically predicted anharmonic $\nu[\text{NHN}]^+$ and $\nu[\text{NDN}]^+$ frequencies for protonated 2,7-dimethoxy-DMAN compared to the experimental results, along with the ISR, X_{12} and barrier height values

	$\nu[\text{NHN}]^+(\text{cm}^{-1})$	$\nu[\text{NDN}]^+(\text{cm}^{-1})$	ISR = $\nu(\text{H})/\nu(\text{D})$	$-X_{12}(\text{cm}^{-1})$	Barrier height (cm^{-1})
DFT	665	331	2.01	326	475
MP2	692	352	1.97	305	462
Expt.	488	235	2.08		

Table 3. Geometrical and spectroscopic characteristics of protonated 2,7- X_2 derivatives of DMAN

	$\angle\text{C}_1\text{C}_2\text{X}$ (deg)	$\angle\text{C}_3\text{C}_2\text{X}$ (deg)	$d(\text{N}\cdots\text{N})$ Å	$\nu[\text{NHN}]$ (cm^{-1})	ISR
2,7- Br_2	124.7(2)	113.4(2)	2.547(3)	560	1.65
2,7- Cl_2	122.8(2)	115.4(2)	2.561(3)	530	1.80
2,7-(OCH_3) ₂	116.0(2)	123.2(3)	2.567(3)	488	2.08

effect in NMR spectra. In agreement with that the $\nu[\text{NHN}]^+$ broad absorption band centred at ca. 1000 cm^{-1} is observed.

It was recently evidenced [55] that also very short OHO hydrogen bonds reveal a low-barrier double-well potential. This was shown in the case of hydrogen bond with the length of 2.393 \AA in 4-cyano-2,2,6,6-tetramethyl-3,5-heptanedione of C_{2v} symmetry. An unequivocal conclusion was based on detailed INS, neutron diffraction and NMR studies. The difference between the two lowest protonic vibrational levels equals to 371 cm^{-1} that convincingly speaks against the single minimum potential. One should mention that in both protonated DMAN and last example of tetramethylated heptanedione the hydrogen bonds are to a large extent isolated.

11 POSSIBILITIES OF NMR SPECTROSCOPY

NMR spectroscopy provides valuable information on the structure and dynamics of the systems with hydrogen bonds, IR and NMR data substantially supplement each other. Most direct information can be derived from spectra of magnetically active nuclei of atoms, participating in hydrogen bridge and neighbouring atoms, such as ^1H , ^2H , ^{13}C , ^{15}N , ^{19}F and ^{31}P , in some cases ^{14}N and ^{17}O . Main parameters, measured in NMR spectroscopy, are chemical shifts and scalar spin–spin couplings between adjacent or closely located nuclei. The chemical shift δ is a characteristic of magnetic shielding of a nucleus by electron shell of a molecule, it is a specific characteristic of a given atom in a molecule. Scalar spin–spin coupling constant J is a characteristic of indirect interaction energy of magnetic moments of non-equivalent nuclei through electron shell of a molecule, it determines the multiplet structure of signals.

Formation of $\text{AH}\cdots\text{B}$ hydrogen bond leads to low-field shift of the proton signal of AH group (decrease of electron magnetic shielding), which grows with the increase of the hydrogen bond energy. Signs and values of the shifts of the signals of A and B nuclei are specific and depend on the interacting functional groups. Scalar spin–spin couplings between nuclei of proton donor and proton acceptor give valuable information about overlapping of electron clouds of partner groups upon formation of hydrogen bond. One feature of NMR spectroscopy is of fundamental importance—it is significantly larger characteristic time τ^* , compared to the optical spectroscopy. The order of magnitude of τ^* is defined by the inverse value of the quantum transitions frequencies in a system studied by the given method. For NMR spectroscopy it is about 10^{-2} – 10^{-5} s for different cases; characteristic time in optical spectroscopy is of the order of 10^{-10} (microwave) to 10^{-16} (UV) regions. On one hand, this complicates NMR study of systems with dynamic equilibrium between different molecular forms (such as hydrogen bonding, tautomeric equilibrium, internal rotation), because when $\tau^* \gg \tau$, where τ is the characteristic time of chemical process, for example, the lifetime of proton between acts of exchange, in NMR spectrum only one average signal of two or more forms participating

in exchange is registered. On the other hand, this gives a unique opportunity to measure kinetic parameters of averaging processes with $\tau \approx \tau^*$, where it is possible to measure directly the lifetime of exchanging forms by NMR lineshape analysis. This can be achieved by changing the conditions of the experiment, which can influence the lifetimes, mainly temperature and concentration, but sometimes also the magnetic field strength (by using several NMR spectrometers). In this sense processes can be described as fast or slow in NMR timescale.

The experience shows that for many systems with hydrogen bond slow exchange conditions $\tau \gg \tau^\circ$ down to $\tau \approx \tau^\circ$ are fulfilled at temperatures below 200–150 K and it is possible to detect separated signals of non-equivalent movable protons [56, 57], ^{15}N nuclei [57, 58], ^{19}F nuclei [59, 60], ^{13}C nuclei [61] and ^{31}P nuclei [62, 63]. In slow exchange regime the tremendous potential of NMR for hydrogen bond investigation is disclosed. For example, proton chemical shift range is about 20 ppm and linewidth for exchangeable protons can be as low as 5 Hz, so that the total number of independent points in ^1H NMR spectrum, which characterizes selectivity of the method, is around 2000 on average spectrometer. Unfortunately, possibility to measure spectra of liquid state samples at low temperatures is limited by the small number of suitable solvents. Well utilized is the freon mixture $\text{CDF}_3/\text{CDCIF}_2$, which has rather high dissolving ability even for ionic compounds and low viscosity down to freezing temperature, below 100 K. 1:1 mixture freezes around 95 K and at this temperature its dielectric constant rises up to 45 [59].

12 POTENTIAL SURFACES OF COMPLEXES WITH INTERMOLECULAR HYDROGEN BOND

12.1 Complexes of Neutral Molecules

Intermolecular hydrogen bond $\text{AH} \cdots \text{B}$ in solution in majority of cases is either linear or close to linear, i.e. angle θ AHB is close to 180° . The dependence of the hydrogen bond energy on the angle is weak, thus it is convenient to build two-dimensional potential energy surface in coordinates $r_1(\text{AH})$, $r_2(\text{HB})$ (or $R = r_1 + r_2$), assuming $\theta = 180^\circ$. If the difference $\Delta \text{p}K_a = \text{p}K_a(\text{AH}) - \text{p}K_a(\text{HB}^+)$ is close to zero, the proton transfer state $\text{A}^- \cdots \text{HB}^+$ is sufficiently populated, which allows to detect it by spectroscopic methods [64, 65]. In other words, on the potential surface of such system there are two minima, corresponding to two stationary states of the complex, which are in the dynamic equilibrium. Enthalpy difference between these two states (relative depth of potential minima) is defined experimentally using van't Hoff's equation for the temperature dependence of the monomolecular equilibrium constant, which is equal to the ratio of concentrations of two forms of complex. Measurements of the equilibrium constant can be performed using optical spectra in UV and IR regions, where characteristic time of method is much shorter than lifetime of

the complex. In NMR spectra, however, it is rarely possible to detect simultaneously resolved signals of tautomeric molecular and ionic complexes. However, for complexes of strong acids but weak proton donors in hydrogen bond the interconversion frequency of two forms in the temperature range 250–90 K can be comparable with the difference of resonance frequencies of these forms. In such systems minima of molecular and ionic complexes on the two-dimensional potential energy surface are located far away from each other and, as a consequence, are separated by the high potential barrier, which makes the lifetime of the proton in each state comparable with the characteristic NMR time. This is the case of many CH–, SH– and NH–proton donors [56]. Strong OH and many NH acids are also strong proton donors, potential barrier between two minima is lower and rate of exchange is so high that even at ~ 100 K in NMR spectrum only average signal of molecular and ionic forms is seen. Although in these cases spectrum is less informative, equilibrium constant can be estimated from the location of the signal between two limiting positions, corresponding to molecular and ionic forms. Signals of these forms usually cannot be measured independently and their chemical shifts are obtained indirectly.

As an example, in Fig. 15 ^1H NMR spectra of thiophenol $\text{C}_6\text{H}_5\text{SH}$ dissolved in freon CHClF_2 in the presence of triethylamine excess obtained at different temperatures are shown [56]. Upon cooling the signal 2.6 ppm of the amine's α -methylene protons shifts to low field and splits into two signals around 150 K. While temperature decreases the chemical shift of the lower field signal, assigned to the tautomeric complex, increases due to the gradual shift of the equilibrium $\text{SH}\cdots\text{N} \rightleftharpoons \text{S}^- \cdots \text{HN}^+$ to the right side. When the proton exchange between these two tautomeric forms becomes slow in the NMR time-scale the signal of the bonding proton splits in to two signals, which correspond to the molecular and ionic complexes. The lineshapes and relative intensities of

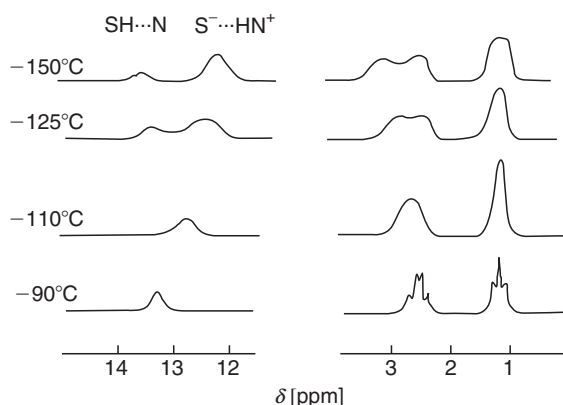


Figure 15. ^1H NMR spectra of thiophenol ($0.05 \text{ mol} \cdot \text{dm}^{-3}$)—triethylamine ($0.1 \text{ mol} \cdot \text{dm}^{-3}$) system in a freon CHClF_2 at various temperatures, reprinted from Ref. [56] by permission granted by Elsevier.

the signals do not depend on concentration. The former are modulated by the exchange rate and the latter are defined by the tautomeric equilibrium. The lineshape analysis allows to determine the lifetime of the complexes and to describe the kinetics of the proton transfer. Analogous experiments were fulfilled in a number of systems of the $\text{RAH} \cdots \text{N}(\text{C}_2\text{H}_5)_3$ type. The employed proton donors RAH, where $\text{AH} = \text{OH}, \text{NH}, \text{SH}, \text{CH}$, were selected in such a way that their proton-donating ability was strongly varied while the acidity stays rather unchanged. The enthalpy of the $\text{RAH} \cdots \text{O} = \text{S}(\text{CD}_3)_2$ complex estimated from IR spectra was employed as a measure of the proton-donating ability. The experimental data obtained for these systems are collected in Table 4.

The enthalpy values of the $\text{AH} \cdots \text{N} \rightleftharpoons \text{A}^- \cdots \text{HN}^+$ process are similar for the studied complexes and are between 13 and 15 $\text{kcal} \cdot \text{mol}^{-1}$. While the proton-donating ability of an acid decreases the rate of the reversible proton transfer diminishes and the activation energy increases. Thus a decrease of the potential well depth for the molecular complex causes an increase of the barrier for the proton transfer. One may conclude that the acidity of RAH defines mostly the depth of the potential well in the ionic complex while the barrier height depends on the hydrogen bond strength in the molecular complex, i.e. the distance between the bridge A, B atoms.

The equilibrium between the molecular and ionic form of hydrogen bonded complexes involving stronger proton donors such as carboxylic acids or phenols was studied using optical spectroscopy methods [64, 65]. In these structures the enthalpy of the proton transfer was found to be always negative. Since the proton transfer in solution is an exothermic process, the second well is always deeper than the first one. The proton transfer is followed by a strong reduction of the entropy due to the ordering of the solvent molecules in the solvation shell of the ionic complex having a higher dipole moment (7–10 D). The structure of strongly hydrogen-bonded complexes dramatically depends on interactions with the environment. Impressive examples are the complexes $\text{HalH} \cdot \text{NH}_3$ (Hal = Cl, Br, I) in inert gas matrices, whose structure changes qualitatively from molecular to ionic one in the row Ne, Ar, Kr, N_2 [66–68].

Table 4. The enthalpy values of hydrogen bonded complexes of acids RAH with $(\text{CD}_3)_2\text{SO}$, coalescence temperature T_c and activation energy E^\ddagger of proton transfer in the complex $\text{RAH} \cdots \text{N}(\text{C}_2\text{H}_5)_3$

Acid RAH	$\text{p}K_a$	ΔH_{DMSO} ($\text{kcal} \cdot \text{mol}^{-1}$)	T_c (K)	E^\ddagger ($\text{kcal} \cdot \text{mol}^{-1}$)
$(\text{CH}_3)_3\text{CCOOH}$	5.1	9.6	<95	<2
CH_3NHNO_2	5.1	7.0	130	2.2
$\text{C}_6\text{H}_5\text{SH}$	6.2	5.2	160	3.4
$(\text{CF}_3)_2\text{CHNO}_2$	5.3	4.4	220	4.7
$\text{CH}_3\text{CH}(\text{NO}_2)_2$	5.1	2.2	315	7.9
$(\text{CF}_3)_2\text{CHCOOCH}_3$	6.2	~1	>340	>10

The solvent plays an important role in the position of the tautomeric equilibrium. Indeed, such equilibrium was not ever observed in gas phase while the proton transfer in complexes formed by neutral molecules is well known, for example, in $\text{BrH} \cdot \text{N}(\text{CH}_3)_3$ as shown by NMR [69]. One may expect that perspective candidates for such study are strong CH- or SH-acids.

For systems with strong hydrogen bond NMR spectroscopy provides an important experimental criterion, which allows to distinguish the complexes with symmetric or nearly symmetric low-barrier potential from complexes with non-symmetric single-well or double-well potential with a high barrier. It is a primary $^1\text{H}/^2\text{H}$ isotope effect—the difference of signals in ^2H and ^1H NMR spectra of complexes containing deuteron and proton in hydrogen bridge $\Delta\delta \equiv \delta(\text{A}^2\text{HB}) - \delta(\text{A}^1\text{HB})$. In some cases the ^3H NMR spectra of compounds enriched with tritium were obtained [70–72]. The basis of this criterion is the change of complex geometry after isotope substitution—the shortening of the bond A–D and further A–T on account of vibration anharmonicity and lesser zero point energy for heavier isotope. Then its shielding increases, hydrogen bond weakens, the distance $\text{H} \cdots \text{B}$ increases more than shortening of the valence bond and the length of hydrogen bridge $\text{R}(\text{A} \cdots \text{B})$ increases [73, 74]. The deuteron signal is shifted to higher field in comparison with proton, the difference of their chemical shifts is negative, $\Delta\delta < 0$. The effect is small for weak hydrogen bonds, it grows with the strength of them, reaches the maximum, for $\text{OH} \cdots \text{O}$ bonds of about -1 ppm, then it decreases, goes through zero and becomes positive, up to $+0.3$ ppm for strongest shortest bonds; the detailed theoretical analyses are given in articles [75, 76].

It is pertinent to add that in the gas phase hydrogen bond may become shorter upon isotope substitution, $R_{\text{D}}(\text{AB}) < R_{\text{H}}(\text{AB})$, according to the data of rotational spectroscopy [77]. This effect is maximum for weak complexes and decreases with the hydrogen bond strength, for complex $\text{ClH} \cdot \text{NH}_3$ it becomes positive. The authors [77] explained it by the opposite influence of H/D substitution on the movements with large amplitudes—stretching vibration $\nu_{\text{s}}(\text{AH})$ and wagging intermolecular vibration ν_{b} . For weak bonds the decrease of zero point vibrations amplitude of ν_{b} dominates, the role of ν_{s} increases with the hydrogen bond strength. Since in liquid phase the positive isotope effect on chemical shifts for uncharged complexes is observed only in few cases of very strong hydrogen bond with “shared” proton, it is believed that in conditions of polar solvent the influence of zero point vibrations on ν_{b} mode on hydrogen bond geometry is insignificant.

In symmetric single minimum potential proton as well as deuteron and triton is located in the centre of bridge, but because of lesser energy of zero-point vibrations and lesser distance between heavy nuclei the amplitude of zero-point vibrations for ^2H and ^3H is less than for ^1H , and average over wave functions of ground state values of their chemical shift proves to be larger, the isotope effect $\Delta\delta > 0$ [70, 94]. When the minimum moves from the centre of bridge the potential curve becomes asymmetric, the distance $r_1(\text{AD})$ becomes less than

$r_1(\text{AH})$ and the opposite influence of anharmonicity on the hydrogen bond strength in H- and D-forms appears, the total effect diminishes. The $\Delta\delta$ value goes through zero, becomes positive and increases [78, 79].

Exclusively strong hydrogen bond, probably the strongest detected up to date between two neutral molecules, is formed in a polar solution between FH and 2,4,6-trimethylpyridine (collidine) [57]. In a $\text{CDF}_3/\text{CDClF}_2$ freon mixture geometry of this bond dramatically depends on temperature. At 190 K the bond is of the molecular type and H is located closer to F than to N. The single well potential curve is asymmetric and the primary isotope effect is negative. Upon cooling $\Delta\delta$ becomes positive, goes through the maximum of 0.27 ppm at 145 K and then decreases again down to 0.2–0.1 ppm at 100 K. That means that the F–H \cdots N bridge contracts first and then lengthens again. The driving force for this contraction is an increase of the solvent polarity due to cooling [59]. The local electric field increases upon cooling because of the ordering of the solvent molecules solvated the complex. This field induces in the complex an extra dipole moment due to the proton transfer from F to N. Thus, the F \cdots H distance increases gradually while the H \cdots N one contracts. We will call the proton position at which the N \cdots F distance is the smallest one as the “quasi-midpoint.” For asymmetric AH \cdots B complexes this point does not necessarily coincide with the geometrical centre of the hydrogen bridge [58]. Further increasing of the dipole moment demands an increase of the N \cdots F distance. Thus, upon cooling geometry of the FH \cdots collidine complex changes gradually from the molecular structure FH \cdots N to the ionic one F $^- \cdots$ HN $^+$ [80].

By using empirical correlation between spectroscopic and geometric characteristics of complex it was shown that the primary isotope effect changes sign when the minimum of the potential curve shifts from the quasi-midpoint by more than ~ 0.06 Å in both sides [57].

Information about the electronic structure of strong hydrogen bond may be obtained from the structure of the NMR signal of the bonding proton. In the $^{19}\text{F} \cdot ^1\text{H} \cdot ^{15}\text{N}$ bridge all nuclei have the spin 1/2. Their mutual interaction through the three-centre four-electrons bond is shown in Fig. 16 [57]. The proton signal is a doublet of doublets whose splitting constants depend on the proton position in the bridge. At high temperatures the proton is strongly coupled to the fluorine, $^1J_{\text{FH}} = 88$ Hz at 180 K. Due to the proton transfer upon cooling this coupling reduces down to 45 Hz near the quasi-midpoint and finally becomes immeasurably small, less than 10 Hz. In contrast, the proton–nitrogen coupling increases upon cooling. It is about -43 Hz at 170 K, becomes equal to $^1J_{\text{FH}}$ near the quasi-midpoint and about -55 Hz at 112 K. The coupling constant between the nitrogen and the fluorine nuclei over the hydrogen bridge does not change much in the inspected temperature interval and is about -96 Hz.

The results of theoretical analysis of a similar complex perfectly correlate with the experimental data and explain the observed effects in detail [81]. It is shown that the strong changes of the $^1J_{\text{FH}}$ and $^1J_{\text{HN}}$ coupling constants are

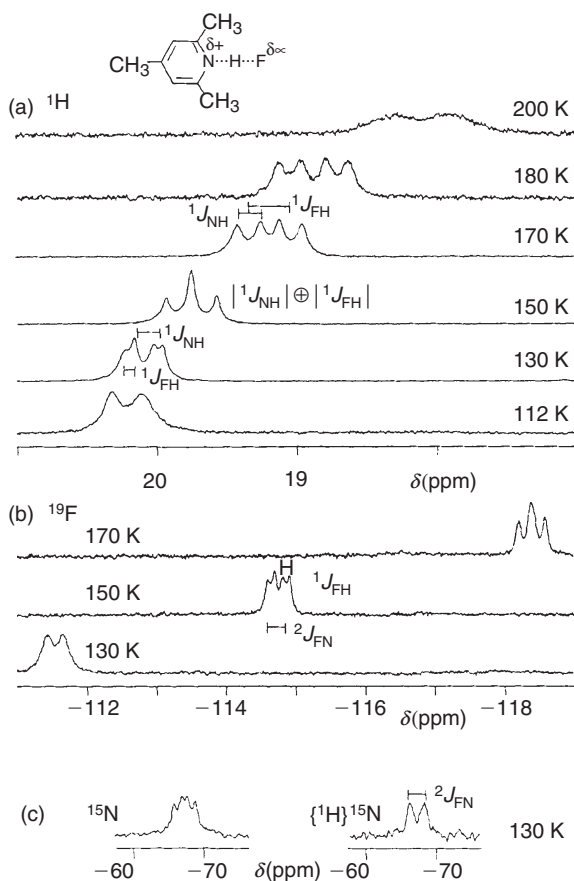


Figure 16. (a) ^1H NMR signals of the hydrogen bond proton of the 1:1 complex between collidine- ^{15}N and HF in $\text{CDF}_3/\text{CDCIF}_2$ of a sample containing a 10-fold excess of collidine; (b) ^{19}F NMR spectra of the same sample (c) ^{15}N spectra with and without proton decoupling at 130 K of a sample containing a 7-fold excess of collidine, reprinted from Ref. [57] by permission granted by the American Chemical Society.

caused by a monotonous increase of the $\text{F}\cdots\text{H}$ distance and the corresponding decrease of the $\text{H}\cdots\text{N}$ distance near the quasi-midpoint or the proton-shared bond where the $\text{F}\cdots\text{N}$ distance does not change much. In all cases the Fermi contact contribution is mostly responsible for the coupling with the exception of the shortest $\text{F}\cdots\text{H}$ distances when the paramagnetic spin-orbit contribution plays a certain role.

A monotonous increase of the potential curve asymmetry is observed for complexes of carboxylic acids with collidine having in the freon mixture the ionic structure at 120–130 K. Here $^1J_{\text{HN}}$ is about -65 Hz for acetic acid, 87 Hz for 2-nitrobenzoic acid and up to -90 and -92 Hz for HCl and HBF_4 [82]. The

structure of these complexes strongly depends on the local electric field and may be dramatically changed in crystal where the dielectric constant $\epsilon \approx 5$ in contrast to ca. 30 in freon. While the crystalline collidine–HCl complex has the ionic structure as well, the benzoic acid forms with collidine in the solid state molecular complex. As a result the difference in the nitrogen chemical shifts in ^{15}N NMR spectra of the latter complex obtained in the freon mixture and crystal is about 60 ppm.

The important regularities were obtained in the study of spectra of complexes with hydrogen bond $\text{AH} \cdots ^{15}\text{N}$ on nuclei ^{15}N of isotopically enriched aromatic bases pyridine and collidine. When proton-donating ability of an acid AH increases the ^{15}N chemical shift monotonously moves towards high field approaching to limiting value, characteristic for a free cation $\text{H}-^{15}\text{N}^+$, in contrast to the chemical shift of proton which passes through the maximum near quasi-midpoint. Thus the ^{15}N chemical shift may be used to detect the minimum on the proton's potential surface. In this row of complexes the secondary isotope effect $\Delta\delta(\text{N}) \equiv \delta(\text{ADN}) - \delta(\text{AHN})$ has the shape of dispersion curve, i.e. it has the maximum in region of strong molecular complexes, goes through zero near quasi-midpoint and then has minimum in region of strong hydrogen bonded zwitterionic complexes [23, 57, 78]. These features help to describe in detail the structure of a hydrogen bonded complex and the shape of its potential surface. It is pertinent to mention here the results of Rospenk et al. [83], where the secondary H/D isotope effect was measured on ^{13}C nuclei of phenyl ring in the row of Mannich bases, substituted 2- $\text{CH}_2\text{N}(\text{C}_2\text{H}_5)_2$ -phenols. The non-linear intramolecular hydrogen bond $\text{OH} \cdots \text{N}(\text{sp}^3)$ exists in these compounds, the strength of which can be varied in wide limits by introducing substitutes in phenyl ring. It was found that when acidity of OH group increases the isotope effect on carbon atom C1OH, $\delta_{\text{C}}(\text{D}) - \delta_{\text{C}}(\text{H})$, changes analogously (with opposite sign) to the secondary isotope effect on nitrogen atom in intermolecular hydrogen bond $\text{OH} \cdots ^{15}\text{N}(\text{sp}^2)$; it goes through zero near quasi-midpoint and has maximum and minimum on both sides of this point. One can think that such behaviour may be rather typical for complexes with strong hydrogen bonds.

12.2 Complexes with Participation of Ions

Very strong bonds are formed between neutral and charged particles—charge assisted hydrogen bonds [84], complexes of neutral proton donors with anions A^- and of neutral acceptors with cations BH^+ . Potential surface of these complexes may be single minimum or double minimum, in dependence on electronegativity of heavy atoms [85, 86]. The potential surface of a centrosymmetrical anion $[\text{AHA}]^-$ or cation $[\text{BHB}]^+$ has the simplest shape. The hydrodifluoride ion $[\text{FHF}]^-$ is most extensively studied experimentally and theoretically, one can assume it to be the limiting case of hydrogen bond with maximum energy $45.8 \text{ kcal} \cdot \text{mol}^{-1}$ [21, 87–89]. As evidenced by X-ray diffraction, vibrational and NMR spectroscopy, this anion in gas, crystal and solution

has centrosymmetric structure, so that its potential surface has one minimum. In deuterated anion the distance $R(\text{F}\cdots\text{F})$ diminishes in crystal by $\sim 0.004 \text{ \AA}$ [90], in gas by $\sim 0.005 \text{ \AA}$ [91]. Therewith the primary isotope effect is positive, $+0.32 \text{ ppm}$, and secondary isotope effect is negative, $\delta(\underline{\text{FDF}}) - \delta(\underline{\text{FHF}}) = -0.37 \text{ ppm}$ [92, 93]. The qualitative treatment was carried out in Refs. [78, 94]; the explanation is given on a basis of comparison of the width of probability density distribution of proton and deuteron in the ground vibrational state (Fig. 17). The thorough analysis of the influence of vibrational effects on NMR spectra of isotope forms of $[\text{FHF}]^-$ anion is accomplished [21]. It is shown that for centrosymmetric ion the contribution of amplitudes of two proton vibrations, antisymmetric and bending, plays the determining role. The contribution of symmetric vibration (the change of effective length of hydrogen bond on deuteration) is negligibly small. The experimentally observed opposite signs of isotope effect on hydrogen and fluorine nuclei resulted in the dominating role of stretching vibration in the first case, and of bending proton vibration in the second case. When passing to complexes with asymmetric proton location, the anharmonic contribution of stretching proton vibration appears and increases, as a result of which the primary H/D isotope effect decreases and changes its sign.

The NMR study of the strong hydrogen bond $^{15}\text{N} \cdot \text{H} \cdot ^{15}\text{N}$ in a complex $(\text{R}-\text{C}\equiv\text{N}\cdots\text{H}\cdots\text{N}\equiv\text{C}-\text{R}) \cdot \text{X}^+$ in solid state led to the similar conclusions

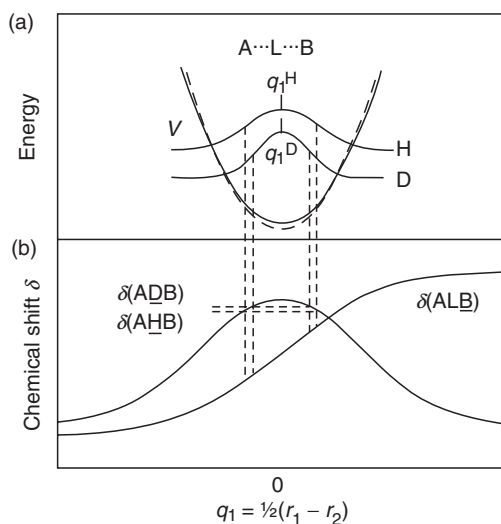


Figure 17. (a) One-dimensional potential curve and squared ground state wave function (schematically) of a symmetric single-well hydrogen bond ALB, L = H, D. (b) Chemical shifts $\delta(\text{ALB})$ (schematically) of B and L as a function of q_1 . The average chemical shift of D is larger than for H because of the maximum of $\delta(\text{ALB})$ and the narrower wave function of D compared with H. By contrast, as $\delta(\text{ALB})$ is a linear function of q_1 , $\delta(\text{AHB}) = \delta(\text{ADB})$, reprinted from Ref. [78] by permission granted by Wiley-VCh.

[23, 79, 80]. Two compounds were studied with symmetric and asymmetric position of a proton between nitrogen atoms ($X^+ = \text{AsPh}_4^+$ and NPr_4^+). On H/D substitution the distance $R(\text{N}\cdots\text{N})$ in the first complex diminishes from 2.62 to 2.60 Å, and in the second one it increases from 2.68 to 2.71 Å. The distances r_1 and r_2 in the first complex remain equal, but in the second complex the length of valence bond $r_1(\text{N}-\text{H})$ 1.16 Å decreases by 0.03 Å, and the length of hydrogen bond $r_2(\text{H}\cdots\text{N})$ 1.49 Å increases by 0.06 Å. Chemical shift of nitrogens signal in the spectrum of symmetrical complex is hardly changed on deuteration, but in the spectrum of asymmetric complex two nitrogen signals shift in opposite directions, the distance between them increases. The secondary isotope effect on nitrogen qualitatively reproduces the primary geometric isotope effect on proton transfer coordinate $q_1 = 1/2(r_1 - r_2)$. Theoretical consideration of a model linear system $(\text{C}\equiv\text{N}\cdots\text{H}\cdots\text{N}\equiv\text{C})^- \cdot \text{Li}^+$, in which the interaction with a cation models the perturbation by external electric field, showed that on approaching a cation the symmetric low-barrier potential loses its symmetry, becomes non-symmetric and its minimum gradually shifts towards one of nitrogen atoms. Hence, the negative H/D effect on geometry (shortening of $R(\text{AB})$ length on deuteration) and positive effect on hydrogen chemical shift (low-field shift of deuteron signal in comparison with proton) allow to identify the systems with single-well potential, with central or nearly central proton location. The NMR criterion is more valuable than the structural one, since it is applicable not only to crystals but to neat liquids and solutions as well.

An interesting approach providing a possibility of measurements of geometric parameters of complexes with hydrogen bond in solutions by the method of nuclear magnetic relaxation is proposed by authors [95, 96]. The measurements of longitudinal magnetic relaxation time T_1 of heavy nuclei were carried out in freon solutions at temperatures 100–150 K in conditions of slow proton and molecular exchange for complexes $\text{FH}\cdots^{15}\text{NCH}$ and $[\text{FHF}]^-$ in three (H,D,T) isotopic modifications. Using these data the ratios of distances $r_1(\text{AT})/r_1(\text{AH})$ and $r_2(\text{TB})/r_2(\text{HB})$ in these complexes were calculated. It was found that in complex $\text{FH}\cdots\text{N}$ the replacement of hydrogen by tritium results in shortening of F–H bond and in lengthening of hydrogen bond $\text{H}\cdots\text{N}$, the distance $R(\text{F}\cdots\text{N})$ increases by 0.02 Å. But in complex $[\text{FHF}]^-$ the reverse effect is observed—the diminution of the distance between heavy atoms. It evidences for some strengthening of hydrogen bond, which manifests itself in positive isotope effect on chemical shift of bridging proton. The obtained value of shortening of $R(\text{F}\cdots\text{F})$ distance 0.008 Å is in accordance with the value of geometric isotope effect for isolated anion in gas phase, found from IR spectrum [90], so that this value is practically insensitive to the phase state and the presence of a counter-ion.

In strong hydrogen bond $[\text{N}\cdots\text{H}\cdots\text{N}]$ in homoconjugated bis-collidinium cation in freon solution the proton signal 19.93 ppm is a triplet with a constant

$^1J_{\text{NH}} = 40$ Hz; the primary isotope effect is $\Delta\delta = -0.81$ ppm [93]. This demonstrates the double-well symmetric potential with fast migration of a proton between two equivalent positions (in slightly disturbed collidinium ion the proton signal of NH^+ group is a doublet with a constant $^1J_{\text{NH}} = 85$ Hz). Similar situation is in protonated proton sponges such like in 1,8-*bis*(dimethylamino)-2,7-dimethoxy naphthalene [97]. $^1\text{H}/^2\text{H}$ primary isotope effect convincingly shows a double-well potential although the NHN bridge is very short, 2.567(3) Å.

In complexes of carboxylic acids with their anions $[\text{AHA}]^-$ hydrogen bond is weaker than in anion $[\text{FHF}]^-$, and the results of experimental and theoretical studies point to double-well potential of proton in a bridge $[\text{OHO}]^-$. The primary isotope effect in ^1H NMR spectrum of hydrogen diacetate anion according to Refs. [61, 93] is negative and large, $\Delta\delta = -0.62$ ppm. An additional information about O-H-O bond is obtained from ^{13}C spectra of carbon atoms adjoining to the hydrogen bridge. The secondary isotope effect on ^{13}C nucleus of carboxylic group $\delta_{\text{C}}(\text{D}) = \delta_{\text{C}}(\text{H}) = -0.20$ ppm is negative; also, it repeats the sign of a primary effect. The authors concluded that the proton potential in this anion is symmetric and has two wells, the same result gives the theoretical analysis. The interaction with solvate shell results in fluctuations of instantaneous form of potential but does not change its double-well character. The fast proton exchange between two wells averages the signals of carboxylic carbon and only one line is revealed in the spectrum [61].

In the row of acetic acid complexes with anions CH_3CO_2^- , $\text{CH}_2\text{ClCO}_2^-$, $\text{CHCl}_2\text{CO}_2^-$, $\text{CCl}_3\text{CO}_2^-$ the $\text{OH}\cdots\text{O}$ hydrogen bond weakens rapidly as one can see from the ^1H chemical shifts—19.25, 16.91, 15.64, 12.04 ppm [98]. In the ^{13}C NMR spectra of asymmetrical complexes $[\text{A}_1 \cdot \text{H} \cdot \text{A}_2]^-$ of this row the signals of two carboxylic carbons are observed separately, the secondary isotope effect on carbon atom of acetic acid decreases rapidly in this row (-0.357 , -0.234 , -0.100 ppm) and exceeds significantly the secondary isotope effect on carbon of chlorosubstituted anion (-0.053 , -0.034 , -0.100 ppm). It shows on hydrogen bond $\text{OH}\cdots\text{O}$ in strongly asymmetric single-well potential [98].

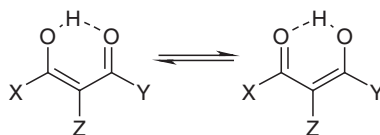
13 INTRAMOLECULAR HYDROGEN BOND

13.1 Enols of β -Diketones

Intramolecular hydrogen bond, as a rule, is non-linear, and the dependence of the energy of a system on the angle AHB θ should be accounted for in building one-dimensional and two-dimensional potential surfaces. The authors [99] advanced a new approach for determination of the type of potential in intramolecular hydrogen bond O-H-O in enols of β -diketones. They suggested the method of representation in one-dimensional form of potential curves describing the profile of proton movement between two oxygen atoms. The difference $r_1(\text{O-H}) - r_2(\text{H}\cdots\text{O})$ at different distances R and angles θ is used as a reaction

coordinate; it was calculated employing Lippincott–Schröder equation. The obtained curves are classified by form and symmetry.

The potential curves of *cis*-enolic form of β -diketones are difficult ones for classification cases of resonance-assisted hydrogen bonds, since parameters of the surface may change strongly for different substituents X, Y, Z. The surface may have either one minimum localized near one of oxygen atoms, or in the centre of the bridge, or two minima of equal ($X = Y$) or different depth ($X \neq Y$). Double-minimum surface corresponds to the existence of two tautomers, being in movable equilibrium with one another. The high rate of mutual conversion gives rise to averaging of signals of two forms, so that it is impossible to distinguish different forms by direct experiment, and one is led to use the indirect arguments. Many examples of such works are given in the review [100]. The important criterion is the temperature dependence of chemical shifts of nuclei forming the hydrogen bridge and adjacent nuclei, mainly ^{13}C , and of scalar spin coupling constants. In case of non-symmetric compounds, $X \neq Y$, one may expect existence of two forms with different energies, and if the energy difference is not very large, the change of state population in operating temperature interval can be measured by the position of averaged signal of these forms. Approximation of $\delta(T)$ dependence by van't Hoff function allows to find unknown parameters, enthalpy and entropy of tautomeric transfer and chemical shifts of each tautomer. Sometimes it is possible to use the independent values of chemical shifts of individual tautomers taken from spectra of model compounds, then the precision may be increased. In a similar way the measurements of tautomeric equilibrium may be carried out by temperature dependence of scalar spin coupling constant of movable proton and adjacent nucleus ^{17}O , ^{13}C or proton ^1H if $X = \text{H}$. Enthalpy difference measured for different dicarbonyl compounds reaches $1.0 \text{ kcal} \cdot \text{mol}^{-1}$, the precision of measurement of relative concentration of tautomers is of few percent [100]. If energy difference is large the fraction of dominating tautomer is indistinguishable from unity and the potential with a good approximation can be assumed the single minimum one (Scheme 1) [99].



Scheme 1

For symmetric substitution, $X = Y$, the equilibrium is degenerate, two wells have equal depths and the population of both states is equal at any temperature. In this case chemical shift does not depend on temperature and scalar spin coupling constant has one half value of the full one. Such behaviour allows to identify the systems with close values of depth of two wells and fast in NMR scale proton migration between them. For example, in ^1H NMR spectrum of enol form of malonedialdehyde ($X = Y = Z = \text{H}$) at 170 K the signal of OH

proton is a triplet on account of average spin–spin interaction with two formyl protons. The effective constant ${}^3J_{\text{OH,H}}$ is equal to average value of interaction constants with these protons $1/2 (13 + 0) = 6.5$ Hz.

It should be noted that in enols of β -diketones (acetyl- and benzoylacetone, dibenzoylmethane) the largest primary negative isotope effect is observed, for deuterium between -0.6 and -0.7 ppm and for tritium between -0.8 and -1.0 ppm [70, 71]. It corroborates the double-well character of proton potential in compounds of this group. Even in the shortest intramolecular OHO bridge in 4-cyano-2,2,6,6-tetramethyl-3,5-heptanedione [55], of 2.393 Å length (see Sect. 10) it was evidenced, based on neutron diffraction and inelastic scattering, a double minimum potential with very low barrier. The authors of the cited paper believe the existence of single minimum potential to be unlikely in compounds of this type.

13.2 Anions of Dicarboxylic Acids

The study of isotope effects in NMR spectra of the other classical examples of the strong intramolecular hydrogen bond with single minimum potential, the hydrogen maleate anion MA and its methyl substituted, hydrogen citraconate anion CA, illustrates the high sensitivity of ${}^{13}\text{C}$ spectra to the small changes of potential curve of a proton [93, 98]. The positive primary isotope effect in both anions, $+0.051$ and $+0.162$ ppm, shows on the low-barrier hydrogen bond with a proton location in the centre of a bond for MA and, for symmetry reasons, slightly shifted from the centre for CA; the proton signal of CA is shifted to low field by 0.075 ppm in comparison with MA (20.915 and 20.840 ppm correspondingly). This shift, as well as considerable difference in primary isotope effects, is likely a consequence of the shorter distance $R(\text{O}\cdots\text{O})$ in CA. Symmetrical MA gives in ${}^{13}\text{C}$ spectrum only one signal 171.057 ppm of carboxylic carbon, after partial deuteration the second signal of D-form appears shifted to higher field by 0.069 ppm. But in the spectrum of CA two carboxylic carbons give different signals 171.578 and 171.265 ppm (Fig. 18). The secondary isotope effect on these nuclei differs significantly, on C1 it is less than in MA, -0.013 ppm, and on C4 it is larger, -0.087 ppm. This means that in asymmetric potential well of CA proton is located slightly closer to carbon C4. It is appropriate to add that the sign of secondary isotope effect on nuclei C2 and C3 is different, -0.25 and $+0.16$ ppm correspondingly. The quantum-chemical consideration could help to understand the nature of these shifts.

14 SYNCHRONOUS TRANSFER OF PROTONS IN CYCLIC COMPLEXES WITH SEVERAL HYDROGEN BONDS

Certain compounds susceptible to self-association form stable cyclic structures with several hydrogen bonds—dimers, trimers, etc. Many-dimensional potential surface of such systems has two minima, corresponding to two

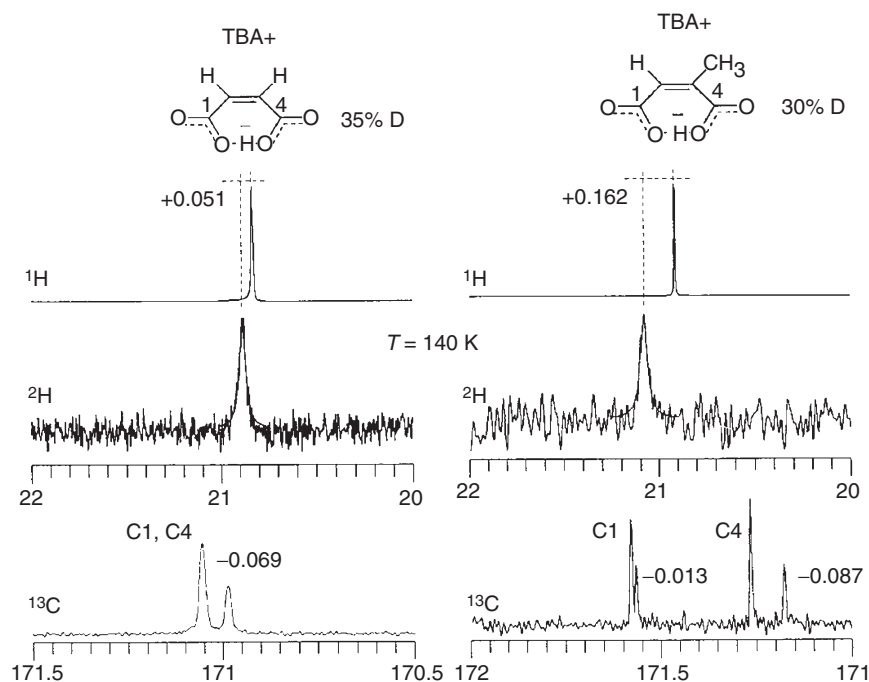


Figure 18. ^1H , ^2H and ^{13}C NMR spectra of partially deuterated hydrogen maleate and hydrogen citraconate in $\text{CDF}_3/\text{CDClF}_2$ (tetrabutylammonium salts), according to Ref. [98].

mirror-symmetrical forms of a complex. These forms are in degenerate equilibrium with one another, the exchange between them occurs through synchronous transfer of protons along hydrogen bonds. The most stable structures are stabilized by resonance interaction in π -electron system in a cycle closed by hydrogen bond (resonance-assisted hydrogen bond [84], therefore the coordinates of heavy atoms also change substantially during the proton transfer. The example of such systems may be well studied by methods of NMR cyclic dimers of carboxylic acids [101–103], and cyclic dimers, trimers and tetramers of pyrazoles [104, 105]. The measurements of the process kinetics enabled to estimate the activation energy of tautomeric transfer—the barrier height of the reaction path profile. At low temperatures the influence of tunnelling reveals itself, the value of kinetic isotope effect for H/D/T forms is determined. Theoretical analysis of the potential surface shape of carboxylic acid dimers showed that the low frequency vibrations make a noticeable contribution to the reaction coordinate of synchronous transfer of protons, an adequate description of experimental results can be realized by the use of at least four-dimensional potential surface [102]. The authors [104] found that the shortening of distances between heavy atoms in hydrogen bridges, the

“shrinking” of a ring, occurs at synchronous transfer of protons in cyclic complexes of pyrazoles; it also evidences the valuable participation of the heavy atom movement in the reaction coordinate.

ACKNOWLEDGMENTS

This research has been supported by the Russian Foundation of Basic Research, grants 03-03-04009 and 05-03-33235. A financial support by the Polish Ministry of Science and Informatics (Grant 4TO9A 05125) is also acknowledged.

REFERENCES

1. G. Fogarasi and P. Pulay (1985) in *Ab Initio Calculation of Force Fields and Vibrational Spectra*, J. Durig (ed.), Vibrational Spectra and Structure, Vol. **14**, Elsevier Science, Amsterdam, p. 125.
2. A. P. Scott and L. Radom (1996) *J. Phys. Chem.* **100**, 16502.
3. O. Henri-Rousseau, P. Blaise and D. Chamma (2002) *Adv. Chem. Phys.* **121**, 241.
4. C. L. Perrin and J. B. Nielson (1997) *Annu. Rev. Phys. Chem.* **48**, 511.
5. Z. Mielke and L. Sobczyk (2005) in *Vibrational Isotope Effects in Hydrogen Bonds*, A. Kohen and H.-H. Limbach (eds.), Isotope Effects in Biology and Chemistry, Taylor & Francis, Boca Raton, 2006, pp. 281–304.
6. A. Warshel (1991) *Computer Modeling of Chemical Reactions in Enzymes and Solution* (J. Wiley, New York).
7. E. R. Lippincott and R. Schröder (1955) *J. Chem. Phys.* **23**, 1099.
8. E. Matsushita and T. Matsubara (1982) *Progr. Theor. Phys.* **67**, 1.
9. T. Saitoh, K. Mori and R. Itoh (1981) *Chem. Phys.* **60**, 161.
10. M. Rospenk and Th. Zeegers-Huyskens (1997) *J. Phys. Chem. A* **101**, 8428.
11. R. L. Somorjai and D. F. Hornig (1962) *J. Chem. Phys.* **36**, 1980.
12. H. Romanowski and L. Sobczyk (1977) *Chem. Phys.* **19**, 361.
13. L. Sobczyk (1996) *Mol. Phys. Rep.* **14**, 19.
14. Y. Guissani and H. Ratajczak (1981) *Chem. Phys.* **62**, 319.
15. J. Laane (1971) *J. Chem. Phys.* **55**, 2514.
16. M. Barroso, L. G. Arnaut and S. J. Formosinho (2005) *Chem. Phys. Chem.* **6**, 363.
17. J. Florián (2002) *J. Phys. Chem. A* **106**, 5046.
18. J. Stare and J. Mavri (2002) *Comput. Phys. Comm.* **143**, 222.
19. C. C. Marston and G. G. Balint-Kurti (1989) *J. Chem. Phys.* **91**, 3571.
20. N. S. Golubev, I. G. Shenderovich, P. M. Tolstoy and D. N. Shchepkin (2004) *J. Mol. Struct.* **697**, 9.
21. N. S. Golubev, S. M. Melikova, D. N. Shchepkin, I. G. Shenderovich, P. M. Tolstoy and G. S. Denisov (2003) *Z. Phys. Chem.* **217**, 1549.
22. I. G. Shenderovich, S. N. Smirnov, G. S. Denisov, V. A. Gindin, N. S. Golubev, A. Dunger, R. Reibke, S. Kirpekar, O. L. Malkina and H.-H. Limbach (1998) *Ber. Bunsenges. Phys. Chem.* **102**, 422.
23. H. Benedict, H.-H. Limbach, M. Wehlan, W. P. Fehlhammer, N. S. Golubev and R. Janoschek (1998) *J. Am. Chem. Soc.* **120**, 2939.
24. T. Dziembowska and Z. Rozwadowski (2001) *Curr. Org. Chem.* **5**, 289.
25. P. E. Hansen (1996) *Isotope Effects on Chemical Shift as a Tool in Structural Studies* (Roskilde Univ. Press, Roskilde).
26. J. Stare, A. Jezierska, G. Ambrožič, I. J. Košir, J. Kidrič, A. Koll, J. Mavri and D. Hadži (2004) *J. Am. Chem. Soc.* **126**, 4437.

27. J. Tomasi and M. Persico (1994) *Chem. Rev.* **94**, 2027.
28. R. M. Czerwinski, T. K. Harris, M. A. Massiah, A. S. Mildvan and C. P. Whitman (2001) *Biochemistry* **40**, 1984.
29. J. Stare, J. Panek, D. Hadži and J. Mavri *J. Phys. Chem. A*, to be submitted.
30. R. Car and M. Parrinello (1985) *Phys. Rev. Lett.* **55**, 2471.
31. D. Sebastiani and U. Rothlisberger (2004) in *Advances in Density-functional-based Modeling Techniques—Recent Extensions of the Car-Parrinello Approach*, P. Carloni and F. Alber (eds.), Quantum Medicinal Chemistry, J. Wiley, New York.
32. J. Stare, J. Panek, J. Eckert, J. Mavri and D. Hadži, to be published.
33. H. J. C. Berendsen and J. Mavri (1993) *J. Phys. Chem.* **97**, 13464.
34. J. Mavri and J. Grdadolnik (2001) *J. Phys. Chem. A* **105**, 2045.
35. N. Došlić, O. Kühn, J. Manz and K. Sundermann (1998) *J. Phys. Chem. A* **102**, 9645.
36. S. B. Braun-Sand, M. Olsson, J. Mavri and A. Warshel, in *Computer Simulation of Proton Transfer in Enzymes and Solution*, R. Schowen, J. P. Klinman and J. T. Hynes (eds.), Handbook of Hydrogen Transfer, in press.
37. C. Sandorfy (1976) in *Anharmonicity and Hydrogen Bonding*, P. Schuster, G. Zundel and C. Sandorfy (eds.), The Hydrogen Bond. Recent Developments in Theory and Experiments, Vol. **2**, North-Holland, Amsterdam, p. 613.
38. C. Sándorfy (1995) *Bull. Pol. Acad. Sci. Chem.* **43**, 7.
39. A. Witkowski (1967) *J. Chem. Phys.* **47**, 3645.
40. Y. Marechal and A. Witkowski (1968) *J. Chem. Phys.* **48**, 3697.
41. M. J. Wójcik (1976) *Int. J. Quant. Chem.* **10**, 747.
42. M. Boczar, K. Szczeponek, M. J. Wójcik and C. Paluszkiwicz (2004) *J. Mol. Struct.* **700**, 39.
43. R. E. Asfin, G. S. Denisov, D. M. Poplevchenkov, K. G. Tokhadze and T. V. Velikanova (2002) *Pol. J. Chem.* **76**, 1223.
44. D. Hadži and S. Bratos (1976) in *Vibrational Spectroscopy of the Hydrogen Bond*, P. Schuster, G. Zundel and C. Sandorfy (eds.), The Hydrogen Bond. Recent Developments in Theory and Experiments, Vol. **2**, North-Holland, Amsterdam, p. 565.
45. G. Zundel (2000) *Adv. Chem. Phys.* **111**, 1.
46. N. D. Sokolov, M. V. Vener and V. A. Savel'ev (1990) *J. Mol. Struct.* **222**, 365.
47. S. Bratos (1975) *J. Chem. Phys.* **63**, 3499.
48. M. Rospenk and L. Sobczyk (2006) *Asian Chem. Lett.* 10(1–2), 7.
49. J. Rossarie, J.-P. Gallas, C. Binet and R. Romanet (1977) *J. Chim. Phys.* **74**, 188.
50. Th. Zeegers-Huyskens and L. Sobczyk (1990) *Spectrochim. Acta A* **46**, 1693.
51. A. J. Bieńko, Z. Latajka, W. Sawka-Dobrowolska, L. Sobczyk, V. A. Ozeryanskii, A. F. Pozharskii, E. Grech and J. Nowicka-Scheibe (2003) *J. Chem. Phys.* **119**, 4313.
52. V. A. Ozeryanskii, A. F. Pozharskii, A. J. Bieńko, W. Sawka-Dobrowolska and L. Sobczyk (2005) *J. Phys. Chem. A* **109**, 1637.
53. L. Sobczyk (2005) *Khim. Fiz.* **24**, 1.
54. R. W. Alder, R. E. Moss and R. B. Sessions (1983) *J. Chem. Soc. Chem. Commun.* 1000.
55. J. A. Belot, J. Clark, J. A. Cowan, G. S. Harbison, A. I. Kolesnikov, Y.-S. Kye, A. J. Schultz, C. Silvernail and X. Zhao (2004) *J. Phys. Chem. B* **108**, 6922.
56. G. S. Denisov and N. S. Golubev (1981) *J. Mol. Struct.* **75**, 311.
57. I. G. Shenderovich, P. M. Tolstoy, N. S. Golubev, S. N. Smirnov, G. S. Denisov and H.-H. Limbach (2003) *J. Am. Chem. Soc.* **125**, 11710.
58. S. N. Smirnov, N. S. Golubev, G. S. Denisov, H. Benedict, P. Schah-Mohammedi and H.-H. Limbach (1996) *J. Am. Chem. Soc.* **118**, 4094.
59. I. G. Shenderovich, A. P. Burtsev, G. S. Denisov, N. S. Golubev and H.-H. Limbach (2001) *Magn. Reson. Chem.* **39**, S91.
60. I. G. Shenderovich, H.-H. Limbach, S. N. Smirnov, P. M. Tolstoy, G. S. Denisov and N. S. Golubev (2002) *Phys. Chem. Chem. Phys.* **4**, 5488.

61. P. M. Tolstoy, P. Schah-Mohammedi, S. N. Smirnov, N. S. Golubev, G. S. Denisov and H.-H. Limbach (2004) *J. Am. Chem. Soc.* **126**, 5621.
62. C. Detering, P. M. Tolstoy, N. S. Golubev, G. S. Denisov and H.-H. Limbach (2001) *Dokl. Phys. Chem.* **379**, 191.
63. N. S. Golubev, S. N. Smirnov and P. M. Tolstoy (2006) *Zhur. Obshch. Khim.*, in press
64. M. M. Habeeb (1997) *Appl. Spectr. Rev.* **32**, 103.
65. A. Jarczewski and C. D. Hubbard (2003) *J. Mol. Struct.* **649**, 287.
66. L. Andrews, X. Wang and Z. Mielke (2001) *J. Phys. Chem. A* **105**, 6054.
67. L. Andrews and X. Wang (2001) *J. Phys. Chem. A* **105**, 6420.
68. L. Andrews and X. Wang (2001) *J. Phys. Chem. A* **105**, 7541.
69. N. S. Golubev and G. S. Denisov (1982) *Khim. Fiz.* **1**, 965.
70. L. J. Altman, D. Laungani, G. Gunnarsson, H. Wennerström and S. Forsén (1978) *J. Am. Chem. Soc.* **100**, 8264.
71. S. Bolvig, P. E. Hansen, H. Morimoto, D. Wemmer and P. Williams (2000) *Magn. Reson. Chem.* **38**, 525.
72. W. Schilf, J. P. Bloxside, J. R. Jones and S. Y. Lu (2004) *Magn. Reson. Chem.* **42**, 556.
73. M. Ichikawa (2000) *J. Mol. Struct.* **552**, 63.
74. H. D. Lutz and B. Engelen (2002) *Trends Appl. Spectr.* **4**, 355.
75. N. D. Sokolov, M. V. Vener and V. A. Savel'ev (1988) *J. Mol. Struct.* **177**, 93.
76. M. V. Vener (1992) *Chem. Phys.* **166**, 311.
77. A. C. Legon and D. J. Millen (1988) *Chem. Phys. Lett.* **147**, 484.
78. H.-H. Limbach, M. Pietrzak, S. Sharif, P. M. Tolstoy, I. G. Shenderovich, S. N. Smirnov, N. S. Golubev and G. S. Denisov (2004) *Chem. Eur. J.* **10**, 5195.
79. H.-H. Limbach, M. Pietrzak, H. Benedict, P. M. Tolstoy, N. S. Golubev and G. S. Denisov (2004) *J. Mol. Struct.* **706**, 115.
80. H.-H. Limbach, G. S. Denisov and N. S. Golubev (2005) in *Isotope Effects in the Biological and Chemical Sciences*, A. Kohen and H.-H. Limbach (eds.), Isotope Effects in Biology and Chemistry, CRC Press, Boca Raton, FL, USA, in press.
81. J. E. Del Bene, R. J. Bartlett and J. Elguero (2002) *Magn. Reson. Chem.* **40**, 767.
82. P. M. Tolstoy, S. N. Smirnov, I. G. Shenderovich, N. S. Golubev, G. S. Denisov and H.-H. Limbach (2004) *J. Mol. Struct.* **700**, 19.
83. M. Rospenk, A. Koll and L. Sobczyk (1995) *J. Mol. Liq.* **67**, 63.
84. G. Gilli and P. Gilli (2000) *J. Mol. Struct.* **552**, 1.
85. S. Gronert (1993) *J. Am. Chem. Soc.* **115**, 10258.
86. S. Gronert and C. Kimura (2003) *J. Phys. Chem. A* **107**, 8932.
87. S. I. Kawahara, T. Uchiwaru and K. Taira (2001) *Chem. Phys.* **273**, 207.
88. A. M. Panich (1995) *Chem. Phys.* **196**, 511.
89. E. A. Moore, A. Healy, M. Mortimer and N. F. Peirson (1993) *J. Mol. Struct. (Theochem)* **285**, 229.
90. W. C. Hamilton and J. A. Ibers (1968) *Hydrogen Bonding in Solids* (W. A. Benjamin, Inc, New York-Amsterdam).
91. K. Kawaguchi and E. Hirota (1986) *J. Chem. Phys.* **84**, 2953.
92. F. Y. Fujiwara and J. S. Martin (1974) *J. Am. Chem. Soc.* **96**, 7625.
93. P. Schah-Mohammedi, I. G. Shenderovich, C. Detering, H.-H. Limbach, P. M. Tolstoy, S. N. Smirnov, G. S. Denisov and N. S. Golubev (2000) *J. Am. Chem. Soc.* **122**, 12878.
94. G. Gunnarsson, H. Wennerstrom, W. Egan and S. Forsén (1976) *Chem. Phys. Lett.* **38**, 96.
95. N. S. Golubev, D. N. Shchepkin and S. M. Melikova (2003) *Khim. Fiz.* **22**, 3.
96. G. S. Denisov, V. A. Gindin, N. S. Golubev, S. S. Ligay, D. N. Shchepkin and S. N. Smirnov (1995) *J. Mol. Liq.* **67**, 217.
97. C. L. Perrin and B. K. Ohta (2001) *J. Am. Chem. Soc.* **123**, 6520.
98. P. M. Tolstoy (2004) *Location of the Proton in Strong Hydrogen Bonds Using Isotope Effects in ¹³C NMR Spectra in Solution*, Thesis, St. Petersburg University; P. M. Tolstoy, N. S. Golubev,

- G. S. Denisov and H.-H. Limbach (2003) *Deprotonation of the Carboxylic Group Monitored by H/D Isotope Effects on ^{13}C NMR Chemical Shift Measured in Slow Exchange Regime*, XV Conference-Workshop "Horizons in Hydrogen Bond Research", Berlin, Germany, 16–20.09.2003.
99. P. Gilli, V. Bertolasi, L. Pretto, V. Ferretti and G. Gilli (2004) *J. Am. Chem. Soc.* **126**, 3845.
 100. A. I. Koltsov (1998) *J. Mol. Struct.* **444**, 1.
 101. B. H. Meier, F. Graf and R. R. Ernst (1982) *J. Chem. Phys.* **76**, 767.
 102. T. Loerting and K. R. Liedl (1998) *J. Am. Chem. Soc.* **120**, 12595.
 103. Q. Xue, A. J. Horsewill, M. R. Johnson and H. P. Trommsdorff (2004) *J. Chem. Phys.* **120**, 11107.
 104. O. Klein, F. Aguilar-Parrilla, J. M. Lopez, N. Jagerovic, J. Elguero and H.-H. Limbach (2004) *J. Am. Chem. Soc.* **126**, 11718.
 105. H.-H. Limbach (2002) in *NMR—A Tool for the Study of the Dynamics of Hydrogen Transfer in Liquids and Solids*, D. M. Grant and R. K. Harris (eds.), Encyclopedia of Nuclear Magnetic Resonance Advances in NMR, Suppl. Vol. **9**, John Wiley & Sons, Ltd, Chichester, p. 520.

CHAPTER 11

MOLECULAR GEOMETRY—DISTANT CONSEQUENCES OF H-BONDING

TADEUSZ M. KRYGOWSKI and JOANNA E. ZACHARA

Department of Chemistry, Warsaw University, Pasteura 1, 02-093 Warsaw, Poland

Abstract The significant influence of H-bonding on π -electron delocalization and distant molecular structure is systematically reviewed. It has been shown that these changes depend monotonically on the H-bonding strength. Two kinds of systems were considered: with intramolecular and intermolecular H-bond. π -Electron delocalization was described by geometry-based index of aromaticity, HOMA as well as by NICSs and Grabowski's resonance parameter, whereas the H-bonding strength by C–O bond length (for phenols), O–H bond length, and $^1\text{H-NMR}$ chemical shift.

Keywords: π -Electron delocalization, H-bonding, HOMA, NICS.

1 INTRODUCTION

Following the classical, Pauling's definition "under certain conditions an atom of hydrogen is attracted by rather strong forces to two atoms, instead of only one, so that it may be considered to be acting as a bond between them. This is called the hydrogen bond." Pauling also states that the hydrogen bond "is formed only between the most electronegative atoms." [1] The IUPAC definitions of hydrogen bonding read: "the hydrogen bond is a form of association between an electronegative atom and a hydrogen atom attached to a second, relatively electronegative atom. It is best considered as an electrostatic interaction, heightened by a small size of hydrogen, which permits proximity of the interacting dipoles or charges. Both electronegative atoms are usually (but not necessarily) from the first row of the Periodic Table, i.e., N, O, or F. With a few exceptions, usually involving fluorine, the associated energies are less than 20–25 kJ/mol. Hydrogen bonds may be intermolecular or intramolecular" [2] and "a particular type of multicenter (three center–four

electron bond) $X-H \cdots Y$ in which the central hydrogen atom covalently linked to an electronegative atom X (C,N,O,S, ...) forms an additional weaker bond with atom Y (N,O,S, ...) in the direction of its lone electron pair orbital. The energy of hydrogen bonds, which is usually in the range of 3–15 kcal/mol (12–65 kJ/mol), results from the electrostatic interaction and also from the orbital interaction of the antibonding $\sigma^*(XH)MO$ of the molecule acting as the hydrogen donor and the nonbonding lone electron pair MO_N of the hydrogen acceptor molecule.” [3] The most general scheme of H-bonded system is



where A and B are atoms/moieties with higher electronegativity than hydrogen, and hydrogen itself is more or less deprived of electron [4].

In general A and B may belong to two different molecules/molecular ions or being connected by a chain of atoms bound by covalent bonds may form one single molecule. In the first case H-bond is called intermolecular and in the other one intramolecular.

Obviously the H-bonded part of a system interacts with the remainder of the molecule and vice versa. These interactions are more or less mutually interrelated. In most cases the attention is paid only to structural aspects of the H-bonded region. Undoubtedly distant structural consequences that result from the H-bonding interactions may be observed in remote parts of molecule(s), to which A and B belong. In limiting cases two situations may be realized:

- a. H-bond affects the remainder of the system in question.
- b. The remainder of the system affects the H-bond region.

None of these two situations is realized alone, in its ideal form. The observed situations are always a blend of both (a) and (b) cases.

It should be pointed out that H-bonding plays a fundamental role in molecular recognition in biological systems and in all systems associated with architecture of crystal or condensed state of matter [5, 6]. These kinds of interactions are in principle of a long-distant type but these aspects will not be discussed in this review.

2 GEOMETRY-BASED INDICATOR OF π -ELECTRON DELOCALIZATION

Molecular geometry is an easy accessible source of chemical information (The Cambridge Structure Database) and hence willingly applied for description and interpretation of chemical systems and processes [7]. According to R. Hoffmann: “There is no more basic enterprise in chemistry than the determination of the geometrical structure of a molecule. Such a determination, when it is well done ends all speculations as to the structure and provides us

with the starting point for understanding of every physical, chemical and biological property of the molecule.” [8]

Thus, undoubtedly, geometry-based analyses of H-bond affecting distant parts of systems in question seem to be well justified. This is particularly right since following the Hellmann–Feynman theorem [9] the distribution of electronic density in the molecule (or any chemical entity) determines the forces acting on the nuclei, which, in turn, define the geometry of the molecule in question. Thus geometry may be a reliable description of electron distribution in a molecule. Applying appropriate references, geometry may be used for the description of π -electron delocalization [10, 11]. One of the earliest invented quantitative descriptors of π -electron delocalization are the geometry-based aromaticity indices [12, 13, 14]. In this review, the Harmonic Oscillator Model of Aromaticity, hereafter abbreviated as HOMA, was chosen for description of changes in geometry and variation in π -electron delocalization.

The HOMA [15] index is defined according to

$$(1) \quad \text{HOMA} = 1 - \frac{1}{n} \sum_{j=1}^n \alpha_j (R_{\text{opt},i} - R_j)^2$$

Its extended version that takes into account different contributions to the decrease of aromaticity is defined as [16]

$$(2) \quad \begin{aligned} \text{HOMA} &= 1 - \left[\alpha_i (R_{\text{opt},i} - R_{\text{av}})^2 + \frac{1}{n} \sum_{j=1}^n \alpha_j (R_{\text{av}} - R_j)^2 \right] \\ &= 1 - \text{EN} - \text{GEO} \end{aligned}$$

In both, Eqs. 1 and 2, n is the number of bonds taken into the summation; α_i is a normalization constant (for C–C, C–N, and C–O bonds $\alpha_{\text{CC}} = 257.7$, $\alpha_{\text{CN}} = 93.52$, $\alpha_{\text{CO}} = 157.38$) fixed to give HOMA = 0 for a model nonaromatic system (e.g., Kekulé structure of benzene for carbocyclic systems) and HOMA = 1 for the system with all bonds equal to the optimal value $R_{\text{opt},i}$ assumed to be realized for full aromatic systems (for C–C, C–N, and C–O bonds $R_{\text{opt,CC}} = 1.388 \text{ \AA}$, $R_{\text{opt,CN}} = 1.334 \text{ \AA}$, $R_{\text{opt,CO}} = 1.265 \text{ \AA}$); R_j stands for bond lengths taken into consideration. In Eq. 2 EN describes the decrease of aromaticity due to the bond elongation whereas GEO—due to the increase of bond alternation; R_{av} stands for average bond length. Applications of HOMA for various π -electron systems were reviewed by Krygowski et al. [10, 11] To demonstrate the behavior of HOMA index as well as GEO and EN terms the values calculated from the experimental geometry of benzene, naphthalene, phenanthrene, and triphenylene are presented in Fig. 1 [17].

Benzene, the archetype of aromatic properties, should have HOMA = 1, but since the reference value of $R_{\text{opt,CC}}$ is an approximate quantity [15], a little deviation from unity is found. For naphthalene, HOMA is significantly lower (0.802) and the decrease of aromaticity is mostly due to the GEO term (0.121)

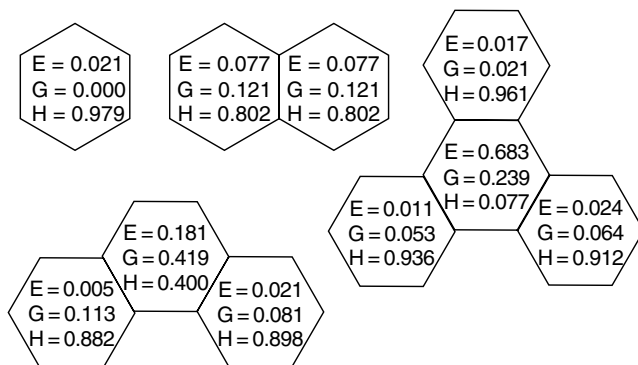


Figure 1. EN (E), GEO (G) and HOMA (H) values for benzene, naphthalene, phenanthrene, and triphenylene calculated from experimental geometry, according to Ref. 17.

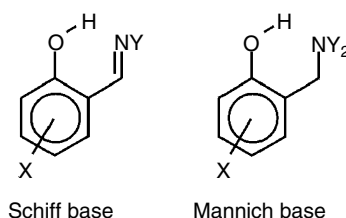
that is greater than the EN term describing mean elongation of bonds. Terminal rings in phenanthrene and triphenylene are aromatic, with HOMA around 0.9, and the dominant structural factor decreasing aromaticity is due to an increase of bond length alternation (GEO term: 0.05–0.1). Interestingly, in both cases the central rings in phenanthrene and triphenylene, respectively, are of low aromatic character but caused by different structural reasons. In the case of phenanthrene this is due to the increase of bond length alternation (GEO = 0.419, comparing to EN = 0.181) whereas for triphenylene this is caused by bond elongation (EN = 0.683 comparing to GEO = 0.239). In summary, HOMA index and its components, GEO and EN terms, provide good information about the structural reasons of decrease of aromaticity of individual rings.

3 CONSEQUENCES OF H-BOND ON THE GEOMETRY OF MOLECULES

The most spectacular cases where the distant structural consequences of H-bonding can be observed are systems in which the proton-donating or proton-accepting or both moieties are attached to π -electron systems. Due to a substantial mobility of π -electrons most examples studied were of this kind.

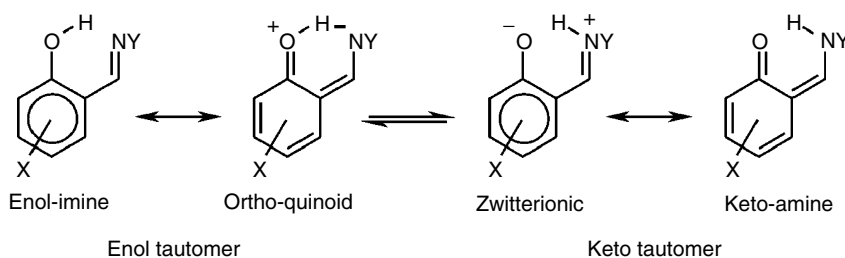
3.1 Schiff and Mannich Bases—Intramolecular H-Bond

To show the difference between the case of H-bonding with the chelate chain enabling π -electron delocalization and without this possibility, let us discuss similarities and differences in the distant structural consequences of H-bonding in *ortho*-hydroxy Schiff and Mannich bases (Scheme 1).



Scheme 1. Structural Schemes of Schiff and Mannich bases.

In the case of *ortho*-hydroxy Schiff base two tautomers are associated with a reorganization of π -electron structure as shown in Scheme 2 [18]. Evidently, in the case of both tautomers the quinoid canonical forms may exist: *ortho*-quinoid for enol tautomer and keto-amine for keto form (Scheme 2).



Scheme 2. Keto-enol tautomeric equilibrium with indication of the most important canonical structures.

In the case of *ortho*-hydroxy Mannich bases, no such possibility exists. Hence, in the *ortho*-hydroxy Mannich and Schiff bases (Scheme 1) the energetics and π -electron delocalization may differ significantly as well as geometry of the quasi-ring built of the H-bonded OCCCN chain. The changes in geometry may also be observed in the aromatic ring.

The first observation is well shown in Fig. 2, where the energy of system is plotted against the elongation of the O–H bond for *ortho*-hydroxy Schiff and Mannich bases [19].

As a result of possibility of cooperative interaction between H-bonding formation and an increase of π -electron delocalization in Schiff base, one observes the minimum on the dependence of energy on O–H interatomic distance. This is absent for Mannich base. Substantial changes in this dependence may also be due to substitution at the nitrogen atom, as it was observed for 2-(*N*-methyl- α -iminoethyl)phenol and 2-(*N*-methyliminomethyl)phenol [20]. Another consequence of H-bonding is a dependence of π -electron delocalization in the ring estimated by HOMA index [11, 15] on the “strength” of H-bonding pictured by O–H interatomic distance [21]. This is shown in Fig. 3. The longer the O–H interatomic distance is, the more negative charge at the oxygen atom appears and thus the stronger resonance with the ring leading in

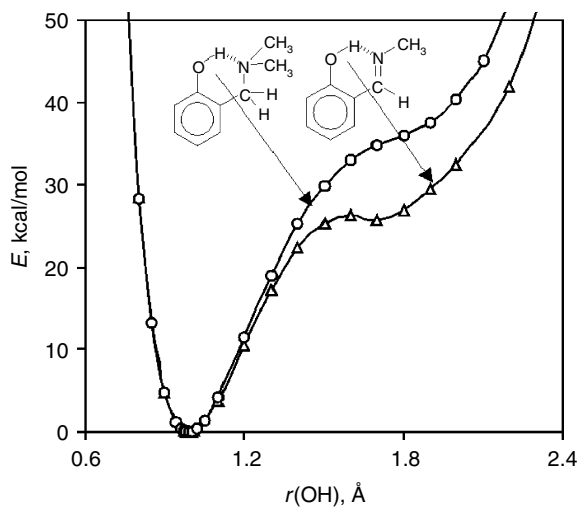


Figure 2. Adiabatic potential curves for the proton movement for 2-(*N*-dimethylaminomethyl)phenol (circles) (Mannich base) and 2-(*N*-methyliminomethyl)phenol (aldimine) (triangles) at MP2/6-31G(d,p) level. Reprinted with permission from Ref. 19. Copyright 2005 John Wiley & Sons, Ltd.

consequence to more quinoid-like structure, i.e., more localized π -electron structure. A similar dependence was observed for the plot of HOMA vs. C–O bond length [21]. The latter is known as a reliable measure of H-bond strength [22] and is often used in this meaning [4].

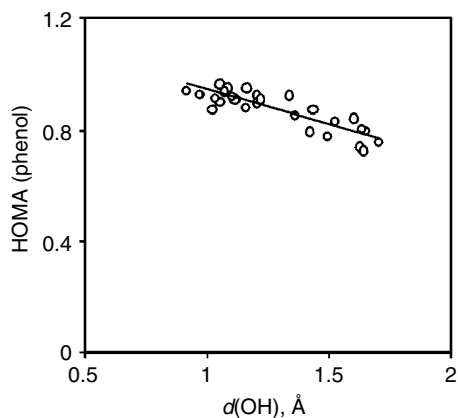


Figure 3. The HOMA (phenol) aromaticity index vs. the $d(\text{OH})$ bond length for crystallographic data for ketamines. Reprinted with permission from Ref. 21. Copyright 2005 John Wiley & Sons, Ltd.

The chelate chain in ketimines involved in the intramolecular H-bonding behaves in an interesting way: the increase of aromaticity of the phenyl ring measured by the use of HOMA is associated with a decrease of resonance energy of the chelate chain estimated by the HOSE model (HOSE—Harmonic Oscillator Stabilization Energy is the energy that must be applied to deform the geometry of the real molecule to its Kekulé structures) [23–25]. Figure 4 presents this dependence.

It means that the increase of stabilization of chelate chain is associated with a decrease of aromaticity, i.e., π -electron delocalization in the ring. A similar situation was observed for the first X-ray determined ionic H-bonding in the crystal state for *ortho*-hydroxy Schiff base—5-nitro-*N*-salicylideneethylamine [26]. It revealed a substantial decrease of aromaticity in the ring for the ionic form, HOMA = 0.732. Polysubstitution of benzene usually decreases the ring aromaticity [27]; the mean HOMA value for 154 molecular geometries of 1,2,4-trisubstituted benzene derivatives, which are topologically equivalent to the studied Schiff base, equals 0.96. This is in line with a value for the neutral form, estimated for an averaged structure of 147 neutral Schiff bases, for which the HOMA = 0.972. Thus the decrease of π -electron delocalization in the ring is unexpectedly large and is due to an increase of weight of the keto–amine form of canonical structures as shown in Scheme 2. These changes are accompanied with the opposite tendency of HOMA values for the spacer; 0.623 for the ionic form and 0.387 for the neutral one. The interrelations are shown in Scheme 3.

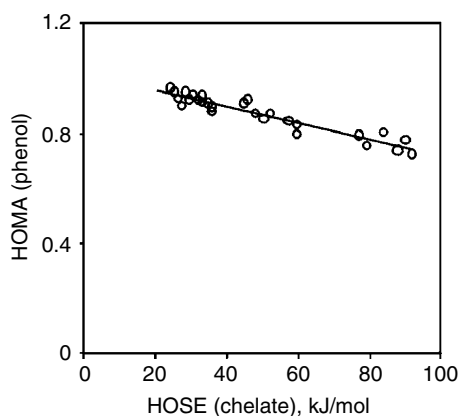
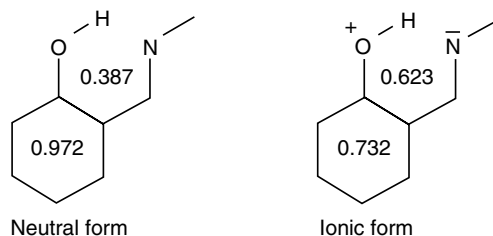


Figure 4. The HOMA (phenol) aromaticity index vs. the HOSE (chelate) destabilization index for crystallographic data for ketimines. Reprinted with permission from Ref. 21. Copyright 2005 John Wiley & Sons, Ltd.



Scheme 3. HOMA values for neutral and ionic forms of *ortho*-hydroxy Schiff base.

The observation is in line with the well-known fact that the double bonded group attached to the ring decreases its aromaticity [28].

3.2 Malonaldehyde—Intramolecularly H-Bonded Quasi-Ring

Various substituted derivatives of malonaldehyde are convenient systems to study the properties of intramolecularly H-bonded chelate chain.

Interrelation between characteristics of H-bonding and overall changes in π -electron delocalization in the chelate chain is shown by the dependence of O–H bond length on HOMA values for seven halogen-substituted malonaldehydes [29]. The longer is the O–H bond, the greater is the HOMA value, as shown in Fig. 5.

Recently Grabowski [30] introduced a resonance parameter describing π -electron delocalization in such systems due to H-bonding formation:

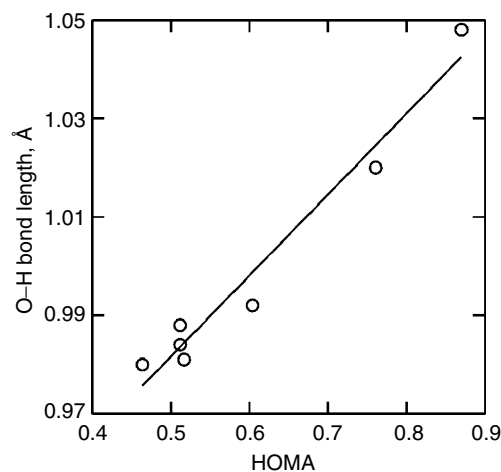
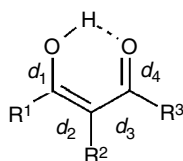


Figure 5. Interrelation between the O–H bond length and HOMA values for variously substituted derivatives of malonaldehyde.

$$\Delta_{\text{rp}} = \frac{1}{2} \left[\frac{\Delta d_1^{\text{o}} - \Delta d_1^{\text{c}}}{\Delta d_1^{\text{o}}} + \frac{\Delta d_2^{\text{o}} - \Delta d_2^{\text{c}}}{\Delta d_2^{\text{o}}} \right]$$

(3) $\Delta d_1^{\text{o}} = d_3^{\text{o}} - d_2^{\text{o}}, \Delta d_2^{\text{o}} = d_4^{\text{o}} - d_1^{\text{o}}$ open conformation
 $\Delta d_1^{\text{c}} = d_3^{\text{c}} - d_2^{\text{c}}, \Delta d_2^{\text{c}} = d_4^{\text{c}} - d_1^{\text{c}}$ closed conformation

where d_i are as shown in Scheme 4; d_i^{c} are for the H-bonded system, whereas d_i^{o} stand for open conformation (Scheme 5).



Scheme 4. Labeling of bonds and substituents in malonaldehyde derivatives.

The Grabowski index, Δ_{rp} , describes π -electron delocalization as a consequence of the intramolecular H-bond formation. To define Δ_{rp} parameter the geometry of the so-called “open conformation” is needed—the situation when the intramolecular H-bond does not exist and this system is a reference state. Figure 6 presents the dependence of HOMA on resonance parameter Δ_{rp} on HOMA.

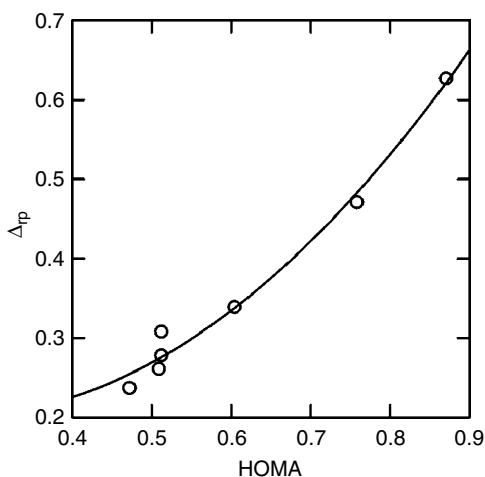
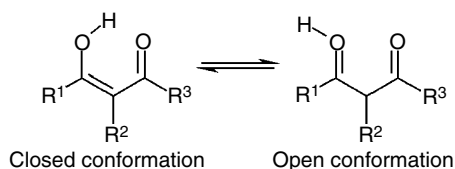


Figure 6. Dependence of resonance parameter Δ_{rp} of the spacer on HOMA values for variously substituted derivatives of malonaldehyde; correlation coefficient for quadratic relationship is 0.990. Reprinted with permission from Ref. 29. Copyright 2005 Springer-Verlag.



Scheme 5. Closed and open conformation of malonaldehyde derivatives.

The non linear dependence of Δ_{rp} on HOMA results from the definitions of these parameters; the first one is a quadratic function of the differences of bond lengths, whereas the other is a linear one. It is worth mentioning here that the main contribution to the variability of HOMA index for chelate chain comes out from the GEO term, i.e., it is due to changes in bond length alternation, whereas the contribution due to the bond elongation is chaotic and insignificant. Figure 7 presents the dependence of EN and GEO on Δ_{rp} .

If the energy of such H-bonding is computed as a difference between the open and closed structures [31] (see Scheme 5) of Cl- and F- substituted derivatives of malonaldehydes, it turns out that an increase of energy is associated with an increase of π -electron delocalization in the chelate chain (OCCCCO), as shown in Fig. 8.

Interestingly, if the computation of energy was done by the use of HF/6-311++G** method, thus taking into account electron correlation only as an averaged electrostatic field, there is practically no dependence. However, if the electron

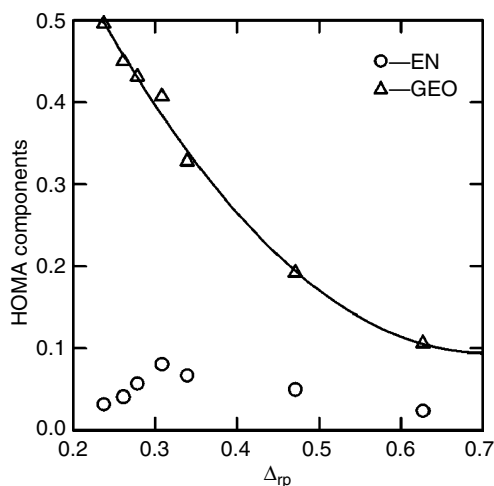


Figure 7. Dependence of HOMA components, EN and GEO terms, on Δ_{rp} for variously substituted derivatives of malonaldehyde. Reprinted with permission from Ref. 29. Copyright 2005 Springer-Verlag.

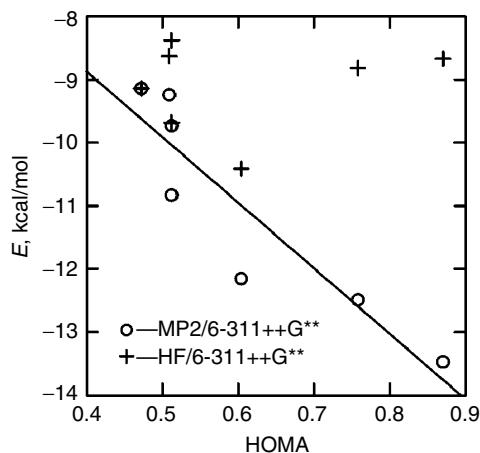


Figure 8. Dependence of H-bonding energy on HOMA values calculated at two levels of theory: HF/6-311++G** and MP2/6-311++G** for variously substituted derivatives of malonaldehyde. Correlation coefficient for the latest relationship is -0.913 . Reprinted with permission from Ref. 29. Copyright 2005 Springer-Verlag.

correlation was taken into account by computation at the MP2/6-311++G** level of theory, the correlation is found which clearly suggests a dependence of π -electron delocalization on energy. It means that for this kind of subtle interaction electron correlation has to be taken into consideration.

The same set of systems was studied by the use of the AIM theory [32, 33]. It was found that electron density in bond critical points (hereafter abbreviated as BCPs) of O–H bond and H \cdots O contact correlated well with HOMA values for the chelate chain as shown in Fig. 9.

3.3 Phenols—Intermolecular H-Bonding

Phenol and its derivatives are convenient systems to study intermolecular H-bonding and its distant influences on molecular structure. Two main ways of analyses are currently used to study these problems: the computational investigations and those based on X-ray structural analysis. Both of them lead to similar conclusions and both are presented in this review.

3.3.1 Analysis based on X-ray structure determination

Analysis of 635 variously substituted phenols in H-bonded complexes [34] revealed that the lengths of both *ipso-ortho* C–C bonds, the C–O bond lengths, and the *ipso* angle are strongly correlated fulfilling the Bent-Walsh rule [35]. The above-mentioned parameters describe geometrical pattern of the close vicinity of the H-bonding. Structural consequences of H-bonding may also be

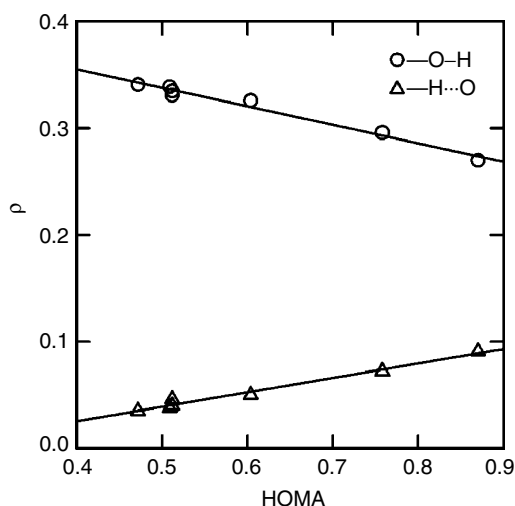


Figure 9. Dependence of electron density in BCP of O–H bond (circles) and O··H contact (triangles) on HOMA values for variously substituted derivatives of malonaldehyde. Correlation coefficients are -0.989 and 0.990 , respectively. Reprinted with permission from Ref. 29. Copyright 2005 Springer-Verlag.

observed in distant parts of molecules, e.g., in the aromatic ring. This may be well described by, e.g., HOMA index.

When the HOMA index calculated for the phenol rings is plotted against the C–O bond length (an approximate measure of H-bonding strength) for 664 H-bonded phenol derivatives retrieved from the Cambridge Structure Database, the dependence looks as in Fig. 10 [36].

Interestingly, of the two HOMA components, the GEO term is clearly related to the H-bonding strength approximated by the C–O bond length [22] (Fig. 11). The other component, EN, does not depend on the C–O bond length at all (Fig. 12).

It is worth mentioning here that a similar dependence is observed for the HOMA vs. α plot. This is shown in Fig. 13. It is an important finding, since very recently Domenicano et al. [37, 38] confirmed that the α angle is a reliable measure of electronegativity of the substituent. In the cases discussed here, it concluded that –OH group influenced by various substituents in the ring and involved in H-bonding with various bases may be treated as a substituent of variable electronegativity approximately measured by the value of α angle.

However, it should be stressed here that in all the above-mentioned cases, the HOMA was estimated from experimental X-ray determined geometry, and hence some interactions from the packing forces may influence the quantities taken into account [39]. This problem is very frequently discussed: how far the crystallographic measurements of molecular geometry are sufficiently reliable

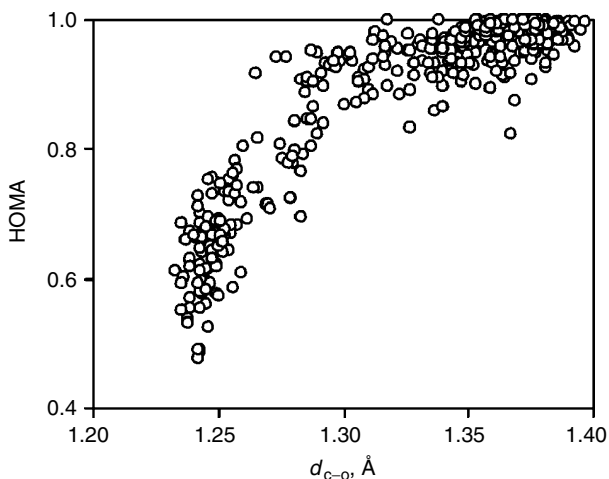


Figure 10. Relationship between HOMA and C–O bond length, d_{C-O} , for variously substituted phenols. Reprinted with permission from Ref. 36. Copyright 2004 American Chemical Society.

to lead to the right conclusions. This is particularly important for systems with H-bonding, since this part of the structure is susceptible to external perturbations [4].

Indeed, when the principal component analysis (PCA) [40, 41] was applied to the structural parameters of the ring of 664 variously substituted phenols interacting with bases in H-bonded complexes [36], it was found that the first

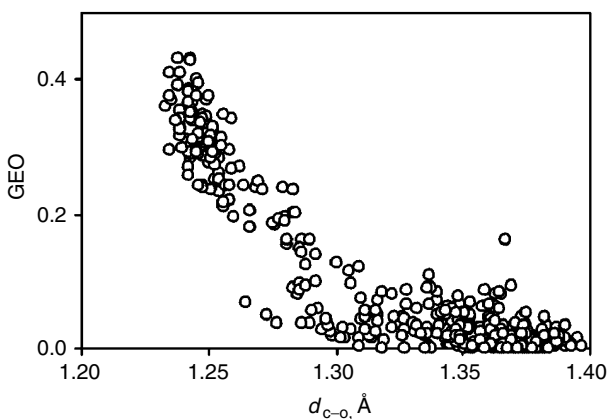


Figure 11. Relationship between GEO term and C–O bond length, d_{C-O} , for variously substituted phenols. Reprinted with permission from Ref. 36. Copyright 2004 American Chemical Society.

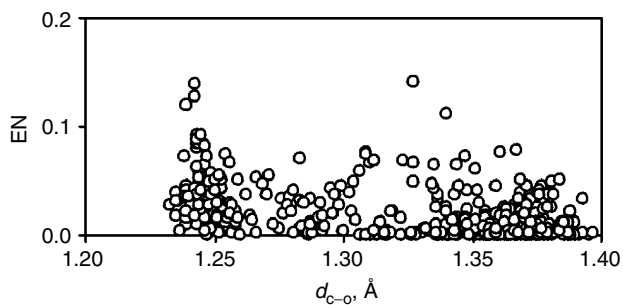


Figure 12. Relationship between EN term and C–O bond length, d_{C-O} , for variously substituted phenols. Reprinted with permission from Ref. 36. Copyright 2004 American Chemical Society.

principal component correlates with the C–O bond length, i.e., the variable not taken into PCA. Figure 14 presents this dependence. However, it should be pointed out, that this first principal component describes only $\sim 50\%$ of the total variance. It is necessary to apply six more principal components to describe the rest of the variance. It is difficult to interpret them and that may suggest a presence of very differentiated sources of distortions from the ideal geometry, as it would be for the isolated systems. For this reason quantum chemical modeling is often used.

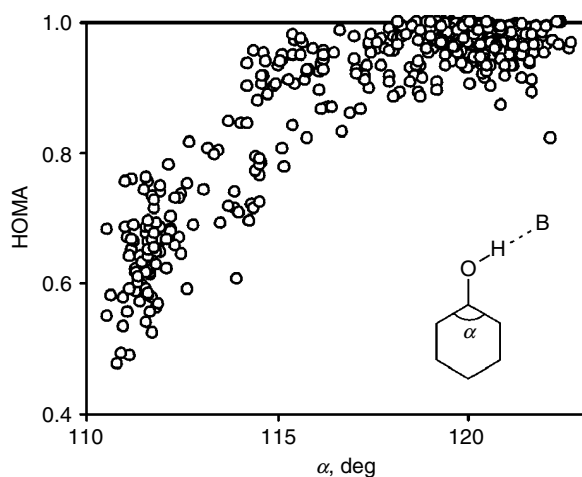


Figure 13. Dependence of HOMA on the ipso angle, α , for variously substituted phenols. Reprinted with permission from Ref. 36. Copyright 2004 American Chemical Society.

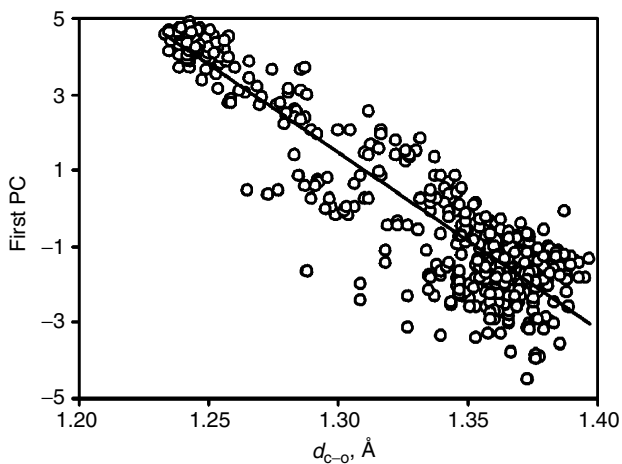
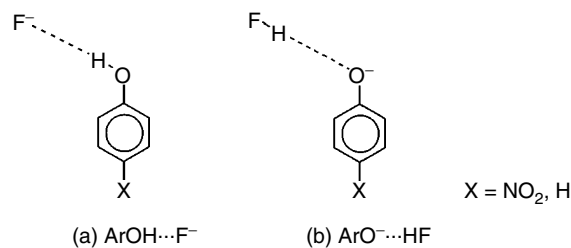


Figure 14. Dependence of first principal component of PCA, when all geometrical parameters of the ring were taken into account, on C–O bond length, d_{C-O} , for variously substituted phenols, $cc = -0.928$. Reprinted with permission from Ref. 36. Copyright 2004 American Chemical Society.

3.3.2 Computational approaches

Ab initio modeling (B3LYP/6–311+G**) was applied to phenol and *p*-nitrophenol complexes with F^- [42]. The fluoride is approaching the molecule of *p*-nitrophenol/phenol along the line being a prolongation of O–H bond direction, as shown in Scheme 6 [42]. Two cases were studied: one with a stronger interaction (6a) when fluoride approaches the –OH group in phenol, and the other, weaker one (6b) when the hydrofluoric acid approaches the oxygen atom in the phenolate anion.



Scheme 6. Modeling of H-bonding interactions.

When the values of HOMA are plotted against O \cdots F distance, which may be considered as an approximate estimate of the “strength” of 6a and 6b interactions, then the dependences are as shown in Fig. 15. Evidently for longer distances the interactions of 6a type weakly affect the π -electron delocalization

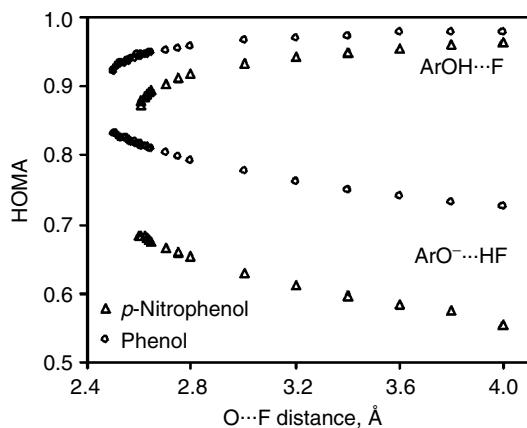
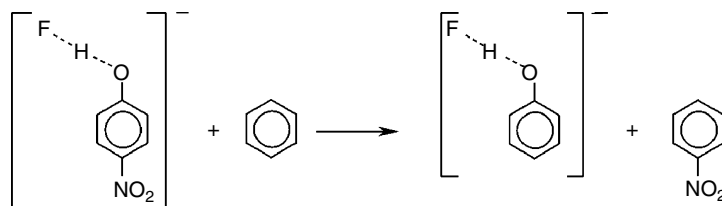


Figure 15. Variation of HOMA values on O...F distance for ArOH...F⁻ and ArO⁻...HF interactions for *p*-nitrophenol and phenol complexes. Reprinted with permission from Ref. 42. Copyright 2004 American Chemical Society.

in the ring—the changes of HOMA are small. In contrast, for 6b-type interactions, the changes in HOMA are significant. The mesomeric interaction of O⁻...HF with the ring and the substituted ring leads to a substantial decrease of the ring aromaticity.

The substituent effect in the system with *para*-NO₂ group leads to a charge transfer from the oxygen atom towards the nitro group and this is associated with an increase of quinoid structure contribution. In consequence it is equivalent to the decrease of π-electron delocalization in the ring. This effect is ruled by the kind and the strength of H-bonding. Energetically it may be described by a Substituent Effect Stabilization Energy (hereafter abbreviated as SESE) [43], which is defined as a difference in energy between the products and the substrates of an appropriate conceived reaction. SESE for nitro interactions were calculated according to the reaction presented in Scheme 7 [42].



Scheme 7. Homodesmotic reaction for estimation of SESE.

Analyzing the plots in Fig. 16, it can be found that the range of variation of SESE values for *p*-nitrophenol...F⁻ complexes (~6 kcal/mol) is greater than for *p*-nitrophenolate...HF complexes (~3 kcal/mol).

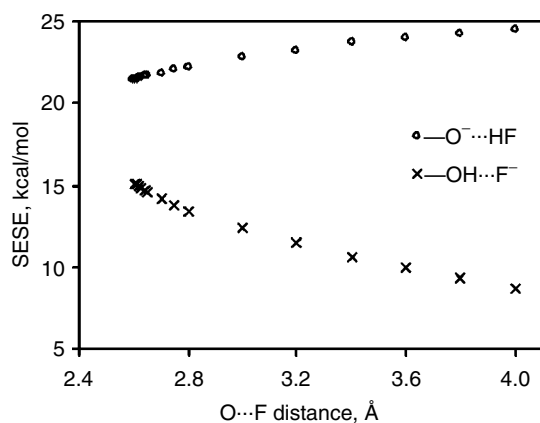


Figure 16. Scatter plots of SESE values for two kinds of H-bonds (Scheme 6) against the O...F distance. Reprinted with permission from Ref. 42. Copyright 2004 American Chemical Society.

In the case of $p\text{-NO}_2\text{PhOH} \cdots \text{F}^-$ interactions (Scheme 6a) the shortening of the O...F distance is associated with an increase of O...H distance and consequently with an increase of the negative charge at the oxygen atom leading to a stronger weight of the quinoid-like structure. In opposition to this, when HF is approaching the oxygen atom (Scheme 6b), the weight of the quinoid structure smoothly decreases. At the distance O...F equal to 4 Å the situation for 6a case resembles the structure of p -nitrophenol, and for 6b case the p -nitrophenolate anion. Obviously the through resonance effect for the first case is substantially weaker than for the second one which results directly from the electron donating power of the substituents, described by the values of substituent constants: σ_{P}^+ for $-\text{OH}$ and $-\text{O}^-$ which are -0.92 and -2.30 , respectively [44].

When the changes in π -electron delocalization are analyzed as a function of the H-bonding strength approximated by the C–O bond length [22] the scatter plot is as in Fig. 17. For $\text{ArOH} \cdots \text{F}^-$ interactions, when $\text{C}_{\text{Ar}}\text{OH}$ is a proton-donating group, the shorter the C–O bond length, the stronger the H-bonding. Opposite that, for $\text{ArO}^- \cdots \text{HF}$ interactions, when $\text{C}_{\text{Ar}}\text{O}^-$ is a proton-accepting system, the shorter the C–O bond, the weaker the H-bond. The changes in H-bond strength cause significant changes in the π -electron delocalization in phenol ring expressed by HOMA values. A similar result is obtained when the delocalization is described by $\text{NICS}(1)_{zz}$ [45] as shown in Fig. 18. In these cases the equivalence of these two descriptors of π -electron delocalization is very high as shown in Fig. 19.

The nature of substituents may affect significantly the H-bond characteristics and associated π -electron delocalization. Analysis of changes of C–O bond length in a set of $para$ -substituted phenol derivatives interacting with fluoride and $para$ -substituted phenolate derivatives interacting with HF allows to show

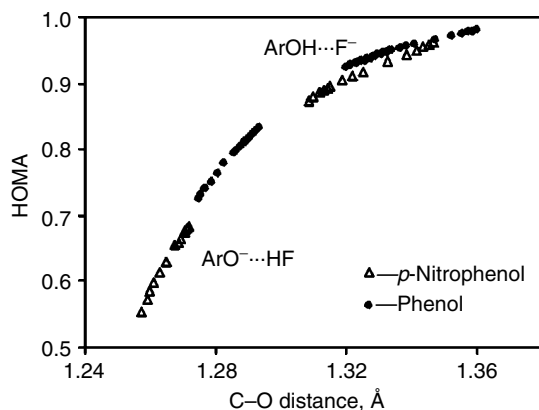


Figure 17. Relationships of HOMA values plotted against C–O bond length for *p*-nitrophenol and phenol complexes with fluoride. Two kinds of interactions are taken into account (Scheme 6). Reprinted with permission from Ref. 42. Copyright 2004 American Chemical Society.

some general dependences [46]. The studied substituents were as follows: $-\text{NO}_2$, $-\text{CHO}$, $-\text{H}$, $-\text{CH}_3$, $-\text{OCH}_3$, $-\text{OH}$. It was found that for the equilibrium structures $[\textit{p}\text{-X-PhO} \cdots \text{H} \cdots \text{F}]^-$, the C–O bond lengths correlate well with the Hammett substituent constants σ_p —as shown in Fig. 20. When O–H distance is taken as a measure of H-bonding strength, the dependence on Hammett's σ_p is also very good (Fig. 21).

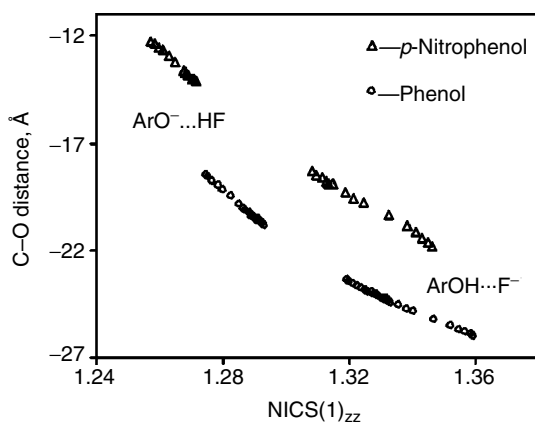


Figure 18. Relationships of NICS(1)_{zz} values plotted against C–O bond length for *p*-nitrophenol and phenol complexes with fluoride. Two kinds of interactions are taken into account (Scheme 6). Reprinted with permission from Ref. 42. Copyright 2004 American Chemical Society.

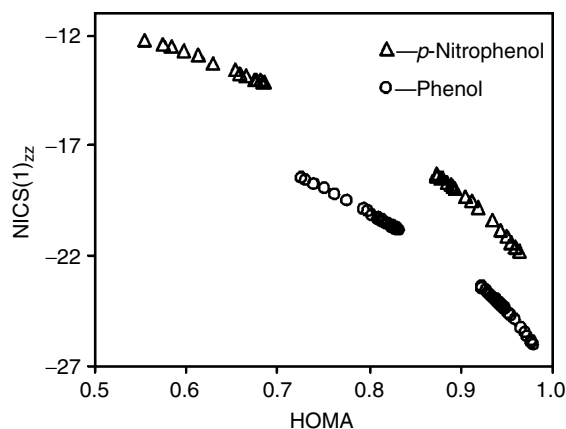


Figure 19. Relationships between $\text{NICS}(1)_{zz}$ and HOMA for *p*-nitrophenol and phenol complexes. Two kinds of interactions were considered (Scheme 6).

In both cases, i.e., equilibrium complexes $[p\text{-X-PhO} \cdots \text{H} \cdots \text{F}]^-$ and phenols, electron-accepting substituents (with $\sigma_p > 0$) increase the contribution of the quinoid-like structure, which in turn leads to a decrease of charge at the oxygen atom. The greater the value of σ_p is, the stronger the mesomeric effect appears. It is worth mentioning that in all equilibrium complexes the proton is transferred to fluoride. In the case of phenols the sensitivity of O–H bond lengths on σ_p is ~ 100 times lower than that for the O \cdots H interatomic distance in equilibrium complexes.

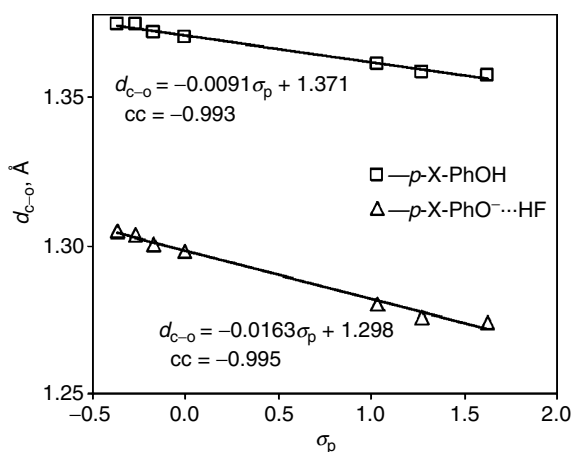


Figure 20. Dependences of C–O bond length, $d_{\text{C-O}}$, in *p*-X-PhOH and optimal structures of $[p\text{-X-PhO} \cdots \text{H} \cdots \text{F}]^-$ on a substituent constant, σ_p (for electron-accepting substituents σ_p^- are used). Reprinted with permission from Ref. 46. Copyright 2005 American Chemical Society.

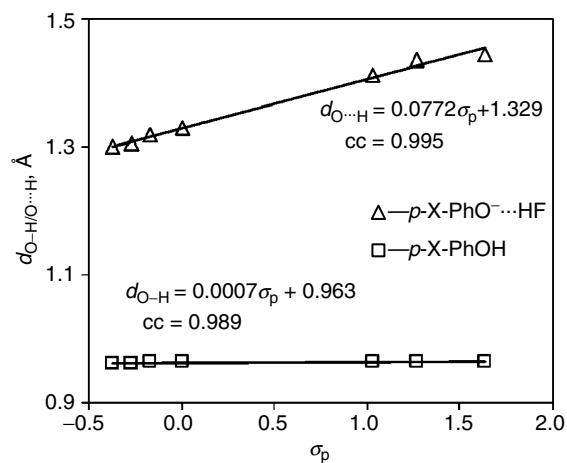


Figure 21. Dependences of the O–H bond length, d_{O-H} , and the O···H contact, $d_{O...H}$, in p -X-PhOH and optimal structures of $[p\text{-X-PhO}\cdots\text{H}\cdots\text{F}]^-$ on a substituent constant, σ_p (for electron-accepting substituents σ_p^- are used). Reprinted with permission from Ref. 46. Copyright 2005 American Chemical Society.

When the fluoride approaches hydrogen in the hydroxyl group at some O···F distance proton is transferred towards fluoride and the hydrofluoric acid is formed. The O···F distance for the proton transfer for variously substituted phenols correlate nicely with the Hammett constants σ_p , as shown in Fig. 22.

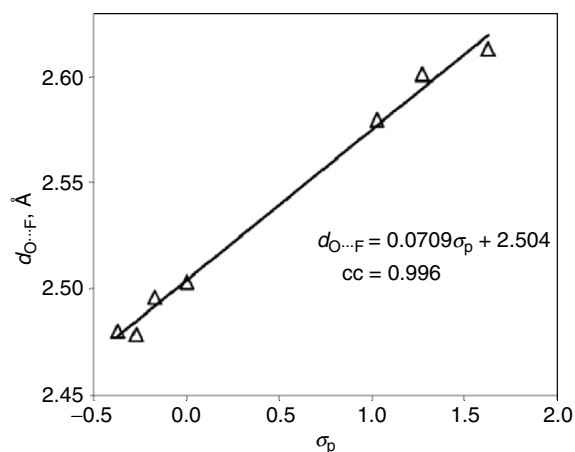


Figure 22. Dependence of the O···F distance for proton transfer, $d_{O...F}$, for $[p\text{-X-PhO}\cdots\text{H}\cdots\text{F}]^-$ complexes on a substituent constant, σ_p (for electron-accepting substituents σ_p^- are used). Reprinted with permission from Ref. 46. Copyright 2005 American Chemical Society.

Interpretation of the above dependence is as follows. The stronger electron-attracting power of the substituent is (more positive value of σ_p), the lesser is the electron density at the oxygen atom in $-\text{OH}$ group, thus the weaker attraction of proton by the oxygen atom, and hence at a longer $\text{O}\cdots\text{F}$ distance proton may be transferred from the hydroxyl group to the fluoride anion.

It is well known that the ^1H NMR chemical shift is often used as an approximate measure of the H-bonding strength [47, 48]. When the ^1H NMR chemical shift of the hydroxyl proton is plotted against the $\text{C}-\text{O}$ bond length, it comes out that those two measures of H-bond strength are equivalent, as shown by the scatter plot in Fig. 23.

Evidently, due to the formerly shown interrelations, there is also a good correlation between the ^1H NMR chemical shift of the proton involved in H-bonding and π -electron delocalization in the ring expressed by HOMA as shown in Fig. 24.

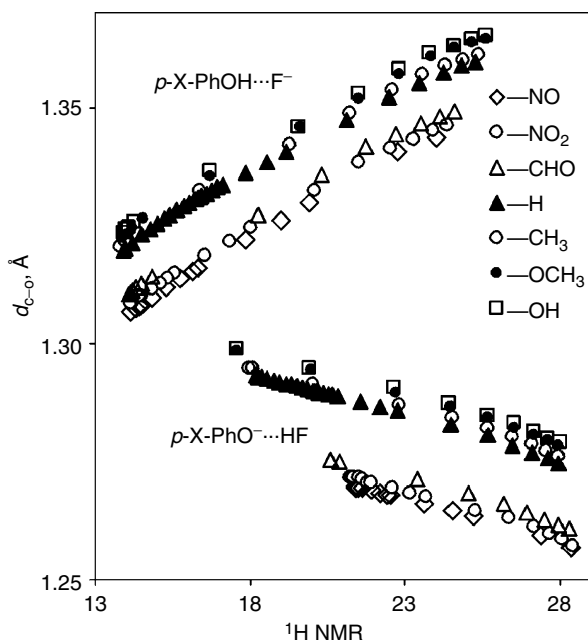


Figure 23. Dependence of two empirical measures of H-bond strength: the ^1H NMR chemical shift of the proton involved and the $\text{C}-\text{O}$ bond length, $d_{\text{C}-\text{O}}$, for $[\text{p-X-PhO}\cdots\text{H}\cdots\text{F}]^-$ complexes. Reprinted with permission from Ref. 46. Copyright 2005 American Chemical Society.

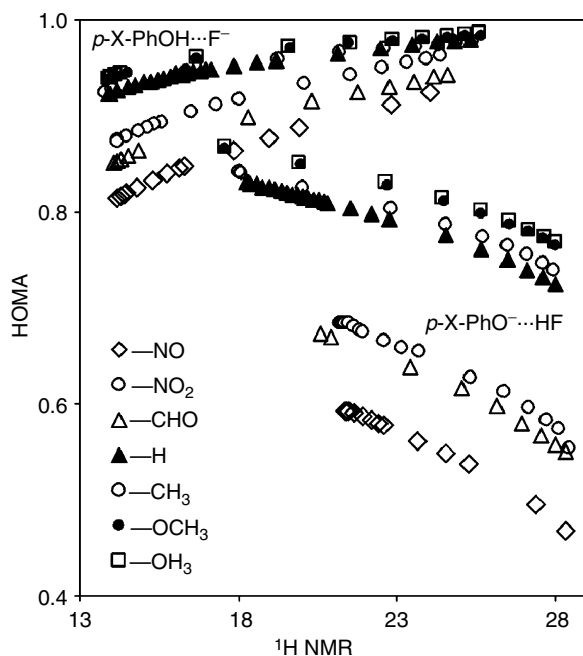


Figure 24. Dependence of the HOMA value on the ^1H NMR chemical shift of the proton involved for $[\text{p-X-PhO}\cdots\text{H}\cdots\text{F}]^-$ complexes. Reprinted with permission from Ref. 46. Copyright 2005 American Chemical Society.

4 CONCLUSIONS

As presented in the numerous examples based on experimental and computational data the H-bonding exerts substantial changes on the molecular geometry of distant parts of the systems in question. These changes are related to the variations in π -electron delocalization and reflect the strength of H-bonding.

REFERENCES

1. L. Pauling *The Nature of the Chemical Bond* (Cornell University Press, Ithaca, New York, 1960).
2. P. Muller (ed) (1994) *Pure Appl. Chem.* **66**, 1077.
3. V. I. Minkin (ed) (1999) *Pure Appl. Chem.* **71**, 1919.
4. L. Sobczyk, S. J. Grabowski and T. M. Krygowski (2005) *Chem. Rev.* **105**, 3513.
5. J.-M. Lehn (1990) *Angew. Chem., Int. Ed.* **29**, 1304.
6. G. A. Jeffrey and W. Saenger, *Hydrogen Bonding in Biological Structures* (Springer-Verlag, Berlin, 1990).
7. H. B. Burgi and J. D. Dunitz (eds), *Structure Correlation* (VCH, Weinheim, 1994).
8. Preface to: L. V. Vilkov, V. S. Mastryukov and N. I. Sadova, *Determination of the Geometrical Structure of Free Molecules* (MIR, Moscow, 1983).
9. H. Hellmann, *Einführung in die Quantenchemie* (Franz Deuticke, Leipzig, 1937); R. P. Feynman (1939) *Phys. Rev.* **56**, 340.

10. T. M. Krygowski and B. T. Stępień (2005) *Chem. Rev.* **105**, 3482 [article].
11. T. M. Krygowski and M. K. Cyrański (2001) *Chem. Rev.* **101**, 1385.
12. A. Julg and P. Francoise (1967) *Theor. Chim. Acta* **8**, 249.
13. J. Kruszewski and T. M. Krygowski (1972) *Tetrahedron Lett.* **36**, 3839.
14. C. W. Bird (1985) *Tetrahedron* **41**, 1409.
15. T. M. Krygowski (1993) *J. Chem. Inf. Comput. Sci.* **33**, 70.
16. T. M. Krygowski and M. K. Cyrański (1996) *Tetrahedron* **52**, 1713.
17. T. M. Krygowski, M. Cyrański, A. Ciesielski, B. Świrska and P. Leszczyński (1996) *J. Chem. Inf. Comput. Sci.* **36**, 1135.
18. J. Jański and A. Koll (2004) *Struct. Chem.* **15**, 353.
19. A. Filarowski (2005) *J. Phys. Org. Chem.* **18**, 686.
20. A. Filarowski, A. Koll and T. Głowiak (2002) *J. Chem. Soc., Perkin Trans. 2*, 835.
21. A. Filarowski, A. Kochel, K. Cieślík and A. Koll (2005) *J. Phys. Org. Chem.* **18**, 986.
22. T. M. Krygowski, J. E. Zachara and H. Szatyłowicz (2005) *J. Phys. Org. Chem.* **18**, 110.
23. T. Więckowski and T. M. Krygowski (1981) *Can. J. Chem.* **59**, 1622.
24. T. M. Krygowski, R. Anulewicz and J. Kruszewski (1983) *Acta Cryst.* **B39**, 732.
25. C. W. Bird (1998) *Tetrahedron* **54**, 4641.
26. T. M. Krygowski, K. Woźniak, R. Anulewicz, D. Pawlak, W. Kołodziejcki, E. Grech and A. Szady (1997) *J. Phys. Chem. A* **101**, 9399.
27. M. K. Cyrański and T. M. Krygowski (1996) *J. Chem. Inf. Comput. Sci.* **36**, 1142.
28. M. K. Cyrański, T. M. Krygowski, M. Wisiorowski, N. J. R. v. E. Hommes and P. v. R. Schleyer (1998) *Angew. Chem., Int. Ed.* **37**, 177.
29. T. M. Krygowski and J. E. Zachara (2005) *Theor. Chem. Acc.* **114**, 229.
30. S. J. Grabowski (2003) *J. Phys. Org. Chem.* **16**, 797.
31. S. J. Grabowski (2002) *Monatsh. Chem.* **133**, 1373.
32. R. F. W. Bader, *Atoms in Molecules: A Quantum Theory* (Oxford University Press, New York, 1990).
33. P. Popelier, *Atoms in Molecules, An Introduction* (Prentice Hall, Pearson Education Ltd, 2000).
34. H. Szatyłowicz and T. M. Krygowski (2004) *Pol. J. Chem.* **78**, 1719.
35. H. A. Bent (1961) *Chem. Rev.* **61**, 275.
36. T. M. Krygowski, H. Szatyłowicz and J. E. Zachara (2004) *J. Chem. Inf. Comput. Sci.* **44**, 2077.
37. A. R. Campanelli, A. Domenicano and F. Ramondo (2003) *J. Phys. Chem. A* **107**, 6429.
38. A. R. Campanelli, A. Domenicano, F. Ramondo and I. Harggitai (2004) *J. Phys. Chem. A* **108**, 4940.
39. J. Bernstein in *Effect of Crystal Environment on Molecular Structure*, A. Domenicano and I. Harggitai (eds), *Accurate Molecular Structures. Their Determination and Importance*, (International Union of Crystallography and Oxford University Press, Oxford, 1992), p. 469.
40. E. R. Malinowski, *Factor Analysis in Chemistry* (Wiley, New York, 2002).
41. R. I. Zalewski in *Principal Component Analysis as a Tool in Organic Chemistry and Food Chemistry*, R. I. Zalewski, T. M. Krygowski and J. Shorter (eds), *Studies in Organic Chemistry. Similarity Models in Organic Chemistry, Biochemistry and Related Fields*, Vol. 42, (Elsevier Science, Amsterdam, 1991), p. 455.
42. T. M. Krygowski, J. E. Zachara and H. Szatyłowicz (2004) *J. Org. Chem.* **69**, 7038.
43. A. Pross, L. Radom and R. W. Taft (1980) *J. Org. Chem.* **45**, 818.
44. C. Hansch, A. Leo and R. W. Taft (1991) *Chem. Rev.* **91**, 165.
45. C. Corminboeuf, T. Heine, G. Seifert, P. v. R. Schleyer and J. Weber (2004) *Phys. Chem. Chem. Phys.* **6**, 273.
46. T. M. Krygowski, H. Szatyłowicz and J. E. Zachara (2005) *J. Chem. Inf. Model.* **45**, 652.
47. V. Bertolasi, P. Gilli, V. Ferretti and G. Gilli (1997) *J. Chem. Soc., Perkin Trans. 2*, 945.
48. T. Dziembowska, B. Szczodrowska, T. M. Krygowski and S. J. Grabowski (1994) *J. Phys. Org. Chem.* **7**, 142.

CHAPTER 12

TOPOLOGY OF X-RAY CHARGE DENSITY OF HYDROGEN BONDS

TIBOR S. KORITSANSZKY

Middle Tennessee State University, Murfreesboro, TN 37132, USA

Abstract Applications of the quantum theory of “Atoms in Molecules” to X-ray charge densities to explore hydrogen bonding in molecular solids are outlined. Uncertainties in the experimental electron density and limitations of local bond-topological and related empirical energetic properties in characterizing hydrogen bonds are discussed. Recent state-of-the-art experimental results—either supporting or contradicting theoretical predictions—are revisited to highlight the importance of interplay between theory and experiment.

Keywords: Electron density; gradient trajectory; bond critical point; interaction line; atomic basin; Laplacian; energy density; local virial; source function; structure factor; pseudoatom; multipole refinement; interaction density.

1 INTRODUCTION

Hydrogen bonding (HB: D–H···A) is usually viewed as a weak interaction between an electronegative acceptor (A) atom with (a) lone-pair(s) and a hydrogen atom (H) involved in a polar covalent bond to a donor atom (D). This textbook definition might sound extremely simple and troublesome at the same time. It is certainly oversimplified considering the important role these interactions are believed to play in driving complex processes, such as phase transitions, or in determining structure, function, and reactivity of complex systems, such as bio-macromolecules [1–3]. It might as well appear complicated, because it presupposes the exact meaning of the concepts mentioned above, all of which are manifestations of the atomic paradigm. This fundamental operative tool of chemistry has been ambiguously defined, until recently, as “a chemical unit” that has recognizable contribution to the “whole”, called molecule. Neither the concept of molecule nor that of the “molecular atom” can, however, directly be deduced from first principles of quantum physics. The

route from the physical system of electrons and nuclei interacting via Coulomb forces to the “chemical system” of interacting atoms forming a stable molecule is far from being straightforward [4]. Traditionally, molecules are identified by their chemical structure, that is, by a definite atomic constitution, configuration, and conformation. The structure hypothesis is necessarily invoked in the interpretation of any observable molecular properties. This is equally true if effects of hydrogen bonding on static, dynamic, and reactive molecular properties—that are readily measurable by spectroscopic, NMR, and diffraction techniques—are to be modeled.

The theoretical foundation of molecular structure is the Born–Oppenheimer (BO) approximation [5], which, by treating the nuclei as classical particles, allows for the separation of nuclear and electronic motion and for the calculation of the electronic energy, in principle, at any frozen nuclear arrangement. The technical difficulties associated with *ab initio* methods severely limit quantum chemical exploration of the BO-energy landscape to sub-domains corresponding to a few internal coordinates of relatively small isolated dimers. While the results of such calculations can correlate well with those of gas-phase measurements, their extrapolation to condensed-phase situations is not justified. A “molecule” in this case, being an integral part of the total system, possesses a temperature- and volume-dependent average structure that can be defined only in relation to a statistical ensemble of all interacting particles. Modeling of such a system at the molecular level requires understanding of interactions at the atomic level, and viewing a subsystem (molecule) in isolation necessarily means neglecting its interaction with its surroundings [6].

Within the framework of Bader’s topological theory [7], atoms are well-defined subsystems with respect to the total system. Their contribution to the properties of the total system can be deduced from the electron density of the total system (ED, ρ). Consequently, an atom in an isolated molecule is different from that in a crystal. The emergence of atom in the latter case does not necessarily mean the emergence of the molecule. Thus, the dilemma of what a molecule in the crystal is, remains unresolved even within the topological theory of structure.

Diffraction methods have been the primary sources of experimental information on structural characteristics of solids, including molecular crystals stabilized by hydrogen bonds. Though single crystal neutron diffraction [8–10] (ND) is particularly well suited for exploring structural properties of HB systems, its applications are necessarily limited due to the demanding experimental efforts involved. The vast majority of information available today is thus based on X-ray diffraction [11] (XRD) performed under standard laboratory conditions. While this method is known to be less accurate for locating hydrogen atoms, in principle, it can lead to an empirical description of atom–atom interactions at the electronic level. This is because X-ray photons

are scattered on electrons whose periodic spatial distribution is “X-ray imaged” into Bragg reflections. If it were possible to maintain kinematic conditions during the entire measurement of an unlimited number of error-free data for a perfect crystal, the ED could be experimentally accessible at any location within the unit cell. This would yield precise knowledge of not only the nuclear positions, but of all electronic properties of a solid-state system. Such absolute measurements are, however, unachievable, and in spite of tremendous recent advancements in technical and theoretical aspects of XRD, critical evaluation of the results remains essential. Nevertheless, general trends emerged from comparative analyses of closely related systems cannot be overlooked, even though experimental uncertainties associated with measurements on individual systems often exceed the error estimates of global figures deduced from measurements on a series of systems.

Figures commonly discussed as recently as a decade ago included internal coordinates in conjunction with the location and height of deformation density peaks [12]. Most recent studies [13], on the other hand, analyze correlations between density-topological indices that require precise parameter estimates of ED models fitted to high quality and resolution intensity data. Significant improvements of experimental conditions over the past few years have resulted in an unprecedented flow of reliable XRD data. Charge-coupled devices (CCD) [14] of increasing covering area and sensitivity have replaced conventional point-detectors (scintillation counters) which had prohibited fast experiments. Near-complete, high resolution, and highly redundant data sets are now being collected routinely in days or even hours [15]. Their analysis, based on advanced models [16, 17] incorporated into sophisticated computer program packages [18–20], allows for almost real-time monitoring of crystal quality and systematic measurement errors. The application of ED-based interpretive tools has made it possible to make unambiguous comparisons of quantum chemical and experimental results [7].

The purpose of this mini-review is to give the reader a taste of recent exciting but often controversy results, covering a period of less than a decade, from systematic topological X-ray charge density studies on HB systems. For purely structural conclusions drawn from standard crystallographic studies we refer to citation classics [21–24]. To put the revolutionary developments mentioned above into perspective, a short overview of theoretical and methodological aspects of the technique is thought to be useful. Chapters, introducing the basics of the topological method and ED measurement, are followed by a critical analysis of experimental uncertainties and limitations addressed in or emerged from recent studies. Given the breadth of applications, no attempt is made here to cover the topic in its entirety. Instead of providing a detailed picture of what has been done, we try to present what has been learned from studies that either confirm or confront each other’s result.

2 TOPOLOGICAL CLASSIFICATION OF ATOMIC INTERACTIONS

Bader's density-based topological theory [7] of "Atoms in Molecules" (AIM) has become a standard interpretive tool of electronic structure studies. There are obvious reasons for the popularity of this method; it provides—on a firm physical basis—a relatively simple, real-space analysis of atomic interactions. Most importantly, the method is applicable to both theoretical and experimental EDs.

Given an analytical expression or a numerical recipe to calculate the molecular or crystalline ED at any spatial point, the topological analysis starts with tracing the trajectories of $\nabla\rho$ (two consecutive points of the path are defined by the infinitesimal gradient vector). Each gradient path originates and terminates at a critical point (CP) where the gradient vanishes ($\nabla\rho(\mathbf{r}_{CP}) = 0$). A CP is designated by the rank of the Hessian matrix (the 3×3 ordered array of the second derivatives of ρ at the CP), and by the algebraic sum of the signs of the principal curvatures (λ_1 , λ_2 , and λ_3 , the eigenvalues of the Hessian at the CP). A CP is distinct from a general point in that it is a terminus or origin of trajectories, while any other point is passed through only by one trajectory (Fig. 1).

A $(3,-3)$ CP, where ρ exhibits a local maximum (typically occurring at nuclear positions), is an attractor in the gradient field, and the topological atom is defined as the union of the attractor and its associated basin. The

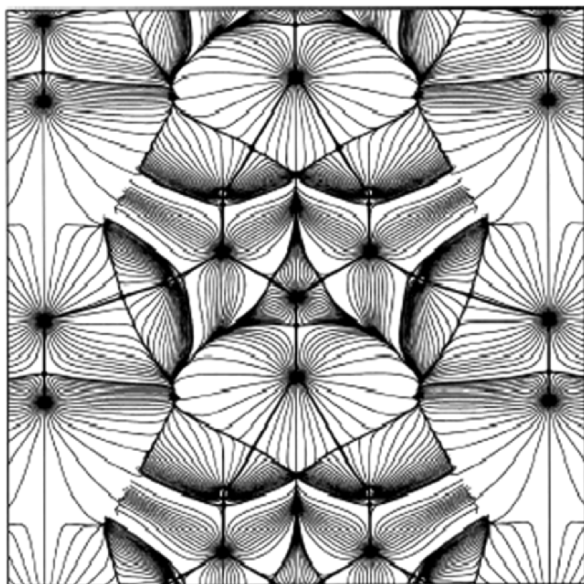


Figure 1. Gradient trajectory map of the crystalline urea in the molecular plane. Bond-paths are indicated by heavy lines, those corresponding to the interaction surface crossing the plane are drawn by weaker, while those originating from a $(3,+3)$ CP and terminating at a $(3,-3)$ CP by the weakest lines. Reprinted with permission from Ref. [78].

interaction between two such attractors results in formation of a (3,-1)CP, a saddle point, called the bond critical point (BCP). The pairs of trajectories, originating at this point and terminating at the two (3,-3)CPs, define the atomic interaction line (IL). Those trajectories that terminate at the BCP span the interatomic surface (IS). These two-dimensional manifolds separate the space into distinct regions encompassing topological atoms.

Since the perpendicular curvatures (λ_1 and λ_2) of ρ at the BCP are negative, charge is locally concentrated here with respect to points on the IS. The parallel curvature (λ_3) is positive at the BCP; thus, charge is locally depleted here relative to points along the IL. The ED and the sum of the principal curvatures, the Laplacian ($\nabla^2\rho(\mathbf{r}_{\text{BCP}}) = \nabla^2\rho_{\text{BCP}} = \lambda_1 + \lambda_2 + \lambda_3$), both taken at the BCP, are thus indicative of the nature of the interaction. Shared interactions (covalent bonds) are dominated by the negative curvatures; the charge concentration is reflected in a relatively large value of ρ_{BCP} and in a large negative value of $\nabla^2\rho_{\text{BCP}}$. For closed-shell interactions (i.e., ionic and van der Waals interactions) on the other hand, the positive curvature of ρ along the IL is dominant, and the charge depletion is reflected in a relatively low value of ρ_{BCP} and a low positive value of $\nabla^2\rho_{\text{BCP}}$.

The Laplacian thus displays where the electronic charge is locally concentrated or depleted [25, 26]. The topology of the valence shell charge concentration (VSCC), the region of the outer shell of an atom over which $\nabla^2\rho < 0$, is in accordance with the Lewis and valence shell electron pair repulsion model. To each local maximum in the VSCC, a pair of bonded or non-bonded electrons can be assigned (Fig. 2).

The value of ρ_{BCP} can serve as a measure of the bond order in non-polar covalent bonds [27, 28]. The accumulation of charge in the binding region is necessary to balance the repulsive force acting between the nuclei. It is thus anticipated that ρ_{BCP} is in a direct relationship with the bond distance, that is, it increases as the bond length decreases. The IL does not necessarily match the internuclear line. It is usually curved from the perimeter of strained rings, or from the edges of cage structures. The deviation of the length of the IL from the internuclear distance is thus an indicator of the strain in a bond [29]. A curved IL suggests that the density is not distributed such as to maximally balance the repulsive forces of the nuclei.

For an excellent review on the density topology in the crystalline state and for a detailed discussion on the interpretation of topological features introduced by the periodicity, symmetry, and cooperative field effects, we refer to a recent work by Gatti [30]. Only two important aspects of the topological approach to solid-state “chemical interactions” highlighted in that work are re-emphasized here.

While topological atoms in an isolated molecule are open domains with infinite boundaries, those in a perfect periodic crystal are defined by closed surfaces. In other words, the atomic basins in a crystal are formed by gradient paths originating from a true minimum ((3,+3)CP) and terminating at a true

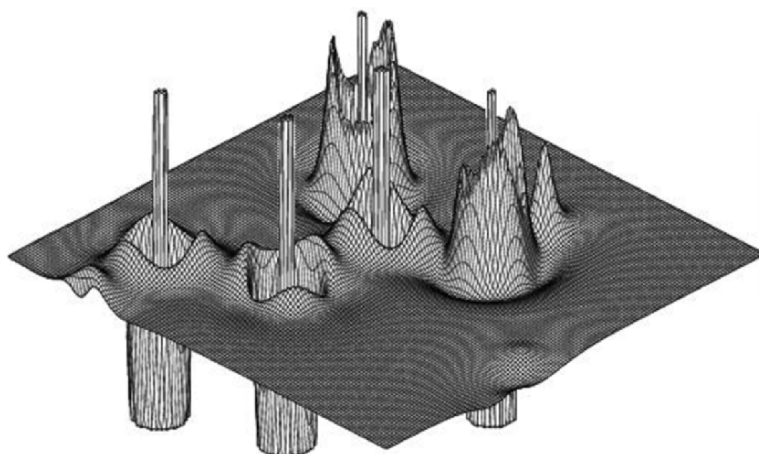


Figure 2. Relief map of the negative Laplacian in the plane of the carboxyl group in glutamic acid. Sharp peaks in the close vicinity of the nuclei represent core charge concentrations. Double maxima in the C–N, C=O, and C–C covalent bonds are bonded VSCCs of the atoms participating in the bond. The two outer maxima at the keto oxygen atom are the non-bonded VSCCs associated with the lone-pair densities. Reprinted with permission from Ref. [77].

maximum ((3,−3)CP) of the ED. The AIM theory declares that the necessary and sufficient condition for bonding is the existence of an IL along which the ED, corresponding to the stationary state of the total system in electrostatic equilibrium, is a maximum with respect to any neighboring line. (The IL in this case is referred to as the bond path (BP), while its length as BPL.) Although this statement is equally valid for the isolated and in-crystal situations, the presence of a BP in one phase does not imply the presence of the same BP in the other phase. “The electron distribution reached at equilibrium is to be seen as the best compromise yielding the lowest energy for the system as a whole, not necessarily for each single pair of atoms embedded in the crystal.” [30] In other words, the energy of the crystal cannot be decomposed into additive terms corresponding to independent pairwise interactions. A recently proposed scheme, one that partitions the total energy into self-basin and basin–basin interaction energies, makes it possible to account also for non-bonded energy terms associated with pairs of atoms not linked by BPs [31].

2.1 Energetic Classification of Atomic Interactions

The Laplacian is related, through the local virial theorem [32, 33], to the electronic kinetic ($G(r) > 0$) and potential energy ($V(r)$) densities

$$(1) \quad \frac{1}{4} \nabla^2 \rho(\mathbf{r}) = 2G(\mathbf{r}) + V(\mathbf{r})$$

This relationship indicates that the potential (kinetic) energy dominates over the total energy ($H(\mathbf{r}) = G(\mathbf{r}) + V(\mathbf{r})$) in those regions of space where charge is locally concentrated (depleted). The combination of the above formulas, provided $G(\mathbf{r})$ is accessible (wavefunction-based studies), leads to simple energetic characterization of chemical bonds [34] (Table 1). For closed-shell interactions ($\nabla^2\rho_{\text{BCP}} > 0$), $|V_{\text{BCP}}|/G_{\text{BCP}} > 2$, while for shared interactions ($\nabla^2\rho_{\text{BCP}} < 0$), $|V_{\text{BCP}}|/G_{\text{BCP}} < 1$.

For calculations based on X-ray charge densities, Abramov [35] proposed to adopt the Kirzhnits [36] formula for $G(\mathbf{r})$:

$$(2) \quad G(\mathbf{r}) = \frac{3(3\pi^2)^{2/3}}{10} \rho(\mathbf{r})^{5/3} + \frac{[\nabla\rho(\mathbf{r})]^2}{72\rho(\mathbf{r})} + \frac{1}{6} \nabla^2\rho(\mathbf{r})$$

This expression, containing only the density and its derivatives, is a good approximation to the “exact” $G(\mathbf{r})$ only in regions of low ρ_{BCP} and $\nabla^2\rho_{\text{BCP}}$ values exhibited by closed-shell interactions [37].

Bader and Gatti [38] suggested a decomposition scheme that divides the total ED into atomic sources on the basis of the local source function (LS)

$$(3) \quad \text{LS}(\mathbf{r}) = -\frac{1}{4\pi} \frac{\nabla^2\rho(\mathbf{r}')}{|\mathbf{r} - \mathbf{r}'|}$$

which is a generating function of the ED, since

$$(4) \quad \rho(\mathbf{r}) = \int \text{LS}(\mathbf{r}, \mathbf{r}') d\mathbf{r}'$$

If the integration is restricted to atomic basins,

$$(5) \quad S(\mathbf{r}, \Omega) = -\frac{1}{4\pi} \int_{\Omega} \frac{\nabla^2\rho(\mathbf{r}')}{|\mathbf{r} - \mathbf{r}'|} d\mathbf{r}', \quad \rho(\mathbf{r}) = \sum_{\Omega} S(\mathbf{r}, \Omega)$$

the source function from atom Ω is obtained which is the measure of an atom's contribution to the ED outside its basin. Making use of the virial expression

Table 1. Classification of atomic interactions on the basis of local topological and energetic properties at the bond critical point

	Shared shell	Intermediate	Closed shell
ρ_{BCP}	Large	Medium	Small
$ \lambda_{1,2} $	$> \lambda_3$		$\ll \lambda_3$
$\nabla^2\rho_{\text{BCP}}$	$\ll 0$	> 0	> 0
H_{BCP}	< 0	< 0	> 0
$H_{\text{BCP}}/\rho_{\text{BCP}}$	$\ll 0$	< 0	> 0
$ V_{\text{BCP}} /G_{\text{BCP}}$	> 2	$1 <, > 2$	< 1

(1), one can give the local source in terms of local kinetic (LG) and potential (LV) energy source contributions [39]:

$$(6) \quad \text{LG}(\mathbf{r}, \mathbf{r}') = \frac{2G(\mathbf{r})}{|\mathbf{r} - \mathbf{r}'|}, \quad \text{LV}(\mathbf{r}, \mathbf{r}') = \frac{V(\mathbf{r})}{|\mathbf{r} - \mathbf{r}'|}$$

Regions where $\nabla^2\rho(\mathbf{r}) > 0$ and $\nabla^2\rho(\mathbf{r}) < 0$ (the potential/kinetic energy dominates) behave, respectively, as source and sink for $\rho(\mathbf{r})$.

2.2 The Topology of Hydrogen Bonds

Because the AIM theory has a firm physical basis, it was quickly adopted in theoretical studies, and almost immediately adapted by experimentalists, to analyze chemical bonding including secondary interactions. The opening of the “topological era” of HB investigations is marked by the appearance of a paper by Koch and Popelier [40], who, based on earlier explorative topological studies, established AIM-based empirical criteria for identifying a D–H···A interaction as a HB formation. These conditions, including four local and four integrated topological properties, are as follows:

- a. The existence of a BCP between, and the associated BP linking, the H- and the A-atoms. The BCP is located closer to the H-nucleus but not necessarily on the BP and the IS, spanned by the trajectories terminating there, is nearly planar.
- b. The ED at the BCP is about an order of magnitude smaller than that in covalent bonds.
- c. The Laplacian exhibits a small positive value indicative for closed-shell interactions. Both ρ_{BCP} and $\nabla^2\rho_{\text{BCP}}$ directly correlate with the interaction energy.
- d. The mutual penetration of H- and A-atoms ($\Delta r(\text{H})$ and $\Delta r(\text{A})$) is measured as the difference between the bonded (r_b) and non-bonded (r_o) atomic radii. The former quantity is defined as the distance of the nucleus to the BCP, while the latter is the distance from the nucleus to an ED contour of 0.001 au ($0.0067 \text{ e}\text{\AA}^{-3}$) of the isolated molecule. This definition allows for the separation of the total penetration ($\Delta r(\text{H}, \text{A}) = \Delta r(\text{H}) + \Delta r(\text{A}) = r_b(\text{H}) - r_o(\text{H}) + r_b(\text{A}) - r_o(\text{A})$) into atomic contributions. A positive value for $\Delta r(\text{H}, \text{A})$ is claimed to be a necessary and sufficient condition for the existence of a HB interaction. Therefore, the $R_o(\text{H} \cdots \text{A})$ separation for which both $\Delta r(\text{H})$ and $\Delta r(\text{A})$ are zero is to be taken as an upper distance limit, where ρ_{BCP} reaches its minimum of 0.002 au ($0.013 \text{ e}\text{\AA}^{-3}$)—an important value to keep in mind for appreciating the following discussion on uncertainties of experimental BCP estimates.
- e–g. The loss of topological charge ($\Delta q(\text{H})$), the decrease of volume ($\Delta v(\text{H})$) and dipolar polarization ($\Delta\mu(\text{H})$) of the H-atom in the complex relative to that in the isolated donor molecule.
- h. The energetic destabilization of the H-atom in the HB measured as the energy deficiency due to complex formation ($\Delta E(\text{H})$).

The above observations are based on calculations on dimers interacting through weak C–H···O contacts. The validation of these criteria for other types of HBs, and for interactions realized in solid-state, has been the subject of a number of subsequent studies [41, 42]. While a detailed review of this material is beyond the scope of this paper, some major points must be addressed, since the quantum chemical description of H-bonded dimers plays an important role in modeling pairwise interactions in solids.

The topological changes accompanying dimer formations of (H₂O)₂, (HF)₂, and (CH₃OH···H₂O) systems were explored by Gálvez et al. [42] at the B3LYP/6-311⁺⁺G(*d*, *p*) level of theory for fully optimized structures but fixed H···A distances. At the equilibrium separations, marked by the minima of the interaction energy curves (represented by Morse type functions for all three dimers), the total ρ_{BCP} values differ only by 0.004 (0.006) eÅ⁻³ for H···F (H···O) from that obtained as the sum of the isolated monomer densities at the BCPs. Though BCPs were found even at $R(\text{H}\cdots\text{A}) = 4.2 \text{ \AA}$, the penetration condition set the limit of HB at $R_{\text{max}}(\text{H}\cdots\text{O}) = 3.1 \text{ \AA}$ and $R_{\text{max}}(\text{H}\cdots\text{F}) = 2.9 \text{ \AA}$ where the interaction energy is purely electrostatic. An important result is that the polarization of the D–H covalent bonds upon dimer formations occurs due to dipolar polarizations of the H-atoms and A-atoms rather than due to charge transfers between the D-sites and H-sites. The energetic destabilization of the H-atoms is balanced, on average, by the stabilization of the donor and acceptor atoms.

Espinosa et al. [34] performed a topological and related energetic analysis on H···F interactions stabilizing simple molecular dimers. The 79 pairs of molecules, neutral, positively and negatively charged complexes, with a wide range of intermolecular separations ($0.8 < R(\text{H}\cdots\text{F}) < 4.2 \text{ \AA}$), provided a sample for exploring the interpretive power of BCP properties in monitoring the strength of pairwise interactions in question. Based on the correlation between $|V_{\text{BCP}}|/G_{\text{BCP}}$ (both derived from the wave function) and $R(\text{H}\cdots\text{F})$, the authors were able to identify a transit region ($1 < |V_{\text{BCP}}|/G_{\text{BCP}} < 2$) between pure shared ($|V_{\text{BCP}}|/G_{\text{BCP}} > 2$) and pure closed-shell ($|V_{\text{BCP}}|/G_{\text{BCP}} < 1$) interactions. This intermediate regime, corresponding to the formation of the bonding molecular orbital, has an upper bound defined by the $H_{\text{BCP}} = 0$ condition (where the closed-shell region starts) and a lower limit defined by the $\nabla^2\rho_{\text{BCP}} = 0$ condition (where the shared-shell region ends). The bond-degree index ($H_{\text{BCP}}/\rho_{\text{BCP}}$), the total energy per electron, was found to be a monotonic function of $R(\text{H}\cdots\text{F})$, changing its sign from negative to positive on passing from shared-shell through transit to the closed-shell regions.

3 ELEMENTS OF EXPERIMENTAL CHARGE DENSITY DETERMINATION

The simplest theory of diffraction [11, 16] relates the intensity distribution of the X-ray wave scattered on a perfect crystal to the distribution of the electrons in the unit cell of volume v_c :

$$(7) \quad I(\mathbf{H}) \propto F(\mathbf{H})^2$$

where F , the complex structure factor amplitude, is the Fourier transform of the ED averaged over vibrational states ($\hat{\rho}$)

$$(8) \quad F(\mathbf{H}) = \int_{V_c} \hat{\rho}(\mathbf{r}) e^{i2\pi\mathbf{H}\mathbf{r}} d\mathbf{r}$$

and \mathbf{H} is the scattering vector, with integral reciprocal-axis components (Miller indices h , k , and l), satisfying the Laue conditions ($\mathbf{H}\mathbf{a}^* = h$, $\mathbf{H}\mathbf{b}^* = k$, and $\mathbf{H}\mathbf{c}^* = l$). This formalism approximates the thermal average of the diffraction intensity with the intensity associated with the average density (Bragg scattering) [43, 44].

Owing to experimental limitations (crystal quality, errors, finite resolution, and the lack of phase information), the direct mapping of the density via Fourier summation

$$(9) \quad \hat{\rho}(\mathbf{r}) = \sum_{\mathbf{H}} F(\mathbf{H}) e^{-i2\pi\mathbf{H}\mathbf{r}}$$

has only a limited information content. The interpretation of F data thus necessarily involves modeling of the density (parameterization) and least-squares (LS) adjusting of the model parameters to the observations. To account for vibrational smearing, the crystalline density has to be partitioned into ‘‘atomic’’ densities (ρ_A), each of which unambiguously assigned to a nucleus at \mathbf{Q}_A :

$$(10) \quad \rho(\mathbf{r}) = \sum_A \rho_A(\mathbf{r} - \mathbf{Q}_A)$$

The harmonic-convolution approximation, according to which the density units rigidly follow the motion of the center to which they are attached, ensures a closed analytic form for the structure factor:

$$(11) \quad F(\mathbf{H}) = \sum_A f_A(\mathbf{H}) t_A(\mathbf{H}) e^{i2\pi\mathbf{H}\mathbf{R}_A}$$

where f_A is the complex atomic scattering factor, \mathbf{R}_A is the equilibrium nuclear position vector and t_A is the temperature factor

$$(12) \quad t_A(\mathbf{H}) = e^{-2\pi^2\mathbf{H}'\mathbf{U}_A\mathbf{H}}$$

which is the Fourier transform of the Gaussian probability density function describing harmonic nuclear displacements ($\mathbf{u}_A = \mathbf{Q}_A - \mathbf{R}_A$):

$$(13) \quad P(\mathbf{u}_A) = (2\pi)^{-3/2} |\mathbf{U}_A|^{-1/2} e^{-(1/2)\mathbf{u}_A' \mathbf{U}_A^{-1} \mathbf{u}_A}$$

The components of the mean-square displacement amplitude matrix (MSDA)

$$(14) \quad \mathbf{U}_A = \langle \mathbf{u}_A \mathbf{u}_A' \rangle$$

are referred to as the atomic displacement parameters (ADP).

The conventional structure factor formalism utilized in standard structure determinations invokes the concept of the promolecule; the superposition of isolated (spherical) atomic densities derived, for example, via the Hartree–Fock procedure [45]. While this model mimics the dominant topological features of the ED (local maxima at the nuclear positions) reasonably well, it completely neglects density deformations due to bonding. Unfortunately, this omission leads to biases in estimates of the structural [46, 47] and thermal parameters [48].

In the course of X-ray ED determination, experimental structure factor amplitudes are LS projected onto the superposition of density units. These units can be products of usual orbital basis functions [49, 50] (density-matrix fitting), or nucleus-centered density functions (pseudoatoms) [51].

3.1 The Pseudoatom Model

In the most widely applied model [52], the atomic decomposition of the ED is retained, but each nucleus-centered spherical density is supplemented by non-spherical functions. The pseudoatom formalism is a finite nucleus-centered multipole expansion of the molecular (crystalline) ED about each nucleus. A pseudoatom is defined as

$$(15) \quad \rho(\mathbf{r}) = \rho_c(r) + P_v \rho_v(\kappa r) + \sum_{l=0}^{l_{\max}} R_l(\kappa' r) \sum_{m=0}^l P_{lm\pm} y_{lm\pm}(\vartheta, \varphi)$$

where R_l and $y_{lm\pm}$ are, respectively, radial density functions (RDF) and density-normalized real spherical harmonics expressed in local spherical polar coordinates (r_A , ϑ_A , φ_A) associated with center (A). The zero-order RDF is taken as a sum of the spherical Hartree–Fock frozen core (ρ_c) and valence densities [45] (ρ_v), while those in the deformation term, are density normalized Slater functions with parameters (n_l and η_l) deduced from single-zeta atomic wave functions [45]

$$(16) \quad R_l = \frac{\eta_l^{n_l+3}}{(n_l + 2)!} \exp(-\eta_l r)$$

The radial deformation of the valence density is accounted for by the expansion–contraction variables (κ and κ'). The ED parameters P_v , $P_{lm\pm}$, κ , and κ' are optimized, along with conventional crystallographic variables (\mathbf{R}_A and \mathbf{U}_A for each atom), in an LS refinement against a set of measured structure factor amplitudes. The use of individual atomic coordinate systems provides a convenient way to constrain multipole populations according to chemical and local symmetries. Superposition of pseudoatoms (15) yields an efficient and relatively simple analytic representation of the molecular and crystalline ED. Density-related properties, such as electric moments electrostatic potential and energy, can readily be obtained from the pseudoatomic properties [53].

3.2 Uncertainties in X-Ray Charge Densities

In spite of its advantageous features and remarkable success, the pseudoatom method has severe limitations; these are partly due to approximations and inadequacies in the model, and partly due to ambiguities associated with the fitting procedure. Since neither the N- nor the V-representability [54] requirement is imposed during the fit, the multipolar density extracted from XRD data is not a “physical” density. It does not necessarily satisfy the positivity requirement and the nuclear cusp condition [55]. Reciprocal-space fitting of a finite number of structure factors in terms of a finite number of multipoles does not necessarily lead to the same density as the direct-space fitting of the same model to a finite number of density points. The pseudoatom electric moments obtained via LS projection do not necessarily add up to the corresponding molecular moments, even if the ED (or F data) is perfectly fitted. Neglecting core polarizations can bias the valence density parameters, especially for atoms beyond the second period. The assumption that the valence density is uniformly deformed upon bond formation, as imposed via the κ -formalism, is in contrast to simple chemical arguments. The restricted flexibility of the single-zeta RDFs of the deformation term in (15) are well-known sources of uncertainties in experimental bond topology [56, 57].

Model inadequacies, in general, and those associated with treating the H-atoms, in particular, can have pronounced effects on experimental densities and related electronic properties. Due to their low scattering power (lack of core electrons) and intense thermal motion (with a considerable anharmonic component), the contribution of H-atoms to XRD intensities is marginal, being in the range of that typical for bonding effects. H-atoms undergo essential density rearrangements upon bond formation and, especially in organic molecules, a considerable amount of charge transfer occurs at the expense of charge on these sites. An inadequate static density model leads to unreliable dynamic parameters and vice versa [48]. Since these uncertainties are “redistributed”, by the electro-neutrality constraint over all valence monopole populations refined, they can significantly bias estimates of properties dominated by atomic net charges (dipole moment, electrostatic potential, field, field gradient, and energy).

The usual practice in modeling the valence deformation of H-atoms is to terminate the expansion at the dipolar level ($l_{\max} = 1$, with a bond directed dipole) and to fix the radial exponents. In addition, H-atoms bonding to the same type of atoms are often constrained to be identical, regardless of their involvement in non-bonded interactions. Model studies on radial functions, obtained by projection of theoretical densities onto nucleus-centered spherical harmonics, show that (a) second neighbors have significant effects on H-atoms, (b) the description of these functions in terms of a single-Slater function (Eq. 16) is inadequate, and (c) an expansion up to the hexadecapolar level is necessary to reach a desired precision of less than $0.05 \text{ e}\text{\AA}^{-3}$ with the pseudoatom model [58].

Uncertainties of the conventional parameters of H-atoms have been addressed since the early applications of X-ray charge density method. Support from ND measurements appears to be essential, because the neutron scattering power is a nuclear property (it is independent of the electronic structure and the scattering angle). The accuracy of nuclear parameters obtained from ND data thus depends mainly on the extent to which dynamic effects (most markedly thermal diffuse scattering) and extinction are correctable. Problems associated with different experimental conditions and different systematic errors affecting the ND and XRD measurements have to be addressed whenever a joint interpretation of these data is attempted. This has become apparent in studies which aimed either to refine XRD and ND data simultaneously [59] (commonly referred to as the X+N method), or to impose ND-derived parameters directly into the fit of XRD data (X–N method) [16]. In order to avoid these problems, usually only the ND parameters of the H-atoms are used and fixed in the XRD refinement (X–(X+N) method).

Results of conventional XRD analyses (independent atom model and isotropic thermal parameters for H-atoms) suffer from well-known biases in parameter estimates. Covalent bonds, in particular those involving H-atoms, are found to be significantly shorter than those derived from ND experiments [46]. Since the D–H distances obtained in such studies are underestimated (often by 0.1–0.2 Å), the corresponding D–H···A geometry is poorly resolved. The usual practice for X-ray charge density studies lacking ND support is to elongate the bonds to H-atoms to match ND mean distances. Additionally, it is necessary to fix the corresponding positions of the idealized H-atoms during the refinement of their isotropic displacement amplitudes using a static scattering model that includes only a monopole and a bond directed dipole (X–X method).

Procedures applicable to correct for the systematic differences between XRD and ND derived ADPs are described in detail by Blessing [60]. One of the most appealing methods makes use of the linear correlation often found between the principal components of the MSDA tensors derived from the two types of experiments. The relationship obtained for the non-hydrogen atoms can be used to modify the ADPs of H-atoms from the ND experiment, thus allowing them for fixing in the refinement of the X-ray charge density.

There are several feasible approaches to estimate the ADPs of H-atoms in the absence of ND parameters. All these methods invoke the assumption that external and internal vibrational modes are uncorrelated, that is, the corresponding MSDA tensors are additive: $U = U_{\text{ext}} + U_{\text{int}}$. The former quantities can be obtained by fitting overall MSDA tensors corresponding to the translation (T), libration (L), and screw-rotation (S) of the molecule as a rigid body [61], to the ADPs of non-hydrogen atoms available at an advanced stage of the X-ray structure factor refinement. Having estimated the T , L , and S tensors in such a way, one can calculate U_{ext} for H-atoms. Unfortunately, this straightforward method has its own drawback; LS-estimated rigid-body tensors are

contaminated by contributions from internal modes, especially for flexible molecules. Numerous models of different levels of sophistication have been proposed for the estimation of U_{int} . These include the use of average values for the bond-parallel and perpendicular MSDAs of H-atoms derived either from ND [62] or infrared spectroscopy [63, 64], the analysis of multi-temperature X-ray data [65, 66], and normal coordinate analysis of the isolated molecule based on ab initio force fields [67].

For a throughout analysis of the performance of different approaches, we refer to a recent study by Madsen et al. [62]. The authors show that the use of idealized D–H distances, in conjunction with a proper model for ADPs of hydrogen sites, is a “must” in the course of the pseudoatom refinement, to extract physically meaningful experimental BCP indices from XRD data. The analysis of X-ray charge density of xylitol, using ND-derived isotropic thermal parameters for H-atoms, results in considerable systematic errors in ρ_{BCP} and $\nabla^2\rho_{\text{BCP}}$ values (even for bonds lacking of H-atoms) as compared to those obtained with the X–N method. The discrepancies can be as large as 20% and 50% for C–H bonds. However, the average error in the position of H-atoms obtained with the idealized D–H distance-constraints is reported to be as small as 0.041(19) Å, with a corresponding mean bond-length deviation of 0.012(8) Å. This finding is consistent with the estimated variation (0.02 Å) reported for O–H distances based on variable-temperature (20–293 K) ND measurements on 2,3,5,6-pyrazinetetracarboxylic acid dihydrate [68]. In the latter work, the $R(\text{H}\cdots\text{O})$ and $R(\text{H}\cdots\text{N})$ distances increased up to 0.03 and 0.06 Å, respectively, with increasing temperature. Nevertheless, the conclusion reached by Madsen et al. [62] that “an improved description of the models for H-atom displacements is necessary for the study of properties intrinsic to the H-atoms, as well as other molecular properties,” should not be neglected when evaluating XRD topological results of HB systems. This conclusion is in contrast to that drawn by Espinosa et al. [69] in a comparative analysis of O–H \cdots A HBs. These authors found that the BCP indices derived from X–X method are in close agreement with those obtained via the X–N or X–(X+N) model.

A temperature dependent X–X+N study (100, 135, 170, and 205 K) on naphthalene [66] addresses the problem of thermal de-convolution, that is, the efficiency of the pseudoatom model to decouple density deformations due to chemical bonding from those due to nuclear motion. The authors analyze the self-consistency of multipole populations, extracted from different temperature XRD data, in terms of statistical distances (d_n) in the parameter space of the same refinement model:

$$(17) \quad d_n(T_1, T_2) = \left(\frac{1}{n} (\mathbf{p}_{T_1} - \mathbf{p}_{T_2})' V^{-1} (\mathbf{p}_{T_1} - \mathbf{p}_{T_2}) \right)^{1/2}$$

where V is the variance–covariance matrix associated with the multipole variables arranged in the n -vector \mathbf{p} . A distance close to unity corresponds to

random errors in the parameter estimates extracted from two different temperature (T_1 and T_2) data sets. Values obtained by using the static density parameters in Eq. 17 at $T_1 = 100$ K are 2.9, 4.7, and 9.5 for $T_2 = 135$, 170 and 205 K, respectively. The analysis reveals “that though the multipole populations exhibit some variation with temperature only the 205 K parameters are significantly different from the rest”, and thus a satisfactory thermal deconvolution could be achieved. The intramolecular bond topology that comes out to be statistically equal in the 100–170 K temperature range is only slightly different from that obtained from periodic crystal and/or isolated-molecule calculations at the B3LYP/6-31G* level (although the discrepancies exceed the experimental standard uncertainties (3σ) even for the C–C bonds and especially for the $\nabla^2\rho_{\text{BCP}}$ values). For the C–H bonds, on the other hand, the experiment (135 K) versus theory comparison reveals differences amounting to 20% and 60% in ρ_{BCP} and $\nabla^2\rho_{\text{BCP}}$, respectively, in spite of relatively small discrepancies in the BCP locations (0.05 Å). This inconsistency is somewhat reversed for the weak C··H and H··X intermolecular interactions. Here the ρ_{BCP} and $\nabla^2\rho_{\text{BCP}}$ differences remain in the 20% range, despite considerable discrepancies in the BCP locations (up to 0.26 Å).

There are additional technical difficulties that prohibit us from making clear-cut statements concerning the experimental uncertainties of topological properties. LS error estimates for BCP properties often suffer from neglecting some of the most important correlations. Standard uncertainties calculated in such a way are considerably underestimated, sometimes by a factor of 5 for ρ_{BCP} and by an order of magnitude for $\nabla^2\rho_{\text{BCP}}$. Studies that report $\rho_{\text{BCP}}(\nabla^2\rho_{\text{BCP}})$ values up to 4 (3) significant figures certainly exaggerate the accuracy achievable by the method. Moreover, procedures to estimate errors in local topological indices (especially those of geometric nature, such as the BCP location, BPL, etc.) and integrated AIM properties are far from trivial.

3.3 Reliability of Experimental Bond-Topological Properties

In view of the above comments, error estimates are usually made on the basis of overall reproducibility of, and matching between independent experimental or theoretical results, rather than on the basis of the precision reachable with a particular measurement and refinement model. There are several approaches that allow us to gain quantitative information on experimental reproducibility and uncertainties. These include the pseudoatom interpretation of error free, theoretical data [56, 57, 70–72], comparative analysis of experimental data sets in terms of different constrained models [73], theory versus experimental comparison of results obtained for the same system [74–76], systematic studies on a series of related compounds [77], and the simultaneous analysis of data collected at different temperatures [66].

The results of such studies appear to be more conclusive for covalent than for hydrogen bonds. The topology of non-polar shared interactions is found to be

more reliably accessible by both theoretical and X-ray methods than that of polar bonds. For example, the statistical spread of experimental ρ_{BCP} ($\nabla^2\rho_{\text{BCP}}$) in bonds common to amino acids is found to be 0.06–0.08 eÅ⁻³ (2.1–2.2eÅ⁻⁵) for C–C and 0.05–0.11 eÅ⁻³ (2.1–4.5 eÅ⁻⁵) for the polar C=O and C–N bonds [77]. These estimates are based on a sample of topological data obtained for 13 amino acids under similar measurement and refinement conditions. The reported values exceed the corresponding variances due to different levels of theory and/or basis sets utilized in the calculations on isolated molecules.

The general agreement between experimental values obtained for ρ at the BCP of covalent bonds and those derived theoretically for the corresponding isolated molecules supports the widely cited error estimate of 0.05 eÅ⁻³. The fact that $\nabla^2\rho_{\text{BCP}}$ is a far less robust index than ρ_{BCP} , as revealed by discrepancies between theory and experiment, has been attributed mainly to the different BCP locations and bond-parallel curvatures obtained by the two methods. Basis set, correlation, and bulk effects are commonly invoked as sources of the discrepancies [74, 78].

A vast amount of quantitative information on crystal field effects has been provided by increasingly affordable periodic quantum chemical methods [79]. Variations in intramolecular BCP properties upon phase transition can be especially pronounced if HB interactions play a dominant role in crystal formation. Theoretical calculations on urea [78], for example, reveal a considerable change in the strength of the bonds to both the H-donor and acceptor atoms in the crystal; the increase in the polarity of the C=O bond ($D[-\nabla^2\rho_{\text{BCP}}] = -67\%$) is accompanied by an increase in the covalent character of the C–N bond ($\Delta[-\nabla^2\rho_{\text{BCP}}] = 18\%$). For the N–H bonds, however, only the bond-parallel curvature is affected markedly ($\Delta\lambda_3 = 11, 18\%$) by the formation of the N–H···O hydrogen bonds.

Such observations immediately raise the question: how reliable are projections of crystal-field effects onto multipoles? The analyses of wavefunction-simulated X-ray data of small model compounds have revealed that the interaction density ($\delta\rho = \rho(\text{crystal}) - \rho(\text{isolated molecule})$) manifests itself in low-order structure factors, and only to an extent that is comparable with the experimental noise [80]. Nevertheless, the multipole refinement was shown to retrieve this low signal (about 1% in F) successfully. A related study on urea, however, demonstrated that this is not the case if random errors of magnitude comparable with the effect of interaction density are added to the theoretical data [81]. The result also implies that indeterminacies associated with the interpretation of non-centrosymmetric structures can severely limit the pseudoatom model in distinguishing between noise and physical effects [82, 83].

A thorough investigation of simulated structure factor data of ammonia provides us with quantitative figures for the accuracy of BCP properties achievable with the pseudoatom projection [72]. The ρ_{BCP} , $\nabla^2\rho_{\text{BCP}}$, and $r_{\text{BCP}}(\text{H})$ indices of the static model density obtained by the multipole refinement of HF/6-311G** static structure factors deviate from the correct values (derived

directly from the target HF density) by 7%, 58%, and 10%, respectively, for the N–H bond and by 75%, 32%, and 16% for the H···N hydrogen bond. It is also important to mention that the fit of a rather limited experimental data appears to be much better than the fit of the same number of theoretical data, irrespective of the level of theory or basis functions used in the calculations. This suggests that the thermally smeared ED lacking sharp density features can be better represented by the limited pseudoatom model than the static ED, and/or the ADPs “are good at” in picking up static deformations.

Of particular relevance to the measurability of crystal-field effects is a recent study that analyzed the experimental BCP properties of 9-ethynyl-9-fluoreno (crystallizes in the centrosymmetric space group $C2/c$ with two molecules in the asymmetric unit) in relation to the extent to which constraints (local pseudo-symmetry and chemical similarity) were imposed on the pseudoatom model [73]. The unconstrained refinement, treating the EDs of the two symmetry-independent molecules independently, and the fully constrained refinement (identical ED for the two molecules with a pseudo-mirror symmetry enforced), lead to the same fit but significantly different estimates for the BCP indices. Differences obtained for the two molecules with the restricted model and thus derived solely from the unconstrained refinement of the conventional variables, amount to $0.02 \text{ e}\text{\AA}^{-3}$, $0.6 \text{ e}\text{\AA}^{-5}$, and 0.003 \AA in ρ_{BCP} , $\nabla^2\rho_{\text{BCP}}$, and r_{BCP} , respectively. The unrestricted refinement, on the other hand, results in significantly larger discrepancies ($0.07 \text{ e}\text{\AA}^{-3}$, $3.0 \text{ e}\text{\AA}^{-5}$), especially for r_{BCP} that increases up to 0.1 \AA . More importantly, the shifts in the BCP locations (of C–C bonds) do not correlate with the differences in any other BCP properties. A related X–X analysis, investigating two crystal forms of two famotidine polymorphs, finds good overall agreement in the BCP indices of chemically equivalent intramolecular bonds for the two molecules [84]. This is also true for the topological charges, including those of the H-atoms. The conformation, dipole moment, electrostatic potential of the two polymorphs, and the electrostatic interaction energy in the two crystals are however fundamentally different. Based on these observations one should conclude that the intramolecular BCP properties are rather insensitive to crystal-field effects.

Another work along this line is concerned about the transferability of topological properties between tetrafluorophthalonitrile and its isomer (tetrafluoroisophthalonitrile), both of which crystallize in orthorhombic space groups ($Pbca$ and $P2_12_12_1$) with, respectively, two and one molecules in the asymmetric unit [85]. Since the molecules lack H-atoms, the driving cohesion forces are expected to be weak secondary interactions. The $mm2$ symmetry possessed by the isolated molecules was imposed in the pseudoatom refinement against 100 K X-ray data. The theoretical and experimental BCP indices are in good agreement for the C–C bonds but no trend appears to exist in the $\nabla^2\rho_{\text{BCP}}$ quantities for the polar bonds. The B3LYP calculations lead to small negative (positive) values for the C–N and (C–F) bonds and predict the equivalent bonds in the three molecules to be identical. The experimental Laplacian values are,

however, all negative and significantly different for the two isomers, as well as for the two molecules in the asymmetric unit. What is suspicious about these results is not so much the discrepancy obtained by the two methods (theory and experiment) but rather the physical significance of the observed spread in the experimental curvatures along the C–F bonds. The variety of the F···F, F··· π , and N··· π type contacts, identified by the topological analysis in the intermolecular regions, seems to suggest a strong and distinct effect of the crystal field on the intramolecular structures. The authors conclude that “the observed differences originate in slightly deviating radial distributions that has a pronounced effect on the topological result—a clear indication of the inadequacy of the BCP as the sole point of interest for bond nature determination.” [85]

The comparison of experimental and theoretical integrated AIM properties can also lead to rather controversy conclusions. The results for naphthalene [66] obtained by the X–N analysis of 100 K data, for example, are consistent with those derived from periodic HF calculations; the mean deviations for the net charges and volumes are about 0.03 e and 0.4 Å [3], respectively. For the crystalline L-tryptophan [86], however, the experimental (100 K synchrotron data) AIM charges and dipole moments are practically identical to those derived from the wavefunction-based density of the isolated molecule at the B3LYP/6-311++G(3d, 3p) level, even for the H-atom involved in a relatively strong ionic O–H···O[(-)] HB ($\rho_{\text{BCP}} = 0.69(1) \text{ e}\text{\AA}^{-3}$ and $\nabla^2\rho_{\text{BCP}} = 4.8(3)\text{e}\text{\AA}^{-5}$) with a formic acid solute present in the unit cell. This lack of HB signal is rather surprising, especially in view of the pronounced charge loss (0.1–0.3 e) found for the H-atoms participating in weak C–H···O interactions in the crystalline coumarin and its derivatives [87].

4 CHARACTERISTICS OF HYDROGEN BONDING FROM TOPOLOGICAL ANALYSES OF X-RAY CHARGE DENSITIES

The main goal of early applications of the AIM theory to experimental densities of HB systems was to explore the interpretive power of the BCP indices in distinguishing between strong (shared-shell) and weak (closed-shell) interactions. Very strong O···H···O type bonds can be found in the crystal structures of dicarboxylic acid salts, with either a symmetric (single-well potential) or quasi-symmetric (double-well potential) arrangements, and of β -diketone enols with a proton being located midway between the keto- and enol-oxygen atoms in a low-barrier potential (resonance-assisted HB) [23].

In the ionic complex of 1,8-bis(dimethylamino)naphthalene with 1,2-dichloromaleic acid, one proton is captured in a N–H···N (cation) and one in a O···H···O (anion) intramolecular HB [88]. The (X+N) study reveals an asymmetric arrangement in the former case; the H-atom is covalently bonded only to one of the N-atoms, strongly polarizes the VSCC of the other, but the N···H BCP is located in a region of positive Laplacian. Although $\nabla^2\rho_{\text{BCP}} < 0$ for both

O···H bonds in the anion, the negative region of the Laplacian is not shared by the VSCCs of either of the O-atoms. Similar situations are found for symmetric intermolecular O···H···O HBs realized in the crystal structures of methylammonium hydrogen succinate monohydrate [89] and methylammonium hydrogen maleate [90]; considerable covalent signal ($\nabla^2 \rho_{\text{BCP}} < 0$) for the O···H interactions, without shared VSCCs with the O-atoms.

The combined ND (20 K) and XRD (8.4 K) study on benzoylacetone [91] provides an experimental verification of the resonance-assisted HB model, according to which the structure is stabilized via π -delocalization [92] of the O=C–C=C–O–H keto–enol group. This is an especially challenging problem, because the diffraction image of a statistically disordered keto–enol system is practically indistinguishable from that of an ordered but delocalized system. The analysis of the ND data excludes the disorder and the experimental BCP indices show fine details of the bonding situation supporting the resonance model; there are clear indications for π -delocalization over the O=C–C=C–O–skeleton but the Laplacian distribution of the O-atoms sharing the proton is well separated.

The fact that the X-ray charge density community has a renewed interest in HB systems is certainly due to a series of papers by Espinosa et al. [93]. Using previously reported experimental BCP properties of 83 D–H···O bonds (with $R(\text{O} \cdots \text{H})$ in the range of 1.56–1.97, 1.65–2.63, and 2.28–2.59 Å, for D = O, N, and C, respectively), the authors examined the energy versus distance correlations. The combination of the local virial equation (1) with Abramov's empirical formula (2) for $G(\mathbf{r})$ resulted in an exponential behavior for both energy densities as the function of the O···H separation (Fig. 3).

Based on the limiting condition for shared-shell interactions ($\nabla^2 \rho_{\text{BCP}} = 0$, $2G_{\text{BCP}} = V_{\text{BCP}}$), a boundary between strong and weak HBs could be drawn, which corresponds to $R_o(\text{O} \cdots \text{H}) = 1.33$ Å and $G_o = 320$ kJ/mol/au. The crucial result however is the simple correlation found between the potential energy density and the dissociation energies (D_e). A sample of D_e data obtained by ab initio calculations on isolated dimers showed also an exponential behavior as the function of $R(\text{O} \cdots \text{H})$. Furthermore, the exponential factor fitted to the theoretical D_e data (3.54(10)) was found to be statistically equal to that fitted to the experimental V_{BCP} values (3.65(18)). Reinterpretation of both data with the same model function sharing the same exponent of 3.6 and adjusting only the linear coefficient led to the following empirical formulas:

$$(18) \quad V_{\text{BCP}} = -50(1.1) \cdot 10^3 e^{-3.6 R(\text{O} \cdots \text{H})}$$

$$(19) \quad D_e = 25.3(6) \cdot 10^3 e^{-3.6 R(\text{O} \cdots \text{H})}$$

which imply the surprisingly simple $E = -D_e = 1/2 V_{\text{BCP}}$ relationship.

In an extended analysis of the same data, Espinosa et al. [94] found similar exponential behaviors for the curvatures of the density at the BCP, based on which, it was possible to establish a linear relationship between G_{BCP} and the

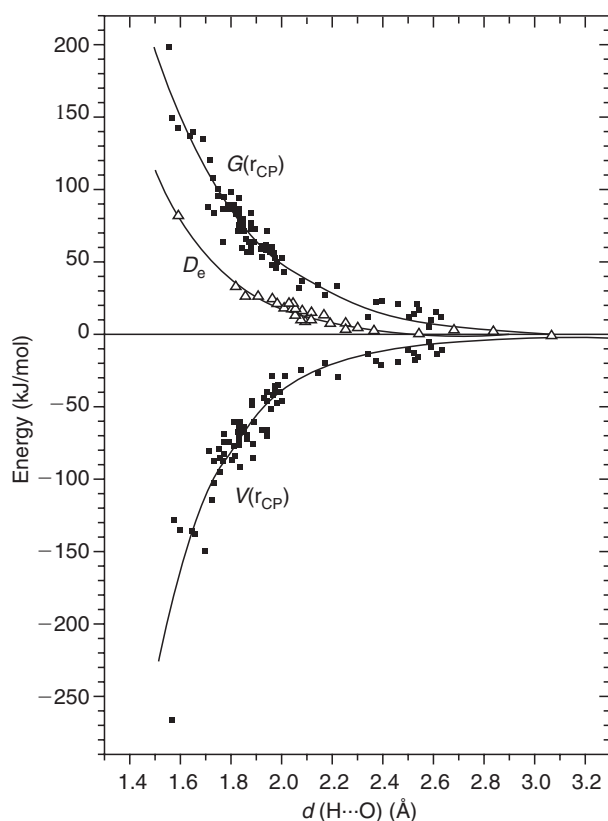


Figure 3. Dependence of the kinetic ($G(r)$) and potential energy density ($V(r)$) at the bond critical point, and the dissociation energy D_e , on the O \cdots H distance. Units are kJ/mol/au [3], kJ/mol, and \AA, respectively. Solid lines correspond to the exponential fitting (18 and 19). Data are from X-ray analyses of 83 (D–H \cdots O, D=C, N, and O) HBs. Reprinted with permission from Ref. [93].

positive, and V_{BCP} and the negative curvatures. This provides a plausible energy-partitioning scheme related to the dilution and concentration of the electrons at the BCP. In a follow-up paper [69], the reliability of the experimental bond-parallel curvatures of HBs was stressed (Fig. 4).

It was also shown that H_{BCP} expressed as a double exponential is proportional to the interaction potential ($U(R) = fH_{\text{BCP}}(R)$), where f was estimated to be the force constant of the O \cdots H hydrogen bond in ice VIII from the values of the local energy densities at the equilibrium O \cdots H separation [95].

Spackman [96] demonstrated that the local kinetic energy density at the BCP, as given by Eq. 2, is rather insensitive to local density rearrangements due to HB formation. Reinterpretation of the above HB data reveals that the observed behavior of G_{BCP} can be well reproduced by a two-atom ED model (spherical

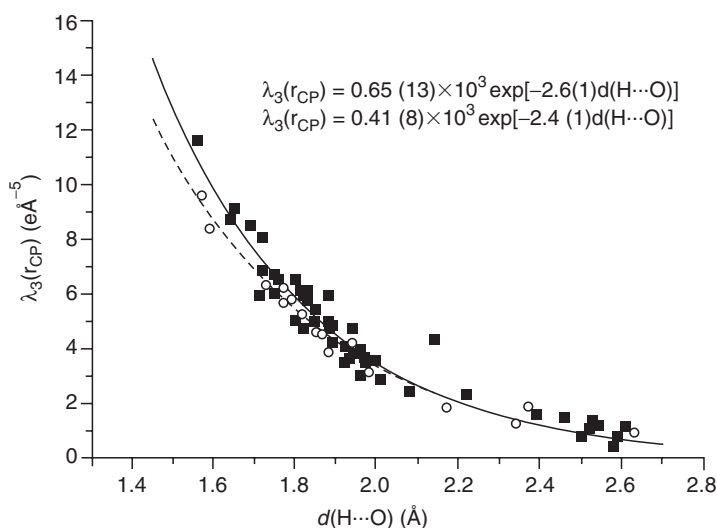


Figure 4. Dependence of bond-parallel curvatures at the bond critical point of D–H···O (D=C, N, and O) HBs on the O···H distance. Data points from X–X and X–(X+N) (or X–N) refinements are represented by filled squares and empty circles, respectively. The corresponding fitted curves are drawn by solid and dashed lines (upper/lower equation). Reprinted with permission from Ref. [69].

H- and O-atoms separated at the experimental distances) without any fitting parameter. The V_{BCP} values are however underestimated in magnitude at short distances because the Laplacian corresponding to the non-interacting density fails to mimic shared-shell charge concentrations.

These observations have inspired a couple of throughout studies on C–H···O contacts to explore the extent of which experimental topological and related energetic figures can distinguish weak HBs from van der Waals contacts [69, 87, 97–99]. It is evident from the entries in Table 2, summarizing the ranges of distances and BCP indices covered in these investigations, that neither ρ_{BCP} nor $\nabla^2\rho_{\text{BCP}}$ carries hardly any information on the strength of the C–H···O HBs. This is especially true for the data in column 1–3 containing values which scatter within the range of experimental uncertainties, and without noticeable correlation with the O···H distance ($\rho_{\text{BCP}}(R_{\text{max}}) = \rho_{\text{BCP}}(R_{\text{min}})$).

The 90 K X–X study on coumarin and its derivatives [87] (column 1 in Table 3) stretches the limit of what local BCP indices can tell us about these weak interactions. The combined analysis of 36 contacts (15 C–H···O and 21 C–H··· π), all satisfying the Koch-Popelier criteria, reveals a narrow range of H···A distances (2.75–2.85 Å) what is believed to correspond to an overlap between the two types of interactions. This observation is fully supported by periodic B3LYP/6-31G** calculations, since the local indices derived by the two methods are in fair agreement. However, the charge depletion at the

Table 2. Experimental local bond-topological properties of C–H···O hydrogen bonds

	[87]	[97]	[98]	[99]	[69]
N	15	7	12	22	10
R_{\min}	2.310	2.298	2.209	2.211	2.219
R_{\max}	2.834	2.949	2.698	2.969	2.591
$\rho_{\text{BCP}}(R_{\min})$	0.04	0.04	0.06	0.11	0.10
$\rho_{\text{BCP}}(R_{\max})$	0.03	0.03	0.06	0.06	0.03
$\text{Min}\rho_{\text{BCP}}$	0.05	0.06	0.06	0.12	0.10
$\text{Max}\rho_{\text{BCP}}$	0.02	0.01	0.03	0.01	0.02
$\nabla^2\rho_{\text{BCP}}(R_{\min})$	0.75	1.1	1.5	1.50	1.56
$\nabla^2\rho_{\text{BCP}}(R_{\max})$	0.52	0.5	0.5	0.27	0.77
$\text{Min}\nabla^2\rho_{\text{BCP}}$	0.93	1.1	1.5	1.57	2.1
$\text{Max}\nabla^2\rho_{\text{BCP}}$	0.52	0.5	0.5	0.23	0.36

First row: reference numbers. N is the number of HBs included in the sample, R_{\min} and R_{\max} are minimum and maximum O···H separations, $\rho_{\text{BCP}}(R_{\min})/\nabla^2\rho_{\text{BCP}}(R_{\min})$ and $\rho_{\text{BCP}}(R_{\max})/\nabla^2\rho_{\text{BCP}}(R_{\max})$ are the density/Laplacian at the BCP corresponding to R_{\min} and R_{\max} . Minimum/maximum values in the sample: $\text{Min}\rho_{\text{BCP}}/\text{Max}\rho_{\text{BCP}}$ and $\text{Min}\nabla^2\rho_{\text{BCP}}/\text{Max}\nabla^2\rho_{\text{BCP}}$. Units are e and Å

H-atoms, as calculated from the topological charges with reference to those in the isolated molecules, is very different; the experimental values being systematically larger than the theoretical ones.

The most detailed analysis by Gatti et al. [99] is concerned about the bonding situation in the crystal structure of 3,4-*bis*(dimethylamino)-3-cyclobutene-1,2-dione stabilized exclusively by C–H···O HBs ($2.351 < R(\text{O} \cdots \text{H}) < 2.942$ Å). The authors supplement the experimental BCP results (derived from 20 K X-ray data via an advanced modeling of the H-atom sites) with those obtained from HF calculations on the crystal, the isolated monomer and dimers at the experimental geometry. For each of the 21 bonded contacts, identified on the basis of their BP, a high degree of directionality ($\angle(\text{C}–\text{H} \cdots \text{O}) \sim 140^\circ$) is found (regardless of the $R(\text{H} \cdots \text{O})$ distance), while the 6 non-bonded interactions can be characterized as bent arrangements of the three atoms ($\angle(\text{C}–\text{H} \cdots \text{O}) \sim 90^\circ$, $2.2 < R(\text{H} \cdots \text{O}) < 3.0$ Å). All bonded HBs are validated against the Koch–Popelier criteria. Changes in the integrated topological properties of the H-atoms suggest that the intramolecular contacts (present also in the isolated monomers) weaken due to the intermolecular HBs formed in the solid state. The theoretical ρ_{BCP} values of the former HBs are scattered around, while the $\nabla^2\rho_{\text{BCP}}$ indices are systematically higher than those derived from the XRD data. The experimental G_{BCP} and V_{BCP} estimates are found to be 30% and 20% lower in magnitude than the theoretical ones. Consequently, the simple relationship between V_{BCP} and D_e established by Espinosa et al. [93] does not seem to be valid for this specific interaction.

In a state-of-the-art X–X+N study, Mallinson et al. [100] explore a wide range of HB interactions found in the crystal structures of five ionic complexes of 1,8-*bis*(dimethylamino)naphthalene with four different acids. The analysis of

63 HBs, covering interactions from weak covalent to weak ionic and classified into five types ($[\text{O}\cdots\text{H}\cdots\text{O}]^-$, $\text{C}-\text{H}\cdots\text{A}$ ($\text{A}=\text{O}$, N , Cl), and $[\text{N}-\text{H}\cdots\text{N}]^+$), reveals new empirical relationships between topological figures. For ρ_{BCP} , G_{BCP} , and V_{BCP} an exponential, while for $\nabla^2\rho_{\text{BCP}}$, a Morse type dependence on BPL was found, in line with earlier observations exploring correlations of the above indices with $R(\text{H}\cdots\text{A})$. The result obtained for $\nabla^2\rho_{\text{BCP}}$ ($R(\text{H}\cdots\text{A})$) resembles closely that found by Espinosa et al. [93] for the $\text{F}-\text{H}\cdots\text{F}$ systems: shared-shell type interactions $\nabla^2\rho_{\text{BCP}} < 0$ with up to $\text{BPL} < 1.3 \text{ \AA}$, a transit region with $1.3 < \text{BPL} < 2.1 \text{ \AA}$, and closed-shell regime with $\text{BPL} > 2.1 \text{ \AA}$. The parameters of the exponential functions describing the energy densities are however significantly different from those in Eqs. 18 and 19.

Gatti and Bertini [39] performed the source-function analysis on theoretical densities (B3LYP/6-31G**) of small-molecule dimers exhibiting prototype $\text{O}-\text{H}\cdots\text{O}$ contacts, such as the isolated, charge-, resonance-, and polarization-assisted HBs. They calculated the LSF profile along the $\text{O}-\text{H}\cdots\text{O}$ interaction line with reference to the $\text{H}\cdots\text{O}$ BCP ($r = r_{\text{BCP}}$), as well as, the percentage source contributions from the donor (%S(D)), hydrogen (%S(H)), and the acceptor (%S(A)) atoms to the same point. The analysis shows that the LSF is positive (nearly zero) along the IL for strong (medium strength) HBs, while %S(H) increases from large negative, through slightly negative to positive values on passing from isolated, through polarized-assisted to charge-assisted HBs. The %S(D) and %S(A) values increase and decrease, respectively, with decreasing strength (increasing $R(\text{H}\cdots\text{O})$) of the HB. The same analysis, when applied to the interaction density, reveals how local charge polarizations due to HB formation contribute to the ED along the IL or at the BCP. It was found, for example, that regions inside the H-atom domain (close to the nucleus) have significantly larger contributions to $\delta\rho$ at the BCP than regions close to the critical point. Both properties appear to be sensitive figures applicable to monitoring the polar character of the HB. The authors' conclusion is in line with the statement quoted in the foregoing paragraph: "This result raises doubts about the use of the BCP properties only when discussing intermolecular interactions in crystals." [39]

Cole et al. [101] combined low temperature (20 K) ND and XRD data of methylbenzylaminopyridine (MBANP) and methylbenzylaminodinitropyridine (MBADNP) to rationalize the different non-linear optical properties of these materials. The former compound possesses a second harmonic generation output that is almost an order of magnitude higher than that of the latter. The distinct behavior of the two systems is attributed to the different solid-state molecular conformations due to different crystal packing. Based on the ND structures, the twist of the pyridine ring observed for MBADNP precludes the formation of the "herringbone" type packing found for MBANP. The $\text{X}-(\text{X}+\text{N})$ analysis shows that of the four candidates for intramolecular contacts, the strongest $\text{N}-\text{H}\cdots\text{O}$ HB is the one which is solely responsible for this intermolecular rearrangement, that is, no other intramolecular contacts can be identified on the basis of ED topology.

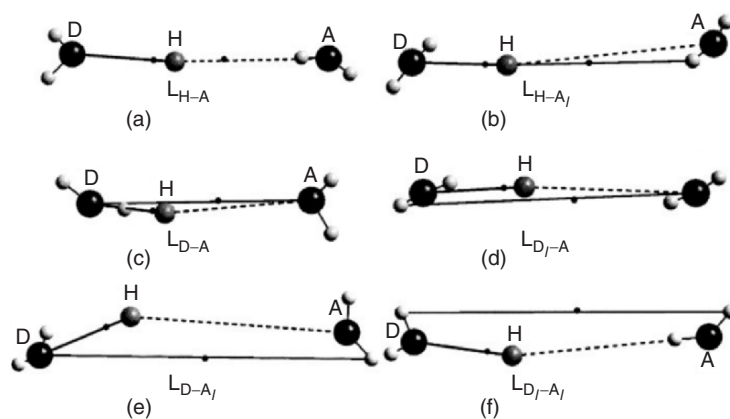


Figure 5. Basic connective motifs found for O–H···O HBs. Large circles: donor (D) and acceptor (A) cores; open circles: hydrogen (H) cores; small circles: lone-pairs; tiny dark circles: BCPs. Reprinted with permission from Ref. [97].

In a comparative X–X analysis of 19 O–H···O hydrogen bonds in 7 molecular crystals, Ranganathan et al. [97] found a geometric pattern in the H···O BCP locations. The sample includes relatively strong and linear, weaker and slightly bent, as well as bi- and trifurcated HBs. Many of these, especially the weak ones, exhibit curved BPs. However, each BCP appears to be located on (or close to) a line joining “cores” and/or “lone-pairs” ((3,-3)CP of $-\nabla^2\rho$) of the participating atoms. The special points defining “new interaction lines” are associated with the core (designated as D, H, and A, corresponding to the donor, hydrogen, and acceptor core) and non-bonded VSCCs (designated as A_I and D_I).

Figure 5 displays the six types of HB motifs, identified by the H–A, H– A_I , D–A, D_I –A, D– A_I , and D_I – A_I links. They resemble the “key-and-lock” arrangement found for other closed-shell interactions. The intermolecular Cl···Cl interactions in the crystalline chlorine, for example, can be viewed as the result of alignments of local charge concentrations ($\nabla^2\rho < 0$) of one atom with local depletions ($\nabla^2\rho > 0$) of the other. [102]

5 CONCLUDING REMARKS

The topological analysis, applicable to both theoretical and experimental EDs, is a sophisticated interpretive tool for exploring fundamental characteristics of chemical bonds. While BCP properties have been proven to possess a vast amount of information on bonding, the widespread view that these local figures are the fingerprints of atom–atom interactions is strictly valid only for diatomics. In extending the local viewpoint to molecular solids, one cannot neglect competing, non-local effects that play an important role in attaining the bal-

ance in electrostatic forces. “In the limiting case of molecular recognition and crystal formation among non-polar molecules, it is probably more instructive to seeing the whole molecule that bonds to another molecule than discussing and justifying cohesion in terms of thousands of unavoidable weak atom–atom contacts. Formation of bond path among couples of facing atoms in this case is more likely the result than the cause of molecular interaction.” as summarized by Gatti. [30]

X-ray charge densities are playing a role of increasing significance in our understanding of bonding in the crystalline state, even though, the method is known to be subject to experimental errors and model ambiguities. The distribution of the uncertainty in the experimental ED ($\sigma[\rho]$ obtained from the LS parameter variances) is far from being uniform. The error function peaks at the atomic regions and exhibits minima in the bond regions. This spatial behavior of $\sigma[\rho(r)]$ has its origin in the characteristics of the Fourier transform and the error distribution of the structure factor data. Sharp (diffuse) density features have diffuse (sharp) scattering power and thus they influence mainly the high- (low) order data, which are usually measured with low (high) relative errors. As a consequence, the signal-to-noise ratio at the BCP of a shared- and closed-shell interaction is anticipated to be high ($\rho_{\text{BCP}} \gg \sigma[\rho_{\text{BCP}}]$) and low ($\rho_{\text{BCP}} \leq \sigma[\rho_{\text{BCP}}]$), respectively. For hydrogen bonds, the BCP is located close to the H-atom lacking of bonded VSCC, and thus λ_3 changes here less erratically than for a polar covalent bond. This might be the reason while the bond-parallel curvature and related energetic properties appear to be reliably obtained experimentally.

The importance of HB studies outlined in this monograph is that they establish simple empirical connections between energetic and local density-topological figures that appear to be valid, to a good approximation, in a wide range of HB interactions regardless of the chemical nature of the acceptor atoms. The simplicity and generality of these relationships also makes their validity questionable. In other words, the possibility of fortuitous error cancellations cannot be excluded, since the results emerge from the combination of the local virial (an exact theorem) and Abramov’s kinetic energy–density expression (an approximate formula) applied to pseudoatoms (subject to experimental uncertainties).

Theoretical studies show that weak C–H···O HBs have an extremely low signal at the BCP. A direct comparison of ρ_{BCP} with that of the promolecule, and the analysis of the interaction density, suggest that these contacts manifest themselves mainly in the basins of the participating atoms rather than at the BCP. Bond analyses relying on local topological figures of a model ED extracted from the X-ray diffraction data must confine with these limitations in order to avoid over-interpretations.

The above argument stresses the importance of adapting the Koch–Popelier criteria [40] in experimental studies, since they include not only local but also integrated topological properties to characterize HBs. New density-based

interpretive tools are being considered that have the potential of revealing non-local effects [37]. Many-center interactions can be unambiguously identified on the basis of source function [39] that enables one to derive the contribution of each topological atom to the density at the BCP. New potential routes to “physically sound” modeling of X-ray diffraction data (density matrix and wave function fitting) are being explored with promising results [103].

REFERENCES

1. G. A. Jeffrey and W. Saenger, *Hydrogen Bonding in Biological Structures* (Springer-Verlag, Berlin, 1991).
2. C. L. Perrin and J. B. Nielson, Strong hydrogen bonds in chemistry and biology, *Annu. Rev. Phys. Chem.* **48**, 511–544 (1997).
3. J. A. Subirana and M. Soler-L'opez, Cations as hydrogen bond donors: a view of electrostatic interactions in DNA, *Annu. Rev. Biophys. Biomol. Struct.* **32**, 27–45 (2003).
4. B. T. Sutcliffe, in: *Intermolecular Interactions*, edited by: W. Gans and J. C. A. Boeyens (Plenum Press, New York, 1998), pp. 25–48.
5. M. Born and R. Oppenheimer, Zur Quantentheorie der Molekeln, *Ann. Phys.* **84**, 457–473 (1927).
6. J. C. A. Boeyens, in: *Intermolecular Interactions*, edited by: W. Gans and J. C. A. Boeyens (Plenum Press, New York, 1998), pp. 3–8.
7. R. F. W. Bader, *Atoms in Molecules: A Quantum Theory* (Oxford Science Publications, Oxford, 1990).
8. B. T. M. Willis, *Thermal Neutron Diffraction* (Oxford University Press, Oxford, 1970).
9. G. E. Bacon, *Neutron Diffraction* (Clarendon Press, Oxford, 1975).
10. F. R. Trouw and D. L. Price, Chemical applications of neutron scattering, *Annu. Rev. Phys. Chem.* **50**, 571–601 (1999).
11. C. Giacovazzo, H. L. Monaco, D. Viterbo, F. Scordari, G. Gilli, G. Zanotti and M. Catti, *Fundamentals of Crystallography* (Oxford University Press, Oxford, 1992).
12. W. H. E. Schwarz, K. Ruedenberg and L. Mensching, Chemical deformation densities. 1. Principles and formulation of quantitative determination, *J. Am. Chem. Soc.* **111**, 6926–6933 (1989).
13. T. S. Koritsanszky and P. Coppens, Chemical applications of X-ray charge density analysis, *Chem. Rev.* **101**, 1583–1628 (2001).
14. S. Kuntzinger, S. Dohaoui, N. E. Ghermani, C. Lecomte and J. A. K. Howard, The use of CCD area detectors in charge-density research. Application to a mineral compound: the -spodumene $\text{LiAl}(\text{SiO}_3)_2$, *Acta Cryst.* **B55**, 867–881 (1999).
15. T. Koritsanszky, R. Flaig, D. Zobel, H. G. Krane, W. Morgenroth and P. Luger, Accurate experimental electronic properties of DL-Proline monohydrate obtained within 1 day, *Science* **279**, 356–358 (1998).
16. P. Coppens, *X-ray Charge Densities and Chemical Bonding* (Oxford University Press, Oxford, 1997).
17. V. G. Tsirelson and R. P. Ozerov, *Electron Density and Bonding in Crystals* (Institute of Physics Publishing, Bristol, 1996).
18. R. F. Stewart and M. A. Spackman, *Valray User's Manual* (Department of Chemistry, Carnegie Mellon University, Pittsburgh, PA, 1983).
19. B. M. Craven, H. P. Weber and X. He, *Technical Report TR-872* (Department of Crystallography, University of Pittsburgh, Pittsburgh, PA, 1987).
20. T. Koritsanszky, T. Richter, P. Macchi, A. Volkov, C. Gatti, S. Howard, P. R. Mallinson, L. Farrugia, Z. Su and N. K. Hansen, *XD: Computer Program Package for Multipole Refinement and Topological Analysis of Electron Densities from Diffraction Data* (2003).

21. G. A. Jeffrey, *An Introduction to Hydrogen Bonding* (Oxford University Press, New York, 1997).
22. G. R. Desiraju and T. Steiner, *The Weak Hydrogen Bond* (Oxford University Press, Oxford, 1999).
23. T. Steiner, The hydrogen bond in the solid state, *Angew. Chem. Int. Ed.* **41**, 48–76 (2002).
24. C. Bolton, F. H. Allen, G. P. Shield and J. A. K. Howard, Intramolecular hydrogen bonds: common motifs, probabilities of formation and implications for supramolecular organization, *Acta Cryst.* **B56**, 849–856 (2000).
25. R. F. W. Bader, R. J. Gillespi and P. J. MacDougall, Physical basis for the VSEPR model of molecular geometry, *J. Am. Chem. Soc.* **110**, 7329 (1988).
26. M. T. Carroll, C. Chang and R. F. W. Bader, Prediction of the structures of hydrogen-bonded complexes using the Laplacian of the charge density, *Mol. Phys.* **63**, 387–405 (1988).
27. D. Cremer and E. Kraka, A description of the chemical bond in terms of local properties of electron density and energy, *Croat. Chem. Acta* **57**, 1259–1281 (1984).
28. R. F. W. Bader and H. Essén, The characterization of atomic interactions, *J. Chem. Phys.* **80**, 1943–1960 (1984).
29. R. F. W. Bader, A bond path: a universal indicator of bonded interactions, *J. Phys. Chem.* **A102**, 7314–7323 (1998).
30. C. Gatti, Chemical bonding in crystals: new directions, *Zeitschrift f. Krist.* **220**, 399–487 (2005).
31. M. Pendás, M. A. Blanco and E. Francisco, Two-electron integrations in the quantum theory of atoms in molecules, *J. Chem. Phys.* **120**, 4581–4592 (2004).
32. J. C. Slater, The virial and the molecular structure, *J. Chem. Phys.* **1**, 687–691 (1933).
33. R. F. W. Bader, P. M. Beddall and J. Peslak Jr., A theoretical development of a virial relationship for spatially defined fragments of molecular systems, *J. Chem. Phys.* **58**, 557–566 (1973).
34. E. Espinosa, I. Alkorta, J. Elguero and E. Molins, From weak to strong interactions: a comprehensive analysis of the topological and energetic properties of the electron density distribution involving X–H···F–Y systems, *J. Chem. Phys.* **117**, 5529–5542 (2002).
35. Yu. A. Abramov, On the possibility of kinetic energy density evaluation from experimental electron density distribution, *Acta Cryst.* **A53**, 264–272 (1997).
36. D. A. Kirzhnits, Quantum corrections to the Thomas–Fermi equation, *Sov. Phys. JETP* **5**, 64–72 (1957).
37. V. T. Tsirelson, The mapping of electronic energy distributions using experimental electron density, *Acta Cryst.* **B58**, 632–639 (2002).
38. R. F. W. Bader and C. Gatti, A Green's function for the density, *Chem. Phys. Lett.* **287**, 233–238 (1998).
39. C. Gatti and L. Bertini, The local form of the source function as a fingerprint of strong and weak intra- and intermolecular interactions, *Acta Cryst.* **A60**, 438–449 (2004).
40. U. Koch and P. L. A. Popelier, Characterization of C–H···O hydrogen bonds on the basis of the charge density, *J. Phys. Chem.* **99**, 9747–9754 (1995).
41. P. L. A. Popelier, Characterization of a dihydrogen bond on the basis of the electron density, *J. Phys. Chem.* **A102**, 1873–1878 (1998).
42. O. Gálvez, P. C. Gomez and L. F. Pacios, Variation with the intermolecular distance of properties dependent on the electron density in hydrogen bond dimmers, *J. Chem. Phys.* **115**, 11166–11184 (2001).
43. R. F. Stewart and D. Feil, A theoretical study of elastic X-ray scattering, *Acta Cryst.* **A36**, 503–509 (1980).
44. R. F. Stewart, Vibrational averaging of X-ray-scattering intensities, *Isr. J. Chem.* **16**, 137–143 (1997).
45. E. Clementi and C. Roetti, Roothan-Hartree-Fock atomic wave functions. Basic functions and their coefficients for ground and certain excited states and ionized atoms, *Z < 54. Atomic Data, Nuclear Data Tables* **14**, 177–478 (1974).

46. F. H. Allen, A systematic pairwise comparison of geometric parameters obtained by X-ray and neutron diffraction, *Acta Cryst.* **B42**, 515–522 (1986).
47. F. H. Allen, J. C. Cole and J. A. K. Howard, A systematic study of coordinate precision in X-ray structure analyses. II. Predictive estimates of e.s.d.'s for the general-atom case, *Acta Cryst.* **A51**, 112–121 (1995).
48. F. L. Hirshfeld, Can X-ray data distinguish bonding effects from vibrational smearing? *Acta Cryst.* **A32**, 239–244 (1976).
49. S. T. Howard, J. P. Huke and C. S. Frampton, Density–matrix refinement for molecular crystals, *Phys. Rev.* **B49**, 7124–7136 (1994).
50. J. A. Snyder and E. D. Stevens, A wave function and energy of the azide ion in potassium azide obtained by a quantum-mechanically constrained fit to X-ray diffraction data, *Chem. Phys. Lett.* **313**, 293–298 (1999).
51. R. F. Stewart, One-electron density functions and many-centered finite multipole expansions, *Isr. J. Chem.* **16**, 124–131 (1977).
52. N. K. Hansen and P. Coppens, Testing aspherical atom refinements on small-molecule data sets, *Acta Cryst.* **A34**, 909–921 (1978).
53. M. A. Spackman, Molecular electric moments from X-ray diffraction data, *Chem. Rev.* **92**, 1769–1797 (1992).
54. R. G. Parr and W. Yang, *Density-Functional Theory of Atoms and Molecules* (Oxford University Press, New York, 1989).
55. T. Kato, On the eigenfunctions of many-particle systems in quantum mechanics, *Comm. Pure Appl. Math.* **10**, 151–177 (1957).
56. A. Volkov and P. Coppens, Critical examination of the radial functions in the Hansen-Coppens multipole model through topological analysis of primary- and refined-theoretical densities, *Acta Cryst.* **A57**, 395–405 (2001).
57. A. Volkov, Yu. A. Abramov and P. Coppens, Density optimized radial exponents for X-ray charge density refinement from *ab initio* calculations. *Acta Cryst.* **A57**, 272–282 (2001).
58. T. Koritsanszky and A. Volkov, Density radial functions for bonded atoms, *Chem. Phys. Lett.* **383**, 431–435 (2004).
59. P. Coppens, R. Boehme, P. F. Price and E. D. Stevens, Electron population analysis of accurate diffraction data. 10. Joint X-ray and neutron data refinement of structural and charge density parameters, *Acta Cryst.* **A37**, 857–863 (1981).
60. R. H. Blessing, On the differences between X-ray and neutron thermal vibration parameters, *Acta Cryst.* **B51**, 816–823 (1995).
61. V. Schomaker and K. N. Trueblood, On the rigid-body motion of molecules in crystals, *Acta Cryst.* **B24**, 63–76 (1968).
62. A. O. Madsen, H. O. Sorensen, C. Flesburg, R. F. Stewart and S. Larsen, Modeling of the nuclear parameters of H atoms in X-ray charge density studies, *Acta Cryst.* **A60**, 550–561 (2004).
63. R. Destro, P. Roversi, M. Barzaghi and R. E. Marsh, Experimental charge density of α -glycine at 23 K, *J. Phys. Chem.* **A104**, 1047–1054 (2000).
64. P. Roversi and R. Destro, Approximate anisotropic displacement parameters for H atoms in molecular crystals, *Chem. Phys. Lett.* **386**, 472–478 (2004).
65. H.-B. Bürgi, S. C. Capelli, A. E. Goeta, J. A. K. Howard, M. A. Spackman and D. S. Yufit, *Chem. Eur. J.* **8**, 3512–3521 (2002).
66. J. Oddershede and S. Larsen, Charge density study of naphthalene based on X-ray diffraction data at four different temperatures and theoretical calculations, *J. Phys. Chem.* **A108**, 1057–1063 (2004).
67. R. Flaig, T. Koritsanszky, D. Zobel and P. Luger, Topological analysis of experimental Electron densities of amino acids: I. D,L-aspartic acid at 20 K, *J. Am. Chem. Soc.* **120**, 2227–2236 (1998).
68. P. Vishweshar, N. J. Babu, A. Nangia, S. A. Mason, H. Puschmann, R. Mondal and J. A. K. Howard, Variable temperature neutron diffraction analysis of a very short O–H \cdots O hydrogen

- bond in 2,3,5,6-pyrazinetetracarboxylic acid dihydrate: synthon-assisted short $O_{\text{acid}}\text{-H}\cdots O_{\text{water}}$ hydrogen bonds in multicenter array, *J. Phys. Chem.* **A108**, 9406–9416 (2004).
69. E. Espinosa, M. Souhassou, M. Lachekar and C. Lecomte, Topological analysis of the electron density in hydrogen bonds, *Acta Cryst.* **B55**, 563–572 (1999).
 70. S. T. Howard, M. B. Hursthouse and C. W. Lehmann, Experimental and theoretical determination of electronic properties in L-dopa, *Acta Cryst.* **B51**, 328–337 (1995).
 71. N. Pèrés, A. Boukhris, M. Souhassou, G. Gavoille and C. Lecomte, Electron density in ammonium dihydrogen phosphate: non-uniqueness of the multipolar model in simple inorganic structures, *Acta Cryst.* **A55**, 1038–1048 (1999).
 72. I. Bytheway, S. G. Chandler and B. N. Figgis, Can a multipole analysis faithfully reproduce topological descriptors of a total charge density? *Acta Cryst.* **A58**, 451–459 (2002).
 73. J. Overgaard, M. P. Waller, J. A. Platts and D. E. Hibbs, Influence of crystal effects on molecular densities in a study of 9-ethynyl-9-fluorenone, *J. Phys. Chem.* **A107**, 11201–11208 (2003).
 74. A. Volkov, Yu. Abramov, P. Coppens and C. Gatti, On the origin of topological differences between experimental and theoretical crystal charge densities, *Acta Cryst.* **A56**, 332–339 (2000).
 75. C. Gatti, R. Bianchi, R. Destro and F. Merati, Experimental vs theoretical topological properties of charge density distribution—an application to the L-alanine molecule studied by X-ray diffraction at 23K, *THEOCHEM, J. Mol. Struct.* **87**, 409–433 (1992).
 76. D. E. Hibbs, J. Overgaard, C. Gatti and T. W. Hambley, The electron density in flavones I. Baicalein, *New J. Chem.* **27**, 1392–1398 (2003).
 77. R. Flaig, T. Koritsanszky, B. Dittrich, A. Wagner and P. Luger, Intra- and intermolecular topological properties of amino acids: a comparative study of experimental and theoretical results, *J. Am. Chem. Soc.* **124**, 3407–3417 (2002).
 78. C. Gatti, V. R. Saunders and C. Roetti, Crystal-field effect on the topological properties of the electron density in molecular-crystals—the case of urea, *J. Chem. Phys.* **101**, 10686–10696 (1994).
 79. V. R. Saunders, R. Dovesi, C. Roetti, M. Causa, N. M. Harrison, R. Orlando, and C. M. Zicovich-Wilson, *CRYSTAL98 User's Manual* (University of Turin, Italy, 1998).
 80. M. A. Spackman, P. G. Byrom, M. Alfredsson and K. Hermansson, Influence of intermolecular interactions on multipole refined electron densities, *Acta Cryst.* **A55**, 30–47 (1999).
 81. R. Y. De Vries, D. Feill and V. G. Tsirelson, Extracting charge density distributions from diffraction data: a model study on urea, *Acta Cryst.* **B56**, 118–123 (2000).
 82. M. A. Spackman and P. G. Byrom, Retrieval of structure-factor phases in non-centrosymmetric space group. Model studies using multipole refinement, *Acta Cryst.* **B53**, 553–564 (1997).
 83. A. El. Haouzi, N. K. Hansen, C. Le. Hénass and J. Protas, The phase problem in the Analysis of X-ray diffraction data in terms of electron-density distributions, *Acta Cryst.* **A52**, 291–301 (1996).
 84. J. Overgaard and D. E. Hibbs, The experimental electron density in polymorphs A and B of the anti-ulcer drug famotidine, *Acta Cryst.* **A60**, 480–487 (2004).
 85. D. E. Hibbs, J. Overgaard, J. A. Platts, M. P. Waller and M. B. Hursthouse, Experimental and theoretical charge density studies of tetrafluorophthalonitrile and tetrafluoroisophthalonitrile, *J. Phys. Chem.* **B108**, 3663–3673 (2004).
 86. S. Scheins, B. Dittrich, M. Messerschmidt, C. Paulmann and P. Luger, Atomic volumes and charges in a system with a strong hydrogen bond: L-tryptophan formic acid, *Acta Cryst.* **B60**, 184–190 (2004).
 87. P. Munshi and T. N. Guru Row, Exploring the lower limit in hydrogen bonds: analysis of weak C–H \cdots O and C–H \cdots π interactions in substituted coumarins from charge density analysis, *J. Phys. Chem.* **109**, 659–672 (2005).
 88. P. R. Mallinson, K. Wozniak, G. T. Smith and K. L. McCormack, A charge density analysis of cationic and anionic hydrogen bonds in a “proton sponge” complex, *J. Am. Chem. Soc.* **119**, 1150–11509 (1997).

89. C. Flensburg, S. Larsen and R. F. Stewart, Experimental density study of methylammonium hydrogen succinate monohydrate. A salt with a very short O–H···O hydrogen bond, *J. Phys. Chem.* **99**, 10130–10141 (1995).
90. D. Madsen, C. Flensburg and S. Larsen, Properties of the experimental crystal density of methylammonium hydrogen maleate. A salt with very short intramolecular O–H···O hydrogen bond, *J. Phys. Chem.* **A102**, 2177–2188 (1998).
91. G. K. H. Madsen, B. B. Iversen, F. K. Larsen, M. Kapon, G. M. Reisner and F. H. Herstein, Topological analysis of the charge density in short intramolecular O–H···O hydrogen bonds. Very low temperature X-ray and neutron diffraction study of benzoylacetone, *J. Am. Chem. Soc.* **120**, 10040–10045 (1998).
92. G. Gilli, F. Belluci, V. Ferretti and V. Bertolasi, Evidence for resonance-assisted hydrogen bonding from crystal–structure correlations on the enol form of the beta-diketone fragment, *J. Am. Chem. Soc.* **111**, 1023–1028. (1989).
93. E. Espinosa, E. Mollins and C. Lecomte, Hydrogen bond strengths by topological analyses of experimentally observed electron densities, *Chem. Phys. Lett.* **285**, 170–173 (1998).
94. E. Espinosa, I. Alkorta, I. Rozas, J. Elguero and E. Mollins, About the evaluation of local kinetic, potential and total energy densities in closed-shell interactions, *Chem. Phys. Lett.* **336**, 457–461 (2001).
95. E. Espinosa and E. Molins, Retrieving interaction potentials from the topology of the electron density distribution: the case of hydrogen bonds, *J. Chem. Phys.* **113**, 5686–5694 (2000).
96. M. A. Spackman, Hydrogen bond energetics from topological analysis of experimental electron densities: recognizing the importance of the promolecule, *Chem. Phys. Lett.* **301**, 425–429 (1999).
97. A. Ranganathan, G. U. Kulkarni and C. N. R. Rao, Understanding the hydrogen bond in terms of the location of the bond critical point and geometry of the lone pairs, *J. Phys. Chem.* **107**, 6073–6081 (2003).
98. K. Wozniak, P. R. Mallinson, C. C. Wilson, E. Hovestreydt and E. Grech, Charge density studies of weak interactions in dipicramine, *J. Phys. Chem.* **106**, 6897–6903 (2002).
99. C. Gatti, E. May, R. Destro and F. Cargnoni, Fundamental properties and nature of C–H···O interactions in crystals on the basis of experimental and theoretical charge densities. The case of 3,4-bis(dimethylamino)-3-cyclobutene-1,2-dione (DMACB) crystal, *J. Phys. Chem.* **A106**, 2707–2770 (2002).
100. P. R. Mallinson, K. Wozniak, C. C. Wilson, K. L. McCormack and D. S. Yufit, Charge density distribution in the “proton sponge” compound 1,8-bis(dimethylamino)naphthalene, *J. Am. Chem. Soc.* **121**, 4640–4646 (1999).
101. M. J. Cole, A. E. Goeta, J. A. K. Howard and G. J. McIntyre, X-ray and neutron diffraction studies of the non-linear optical compounds MBANP and MBADNP at 20 K: charge-density and hydrogen-bonding analyses, *Acta Cryst.* **B58**, 690–700 (2002).
102. V. G. Tsirelson, P. F. Zou, T.-H. Tang and R. F. W. Bader, Topological definition of crystal structure: determination of bonded interactions in solid molecular chlorine, *Acta Cryst.* **A51**, 143–153 (1995).
103. D. J. Grimwood, I. Bytheway and D. Jayatilaka, Wave functions derived from experiment. V. Investigation of electron densities, electrostatic potentials and electron localization functions for noncentrosymmetric crystals, *J. Comp. Chem.* **24**, 470–483 (2003).

CHAPTER 13

STRUCTURE–PROPERTY RELATIONS FOR HYDROGEN-BONDED SOLIDS

Specific Features of Hydrogen Bonds at Structural Transformations and in Polymorphs

A. KATRUSIAK

Faculty of Chemistry, Adam Mickiewicz University, Grunwaldzka 6, 60-780 Poznań

Abstract A brief account of the structure–property relations in hydrogen-bonded molecular and ionic crystals has been highlighted. The selected relations include intramolecular and intermolecular hydrogen bonds, thermodynamic and structural characteristics of phase transitions, occurrence of the tricritical point, quantitative interdependence of hydrogen-bond dimensions and the critical temperature, anomalous thermal expansion of the H-bonded crystals, colour changes, and ferroelectricity. The quantitative analysis of the contribution of the hydrogen bonds is based on the interplay between the H-bond geometry and the local field of the crystal environment. The examples selected for illustrating the structure–property relations include H₂O ices, OH–O, and NH–N bonded ferroelectrics and relaxors.

Keywords: Hydrogen bond; structure–property relation; phase transition; critical temperature; tricritical point; colour; ferroelectricity; proton disordering; spontaneous polarization; anomalous thermal expansion; polymorphism.

1 INTRODUCTION

Physical properties of any material depend on its microscopic structure. The same concerns the hydrogen-bonded crystals. The structural features of hydrogen bonds, patterns of hydrogen bonds, and the coupling between hydrogen-bond dimensions and crystal lattice, as well as transformations of hydrogen bonds and hydrogen-bonded networks can be directly related to specific properties of crystals, such as their anomalous thermal expansion, changes of the thermodynamic character of the phase transitions, spontaneous polarization, or colour. The bistable homonuclear hydrogen bonds are very appealing, as the H-transfers can change polarization of the molecule, of the aggregate, and the

macroscopic dielectric properties of the crystal. Hydrogen bonds are abundant in nature [1], and relatively low energy is required for their transformation—therefore they are very attractive objects for studies, either for purely scientific reasons aimed at a better understanding of molecular and biological systems, or for potential practical applications. However, despite these advantages, presently there are no commercial electronic or mechanic devices based on hydrogen-bonded materials.

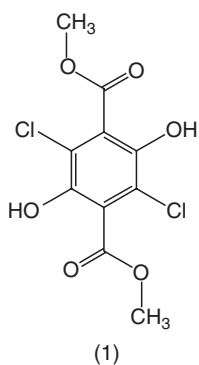
The variety of hydrogen bonds is immense, and they can be classified in different manners [1]. In fact for decades controversies have concerned the definition of the hydrogen bond itself. While it is clear what the strong hydrogen bonds are, there are different attitudes toward the weaker types of hydrogen bonds, such as those involving the CH groups [2], even though the longest H-bonds limit is constantly extended toward the weaker bonds. Because of this very broad scope of the subject of H-bonding interactions, only several selected aspects of structure–property relations of hydrogen-bonded systems will be exemplified in this chapter. For the purpose of illustrating the properties of hydrogen-bonded materials, it is convenient to focus on strong hydrogen bonds, which are clearly distinguishable from other cohesion forces. Moreover, the specific feature of the hydrogen bonds—such as the possibility of reversing the H-bond polarization by the H-transfer to the opposite atom ($\text{OH}\cdots\text{O}$ transforming into $\text{O}\cdots\text{HO}$)—is facilitated in strong hydrogen bonds, and much less likely in the weak ones. In the strong hydrogen bonds, the potential energy barrier separating the two minima is low, and the H-atom can be easily activated to overcome it. On the other hand, there are relatively few substances, the structure of which is totally dominated by the hydrogen bonding, like in H_2O ices. When analysing the structure–property relations, it is necessary to include all the structural features, such as the molecular conformation, molecular arrangement, symmetry and other interactions (van der Waals, electrostatic) in the crystal lattice. It is apparent that the contribution of very weak hydrogen bonds for the properties of crystals is relatively small, and would be more difficult to extract from other structural factors contributing to the crystal properties. The formation of H-bonding network in water as the cause of anomalous expansion below 4°C and on freezing is perhaps the best known example of the H-bonded structure-to-property relations. However, there are practically no other so commonly comprehended hydrogen-bonded substances. The understanding of hydrogen-bonded materials definitely requires that the arrangement of hydrogen-bonded molecules be taken into account, and cannot be limited to the hydrogen bonds only. When neglecting other structural factors, one can arrive to conclusions contradicting the experimental evidence [3]. Meanwhile, it is essential to have a theory capable of predicting the properties of hydrogen-bonded systems and their quantitative characteristics. The observations of the properties of H-bonded structures are perhaps most spectacular in these materials, where the H-bonds are strong and undergo

transformations. The mechanism of the hydrogen-bond transformations described for a specific type of hydrogen bonds can be generalized also to other types of hydrogen bonds. For example, it can be shown that $\text{OH}\cdots\text{O}$, $\text{NH}\cdots\text{N}$, and even heteronuclear hydrogen bonds may have common features, although they may transform in different manners. The discussion in this chapter will be mainly focused on the strong $\text{OH}\cdots\text{O}$ bonds. Some selected examples of the hydrogen-bond transformations will be given. It will be also shown that the H-bond structure can be directly or indirectly connected with the macroscopic properties of the crystal. The main aim of this chapter is to present a very brief introduction to the structural models of physical properties. It was not attempted to review completely the structural models of hydrogen-bonded materials.

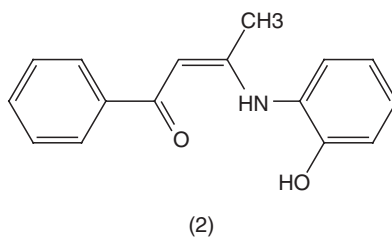
2 INDIRECT H-BOND–PROPERTY RELATIONS

In most cases, the property of a hydrogen-bonded substance is not directly related to the hydrogen-bond structure. Such relations are beyond the scope of this chapter; however, a few examples will be given below for illustration. The very spectacular properties are those of colour changes.

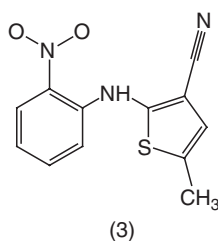
3,6-Dichloro-2,5-dihydroxyterephthalate (1) is frequently cited as an example of macroscopic properties transforming in this manner: the hydrogen bonds control the conformation of the molecule, the conformation of the molecule in turn controls the molecular electronic structure responsible for the colour of the substance. These colour transformations were already observed by Hantzsch in 1915 [4], and the molecular interpretation of these transformations was given by Byrn et al. [5] after determining the crystal structures of the yellow and colourless crystals of the substance. In the yellow form, the ester groups are held within the molecular plane by the intramolecular $\text{OH}\cdots\text{O}$ hydrogen bonds, and owing to the π -electron conjugation between the phenyl ring and ester groups (terephthalate), the substance enquires a yellow tint. In another phase of (1), intramolecular $\text{OH}\cdots\text{Cl}$ hydrogen bonds are formed, and the ester groups are rotated to form dihedral angles of 86.5° and 72.6° with the phenyl ring in two symmetry-independent molecules. In the consequence of this rotation, the conjugation between the phenyl and ester groups breaks, and the crystal becomes colourless. In the third light-yellow form of (1) discovered later, the ester groups are inclined by about 40° to the phenyl ring, and this conformation is stabilized both by intramolecular and intermolecular $\text{OH}\cdots\text{O}$ hydrogen bonds [6, 7]. The sequence of thermodynamic stability of these three phases is yellow > light-yellow > colourless at ambient conditions, while above 360 K it changes to colourless > yellow > light-yellow [8]. It is obvious that the crystal colour depends on the molecular electronic structure and conformation. Thus the hydrogen-bond transformations indirectly lead to the colour change.



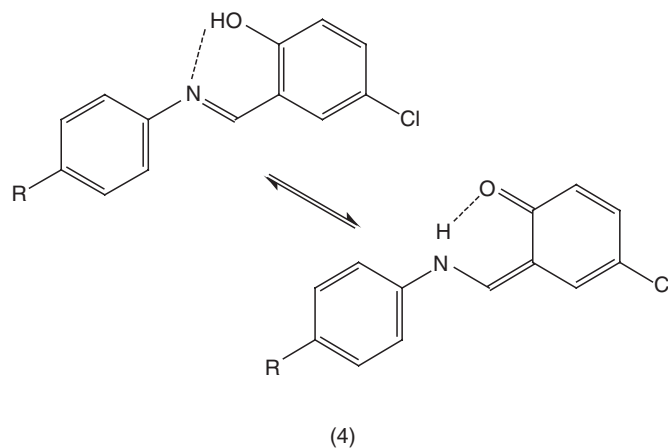
Analogous interdependence between the hydrogen bonding, molecular conformation, and crystal colour has been observed and discussed in a number of other compounds. For example, 1-phenyl-3-(2-hydroxyphenylamino)-2-buten-1-one (2) forms orange and light-yellow crystal forms, depending on the orientation of the phenol ring about the N–C bond [9].



Similarly, the conformation of 5-methyl-2-[(2-nitrophenyl)amino]-3-thiophene-carbonitrile (3) forms seven (if not more) polymorphs, the colour of which ranges from yellow to red depending on the molecular conformation [10–12].

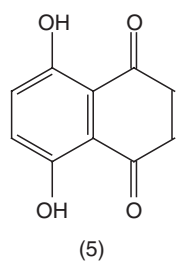


Another mechanism of H-transfer in intramolecular OH...N bond, without breaking the hydrogen bonds and without conformation change, leading to colour changes was observed in N-salicylideneanilines (4) in the function of temperature [13].



3 H-DISORDERING IN INTRAMOLECULAR H-BONDS

Naphthazarin (5) is known to form three polymorphs, labelled A, B, and C, and naphthazarin C undergoes a phase transition at $T_c = 110\text{K}$ induced by the onset of ordering of the hydrogen bonds [14]. This phase transition illustrates the ability of the H-bonding protons to disorder between the donor and acceptor sites. The dynamical disorder of the H-atom is coupled to the electronic structure of the molecule, its geometrical dimensions [15], and to the molecular and crystal symmetry. Above T_c the single and double bonds become delocalized, and in crystal lattice molecules become centrosymmetric. The onset of the H-ordering below T_c lowers the space-group symmetry of the crystal from $P2_1/c$ to Pc . Generally, owing to the symmetry change, the crystal may acquire new properties, like piezoelectricity, ferroelectricity, or ferroelectricity.



4 H-DISORDERING IN INTERMOLECULAR H-BONDS

The dynamical disordering of protons in intermolecular hydrogen bonds is quite common. Such a H-disordering often changes the crystal symmetry and those properties of the crystal, which are symmetry-dependent. Naturally, there

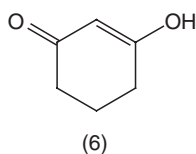
are many crystals, the symmetry of which does not change when the proton dynamically disorders in the hydrogen bonds—perhaps the best known examples are most of carboxylic acids and H₂O ice *I_c*. The transformations in the carboxylic acids and in H₂O ice *I_c* are quite different. In the carboxylic-acid dimers, the H-atom ordering in one of the sites in the –OH···O= bond is strongly coupled to the H-ordering in the other oppositely polarized =O···HO– hydrogen bond. But most importantly, the H-disordering in the carboxylic-acid dimers is clearly coupled to the mutual arrangement of the molecules. For the disordered H-atoms both the C–O···O at each carboxyl group are similar, while they differ by ca. 5° when the H-atoms are ordered [15, 16]. The H-site-arrangement coupling is a very important and general property, which is characteristic practically for all hydrogen-bonded crystals, and can be used for qualitative analysis of crystal properties [16, 17].

In the crystals of *I_c* ice, the freezing of the H-dynamics leads to the static disorder of the H-atoms, except for the doped crystal [18]. However, for both carboxylic dimers and ice, despite the apparent differences of the mechanisms of the H-atom disordering, there are common features resulting from the symmetry relations between the hydrogen-bonded groups [16]. It can be shown that the molecular arrangement and dimensions of hydrogen bonds are interdependent.

5 COMPETING STRAINS IN H-BONDS AND OTHER INTERACTIONS

It can be stated that in general there is always some discrepancy between the ideal dimensions of a hydrogen bond, such that would be assumed in an isolated molecule or dimer, and the dimensions of the hydrogen-bonded aggregate in the crystal lattice. The reason for this discrepancy is that the hydrogen-bonded molecules/ions are located in the crystal environment where they interact via van der Waals and electrostatic forces. Thus the crystal structure is a compromise between the arrangements favoured by the directional hydrogen bonds, and the close-packing arrangements favoured by other, mainly central interactions. This compromise can be regarded in the terms of strains in the hydrogen bonding and in the molecular packing. For bistable hydrogen bonds, the crystal environment can favour one of the H-sites. Such a situation was observed in the crystals of 1,3-cyclohexanedione (6—in the enolized form), where at ambient conditions the H-atom is ordered at one of the sites in the –OH–O= bond linking the molecules into chains. The modification of this hydrogen-bond environment below 286 K at the pressure of 0.1 MPa, or above 8 MPa at 296 K, forces the H-atom to move to the opposite site at the other oxygen atom [19, 20]. The H-site in the hydrogen bond is clearly coupled with angular displacements of the hydrogen-bonded molecules. This coupling has significant structural and thermodynamic consequences. It was shown that the H-transfers in bistable hydrogen bonds could occur

only for specific types of hydrogen-bonded networks. There are crystal structures where the molecular rotations following the H-transfers can mutually compensate, and other structures, where these rotations would accumulate. In the first type of structures the H-transfer is possible, while in the latter it is highly unlikely. The arrangements of H-bonded molecules can be clearly classified by specifying the conformations and configurations of hydrogen bonds forming the supramolecule, and their ability to undergo H-transfers easily predicted [21]. For example, no H-transfers could occur in the structure of polymorph γ of 1,3-cyclohexanedione, where the symmetry-independent molecules are bonded consecutively by *anti-anti* and *syn-syn* $-\text{OH}\cdots\text{O}=\text{C}$ bonds; similarly no H-transfer has been observed in the inclusion compound with benzene where the 1,3-cyclohexanedione molecules are linked by *syn-anti* hydrogen-bonded into hexameric cyclomers [21].



It can be observed in Fig. 1 that the molecular orientation within a hydrogen-bonded aggregate formed by a bistable hydrogen bond can favour one of the H-sites. Naturally, this coupling also works in the opposite direction—the H-site modifies the arrangement of the H-bonded molecules or ions. This interdependence can be used for determining which of the H-sites is

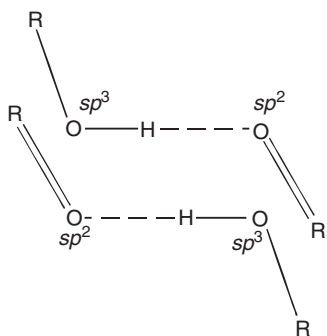


Figure 1. The interdependence of the H-atom site in the hydrogen bond, and the orientation of the $-\text{O}\cdots\text{HO}=\text{C}$ bonded molecules (moieties). In this schematic drawing the hydrogen bond is linear (the $\text{O}-\text{H}-\text{O}$ angle is 180°) and the $\text{R}-\text{O}-\text{H}$ and $\text{H}-\text{O}-\text{R}$ angles assume ideal openings for the sp^3 and sp^2 hybridizations of 109° and 120° , respectively. The upper drawing shows the hydrogen bond with the H-atom at the left-hand site, and in the drawing below the H-atom is moved to the right-hand site. R stands for the rest of the molecule/ion, which in these drawings is located at the atom covalently bonded to the oxygen.

occupied, by analysing the positions of non-H atoms in the structures, where the experimental measurements are not sufficiently precise to allow the H-location [22].

6 COUPLING OF THE H-SITE AND CRYSTAL STRUCTURE IN DISORDERED PHASES

When the H-atom becomes dynamically disordered in the hydrogen bond, the electronic structures of the hydrogen-bonded atoms are switched over in the rhythm of the H-hopping. The electronic structure of the H-donor and acceptor atoms controls the O–H and H···O lengths as well as the R–O–H and H–O–R angles. When the H-atom becomes disordered between the H-donor and acceptor groups, the only way to preserve these dimensions is to bend the O–H···O angle as shown in Fig. 2. At the same time the O–R bonds, owing to the relatively large mass of the non-H atoms and large frequency of the H-hopping (of ca. 10^{10} Hz), become averaged.

The bending of the O–H···O angle is indeed observed in the structures, where the H-atom becomes disordered [16, 21]. Although this property has been discussed here for the OH–O bond, analogous interdependence between the H-site and molecular/ionic arrangement is also observed for other hydrogen bonds, for example NH···N [23].

7 AN EASY INTERPRETATION OF ORDER–DISORDER PHASE TRANSITIONS

The dynamical H-disordering in hydrogen bonds is often connected with phase transitions. For example, KH_2PO_4 is ferroelectric below $T_c = 122$ K, and it

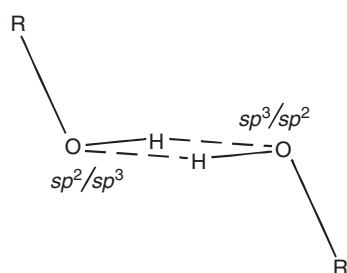


Figure 2. The time-averaged structure of disordered hydrogen bond (compare Fig. 1). Two half-occupied sites of the H-atom have been shown. The electronic structure of the oxygen atoms is repeatedly switched between sp^3 and sp^2 hybridizations, following the H-hopping. The two hydrogen-bonded groups are symmetry-related, and the O–H···O angle(s) are bent from ideal 180° to satisfy the boundary conditions required by the coexistence of different R–O–H and H···O–R angles (of 109° and 120° , respectively, in this drawing).

becomes paraelectric above T_c when the H-atoms disorder in the hydrogen bonds [24]. This is a prototypical structure for a large group of substances, termed KDP-type ferroelectrics. This group of materials includes RbH_2PO_4 , CsH_2PO_4 , PbHPO_4 , CsHSO_4 , RbHSeO_4 , or antiferroelectric squaric acid ($\text{C}_4\text{H}_2\text{O}_4$). Although the structural mechanism of the H-bond transformation in these materials is in principle very simple, it soon became apparent that certain features of the transformation could not be explained. These features can be straightforwardly explained by assuming the simple mechanism of the H-transition presented above. Below, several main features of the $-\text{OH}\cdots\text{O}=\text{O}$ bonded structures have been explained.

7.1 Displacive and Order–Disorder Character of the Phase Transition

Initially, it appeared that the phase transitions are purely of the order–disorder type [24]. However, it soon became apparent that atomic displacements also contribute to these phase transitions. These displacements are easy to identify, when one compares the molecular arrangements in the ordered $-\text{OH}\cdots\text{O}=\text{O}$ bonds in Fig. 1, with the arrangement of these molecules linked by the disordered bond in Fig. 2. The hydrogen-bonded molecules/ions must rotate before the two H-sites become symmetry-equivalent in the paraelectric phase above T_c . These rotations, usually of few degrees, can be termed as angular displacements. In other words, these angular displacements measure the distortions of the ferroelectric structure where the H-atom ordered from the paraelectric structure where the H-atom is dynamically disordered in two equivalent sites.

7.2 The Role of Atomic Displacements in KDP-Type Phase Transitions

The molecular displacements introduced above (in Sect. 7.1) can be used for characterizing various properties of hydrogen-bonded structures. For example, one can argue that for short H-bonds the reorientation of the molecules/ions requires more energy than the activation of the light H-atom hopping. Consequently, the critical temperature of the ferroelectric–paraelectric phase transition may depend more on the angular displacements of the H-bonded molecules than on dimensions of the hydrogen bond (such as $\text{O}\cdots\text{O}$ or $\text{H}-\text{O}$ distances). Indeed, it was shown that T_c correlates with the angular displacement of the H-bonded molecules [17]. This correlation testifies that the displacive character is important in these phase transitions.

7.3 T_c Determination from Structural Data

The angular displacements can be employed for calculating from structural data the critical temperature of the phase transition: the smaller is the difference between the orientations of the H-donor and H-acceptor groups, the lower is the critical temperature at which these two groups can assume the same

orientation. Thus for the molecules of similar molecular weight, the regression between the angular-displacements vs. T_c s in prototypic crystals can be used for assessing the T_c for a given substance, for which only the ferroelectric structure is known [17]. The angular displacement can be easily calculated as the difference between the so-called Donohue angles $R-O \cdots O$ on the H-donor and acceptor sides [25].

7.4 The H/D-Isotope Effect

It is a well-known property of the KDP-type ferroelectrics that the deuteration of the hydrogen bonds considerably increases the critical temperature of the phase transition. This feature can be attributed to the lengthening of the $O \cdots O$ distance caused by deuteration [26], but it can be also observed that the deuteration increases the difference between the orientation of the donor and acceptor groups. It occurs that lengthening of short hydrogen bonds increases the angular displacements; the displacements are also increased by deuteration [17]. Thus the deuteration increases not only the distance between the two H-sites, and the height of the energy barrier between them, but also the angular displacements between the H-bonded molecules.

7.5 Thermodynamic Character of the Phase Transitions

According to Erenfest's classification, there are *first-order* and *second-order* phase transitions. The first-order transitions are discontinuous, and the second-order transitions are continuous. The KDP-type phase transitions for many years were regarded as purely continuous ones. Then it was shown by Kobayashi et al [27], that there is a discontinuity in the temperature dependence of the unit-cell dimensions of the KDP crystal, and a hysteresis around T_c . This testified that the phase transition has some first-order contribution. Other characteristic features of first-order phase transitions are the latent heat and volume change at T_c .

7.6 Anomalous Thermal Expansion

It can be shown that in the KDP-type structures the anomalous thermal expansion of the crystal results from the geometrical effects of the H-atom disordering in the hydrogen bond [16]. As can be seen from Figs. 1 and 2, the hydrogen bond $O-H \cdots O$ angle becomes bent when the H-atom disorders in the paraelectric phase. Because there are no reasons for changes in the $O-H$ and $H \cdots O$ lengths (the electronic structure of the oxygen atoms is switched over, but not changed to other hybridizations), the bending of the $O-H-O$ angle shortens the $O \cdots O$ distance. This shortening induces some anomaly in the thermal expansion. When temperature rises, the crystal expands till T_c , when the H-atom becomes disordered and the $O \cdots O$ distance contracts. This contraction induces an anomaly in the thermal expansion at T_c . It can be shown

that KDP crystals exhibit the anomalous expansion in the direction of hydrogen bonds in their structures. Naturally, the anomalous volume change is derived from the anomalous thermal expansion of the unit-cell dimensions.

7.7 Tricritical Point

It was postulated by Landau that the first-order character of the Landau-type phase transitions (i.e., the transitions for which a group–subgroup relation exists between the symmetries of the transforming phases) is reduced by pressure till the so-called tricritical point when the phase transition becomes purely continuous [28, 29]. The structural origin of the tricritical point can be illustrated for the KDP-type ferroelectrics [30]. Intermolecular central forces intensify with pressure, which reduces the angular displacements and the distortions of the crystal structure from the paraelectric phase. The reduction of angular displacements is equivalent to bending of the O–H–O angle and to squeezing of the O···O distance in an analogous way as in the ferroelectric structure approaching T_c (as described above).

Thus compressing the structure can also induce the strains of the hydrogen bond, similar to those induced by the H-atom disordering. When the O···O distance is squeezed to the same length as caused by the H-disordering, the H-disordering will cause no further shortening and the phase transition becomes continuous. This simple structural model allows the tricritical temperature and pressure to be calculated with a good agreement with the experimentally determined tricritical point [30, 31, 32].

7.8 Accurate H-Bond Dimensions

The simple model relating the ordered and disordered structures allows one to calculate precisely the dimensions of disordered hydrogen bonds. The magnitudes of several features can be precisely calculated. For example, one can evaluate accurately the shortening of the O···O distance, or angular displacement, the inclination of the H···H hopping trajectory to the O···O line, and the distance between the half-occupied H···H sites [16].

7.9 Which is First? The Hen and Egg Problem

One can also wonder, which is the original cause of the ferroelectric–paraelectric phase transitions in KDP-type crystals: the H-hopping or the vibrations (rotations) of the H-bonded molecules. It has been shown that the angular displacements and the H-sites are coupled, thus the vibrations of molecules destabilize and facilitate the H-hopping. This coupling is essential for understanding the interactions between the lattice-mode vibrations in crystals, and the transformations in hydrogen bonds. Also other features of the KDP crystals, like the existence of soft modes, can be explained in this way.

8 NEW EXCITING MATERIALS

Presently hydrogen-bonded ferroelectric materials have not got any practical and commercial applications as electronic devices. The main disadvantages of the hydrogen-bonded crystals are the relatively weak spontaneous polarization, when compared to that of the best inorganic ferroelectrics, and low stability and durability of these materials. It was shown recently that $\text{NH}\cdots\text{N}$ -bonded molecules and ions can form ferroelectric crystals with a very high spontaneous polarization [33, 34, 35]. The $\text{NH}\cdots\text{N}$ hydrogen bonds are considerably different than the $\text{OH}\cdots\text{O}$ bonds, nonetheless the H-site in the bistable $\text{NH}\cdots\text{N}$ hydrogen bonds is coupled to the orientation of the hydrogen-bonded molecules or ions, and to the positions of the counterions [23]. Thus the lattice-type vibrations can be coupled to the H-sites in the hydrogen bonds.

The $\text{NH}\cdots\text{N}$ -bonded crystals revealed yet another exciting property of the hydrogen-bonded materials. In a typical ferroelectric crystal, domains of different spontaneous polarization are formed, as illustrated in Fig. 3a. Most recently also relaxor behaviour has been observed in the dabco monosalts [36]. In the relaxor materials, small nano-sized domains are formed, which have properties considerably different from the bulk of the crystal (see Fig. 3b). The structure of these domains may be different, although it should be stabilized by their surroundings. The properties of these nanoregions can considerably influence the macroscopic properties of the crystal, which despite the

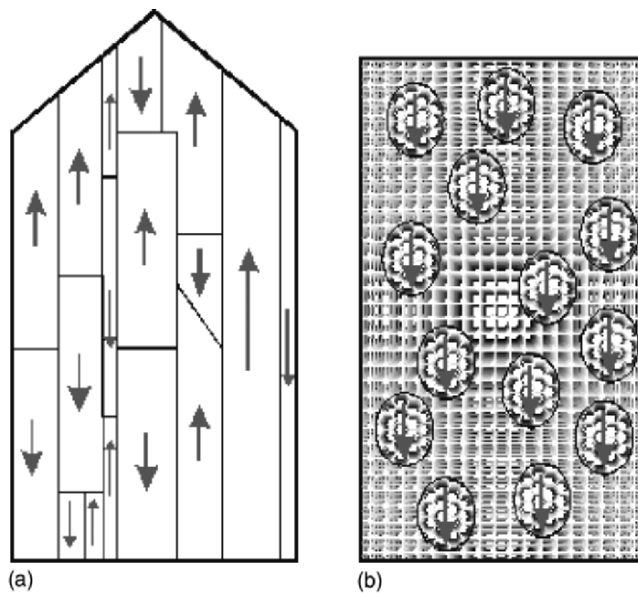


Figure 3 (see color section). A schematic illustration of the domain structure in a ferroelectric crystal (a), and of a relaxor with the polarization of nanoregions pooled in one direction (b).

centrosymmetric bulk structure can exhibit a considerable polarization. Inorganic relaxors based on inorganic mixed perovskite structures find numerous applications in electronics.

9 CONCLUSIONS

It can be shown that certain characteristics are common to all the hydrogen-bonded materials. Although this chapter has been mainly focused on the KDP-type crystals, the hydrogen bonds may transform also in different manners than the H-hopping from one site to the other over the energy barrier. For example, one can apply similar criteria to the structures where the H-atom is moved to the other site of the hydrogen bond over the potential energy barrier separating the two energy wells, such as the transformation between two static H-bonds (i.e., in 1,3-cyclohexanedione phases), or between the static and dynamic disorder in H₂O ices [37], or in HCl crystals where the dynamics of the disordered phases is dominated by the rotations of the molecules, and in alcohols or other materials, such as orthoboric acid H₃BO₃, where the hydrogen-bonded groups rotate [22]. Relatively simple principles govern the contribution of the hydrogen bonds to the thermal expansion of the crystals, and it is possible to predict several properties of these materials. For example, it is possible to determine accurately the tricritical point for KDP-type ferroelectrics, or to assess the temperature of paraelectric–ferroelectric phase transitions from the structural data. Thus it appears that structural transformations of hydrogen bonds, often regarded as weak and complex interactions difficult for theoretical description, can be successfully predicted for various substances and at varied thermodynamical conditions. This information can be further applied for understanding the behaviour and properties of any materials with hydrogen-bonded aggregates in their structure. The understanding of the structure–property relations for hydrogen-bonded crystals can also prove useful for understanding the functions of H-bonds in biological systems, and for validating results of structural analysis.

By no means, this short chapter could include all the types of hydrogen-bonded materials, or all types of transformations of hydrogen bonds. It was only aimed to present very briefly a few selected examples, and only one structural approach to the structural transformations has been presented. Some of the important classes of hydrogen-bonded materials have not been even mentioned, for example the hydrogen-bonded ionic conductors [38–40].

REFERENCES

1. Jeffrey, G.A. and Saenger, W. (1991). *Hydrogen Bonding in Biological Structures*. Springer-Verlag, Berlin, Heidelberg.
2. Donohue, J. (1968). Selected topics in hydrogen bonding. In *Structural Chemistry and Molecular Biology* (Eds. A. Rich and N. Davison). Freeman, San Francisco. pp. 443–465.

3. Dalal, N., Klymachyov, A. and Bussmann-Holder, A. (1998). Coexistence of order–disorder and displacive features at the phase transitions in hydrogen-bonded solids: squaric acid and its analogs. *Phys. Rev. Lett.* **81**, 5924–5927.
4. Hantzsch, A. (1915). Die Chromoisomerie der *p*-Dioxy-terephthalsäure-Derivate als Phenol–Enol–Isomerie. *Ber. Deutschen Chem. Ges.* **48**, 797–816.
5. Byrn, S.R., Curtin, D.Y. and Paul, I.C. (1972). The X-ray crystal structures of the yellow and white forms of dimethyl-3,6-dichloro-2,5-dihydroxyterephthalene and a study of the conversion of the yellow form to the white form in the solid state. *J. Am. Chem. Soc.* **94**, 890–898.
6. Richardson, M.R., Yang, Q., Novotny-Begger, E. and Dunitz, D.J. (1990). Conformational polymorphism of dimethyl 3,6-dichloro-2,5-dihydroxyterephthalate. II. Structural, thermodynamic, kinetic and mechanistic aspects of phase transformations among the three crystal forms. *Acta Cryst. B* **46**, 653–660.
7. Yang, Q.-C., Richardson, M.F. and Dunitz, J.D. (1989). Conformational polymorphism of 3,6-dichloro-2,5-dihydroxyterephthalate. I. Structures and atomic displacement parameters between 100 and 350 K for three crystal forms. *Acta Cryst. B* **45**, 312–323.
8. Ceolin, R., Toscani, S., Agafonov, V. and Dugne, J. (1992). Phenomenology of polymorphism. I. Pressure–temperature representation of trimorphism: general rules; application to the case of 3,6-dichloro-2,5-dihydroxyterephthalate. *J. Solid State Chem.* **98**, 366–378.
9. Głowiak, T. and Sobczak, J.M. (1992). Crystal and molecular structure of 1-phenyl-3-(2-hydroxyphenylamino)-2-buten-1-one. *J. Crystallogr. Spectr. Res.* **22**, 673–678.
10. Yu, L., Stephenson, G.A., Mitchell, C.A., Bunnell, C.A., Snorek, S.V., Bowyer, J., Borchardt, T.B., Stowell, J.G. and Byrn, S.R. (2000). Thermochemistry and conformational polymorphism of a hexamorphic crystal system. *J. Am. Chem. Soc.* **122**, 585–591.
11. Stephenson, G.A., Borchardt, T.B., Byrn, S.R., Bowyer, J., Bunnell, S.A., Snorek, S.V. and Yu, L. (1995). Conformational and color polymorphism of 5-methyl-2-[(2-nitrophenyl) amino]-3-thiophenecarbonitrile. *J. Pharm. Sci.* **84**, 1385–1386.
12. Yu, L. (2002). Color changes caused by conformational polymorphism: optical crystallography, single-crystal spectroscopy, and computational chemistry. *J. Phys. Chem. A* **106**, 544–550.
13. Ogawa, K., Kasahara, Y., Ohtani, Y. and Harada, J. (1998). Crystal structure change for the thermochromy of N-salicylideneanilines. The first observation by X-ray diffraction. *J. Am. Chem. Soc.* **120**, 7107–7108.
14. Herstein, F.H., Kapon, M., Reisner, G.M., Lehmann, M.S., Kress, R.B., Wilson, R.B., Shiau, W.-L., Duesler, E.N., Paul, I.C. and Curtin, D.Y. (1985). Polymorphism of naphthazarin and its relation to solid-state proton transfer. Neutron and X-ray diffraction studies of naphthazarin. *Proc. Royal Soc. London A* **399**, 295–319.
15. Katrusiak, A. (1996). Macroscopic and structural effects of hydrogen-bond transformations. *Crystallogr. Rev.* **5**, 133–180.
16. Katrusiak, A. (1993). Geometric effects of H-atom disordering in hydrogen-bonded ferroelectrics. *Phys. Rev. B* **48**, 2992–3002.
17. Katrusiak, A. (1995). Coupling of displacive and order–disorder transformations in hydrogen-bonded ferroelectrics. *Phys. Rev. B* **51**, 589–592.
18. Tajima, Y., Matsuo, T. and Suga, H. (1984). Calorimetric study of phase transition in hexagonal ice doped with alkali hydroxides. *J. Phys. Chem. Solids* **45**, 1135–1144.
19. Katrusiak, A. (1990). High-pressure X-ray diffraction study on the structure and phase transition of 1,3-cyclohexanedione crystals. *Acta Cryst. B* **46**, 246–256.
20. Katrusiak, A. (1991). Structure and phase transition of 1,3-cyclohexanedione crystals as a function of temperature. *Acta Cryst. B* **47**, 398–404.
21. Katrusiak, A. (1992). Stereochemistry and transformation of –OH–O= hydrogen bonds. Part I. Polymorphism and phase transition of 1,3-cyclohexanedione crystals. *J. Mol. Struct.* **269**, 329–354.

22. Katrusiak, A. (1998). Modelling hydrogen-bonded crystal structures beyond resolution of diffraction methods. *Pol. J. Chem.* **72**, 449–459.
23. Katrusiak, A. (1999). Stereochemistry and transformations of NH–N hydrogen bonds. Part I. Structural preferences for the H-site. *J. Mol. Struct.* **474**, 125–133.
24. Slater, J.C. (1941). Theory of the transition in KH_2PO_4 . *J. Chem. Phys.* **9**, 16–33.
25. Katrusiak, A. (1996). Stereochemistry and transformation of –OH–O= hydrogen bonds. Part II. Evaluation of T_c in hydrogen-bonded ferroelectrics from structural data. *J. Mol. Struct.* **374**, 177–189.
26. Ichikawa, M. (1978). The O–H vs. O···O distance correlation, the geometric isotope effect in OHO bonds, and its application to symmetric bonds. *Acta Cryst. B* **34**, 2074–2080.
27. Kobayashi, J., Uesu, Y., Mizutani, I. and Enomoto, Y. (1970). X-ray study on the thermal expansion of ferroelectric KH_2PO_4 . *Phys. stat. solidi (a)* **3**, 63–69.
28. Landau, L.D. (1937). On the theory of phase transitions I. *Zh. Eksp. Teoret. Fiz.* **7**, 19–32 [in Russian]; *Sov. Phys. JETP* **26**.
29. Landau, L.D. and Lifschitz, E.M. (1976). *Statisticheskaya Fizika*. Izdatielstvo Nauka, Moscow, p. 536.
30. Katrusiak, A. (1996). Structural origin of tricritical point in KDP-type ferroelectrics. *Ferroelectrics* **188**, 5–10.
31. Bastie, P., Vallade, M., Vettur, C., Zeyen, C.M.E. and Meister, H. (1981). Neutron diffractometry investigation of the tricritical point of KH_2PO_4 . *J. Physique* **42**, 445–458.
32. Schmidt, V.H., Western, A.B. and Baker, A.G. (1976). Tricritical point in KH_2PO_4 . *Phys. Rev. Lett.* **37**, 839–842.
33. Szafranski, M., Katrusiak, A. and McIntyre, G.J. (2002). Ferroelectric order of parallel bistable hydrogen bonds. *Phys. Rev. Lett.* **89**, 215507-1–4.
34. Szafranski, M. and Katrusiak, A. (2000). Thermodynamic behaviour of bistable $\text{NH}^+–\text{N}$ hydrogen bonds in monosalts of 1,4-diazabicyclo[2.2.2]octane. *Chem. Phys. Lett.* **318**, 427–432.
35. Katrusiak, A. and Szafranski, M. (1999). Ferroelectricity in NH–N hydrogen-bonded crystals. *Phys. Rev. Lett.* **82**, 576–579.
36. Szafranski, M. and Katrusiak, A. (2004). Short-range ferroelectric order induced by proton transfer-mediated ionicity. *J. Phys. Chem.* **108**, 15709–15713.
37. Katrusiak, A. (1996d). Rigid H_2O molecule model of anomalous thermal expansion of ices. *Phys. Rev. Lett.* **77**, 4366–4369.
38. Pavlenko, N.I. (2000). Peierls instabilities in quasi-one-dimensional quantum double-well chains. *Phys. Rev. B* **61**, 4988–4993.
39. Pavlenko, N.I. (2000). Proton hopping conductivity in quasi-one-dimensional hydrogen-bonded chains. *Phys. Stat. Solidi B* **218**, 295–298.
40. Pietraszko, A., Hilczer, B. and Pawlowski, A. (1999). Structural aspects of fast proton transport in $(\text{NH}_4)_3\text{H}(\text{SeO}_4)_2$ single crystals. *Solid State Ionics* **119**, 281–288.

CHAPTER 14

UNREVEALING THE NATURE OF HYDROGEN BONDS: π -ELECTRON DELOCALIZATION SHAPES H-BOND FEATURES

Intramolecular and Intermolecular Resonance-Assisted Hydrogen Bonds

SŁAWOMIR J. GRABOWSKI^{1,2} and JERZY LESZCZYŃSKI²

¹*Department of Physics and Chemistry, University of Łódź, ul.Pomorska 149/153, 90-236 Łódź, Poland*

²*Computational Center for Molecular Structure and Interactions, Department of Chemistry, Jackson State University, Jackson, MS 39217, USA*

Abstract In this chapter we discuss the influence of π -electron delocalization on the properties of H-bonds. Hence the so-called resonance-assisted hydrogen bonds (RAHBs) are characterized since such systems are mainly classified in the literature as those where π -electron delocalization plays a very important role. Both the intramolecular and intermolecular RAHBs are described. RAHBs are often indicated as very strong interactions; thus, their possible covalent nature is also discussed. Examples of the representative crystal structures as well as the results of the ab initio and DFT calculations are presented. Additionally the RAHB systems, and the other complexes where π -electron delocalization effects are detectable, are characterized with the use of the QTAIM (Quantum Theory “Atoms in Molecules”) method. The decomposition scheme of the interaction energy is applied to expand the knowledge of the nature of the RAHBs.

Keywords: Resonance-assisted hydrogen bond (RAHB); electron density; intramolecular H-bonds; intermolecular H-bonds π -electron delocalization; topological parameters; critical points; QTAM (Quantum Theory “Atoms in Molecules” method); covalent hydrogen bonds; interaction energy decomposition scheme.

1 INTRODUCTION

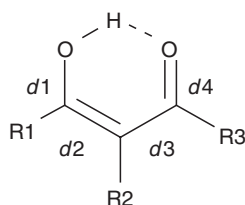
Among many leading factors, π -electron delocalization is a very common effect influencing the characteristics of molecules and very often participating in chemical and biochemical processes [1, 2]. The influence of π -electron

delocalization on intramolecular and intermolecular interactions was also noticed [2, 3]. Among various types of interactions the hydrogen bond plays a special role [1, 4] as discussed in all chapters of this volume. Hence the influence of π -electron delocalization on hydrogen bonding interactions is the subject of this chapter. The latter interrelation is known in literature as a special type of cooperativity [1], and hydrogen bonds where such an effect exists are called resonance-assisted hydrogen bonds (RAHBs) [5]. The first observations connected with the concept of RAHB are those of Huggins [6] who analyzed the $\text{O}-\text{H}\cdots\text{O}=\text{C}$ chains in carboxylic acids and carboxylate hydrates. Also Coulson has found that because of chains of molecules connected through $\text{O}-\text{H}\cdots\text{O}$ bonds the $\text{O}\cdots\text{O}$ distance in crystals of β -oxalic acid is decreased from 2.8 to 2.5 Å [7]. This indicates that H-bonds are stronger due to such connections. It was also pointed out that for the cyclic dimers of carboxylic acids the double hydrogen bonding is stronger due to the effect of resonance, resulting from the existence of two resonance forms [8]. The centrosymmetric dimers of carboxylic acids were later classified as one of the most frequently occurring types of RAHB [5]. Emsley [3] has found that for the $\text{HO}-\text{C}=\text{C}=\text{O}$ conjugated systems the π -electron delocalization is greater if an intramolecular H-bond or a chain of intermolecular H-bonds exist. In other words, the H-bond interaction enhances the effect of π -electron delocalization. This is, for example, observed for the chain of β -diketone molecules.

Gilli and coworkers postulated the reverse dependence as one of the main features of RAHBs. This means that the π -electron delocalization causes a strengthening of the hydrogen bond [5, 9]. Their statement was contested in recent studies; hence, the idea of an RAHB type of interaction was questioned [10, 11]. However, in our opinion, the recent findings and reservations need further investigations. Additionally, the RAHB idea provides many results and generalizations useful in different areas of structural chemistry. These are the reasons why, in spite of the recent controversies, the aim of this chapter is to present and to characterize the systems which might be classified as RAHBs. Hydrogen bonds where the π -electron delocalization is detected exist very often in the solid state, in liquids, and in the gas phase, and the description of such species is of continuous interest.

2 INTRAMOLECULAR RAHBs

As was mentioned in the introduction, H-bonds exist within species where π -electron delocalization occurs, among them in RAHBs. These types of systems were analyzed early on. However, the systematization of such interactions was given in detail by Gilli and coworkers [5, 9]. The authors characterized the features of homonuclear $\text{O}-\text{H}\cdots\text{O}$ intramolecular RAHBs. For example, H-bonds in malonaldehyde and its simple derivatives may be classified as RAHBs since a system of conjugated double and single bonds are contained there (Scheme 1).



Scheme 1

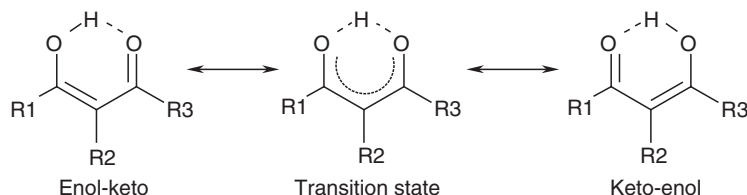
The characteristics of the intramolecular O–H···O RAHBs summarized by Gilli and coworkers are as follows:

- there is equalization of the $d2$ and $d3$ bond lengths,
- there is equalization of the $d4$ and $d1$ bond lengths, and
- as an effect of π -electron delocalization and the equalization mentioned above of the corresponding bonds, there is a strengthening of the O–H···O bond leading to a shortening of the O···O distance.

It was also pointed out that in extreme cases there is a movement of the proton toward the middle of the O···O distance, shortening of the latter to 2.4 Å or even less and hence causing equalization of the H···O contact and the O–H bond. Such extreme cases are characterized as short strong hydrogen bonds (SSHBs) [12]. Two geometrical parameters, being in principle the internal coordinates, were introduced: $q1 = d1 - d4$ and $q2 = d3 - d2$. Linear relationship between them was found. The Q -parameter ($Q = q1 + q2$) may be treated as the descriptor of the π -electron delocalization. Gilli and coworkers also introduced the λ -parameter (see Chapt. 2 of this volume).

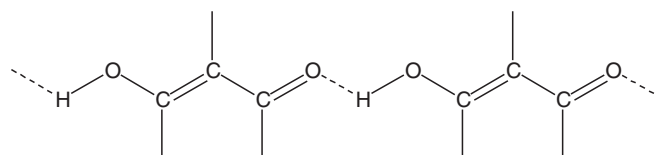
$$(1) \quad \lambda = (1 - Q/Q_0)/2$$

Q_0 is calculated in the same way as the Q -value but relates to the single and double reference CO and CC bonds, theoretically the bonds not involved in the conjugated system of double and single bonds. Q_0 amounts to 0.320 according to the early reference bonds proposed by Gilli and coworkers [9]. The λ -parameter is a descriptor which, similar to the Q -parameter, indicates the degree of the π -electron delocalization. If it is equal to 0, then it corresponds to the enol–keto form; $\lambda = 1$ stands for the keto–enol form; and $\lambda = 1/2$ corresponds to the full equalization of the bond lengths mentioned above. The latter is also applied to the transition state of the C–O–H···O=C \leftrightarrow C=O···H–O–C proton transfer reaction (Scheme 2).



Scheme 2

There is no difference between the enol–keto and keto–enol O–H...O H-bridge and no difference for the double–single conjugated bonds, especially if R1 and R3 substituents are equivalent. Hence Buemi and Zuccarello [13] proposed to use $\lambda = (1 - Q/Q_0)$ since in such a case 0 corresponds to the system with the lack of π -electron delocalization and $\lambda = 1$ to the full delocalization with the movement of H-atom to the middle of O...O distance or nearly so. It is worth mentioning that, similar for intramolecular H-bonds, an enhancement of H-bond strength may be observed for intermolecular interactions [3, 5]. Scheme 3 presents an example of a system often found in crystal structures.



Scheme 3

Bertolasi et al. [9] analyzed the influence of substituents on the stability of tautomeric forms of intramolecular RAHB systems (Scheme 1). They have stated that the enol–keto form (Scheme 2) is stabilized by the following factors: R1 is the electron-withdrawing substituent; R3 is the electron-donating substituent; or there is an additional H-bond between the outer proton-donating species and the C=O carbonyl group acting as an acceptor. These statements were partly supported by the results of *ab initio* calculations. The fluoro and chloro derivatives of malonaldehyde (R1, R2, R3 = H, Cl, F) were analyzed at the MP2/6-311++G(*d,p*) level of approximation [14]. Table 1 presents some of the geometrical and topological parameters for these species.

These results are in excellent agreement with the statements presented by Bertolasi et al. [9]. One can observe the interrelation between all collected parameters. For the strongest H-bonds there is the greatest elongation of the O–H proton donating bond. This is for R1 = F or Cl—the electron-withdrawing substituents. For these species also the H...O contacts are the shortest, and also the systems are closer to linearity than the other ones.

The Bader theory [15] was also applied for the systems collected in Table 1. It is well known that electron density at the proton...acceptor bond critical point (BCP) correlates with the H-bond energy and other parameters describing the H-bond strength [16] (Chaps. 1, 3, and 9). The latter value, $\rho_{\text{H}\cdots\text{O}}$, is the greatest for R1 = F and Cl (enol–keto form, Scheme 2). It is worth mentioning that the Q -parameter reflecting the π -electron delocalization is the smallest one for these RAHBs. For greater π -electron delocalization, there is a higher degree of equalization of the corresponding bonds, and the hydrogen bond is stronger.

Also the R3 substituent, if this is the electron-donating group, should cause greater π -electron delocalization of the RAHB system. Table 1 shows the action of the R3 electron-withdrawing substituents, Cl and F, which should

Table 1. Geometrical (in Å, degrees) and topological (a.u.) parameters for O–H···O H-bonds of malonaldehyde and its derivatives

R1, R2, R3	Q	O–H	H···O	O–H···O	$\rho_{\text{H}\cdots\text{O}}$	$\nabla^2\rho_{\text{H}\cdots\text{O}}$
H, H, H	0.160	0.992	1.687	148.4	0.050	0.139
H, F, H	0.184	0.984	1.776	145.8	0.040	0.123
H, Cl, H	0.178	0.988	1.717	147.1	0.046	0.135
H, H, F	0.210	0.980	1.825	143.8	0.035	0.116
H, H, Cl	0.191	0.981	1.793	144.3	0.038	0.122
F, H, H	0.083	1.049	1.449	155.0	0.091	0.139
Cl, H, H	0.121	1.020	1.540	153.2	0.072	0.150

act on opposite sides as the electron-donating substituents. F and Cl should hamper the π -electron delocalization and hence weaken the hydrogen bond. This is supported by the results of Table 1 since for R3 = F and Cl the hydrogen bonds are weakest, and the O–H bond elongations as an effect of H-bond formation are smallest. Besides, the H···O distances being the longest, the systems are far from linearity, and the electron densities at the H···O BCPs are the smallest if one compares them with the other species of Table 1. Figure 1 shows the relationship between the Q -parameter and the electron density at H···O BCP. Since the latter may be treated as a descriptor of the H-bond strength [16], then one may note that the π -electron delocalization enhances the

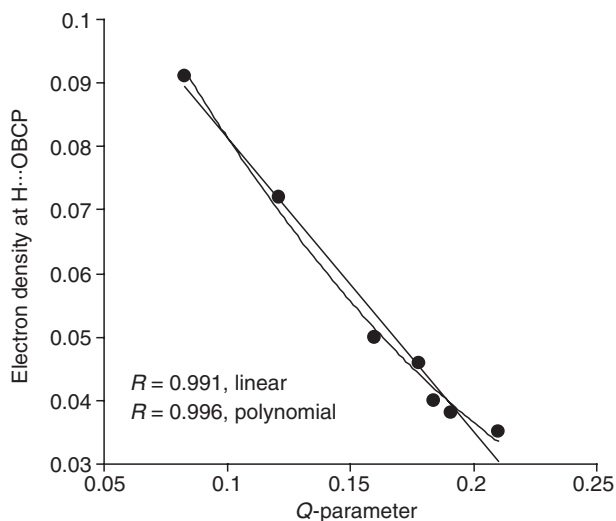


Figure 1. The correlation between the Q -parameter and electron density at H···O BCP (a.u.). The linear correlation coefficient amounts to 0.991 and the correlation coefficient for the second order polynomial regression is equal to 0.996.

H-bond strength. The linear correlation as well as the slightly better polynomial correlation is presented (the polynomial of the second order). Laplacian values of the electron density at $\text{H}\cdots\text{O}$ BCP (Table 1) also confirm the relations mentioned above since they are the greatest for $\text{R1} = \text{F}$ and Cl and the smallest for $\text{R3} = \text{F}$ and Cl .

It is worth mentioning that the RAHB systems are often found and investigated in crystal structures of organic compounds. Gilli et al. [5] have found similar dependencies as that presented in Fig. 1. They have taken into account the components of crystal structures containing a β -diketone fragment involved in intramolecular or intermolecular RAHB. For such a sample they have found the relationship presented in Fig. 2. This figure displays the dependence between the λ -parameter and $\text{O}\cdots\text{O}$ distance described above. Since the first parameter corresponds to the π -electron delocalization and the second one roughly reflects the H-bond strength, this relation reflects the same findings as those depicted in Fig. 1.

It is worth mentioning that six-membered rings, among them those classified as RAHBs, are very common in crystal structures. Etter [17] has pointed out that hydrogen bonds as relatively strong interactions influence the arrangement of molecules in crystals. She has specified the rules for the existence of that kind

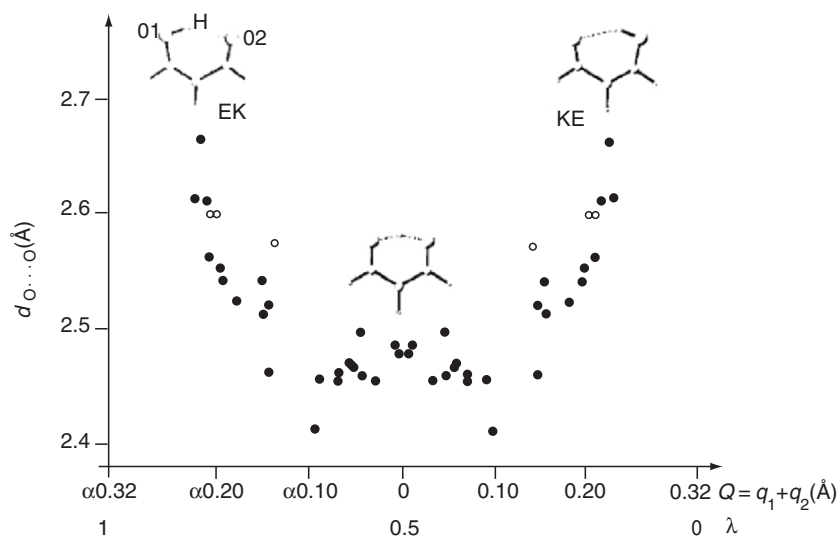


Figure 2. The dependence between the λ -parameter and the $\text{O}\cdots\text{O}$ distance (in Å). The enol–keto form corresponds to the λ -values close to unity and the keto–enol form to that value close to zero. The full equalization of CC and CO bonds is for λ -values equal to 0.5. Full circles designate the systems with intramolecular RAHBs while empty circles the intermolecular RAHBs. The Q -parameter is also indicated. (Reprinted with permission from Ref. [5]. Copyright 1989 American Chemical Society.)

of interaction in crystals. The main rules are as follows: all good proton donors and good acceptors are used in hydrogen bonding; six-membered-ring intramolecular hydrogen bonds form in preference to intermolecular hydrogen bonds; and the best proton donors and acceptors remaining after intramolecular hydrogen-bond formation form intermolecular hydrogen bonds to one another. The terms “good proton donors” and “good proton acceptors” were introduced by Donohue [18]. Good proton donors are those of carboxylic acids, amides, ureas, anilines, imides, and phenols, while good proton acceptors occur for acid and amide carbonyl groups, sulfoxides, phosphoryls, nitroxides, and amine nitrogens.

One can see that the formation of six-membered rings and intramolecular RAHBs should be preferred in crystals. Figure 3 presents an example of such species in the crystal structure of benzylacetone [19].

This is the classical example of RAHB since the H-atom is moved toward the middle of the O···O distance; the O(1)–H(X1) and O(2)–H(X1) bonds are equal to 1.329(11) and 1.245(11) Å, respectively. One can see that it is not exactly the center of the H-bridge. Figure 3 also shows the longest ellipsoid axis of the thermal motion of H(X1) in accordance with the O···O direction. This means that the hydrogen atom is asymmetrically placed in a large potential well. There is also the meaningful equalization of the bonds within the ring since C(2)–O(1), C(4)–O(2), C(2)–C(3), and C(3)–C(4) are equal to 1.286(4), 1.293(4), 1.414(4), and 1.405(4) Å, respectively. For the crystal structure of benzylacetone the charge density obtained from X-ray and neutron diffraction measurements has also been analyzed using multipolar refinement and topological

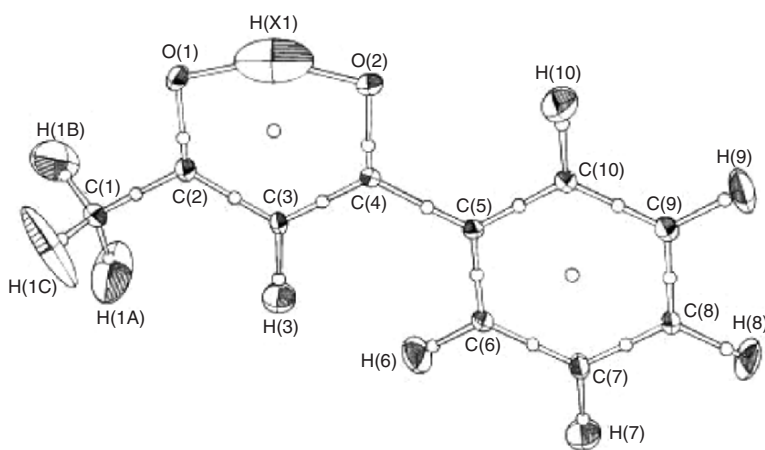


Figure 3. The molecular structure of benzylacetone showing atom numbering and 50% probability ellipsoids determined by refinement of the 20K neutron data. Open circles correspond to critical points determined in the topological analysis. (Reprinted with permission from Ref. [19]. Copyright 1998 American Chemical Society.)

analysis based on “the atoms in molecules” (AIM) theory. It is important to note that for both H···O interactions (H(X1)–O(1) and H(X1)–O(2)) the Laplacian of electron density at the corresponding H···O bond critical points is negative. It is for the shorter H···O distance, e.g., covalent bond, as well as for the longer one, e.g., H-bond contact. Interestingly, this supports the idea of the covalent nature of some strong hydrogen bonds.

The idea of the covalent nature of short H-bonds is analyzed later in this chapter in detail. This is not a new idea, originally claimed by Pauling [20] who stated the covalent nature of the H-bond for the (FHF)[−] ion. The covalency of H-bonds was also discussed early on by Coulson and Danielsson [21]; and this topic was analyzed in more recent studies [22]. Gilli et al. [23] introduced the so-called electrostatic-covalent H-bond model (ECHBM) where the following features were summarized:

- weak H-bonds are electrostatic interactions but become increasingly covalent if their strength increases,
- very strong H-bonds are in principle three-center–four-electron covalent bonds,
- the strongest H-bonds should be homonuclear and symmetrical since only in such a case two valence bond resonance forms are isoenergetic and may mix effectively,
- the last statement may be expressed as the condition of minimum difference between the proton acceptor and the proton donor affinities.

The authors also indicated that there are three ways to make a H-bond stronger, particularly an interaction where the covalent nature is detected: by addition of an electron, by its rejection, and by π -electron delocalization. In such a way one can point out three types of H-bonds: negatively charge-assisted H-bonds (CAHB(−)), positively charge-assisted H-bonds (CAHB(+)), and RAHBs. The latter are analyzed in this chapter.

3 HETERONUCLEAR INTRAMOLECULAR RESONANCE-ASSISTED HYDROGEN BONDS

It was pointed out in the previous section that the effective mixing of two RAHB tautomeric forms leads to the enhancement of H-bond strength since it is connected with greater π -electron delocalization. This may be fulfilled effectively for homonuclear H-bonds such as O–H···O systems. According to these conditions, heteronuclear hydrogen bonds are not as strong as homonuclear bonds. However, the occurrence of heteronuclear RAHBs in crystal structures and especially their role in different processes, among them biochemical reactions, is well known [1]. Crystal structures where N–H···O RAHBs exist were often investigated. Among them are ketohydrazone [24], nitrosoenamines [24b], cumarine derivatives and chromone derivatives [25], and other classes of compounds investigated with the use of neutron and X-ray diffraction techniques.

The phosphorohydrazone derivatives of chromone seem to be very interesting due to their potential biological activity and the possible application in cancer chemotherapy. Figures 4 and 5 present the molecular structures of two such compounds: (*E*)-3-{[(diphenoxyphosphoryl)-2-methylhydrazone]-methylene}-

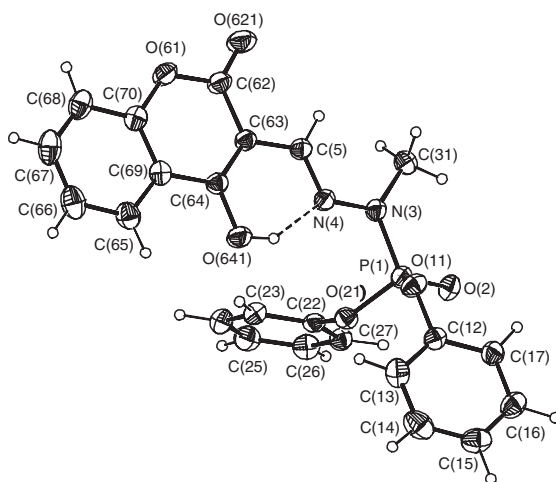


Figure 4. The molecular structure of **1** with an atom labeling scheme. The displacement ellipsoids are drawn at 30% probability level. (Reprinted with permission from Ref. [25a]. Copyright 2002 American Chemical Society.)

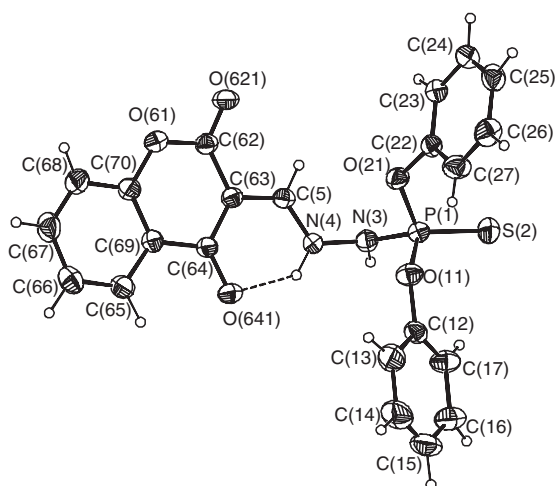
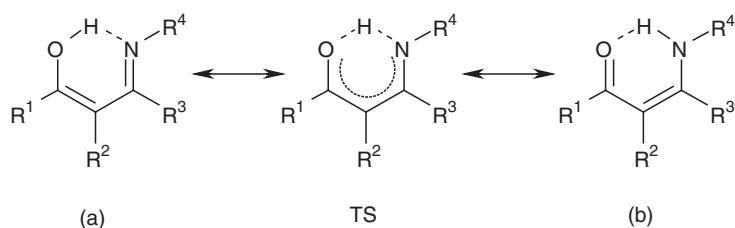


Figure 5. The molecular structure of **2** with an atom labeling scheme. The displacement ellipsoids are drawn at a 30% probability level. (Reprinted with permission from Ref. [25a]. Copyright 2002 American Chemical Society.)

4-hydroxy-2*H*-1-benzopyran-2-one (**1**) and 3-[[[(diphenoxythio-phosphoryl)-hydrazine]-methylidene]-3,4-dihydro-2*H*-1-benzopyran-2,4-dione (**2**) which have been determined by the X-ray diffraction method [25a]. One can observe the existence of six-membered rings with intramolecular H-bonds for both structures, O–H···N for structure **1** and N–H···O for structure **2**.

One can see that there is only a slight difference between the N-substituents of the molecular structures **1** and **2**. This indicates that this kind of substituent may strongly effect the proton affinity of the nitrogen atom and influence the N–H···O or O–H···N types of H-bond interactions (Scheme 4). The only difference between the structures analyzed here, except for the intramolecular H-bond mentioned above, is the R4 substituent which is N(CH₃)–P(O)(OC₆H₅)₂ for **1** and NH–P(S)(OC₆H₅)₂ for **2**.



Scheme 4

This is in line with the approach of Bürgi and Dunitz [26] that each of the crystal structures may be treated as a frozen state corresponding to the particular stage of the reaction. Accordingly the **1** and **2** crystal structures correspond to different stages of the reaction of the proton transfer: N···H–O ⇌ N–H···O. In order to explain the influence of substituents on the proton affinities of nitrogen and oxygen atoms, model ab initio calculations were performed [25a]. The simple enaminones were considered. Table 2 shows the geometrical

Table 2. The geometrical (in Å and degrees) and energetic (kcal/mol) parameters for two tautomeric forms of the simple enaminones; the results for transition states of corresponding proton transfer reactions are also included; there is also the difference in energies between the considered system and the most energetically stable system (hence 0 designates the most stable system)

R1, R2, R3, R4	Form	O···N	∠O···H···N	Difference
H, H, H, H	a	2.580	148.0	5.9
	TS	2.390	152.7	8.4
	b	2.705	128.2	0
F, H, H, H	b	2.765	125.0	–
	a	2.668	141.3	0
H, H, H, F	TS	2.367	142.8	11.8
	b	2.591	118.5	8.8
	a	2.813	141.3	–

and energetic parameters for the corresponding intramolecular H-bonds of the selected systems optimized within the MP2/6-311++G(*d,p*) level of theory. One can see that for the unsubstituted species (all R are hydrogen atoms) the (b) tautomeric form with N–H···O intramolecular H-bond is energetically favorable. The potential barrier height for the proton transfer reaction amounts to 8.4 kcal/mol and the form with the O–H···N hydrogen bond is characterized by an energy higher by 5.9 kcal/mol than for form (b). If the R1 substituent is a fluorine atom, then only form (b) exists since such a substituent decreases the proton affinity of the oxygen atom. As a result the H-atom is covalently bonded to nitrogen, and form (a) does not exist at all. The optimizations performed for the latter form lead to form (b); in other words, form (a) collapses into form (b). The other interesting results are for R4 substituents attached to nitrogen. If R4 is an F-atom, then form (a) with O–H···N is more stable since the F-substituent decreases the proton affinity of nitrogen. The lithium atom as an electron donating substituent in the R4 position causes an increase in proton affinity of the nitrogen center; hence, only form (b) exists with N–H···O hydrogen bonding.

There are also other interesting results included in Table 2. One can observe that the O···N distances are shorter for systems characterized by higher energies, accordingly the O···H···N angles are greater, closer to linearity. This means that there are stronger hydrogen bonds for the less stable systems. As was pointed out by Gilli et al. [27] this is in line with the Leffler–Hammond rule [28]. The results collected in Table 2 are supported by topological parameters derived from the Bader theory (Table 3). The electron densities at the BCPs correspond to covalent bonds and to proton···acceptor contacts; the corresponding Laplacian values are negative and positive, respectively. In such a way it is possible to detect that, for the unsubstituted species (all R-substituents are H-atoms), the N–H···O hydrogen bond exists. The remaining electron densities and Laplacians are in excellent agreement with

Table 3. The topological (in a.u.) parameters for two tautomeric forms of simple enamines; the results for the transition states of corresponding proton transfer reactions are also included; the electron densities at BCPs and their Laplacians for H···O and H···N interactions are considered

R1, R2, R3, R4	Form	$\rho(\text{O,H})$	$\rho(\text{N,H})$	$\nabla^2\rho(\text{O,H})$	$\nabla^2\rho(\text{N,H})$
H, H, H, H	a	0.3153	0.0564	–2.175	0.117
	TS	0.1817	0.1589	–0.379	–0.863
	b	0.0276	0.3287	0.102	–1.825
F, H, H, H	b	0.0219	0.3322	0.084	–1.812
H, H, H, F	a	0.3394	0.0370	–2.413	0.108
	TS	0.1173	0.2225	0.083	–0.086
	b	0.0293	0.3270	0.112	–1.975
H, H, H, Li	b	0.0292	0.3234	0.100	–1.561

the geometrical parameters collected in Table 2, indicating the existence of N–H···O or O–H···N H-bonds. The results concerning transition states are worth mentioning. For all R = H both H···N and H···O interactions are characterized by relatively high values of electron density at BCP. Both corresponding Laplacians are negative, indicating the covalent character of N···H and O···H interactions. The situation is slightly different if the R4 substituent is a fluorine atom. In such a case the proton affinity of nitrogen is decreased causing the movement of a proton to an oxygen atom. For the transition state, the hydrogen is more strongly connected with nitrogen than with oxygen since for the latter interaction the electron density at the corresponding BCP is smaller, and the Laplacian is positive. For the N···H interaction the negative value of Laplacian is predicted indicating the covalent nature of interaction.

It seems that the substituents are very important factors governing the proton affinities of acceptors and donors and hence steer the strength and type of hydrogen bonding. However there are also other factors, for example, the steric effects investigated for the Schiff and Mannich bases [29] as well as the orientation of substituents relative to the remaining fragments of the molecules [30]. The last interrelations were investigated for crystal structures of coumarines with intramolecular N–H···O and O–H···N RAHBs.

Figure 6 shows a very interesting case of phosphorocoumarine [25b] where the bifurcated hydrogen bonds (two donors: C–H and N–H bonds and O-atom as an accepting center) are influenced by the intramolecular O–H···N hydrogen bond (Fig. 6—O(641)–H(641)···N(4)). It is interesting to note that for this structure there is the less often occurring intramolecular O–H···N. It may be explained by the notion that the nitrogen···nitrogen connection N(3) atom being electronegative decreases the proton affinity of the N(4) center, and hence the hydrogen is covalently connected with the O-atom within the resonance-assisted O–H···N hydrogen bond.

It is worth mentioning that there are numerous studies of intramolecular RAHBs. For example, one can refer to the sound studies of Buemi and Zuccarello [13, 31]. There are investigations of homonuclear and heteronuclear intramolecular RAHBs [13, 31, 32], and not only were O–H···O, N–H···O, and O–H···N studied, but also other more “exotic” systems such as O–H···S [33] and intramolecular RAHBs with S, Se, and Te as the proton donors and acceptors [34]. Very recently DFT and ab initio calculations were performed on intramolecular RAHBs with different donors and acceptors [35], and such species containing C–H···Y (Y = O, N, S) were analyzed [35, 36].

It is always of great interest to extend the understanding of the nature of interaction of RAHBs. For this purpose it is possible to apply the scheme of the decomposition of interaction energy. Such an approach was described in Chaps. 4 and 5 of this volume and may be applied for intermolecular interactions. The intermolecular RAHBs will be analyzed in the next sections.

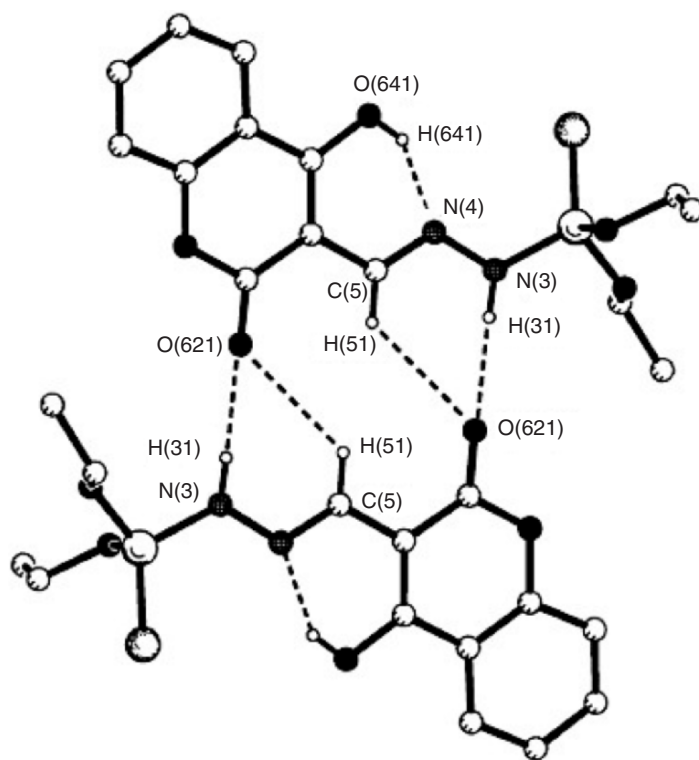


Figure 6. The molecular structure of a dimer of phosphorocoumarine with an atom labeling scheme for H-bonds. There is the bifurcated H-bond with O(621) accepting center and two donating bonds (C(5)–H(51) and N(3)–H(31)—two such connections related through the inversion center) and the RAHB (O(641)–H(641)···N(4)). (Reprinted with permission from Ref. [25b]. Copyright 2003 American Chemical Society.)

4 THE DECOMPOSITION OF INTERACTION ENERGY

It is often stated in different monographs and review articles that hydrogen bonding is an electrostatic interaction [1, 4, 20]. This was pointed out by Pauling and later by others. Deeper insight into the physical nature of interactions of molecular complexes may be obtained by analysis of the interaction energy components. To accomplish this task for hydrogen bonding the results of the decomposition of the interaction energy were presented in previous chapters (Chaps. 4 and 5). It is worth mentioning that the most often applied decomposition scheme is that of Kitaura and Morokuma [37]. According to this approach the Hartree–Fock interaction energy is decomposed in the following way:

$$(2) \quad E(\text{HF}) = \text{ES} + \text{EX} + \text{CT} + \text{POL}$$

The energy correlation term is usually calculated as a difference between the energy calculated within the method taking into account the correlation and the Hartree–Fock energy. For example, for MP2 results,

$$(3) \quad \text{CORR} = E(\text{MP2}) - E(\text{HF})$$

The term ES, the electrostatic energy term, represents the Coulombic interaction energy between the charge distributions of two subunits of the complex considered. EX, the exchange term, corresponds approximately to the steric repulsion of electron clouds. The polarization interaction energy term (POL) is connected with the internal redistribution of the electron density. Charge transfer term CT corresponds to the shift of electron charge between interacting subunits. The term CORR is connected with correlation. For example, EC, EX, POL, CT, and CORR contributions to the binding energy of the water dimer calculated at the MP2/6-31+G(*d,p*) level of approximation and within the Morokuma–Kitaura approach are equal to -7.6 , $+4.2$, -0.7 , -0.9 , and -0.3 kcal/mol, respectively [38]. One can see that the most important attractive interaction energy term for this complex connected through the O–H \cdots O hydrogen bond is the electrostatic term. This is in line with the statement that the H-bond in the interaction is primarily electrostatic in nature.

Despite the fact that the Kitaura–Morokuma approach allows insight into the nature of interaction to be obtained, it has also a lot of limitations. One of the most important is that the binding energy and its components are not free of the basis set superposition error [39]. Another variation-perturbation scheme of the decomposition of the interaction energy was previously proposed [40]. The starting wave functions of the subsystems are obtained in this approach in the dimer-centered basis set (DCBS); hence, the following interaction energy components free of BSSE can be obtained:

$$(4) \quad \Delta E = E_{\text{EL}}^{(1)} + E_{\text{EX}}^{(1)} + E_{\text{DEL}}^{(\text{R})} + E_{\text{CORR}}^{(2)}$$

where $E_{\text{EL}}^{(1)}$ is the first order electrostatic term describing the Coulomb interaction of the static charge distributions of both molecules; $E_{\text{EX}}^{(1)}$ is the repulsive first order exchange component resulting from the Pauli exclusion principle and is defined as the difference of the Heitler–London energy and the electrostatic term. $E_{\text{DEL}}^{(\text{R})}$ and $E_{\text{CORR}}^{(2)}$ correspond to higher order delocalization and correlation terms.

Table 4 presents the results of the decomposition of the interaction energy for different H-bonded systems [41]. The ionic Na⁺Cl[−] system is also included.

One can see that for typical hydrogen bonds, O–H \cdots O and F–H \cdots O for dimer of water and the FH \cdots OCH₂ complex, respectively, the electrostatic term is the most important attractive term. In all of these cases the electrostatic term outweighs the exchange term, and hence the first order interaction energy component $\Delta E^{(1)}$ is negative. This is again in line with conditions that the H-bond is predominantly an electrostatic interaction. Table 4 contains also the

Table 4. The interaction energy terms (in kcal/mol) for various H-bonded complexes, calculations at the MP2/6-311++G(d,p) level of approximation

System	$E_{\text{EL}}^{(1)}$	$E_{\text{EX}}^{(1)}$	$E_{\text{DEL}}^{(R)}$	$E_{\text{CORR}}^{(2)}$	ΔE_{MP2}^*
HOH...OH ₂	-8.750	6.776	-2.190	-0.293	-4.457
FH...OCH ₂	-8.869	5.018	-2.647	1.060	-5.438
HCCH...OH ₂	-4.785	3.386	-1.059	-0.010	-2.468
HCCH... π	-2.126	2.206	-0.544	-0.591	-1.056
Na + Cl ⁻	-142.285	25.285	-10.342	0.181	-127.161

$$*\Delta E_{\text{MP2}} = \Delta E_{\text{SCF}} + E_{\text{CORR}}$$

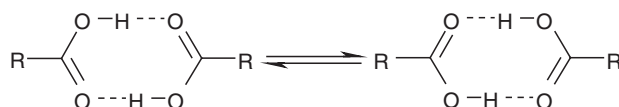
$$\Delta E^{(1)} = E_{\text{EL}}^{(1)} + E_{\text{EX}}^{(1)}, \Delta E_{\text{SCF}} = \Delta E^{(1)} + E_{\text{DEL}}^{(R)}$$

complex with an acetylene molecule as a proton donating system and the O-atom of water as an acceptor center; the complex is connected through the C-H...O H-bond. One can see that in this case the electrostatic term is the most important attractive term and that it outweighs the exchange interaction energy term. In the case of the T-shaped dimer of acetylene, there is the C-H... π interaction where the first order interaction energy component is positive, and the system is stable due to the delocalization and correlation terms. The results for the ionic system, Na⁺Cl⁻, are included in Table 4 for comparison. There is the most important electrostatic interaction energy term and the remaining attractive components: delocalization and correlation are negligible in comparison with the first one. One may observe the same trend for the exchange term which is almost ten times smaller than the electrostatic term. As the main conclusion it may be pointed out that for H-bonded systems the electrostatic component is mainly responsible for the stability of the complex; the other attractive terms are much less important. It is worth mentioning that for hydrogen bonding the difference between the electrostatic term and the remaining attractive terms (delocalization and correlation) is not so high as for ionic interactions.

5 INTERMOLECULAR RESONANCE-ASSISTED HYDROGEN BONDS

There are also intermolecular RAHBs such as those existing in dimeric structures of centrosymmetric carboxylic acids. The intermolecular RAHBs also exist in other systems mentioned by Gilli and coworkers such as amide dimers, amide-amidine couplings, and DNA base pairs [5]. The latter systems were investigated extensively [42] and also in terms of the π -electron delocalization effects [43]. Since it was pointed out that some of the intramolecular homonuclear RAHBs may be treated as partly covalent in nature, the decomposition of the interaction energy for these intermolecular RAHBs provides a powerful tool to better understand the nature of such connections and to investigate what does the term "covalent" exactly mean.

There are several interesting effects connected with carboxylic groups connected through the double O–H···O hydrogen bond. Such effects as dynamic disorder, orientational disorder, and mesomeric effect of the carboxylic group were investigated, especially in crystal structures [44]. The strengthening of hydrogen bonds in these dimers is often the result of the existence of such effects but may be also explained within the conditions related to the RAHBs. For centrosymmetric dimers of carboxylic acids there are often similar effects such as equalization of C=O and C–O bonds for malonaldehyde and its derivatives. One can also observe the double movement of protons to the middle of the O···O distances for extremely strong O–H···O hydrogen bonds. To explain such a situation in terms of the RAHB model one may claim that this is possible if there is an effective mixing of two tautomeric forms (Scheme 5).



Scheme 5

In such a case it is also possible to apply the conditions proposed by Bürgi and Dunitz [26]. The results obtained for the different crystal structures may be treated as the frozen states of the double proton transfer reaction (Scheme 5). Figure 7 displays such a reaction path.

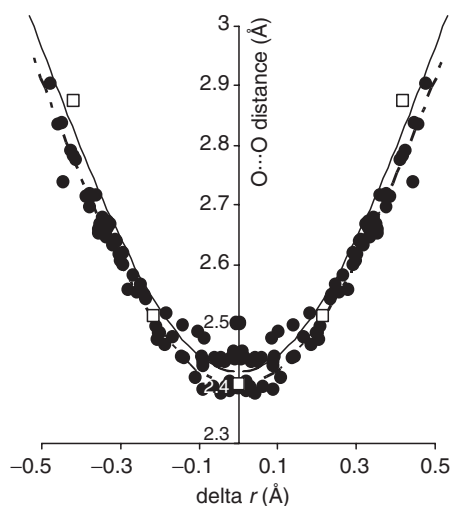


Figure 7. The reaction path for the proton transfer reaction, the variables corresponding to coordinate axes in Å, and empty squares represent ab initio results for the formic acid dimer. The solid line as well as the broken line corresponds to the BV model; for the latter the constants proposed by Gilli et al. were applied. (Reprinted with permission from [Ref. 2]. Copyright 2005 American Chemical Society.)

Full circles (Fig. 7) designate the results obtained by accurate neutron diffraction measurements of crystal structures of organic and metal organic compounds containing the C–O–H···O=C system. The vertical axis indicates the O···O distance for the O–H···O hydrogen bond; the horizontal axis designates the distance of the proton from the middle of O···O. Thus the systems taken from crystal structures and characterized by an O···O distance of about 2.4 Å correspond to the transition state of the proton transfer reaction C–O–H···O=C \leftrightarrow C=O···H–O–C. The solid and broken lines were obtained from the bond valence (BV) model [45] and differ between themselves by the choice of constant parameters. There are also empty squares in Fig. 7 which are the result of high level ab initio calculations on the double proton transfer for the formic acid dimer [46]. One can see that the reaction path (Fig. 7) obtained from the neutron diffraction results is in excellent agreement with the ab initio calculations as well as with the simple semi-empirical BV model.

There have been other investigations of intermolecular RAHBs such as of the pyrrole-2-carboxylic acid (PCA). The infrared and Raman spectroscopic studies of this compound indicate the formation of cyclic dimer species in the solid state [47]. These studies are supported by the results of DFT and ab initio calculations. Three types of dimers of PCA are possible. Figure 8 shows the molecular graphs of those species.

These dimers were analyzed at the B3LYP/6-311+G(*d*) level of approximation, and it was found that the theoretically estimated IR frequencies for the B and C dimers are very close to the experimentally observed absorptions [47]. PCA exists in solution and in the solid state in only one conformation, most likely in the *cis*-form, where the C=O bond of the carboxylic group and the N–H bond of the pyrrole ring are at the same side. This form exists for the B and C dimers. These findings were supported by X-ray crystal structure determination of PCA [48] (Fig. 9) since in crystals both B and C dimers exist while the A dimer does not.

It is worth mentioning that more accurate calculations of these three dimers of PCA were performed at the MP2/6-311++G(*d,p*) and B3LYP/6-311++G(*d,p*) levels of approximation (BSSE included) [48]. It was found that the formation of the A and B dimers leads to significant equalization of the C–O and C=O bonds as an effect of π -electron delocalization. Such an effect is also observed for the C dimer, but it is not as meaningful as for A and B. The H-bond energy (single O–H···O or N–H···O interaction) amounts to -7.9 , -7.4 , and -6.3 kcal/mol for the A, B, and C dimers, respectively (MP2/6-311++G(*d,p*) level). It should be noted that the double proton transfer for the A configuration leads to the B-type dimer. For the corresponding transition state there is practically full equalization of the C=O and C–O bonds since their lengths are equal to 1.270 and 1.282 Å, respectively, at the MP2/6-311++G(*d,p*) level. The difference between the OH bond and the H···O contact for such a transition state disappears. Both corresponding distances are equal to 1.201 Å. Also, the electron densities at both H···O critical points are high, as

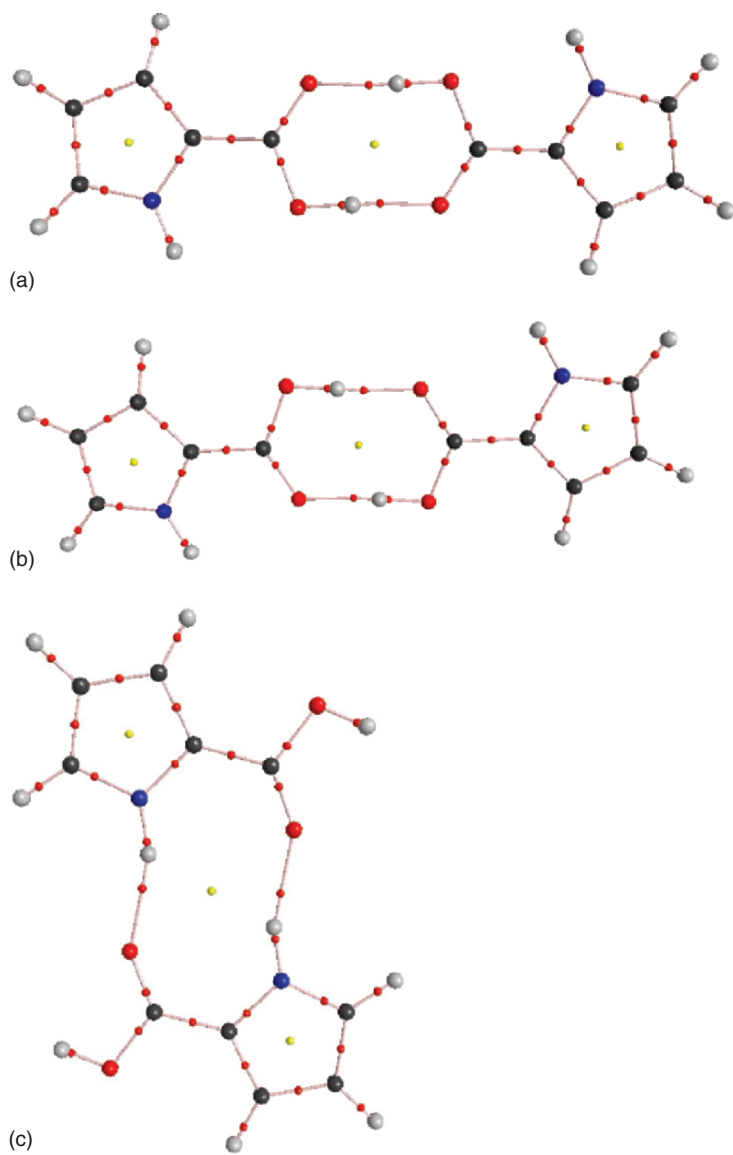


Figure 8. (a) PCA—dimer A. (b) PCA—dimer B. (c) PCA—dimer C. (Reprinted with permission from Ref. [49]. Copyright 2005 American Chemical Society.)

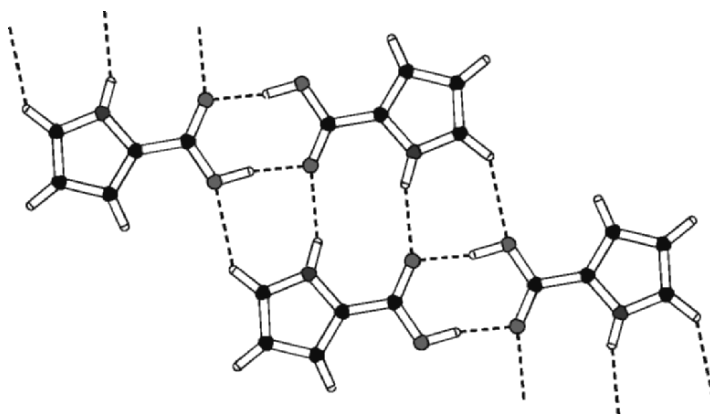


Figure 9. PCA—crystal structure motif containing B and C species. (Reprinted with permission from Ref. [48]. Copyright 2004 American Chemical Society.)

for covalent bonds since they are equal to 0.1734 and 0.1664 a.u. The corresponding Laplacian values amount to -0.3629 and -0.2870 a.u. indicating the covalent nature of both interactions. Gilli et al. [27] have pointed out that such results are in line with the Leffler–Hammond rule that, for systems closer to the transition state, the H-bond interaction is stronger. This is fulfilled for the PCA dimers. For results obtained at the MP2/6-311++G(*d,p*) level the A configuration is slightly closer to TS and the H-bond is stronger here than for the B configuration. For TS the H-bond is strongest as indicated by the displayed topological parameters.

To explore the nature of these intermolecular RAHBs the decomposition of the interaction energy was performed for dimers of PCA as well as for simple centrosymmetric related dimers of formic acid, acetic acid, and formamide [49]. The appropriate results are collected in Table 5. One can observe that for all systems connected through O–H···O H-bonds (formic acid, acetic acid, PCA(A), and PCA(B) dimers) the first order electrostatic interaction energy term is balanced by the exchange term; hence, the first order interaction energy term $\Delta E^{(1)}$ is close to zero, and the other most important attractive term is the delocalization interaction energy. The situation is different for dimers connected through heteronuclear N–H···O bonds (formamide and PCA(C) dimers). In these cases the electrostatic term outweighs the exchange term, and the first order interaction energy term $\Delta E^{(1)}$ is negative. Also the delocalization term is not as significant as it is for homonuclear O–H···O H-bonds.

Hence it seems that for stronger RAHBs the delocalization becomes more important, and the electrostatic interaction energy is less significant than for

Table 5. The interaction energy terms (in kcal/mol) for various PCA dimers and related species, calculations at the MP2/6-311++G(*d,p*) level of approximation

System	$E_{\text{EL}}^{(1)}$	$E_{\text{EX}}^{(1)}$	$E_{\text{DEL}}^{(R)}$	$E_{\text{CORR}}^{(2)}$	ΔE_{MP2}^*
Formic acid	-30.1	30.0	-14.3	0.9	-13.6
Acetic acid	-32.2	32.3	-15.2	0.5	-14.5
Formamide	-23.4	19.8	-8.5	0.0	-12.1
PCA(A)	-36.7	37.6	-18.6	0.6	-17.1
PCA(B)	-34.8	36.1	-17.3	0.3	-15.7
PCA(C)	-19.9	16.1	-6.9	-1.4	-12.1

$$*\Delta E_{\text{MP2}} = \Delta E_{\text{SCF}} + E_{\text{CORR}}$$

$$\Delta E^{(1)} = E_{\text{EL}}^{(1)} + E_{\text{EX}}^{(1)}$$

weaker, mainly heteronuclear N–H···O RAHBs. This may be a common characteristic of H-bonds. For stronger H-bonds with shorter proton···acceptor distances, the nature of such interactions is not mainly electrostatic as was stated by Pauling in the early definition, but the other interaction energy terms are dominant. It was clearly expressed for very strong dihydrogen bonds [41]. For the complex of the hydronium ion as the proton donor and beryllium hydride as an acceptor and simple related complexes, full geometry optimizations were performed. The calculations were performed using the second order Møller–Plesset perturbation method (MP2) [50]. The 6-311++G(*d,p*) basis set [51] was used; 6-311++G(*d,p*) as well as the Dunning type basis sets [52] were applied: aug-cc-pVDZ and aug-cc-pVTZ. Full optimizations have been performed at the MP2/6-311++G(*d,p*) and MP2/aug-cc-pVDZ levels of theory. All results of these optimizations correspond to energy minima since no imaginary frequencies were found. The single point MP2 calculations have been carried out with the aug-cc-pVTZ basis set and for the reference geometry as optimized at the MP2/aug-cc-pVDZ level of theory. Figure 10 shows the molecular graph of the simplest complex of hydronium ion and beryllium species –Be₂H₂.

Table 6 presents the results of the decomposition of the interaction energy. These are very interesting findings. The binding energies were calculated within

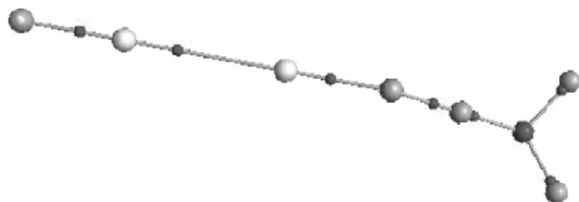


Figure 10. The molecular graph of the H₂OH⁺···HBeBeH complex; big circles correspond to attractors, small ones to bond critical points. (Reprinted with permission from Ref. [41]. Copyright 2005 American Chemical Society.)

Table 6. The interaction energy terms (in kcal/mol) for the $\text{H}_2\text{OH}^+ \cdots \text{HBeH}$ complex and related species, calculations at the MP2/aug-cc-pVTZ level of approximation

System	$E_{\text{EL}}^{(1)}$	$E_{\text{EX}}^{(1)}$	$E_{\text{DEL}}^{(R)}$	$E_{\text{CORR}}^{(2)}$	ΔE_{MP2}^*
$\text{H}_2\text{OH}^+ \cdots \text{HBeH}$	-12.0	19.9	-24.4	-4.2	-20.8
$\text{H}_2\text{OH}^+ \cdots \text{HBeBeH}$	-16.9	27.6	-37.0	-5.0	-31.3
$\text{H}_2\text{OH}^+ \cdots \text{HBeF}$	-6.5	16.6	-20.2	-4.6	-15.1
$\text{HClOH}^+ \cdots \text{HBeH}$	-12.5	26.1	-32.7	-6.3	-25.4
$\text{Cl}_2\text{OH}^+ \cdots \text{HBeH}$	-12.8	33.4	-45.7	-8.3	-33.4
$\text{Cl}_2\text{OH}^+ \cdots \text{HBeF}$	-7.0	27.4	-34.7	-8.9	-23.2

$$*\Delta E_{\text{MP2}} = \Delta E_{\text{SCF}} + E_{\text{CORR}}$$

$$\Delta E^{(1)} = E_{\text{EL}}^{(1)} + E_{\text{EX}}^{(1)}$$

the supermolecular approach; as a result, the deformation energy of the complexation is not taken into account. One can see that for some of the systems the absolute value of the binding energy exceeds 30 kcal/mol. Additionally, for all cases, the first order interaction energy term is positive since the exchange term prevails over the electrostatic term, and the delocalization is mostly responsible for the stability of the systems considered.

Figure 11 presents the dependencies between the $\text{H} \cdots \text{H}$ intermolecular distance: proton \cdots acceptor (acceptor is the negatively charged hydrogen atom) and the interaction energy components.

One can see that the delocalization and exchange components are mainly responsible for the strength of the analyzed dihydrogen bonds since these terms correlate with the $\text{H} \cdots \text{H}$ distance. These terms increase (their absolute values) with a decrease in intermolecular distance. The other attractive terms

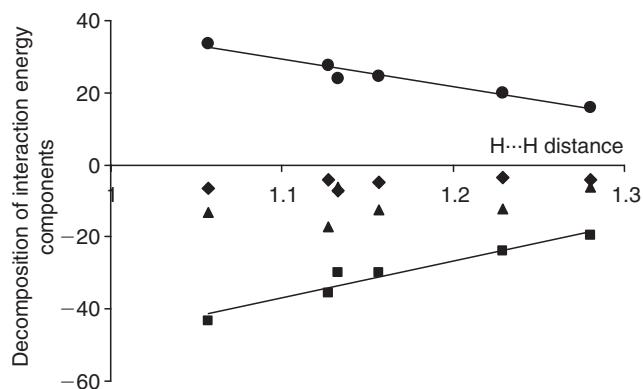


Figure 11. The relationships between the $\text{H} \cdots \text{H}$ intermolecular distance (in Å) and the interaction energy terms (in kcal/mol), circles—exchange, squares—delocalization, triangles—electrostatic and twisted squares—correlation. (Reprinted with permission from Ref. [41]. Copyright 2005 American Chemical Society.)

(correlation and electrostatic) do not correlate with H···H distance and are of much less importance. It is also worth mentioning that almost for all complexes considered the Laplacian of electron density at H···H BCP is negative, or at least the H_C value (the electron energy density at BCP) is negative. This shows that dihydrogen bonds, O–H···H–Be, are covalent in nature. Such covalency is connected with the importance of exchange and delocalization interaction energy terms.

It was pointed out that the AIM parameters for some intramolecular RAHBs indicate the covalent nature of these interactions. This was described in this chapter for benzylacetone and for the transition states of proton transfer reactions. The SSHBs were also analyzed [12], and the AIM results indicate negative values of Laplacian for the proton···acceptor bond critical point. There are also very interesting results for intermolecular RAHBs. The H_C values for intermolecular H···O contacts of formic and acetic acids are negative [49]. This is often described as the partly covalent nature of the interaction (Chap. 9). However, for the formamide dimer where heteronuclear N–H···O RAHBs exist, neither the Laplacian nor H_C for the intermolecular (N)H···O contact is negative. This may be explained within the principle of the minimal proton affinity difference [53] between donor and acceptor. Such a difference is close to zero for homonuclear O–H···O H-bonds, especially for symmetrical systems, while that value is greater for N–H···O interactions. For the latter there is the greater proton affinity of nitrogen than for the oxygen accepting center. This is observed for the structure of PCA discussed here since O–H···O interactions for the A and B forms of dimeric PCA are stronger than N–H···O interactions for the C-conformation. Similarly weaker N–H···O interactions were found for dimers of Pyrrole-2-Carboxamide [54] in the crystal structure (Fig. 12). The binding energy for that dimer (calculated at the MP2/6-311++G(*d,p*) level, BSSE included) is equal to -13.6 kcal/mol (it corresponds to the energy of two symmetrically equivalent N–H···O H-bond energies).

To provide more insight into the nature of heteronuclear intermolecular RAHBs, ab initio calculations at the MP2/6-311++G(*d,p*) level of approximation and QTAIM (Quantum Theory “Atoms in Molecules”) calculations were performed for the formamide dimer (Fig. 13) and its simple fluoro derivatives [55]. In these derivatives the fluoro substituents have replaced the H-atom connected with the carbon and/or H-atom not participating in the hydrogen bond interaction and connected with nitrogen.

Additionally the corresponding tautomeric forms with double O–H···N H-bonds were also considered as well as the transition states corresponding to the C–N–H···O=C \leftrightarrow C=N···H–O–C proton transfer reaction. Finally, all N···H (N–H) and H···O (O–H) interactions of N–H···O and O–H···N systems were collected and analyzed. The findings are as follows. For N–H···O hydrogen bonds for N–H BCPs, the Laplacian values are negative, while for H···O contacts, they are positive indicating that these interactions are covalent and noncovalent, respectively. For O–H···N hydrogen bonds, the situation is

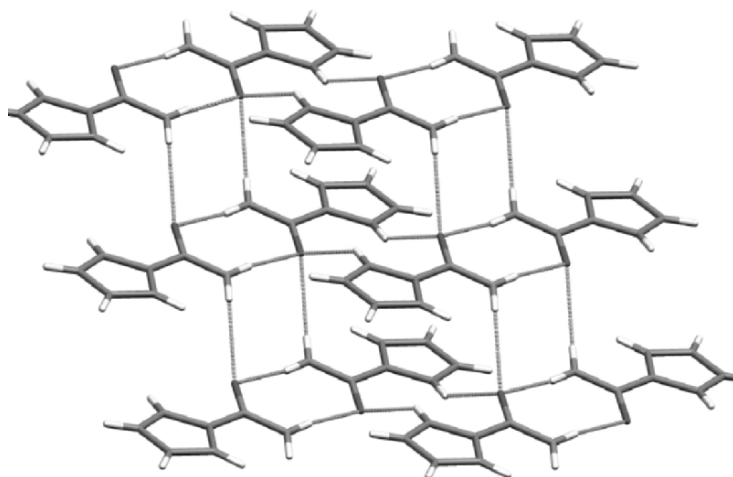


Figure 12 (see color section). Pyrrole-2-Carboxamide—crystal structure motif containing centrosymmetric dimers with double N–H···O H-bonds.

the same as for N–H···O. There are O–H covalent bonds and H···N contacts. However, the latter interactions are characterized by positive Laplacian values and negative H_C values. This may indicate the partially covalent nature of such interactions. It is worth mentioning that for H···O contacts of N–H···O systems, the H_C values are positive. For transition states, both H···O and H···N interactions within the N···H···O H-bonds are characterized by negative Laplacian values of electron density of the corresponding BCP. These findings are in line with the minimum difference of the proton affinities of the donor and acceptor principle, with the Leffler–Hammond rule and the transition state model for H-bonds introduced recently by Gilli et al. [27]. It was

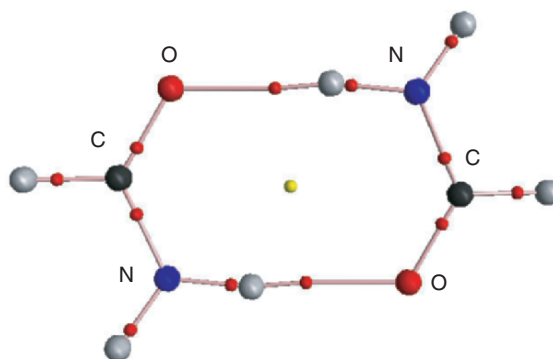


Figure 13. Molecular graph of formamide dimer.

found that N···H···O H-bonds for transition states are the strongest; next are O–H···N interactions being often close to the corresponding TSs; and the N–H···O H-bonds being far from the TSs are the weakest.

6 CONCLUDING REMARKS

Hydrogen bonds affected by π -electron delocalization are often classified as RAHBs. These interactions are usually stronger than typical hydrogen bonds that have primarily electrostatic character. For some very strong RAHBs, short proton···acceptor distances were detected, and it is sometimes pointed out that they are covalent in nature. What does it mean is that these interactions are covalent in nature? The QTAIM indicates that for such interactions the Laplacian value of the electron density at the proton···acceptor bond critical is negative, or at least the electron energy density at BCP is negative. An analysis of the interaction energy components shows that, for hydrogen bonds covalent in nature, the delocalization interaction energy term is the most important attractive contribution. The delocalization term as well as the exchange component strongly correlates with the proton···acceptor distance. These conditions are also fulfilled for very strong intermolecular homonuclear RAHBs.

ACKNOWLEDGMENT

The authors thank the State Committee for Scientific Research (KBN No. 3T09A 138 26), NSF CREST No. HRD-0125484, NSF EPSCoR 02-01-0067-08/MSU, and ONR Grant N00014-98-1-0592 for financial support.

REFERENCES

1. G.A. Jeffrey, *An Introduction to Hydrogen Bonding* (Oxford University Press, New York, 1997).
2. L. Sobczyk, S.J. Grabowski and T.M. Krygowski (2005) *Chem. Rev.* **105**, 3513.
3. J. Emsley (1984) *Struct. Bonding* **57**, 147.
4. G.A. Jeffrey and W. Saenger, *Hydrogen Bonding in Biological Structures* (Springer-Verlag, Berlin, 1991).
5. G. Gilli, F. Belluci, V. Ferretti and V. Bertolasi (1989) *J. Am. Chem. Soc.* **111**, 1023.
6. M.L. Huggins (1936) *J. Org. Chem.* **1**, 405.
7. C.A. Coulson, *Valence* (Oxford University Press, Oxford, 1952).
8. H.A. Staab, *Einführung in die Theoretische Organische Chemie* (Verlag Chemie, Weinheim/Bergstr, 1959).
9. V. Bertolasi, P. Gilli, V. Ferretti and G. Gilli (1991) *J. Am. Chem. Soc.* **113**, 4917.
10. I. Alkorta, J. Elguero, O. Mó, M. Yañez and J.E. del Bene (2004) *Mol. Phys.* **102**, 2563.
11. I. Alkorta, J. Elguero, O. Mó, M. Yañez and J.E. del Bene (2005) *Chem. Phys. Lett.* **411**, 411.
12. (a) J.A. Gerlt, M.M. Kreevoy, W.W. Cleland and P.A. Frey (1997) *Chem. Biol.* **4**, 259. (b) C.L. Perrin and J.B. Nielson (1997) *Annu. Rev. Phys. Chem.* **48**, 511. (c) V. Guallar, M. Moreno, J.M. Lluch, F. Arnat-Guerri and A. Douhal (1996) *J. Phys. Chem.* **100**, 19789. (d) M. Garcia-Viloca, A. González-Lafont and J.M. Lluch (1997) *J. Phys. Chem. A* **101**, 3880. (e) M. Garcia-Viloca, R. Gelabert, A. González-Lafont, M. Moreno, and J.M. Lluch (1997) *J. Phys. Chem. A* **101**, 8727. (f) M. Garcia-Viloca, A. González-Lafont and J.M. Lluch (1997) *J. Am. Chem. Soc.* **119**, 1081.

13. G. Buemi and F. Zuccarello (2004) *Chem. Phys.* **306**, 115.
14. S.J. Grabowski (2001) *J. Mol. Struct.* **562**, 137.
15. R.F.W. Bader, *Atoms in Molecules. A Quantum Theory* (Oxford University Press, New York, 1990).
16. (a) O. Galvez, P.C. Gomez and L.F. Pacios (2001) *Chem. Phys. Lett.* **337**, 263. (b) O. Galvez, P.C. Gomez and L.F. Pacios (2001) *J. Chem. Phys.* **115**, 11166. (c) O. Galvez, P.C. Gomez and L.F. Pacios (2003) *J. Chem. Phys.* **118**, 4878. (d) L.F. Pacios (2004) *J. Phys. Chem. A* **108**, 1177. (e) S.J. Grabowski (2001) *J. Phys. Chem. A* **105**, 10739. (f) C. Gatti, F. Cargnoni and L. Bertini (2003) *J. Comput. Chem.* **24**, 422.
17. M.C. Etter (1990) *Acc. Chem. Res.* **23**, 120.
18. J. Donohue (1952) *J. Phys. Chem.* **56**, 502.
19. G.K.H. Madsen, B.B. Iversen, F.K. Larsen, M. Kapon, G.M. Reisner and F.H. Herbstein (1998) *J. Am. Chem. Soc.* **120**, 10040.
20. L. Pauling, *The Nature of the Chemical Bond* (Ithaca, NY, Cornell University Press, Ithaca, New York, 1960).
21. (a) C.A. Coulson and U. Danielsson (1954) *Ark. Fys.* **8**, 239. (b) C.A. Coulson and U. Danielsson (1954) *Ark. Fys.* **8**, 245. (c) G.C. Pimentel (1951) *J. Chem. Phys.* **19**, 446. (d) C. Reid (1959) *J. Chem. Phys.* **30**, 182. (e) P.A. Kollman and L.C. Allen (1970) *J. Am. Chem. Soc.* **92**, 6101. (f) E.D. Stevens, M.S. Lehmann and P. Coppens (1977) *J. Am. Chem. Soc.* **99**, 2829. (g) P.J. Desmeules and L.C. Allen (1980) *J. Chem. Phys.* **72**, 4731.
22. (a) T.K. Ghanty, V.N. Staroverov, P.R. Koren and E.R. Davidson (2000) *J. Am. Chem. Soc.* **122**, 1210. (b) T.W. Martin and Z.S. Derewenda (1999) *Nature Struct. Biol.* **6**, 403. (c) J.J. Dannenberg, L. Haskamp and A. Masunov (1999) *J. Phys. Chem. A* **103**, 7083.
23. (a) P. Gilli, V. Bertolasi, V. Ferretti and G. Gilli (1994) *J. Am. Chem. Soc.* **116**, 909. (b) G. Gilli and P. Gilli (2000) *J. Mol. Struct.* **552**, 1.
24. (a) P. Gilli, V. Bertolasi, V. Ferretti and G. Gilli (2000) *J. Am. Chem. Soc.* **122**, 10405. (b) P. Gilli, V. Bertolasi, L. Pretto, A. Lyčka and G. Gilli (2002) *J. Am. Chem. Soc.* **124**, 13554.
25. (a) A.J. Rybarczyk-Pirek, S.J. Grabowski, M. Małecka and J. Nawrot-Modranka (2002) *J. Phys. Chem. A* **106**, 11956. (b) A.J. Rybarczyk-Pirek, S.J. Grabowski and J. Nawrot-Modranka (2003) *J. Phys. Chem. A* **107**, 9232. (c) M. Małecka, S.J. Grabowski and E. Budzisz (2004) *Chem. Phys.* **297**, 235.
26. (a) J.D. Dunitz, *X-Ray Analysis and the Structure of Organic Molecules* (Cornell University Press, Ithaca, 1979). (b) H.-B. Bürgi (1975) *Angew. Chem. Internat. Edit.* **14**, 460.
27. P. Gilli, V. Bertolasi, L. Pretto, L. Antonov and G. Gilli, (2005) *J. Am. Chem. Soc.* **127**, 4943.
28. (a) J.E. Leffler (1953) *Science* **117**, 340. (b) G.S. Hammond (1955) *J. Am. Chem. Soc.* **77**, 334.
29. (a) A. Filarowski, A. Koll and T. Głowiak (2002) *J. Chem. Soc. Perkin Trans. 2*, 835. (b) A. Filarowski and A. Koll (1998) *Vibr. Spectr.* **17**, 123. (c) A. Filarowski, A. Koll, T. Głowiak, E. Majewski and T. Dziembowska (1998) *Ber. Bunsenges. Phys. Chem.* **102**, 393. (d) A. Filarowski, A. Koll and T. Głowiak (1999) *Monatsh. Chem.* **130**, 1097. (e) A. Filarowski, A. Koll, A. Karpfen and P. Wolschann (2004) *Chem. Phys.* **297**, 323.
30. A.J. Rybarczyk-Pirek, A.T. Dubis, S.J. Grabowski and J. Nawrot-Modranka (2006) *Chem. Phys.* **320**, 247.
31. (a) G. Buemi and F. Zuccarello (2000) *J. Mol. Struct. (Theochem)* **506**, 213. (b) G. Buemi (2000) *J. Mol. Struct. (Theochem)* **499**, 21. (c) G. Buemi and F. Zuccarello (2002) *J. Mol. Struct. (Theochem)* **581**, 71. (d) G. Buemi and F. Zuccarello (2005) *J. Mol. Struct. (Theochem)* **719**, 137. (e) G. Buemi (2002) *Chem. Phys.* **277**, 241. (f) G. Buemi (2002) *Chem. Phys.* **282**, 181. (g) G. Buemi (2004) *Chem. Phys.* **300**, 107.
32. (a) M. Cuma, S. Scheiner and T. Kar (1999) *J. Mol. Struct. (Theochem)* **467**, 37. (b) S. Wojtulewski and S.J. Grabowski (2003) *J. Mol. Struct.* **645**, 287.
33. L. González, O. Mó and M. Yáñez (1999) *J. Org. Chem.* **64**, 2314.
34. P. Sanz, M. Yáñez and O. Mó (2002) *J. Phys. Chem. A* **106**, 4661.
35. S. Wojtulewski and S.J. Grabowski (2003) *Chem. Phys. Lett.* **378**, 388.

36. S. Wojtulewski and S.J. Grabowski (2005) *Chem. Phys.* **309**, 183.
37. K. Kitaura and K. Morokuma (1976) *Int. J. Quantum Chem.* **10**, 325.
38. Y. Gu, S. Kar and S. Scheiner (1999) *J. Am. Chem. Soc.* **121**, 9411.
39. S.F. Boys and F. Bernardi (1970) *Mol. Phys.* **19**, 553.
40. (a) W.A. Sokalski, S. Roszak and K. Pecul (1988) *Chem. Phys. Lett.* **153**, 153. (b) W.A. Sokalski and S. Roszak (1991) *J. Mol. Struct. (Theochem)* **234**, 387. (c) R.W. Gora, W. Bartkowiak, S. Roszak and J. Leszczynski (2002) *J. Chem. Phys.* **117**, 1031. (d) R.W. Gora, W. Bartkowiak, S. Roszak and J. Leszczynski (2004) *J. Chem. Phys.* **120**, 2802.
41. S.J. Grabowski, W.A. Sokalski and J. Leszczynski (2005) *J. Phys. Chem. A* **109**, 4331.
42. (a) J. Sponer, J. Leszczynski and P. Hobza (1996) *J. Phys. Chem.* **100**, 1965. (b) J. Florian and J. Leszczynski (1996) *J. Am. Chem. Soc.* **118**, 3010. (c) N.U. Zhanpeisov, J. Sponer and J. Leszczynski (1998) *J. Phys. Chem. A* **102**, 10374. (d) N.U. Zhanpeisov and J. Leszczynski (1998) *J. Phys. Chem. B* **102**, 9109. (e) Y. Podolyan, Y.V. Rubin and J. Leszczynski (2000) *J. Phys. Chem. A* **104**, 9964.
43. C.F. Guerra, F.M. Bickelhaupt, J.G. Snijders and E.J. Baerends (1999) *Chem. Eur. J.* **5**, 3581.
44. L. Leiserowitz (1976) *Acta Cryst.* **B32**, 775.
45. (a) I.D. Brown (1978) *Chem. Soc. Rev.* **7**, 359. (b) I.D. Brown and D. Altermat (1985) *Acta Cryst.* **B41**, 244. (c) I.D. Brown (1992) *Acta Cryst.* **B48**, 553.
46. Y. Kim (1996) *J. Am. Chem. Soc.* **118**, 1522.
47. A.T. Dubis, S.J. Grabowski, D.B. Romanowska, T. Misiaszek and J. Leszczynski (2002) *J. Phys. Chem. A* **106**, 10613.
48. S.J. Grabowski, A.T. Dubis, D. Martynowski, M. Glowka, M. Palusiak and J. Leszczynski (2004) *J. Phys. Chem. A* **108**, 5815.
49. R.W. Gora, S.J. Grabowski and J. Leszczynski (2005) *J. Phys. Chem. A* **109**, 6397.
50. C. Møller and M.S. Plesset (1934) *Phys. Rev.* **46**, 618.
51. (a) A.D. McLean and G.S. Chandler (1980) *J. Chem. Phys.* **72**, 5639. (b) M.J. Frisch, J.A. Pople and J.S. Binkley (1984) *J. Chem. Phys.* **80**, 3265. (c) R. Krishnan, J.S. Binkley, R. Seeger and J.A. Pople (1980) *J. Chem. Phys.* **72**, 650. (d) T. Clark, J. Chandrasekhar, G.W. Spitznagel and P.v. R. Schleyer (1983) *J. Comput. Chem.* **4**, 294.
52. (a) D.E. Woon and T.H. Dunning, Jr. (1993) *J. Chem. Phys.* **98**, 1358. (b) R.E. Kendall, T.H. Dunning, Jr. and R.J. Harrison (1992) *J. Chem. Phys.* **96**, 6796.
53. (a) Z. Malarski, M. Rospenk, L. Sobczyk and E. Grech (1982) *J. Phys. Chem.* **86**, 401. (b) L. Sobczyk (1998) *Ber. Bunsen-Ges. Phys. Chem.* **102**, 377.
54. S.J. Grabowski, A. Dubis, M. Palusiak and J. Leszczynski (2006) *J. Phys. Chem. B* **110**, 5875.
55. S.J. Grabowski, W.A. Sokalski and J. Leszczynski (2006) *J. Phys. Chem. A* **110**, 4772.

INDEX

- π -electron delocalization 13, 72, 418–420, 421, 423, 425–432, 487–499
- π -delocalization energy 77–80
- π -delocalization 520
- α -helix 8, 30, 31, 263
- β -diketones 67, 70, 75, 76, 409–411
- λ -parameter 71, 72, 73, 489, 492
- σ -type H-bonds 159
- π -type H-bonds 159
- χ -type H-bonds 159
- $[(\eta^5\text{-C}_5\text{H}_5)_2\text{MoH}(\text{CO})]^+$ structure 259
- $[\text{IrH}(\text{OH})(\text{PH}_3)_4][\text{PF}_6]$ complex 252
- $[\text{IrH}(\text{OH})(\text{PMe}_3)_4][\text{PF}_6]$: cation 251
- $[\text{IrH}_3(\text{HNCHNH}_2)(\text{PH}_3)_2]$ complex 252
- $[\text{MnH}(\text{CO})_5]$ dimer 257
- $[\text{ReH}_5(\text{PPh}_3)_3] \cdots \text{indole} \cdots \text{benzene}$ 254
- 1, 2, 4, 5-tetrafluorobenzene—water complex 280
- 1-fluoro-cyclopropane-carboxylic acid 82
- 3, 3-difluorobutan-1-ol 82
- 3-fluorobutan-1-ol 82
- ab initio computational packages 59
- ab initio methods 57–62, 384
- acceptor groups 55, 77, 112, 113, 116, 135, 137, 144, 211, 213, 216, 217, 321, 478, 479, 480
- accumulation of electron density 201, 345
- acetylene 228, 237, 238, 345, 501
- acidity constants 69
- acidity of a CH group 228
- Ac-L-Ala-NMe₂ dimer 277
- Adenine–Uracil (AU) dimer 271, 272
- adiabatic potential curves 422
- agostic bonds 247
- AIM (“atoms in molecules”) 2, 12–14, 16, 23, 24, 28, 34, 111, 115–116, 119–130
- AIM 2000 program 35, 350
- AIM atomic charges 116, 126, 128
- AIMDELOC program 350
- AIMPAC package 350
- ammonia interactions 156, 158
- angular displacements 476, 479, 480
- anharmonic potential energy shape 391–395
- anharmonic potentials 379, 380
- anharmonic systems 384
- anharmonicity effect 86–88
- anharmonicity of the stretching protonic vibrations 377–378
- anion \cdots anion dimers 233
- anions of dicarboxylic acids 411
- anomalous thermal expansion 471, 480–481
- anthracene 352, 353, 354, 359
- antisymmetric many-electron wave function 345
- aromatic hydrocarbons 350, 358, 359
- atomic basins 116, 128, 129, 340, 342, 343, 350, 446, 447
- atomic dipolar polarizations 14, 56, 448
- atomic displacement parameters (ADP) 451
- atomic energies 349, 350, 354, 356, 357, 358, 360, 362, 363
- atomic polarisabilities 344
- B3LYP 55, 60, 62, 63, 64, 65, 115, 150, 174, 208, 387, 390
- base pairs 7, 8, 28–30
- basis set superposition error (BSSE) 11, 12, 16, 33, 62–63, 115, 151, 210, 500
- Be₂ dimer 210
- benzene dimer 55, 163
- benzene 237, 279, 345, 419
- benzylacetone 493, 508
- beryllum hydride 506
- BH₃NH₃ 55, 338
- biphenyl 354–356

- bistable hydrogen bonds 376, 377
- blue-shifted hydrogen
 - bond—concept 318–329
- blue-shifted hydrogen
 - bonds—examples 318–323
- blue-shifting hydrogen bonds 3–4, 299–317
- bond component 200
- bond critical point (BCP) 12, 56, 115, 185, 201, 230, 342, 344, 345, 445
- bond degree index 449
- bond ellipticity 345
- Bond Order (BO) 344, 346, 445
- Bond Path (BP) 12, 13, 31, 56, 124, 342, 344, 345, 351, 352, 355, 363, 446, 465
- Bond Valence (BV) model 503
- Bond-path length (BPL) 446, 455, 463
- Born–Oppenheimer (BO) surface 380
- Born–Oppenheimer approximation 442
- Bragg scattering 450
- Bürgi and Dunitz rule 496, 502

- Cage Critical Point (CCP) 17, 362
- calculation of NMR isotope
 - effects 385–387
- calixarenes 90–91
- Cambridge Structure Database (CSD) 194, 206, 211, 215, 246, 367, 368, 418, 428
- carbonylamine 53, 68, 78
- carboxylic acids 232, 402, 405, 409, 411, 412, 458, 476, 488, 493, 501–506
- Car–Parrinello simulation 388–390
- cation···cation dimers 233
- CCSD 11, 151, 164
- C–H bond acidity 265
- CH proton donors 278
- C–H···H–M short contacts 256
- C–H···O hydrogen bonds 219–232, 264, 265, 266
- C–H··· π interactions 159, 237, 238
- CH···O interaction energies for amino acids 276
- CH···O=C interactions 266
- CH···X hydrogen bonding 193–244
- C–H···B hydrogen bonds—
 - examples 299–301
- C–H···S interactions 237

- C–H···X intermolecular interactions 270
- CH₄ dimer 339
- Charge assisted hydrogen bonds (CAHBs) 69, 205, 398, 406, 463, 494
- charge density 112, 246, 449–451
- charge transfer effect 167, 169
- charge transfer term 500
- charge transfer 432, 449, 452
- Charge-coupled device (CCD) 443
- charge-induced bonds 233–234
- charge-quadrupole term 198
- charge-transfer components 199
- CISD 350
- classification of bonding interactions 347
- closed-shell interaction 122, 124, 200, 338, 339, 342, 345, 347, 358, 367, 368, 445, 447, 448, 449, 458, 463
- Co···H distance 249
- colour changes 473, 474
- Complete basis set (CBS) 60, 164
- Compton profile anisotropies 110
- conformation changes 463
- conjugated bonds 490
- continuous phase transition 481
- contour plot of the electron density 340
- conventional hydrogen bond donors 295
- conventional hydrogen bonding 2–4
- convolution 450
- cooperative effect 150, 172–174
- cooperative effects in H₂O 217
- coordination chemistry 171–172
- core density 451
- correlation energy 60, 61, 80, 84, 151, 500–501
- Coulombic correlation 350
- Coumarines* 498, 499
- counterpoise corrections 16, 62, 210, 339
- coupling of protonic stretching
 - vibrations 378
- coupling parameter 71
- covalency 3, 32–35, 110, 494
- covalent bond—AIM characteristics 122, 124, 246–247, 445
- covalent bond 129, 247, 344, 441, 445
- covalent H-bonds 32, 494
- covalent/shared interaction 342
- Critical point (CP) 56, 115, 230, 342
- critical temperature 479, 480

- crystal engineering 9
crystal-field effects 388, 457–458
cyclic peptides 182–183
- decomposition of interaction energy 151–152, 249, 256, 258, 499–501
deformation density 443
delocalisation index $\delta(A, B)$ 346
delocalisation indices 350
delocalization energy term 500
density radial function (RDF) 451, 452
deprotonated dicarboxylic acids 232
DFT 5, 7, 11, 60, 111, 115, 208, 350, 383, 390
Dibenz[*a, j*]anthracene 354
diffuse functions 60, 150
dihydrogen bonds 13, 54, 55, 83–84, 246, 251–259, 338–340, 506–508
Dimer-centred basis set (DCBS) 500
dimeric complexes of H₂O 211
dipole momentum 198, 452
dipole–dipole term 338
disorder 459, 475, 502
disordered H-bond dimension 478
dispersion component 205, 213
dispersion interaction energy 3, 11, 12, 151, 158, 161, 168, 200, 295, 297, 316
displacive phase transition 479
dissociation energy 24, 358, 380, 460
DNA 7–12, 28–30
DNA base pairing 8, 263
donor groups 109, 110, 112, 116, 119, 123, 143, 213, 215, 298
double minimum potential 378
Dunning basis sets 5, 12, 60
- edge-to-face interactions 163–171
Ehrenfest forces 360
electron density—isocontours 119, 131
electron density—topological descriptors 115, 119–126
electron density (ED) 457
electron density 4, 13, 14, 17, 18, 19, 20, 21, 22, 23, 24, 27, 30, 31, 32, 56, 111, 112, 113, 115–116, 119, 124, 195, 216, 239, 338, 340, 344, 350
electron density at the BCP 356
electron donating substituents 490
- electron localization function (ELF) 86, 112, 113, 117–118, 135–142
electronegative elements 111, 246, 264, 338
electronegativities 86, 294
electronegativity of carbon 263
electronic energy 64, 150, 346, 442
electron-withdrawing substituents 40, 80, 169, 300, 315, 490
electrostatic forces 465, 476
electrostatic interaction energy 3, 111, 156, 158, 167, 172, 198, 199, 246, 249, 337, 418, 457, 494, 499, 500, 505
electrostatic potentials 112, 116–117, 130–135
Electrostatic-covalent H-bond model (ECHB) 32, 494
Empirical valence bond (EVB) method 380, 383, 384
energy of H-bond formation 296
enol–keto form 489, 490
enols 409–411, 458
enzyme catalysis 8, 177–179
equilibrium geometry 324, 327, 345, 349, 357, 360
Erenfest's classification 480
error distribution 465
Espinosa's relationship 459
ethylene 345
Etter's rules 239, 492
exchange energy term 11, 151, 158, 161, 167, 199, 200, 256, 315, 316, 500, 501, 507
excited vibrational levels 378, 392
experimental uncertainties 443, 448, 461, 465
- ferroelectrics 479, 481
first-order density matrix 351
first-order phase transitions 480
fold catastrophe 355
formaldehyde 5, 230, 273, 326, 329
formamide dimer 113, 228, 505–506
formamide–formic acid complex 113
formazan 68
formic acid dimer 113, 502, 503
Fourier transform 450, 465
frequency isotope effects 395–396
furan crystal 367

- GAMESS program 59
Gaussian program 11, 59, 87, 115
glyoxalmonoxime 74
good acceptors 493
good proton donors 493
Grabowski's measure of H-bond strength 14–15
gradient trajectory, path 444, 445
gradient vector field of the electron density 56, 118, 340, 342
Graph sets: motifs 213–217
guanosine geometries 273
- H/D isotope effects 384
H···H interaction 363, 364
H···H contacts 350–358
Hammett's substituent constants 163, 164, 167, 434
Harmonic Ansatz 324–426
harmonic approximation 324, 327, 377, 380, 384
harmonic potential 382
Hartree–Fock method (HF) 11, 58, 60, 62, 208, 350, 383, 390, 499–500
hexafluoroacetylacetone 68
H-bond in amphi-ionophores 182–183
HCOOH/HCONH₂ pair 274
Heitler–London energy 500
Hellmann–Feynman theorem 419
Hessian matrix of electron density 124
Hessian 444
heteronuclear intramolecular H-bonds 77–84
heteronuclear intramolecular RAHBs 494–499
high level calculations 13, 30, 59, 61–62
HOMA 419–420
HOMO 151, 158
HOSE—harmonic oscillator stabilization energy 423
hydrated anion clusters 171
hydration 6, 8, 20, 171–172
hydrogen bonding—AIM characteristics 12, 13, 122, 230
hydrogen bonding—AIM criteria 14, 448–449
hydrogen bonding—characteristics 494
hydrogen bonding—definition 2, 195, 238, 245–246, 254, 297, 417, 494
hydrogen bonding—energy 62, 149, 203, 270, 400
hydrogen bonding—experimental evidences 4, 7, 20
hydrogen bonding—geometry 57, 202
hydrogen bonding—IR spectroscopy 203
hydrogen bonding—NMR spectroscopy 203
hydrogen bonding—rotational spectroscopy of gas-phase complexes 203
hydrogen bonding—types 3–4
hydrogen bonding in proteins 8, 30
hydrogen bonds—classification 2–4, 52–56
hydrogen–hydrogen bonding 358, 360
hydronium ion 506
hysteresis 480
- ice I_h polymorph 217
ice 217, 460, 472
induction energy 158, 168
integrated topological properties 14, 23, 118, 124, 346, 448, 455, 458, 462, 465
interaction density 456, 463, 465
Interaction line (IL) 56, 124, 445
Interatomic surface (IS) 340, 342, 361, 445
intermolecular hydrogen bonds 62–63
intermolecular hydrogen–hydrogen bonding 365–367
Intermolecular perturbation theory (IMPT) 199–200
intermolecular RAHBs 501–506
intramolecular dihydrogen bonds 83–84, 254
intramolecular H-bonds—H-bond energy 63–64
intramolecular hydrogen bonds—energetics 69–70, 361–369
intramolecular hydrogen bonds 63–64, 67, 76, 77, 270, 409–411
intramolecular hydrogen–hydrogen bonding—examples 361–365
intramolecular RAHBs 488–501
inverse hydrogen bonds 55, 338

- ionic bonds 51, 195, 200
ionic character 501
ionic hydrogen bonding 27, 180
ionic interaction—AIM
 characteristics 14, 200–201, 344, 347, 445
ionic system, Na⁺Cl 500
IR spectra 7, 11, 86–88, 391–395
isolated hydrogen bonds 203, 204
isotope effect 66, 381, 384, 385–387, 395, 403–407
isotropic displacement amplitude 453
- KDP ferroelectrics 479, 480, 481, 482
keto–enol forms 489, 492
kinetic electron energy density at
 BCP 124, 345
kinetic and potential energy density 124, 125, 230, 342, 345
Kitaura–Morokuma approach 499, 500
Koch–Popelier criteria 12–13, 56–57, 120
- Landau phase transition 481
Laplacian of electron density 13, 14, 15, 22, 26, 31, 56, 115, 124, 143, 246, 249, 252, 344–345, 348, 445, 446, 448, 458, 494, 497
latent heat 480
lattice-mode vibrations 481
least-squares refinement 450
Leffler–Hammond rule 497, 505, 509
Lennard–Jones potential 12, 67
Lippincott–Schröder function 66, 67, 381–383, 410
local coordinate system 451
local source function 447
local virial theorem 345, 446, 465
localized Wannier functions 110
Low barrier hydrogen bonds (LBHBs) 65, 69, 110
LUMO 151, 158
- malonaldehyde 53, 54, 63, 66, 68, 70, 72, 73, 74, 76, 78, 79, 80, 424, 488
malondialdehyde 83
Mannich bases 394, 395, 396, 406, 420–424, 498
matrix diagonalization procedures 385
- mean-square displacement amplitudes (MSDA) 450
metallic bond—AIM characteristics 347
methane–water interaction 205, 219, 220
methanol–water complex 113
microsalvation 6–7
model ambiguities 465
modified Morse potential 380
molecular graph 342
molecular hydration 6–7
Morse potential 380–383
MP2 method 12, 208, 210, 220
multipolar refinement 350, 363
multipole expansion 451
multipole population 451, 454, 455
multireference methods 210
mutual penetration 14, 137, 144, 448
- N*, *N*-dimethylformamide dimer 275
nanotubes 150, 174–176
naphthalene 419, 420
NBO populations 19, 111, 116, 126–130, 143
neutron diffraction (ND) 211
N–H···Co hydrogen bonds 249
N–H···N hydrogen bonds 66, 77, 249
NH···O hydrogen bonds 54, 66, 78, 81
N–H···N intramolecular H-bonds 77
NHN ferroelectrics 482
NICS 433
nitrosoethanol 74, 75
N-methyl maleimide–acetone complex 279
N-methyl maleimide–water complex 279
NMR spectroscopy 10, 204, 399
N-substituents 496
nuclear cusp condition 452
nucleic acids 7–8, 264, 265, 266
- OH stretching modes 66, 73, 79, 86, 389
O–H···Mo contact 250
OH···O hydrogen bonds 70, 76, 211–212
OH···π hydrogen bond 263
O–H···O interactions in crystals 211–212
one-dimensional potential energy curves 378–379
open quantum system 343
optimized geometry 111, 449

- order-disorder phase transitions 478
organometallic complexes 246
Os-H···H-N interaction 254
overlap integral of two spin orbitals 346
overtones 378, 391
- pairs of acetic acid molecules 270, 506
partially covalent H-bond 509
partitioning of the molecular energy into
 atomic contributions 347-349
Pauli exclusion principle 500
phase transitions 478, 479-481
phenanthrene 351, 352, 353, 361, 419
phenol systems 159
phenols 427-431
phenol-water clusters 20-23
phenol-water complexes 162
phosphine oxides 250
phosphorocoumarine 498
picolinic acid N-oxide—free energy
 surface 384-387
picolinic acid N-oxide 384
 π -systems 158-163
plot of the electron density
 distribution 340
Poincaré-Hopf relationship 351
Poisson's equation 112
polar systems 156-158
polar-covalent bond 342, 347
polarizability 167, 199, 219, 393
polarizability-driven inductive effect 167
Polarization-assisted hydrogen bonds
 (PAHBs) 69
polarization component 168, 169
polarization interaction energy term 316,
 500
polarization 3, 4, 155, 169, 173,
 199, 217
polarized basis sets 60
polypeptides 30-32
polymorphism 474, 475, 477
Popelier's criteria 12-13, 56-57, 120
Pople basis sets 5
post-self-consistent field (SCF)
 configuration interaction
 methods 350
potential electron energy density at
 BCP 124, 342
- potential surfaces—complexes with
 intermolecular hydrogen
 bond 400-406
principal curvatures 444, 445
probability density function 407, 450
promolecule 239, 451, 465
protein secondary structure 8-9
proteins 8, 9, 30, 266, 268, 271
proton acceptor 2, 4, 201, 205, 211, 228,
 229, 265, 294
proton affinities 69, 496, 498, 509
proton donor 2, 155, 156, 201, 205, 211,
 216, 228, 250, 255, 263, 267
proton motion—quantum-dynamical
 simulation 386, 387, 388
proton nuclear magnetic resonance
 (¹HNMR) chemical shifts 296
proton transfer pathway 70
proton transfer reaction 225, 383, 489,
 496, 457, 502
protonated 2,7-dimethoxy-DMAN 398
proton-stretching vibrational mode 296
pseudoatom model 451, 452
pseudoatom 451
pyridine 158, 394
pyrimidine dimer 273
pyrrole 87, 158, 503
pyrrole-2-carboxamide 508
pyrrole-2-carboxylic acid (PCA) 503
- QCISD 61, 210, 350
QCISD(T) 210
Q-parameter 489, 490, 491, 492
Quantum Theory of Atoms in Molecules
 (QTAIM) 339-341
- reaction path for the proton transfer
 reaction 502
relaxor 482, 483
repulsive interaction 67, 91, 150, 339, 363,
 368
Resonance-assisted hydrogen bonds
 (RAHBs) 54, 67, 69, 70, 71, 488-499
resonance energy 78, 351, 423
resonance parameter 71, 424, 425
rigid-body motion 453
Ring critical point (RCP) 16, 17, 32, 351,
 355

- RNA 7–8
rotation barrier 59, 68, 77–80
Ru–H···H–O bond 255
Ru–H···Si contacts 251
- SAPT 151, 158, 161, 168
scattering angle 453
scattering factor 450
scattering vector 450
Schiff bases 420–424, 498
Schwinger's principle 343
SCVS corrections scale 350
second-order phase transitions 480
Self-consistent reaction field (SCRf)
 method 6, 81, 89
semiempirical methods 57–59
S–H···S intramolecular H-bonds 66, 79,
 80, 81
shared-shell interaction 342, 344, 345–
 347, 445, 447
shared-shell interatomic interactions 122
short H···H contacts 338, 367
short H-bond 172–175, 297, 479, 494
Short strong hydrogen bond (SSHB) 110,
 177, 489, 508
Si···H distances 250
six-membered rings 64, 195, 351, 492, 493,
 496
Slater determinant 13
Slater Type Orbitals (STO) 60
soft modes 481
solvent effect 89, 151
SPARTAN program 59
spherical atom 451
spherical harmonics 451, 452
stabilization energy 5, 12, 16, 17, 20, 25,
 26, 30, 33
statistical distance 454
steric repulsion of electron clouds 500
strength of a chemical bond 203, 284, 344
strong O–H···O hydrogen bonds 502
strong symmetric hydrogen bonds 295
structure factor 450–451, 452, 453
structure property relations 471–485
substituent constants 435, 436
substituent effect stabilization energy
 (SESE) 432
substituent effect 80, 163–171
supermolecular approach 151, 507
supramolecular synthons 215
- T*, *L* and *S* tensors 453
tautomeric forms 70, 79, 401, 490, 494,
 496–497, 502, 508
temperature factor 450
tetra-*tert*-butylcyclobutadiene 362
tetra-*tert*-butylindacene 362
tetra-*tert*-butyltetrahedrane 362
Theoretical force-field model 323–329
thermal expansion 480, 483
time-dependent Schrödinger equation 384
topological analysis 118, 456–464
topological partitioning of molecules 343
total electron energy density at BCP 19,
 28, 345, 346
trace of Hessian matrix 124, 344
transferable interaction potentials 12
transition state 64, 70, 177, 255,
 355, 489
tricritical point 481
triphenylene 419, 420
T-shaped dimer of acetylene 501
- unconventional hydrogen bonds 91, 246,
 259, 263
Uracil–uracil (UU) dimer 272
UV spectra 10
- valence deformation 452
valence density 451, 452
Valence shell charge concentration
 (VSCC) 445, 446, 458, 459,
 464, 465
Valence shell electron pair repulsion
 model (VSEPR) 136
van der Waals bonds 200, 201, 215, 219
van der Waals cutoff criterion 295
van der Waals interaction—AIM
 characteristics 338, 342
van der Waals interactions 13, 35, 109,
 201, 246, 302, 445
van der Waals radii 2, 57, 203, 248
very strong hydrogen bond 34, 66, 69,
 297, 378, 403, 458, 494, 510

CHALLENGES AND ADVANCES IN COMPUTATIONAL CHEMISTRY AND PHYSICS

1. M.G. Papadopoulos, A.J. Sadlej and J. Leszczynski (eds.): *Non-Linear Optical Properties of Matter. From Molecules to Condensed Phases*. 2006
ISBN 1-4020-4849-1
2. S.J. Grabowski (ed.): *Hydrogen Bonding. New Insights*. 2006
ISBN 1-4020-4852-1
3. J. Šponer and F. Lankas (eds.): *Computational studies of RNA and DNA*. 2006
ISBN 1-4020-4794-0